

Lecture Notes in Civil Engineering

Antonio Coppola
Giovanni Carlo Di Renzo
Giuseppe Altieri
Paola D'Antonio *Editors*

Innovative Biosystems Engineering for Sustainable Agriculture, Forestry and Food Production

International Mid-Term
Conference 2019 of the Italian
Association of Agricultural Engineering
(AIIA)

 Springer

Lecture Notes in Civil Engineering

Volume 67

Series Editors

Marco di Prisco, Politecnico di Milano, Milano, Italy

Sheng-Hong Chen, School of Water Resources and Hydropower Engineering,
Wuhan University, Wuhan, China

Ioannis Vayas, Institute of Steel Structures, National Technical University of
Athens, Athens, Greece

Sanjay Kumar Shukla, School of Engineering, Edith Cowan University, Joondalup,
WA, Australia

Anuj Sharma, Iowa State University, Ames, IA, USA

Nagesh Kumar, Department of Civil Engineering, Indian Institute of Science
Bangalore, Bangalore, Karnataka, India

Chien Ming Wang, School of Civil Engineering, The University of Queensland,
Brisbane, QLD, Australia

Lecture Notes in Civil Engineering (LNCE) publishes the latest developments in Civil Engineering - quickly, informally and in top quality. Though original research reported in proceedings and post-proceedings represents the core of LNCE, edited volumes of exceptionally high quality and interest may also be considered for publication. Volumes published in LNCE embrace all aspects and subfields of, as well as new challenges in, Civil Engineering. Topics in the series include:

- Construction and Structural Mechanics
- Building Materials
- Concrete, Steel and Timber Structures
- Geotechnical Engineering
- Earthquake Engineering
- Coastal Engineering
- Ocean and Offshore Engineering; Ships and Floating Structures
- Hydraulics, Hydrology and Water Resources Engineering
- Environmental Engineering and Sustainability
- Structural Health and Monitoring
- Surveying and Geographical Information Systems
- Indoor Environments
- Transportation and Traffic
- Risk Analysis
- Safety and Security

To submit a proposal or request further information, please contact the appropriate Springer Editor:

- Mr. Pierpaolo Riva at pierpaolo.riva@springer.com (Europe and Americas);
- Ms. Swati Meherishi at swati.meherishi@springer.com (Asia - except China - and Australia/NZ);
- Ms. Li Shen at li.shen@springer.com (China).

Indexed by Scopus

More information about this series at <http://www.springer.com/series/15087>

Antonio Coppola · Giovanni Carlo Di Renzo ·
Giuseppe Altieri · Paola D'Antonio
Editors

Innovative Biosystems Engineering for Sustainable Agriculture, Forestry and Food Production

International Mid-Term Conference 2019
of the Italian Association of Agricultural
Engineering (AIIA)

 Springer

Editors

Antonio Coppola
Università degli Studi della Basilicata
Potenza, Italy

Giovanni Carlo Di Renzo
Università degli Studi della Basilicata
Potenza, Italy

Giuseppe Altieri
Università degli Studi della Basilicata
Potenza, Italy

Paola D'Antonio
Università degli Studi della Basilicata
Potenza, Italy

ISSN 2366-2557

ISSN 2366-2565 (electronic)

Lecture Notes in Civil Engineering

ISBN 978-3-030-39298-7

ISBN 978-3-030-39299-4 (eBook)

<https://doi.org/10.1007/978-3-030-39299-4>

© Springer Nature Switzerland AG 2020

This work is subject to copyright. All rights are reserved by the Publisher, whether the whole or part of the material is concerned, specifically the rights of translation, reprinting, reuse of illustrations, recitation, broadcasting, reproduction on microfilms or in any other physical way, and transmission or information storage and retrieval, electronic adaptation, computer software, or by similar or dissimilar methodology now known or hereafter developed.

The use of general descriptive names, registered names, trademarks, service marks, etc. in this publication does not imply, even in the absence of a specific statement, that such names are exempt from the relevant protective laws and regulations and therefore free for general use.

The publisher, the authors and the editors are safe to assume that the advice and information in this book are believed to be true and accurate at the date of publication. Neither the publisher nor the authors or the editors give a warranty, expressed or implied, with respect to the material contained herein or for any errors or omissions that may have been made. The publisher remains neutral with regard to jurisdictional claims in published maps and institutional affiliations.

This Springer imprint is published by the registered company Springer Nature Switzerland AG
The registered company address is: Gewerbestrasse 11, 6330 Cham, Switzerland

Preface

The Mid-Term Conference of the Italian Association of Agricultural Engineering (AIIA) is part of a series of conferences, seminars and meetings that AIIA periodically promotes and organizes, also together with other entities and associations, involving stakeholders, public and private, with the aim of facilitating the encounter of research and training, innovation and development demand, and to promote the creation and dissemination of new knowledge in the sector.

This particular 2019 Mid-Term AIIA Conference will deal with the following major topic:

Innovative Biosystems Engineering for Sustainable Agriculture, Forestry and Food Production

The specific subjects will include the following:

- Agricultural hydraulics;
- Water resources management in agriculture and forestry ecosystem;
- Design and management of Farm and District-Scale Irrigation Systems;
- Remote Sensing in agricultural and forestry systems;
- Monitoring and modelling of the interactions among soil hydrological, plant and atmosphere;
- Processes, and agricultural management practices;
- Soil and contaminant hydrology;
- Forestry hydraulics and hydraulics protection of agricultural and forestry systems;
- Bioengineering Techniques for soil protection and slope stabilization;
- Rural buildings, facilities and territory;
- Spatial and landscape analysis;
- Planning and design of rural areas;
- Mechanization and technologies for agricultural production;
- Agricultural electrification and energy usage;

- Ergonomics and work organization;
- Computer and communication technologies;
- Machines and facilities for agricultural products and food processing.

The sustainable development of agriculture, forestry and food production sectors is closely related to the research developments in the field of biosystems engineering.

On one side, biosystems research is oriented to efficiently produce and process biological resources to satisfy the demand of consumers and a wide range of industries for food, feed, bioenergy and bio-based products. At the same time, it provides and develops engineering-based methodologies and decision support tools for management and protection of soil, water and environmental resources; design of structures, facilities, equipment and infrastructures; planning and design of rural areas and landscape; mechanization and technologies for agricultural production; agricultural electrification and energy usage; ergonomics and work organization and safety; computer and communication technologies.

The aim of this Conference is to stimulate contributions related to the engineering technological applications to the agriculture, forestry and agri-food sectors. Researchers involved in activities related to Biosystems and Agricultural Engineering, as well as Agricultural, Forestry and Food Engineers, farm and food company managers have been invited to present their contributions at the Conference.

This book focuses on the challenges to implement sustainability in diverse contexts in the fields of biosystems engineering for sustainable agriculture, forestry and food production. As the production systems are mainly based on the agricultural sector, the research has taken up the challenge of the sustainable use of renewable and non-renewable resources showing some possible solutions in order to have a sustainable production.

The book consists of seven parts, offering a broad and multidisciplinary approach of some interesting solutions in the field of innovative biosystems engineering, each part corresponds to the seven technical sections composing the AIIA association.

- Part I—Land and Water Use;
- Part II—Rural Buildings, Equipment and Territory;
- Part III—Mechanization and Technologies for Agricultural Production;
- Part IV—Agricultural Electrification and Use of Energy;
- Part V—Ergonomics and Work Organization;
- Part VI—Machines and Plants for Processing Agricultural Production;
- Part VII—Information and Communication Technologies.

We wish to thank colleagues and technicians who participated in the Conference and supported us. We would like also to thank all the authors who have presented their contributions to the Conference. Finally, we would like also to express our

gratitude to the President of the AIIA Association and to the Presidents of the seven AIIA Sections who have taken the responsibility to organize the review and revision of the presented works making thus possible the realization of this book.

Potenza, Italy

Antonio Coppola
Giovanni Carlo Di Renzo
Giuseppe Altieri
Paola D'Antonio

Introduction

The contribution of agricultural and biosystems engineering to meet the sustainable agriculture challenges and contributing to economic growth

The Italian Association of Agricultural Engineering (AIIA)

AIIA was founded in 1959, as a national association belonging to the Commission Internationale du Génie Rural (CIGR). AIIA adheres to the CIGR in all its direct and indirect forms and represents it nationally. AIIA also adheres to the European Society of Agricultural Engineers (EurAgEng), a European member of the CIGR. Furthermore AIIA, along with other scientific societies pertaining to the agricultural, forestry, agro-industrial and environmental sectors, is a part of the Italian Society of Agricultural Scientific Societies (AISSA). The AIIA coordinates and develops all the activities in the field of agricultural and biosystems engineering, i.e. those scientific and technical disciplines related to engineering applied to agricultural and forestry systems. Moreover, AIIA promotes the exchange of experiences and research results among scholars and professionals. AIIA fosters initiatives involving the application of engineering principles to the processes at the basis of land use and territorial development in order to study, model and enhance biological systems for sustainable agriculture, food production, land use and environment safety. AIIA is particularly active in networking between scholars and experts in the various sectors of agricultural and biosystems engineering, with reference to research, innovation, development, technology transfer and training. AIIA periodically promotes and organizes, also together with other institutions and associations, conferences, seminars and meetings involving stakeholders, public and private, with the aim of facilitating the encounter of research and training, innovation and development demand, and to promote the creation and dissemination of new knowledge in the sector.

In particular, the Italian Association of Agricultural Engineering pursues the following aims:

- Bring its technical and scientific contribution to questions of general interest in the field of agricultural engineering;
- Foster relations between scholars and operators dedicated to agricultural engineering;
- Promote the development of agricultural engineering in its various branches;
- Encourage, coordinate and perform—also on behalf of third parties—research in the field of agricultural engineering, also by setting up specific centres;
- Encourage the training of technicians specialized in agricultural engineering by means of teaching courses, scholarships and similar facilities;
- Promote activities and events for dealing with historical and cultural issues concerning agricultural engineering;
- Promote and maintain connections with similar Italian and foreign institutions;
- Promote study events for dealing with issues and problems of a scientific and technical nature relevant to agricultural engineering.

The *Journal of Agricultural Engineering* (JAE), an international journal with peer review and open access, is the official organ of the Association.

The Italian Association of Agricultural Engineering is divided into the following Technical Sections:

- Part I—Land and Water Use;
- Part II—Rural Buildings, Equipment and Territory;
- Part III—Mechanization and Technologies for Agricultural Production;
- Part IV—Agricultural Electrification and Use of Energy;
- Part V—Ergonomics and Work Organization;
- Part VI—Machines and Plants for Processing Agricultural Production;
- Part VII—Information and Communication Technologies.

Members of AIIA are professors and researchers of Universities and Research Institutes, and scholars, experts, technicians, professionals, companies active in research and training in the field of agricultural and biosystems engineering in Italy.

Giacomo Scarascia Mugnozza
President of the Italian Association
of Agricultural Engineering (AIIA)

The Context

In the past century, considerable advances were made in discovering fundamental principles in several scientific disciplines, which created major breakthroughs in management and technology for agricultural systems. However, in the twenty-first century, agricultural research has more difficult and complex problems to solve. Growing environmental awareness of the general public is challenging producers to change farm management practices and protect water, air and soil quality, while staying economically profitable. At the same time, market-based global competition

in agricultural production and global climate change are threatening the economic viability of traditional agricultural systems, and now require the development of dynamic new production systems. Site-specific optimal management of spatially variable soils and available water resources, associated with optimal selection of crops, can help achieve both production and environmental objectives. Fortunately, new technologies can provide a vast amount of real-time information about soil and crop conditions via remote sensing or ground-based instruments which, combined with near-term weather forecasting, can be utilized to develop a whole new level of site-specific management.

Agricultural engineering recognizes the importance of multidisciplinary approaches to develop and deliver know-how and technological solutions in tackling problems at full scale, in real-time and on real-life systems, (Munack 2000).

The used approaches share much common ground with environmental concerns, and the development of methods and systems to deal with the underlying biological system complexity and uncertainty is a major scientific challenge. Agricultural systems are often sensitive to many interacting environmental variables and processes, and solutions frequently involve understanding, monitoring and controlling complex processes in order to improve productivity and minimize environmental emissions and impacts.

The Vision in the Twenty-First Century

There is today real demand for further innovation and its translation into practice in the agricultural context. A wide range of physical sciences and engineering disciplines can make a substantial contribution to the future of agriculture. The following Table 1 provides a synopsis of the sciences involved in different agricultural/environmental applications.

Table 1 Agricultural engineering applications in the context of wider sciences (Source Munack 2000)

	MATHEMATICAL MODELING	SENSORS	REMOTE SENSING	NANOTECHNOLOGY	FLUID DYNAMICS	SOIL PHYSICS	DATA MINING AND PATTERN	ROBOTICS	SURFACE CHEMISTRY
PRODUCT QUALITY	X	X						X	X
ENVIRONMENTAL POLLUTION	X	X	X		X	X			
LOGISTICS	X							X	
ENVIRONMENTAL CONTROL	X	X			X				
IRRIGATION MANAGEMENT	X	X	X		X	X	X	X	
FERTILIZERS AND PESTICIDES				X			X		X
WITHIN-FIELD PRECISION		X					X	X	
SELECTIVE HARVESTING			X					X	
POST-HARVEST MANAGEMENT		X							
LIVESTOCK SYSTEMS	X	X	X	X	X		X	X	
SOIL AND WATER MANAGEMENT	X	X	X		X	X	X		X

Advances in sensing, control engineering, mechanical and hydraulic engineering, robotics and mechatronics, data management, will all contribute to global challenges solutions (Cavalli and Monarca 2011; Scarascia Mugnozza et al. 2011; Gandolfi and Lenzi 2011). Similarly, the ways in which engineering advances will demonstrate their impact is very varied. The sections below serve to emphasize opportunities in different areas of application.

Precision Agricultural Management

Precision Crop Management and Harvesting

(i) Advanced sensing techniques will provide real-time information on the health status of crops (nutrient levels, presence of disease) and soils (nutrient levels); (ii) Appropriate combination of data with crop and system models, will provide early warning of risks and suggest mitigation strategies; (iii) Appropriate interpretation of the relationship between spatial variability of biochemical–physiological response of plants and vegetation, which can be detected by remote sensing observation, and of the stress factors (water, nutrient and salinity stress) may help to adopt spatially variable crop management to maximize productivity and minimize wastage of inputs; (iv) With robotics systems increasingly available, crop quality sensing at harvest will allow to optimize harvest time and sorting to be integrated with the harvesting process.

Precision Control of Pest and Disease

(i) Biosensors will provide early warning of pest or disease outbreaks; (ii) Further improvements to chemical application, through innovative atomization and improved spray handling, will allow optimizing target coverage and efficacy by minimizing losses and environmental impact; (iii) Mechatronics and automation technologies will allow crop management with autonomous machines, including the identification and eradication of weeds by non-chemical means.

Precision Livestock Management

Controlling Animal Health and Welfare

(i) Guidance to animal management both in the field and in housed systems will be improved by animal monitoring systems, including environmental sensors, machine vision, acoustic monitors and gas detectors; (ii) Biosensors will be actively used for monitoring key health and welfare indicators in real time; (iii) Coupling direct observations on the performance of individual animals and animal growth models, will provide early health warning systems to identify and control nutrition and environmental problems.

Controlling Environmental Impacts

(i) Innovative housing and aeration design will improve the control of ventilation and the aerial environment for animals; (ii) Greenhouse gases and other emissions in livestock housing systems will be minimized by environmental control sensors; (iii) Innovative chemical engineering techniques will improve waste treatment and recycling of water and nutrients.

Agriculture and Environment: New Challenges for Engineers

Progress in biological sciences, associated with engineering research and innovations will provide many benefits for agricultural systems, which can be summarized as follows:

Balancing Future Demand and Supply Sustainably

Innovation in agricultural engineering is going to be a crucial contributor to the delivery of agricultural outputs under sustainable intensification conditions. New science and innovative technologies will open up new practices that will both increase production and reduce or reuse waste streams.

Advances in Precision Farming to Enhance Crop Productivity

Advances in precision farming are already supplying considerable understandings of the variability of current production systems (yields can vary considerably in different regions of the same field), Anyway, more precisely controlled input (at scales down to a few meters or individual plants) may still produce benefits in terms of increased productivity, reduced inputs and lower environmental impacts. Timings and quantities of fertilizers and pesticides can be adjusted to much current locally crop state and can be coupled to predictions of future changes in growth rates or disease pressure. Future advances in application technologies and in crop management regimes will allow minimizing gas emissions from soils. Better planning and scheduling of machine operations have the potential to reduce costs by 20%.

Improved Animal Health and Welfare Through Real-Time Monitoring and Diagnostics

Real-time monitoring will allow recognizing health and welfare problems. Biosensors to identify changes in physiological state or exposure to pathogens will become feasible for use in intensive systems, and even in extensive ones through the use of remote tracking and monitoring systems. This real-time monitoring can improve productivity and quality, while also addressing welfare and environmental

impact issues. Improved dairy cow fertility management through estrus sensing has been estimated to be able to deliver 15% reduction in methane emissions, for example.

Meeting the Challenges of a Low Emission World

Concerns about energy demand and climate change require that improvements be made in environmental control and emissions from the biological processes on which farming depends. Engineering advances to optimize performance in energy use for land management and in renewable energy production will be crucial if agriculture is to play its part in averting damage to climate and environment. The complexity of farming systems calls for an interdisciplinary approach to these problems, and combinations of new biological concepts and new engineering techniques are needed.

Reduced Emissions and Other Waste from Livestock

Innovative approaches to managing and handling waste, both on-farm and through cooperative actions with other waste generators, have the potential to enhance the return of plant nutrients to the land and maximize crop nutrient value while minimizing liquid and gaseous emissions of pollutants, including greenhouse gases. Effective management of livestock waste may also provide on-farm energy, e.g. through anaerobic digestion and pyrolysis.

Sensors based on simple physical methods or on more sophisticated techniques using near-infrared spectroscopy or hyperspectral reflectance analysis may be used to determine the nutrient content of the waste stream before land spreading, or even in real time during land spreading, so that application rates can be matched to local crop nutrient requirements within the field. Optimizing application systems will allow the manure in the soil to be distributed appropriately, to control losses of gases such as ammonia or nitrous oxide, and ensure rapid nutrient availability for the crop. High capacity distribution machinery will allow timely application within narrow periods when crop requirements, soil conditions and the demands of regulations come together.

Optimizing Energy Use in Farm Machines

Fuel economy has become a major concern to the industry following price increases, and is now strongly studied. Tractors and other agricultural machines mostly use diesel engines. These are characterized by more sustained and often continuous full-power operation and cooling concerns due to slower vehicle speed and often dusty operating conditions.

New Contributions to Assess the Interactions Among Soil Physical Processes, Plant and Atmospheric Processes, Agricultural Water Management, Soil Environment and Climate Change

Interpreting and controlling the interaction between farming systems and management processes, including soil and water processes, will allow innovative technologies to deliver real benefits to maintain ecosystem services for feeding the world.

The Soil–Plant–Atmosphere Continuum as a Hydraulic System

Water uptake is a key component of the soil hydrological balance and is of concern for a range of hydrological, agricultural and ecological applications, as it controls, either directly or indirectly, the partitioning of infiltrating water into evaporation, transpiration and deep percolation fluxes. It is a dynamic process influenced by soil, plant and climate conditions. It depends on a number of factors such as soil water pressure head, soil hydraulic conductivity, osmotic head (in saline condition), evaporative demand, rooting depth, root density distribution and plant properties. Soil physicists and hydrologists have skills to apply analytical and numerical techniques to model water flow in hydraulic systems and to quantify water transport in plants. The challenge to modelling water uptake and transport in plants is that water flow is controlled by a biological entity, the plant, which senses environmental conditions such as light, temperature and humidity, and continuously adjusts flow rates to maintain its own internal water status. Water potential gradients between the soil and the atmosphere drive the flow. This results in a dynamic hydrologic flow system controlled by both physical and biological parameters. Since plant hydrology and plant structure are closely tied, an understanding of plant hydraulic relationships is essential if we are to model plant properties like leaf and stem sizes and arrangement. A sophisticated approach to the issue would be to combine plant hydrology with an L-Systems description of plant architecture (Prusinkiewicz and Lindenmayer 1990). Forestry researchers have made advances in modelling such systems, but more work is necessary, especially in the area of xylem hydraulics (Sperry et al. 2003).

Transpiration and Carbon Dioxide Fluxes at the Vegetation-Atmosphere Interface

Most of the models simulating agro-hydrological systems should be improved with respect to the effect of water stress on transpiration, C assimilation (photosynthesis), C allocation, canopy temperature and the resulting water use efficiency for production. So far, simple stress factor approach has been mostly adopted to simulate transpiration. In some models, daily crop water stress is calculated as $1 - AT/PT$, where AT is the daily actual water uptake and PT is daily potential transpiration (Hanson 2000; Sudar et al. 1981). In principle, models should rely on stomatal resistance to simulate transpiration (see for example RZWQM model, Farahani and Ahuja 1996). Stomatal behaviour is an important regulator of water flow from the soil and plant to the atmosphere and control mechanisms are still largely unknown.

Are stomata responsive to leaf water potential or soil water potential or both, or other factors such as temperature and chemical signals? Coupled models of photosynthesis and transpiration with an energy balance hold the greatest potential to appropriately model and analyse these issues (Buckley et al. 2003; Tuzet et al. 2003). This would provide a more physiologically based approach taking into account processes that plants have developed to optimize C assimilation and minimize water loss under all conditions of water availability and especially water-deficit situations. Application of such models in forestry has provided good representations of plant response to water stress (Misson et al. 2004). Many of the parameters in these models can be determined using photosynthetic gas flux equipment and sap flow measurements.

Agricultural engineers are well qualified to tackle the above biophysics and energy balance problems.

Better Use of Irrigation Water to Support Production

Water scarcity and quality degradation are set to become the main environmental problems for all countries in the Mediterranean region in the near future. Due mainly to population growth, pressure on agriculture and demand for water to irrigate food crops have also increased. In Mediterranean countries the irrigated area has more than doubled in 40 years, totalling 24,200,000 ha in 2009 (17.8 million in Mediterranean Europe and 6.4 million in Northern Africa). However, in many countries, irrigation practice is often wasteful and highly inefficient. In an attempt to tackle the problem in Italy and other Mediterranean regions, open-channel irrigation systems have been (or are going to be) converted into pressurized pipeline networks. In most cases, the “on-demand” method for water distribution has been adopted to replace the old rotational schedule (Lamaddalena and Sagardoy 2000; D’Urso 2001; Schultz and De Wrachien 2002; Galelli et al. 2010; Coppola et al. 2019).

However, experience shows that even for on-demand pressurized irrigation systems the performance of distribution networks is still frequently far from acceptable in terms of efficiency for both (1) economic/political and (2) technical reasons.

In this context, the use of decision support systems (DSS) may significantly enhance the management of on-demand irrigation systems. Advanced technical tools are nowadays available for monitoring and simulating the various physical processes involved in an irrigation system. Such tools can be used in an integrated way for estimating irrigation water demand and scheduling water use, and thus for simulating the operation of on-demand irrigation networks, under varying soil and weather conditions, crop management options and irrigation technologies.

In general, by integrating the above technical tools with economic instruments, such systems may facilitate the decision-making process on the quantities of water to be allocated to agricultural consumers. Such tools may take into account the most profitable cropping patterns given any water restrictions imposed by existing hydrological conditions, as well as the potential yields in each irrigation district according to its production characteristics, irrigation efficiency, economic scenario and external factors such as agricultural policies.

Processes at the Watershed Scale

Going from field to watershed scale, several processes come into play, such as subsurface flow of water and chemicals to a channel or a stream, flow of field surface runoff through riparian zones, chemical transport in channels and streams. In addition, there may be related to soil erosion processes. Agricultural engineers and soil physicists can contribute to quantification and modelling of some of these processes at this scale as well. Some examples of past contributions in this area are the work on subsurface interflow (Lehman and Ahuja 1985), tile flow (Johnsen et al. 1995), gully erosion (Zheng et al. 2000), and buffer strips (Seobi et al. 2005). Watershed models have been developed that include the above processes, such as the SWAT, AnnAGNPS and REMM models (Arnold et al. 1998; Lowrance et al. 2000; Bingner and Theurer 2001). These models simplify the simulation of physical processes for large simulation units. However, agricultural engineers and soil hydrologist can help improve these simulations by ensuring that field-scale effects are appropriately aggregated up to the watershed scale.

Modelling Climate Change, Soil Environment and Agriculture

Agricultural engineers may significantly contribute to the evaluation of the contribution of agricultural practices on global warming and, inversely, the impact of climate change on soil agricultural systems. Specifically, important contributions may come in the following issues: (i) Quantifying the impact of agricultural soils and current management practices to climate change; (ii) Assessing the effects of climate change on the soil environment, crop growth and agricultural systems, and to identify potential management changes to mitigate the adverse effects.

Agricultural soils and management contribute to climate change primarily through the emission of greenhouse gases, such as CO₂, CH₄, N₂O, NO and NH₃. Models are needed to quantify these emissions as functions of several dynamic variables and aggregate the results over large spatial areas and long timescales. Some models are available (Li 2000) that need more extensive evaluation and improvement.

Climate changes have impacts on the soil environment, especially soil water and temperature, and a number of related processes, such as evapotranspiration, runoff and erosion. Models are needed to quantify these influences in different agricultural systems and to identify strategies for mitigating any adverse effects (e.g. Tubiello et al. 2000).

Land-Use Change Impacts on Floods at the Catchment Scale

Agricultural engineers may also contribute to quantify the land-use change effects on floods. The intensification of agricultural practices has heavily modified natural landscapes. Tillage has frequently created dense soil layers inducing preferential lateral flow and reducing the filtering and buffering potential of soil horizons. Hillslopes have been modified for agricultural production, thus changing flow paths, flow velocities and water storage, and consequently flow connectivity and

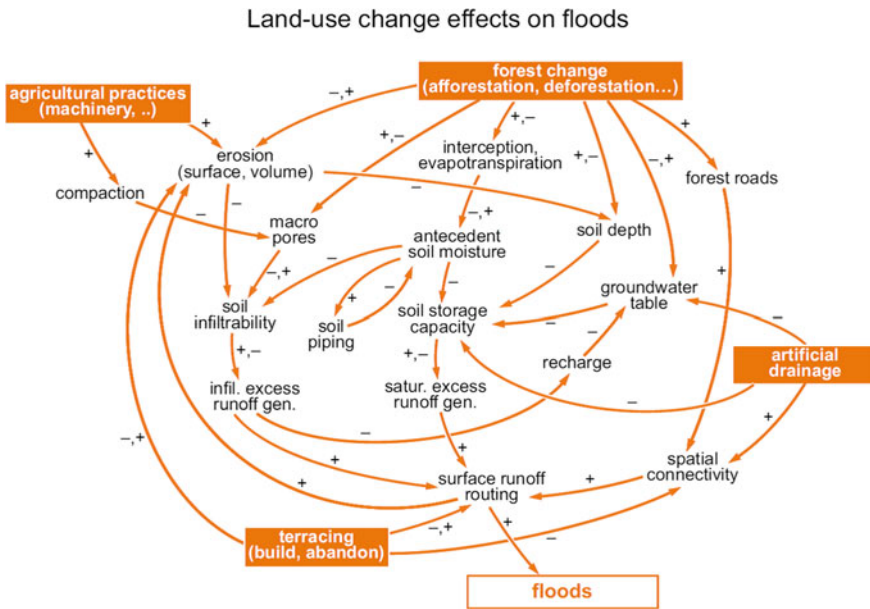


Fig. 1 Diagram of process interactions in land-use changing effects on floods at the catchment scale. Plus and minus signs indicate whether an increase in the variable increases or decreases another variable (Source Rogger et al. 2017)

concentration times. Large areas have been deforested or drained, thus either increasing or decreasing antecedent soil moisture and triggering erosion. In general, an increase in vegetation cover is expected to lead to a decrease in mean streamflow due to increased canopy interception and vegetation transpiration, and that a decrease in vegetation cover will lead to an increase in streamflow. However, the exact role of land-use change in modifying all these processes and thus the hydrological behaviour of a river basin is still to be determined. Also, our ability to predict the impacts of vegetation changes on streamflow regimes (e.g. low flow) across different spatio-temporal scales is still limited. The complexity of the issue is clearly illustrated in Fig. 1 (Rogger et al. 2017).

Concluding Remarks

The above review describes, in our judgment, the most important knowledge gaps that have been encountered by developers of agricultural and environmental system models. Acquisition of more knowledge in the above areas and its calibration will require both innovative experimental research and the development of new concepts, theories and models. Exciting and potentially high-impact areas of further research lie at the interface of several disciplines. Agricultural engineers are uniquely qualified to

tackle such challenges and make highly original and much-needed contributions. Integrated within agricultural systems, such research will create breakthroughs in the knowledge that will help solve the main practical problems that agriculture is facing in the twenty-first century. To take advantage of the opportunities indicated above it will require a supply of high-quality researchers, educators innovators, and technicians along with appropriate facilities. Therefore, we need to develop education, research and training in engineering for agriculture.

Antonio Coppola
Giovanni Carlo Di Renzo
Giuseppe Altieri
Paola D'Antonio

School of Agricultural, Forestry
Food and Environmental Science
University of Basilicata
Potenza, Italy

References

- Arnold, J. R., Srinivasan, R., Muttiah, R. S., & Williams, J. R. (1998). Large area hydrologic modeling and assessment, Part 1: Model development. *Journal of the American Water Resources Association*, 34, 73–89.
- Bingner, R. L., & Theurer, F. D. (2001). AnnAGNPS: Estimating sediment yield by particle size by sheet and rill erosion. p. I-1-I-7. In *Proceeding Sediment Monitoring, Modeling, and Managing, 7th Federal Interagency Sedimentation Conference*, Reno, NV. 25–29 March, 2001. U.S. Dep. of Interior, U.S. Geological Survey, Reston, VA.
- Buckley, T. N., Mott, K. A., & Farquhar, G. D. (2003). A hydro mechanical and biochemical model of stomatal Conductance. *Plant, Cell & Environment*, 26, 1767–1785.
- Cavalli, R., & Monarca, D. (2011). Lo stato e le prospettive della ricerca nel settore AGR/09. Convegno di Medio Termine dell'Associazione Italiana di Ingegneria Agraria Belgirate, 22–24 settembre 2011.
- Enquist, B. J. (2003). Cope's Rule and the evolution of long-distance transport in vascular plants: Allometric scaling, biomass partitioning and optimization. *Plant, Cell & Environment*, 26, 151–161.
- Farahani, H. J., & Ahuja, L. R. (1996). Evapotranspiration modeling of partial canopy/residue-covered fields. *Transactions of the ASAE*, 39, 2051–2064.
- Gandolfi, C., & Lenzi, M. A. (2011). Stato e prospettive della ricerca nel settore Idraulica Agraria e Sistemazioni Idraulico-Forestali. Convegno di Medio Termine dell'Associazione Italiana di Ingegneria Agraria Belgirate, 22–24 september 2011.
- Hanson, J. D. (2000). Generic crop production model for the root zone water quality model. p. 529–556. In L. R. Ahuja et al. (Ed.). *The root zone water quality model*. Highlands Ranch, CO: Water Resources Publications LLC.
- Johnsen, K. E., Liu, H. H., Dane, J. H., Ahuja, L. R., & Workman, S. R. (1995). Simulating fluctuating water tables and tile drainage with the Root Zone Water Quality Model and a new model WAFLOWM. *Transactions of the ASAE*, 38, 75–83.
- Lehman, O. R., & Ahuja, L. R. (1985). Interflow of water and tracer chemical on sloping field plots with exposed seepage faces. *Journal of Hydrology (Amsterdam)*, 76, 307–317.

- Li, C. S. (2000). Modeling trace gas emissions from agricultural ecosystems. *Nutrient Cycling in Agroecosystems*, 58, 259–276.
- Lowrance, R. R., Altier, L. S., Williams, R. G., Inamdar, S. P., Bosch, D. D., Hubbard, R. K., et al. (2000). The riparian ecosystem management model. *Journal of Soil and Water Conservation*, 55, 27–36.
- Meinzer, F. C., Clearwater, M. J., & Goldstein, G. (2001). Water transport in trees: Current perspectives, new insights and some controversies. *Environmental and Experimental Biology*, 45, 239–262.
- Misson, L., Panek, J. A., & Goldstein, A. H. (2004). A comparison of three approaches to modeling leaf gas exchange in annually drought-stressed ponderosa pine forests. *Tree Physiology*, 24, 529–541.
- Munark, A. (2000). Tasks for agricultural engineering research: New challenges-new trends? *Modelling and Control in Agriculture, Horticulture and Post-Harvest Processing*, Wageningen, The Netherlands.
- Prusinkiewicz, P., & Lindenmayer, A. (1990). *The algorithmic beauty of plants*. New York: Springer.
- Rogger, M., Agnoletti, M., Alaoui, A., Bathurst, J. C., Bodner, G., Borga, M., et al. (2017). Land use change impacts on floods at the catchment scale: Challenges and opportunities for future research. *Water Resources Research*, 53, <https://doi.org/10.1002/2017WR020723>.
- Rosenzweig, V., & Hillel, D. (1995). Updated 2004. Potential impacts of climate change on agriculture and food supply. Consequences 1(2). U.S. Climate Change Information Office, Washington, DC.
- Scarascia Mugnozza, G., Cascone, G., & Tassinari, P. (2011). Stato dell'arte e prospettive della ricerca nel settore delle Costruzioni Rurali e Territorio Agroforestale. Convegno di Medio Termine dell'Associazione Italiana di Ingegneria Agraria Belgirate, 22–24 september 2011.
- Schultz, B., & De Wrachien, D. (2002). Irrigation and drainage systems research and development in the 21st century. *Irrigation and Drainage*, 51(4), 311–327 <https://doi.org/10.1002/ird.67>.
- Seobi, T., Anderson, S. H., Udawatta, R. P., & Gantzer, C. J. (2005). Influence of grass and agroforestry buffer strips on soil hydraulic properties for an Albaqualf. *Soil Science Society of America Journal*, 69, 893–901.
- Sperry, J. S., Stiller, V., & Hacke, U. G. (2003). Xylem hydraulics and the soil-plant-atmosphere continuum: Opportunities and unresolved issues. *Agronomy Journal*, 95, 1362–1370.
- Tardieu, V., & Davies, W. J. (1993). Integration of hydraulic and chemical signaling in the control of stomatal conductance and water status of drought plants. *Plant, Cell & Environment*, 16, 341–349.
- Tubiello, E. N., Donatelli, M., Rosenzweig, C., & Stockle, C. O. (2000). Effects of climate change and elevated CO₂ on cropping systems: Model predictions at two Italian locations. *European Journal of Agronomy*, 12, 179–189.
- Tuzet A., Perrier A., & Leuning R. (2003). A coupled model of stomata conductance, photosynthesis and transpiration. *Plant, Cell & Environment*, 26, 1097–1116.
- Tyree, M. T. (1997). The Cohesion-Tension theory of sap ascent: Current controversies. *Journal of Experimental Botany*, 48, 1753–1765.
- Zheng, F. L., Huang, C., & Darrell Norton, V. (2000). Vertical hydraulic gradient and run-on water and sediment effects on erosion processes and sediment regimes. *Soil Science Society of America Journal*, 64, 4–11.

Contents

Land and Water Use

A Comprehensive Check of Usle-Based Soil Loss Prediction Models at the Sparacia (South Italy) Site	3
V. Bagarello, V. Ferro and V. Pampalone	
Evaluating the Effects of Forest Cover Changes on Sediment Connectivity in a Catchment Affected by Multiple Wildfires	13
Lorenzo Martini, Lorenzo Faes, Cordelia Scalari, Giacomo Pellegrini, Andrés Iroumé, Mario Aristide Lenzi and Lorenzo Picco	
A Check of Water Drop Impact Effects on Surface Soil Saturated Hydraulic Conductivity	21
F. Todisco, V. Bagarello, L. Vergni and A. Vinci	
On the Description of Soil Variability Through EMI Sensors and Traditional Soil Surveys in Precision Agriculture	29
Bianca Ortuani, Enrico Casati, Camilla Negri and Arianna Facchi	
Drought Variability and Trend Over the Lombardy Plain from Meteorological Station Records	39
C. Gandolfi, A. Facchi, A. Crespi, M. Rienzner and M. Maugeri	
Biodegradable Geosynthetics for Geotechnical and Geo-Environmental Engineering	49
Alessio Cislaghi, Paolo Sala, Gigliola Borgonovo, Claudio Gandolfi and Gian Battista Bischetti	
Comparison of Different Methods for Topographic Survey of Rural Canals	59
Daniele Masseroni, Daniele Passoni, Alessandro Castagna, Luca Civelli, Livio Pinto and Claudio Gandolfi	

Hydraulic Modeling of Field Experiments in a Drainage Channel Under Different Riparian Vegetation Scenarios	69
G. F. C. Lama, A. Errico, S. Francalanci, G. B. Chirico, L. Solari and F. Preti	
Groundwater Recharge Through Winter Flooding of Rice Areas	79
Arianna Facchi, Camilla Negri, Michele Rienzner, Enrico Chiaradia and Marco Romani	
Evaluation of Green Roof Ageing Effects on Substrate Hydraulic Characteristics	89
V. Alagna, V. Bagarello, P. Concialdi, G. Giordano and M. Iovino	
Influence of Site and Check Dam Characteristics on Sediment Retention and Structure Conservation in a Mexican River	99
Manuel E. Lucas-Borja, Demetrio A. Zema, Yang Yu, Mary Nichols, Giuseppe Bombino, Pietro Denisi, Antonino Labate, Bruno G. Carrà, Xu Xiangzhou, Bruno T. Rodrigues, Artemi Cerdà and Santo Marcello Zimbone	
Comparing LAI Field Measurements and Remote Sensing to Assess the Influence of Check Dams on Riparian Vegetation Cover	109
G. Romano, G. F. Ricci and F. Gentile	
SIRR-MOD—A Decision Support System for Identifying Optimal Irrigation Water Needs at Field and District Scale	117
G. Dragonetti, A. Sengouga, A. Comegna, N. Lamaddalena, A. Basile and A. Coppola	
Modeling the Effect of Different Management Practices for Soil Erosion Control in a Mediterranean Watershed	125
Giovanni Francesco Ricci, Anna Maria De Girolamo and Francesco Gentile	
The Benefit of Continuous Modelling for Design Hydrograph Estimation in Small and Ungauged Basins	133
S. Grimaldi, A. Petroselli, R. Piscopia and F. Tauro	
A Theoretical Approach to Improve the Applicability of the Catchment Connectivity Index	141
Giuseppe Bombino, Carolina Boix-Fayos, Maria Francesca Cataldo, Daniela D’Agostino, Pietro Denisi, Joris de Vente, Antonino Labate and Demetrio Antonio Zema	
On the Performance of a Novel Hybrid Constructed Wetland for Stormwater Treatment and Irrigation Reuse in Mediterranean Climate	151
Delia Ventura, Salvatore Barbagallo, Simona Consoli, Mirco Milani, Alessandro Sacco, Ruggero Rapisarda and Giuseppe Luigi Cirelli	

Rural Buildings, Equipment and Territory

Urban Agriculture, Cui Prodest? Seattle’s Picardo Farm as Seen by Its Gardeners 163
 M. E. Menconi, P. Borghi and D. Grohmann

Evaluation of Greenwalls Efficiency for Building Energy Saving 169
 C. Bibbiani, C. Gargari, C. A. Campiotti, G. Salvadori and F. Fantozzi

Modelling of the Thermal Effect of Green Façades on Building Surface Temperature in Mediterranean Climate 179
 I. Blanco, G. Scarascia Mugnozza, G. Vox and E. Schettini

Heat Fluxes in a Green Façade System: Mathematical Relations and an Experimental Case 189
 Fabiana Convertino, Giacomo Scarascia Mugnozza, Evelia Schettini and Giuliano Vox

Odor Nuisance in the Livestock Field: A Review 199
 C. Conti, M. Guarino and J. Bacenetti

Spatial Analysis of the Impact of Rural Buildings on the Agro-Forestry Landscape Using GIS 207
 Giuseppe Cillis, Dina Statuto and Pietro Picuno

Milk-Production in Barns with Compost Bedding and Free Stall: A Profitability Analysis 215
 Marcos A. Lopes, Gustavo R. de O. Silva, André L. R. Lima, Geraldo M. da Costa, Flávio A. Damasceno, Vítor P. Barros and Matteo Barbari

Thermal Environment Inside Mechanically Ventilated Greenhouses: Results from a Long-Term Monitoring Campaign 223
 Andrea Costantino, Lorenzo Comba, Giacomo Sicardi, Mauro Bariani and Enrico Fabrizio

Physical Properties of Cement Panels Reinforced with Lignocellulosic Materials 231
 Patrícia Ferreira Ponciano Ferraz, Matheus da Rocha Coutinho Avelino, Victor Rezende Carvalho, Isabela Moreira Albano da Silva, André Luiz de Lima Domingos, Rafael Farinassi Mendes, Jaqueline de Oliveira Castro, Leonardo Conti and Giuseppe Rossi

Physical Properties of Miscanthus Grass and Wheat Straw as Bedding Materials for Dairy Cattle 239
 Patrícia Ferreira Ponciano Ferraz, Giuseppe Rossi, Leonardo Conti, Gabriel Araújo e Silva Ferraz, Lorenzo Leso and Matteo Barbari

Innovative Tensile Structures for Protected Crop Facilities	247
Silvana Fuina, Giacomo Scarascia-Mugnozza and Sergio Castellano	
Analysis of the Evolution of a Rural Landscape by Combining SAR Geodata with GIS Techniques	255
Giuseppe Cillis, Aimé Lay-Ekuakille, Vito Telesca, Dina Statuto and Pietro Picuno	
Smart Dairy Farming: Innovative Solutions to Improve Herd Productivity	265
C. Arcidiacono, M. Barbari, S. Benni, E. Carfagna, G. Cascone, L. Conti, L. di Stefano, M. Guarino, L. Leso, D. Lovarelli, M. Mancino, S. Mattoccia, G. Minozzi, S. M. C. Porto, G. Provolo, G. Rossi, A. Sandrucci, A. Tamburini, P. Tassinari, N. Tomasello, D. Torreggiani and F. Valenti	
A Methodology to Support Planning and Design of Suburban Agricultural Areas	271
P. Russo, P. Lanteri and A. D’Emilio	
Modeling Soil Thermal Regimes During a Solarization Treatment in Closed Greenhouse by Means of Symbolic Regression via Genetic Programming	279
A. D’Emilio	
Comparison of the Efficiency of Plastic Nets for Shading Greenhouse in Different Climates	287
Dina Statuto, Ahmed M. Abdel-Ghany, Giuseppe Starace, Paolo Arrigoni and Pietro Picuno	
Planning the Flows of Residual Biomass Produced by Wineries for Their Valorization in the Framework of a Circular Bioeconomy	295
Canio Manniello, Dina Statuto, Andrea Di Pasquale and Pietro Picuno	
Effects of Feeding Frequency on the Behavior Patterns of Dairy Cows in an Automatic Feeding System	305
G. Mattachini, A. Finzi, E. Riva and G. Provolo	
Shading Screens Characterization by Means of Wind Tunnel Experiments and CFD Modeling	313
E. Santolini, D. Torreggiani and P. Tassinari	
Damages to Rural Buildings and Facilities Observed in the Aftermath of 2012 Emilia Earthquakes	323
M. Bovo, A. Barbaresi, D. Torreggiani and P. Tassinari	

Proposal of a Web-Based Multi-criteria Spatial Decision Support System (MC-SDSS) for Agriculture 333
 Giuseppe Modica, Maurizio Pollino, Luigi La Porta and Salvatore Di Fazio

The Apulian Territory and the Typical Local Farmhouses: A Case of Study Through Landscape Analysis 343
 E. Liano, I. Blanco and G. Scarascia Mugnozza

Enhancement of the Roman Bridge of Canosa in the Ofanto Valley Rural Landscape 351
 Enrico Liano, Silvana Fuina, Marcio A. Alberti and Giacomo Scarascia-Mugnozza

Mechanization and Technologies for Agricultural Production

Economic and Environmental Performances of a New Double Wheel Rake 363
 J. Bacenetti, L. Bava, D. Lovarelli, A. Fusi and G. Repposi

Environmental Impact Alternatives for Soil Tillage and Sowing: Farmer or Contractor? 373
 J. Bacenetti, D. Facchinetti, D. Lovarelli and D. Pessina

A Biomass-Fueled Flamer for In-Row Weed Control in Vineyards: An Economic Evaluation 381
 Gianfranco Pergher, Rino Gubiani and Matia Mainardis

N-TRE: A Model for the Evaluation of the Narrow Tractors Real Efficiency 389
 Lavinia Eleonora Galli, Davide Facchinetti and Domenico Pessina

Controlled Mechanical Ventilation to Reduce Primary Energy Consumption in Air Conditioning of Greenhouses 399
 C. Perone, P. Catalano, F. Giametta, G. La Fianza, L. Brunetti and B. Bianchi

Efficiency of Tractor Drawbar Power Taking into Account Soil-Tire Slippage 409
 M. Cutini, M. Brambilla, C. Bisaglia, D. Pochi and R. Fanigliulo

Design and Assessment of a Test Rig for Hydrodynamic Tests on Hydraulic Fluids 419
 Daniele Pochi, Roberto Fanigliulo, Renato Grilli, Laura Fornaciari, Carlo Bisaglia, Maurizio Cutini, Massimo Brambilla, Angela Sagliano, Luigi Capuzzi, Fulvio Palmieri and Giancarlo Chiatti

Evaluation of Potential Spray Drift Generated by Different Types of Airblast Sprayers Using an “ad hoc” Test Bench Device	431
M. Grella, P. Marucco and P. Balsari	
Influence of Ploughshare Wear on Plough Efficiency	441
Giovanni Molari, Massimiliano Varani and Michele Mattetti	
Brotweg—A Path of Bread in an Alpine Environment: New Mechanical Solutions for Grain Processing in Steep Mountain Slopes	449
Sabrina Mayr, Riccardo Brozzi, Alice Cervellieri, Thomas Desaler, Raimondo Gallo, Josef Gamper, Bernhard Geier, Laurin Holzner, Pasqualina Sacco and Fabrizio Mazzetto	
The H2020 INNOSETA Project	457
Fabrizio Gioelli, Paolo Marucco, Floriana Nuzzo and Paolo Balsari	
Sprayer Inspection in Sicily on the Basis of Workshop Activity	463
Emanuele Cerruto, Giuseppe Manetto, Domenico Longo and Rita Papa	
Evaluation on the Stability of Tree Used as Anchors in Cable Yarding Operations: A Preliminary Test Based on Low-Cost MEMS Sensors	473
L. Marchi, O. Mologni, S. Grigolato and R. Cavalli	
Modelling of Agricultural Machinery Trends for Power, Mass, Working Width and Price	481
Francesco Marinello, Tatevik Yezekyan, Giannantonio Armentano and Luigi Sartori	
High Accuracy Site-Specific Secondary Data for Mechanical Field Operations to Support LCA Studies	491
Marco Fiala and Luca Nonini	
Assessment of Forest Biomass and Carbon Stocks at Stand Level Using Site-Specific Primary Data to Support Forest Management	501
Luca Nonini, Calogero Schillaci and Marco Fiala	
Sensors and Electronic Control Unit for Optimize Rotary Harrow Soil Tillage Operation	509
Francesco Marinello, Filippo Pegoraro and Luigi Sartori	
LIFE-Vitisom: An EU Project for the Set-up of VRT Organic Fertilization in Vineyard	519
Domenico Pessina, Davide Facchinetti and Lavinia Eleonora Galli	
Real-Time Measurement of Silage Moisture Content During Loading of a TMR Mixer Wagon: Preliminary Results	531
V. Perricone, A. Costa, A. Calcante, A. Agazzi, M. Lazzari, G. Savoini, M. Chiara, E. Sesan and F. M. Tangorra	

The Response Surface Methodology as a Tool to Evaluate the Effects of Using Diesel-Biodiesel-Bioethanol Blends as Farm Tractor Fuel 539
 Marco Bietresato, Carlo Caligiuri, Anna Bolla, Massimiliano Renzi and Fabrizio Mazzetto

An Approach to the Development of an Integrated Real-Time Engine Test System for Agricultural Machines: Conceiving, Implementation, Set-up and First Tests 551
 Marco Bietresato, Matteo Malavasi and Fabrizio Mazzetto

Development and Implementation of an Ultra-Low Volume (ULV) Spraying Equipment Installed on a Commercial UAV 563
 Alberto Sassu, Luca Ghiani, Antonio Pazzona and Filippo Gambella

Agricultural Electrification and Use of Energy

Life Cycle Impact Assessment of Carrot Cultivation and Processing: An Italian Case Study for a Small Family Company in the Marche Region 575
 A. Ilari, D. Duca, G. Toscano, V. Vecchiarelli and E. Foppa Pedretti

Does Precision Photovoltaic Irrigation Represent a Sustainable Alternative to Traditional Systems? 585
 Giuseppe Todde, Maria Caria, Antonio Pazzona, Luigi Ledda and Luis Narvarte

Development of an Energy Efficiency Index for Agricultural Tractors Based on OECD Codes Data 595
 C. Carnevali and S. Angelelli

Evaluation of Coaxial Pipes for Basal Heating as Alternative for Energy Saving in Heating System for Leafy Vegetables 603
 M. Fedrizzi, C. Terrosi, S. Cacini, G. Burchi, M. Cutini, M. Brambilla, C. Bisaglia, M. Pagano, S. Figorilli, C. Costa and D. Massa

Energy Monitoring of Fully Automated Dairy-Farm: A Case Study 611
 Andrea Pezzuolo, Francesco Marinello, Luigi Sartori and Stefano Guercini

Comparison of Environmental Impact of Two Different Bioelectricity Conversion Technologies by Means of LCA 619
 Mauro Villarini, Sara Rajabi Hamedani, Vera Marcantonio, Andrea Colantoni, Massimo Cecchini and Danilo Monarca

Ergonomics and Work Organization

Spatial Analysis for Detecting Recent Work Accidents in Agriculture in Italy 631

Massimo Cecchini, Ilaria Zambon, Danilo Monarca, Francesca Piccioni, Alvaro Marucci and Andrea Colantoni

A Bottom-Up Approach to Tractor Safety: Improving the Handling of Foldable Roll-Over Protective Structures (FROPS) Through User-Centred Design 645

Lucia Vigoroso, Federica Caffaro, Margherita Micheletti Cremasco, Ambra Giustetto, Giuseppe Paletto and Eugenio Cavallo

Technical and Economic Evaluation of Urban Trees Pruning by Climbing Arborists 653

M. Biocca, P. Gallo and G. Sperandio

First Tests on a Prototype Device for the Active Control of Whole-Body Vibrations on Agricultural Tractors 661

Daniele Pochi, Laura Fornaciari, Renato Grilli, Monica Betto, Stefano Benigni and Roberto Fanigliulo

Effects of Rod and Oscillating Frequency on the Vibrations Transmitted to Hand-Arm System by Four Olive Portable Harvesters 671

Giuseppe Manetto, Emanuele Cerruto and Rita Papa

Perceived Barriers to the Adoption of Smart Farming Technologies in Piedmont Region, Northwestern Italy: The Role of User and Farm Variables 681

Federica Caffaro and Eugenio Cavallo

Effect of Different Axial Fans Configurations on Airflow Rate 691

S. Failla, E. Romano, D. Longo, C. Bisaglia and G. Schillaci

Machines and Plants for Processing Agricultural Production

Use of Ultrasound in the Extraction Process of Virgin Olive Oil and Influence on Malaxation Time 703

Mauro Pagano, Roberto Tomasone, Carla Cedrola, Marco Fedrizzi, Gianluca Veneziani and Maurizio Servili

An Innovative Vat for the Continuous Recovery of Volatile Compounds During Fermentation 713

Giulia Angeloni, Lorenzo Guerrini, Piernicola Masella, Agnese Spadi, Fabio Baldi and Alessandro Parenti

Effect of Packaging Technology on the Quality of Pre-cooled Clementine Fruit 723
 F. Genovese, G. C. Di Renzo, G. Altieri, L. Scarano and M. C. Strano

Optimization of Donkey Milk Pasteurization Process 735
 A. Matera, G. Altieri, F. Genovese and G. C. Di Renzo

Effect of Materials and Assembly Methods on Gas Selectivity of Blow[®] Device 745
 A. Matera, G. Altieri, F. Genovese and G. C. Di Renzo

Information and Communication Technologies

Monitoring of Coffee Tree Growth Through Crop Surface Models and MGRVI with Images Obtained with RPA 757
 Gabriel Araújo e Silva Ferraz, Luana Mendes dos Santos, Marco Thulio Andrade, Leticia Aparecida Gonçalves Xavier, Diogo Tubertini Maciel, Patricia Ferreira Ponciano Ferraz, Giuseppe Rossi and Matteo Barbari

A Prototype of Service Oriented Architecture for Precision Agriculture 765
 S. Lanucara, A. Oggioni, S. Di Fazio and G. Modica

A Method to Implement a Monitoring System Based on Low-Cost Sensors for Micro-environmental Conditions Monitoring in Greenhouses 775
 Elio Romano, Massimo Brambilla, Pietro Toscano and Carlo Bisaglia

An Innovative Methodology to Be More Time-Efficient When Analyzing Data in Precision Viticulture 783
 Monica F. Rinaldi, Raimondo Gallo, Gabriele Daglio and Fabrizio Mazzetto

AgroBot Smash a Robotic Platform for the Sustainable Precision Agriculture 793
 D. Sarri, S. Lombardo, R. Lisci, V. De Pascale and M. Vieri

Use of a Multirotor-UAV Equipped with a Multispectral Camera to Detect Vineyard Diseases: A Case Study on Barbera and Dolcetto Cultivars 803
 Gabriele Daglio, Raimondo Gallo, Monica F. Rinaldi, Nadia Massa, Valeria Todeschini and Fabrizio Mazzetto

An Ontology-Based Study for the Design of a Database for Data Management in Precision Farming 811
 S. Chiappini, A. Galli, E. S. Malinverni, P. Zingaretti, R. Orsini, M. Fiorentini and S. Zenobi

A Skyline Deflection Analysis Methodology for Timber Volume Estimation in Yarding Operations	819
Raimondo Gallo, Luca Marchi, Stefano Grigolato, Raffaele Cavalli and Fabrizio Mazzetto	
Neural Network Algorithms for Real Time Plant Diseases Detection Using UAVs	827
Mariano Crimaldi, Vincenzo Cristiano, Angela De Vivo, Marco Isernia, Plamen Ivanov and Fabrizio Sarghini	
Use of UAVs and Canopy Height Model Applied on a Time Scale in the Vineyard	837
Luca Ghiani, Alberto Sassu, Vanessa Lozano, Giuseppe Brundu, Davide Piccirilli and Filippo Gambella	
Development of a Matlab Code for the Evaluation of Spray Distribution with Water-Sensitive Paper	845
Luca Ghiani, Alberto Sassu, Davide Piccirilli, Gian Luca Marcialis and Filippo Gambella	
Detection and Monitoring of Alien Weeds Using Unmanned Aerial Vehicle in Agricultural Systems in Sardinia (Italy)	855
Vanessa Lozano, Giuseppe Brundu, Luca Ghiani, Davide Piccirilli, Alberto Sassu, Maria Teresa Tiloca, Luigi Ledda and Filippo Gambella	
Experimental Methodology for Prescription Maps of Variable Rate Nitrogenous Fertilizers on Cereal Crops	863
Costanza Fiorentino, A. R. Donvito, P. D'Antonio and S. Lopinto	
Monitoring Onion Crops Using UAV Multispectral and Thermal Imagery: Preliminary Results	873
Gaetano Messina, Salvatore Praticò, Biagio Siciliani, Antonio Curcio, Salvatore Di Fazio and Giuseppe Modica	

Land and Water Use

Introduction

Prof. Antonio Coppola

President of the 1st Section of the Italian Association of Agricultural Engineering
'Land and Water Use'

The 1st Section promotes scientific progress in the methods, tools and technologies for the monitoring and modeling of water resources and soils in agricultural-forestry systems. The priority areas of investigation and intervention are those of agricultural areas and rural and forest areas, with an open vision to interactions with near-urban areas. Principles of hydraulics and soil hydrology are applied to manage and protect water and soil resources in both agricultural and forest contexts.

Traditional fields of interest are in the Monitoring and Modelling water resources in the agricultural and forestry systems; Quantitative and qualitative monitoring of water resources in agricultural and forest soils; Management of irrigation water; Processes at watershed scale; Land use change impacts on floods at the hillslope and catchment scale.

New contributions of the 1st Section are in: Quantifying interactions among soil physical processes, plant and atmospheric processes; Developing Decision Support Systems for agricultural water management; Quantifying the effects of climate change on water resources and agricultural-forestry systems; Quantifying transpiration and carbon dioxide fluxes at the canopy-atmosphere interface under water stress; Quantifying and maintaining ecosystem services.

Specific topics of interest, even if not exhaustive, are: Soil Hydrological characterization; Spatial variability of soil hydrological properties and stochastic approaches in natural porous media; Hydrological balance at different spatial and temporal scales; Conceptualization, modelling and prediction of water flow velocity, pathways and patterns on forest and agricultural hillslopes; Numerical modelling of soil water and solute transport in the Soil-Plant-Atmosphere continuum system; Irrigation with conventional and non-conventional water resources; Remote sensing of hydrological processes in agri-forestry systems; Irrigation, drainage, reclamation in agriculture; Design and Planning of water systems for agriculture and the agri-food industry; Irrigation at field and district scale; Irrigation networks; Groundwater pollution risk

within agricultural watershed; Groundwater resources estimates; Forest hillslope hydrology; Surface flows in natural watercourses; Intervention techniques for river bed and slope consolidation; Hydraulic interventions for land conservation; Design of intensive works of forest hydraulic engineering; Hydraulic-forest problems at the catchment scale, also resorting to interventions of natural engineering.

A Comprehensive Check of Usle-Based Soil Loss Prediction Models at the Sparacia (South Italy) Site



V. Bagarello, V. Ferro and V. Pampalone

Abstract At first, in this paper a general definition of the event rainfall-runoff erosivity factor for the USLE-based models, $REF_e = (Q_R)^{b_1}(EI_{30})^{b_2}$, in which Q_R is the event runoff coefficient, EI_{30} is the single-storm erosion index and b_1 and b_2 are coefficients, was introduced. The rainfall-runoff erosivity factors of the USLE ($b_1 = 0, b_2 = 1$), USLE-M ($b_1 = b_2 = 1$), USLE-MB ($b_1 \neq 1, b_2 = 1$), USLE-MR ($b_1 = 1, b_2 \neq 1$), USLE-MM ($b_1 = b_2 \neq 1$) and USLE-M2 ($b_1 \neq b_2 \neq 1$) can be defined using REF_e . Then, the different expressions of REF_e were simultaneously tested against a dataset of normalized bare plot soil losses, A_{eN} , collected at the Sparacia (south Italy) site. As expected, the poorest A_{eN} predictions were obtained with the USLE. A distinction was made among the four power-type models since the fitting to the data was poor with the USLE-MR as compared with the other three models. Estimating two distinct exponents (one for EI_{30} and another for Q_R , USLE-M2) instead of a single exponent (USLE-MB, USLE-MR, USLE-MM) did not appreciably improve soil loss prediction. The USLE-MB and the USLE-MM were the best performing models.

Keywords Soil erosion · Event soil loss · Soil loss prediction · USLE-type erosion models

1 Introduction

Improving soil erosion empirical models, such as those USLE-based, has a large interest since these models require few input data and are able to provide sufficiently reliable soil loss predictions for many practical purposes.

V. Bagarello · V. Pampalone (✉)

Department of Agricultural, Food and Forest Sciences, University of Palermo, Viale Delle Scienze, 90128 Palermo, Italy

e-mail: vincenzo.pampalone@unipa.it

V. Ferro

Department of Earth and Marine Science, University of Palermo, Via Archirafi 20, 90123 Palermo, Italy

© Springer Nature Switzerland AG 2020

A. Coppola et al. (eds.), *Innovative Biosystems Engineering for Sustainable Agriculture, Forestry and Food Production*, Lecture Notes in Civil Engineering 67,

https://doi.org/10.1007/978-3-030-39299-4_1

According to Bagarello et al. (2018a), the general definition of the event rainfall-runoff erosivity factor, REF_e , in a USLE-based model is:

$$REF_e = (Q_R)^{b_1} (EI_{30})^{b_2} \quad (1)$$

in which Q_R is the event runoff coefficient, equal to the ratio between the event runoff volume per unit plot area, V_e (mm), and the corresponding rainfall depth, P_e (mm), EI_{30} ($\text{MJ mm ha}^{-1} \text{h}^{-1}$) is the single-storm erosion index (Wischmeier and Smith 1978), and b_1 and b_2 are coefficients. The rainfall erosivity factor of the USLE is obtained from Eq. (1) for $b_1 = 0$ and $b_2 = 1$. The condition $b_1 = b_2 = 1$ corresponds to the rainfall-runoff erosivity factor of the USLE-M (Kinnell and Risse 1998). When $b_1 = b_2$ is different from 1, the USLE-MM rainfall-runoff erosivity factor is obtained (Bagarello et al. 2015). The case $b_1 \neq 1$ and $b_2 = 1$ was named USLE-MB by Bagarello et al. (2018a). The last two cases are $b_1 = 1$ and $b_2 \neq 1$, here named USLE-MR, and $b_1 \neq b_2$ with both exponents which differ from one (USLE-M2).

The II-theorem of the dimensional analysis and the self-similarity theory yield rainfall-runoff erosivity factors corresponding exclusively to the conditions $b_1 = 0$ and $b_2 = 1$ (USLE) (Ferro 2010), $b_1 = b_2 = 1$ (USLE-M) (Di Stefano et al. 2017) and $b_1 \neq 1$ and $b_2 = 1$ (USLE-MB) (Bagarello et al., 2018a). Therefore, these three models can be considered theoretically supported and are characterized by common measurement units of the soil erodibility factor. However, a theoretically supported model should not be expected to necessarily perform well or better than an empirical based one. For example, for the Masse (Umbria, central Italy) and Sparacia (Sicily, southern Italy) experimental stations, Bagarello et al. (2018b) recognized that a correct specification of the model (normality and homoscedasticity of residuals) was detectable for the USLE-MM but not for the USLE-M.

The models can also be considered to differ by the perceivable physical soundness. For example, $b_1 > 1$ agrees with the mathematical expression of the flow transport capacity (Bagarello et al. 2018b) and a b_2 exponent equal to one is consistent with Wischmeier and Smith (1978) since these authors established a linear relationship between soil loss and the rainfall erosivity factor EI_{30} and they also stated that EI_{30} reflects the combined potential effect of raindrop splash and runoff scour on soil erosion (Yin et al. 2017). Consequently, the USLE-MB ($b_1 \neq 1$ and $b_2 = 1$) is conceptually justified while the USLE-MR ($b_1 = 1$ and $b_2 \neq 1$) can be considered a merely empirical choice. However, taking into account that models making use of a linear relationship between A_{eN} and Q_R (USLE-M) or a power relationship between A_{eN} and EI_{30} (USLE-MM) have also been developed and positively tested, verifying the USLE-MR could have some practical reason of interest. Using a dataset developed at the Sparacia site, the general objective of this investigation was comparing all possible expressions of REF_e for: (i) quantitatively establishing the advantage of considering more input data, such as the runoff coefficient, for soil loss prediction (e.g., from USLE to USLE-M); (ii) determining, for an input information including single-storm erosion index and runoff coefficient, what happens if an additional

model parameter is estimated instead of fixing it equal to unity. The required experimental information does not vary between the USLE-M and the USLE-MB, USLE-MR and USLE-MM but the models differ by their parameterization; (iii) verifying if considering two possibly different exponents for EI_{30} and Q_R could be advantageous from a practical point of view, i.e. appropriate to improve soil loss predictions. In this case, the question is to see if, with an experimental information made by EI_{30} and Q_R , there is still space for additional improvements in soil loss predictions, although with a model needing calibration of more parameters.

2 Materials and Methods

The experimental station for soil erosion measurement Sparacia of the Agricultural, Food and Forest Sciences Department of the Palermo University is located in western Sicily, south Italy, approximately 100 km south of Palermo. The soil at the experimental station has a clay texture (62% clay, 33% silt, 5% sand). The experimental station includes plots with lengths of 11–44 m, widths of 2–8 m and steepness of 9–26%. All plots are maintained in continuous fallow and are equipped by a recording rain-gauge operating with a 1-min temporal resolution. Runoff and associated sediments from each plot are intercepted by a gutter placed at the lower end of the plot, and collected into a storage system. Total runoff and soil loss are measured after each erosive event, i.e. an event producing measurable runoff and sediment, or occasionally after a series of events if they are separated by a short time interval. The applied runoff and sediments measurement procedures were described in other papers (e.g., Bagarello et al. 2015; 2018a; Carollo et al. 2016) and they were not repeated here for brevity reasons. For each erosive event, total rainfall depth, P_e (mm), is measured and the rainfall erosivity index, EI_{30} ($\text{MJ mm h}^{-1}\text{ha}^{-1}$), is calculated according to Wischmeier and Smith (1978). For each individual plot, total runoff per unit area, Q_e (mm), and the associated soil loss per unit area, A_e (Mg ha^{-1}), are measured and the runoff coefficient $Q_R = Q_e/P_e$ is calculated. In this investigation, the topographic factor, LS (Wischmeier and Smith 1978), was calculated for each plot according to Nearing (1997) and Renard et al. (1997). The normalized soil loss, A_{eN} (Mg ha^{-1}), was then calculated for each individual A_e value as A_e/LS . The used dataset was developed in the period from January 16, 2002 to March 20, 2018 and it included a total of $N = 641$ A_{eN} data and the associated P_e , EI_{30} and Q_R values.

The performances of the six investigated models were tested against the complete calibration dataset ($N = 641$ data pairs) by both visual inspection of the scatter-plots of predicted against measured normalized soil loss values and calculation of several quantitative statistics. In particular, in addition to the coefficient of determination of the regression, R^2 , the root mean square error, $RMSE$, the Nash-Sutcliffe (1970) model efficiency index, $NSEI$, the $BIAS$, the percentage number of under- and over-estimations, p_{ue} and p_{oe} , respectively, the discrepancy factor, DF , between the experimental and the predicted A_{eN} values, and the absolute value of the normalized soil loss prediction error, $|E_r|$, were calculated. The $BIAS$ is given by:

$$BIAS = \frac{\sum_{i=1}^N (A_{eN,m} - A_{eN,c})_i}{N} \quad (2)$$

where $A_{eN,m}$ is the measured normalized soil loss and $A_{eN,c}$ is the normalized soil loss predicted by the model. The p_{ue} and p_{oe} percentages are determined by counting the number of cases yielding $A_{eN,c} < A_{eN,m}$ and $A_{eN,c} > A_{eN,m}$, respectively. The DF value is calculated for a given data pair as the highest value between the measured and the predicted normalized soil loss divided by the lowest of these two values:

$$DF = \frac{\max(A_{eN,m}, A_{eN,c})}{\min(A_{eN,m}, A_{eN,c})} \quad (3)$$

Finally, $|Er|$ (%) is calculated for each data pair as:

$$|Er| = 100 \left| \frac{A_{eN,c} - A_{eN,m}}{A_{eN,m}} \right| \quad (4)$$

3 Results and Discussion

The tested soil loss prediction equation has the following general form:

$$A_{eN} = K \times REF_e = K(Q_R)^{b_1} (EI_{30})^{b_2} \quad (5)$$

where K is the soil erodibility factor, whose measurement units depend on the chosen expression for the rainfall-runoff erosivity factor REF_e .

The following models were obtained in this investigation:

$$A_{eN} = 0.0391 EI_{30} \text{ USLE} \quad (6)$$

$$A_{eN} = 0.2617 Q_R EI_{30} \text{ USLE} - M \quad (7)$$

$$A_{eN} = 0.2327 EI_{30} Q_R^{1.5202} \text{ USLE} - MB \quad (8)$$

$$A_{eN} = 0.0144 EI_{30}^{1.3127} Q_R \text{ USLE} - MR \quad (9)$$

$$A_{eN} = 0.0246 (Q_R EI_{30})^{1.4263} \text{ USLE} - MM \quad (10)$$

$$A_{eN} = 0.0605 Q_R^{1.5102} EI_{30}^{1.2801} \text{ USLE} - M2 \quad (11)$$

Table 1 Performance statistics of the six tested models against $N = 641$ soil loss data

Model	R^2	RMSE	NSEI	BIAS	P_{ue}	P_{oe}
USLE	0.320	10.613	0.320	-1.554	19.5	80.5
USLE-M	0.688	7.184	0.688	-1.180	19.8	80.2
USLE-MB	0.634	9.197	0.489	2.344	50.9	49.1
USLE-MR	0.384	9.832	0.416	2.800	51.5	48.5
USLE-MM	0.717	6.474	0.747	1.436	50.4	49.6
USLE-M2	0.721	7.065	0.698	1.661	51.3	48.7
Model	DF				Erl	
	Max	Mean	Median	<3	<200%	
USLE	3805.0	88.0	5.75	33.1	37.4	
USLE-M	271.0	12.3	4.46	41.0	43.3	
USLE-MB	90.2	4.48	2.50	59.9	80.3	
USLE-MR	86.2	5.03	2.86	52.6	77.4	
USLE-MM	95.6	4.47	2.28	61.0	80.0	
USLE-M2	92.6	4.42	2.28	62.1	80.3	

For each model, Table 1 lists the performance statistics (R^2 , $RMSE$, $NSEI$, $BIAS$, p_{ue} , p_{oe} , DF , $|Erl|$) and Fig. 1 shows the comparison between the predicted and the measured values of A_{eN} .

The performances of the USLE were poor with reference to all considered statistics because $A_{eN,c}$ varied over slightly more than two orders of magnitude against a variation of even more than five orders of magnitude for $A_{eN,m}$. In particular, the 80% of the normalized soil loss values were overestimated, the mean DF value was close to two orders of magnitude, and relatively reliable A_{eN} predictions (i.e. $DF < 3$; Bagarello et al., 2012) were only obtained for nearly one third of the considered events. Very large errors, i.e. $|Erl| > 200\%$, were detected for the 62.6% of the events.

Including the runoff coefficient in the soil loss prediction model improved all considered performance indices and also made the predicted A_{eN} values closer to the measured ones. In particular, as compared with the USLE, the USLE-M was characterized by more than two fold R^2 and $NSEI$ values, a lower $RMSE$ by 32%, a $\max(DF)$ that decreased by 14 times, a mean DF 7.2 times lower and a median DF 1.29 times lower. Moreover, relatively reliable A_{eN} predictions ($DF < 3$) were obtained more frequently, i.e. in the 41% of the cases. However, $|Erl| > 200\%$ was still detected for the majority of the cases, i.e. the 56.7% of the events, and overestimation of A_{eN} continued to prevail at a similar rate to that detected for the USLE, i.e. for approximately the 80% of the events. The increased predictive ability of the model due to the use of the runoff coefficient was expected from a qualitative point of view (e.g., Kinnell and Risse, 1998) but the quantification of the performance differences between the USLE and the USLE-M appears rather novel since it was not provided with this detail (Table 1) in other investigations.

Introducing an exponent in the erosivity term (USLE-MB, USLE-MR, USLE-MM) did not improve the classical statistical indices (R^2 , $RMSE$, $NSEI$, $BIAS$) which

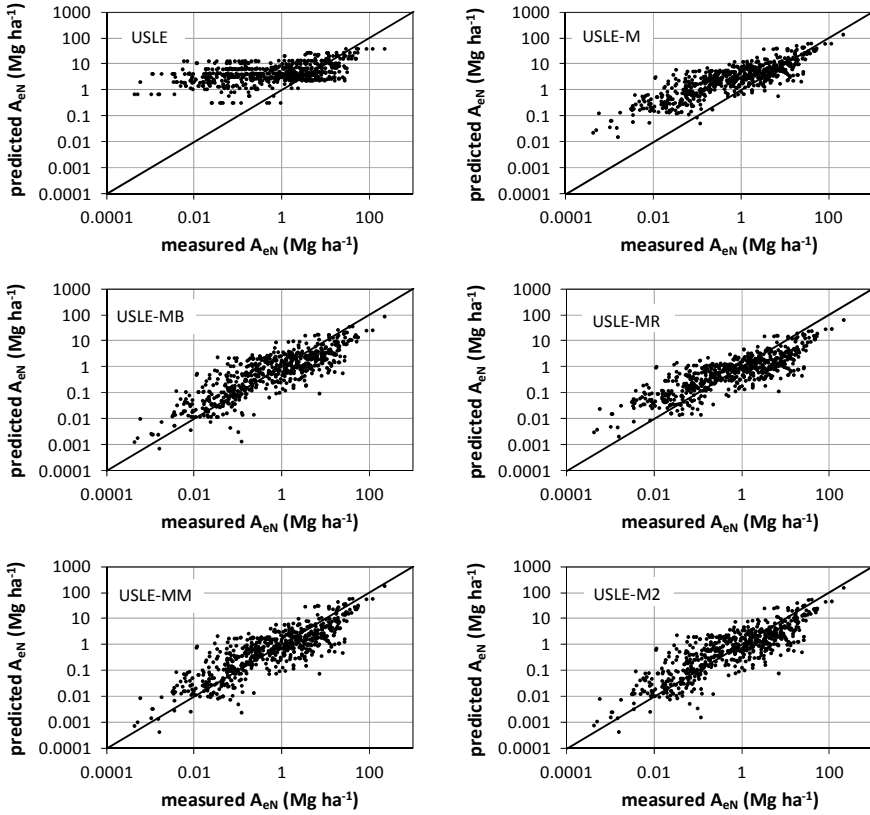


Fig. 1 Comparison between the predicted and the measured normalized soil loss values, A_{eN} , for the six tested models

are generally used to represent the model's global performances. In particular, the USLE-MM performed better than the USLE-M in terms of R^2 , $RMSE$ and $NSEI$ but not of $|BIAS|$. However, developing power-type models was appropriate to effectively balance the number of over- and under-estimations ($p_{ue} = 50\text{--}52\%$ and $p_{oe} = 48\text{--}50\%$, depending on the model), to appreciably reduce maximum (86–96 against 271 for the USLE-M), mean (4.5–5.0 against 12.3) and median (2.3–2.9 against 4.5) values of DF , to increase the number of cases yielding relatively reliable A_{eN} predictions (53–61% of the events against 41%), and to substantially reduce the number of events for which soil loss predictions were particularly poor ($|Er| > 200\%$ in the 19.7–22.6% of the cases against 56.7%). The three power-type models showed some differences. In particular, the USLE-MM performed statistically better than the USLE-MB but these two models yielded very similar p_{ue} , p_{oe} and DF values, being occasionally the USLE-MB even better than the USLE-MM. In general, the USLE-MR performed worse than the other two models.

As compared with the USLE-M, the USLE-MB yielded systematically lower A_{eN} predictions ($0.03 < A_{eN}(\text{USLE-MB})/A_{eN}(\text{USLE-M}) < 0.80$, depending on the event) (Fig. 2a) and a near systematic under-prediction was also detected for the USLE-MM ($0.03 < A_{eN}(\text{USLE-MM})/A_{eN}(\text{USLE-M}) < 1.34$) since the latter model yielded a higher A_{eN} prediction than the USLE-M in a single case (Fig. 2a). The A_{eN} predictions obtained with the USLE-MB and the USLE-MM differed at the most by 3.8 times since the ratios between corresponding values varied from 0.4 to 3.8 (mean = 1.08, median = 1.03). The lowest $A_{eN}(\text{USLE-MB})/A_{eN}(\text{USLE-MM})$ ratios were associated with the most severe events (Fig. 2b) but a clear trend of these ratios with A_{eN} was not detectable. Therefore, the USLE-MB and the USLE-MM generally yielded relatively similar normalized soil loss predictions (Fig. 2b) whereas the USLE-M yielded appreciably higher A_{eN} values than the other two models especially for the less severe events. The three tested models were characterized by more similar performances in the most severe conditions.

Estimating separately an exponent for EI_{30} and another exponent for Q_R (USLE-M2) did not improve the general performances of the soil erosion model (Table 1). In particular, very slightly higher R^2 value, lower mean of DF , and higher percentages of events for which DF did not exceed 3 as compared with the single-exponent models were detected. There was not any numerical improvement with reference to the other indices, suggesting that the more parameterized soil loss prediction model did not allow any perceivable improvement in the erosion estimates.

Even if the inclusion of the runoff coefficient in the empirical soil prediction model improved the quality of the event soil loss predictions, a great importance was found to have the mathematical structure of the model since very different results were obtained using the same experimental information. The USLE-MB and the USLE-MM appeared to be the best choices among the possible alternatives. On the whole, these two models performed similarly in terms of both over- (50.4–50.9%, depending on the model, Table 1) and under-estimation (49.1–49.6%) percentages and discrepancy factors (e.g., means = 4.47–4.48). The USLE-MM was characterized by better statistical indices (R^2 , $RMSE$, $NSEI$, $BIAS$) than the USLE-MB. Unlike

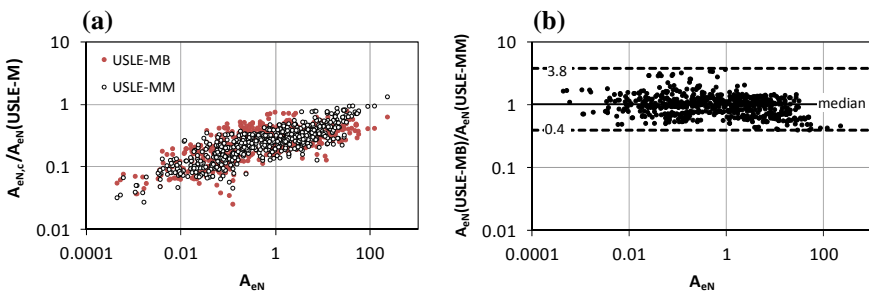


Fig. 2 Ratios between normalized soil loss, A_{eN} (Mg ha^{-1}), predictions obtained with different models plotted against the measured A_{eN} values

the former model, the latter one can be deduced by applying the dimensional analysis and self-similarity and it yielded better performances in terms of $\max(DF)$.

4 Conclusions

Predicting event soil loss at the plot scale by empirical models is interesting from a practical point of view. Empirical models have to be consistent with the main physical processes that control soil erosion at the considered temporal and spatial scales. The persisting interest for the USLE-type models has probably to be attributed to both the simplicity of the model and to its approximate soundness from a physical point of view. A comprehensive analysis of all possible expressions of the event rainfall-runoff erosivity factor for a USLE-type model was carried out at the Sparacia (south Italy) experimental site. The inclusion of the runoff coefficient in the empirical soil erosion model did not assure soil loss predictions of an acceptable quality, while the mathematical structure of the model affected the results obtained using the same experimental information. In particular, including rainfall erosivity factor EI_{30} and runoff coefficient Q_R and using a site-appropriate parameterization of the USLE-type model, the highest discrepancy factor between predicted and measured event soil losses decreased from more than 250 to less than 100. Better performances were obtained with the USLE-MB and the USLE-MM as compared with the USLE, USLE-M, USLE-MR and USLE-M2. Increasing the number of calibration parameters (i.e. USLE-M2) was not a good choice since the performances of the USLE-M2 were comparable to those detected for the single-exponent models (the USLE-MB and the USLE-MM).

Acknowledgements All authors set up the research and contributed to both analyze the data and write the manuscript.

References

- Bagarello, V., Di Stefano, C., Ferro, V., Giordano, G., Iovino, M., & Pampalone, V. (2012). Estimating the USLE soil erodibility factor in Sicily, south Italy. *Applied Engineering in Agriculture*, 28(2), 199–206.
- Bagarello, V., Ferro, V., & Pampalone, V. (2015). A new version of the USLE-MM for predicting bare plot soil loss at the Sparacia (South Italy) experimental site. *Hydrological Processes*, 29, 4210–4219.
- Bagarello, V., Di Stefano, C., Ferro, V., and Pampalone, V. (2018a). Comparing theoretically supported rainfall-runoff erosivity factors at the Sparacia (South Italy) experimental site. *Hydrological Processes* 32, 507–515.
- Bagarello, V., Ferro, V., Giordano, G., Mannocchi, F., Todisco, F., and Vergni, L. (2018b). Statistical check of USLE-M and USLE-MM to predict bare plot soil loss in two Italian environments. *Land Degradation & Development* 29, 2614–2628.

- Carollo, F. G., Di Stefano, C., Ferro, V., Pampalone, V., & Sanzone, F. (2016). Testing a new sampler for measuring plot soil loss. *Earth Surface Processes and Landforms*, *41*, 867–874.
- Di Stefano, C., Ferro, V., & Pampalone, V. (2017). Testing the USLE-M family of models at the Sparacia experimental site in South Italy. *Journal of Hydrological Engineering*, *22*(05017012), 1–11.
- Ferro, V. (2010). Deducing the USLE mathematical structure by dimensional analysis and self-similarity theory. *Biosystems Engineering*, *106*(2), 216–220.
- Kinnell, P. I. A., & Risse, L. M. (1998). USLE-M: empirical modeling rainfall erosion through runoff and sediment concentration. *Soil Science Society America Journal*, *62*, 1667–1672.
- Nash, J. E., & Sutcliffe, J. E. (1970). River flow forecasting through conceptual models, part 1—a discussion of principles. *Journal of Hydrology*, *10*, 282–290.
- Nearing, M. A. (1997). A single continuous function for slope steepness influence on soil loss. *Soil Science Society of America Journal*, *61*, 917–919.
- Renard, K. G., Foster, G. R., Weesies, G. A., McCool, D. K., & Yoder, D.C. (1997). *Predicting soil erosion by water: a guide to conservation planning with the Revised Universal Soil Loss Equation (RUSLE)* (Vol. 703). USDA Agriculture Handbook. Washington, DC.
- Yin, S., Nearing, M. A., Borrelli, P., & Xue, X. (2017). Rainfall erosivity: an overview of methodologies and applications. *Vadose Zone Journal*, *16*, 1–16.
- Wischmeier, W. H., & Smith, D. D. (1978). *Predicting rainfall-erosion losses – A guide to conservation farming* (Vol. 537). USDA, Agr. Handbook, Blacksburg, VA.

Evaluating the Effects of Forest Cover Changes on Sediment Connectivity in a Catchment Affected by Multiple Wildfires



Lorenzo Martini, Lorenzo Faes, Cordelia Scalari, Giacomo Pellegrini, Andrés Iroumé, Mario Aristide Lenzi and Lorenzo Picco

Abstract Wildfire-related impacts on the hydrogeomorphic properties of river basins is scarcely studied in South American sites. Fire affects river systems by altering the forest cover, decreasing the soil infiltration capacity, modifying the sediment yields and leading to channel instability. To study the effect of the disturbance in the sediment routing, the analysis of changes in sediment connectivity, i.e. the degree of linkage between source and sink areas, has been recently used. The main aim of the present research is to adapt and apply the Index of Connectivity (IC) in a Chilean catchment affected by subsequent wildfires in 2002 and 2015. Specific objectives involve the derivation of fire severity maps of both wildfires, and the development of a weighting factor, which properly represents the impedance to sediment fluxes. We made use of satellite images and sampling plots to carry out the fire severity maps and then the Normalized Difference Vegetation Index (NDVI) for the computation of the weighting factor maps used in the connectivity analysis. The results demonstrated not only the applicability of this approach, which permitted to highlight the changes in IC patterns but even the predominant changes in forest cover as well as the preferential sources of sediment within the basin.

Keywords Wildfires · Fire severity · Land cover change · Sediment connectivity · Chile

L. Martini (✉) · L. Faes · C. Scalari · G. Pellegrini · M. A. Lenzi · L. Picco
Department of Land, Environment, Agriculture and Forestry, Università Degli Studi Di Padova,
Viale Dell'Università 16, 35020 Legnaro, Italy
e-mail: lorenzo.martini.2@phd.unipd.it

A. Iroumé
Faculty of Forest Sciences and Natural Resources, Universidad Austral de Chile, Valdivia, Chile

L. Picco
Faculty of Engineering, Universidad Austral de Chile, Valdivia, Chile

Rina–Natural and Anthropogenic Risks Research Center, Universidad Austral de Chile, Valdivia, Chile

© Springer Nature Switzerland AG 2020

A. Coppola et al. (eds.), *Innovative Biosystems Engineering for Sustainable Agriculture, Forestry and Food Production*, Lecture Notes in Civil Engineering 67,
https://doi.org/10.1007/978-3-030-39299-4_2

1 Introduction

Among large natural disturbances affecting river systems, wildfires are often indicated as major agents for land and soil degradation (Shakesby 2011) and for geomorphological changes in densely vegetated catchments (Neary et al., 2005). The hydrogeomorphic response to wildfires has been deeply studied in forested catchments: decrease of root resistance; reduction of soil infiltration capacity (Swanson, 1981), exacerbation of soil erosion (Shakesby, 2011), water runoff and sediment yield increase (Benavides-Solorio and MacDonald, 2001; Neary et al., 2005) are few out of many effects reported in areas affected by wildfire. Furthermore, specific effects on river morphology have been documented due to the increase of in-channel wood recruitment (Benda et al., 2003) and the alteration of channel stability (e.g. channel aggradation) (DeBano et al., 1998). The effects of fire strongly depend on the intensity, duration, pre-fire disturbance history (Brogan et al., 2019) as well as from the topography, vegetation, geology and climate of the area affected (Swanson 1981). In addition, human activities are becoming a further propellant factor for wildfire's occurrence and damages. In this context, the assessment of fire severity, which often encompasses the properties of intensity and duration, is extremely important to quantify the fire-related impact and still represents a major challenge.

In river basins, the spatial distribution of wildfire-induced effects, especially those regarding sediment transfer, is determined by the spatial arrangement of the sediment sources and their capability to deliver sediment into the stream network. In the cascade process, the chance of sediments to reach specific compartments of the catchment is strictly related to the structural properties of the system itself (Hooke 2003; Heckmann et al., 2018). The evolving studies in the field of connectivity are becoming fundamental to understand the efficiency of sediment transfer within geomorphic systems (Heckmann et al., 2018). The assessment of the degree of linkage between two compartments, potentially (de)coupled, can be ensured thanks to the Index of Connectivity (IC) (Borselli et al., 2008; Cavalli et al., 2013). The IC performs a characterization of the sediment paths prone to deliver sediment from sources to sinks primarily according to the topographic conditions. Initially, such topography-based index gave positive results in alpine catchments, typically with steep slopes, high sediment availability and scattered vegetation (Cavalli et al., 2013; Rainato et al., 2018). Afterwards, the IC have been widely used to analyse various catchments after natural or human disturbances (Heckmann et al., 2018; Persichillo et al., 2018; Llana et al., 2019). Nevertheless, the analysis of sediment connectivity in response to wildfires is scarcely considered (Ortíz-Rodríguez et al., 2019) even if their capability to mobilize sediments have been largely documented.

The present study aims to analyse the variations in sediment connectivity in a catchment affected by two subsequent wildfires. Specific objectives regards (i) the assessment of fires severity (ii) the development of IC by means of open source Digital Elevation Model (DEM) and satellite images (iii) comparison of wildfire and IC spatial patterns for land management purposes.

2 Study Area

The study area is the Rio Toro catchment, an 18 km² basin located in southern Chile (Araucanía Region). The Chilean territory is known for the high occurrence of large wildfires (between one and eight thousands per year, in the last 20 years), which represents a cause of loss of native forests, a major threat for human settlements and a destabilizing factor for river systems (Úbeda and Sarricolea 2016; Mazzorana et al. 2019). In this context, the Rio Toro catchment was affected by the occurrence of two major wildfires in 2002 and 2015. The former burned almost 20000 ha in the Araucanía Region (González et al., 2005). The climate of the area is temperate warm humid with mean annual precipitation of 2480 mm (Comiti et al., 2008; Mao et al., 2008), promoting the growth of endemic *Nothofagus* spp. in the downstream part and *Araucaria araucana* in the uppermost part. The thick understorey is mainly composed by native bamboo (*Chusquea* spp.), which takes advantage of the large gaps offered by *Araucaria aruacana* forest (Ulloa et al., 2015). The catchment’s altitude ranges from 762 m a.s.l. in the northern areas to 1816 m a.s.l. The water course flows from S–E to N–W for about 7 km, exhibiting plane-bed/step-pool channel morphology (Comiti et al., 2008).

3 Materials and Methods

The study was carried out in two main phases: i) the assessment of fire severity for both wildfires (2002 and 2015) by means of the spectral vegetation index difference Normalized Burn Ratio (dNBR)(Key and Benson, 2006) and ii) the analysis of sediment connectivity changes thanks to the IC (Fig. 1).

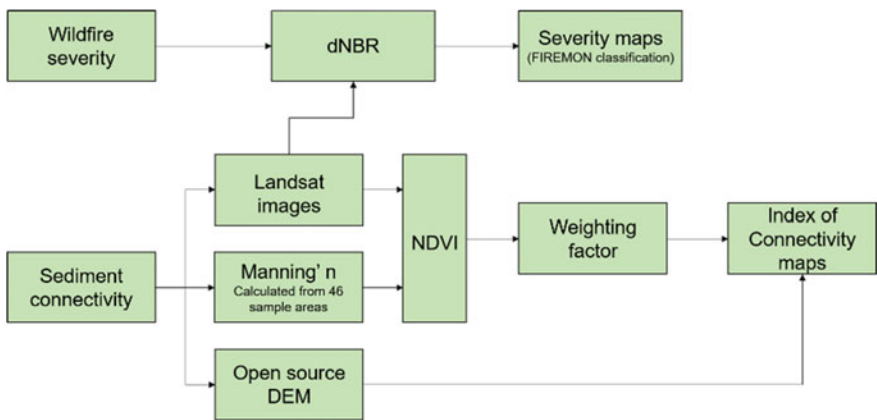


Fig. 1 Flowchart describing the procedure to carry out the wildfire severity and the IC

The two phases rely upon open-source remote sensing data and field surveys in order to carry out the fire severity and IC maps.

3.1 Fire Severity

The severity of the two wildfires has been assessed using the classification system FIREMON (Fire Effects Monitoring and Inventory System) included in the Landscape Assessment section (Key and Benson, 2006). This approach requires aggregate information about fire effects among large areas by using remote sensing data to perform the dNBR. The dNBR, calculated using Landsat 7 products, allows the quantitative detection of the differences of reflectance between the pre and post-fire surfaces (further information in Key and Benson, 2006). The resulting fire severity maps have been presented by highlighting only the high—moderate high classes due to major interest.

3.2 Index of Connectivity

The analysis of sediment connectivity has been carried out thanks to the IC (Borselli et al., 2008; Cavalli et al., 2013) in order to adapt it to mountainous catchments, typically showing lack of vegetation, steep slopes and high sediment availability. The IC is computed according to the logarithmic form described in the Eq. (1):

$$IC = \log_{10} \left(\frac{\bar{W} \bar{S} \sqrt{A}}{\sum_i \frac{d_i}{S_i W_i}} \right) \quad (1)$$

where W is the weighting factor, representing the impedance to sediment fluxes given by the structural characteristics of surface roughness, S (m/m) is the slope, A (m²) is the area contributing to a specific point, d_i (m) is the length of the path between the upslope and downslope component (represented by numerator and denominator, respectively).

The topographic information required to derive the IC is given by an open source DEM obtained from the satellite mission ALOS PALSAR. The DEM has 12,5 m resolution and it can be downloaded from the Alaskan Facility Service (ASF) website (<https://www.asf.alaska.edu>). The DEM constitutes the basis for the IC analysis which accounts the land cover changes for two periods before and after both wildfires to carry out coherent Weighting factors (see Sect. 3.2.1). The IC changes have been verified with the Wilcoxon signed ranked in order to test statistical differences in the medians between pre and post-wildfires years (p-value < 0,05). The differences have been classified in seven main classes to highlight the major differences in IC.

3.2.1 Weighting Factor

The weighting factor (W factor) represents the impedance to sediment fluxes, which can be derived from the measure of the surface roughness. In this work, the W factors have been carried out according to a methodology involving first the computation of a Manning's coefficient for the overland flow for 46 ground samplings and then the propagation of the coefficient to the whole catchment thanks to the correlation with the Normalized Difference Vegetation Index (NDVI). Similar methodologies have been proposed by other authors (e.g. Mishra et al., 2019) to extend land cover parameters (such the C factor in the Revised Universal Soil Loss Equation) at catchment scale by correlating them with the NDVI. In this study, the Manning's n for the overland flow was used instead of the much-used C factor to represents the impedance to sediment fluxes. The Manning's n was calculated using the pre-existing adjustment tables of Arcement and Schneider (1989), which calculate an overall coefficient (n) according to specific parameters observed in the field. The coefficient was calculated for 46 sampling plots (10 × 10 m) scattered all over the Rio Toro catchment. Finally, four W factor maps have been produced to support the computation of IC in four different years (pre and post-wildfires, 2001, 2003, 2015, 2016).

4 Results and Discussion

Our results regarding the severity of the two wildfires show that in both cases the areas classified as high-moderate high covers more than 20% of the whole catchment. However, as expected, an outstanding difference is evident between the results of the two wildfires (Fig. 2). The wildfire's high-moderate high severity areas, in fact, are much more widen in 2002 (Fig. 2a) than 2015 (Fig. 2b), 12 km² and 3,6 km², respectively. This outstanding difference could be caused by the intrinsic bias in the 2015 severity map, which inevitably takes into account the 2002 post-wildfire condition for the computation of the dNBR. This is in accordance with Brogan et al. (2019), who defined as the pre-disturbance history can drastically impose either a decrease or an increase of catchment's sensitivity. The difference of IC (DoIC) values are also presented in Fig. 2. The DoIC highlights similar spatial patterns among the IC variations and the high-moderate high fire severity areas. The areas classified as high and medium-high fire severity partially corresponds to the areas where the IC difference is higher as well, which are mainly located in the central part of the catchment. In both maps, there is an evident increase in IC values: mean values from -2,32 (2001) to -2,16 (2003) and from -2,24 (2015) to -2,18 (2016); maximum values from 2,52 (2001) to 2,59 (2003) and from 2,55 (2015) to 2,57 (2016). This results is mainly associated with the important reduction of forest cover and major increase of potential erodible areas. The difference in IC was documented also in the Mexican site studied by Ortíz-Rodríguez et al. (2019), which also found similar proportion between the higher IC patterns and the burned areas. The higher differences in IC are more evident along the slopes close to the channels, which represent the primary

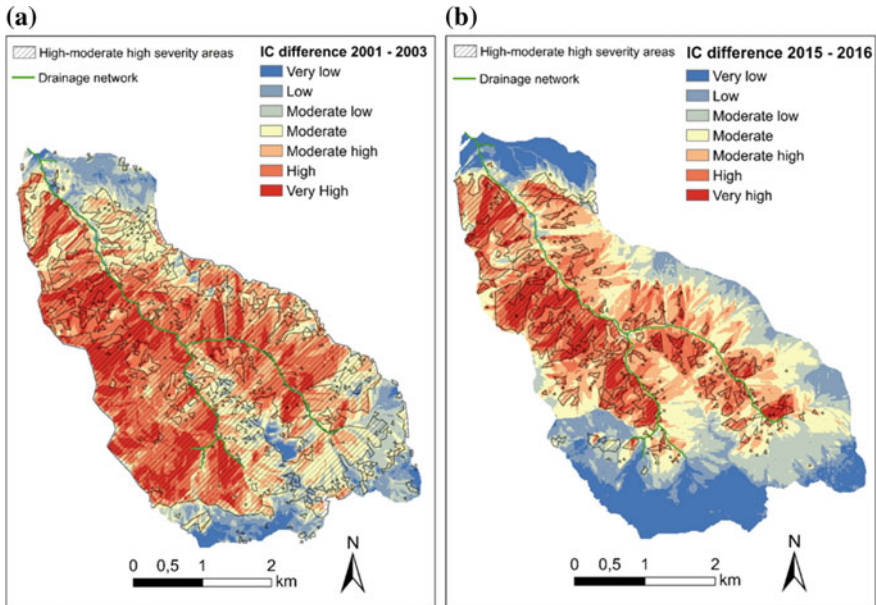


Fig. 2 Difference of the Index of Connectivity calculated between pre and post-wildfire periods: **a** first wildfire in 2002; **b** second wildfire in 2015. High—moderate high fire severity areas are represented by dashed areas

sink for the sediment fluxes from hillslope-channel perspective. Considering these results, the Rio Toro catchment could face two intertwined trends that will promote the sediment yields towards the stream network: the increase of sediment connectivity suggested by higher IC values and the increase of slope erodibility due to the loss of forest cover.

5 Conclusions

In the present study, an application of the Index of Connectivity have been carried out in order to assess the importance of land cover changes, caused by a natural disturbance, to the sediment connectivity. The strong relationship between the two components was evident from the results, which highlights the spatial overlaps between IC changes and fire severity. Indeed, when considering the analysis of sediment dynamics in forested catchments, the vegetation characteristics cannot be neglected. Particularly, this correlation is even more important in post-disturbance scenarios, where the variations of land cover and sediment connectivity are emphasised. In this way, further analysis in the field of sediment connectivity applied in wildfire-affected areas could provide helpful information for land managers.

Acknowledgements The present research activity was developed within the framework of projects FONDECYT 1170413 and CONICYT-ITAL170004.

References

- Arcement, G.J., Schneider, V.R., 1989. Guide for selecting Manning's roughness coefficients for natural channels and floodplains. USGS Water-Supply Paper 2339.
- Benavides-Solorio, J., & MacDonald, L. H. (2001). Post-fire runoff and erosion from simulated rainfall on small plots. *Colorado Front Range. Hydrological Processes*, 15(15), 2931–2952. <https://doi.org/10.1002/hyp.383>.
- Benda, L., Miller, D., Sias, J., Martin, D., Bilby, R., Veldhuisen, C., et al. (2003). Wood Recruitment Processes and Wood Budgeting. *American Fisheries Society Symposium*, 37(January), 49–73.
- Borselli, L., Cassi, P., & Torri, D. (2008). Prolegomena to sediment and flow connectivity in the landscape: A GIS and field numerical assessment. *CATENA*, 75(3), 268–277. <https://doi.org/10.1016/j.catena.2008.07.006>.
- Brogan, D. J., MacDonald, L. H., Nelson, P. A., & Morgan, J. A. (2019). Geomorphic complexity and sensitivity in channels to fire and floods in mountain catchments. *Geomorphology*, 337, 53–68. <https://doi.org/10.1016/j.geomorph.2019.03.031>.
- Cavalli, M., Trevisani, S., Comiti, F., & Marchi, L. (2013). Geomorphometric assessment of spatial sediment connectivity in small Alpine catchments. *Geomorphology*, 188, 31–41. <https://doi.org/10.1016/j.geomorph.2012.05.007>.
- Comiti, F., Andreoli, A., Mao, L., & Lenzi, M. A. (2008). Wood storage in three mountain streams of the Southern Andes and its hydro-morphological effects. *Earth Surface Processes and Landforms*, 33, 244–262. <https://doi.org/10.1002/esp.1541>.
- DeBano, L. F., Neary, D. G., & Ffolliott, P. F. (1998). *Fire's effects on ecosystems*. New York: Wiley.
- González, M. E., Veblen, T. T., & Sibold, J. S. (2005). Fire history of Araucaria-Nothofagus forests in Villarica National Park. *Chile Journal of Biogeography*, 32(7), 1187–1202. <https://doi.org/10.1111/j.1365-2699.2005.01262.x>.
- Heckmann, T., Cavalli, M., Cerdan, O., Foerster, S., Javaux, M., Lode, E., & Brardinoni, F. (2018). Indices of sediment connectivity: Opportunities, challenges and limitations. *Earth-Science Review*, 1–32. <https://doi.org/10.1016/J.EARSCIREV.2018.08.004>.
- Hooke, J. (2003). Coarse sediment connectivity in river channel systems: A conceptual framework and methodology. *Geomorphology*, 56(1–2), 79–94. [https://doi.org/10.1016/S0169-555X\(03\)00047-3](https://doi.org/10.1016/S0169-555X(03)00047-3).
- Key, C. H., & Benson, N. C. (2006). Landscape assessment: Sampling and analysis methods. General Technical Report RMRS-GTR-164-CD.
- Llena, M., Vericat, D., Cavalli, M., Crema, S., & Smith, M. W. (2019). The effects of land use and topographic changes on sediment connectivity in mountain catchments. *Science of the Total Environment*, 660, 899–912. <https://doi.org/10.1016/j.scitotenv.2018.12.479>.
- Mao, L., Uyttendaele, G. P., Iroumé, A., & Lenzi, M. A. (2008). Field based analysis of sediment entrainment in two high gradient streams located in Alpine and Andine environments. *Geomorphology*, 93(3–4), 368–383. <https://doi.org/10.1016/j.geomorph.2007.03.008>.
- Mazzorana, B., Picco, L., Rainato, R., Iroumé, A., Ruiz-Villanueva, V., Rojas, C., & Melnick, D. (2019). Cascading processes in a changing environment: Disturbances on fluvial ecosystems in Chile and implications for hazard and risk management. *Science of The Total Environment*, 655(November 2018), 1089–1103. <https://doi.org/10.1016/j.scitotenv.2018.11.217>.
- Mishra, K., Sinha, R., Jain, V., Nepal, S., & Uddin, K. (2019). Towards the assessment of sediment connectivity in a large Himalayan river basin. *Science of the Total Environment*, 661, 251–265. <https://doi.org/10.1016/j.scitotenv.2019.01.118>.

- Neary, D. G., Ryan, K. C., & DeBano, L. F. (2005). Wildland fire in ecosystems—Effects of fire on soil and water: U.S. Department of Agriculture Forest Service General Technical Report RMRS-GTR-42, Vol. 4, 250 p.
- Ortiz-rodríguez, A. J., Muñoz-robles, C., & Borselli, L. (2019). Changes in connectivity and hydrological efficiency following wildland fires in Sierra Madre Oriental, Mexico. *Science of The Total Environment* 655, 112–128. <https://doi.org/S0048969718345923>.
- Persichillo, M. G., Bordoni, M., Cavalli, M., Crema, S., & Meisina, C. (2018). The role of human activities on sediment connectivity of shallow landslides. *Catena*, 160(August 2016), 261–274. <https://doi.org/10.1016/j.catena.2017.09.025>.
- Rainato, R., Picco, L., Cavalli, M., Mao, L., Neverman, A. J., & Tarolli, P. (2018). Coupling Climate Conditions, Sediment Sources and Sediment Transport in an Alpine Basin. *Land Degradation and Development*, 29(4), 1154–1166. <https://doi.org/10.1002/ldr.2813>.
- Shakesby, R. A. (2011). Post-wildfire soil erosion in the Mediterranean: Review and future research directions. *Earth-Science Reviews*, 105(3–4), 71–100. <https://doi.org/10.1016/j.earscirev.2011.01.001>.
- Swanson, F. J. (1981). Fire and geomorphic processes. *Fire Regimes and Ecosystem Properties*, 401–420.
- Úbeda, X., & Sarricolea, P. (2016). Wildfires in Chile: A review. *Global and Planetary Change*, 146, 152–161. <https://doi.org/10.1016/j.gloplacha.2016.10.004>.
- Ulloa, H., Iroumé, A., Picco, L., Korup, O., Lenzi, M. A., Mao, L., & Ravazzolo, D. (2015). Massive biomass flushing despite modest channel response in the Rayas River following the 2008 eruption of Chaitén volcano, Chile. *Geomorphology*, 250(May 2008), 397–406. <https://doi.org/10.1016/j.geomorph.2015.09.019>.

A Check of Water Drop Impact Effects on Surface Soil Saturated Hydraulic Conductivity



F. Todisco, V. Bagarello, L. Vergni and A. Vinci

Abstract The post-tillage dynamics of the surface soil saturated hydraulic conductivity, K_s , was studied at the Masse experimental station (central Italy, silty-clay-loam soil). A sequence of experiments was performed by rainfall simulation on two replicated micro-plots (width 1 m, length 0.92 m, slope 16%) established on bare soil. Each high-intensity rainfall simulation was preceded by a low-intensity wetting phase. The soil water content, w , was measured before wetting and both before and after simulation. Runoff was measured at 5 min intervals. The infiltration rate was calculated as the difference between rainfall intensity and runoff rate. Finally, K_s was assumed to be equal to the infiltration rate under the nearly steady conditions reached at the end of each simulation. The pre-wetting w values were quite low and they increased during wetting, reaching at the end of this phase a value that remained more or less stable during the simulation phase. Consequently, all changes of K_s were expected to be specifically attributable to mechanical modifications of the porous medium due to the raindrop impact. For each individual experiment, K_s decreased with cumulative rainfall energy, E , according to an exponential or power relationship, denoting that raindrop impact had a noticeable effect on K_s when it occurred on an initially tilled soil. The developed experimental methodology appears usable to determine raindrop impact effects on the surface soil K_s in highly controlled field conditions and it could be applied to develop K_s versus E relationships usable for numerically simulating surface soil hydrological processes.

Keywords Tillage · Infiltration · Rainfall simulation · Rainfall kinetic energy

F. Todisco (✉) · L. Vergni · A. Vinci

Dipartimento di Scienze Agrarie, Alimentari e Ambientali (DSA3), Università di Perugia, Borgo XX Giugno 74, Perugia, Italy

e-mail: francesca.todisco@unipg.it

V. Bagarello

Dipartimento di Scienze Agrarie, Alimentari e Forestali (SAAF), Università di Palermo, Viale delle Scienze, Palermo 90128, Italy

© Springer Nature Switzerland AG 2020

A. Coppola et al. (eds.), *Innovative Biosystems Engineering for Sustainable Agriculture, Forestry and Food Production*, Lecture Notes in Civil Engineering 67,

https://doi.org/10.1007/978-3-030-39299-4_3

1 Introduction

The hydraulic conductivity of the soil expresses the aptitude of the porous medium to transmit water and therefore has a strategic importance in the surface runoff response and in the dynamics of hydrological processes. Generally, the hydraulic conductivity shows high space-time variability due to variations of both soil physical properties and water content (Mualem et al. 1990; Assouline and Mualem 2006; King and Bjomeberg 2012; Bagarello et al. 2019). The temporal variability is further accentuated in soils subject to mechanical processing like tillage which temporarily changes the structure of the soil surface layer where the infiltration processes take place (Coutadeur et al. 2002). An increase in saturated soil hydraulic conductivity K_s resulting from tillage has been frequently observed (Haruna et al. 2018; Chahinian et al. 2006; Heard et al. 1988; Carter and Kunelius 1986) and it can be generally attributed to an increment of both total porosity and macropores to micropores ratio. However, in some particular circumstances, a reduction of K_s after tillage was also observed (Bhattacharyya et al. 2006; Joschko et al. 1992) as a consequence of a cancellation or reduction of the pores connectivity present in the no-tilled soil.

The increase of K_s after tillage is always temporary (Haruna et al. 2018) and is followed by a progressive reduction, whose dynamics is affected by the soil type, the agronomic practices and environmental factors, primarily including rainfall. The knowledge of the dynamics of K_s in tilled soils is expected to have practical interest in the calibration and application of hydrological models, but this dynamics has been analyzed a few times in the literature. For example Chahinian et al. (2006), studying the dynamics of different hydraulic properties in tilled silty-clay-loam soils, found that K_s decreased from a maximum value just after tillage to a minimum value after soil reconsolidation, with a rate dependent on the amount of rainfall that occurred since tillage. A similar dynamics was observed in a sandy-clay-loam soil by Ndiaye et al. (2005).

In this paper, the temporal modifications of the saturated soil hydraulic conductivity since tillage were analyzed for a silt-clay-loam soil in highly controlled rainfall simulation experiments. Unlike most of the works in the literature, in which the K_s reduction is expressed in terms of cumulative rainfall depth, here the process has been described according to the cumulative rainfall kinetic energy.

2 Materials and Methods

The post-tillage dynamics of the saturated soil hydraulic conductivity was studied using the nozzle-type rainfall simulator installed at the Masse experimental station (Agricultural and Forest Hydraulics Research Division, Department of Agricultural, Food and Environmental Sciences of the University of Perugia). The station is located 20 km south of Perugia, in the Region of Umbria (Central Italy). Detailed information on the experimental site can be found in Todisco et al. (2012) and Vinci et al. (2016).

The rainfall simulator is placed over two replicated micro-plots with width 1 m, length 0.92 m, and slope 16%. Each micro-plot is surrounded by a can, laid on the soil surface, with walls of a few centimeters and an outlet at the bottom end. This can is used to measure rainfall falling outside the plot (Vergni et al. 2018). The soil texture is silty-clay-loam with 16, 51 and 34% of sand, silt and clay, respectively. The gravel content is negligible and the organic matter content is about 1%. The soil structure is massive when wet, and upon drying breaks into weak fine subangular blocky.

The nozzles are centered over each plot at a height of 2.8 m above the ground and the experiments are simultaneously replicated in the two micro-plots. Two types of wide angle square Full Jet nozzles, provided by Jetsystem srl (<https://www.jetsystemsrl.it>), were used in the experiments: the 14WSQ nozzle (intensity of about 40 mm/h and kinetic energy of $9.5 \text{ J mm}^{-1} \text{ m}^{-2}$) and the 30WSQ nozzle (intensity of about 70 mm/h and kinetic energy of $14.5 \text{ J mm}^{-1} \text{ m}^{-2}$). More technical features of the simulator and of the rainfall characteristics can be found in Vergni et al. (2018).

The experiments were carried out according to the following scheme: tillage, wetting 1 phase (rainfall with low intensity, i.e. 40 mm/h, and low kinetic energy), simulation 1 phase (rainfall with high intensity, i.e. 70 mm/h, and high kinetic energy), suspension for some days, wetting 2 phase, simulation 2 phase, suspension for some days, wetting 3 phase, simulation 3 phase. This type of experiment was replicated two times on plot 1 and three times on plot 2, with a pause of a few months between two replicated experiments on a plot. The duration of the wetting phase was 30 min with the exception of wetting 1 and wetting 2 of the first experiment whose durations were 125 and 45 min, respectively. The simulation phase started a few minutes after the wetting phase and its duration varied between 60 and 120 min.

The surface soil (upper 5 cm) water content, w , was measured by the gravimetric method before wetting and both before and after simulation. Runoff was measured at 5 min intervals. The infiltration rate was calculated as the difference between rainfall intensity and runoff rate. Finally, K_s was assumed to be equal to the infiltration rate under the nearly steady conditions reached at the end of each simulation phase (White et al. 1989), which implied that lateral expansion of soil water during the wetting phase was considered to induce an approximately one-dimensional infiltration process during simulation. For each individual experiment, the relationship between K_s and the energy, E , dissipated at the soil surface after tillage was examined by considering two alternative scenarios: (i) energy of the simulation phase only, E_s ; and (ii) total energy, i.e. also including the energy dissipated for wetting (E_w).

3 Results

The pre-wetting water contents w were quite low and they increased during wetting, reaching at the end of this phase a value that remained more or less stable during the simulation phase (Fig. 1).

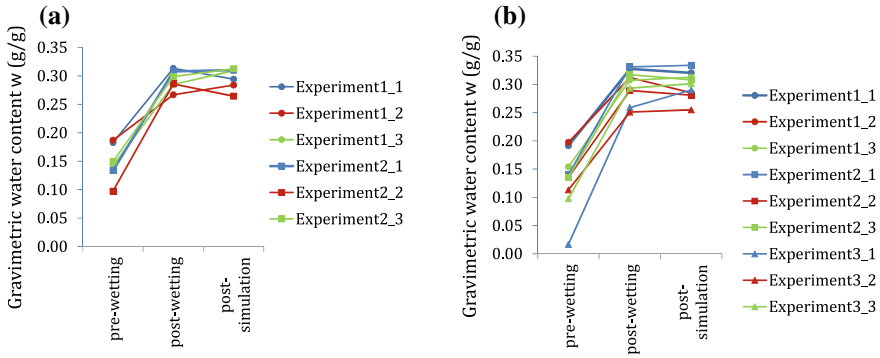


Fig. 1 Variations of the gravimetric water content w in plot 1 (a) and plot 2 (b) during the three phases of each simulation. Each experiment started from tillage and included a series of three simulations (1, 2, 3)

Consequently, all changes in K_s were expected to be specifically attributable to mechanical modifications of the porous medium occurring as a consequence of raindrop impact.

The 5-minute dynamics of rainfall, R (mm/h), runoff, r (mm/h), and infiltration, ir (mm/h), rates during the three simulations carried out in each experiment are given in Fig. 2.

With simulation 1, runoff started to occur almost always (i.e. for four experiments out of five) some time (half an hour or more) after rainfall beginning. In simulations 2 and 3, runoff started to occur, in most cases (nine times out of 10), concurrently with rainfall.

In the passage from simulation 1–3, the five experiment yielded some common results including the following ones: (i) the initial value of r increased and the initial value of ir decreased; (ii) in all but two cases, at the beginning of the simulation ir was greater than r ; (iii) the interception point between ir and r tended to move towards the left. In other words, the instantaneous condition of equality between infiltration and runoff rates, i.e. $ir = r$, occurred earlier during subsequent simulations and approached the simulation starting time.

On average, the decrease of K_s was noticeable in the passage from simulation 1 (25.7 mm/h) to simulation 2 (8.4 mm/h, -67.2%) but it was less pronounced in the passage from simulation 2 to simulation 3 (5.1 mm/h, -39.4% , Fig. 3). The variability of K_s among experiments was highest for the first simulation ($CV = 77\%$) and it decreased to a nearly constant value for the two subsequent simulations ($CV = 41\text{--}44\%$).

For each individual experiment, K_s decreased with E (E_s or $E_w + E_s$) according to an exponential or power relationship, denoting that raindrop impact had a noticeable effect on K_s when it occurred on an initially tilled soil. For some experiments, the K_s versus E relationships were excellent (coefficient of determination, $R^2 \approx 1$) while, in other cases, they appeared less robust ($R^2 > 0.7$) even though the general decreasing

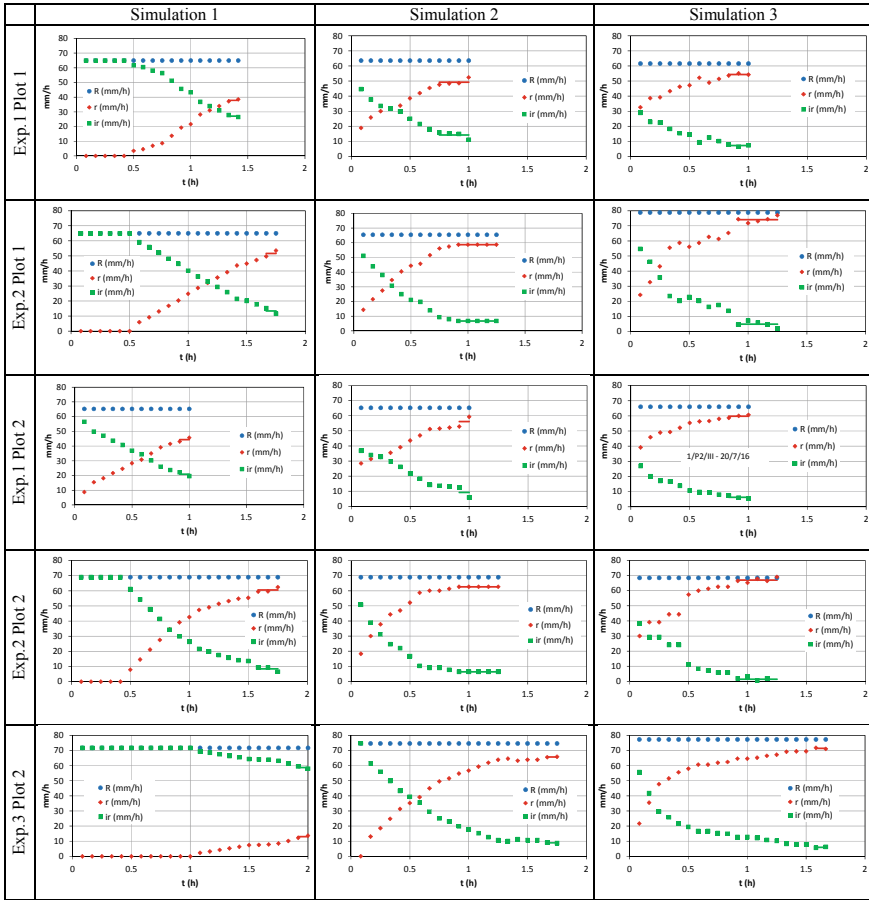
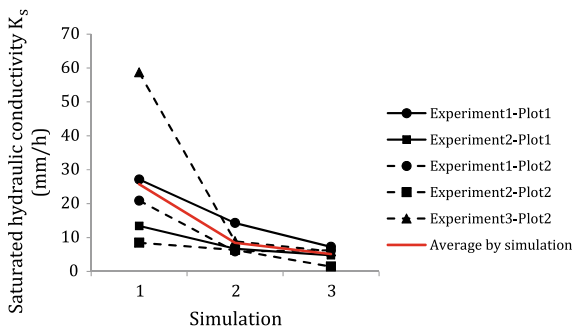


Fig. 2 Five-minute dynamics of rainfall, R , runoff, r , and infiltration, ir , rates in the three simulations of each experiment

Fig. 3 Variations of the saturated soil hydraulic conductivity K_s during the three simulations forming part of the same experiment. The red line indicates the K_s value averaged by simulation



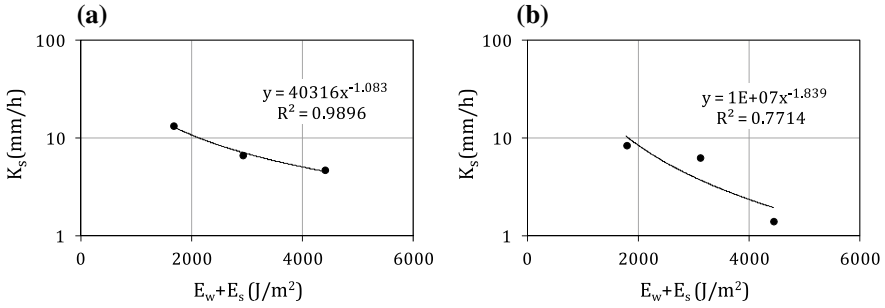


Fig. 4 Relationship between the dissipated kinetic energy (including both wetting and event phases) and the saturated soil hydraulic conductivity, K_s , for two exemplificative cases: II experiment on plot 1 **(a)** and II experiment on plot 2 **(b)**

trend was always captured. Two examples (the best and the worst respectively) are shown in Fig. 4a and b. For these relationships, fitted on only three points, the exponent was very variable ($1.1 \div 2.3$) and strongly influenced by the initial and final values of K_s .

Decreasing relationships between K_s and the dissipated energy were E also observed considering all the experimental data together (Fig. 5), although in this case the goodness of the fit decreased appreciably, probably as a consequence of the fact that each experiment started from a more or less different K_s value.

The goodness of the fit was similar for the K_s versus $E_w + E_s$ and K_s versus E_s relationships (Fig. 5a and b, respectively). Therefore, the dissipated energy during the simulation phase of the experiment had a prevalent effect on the K_s dynamics.

The relationship between the cumulative rainfall P_{cum} and K_s was also analyzed. The exponent (-1.43) was very similar to that obtained using the dissipated kinetic energy $E_w + E_s$ (-1.42 , Fig. 5a), with a slightly lower goodness of fit ($R^2 = 0.42$). This modest difference in the use of P_{cum} or E could depend on the fact that the events were simulated with constant intensity (excluding the almost negligible contribution

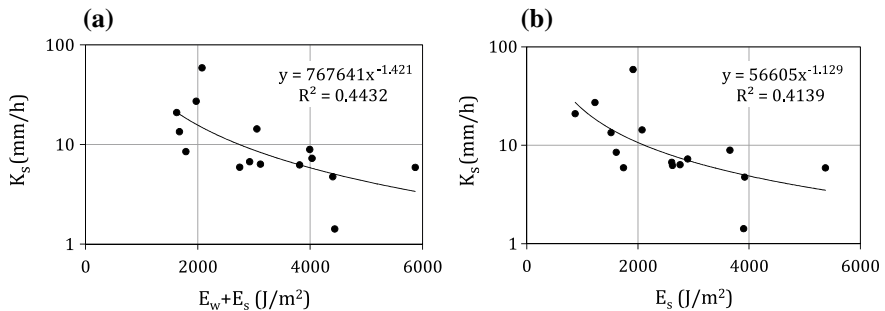


Fig. 5 Relationship between the dissipated kinetic energy and the saturated soil hydraulic conductivity, K_s , including **(a)** or not including **(b)** the dissipated energy during the wetting phase

of the wetting phase). Surely, a greater variability in intensity (and therefore in E) could highlight a greater performance of the K_s versus E relationships compared to those K_s versus P_{cum} .

4 Conclusions

In conclusion, raindrop impact had a noticeable effect on K_s , with a high reduction of both the average value and its variability, when it occurred on an initially tilled soil. An event with similar perturbative characteristics had a more limited effect on K_s (smaller decrease of the mean value and unchanged variability) when it fell on a surface that was already subjected to a previous disturbance process after tillage.

The developed experimental methodology appears usable to determine raindrop impact effects on the surface soil K_s in highly controlled field conditions and it could be applied to develop K_s versus E relationships usable for numerically simulating surface soil hydrological processes. Further experiments could contribute to derive a more robust database. Moreover, the assumption of an approximately one-dimensional infiltration process during the simulation phase requires specific testing due to the presence of the can around the plot.

References

- Assouline, S., & Mualem, Y. (2006). Runoff from heterogeneous small bare catchments during soil surface sealing. *Water Resource Research*, *42*, W12405.
- Bagarello, V., Baiamonte, G., & Caia, C. (2019). Variability of near-surface saturated hydraulic conductivity for the clay soils of a small Sicilian basin. *Geoderma*, *340*, 133–145.
- Bhattacharyya, R., Prakash, V., Kundu, S., & Gupta, H. S. (2006). Effect of tillage and crop rotations on pore size distribution and soil hydraulic conductivity in sandy clay loam soil of the Indian Himalayas. *Soil Tillage Research*, *86*, 129–140.
- Carter, M. R., & Kunelius, H. T. (1986). Comparison of tillage and direct drilling for Italian ryegrass on the properties of a fine sandy loam soil. *Canadian Journal of Soil Science*, *66*, 197–207.
- Chahinian, N., Moussa, R., Andrieux, P., & Voltz, M. (2006). Accounting for temporal variation in soil hydrological properties when simulating surface runoff on tilled plots. *Journal of Hydrology*, *326*, 135–152.
- Coutadeur, C., Coquet, Y., & Roger-Estrade, J. (2002). Variation of hydraulic conductivity in a tilled soil. *European Journal of Soil Science*, *53*, 619–628.
- Haruna, S. I., Anderson, S. H., Nkongolo, N. V., & Zaibon, S. (2018). Soil hydraulic properties: Influence of tillage and cover crops. *Pedosphere*, *28*(3), 430–442.
- Heard, J. R., Kladvik, E. J., & Mannering, J. V. (1988). Soil macroporosity, hydraulic conductivity and air permeability of silty soils under long-term conservation tillage in Indiana. *Soil Tillage Research*, *11*, 1–18.
- Joschko, M., Sochtig, W., & Larink, O. (1992). Functional relationship between earthworm burrows and soil water movement in column experiments. *Soil Biology & Biochemistry*, *24*, 1545–1547.
- King, B. A., & Bjomeberg, D. L. (2012). Droplet kinetic energy of moving spray-plate center-pivot irrigation sprinklers. *Transactions of the ASABE*, *55*(2), 505–512.

- Mualem, Y., Assouline, S., & Rohdenburg, H. (1990). Rainfall induced soil seal (A) A critical review of observations and models. *CATENA*, *17*(2), 185–203.
- Ndiaye, B., Esteves, M., Vandervaere, J. P., Lapetite, J. M., & Vauclin, M. (2005). Effect of rainfall and tillage direction on the evolution of surface crusts, soil hydraulic properties and runoff generation for a sandy loam soil. *Journal of Hydrology*, *307*, 294–311.
- Todisco, F., Vergni, L., Mannocchi, F., & Bomba, C. (2012). Calibration of the soil loss measurement method at the Masse experimental station. *CATENA*, *91*, 4–9.
- Vergni, L., Todisco, F., & Vinci, A. (2018). Setup and calibration of the rainfall simulator of the Masse experimental station for soil erosion studies. *CATENA*, *167*, 448–455.
- Vinci, A., Todisco, F., & Mannocchi, F. (2016). Calibration of manual measurements of rills using Terrestrial Laser Scanning. *CATENA*, *140*, 164–168.
- White, I., Sully, M. J., & Melville, M. D. (1989). Use and hydrological robustness of time-to-incipient-ponding. *Soil Science Society of America Journal*, *53*, 1343–1346.

On the Description of Soil Variability Through EMI Sensors and Traditional Soil Surveys in Precision Agriculture



Bianca Ortuani, Enrico Casati, Camilla Negri and Arianna Facchi

Abstract In Precision Agriculture electromagnetic induction (EMI) sensors are generally used to obtain soil electrical conductivity (EC) maps for the delineation of homogeneous management zones (MZ). EC measurements are related to many physical-chemical soil properties and, moreover, are average values referred to the soil depth explored by the sensor. Consequently, the following questions arise: how reliable are EC measurements to describe soil variability, compared to the data provided by a pedological survey? To which extent MZs correspond to pedological units in a soil map? Texture analysis was conducted on 38 soils samples collected at three depths with a manual auger in a rice farm (province of Pavia, Italy) characterized by sandy-loamy soils. Four pedological units were recognized, mainly based on differences in clay content distribution with depth. Four MZs were recognized from the EC maps. MZ and pedological soil maps showed similar spatial distributions of soil types, particularly at field scale. However, at the farm scale, different MZs may correspond to the same pedological unit, because of the different soil properties to which the two classification approaches are sensitive: clay contents for pedological soil mapping, and sand contents for MZ mapping. Finally, ANOVA was carried out to evaluate the statistical significance of this result.

Keywords Traditional soil survey · EMI sensor · Precision agriculture · Homogeneous management zones

1 Introduction

The agronomic and irrigation practices in Precision Agriculture consider the distribution of the inputs (i.e. nutrients and water) with different rates according to the spatial variability of soil properties within the field. Consequently, a detailed description of the soil variability at the field scale is required. To achieve this goal through a

B. Ortuani (✉) · E. Casati · C. Negri · A. Facchi
Dipartimento di Scienze Agrarie e Ambientali – Produzione, Territorio, Agroenergia, Università degli Studi di Milano (DiSAA-UNIMI), via Celoria 2, 20133 Milan, Italy
e-mail: bianca.ortuani@unimi.it

© Springer Nature Switzerland AG 2020

A. Coppola et al. (eds.), *Innovative Biosystems Engineering for Sustainable Agriculture, Forestry and Food Production*, Lecture Notes in Civil Engineering 67,
https://doi.org/10.1007/978-3-030-39299-4_4

traditional soil survey, a very dense sampling network should be designed, with high economic cost and time consumption. Since the 1990s, electromagnetic induction (EMI) sensors have been adopted to measure soil properties through quick and non-invasive surveys. These sensors measure the soil electrical conductivity (EC), related to both physical and chemical soil properties. Many studies deal with the delineation of homogeneous Management Zones (MZ) (Corwin et al. 2003; Moral et al. 2010; Scudiero et al. 2013), and the soil properties mapping from the EC maps (André et al. 2012; Doolittle et al. 2002; Fortes et al. 2015; Hedley et al. 2010, 2013; Moral et al. 2010; Priori et al. 2013). This work aims to provide elements to answer these questions: how reliable are EC measurements acquired by EMI sensors to describe soil variability, compared to data provided by a traditional survey? To which extent do MZs correspond to units in a soil map?

2 Materials and Methods

2.1 Study Area

The study area is located in the administrative boundary of Zeme (province of Pavia, Italy), about 50 km south west of the city of Milan. The study area extends for 35.6 hectares, with an average altitude of 104.7 m a.s.l. This area includes 9 adjacent paddies in some of which the winter flooding has been practiced since 2004 and it has been gradually extended to the others. The data used for this study were collected from the end of September 2017 (before winter flooding) to the middle of March 2018 (before spring flooding). The EMI survey was carried out in September 2017, before winter flooding and after a few days of rain events in order to have optimal conditions for the survey, with soil water content near field capacity.

2.2 Traditional Soil Survey and Soil Map

An intensive soil survey was performed to describe the soil variability within the study area, starting from the regional soil map at scale 1:50.000 (ERSAF 2004). Soils were investigated by hand auger drilling till the depth of 120 cm; samples were taken from the surface horizon and from the main horizons recognized at two depth ranges, from 50 to 70 cm and from 90 to 110 cm. The texture was analyzed according to the national methods (Colombo and Miano 2015), to measure the apparent granulometry without destroying organic or iron cements. Particle-size classes from Soil Taxonomy families' definition rules (Soil Survey Staff 2014) were applied to all samples to map the soil variability at farm scale by defining site specific soil units. The soil map was constructed by taking into account the morphology of the area, and by clustering the soils according to the vertical sequence of different particle size classes

with respect to the sampling depths. Despite the overall flat position, the study area alternates relatively elevated surfaces, corresponding to ancient sandy river ridges, and lowlands, lowered of about ten meters. Repeated leveling and expansion of the fields progressively disguised this original pattern, with a remarkable movement of soil materials on surface. Because of this leveling trend, the original height differences among the fields were reduced to few meters, and the soil texture in the surface horizons were almost uniform all over the farm, while the differences in soils are mainly due to the granulometry of the deeper horizons.

2.3 EMI Survey and MZ Map

The EMI survey was carried out by using the multi-frequency sensor Profiler–EMP 400 (GSSI, USA). This instrument can acquire data for three different frequencies simultaneously, selected in the range 1–16 kHz, allowing the exploration of different soil depths with one survey. Moreover, with a distance between transmitting and receiving antennas equal to 1.21 m, the Depth of Exploration (DoE) varies from 1 m to several meters, depending on the frequency; for each frequency, DoE depends on the soil type as well. The sensor was used to collect data in the vertical dipole orientation mode, thus the EC values measured at 15 kHz were most sensitive to the soil properties at about 0.5 m of depth (McNeil 1990). The EC measurements acquired for each frequency of the EMI sensor were interpolated to obtain EC maps relative to different soil depths. The EC maps were combined through the Principal Component Analysis (PCA), to elaborate maps—i.e. maps of the Principal Components (PC maps)—describing both the horizontal soil variability for each DoE and the vertical soil variability along the soil profile. Finally, a Cluster Analysis (CA) was applied to the PC maps, to delineate MZs accounting for both the horizontal and the vertical soil variability. Particularly, the CA considered the PC maps representing most of the variability of the EC maps. CA was carried out with the Management Zone Analyst (MZA) software, implementing an unsupervised fuzzy classification method and determining the optimal number of MZs (Fridgen et al. 2004).

3 Results

3.1 Traditional Soil Survey and Soil Map

According to the Regional soil map 1:50.000, the study area includes three consoziations of soils, in which Haplustalfs prevail (Soil Survey Staff 2014). Typic, Ultic and Aquic are the most representative subgroups, while particle-size class ranges from coarse loamy—the more diffuse—to fine loamy, and surface horizons are characterised by sandy loam surface texture. All soils are developed in alluvial (from

medium to coarse) sandy, non calcareous materials (early Holocene). However, the study area is characterized by Anthraquic Haplustalfs coarse or fine loamy soils, due to a continuous rice cultivation. Starting from the variability representation provided by the Regional soil map, soils were investigated by hand auger drilling till the depth of 120 cm in 38 pits distributed within the area. Moreover, three soil profiles were opened and described, and texture, bulk density, reaction and organic carbon were measured for samples collected from their horizons. All the soils were deep (>100 cm) and characterized by the presence in sequence of Ap horizons (i.e. corresponding to A layer, the surface layer, from 0 to 40 cm), brown Bt horizons (i.e. corresponding to B layer, the intermediate layer, from 50 to 70 cm) with increasing clay content, passing gradually to the unweathered parent materials (i.e. corresponding to C layer, the deepest layer, from 90 to 110 cm). Data relative to the A, B and C layers are described in Table 1.

The samples collected from the horizons in A, B and C layers were classified according to the Soil Taxonomy particle-size rules. The sandy and loamy sand textural classes were combined in sandy class (S). The sandy loam, loam and sandy clay loam textural classes were distinguished in two classes: coarse loamy (CL) class, characterized by materials with clay content less than 18%, and fine loamy (FL), characterized by materials with clay content greater than 18%. Finally, each drilling pit was characterized by a sequence of classes assigned to the A, B and C layers. Six sequences were recognized, corresponding to four main types of soil in the area (Table 2): (1) the sequence CL/S/S describes Sandy (S) soils; (2) the sequences

Table 1 Texture of the three soil horizons within the study area

Layers	Depth (m)	Sand (%) (mean \pm dev)	Silt (%) (mean \pm dev)	Clay (%) (mean \pm dev)
Surface (A)	0–0.4	49.0–74.7 (62.2 \pm 5.6)	20.8–37.9 (28.3 \pm 4.2)	4.6–14.4 (9.5 \pm 2.1)
Intermediate (B)	0.5–0.7	29.1–81.0 (47.5 \pm 10.4)	11.0–48.5 (39.5 \pm 8.5)	4.6–24.6 (13.0 \pm 3.5)
Deeper (C)	0.9–1.1	20.1–95.1 (43.6 \pm 16.3)	3.0–54.7 (37.0 \pm 12.0)	1.9–25.6 (19.4 \pm 6.1)

Table 2 Clay and sand average contents (%) in layers A, B, C, for the different soil-types and map units

Soil types	Map units	No. points	Clay (%)			Sand (%)		
			A	B	C	A	B	C
CL/FL/FL	FL	2	58.1	46.8	38.9	11.5	19.1	58.1
CL/FL/CL	FL	2	59.2	43.2	69.1	10.4	19.4	59.2
CL/CL/FL	FL	13	61.5	56.7	50.3	9.4	12.8	61.5
CL/CL/CL	CL	16	62.9	60.3	57.7	9.5	12.0	62.9
CL/CL/S	DS	4	61.9	65.7	86.1	9.6	13.6	61.9
CL/S/S	S	1	61.9	65.7	86.1	9.6	13.6	5.1
CL/FL/FL + CL/FL/CL + CL/CL/FL	FL	17	60.8	54.0	51.2	9.8	14.3	19.5



Fig. 1 Soil map from the traditional soil survey

CL/FL/FL, CL/FL/CL, CL/CL/FL describes Fine Loamy (FL) soils, with an increment of clay in the subsurface layer; (3) the sequence CL/CL/CL describes Coarse Loamy (CL) soils, with no increment in clay content throughout the explored depth; (4) the sequence CL/CL/S describes Deep Sandy (DS) soils, with sandy horizons in the deeper layers and the highest clay content in the B layer. The soil map was prepared, considering four main soil-type units (Fig. 1): (1) S, covering a small area in the northern border of the farm; (2) FL, covering the western part of the farm, part of the central fields and a limited area in the eastern part of the farm, corresponding to the surfaces (around the alluvial mounds) with the highest elevation; (3) CL, interesting a great part of the lowermost fields; (4) DS, distributed in a narrow stripe probably attributable to a small watercourse now buried.

3.2 *EMI Survey and MZ Map*

The EC measurements were acquired along parallel lines 10 m apart, and two frequencies, namely 15 and 13 kHz, were used to explore two soil depths, about 1.5 m and about 2–3 m, respectively. The survey carried out in September 2017 did not cover two paddy fields (Fig. 2), due to the time constraints related to the winter flooding practice adopted in the farm. Consistent rains after winter flooding and before the summer flooding did not allow to complete the EMI survey to cover the entire study area.



Fig. 2 Homogeneous management zones map obtained by the PCA and CA. EC values characterizing each MZ are also reported

For each frequency, the EC data were interpolated to obtain the EC maps. In the surveyed farm area, EC varies between 0.3 and 18.0 mS m^{-1} , which is consistent with the EC values for soils from sandy to sandy loam. Even though the soil sampling depths were not greater than 1.5 m, PCA was applied to the EC maps relative to both 15 and 13 kHz frequencies, since in this case their spatial patterns were very similar. CA was applied to the PC map representing the 98% of the variability of both the EC maps. Finally, the MZ map (Fig. 2) was obtained, with the optimal number of four zones.

3.3 Comparison Between Soil Map and MZ Map

As a first step, a visual comparison between the soil map and the MZ map was carried out. The S unit was not considered for its very small extension within the farm area. The FL unit was generally associated with the MZs characterised by low EC values, despite the relatively low sand content and the relatively high clay content in the C layer (Table 2). Reasonably, mostly the upper horizons (characterised by low clay contents, as shown in Table 2) affected the EC measurements, just because of the low sand content in the A layer. The FL unit generally corresponded to the MZs 3 and 4, with the exception of the areas shown in Fig. 2 with red solid circles; in these areas, the observed soil depths were characterised by relatively high sand content

Table 3 ANOVA results for the sand contents in the A layer

Zones	No. points	Sand (%)		
		Min	Range	Mean \pm st. dev
MZs 1 + 2	9	52.28	65.33	59.13 \pm 4.78 ^a
MZs 3 + 4	11	58.51	74.68	65.99 \pm 5.64 ^a

^ap value for homoscedasticity of variance is 0.377 (Levene test)

($\geq 60\%$) in the A layer, and/or relatively high clay content ($>12\%$) in the B layer. In the areas shown with dashed red circles, the correspondence with MZ 2 rather than with MZ 3 is probably due to the fuzzy limits between the zones. The CL unit generally corresponded to the MZs 1 and 2, with the exception of the areas shown in Fig. 2 with purple circles, where the observed soil depths were characterised by high sand content (from 60 to 75%) in the A layer. The DS unit corresponded to the MZ 2, as expected (the clay content is maximum in the B layer at depths for which the sensitivity of EMI sensor is the highest). Anyway, the DS unit corresponded to MZ 4 in the areas shown in Fig. 2 with yellow circles; in these areas, the soil depths observed in some sampling points revealed a relatively high sand content ($>60\%$) in the A layer, with increasing values in the B layer. Finally, in most of the cases, the exceptions in the correspondence between soil map units and MZs were due to the properties of the EC measurements, which are average values throughout the explored soil depth. Moreover, the DoE depends on the type of soil, increasing with increasing sand contents in the surface layers. A statistical analysis of variance (ANOVA) was conducted to analyse the significant differences in the sand content of the A horizon among the different MZs. Two cases were analysed, considering MZ 1 together with MZ 2 (i.e. zone with high EC values), and MZ 3 with MZ 4 (i.e. zone with low EC values), in order to carry out a balanced ANOVA. The zones with high and low EC values were characterised by significantly ($p = 0.01$) different mean values of sand contents, respectively 59.13% and 65.99% (Table 3). The significant differences in sand contents explained the behaviour in the correspondence between soil map units and MZs; the same soil map unit, if including areas with sand contents in surface horizons lower and greater than 60%, might correspond to different MZs. As matter of fact, the EC values significantly decreased in MZs 3 and 4, where sand contents in surface horizons were greater than 60%, respect to the EC values in MZs 1 and 2 (sand contents in surface horizons mostly less than 60%).

4 Conclusions

MZ map derived from EC measurements acquired by EMI sensor and soil map obtained from the textural data acquired by a traditional soil survey showed similar spatial distributions of soil types. However, somewhere the same soil unit may correspond to different MZs. This behavior was principally due to the different soil

properties to which the two classification methods (for soil and MZ maps) are mainly sensitive, respectively clay and sand contents. Even though soils in different areas had similar distributions of clay contents throughout the soil depths (i.e. the soils belong to the same unit of the soil map), the EC values measured in those areas may be significantly different (i.e. the soils belong to different MZs), if the sand contents in the surface layer were significantly different. Indeed, in this case, the DoEs of the EMI sensor are different, hence the EC measurements (which are average values throughout the explored soil depths) may be different depending on the properties of the deeper soil depths. Moreover, the EMI survey provided a description of soil variability at field and farm scales more detailed than the traditional soil survey, due to the high number of EC measurement points. Indeed, the MZ map appeared somewhere fragmented, and this behavior induced somewhere differences between soil and MZ maps. Finally, this study stressed how the differences in the correspondence between MZs and soil units occurred somewhere do not depend on unreliable description of soil variability through EMI survey, but rather to the different DoEs depending on the local properties of the shallow soils. As a concluding remark, this work highlights how traditional soil surveys in at least a few sampling points within each MZ should always be carried out to better investigate the relationships between MZs and soil units.

Acknowledgements The activity presented is conducted in the context of the RISTEC project, co-funded by Regione Lombardia (Operation 1.2.01—EU-RDP 2014–2020).

References

- André, F., van Leeuwen, C., Saussez, S., van Durmen, R., Bogaert, P., Moghadas, et al. (2012). High-resolution imaging of a vineyard in south of France using ground-penetrating radar, electromagnetic induction and electrical resistivity tomography. *The Journal of Applied Geophysics*.
- Colombo, C., Miano, T. (2015) *Metodi di Analisi Chimica del Suolo*, 3rd version, Bari.
- Corwin, D. L., Lesch, S. M., Shouse, P. J., Sopper, R., & Ayars, J. E. (2003). Identifying soil properties that influence cotton yield using soil sampling directed by apparent soil electrical conductivity. *Agronomy Journal*, 95, 352.
- Doolittle, J. A., Indorante, S. J., Potter, D. K., Hefner, S. G., & McCauley, W. M. (2002). Comparing three geophysical tools for locating sand blows in alluvial soils of southeast Missouri. *Journal of Soil and Water Conservation*, 57, 175–182.
- Fortes, R., Millán, S., Prieto, M. H., & Campillo, C. (2015). A methodology based on apparent electrical conductivity and guided soil samples to improve irrigation zoning. *Precision Agriculture*, 16, 441–454.
- Fridgen, J. J., Kitchen, N. R., Sudduth, K. A., Drummond, S. T., Wiebold, W. J., & Fraisse, C. W. (2004). Management zone analyst (MZA): Software for subfield management zone delineation. *Agronomy Journal*, 96, 9.
- Hedley, C. B., Bradbury, S., Ekanayake, J., Yule, I. J., Carrick, S. (2010). Spatial irrigation scheduling for variable rate irrigation. In *Proceedings of the New Zealand Grassland Association* (vol. 72, pp. 97–102).

- Hedley, C. B., Roudier, P., Yule, I. J., Ekanayake, J., & Bradbury, S. (2013). Soil water status and water table depth modelling using electromagnetic surveys for precision irrigation scheduling. *Geoderma*, *199*, 22–29.
- McNeil, J. D. (1990). *Geonics EM38 ground conductivity meter: EM38 operating manual*. Ontario, Canada: Geonics Limited.
- Moral, F. J., Terrón, J. M., & Marques da Silva, J. R. (2010). Delineation of management zones using mobile measurements of soil apparent electrical conductivity and multivariate geostatistical techniques. *Soil and Tillage Research*, *106*, 335–343.
- Priori, S., Martini, E., Andrenelli, M. C., Magini, S., Agnelli, A. E., Bucelli, P., et al. (2013). Improving wine quality through harvest zoning and combined use of remote and soil proximal sensing. *Soil Science Society of America Journal*, *77*, 1338.
- Scudiero, E., Teatini, P., Corwin, D. L., Deiana, R., Berti, A., & Morari, F. (2013). Delineation of site-specific management units in a saline region at the Venice Lagoon margin, Italy, using soil reflectance and apparent electrical conductivity. *Computers and Electronics in Agriculture*, *99*, 54–64.
- Soil Survey Staff. (2014). *Key to soil taxonomy* (12th ed.).

Drought Variability and Trend Over the Lombardy Plain from Meteorological Station Records



C. Gandolfi, A. Facchi, A. Crespi, M. Rienzner and M. Maugeri

Abstract The spatial and temporal variability of droughts over the period 1951–2017 for a portion of Lombardy plain (Northern Italy) was reconstructed starting from a quality-checked and homogenized database of long precipitation and temperature station records covering the study region. The monthly meteorological series were interpolated over the period 1951–2017 onto a 30-arc second resolution grid covering the area by means of an anomaly-based procedure and the gridded fields were used to extract for each cell the series of two standardized drought indices: Standardized Precipitation Index (SPI) and Standardized Precipitation-Evapotranspiration Index (SPEI). SPI and SPEI trend analyses were performed on annual and seasonal scales at both regional and grid-point levels. Theil-Sen test on SPI values highlighted a significant drying tendency (Mann-Kendall p -value <0.05) for summer only (-0.14 decade $^{-1}$), while SPEI series exhibited a more negative summer trend (-0.22 decade $^{-1}$) and significant reductions also in spring and annual values (-0.14 and -0.17 decade $^{-1}$, respectively), suggesting an increase of evapotranspiration rates driven by higher temperature. Moreover, the trend analyses at grid cell level highlighted a greater negative and significant tendency for the western and southern part of the domain. Similar outcomes were obtained by assessing the temporal evolution of drought features over the decades in terms of frequency, duration and severity.

Keywords Drought · SPI · SPEI · Trend analysis · Observations

C. Gandolfi (✉) · A. Facchi · A. Crespi · M. Rienzner
Department of Agricultural and Environmental Sciences, Università degli Studi di Milano, via
Celoria 2, 20133 Milan, Italy
e-mail: claudio.gandolfi@unimi.it

M. Maugeri
Department of Environmental Science and Policy, Università degli Studi di Milano, via Celoria 2,
20133 Milan, Italy

© Springer Nature Switzerland AG 2020
A. Coppola et al. (eds.), *Innovative Biosystems Engineering for Sustainable Agriculture, Forestry and Food Production*, Lecture Notes in Civil Engineering 67,
https://doi.org/10.1007/978-3-030-39299-4_5

1 Introduction

Variations in hydrological regime are expected in the future at global scale driven by increasing temperature. Extreme events, in term of both intense precipitation and droughts, could become more frequent and severe with relevant negative impacts on ecosystems and on several human activities, such as agriculture (IPCC 2014, 2018). However, the distribution of climate change and impacts could be highly variable in space: in Europe for example wetting tendencies in the North and drier regimes in Mediterranean areas were depicted, especially for summer and spring (Spinoni et al. 2018). The temporal variability in hydrological regime is generally analyzed by means of standardized drought indicators, the most common ones are computed from meteorological records, such as precipitation and water deficits due to evapotranspiration (Tsakiris et al. 2007; Vicente-Serrano et al. 2014). In Italy, a general increase in drought events was pointed out for Central and Southern regions over recent decades by several studies, even though the observed trends are strongly influenced by the analyzed period and the surface heterogeneity (Buttafuoco et al. 2015; Vergni and Todisco 2011; Piccarreta et al. 2004). Drought characterization over Northern Italy, especially for the Po Plain and Pre-Alps, is less systematically discussed in scientific literature. However, an increasing drought occurrence was observed for the area, especially during the most recent decades (Stagge et al. 2017; Brunetti et al. 2009). Improving the available information about the variability of water resources in the Po plain could support water managements and adaptation strategies, especially for agricultural that highly relies on irrigation.

In this framework, the spatio-temporal trend and variability of droughts were investigated over a portion of Po Plain in Lombardy ($9^{\circ}12' - 10^{\circ}30'E$ and $45^{\circ}00' - 45^{\circ}45'N$) for the period 1951–2017. The monthly series of Standardized Precipitation Index (SPI) and of Standardized Precipitation-Evapotranspiration Index (SPEI) were reconstructed by using a dense database of checked and homogenized precipitation and temperature records covering the area. Trends in SPI and SPEI seasonal and annual records as well as in main drought features were evaluated at both regional and grid point scales over both the whole 1951–2017 interval and on shorter time windows.

2 Data and Methods

The study area is located in the middle of Northern Italy and covers about 8500 km² encompassing the central part of southern Lombardy and, to a lesser extent, the northern Emilia-Romagna ($9^{\circ}12' - 10^{\circ}30'E$ and $45^{\circ}00' - 45^{\circ}45'N$, Fig. 1). In particular, the domain includes the lower part of Adda river basin and it is largely characterized by a flat surface, with pre-Alpine reliefs occurring in the northernmost part only. In the area, intensive agriculture, mainly based on maize and pasture, is practiced by using an extensive irrigation network supplied by water from main rivers.

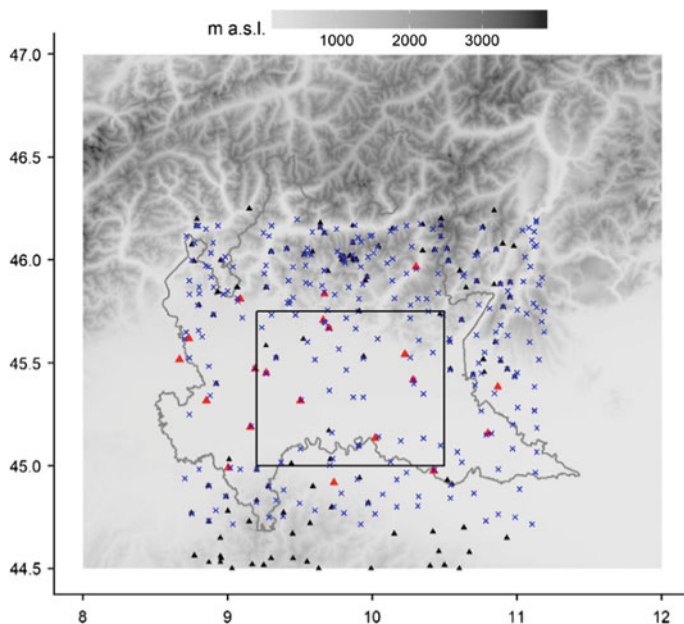


Fig. 1 Study domain (black box) and station distribution: blue crosses are precipitation sites, red triangles are temperature series and the blue triangles report the 1961–1990 monthly temperature normals added for climatology interpolation

42 monthly precipitation series and 13 monthly maximum and minimum temperature series were retrieved for the domain, or very close to it, spanning the period 1951–2017. In addition, in order to better represent the borders, the further available series for stations located within a larger box centered on the study area were included, reaching more than 100 sites for precipitation and 20 sites for temperature.

The series were retrieved from the regional services (ARPA Lombardia, ARPA Emilia-Romagna, ARPA Veneto, ARPA Piemonte), the archives of the former Italian Hydrographic Service and previous projects focusing on historical data collection and homogenization. Temperature series were checked for quality and homogeneity by means of the Craddock test (Craddock 1979) and homogenization was applied on 8 maximum and minimum temperature series, while precipitation records were not checked since they were derived from the database already analyzed by Crespi et al. (2018a) for assessing the hydrological cycle over the upper Adda basin.

The 1951–2017 monthly precipitation and mean temperature, as average of maximum and minimum values, records were interpolated onto a 30-arc second resolution Digital Elevation Model (DEM) covering the domain by means of the anomaly method (see, e.g., New et al. 2000; Isotta et al. 2014; Scapin et al. 2015). The gridded fields are obtained by superimposing a field of long-term means, i.e. 30-year climatologies, and the field of anomalies, i.e. the departures from the normals. The 1961–1990 precipitation and temperature normals were computed for all stations

after filling the monthly gaps in the 30-year period and for both variables they were interpolated by applying a local weighted linear regression versus elevation (Daly et al. 2002; Brunetti et al. 2014; Crespi et al. 2018b). In order to improve the data coverage for climatology interpolation, the temperature database was integrated with the 1961–1990 monthly normals of 125 sites located within the outer box and retrieved from the database used in Brunetti et al. (2014).

The station monthly anomalies, i.e. differences for temperature and ratios for precipitation from the normals, were gridded by means of the weighted averaging scheme described in Crespi et al. (2018b). The 1951–2017 monthly series in absolute values were finally computed by adding (multiplying) the gridded temperature (precipitation) anomalies to (times) the gridded climatologies.

1951–2017 SPI and SPEI series were computed both at cell level from the interpolated fields and at regional level as areal average of all points in the domain. The deficit series used to derive SPEI were computed as the difference between monthly precipitation and potential evapotranspiration (PET). PET was calculated by Thornthwaite's equation (Thornthwaite 1948) based on mean temperature only and, therefore, suitable for climatic reconstruction in the past when other meteorological observations are very few. Trends analyses were assessed by means of Theil-Sen and Mann-Kendall tests, hereafter referred as TS and MK respectively. The 1951–2017 regional SPI and SPEI series were computed by averaging the gridded precipitation and deficit series of all grid cells and on accumulation periods of 3 and 12 months (SPI-3, -12, SPEI-3, -12). Trend evaluation was performed at seasonal scale by considering SPI-3 and SPEI-3 values in February for winter, May for spring, August for summer and November for autumn and on annual scale by extracting SPI-12 and SPEI-12 values in December.

3 Results and Discussion

The TS test on SPI values highlighted a significant drying tendency (MK p-value < 0.05) for summer only ($-0.14 \text{ decade}^{-1}$), while SPEI series exhibited a more negative summer trend ($-0.22 \text{ decade}^{-1}$) and significant reductions also in spring and annual values (-0.14 and $-0.17 \text{ decade}^{-1}$, respectively), suggesting an increase of evapotranspiration rates driven by higher temperature since precipitation do not show relevant variations.

The trend assessment performed on SPI and SPEI values computed at grid cell level allow to show the spatial variability of the indices. Areas exhibiting significant seasonal trends were found out in summer for SPI and in summer and spring for SPEI (Fig. 2a, c, d). Trends are negative and significant over the whole domain for SPEI while SPI gridded series experience significant negative trends over half domain and with lower TS slopes. Both indices show the most drying tendency in the south and the western parts of domain where SPEI trends reach $-0.25 \text{ decade}^{-1}$. As shown in Fig. 2b, e, annual SPI and SPEI trends are negative over the whole region with significant values in the western and south-western domain, respectively, where the

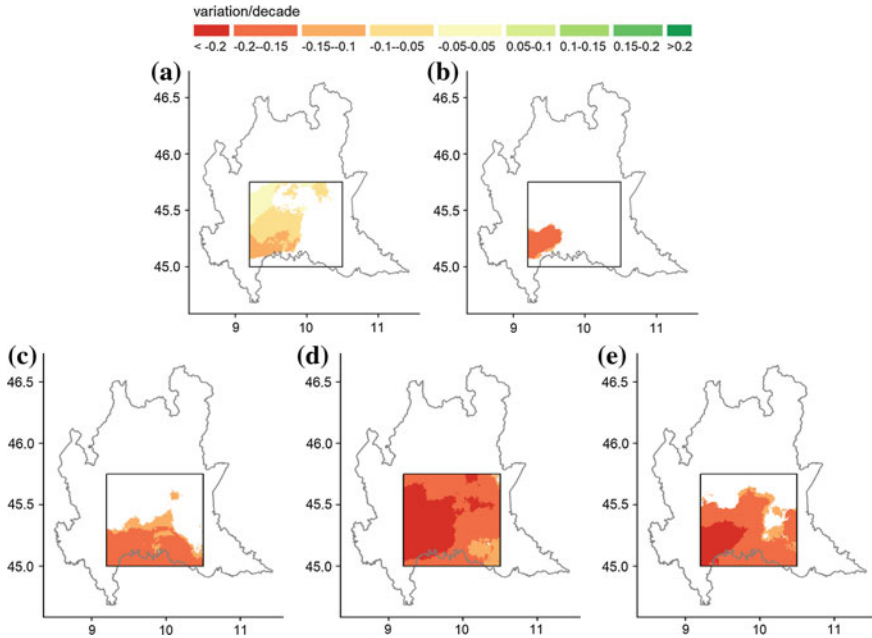


Fig. 2 Distribution of SPI (a, b) and SPEI (c, d, e) significant trends in a summer and b year for SPI and in c spring, d summer and e year for SPEI

decrease turned out to be lower than $-0.15 \text{ decade}^{-1}$ for both indices. This area is at the very center of the Po plain, where the flat terrain is surrounded by the Prealps in the North, the close Apennines in the South and the Mediterranean influence is lower so that higher temperature, and therefore higher PET, could be enhanced.

Specific drought features and their variability over subsequent decades were evaluated for each grid cell. In particular, the frequency of events (DF), the total severity (TSD) and total duration (TDD) were computed from monthly SPI and SPEI series for 1951–1960, 1961–1970, 1971–1980, 1981–1990, 1991–2000 and 2001–2010. Drought starts in the month experiencing index values below -1 and ends when it returns positive for at least two consecutive months (McKee et al. 1993). Drought duration corresponds to the number of months between the start and the end (not included) of each episode, while severity is the absolute value of the integral area under the index curve. DF, TSD and TDD are the sum of number, intensity and duration of drought events occurred over the considered period, respectively (Spinoni et al. 2014). For each grid cell, the spatio-temporal variability of the series of 6 decadal values for each drought feature was evaluated by applying a linear trend analysis and significance was computed by Student t-test with confidence level of 95%. For both indices, trends are positive for south-western and south-eastern areas and lower, or even slightly negative for SPI indicators, in the central part of the domain.

DF increases in the south-western part, while TDS and TDD show positive tendencies, especially for indicators extracted from SPEI, also in the south-eastern portion. Trends for SPI-3 indicators are not significant, except for very limited areas, while significance for all the indicators derived from SPEI is more evident and concerns the western and eastern areas, where TDD increases at a rate of more than 10 months per decade (Figs. 3 and 4). Since trend analyses are based on 6 points only, the outcomes are first indications of current tendencies and hot-spot area locations. Further analyses are needed to improve the drought characterization over the domain.

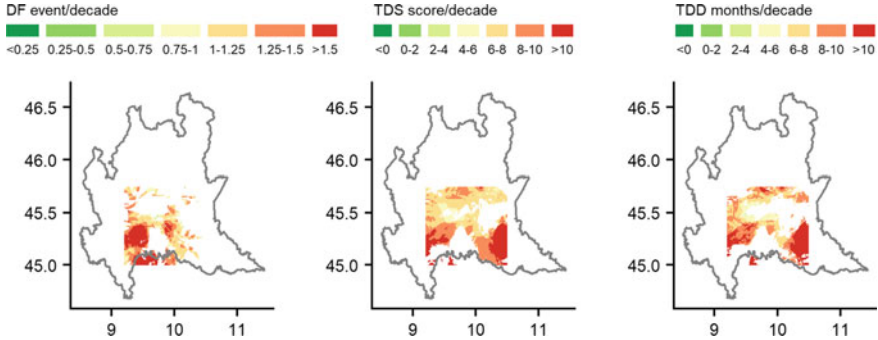


Fig. 3 Distribution of significant trends in decadal drought indicators (drought frequency DF, total drought severity TDS and total drought duration TDD) extracted from the monthly SPI series

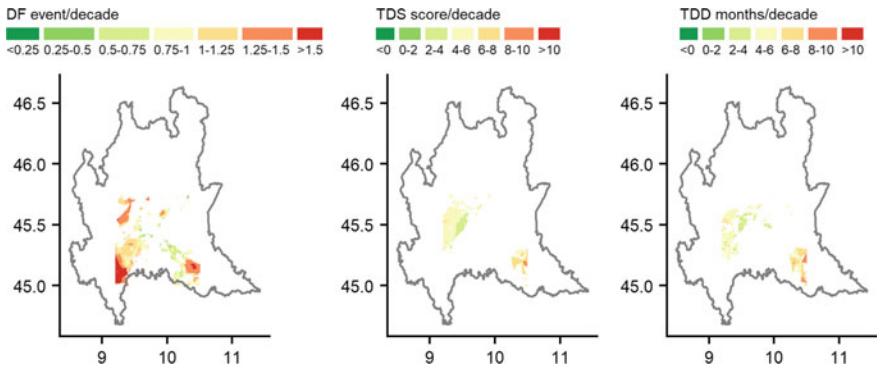


Fig. 4 Distribution of significant trends in decadal drought indicators (drought frequency DF, total drought severity TDS and total drought duration TDD) extracted from the monthly SPEI series

4 Conclusions

The spatio-temporal variability of the hydrological regime over a 67-year period in a portion of Po Plain (Northern Italy) was investigated by considering the meteorological drought indices SPI and SPEI. The 1951–2017 gridded datasets of mean monthly temperature and total precipitation were computed at 30-arc second resolution by means of an anomaly-based interpolation approach. PET was estimated by Thornthwaite equation and gridded deficit was also computed by subtracting PET field from total monthly precipitation values. SPI and SPEI were extracted over cumulated periods of 3 and 12 months at both cell level and regional scale and seasonal and annual trends were evaluated. Significant drying tendencies were found out in summer for SPI ($-0.14 \text{ decade}^{-1}$) and in spring, summer and year for SPEI (-0.14 , -0.22 and $-0.17 \text{ decade}^{-1}$, respectively). The more relevant SPEI signal suggests a greater role of evapotranspiration driven by higher temperatures. The trend analysis at grid cell indicated that the area mostly experiencing drying tendencies are located in the south-western part, especially for annual indices.

Drought indicators in terms of frequency, total severity and total duration were computed over subsequent 10-year intervals spanning the whole study period and trend analysis was performed. Except for very limited areas, no significance emerges for SPI-based indicators. Indicators computed from SPEI show more relevant tendencies with hot spots located in the south-western and south-eastern parts of the domain.

Further analyses are ongoing to better investigate the observed tendencies in drought indices and to identify the main drivers for the different zones; an extension of the study area is also foreseen in order to get a more comprehensive description of the hydrological cycle variability over Po Plain.

Acknowledgements The activity presented in the paper is part of the research grant “SO-WATCH—Soft path WATER management adaptation to CHanging climate”, funded by Fondazione CARIPO (www.fondazionecriplo.it).

References

- Brunetti, M., Lentini, G., Maugeri, M., Nanni, T., Auer, I., Böhm, R., et al. (2009). Climate variability and change in the Greater Alpine Region over the last two centuries based on multi-variable analysis. *International Journal of Climatology*, 29, 2197–2225. <https://doi.org/10.1002/joc.1857>.
- Brunetti, M., Maugeri, M., Nanni, T., Simolo, C., & Spinoni, J. (2014). High-resolution temperature climatology for Italy: Interpolation method intercomparison. *International Journal of Climatology*, 34(4), 1278–1296.
- Buttafuoco, G., Caloiero, T., & Coscarelli, R. (2015). Analyses of drought events in Calabria (Southern Italy) using standardized precipitation index. *Water Resources Management*, 29, 557–573. <https://doi.org/10.1007/s11269-014-0842-5>.
- Craddock, J. (1979). Methods of comparing annual rainfall records for climatic purposes. *Weather*, 34, 332–346. <https://doi.org/10.1002/j.1477-8696.1979.tb03465.x>.

- Crespi, A., Brunetti, M., Maugeri, M., Ranzi, R., & Tomirotti, M. (2018a). 1845–2016 gridded dataset of monthly precipitation over the upper Adda river basin: A comparison with runoff series. *Advances in Science and Research*, 15, 173–181. <https://doi.org/10.5194/asr-15-173-2018>.
- Crespi, A., Brunetti, M., Lentini, G., & Maugeri, M. (2018b). 1961–1990 high-resolution monthly precipitation climatologies for Italy. *International Journal of Climatology*, 38, 878–895. <https://doi.org/10.1002/joc.5217>.
- Daly, C., Gibson, W. P., Taylor, G. H., Johnson, G. L., & Pasteris, P. (2002). A knowledge-based approach to the statistical mapping of climate. *Climate Research*, 22, 99–113. <https://doi.org/10.3354/cr022099>.
- IPCC. (2014). In R. K. Pachauri, L. A. Meyer (Eds.), *Climate Change 2014: Synthesis Report. Contribution of Working Group II to the Fifth Assessment Report of the Intergovernmental Panel on Climate Change, Core Writing Team*. Geneva, Switzerland: IPCC, 151 pp.
- IPCC. (2018). Global Warming of 1.5 °C. In V. Masson-Delmotte, P. Zhai, H.-O. Pörtner, D. Roberts, J. Skea, P. R. Shukla, A. Pirani, W. Moufouma-Okia, C. Péan, R. Pidcock, S. Connors, J. B. R. Matthews, Y. Chen, X. Zhou, M. I. Gomis, E. Lonnoy, Maycock, M. Tignor & T. Waterfield (Eds.), *World meteorological organization*, Geneva, Switzerland.
- Isotta, F. A., Frei, C., Weigluni, V., Perčec Tadić, M., Lassègues, P., Rudolf, B., et al. (2014). The climate of daily precipitation in the Alps: development and analysis of a high-resolution grid dataset from pan-Alpine rain-gauge data. *International Journal of Climatology*, 34, 1657–1675. <https://doi.org/10.1002/joc.3794>.
- McKee, T. B., Doesken, N. J., & Kleist, J. (1993). The relationship of drought frequency and duration to time scales. In *Proceedings of the 8th Conference on Applied Climatology* (Vol. 17, pp. 179–183). Boston, MA: American Meteorological Society.
- New, M., Hulme, M., & Jones, P. (2000). Representing twentieth-century space-time climate variability. Part II: Development of 1901–96 monthly grids of terrestrial surface climate. *Journal of Climate*, 13, 2217–2238. [https://doi.org/10.1175/1520-0442\(2000\)013%3c2217:rtcstc%3e2.0.co;2](https://doi.org/10.1175/1520-0442(2000)013%3c2217:rtcstc%3e2.0.co;2).
- Piccarreta, M., Capolongo, D., & Boenzi, F. (2004). Trend analysis of precipitation and drought in Basilicata from 1923 to 2000 within a southern Italy context. *International Journal of Climatology*, 24, 907–922. <https://doi.org/10.1002/joc.1038>.
- Scapin, S., Apadula, F., Brunetti, M., & Maugeri, M. (2015). The sensitivity of present-time electricity demand on past climate change: a case study for Italy. *Earth Perspectives*, 4, 2194–6434. <https://doi.org/10.1186/s40322-015-0030-7>.
- Spinoni, J., Naumann, G., Carrao, H., Barbosa, P., & Vogt, J. (2014). World drought frequency, duration, and severity for 1951–2010. *International Journal of Climatology*, 34, 2792–2804. <https://doi.org/10.1002/joc.3875>.
- Spinoni, J., Vogt, J. V., Naumann, G., Barbosa, P., & Dosio, A. (2018). Will drought events become more frequent and severe in Europe? *International Journal of Climatology*, 38, 1718–1736. <https://doi.org/10.1002/joc.5291>.
- Stagge, J. H., Kingston, D. G., Tallaksen, L. M., & Hannah, D. M. (2017). Observed drought indices show increasing divergence across Europe. *Scientific Reports*, 7, 14045. <https://doi.org/10.1038/s41598-017-14283-2>.
- Thornthwaite, C. W. (1948). An approach toward a rational classification of climate. *Geographical Review*, 38(1), 55–94. <https://doi.org/10.2307/210739>.
- Tsakiris, G., Pangalou, D., & Vangelis, H. (2007). Regional drought assessment based on the reconnaissance drought index (RDI). *Water Resources Management*, 21, 821–833. <https://doi.org/10.1007/s11269-006-9105-4>.
- Vergni, L., & Todisco, F. (2011). Spatio-Temporal variability of precipitation, temperature and agricultural drought indices in central Italy. *Agricultural and Forest Meteorology*, 151, 301–313. <https://doi.org/10.1016/j.agrformet.2010.11.005>.

Vicente-Serrano, S. M., Lopez-Moreno, J. I., Beguería, S., Lorenzo-Lacruz, J., Sanchez-Lorenzo, A., García-Ruiz, J. M., et al. (2014). Evidence of increasing drought severity caused by temperature rise in southern Europe. *Environmental Research Letters*, 9, 044001. <https://doi.org/10.1088/1748-9326/9/4/044001>.

Biodegradable Geosynthetics for Geotechnical and Geo-Environmental Engineering



Alessio Cislaghi, Paolo Sala, Gigliola Borgonovo, Claudio Gandolfi and Gian Battista Bischetti

Abstract Among the commonly used plastic materials in geotechnical engineering, the most significant fraction consists in the geosynthetics. The use of these products involves environmental risks associated with their degradation. Hence, a strong interest in biodegradable polymers of natural origin has been increasing, for finding alternative materials with adequate mechanical properties for geotechnical and geo-environmental applications. The main aim of this study is to test a bio-based, biodegradable and eco-compatible polymer, able to replace polypropylene and other synthetic materials in the production of geosynthetics. For this purpose, Poly(lactic acid) or PLA, one of the most common bioplastic polymer material commonly used as filament for 3D printers, was investigated. The chemical structure of PLA was determined by ^1H NMR and the optical purity determination by polarimetry. PLA filament was used to print samples of uniaxial and biaxial geogrid at 1:5 scale using a professional 3D printer. Subsequently, tensile tests were performed on the filament and on prototype geogrids. Tensile tests measured a maximum tensile resistance of 51.96 MPa for the filament and 12.96 kN/m for uniaxial geogrid prototypes. The mechanical properties of PLA were found to be comparable to petroleum derivatives. These results are encouraging and can support the utilization of PLA for innovative biodegradable geosynthetics production, which could represent an alternative to non-biodegradable products, particularly when used in combination with live plants. In view of practical applications, however, research is still needed to determine the degradation of their mechanical properties over time.

A. Cislaghi (✉) · P. Sala · C. Gandolfi · G. B. Bischetti
Department of Agricultural and Environmental Sciences, University of Milan, Via Celoria 2,
20133 Milan, Italy
e-mail: alessio.cislaghi@unimi.it

A. Cislaghi · G. B. Bischetti
Centre of Applied Studies for the Sustainable Management and Protection of Mountain Areas
(Ge.S.Di.Mont.), University of Milan, Via Morino 8, 25048 Edolo (Brescia), Italy

G. Borgonovo
Department of Food, Environmental and Nutritional Sciences, University of Milan, Via Celoria 2,
20133 Milan, Italy

© Springer Nature Switzerland AG 2020

A. Coppola et al. (eds.), *Innovative Biosystems Engineering for Sustainable Agriculture, Forestry and Food Production*, Lecture Notes in Civil Engineering 67,
https://doi.org/10.1007/978-3-030-39299-4_6

Keywords Geosynthetics · Biopolymer · PLA · Geogrid · Tensile strength

1 Introduction

Plastics are among the most common materials in Construction and Demolition sector (CaD), one of the most challenging in reaching the ambitious objectives proposed by the European Commission's Waste Framework Directive 2008/98/EC in terms of recycling and eco-compatibility (EC 2015, 2018). Among the plastics used in CaD sector, a significant amount is composed by geosynthetics. Geosynthetics are polymeric products, such as geotextiles, geogrids, geonets etc., used in contact with soil and/or rock and mainly applied in civil and environmental engineering (Wiewel and Lamoree 2016). The global market of geosynthetics is approximately of 6,125 million square meters per year, for 5.76 USD Billion value and still growing (Müller and Saathoff 2015). Most of geosynthetics are fabricated from petroleum-based polymers such as the polyolefin and polyester family. Polypropylene covers almost the whole total production (~90%), whereas polyethylene accounts for the remaining part (Wiewel and Lamoree 2016). Surely, petroleum-based polymers are high performing in terms of mechanical resistance and durability, but the exposure to common environmental conditions over time could lead to micro-plastics particles (below 5 mm) releasing and leaching of eco-toxic compounds (Browne et al. 2007). The increase of environmental consciousness has led to an increasing interest in using natural and biodegradable products, such as the biopolymers, to replace the synthetic materials. The recent research highlighted how biopolymers can provide a good and cost-effective alternative to the conventional materials in several engineering applications, such as the construction of temporary roads, the basal reinforcement of embankments or the control of surface erosion (Maneecharoen et al. 2013). Until now, a wide variety of biodegradable composites reinforced with natural fiber composites (bamboo, banana, hemp, etc.) has been proposed and tested with encouraging results (Pickering et al. 2016); blending with polymeric matrix was also shown to be a viable option (Farrington et al. 2005). Among the available biodegradable biopolymers, poly(lactic acid) or polylactide (PLA) is one of the most common. PLA is a thermoplastic, high-strength, high-modulus biopolymer that can be easily processed to fabricate a wide range of products. PLA has already been investigated/used for several applications such as food technology, medical engineering, pharmaceutical, packaging and agriculture (Garlotta 2001), whereas very few are the studies focusing on geocomposites production (Bhatraju and Kumar 2018). Producing geosynthetics with PLA and/or PLA-based composites can potentially ensure several advantages in terms of sustainability and eco-compatibility. In fact, PLA is (i) prepared from renewable agriculture-based feedstock, which are fermented into lactic acid; (ii) recyclable and compostable (Drumright et al. 2000); and (iii) slowly degradable (Rasal et al. 2010) into non-toxic substances, as water, carbon dioxide and humus (Tuominen et al. 2002). The aim of this work is to investigate the chance to produce geosynthetics for geotechnical applications with PLA, in view of its high sustainability and

favorable mechanical properties. Moreover, PLA is easily available on the market and suitable for prototypes construction. Specific objectives are to investigate the chemical and mechanical characteristics of PLA and to test the tensile behavior of small-scaled model geogrids produced through a 3D printing process.

2 Materials and Methods

2.1 Selection of Biopolymer

An accurate analysis of the wide spectrum of biodegradable and non-toxic materials already available on the global market and, in particular, of those commercialized as consumables for 3D printers was conducted. The research focused on those biopolymers characterized by elevate mechanical properties, comparable with petroleum derivatives. Neat PLA was selected for the present study because it is surely the most diffuse biopolymer in the field of 3D printing and shows also an ultimate tensile strength (TS) variable between 25 and 70 MPa and an average Young's modulus of 3500 MPa (Muller et al. 2017). PLA is readily available on the market as cheap filament with standard diameter of 1.75 mm or 2.85 mm, suitable for 3D printers.

2.2 Physical, Mechanical and Chemical Characterization of Biopolymer

Neat PLA filament (Orbi-Tech®, Germany) was selected and characterized in detail, besides the physical properties provided in the producer's technical sheet, such as a glass transition temperature of 50 °C, a melting temperature of 210 °C and a Young's modulus of 3310 MPa.

Chemical structure of PLA samples was obtained through optical purity analysis and ¹H-NMR spectroscopy. Such procedure verified the chemical purity of the lactic acid monomer, the presence of carboxylic acid impurities that could retard the polymerisation of lactic acid and could affect the other properties. Specific optical rotation ($[\alpha]_D$) was registered with a JASCO P-2000 polarimeter, at 25 °C with a wavelength of 589 nm. PLA samples were solubilized in chloroform (CHCl₃) at a concentration of 1.00 g/dL. Equation 1 defines the percentage of optical purity (OP):

$$OP(\%) = \frac{[\alpha]_{589}^{25}}{-156} \cdot 100 \quad (1)$$

where $[\alpha]$ is the specific rotation observed and -156 is the specific rotation for L-lactic acid enantiomerically pure PLA, at a concentration of 1 g/dL at 25 °C (Marques et al. 2012). ¹H NMR spectra were recorded at 25 °C with a Bruker AV

600 spectrometer at 600 MHz. Samples were prepared solubilizing PLA in CDCl_3 in a range of concentration of 1–10 mg/mL.

Mechanical tests were conducted through a Universal Testing Machine (MTS tensile test machine) mounting TH240 g universal clamps (with a distance between the jaws of 10 cm) that avoided sample damage at the clamping points (ASTM D638). Tensile force was exerted by a system of gears at a rate of 10 mm/min and it was measured as a function of the strain by a load cell (F.S. = 5000 N). The tensile force (N) at the point of rupture was taken as the peak load, and the related stress (MPa) was calculated by dividing the breaking force by the cross-sectional area of the filament (mm^2). For model geogrids, the stress (kN/m) was calculated by dividing the breaking force by the sample's width.

2.3 Prototype Samples Building and Testing

A common approach adopted in geotechnical research is based on model test results. However, due to the cost and difficulties associated with model preparation, full-scale model tests/studies are rare compared to small-scale tests. 3D printing has become a revolutionary technology that has also been adopted in geotechnical research. For instance, Stathas et al. (2017) proposed and successfully fabricated standard prototypes of model geogrids at a scale of 1:10 through a 3D printing process for the centrifuge model testing under 1-g and 10-g condition.

According to the technical specifications of the geotechnical literature (e.g., Springman et al. 1992; Viswanadham and König 2004) the tensile strength of model geogrids used in 1:N reinforced-soil models must be $1/N^2$ of that of full-scale geogrids when the test is carried out under 1-g condition, or n/N^2 of that of prototype (geogrids) under n-g condition in centrifuge tests. Note that N represents the scale of a reduced model (e.g., 1:10), and n is the level of gravity (e.g., 10-g) to which the model is subjected (usually n is set equal to N).

For this study two different model geogrids, uniaxial and biaxial, were designed and tested on a scale of 1:5 so that they could be used to investigate the behavior of geosynthetics-reinforced soil structures in 5-g centrifuge models. The design adopted for the geogrids was obtained modifying the scale of the design adopted by Stathas et al. (2017) from 1:10 to 1:5. The prototypes were produced with a Sharebot NG 2 printer using the Fused Filament Fabrication, a common 3D printing process for thermoplastic materials that uses a continuous filament (as shown in Fig. 1). The dimensions of the prototype samples were 50 mm width \times 150 mm length, and 1 mm thick. Tensile tests were carried out on the raw filaments characterized by 1.75 and 2.85 mm diameter and on the 3D printed geogrids samples.

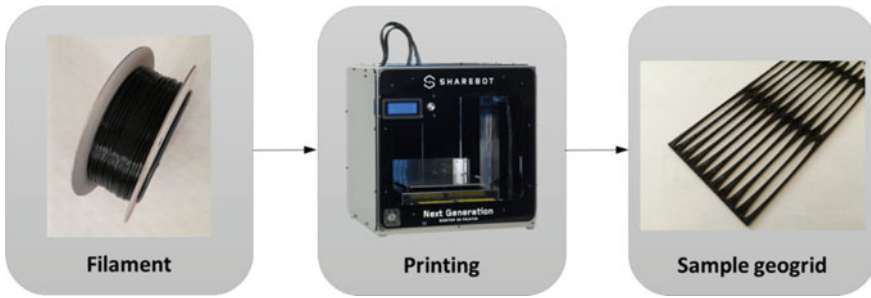


Fig. 1 3D printing process of model geogrids from filament to sample geogrid

3 Results

3.1 Chemical and Mechanical Characterization of Biopolymers

In terms of chemical properties, PLA samples showed an average $[\alpha]_D$ value of $-128.70 \pm 1.40^\circ$ and an OP of $81.96 \pm 0.52\%$. The data obtained, compared with the literature (Marques et al. 2012), showed how the PLA sample was mainly composed by the L-lactic acid enantiomer with a not substantial amount of impurities.

PLA structure was confirmed by the NMR analysis. In the protonic spectrum a quartet and a doublet were observed at 5.15 and 1.57 ppm. Those signals are typical of the CH and CH₃ groups of the polymeric chain. In the spectrum, were also visible a weak quartet at 4.35 ppm (compatible with the terminal CH) and weak high-field peaks.

From the mechanical point of view, the observations during the tensile tests exhibited the common characteristics of the stress-strain curve of plastic materials as shown in Fig. 2. These features can be identified as three principal stages:

- The linear elastic region, where the stress is proportional to the strain and the material undergoes only elastic deformation. The end of the stage is the initiation

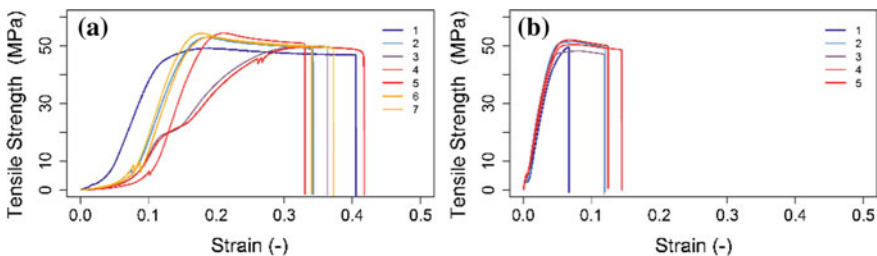


Fig. 2 a Stress-strain curve of the seven tests (1, 2, ...7) conducted on 1.75 mm PLA filaments; b stress-strain curve of the five tests (1, 2, ...5) conducted on 2.85 mm PLA filaments

point of plastic deformation. The stress component of this point is defined yield strength.

- The strain hardening region, which starts as the strain goes beyond yielding point, and ends at the ultimate strength point that is the maximal tensile stress shown in the stress-strain curve (that corresponds to the maximum tensile strength, TS).
- The necking region, where the local cross-sectional area becomes significantly smaller than the average. During this stage irreversible plastic deformation of the material occurs.

Mechanical characterization of PLA shows how the 1.75 mm filament has a peak tensile load of 124.99 ± 5.72 N, corresponding to TS of 51.96 ± 2.38 MPa. Tests conducted on 2.85 mm filament highlighted a peak tensile load of 303.99 ± 31.38 N, TS of 47.65 ± 4.92 MPa and a shorter plastic deformation phase, compared with 1.75 mm filament (Fig. 2b).

3.2 Prototype Samples Building and Testing

Mechanical tests conducted on the uniaxial geogrid prototypes gave a maximum tensile load of 681.54 ± 163.67 N and a TS of 12.66 ± 3.20 kN/m. Figure 3 shows all the tests and highlights the different shapes of the stress-strain curves. The variability in the trends of the curves could be due to the 3D printing process that produced prototypes with microscopic imperfections within a tolerance margin depending on the printer and caused by a possible variation of the extrusion temperature.

Biaxial prototype geogrids showed an average peak load of 192.92 ± 72.76 N. Consequently, a lower ultimate tensile strength was obtained (3.79 ± 178 kN/m).

A certain variability was still recorded between the stress-strain curves. In particular, tests [1] and [2] showed a long plastic deformation phase, while its nearly absent in the other cases (Fig. 3b). As expected, if tested in machine direction, uniaxial prototype geogrids exhibited a higher tensile strength than the biaxial samples that,

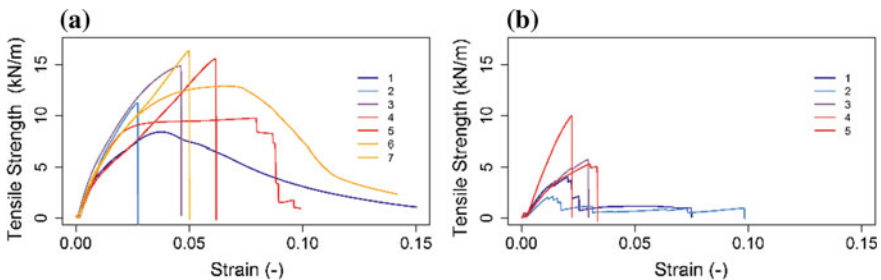


Fig. 3 **a** stress-strain curve of the seven tests (1, 2, ...7) conducted on uniaxial prototype geogrid **b** stress-strain curve of the five tests (1, 2, ...5) conducted on biaxial prototype geogrid

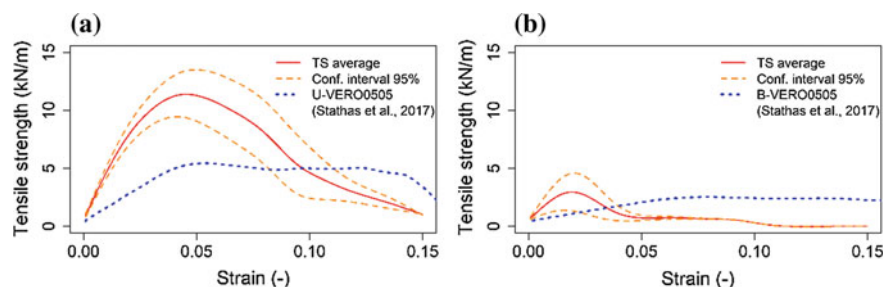


Fig. 4 Comparison between uniaxial **(a)** and biaxial **(b)** model geogrid with literature (Stathas et al. 2017) at 1:5 scale

conversely, provided a more uniform tensile in two orthogonal directions instead of a single one.

The obtained results were compared with those measured in the work of Stathas et al. (2017), once converted to 1:5 scale. The comparison highlighted that the uniaxial prototype geogrids of neat PLA pointed out a greater tensile resistance (12.66 kN/m) respect than the same ones produced with Verowhiteplus, a photopolymerising resin composed of acrylic compounds, as shown in Fig. 4a, despite the greater tensile strength (58 MPa) of the raw material compared with PLA. PLA-based biaxial geogrid resulted slightly more resistant than Verowhiteplus-based (Fig. 4b), with a tensile strength of 3.79 kN/m versus 2.4 kN/m. However, despite the lower tensile strength, acrylic resin resulted to be more elastic than PLA in both uni- and bi-axial prototypes.

4 Discussion and Conclusions

In the present study, the chemical and mechanical properties of PLA, a biodegradable biopolymer, were investigated in view of its use for geosynthetics production, as an alternative to petroleum-based polymers. PLA emerged as the best candidate for this application among the variety of biodegradable materials available on the market and already largely used in other fields, such as packaging, that we analysed prior to the study. The chemical and mechanical characterization showed that sample PLA is composed of approximately 82% L-lactic acid and has a tensile strength of 51.96 ± 2.38 MPa in form of 1.75 mm filament and 47.65 ± 4.92 MPa in form of 2.85 mm filament.

The production of small-scaled standard geogrid through a 3D printer allowed a robust comparison with other produced with different materials. In particular, PLA-made uniaxial geogrids resulted to be approximately 50% more resistant than Verowhiteplus ones at the same scale. The PLA biaxial geogrid performance, even if higher than the models realized by Stathas et al. (2017), showed a high variability, probably due to the difficulty to reproduce this specific geometry during the 3D

printing process. Despite the higher tensile strength, PLA prototypes resulted to be less elastic than those produced with the acrylic resin that present an elongation at break up to 25%.

Finally, the biodegradable PLA or PLA-based polymers could be reliable and robust materials for the use in the field of civil, geotechnical and bioengineering. Further investigations on their mechanical degradation under different field conditions (water, soil, rooted-soil, etc.) and estimation of durability, will allow to establish if these materials may actually represent an alternative to the petroleum-based products that cause serious impacts on the environment. Clearly, there is still a gap in terms of tensile strength between biopolymer-made and petroleum-based geosynthetics, but their use in combination with live plants—where the root system development initially supports and then gradually substitutes the biodegradable products in soil reinforcement—represents a promising research field.

References

- Bhatraju, N. S., & Kumar, K. K. (2018). To learn on construction of pavement by using geotextile. *International Journal of Innovative Technology and Research*, 6, 7867–7869.
- Browne, M. A., Galloway, T., & Thompson, R. (2007). Microplastic—an emerging contaminant of potential concern? Learned discourses. *Integrated Environmental Assessment and Management*, 3, 559–561. <https://doi.org/10.1002/ieam.5630030412>.
- Drumright, R. E., Gruber, P. R., & Henton, D. E. (2000). Polylactic acid technology. *Advanced Materials*, 12, 1841–1846.
- European Commission. (2015). Communication from the Commission to the European Parliament, the Council, the European Economic and Social Committee and the Committee of the Regions, Closing the loop—An EU action plan for the Circular Economy. COM(2015) 614 final.
- European Commission. (2018). Communication from the Commission to the European Parliament, the Council, the European Economic and Social Committee and the Committee of the Regions, A European Strategy for Plastics in a Circular Economy. COM (2018) 28 final.
- Farrington, D. W., Davies, J. L. S., & Blackburn, R.S. (2005). Poly(lactic acid) fibers. In: *Biodegradable and sustainable fibres* (pp. 191–220). Elsevier Science Publishers, Elsevier.
- Garlotta, D. (2001). A literature review of poly(lactic acid). *Journal of Polymers and the Environment*, 9, 63–84.
- Manecharoen, J., Htwe, W., Bergado, D. T., & Baral, P. (2013). Ecological erosion control by Limited Life Geotextiles (LLGs) as well as with vetiver and ruzi grasses. *Indian Geotechnical Journal*, 43, 388–406. <https://doi.org/10.1007/s40098-013-0061-7>.
- Marques, D. S., Gil, M. H., & Baptista, C. M. S. G. (2012). Bulk polytransesterification of L-Lactic acid esters: an alternative route to synthesize poly(lactic acid). *Journal of Applied Polymer Science*, 125, E283–E289.
- Muller, J., González-Martínez, C., & Chiralt, A. (2017). Combination of poly(lactic acid) and starch for biodegradable food packaging. *Materials*, 10, 952. <https://doi.org/10.3390/ma10080952>.
- Müller, W. W., & Saathoff, F. (2015). Geosynthetics in geoenvironmental engineering. *Science and Technology of Advanced Materials*, 16, 034605. <https://doi.org/10.1088/1468-6996/16/3/034605>.
- Pickering, K. L., Aruan Efendy, M. G., & Le, T. M. (2016). A review of recent developments in natural fibre composites and their mechanical performance. *Composites Part A Applied Science and Manufacturing*, 83, 98–112. <https://doi.org/10.1016/j.compositesa.2015.08.038>.
- Rasal, R. M., Janorkar, A. V., & Hirt, D. E. (2010). Poly(lactic acid) modifications. *Progress in Polymer Science*, 35, 338–356. <https://doi.org/10.1016/j.proppolymsci.2009.12.003>.

- Springman, S. M., Bolton, M., Sharma, J., & Balachandran, S. (1992). Modelling and instrumentation of a geotextile in the geotechnical centrifuge. In: H. Ochiai, S. Hayashi, & J. Otani (Eds.), *Proceedings of International Symposium on Earth Reinforcement Practice* (pp. 167–172). Kyushu, Rotterdam: Balkema.
- Stathas, D., Wang, J. P., & Ling, H. I. (2017). Model geogrids and 3D printing. *Geotextiles and Geomembranes*, 45, 688–696. <https://doi.org/10.1016/j.geotextmem.2017.07.006>.
- Tuominen, J., Kylmä, J., Kapanen, A., Venelampi, O., Itävaara, M., & Seppälä, J. (2002). Biodegradation of lactic acid based polymers under controlled composting conditions and evaluation of the ecotoxicological impact. *Biomacromolecules*, 3, 445–455. <https://doi.org/10.1021/bm0101522>.
- Viswanadham, B. V. S., & König, D. (2004). Studies on scaling and instrumentation of a geogrid. *Geotextiles and Geomembranes*, 22(5), 307–328.
- Wiewel, B. V., & Lamoree, M. (2016). Geotextile composition, application and ecotoxicology: a review. *Journal of Hazardous Materials*, 317, 640–655. <https://doi.org/10.1016/j.jhazmat.2016.04.060>.

Comparison of Different Methods for Topographic Survey of Rural Canals



Daniele Masseroni, Daniele Passoni, Alessandro Castagna, Luca Civelli, Livio Pinto and Claudio Gandolfi

Abstract The topographic survey of rural canal network is a crucial task to allow a sustainable irrigation management and planning in rural areas and, always more frequently, to control the interactions with urban areas (flood protection, in particular). However, to date, datasets of canal and ditch geomorphological characteristics, such as layout, cross-sections, slopes and canal bed characteristics, are almost completely absent, or unreliable. This work tests the use of four different data sources—two from remote sensing and two from ground survey—for detecting the geometrical characteristics of rural canals at increasingly high resolution, providing cross sections and slopes over a pilot study domain of about two hectares located in south Milan (Italy). Specifically, rural canal geometries were obtained from the processing of data from (i) a Lidar and a photogrammetric flight at different altitude (ii) a ground-fixed laser scanner and (iii) a GPS spot acquisition to complete surveys with a further level of detail. 3D models of the rural canals were obtained from the processing of the data of each of the three sources. Results of the comparison of the models are presented, focusing on canal cross sections, slope, and bed characteristics; moreover, the impact of these differences on the flow and storage capacity of the channels will be discussed and, finally, an assessment of the costs of data acquisition and processing is provided.

Keywords High resolution topography · Rural canals · Agrarian landscape · 3D surface models

D. Masseroni (✉) · A. Castagna · L. Civelli · C. Gandolfi
Department of Agricultural and Environmental Sciences, Università degli Studi di Milano, Via
Celoria 2, 20133 Milan, Italy
e-mail: daniele.masseroni@unimi.it

D. Passoni · L. Pinto
Department Civil and Environmental Engineering, Politecnico of Milan, P.zza Leonardo da Vinci
32, 20133 Milan, Italy

© Springer Nature Switzerland AG 2020

A. Coppola et al. (eds.), *Innovative Biosystems Engineering for Sustainable Agriculture, Forestry and Food Production*, Lecture Notes in Civil Engineering 67,
https://doi.org/10.1007/978-3-030-39299-4_7

1 Introduction

In Northern Italy, the rural canal network consists generally of open mains, sub-mains, and lateral ditches, located both on the field boundaries but also within the plots. The whole network is subdivided into different irrigation and drainage districts, each managed and monitored mainly by irrigation and land reclamation consortiums, either of public or private interest. Each of them has the responsibility to control, maintain and modernize the rural canal network, mainly to guarantee the satisfaction of crop water needs and the hydraulic safety of the territory from flooding. A proper planning of actions and decisions, especially for complex rural canal systems, relies on a correct network characterization, starting from information about network topology and geometry (Cazorzi et al. 2013).

Concerning the network topology, if one does not consider field surveys, the only available source is the official cartography (Regional Technical Maps (RTM)—1:5000 scale). The provided information refers to the time when the map was produced. In Italy, the updating of the RTM is supposed to be done approximately every 10–15 years, but no specific regulation exists: each regional government makes its own rules and specifications. It is therefore clear that users, when working with the RTM, must cope with the uncertainty deriving from information, that may not account for all the changes the rural canal network has been subjected to (Tarolli et al. 2009).

When dealing with the geometric characterization of the network, canal geometries can vary widely from the diversion points to the individual plots, and no information about canal widths, cross sections and slopes are generally available, unless they are derived with large investments in field surveys (Lagacherie et al. 2004).

Recent advances in data collection technology, such as airborne and terrestrial laser scanning, enabled rapid acquisition of topographic information (Ackermann 1999; Kraus and Pfeifer 2001; Slatton et al. 2007; Tarolli et al. 2009). Digital Surface Models (DSM) can be derived from this kind of topographic surveys, with a better level of resolution passing from in-flight to ground mode of detection (Bailly et al. 2008). In particular, LiDAR data, which cover large areas of Italian regions, are nowadays readily available (see “<http://www.pcn.minambiente.it/mattm/servizio-di-scaricamento-wfs/>”) for public authorities responsible for land management for the development of methods and actions aimed at solving geomorphological and hydrological problems (Passalacqua et al. 2010; Pirotti and Tarolli 2010; Sofia et al. 2011). However, these data currently have at most 1 m of resolution and they could be unsuitable for detecting accurately the geomorphological characteristics of rural canal network down to the plot level.

Therefore, if on the one hand the application of LiDAR or photogrammetric flights could be good candidates for a fast large-scale detection of rural canal features, on the other hand they could be unsuitable to characterize canal geometries with an adequate level of accuracy (especially when small ditches and vegetated canals are considered). Conversely, field surveys for large areas (about km²) are cost-prohibitive and time-consuming (Zhang et al. 2018).

In light of these considerations, it becomes essential to compare canal geometries (i.e. cross-sections and slopes) obtained by different types of topographic surveys, in order to evaluate the precision of each survey technique and its reliability in providing rural canal geometries in a large-scale prospective.

In this research, cross sections and slopes of rural canals obtained by LiDAR data were compared with those obtained by aerial images provided by an unmanned aerial vehicle (drone) and by ground-based measurements (respectively carried out through a terrestrial laser scanner and GPS). DSMs of different portions of two rural canals belonging to a typical Northern Italy agrarian landscape were extracted from the results of topographic surveys. Rural canal characteristics were derived from DSM raster maps with different levels of resolution, while accuracy in geometries was assessed from a combination of metrics which compare aerial and ground-based cross-section and slope patterns. A rough estimation of costs of each topographic data acquisition was also presented to understand the sustainability and scalability of the different survey solutions.

2 Area Test and Data Capture

The pilot study area is characterized by four unlined ditches located in a rural area in the southern part of Milan (between Parco Agricolo Sud Milano and Parco del Ticino) (Fig. 1). They have the typical geometrical features of Northern Italy rural canal network and are mainly intended to supply water for irrigation, as well as to drain the water excesses from the surrounding fields.

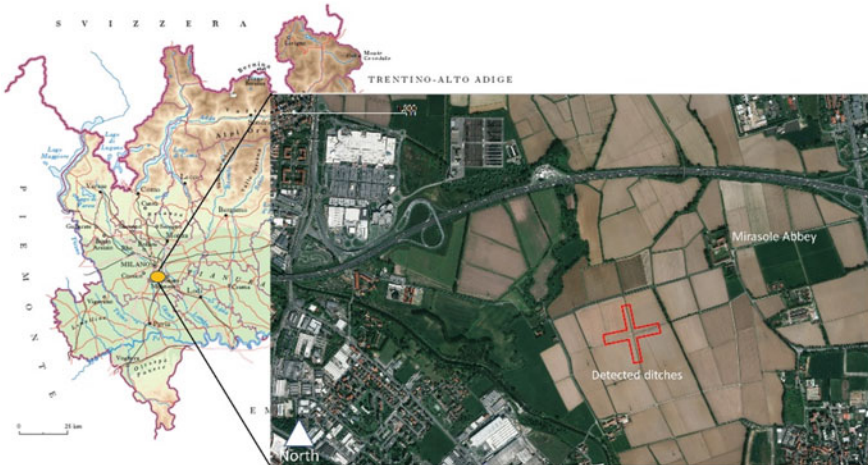


Fig. 1 Location of area test

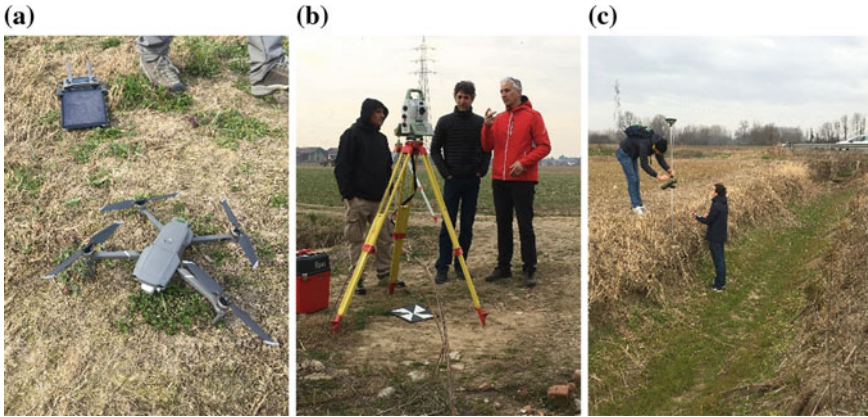


Fig. 2 a drone; b ground-fixed laser scanner; c GPS data acquisitions

Concerning the data acquisition, the density of survey points obtained by LiDAR is about 1.5 points per square meter (i.e. about 1 m of ground resolution). The DSM elevation presents an accuracy of ± 1 s (standard deviation), corresponding to an error lower than ± 15 cm, while the planimetric accuracy is 2 s i.e. within ± 30 cm. Subsequently, LiDAR data were compared with those obtained by a photogrammetric flight carried out at 30 m altitude through a DJI Mavic 2 Pro unmanned aerial vehicle (UAV) equipped with 20 megapixel camera with ground resolution of about 1 cm and vertical error of about 5 cm and a ground-fixed Leica Nova MS60 MultiStation with a ground resolution about 1×1 mm and vertical error of about 2 mm. Moreover, GPS spot acquisitions carried out by a GPS GNSS Leica GS14 with horizontal and vertical resolution of about 1.5 cm and 2 cm, allowed to complete surveys with a further level of detail (see Fig. 2a–c, respectively for UAV, ground station and ground GPS).

The topographic surveys were carried out at the end of February when the water in the canals is not yet present. Concerning drone acquisitions, the vehicle is characterized by limited weight (~ 900 g) and a payload of 300 g. These features make it suitable for photogrammetric flights over limited areas (about 0.03 km²) to obtain very high spatial resolution images. The propulsion is electric, with a maximum flight time around 15 min. The nominal cruise speed is ~ 18 km h⁻¹, with a radio link range about 0.5 km from the master station on the ground. The quadcopter is able to perform pre-planned flights in a fully automated mode, since it continuously analyzes data from the onboard GPS/IMU system. However, the operator can always recover full control of the system. The study area is classified in the context of noncritical operations, conducted in Visual Line of Sight (VLoS). For this situation, the rules of the Italian Civil Aviation Authority (Ente Nazionale Aviazione Civile, ENAC) require that the pilot can maintain a direct eye contact with the UAV, to monitor the flight with respect to other aircraft, infrastructure and people in order to avoid collisions. Flight plan for each detected ditch is organized in 3 strips (with about

85% of overlapping) along their longitudinal direction. The photogrammetric block was lastly georeferenced using 8 Ground Control Points (GCPs), marked with square targets of size $0.30 \times 0.30 \text{ m}^2$ divided in black and white triangles.

Concerning the laser scanner, it was mounted on a tripod (~150 cm height) on a small bridge in the middle of the canals in order to achieve a full panoramic of ditches around the four cardinal directions (i.e. North, South, East and West) through a single point of stationing. The raw data of laser scanner were processed with Cloud Compare software which is able to build the 3D point cloud and to extract directly the oriented DSM. Lastly, the GPS acquisitions were carried out manually moving inside the canals in transverse and longitudinal directions. All data was oriented in WGS84-32 N geographical system.

3 Results and Discussion

Cross sections as detected by different topographic survey techniques are reported in Fig. 3. In general, LiDAR significantly underestimates the depth of canals, reducing the bed size and increasing sides slopes. However, all topographic survey techniques describe quite well the shape and the pattern of the canals.

Drone acquisitions are in good agreement with ground surveys (i.e. GPS and laser scanner) only referring to East-West flight direction (i.e. Fig. 3b, d), while in

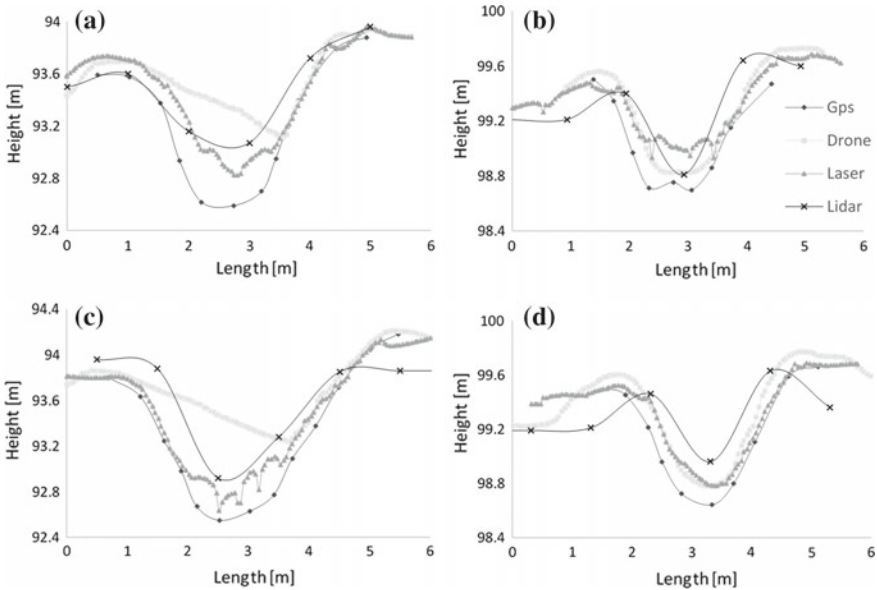


Fig. 3 Comparison of cross sections obtained by different data sources (LiDAR, Laser Scanner, Drone and GPS) in North-South direction (a-c) and East-West direction (b-d)

the North-South direction (i.e. Fig. 3a, c) an unexpected cross section layout occurs. This is mainly due to the shadow that the left side of the embankment cast inside the canal at the time of the UAV acquisition. This problem was also found in previous studies of Kraus and Pfeifer (2001), where complex shadow removal algorithms were applied for reducing the data defects.

Comparing, in pairs, the different topographic survey methodologies (Fig. 4), drone-GPS, drone-laser scanner and laser scanner-GPS offer mutually consistent measurements (R^2 higher than 0.80), while R^2 coefficient is less than 0.6 if LiDAR-GPS, LiDAR-laser scanner and LiDAR-drone couple of data are considered. Our

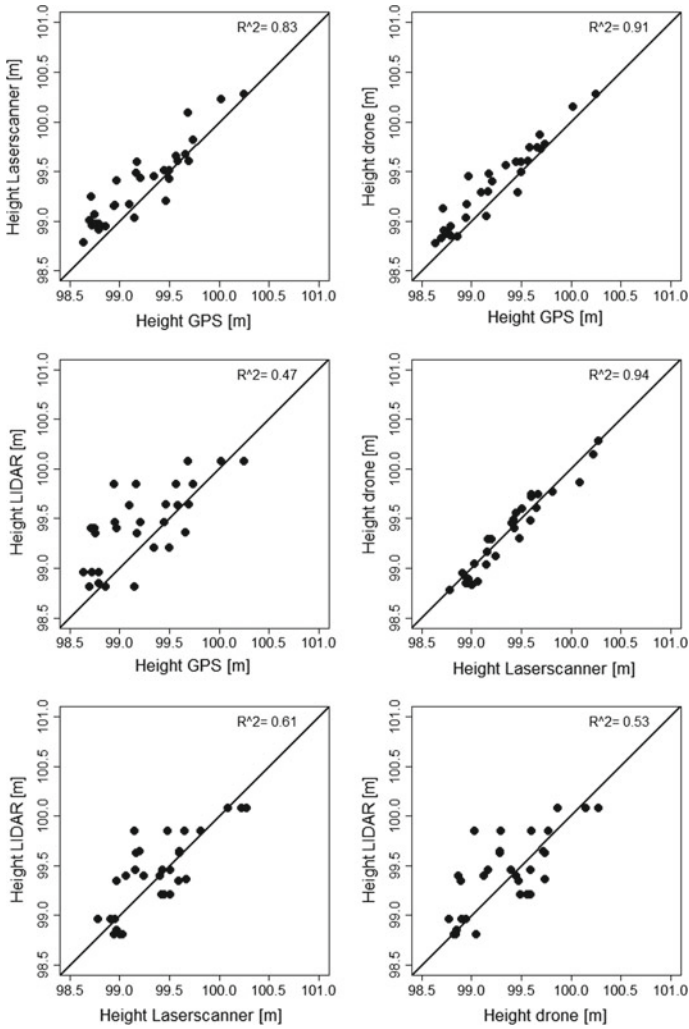


Fig. 4 Differences in topographic surveys with different level of resolutions

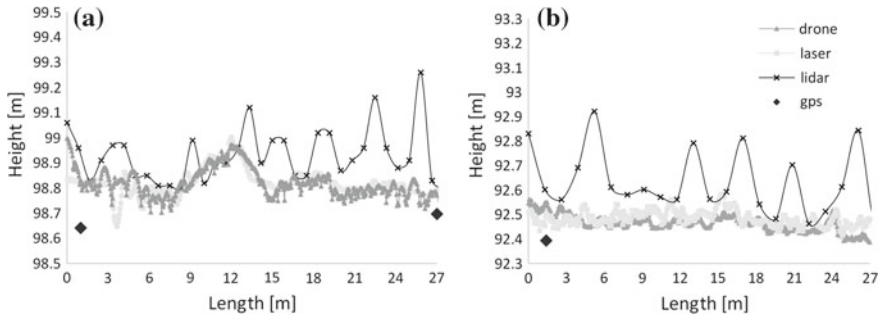


Fig. 5 Longitudinal profile obtained by different source of data (LiDAR, drone, laser scanner and GPS). **a** North-South direction and **b** East-West direction

results show a good concordance only among ground-based survey techniques or very proximal ground detections. This makes unreliable the 1 m LiDAR acquisitions for an accurate large-scale detection of rural canal geometrical characteristics, especially when small ditches are surveyed. However, the good alignment among canal shapes showed in Fig. 3, enables to envisage the use of LiDAR data as a reliable support dataset for extracting the topology of the rural canal network in a large-scale prospective.

A canal branch about 27 m long (both in North–South and in East–West direction) was considered for comparing slopes obtained by the different topographical surveys. The oscillation of LiDAR signal is very high both in North–South and in East–West as shown in Fig. 5a and b, respectively. Differences between peaks and valleys of LiDAR signal can reach 30 cm over a mean canal slope of about 3‰. This makes 1 m LiDAR data inapplicable to derive the channel flow-direction, especially in the study area context where very low canal slopes occur. Conversely, drone and laser scanner acquisitions provide more accurate data, quite consistent with GPS measurements.

A rough estimation of potential flow (calculated by Chezy formula—considering a maximum cross-section degree of filling) and storage capacity of the canal branch was provided first by using LiDAR data and then by laser scanner acquisitions. The underestimation in flow and volume capacities obtained using the LiDAR data is about 35% and 20% respectively, confirming the inadequacy of LiDAR data of 1 m of resolution to describe hydraulic features of small rural canals (i.e. lower than 1–2 m of cross-section).

Concerning the cost of data acquisitions, the LiDAR data are free of charge and freely downloadable after the sending a written request at the Environmental Ministry electronic mailbox. The UAV acquisitions are affordable for small areas (about 8 €/hectare, including post-processing) but quite cost-prohibitive if large areas have to be detected. Laser-scanner and GPS measurements are cost-prohibitive for large scale applications because, on average, no more than one hectare (about 400 m of canals) can be surveyed daily.

4 Conclusions

The work presents the results of different topographic survey methodologies for detecting rural canal geomorphological characteristics. In flight-mode and ground-based measurements with different levels of resolution were compared. The results show that LiDAR data, currently available with a ground resolution of 1 m, can be useful for detecting topological features of the rural canal network, but they are inapplicable for extracting canal geometries and flow-directions. Drone acquisitions are more consistent with ground-based measurements (i.e. laser-scanner and GPS), but shadows on the ground surface can cause errors in the results, if not appropriately corrected. In light of these considerations, only a combination of different topographic survey technique appears suitable to detect the geomorphological characteristics of rural canals with an adequate level of detail over large areas. From a methodological point of view, we believe that this work represents an interesting scalable approach that can be easily applied in different rural areas, in addition to those presented in this paper, with modest time-consuming and costs.

Acknowledgements The activity presented in the work is part of the research funded by Fondazione Sviluppò Ca' Granda on the detection of rural canal characteristics.

References

- Ackermann, F. (1999). Airborne laser scanning—present status and future expectations. *ISPRN Journal of Photogrammetry and Remote Sensing*, 54, 64–67.
- Bailly, J. S., Lagacherie, P., Millier, C., Puech, C., & Kosuth, P. (2008). Agrarian landscapes linear features detection from LiDAR: Application to artificial drainage networks. *International Journal of Remote Sensing*, 29(12), 3489–3508.
- Cazorzi, F., Fontana, G. D., Luca, A. D., Sofia, G., & Tarolli, P. (2013). Drainage network detection and assessment of network storage capacity in agrarian landscape. *Hydrological Processes*, 27(4), 541–553.
- Kraus, K., & Pfeifer, N. (2001). Advanced DTM generation from LIDAR data. *International Archives of Photogrammetry and Remote Sensing XXXIV-3/W4*, 23–35.
- Lagacherie, P., Diot, O., Domange, N., Gouy, V., Floure, C., Kao, C., et al. (2004). An indicator approach for describing the spatial variability of human-made stream network in regard with herbicide pollution in cultivated watersheds. *Ecological Indicators*, 6, 265–279.
- Passalacqua, P., Tarolli, P., & Fofoula-Georgiou, E. (2010). Testing space-scale methodologies for automatic geomorphic feature extraction from lidar in a complex mountainous landscape. *Water Resources Research*, 46, W11535. <https://doi.org/10.1029/2009WR008812>.
- Pirotti, F., & Tarolli, P. (2010). Suitability of LiDAR point density and derived landform curvature maps for channel network extraction. *Hydrological Processes*, 1187–1197. <https://doi.org/10.1002/hyp.7582>.
- Slatton, K. C., Carter, W. E., Shrestha, R. L., & Dietrich, W. E. (2007). Airborne laser swath mapping: Achieving the resolution and accuracy required for geosurficial research. *Geophysical Research Letters*, 34, L23S10.
- Sofia, G., Tarolli, P., Cazorzi, F., & Dalla Fontana, G. (2011). An objective approach for feature extraction: Distribution analysis and statistical descriptors for scale choice and channel network

identification. *Hydrology and Earth System Sciences*, 15, 1387–1402. ISSN: 1027-5606. <https://doi.org/10.5194/hess-15-1387-2011>.

Tarolli, P., Arrowsmith, J. R., & Vivoni, E. R. (2009). Understanding earth surface processes from remotely sensed digital terrain models. *Geomorphology*, 113, 1–3.

Zhang, H., Yang, J., Baartman, J. E., Li, S., Jin, B., Han, W., et al. (2018). Quality of terrestrial data derived from UAV photogrammetry: A case study of Hetao irrigation district in northern China. *International Journal of Agricultural and Biological Engineering*, 11(3), 171–177.

Hydraulic Modeling of Field Experiments in a Drainage Channel Under Different Riparian Vegetation Scenarios



G. F. C. Lama, A. Errico, S. Francalanci, G. B. Chirico, L. Solari and F. Preti

Abstract A hydraulic model was implemented for interpreting the real-scale hydraulic tests conducted in a vegetated drainage channel, colonized by dormant *Phragmites australis* (Cav.) Trin. ex Steud. (common reed), located in the San Rossore-Migliarino-Massaciuccoli Regional Park (Tuscany, Italy). The hydraulic tests encompassed six flow rates and three vegetation scenarios: (a) natural scenario, with common reed fully covering the drainage channel; (b) side vegetation scenario, achieved by removing the in-stream reed just in the central portion of the channel, with two lateral buffers of undisturbed vegetation and (c) unvegetated scenario, corresponding to the complete removal of the riparian reed plants. The outputs of the simulation were compared with the experimental flow average velocities and vegetative Manning's roughness coefficient, obtained from measured punctual flow velocities by means of an acoustic Doppler velocimeter (ADV) and a propeller-type current meter, respectively located at the upstream and downstream cross sections of the experimental stretch of the drainage channel. The results of this study are

G. F. C. Lama (✉) · G. B. Chirico
Department of Agricultural Sciences, University of Naples Federico II, Via Università 100, 80055 Portici, Italy
e-mail: giuseppefrancescocesare.lama@unina.it

G. B. Chirico
e-mail: giovannibattista.chirico@unina.it

A. Errico · F. Preti
Department of Agricultural, Food, Environmental and Forestry Sciences and Technologies, University of Florence, Via San Bonaventura 13, 50145 Florence, Italy
e-mail: alessandro.errico@unifi.it

F. Preti
e-mail: fedrico.preti@unifi.it

S. Francalanci · L. Solari
Department of Civil and Environmental Engineering, University of Florence, Via Santa Marta 3, 50139 Florence, Italy
e-mail: simona.francalanci@unifi.it

L. Solari
e-mail: luca.solari@unifi.it

© Springer Nature Switzerland AG 2020
A. Coppola et al. (eds.), *Innovative Biosystems Engineering for Sustainable Agriculture, Forestry and Food Production*, Lecture Notes in Civil Engineering 67,
https://doi.org/10.1007/978-3-030-39299-4_8

discussed for assessing the impact of the vegetation management scenarios on both hydraulic conveyance and riparian habitat functionality of the examined vegetated drainage channel.

Keywords Riparian plants management · Real scale experiments · Hydraulic modeling · Flow velocity field · Vegetative manning's roughness coefficient

1 Introduction

The interaction between riparian vegetation and water flow in vegetated waterbodies is the main objective of Ecohydraulics, from both experimental and numerical perspectives (Errico et al. 2018; Pasquino et al. 2019; Wang and Zhang 2019). This interaction sensibly modifies the cross sectional hydrodynamic patterns inside the waterbodies (i.e. velocities and water levels), with notable impacts on hydraulic conveyance (Rhee et al. 2008) and riparian habitat functionality (Fierro et al. 2017; Errico et al. 2019a). For these reasons, the attention of waterbodies' managers is nowadays focused on identifying sustainable practices of riparian vegetation management for balancing these two needs. This is still an open research question, because of the unpredictable effects of riparian vegetation distribution on the aquatic and terrestrial ecosystems and the wide range of interaction which can occur between plants and water flow.

The aim of the present study is to evaluate the effect of different vegetation scenarios on the flow features in a drainage channel covered by dormant *Phragmites australis* (Cav.) Trin. ex Steud. (common reed) plants, situated in the San Rossore-Migliarino-Massaciuccoli Regional Park (Tuscany, Italy), by means of a hydraulic model of the channel flow applied to reconstruct experimental tests carried out in November 2017.

The hydraulic model was implemented by considering variable vegetative Manning's roughness coefficients for describing the effects of the different vegetation management scenarios. The model outcomes in terms of flow averaged velocity and Manning's n were compared with those derived from the field experiments. The comparison between estimated and measured results was carried out for validating the model, in order to extend the simulation to other vegetation management scenarios and providing to waterbodies managers predictive indications on the effect of riparian vegetation on both riparian habitat functionality and hydraulic conveyance within the drainage channel.

2 Materials and Methods

2.1 Field Experiments

The experiments took place in a vegetated drainage channel covered by dormant common reed plants, located in a lowland belonging to the San Rossore-Migliarino-Massaciuccoli Regional Park (Tuscany, Italy), in hydraulic connection with the Massaciuccoli Lake (Fig. 1a). Inside the 500 m long drainage channel, characterized by an almost null slope angle, a stretch 70 m long was selected for the real-scale hydraulic experiments. Discharge rates and boundary conditions were controlled by means of a pumping system located at the extremes of the 500 m long channel, to ensure steady flow conditions in the 70 m long stretch (Errico et al. 2019a). The tests were conducted with six flow rates (Errico et al. 2019a) and three different vegetation management scenarios: (a) one flow rate ($Q_N = 0.13 \text{ m}^3\text{s}^{-1}$) under a natural scenario, i.e. with reed plants in natural abandonment; (b) two flow rates ($Q_{S1} = 0.16 \text{ m}^3\text{s}^{-1}$ and $Q_{S2} = 0.33 \text{ m}^3\text{s}^{-1}$) for the side vegetation scenario, obtained by removing the reed plants for a 2.70 m wide central region of the channel, leaving two buffers of undisturbed vegetation at channel sides; and (c) three flow rates ($Q_{U1} = 0.09 \text{ m}^3\text{s}^{-1}$, $Q_{U2} = 0.18 \text{ m}^3\text{s}^{-1}$ and $Q_{U3} = 0.28 \text{ m}^3\text{s}^{-1}$) for the unvegetated scenario, obtained with the total cut of reed plants from the channel. Hereinafter, the six flow rate regimes are indicated as N, S₁, S₂, U₁, U₂ and U₃, respectively. Surface water levels were measured in four cross sections (Fig. 1b), while the velocity was measured at just the upstream and downstream cross sections. The plants were in emergent condition, as the plants' height was higher than the water level.

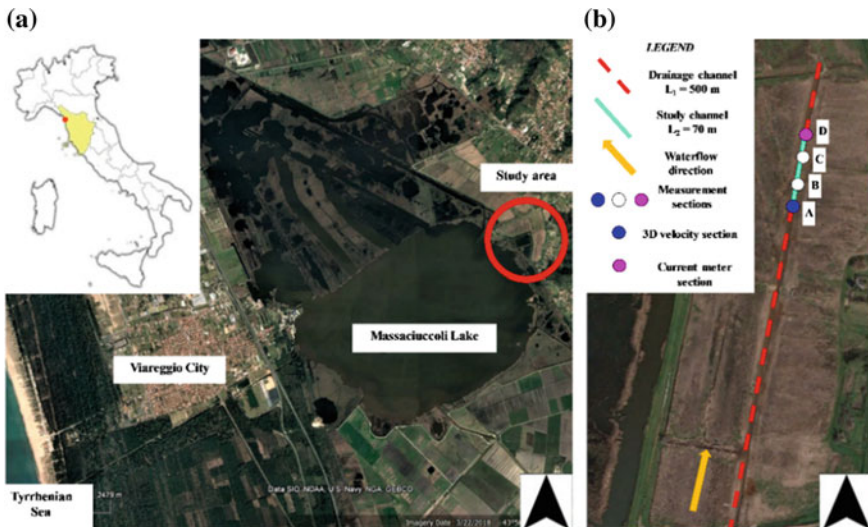


Fig. 1 a Study area and b experimental setup of the field experiments

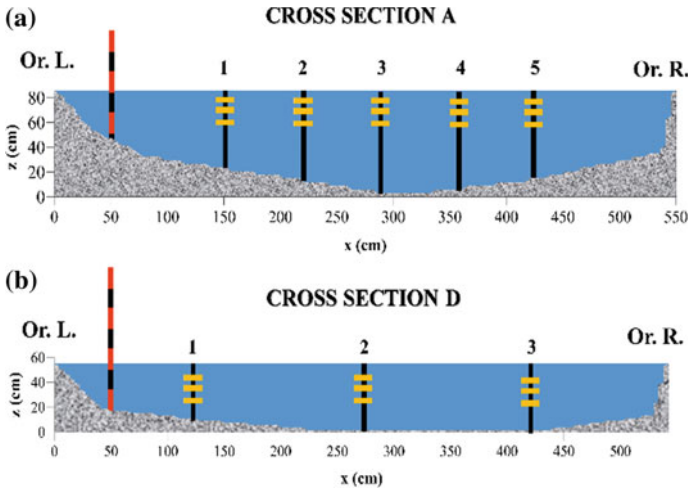


Fig. 2 Flow velocity measuring verticals at upstream (a) and downstream cross section (b)

As shown in Fig. 1b, 3D velocity data were acquired by means of an acoustic Doppler velocimeter (ADV), equipped with a down-looking 4-beam probe and by a propeller-type current meter, respectively located at the upstream and downstream cross sections (Errico et al. 2019a, b), which shape is assimilable to a trapezoidal geometry, having an inclination of the banks ranging from 20° to 35° , respectively for the orographic right and left banks. ADV measurements were conducted considering a regular grid, consisting of 3 points for 5 verticals (Fig. 2a), while, at downstream cross section, the number of verticals was reduced to 3, for a total of 9 points (Fig. 2b).

The ADV measurements are more accurate than current meter ones because the ADV does not interfere with the target since the sampling volume is 0.05 m far from it, while the propeller largely interact with the flow; moreover, the ADV make a continuous acquisition, while the current meter gives the number of propeller's revolutions in 10 min, from which it can be assessed just a time average velocity. So, the ADV velocities, characterized by an accuracy of $\pm 0.5\%$ as declared by the manufacturer (Nortek[®]), were considered as reference for the comparisons. The water levels were monitored by means of graduated piezometers at the four cross sections, quoted by means of total station theodolites. The flow was considered stationarity when the water level in each of them was stable for 30 min, with an accepted residual of ± 0.0001 m.

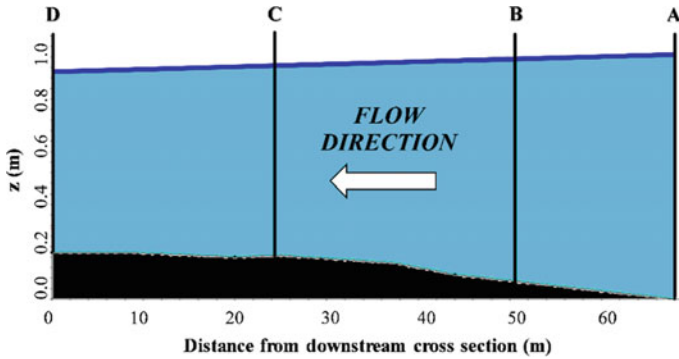


Fig. 3 Longitudinal profile of the water surface, with the four cross sections (black vertical lines)

2.2 Hydraulic Model

HEC-RAS (Hydrologic Engineering Center—River Analysis System) freeware software (<https://www.hec.usace.army.mil/software/hecras/>) was employed for the hydraulic simulation of the examined vegetated drainage channel.

In Fig. 3 is represented the water surface profile in the channel. The water level at the downstream cross section was used as a boundary condition since the flow in the drainage channel was sub-critical. Three flow rates were used in the model: Q_N , Q_{S1} and Q_{S2} , corresponding to N, S_1 and S_2 scenarios, respectively. The influence of vegetation on the channel flow under the different vegetation scenarios was assessed by calibrating the Manning’s n coefficients to fit the observed surface water level profile. The cross sectional variability of the vegetation density in the S_1 and S_2 scenarios was modelled by splitting the channel into three portions according to the Divided Channel Method, combined with Horton’s composite section method (Horton 1933).

3 Results and Discussions

3.1 Real-Scale Experiments

Cross sectional flow velocity fields were obtained by interpolating the punctual measurements at the channel upstream and downstream cross sections, imposing a null value along the wetted perimeter, corresponding to the channel’s bed and banks.

The flow fields in Fig. 4 refer to the N scenario with a discharge $Q_N = 0.13 \text{ m}^3\text{s}^{-1}$.

It can be easily noticed from Fig. 4a that the velocity field at the upstream cross section was highly influenced by the vegetation covering the entire wetted perimeter, with a low velocity peak (0.10 ms^{-1}) in the upper region of the cross section, and a

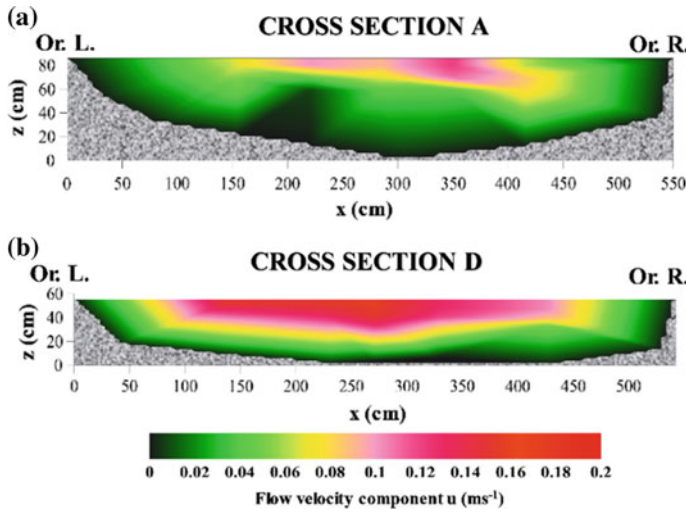


Fig. 4 Flow velocity u at upstream (a) and downstream (b) cross sections for $Q_1 = 0.13 \text{ m}^3 \text{ s}^{-1}$

significant reduction of the effective cross sectional wetted area, with a water depth of 81 cm, corresponding to the bankfull level. As shown in Fig. 4b, at downstream cross section, where vegetation was absent in all the experiments, the flow velocity field assumed a very regular and symmetric pattern, with a peak velocity value (0.17 ms^{-1}) at the center of the cross section and a water depth of 60 cm. The experimental averaged flow velocities and Manning's n are expressed according to the following Eq. (1) and Eq. (2):

$$U_{mi} = \frac{Q_i}{\Omega_i}, \quad (1)$$

$$n_{mi} = \frac{J_i^{\frac{1}{2}} R_i^{\frac{2}{3}}}{U_{mi}}, \quad (2)$$

where Q_i and Ω_i are the flow rates and the cross sectional wetted areas (Eq. (1)), while J_i and R_i are the slopes of the total energy and the hydraulic radius (Eq. (2)). Subscript i is used for referring to the three vegetation scenarios: (1) N, (2) S_1 and (3) S_2 .

3.2 Hydraulic Model Results

The comparison between model results and field measurements was done at upstream cross section, which can represent the plant distribution (Errico et al. 2019b) of the

Table 1 Measured (U_m) and estimated (U_e) average flow velocities and measured (n_m) and estimated (n_e) Manning’s n coefficients at the upstream cross section, for N, S₁ and S₂ scenarios

Scenario	Q (m ³ s ⁻¹)	U _m (ms ⁻¹)	U _e (ms ⁻¹)	n _m (sm ^{-1/3})	n _e (sm ^{-1/3})
N	0.13	0.035	0.041	0.495	0.650
S ₁	0.16	0.051	0.064	0.129	0.115
S ₂	0.33	0.100	0.072	0.268	0.185

entire channel. Average flow velocities and Manning’s n for the three examined flow rates are compared in Table 1, corresponding to N, S₁ and S₂ vegetation scenarios.

After the first run corresponding to N scenario, it was possible to estimate an equivalent Manning’s coefficient n of 0.65 sm^{-1/3}. Then, for the S₁ and S₂ scenarios, miming vegetation removal for a 2.70 m wide central region of the channel, and leaving two side buffers of undisturbed vegetation, the value of n = 0.65 sm^{-1/3}, as assessed for the N scenario, was imposed for the side buffers, while it was calibrated for the central clean, till the predicted water levels at the four cross sections converged to the measured ones (Fig. 5).

Measured and estimated average flow velocities and Manning’s n exhibited a good correlation, characterized by values of Root Mean Square Errors (RMSE) respectively equal to 0.02 ms⁻¹ and 0.10 sm^{-1/3}. The correlation between the measured and the estimated (or simulated) water flow features is comparable with that obtained by previous studies in similar conditions. Galema (2009), by exploiting a dataset from Stone and Shen (2002), which referred to the case of emergent rigid plants, as the reed analyzed in the present study. Similar results were also obtained by Vinatier et al. (2017), who simulated the plants’ cross sectional distribution with 3D voxels grids (i.e. volumetric picture elements). The authors achieved prediction performances similar to the present case study by comparing observed and simulated vegetative

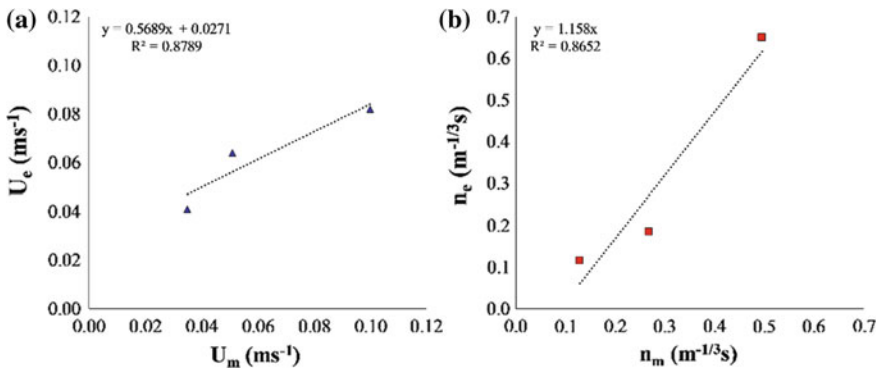


Fig. 5 Comparisons between measured and estimated averaged flow velocities (purple triangles) (a) and vegetative Manning’s n (red squares) (b) at the upstream cross section for N, S₁ and S₂ scenarios

Manning's n for different species (*Asparagus acutifolius*, *Elytrigia repens*, *Lythrum salicaria* and *Scirpoides holoschoenus*).

4 Conclusions

A hydraulic model was employed for reproducing the outcomes of field tests conducted in a drainage channel covered by dormant common reed in order to evaluate the effects of different vegetation management scenarios on average flow velocity and vegetative Manning's roughness coefficient n . Two vegetation scenarios were simulated: natural cover (N scenario) and side vegetation cover (according to two configurations: S₁ and S₂ scenarios). For the three flow rates examined within the present study, it was observed that the measured and the estimated average flow velocities and vegetative Manning's roughness coefficient exhibited a high correlation, testified by values of Root Mean Square Error (RMSE) respectively equal to 0.02 ms^{-1} and $0.10 \text{ sm}^{-1/3}$. The achieved predictive performances are comparable with those obtained by previous authors for similar experimental conditions (Galema 2009; Vinatier et al. 2017).

Acknowledgements Part of the research was funded by the Interreg EU project "Assistere l'adattamento ai cambiamenti climatici dei sistemi urbani dello spazio transfrontaliero—ADAPT, Interreg. Italia-Francia Marittimo 2014–2020 CUP B19J1600289000". The Authors thank Consorzio di Bonifica 1 Toscana Nord for funding the tests, Eng. Leonardo Giannecchini and Eng. Daniele Maffi for their support.

References

- Errico, A., Pasquino, V., Maxwald, M., Chirico, G. B., Solari, L., & Preti, F. (2018). The effect of flexible vegetation on flow in drainage channels: Estimation of roughness coefficients at the real scale. *Ecological Engineering*, *120*, 411–421.
- Errico, A., Lama, G. F. C., Francalanci, S., Chirico, G. B., Solari, L., & Preti, F. (2019a). Flow dynamics and turbulence patterns in a drainage channel colonized by common reed (*Phragmites australis*) under different scenarios of vegetation management. *Ecological Engineering*, *133*, 39–52.
- Errico, A., Lama, G. F. C., Francalanci, S., Chirico, G. B., Solari, L., & Preti, F. (2019). Validation of global flow resistance models in two experimental drainage channels covered by *Phragmites australis* (common reed). In *38th IAHR World Congress*, Panama City.
- Fierro, P., Bertràn, C., Tapia, J., Haunstein, E., Peña-Cortés, F., Vergara, C., et al. (2017). Effects of local land-use on riparian vegetation, water quality, and the functional organization of macroinvertebrate assemblages. *Science of Total Environment*, *609*, 724–734.
- Galema, A. (2009). Vegetation resistance; evaluation of vegetation resistance models for flood management. *Master Thesis, University of Twente*, Enschede, The Netherlands.
- Horton, R. E. (1933). Separate roughness coefficients for channel bottoms and sides. *Engineering News-Record*, *111*(22), 652–653.

- Pasquino, V., Saulino, L., Pelosi, A., Allevalo, E., Rita, A., Todaro, L., et al. (2019). Hydrodynamic behaviour of European black poplar (*Populus nigra* L.) under coppice management along Mediterranean river ecosystems. *River Research and Applications*, 34, 586–594.
- Rhee, D. S., Woo, H., Kwon, B. A., & Ahn, H. K. (2008). Hydraulic resistance of some selected vegetation in open channel flows. *River Research and Applications*, 24, 673–687.
- Stone, B. M., & Shen, H. T. (2002). Hydraulic Resistance of flow in channels with cylindrical roughness. *Journal of Hydraulic Engineering*, 128(5), 500–506.
- Wang, J., & Zhang, Z. (2019). Evaluating riparian vegetation roughness computation methods integrated within Hec-RAS. *Journal of Hydraulic Engineering*, 145(6).
- Vinatier, F., Bailly, J. S., & Belaud, G. (2017). From 3D grassy vegetation point cloud to hydraulic resistance: Application to close-range estimation of Manning coefficients for intermittent open channels. *Ecohydrology*, 10(8), e1885.

Groundwater Recharge Through Winter Flooding of Rice Areas



Arianna Facchi, Camilla Negri, Michele Rienzner, Enrico Chiaradia and Marco Romani

Abstract Starting from October 2017, the hydrological balance of a 36 hectares' rice area located in Lomellina (PV), where the practice of winter flooding has been adopted since 2004, has been under investigation. Flow meters were installed on the irrigation and drainage channels, piezometers were positioned inside and outside the study area, and a soil survey was performed. A conceptual hydrological model simulating the water balance at the paddy field scale was developed and calibrated. Main results show that: (a) irrigation efficiency of the pilot area during the first summer season is well in line with those found for other paddy areas in the region; (b) higher percolation rates are observed in wintertime compared to summer season; (c) despite the higher percolation, groundwater level reached in winter season is slightly lower than in summer, and the groundwater depletion after the end of the flooding period is faster compared to that observed after the summer flooding; (d) to maintain higher groundwater levels at the beginning of the cropping season, which would increase irrigation efficiency, winter flooding should be maintained longer over time and involve larger paddy areas.

Keywords Winter flooding · Groundwater recharge · Hydrological model · Irrigation efficiency · Paddy

1 Introduction

Recent research suggests that groundwater overdraft can be mitigated by diverting flood waters onto agricultural lands for direct groundwater recharge (Bachand et al. 2016). This technique is often called Ag-MAR (where Ag is for Agricultural and

A. Facchi (✉) · C. Negri · M. Rienzner · E. Chiaradia
Dipartimento di Scienze Agrarie e Ambientali – Produzione, Territorio, Agroenergia, Università degli Studi di Milano (DiSAA-UNIMI), Via Celoria 2, 20133 Milano, Italy
e-mail: arianna.facchi@unimi.it

M. Romani
Centro Ricerche Riso, Ente Nazionale Risi (CRR-ENR), Strada per Cerretto 4, 27030, Castello d'Agogna, Pavia, Italy

© Springer Nature Switzerland AG 2020
A. Coppola et al. (eds.), *Innovative Biosystems Engineering for Sustainable Agriculture, Forestry and Food Production*, Lecture Notes in Civil Engineering 67,
https://doi.org/10.1007/978-3-030-39299-4_9

MAR for Managed Aquifer Recharge) and is usually carried out during wintertime, when water is abundant since it is not used for irrigation (Niswonger et al. 2017). Recently, Ag-MAR has been adopted in a few agricultural areas of the USA, particularly in California. In Europe, the implementation of winter flooding (WF) of rice paddies has been promoted since the late nineties as an environmentally friendly technique to degrade straw residue as well as to provide foraging habitats to winter waterfowl and other wildlife. However, in Northern Italy it was introduced as an agro-environmental measure in the EU-RDP 2014-2020 and thus it has been adopted only recently. If only a few studies in recent years have focused on biodiversity and agronomic effects of winter flooding, no studies have investigated its impacts on the hydrological balance of rice areas in terms of both groundwater recharge and possible increase of irrigation efficiency during summertime (as a consequence of a higher soil water content and/or a higher groundwater level at seeding time).

2 Materials and Methods

2.1 Study Area

The study area is located in Zeme (PV, Italy), about 50 km south-west of the city of Milan, in the middle of the main Italian rice growing area, between Lombardy and Piedmont. The study area is cropped with rice and it extends for about 36 hectares (9 adjacent paddies). Winter flooding has been practiced since 2004–2008 in 5 fields (old WF fields), and it was extended to the rest of the paddies in 2016 (new WF fields) with the introduction of EU-RDP 2014–2020. Some maize fields (for a total of 6 ha) are also located within the study area. The farm is surrounded by other rice farms most of which do not practice winter submersion. A soil survey was carried out to characterize the area. The information garnered with the survey was used to describe the soil distribution and the average depth of impervious layer (low conductivity layer or LCL hereafter), often being the hardpan. A rather high variability amongst and within the fields, but a fairly even depth and thickness of the LCL (horizon between 30–50 cm depth) were observed. Given the topography of the study area, in which the altitude decreases from west to east, it was decided, with respect to the groundwater depth, to divide the area in two main blocks. The first block (high WF fields, 4 paddies) is comprised of all the fields surrounding the Z1 piezometer, having an average altitude of 105 m a.s.l. The second block (low WF fields, 5 paddies) is comprised of all the fields surrounding the Z2 piezometer, having an average altitude of 104 m a.s.l. (Z1 and Z2 are shown in Fig. 1).

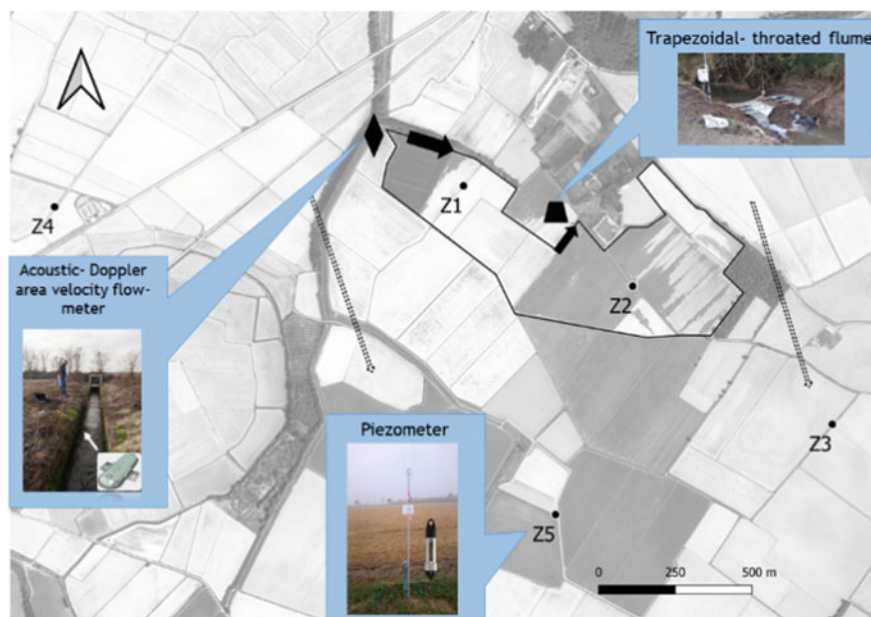


Fig. 1 Study area and position of the monitoring devices. Piezometers (from Z1 to Z5) are shown by black dots, the acoustic-Doppler inflow-meter by a diamond, and outflow flumes by a trapezoid. The main groundwater flow direction is shown by dashed arrows, while surface water flow direction by black arrows

2.2 Irrigation Management

Data related to the irrigation management during winter and summertime were provided by the farmer. In particular, winter water management consists of irrigating all rice fields from October to the end of January, keeping ponding water at about 10–25 cm above the soil surface. While winter management is uniform all over the farm (all fields are submerged more or less at the same time), summer management follows either traditional flooding or dry seeding and delayed flooding practices. In the farm, traditional flooding sowing is followed by a dry period for enhancing root development (1 month), a second water flooding (1 month), a second drainage period followed by flooded conditions until the final drying (about 3 weeks before harvest). In the case of dry seeding and delayed flooding, the first submersion is conducted about one month after sowing and is followed by a drying period and a second flooding lasting until the final drying. Maize fields were border irrigated two times during the cropping season 2018 by means of a pump coupled with a tractor taking water from the ditch supplying the rice fields. The amount of water diverted to maize fields was computed (by measuring motor rpm and irrigation duration, and by applying the relationship provided by the pump manufacturer). The discharge was then removed from the water inputs, obtaining water inflow to the paddies. Lastly, a single field

(‘Zan 16–18’), was managed differently during the first winter, being kept flooded from October 2017 to April 2018.

2.3 Surface Water Inflow, Outflow and Groundwater Levels

The surface water inflow discharge in the irrigation channel providing water to the nine fields of the study area was measured using an acoustic-Doppler area-velocity flow meter (SonTek-IQ Standard), while two trapezoidal long-throated flumes were used in combination with pressure transducers to measure the surface water outflow discharge in the drainage channel collecting tailwater. The flumes were self-made, and designed to fit a maximum discharge of 120 l s^{-1} each. Flow rate curves were estimated using the WinFlume software (U.S.B.R., USA), as illustrated in Chiaradia et al. (2015). Groundwater levels were monitored using five piezometers: two located inside and three outside the area. Wells were made of 4.5 meters PVC pipes (the lower 1.5 m were windowed) installed into holes drilled with a manual auger, pressure transducers were positioned inside the wells in order to continuously measure water levels. Figure 1 shows the devices installed. The study site was instrumented in October 2017; thus, data of two winters (2017–2018 and 2018–2019) and one summer (2018) seasons are shown in this paper.

2.4 Semi-distributed Conceptual Model: Set up and Calibration

Since water flow measurements were taken at the inlet irrigation channel and outlet drainage channel, respectively delivering irrigation water and collecting tailwater from the nine fields, discharge inflow and outflow of each paddy field are actually unknown.

A semi-distributed model was set up with the aim to gain a deeper knowledge of the system’s processes, providing an estimation of all the water fluxes and storages at the field scale, to double-check measured fluxes and irrigation scheduling reported by the farmer in the farm-diary, as well as to investigate the relevance of groundwater levels, thickness of ponding water levels within the paddies, and soil properties (i.e., saturated hydraulic conductivity of the LCL) on percolation losses. The model was built setting the water amount available for irrigation within the study area as the difference between irrigation inflow (Q_{in}) and outflow (Q_{out}), while the time for the water to travel from the inlet to the outlet of the system, the water storage in the channels and the lateral seepage through the bounds were considered to be negligible. In particular, when the difference between Q_{in} and Q_{out} was positive, the water flux was considered entering the system, and vice versa if negative. Each of the nine paddy fields was simulated as two tanks in series: the first tank being the top soil

(0–30 cm, above the LCL), the second being the ponding water above the paddy. Equation 1 defines the balance equation for each paddy:

$$\Delta S_{w,t} + \Delta S_{s,t} = \gamma \Delta(Qin_t - Qout_t) + R_t - ET_t + P_t \quad (1)$$

where: t is the hourly time index, $\Delta S_{w,t}$ is the variation in ponding water, $\Delta S_{s,t}$ is the variation in water storage within the first 0–30 cm of soil profile, Qin_t and $Qout_t$ are the measured irrigation inflow and outflow, R_t is the rain, ET_t is the evapotranspiration and P_t is the percolation term of the equation. All the terms of Eq. 1 are expressed in millimetres, with the exception of Qin_t and $Qout_t$ ($Ll\ s^{-1}$) and γ is a conversion factor which accounts for the fields' area. The terms $\Delta S_{w,t}$ and $\Delta S_{s,t}$ are considered mutually exclusive: when the soil tank is full (the upper soil is saturated, $\Delta S_{s,t} = 0$), the value of the right hand side of Eq. 1 is allocated only to $\Delta S_{w,t}$; when the water tank is empty ($\Delta S_{w,t} = 0$) that value in the right hand side of Eq. 1 is allocated only to $\Delta S_{s,t}$. The water inflow/outflow (Qin_t and $Qout_t$) to/from a single field was considered different from zero only if the corresponding inlet/outlet was open, according to the farm-diary provided by the farmer. For each hour, the total amount of incoming/outcoming water was split among the fields with open inlet/outlet according to their area and ponding water level (computed by the model at the previous time step). Evapotranspiration (ET_t), considered as potential when the water content of the shallow soil (0–30) was over the field capacity, was calculated according to the FAO *ET_o* multiplied by a single crop coefficient (Kc_t) (Allen et al. 1998). When the soil was dry, a stress coefficient was taken into account according to the FAO-56 method (Allen et al. 1998). During winter flooding, the Kc for ponded water suggested by Allen et al. (1998) was adopted ($Kc = 1.05$), while during the agricultural season, rice phenology was estimated from Sentinel-2 (ESA) images. The crop coefficients (Kc_t) for the two irrigation treatments (i.e. wet and dry seeding) were derived from a previous study carried out in the same area (Chiaradia et al. 2015; Cesari de Maria et al. 2017). In presence of ponding water in the field and rice Kc lower than 1.05, the latter value was adopted. When the soil tank is full (saturated soil), the percolation term (P_t) was computed through the Darcy law (following the approach described in Facchi et al. 2018); in case of unsaturated soil the percolation was strongly reduced, and it was set to zero as the soil moisture dropped below the field capacity. For each of the nine paddies, the model simulates: ponding water level (state variable), soil water content (state variable) and percolation (Darcy law). According to Facchi et al. 2018, percolation through the LCL can be computed once the following data are known: depth and thickness of the LCL (measured during the soil survey), ponding water levels (state variable), distance between the groundwater table and the lower side of the LCL (depending on the groundwater level), and the saturated hydraulic conductivity of the LCL (Ks). The groundwater level is measured in the center of two groups of fields (high and low; Fig. 1). However, the average groundwater level for each field was unknown as, especially during the winter, the water table is expected to be subject to border effects while approaching the borders of the submerged area. To account for this, the average groundwater level under the fields in each one of the two blocks was assumed

Table 1 Water fluxes and storages considered by the semi-distributed conceptual model

Dataset	Type of data
Rain, Q_{in}	Measured data
Q_{out}	Measured data
Groundwater table depth	Measured data
Depth of ponding water/soil desaturation	Simulated by the model
Summer evapotranspiration	Simulated by the FAO-PM equation, with crop coefficient (K_c) based on a previous study in the same rice area
Winter evaporation	Simulated by the FAO-PM equation with a constant crop coefficient for water ($K_c = 1.05$)
Groundwater recharge	Simulated by using the Darcy's law under flooded conditions (K_s of the LCL is the calibration parameter), as in Facchi et al. (2018)

to be the one measured by the piezometers ($Z1$ or $Z2$) added to an offset ($\delta 1$ and $\delta 2$) obtained by calibration. With respect to hydraulic conductivities, two K_s values were calibrated: one for the old WF fields, $K_{s_{old}}$, and one for the new WF fields, $K_{s_{new}}$. During the calibration for the summer season 2018 it turned out that calibrating the K_s of 'Zan 16–18' ($K_{s_{16-18}}$) was mandatory for achieving satisfactory results. Calibration procedures were carried out through the MATLAB Global Calibration Toolbox using an objective function based on the difference between simulated and expected levels of ponding water in the paddy fields. Such expected levels are varying throughout the year, according to the phenological phases of rice and to what reported by the farmer. Table 1 summarizes water fluxes and storages considered in the model, highlighting measured and simulated ones.

3 Results and Discussion

3.1 Hydrological Balance

Table 2 summarizes the main results concerning the quantification of water fluxes and storages during winter and summer seasons in the study area. In winter the balance is computed from the start of the submersion to the drying of the fields (11-Oct-2017 to 25-Jan-2018; 14-Oct-2018 to 24-Jan-2019). In the summer period the balance was computed from 11-Apr-2018 (when the first field was water-seeded) to the 19-Aug-2018 (harvest occurred on 21-Sep-2018 on average), while the results shown in parenthesis refer only to the time period in which 100% of the fields were flooded (21-May-2018 to 19-Aug-2018). The results show that wintertime percolation rates are two fold those observed during the summer season. This could be due to higher ponding water levels within the fields, lower evaporative processes,

Table 2 Results of the hydrological balance for the study area

Variables	First winter	First summer	Second winter
Length of flooding (days)	106	130 (90)	102
Rain (mm)	117.0	260.4 (114.4)	179.8
Qin-Qout (mm)	4185.6	2388 (2030)	4141.4
Average groundwater depth Z1 (cm)	81	128 (76)	124
Average groundwater depth Z2 (cm)	147	139 (101)	158
Total storage variation ($\Delta S_w + \Delta S_s$) (mm)	149.6	29.6 (17.7)	63.2
Average ponding water depth (cm)	13.9	(12.5)	14.5
ETc (mm)	52.4	607.0 (503.0)	67.6
ETc (mm) ^a	–	712.6	–
Percolation (mm)	4100	2009 (1624)	4190
Percolation rate (mm day ⁻¹)	38.5	15.4 (17.9)	40.5
Percolation efficiency (%): Percolation/(Qin – Qout + Rain)	95.3	75.8 (75.7)	96.9
WUE (%): ET/(Qin – Qout + Rain) ^a	1.2	26.4	1.6

^acomputed on the entire season (from seeding to harvest) in the case of summertime

lower groundwater levels and, also, by higher paddy soil hydraulic conductivities in wintertime (discussed in Sect. 3.2).

3.2 Results of Calibration

The calibration process was carried out independently on the first winter and first summer. The second winter was then used to verify the calibration of the first winter.

Table 3 shows calibration results. Parameters obtained for the first winter, when used in the summer of 2018, produced ponding water levels rarely different from zero, while the summer parameters produced ponded water levels far above the physical limits of the system (more than 25 cm, which is the height of the levees). This difference is underlined by the calibrated Ks values, which halve in summer with

Table 3 Results of model calibration, including Ks (cm day⁻¹) and offsets (cm)

	Ks _{new} (cm d ⁻¹)	Ks _{old} (cm d ⁻¹)	Ks ₁₆₋₁₈ (cm d ⁻¹)	Offset high (cm)	Offset low (cm)
Winter 2017-18	0.90	0.49	0.49	–28	82
Summer 2018	0.45	0.29	0.08	0	0

respect to wintertime. Moreover, this is also confirmed by the percolation rate, which is found to be about 40 cm d^{-1} in wintertime and about 20 cm d^{-1} in summer, showing a difference that cannot be justified only on the basis of the difference in water ponding level and groundwater table depth values in the two seasons. Furthermore, old WF fields show calibrated K_s values lower than those found for new WF fields (on average about 60%, both in winter and summer times). Summer K_s value for the field ‘Zan 16–18’ is below that for old WF fields, probably due to the long submersion time.

With respect to calibrated offsets, summer offsets equal to zero are explained by the fact that in the summertime the farm is surrounded by flooded paddies, hence the groundwater table is not subject to border effects. On the contrary, in wintertime the groundwater table depth below the fields tends to be lower than the one measured in Z1 in the topographically higher block of fields (negative offset), and higher than in Z2 in the case of lower fields. Parameters calibrated for the winter 2017–2018 were used for the following winter (2018–2019; validation period) producing very good results, as ponding water levels in the fields were well in accordance with data reported in the farm-diary.

Data that is being collected in the 2019 summer season will be indispensable for obtaining more information to better explain the highlighted differences between winter and summer flooding periods.

3.3 Groundwater Levels

Groundwater levels measured during the first 18 months of investigation (October 2017–March 2019) are illustrated in Fig. 2. Despite the higher percolation rate, the groundwater level reached in the winter season is slightly lower than in the summer, and the groundwater depletion after the end of the flooding period is faster (about 1 month) compared to that observed after the summer flooding (2–2.5 months).

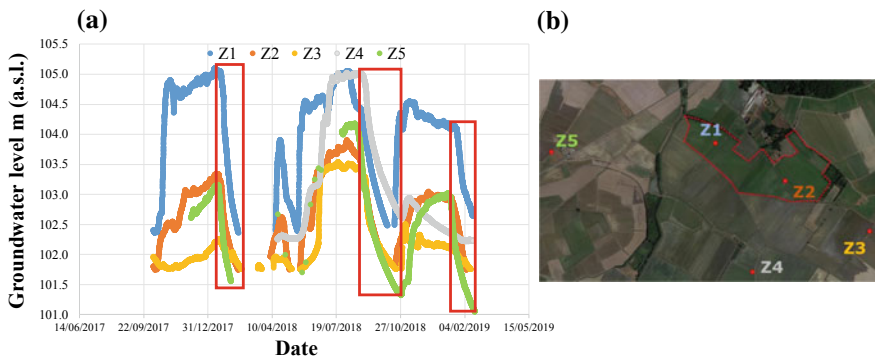


Fig. 2 Groundwater levels (m a.s.l.) monitored in the study area. Colours in (a) correspond to piezometers in (b). Red boxes highlight the groundwater depletion rates after the flooding periods

4 Conclusions

The results of the first 18 months of investigation (October 2017–March 2019) showed that: (a) WF proved to be very effective in recharging the groundwater reservoir, providing percolation rates doubled compared to those observed during summer months because of higher ponding water levels within the fields, lower evaporative processes, lower groundwater levels and probably also to higher soil hydraulic conductivities; (b) despite the higher percolation rate, the groundwater level reached in the winter season is slightly lower than in the summer, and the groundwater depletion after the end of the flooding period is faster (about 1 month) compared to that observed after the summer flooding (2–2.5 months), probably due to the larger and more compacted portion of territory flooded during summer months; (c) as a consequence, to maintain higher groundwater levels at the beginning of the cropping season, which would increase the irrigation efficiency, winter flooding should be maintained longer over time and should involve larger paddy areas.

Acknowledgements The authors wish to acknowledge Regione Lombardia for co-founding the RISTEC project (Operation 1.2.01 EU-RDP 2014–2020).

References

- Allen, R. G., Pereira, L. S., Raes, D., & Smith, M. (1998). FAO Irrigation and drainage paper No. 56. Rome Food Agric. Organ. U. N. 26–40.
- Bachand, P. A. M., Roy, S. B., Stern, N., Choperena, J., Cameron, D., & Horwath, W. R. (2016). On-farm flood capture could reduce groundwater overdraft in Kings River Basin. *California Agriculture*, 70, 200–207.
- Cesari de Maria, S., Bischetti, G. B., Chiaradia, E. A., Facchi, A., Miniotti, E. F., Rienzner, M., et al. (2017). The role of water management and environmental factors on field irrigation requirements and water productivity of rice. *Irrigation Science*, 35, 11–26.
- Chiaradia, E. A., Facchi, A., Masseroni, D., Ferrari, D., Bischetti, G. B., Gharsallah, O., et al. (2015). An integrated, multisensor system for the continuous monitoring of water dynamics in rice fields under different irrigation regimes. *Environmental Monitoring and Assessment*, 187, 586.
- Facchi, A., Rienzner, M., Cesari de Maria, S., Mayer, A., Chiaradia, E. A., Masseroni, D., et al. (2018). Exploring scale-effects on water balance components and water use efficiency of toposequence rice fields in Northern Italy. *Hydrology Research*, 49, 1711–1723.
- Niswonger, R. G., Morway, E. D., Triana, E., & Huntington, J. L. (2017). Managed aquifer recharge through off-season irrigation in agricultural regions. *Water Resources Research*, 53, 6970–6992.

Evaluation of Green Roof Ageing Effects on Substrate Hydraulic Characteristics



V. Alagna, V. Bagarello, P. Concialdi, G. Giordano and M. Iovino

Abstract The vegetated substrate of green roofs may undergo various chemical and physical changes with time. Minidisk infiltrometer (MDI) tests were conducted to assess the short-term variations of the near-saturated hydraulic conductivity, K_0 , in the extensive green roof test plot established at the University of Palermo. Sampling was repeated four times: before planting (Age 0) and then after four months (Age 1), seven months (Age 2) and ten months (Age 3). A total of 144 infiltration tests were conducted at two pressure heads, $h_0 = -3$ cm and $h_0 = -0.5$ cm and infiltration data analysed by the Zhang (Soil Science Society of America Journal 61(4):1024–1030, 1997) model. Both $K_{.3}$ and $K_{.0.5}$ underwent temporal variations resulting in final values that were higher by a factor of 3.0 and 1.4, respectively, than the initial ones. Compaction and washing off of fine particles explained the observed trend in K_0 as the lower part of the growing media enriched in fine particles and resulted in higher bulk density than the upper one. The results showed that the hydraulic properties of the growing substrate were subjected to short term modifications that may influence the hydrological performance of the green roof.

Keywords Green roofs · Growing substrate · Minidisk infiltrometer · Near-saturated soil hydraulic conductivity

1 Introduction

Green roofs can contribute to mitigate urban storm water effects by reducing the total runoff volume, peak flow rate, and delaying peak discharge time into the sewer systems (Li and Babcock 2013). The retention of rainfall and the detention of runoff are the two main processes that determine the green roof hydrological performance

V. Alagna

Department of Agricultural and Food Sciences, University of Bologna, Bologna, Italy

V. Bagarello · P. Concialdi · G. Giordano · M. Iovino (✉)

Department of Agricultural, Food and Forest Sciences, University of Palermo, Palermo, Italy
e-mail: massimo.iovino@unipa.it

© Springer Nature Switzerland AG 2020

A. Coppola et al. (eds.), *Innovative Biosystems Engineering for Sustainable Agriculture, Forestry and Food Production*, Lecture Notes in Civil Engineering 67,
https://doi.org/10.1007/978-3-030-39299-4_10

(De-Ville et al. 2018). Growth media influence both retention, i.e., the volume subsequently lost via evapotranspiration that does not become runoff, and detention, i.e., the volume that is temporary stored as it passes through the roof layers. However, while the water retention capacity of the growing media is mostly influenced by the pore size distribution, the detention performance is largely influenced by hydraulic conductivity, as this property defines the speed with which water can flow through a substrate.

Due to various chemical and physical changes, the growing media of a green roof may undergo hydrologic changes over time (Czemiel Berndtsson 2010). Getter et al. (2007) found that the pore volume doubled (from 41 to 82%) and the water-holding capacity increased from 17 to 67% after 5 years of usage. However, a review of data from 18 studies did not show any significant effect of green roof age on the annual runoff volume (Mentens et al. 2006). Studies addressing the short-term changes of hydraulic characteristics of green roofs are lacking. De-Ville et al. (2018) found that the sub-annual (seasonal) variation in retention and detention performance of green roof may be greater than the long-term ones. Time variable hydrophobicity of the substrate was hypothesised as responsible of short-term trends. However, in the study by De-Ville et al. (2018) the variation in detention performance were inferred from overall hydrological functioning of the green roof whereas a specific assessment of the hydraulic characteristics of the growing substrate was not conducted.

Measurement of soil hydraulic conductivity is time-consuming and, given to its small scale spatial variability, estimation of a representative value, even at the plot scale, needs to sample a large number of tests (Bagarello et al. 2013). Especially close to saturation, hydraulic conductivity should be measured directly in the field to minimize disturbance of macropores connectivity while maintaining its functional connection with the surrounding soil (Angulo-Jaramillo et al. 2016). In situ infiltrometer techniques are becoming very popular because the experiments are relatively easy, rapid and inexpensive (Alagna et al. 2016). The mini disk infiltrometer (MDI, Decagon Devices Inc., Pullman, WA), due to its compact size, is particularly suitable for applications in sites where extremely variable microtopography or dense vegetation limit the use of larger infiltrometers (Gadi et al. 2017). Moreover, it samples the upper surface layer with a minimum disturbance, thus preventing alteration of the sampled pore space (Alagna et al. 2013). Either steady-state or transient solutions have been proposed to determine soil hydraulic conductivity from MDI data (Dohnal et al. 2010) but, due to the limited depth of the growing media, steady state approaches can be hindered by violations of homogeneous and isotropic soil assumption. Furthermore, transient flow means shorter experiments and increased number of sampling points, which is of particular interest for spatial/temporal variability studies (Vandervaere et al. 2000).

The transient method proposed by Zhang (1997) consist of fitting the two-term model (Philip 1957) to the measured cumulative infiltration data and then estimating soil sorptivity and near-saturated hydraulic conductivity from the model coefficients, C_1 and C_2 . Zhang's idea to relate the coefficient C_2 only to gravity forces was questioned as sorptivity accounting for lateral capillarity flow from a circular source should appear in coefficient C_2 (Angulo-Jaramillo et al. 2016). Notwithstanding this,

the Zhang's model (ZH) seems to provide a useful procedure (Dohnal et al. 2010) and has been frequently used to analyse the data collected by the MDI (Gadi et al. 2017; Li et al. 2005; Lichner et al. 2007).

The present study investigated the temporal changes in the substrate near-saturated hydraulic conductivity of an extensive green roof. At this aim, MDI experiments were conducted at the time of vegetation planting and then repeated three times during the first year of green roof functioning.

2 Materials and Methods

The extensive green roof experimental plot at the Department of Agricultural, Food and Forest Sciences of University of Palermo was settled in October 2017 (Fig. 1). It covers a plane surface of 18 m² (3 m width by 6 m long) directly connected to a drainpipe instrumented with a discharge measurement system specifically calibrated to measure the drainage flow. The green roof was built with "Mediterranean green roof system" supplied by HARPO verdepensile (Trieste, Italy). The system is around 11 cm thick and consists of a drainage and accumulation bottom layer and an overlying growing substrate (approximately 8 cm high) made of a mixture of lapillus, pumice and zeolites (total mineral fraction 80% by weight), with compost and acidic peat.

The green roof was planted in January 2018 with *Sedum sediforme* at a density of 70 sprouts m⁻². Negligible plant failure were observed during the monitoring period. The water retention characteristic of the substrate was determined by a combination of hanging water column apparatus and pressure plate extractors on four replicated soil cores (diameter $d = 8$ cm, height $h = 5$ cm) packed at a bulk density value close



Fig. 1 Experimental green roof plot at the time the first sampling campaign (Age 0) (a); MDI device used for infiltration tests (b)

to the mean value measured in the experimental plot ($\rho_b = 0.828 \text{ g cm}^{-3}$). Infiltration tests were performed by a MDI manufactured by Decagon (Decagon Devices, Inc., Pullman, WA) having a disk radius, r_0 , of 2.25 cm. Two sampling sites were randomly established inside each of the 18 blocks ($1 \times 1 \text{ m}^2$) in which the experimental plot was subdivided and infiltration tests were conducted at pressure head, h_0 , values of -0.5 cm and -3 cm to explore different near-saturated soil conditions. A total of 144 infiltration tests were conducted during the four sampling campaigns. The first sampling campaign was conducted on December 2017 some days before vegetation planting (Age 0). The second, third and fourth sampling campaigns were conducted on April 2018 (Age 1), July 2018 (Age 2) and October 2018 (Age 3). Each campaign was completed in maximum three days to explore similar initial soil water content. Mean daily air temperature at each age was 13.8, 18.4, 29.5 and 25.7 °C, respectively. The sampling surface was carefully levelled before MDI application, to assure a good hydraulic contact between the porous disk and the soil. Visual readings of the water level in the MDI supply tube were taken at fixed time intervals until the complete emptying of the reservoir.

Fitting of the ZH model to the cumulative infiltration, I (mm), vs. time, t (h), data was conducted by a non-linear fitting technique. Given capillarity can be ignored at long times, estimation of soil hydraulic conductivity is expected to be more accurate as time increases (Zhang 1997). Thus, no time limitation was considered and estimation of C_1 and C_2 was obtained from the entire $I(t)$ data. The near-saturated soil hydraulic conductivity, K_0 (mm h^{-1}), was estimated by:

$$K_0 = \frac{C_2}{A_2} \quad (1)$$

in which A_2 is dimensionless coefficient that depends on the parameters n and α of the van Genuchten (1980) water retention model:

$$A_2 = \frac{11.65(n^{0.1} - 1)\exp[7.5(n - 1.9)\alpha h_0]}{(\alpha r_0)^{0.91}} \quad (2)$$

According to the measured water retention characteristic, $n = 1.6615$ and $\alpha = 0.0149 \text{ cm}^{-1}$ were assumed. Soil hydraulic conductivity data were corrected to account for the effect of temperature on water viscosity (Bagarello and Iovino 2010).

The experimental plot was also sampled at the end of the monitoring period (i.e., November 2018) to detect any change in substrate bulk density and particle size distribution. Eight undisturbed soil cores were collected at randomly selected points by gently pushing stainless steel cylinders ($d = 8.5 \text{ cm}$, $h = 11 \text{ cm}$) into the growing substrate. Soil outside the cylinder's wall was progressively removed during sampling to limit soil compaction due to the applied pressure. Soil samples were then sectioned in laboratory to determine the dry bulk density and the PSD of the upper (i.e., 0 to 4 cm depth) and lower (i.e. 4 to 8 cm depth) halves of the substrate. Nine particle size fractions in the range 9.53 to 0.25 mm were determined by mechanical sieving. Presence of roots was annotated and, when possible, their weight was determined.

The statistical frequency distribution of K_0 data was assumed to be ln-normal as commonly found for this soil property (Warrick 1998) also considering the heterogeneous nature of this anthropogenic porous media. Therefore, geometric means and associated coefficients of variation, CVs, were calculated to summarize the data using the appropriate ln-normal equations (Lee et al. 1985). Comparison among mean K_0 data collected at the different sampling campaigns were conducted by a Tukey Honestly Significant Difference test ($P = 0.05$).

3 Results and Discussion

The growing substrate went through modifications during the first year of operation (Table 1). Between Age 0 and Age 1, no change in near-saturated hydraulic conductivity ($K_{-0.5}$) or a reduction (K_{-3}) was observed. In particular, K_{-3} decreased by a factor of 2.3 while the associated CV increased more than two-fold and the minimum value decreased by a factor of 7. The third sampling campaign (July) resulted in a significant increase of both K_{-3} and $K_{-0.5}$. Compared to the values at the time of installation (Age 0), the mean hydraulic conductivity increased by a factor of 3–3.7 depending on the applied pressure head (Table 1). Spatial variability was comparable (K_{-3}) or lower than that observed at Age 0. In the following three months (July to October), a reduction of unsaturated hydraulic conductivity was observed that was significant at the highest pressure head given that $K_{-0.5}$ decreased by a factor of two (Table 1). The spatial variability of K_{-3} was unaffected while it increased for $K_{-0.5}$. The near-saturated hydraulic conductivity at the end of the monitoring period was significantly higher than the initial one by a factor of 3.0 and 1.4 at $h_0 = -3$ and -0.5 cm, respectively.

Temporal modifications of growing substrate hydraulic conductivity were more considerable at the lower pressure head value, that is for the relatively smaller pore classes. Soil compaction and washing off of fine particles could explain the observed trend in K_0 . Between the first two sampling dates, a total of 440.6 mm of rainfall occurred that is around 59% of the average year precipitation for the area of Palermo (period 2003–2017). Compaction due to the kinetic energy of raindrops and occlusion

Table 1 Statistics of near-saturated soil hydraulic conductivity, K_0 (mm h^{-1}), estimated at the different sampling campaigns

	K_{-3}				$K_{-0.5}$			
	Age 0	Age 1	Age 2	Age 3	Age 0	Age 1	Age 2	Age 3
<i>N</i>	18	18	18	18	18	18	18	18
min	0.68	0.06	2.37	2.20	2.31	4.23	13.04	3.81
max	2.71	1.63	9.67	9.56	14.39	15.67	36.95	20.19
GM	1.45a	0.62b	5.38c	4.38c	8.13a	8.06a	24.36c	11.52b
CV%	42.3	129.9	51.2	48.0	54.7	29.3	24.4	53.0

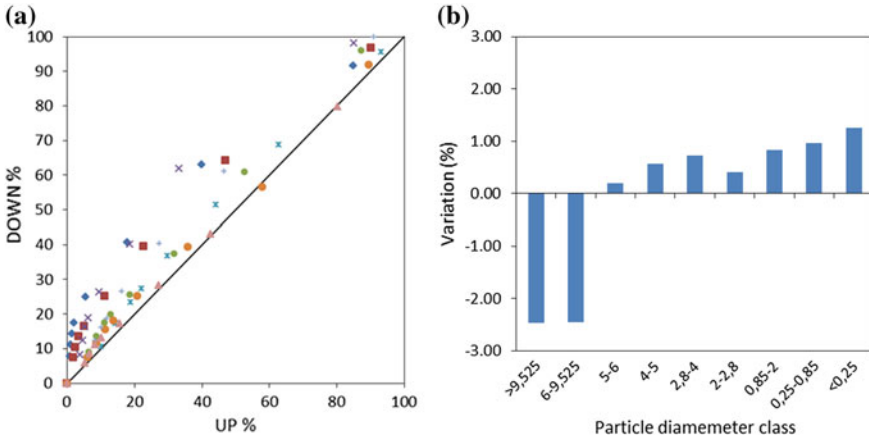


Fig. 2 Comparison between particle size distribution of the upper (0–4 cm, UP) and lower (4–8 cm, DOWN) layer of the growing substrate after ten months. Mass fraction of particle (%) having a diameter lower than a fixed one (a), and mean variation (%) of mass fraction for lower layer (b)

of smaller pores due to mobility of detached particles can be the main cause for the initial reduction of K_{-3} . Smaller particles are relatively more susceptible to structural changes due to the mechanical actions and the highest spatial variability observed at Age 1 is another indirect sign that these fractions underwent larger modifications.

As a consequence of heavy rainfall, fine particles were also washed off from the surface layer thus determining the increase of K_0 that was observed at the successive sampling dates. Figure 2a compares the final percentage mass fraction of particles having a diameter lower than a fixed value for the upper (0–4 cm) and the lower (4–8 cm) part of the growing substrate. Identity line stands for no modification. For seven out of eight samples, a modification of particle size distribution between the two layer was observed. As a matter of fact, after ten months of operation, the particle size distribution of the lower layer showed a higher frequency of fine particles (diameter, ϕ , smaller than 6 mm) and a lower frequency of coarse ones ($\phi > 6$ mm) (Fig. 2b).

According to these findings, washing off of fine particles occurred as confirmed also by the bulk density increase in the lower layer. Indeed, the mean bulk density of the 4–8 cm layer ($\rho_b = 0.985 \text{ g cm}^{-3}$, CV = 9.5%, $N = 8$) was significantly higher than the one of the surface layer ($\rho_b = 0.707 \text{ g cm}^{-3}$, CV = 13.8%, $N = 8$). This is also an expected consequence of the composition of the growing media that is a mixture of large and relatively lighter pumice particles with small and more massive mineral particles. As a consequence of selective migration, the surface layer become lighter and more porous. The reduction of K_0 occurring between Age 2 and Age 3 can be attributed to the mechanical consolidation due to root development that was particularly effective between July and October (Fig. 3). Root residues were observed into both the upper and lower part of each sample. Despite not accurately measurable, the mean root density (RD) was higher in the upper layer (RD = 0.84%) as compared to lower layer (RD = 0.12%). It is expected that roots develop into

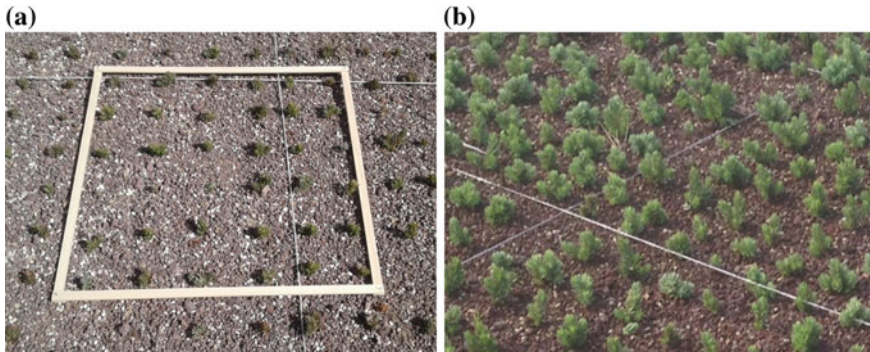


Fig. 3 Sedum stages at the Age 2 (a) and Age 3 (b) sampling dates

relatively larger pores of the upper layer, thus the observed reduction in $K_{-0.5}$, and not in K_{-3} , between Age 2 and Age 3 is consistent with this hypothesis.

The MDI experiment, that basically sampled the upper layer, was able to detect such temporal trend and, therefore, it can be considered suitable for investigating the temporal variations of growing media hydraulic characteristics due to ageing. It should be considered that MDI tests were conducted only at the surface layer and, probably, an analysis conducted at different depths could have contributed to better understand the effect of ageing on the temporal variability of growing substrate K_0 . However, the collected results consistently showed that growing substrate underwent significant modifications of physical and hydraulic properties, even in relatively short time, essentially due to washing off of fine particles from the upper layer followed by mechanical consolidation as plant roots developed.

4 Conclusions

Due to its compact size and limited disturbance of the sampled surface, the MDI proved to be valuable device for assessing the differences in pore size arrangement of a growing substrate due to compaction, disruption and migration of fine particles. Unsaturated hydraulic conductivity at the end of the ten months monitoring period was higher than the initial one by a factor of 1.4–3.0, depending on the applied pressure head at the MDI disk. More in detail, a higher temporal variability in K_{-3} was observed as compared to $K_{-0.5}$ that was attributed to larger changes occurring for the relatively smaller pore classes. Soil compaction and washing off of fine particles, that are more susceptible to the mechanical disruption operated by rainfall, were considered the main causes of the observed modifications. As matter of fact, the bulk density and the relative percentage of fine particles increased in the lower part of the growing media (i.e. 4 to 8 cm depth) as compared to the upper one (0 to 4 cm). A role was played also by the roots growth that determined a reduction of

$K_{0.5}$ as a consequence of larger pore occlusions. It was concluded that the hydraulic conductivity of the growing substrate may undergo considerable changes, even in relatively short time, that directly affect the detention time of the green roof. In particular, an increase of hydraulic conductivity by a factor of two is expected to reduce by a similar factor the time delay in the hydrograph peak thus threaten the green roof hydrological performance.

Acknowledgements This work was supported by the Ministero dell'Istruzione, dell'Università e della Ricerca of Italy [PRIN 2015—GREEN4WATER—CUP B72F16000550005]

References

- Alagna, V., Bagarello, V., Di Prima, S., Giordano, G., & Iovino, M. (2013). A simple field method to measure the hydrodynamic properties of soil surface crust. *Journal of Agricultural Engineering*, *XLIV*(s2), e14.
- Alagna, V., Bagarello, V., Di Prima, S., & Iovino, M. (2016). Determining hydraulic properties of a loam soil by alternative infiltrometer techniques. *Hydrological Processes*, *30*, 263–270.
- Angulo-Jaramillo, R., Bagarello, V., Iovino, M., & Lassabatere, L. (2016). *unsaturated soil hydraulic properties, infiltration measurements for soil hydraulic characterization*. Springer International Publishing, Cham, pp. 181–287.
- Bagarello, V., Di Stefano, C., Iovino, M., & Sgroi, A. (2013). Using a transient infiltrometric technique for intensively sampling field-saturated hydraulic conductivity of a clay soil in two runoff plots. *Hydrological Processes*, *27*(24), 3415–3423.
- Bagarello, V., & Iovino, M. (2010). Conducibilità idraulica del suolo. Metodi di misura nelle applicazioni idrologiche. Hoepli, Milano. 382 pp. (in Italian).
- Czemieli Berndtsson, J. (2010). Green roof performance towards management of runoff water quantity and quality: A review. *Ecological Engineering*, *36*(4), 351–360.
- De-Ville, S., Menon, M., & Stovin, V. (2018). Temporal variations in the potential hydrological performance of extensive green roof systems. *Journal of Hydrology*, *558*, 564–578.
- Dohnal, M., Dusek, J., & Vogel, T. (2010). Improving hydraulic conductivity estimates from mini-disk infiltrometer measurements for soils with wide pore-size distributions. *Soil Science Society of America Journal*, *74*(3), 804.
- Gadi, V. K., Tang, Y.-R., Das, A., Monga, C., Garg, A., Berretta, C., et al. (2017). Spatial and temporal variation of hydraulic conductivity and vegetation growth in green infrastructures using infiltrometer and visual technique. *CATENA*, *155*, 20–29.
- Getter, K. L., Rowe, D. B., & Andresen, J. A. (2007). Quantifying the effect of slope on extensive green roof stormwater retention. *Ecological Engineering*, *31*(4), 225–231.
- Lee, D. M., Reynolds, W. D., Elrick, D. E., & Clothier, B. E. (1985). A comparison of 3 field methods for measuring saturated hydraulic conductivity. *Canadian Journal of Soil Science*, *65*(3), 563–573.
- Li, X.-Y., González, A., & Solé-Benet, A. (2005). Laboratory methods for the estimation of infiltration rate of soil crusts in the Tabernas Desert badlands. *CATENA*, *60*(3), 255–266.
- Li, Y., & Babcock, R. W., Jr. (2013). Green roof hydrologic performance and modeling: A review. *Water Science and Technology*, *69*(4), 727–738.
- Lichner, L., Hallett, P. D., Feeney, D. S., Dugova, O., Sir, M., & Tesar, M. (2007). Field measurement of soil water repellency and its impact on water flow under different vegetation. *Biologia*, *62*(5), 537–541.
- Mentens, J., Raes, D., & Hermy, M. (2006). Green roofs as a tool for solving the rainwater runoff problem in the urbanized 21st century? *Landscape Urban Plan*, *77*(3), 217–226.

- Philip, J. R. (1957). The theory of infiltration: 1. The Infiltration equation and its solution. *Soil science*, 83(5), 345–358.
- van Genuchten, M. T. (1980). Closed-form equation for predicting the hydraulic conductivity of unsaturated soils. *Soil Science Society of America Journal*, 44(5), 892–898.
- Vandervaere, J.-P., Vauclin, M., & Elrick, D.E. (2000). Transient Flow from Tension Infiltrometers I. The Two-Parameter Equation. *Soil Science Society of America Journal*, 64(4), 1263–1272.
- Warrick, A. W. (1998). *Appendix 1: Spatial variability*. pp. 655–675. In D. Hillel (ed.), *Environmental Soil Physics*, Academic Press, San Diego.
- Zhang, R. D. (1997). Determination of soil sorptivity and hydraulic conductivity from the disk infiltrometer. *Soil Science Society of America Journal*, 61(4), 1024–1030.

Influence of Site and Check Dam Characteristics on Sediment Retention and Structure Conservation in a Mexican River



Manuel E. Lucas-Borja, Demetrio A. Zema, Yang Yu, Mary Nichols, Giuseppe Bombino, Pietro Denisi, Antonino Labate, Bruno G. Carrà, Xu Xiangzhou, Bruno T. Rodrigues, Artemi Cerdà and Santo Marcello Zimbone

Abstract Previously, in a large river of Mexico regulated by more than 200 check dams, we demonstrated that vegetation cover and channel characteristics were the dominant factors on the structure conditions and capacity to store sediments. This study focuses on other categorical (i.e., check dam type and location, soil texture and land use) and numerical (i.e. water discharge, check dam dimensions) variables, to whom statistical analysis is applied, in order to assess their influence on sediment filling degree and conditions (functional or destroyed) of the check dams in the same river. ANOVA has shown that: (i) check dam type (gabion or stone) and location (headwater, middle or valley reaches), and soil texture significantly influence the sediment filling degree of structures; (ii) vegetation cover of the drained sub-watersheds, water discharge, channel width and check dam upstream depth significantly affect the structure conditions (functional or destroyed). PCA has provided two derivative variables, related to the geomorphological characteristics of channels and vegetation cover, to whom sediment retention behind check dams is related.

M. E. Lucas-Borja · B. T. Rodrigues

Departamento de Ciencia y Tecnología Agroforestal y Genética, Universidad de Castilla La Mancha, Campus Universitario, 02071 Albacete, Spain

D. A. Zema (✉) · G. Bombino · P. Denisi · A. Labate · B. G. Carrà · S. M. Zimbone

Department “Agraria”, University “Mediterranea” of Reggio Calabria, Località Feo di Vito, 89122

Reggio Calabria, Italy

e-mail: dzema@unirc.it

Y. Yu

Department of Sediment Research, China Institute of Water Resources and Hydropower Research, Beijing 100048, China

M. Nichols

Southwest Watershed Research Center, USDA-ARS, 2000 E. Allen Rd, Tucson, AZ, USA

X. Xiangzhou

School of Hydraulic Engineering, Dalian University of Technology, Dalian 116024, China

A. Cerdà

Soil Erosion and Degradation Research Group, Department of Geografia, University of Valencia, Blasco Ibáñez, 28, 46010 Valencia, Spain

© Springer Nature Switzerland AG 2020

A. Coppola et al. (eds.), *Innovative Biosystems Engineering for Sustainable Agriculture,*

Forestry and Food Production, Lecture Notes in Civil Engineering 67,

https://doi.org/10.1007/978-3-030-39299-4_11

Keywords Soil erosion · Vegetation cover · Land use · Soil characteristics · Regulated river · Water discharge

1 Introduction

Check dams have been installed for controlling water flow and conserving soil in watersheds of many regions all over the world, as, for instance, in Italy, Ethiopia, Spain, China and USA (Abbasi et al. 2019). However, their desired impacts on river hydrology, geomorphology and ecology are sometimes not achieved, due to reasons such as poor construction quality, improper location and inadequate design. From many examples worldwide, it appears that, after construction, the most important features that influence check dam function within the watershed system are sediment storage capacity and structural conditions (Nyssen et al. 2004; Lucas-Borja et al. 2018). However, there is limited information describing the influence of structure characteristics and site factors (such as river hydrology, channel and check dam geometry as well as land use and soils), on conditions of the check dams and their effectiveness for soil conservation at the watershed scale (Castillo et al. 2007) moreover, porous rock check dams are not deeply researched (Nichols and Polyakov 2019). In a previous work, vegetation cover and channel characteristics have been shown to be dominant factors influencing the *post operam* conditions of check dams and their ability to store sediments in a large regulated river of Mexico (Lucas-Borja et al. 2018). A more comprehensive evaluation of the influence of other factors (for instance, site and check dam characteristics as well as channel hydrology) on functioning (in terms of sediment storage) and conditions (intact or destroyed) of check dams may be of help to watershed managers, in order to reduce check dam failure, accomplish the expected response, and increase the confidence in using check-dams as restoration tools at the watershed level. We hypothesize that check dam and channel dimensions, site features (e.g., soil and land use of the drained sub-watersheds), sediment filling degree behind the structures and hydrology may influence the structural conditions and functioning of the control works installed in the watershed.

To address these hypotheses, the ANalysis Of VAriance (ANOVA) and Principal Component Analyses (PCA) have been applied to the large dataset of check dam and site characteristics of the regulated watershed studied by Lucas-Borja et al. (2018). In more detail, ANOVA has separately evaluated the influence of some categorical and numerical variables (measuring as many site and check dam characteristics) on sediment filling degree and condition (functional or destroyed) of the check dams. PCA was used to link the derivative variables (principal components) to the numerical original variables, explaining check dam functioning.

2 Materials and Methods

2.1 The Studied Watershed

The watershed under investigation (Culiacan River, Mexico), which covers a total area of 10368 km², drains into the Sinaloa reservoir at an elevation of 128 m after running 25.3 km from the headwater (Fig. 1). Topography ranges from mountains to lower lying hilly areas and plains. Average annual precipitation is 860 mm, mostly occurring in summer, and the mean annual temperature is 25 °C. The watershed is covered mainly by cropland (sorghum and corn) and protective forest. Soils can be classified as *Eutric regosols*, *Cromic vertisol* and *Haplic feozem*. In the watershed drainage network, approximately 270 small, temporary, stone check dams were recently built (2011–2015) across swales and drainage ditches. Many of these check dams are intact, but others have failed or damaged. The maximum height of the stone check dams is 3 m; to increase their stability, the base of each check dams is embedded into the soil approximately at 1 m depth. The structures were built as part of an “emergency” strategy to potentially control the channel grade and mitigate channel erosion; thus, it was expected that these control works would start functioning immediately after their installation, and this short-term monitoring activity can verify that they are functioning as anticipated.

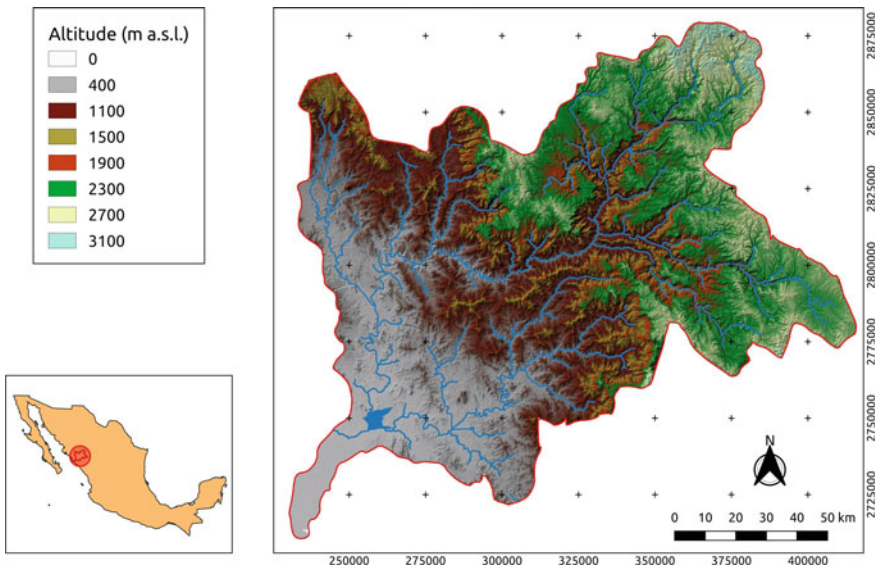


Fig. 1 Geographical location and map of Culiacan River (Mexico) with the location of the Sinaloa reservoir

2.2 Data Collection

The check dam dataset has been prepared using a combination of field surveys (measuring check dam and channel geometry) and remotely sensed data (for vegetation cover, land use and soil characteristics of the drained sub-watersheds) and digital terrain models (for the original and regulated channel profiles). A complete dataset was available for 206 out of the 273 check dams installed in the watersheds. Field data included both categorical and numerical variables. Categorical data for the check dams were *type* (gabion or stone), *condition* (functional or destroyed, related to check dam conservation), and *location* (headwater, middle or valley reaches). For each treated sub-watershed, *soil type and texture*, and *land use* were determined (Table 1).

The numerical variables were related to: *check dam dimensions* (width, and upstream and downstream height); *site features* (longitudinal slope and vegetation cover of the drained sub-watershed); *sediment retention* (initial capacity and filling degree); *channel geometry* (mean width and length) and *hydrology* (water discharge) associated with each check dam. In the absence of direct measures, water discharge in the active channel was estimated using Manning's equation based on channel dimensions and riverbed roughness. As regards check dam condition, each structure is classified as functional, if it is completely or partially filled with sediments, or destroyed, if it has completely collapsed and thus it is not functioning. With regards

Table 1 Categorical data related to check dam and drained sub-watershed characteristics (Culiacan River, Mexico)

Check dam			Soil characteristics of the drained sub-watershed		
Condition	Type	Location	Type	Texture	Land use
Functional (189)	Gabion (106)	Headwater (44)	Haplic Feozem (46)	Loamy-silty (93) Sandy-loamy (95)	Farming/grazing (13) Forest (175)
	Stone (82)	Middle (31) Valley (113)	Eutric Regosol (57) Cromic Vertisol (85)		
Destroyed (17)	Gabion (8)	Headwater (5)	Haplic Feozem (14)	Loamy-silty (14) Sandy-loamy (3)	Farming/grazing (4) Forest (13)
	Stone (9)	Middle (8) Valley (4)	Eutric Regosol (3) Cromic Vertisol (0)		

Note in brackets the number of check dams in each class is reported

to the sediment stored behind each check dam, the initial storage capacity and filling degree of sediments—the latter considered as the ratio of actual sediment storage and the initial storage capacity—were estimated from the regulated and the original longitudinal profiles, and from check dam dimensions. It has been assumed that the deposited sediment volume behind a check dam has a prismatic shape with a trapezoidal section.

2.3 Statistical Processing

ANOVA was used to evaluate the influence of: (i) the categorical variables (check dam type and location as well as soil type, texture and land use of the drained sub-watersheds) on sediment filling degree of functional check dams; (ii) the numerical variables (check dam dimensions, site features, sediment retention, channel geometry and hydrology) on check dam condition. The post hoc LSD (least square difference) test was used to explore statistical differences between the different levels of each studied variable. PCA was applied to the numerical variables, considered as explanatory, in order to elucidate their influence on sediment filling degree of the check dams (considered as response variable). PCA was carried out after standardisation and orthogonal transformation of the original variables. All statistical analyses were conducted using the R software version 3.2.4.

3 Results and Discussions

In the experimental watershed, the sediment filling degree of functional check dams is significantly influenced by the construction type and location (Table 2). The importance of the material and technique used for check dam construction in their integrity

Table 2 Results of the ANOVA used to evaluate the influence of categorical variables on sediment filling degree of functional check dams in the Culiacan River (Mexico)

Categorical (explanatory) variable	Response variable	
	(sediment filling degree of check dam)	
	F value	Pr (>F)
Check dam ⁺ type	47.90	0.0001***
Check dam ⁺ location	15.59	0.0001***
Sub-watershed land use	1.08	0.2994
Sub-watershed soil type	1.63	0.3800
Sub-watershed soil texture	8.38	0.0043**

Note *** = $p < 0.001$; ** = $p < 0.01$; * = $p < 0.05$; + Only functional check dams are considered

and functioning was stated also by other authors (i.e., Nyssen et al. 2004; Zhou et al. 2004).

The results of the LSD tests have demonstrated that the sediment filling degree is higher for check dams made of stone and located at the middle reaches compared to structures made of gabions and installed in middle and valley reaches, respectively (Table 3). The first evidence may be due to the higher porosity of gabions to water and sediments compared to stones, while the second evidence may be explained by the buffering effect of banks in some upper and valley reaches, which store sediment before entering in the river channel.

Vegetation cover, sediment filling degree, water discharge, channel width and check dam upstream depth are the factors that significantly influence check dam conditions (Table 4). As a matter of fact, in those streams, where channels are narrower and vegetation cover is more developed, water discharge and sediment flows are lower; thus the dynamic actions on check dams decrease with higher structure

Table 3 Sediment filling degree (mean \pm standard error) for each categorical variable of functional check dams in the Culiacan River (Mexico)

Check dam						
Type			Location			
Gabion	Stone		Headwater	Middle reach	Valley reach	
54.6 \pm 2.5a	81.2 \pm 2.8b		54.2 \pm 3.3a	79.7 \pm 3.2b	62.5 \pm 3.8a	
Sub-watershed						
Soil type			Soil texture		Land use	
Haplic Feozem	Eutric Regosol	Cromic Vertisol	Loamy-silty	Sandy-loamy	Farming/grazing	Forest
62.0 \pm 3.1a	45.0 \pm 8.4a	45.4 \pm 8.5a	64.5 \pm 2.7a	87.6 \pm 7.6b	59.6 \pm 6.7a	67.0 \pm 2.7a

Note different lowercase letters indicate statistically significant differences ($p < 0.05$) according to the LSD test

Table 4 Results (mean \pm standard error) of ANOVA to evaluate the influence of numerical variables on condition of check dams in the Culiacan River (Mexico)

Check dam condition	Site features		Sediment retention		Hydrology
	Longitudinal slope (%)	Vegetation cover (%)	Initial capacity (m ³)	Sediment filling degree (%)	Water discharge (m ³ /s)
Functional	7.12 \pm 0.48a	15.66 \pm 1.89a	67.23 \pm 5.72a	44.84 \pm 1.38a	15.68 \pm 3.59a
Destroyed	7.84 \pm 1.16a	46.47 \pm 7.82b	80.26 \pm 9.31a	0.08 \pm 0.02b	40.37 \pm 19.93b
	Channel geometry		Check dam dimensions		
	length (m)	width (m)	Downstream depth (m)	Upstream depth (m)	width (m)
Functional	15.47 \pm 0.73a	6.93 \pm 0.29a	1.10 \pm 0.09a	0.51 \pm 0.02a	6.53 \pm 0.23a
Destroyed	14.61 \pm 1.89a	8.54 \pm 0.75b	1.14 \pm 0.09a	0.63 \pm 0.05b	7.15 \pm 0.98a

Note different lower case letters indicate statistically significant differences ($p < 0.05$) according to the LSD test

stability (Lucas-Borja et al. 2018; Keesstra et al. 2018). Destroyed check dams are associated to a reduced functioning, since their sediment wedge has lower sediment filling degree and higher upstream depth compared to functional structures. The longitudinal slope and length of channels do not significantly affect the check dam condition (Table 4). This could be explained by the relatively relief of the watershed (with less than 150 m difference in elevation between the upper and the lower part of the watershed) and the very similar channel length between two consecutive check dams in many reaches.

PCA applied to the numerical factors (explanatory variables) and sediment filling degree of check dams (response variable) has provided two Principal Components (PCs), which together explain more than 70% of the variance of the original variables. Channel width (factor loading of 0.455) and length (0.378), as well as the initial capacity of sediment retention (0.355) and check dam downstream depth (0.432) are associated to PC1, while only the vegetation cover is associated to the PC2 (factor loading of -0.957) (Fig. 2). The remaining variables—longitudinal slope, check dam upstream depth and width, and water discharge—have lower influence on both PCs. Clearly and as expected (e.g., Zema et al. 2018; Lucas-Borja et al. 2018), the two selected PCs are separately related to different parameters, linked to geomorphological factors (PC1) and ecological features (PC2). These results are consistent with findings of other studies focusing the effects of check dams on river

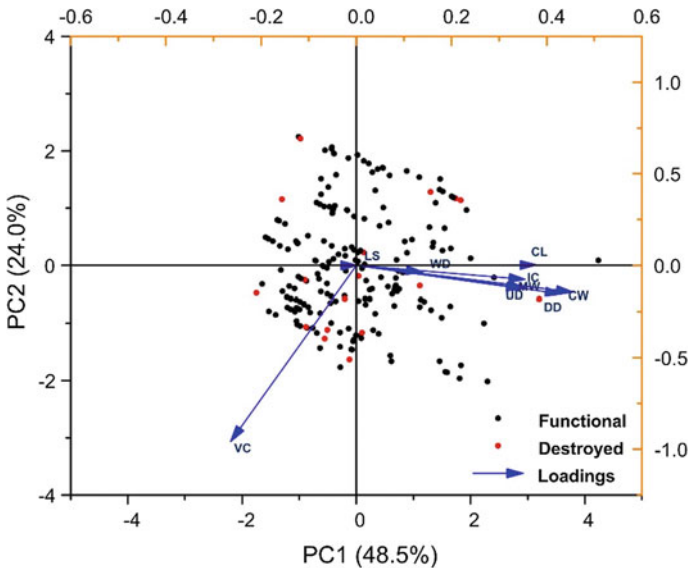


Fig. 2 Biplot of PCA applied to numerical factors (explanatory variables) and sediment filling degree (response variable) of check dams in the Culiacan watershed (Mexico). (VC: Vegetation cover, LS: Longitudinal slope, CL: Channel length, CW: Channel width, IC: Initial sediment capacity, WD: Water discharge, UD: Upstream depth of check dam, DD: Downstream depth of check dam, MW: Mean width of check dam)

geomorphology and ecology (e.g., Bombino et al. 2019). Moreover, and unexpectedly (e.g, differently from findings of Zema et al. 2018), the hydraulic regime of the sub-watershed has not found to be an influencing factor on the sediment retention. This may be explained by the fact that the disruptive action exerted on the check dam during a flood can be mainly due to the sediment flow rather than the water discharge. No clusters of functional and destroyed check dams are evident from the analysis (Fig. 2).

4 Conclusions

This study has demonstrated that, among the hypothesized site and check dam characteristics of a large regulated watershed in Mexico, location (headwater, middle or valley reaches) and type (gabion or stone) of the structures as well as the soil texture significantly influence the sediment filling degree of check dams, while soil type and land use play a minor influence on sediment retention. The structural conditions (functional or destroyed) of the check dams are significantly influenced by the vegetation cover, water discharge and channel width, but not by the longitudinal slope and length of the channels where the structures are installed. PCA has provided two derivative variables, which are mainly related to channel dimensions and vegetation cover, respectively, thus demonstrating the influence of river features on sediment retention behind check dams. The output of these statistical models has allowed the identification of the dominant factors affecting both the structural condition of the check dams and their capacity to store sediment. Overall, the influence of check dam construction technique and location as well as vegetation cover and water discharge must be considered with care in developing the best strategies for soil conservation in watersheds regulated with check dams.

Acknowledgements Yang Yu received the National Natural Science Foundation of China (41501091) and the young elite scientist sponsorship program by China Association for Science and Technology (2017 to 2019).

References

- Abbasi, N. A., Xu, X., Lucas-Borja, M. E., Dang, W., & Liu, B. (2019). The use of check dams in watershed management projects: Examples from around the world. *Science of the Total Environment*, 676, 683–691.
- Bombino, G., Zema, D. A., Denisi, P., Lucas-Borja, M. E., Labate, A., & Zimbone, S. M. (2019). Assessment of riparian vegetation characteristics in Mediterranean headwaters regulated by check dams using multivariate statistical techniques. *Science of the Total Environment*, 657, 597–607.
- Castillo, V. M., Mosch, W. M., García, C. C., Barberá, G. G., Cano, J. N., & López-Bermúdez, F. (2007). Effectiveness and geomorphological impacts of check dams for soil erosion control in a semiarid Mediterranean catchment: El Cárcavo (Murcia, Spain). *Catena*, 70, 416–427.

- Keesstra, S., Nunes, J., Novara, A., Finger, D., Avelar, D., Kalantari, Z., et al. (2018). The superior effect of nature based solutions in land management for enhancing ecosystem services. *Science of the Total Environment*, 610, 997–1009.
- Lucas-Borja, M. E., Zema, D. A., Guzman, M. D. H., Yang, Y., Hernández, A. C., Xiangzhou, X., et al. (2018). Exploring the influence of vegetation cover, sediment storage capacity and channel dimensions on stone check dam conditions and effectiveness in a large regulated river in México. *Ecological Engineering*, 122, 39–47.
- Nichols, M. H., & Polyakov, V. O. (2019). The impacts of porous rock check dams on a semiarid alluvial fan. *Science of the Total Environment*, 664, 576–582.
- Nyssen, J., Veyret Picot, M., Poesen, J., Moeyersons, J., Haile, M., Deckers, J., et al. (2004). The effectiveness of loose rock check dams for gully control in Tigray, northern Ethiopia. *Soil Use and Management*, 20, 55–64.
- Zema, D. A., Bombino, G., Denisi, P., Lucas-Borja, M. E., & Zimbone, S. M. (2018). Evaluating the effects of check dams on channel geometry, bed sediment size and riparian vegetation in Mediterranean mountain torrents. *Science of the Total Environment*, 642, 327–340.
- Zhou, Xu X, Zhang, H., & Zhang, Y. (2004). Development of check-dam systems in gullies on the Loess plateau, China. *Environmental Science & Policy*, 7, 79–86.

Comparing LAI Field Measurements and Remote Sensing to Assess the Influence of Check Dams on Riparian Vegetation Cover



G. Romano, G. F. Ricci and F. Gentile

Abstract The Cammarota stream is located in Northern Puglia (Southern Italy) and is characterized by the presence of intact and destroyed check dams. Here in-fields measurements of the Leaf Area Index (LAI) were conducted to detect the variability of riparian vegetation along fifty-three riverbed transects. The observed values ranged from 0.26 to 5.71. The lower ones were found in those reaches where destroyed or strongly damaged check dams are located, and, consequently, riverbed erosive processes are present. The higher LAI values were found in those reaches with the presence of intact or slightly damaged check dams, characterized by a higher geomorphological stability. LAI measurement were also conducted in a nearby stream, named Vallone della Madonna, with intact check dams and sound riparian vegetation. Here the observed values of LAI ranged between 4.08 and 5.93, which are similar to those found in the Cammarota reaches with good geomorphological conditions. LAI values from both streams were also retrieved from Landsat 8 and Pleiades 1A satellite images using three different equations to derive LAI values from the Normalized Difference Vegetation Index (NDVI) and its corrected form. A statistical analysis was performed for every formula used.

Keywords Check dams · Riparian buffers · Mediterranean stream · Leaf area index · Normalized difference vegetation index · Satellite images

1 Introduction

The morphology of watercourses, and indirectly the riparian vegetation features, can be modified after the building of check dams (Gentile et al. 1998, Bombino et al. 2014). Gentile et al. (2008) observed processes of renaturalization, upstream and downstream of numerous monitored works in several Northern Apulian streams. Moreover, Ricci et al. (2019) highlighted vegetation retreat processes where riverbed

G. Romano · G. F. Ricci (✉) · F. Gentile
Department of Agricultural and Environmental Sciences (DISAAT), Univ. di Bari “a. Moro”, Via
G. Amendola 165, 70126 Bari, Italy
e-mail: giovanni.ricci@uniba.it

© Springer Nature Switzerland AG 2020
A. Coppola et al. (eds.), *Innovative Biosystems Engineering for Sustainable Agriculture, Forestry and Food Production*, Lecture Notes in Civil Engineering 67,
https://doi.org/10.1007/978-3-030-39299-4_12

instability takes place, after the destruction of check dams. Therefore, the state of conservation of these works plays an important role in preserving their functions (Lucas-Borja et al. 2018). Monitoring the check dams in the years after their implementation is necessary to evaluate their operating status and the existing fluvial processes (Ramos-Diez et al. 2016; Piton et al. 2017).

The relationships between riverbed stability and riparian vegetation can be investigated evaluating the structure of the riparian buffers and estimating vegetation indices (VIs). To assess the VIs directly in-field could be expensive and time consuming, hence the use of remote sensing can be useful when there is a necessity to broaden the analysis at the watershed scale (Ricci et al. 2019). In this case a multiscale approach is required comparing in situ and remote sensing data related to several VIs such as the Leaf Area Index (LAI) (Nagler et al. 2001). LAI, physically the one-sided leaf area per unit ground area (Novelli et al. 2016), is an indicator of ecological plant processes (Pierce and Running 1988) and can be used to describe the main characteristics of the plant canopy (Kamal et al. 2016). Moreover, LAI can be estimated from both satellite data and in situ monitoring, thus it is one of the most used indices to compare remote sensing retrievals and field observations.

In this study, a multiscale approach, based on in situ measurements and remote sensing was applied with the following aims: (i) to assess the variability of the LAI of riparian vegetation in two Mediterranean streams characterized by the presence of intact and destroyed check-dams; (ii) to test the performances of Landsat 8 and Pleiades 1A data (30 m and 2 m pixel size, respectively) in detecting the LAI of riparian vegetation.

2 Materials and Methods

2.1 Study Area

The study area includes the Cammarota (C) and the Vallone della Madonna (VdM) streams (Fig. 1), which flow in the territory of Deliceto (northwestern Puglia, Southern Italy). Both streams are tributaries of the Carapelle torrent and are located in its upper part. The most frequent tree species are Elm (*Ulmus minor* Mill.) and Hornbeam (*Carpinus orientalis* Mill.) with a frequency of about 65% in the C and of 100% in VdM. Blackberry (*Rubus ulmifolius* Schott.) and Common reed (*Phragmites Australis* Cav.) are the most frequently occurring shrubs. Additional information about the Carapelle torrent and the two studied streams can be found in Ricci et al. (2019).

Along the monitored section of C 28 check dams are present of which 15 destroyed, 3 damaged and 10 intact. The destroyed check dams are the main cause of the active erosion processes in the stream. Hence, C was divided in four reaches (Ri), based on the conservation state of the check dams and the erosion processes, as follow (Fig. 1):

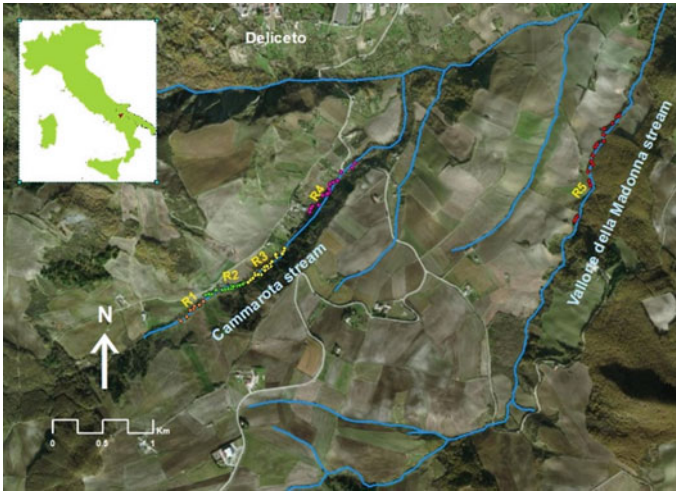


Fig. 1 Reaches (R1–R4) of the Cammarota stream and reach (R5) of the Vallone della Madonna stream

- R1—Upstream reach, with three intact and one damaged check dams; without bank erosion and vegetation stratified in regular pattern.
- R2—Incipient erosion reach, with three intact and functioning check dams, one damaged and five destroyed; eroded riverbed and presence of vegetation less dense or completely absent in the much eroded parts of the reach.
- R3—Full erosion reach, with nine destroyed works; extremely eroded watercourse vegetation almost absent where the erosive phenomena are more relevant.
- R4—Downstream reach, with four intact, one slightly damaged and one destroyed check dams, very low erosion and stratified riverbed vegetation.

The monitored reach of VdM (named R5, Fig. 1) is characterized by intact check dams without erosion in the riverbed or on the banks.

2.2 Field Measurement and Images Processing

The LAI 2200 Plant Canopy Analyzer was used to detect the LAI in-fields from May 2015 to July 2015 along transects from one bank to the other (LI-COR Inc., 2010). The width of the cross section ranged from 10 to 20 m. The transects were conducted in correspondence of a check dam or in the middle of two consecutive check dams. A total of 64 transect were measured of which 53 in C and 11 in VdM. To register the transects and the check dam positions a Garmin GPSMAP 76CSx was used.

Multispectral data were acquired from medium and high resolution imagery provided by Landsat 8 and Pleiades 1A satellites, respectively. Landsat data, with a pixel resolution of 30 m (<https://landsat.usgs.gov/landsat-8>), have been frequently used for

land cover studies (Romano et al. 2018) while rarely for the analysis of riparian vegetation in streams with narrow cross sections (Ricci et al. 2019). Pleiades constellation provides multispectral data with a pixel resolution of 2 m in the visible bands (Vanhellemont and Ruddick 2018). The satellite images used in this work were acquired by OLI sensors on June 1 and July 3, 2015, and by Pleiades devices on 20 July, 2015. A radiometric and an atmospheric correction were performed for each image to improve the product data accuracy and better compare data sets over a multiple time period. Subsequently, following Ricci et al. (2019) the corrected Normalized Difference Vegetation Index (NDVIC) was computed using the formula suggested by Nemani et al. (1993) with the aim of reduce the near-infrared response in open areas with dense ground vegetation or highly reflective canopies and improve the correlation accuracy between the NDVI and LAI (Nemani et al. 1993). Three equations to derive LAI values from the NDVIC were used: a simple linear equation suggested by Caraux-Garson (Caraux-Garson et al. 1998; Milella et al. 2012) and two non-linear relationships proposed respectively by Lambert-Beer (Lacaze et al. 1996) and Campbell and Norman (Campbell and Norman 1998; Walthall et al. 2004). More information about the equation used can be found in Ricci et al. (2019).

3 Results and Discussion

The values of LAI in-field measurements (LAIobs) were rather different in the four reaches of C caused by the different state of conservation of the watercourse (Fig. 2). R1 and R4 showed similar values of LAIobs while a progressive decrease was

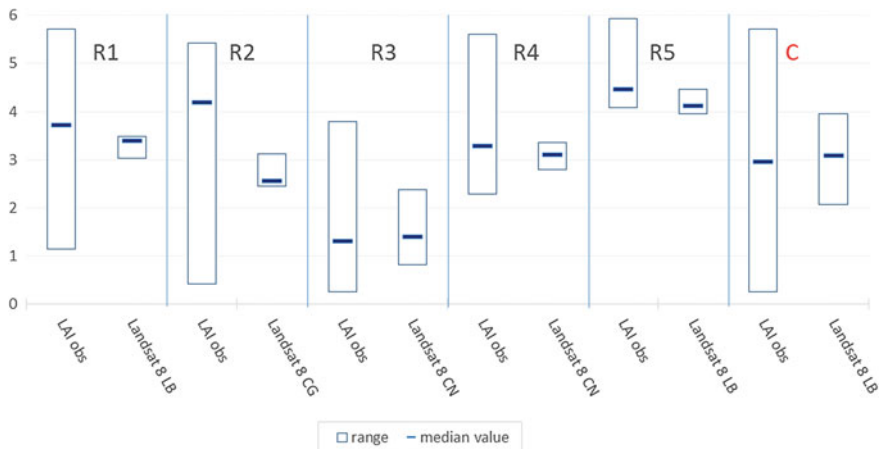


Fig. 2 Comparison between the ranges and median observed Leaf Area Index (LAIobs) values and LAI values derived from Landsat 8 images. (C), Cammarota stream including all the reaches from R1 to R4; (R5), Vallone della Madonna

observed in R2 and in R3. Generally vegetation in C is greatly fragmented due to the erosive processes in the different reaches. In the incipient erosion reach R2 and in the eroded reach R3 a decrease of vegetation was observed due to the increase of the erosive processes and the malfunctioning or the collapse of the check dams. The median value of LAI_{Obs} detected in R2, is higher than those observed in R1 and R4 reaches because of the colonization of opportunistic vegetation, such as Blackberry, during the initial stages of the erosion processes. R5 instead, showed higher values of LAI_{Obs} (Fig. 2), both in terms of median and range. Indeed, in R5, where no active erosive processes were monitored, riparian vegetation is multi-stratified with the shrubs that interpenetrates the arboreal layers. Consequently, a more marked presence of typical vegetation species of the area, such as Elm, Hornbeam and Downy oak, was detected.

A graphical analysis was performed to compare the ranges and median LAI_{Obs} values with those retrieved from Landsat 8 in the study reaches (Fig. 2). In terms of median values, the Lambert-Beer (LB) equation resulted as the most suitable for all the reaches characterized by geomorphological stability (R1, R4 and R5) as well as for the entire C reach. The Campbell-Norman (CN) equation resulted as the more accurate formula for the eroded reach R3, while none of the equations was a good predictor in R2 because of the high variability of LAI_{Obs} caused by the incipient erosive processes.

A low descriptor was found in the case of R2 for the high variability of this reach, both in terms of vegetation and stream bank erosion. The limit, in the case of the Landsat images, is due to the spatial resolution of 30 m that makes it difficult to find a pure pixel of vegetation or bare soil to insert in the equations (Wu et al. 2004; Hu et al. 2007). LB represents the best performed equation although it needs an improving of the De Jong (1994) coefficients, which aren't site-specific but generic for Mediterranean environments.

The analysis of Fig. 2 highlights a good correspondence for Landsat data, comparing the median values of LAI_{Obs} and LAI retrieved in all the reaches, except for R2. It also indicates that the ranges of LAI values derived from remote sensing is narrower than those observed. It can be ascribed to the ability of the canopy cover analyzer to better detect the variability of the vegetation cover compared to satellite images. Landsat images, because of their spatial resolution, could include in one "mixed pixel" (Lu and Weng 2004) several land cover types such as, as in the case of the study area, riparian vegetation, surrounding wheat fields and orchards, which negatively affect the images accuracy. In order to limit this problem, pixels with less than 75% of riparian vegetation were excluded from the analysis according to Chen et al. (2005).

To improve the performance of satellite images in retrieving LAI values in the reaches characterized by higher variability (R2 and R3), a satellite image with higher resolution (Pleiades) was used. In Table 1 LAI_{Obs} are compared with LAI retrieved from Landsat 8 and from Pleiades. Regarding the latter, for R2 the most suitable equation was LB while for R3 was the Caraux-Garson (CG). The values obtained were comparable with those retrieved from the Landsat 8.

Table 1 Comparison between the observed LAI values and LAI values retrieved from satellite data

	LAIobs	LAI Landsat 8 CG	LAI Pleiades 1A LB	
Min	0.43	2.45	1.87	R2
Max	5.43	3.12	3.92	
Median	4.19	2.56	2.90	
		CN	CG	
Min	0.26	0.83	1.89	R3
Max	3.80	2.38	3.27	
Median	1.32	1.41	2.68	

In R2 both the Landsat 8 and the Pleiades showed not good performances in terms of statistical indices. In this reach R^2 , NSE and PBIAS are respectively 0.04, -0.43 and 24.12 for the Landsat 8 and respectively 0.31, -0.03 and 22.34 for the Pleiades. This shows that a good descriptor wasn't found in the case of R2 caused by the high variability of this reach, both in terms of vegetation and stream bank erosion, which wasn't detected by satellite imagery neither with medium or high pixel resolution.

In sum, it can be observed that the evaluation of the characteristics of riparian vegetation of streams with narrow cross sections is possible with medium resolution satellite images. Moreover, Landsat images are open access and allow the users to carry out historical analyses to obtain information about the areas where detailed in-field studies should be conducted. The methodology adopted in this study could be useful when considering a comprehensive analysis of check dams' efficiency (Piton et al. 2017). The analysis of high resolution images (Pleiades in this study) shows that there isn't an improvement of the estimation performance in the reaches characterized by strong erosion processes and high variable vegetation, where the medium resolution images show low performances.

4 Conclusions

This study analyzed the effect of check dams on variability of riparian vegetation in a Mediterranean stream by means of in-field measurements of the LAI and its retrieval from Landsat 8 and Pleiades satellite data. The study was carried out in the Cammarota stream, with active erosion processes, and the results were compared with those found in the Vallone della Madonna stream, presenting steady geomorphological conditions.

Highly variable LAI values were observed in the Cammarota riparian environment, whereas the eroded reach R3 showed low LAI values because of the presence of destroyed check dams and scarce vegetation. Conversely, high LAI values were detected in reaches R1 and R4, with functioning check dams. It could be concluded that the intact check dams in the studied streams had positive effects on riparian vegetation, making it possible the progressive introduction of broadleaved heliophiles (Hornbeam, Manna ash, Downy oak) in the Vallone della Madonna stream.

The comparison between LAI values detected in-field and those retrieved from remote sensing images highlights the limitations of extracting reliable information on vegetation indices in the analyzed riparian context, as a consequence of the resolution of the considered images and the narrow stream cross sections. However, Landsat data can be useful to conduct preliminary studies on the possible long-term effects of the check dams in such territorial context before further in-field measurements. A limited effect in improving the performance of satellite images using higher resolution products like Pleiades was found in the reaches characterized by intense erosive processes. This result should be better analyzed taking into account also different types of images such as Sentinel 2, characterized by a resolution between that of Landsat 8 and that of Pleiades.

References

- Bombino, G., Boix-Fayos, C., Gurnell, A. M., Tamburino, V., Zema, D. A., & Zimbone, S. M. (2014). Check dam influence on vegetation species diversity in mountain torrents of the Mediterranean environment. *Ecohydrology*, 7, 678–691. <https://doi.org/10.1002/eco.1389>.
- Campbell, G. S., & Norman, J. M. (1998). *An introduction to environmental biophysics* (p. 268). New York: Springer.
- Caraux-Garson, D., Lacaze, B., Scala, F., Hill, J., & Mehel, W. (1998). Ten years of vegetation cover monitoring with Landsat TM remote sensing, an operational approach of DeMon-2 in Languedoc, France. *Symposium on operational remote sensing for sustainable development*, Enschede, Netherlands.
- Chen, D., Huang, J., & Jackson, T. J. (2005). Vegetation water content estimation for corn and soybeans using spectral indices derived from MODIS near- and short-wave infrared bands. *Remote Sens. Environ.*, 98, 225–236. <https://doi.org/10.1016/j.rse.2005.07.008>.
- De Jong, S. M. (1994). Derivation of vegetative variables from a Landsat TM image for modelling soil erosion. *Earth Surface Processes and Landforms*, 19, 165–178.
- Gentile, F., Moretti, F., & Puglisi, S. (2008). Preliminary study about renaturalisation induced by watershed management works in Sub-Appennino Dauno area (Apulian Region, Southern Italy). *QJM* 28/2, 377–389, Nuova Bios (in Italian).
- Gentile, F., Puglisi, S., & Trisorio Liuzzi, G. (1998). Some aspects of linear erosion control in Mediterranean watersheds. *Quaderni di Idronomia Montana*, 17, 77–89.
- Hu, Z. Q., He, F. G., Yin, J. Z., Lu, X., Tang, S. L., Wang, L. L., & Li, X. J. (2007). Estimation of fractional vegetation cover based on digital camera survey data and a remote sensing model. *Journal of China University of Mining and Technology*, 17(1), 0116–0120. [https://doi.org/10.1016/S1006-1266\(07\)60025-X](https://doi.org/10.1016/S1006-1266(07)60025-X).
- Kamal, M., Phinn, S., & Johansen, K. (2016). Assessment of multi-resolution image data for mangrove leaf area index mapping. *Remote sensing of Environment*, 176, 242–254. <https://doi.org/10.1016/j.rse.2016.02.013>.
- Lacaze, B., Caselles, V., Coll, C., Hill, H., Hoff, C., & De Jong, S., et al. (1996). Integrated approach to desertification mapping and monitoring in the Mediterranean basin. *Final report of De-Mon I Project*, Joint Research Centre of European Commission, Ispra (VA), Italy.
- LI-COR, (2010). LAI-2200C plant canopy analyzer. Lincoln, Nebraska: LI-COR Inc.
- Lu, D., & Weng, Q. (2004). Spectral mixture analysis of the urban landscape in Indianapolis with Landsat ETM+ imagery. *Photogrammetric Engineering and Remote Sensing*, 70(9), 1053–1062. <https://doi.org/10.14358/PERS.70.9.1053>.

- Lucas-Borja, M. E., Zema, D. A., Hinojosa Guzman, M. D., Yang, Y., & Hernández, A. C. et al. (2018). Exploring the influence of vegetation cover, sediment storage capacity and channel dimensions on stone check dam conditions and effectiveness in a large regulated river in Mexico. *Ecological Engineering*, 122, 39–47. <https://doi.org/10.1016/j.ecoleng.2018.07.025>.
- Milella, P., Bisantino, T., Gentile, F., Iacobellis, V., & Trisorio Liuzzi, G. (2012). Diagnostic analysis of distributed input and parameter dataset in Mediterranean basin streamflow modeling. *Journal of Hydrology*, 472–473, 262–276.
- Nagler, P. L., Glenn, E. P., & Huete, A. R. (2001). Assessment of spectral vegetation indices for riparian vegetation in the Colorado River delta, Mexico. *Journal of Arid Environments*, 49, 91–110. <https://doi.org/10.1006/jare.2001.0844>.
- Nemani, R., Pierce, L., Running, S., & Band, L. (1993). Forest ecosystem processes at the watershed scale: Sensitivity to remotely-sensed Leaf Area Index estimates. *International Journal of Remote Sensing*, 14, 2519–2534. <https://doi.org/10.1080/01431169308904290>.
- Novelli, A., Tarantino, E., Fratino, U., Iacobellis, V., Romano, G., & Gentile F. (2016). A data fusion algorithm based on the Kalman filter to estimate leaf area index evolution in durum wheat by using field measurements and MODIS surface reflectance data. *Remote Sensing Letters*, 7(5), 476–484. <https://doi.org/10.1080/2150704X.2016.1154219>.
- Pierce, L. L., & Running, S. W. (1988). Rapid estimation of coniferous of forest leaf area index using portable integrating radiometer. *Ecology*, 69, 1762–1767.
- Piton, G., Carladous, S., Recking, A., Tacnet, J. M., Liébault, F., Kuss, D., et al. (2017). Why do we build check dams in Alpine streams? An historical perspective from the French experience. *Earth Surface Processes and Landforms*, 42(1), 91–108. <https://doi.org/10.1002/esp.3967>.
- Ramos-Diez, I., Navarro-Hevia, J., Fernández, R. S. M., Díaz-Gutiérrez, V., & Mongil-Manso, J. (2016). Geometric models for measuring sediment wedge volume in retention check dams. *Water Environment Journal*, 30(1–2), 119–127.
- Ricci, G. F., Romano, G., Leronna, V., Gentile, F. (2019). Effect of check dams on riparian vegetation cover: A multiscale approach based on field measurements and satellite images for Leaf Area Index assessment. *Science of the Total Environment*, 657, 827–838. <https://doi.org/10.1016/j.scitotenv.2018.12.081>.
- Romano, G., Abdelwahab, O. M. M., Gentile, F. (2018). Modeling land use changes and their impact on sediment load in a Mediterranean watershed. *CATENA*, 163, 342–353. <https://doi.org/10.1016/j.catena.2017.12.039>.
- Vanhellemont, Q., & Ruddick, K. (2018). Atmospheric correction of metre-scale optical satellite data for inland and coastal water applications. *Remote Sensing of Environment*, 216, 586–597. <https://doi.org/10.1016/j.rse.2018.07.015>.
- Walthall, C. L., Dulaney, W. P., Anderson, M. C., Norman, J., Fang, H., Liang, S., Timlin, D. J., & Pachevsky, Y. (2004). Alternative approaches for estimating leaf area index (LAI) from remotely sensed satellite and aircraft imagery. *Proceedings of SPIE*, 5544, <https://doi.org/10.1117/12.559863>.
- Wu, B., Li, M., Yan, C., & Zhou, W. (2004). Developing method of vegetation fraction estimation by remote sensing for soil loss equation: A case in the Upper Basin of Miyun Reservoir. *International Geoscience and Remote Sensing Symposium (IGARSS)* 6, pp. 4352–4355. <https://doi.org/10.1109/IGARSS.2004.1370101>.

SIRR-MOD—A Decision Support System for Identifying Optimal Irrigation Water Needs at Field and District Scale



G. Dragonetti, A. Sengouga, A. Comegna, N. Lamaddalena, A. Basile and A. Coppola

Abstract SIRR-MOD is a DSS integrating two numerical modules: (1) A agro-hydrological model (named FLOWS-HAGES) for simulating flow of water and solutes in heterogeneous agri-environmental systems; (2) A model for simulating the hydraulics of the irrigation network (named COPAM). FLOW-HAGES provides a daily list of hydrants opening based on water or crop criteria. Then, an optimal sequence of hydrants may be established by passing the volumes to be delivered to a model (COPAM) for simulating the hydraulics of the irrigation network, in order to guarantee that the discharges flowing inside the distribution pipes network are delivered under optimal pressure head distribution. In this paper, we only illustrated the potential of FLOWS-HAGES model in simulating the daily evolution of: soil water contents and pressure heads in the soil profile; water uptake; stress periods for each crop; return fluxes to the groundwater under pressurized irrigation systems and climatic conditions at district level. This methodology has been applied to establish irrigation scheduling over the irrigation season for sector 6 of the Irrigation District 10 in the “Sinistra Ofanto” irrigation system. Irrigation water volumes calculated by FLOWS-HAGES model were compared to the volumes delivered by farmers, showing irrigation simulated by the model more frequent than those supplied by the farmers and with lower irrigation volumes.

Keywords Irrigation scheduling · Agro-hydrological simulation models · Soil water pressure head · Water stress

G. Dragonetti (✉) · N. Lamaddalena
Department of Land and Water, Mediterranean Agronomic Institute (IAMB), Bari, Italy
e-mail: dragonetti@iamb.it

A. Sengouga · A. Comegna · A. Coppola
School of Agricultural, Forestry, Food and Environmental Sciences (SAFE), University of Basilicata, Potenza, Italy

A. Basile
Italian National Research Council (CNR), Institute for Mediterranean Agriculture and Forest Systems (ISAFOM), Ercolano, Italy

© Springer Nature Switzerland AG 2020
A. Coppola et al. (eds.), *Innovative Biosystems Engineering for Sustainable Agriculture, Forestry and Food Production*, Lecture Notes in Civil Engineering 67,
https://doi.org/10.1007/978-3-030-39299-4_13

1 Introduction

The rapid growth of the world population has increased the use of water in agriculture. In Mediterranean countries the irrigated area became more than double in the last 40 years. However, frequently irrigation management is inefficient and wasteful (Hsiao et al. 2007). To partially solve the problem, in Italy and other Mediterranean regions, open channel irrigation systems have been converted into pressurized pipeline networks. However, the performance of distribution networks under on-demand pressurized irrigation system is still inefficient because of (i) economics and political and (ii) technical issues, which are both clarified below.

- (i) Even for on-demand irrigation distribution, the irrigation water is frequently overused, due to the price of water below the cost of provision, frequently for political reasons. Water is delivered to the farmer at a price calculated on the basis of the irrigated area, regardless of the actual amount of water needed. This form of irrigation management naturally leads to over-irrigation, with losses of water and nutrients on one side and sometimes with problems of rising water tables, waterlogging and upward movement of salts.
- (ii) In the on-demand irrigation networks, the behavior of single farmers, once aggregated at district scale, determines the total water discharge to be delivered to the irrigation network. Under these conditions, the manager of the distribution network has only minor control on the water scheduling and thus on the performance of distribution network. Being unknown a priori when any of the single farmers decide to irrigate, discharges flowing in the distribution network and the pressure head distributions are also unknown. There may be case were the capability of the conveyance hydraulic system may not be able to provide the discharge the farmers require at a given time. Also, under changing discharges, the pressure head in the system can be subject to high fluctuation, with consequent impacts on the distribution uniformity and efficiency of on-farm irrigation systems, also in terms of energy to be spent for water distribution (Lamaddalena and Sagardoy 2000).

The twofold nature of the problem requires corresponding economics and technical solutions. On one side, solutions require a change of attitude in the management of irrigation water by appropriately quantifying the profitability of irrigation water and by incentivizing the farmers to maximize the economical return per unit of water (water productivity). On the other side, irrigation managers, provided with appropriate decision support tools (DSS), could be able to identify properly the actual crop water requirements and to determine the optimal timing, quantity, and quality of irrigation water to be supplied to each farm in order to maximize the crop yield, while minimizing deep percolation fluxes of water and nutrients, and thus water losses and groundwater degradation.

Based on these premises, the aim of this study is to illustrate the potential of a physically-based module (FLOW-HAGES) to simulate the different physical processes involved in an irrigation system and thus for identifying optimal irrigation

water needs at district scale over the course of an irrigation season. The model was applied to one case study located in the sector 6 of irrigation District 10 in the “Sinistra Ofanto” irrigation system.

2 Materials and Methods

2.1 Case Study: Sector 6 of Capitanata Irrigation Network—Hydrogeological Characteristics and Crop Pattern

The study area is located at the Consorzio per la Bonifica della Capitanata (CBC), Apulia, southern Italy which belongs to the Capitanata Irrigation Network. District 10 operates with a pressurized on-demand delivery schedule and with a “low-zone”, where the water is supplied to farms by gravity. Irrigation water comes from a storage reservoir, and water is supplied by Capacciotti dam (50,000 m³ of capacity). Here, FLOWS-HAGES model was applied to one operation unit (Sector 6), served by 31 hydrants and covering a total cultivated area of 129 ha. To determine the pedological and hydraulic characteristics five sites were also selected and dug for each soil. Disturbed soil samples were collected to determine soil texture (Gee and Or 2002).

Hydraulic properties of each horizon for each profile were also determined by using both laboratory and field methods. At shallower horizon, field infiltration measurements were carried out by using tension infiltrometer (Ankeny et al. 1991; Coppola et al. 2011; Basile et al. 2012) and the data were elaborated by DISC code (Šimůnek et al. 2000). At deeper soil horizons, hydraulic properties were determined by laboratory Stackman apparatus on undisturbed soil samples (7.6 cm diameter and 7 cm height). Then a simple Thiessen polygon technique was used to extend the soil hydraulic properties measured in these 5 soil profiles to all fields in sector 6.

With regards to the crop pattern, the sector 6 includes mainly grapevines, peaches and cereals (Fig. 1). According to the relative spatial distribution for the year 2016 (source CBC), vineyards cover almost half (46%) the total study area; early peach account for one fifth of the total area (21%); table grapes, apricots and olives represents a smaller fraction (2%). For the year 2016, the overall water consumption of farmers was about 125,000 m³.

2.2 FLOW-HAGES Model

FLOW-HAGES model simulates flow and solute transport in heterogeneous agri-environmental systems. Vertical transient water flow and solute transport are simulated by numerically solving a 1D form of the Richards equation with a sink term for root uptake and the Advection-Dispersion Equation (ADE), respectively.

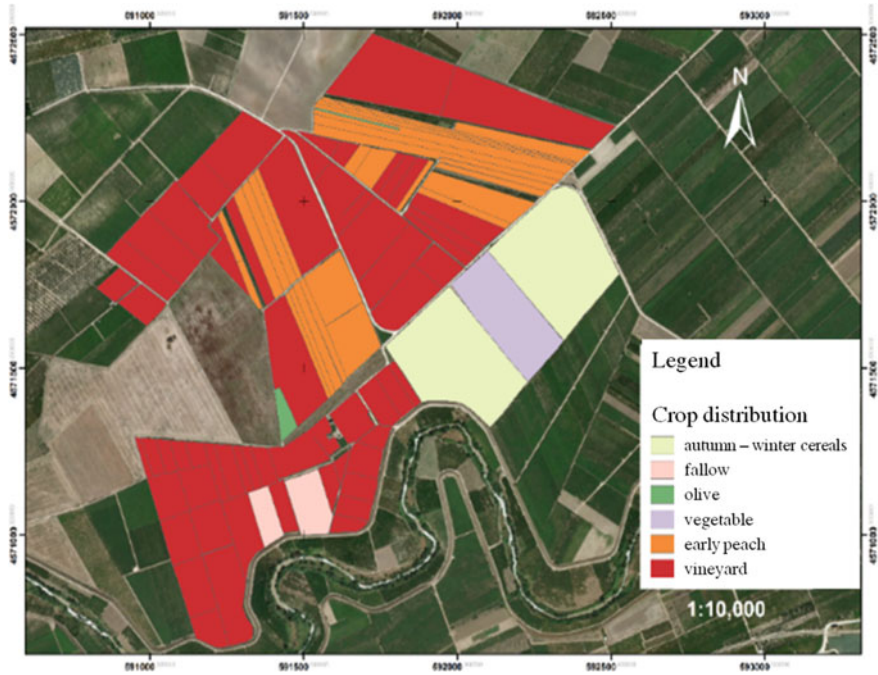


Fig. 1 Crop pattern of Sector 6 of District 10 “Sinistra Ofanto”

The numerical code is based on a standard finite difference scheme (Coppola et al. 2009, 2006, 2018) and written in Matlab.

In this study, daily potential evapotranspiration and rain were assumed at the upper boundary, whereas free drainage was assumed as bottom boundary condition.

The criterion adopted by the model to calculate the time and the irrigation volume is illustrated in the Fig. 2a, b.

The model calculates the average pressure head in the root zone, hav . In the case hav remains higher than the threshold pressure head, $hcrit$, inducing water stress for the specific crop considered, no irrigation is required (Fig. 2a); in other words the average pressure head h is above the stress conditions. The irrigation starts whenever hav becomes lower than $hcrit$ (Fig. 1b). In this condition, the model calculates the gross irrigation height, Irr_{gross} , as the difference between the storage at the field capacity and the actual water storage in the root zone:

$$Irr_{gross} = \int_0^{D_{root}} (\theta_{fc} - \theta(z))dz \text{ (cm of water)} \tag{1}$$

At day t , net irrigation, Irr_{net} is calculated as difference between Irr_{gross} and the rain falling at the irrigation time:

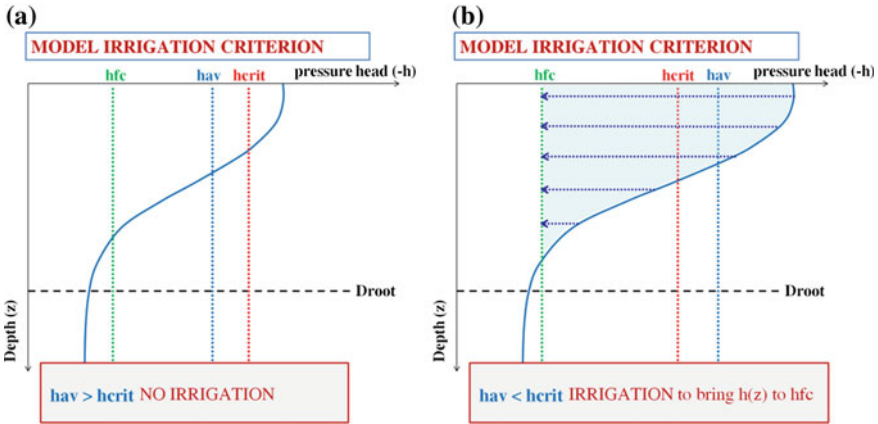


Fig. 2 Graphical view of the criterion used by the model to calculate the time for irrigation and the irrigation volume. **a** $hav > hcrit$, no irrigation is required; **b** $hav < hcrit$, irrigation is required to bring the pressure head at the field capacity, hfc

$$Irr_{net} = Irr_{gross} - rainfall(\text{cm of water}) \tag{2}$$

and irrigation water is not supplied if the rainfall exceeds Irr_{gross} .

At the irrigation network management level, the actual irrigation amount (cm), Irr_{act} , is calculated by dividing Irr_{net} by the farm irrigation efficiency, IE, of the irrigation system used for each crop tested.

To satisfy Irr_{act} at day t , the duration of a hydrant opening, t_{irr} , is obtained as:

$$t_{irr} = Irr_{act}Ak/q \tag{3}$$

where $q(l/h)$ is the nominal discharge of the hydrant considered, $A(\text{ha})$ the area to be irrigated and k a factor to account for the different dimensions in the equation.

FLOW-HAGES model identifies the list of hydrants to be opened at day t , by repeating the approach described above for each crop area included in the irrigation sector.

3 Results and Discussions

Here, one FARM case study is illustrated as representative of the applied methodology. The outputs of FLOWS-HAGES model are obtained by simulating water dynamics and distribution in the soil profile under two scenarios: (1) by assuming the time and volume of irrigation supplied by the farmer; (2) using the model criteria (as described in the Sect. 2). Assuming that water volumes requirement from simulation represent the optimum level, they were compared with volumes actually

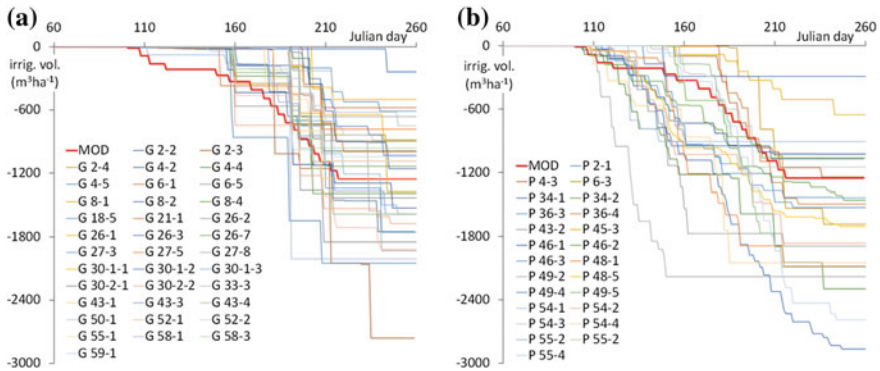


Fig. 3 Cumulative irrigation volumes based on farmer and model (the bold red line) for grape (a) and peach (b)

delivered by the consortium. This way it was possible to estimate irrigation efficiency both at field and district scale.

The rainfall and evapotranspiration data used as input model refers to the year 2016. The cumulative irrigation volumes actually supplied by the farmers for the most representative crops in the area, grapevines (G) and peaches (P), are shown in the Fig. 3. In the figures, the red bold line indicates the calculated irrigation volumes for each of the two crops, which is roughly the average of the farmers irrigation volumes and is assumed to represent the optimal behavior of farmers, assuming no soil hydraulic variability in the irrigation sector.

The figures show a large variability of farmer behavior in irrigating the same crop. When the irrigation applied by the farmer is higher or lower than that simulated, the farmer is overestimating or underestimating the water needs. In the first case, water and nutrients are lost by deep percolation, in the second the farmer is inducing water stress.

The graphs in the Fig. 4 show, for table grape (G): (a) the irrigation volumes (daily and cumulative) calculated by model; (b) the irrigation volumes actually supplied by the farmer, (c) the pressure head trend at 40 cm depth, (d) the percolation fluxes at 80 cm.

In the graph (c) the horizontal line represents the critical pressure head (h_{crit}) selected for the grape crop. It can be observed how the model allows the pressure head to remain regularly above the critical value, with frequent irrigation and low volumes applied. The low volumes have major implications in terms of overall discharge to be supplied at the head of the irrigation sector. By contrast, the actual behavior of the farmer induces the pressure head to be lower than threshold value (water stress conditions) for a long period. This can be explained by the fact that the farmer irrigates less frequently with higher volumes. In other words, the farmer induces stress periods alternating with large irrigation supplies. This behavior is reflected in the generally lower deep percolation fluxes coming from the model irrigation criterium as compared to those coming from the farmer behavior (d).

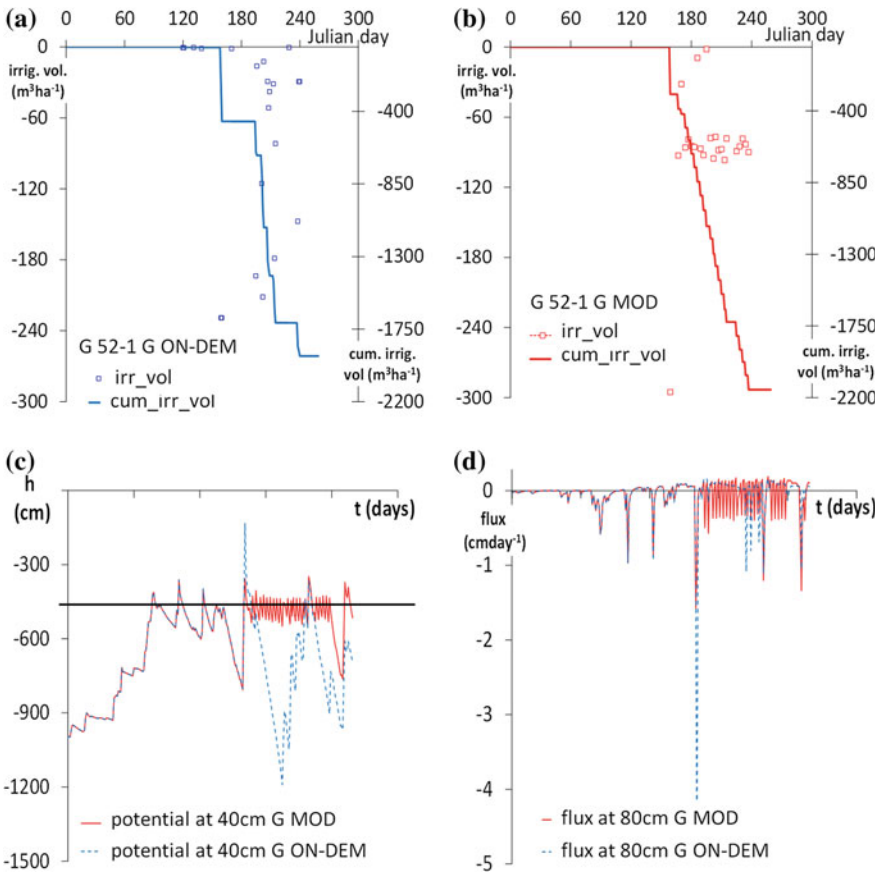


Fig. 4 **a** Irrigation volumes (both per single day and cumulative) calculated by the model (MOD); **b** irrigation volumes actually supplied by the farmer (ON-DEM); **c** pressure head at 40 cm depth; **d** percolation fluxes at 80 cm. All the graphs refer to the hydrant labeled as G 52-1

4 Conclusions

In this paper we shortly described the potential of an irrigation management tool to simulate district-level water scheduling over the course of an irrigation season. The tool is largely based on the use of mathematical models for the simulation of soil water movement in the unsaturated zone. This is a precise approach to rational irrigation and the key to saving irrigation water. Compared to other similar existing approaches, the soil water balance is calculated by solving the partial differential equation known as the Richards equation. Additionally, the tool takes into account the spatial variability of the soil hydraulic parameters. The model provides a way to establish the right frequency and amount of irrigation to keep the pressure head

above the critical value by minimizing both the stress periods and the water (and nutrients) lost by deep percolation fluxes.

Acknowledgements The study was carried out thanks to the dataset (irrigation volumes, meteorological data) provided by the Consorzio di Bonifica della Capitanata (CBC), Foggia, Italy.

References

- Ankeny, M., Ahmed, M., Kaspar, T., & Horton, R. (1991). Simple field method for determining unsaturated hydraulic conductivity. *Soil Science Society of America Journal*, 55, 467–470.
- Basile, A., Buttafuoco, G., Mele, G., & Tedeschi, A. (2012). Complementary techniques to assess physical properties of a fine soil irrigated with saline water. *Environmental Earth Science*, 66, 1797–1807.
- Coppola, A., Randazzo, L., Basile, A., & Fenu, C. (2018). FLOWS-HAGES (FLOW of Water and Solutes in Heterogeneous AGri-Environmental Systems): A MatLab Code for the Transport of Water and Solutes in Unsaturated Soils with Vegetation in Heterogenous Systems; D. S. U. o. B. Tech. Rep. Soil and Contaminant Hydrology Laboratory: Potenza, Basilicata, Italy.
- Coppola, A., Basile, A., Wang, X., Comegna, V., Tedeschi, A., Mele, G., et al. (2011). Hydrological behaviour of microbiotic crusts on sand dunes: Example from NW China comparing infiltration in crusted and crust-removed soil. *Soil and Tillage Research*, 117, 34–43.
- Coppola, A., Comegna, V., Basile, A., Lamaddalena, N., & Severino, G. (2009). Darcian preferential water flow and solute transport through bimodal porous systems: Experiments and modelling. *Journal of Contaminant Hydrology*, 104, 74–83.
- Coppola, A., & Randazzo, L. A. (2006). MatLab code for the transport of water and solutes in unsaturated soils with vegetation. In Tech. Rep. Soil and Contaminant Hydrology Laboratory, University of Basilicata, Potenza, Italy.
- Gee, G. W., & Or, D. (2002). Particle-size analysis. In *Methods of soil analysis, Part4. Physical methods. Soil Science Society of America Journal. Book Series*, 5, 255–293.
- Hsiao, T., Steduto, P., & Fereres, E. (2007). A systematic and quantitative approach to improve water use efficiency in agriculture. *Irrigation Science*, 25, 209–231.
- Lamaddalena, N., & Sagardoy, J. (2000). *Performance analysis of on-demand pressurized irrigation systems*. Food and Agriculture Organization of the United Nations 92-5-1044377-6, <https://doi.org/10.13140/2.1.1127.5849>.
- Šimůnek, J., van Genuchten, M. T., & Sejna, M. (2000). The DISC Computer Software for Analyzing Tension Disc Infiltrometer Data by Parameter Estimation, Version 1.0; US Salinity Laboratory: Riverside, CA, USA.

Modeling the Effect of Different Management Practices for Soil Erosion Control in a Mediterranean Watershed



Giovanni Francesco Ricci, Anna Maria De Girolamo and Francesco Gentile

Abstract To counteract the threat of soil erosion, European countries are called to identify the high-risk erosion areas and to adopt Best Management Practices (BMPs). The Soil and Water Assessment Tool (SWAT) was used to identify the critical source areas, for the current management, in the Carapelle watershed, an agricultural watershed located in the Puglia region (Southern Italy). SWAT was calibrated and validated both manually and automatically, using SWAT-CUP, for runoff and sediment load at daily time scale for a 5-years period. Results show that in the Carapelle the average annual sediment load is $5.95 \text{ t ha}^{-1} \text{ y}^{-1}$. A threshold of sediment yield $10 \text{ t ha}^{-1} \text{ y}^{-1}$ was selected to discretize the high erosion-risk areas, resulting in 59 HRUs characterized by agricultural land use. Three BMPs scenarios, based on the regional policies, were modeled: contour farming, no-tillage and reforestation. No-tillage is the most effective scenario, reducing soil erosion to 4.20 t ha^{-1} . The study offers to watershed managers a methodology to discretize the high erosion-risk areas, test and choose the most effective BMPs for sediment load reduction.

Keywords Soil erosion · SWAT model · Best management practices (BMPs) · Rural development program

1 Introduction

Soil erosion is one of the main threats for soils worldwide, as well as in Europe. The European Soil Data Centre (ESDAC) estimated that about 20% of the European soils are eroded by wind and water (Jones et al. 2012). Intensive agricultural activity together with steep topography, deforestation and overgrazing leads to increase soil erosion (Pimentel and Burgess 2013). The Soil Thematic Strategy (EC 2006) focuses

G. F. Ricci · F. Gentile (✉)

Department of Agricultural and Environmental Sciences, University of Bari Aldo Moro, Via Giovanni Amendola 165/A, 70126 Bari, Italy
e-mail: francesco.gentile@uniba.it

A. M. De Girolamo

Water Research Institute, National Research Council, 70132 Bari, Italy

© Springer Nature Switzerland AG 2020

A. Coppola et al. (eds.), *Innovative Biosystems Engineering for Sustainable Agriculture, Forestry and Food Production*, Lecture Notes in Civil Engineering 67,
https://doi.org/10.1007/978-3-030-39299-4_14

the attention on limiting the sediment yield (SY) production. Each member state is required to identify areas of high risk of erosion where specific conservation measures can be applied which can be called Best Management Practices (BMPs) (Vigiak et al. 2016). Contour farming, hill ponds, no tillage, reforestation and strip cropping are some of the main BMPs, which have been used in croplands (Arabi et al. 2008; Mtibaa et al. 2018). The European Union (EU) encouraged the application of BMPs by agricultural financing programs such as the Community Agricultural Policy (PAC) (Coderoni and Esposito 2018). These funding are often subordinated to the maintenance of the Good Agricultural Environmental Conditions (GAEC), which are a series of measures to counteract soil erosion (Panagos et al. 2016).

In Italy, where soil erosion is a threat especially in croplands (Ricci et al. 2018), the maintenance of the GAEC is addressed by the D.M. 1867/2018 of the Ministry of Agricultural, Food and Forestry Policies (MiPAAF) about the Cross-Compliance Standard and the minimum land management that meets specific local conditions (MiPAAF 2018). The financing of the agricultural system is addressed by the Rural Development Programme (in Italian: Programma di Sviluppo Rurale; PSR), which is a seven-year program. In particular, the actual program (PSR 2014–2020) with the target items 8 and 10 aims to increase forested areas and improve the management of agricultural lands.

In this study, the Soil and Water Assessment Tool (SWAT) (Arnold et al. 1998) was used to estimate runoff and sediment load (SL) in the Carapelle, a medium-size agricultural watershed located in Southern Italy. In particular, the study aims (i) to identify high risk erosion areas at the current management conditions; (ii) to evaluate the effect of three specific BMPs scenarios, based on actual national and regional policies, in reducing soil erosion at the watershed and sub-watershed scale.

2 Study Area

The study area is the Carapelle watershed located in the Puglia region (South Italy) (Fig. 1). The watershed area is 506 km², while the main stream length is 52.16 km; the elevation ranges from 120 to 1089 m a.s.l. Precipitation is characterized by high spatial as well as seasonal variability (between 450 and 800 mm y⁻¹), which influence watershed hydrology and sediment transport processes. The gauging station at the outlet (41° 17' 50.347" N; 15° 36' 2.583" E; Ortona Village) is equipped with two monitoring systems, one for the streamflow measurements and the other for the suspended sediment concentration (Gentile et al. 2008). Measured data are available for a 5-years period (2007–2011). Agriculture is the main economic activity in the watershed. The main crops are winter wheat (75% of the area) and olive tree cultivation, while forest and pasture are prevalent in mountainous areas (Aquilino et al. 2014). Urban settlements are limited to a few small villages. The traditional cultivation method adopted for winter wheat is a 4-year crop rotation (wheat, wheat, wheat and clover). Plowing is carried out up and down slopes (25–40 cm depth).

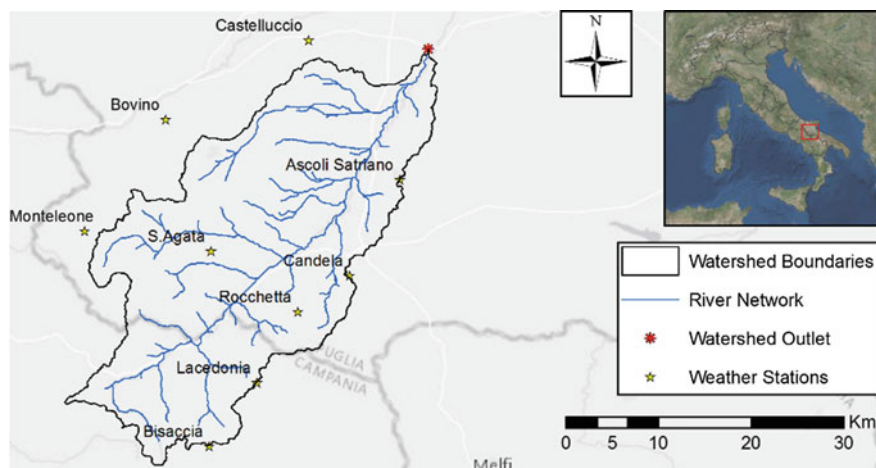


Fig. 1 Study area: the Carapelle watershed (Puglia, SE Italy)

3 Methodology

3.1 Model Set-up, Calibration and Validation

The semi-distributed and continuous hydrological model, SWAT version 2015 (Arnold et al. 2012a) was run at daily timescale from 2004 to 2011 with the first three years used to warm up the model. Using a threshold of 200 ha, 115 sub-watersheds were identified. To keep the proportion of the main soil type, slope and land uses in every sub-watershed, 451 Hydrological Response Units (HRUs) were identified applying percentage thresholds of 5, 25, and 25% for soil type, slope and land uses, respectively. A Digital Elevation Model (20 m \times 20 m), a land use map (100 m resolution), 9 soil profiles and 8 weather stations were used to set up the model. A detailed description of the SWAT model, and input data can be found in Abdelwahab et al. (2018). Measured streamflow and SL data (2007–2011) were split into two periods (Arnold et al. 2012b), one for the calibration (2007 to 2009) and one for the validation (2010 to 2011). A sensitivity analysis was performed with the SWAT-CUP tool using the Sequential Uncertainty Fitting version 2 (SUF2). The most sensitive parameters and their calibrated values are reported in Abdelwahab et al. (2018) and Ricci et al. (2018). The parameters were changed manually to reach a correspondence between the simulated and the observed curves (Jeong et al. 2010). Then, to find the best value, the SWAT-CUP automatic procedure was used considering the Nash and Sutcliffe efficiency (NSE) objective function >0.5 (Ricci et al. 2018).

3.2 *BMPs Evaluation and Parameterization*

Three BMPs scenarios were implemented: contour farming (BMP1), which although not financed by the PSR is suggested in the GAEC; no tillage (BMP2), which is supported by the PSR measure 10.1.3; reforestation (BMP3), which is supported by the PSR measure 8.1 (Table 1). A description of the effects of the BMPs can be found in the Natural Resources Conservation Service (NRCS) conservation practice (USDA-NRCS 2017). In the actual conditions (Baseline scenario), areas under severe erosion risk (HRUs) were discretized considering a threshold of $SY > 10 \text{ t ha}^{-1}$ (Kuhlman et al. 2010). Then, 59 target HRUs (Table 1), all characterized by the cultivation of winter wheat, were identified. As to practice contour farming the slope cannot overtake 20% for tractor over-turning risk, a second criteria of discretization, based on the slope ($<20\%$) was considered for BMP1, which resulted in 44 HRUs (Table 1). BMP2 had no constraints, therefore it was applied to all the 59 HRUs. Reforestation was applied only in the HRUs where it is difficult to apply the traditional tillage techniques (slope $> 20\%$) and the productivity is low. Hence, 15 HRUs were selected (Table 1). To reflect the effect of the BMPs scenarios, SWAT parameters were modified as suggested by Arnold et al. (2012a) and Ullrich and Volk (2009) (Table 1).

Table 1 SWAT parameterization for simulating the BMPs scenarios

BMP code and name	Selected criteria	Number of target HRUs	Modified parameters in SWAT simulations
BMP1: Contour farming	Erosion $> 10 \text{ t ha}^{-1}$ Slope $< 20\%$ (tractor overturning risk)	44	CNII table provided by Arnold et al. (2012a) considering the contoured w/residue values USLE_P values provided by Arnold et al. (2012a) for slope classes
BMP2: No tillage	Erosion $> 10 \text{ t ha}^{-1}$	59	Removing tillage operation in target HRUs BIOMIX set to 0.4 OV_N set to 0.320 CNII decreased by 2
BMP3: Reforestation	Erosion $> 10 \text{ t ha}^{-1}$ Slope $> 20\%$	15	Change of the land use in the target HRUs CNII values for forest in the table provided by Arnold et al. (2012a)

Table 2 SWAT model performances results for calibration and validation at daily time scale. Coefficient of determination (R^2), Nash and Sutcliffe efficiency (NSE), Percent Bias (PBIAS)

	Streamflow		Sediment load	
	Calibration	Validation	Calibration	Validation
R^2	0.6	0.5	0.5	0.5
NSE	0.6	0.5	0.5	0.5
PBIAS	+5.3	-17.2	-2.8	5.1

4 Results and Discussions

4.1 Modeling Streamflow and Sediment Load in Actual Conditions

The SWAT model shows satisfactory results in simulating streamflow and SL at daily time scale in the Baseline scenario (Table 2). The processes acting in the watershed influence hydrological modeling in complex environments such as the Mediterranean areas (Ricci et al. 2018). In this case, SWAT shows an underestimation in the SL validation. This because some typical processes of the Mediterranean streams, such as bank collapse, are not included in the Modified USLE (MUSLE) equation (Abouabdillah et al. 2014).

For the study period, at the watershed scale, the average annual streamflow is 180 mm, equivalent to 27% of the rainfall and the average annual SL is 5.95 t ha⁻¹ yr⁻¹. The production of SY in the Carapelle watershed is mainly related to steep-slope areas and to the winter wheat cultivation.

4.2 Modeling BMPs

Every BMPs scenario reduces the average annual SL at the outlet. BMP2 decreases the SL of 29% (4.20 t ha⁻¹), while BMP1 of 22% (4.61 t ha⁻¹) and BMP3 of 15% (5.04 t ha⁻¹). Figure 2 shows the ranges of SY values, calculated for the sub-watersheds related to the 59 target HRUs, for the baseline and the three scenarios. Considering the median values, Baseline shows a SY of 5.13 t ha⁻¹, BMP2 reduces the SY to 2.30 t ha⁻¹ and BMP1 to 3.84 t ha⁻¹. BMP3 shows a median value higher than BMP2 since this practice is applied in only 15 of the 59 target HRUs.

Figure 3 shows the spatial distribution of the SY (t ha⁻¹) at the sub-watershed scale for the Baseline and the different BMPs scenarios. BMP1 and BMP2 scenarios show a decrease of SY of 29% and 37% respectively compared to the Baseline scenario in the sub-watersheds related to the 59 target HRUs. BMP3 shows a reduction only of the 19%, while highlights the highest decrease of SY in a single sub-watershed (from 8.74 to 0.17 t ha⁻¹).

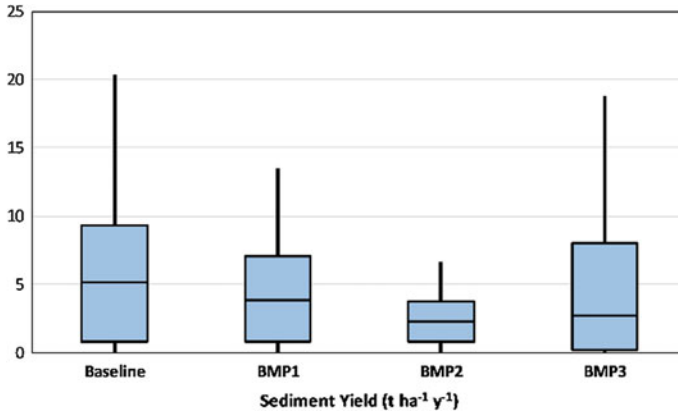


Fig. 2 Box plots of sediment yield including only the sub-watersheds related to the 59 target HRUs. The horizontal line within the box indicates the median values, boundaries indicate the 25th and the 75th percentile, whiskers indicate the 5th and the 95th percentile

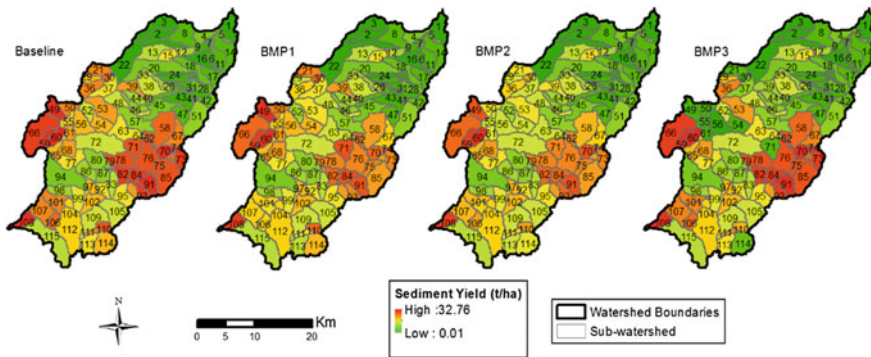


Fig. 3 Spatial distribution of the annual sediment yield ($t\ ha^{-1}$) for the Baseline and for the different BMPs scenarios

Summarizing the results, BMP2 produces the higher SL reduction at the watershed outlet as well as the higher SY reduction at sub-watershed level. No tillage indeed contributes to increase the surface roughness (OV_N) (Ullrich and Volk 2009) and, improves the soil fertility and humidity, especially in the semi-arid areas (De Vita et al. 2007). BMP1 highlights a fair reduction of SY. The change of the direction of plowing (from perpendicular to parallel to the slope lines) in the contour farming leads to impound water in small depressions and, consequently reduce the surface runoff and the SY (Arabi et al. 2008). For this reason, contour farming is defined as a structural practice useful to decrease sheet and rill erosion (Ginzky et al. 2017). At the single sub-watershed scale, BMP3 shows the highest SY reduction. Indeed, forests can decrease the effect of the raindrop splashes and improve the soil protection from the detachment from surface litters (Xiao et al. 2015). At the basin scale, BMP3

generates apparently the worst result in terms of sediment reduction only because it is applied in a limited area with slope higher than 20%.

5 Conclusions

In the present study, the impact of conservation measures in areas under high risk of erosion was estimated. The SWAT model was used to estimate the SL at the watershed scale in current conditions as well as considering new management scenarios. The study area is an agricultural watershed located in S-E Italy where soil erosion is due to the conventional tillage. 59 HRUs were discretized as target areas using a threshold of $SY > 10 \text{ t ha}^{-1}$. No tillage was the BMP scenario with the highest SL reduction at the outlet as well as with the highest SY reduction at sub-watershed scale. Reforestation instead was the least effective at the basin scale because it was applied only on the steep slope areas, where reforestation is the best solution to prevent the soil particle detachment. Contour farming could be considered a good alternative to the conventional tillage because, only changing the direction of plowing, produced a good reduction of the SY in non-steep slope areas. As the choice of the most appropriate BMP has to be done considering the characteristics of the target areas, the proposed methodology can be helpful to this aim. Based on the results obtained in term in SL reduction, further analysis are needed to estimate the economic feasibility of the different BMPs both for the public and the private sector.

References

- Abdelwahab, O. M. M., Ricci, G. F., De Girolamo, A. M., & Gentile, F. (2018). Modelling soil erosion in a Mediterranean watershed: Comparison between SWAT and AnnAGNPS models. *Environmental Research*, 166, 363–376. <https://doi.org/10.1016/j.envres.2018.06.029>.
- Abouabdillah, A., White, M., Arnold, J. G., De Girolamo, A. M., Oueslati, O., & Maataoui, A. et al. (2014). Evaluation of soil and water conservation measures in a semi-arid river basin in Tunisia using SWAT British Society of Soil Science <https://doi.org/10.1111/sum.12146>.
- Aquilino, M., Novelli, A., Tarantino, E., Iacobellis, V., & Gentile, F. (2014). Evaluating the potential of GeoEye data in retrieving LAI at watershed scale. In *Proceedings of SPIE—The International Society for Optical Engineering*, 9239, Art. No. 92392B. <https://doi.org/10.1117/12.2067185>.
- Arabi, M., Frankenberger, J. R., Engel, B. A., & Arnold, J. G. (2008). Representation of agricultural conservation practices with SWAT. *Hydrological Processes*, 22, 3042–3055. <https://doi.org/10.1002/hyp.6890>.
- Arnold, J. G., Kiniri, J. R., Srinivasan, R., Williams, J. R., Haney, E. B., & Neitsch S. L. (2012a). Soil & Water Assessment Tool: Input/Output Documentation Version 2012. Texas Water Resource Institute.
- Arnold, J. G., Moriasi, D. N., Gassman, P. W., Abbaspour, K. C., White, M. J., Srinivasan, R., et al. (2012b). SWAT: Model use, calibration, and validation. *Transactions ASABE*, 55, 1491–1508.
- Arnold, J. G., Srinivasan, R., Mutiah, R. S., & Williams, J. R. (1998). Large area hydrologic modeling and assessment—Part 1: Model development. *Journal of the American Water Resources Association*, 34(1), 73–89. <https://doi.org/10.1111/j.1752-1688.1998.tb05961.x>.

- Coderoni, S., & Esposti, R. (2018). CAP payments and agricultural GHG emissions in Italy. A farm-level assessment. *Science of the Total Environment*, 627, 427–437. <https://doi.org/10.1016/j.scitotenv.2018.01.197>.
- De Vita, P., Di Paolo, E., Fecondo, G., Di Fonzo, N., & Pisante, M. (2007). No-tillage and conventional tillage effects on durum wheat yield, grain quality and soil moisture content in southern Italy. *Soil and Tillage Research*, 92(1–2), 69–78. <https://doi.org/10.1016/j.still.2006.01.012>.
- European Commission (EC). (2006). Commission staff working document “Impact Assessment of the Thematic Strategy on Soil Protection” (SEC(2006)620) Available online: <http://eur-lex.europa.eu/legal-content/EN/TXT/?uri=CELEX:52006PC0232>. Accessed 15 December 2016.
- Gentile, F., Bisantino, T., Corbino, R., Milillo, F., Romano, G., & Trisorio Liuzzi, G. (2008). Sediment transport monitoring in a Northern Puglia watershed. *WIT Transactions on Engineering Sciences*, 60, 153–161. <https://doi.org/10.2495/DEB080161>.
- Ginzky, H., Dooley, E., Heuser, I. L., Kasimbazi, E., Markus, T., & Qin, T. (2017). *International Yearbook of Soil Law and Policy*. Springer.
- Jeong, J., Kannan, N., Arnold, J. G., Glick, R., Gosselink, L., & Srnivasan, R. (2010). Development and integration of subhourly rainfall-runoff modeling capability within a watershed model. *Water Resources Management*, 24(15), 4505–4527.
- Jones, A., Panagos, P., Barcelo, S., Bouraoui, F., Bosco, C., Dewitte, O., et al. (2012). *The State of soil in Europe: A contribution from JRC to the European environmental agency's environment state and outlook report—SOER 2010*. Luxembourg: Publications Office.
- Kuhlman, T., Reinhard, S., & Gaaff, A. (2010). Estimating the costs and benefits of soil conservation in Europe. *Land Use Policy*, 27(1), 22–32. <https://doi.org/10.1016/j.landusepol.2008.08.002>.
- MiPAAF. (2018). De Decreto del Ministero delle Politiche Agricole Alimentari e Forestali (MiPAAF) n. 1867 del 18 gennaio 2018. Pubblicato sulla G.U.R.I n. 74 del 29/3/2017, Disciplina del regime di condizionalità ai sensi del regolamento (UE) n. 1306/2013 e delle riduzioni ed esclusioni per inadempienze dei beneficiari dei pagamenti diretti e dei programmi di sviluppo rurale.
- Mtibaa, S., Hotta, N., & Irie, M. (2018). Analysis of the efficacy and cost-effectiveness of best management practices for controlling sediment yield: A case study of the Joumine watershed. *Tunisia. Science of the Total Environment*, 616–617(2018), 1–16. <https://doi.org/10.1016/j.scitotenv.2017.10.290>.
- Panagos, P., Imeson, A., Meusburger, K., Borrelli, P., Poesen, J., Alewell, C. (2016). Soil conservation in Europe: Wish or reality? *Land Degradation and Development*, 27(6), 1547–1551. <https://doi.org/10.1002/ldr.2538>.
- Pimentel, D., & Burgess, M. (2013). Soil erosion threatens food production. *Agriculture*, 3, 443–463. <https://doi.org/10.3390/agriculture3030443>.
- Ricci, G. F., De Girolamo, A. M., Abdelwahab, O. M., & Gentile, F. (2018). Identifying sediment source areas in a Mediterranean watershed using the SWAT model. *Land Degradation and Development*, 29, 1233–1248. <https://doi.org/10.1002/ldr.2889>.
- Ullrich, A., & Volk, M. (2009). Application of the soil and water assessment tool (SWAT) to predict the impact of alternative management practices on water quality and quantity. *Agricultural Water Management*, 96, 1207–1217. <https://doi.org/10.1016/j.agwat.2009.03.010>.
- United States Department of Agriculture—National Conservation Practice Standards. 20017. National Conservation Practice Standards. Available online at https://www.nrcs.usda.gov/wps/portal/nrcs/detailfull/national/technical/cp/ncps/?cid=nrcs143_026849.
- Vigiak, O., Malagó, A., Bouraoui, F., Grizzetti, B., Weissteiner, C. J., & Pastori, M. (2016). Impact of current riparian land on sediment retention in the Danube River Basin. *Sustainability of Water Quality and Ecology*, 8, 30–49. <https://doi.org/10.1016/j.swaqe.2016.08.001>.
- Xiao, L., Yang, X., Chen, S., & Cai, H. (2015). An assessment of erosivity distribution and its influence on the effectiveness of land use conversion for reducing soil erosion in Jiangxi, China. *CATENA*, 125, 50–60. <https://doi.org/10.1016/j.catena.2014.10.016>.

The Benefit of Continuous Modelling for Design Hydrograph Estimation in Small and Ungauged Basins



S. Grimaldi, A. Petroselli, R. Piscopia and F. Tauro

Abstract Estimating the design hydrograph (DH) is a crucial problem in practical hydrology and hydraulics. The development of reliable DHs is particularly challenging in small and ungauged basins due to the lack of observed discharge data that are needed for calibrating advanced models. For such basins, the modeler is often forced to adopt simple and conceptual modelling like the so called event-based approach. It consists in selecting a design rainfall event, which is related to an assigned return period, estimating the rainfall excess and then transforming it into the DH. In recent years, the continuous modelling approach was introduced. This relies on generating a long synthetic rainfall time series at sub-daily resolution that feeds a continuous rainfall–runoff model. Then, a discharge time series is produced that allows for estimating the DH. In this work, we would like to emphasize the added value of the continuous modelling approach in providing a more reliable estimation of the DH.

Keywords Continuous modelling · COSMO4SUB · Design hydrograph · EBA4SUB · Event-based approach · Rainfall-runoff modelling

1 Introduction

The design hydrograph (DH) estimation for small and ungauged watersheds is a fundamental topic in hydrology. In the literature, two distinct approaches for evaluating the DH can be found, the so called ‘event-based’ and ‘continuous simulation’

S. Grimaldi (✉) · F. Tauro

Department for Innovation in Biological, Agro-Food and Forest Systems (DIBAF), University of Tuscia, via San Camillo de Lellis snc, 01100 Viterbo, Italy
e-mail: salvatore.grimaldi@unitus.it

A. Petroselli

Department of Economics, Engineering, Society and Enterprise (DEIM), University of Tuscia, Via San Camillo de Lellis snc, 01100 Viterbo, Italy

R. Piscopia

Freelance, Via Flaminia 793, 00191 Rome, Italy

© Springer Nature Switzerland AG 2020

A. Coppola et al. (eds.), *Innovative Biosystems Engineering for Sustainable Agriculture, Forestry and Food Production*, Lecture Notes in Civil Engineering 67,
https://doi.org/10.1007/978-3-030-39299-4_15

approaches. The popular ‘event-based’ scheme defines the DH through the rainfall-runoff transformation of a design hyetograph characterized by an assigned return period (Tr). The more recent ‘continuous simulation’ approach consists in generating a long synthetic rainfall time series and transforming it through a continuous rainfall-runoff model (Moretti and Montanari 2008; Grimaldi et al. 2012a, b).

The event-based procedure is widely applied since it is based on the easily available DDF curves, however this approach involves some assumptions whose effects are difficult to quantify, including the simplified hyetograph shape, the concept of critical rainfall duration, the lack of information about the antecedent soil wetness conditions and the hypothesis that the design storm and the DH have the same return period (Verhoest et al. 2010). In order to overcome such drawbacks, in the last years continuous modelling approaches have been developed and many Authors have evaluated their performances with respect to event-based methods (Nnadi et al. 1999; Alfieri et al. 2008; Viglione and Bloschl 2009; Nishat et al. 2010).

In this contribution, we compare the continuous and the event-based approaches within two different and recently developed frameworks, with the aim of investigating the influence of the AMC (Antecedent Moisture Condition) on the estimated design peak discharge.

2 Materials and Methods

2.1 Data Set

The selected case study is the Vezza river basin, a right tributary of the Tiber river located in the Lazio Region, central Italy (Fig. 1). The watershed outlet was selected at the confluence with the Tiber river, determining a total contributing area equal

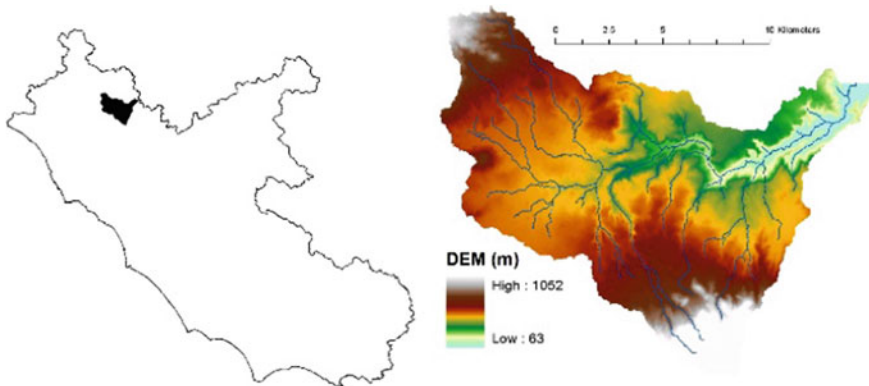


Fig. 1 Vezza river basin case study. Localization (left), DEM and drainage network (right)

to 168.1 km². A Digital Elevation Model (DEM) at 20 m resolution was retrieved thanks to IGMI, while the land cover was extracted using the CORINE European database.

Rainfall data, consisting in 71 years (from 1928 to 2015, with gaps) of annual maxima observations with durations of 1, 3, 6, 12, and 24 h, plus 22 years (from 1994 to 2015) at high resolution (from 1 min to 15 min) were retrieved from the Viterbo raingauge station, that is nearest to the watershed centroid.

Rainfall observations were used as input of the HyetosR 1.1 software according the methodology described in Grimaldi et al. (2016), for generating a synthetic rainfall timeseries of 500 years at 1-hour resolution. Such synthetic rainfall timeseries represents the input data for the event-based and the continuous modelling approaches, as explained in the following.

2.2 *Event-Based Modelling Approach*

The 500 years synthetic rainfall timeseries was analyzed extracting the 500 annual maxima of cumulative values with the standard durations of 1, 3, 6, 12, and 24 h. Such values allowed the development of the DDF curves, which were based on the empirical Weibull formulation for return periods of 10, 20, 50 and 100 years. The DDF curves were used as input rainfall data of the Event-Based Approach For Small and Ungauged Basins (EBA4SUB) conceptual rainfall-runoff model (Grimaldi and Petroselli 2015; Piscopia et al. 2015; Petroselli and Grimaldi 2018).

The framework consists in a series of modules typical of the event-based procedures: design gross rainfall estimation, design hyetograph selection, excess rainfall estimation, and rainfall-runoff transformation.

In the present contribution, the rectangular hyetograph was selected for the design gross rainfall estimation, assuming a rainfall duration equal to the basin concentration time (8 h), estimated using the Giandotti formula.

The excess rainfall estimation was performed applying the SCS-Curve Number method (NRCS 2008), with the Curve Number (CN) value automatically estimated from the land cover data and assuming a Hydrologic Soil Group B. The CN estimation was performed both in Antecedent Moisture Condition (AMC) II (average condition for soil moisture; CN 68.1) and in the AMC III condition (wet soil; CN 82.9).

It is noteworthy that usually EBA4SUB estimates the excess rainfall employing the CN4GA (Grimaldi et al. 2013a, b) module, that combines the SCS-Curve Number method with the Green-Ampt infiltration scheme. But in this specific analysis, in order to reduce the computational time of the continuous modelling, we refer to the classical SCS-CN method, being aware that for sub-hourly time resolution it is not appropriate and a proper version should applied, like CN4GA.

The rainfall-runoff transformation was performed using the width function-based instantaneous unit hydrograph (WFIUH-1par) (Grimaldi et al. 2012a, b), calibrating the WFIUH by imposing that its center of mass is equal to the basin lag time (TL). TL is estimated from concentration time (Tc) according to the $TL = 0.6 Tc$ relationship.

The analysis was conducted at 1 h time resolution and allowed the DH estimation, with the corresponding peak discharges, for the specified return periods.

2.3 Continuous Modelling Approach

The 500 years synthetic rainfall timeseries was used as input data of the simulation framework named COSMO4SUB (CONTinuous Simulation MODEL For Small and Ungauged Basins). COSMO4SUB (Grimaldi et al. 2012a, b) consists in a multi-step procedure characterized by a rainfall generator, an infiltration and rainfall excess model, and a rainfall-runoff model.

Regarding the second step, the excess rainfall estimation was performed as above applying again the SCS-Curve Number method (NRCS 2008), with the model changing automatically the AMC condition based on the cumulative value of rainfall occurred in the previous 5 days.

Regarding the third step, the same WFIUH-1par of the event-based modelling approach was used. The analysis was performed again at 1 h timescale.

At the end of the COSMO4SUB simulation, 500 years of continuous runoff at 1 h time resolution were available. From the resulting runoff time series, the 500 annual maxima of runoff were selected and their return period was estimated applying the empirical Weibull formulation for 10, 20, 50 and 100 years.

3 Results and Discussion

In Fig. 2, the DDF curves obtained analyzing the 500 years synthetic rainfall timeseries are shown. In Table 1 and Fig. 3, the design peak discharges (Q_p), resulting from both approaches are reported and shown.

Fig. 2 The DDF curves obtained with the empirical Weibull formulation on the 500 years synthetic rainfall timeseries

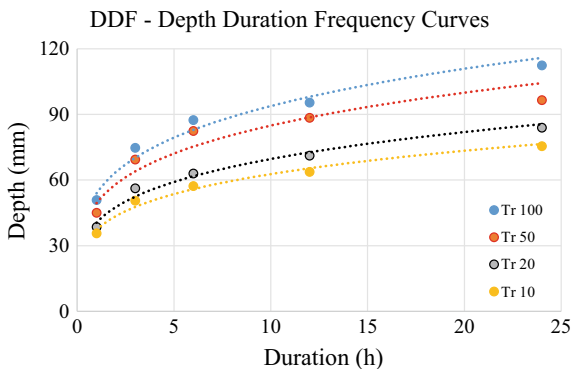
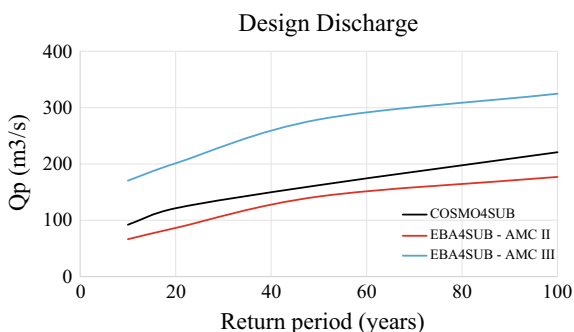


Table 1 The obtained design peak discharge values

Tr	COSMO4SUB	EBA4SUB (AMC-II)	EBA4SUB (AMC-III)	Differences (%) COSMO4SUB/ EBA4SUB (AMC II)	Differences (%) COSMO4SUB/ EBA4SUB (AMC III)
(y)	Qp (m ³ /s)	Qp (m ³ /s)	Qp (m ³ /s)		
10	92.1	66.4	170.4	27.9	-85.1
20	121.4	86.4	201.2	28.8	-65.7
50	162.3	142.2	279.0	12.4	-71.9
100	220.9	177.0	324.8	19.9	-47.0

Fig. 3 Relationship between design peak discharge and return period for the investigated approaches

Differences between the two modelling approaches are evident. The first clear comment concerns the obtained wide range, for each return period, given by the two EBA4SUB applications. For instance, for Tr 100 years, Qp ranges from 177 m³/s (AMC II) to 324.8 m³/s (AMC III). This circumstance highlights the critical role of AMC and how subjective is the event-based approach for determining the design hydrograph and peak discharge.

Conversely, it is noteworthy that the continuous modelling is able to automatically adjust AMC based on rainfall data. In doing so, the design Qp values obtained with COSMO4SUB are positioned always inside the range of values provided by EBA4SUB.

4 Conclusions

In this contribution a preliminary analysis is illustrated to highlight the benefit of continuous modelling compared to the well-known event-based approach for the estimation of the design peak discharge. Specifically, a case study demonstrates the relevant role of the Antecedent Moisture Condition (AMC) on the final results. Notably, in the event-based approach, AMC is arbitrarily selected by the analyst,

while in the continuous modelling it is automatically determined using the synthetic rainfall input.

This is only one among the numerous benefits of the continuous framework that allows to avoid several modelling choices present in the event-based approach, including hyetograph shape, critical rainfall duration, and antecedent moisture condition. This works supports the fact that the major drawback of the event-based approach is due to the high level of subjectivity of this procedure that significantly affects final results.

References

- Alfieri, L., Laio, F., & Claps, P. (2008). A simulation experiment for optimal design hyetograph selection. *Hydrological Processes*, *22*, 813–820.
- Grimaldi, S., Petroselli, A., & Serinaldi, F. (2012a). A continuous simulation model for design hydrograph estimation in ungauged watersheds. *Hydrological Sciences Journal*, *57*(6), 1035–1051.
- Grimaldi, S., Petroselli, A., & Serinaldi, F. (2012b). Design hydrograph estimation in small and ungauged watersheds: Continuous simulation method versus event-based approach. *Hydrological Processes*, *26*(20), 3124–3134.
- Grimaldi, S., Petroselli, A., & Romano, N. (2013a). Green-Ampt Curve Number mixed procedure as an empirical tool for rainfall-runoff modelling in small and ungauged basins. *Hydrological Processes*, *27*(8), 1253–1264.
- Grimaldi, S., Petroselli, A., & Romano, N. (2013b). Curve-Number/Green-Ampt mixed procedure for streamflow predictions in ungauged basins: Parameter sensitivity analysis. *Hydrological Processes*, *27*(8), 1265–1275.
- Grimaldi, S., & Petroselli, A. (2015). Do we still need the rational formula? An alternative empirical procedure for peak discharge estimation in small and ungauged basins. *Hydrological Sciences Journal*, *60*, 66–67.
- Grimaldi, S., Petroselli, A., Salvadori, G., & De Michele, C. (2016). Catchment compatibility via copulas: a non-parametric study of the dependence structures of hydrological responses. *Advances in Water Resources*, *90*, 116–133.
- Moretti, G., & Montanari, M. (2008). Inferring the flood frequency distribution for an ungauged basin using a spatially distributed rainfall-runoff model. *Hydrology and Earth System Sciences*, *12*, 1141–1152.
- Nishat, S., Guo, Y., & Baetz, B. W. (2010). Antecedent soil moisture conditions of different soil types in South-western Ontario, Canada. *Hydrological Processes*, *24*, 2417–2424.
- Nnadi, F. N., Kline, F. X., Wary, H. L., & Wanielista, M. P. (1999). Comparison of design storm concepts using continuous simulation with short duration storms. *Journal of the American Water Resources Association*, *31*(1), 61–85.
- NRCS (Natural Resources Conservation Service). (2008). National engineering handbook—part 630, Hydrology. U.S. Department of Agriculture, Washington, DC, USA.
- Petroselli, A., & Grimaldi, S. (2018). Design hydrograph estimation in small and fully ungauged basin: A preliminary assessment of the EBA4SUB framework. *Journal of Flood Risk Management*, *11*, 197–210.
- Piscopia, R., Petroselli, A., & Grimaldi, S. (2015). A software package for the prediction of design flood hydrograph in small and ungauged basins. *Journal of Agricultural Engineering 2015 XLVI*, *432*, 74–84.

- Verhoest, N. E. C., Vandenberghe, S., Cabus, P., Onof, C., Meca-Figueras, T., & Jameleddine, S. (2010). Are stochastic point rainfall models able to preserve extreme flood statistics? *Hydrological Processes*, *24*, 3439–3445.
- Viglione, A., & Blöschl, G. (2009). On the role of storm duration in the mapping of rainfall to flood return periods. *Hydrology and Earth System Sciences*, *13*, 205–216.

A Theoretical Approach to Improve the Applicability of the Catchment Connectivity Index



Giuseppe Bombino, Carolina Boix-Fayos, Maria Francesca Cataldo, Daniela D'Agostino, Pietro Denisi, Joris de Vente, Antonino Labate and Demetrio Antonio Zema

Abstract Several frameworks to evaluate the sediment connectivity—the physical linkage of sediment through the channel system—in a catchment have been proposed and verified in several environmental contexts. A simple but effective index (“catchment connectivity index”, CCI), considering the geomorphological characteristics of the channels and the connectivity between hillslopes and channels was proposed for estimating the sediment connectivity in Spanish rivers. The procedure to calculate the CCI is improved in this study, which suggest a modified index (“mCCI”) to make simpler and more realistic the hydrological and geomorphological description of the landscape elements influencing the sediment connectivity. The new procedure to calculate the mCCI reduces the need of many field surveys (whose output is often affected by errors when carried out by low-experience operators) and makes quicker the CCI application on a catchment scale (thanks to the large use of GIS).

Keywords Connectivity · Sediment source · Hillslope-channel connection · Geo-morphological factor · CCI

1 Introduction

The concept of connectivity is taken to mean the physical linkage of sediment through the channel system, which is defined as the transfer of sediment from one zone or location to another and the potential for a specific particle to move through the system. Sediment connectivity of the river system depends on the spatial variability, organization and internal connectivity of landform elements as well as its adaptability and type of response to any change (Borselli et al. 2008). Thus, it is possible to

G. Bombino (✉) · M. F. Cataldo · D. D'Agostino · P. Denisi · A. Labate · D. A. Zema
Department AGRARIA, University “Mediterranea” of Reggio Calabria, Loc. Feo di Vito, 89122
Reggio Calabria, Italy
e-mail: giuseppe.bombino@unirc.it

C. Boix-Fayos · J. de Vente
Departamento de Conservación de Suelos y Agua y Manejo de Residuos Orgánicos, Grupo de
Erosión y Conservación de Suelos, CEBAS-CSIC, Campus de Espinardo, 30100 Murcia, Spain

© Springer Nature Switzerland AG 2020

A. Coppola et al. (eds.), *Innovative Biosystems Engineering for Sustainable Agriculture, Forestry and Food Production*, Lecture Notes in Civil Engineering 67,
https://doi.org/10.1007/978-3-030-39299-4_16

investigate the overall complexity and heterogeneity of a given river system, from the relationships between its components, such as their location and extension (Brierley et al. 2006).

In the past decade the scientific literature has shown a large interest in studying sediment movement within a catchment. Sediment connectivity evaluates the sediment sources, transport and storage from hillslopes along the channels to the outlet point. Besides studying the sediment connectivity as resulting from natural processes, it is necessary to identify sediment barriers in channels, such as the retention sites due to check-dams and deposition areas between hillslopes and channels as well as the changes in the drainage area; these factors are partly responsible for the development of hillslope-channel connection (coupling), for the evolution of channel morphology (lateral erosion, bed incision, narrowing, aggradation, degradation) and for changes in the sediment balance at the catchment scale (Quiñonero-Rubio et al. 2013). Such factors must be taken into account with particular care to study the sediment connectivity of the Mediterranean torrents, where the local meteorological drivers (precipitation and temperature) coupled with the climate (semi-arid), hydrology (intermittent flow regime) and geo-morphology (high gradient, steep and coarse-grained riverbed) make these water courses particularly prone to the hydrogeological and flooding risk.

A number of frameworks to evaluate sediment connectivity in a catchment have been proposed and widely verified (e.g. Borselli et al. 2008; Cavalli et al. 2013; Grauso et al. 2018). A simple but effective index (“catchment connectivity index”, CCI) was proposed by Quiñonero-Rubio et al. (2013). CCI considers geomorphological characteristics of the channels and the connectivity slope-channel. The developers tested CCI estimating the sediment connectivity of Alto Taibilla river (SE Spain) under different historical land use patterns including hydrological control works. Some of the strengths of this index are: the inclusion of geomorphological factors, the connectivity evaluation at different spatial scales, the inclusion of transversal and longitudinal connectivity and the combination of different data sources (modelling, field data and orthophoto-interpretation). However, the procedure to calculate this index can be improved by a more efficient description of the hydrological and geomorphological parameters composing CCI; moreover, the CCI applicability can be made easier for the operators with less field experience.

To achieve these goals, this paper proposes the “modified CCI” (mCCI) that is a revised version of the original CCI of Quiñonero-Rubio et al. (2013). The mCCI minimises the need of direct surveys (whose reliability strictly depend on the ability and experience of the field operators) thanks to the use of sub-indices directly determined by GIS software, with the possibility of future use of remote sensing data.

2 The Original CCI of Quiñonero-Rubio et al. (2013)

Acknowledged the complexity and the importance of the movement of sediments within the hydrographic basin, Quiñonero-Rubio et al. (2013) developed an experimental index, mainly based on field surveys, which give a measure of the degree of

sediment connectivity in a watershed. The proposed is based on a semi-quantitative assessment of hydrological and geomorphological factors (Eq. 1), using remote sensing (analysis of aerial photography), hydrological modelling (waTEM/SEDEM model De Vente et al. 2008), GIS analysis and field observations. Thus, the authors defined the original CCI as follows:

$$CCI = \left(\frac{TC_{av}}{TC_{max}} \right) \cdot \left(\frac{100 - TE_{av}}{100} \right) \cdot \left(\frac{GF_{av}}{GF_{max}} \right) \cdot \left(\frac{SP_{av}}{SP_{max}} \right) \cdot \left(\frac{FC_{av}}{FC_{av_max}} \right) \quad (1)$$

where TC (Transport Capacity) is the sediment transport capacity within the catchment (hillslopes and channels), TE (Trap Efficiency) is the capacity of sediment retention behind check dams, GF is the Geomorphological Factor, SP (Stream Power) is the sediment transport capacity in channels, and FC (Flow Conditions) expresses the conditions of flow channels (continuous or ephemeral). The subscripts 'av' and 'max' indicate, respectively, the average and the maximum value of these factors within the catchment. The range of each factor is 0 to 1, that is, from a lower to higher connectivity, respectively.

TC (Eq. 2), has different values according to different land use scenarios by the ktc parameter. TC is given by the following equation:

$$TC = ktc \cdot R \cdot K \cdot A^{1.4} \cdot S^{1.4} \quad (2)$$

where R and K are RUSLE factors, determining rainfall erosivity and soil erodibility, A is the contributing area and S is the terrain slope. The values of ktc derive from a reclassification of the RUSLE C factor values, shown by a related map according to the C distribution for each land use (Borselli et al. 2008). The area covered by the channels is considered in the analysis. Values of ktc are calibrated assuming as optimal those obtained in previous works where the model was calibrated by WaTEM/SEDEM (optimizing values: ktc -low = 2×10^{-6} and ktc -high = 2×10^{-5}) (Boix-Fayos et al. 2008; Quiñonero-Rubio et al. 2016).

TE (Eq. 3), limits the transfer of sediment downstream, since the material is stored into drainage areas artificially created by the check dam; this factor is the trap efficiency proposed by Brown (1943):

$$TE = 100 \cdot \left(1 - \frac{1}{1 + 0.0021 \cdot D \cdot \frac{C}{W}} \right) \quad (3)$$

where C is the reservoir storage capacity (m^3), W is the catchment area (km^2), D is a value ranging from 0.046 to 1 (with a mean value of 0.1), all of them being dependent on the characteristics of the artificial reservoir.

GF explains the degree (that is, the fraction) of sediment connectivity of a sub-catchment due to geomorphological conditions at the confluence of a tributary channel with the main channel of a catchment. It can have values of 1 or 0.5 depending whether the tributary channel is connected or not to the main channel, respectively.

SP (Stream Power, Eq. 4), unlike *TC* slopes, does not consider changes in land use, being only oriented to sediment transport through the channels, not from hillslopes. As suggested by Prosser and Rustomji (2000):

$$SP = A^m \cdot S^n \quad (4)$$

SP is proportional to the drainage area (*A*) and terrain slope (*S*); *m* and *n* are two empirical values, equal to 1.4 in the work of Quiñonero-Rubio et al. (2013).

FC expresses the continuity and persistence of flow in the channels, with values of 1 or 0.5 depending whether flow is permanent or ephemeral, respectively.

Thanks to the standardization, the range of possible values for each factor is 0 to 1, from a lower to a higher connectivity, respectively.

3 Suggested Improvements of CCI (MCCI)

Modifications are made on all CCI factors (*TC*, *TE*, *GF*, *FC*), except *SP*, which is implemented only by a different standardization.

The use of WaTEM/SEDEM model provides only two values for the subfactor *ktc* of *TC* (*ktc*-low and *ktc*-high), which do not express in detail the variability of land cover of an area. For this reason, in the mCCI the USLE-C factor (better consolidated in literature) is instead proposed in the mCCI to obtain more than two classes.

For *TE* factor, Brown (1943) proposed values of *D* close to 1 (i.e., high *TE*) for reservoirs in regions with smaller and more variable runoff). More specifically, the original *TE* of Brown (1943) depends on the *C/W* ratio. However, the use of this ratio could lead to very different *TE* values (Brune 1953), since *TE* depends on runoff volumes or other hydrological characteristics (whose values are often not available in the Mediterranean catchments). Since the *TE* of CCI may be affected by a large error, which weighs on the overall CCI value, the *TE* expression of Brown is replaced in the mCCI by an index ($TE = 1 - V_s$) that provides a more accurate estimate of the ability of an artificial reservoir (such as a check dam) to store sediment in the channel. *TE* expresses the residual capacity of a barrier to store sediment, that is, the difference between the total trap capacity (equal to 1) and the volume of sediment effectively retained behind the barrier (*V_s*). This sedimentary zone can be considered as a prism with a trapezoidal section. Based on the height and surface area, the parameter *V_s* can be estimated by Eq. (5) (Castillo et al. 2007; Zema et al. 2014).

$$V_s = \frac{1}{2} w_s \cdot l_s \cdot h = \frac{1}{2} S h \quad (5)$$



Fig. 1 Sedimentary zone behind a check dam in a Mediterranean ephemeral torrent

where V_s (m^3), l_s (m), w_s (m), S (m^2), h (m) are the volume, the longitudinal length, the average width, the surface area and the height of the sedimentary zone, respectively.

The limit of the sedimentary wedge/area can be identified upstream of each barrier by the changes in longitudinal gradients or surface grain size. The surface of this sediment wedge can be mapped by GPS (Fig. 1).

Whereas the equation for calculating TE in the original expression of CCI has an empirical nature (mainly in the estimation of the parameter D , C and W), the TE proposed in the mCCI can be derived from the actual feature (shape and geometry) of a geomorphological feature of a channel and estimated by aerial maps or, in its absence, by field surveys with low possibility of errors.

In the CCI the GF and FC factors are calculated in fieldwork and, as explained above, the errors in their estimation (depending on the ability and experience of the field operators) can be high when the surveyor has low skills and experience. In order to make more realistic the evaluation and reduce the errors for the GF sub-index, the use of the terrain profile curvature (longitudinal and tangential directions) is proposed in the mCCI. Longitudinal curvature belongs to the vertical plane parallel to the slope direction, identified by Shary (1995) and Florinsky (1998) as “vertical curvature”. It measures the slope variability and influences the surface water flow velocity and thus the downstream flow of water and sediment.

GF values can be easily calculated by a common GIS based on a DEM of the study catchment. GIS calculates longitudinal curvature as the second derivative of the terrain local slope, in a 3×3 moving window surrounding a given cell of DEM. The tangential curvature is calculated as for the longitudinal value, but it is estimated in the perpendicular direction to the steepest slope. After the standardization, GF ranges from 1 (negative values of curvature, that is, concave terrain) to 0 (for higher values of curvature, that is, convex shape of terrain). Therefore, GF factor gives

information about the local shape of the terrain (convexity or concavity) using the values of longitudinal and tangential curvatures. There is a reduction or a lack of connectivity in correspondence of sediment accumulation (buffers) originated by natural (floodplain areas or areas with very low slope) or artificial (flat agricultural areas occupying and filling ephemeral channels) conditions (Quiñonero-Rubio et al. 2013).

The terrain profile curvature by GIS procedure in the mCCI, is able to better discriminate—compared to the CCI, relying to field observations—the connections between main channel and tributaries at the pixel scale. Furthermore, GIS approach is able to overcome the limit reported by Heckmann et al. (2018), who stated that (dis) connectivity operates at landform scale and not at raster cell scale.

Perennial rivers are characterized by a permanent water flow, while intermittent torrents typically alternate prolonged periods of minimum flow to flash flood events in response to the large temporal variability of precipitation. In CCI the FC factor discriminates permanent ($FC = 1$) and discontinuous flow ($FC = 0.5$). The original FC factor of Quiñonero-Rubio et al. (2013) is replaced in the mCCI by the difference (if positive, otherwise FC has a value of 0.5) of: (a) short-term precipitation given by flow duration curves at a return interval of two years (which determines the most frequent hydrological regime in Mediterranean torrents) and a duration equal to the catchment concentration time, tc ; (b) the initial abstraction (Ia), calculated by SCS-CN method. In other words, when the precipitation depth exceeds Ia , the channel has permanent flow and $FC = 1$, otherwise FC is set to 0.5.

As outlined above, the CCI requires the standardization of all factors, made by Eq. (6). If this equation is applied to the factors of the mCCI, in some cases (extreme values of DEM), the standardization provides very small values, which may become unrealistic. In the mCCI a different standardization method (Eq. 7) is proposed for all factors, except for GF , where the Eq. (8) is assumed, and for TE , which, unlike the other factors, is directly expressed as a percentage.

$$\frac{x_{avg}}{x_{max}} \quad (6)$$

$$\frac{x - x_{min}}{x_{max} - x_{min}} \quad (7)$$

$$\frac{x_{max} - x}{x_{max} - x_{min}} \quad (8)$$

Contrarily to the range of values of the CCI, the mCCI index is expressed as the binary logarithm of the product among the factors, in order to reproduce the very large range of values of the sediment connectivity. All mCCI factors being in the range $[0, 1]$, the binary logarithm is in the range $[-\infty, 0]$. To avoid negative values, the absolute value of the mCCI is taken. Accordingly, the mCCI is calculated using Eq. (9):

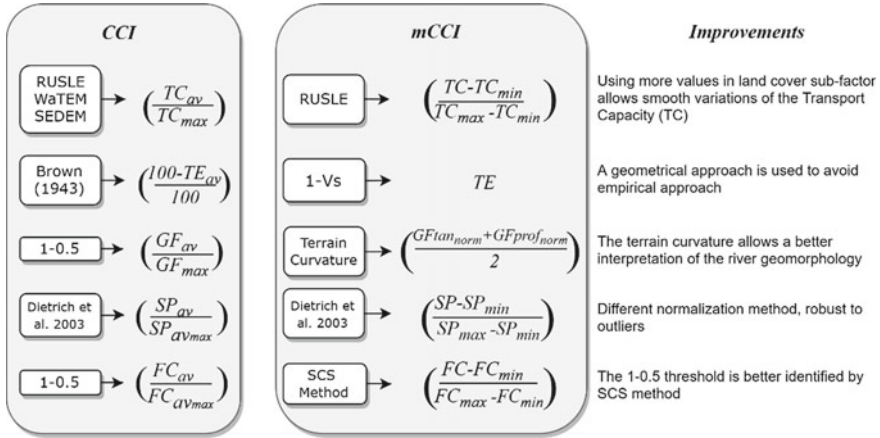


Fig. 2 Comparison of methods to calculate CCI and mCCI

Table 1 Main differences between CCI and mCCI

CCI	mCCI
Gives the sediment connectivity at the catchment or sub-catchment scales	Gives the sediment connectivity for each cell of DEM with the possibility to calculate at different spatial scales
Requires geomorphological training	Does not require experience for field operators
Some factors are binary in nature and left to the evaluation of operators	Every factor is continuous
Not automatable calculations for some factors	Quick and automatable calculation of all factors

$$mCCI = \left| \log_2 \left[\left(\frac{TC - TC_{min}}{TC_{max} - TC_{min}} \right) \cdot \left(\frac{GF_{tan_norm} + GF_{prof_norm}}{2} \right) \cdot \left(\frac{SP - SP_{min}}{SP_{max} - SP_{min}} \right) \cdot \left(\frac{FC - FC_{min}}{FC_{max} - FC_{min}} \right) \cdot TE \right] \right| \quad (9)$$

Figure 2 compares the sub-factors and the calculation procedures of CCI and mCCI, while Table 1 explains the main differences between the two indexes.

4 Conclusions

This study reports a theoretical approach to improve the applicability of the CCI of Quiñonero-Rubio et al. (2013). A modified CCI (mCCI) is suggested by improving the calculation methods of CCI. Some factors of the original index are replaced by alternative methods, which are based on DEM. This reduces the need of field

surveys and allows the almost complete automation of the procedure. The proposed mCCI may be used not only for the analysis of sediment connectivity of the individual elements of a catchment (spatial domain), but it allows also the possibility to catch the evolution of river connectivity from a diachronic perspective (temporal domain). The mCCI can be used as analytical tool to evaluate the influence of past or future changes in land use, climate and anthropogenic actions by comparing scenarios of torrent connectivity. Practical applications in different environmental contexts are expected in order to verify the efficacy and efficiency of the suggested improvements. Finally, the mCCI could be more reliable in the case of high-resolution DEM availability (e.g., LIDAR), which may allow a more realistic estimation of the geomorphological factors of the index.

References

- Brierley, G. J., Fryirs, K., & Jain, V. (2006). Landscape connectivity: The geographic basis of geomorphic applications. *Area*, 38, 165–174.
- Boix-Fayós, C., De Vente, J., Martínez-Mena, M., Barberá, G. G., & Castillo, V. (2008). The impact of land use change and check-dams on catchment sediment yield. *Hydraulic Proceedings*, 22, 4922–4935.
- Borselli, L., Cassi, P., & Torri, D. (2008). Prolegomena to sediment and flow connectivity in the landscape: A GIS and field numerical assessment. *CATENA*, 75, 268–277.
- Brown, C. B. (1943). Discussion of Sedimentation in reservoirs, by J. Witzig. *Transactions of the American Society of Civil Engineers*, 69, 1493–1500.
- Brune, G. M. (1953). Trap efficiency of reservoirs. *Transactions of the American Geophysical Union*, 34(3), 407–418.
- Castillo, V. M., Mosch, W. M., Conesa, García C., Barberá, G. G., Navarro Cano, J. A., & López-Bermúdez, F. (2007). Effectiveness and geomorphological impacts of check dams for soil erosion control in a semiarid Mediterranean catchment: El Cárcavo (Murcia, Spain). *CATENA*, 70(3), 416–427.
- Cavalli, M., Trevisani, S., Comiti, F., & Marchi, L. (2013). Geomorphometric assessment of spatial sediment connectivity in small Alpine catchments. *Geomorphology*, 188, 31–41.
- De Vente, J., Poesen, J., Verstraeten, G., Van Rompaey, A., & Govers, G. (2008). Spatially distributed modelling of soil erosion and sediment yield at regional scales in Spain. *Global and Planetary Change*, 60, 393–415.
- Florinsky, I. V. (1998). Accuracy of local topographic variables derived from digital elevation models. *International Journal of Geographical Information Science*, 12, 47–61.
- Grauso, S., Pasanisi, F., & Tebano, C. (2018). Assessment of a simplified connectivity index and specific sediment potential in river basins by means of geomorphometric tools. *Geosciences*, 8(2), 48.
- Heckmann, T., Cavalli, M., Cerdan, O., Foerster, S., Javaux, M., & Lode, E. et al. (2018). Indices of sediment connectivity: Opportunities, challenges and limitations. *Earth-Science Reviews*.
- Prosser, I. P., & Rustomji, P. (2000). Sediment transport capacity relations for overland flow. *Progress in Physical Geography*, 24, 179–193.
- Quiñonero-Rubio, J. M., Boix-Fayós, C., & De Vente, J. (2013). Desarrollo y aplicación de un índice multifactorial de conectividad de sedimentos a escala de cuenca. *Cuadernos de Investigación Geográfica*, 39, 203–223.

- Quiñonero-Rubio, J. M., Nadeu, E., Boix-Fayos, C., & de Vente, J. (2016). Evaluation of the effectiveness of forest restoration and check-dams to reduce catchment sediment yield. *Land Degradation & Development*, 27(4), 1018–1031.
- Shary, P. (1995). Land surface in gravity points classification by a complete system of curvatures. *Mathematical Geology*, 27(3), 373–390.
- Zema, D. A., Bombino, G., Boix-Fayos, C., Tamburino, V., Zimbone, S. M., Fortugno, D. (2014). Evaluation and modeling of scouring and sedimentation around check dams in a Mediterranean torrent in Calabria, Italy. *Journal of Soil and Water Conservation*, 69(4), 316–329.

On the Performance of a Novel Hybrid Constructed Wetland for Stormwater Treatment and Irrigation Reuse in Mediterranean Climate



Delia Ventura, Salvatore Barbagallo, Simona Consoli, Mirco Milani, Alessandro Sacco, Ruggero Rapisarda and Giuseppe Luigi Cirelli

Abstract Decentralized water treatment facilities (DWFTs) have been described as one of the best practices (BMPs) for promoting effective water management programs in the framework of the circular economy, with the aim to ease the exploitation of freshwater supply. In many Mediterranean regions, wastewater (WW) reuse practice is still struggling for being accepted and it's clearly affected by legislation gaps and discrepancy among national and European perspectives. This work mainly investigates some issues related to stormwater and conventional WW reuse feasibility for green areas irrigation, after being treated by a pilot hybrid constructed wetland (H-CW) in Mediterranean climate. Experimental results are promising and suggest as viable the reclaimed water use in green area irrigation. Nevertheless, at the light of the EU guidelines proposal, the effluent water quality hereby reported fulfilled the minimum requirements for the intended use above mentioned, but did not fully comply the stringent Italian standards.

Keywords Decentralized water · Treatment · Stormwater · Reuse · Legislation · Metals

1 Introduction

Future urban scenarios could benefit from decentralized water treatment facilities (DWFTs) for effective water management of conventional and unconventional sources. In fact, De Feo et al. (2014) pointed out the unfeasibility to extend existing centralized water and wastewater (WW) systems to cope with the increasing level of urbanization, with consequent extra water demand and waste loads. Many WW facilities still remain vulnerable to the adverse effects of climate variability, with different frequencies in drought and flood all over the world. Moreover, in developed economies, like European Member States (MS), many infrastructures are

D. Ventura (✉) · S. Barbagallo · S. Consoli · M. Milani · A. Sacco · R. Rapisarda · G. L. Cirelli
Department of Agriculture, Food and Environment, University of Catania, Via S. Sofia 100, 95123
Catania, Italy
e-mail: delia.ventura@phd.unict.it

© Springer Nature Switzerland AG 2020

A. Coppola et al. (eds.), *Innovative Biosystems Engineering for Sustainable Agriculture, Forestry and Food Production*, Lecture Notes in Civil Engineering 67,
https://doi.org/10.1007/978-3-030-39299-4_17

ageing, while developing countries are facing challenging and costly investments for upgrading poor sewerage and drainage systems (SDS). In Italy, WW collection and treatment is largely lacking and insufficient, as reported by the European Community (EC), that considers 620 agglomerations in 16 regions in breach of the EU rules (EC 2019). In particular, several EC infringement procedures and one condemnation of the Court of Justice, highlight absent or not complying infrastructures in 62 (>10.000 PE) and 5 (>2.000 PE) agglomerations in Sicily (CSEI, 2018). Begum et al. (2008) already described several stormwater reuse techniques used around the world, and sensitive urban design systems (SUDS) for urban green areas and sport fields irrigation have been particularly proposed. However, as reported by Goonetilleke et al. (2017), stormwater are still globally undervalued, because of related uncertainty and unreliability due to seasonal supply and therefore to quantitative and qualitative issues that could complicate the implementation of storage and treatment planning and designing strategies. In order to reduce the consequent counterproductive effects of combined quantitative and qualitative constraints, such as increased management and treatment costs, the intended use is a key concept allowing to use different water, with highly variable quality. To this aim, the adoption and the application of suitable existing technologies should be fitted for given water reuse purposes. Regarding to that, the possibility to increase and define technical knowledge and management guidance can turn it into the chance to knowingly relay on extensive, more adaptive and self-supporting DWTFs. In the case of first flush rain water and stormwater runoff, Italian normative (Legislative Decree 152/06, Art. 113), specified that the Regions, subject to the authorization of the Ministry of the Environment, can regulate and manage, by means of specific rules and “case by case”, these resources. On this regard, Lombardy and Emilia Romagna have promulgated the appropriate regional regulations, while the Sicily region, among others, does not have anyone yet. Stormwater runoff have been compared to industrial WW and their reuse, as well as for domestic and urban WW, is regulated by the Ministerial Decree (M.D.) 185/2003. However, the strictness of this law, which is reflected in costly monitoring activity, the absence of clear standard limits for specific intended use, and also the increasing tariffs to the expense of consumers for covering the reuse costs, generally discourages the spread of this practice (Ventura et al. 2019a). To optimize costly and time—consuming microbial monitoring analyses for WW reuse, the Italian Superior Institute of Health (Bonadonna et al. 2002) already proposed *Clostridium perfringens* as an effective indicator for old faecal contamination. However, the latter has never been included in the Italian standard limits for water reuse (M.D. 185/2003). Also the recent EU proposal for water reuse (European Commission, 2018) recommended *Escherichia coli* and *Clostridium perfringens*, respectively, as the most appropriate indicators for pathogenic bacteria and protozoa assessment. Masi et al. (2018), highlighted how generally people are not willing to pay for wastewater reuse service and there is a need to demonstrate the reliability of costs-saving treatment technologies on the long term. The EU proposal for water reuse (2018) could be considered, in this context, as a first important step for easing and conforming its promotion and actualization at national level (Ventura et al. 2019a). Despite CWs are well known treatment technologies and largely applied since several decades at

international level (e.g. in Germany, since the end of 70's), however, there is a need to fill the knowledge gap on their technical performances, management procedures and design criteria (CSEI, 2018). As a step forward of previous case study on the reliability of a pilot hybrid constructed wetland (H-CW) in treating typical stormwater runoff contaminants (metals and polycyclic aromatic hydrocarbons, PAHs) and alternative conventional rich-nutrient WW in the favorable climate of Mediterranean area (Ventura et al. 2019b), this work mainly aims at investigating some issues related to treated WW reuse feasibility for green areas irrigation, with special regard to Italian and EU legislations.

2 Case Study

The H-CW is constituted by two identical parallel lines (1–2), with a common inlet (stabilization pond, monitoring points: in unit #1, out unit #2), a sub-surface horizontal flow bed (HF1-HF2, monitoring point: out unit #3), planted with *Canna indica*, and a free-water surface unit (FWS1-FWS2, monitoring point: out unit #4) with floating *Typha latifolia*, for each line. For further details on H-CW design, operating, site location, monitoring steps, metals and PAHs analytical methods, as also statistical approach, refer to Ventura et al. (2019b). For conventional water quality and overall removal efficiency (RE, %) relate to Marzo et al. (2018). Also, microbial indicators and pathogens were monitored: *Escherichia coli* and *Costridium perfringens* spore were analysed with the method of membrane filtration and culturing on suitable agar media.

Overall, water quality parameters are shown as averaged values from treatment line 1 and 2 since non-parametric data analysis did not reveal any significant differences (Kruskal-Wallis test p-values >0.05). In Table 1, mean values of main physical parameters for each period are reported, at the general inlet and outlet of the hybrid system as also relative P-values for the latter (caption a). Electrical conductivity (EC) and dissolved oxygen (DO) values varied among I, II and III periods, along the treatment units (data not show), and generally between the inlet and the outlet of the plant, due to the different quality of WW treated, the seasonality and the hydraulic regime of each bed. The system design can clearly determine very variable biological and chemical dynamics occurring in within, particularly when a hybrid CW is set up. In fact, thanks to the arrangement of different CWs types all potential pollutants removal mechanisms can be exploited (Stefanakis and Akrotas 2016). Among the parameters reported in Table 1, the EC should be considered together with the SAR index for a proper evaluation of the ultimate effect on water infiltration rate for pursuing suitable irrigation management practices (FAO 1994). In Fig. 1a the relationship between these two parameters in terms of soil structural stability is plotted, as already described by ANZECC (2000). The Fig. 1b reports the mean EC and SAR values observed at the inlet and the outlet of the hybrid CW during the SBR effluent (I period) and runoff (II-III period) treatment. After the treatment, in both cases, a quite increase of both parameters can be noted. The EC increment could be explained

Table 1 Average values and standard deviation (SD, \pm) of physical parameters recorded at H-CW Inlet and Outlet during the three monitoring periods; dissolved oxygen (DO), electrical conductivity (EC, at 20 °C), pH and T (°C)

Period	I		II		III	
	Inlet	Outlet	Inlet	Outlet	Inlet	Outlet
DO (mg L ⁻¹)	6.7 (1.8)	5.6 (2.5) ^{a1}	4.9 (1.5)	8.4 (2.3) ^{a0.08}	3.1 (0.7)	3.3 (0.1) ^{a0.59}
EC (μ S cm ⁻¹)	1910 (388)	2851 (1443) ^{a0.87}	114 (14)	471 (291) ^{a0.35}	160 (73)	218 (30) ^{a0.07}
pH	7.5 (0.3)	7.2 (0.2) ^{a0.57}	6.7 (0.9)	7.5 (0.8) ^{a0.92}	6.7 (0.7)	7.4 (0.01) ^{a0.91}
T (°C)	28.9 (3.1)	26.5 (3) ^{a0.87}	15.2 (1.9)	15.21 (1.4) ^{a0.75}	23.9 (6.1)	21.7 (0.2) ^{a0.75}

^aKruskal-Wallis test p-values calculated between identical treatment units (FWS1-FWS2: outlet point)

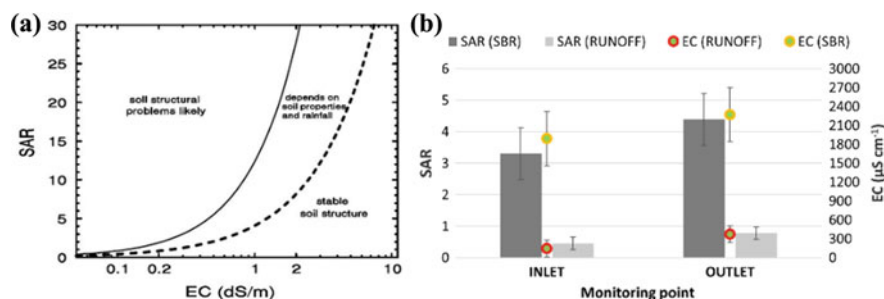


Fig. 1 Mean EC and SAR values detected at the inlet and outlet points of the hybrid CW during runoff and SBR effluent treatment (a); the relationship between SAR and EC for soil structural stability (b), as it appears in ANZECC (2000). Note that 1 dS m⁻¹ = 1000 μ S cm⁻¹

by evapotranspiration (ET) processes taking place in the treatment beds, while the photosynthetic activity occurring in the FWS units could have risen the pH values (as referred in Table 1), causing cations precipitation like Mg²⁺ and Ca²⁺ and therefore a slight SAR increase. By comparing the two graphs, it seems that in this case, the CW treatment train could have played a positive role by making more favourable the EC and SAR relationship in the perspective of WW reuse for irrigation. However, too high proportion of sodium (Na⁺) ions relative to Mg²⁺ and Ca²⁺ could degrade the soil stability and reduce plants growth. Finally, the SAR index was always within the Italian standard limits for water reuse.

In Fig. 2, concentrations of main water quality parameters during SBR effluent treatment (I period) are reported as boxplots, at the inlet, the HF outlet and the final

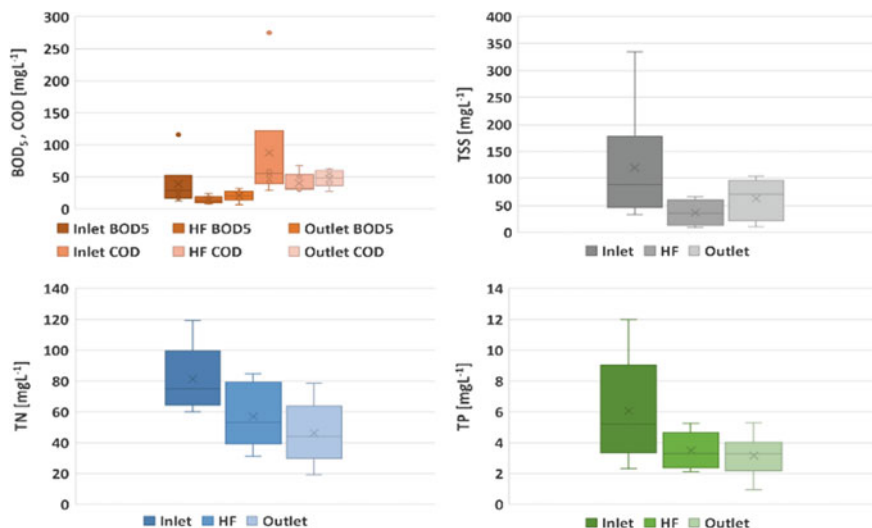


Fig. 2 Boxplots of the concentrations of conventional quality parameters (BOD₅, COD, TSS, TN and TP) detected in water samples collected at the inlet, the HF outlet, and the final outlet of the H-CW, during I monitoring period (SBR effluent treatment)

outlet of the H-CW system. By comparing the partial RE (%) observed at the HF outlet and the overall one (respectively: 64–45 TSS, 50–25 BOD₅, 35–16 COD, 25–38 TN, 35–41 TP), it was evident that the sub-surface horizontal flow units had better performance for organic matter and TSS removal, while the free water surface units for nutrients depletion. These trends were probably due to the instability of the novel system (data were collected since the start-up phase of the system and during the first year and a half of operations): macrophytes growth was, in fact, quite limited (FWS units were replanted after 6 months because the floating support was damaged and replaced) and algal proliferation occurred during warmer seasons was not confined and retained by the typical *Typha latifolia* huge root system, that was expected to act as a final filter. Outlet concentrations of TSS, BOD₅, COD, TN and TP were respectively: 62.5 (±37), 20.3 (±8), 47 (±13), 3.2 (±1.5), 46.3 (±21). These values were generally not complying with the Italian standard limits for reuse (Table 2), except for COD and TP, but confirmed the self-defeating strictness of this legislation. According to the Table 2 of the European proposal for water reuse (EU 2018) on reclaimed water quality criteria for agricultural irrigation in case of non-food crops (quality classes B and C), BOD₅ and SST limits refer to those reported in the European Directive on urban wastewater treatment (91/271/EEC): respectively 25 mg L⁻¹ and 35 (<10.000 PE) or 70 mg L⁻¹ (2.000-10.000 PE), while COD and nutrients limits are not reported. However, among the environmental hazards linked to reclaimed water use in agriculture, the same EU proposal cites the nutrients imbalance (the others are salinization, sodicity and toxicity) and reminds the importance of MS in knowledge gathered in order to limit concrete environmental risks.

Table 2 Physical-chemical (mgL^{-1}), trace metals (mgL^{-1}), and microbiological (CFU 100 mL^{-1}) Italian standard limits for wastewater discharge and reuse

Italian standard limits	TSS	BOD ₅	COD	TN	TP	Tot Cr	Fe	Ni	Pb	Cu	Zn	<i>E. coli</i>
WW discharge ^a	80	40	160	35 ^c	10	2	2	2	0.2	0.1	0.5	5.0×10^{3d}
WW reuse ^b	10	20	100	15	2	0.1	2	0.2	0.1	1	0.5	100 ^e

^aLegislative Decree 152 (2006),

^bMinisterial Decree 185 (2003),

^cLimit for discharge into surface water bodies (as the rough sum of NH_4 , N-NO_2 and N-NO_3),

^dRecommended value for PE: > 2,000,

^eMaximum value in 80% of samples, 100 is the max punctual value permitted; in case of natural systems, like lagooning and constructed wetlands, limits increase up to 50 UFC 100 mL^{-1} (80% of samples) and 200 UFC 100 mL^{-1} (max punctual value)

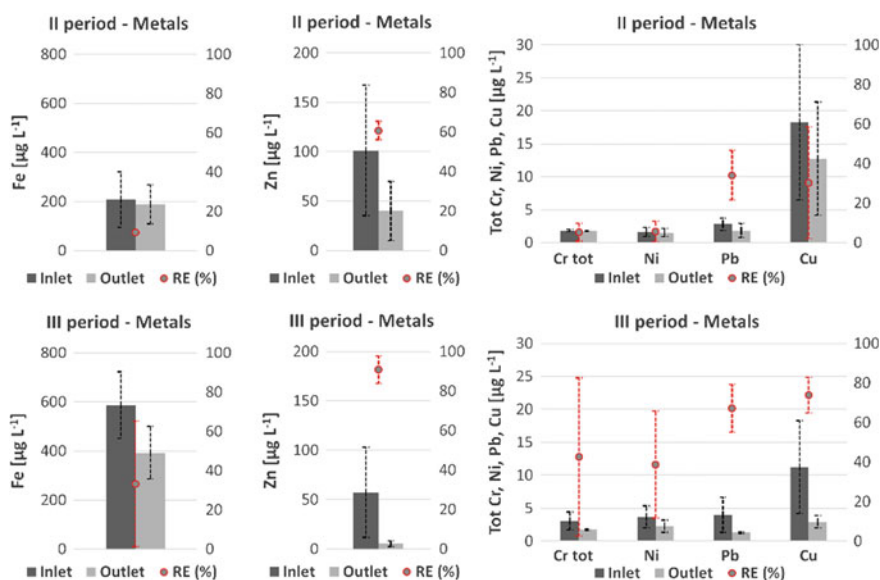


Fig. 3 Mean metals concentrations ($\mu\text{g L}^{-1}$), SD, removal efficiency (RE, %) (red points) and SD at the hybrid CW inlet (monitoring point #1) and outlet (monitoring point #4) during runoff treatment (II–III monitoring periods)

The presence of metals in stormwater runoff is strongly influenced by rainfall events and intensity, the hydraulic loads entering the treatment system and the physical state they are found in (dissolved or particle-bound). Physical form, together with temperature, conductivity and pH variations can foster metals release in water and are crucial in major metals removal processes, like their association with granular media, precipitation as salts and biological uptake. Figure 3 reports mean metals concentrations ($\mu\text{g L}^{-1}$) and relative removal efficiency during II and III monitoring periods. They were always very low and clearly below the values imposed by Italian standard limits for reuse (Table 2), but a slight increase between II and III periods (except for Zn and Cu), allowed to observe higher RE during the last one (ranging from 33% (± 32) for Fe to 91% (± 7) for Zn). Mean *E. coli* concentrations (log UFC 100 ml⁻¹) were at the inlet and the outlet during I, II and III periods, respectively: 4.1 (± 0.12) and of 1.5 (± 0.4), with an overall RE of 2.6 (± 0.4); 2 (± 0.3) and 0.4 (± 0.2), with an overall RE of 1.6 (± 0.2); 1.5 (± 1.3) and 0.09 (± 0.2) with an overall RE of 1.4 (± 0.6). Mean *C. perfringens* concentrations (log UFC/100 ml) were at the inlet and the outlet during I, II and III periods, respectively: 3.3 (± 0.2) and 1.3 (± 0.2) with an overall RE of 2 (± 0.3); 2.6 (± 0.3) and 0.8 (± 0.1) with an overall RE of 1.8 (± 0.4); during the III period, *C. perfringens* was not determined. H-CWs pathogens removal efficiency has been generally evaluated up to 4 u-log, and in some case, depending on the initial microbial load, further disinfection technology must be used. Thanks to the combination of different CWs types (which can promote prolonged HRTs like usually HSF units do, and high DO concentrations ensured by

VF stages), however, all potential pathogen removal mechanisms can be encouraged (Stefanakis and Akratos, 2016). In this study, different effects of various treatment units, in function of the indicator or pathogen considered were observed, since main RE of *E. coli* occurred at the FWS outlet, while *C. perfringens* was removed already at the HF outlet. The latter is an obligate anaerobic, but in spite of its resistance to environmental changes and disinfection processes, perhaps could have been inhibited by possible microbial predation activities and/or unfavourable environmental conditions occurrence (like atmospheric oxygen transferring in the rhizosphere of *Canna indica*). Finally, the sum of the PAHs species analysed at the system inlet, had an average concentration of $0.038 \mu\text{g L}^{-1}$ (± 0.017), which was clearly below respectively to 0.01 and 0.001mg L^{-1} , the Italian standard limits relative to the total organic aromatic compounds and benzene for water reuse. However, despite the low concentrations detected, the overall removal efficiency was 81% (± 31), and 78% (± 11) was already observed at the outlet of the Pond. This could be in agreement with the major removal mechanism of PAHs in CWs described by Wojciechowska in terms of sedimentation (2013).

3 Conclusions

The novel H-CW system exhibited positive performance even treating two types of WW, highly different in terms of nutrient-richness. On this regard, main considerations are reported by Ventura et al. (2019b). However, there is still a strong discrepancy between the Italian legislation for water reuse and the guidelines proposed by the EU, which clearly would require an implementation process for being integrated at national level. Even when considering conventional parameters and microbial indicators for water quality monitoring for reuse, quantitative and qualitative differences appear obvious. Therefore, the overcoming of this gap probably remains a key point to make effective the WW reuse practice in Italy, also because the intended use would be finally considered. Valuable resource like stormwater runoff would be then valorized. In fact, at the light of EU guidelines proposed, the effluent water quality reported in this case study would fulfil the minimum requirements for reuse in green area irrigation, in contrast with the stringent Italian standard limits, which would not be fully complied.

Acknowledgements The research was performed within the international research joint project, WATinTECH (WATERWORKS 2014- ID 196), and “GREENWATER—Le infrastrutture verdi per la gestione e la tutela delle risorse idriche” (PRIN 2015 Programme) (grant N. PRIN2015 AKR4HX), both funded by the Italian Ministry of University and Research.

References

- ANZECC. (2000). Australian and New Zealand guidelines for fresh and marine water quality. (Australian Water Association).
- Bonadonna, L., Briancesco, R., D'Angelo, A. M., & Marini, R. (2002). Clostridium perfringens as an environmental pollution indicator and its hygienic role. Istituto Superiore di Sanità, 39 p. Rapporti ISTISAN 02/8.
- De Feo, G. De, Antoniou, G., Fardin, H. F., El-gohary, F., Zheng, X. Y., & Reklaityte, I., et al. (2014). The historical development of sewers worldwide. (June), *Sustainability*, 3936–3974. <https://doi.org/10.3390/su6063936>
- EC, European Commission (2019). http://europa.eu/rapid/press-release_IP-19-1475_en.htm. Accessed 08 July 2019.
- EU, European Union (2018). http://ec.europa.eu/environment/water/pdf/water_reuse_regulation.pdf448. Accessed June 7, 2018.
- FAO (1994). <http://www.fao.org/3/T0234e/T0234E04.htm>. Accessed 08 July 2019.
- Goonetilleke, A., Liu, A., Managi, S., Wilson, C., Gardner, T., Bandala, E. R., et al. (2017). Stormwater reuse, a viable option: Fact or fiction? *Economic Analysis & Policy*, 56, 14–17. <https://doi.org/10.1016/j.eap.2017.08.001>.
- Legislative Decree 152. (2006). Decreto Legislativo 3 aprile 2006, n.152, 'Normative requirements on the environment', GU n. 88, April 14th 2006.
- Marzo, A., Ventura, D., Cirelli, G. L., Aiello, R., Vanella, D., Rapisarda, R., et al. (2018). Hydraulic reliability of a horizontal wetland for wastewater treatment in Sicily. *Science of the Total Environment*, 636(September), 94–106.
- Masi, F., Rizzo, A., & Regelsberger, M. (2018). The role of constructed wetlands in a new circular economy, resource oriented, and ecosystem services paradigm. *Journal of Environmental Management*, 216, 275–284.
- Ministerial Decree 185. (2003). Decreto Ministeriale 12 giugno 2003, n. 185. 'Technical standards for wastewater reuse', GU n. 169, July 23th 2003.
- Stefanakis, A. I., & Akratos, C. S. (2016). Removal of pathogenic bacteria in constructed wetlands: Mechanisms and mechanisms and efficiency, (October). *Phytoremediation*. <https://doi.org/10.1007/978-3-319-41811-7>.
- Ventura, D., Consoli, S., Barbagallo, S., Marzo, A., Vanella, D., Licciardello, F., et al. (2019a). How to overcome barriers for wastewater agricultural reuse in Sicily (Italy)? *Water*, 11(2), 335. <https://doi.org/10.3390/w11020335>.
- Ventura, D., Barbagallo, S., Consoli, S., Ferrante, M., Milani, M., Licciardello, F., et al. (2019b). On the performance of a pilot hybrid constructed wetland for stormwater recovery in Mediterranean climate. *Water Science and Technology*, 79(6), 1051–1059. <https://doi.org/10.2166/wst.2019.103>.
- Wojciechowska, E. (2013). Removal of persistent organic pollutants from landfill leachates treated in three constructed wetland systems. *Water Science and Technology*, 68(5), 1164–1172. <https://doi.org/10.2166/wst.2013.316>.

Rural Buildings, Equipment and Territory

Introduction

Prof. Patrizia Tassinari

President of the 2nd Section of the Italian Association of Agricultural Engineering ‘Rural Buildings, Facilities and Territory’

The research, innovation and education activities of the scientific community of the 2nd Section of the Italian Association of Agricultural Engineering ‘Rural Buildings, Facilities and Territory’ contribute to 11 of the 17 sustainable development goals of the United Nations, and in particular: Zero hunger (Food security and sustainable agriculture), Good health and well-being, Quality education, Affordable and clean energy, Industry, innovation and infrastructure, Reduced inequalities, Sustainable cities and communities, Responsible consumption and production, Climate action (To combat climate change and its impacts), life below water, life on land (Protect, restore and promote sustainable use of terrestrial ecosystems).

The main topics studied by the scholars are related to the plant production chain (protected cultivation structures and materials, precision systems), to the animal production chain (livestock buildings, PLF, livestock wastes), and to the agri-industrial production chain (structures for conditioning, processing and preserving vegetal and animal products), as well as to vegetal and agri-industrial wastes and by-products and biomass. Significant and growing attention is also paid to environmental, landscape and territorial resources, with reference to both rural, peri-urban and urban areas, and in particular to the themes of territory and environment, landscape, green systems and infrastructure, cultural resources and heritage.

Both studies on the built system and territorial systems are conducted with innovative methodological approaches, such as: probabilistic-previsional models and simulations—optimization algorithms, spatial analysis/statistics, ICT—smart systems—machine learning—computer vision—big data—IoT—artificial intelligence, remote sensing and proximal remote sensing, risk and vulnerability evaluation, circular approach—life-cycle analysis and life-cycle cost analysis, performance evaluation.

Interdisciplinary and cross-sector approaches characterize most of the research works of the scholars, in line with what is required by the evolution of knowledge itself, by the ever-increasing complexity of the needs of the productive and

socio-economic world, and by the challenges related to environmental protection (resilience, regeneration, circularity) and to a general improvement in the welfare conditions of ecosystems (safety, health, well-being).

Urban Agriculture, Cui Prodest? Seattle's Picardo Farm as Seen by Its Gardeners



M. E. Menconi, P. Borghi and D. Grohmann

Abstract The urban green network provides various ecosystem services that are crucial assets in determining cities' sustainability. Urban agriculture is a type of urban green space that is experiencing a growing interest among Institutions and researchers. This paper analyses its benefits, as perceived by the urban gardeners, using an open-questions survey. The case study is a community garden in Seattle, called Picardo farm. The results show how the citizens involved in community gardens are aware of a variety of values linked with the urban agriculture, that provides outdoor activities, food production, connection with nature, wellbeing, education, and positive social interactions. A significative strength of the community gardens regards the ability to build site-specific cohesive communities, guaranteeing constant stewardship of the place where they are located. Finally, the results show that urban agriculture is a complementary form of urban green space provision with distinctive values of respect to other urban green spaces.

Keywords Gardeners' perception · Community gardens · Place attachment · Wellbeing · Sense of belonging · Urban green system

1 Introduction

Urban agriculture has many types of functional dimensions: allotment gardens, educational gardens, therapeutic gardens, community gardens, squatter gardens, and urban farming (Lohrberg et al. 2015). Every dimension offers interesting and innovative aspects for the planning of sustainable urban green systems (United Nations 2016; FAO 2019; Bill et al. 2016; Weidner et al. 2019).

This paper aims to outline the role of the community gardens in urban green networks, by analyzing the benefits of one of them in Seattle (USA), as perceived by its gardeners.

M. E. Menconi · P. Borghi · D. Grohmann (✉)

Department of Agricultural, Food and Environmental Sciences, University of Perugia, Perugia, Italy

e-mail: david.grohmann@unipg.it

© Springer Nature Switzerland AG 2020

A. Coppola et al. (eds.), *Innovative Biosystems Engineering for Sustainable Agriculture, Forestry and Food Production*, Lecture Notes in Civil Engineering 67,
https://doi.org/10.1007/978-3-030-39299-4_18

2 Method

2.1 Study Area

The study area is the Picardo farm in Seattle (Fig. 1).

This community garden started in 1973 and has inspired the Municipality of Seattle to develop a public program dedicated to urban community gardens, called Municipal P-Patch Community Gardening program (Hou and Grohmann 2018). P-Patch Program coordinates the planning, development, and management of community gardens, through the search of suitable areas, the production of a regulatory framework, and the organization of various social aspects, such as the land-banking, the promotion of edible planting, and the food banking (Hou and Grohmann 2018). “P” of P-Patch stands for “Picardo,” the name of the family who owned the land since the 1920s, and that opened the area to shared uses with the local community (Murakami 2005). In 1975, the area occupied by Picardo farm was bought by the City of Seattle.

Picardo farm covers 1.2 hectares, subdivided into 281 plots. Every plot is assigned to a gardener that freely manages its uses. The 85% of the 281 gardeners are white or Caucasian; they are aged 25 to 80. Gardeners can use shared services (furniture, water, kindergarten) and must to do 8 h/year working with shared purposes. There is a volunteer team of 4 people for organizing the community, called *garden leaders*.



Fig. 1 Picardo farm

2.2 Gardeners’ Survey

The method uses a survey of two open questions for understanding the strengths and weaknesses of the farm, as perceived by its 281 gardeners. The survey is hosted on the website of P-Patch, and it has these questions: “What do you like best about coming to Picardo farm?”, and “What do you like least about coming to Picardo farm?”. It gives a maximum of 500 words for every answer.

The method searches for recurrence keywords in the answers building clusters through this process. An answer could belong to more clusters if the respondent lists more themes in common with the others or if he gives positive and negative considerations for the same theme. In these cases, the same answer is counted more times.

3 Results and Discussion

The resulting clusters are eleven, belonging to six recurrence keywords: *gardening activity*, *social interactions*, *place*, *health*, *education*, and *connection with nature* (Table 1).

All the keywords have two clusters corresponding to positive and negative evaluations, except for *connection with nature* that has only a positive cluster.

These clusters outline the main themes linked to community gardens, as perceived by gardeners. Having 11 clusters, an answer can be counted maximum up to 11 times if it reports statements referring to all the clusters. On average, every respondent gave an answer belonging to 3 positive clusters and 1 negative cluster.

Table 1 The table shows the number of respondents that gave answers belonging to the listed themes and linked with strengths (column “BEST”, with 6 clusters), and weakness (column “LEAST, with five clusters) of Picardo farm, respectively. The results of the Pearson’s Chi-squared test are X-squared = 262.06, df = 5, p-value < 2.2e-16 (for column BEST) and X-squared = 198.01, df = 4, p-value < 2.2e-16 (for column LEAST)

Number of answers linked to theme:	What do you like		Total answers	(%)
	BEST	LEAST		
	About coming to Picardo Farm?			
Gardening activity	216	84	300	26
Social interactions	183	121	304	26
Place	183	34	217	19
Health	163	3	166	14
Education	81	34	115	10
Connection with nature	67	–	67	6
Total	893	276	1169	100

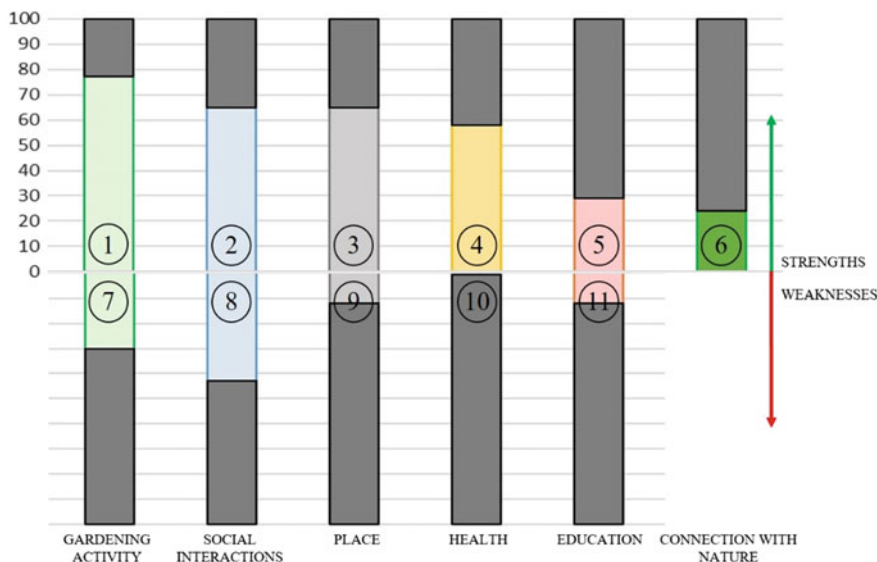


Fig. 2 For every cluster, the figure shows the percentage of respondents that gave answers belonging to it. The clusters numbered 1 to 6 correspond to themes linked to strengths (green arrow), and the clusters numbered 7 to 11 correspond to weaknesses (red arrow) of Picardo farm

Figure 2 shows that spontaneous appreciation is distributed among these themes: pleasure in producing organic, and fresh food and in “getting dirty” (cluster n.1; 77% of respondents); positive social interactions and increasing sense of community within the gardens of Picardo farm (cluster n.2; 65% of respondents); good quality of soil, good exposure, water availability and sense of belonging with the place (cluster n.3; 65% of respondents); wellbeing thanks to spending time outdoors, and healthy diet (cluster n.4; 58% of respondents); increase of education about food production and consumption (cluster n.5; 29% of respondents); and connection with nature observing seasonal changes, and increasing sustainability and self-resilience (cluster n.6; 24% of respondents).

The weaknesses of Picardo farm mainly refer to negative social interactions linked to difficulties concerning on the one side the shared management of the devices used for watering (hoses, keys, waiting time), and of the compost bins, and on the other to unfriendly gardeners, and people that do not understand the rules (cluster n.8; 43% of respondents). The respondents complain about the distant parking (cluster n.9; 12% of respondents), and the effort needed to manage the plot, especially for controlling invasive plants (cluster n.7; 30% of respondents). Furthermore, for bringing heavy loads in and out, some of them have health issues (cluster n.10; 1% of respondents). Regarding education, the gardeners see as a problem the gentrification of the community and a lack of strong leadership (cluster n.11; 12% of respondents).

As showed in Table 1, the 281 respondents listed 1169 aspects of Picardo farm, and 24% refers to problems. These not always correspond to the weaknesses of

the farm. Indeed, in participatory management, the unanimous agreement generally reflects a lack of interest (Menconi et al. 2017). Mostly, the respondents that gave negative answers to a cluster also gave very positive answers to the specular cluster (the cluster numbered 1 is specular to 7, 2 to 8, 3 to 9, 4 to 10, and 5 to 11), showing a clear sense of belonging with the place. In other words, the more an issue is felt by the participants, regardless of whether the reaction to the phenomenon is positive or negative, the more it means that the element is cared for. In the end, the recurrence of this dynamic for all the main themes shows a strong relationship between the gardeners and the farm.

This is the first community garden in Seattle. The respondents work at Picardo farm for over four years and, few of them, for over 20. On average, this is an extended period, which allowed a “slow process” to increase the sense of belonging with the territory (Menconi et al. 2018). Furthermore, the gardeners frequent the farm at least 2–3 times a week. This continuous effort helps for the ongoing construction and maintenance of the structures of community feeling (Neals and Walters 2008). Overall, these results show constructive conflicts and a secure attachment to the place.

The resulting variety of clusters shows as community gardens are an approach win-win for the ecosystem services matching. Considering the complex synergies and trade-offs that complicate ecosystem services supply-demand dynamics (Wang et al. 2019), this kind of land use represents an interesting choice. Picardo farm provides various ecosystem services that could be crucial assets in determining Seattle's sustainability if linked within a network with other green urban areas (Cortinovis et al. 2019).

4 Conclusions

In the present study, open questions surveys with urban gardeners have been carried out to evaluate their perception regarding the strengths and weaknesses of community gardens.

Generally, the results showed how the citizens involved in community gardens are aware of the variety of values linked with this activity or, in other words, how the community gardens attract or generate aware citizens.

Respect to other urban green spaces, the strengths of the community gardens, in addition to food production, regard the ability to build site-specific cohesive communities. Indeed, the higher values linked to the theme “social interactions” refer to the cohesion between gardeners that manage the place, and the higher values linked to the “attachment to place” refer to site-specific characteristics of the place (quality of soil, exposure, water availability, beauty). These considerations show as these communities guarantee constant stewardship of the place where they are located.

Finally, the results show as a community garden is a complementary form of green space provision with distinctive values, and it is an approach win-win for the ecosystem services matching.

Acknowledgements The authors would like to thank the garden leaders of Picardo farm for their invaluable help in organizing and supporting the creation and diffusion of the survey, and for their work with the community.

References

- Bell, S., Fox-Kamper, R., Keshavarz, N., Benson, M., Caputo, S., Noori, S., & Voigt, A. (2016). *Urban allotment gardens in Europe*. Routledge.
- Cortinovis, C., Haase, D., Zanon, B., & Geneletti, D. (2019). Is urban spatial development on the right track? Comparing strategies and trends in the European Union. *Landscape and Urban Planning, 181*, 22–37.
- FAO. FAO's role in urban agriculture. Retrieved from: <http://www.fao.org/urban-agriculture/en/> (March, 2019).
- Hou, J., & Grohmann, D. (2018). Integrating community gardens into urban parks: Lessons in planning, design and partnership from seattle. *Urban Forestry & Urban Greening, 33*, 46–55.
- Lohrberg, F., Licka, L., Scazzosi, L., & Timpe, A. (2015). *Urban Agriculture Europe*. COST-action. Jovis publisher. Retrieved from: www.jovis.de/en/books/product/urban-agriculture-europe.html. Accessed 11 June 2019.
- Menconi, M. E., Artemi, S., Borghi, P., & Grohmann, D. (2018). Role of local action groups in improving the sense of belonging of local communities with their territories. *Sustainability, 10*, 4681.
- Menconi, M. E., Grohmann, D., & Mancinelli, C. (2017). European farmers and participatory rural appraisal: A systematic literature review on experiences to optimize rural development. *Land use Policy, 60*, 1–11.
- Murakami, K. (2005). Do you know why they're called P-patches?. Retrieved from: www.seattle.gov/neighborhoods/programs-and-services/p-patch-community-gardening/p-patch-list/picardo-farm. Accessed 11 June 2019.
- Neals, S., & Walters, S. (2008). Rural Be/longing and rural social organizations: conviviality and community-making in the english countryside. *Sociology, 42*, 279–297.
- United Nations. (2016). *New Urban Agenda Habitat III*. United Nations Conference on Housing and Sustainable urban Development, Oct. 17–20, Quito, Ecuador.
- Wang, L., Zheng, H., Wen, Z., Liu, L., Robinson, B. E., Li, R., et al. (2019). Ecosystem service synergies/trade-offs informing the supply-demand match of ecosystem services: Framework and application. *Ecosystem Services, 37*, 100939.
- Weidner, T., Yang, A., & Hamm, M. W. (2019). Consolidating the current knowledge on urban agriculture in productive urban food systems: Learnings, gaps and outlook. *Journal of Cleaner Production, 209*, 1637–1655.

Evaluation of Greenwalls Efficiency for Building Energy Saving



C. Bibbiani, C. Gargari, C. A. Campiotti, G. Salvadori and F. Fantozzi

Abstract The research moves from thermo-hygrometric data collected during a campaign to monitor energy exchanges at “Building F92” ENEA ‘La Casaccia’, with particular reference to the sections of the building facing south-east, south-west, screened by a green wall. In spring 2018, ENEA installed many sensors to detect parameters such as air temperature, internal and external surface temperature of walls, solar irradiation, wind speed, on the one hand, to validate the reliability of the parameters that can be extrapolated from the critical analysis of data, on the other to derive indications for a possible schematization of the contribution offered by the green-wall to the improvement of the conditions of indoor comfort. The research focused on the interpretation of the values measured by the sensors for the validation of simplified calculation models available in bibliography. The analysis allowed the extrapolation of data useful for the calculation of the K_v -parameter, the so-called “green factor”, an index describing the contribution to indoor cooling offered by the green-wall. The evaluation of the K_v -parameter demonstrates the substantial contribution of the green-wall to the reduction of the energy flux entering the opaque wall.

Keywords Green-wall · Building energy saving · Green factor

C. Bibbiani (✉)

Department of Veterinary Sciences, University of Pisa, Viale delle Piagge 2, 56124 Pisa, Italy
e-mail: carlo.bibbiani@unipi.it

C. Gargari · G. Salvadori · F. Fantozzi

Department of Energy Systems, Territory and Construction Engineering (DESTEC), University of Pisa, Via Diotisalvi 2, 56126 Pisa, Italy

C. A. Campiotti

ENEA - Italian National Agency for New Technologies, Energy and Sustainable Economic Development - Technical Unit Energy Efficiency - Agriculture Unit, Via Anguillarese 301, 00123 Rome, Italy

© Springer Nature Switzerland AG 2020

A. Coppola et al. (eds.), *Innovative Biosystems Engineering for Sustainable Agriculture, Forestry and Food Production*, Lecture Notes in Civil Engineering 67,
https://doi.org/10.1007/978-3-030-39299-4_19

Nomenclature

U	Thermal transmittance of the opaque element, $\text{W/m}^2 \text{K}$
K_v	Green constant, –
α	Absorption coefficient of the opaque wall, –
I	Solar radiation incident on the outer surface, W/m^2
h_e	Coefficient of convective exchange, $\text{W/m}^2 \text{K}$
T_{se}	Surface temperature of the opaque wall not subjected to effects of the green wall, K
T_{sev}	Surface temperature of the opaque wall subjected to effects of the green wall, K
T_{ae}	Temperature of the external environment, K
Hc	Convection coefficient, $\text{W/m}^2 \text{K}$
hr	Irradiation coefficient, $\text{W/m}^2 \text{K}$
v	Wind speed near the surfaces, m/s
\mathcal{E}	Emissivity of the surface, –
hro	Irradiation coefficient of a black body:
σ	Stefan-Boltzmann constant of $5.67 \times 10^{-8} \text{W/m}^2 \text{K}^4$
T_m	Average thermodynamic temperature of the surface and of the neighboring surfaces, which will be assumed equal to the temperature of the leaf layer.

1 Introduction

Green roofs and walls are considered a solution to many urban problems, including the mitigation of the urban heat island phenomenon, noise attenuation, air pollution reduction, rainwater management, quality of air and water and biodiversity support (Capiotti et al. 2011). They are often addressed as the best constructive choice for increasing environmental sustainability in an urban environment (Gargari et al. 2016). The function of the green wall is to shield the surface of the building that would otherwise be exposed to direct solar radiation in order to reduce the energy absorbed by the wall and, consequently, transmitted inside (Flores Larsen et al. 2015). The presence of the green wall, therefore, is aimed at mitigating the high temperatures inside the building in the hottest periods and allows the reduction of the energy requirement necessary for the summer conditioning. Because the building sector in Europe is responsible of 40% of the total end-energy consumed, there is increasing interest in using this “green option” to improve the envelope heat transfer resistance, and therefore the energy efficiency of the buildings (Kumar and Kaushik 2005; Lazzarin et al. 2005). As such, the green roofing and facades technology is being to become commonly applied, especially in the buildings of new construction industry. In order to evaluate the performance of green walls in terms of cooling load demand variation, a model was developed to describe the dynamic thermal behavior of different green walls realized with various plant species (Ariaudo et al. 2009). This

paper reports a validation of the proposed “Green Factor” (Kv) based on measured environmental parameters, in order to describe the contribution to cooling offered by the green-wall and the consequent reduction of the energy flux entering into the building.

2 Materials

The building under study is located at the ‘Casaccia’ Research Center, the largest ENEA laboratory and plant complex. The project activities were carried out on the “F92 building”, called “School of Energies”. It is a single-family house, with a semi-underground floor, two above-ground with flat roof, with a total area of about 230 sq. meters, a green roof and the installation of a green wall (Fig. 1). The structure, different from the “ordinary” buildings of that time, turns out to be made with good insulating-performance materials and innovative technological solutions, such as to reach an overall thermal transmittance value of the vertical wall equal to 0.3 W/m² K.

Sensors have been installed at the F92 building to measure the surface temperature of the walls, air speed, relative humidity, global solar radiation (and its photosynthetic component) on the outside and inside the green wall, as described by Campiotti and his team (Campiotti et al. 2016, 2017). The green wall with metal structure was installed on the south corner of the F92 building in 2017, but the full growth of leaves was completed only in 2018. Starting from October 2017, many other sensors for the measurement of thermo-hygrometric parameters were installed.

The sensors installed in the building are listed below:



Fig. 1 Evolution of the green wall from March to September 2018

- SW and SE walls: air temperature and relative humidity; leaf temperature; external surface wall temperature; global solar radiation on the external surface of the green wall; global solar radiation on the external surface of the shielded wall; PAR radiation; wind speed and wind direction;
- Internal environments: Radiant temperature; air temperature and relative; internal surface temperature.

The research focused in particular on the analysis of data extrapolated from the measurements of the sensors on the South-West wall, considering the most significant sensor pairs for the objectives of this study.

The South-West wall is in fact equipped with a double pair of sensors of internal-external T° , placed both on the side of the wall completely exposed to sun radiation, and inside the interspace on the portion of the wall shielded by the green wall.

3 Methods

The research examined the data recorded by the sensors during the period June-October 2018. The array of the sensors allows to evaluate both the incoming thermal flux (Φ_S) and (Φ_V) on the masonry parts exposed to the sun and shielded by the green wall, respectively, the reduction factor of the solar radiation “ τ ”, and finally ‘Kv’ the green factor.

The equations that provide the value of the difference between the incoming thermal flux (Φ_S) and (Φ_V), defined ($\Delta\Phi$) can be written (Ariaudo et al. 2009) as:

$$\frac{\Delta\phi}{A} = U \frac{K_v \alpha I}{h_e} \quad (1)$$

$$K_{v1} = \frac{T_{se} - T_{sev}}{T_{se} - T_{ae}} \quad (2)$$

$$h_e = h_c + h_r \quad (3)$$

$$h_c = 4 + 4v \quad (4)$$

$$h_r = \varepsilon \times h_{ro} \quad (5)$$

$$h_{ro} = 4 \times \sigma \times T_m^3 \quad (6)$$

Starting from Eq. (1), Kv value can be derived as well, which will be called Kv2, from measurements in part independent of those used to derive Kv1. In fact:

$$K_{v2} = \frac{\Delta\phi}{AU\alpha I} h_e \quad (7)$$

Therefore, the problem moves to the evaluation of both the difference Δ between the incoming thermal flux (Φ_S) and (Φ_V), and the convective exchange coefficient ‘ h_e ’.

4 Results and Discussion

Months from June to October 2018 were analyzed, taking into consideration 4 weeks (one for each month). To validate data of the radiation sensors, the ‘ τ ’ ratio, that is the fraction of radiation that filters through the green wall, relative to each month has been calculated as shown in the Fig. 2.

The ‘ τ ’ ratio ‘, which varies according to the leaf coverage or the LAI index (Leaf Area Index), shows decreasing values from June to September (average value from 0.3 to 0.2), and then increases again in October concurrently with the fall of part of the leaf layer (value > 0.3).

The validity of Eq. (7) is assumed by the theory that identifies the exact moment in which calculation the value of K_v should be done, that is when the surface temperature of the opaque wall behind the green wall (T_{sev}) reaches its maximum. The results of the elaborations show that the maximum values of T_{sev} are generally synchronous with the peaks of the radiation ‘ αI ’ measured on the part of the wall subject to the effects of the green wall.

Figure 3 shows both the values of the green factor ‘ K_{v1} ’ and ‘ K_{v2} ’, reported in the table below (Table 1).

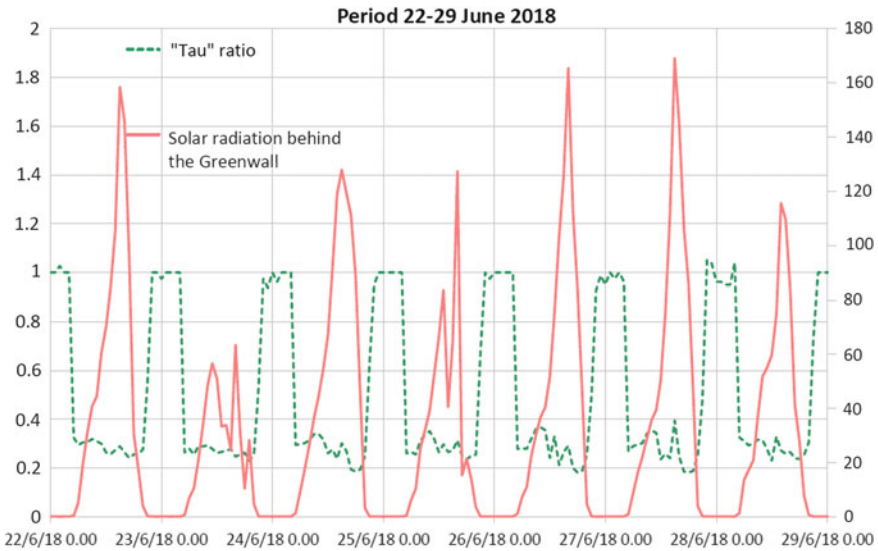


Fig. 2 SW-wall. Radiation behind the green wall and ‘ τ ’ ratio. June 2018

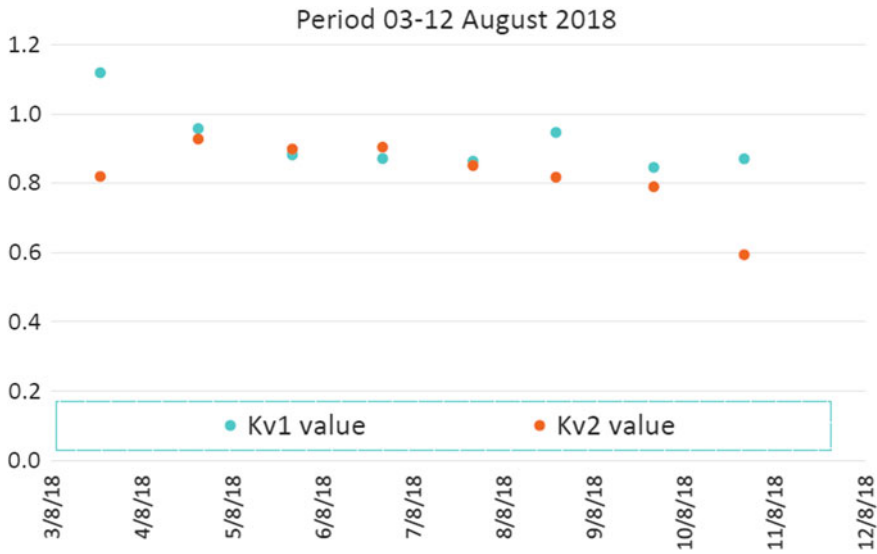


Fig. 3 SW-wall. Values of the green factor 'Kv1' and 'Kv2'. August 2018

From mid-September onwards, both Kv1 and Kv2 seem to deviate from the average of the summer months, probably due to the incorrect evaluation of the ' h_e ' coefficient to be clarified with more in-depth dynamic analysis based on measurements of thermal fluxes by heat flow-meter, anemometer, and air temperature sensors to be installed near the bare wall itself.

Figure 4 shows the trend of the Kv1/Kv2 ratio, the temperature of the external wall surface ' T_{sev} ' protected by the green wall, and the radiation inside the gap between the green wall and the wall itself.

Moreover, the value of Kv1/Kv2 is highlighted in correspondence with the maximum surface temperature of the opaque wall (point circled in blue, on the red dashed-line) subject to the effects of the green wall.

From the values of the Kv1/Kv2 ratio it can be seen that during the three summer months a great stability around the calculation point, and moreover that the two methods of evaluation of Kv lead to a good correspondence of the two estimations, implicitly giving a verification of multiple measurements of such a complex phenomenon as the convective heat exchange around the green wall.

Given the non-perfect evaluation of both the thermal fluxes and the thermal exchange coefficient ' h_e ', for the bare wall, it is therefore not possible to derive from Eq. (1) an estimation of the convective exchange coefficient h_{e^*} behind the green wall. This impossibility therefore translates into the failure to define an equivalent resistance ' Req '.

Table 1 Values of the green factor 'Kv1' and 'Kv2', and their ratio

Kv1	Kv2	Date	Kv1/Kv2 ratio	Kv1	Kv2	Date	Kv1/Kv2 ratio
0.82	0.74	22/6/18	1.11	0.69	0.58	14/9/18	1.19
–	0.67	23/6/18	–	0.70	0.57	15/9/18	1.23
0.75	0.55	24/6/18	1.38	0.73	0.52	16/9/18	1.38
0.82	0.69	25/6/18	1.18	0.75	0.65	17/9/18	1.16
0.72	0.43	26/6/18	1.67	0.81	0.65	18/9/18	1.23
0.71	0.48	27/6/18	1.48	–	0.46	19/9/18	–
0.71	0.63	28/6/18	1.14	–	0.45	20/9/18	–
0.86	0.64	29/6/18	1.36				
0.84	0.80	13/7/18	1.05	0.79	0.40	14/10/18	2.00
0.83	0.82	14/7/18	1.02	0.80	0.50	15/10/18	1.59
0.85	0.77	15/7/18	1.10	0.87	0.43	16/10/18	2.00
–	0.67	16/7/18	–	0.89	0.42	17/10/18	2.13
0.83	0.63	17/7/18	1.32	0.74	0.42	18/10/18	1.78
0.85	0.75	18/7/18	1.13	0.74	0.61	19/10/18	1.22
0.84	0.76	19/7/18	1.12	0.74	0.44	20/10/18	1.70
0.88	0.79	20/7/18	1.11	0.78	0.51	21/10/18	1.54
–	0.82	3/8/18	–				
0.96	0.93	4/8/18	1.03				
0.88	0.90	5/8/18	0.98				
0.87	0.90	6/8/18	0.96				
0.86	0.85	7/8/18	1.01				
0.95	0.82	8/8/18	1.16				
0.85	0.79	9/8/18	1.07				
0.87	0.59	10/8/18	1.47				

5 Conclusions

The analysis of data was focused on some months due to the full growth of the plant screen on the wall, which reached full coverage only from June 2018 onward.

That said, the analysis confirmed the reliability in the application of the two formulas for the calculation of the “green factor” Kv, adopted to represent the contribution of the green wall to the control of the thermal flux entering the screen, with the serious limitation of the validity of the analysis at the exact time when the superficial temperature of the wall reaches its maximum. Nevertheless, a good stability of Kv value can be detected within each day. The two formulas lead to comparable experimental Kv values.

The ratios of the Kv1/Kv2 values detected oscillate on average between 1.1 and 1.4 in the summer period, showing a good congruence of the two calculations methods,

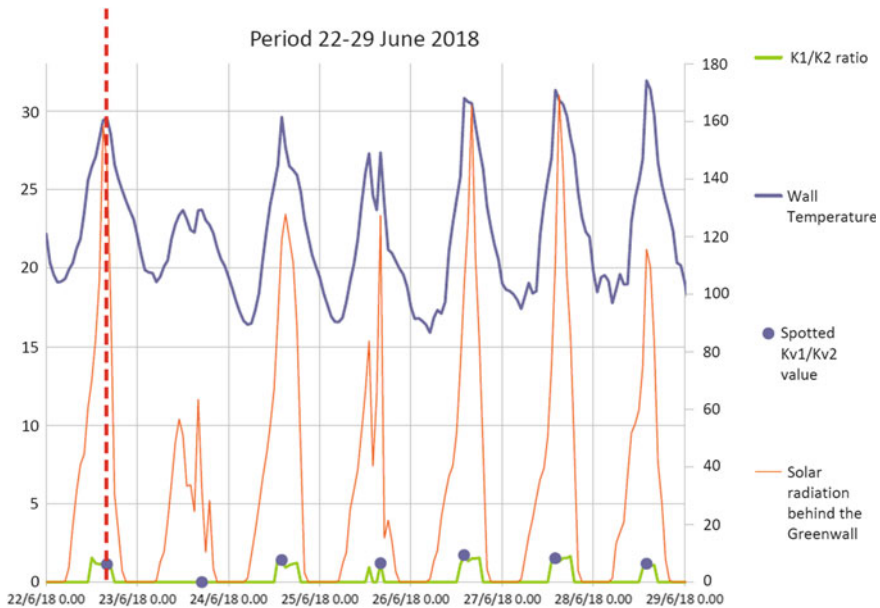


Fig. 4 SW-wall. $Kv1/Kv2$ ratio trend; external wall surface temperature protected by the green screen; radiation inside the interspace between the green wall and the wall. June 2018

while they rise to 1.6–1.7 in autumn when the incidence of the Sun is less effective and/or the leaf-coverage is naturally reduced.

It has also been noted that in order to define an equivalent resistance ‘Req’ related to the green wall it is necessary to analyze by transitory-state approach the complex thermal exchange phenomena occurring between the building and the green wall itself.

Acknowledgements We thank the National Agency for New Technologies, Energy and Sustainable Economic Development (ENEA) for the granting of experimental data collected at the F92 building, ENEA Casaccia Research Center. The research and development activities of general interest for the national electricity system are financed by the Ministry of Economic Development (MiSE), with the Three-Year Research Plan in the so-called National Electric System 2015–2017, within the 2015–2017 Program Agreement stipulated to ENEA, the Annual Implementation Plan (PAR) 2018, as part of Project D.1 “Technologies for building buildings of the future”, Research Theme: Intelligent Buildings.

References

- Ariaudo, F., Corgnati, S. P., Fracastoro, G. V., & Raimondo, D. (2009). Cooling load reduction by green walls: Results from an experimental campaign. In *Conference Paper IV International Building and Physics Conference*, Istanbul, June.

- Campiotti, C. A., Bibbiani, C., Alonzo, G., Giangiaco, G., Ragona, R., & Viola C. (2011). Green roofs and green façades for improving sustainability of towns. *Journal of Sustainable Energy*, *II*(3), 24–29.
- Campiotti, C. A., Giagnacovo, G., Latini, A., Margiotta, F., Nencini, L., Pazzola, L., & Puglisi, G. (2016). *Le coperture vegetali per la sostenibilità energetica ed ambientale degli edifici*, ENEA, Report Ricerca di Sistema Elettrico, RdS/PAR2016/075.
- Campiotti, C., Cancellara, A., Consorti, L., Giagnacovo, G., Marani, & S., Margiotta, F. et al. (2017). *L'uso della vegetazione per aumentare l'efficienza energetica degli edifici e l'impiego di sistemi di climatizzazione rinnovabile*. ENEA, Report Ricerca di Sistema Elettrico, RdS/PAR2017/084.
- Flores Larsen, S., Filippin, C. A., & Lesino, G. (2015). Modeling double skin green facades with traditional thermal simulation software. *Solar Energy*, *121*, 56–67.
- Gargari, C., Bibbiani, C., Fantozzi, F., & Campiotti, C. A. (2016). Environmental impact of Green roofing: the contribute of a green roof to the sustainable use of natural resources in a life cycle approach. *Agriculture and Agricultural Science Procedia*, *8*, 646–656.
- Kumar, R., & Kaushik, S. C. (2005). Performance evaluation of green roof and shading for thermal protection of buildings. *Building and Environment*, *40*, 1505–1511.
- Lazzarin, R. M., Castellotti, F., & Busato, F. (2005). Experimental measurements and numerical modelling of a green roof. *Energy and Buildings*, *37*, 1260–1267.

Modelling of the Thermal Effect of Green Façades on Building Surface Temperature in Mediterranean Climate



I. Blanco, G. Scarascia Mugnozza, G. Vox and E. Schettini

Abstract Urban Green Infrastructures (UGIs) improve the supply of urban ecosystem services. UGIs can provide benefits such as better urban climate conditions and lower temperature of urban air. They can also limit the development of extreme temperatures on buildings surface, in particular in Mediterranean climate areas. Green façades permit the physical shading of the building envelope, produce a cooling effect by means of evapotranspiration in summer, and improve the thermal insulation in winter. A reduction of the thermal flows between exterior and interior and more sustainable buildings can be obtained. A three years experimental test was carried out at the University of Bari (Italy) for assessing the thermal performance of two green façades characterized by two different climbing plants (*Pandorea jasminoides variegated* and *Rhynchospermum jasminoides*). The selected plants well adapt to the local climate, growing quickly and vigorously. The environmental conditions and several climatic parameters on the walls were monitored during the field test. The temperature on the external surface during July 2015 was used for fitting a regression model. The model was validated on July 2016. It can be applied for predicting the two green façades performance in a Mediterranean climate only by using an input dataset on climate conditions.

Keywords Greenery systems · Microclimate · Regression model · Urban green infrastructures

I. Blanco (✉)

Department of Biological and Environmental Sciences and Technologies (DiSTeBA), University of Salento, S.P. 6, Lecce-Monteroni, 73100 Lecce, Italy
e-mail: ileana.blanco@uniba.it

G. Scarascia Mugnozza · G. Vox · E. Schettini

Department of Agricultural and Environmental Science (DISAAT), University of Bari, via Amendola 165/a, 70126 Bari, Italy

© Springer Nature Switzerland AG 2020

A. Coppola et al. (eds.), *Innovative Biosystems Engineering for Sustainable Agriculture, Forestry and Food Production*, Lecture Notes in Civil Engineering 67,
https://doi.org/10.1007/978-3-030-39299-4_20

1 Introduction

Urban Green Infrastructures (UGIs) are vegetation elements and systems, located within the urban environment, that have the ability of alleviating the negative impacts of urbanization (Mekala and Hatton MacDonald 2018). UGIs not only improve the supply of urban ecosystem services, but also contribute to improving urban climate conditions, reducing the temperature of urban air and limiting the maximum surface temperature, particularly in Mediterranean climate areas (Mekala and Hatton MacDonald 2018; Norton et al. 2015; Vox et al. 2017). Vertical greenery systems (VGSs) are a typology of UGIs. They are characterized by climbing plants or shrubs which grow along building vertical walls, also by using supporting structures such as trellises (Afshari 2017). VGSs can be used in new buildings design or in existing buildings retrofitting for energy efficiency improvement. They have the ability to reduce the energy consumption for air conditioning in summer, to increase the thermal insulation in winter and to improve indoor microclimate and building indoor air temperature (Gago et al. 2013; Cheng et al. 2010; Pérez et al. 2011), due to the cooling, shading, insulation and wind barrier effects (Pérez et al. 2011; Afshari 2017; Blanco et al. 2017).

A green façade is the simplest technology in the field of engineered VGSs. Plants grow vertically on the walls of the building; they can be rooted in the ground at the base of buildings or at different heights of the façade, by using planters, or in some cases on the rooftop (Vox et al. 2017). Experimental results on green façades thermal performance are very heterogeneous due to the several factors they depend on and are often based on short time periods (Blanco et al. 2018). Simulation results based on the development and application of “engineered models” (Fumo 2014) need the input of detailed physical information on the building and several assumptions are made on the plants. Few simulation results were validated with experimental data (Pérez et al. 2014; Hunter et al. 2014; Raji et al. 2015). On the contrary statistical approaches can be easily developed for predicting the green façades thermal performance; they require experimental data and no detailed information on the building (Yildiz et al. 2017; Fumo and Rafe Biswas 2015).

The relationship between the thermal benefits provided by green façades on the building and the external climate conditions needs further research and experimental studies, in particular in summer Mediterranean climate conditions.

This study develops a statistical model, an autoregressive linear one, for the analysis of the thermal performance, in the summer period, of two green façades built at the University of Bari (South Italy). The performance of two evergreen climbing plants, *Rhynchospermum jasminoides* and *Pandorea jasminoides variegated*, was compared. The model can be used for predicting the external surface temperature difference between a bare reference wall and the wall behind the green covers.

2 Materials and Methods

An experimental test was carried out at the experimental farm of University of Bari in Valenzano (Bari, Italy), at latitude $41^{\circ} 05' N$, longitude $16^{\circ} 53' E$, altitude 85 m ASL. Three identical building wall prototypes were designed and built in small scale. The construction technique used refers to a typical Mediterranean building wall. The walls were built south oriented and were made of perforated bricks, joined with mortar, covered with a layer of plaster. They were 1.00 m wide, 1.55 m high and 0.22 m thick. The thickness was 0.20 m and 0.02 m for the masonry and the plaster coating, respectively. The masonry and the plaster coating were characterized by thermal conductivity coefficients of $0.28 \text{ Wm}^{-1}\text{K}^{-1}$ and $0.55 \text{ Wm}^{-1}\text{K}^{-1}$, respectively. The heat capacity coefficient of the masonry was $840 \text{ Jkg}^{-1}\text{K}^{-1}$. The heat capacity coefficient of the plaster coating was $1000 \text{ Jkg}^{-1}\text{K}^{-1}$. The prototypes were protected on the backside with sheets of expanded polystyrene, in order to shade and insulate the internal side of the walls (Fig. 1). A colored shading net was positioned on the sheets of expanded polystyrene for reducing the effect of the incident solar radiation.

Two façades were covered with two evergreen plants, *Rhynchospermum jasmynoides* and *Pandorea jasminoides variegated*, starting from June 2014. These plants well adapt to the climatic conditions of the experimental area. The Plant Leaf Area Index (LAI) of the plants, fully developed, ranged throughout the year in the range 2.0–4.0 for *Rhynchospermum jasmynoides* and 1.5–3.5 for *Pandorea jasminoides variegated*. The LAI was measured with an AccuPAR PAR/LAI Ceptometer (model LP-80, Decagon Devices Inc., Pullman, WA, USA). An iron net was placed 0.15 m from the front of the walls for supporting the plants growing. An irrigation drip system and an N: P: K 12:12:12 fertilizer were used. The third façade was left uncovered and used as control.



Fig. 1 The experimental walls at University of Bari and the location of the sensors measuring the temperature of the external plaster surfaces (yellow point); the left wall is the control wall, the central green façade is screened with *Pandorea jasminoides variegated* and the right façade with *Rhynchospermum jasmynoides*

The following parameters were collected: the temperature of the plaster on the external surface of the walls, the external air temperature and relative humidity, the solar radiation on a horizontal and on a vertical plane, the wind velocity and direction. The data, measured with a frequency of 60 s and averaged every 15 min, were stored on a data logger (CR10X, Campbell, Logan, USA). The temperature of the external plaster surfaces was measured using thermistors with an accuracy of ± 0.15 °C (Tecno.EL s.r.l., Formello, Rome, Italy). The thermistors were placed inside the plaster layer; they were located as shown in Fig. 1. The sensors described afterwards were placed on a weather station about 10 m away from the experimental walls. The external air temperature and relative humidity were measured by Hygroclip-S3 sensors having an accuracy of ± 0.1 °C and $\pm 0.8\%$, respectively (Rotronic, Zurich, Switzerland). The solar radiation was measured in the wavelength range 0.3–3.0 μm by means of pyranometer with an accuracy of 10 Wm^{-2} (model 8-48, Eppley Laboratory, Newport, RI, USA). A Young Wind Sentry anemometer (Young Company, Traverse City, MI, USA) was used for measuring the wind speed and direction, with an accuracy of 0.5 ms^{-1} and of $\pm 5^\circ$, respectively. All sensors were shielded from solar radiation.

In this study the regression analysis method was used for analyzing the functional equation that relates the difference between the external surface temperature of the control wall and of the green façades (the dependent variable) and the external ambient parameters (the predictors) (Yildiz et al. 2017; Fumo and Rafe Biswas 2015). The predictors used in the statistical model were the external air temperature and relative humidity, the horizontal and vertical solar radiation, the wind velocity and direction. The model used is a multiple linear regression, as follows:

$$Y_t = \beta_0 + \beta_1 Y_{t-1} + \beta_2 X_{1,t} + \beta_3 X_{2,t} + \beta_4 X_{3,t} + \beta_5 X_{4,t} + \beta_6 X_{5,t} + \beta_7 X_{6,t} + \varepsilon_t \quad (1)$$

Y_t , the dependent variable, is the difference between the external surface temperature of the control wall and of the green façade at time t . t corresponds to the quarters of hours analyzed. The variable Y_{t-1} is the difference between the external surface temperature of the control wall and of the green façade at time $t-1$. $X_{1,t}$ is the external air temperature, $X_{2,t}$ is the horizontal solar radiation, $X_{3,t}$ is the external air relative humidity, $X_{4,t}$ is the wind velocity, $X_{5,t}$ is the wind direction, and $X_{6,t}$ is the vertical solar radiation, at time t . β_0 is the intercept; β_i , with $i = 1, \dots, 7$, are the regression parameters of the model. ε_t is an error; it stands for the difference between the observed data and the predicted data.

Equation (1) was fitted using the data gathered during July 2015 and was applied for predicting the temperature difference values during July 2016. The Regression Tool in Excel's Data Analysis add-in and the Least Squares Method were used in the statistical analysis.

3 Results and Discussion

During July 2015 the field was characterized by: external air temperature values ranging from 18.6 °C to 40.7 °C; an average external air relative humidity of 48.8%; an average wind velocity of 2.1 ms⁻¹; a monthly value of cumulative solar radiation of 802 MJ m⁻² and 304 MJ m⁻² on a horizontal and on a vertical plane, respectively. During July 2016 the field was characterized by: external air temperature values ranging from 15.5 °C to 38.9 °C; an average external air relative humidity of 52.8%; an average wind velocity of 2.2 ms⁻¹; a monthly value of cumulative solar radiation of 760 MJ m⁻² and 278 MJ m⁻² on a horizontal and on a vertical plane, respectively.

The data measured during July 2015 were grouped in five slots defined based on the solar radiation on a horizontal surface (I_{hor}) values, as follows:

$$\begin{aligned} I_{\text{hor } 200} &: I_{\text{hor}} < 200 \text{ W m}^{-2}; \\ I_{\text{hor } 200-400} &: 200 \leq I_{\text{hor}} < 400 \text{ W m}^{-2}; \\ I_{\text{hor } 400-600} &: 400 \leq I_{\text{hor}} < 600 \text{ W m}^{-2}; \\ I_{\text{hor } 600-800} &: 600 \leq I_{\text{hor}} < 800 \text{ W m}^{-2}; \\ I_{\text{hor } 800} &: I_{\text{hor}} \geq 800 \text{ W m}^{-2}. \end{aligned}$$

A statistical model was developed for each green façade and for each slot. Thus, each model was developed on data related to an almost similar thermal performance of the green façades.

The data observed during July 2015 were used for developing the regression models. Only the predictors with a p-value < 0.01 have been incorporated in the regression models. Tables 1 and 2 report the estimated regression parameters for each solar radiation slot and also the related parameters of quality analysis: the adjusted coefficient of determination R_{adj}^2 and the Root-mean-square error RMSE. R_{adj}^2 explains the goodness of the fit by the trained models; R_{adj}^2 values are very high for each model, therefore they indicate a good fitting. The RMSE values are low; they vary in the range 0.05–0.12 °C and 0.06–0.11 °C in the model regarding *Rhynchospermum jasminoides* and *Pandorea jasminoides variegated*, respectively (Tables 1 and 2). They indicate that the dispersion of the data around the regression line is small.

Each model was then used for the prediction of the performance of the green façades in July 2016. Figures 2 and 3 show the difference between the external surface temperature of the control wall and of the green façades; the values calculated with the regression models are compared with the data observed during the experimental test. Data are shown for 24 July 2016.

The maximum wall external surface temperature difference between the control and the green façade covered with *Rhynchospermum jasminoides* (Fig. 2) was 5.8 °C and 4.8 °C considering the experimental values and the predicted values, respectively. The minimum difference was -1.8 °C and -1.3 °C for the experimental values and the predicted values, respectively.

The maximum wall external surface temperature difference between the control and the green façade covered with *Pandorea jasminoides variegated* (Fig. 3) was 5.7 °C and 5.5 °C for the experimental values and the predicted values, respectively.

Table 1 Estimated regression coefficients and quality model parameters for the green façade covered with *Rhynchospermum jasmynoides*, for July 2015

Predictor variables	Y_{t-1}	$X_{1,t}$	$X_{2,t}$	$X_{3,t}$	$X_{4,t}$	$X_{5,t}$	$X_{6,t}$	Quality model parameters		
		External air temperature	External horizontal solar radiation	External air relative humidity	Wind velocity	Wind direction	External vertical solar radiation			
Estimated regression coefficient										
	$\hat{\beta}_0$	$\hat{\beta}_1$	$\hat{\beta}_2$	$\hat{\beta}_3$	$\hat{\beta}_4$	$\hat{\beta}_5$	$\hat{\beta}_6$	$\hat{\beta}_7$	R^2_{adj}	RMSE
$I_{hor\ 200}$	-0.4798	0.8907	0.0044	-0.0007	0.0018	0.0174	0.0003	0.0043	0.99	0.05
$I_{hor\ 200-400}$	-0.1892	0.9296		-0.0012			0.0004	0.0048	1.00	0.08
$I_{hor\ 400-600}$	-0.5835	0.9487			0.0040		0.0005	0.0024	1.00	0.10
$I_{hor\ 600-800}$	-0.9786	0.8953	0.0166	0.0007	0.0063	-0.0705		0.0007	0.99	0.12
$I_{hor\ 800}$	-0.4735	0.9125			0.0024	-0.0434	-0.0007	0.0030	0.99	0.08

Table 2 Estimated regression coefficients and quality model parameters for the green façade covered with *Pandorea jasminoides variegata*, for July 2015

Predictor variables	Y_{t-1}	$X_{1,t}$	$X_{2,t}$	$X_{3,t}$	$X_{4,t}$	$X_{5,t}$	$X_{6,t}$	Quality model parameters		
		External air temperature	External horizontal solar radiation	External air relative humidity	Wind velocity	Wind direction	External vertical solar radiation			
Estimated regression coefficient										
	$\hat{\beta}_0$	$\hat{\beta}_1$	$\hat{\beta}_2$	$\hat{\beta}_3$	$\hat{\beta}_4$	$\hat{\beta}_5$	$\hat{\beta}_6$	$\hat{\beta}_7$	R^2_{adj}	RMSE
$I_{hor\ 200}$	-0.1916	0.9451	-0.0043		0.0008	0.0147	0.0006	0.0016	0.97	0.10
$I_{hor\ 200-400}$	-0.1257	0.8761		-0.0018		-0.0271	0.0003	0.0074	1.00	0.06
$I_{hor\ 400-600}$	-0.2503	0.8955		-0.0006	0.0024	-0.0317		0.0040	0.99	0.10
$I_{hor\ 600-800}$	-0.8280	0.8252	0.0234	0.0002	0.0043	-0.0821	-0.0003	0.0020	0.99	0.11
$I_{hor\ 800}$	-0.2449	0.8803		-0.0004		-0.0575	-0.0004	0.0040	0.99	0.08

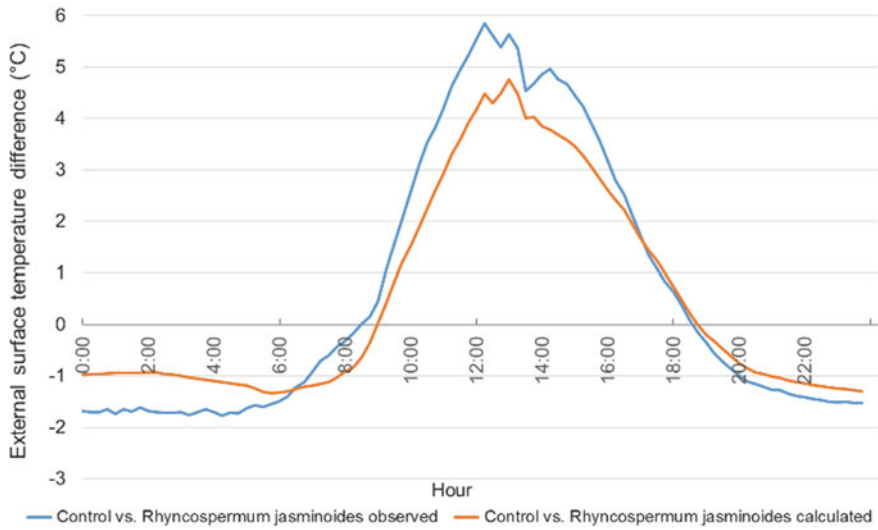


Fig. 2 Difference of the wall external surface temperature between the control and the green façade covered with *Rhynchospermum jasminoides*: data observed at the experimental field and values calculated; 24/07/2016

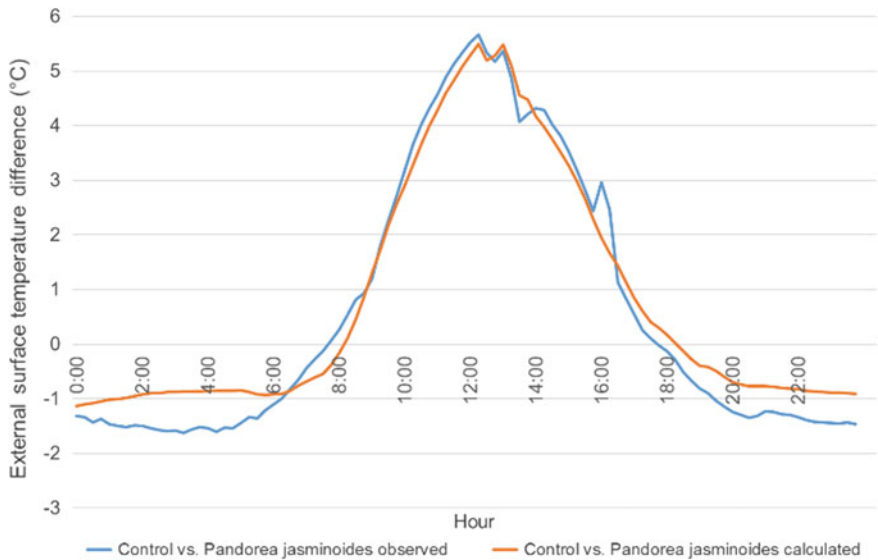


Fig. 3 Difference of the wall external surface temperature between the control and the green façade covered with *Pandorea jasminoides variegated*: data observed at the experimental field and values calculated; 24/07/2016

The minimum difference was -1.6 °C and -1.1 °C for the experimental values and the predicted values, respectively. The models show a good predicting performance.

One-way ANOVA analysis at a 95% probability level was performed for the selected period of the testing month and the mean values of the experimental data and the calculated data were evaluated. No statistically significant differences were found for both the green façades.

4 Conclusions

The thermal performance of residential and rural building envelopes can be improved by exploiting the high potential of VGSs. In this study, the thermal performance of two green façades, equipped with two climbing plants (*Rhynchospermum jasminoides* and *Pandorea jasminoides variegated*) was explored during the summer period in Mediterranean climatic conditions. The use of the green layers led to a significant reduction of the daylight temperatures on the walls external surface during warm days.

The multiple linear regression method was used for developing a model on the external surface temperature. The external environmental parameters were used as input data for the model. The model was trained on July 2015 data, and tested on July 2016. The model is able to predict the wall external surface temperature difference between an uncovered reference wall and the wall behind the green layers. The model shows a good predicting performance. It may prove useful in comparing the effect on building envelopes of different vertical greenery solutions in similar Mediterranean climatic contexts, by making forecasts. Future research could be addressed to evaluate the influence of other plants type and to collect additional experimental data for refining the model on a larger training data set.

Acknowledgements The contribution to programming and conducting this research must be equally shared between the Authors. The present work has been carried out under the “Studio di tecniche di realizzazione di un prototipo di edificio con parete verde a microclima controllato per testare il modello del flusso energetico tra la parete verde e la superficie dell’edificio”; Sistema Elettrico Nazionale, Progetto D.1 ‘Tecnologie per costruire gli edifici del futuro’, Piano Annuale di Realizzazione (PAR) 2018”, Accordo di Programma Ministero dello Sviluppo Economico–ENEA funded by the Italian Ministry of Economic Development.

References

- Afshari, A. (2017). A new model of urban cooling demand and heat island-application to vertical greenery systems (VGS). *Energy and Buildings*, 157, 204–217.
- Blanco, I., Schettini, E., Scarascia Mugnozza, G., Campiotti, C. A., Giagnacovo, G., & Vox, G. (2017). Vegetation as a passive system for enhancing building climate control. *Acta Horticulturae*, 1170, 555–562.

- Blanco, I., Schettini, E., Scarascia Mugnozza, G., & Vox, G. (2018). Thermal behaviour of green façades in summer. *Journal of Agricultural Engineering*, 49(3), 183–190.
- Cheng, C. Y., Cheung, K. K. S., & Chu, L. M. (2010). Thermal performance of a vegetated cladding system on facade walls. *Building and Environment*, 45, 1779–1787.
- Fumo, N. (2014). A review on the basics of building energy estimation. *Renewable and Sustainable Energy Reviews*, 31, 53–60.
- Fumo, N., & Rafe Biswas, M. A. (2015). Regression analysis for prediction of residential energy consumption. *Renewable and Sustainable Energy Reviews*, 47, 332–343.
- Gago, E. J., Roldan, J., Pacheco-Torres, R., & Ordóñez, J. (2013). The city and urban heat islands: A review of strategies to mitigate adverse effects. *Renewable and Sustainable Energy Reviews*, 25, 749–758.
- Hunter, A. M., Williams, N. S. G., Rayner, J. P., Aye, L., Hes, D., & Livesley, S. J. (2014). Quantifying the thermal performance of green façades: A critical review. *Ecological Engineering*, 63, 102–113.
- Mekala, G. D., & Hatton MacDonald, D. (2018). Lost in transactions: Analysing the institutional arrangements underpinning urban green infrastructure. *Ecological Economics*, 147, 399–409.
- Norton, B. A., Coutts, A. M., Livesley, S. J., Harris, R. J., Hunter, A. M., & Williams, N. S. G. (2015). Planning for cooler cities: A framework to prioritise green infrastructure to mitigate high temperatures in urban landscapes. *Landscape and Urban Planning*, 134, 127–138.
- Pérez, G., Coma, J., Martorell, I., & Cabeza, L. F. (2014). Vertical greenery systems (VGS) for energy saving in buildings: A review. *Renewable and Sustainable Energy Reviews*, 39, 139–165.
- Pérez, G., Rincón, L., Vila, A., González, J. M., & Cabeza, L. F. (2011). Green vertical systems for buildings as passive systems for energy savings. *Applied Energy*, 88(12), 4854–4859.
- Raji, B., Tenpierik, M. J., & Van Den Dobbelaar, A. (2015). The impact of greening systems on building energy performance: A literature review. *Renewable and Sustainable Energy Reviews*, 45, 610–623.
- Vox, G., Blanco, I., Fuina, S., Campiotti, C. A., Scarascia Mugnozza, G., & Schettini, E. (2017). Evaluation of wall surface temperatures in green facades. *Proceedings of the Institution of Civil Engineers-Engineering Sustainability* 170 (6), 334–344.
- Yildiz, B., Bilbao, J. I., & Sproul, A. B. (2017). A review and analysis of regression and machine learning models on commercial building electricity load forecasting. *Renewable and Sustainable Energy Reviews*, 73, 1104–1122.

Heat Fluxes in a Green Façade System: Mathematical Relations and an Experimental Case



Fabiana Convertino, Giacomo Scarascia Mugnozza, Evelia Schettini and Giuliano Vox

Abstract The need of greater environmental sustainability in today's living contexts can be significantly coped through the introduction of green infrastructures. Their benefits concern improvement of climate and comfort conditions. Among green infrastructures, vertical greenery systems, applied to buildings, contribute to the energy efficiency of buildings and to the improvement of outdoor and indoor microclimatic conditions. Green façades, a typology of vertical greenings, allow a considerable energy saving for air conditioning, by reducing the surfaces temperature of buildings and increasing the envelope thermal insulation. A realistic description of the functioning of green façades is essential to comprehend the real extent of their advantages. This paper aims to provide a first answer to the need of energy simulation models for green façades' thermal behavior. The paper proposes a theoretical and an experimental approach. The main heat fluxes involved into the green façade system are investigated and described, by resorting to a schematic representation. The defined mathematical relations are applied to data collected during an experiment on a green façade conducted at the University of Bari. This work represents a contribution to the development of a model to forecast the thermal behavior of green façades and of the microclimate of buildings equipped with them.

Keywords Vertical greenings · Energy saving · Heat flux · Green layer · Evapotranspiration

1 Introduction

Green Infrastructures (GIs) have been defined as “strategically planned network of natural and semi-natural areas with other environmental features designed and managed to deliver a wide range of ecosystem services” (European Commission 2013). GIs introduced in urban contexts allow to counteract the urbanization negative and

F. Convertino (✉) · G. Scarascia Mugnozza · E. Schettini · G. Vox
Department of Agricultural and Environmental Science (DISAAT), University of Bari “Aldo Moro”, Via Amendola 165/A, 70126 Bari, Italy
e-mail: fabiana.convertino@uniba.it

© Springer Nature Switzerland AG 2020
A. Coppola et al. (eds.), *Innovative Biosystems Engineering for Sustainable Agriculture, Forestry and Food Production*, Lecture Notes in Civil Engineering 67,
https://doi.org/10.1007/978-3-030-39299-4_21

dangerous consequences and to improve the environmental quality. GIs comprise a huge amount of planned and unplanned green systems and, among these, green solutions for buildings deserve particular attention (Norton et al. 2015). Vertical green systems (VGSs) are technologies that include vegetal layers on building walls. VGSs can be mainly distinguished into green façades and living walls. The benefits deriving from the VGSs introduction in buildings are several and at different scales, especially in Mediterranean areas (Blanco et al. 2017). VGSs allow to reduce energy consumption for air conditioning in summer and to improve thermal insulation in winter (Bianco et al. 2017; Vox et al. 2018). Vertical greenings act as passive technology for enhancing the energy efficiency of buildings and for mitigating the heat events due to urban heat island. VGSs improve indoor and outdoor microclimatic conditions. They reduce the ambient temperatures, in warm period, and improve human thermal comfort (Cameron et al. 2014; Pérez et al. 2014). The green vegetal layer works as a solar barrier, lowering the external surfaces temperature during daytime, and as a thermal barrier at night-time (Jim and He 2011; Schettini et al. 2018). Additional significative advantages given by the vegetation layer are the cooling effect due to the evapotranspiration process of plants and to the interaction of vegetation with air flows (Bowler et al. 2010; Perini et al. 2011).

The comprehension of the energy behavior of VGSs is necessary to fully understand their functions and to obtain the maximum benefit from their application. This is particularly difficult due to the numerous and complex variables involved and since VGSs are living systems, responding to environmental conditions in very complicated ways. These are the main reasons of the poor availability of detailed realistic energy models and of VGSs simulation tools.

Especially in the last years, researchers have focused on this criticality. Some of them concentrated on the shading function of the green layer, others proposed the thermal electrical analogy, others followed the energy balance approach (Ip et al. 2010; Kontoleon and Eumorfopoulou 2010; Malys et al. 2014; Susorova et al. 2013).

This research aims to investigate the energy behavior of a green façade (GF) system. It was studied by schematizing it through the different layers that compose it and the heat fluxes occurring (Convertino et al. 2019). Heat balance equations for each layer were proposed. The attention was focused on the green layer energy balance. The validation of the proposed mathematical model was based on the use of experimental data.

This study represents a first step towards the modeling of the GF systems and the development of specific tools to be implemented in building simulation software.

2 Materials and Methods

The study of the heat fluxes in a GF system was based on a schematization of the layers that compose it and on the identification of the main heat transfer mechanisms (Fig. 1). The external air (ea), the green layer of vegetation (gl), the air gap (ag) behind the plant, the external (ew) and the internal (iw) surfaces of the building wall

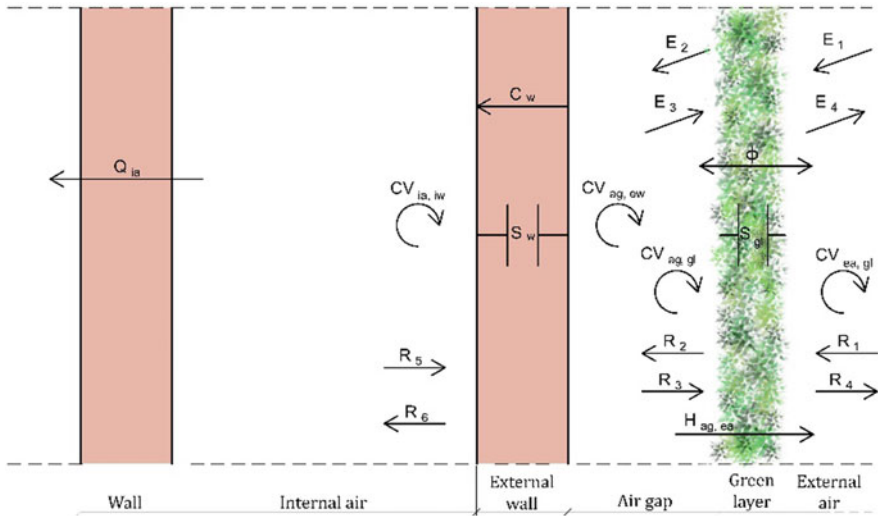


Fig. 1 Schematic representation of the layers and the energy fluxes in the green façade system

and the internal air (ia) of the building were the system considered components. The heat fluxes by radiation, convection, conduction and also by the evapotranspiration process of the plants were identified. A heat balance equation was written for each layer. It was chosen a one-dimensional model and the only considered fluxes were those normal to the wall.

2.1 Energy Balance Equations

The main heat transfer mechanisms are the radiative ones both in the solar wavelength range ($0.3\text{--}3\ \mu\text{m}$; E) and in the longwave infrared (LWIR) range ($>3\ \mu\text{m}$; R) and the convective one (CV). There is also a quantity of heat stored into the layers (S). The plant evapotranspiration (Φ) constitutes the latent heat exchange. Heat exchanged by ventilation (H), conduction (C), and air conditioning (Q) were included in the balance of the air gap, external surface of the wall and internal air of the building, respectively.

The energy balance for each layer was written (see Table 1 and Notation list).

Notation list			
C	Heat transfer by conduction [W m^{-2}]	r	Resistance [s m^{-1}]
C_{pa}	Specific heat of air at constant pressure [$\text{J kg}^{-1}\ \text{K}^{-1}$]	S	Heat storage [W m^{-2}]

(continued)

(continued)

Notation list			
CV	Heat transfer by convection [W m^{-2}]	T	Temperature [K]
E	Solar radiation [W m^{-2}]	γ	Psychrometric constant = $66.7 [\text{Pa K}^{-1}]$
e	Air vapour pressure [Pa]	ε	Emissivity [%]
e_s	Air vapour pressure at saturation [Pa]	ρ	Solar reflectivity [%]
F	View factor	ρ_a	Air density [kg m^{-3}]
H	Heat transfer by ventilation [W m^{-2}]	σ	Stefan-Boltzmann constant = $5.6697 \times 10^{-8} [\text{W m}^{-2} \text{K}^{-4}]$
h	Convective coefficient [$\text{W m}^{-2} \text{K}^{-1}$]	τ	Solar transmissivity [%]
Q	Heat exchanges for air conditioning [W m^{-2}]	Φ	Evapotranspiration [W m^{-2}]
R	Heat transfer by LWIR radiation [W m^{-2}]		
Subscripts			
a	Air	gl	Green layer
ag	Air gap	ia	Internal air
e	Aerodynamic or external	iw	Internal surface of the wall
ea	External air	s	Stomatal or internal
ew	External surface of the wall	w	External building wall

2.2 The Green Layer Energy Balance Equation and Its Terms

The green layer energy balance was analyzed in detail. Equation (1) was rewritten by neglecting the term S, since it is small compared to all other terms and by equating all the sensible terms to the latent one. The green layer energy balance became:

$$E_1 - E_4 - E_2 + E_3 + \varepsilon_{gl} \cdot (R_1 + R_3) - (R_4 + R_2) + CV_{ea,gl} + CV_{ag,gl} = \Phi \quad (6)$$

Table 1 Energy balance equations for each layer of the green façade system

Layer	Energy balance equation	
Green layer	$E_1 - E_4 - E_2 + E_3 + \varepsilon_{gl}(R_1 + R_3) - (R_4 + R_2) + CV_{ea,gl} + CV_{ag,gl} + S_{gl} - \Phi = 0$	(1)
Air gap	$CV_{ag,ew} - CV_{ag,gl} - H_{ag,ea} = 0$	(2)
External wall surface	$E_2 - E_3 + \varepsilon_{ew}R_2 - R_3 - CV_{ag,ew} - C_w - S_w = 0$	(3)
Internal wall surface	$\varepsilon_{iw}R_5 - R_6 - CV_{ia,iw} = 0$	(4)
Internal air	$CV_{ia,iw} - Q_{ia} = 0$	(5)

where: E_1 is the solar radiation on a vertical surface, and E_2 , E_3 , and E_4 are equal to:

$$E_2 = \tau_{gl} \cdot E_1 \quad (7)$$

$$E_3 = \rho_{ew} \cdot \tau_{gl} \cdot E_1 \quad (8)$$

$$E_4 = \rho_{gl} \cdot E_1 \quad (9)$$

where: ρ_{gl} and τ_{gl} are the green layer solar reflectivity and transmissivity, respectively, and ρ_{ew} is the external wall surface solar reflectivity.

Concerning the LWIR terms, R_1 includes the radiation coming from the sky (R_{sky}) and from the ground (R_{ground}), and was calculated as:

$$R_1 = R_{sky} + R_{ground} \quad (10)$$

with:

$$R_{ground} = \sigma \cdot F_{ground} \cdot T_{ground}^4 \quad (11)$$

$$R_{sky} = \sigma \cdot F_{sky} \cdot T_{sky}^4 \quad (12)$$

calculated according to the Stefan-Boltzmann law, and where: σ is the Stefan-Boltzmann constant; F_{ground} and F_{sky} are the ground and the sky view factors, respectively; T_{ground} and T_{sky} are the ground and the sky temperature, respectively. T_{sky} , for clear sky conditions, was calculated from the external air temperature (T_{ea}) as:

$$T_{sky} = 0.0552 \cdot T_{ea}^{1.5} \quad (13)$$

The terms R_2 and R_4 refer to the LWIR emissions from the green layer, and R_3 to those from the building external surface:

$$R_2 = R_4 = \sigma \cdot \varepsilon_{gl} \cdot T_{gl}^4 \quad (14)$$

$$R_3 = \sigma \cdot \varepsilon_{ew} \cdot T_{ew}^4 \quad (15)$$

The convective heat flux between the external air and the green layer ($CV_{ea,gl}$) was:

$$CV_{ea,gl} = \rho_a \cdot C_{pa} \cdot (T_{ea} - T_{gl}) \cdot r_e^{-1} \quad (16)$$

where: ρ_a is the air density, C_{pa} is the specific heat of air at constant pressure, and r_e is the external or aerodynamic resistance of the plant.

The green layer exchange by convection with the air gap ($CV_{ag,gl}$) was evaluated as:

$$CV_{ag,gl} = h_{ag} \cdot (T_{ag} - T_{gl}) \quad (17)$$

where h_{ag} is the convective heat transfer coefficient.

The latent heat transfer (Φ), due to the plant evapotranspiration, was calculated as:

$$\Phi = \rho_a \cdot C_{pa} \cdot (e_{s,gl} - e_a) \cdot \gamma^{-1} \cdot (r_s + r_e)^{-1} \quad (18)$$

where: $e_{s,gl}$ and e_a are the green layer air vapour pressure at saturation and the air vapour pressure, respectively; γ is the psychrometric constant; r_s is the stomatal resistance.

2.3 Model Application to Experimental Data and Main Assumptions

The energy balance model of the green layer was applied to experimental data relating to a GF realized at the University of Bari. In this system, the green layer was made up of *Pandorea jasminoides* variegated, an evergreen climbing plant, and an iron net, 15 cm far from the building wall, as supporting structure.

The measured parameters used were: external air temperature and relative humidity, wind speed, solar radiation, green layer and wall external surface temperature.

The main assumptions underlying the model application concern: the neglect of vertical fluxes of energy and of the heat storage in the leaves and the selection of a significative day within the two-years (2015–2016) measurement campaign.

3 Results and Discussion

The energy model was applied to a summer clear day, 1 August 2015. Significant measured parameters are shown in Fig. 2. The analysis of relationships between solar radiation, external air, green layer and external surface temperatures is useful to understand the functioning of the GF. There is a certain displacement between curves. The values of vegetation temperature were lower than those of the external air temperature. The wall surface temperature was lower than the air and green layer temperatures at daytime. The lower temperature of the external wall surface, in warm periods, is one of the most relevant benefits of GFs on buildings functioning.

Figure 3 shows the main sensible contributions of the energy balance. Positive values stand for heat quantities gained by the green layer, while negative ones are

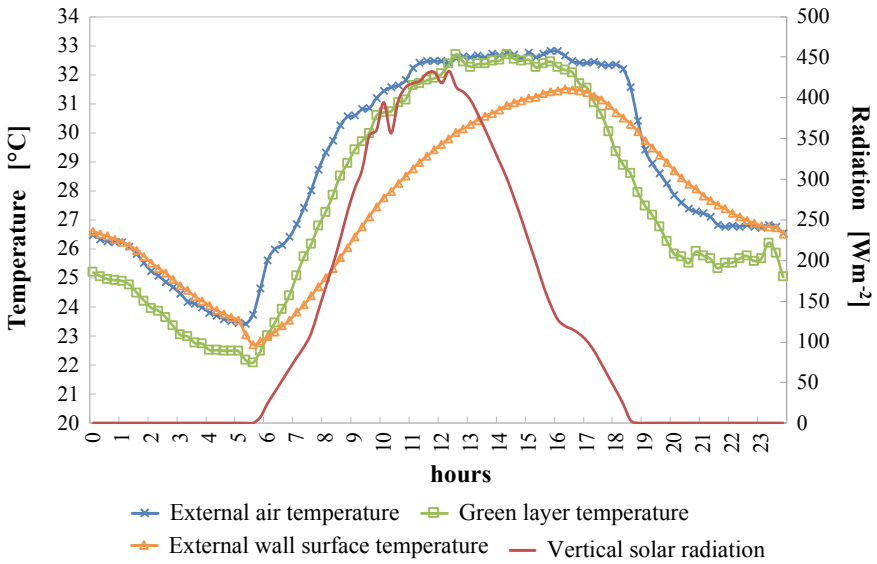


Fig. 2 Measured values of external air temperature, green layer temperature, external surface temperature of the wall behind the vegetation and solar radiation on a vertical surface; 1 August 2015

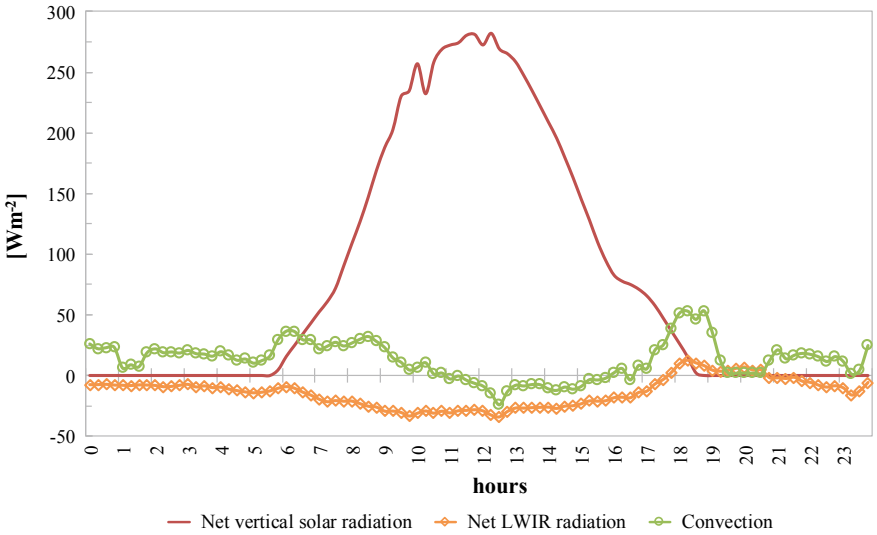


Fig. 3 Calculated sensible heat fluxes for the green layer: net vertical solar radiation, net LWIR radiation and heat convection; 1 August 2015

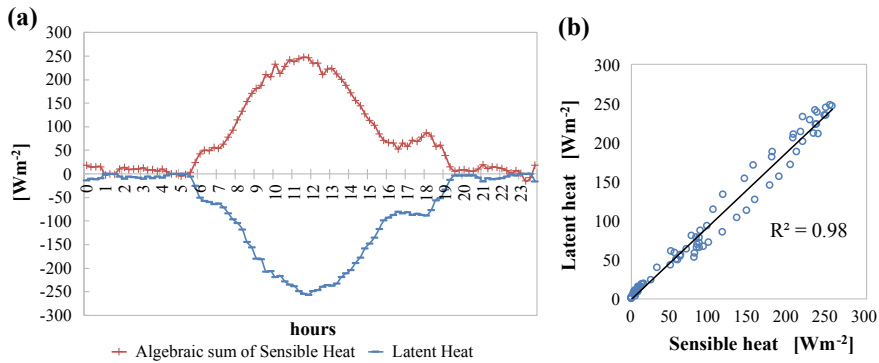


Fig. 4 Algebraic sum of calculated sensible heat contributions and latent heat: curves trend (a) and correlation analysis (b); 1 August 2015

energy losses for it. The vertical solar radiation was quantitatively the most significant term. It has an almost normal course, with the peak value around noon. The LWIR radiative and the convective fluxes were, generally, lower than solar radiation one and had also negative values. Convective flux had a jagged trend, since it was influenced by wind speed.

The algebraic sum of the sensible heat contributions and the latent one are plotted in Fig. 4a. While the sensible heat was absorbed by vegetation, evapotranspiration is the main mechanism to disperse heat. The sensible and the latent curves showed almost perfectly equal and opposite values. As required by the energy balance, their sum was nearly zero (Eq. 6). A correlation analysis was also carried out (Fig. 4b); the coefficient of determination R^2 was equal to 0.98, that means a good agreement between the two terms. Therefore, the energy balance of the green layer can be considered verified.

4 Conclusions

In this research, the heat flow mechanisms involved in green façade systems were defined. A heat balance equation for each of the system identified layer was written. The energy balance model considers the main sensible (solar radiation, infrared radiation, convection) and latent (evapotranspiration) contributions. The attention was pointed to the green layer energy balance. The balance of the vegetated layer was analyzed and validated through experimental data. The comparison between the mathematical model and the measured values allowed to assess the reliability and validity of the approach. This research could be considered a first significant step towards the definition of tools, specific for green façades, to be used in simulating building microclimate models.

Acknowledgements The contribution to programming and conducting this research must be equally shared between the Authors. The present work has been carried out under the “Studio di tecniche di realizzazione di un prototipo di edificio con parete verde a microclima controllato per testare il modello del flusso energetico tra la parete verde e la superficie dell’edificio”; Sistema Elettrico Nazionale, Progetto D.1 ‘Tecnologie per costruire gli edifici del futuro’, Piano Annuale di Realizzazione (PAR) 2018”, Accordo di Programma Ministero dello Sviluppo Economico—ENEA funded by the Italian Ministry of Economic Development.

References

- Bianco, L., Serra, V., Larcher, F., & Perino, M. (2017). Thermal behaviour assessment of a novel vertical greenery module system: First results of a long-term monitoring campaign in an outdoor test cell. *Energy Efficiency*, *10*, 625–638.
- Blanco, I., Schettini, E., Scarascia Mugnozza, G., Campiotti, C. A., Giagnacovo, G., & Vox, G. (2017). Vegetation as a passive system for enhancing building climate control. *Acta Horticulturae*, *1170*, 555–561.
- Bowler, D. E., Buyung-Ali, L., Knight, T. M., & Pullin, A. S. (2010). Urban greening to cool towns and cities: A systematic review of the empirical evidence. *Landscape and Urban Planning*, *97*, 147–155.
- Cameron, R. W. F., Taylor, J. E., & Emmett, M. R. (2014). What’s “cool” in the world of green façades? How plant choice influences the cooling properties of green walls. *Building and Environment*, *73*, 198–207.
- Convertino, F., Vox, G., & Schettini, E. (2019). Heat transfer mechanisms in vertical green systems and energy balance equations. *International Journal of Design & Nature and Ecodynamics* *14*, 7–18.
- European Commission. (2013). Building a Green Infrastructure for Europe.
- Ip, K., Lam, M., & Miller, A. (2010). Shading performance of a vertical deciduous climbing plant canopy. *Building and Environment*, *45*, 81–88.
- Jim, C. Y., & He, H. (2011). Estimating heat flux transmission of vertical greenery ecosystem. *Ecological Engineering*, *37*, 1112–1122.
- Kontoleon, K. J., & Eumoropoulou, E. A. (2010). The effect of the orientation and proportion of a plant-covered wall layer on the thermal performance of a building zone. *Building and Environment*, *45*, 1287–1303.
- Malys, L., Musy, M., & Inard, C. (2014). A hydrothermal model to assess the impact of green walls on urban microclimate and building energy consumption. *Building and Environment*, *73*, 187–197.
- Norton, B. A., Coutts, A. M., Livesley, S. J., Harris, R. J., Hunter, A. M., & Williams, N. S. G. (2015). Planning for cooler cities: A framework to prioritise green infrastructure to mitigate high temperatures in urban landscapes. *Landscape and Urban Planning*, *134*, 127–138.
- Pérez, G., Coma, J., Martorell, I., & Cabeza, L. F. (2014). Vertical Greenery Systems (VGS) for energy saving in buildings: A review. *Renewable and Sustainable Energy Reviews*, *39*, 139–165.
- Perini, K., Ottelé, M., Fraaij, A. L. A., Haas, E. M., & Raiteri, R. (2011). Vertical greening systems and the effect on air flow and temperature on the building envelope. *Building and Environment*, *46*, 2287–2294.
- Schettini, E., Vox, G., Blanco, I., Campiotti, C. A., & Scarascia Mugnozza, G. (2018). Green walls for building microclimate control. *Acta Horticulturae*, *1215*, 73–76.
- Susorova, I., Angulo, M., Bahrami, P., & Stephens, Brent. (2013). A model of vegetated exterior facades for evaluation of wall thermal performance. *Building and Environment*, *67*, 1–13.
- Vox, G., Blanco, I., & Schettini, E. (2018). Green façades to control wall surface temperature in buildings. *Building and Environment*, *129*, 154–166.

Odor Nuisance in the Livestock Field: A Review



C. Conti, M. Guarino and J. Bacenetti

Abstract The development of residential areas near farms, and the intensification and specialization of livestock activities have led to a considerable increase in the potential of odor impact on nearby residents. The manure management system is the principal cause of odor nuisance to the surrounding neighborhood. Ammonia, hydrogen sulfide, and volatile organic compounds are the principal odorous compounds emitted from farms. Their impact depends on animal species (pig, cattle, poultry, etc.), farm management, FIDOL factors, topography, and meteorological conditions. Thus, reducing nuisance episodes is a relevant air quality issue. Different types of atmospheric dispersion models (Gaussian, Lagrangian or Eulerian) can be used to predict the impact of odors on nearby communities, and to plan setback distances, aimed at maintaining adequate buffer zones between livestock units and residents. The aim of this review was to investigate, through the analysis of the published literature, air dispersion models used to determine setback distances, aimed at protecting neighbors from odor discomfort.

Keywords Odor · Livestock · Air dispersion models · Setback distances

1 Introduction

Since several times, odors have received increasing attention among atmospheric pollutants (Mielcarek and Rzeznik 2015). Intensive livestock farming and animal production operations are among the major sources of complaints of people living near these production facilities (Bibbiani and Russo 2012). Odors from livestock units and operations are the result of many different compounds, mainly ammonia

C. Conti (✉) · M. Guarino · J. Bacenetti

Department of Environmental Science and Policy, Università degli Studi di Milano, Via Giovanni Celoria 2, 20133 Milan, Italy
e-mail: cecilia.conti@unimi.it

© Springer Nature Switzerland AG 2020

A. Coppola et al. (eds.), *Innovative Biosystems Engineering for Sustainable Agriculture, Forestry and Food Production*, Lecture Notes in Civil Engineering 67,
https://doi.org/10.1007/978-3-030-39299-4_22

(NH₃), hydrogen sulfide (H₂S) and volatile organic compounds (VOCs) (Blanes-Vidal et al. 2012), deriving almost totally from manure and urine (Barth et al. 1984; Kreis 1978; Lemay 1999).

The impact of odors on the surrounding communities depends on several factors, such as the amount of odor emitted, the distance from the site, weather conditions, topography, and odor sensitivity and tolerance of the neighbors (Danuso et al. 2015; Guo et al. 2004) other than from the combination of the FIDOL factors (Frequency, Intensity, Duration, Offensiveness, and Location) (de Melo et al. 2012). They may affect humans in various ways, ranging from annoyance to documented health effects, leading to a reduced quality of life (Blanes-Vidal 2015; Radon et al. 2004). The relevance of the odors on public health and the increasing citizens complaints to public health agencies have led Authorities and Governments to tackle the problem (Nicell 2009). Several countries have developed setback guidelines aimed at maintaining adequate buffer zones between livestock units and residents to protect people from odor nuisance (Guo et al. 2004; Zhou et al. 2005). Atmospheric dispersion models are commonly used to evaluate the impact of odors on receptors (Schaubberger et al. 2001). They are mathematical models used to predict the downwind odor concentration considering odor emission rates, topography and meteorological data. They provide estimates of odor levels in both current and future emission scenarios, thus having both a predictive (in case of facilities already realized) and a descriptive function (facilities to be built) (Capelli et al. 2013; Danuso et al. 2015). Given the complexity of the problem, the aim of this review was to assess, through the analysis of the published literature, the dispersion models that can be applied for planning setback distances.

2 Materials and Methods

44 scientific studies on odors in livestock field published till 2019 were reviewed. The agricultural sector was analyzed because it is one of the major responsible for odor impact. A systematic search of scientific literature was carried out in order to find studies, which addressed odors impact assessment. The inserted keywords were “Odor”, “Livestock”, “Dispersion models” and “Setback distance”. Articles with the title and/or abstract description unfitting these themes were not considered. The checked databases were Scopus (www.scopus.com) and Web of Science (www.isiwebofknowledge.com), which were visited last time in May 2019. Only literature reported in English was included in the review scope. All types of studies (i.e. original field investigations, modeling studies, air dispersion studies, and review articles) were included in the selection, except for patents, letters, and conference abstracts. Finally, the resulting list of articles to be reviewed was agreed upon by the authors (Fig. 1).

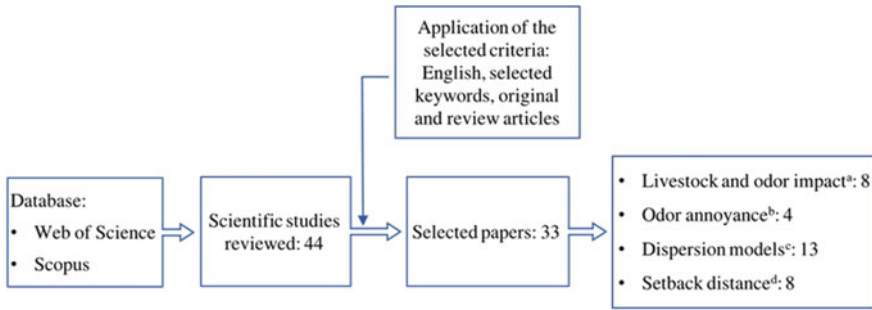


Fig. 1 Systematic mapping process ^aBarth et al. (1984), Bibbiani and Russo (2012), Hansen et al. (2012), Kreis (1978), Lemay (1999), Mielcarek and Rzeznik (2015), Nicell (2009), Stowell et al. (2005)

^bBlanes-Vidal (2015), Blanes-Vidal et al. (2012), Nimmermark (2004), Radon et al. (2004)

^cCapelli and Sironi (2018), Capelli et al. (2013), Danuso et al. (2015), de Melo et al. (2012), Guo et al. (2001), Nimmermark et al. (2005), Ranzato et al. (2012), Schauberger and Piringer (2001), Schulte et al. (2007), Wilson and Sawford (1996), Yu et al. (2010), Zhou et al. (2005), Zhu et al. (2000)

^dGuo et al. (2004, 2005), Jacobson et al. (2000, 2005), OMAFRA (1995a, b), Schauberger et al. (2001, 2002)

3 Atmospheric Dispersion Models

The release of odorous components, from husbandry practices, and the repeated exposure to intense malodor, are a concern for the health of animals and agricultural workers and for people living near the production facilities, especially in densely populated areas (Bibbiani and Russo 2012; Capelli et al. 2013; Hansen et al. 2012; Nimmermark 2004). Residents living close to livestock facilities reported more physical and non-specific health symptoms compared to people living further (Blanes-Vidal et al. 2012). To overcome such problems, different air dispersion models are available and have been applied to simulate odor dispersion from agricultural sources and used for measuring odor impact on the nearby communities (Yu et al. 2010). Most of them are Gaussian models, but also Lagrangian and Eulerian models can be used.

Gaussian models are the most widely used (Yu et al. 2010). According to Gaussian plume model, meteorological conditions and emission are assumed time-invariant, mass is conserved, the wind is considered absent in calm conditions and complex terrain is not considered (Danuso et al. 2015). Puff models are an evolution of classical Gaussian models since they represent the emission in a series of puffs, each moved by wind (center of gravity) and with an internal Gaussian distribution (Zhou et al. 2005). Differently, from plume models, they do not assume steady-state conditions and they allow to simulate calm wind conditions and consider three-dimensional space characteristics (Yu et al. 2010).

In Lagrangian models each air parcel is assumed to move in the atmosphere along trajectories determined by the wind field, the buoyancy, and the turbulence effects (Wilson and Sawford 1996). The Eulerian model is similar to the Lagrangian model

with the exception that it utilizes a fixed reference grid, instead of the moving grid of the Lagrangian model, and in each grid is calculated the average concentration of pollutant particles (Danuso et al. 2015) Compared to Gaussian models they are more accurate but they require a higher computing power.

As mentioned above, several models (e.g. AERMOD, AODM, LODM, INPUFF-2, CALPUFF, etc.) have been applied to simulate odor dispersion from agricultural sources. AERMOD, a plume model, is the U.S. EPA preferred air dispersion model. Schulte et al. (2007) reported that when modeled as a point source, predicted odor concentrations were generally lower than measured, whereas when modeled as an area source, AERMOD greatly under-predicted odor concentrations. The main advantage of this model is that it considers topographic features and meteorological conditions and it is suited for near-field dispersion.

Among puff models, INPUFF-2 and CALPUFF are the most widely used (Yu et al. 2010). INPUFF-2 was developed by the U.S. Environmental Protection Agency (USEPA), it is capable of addressing the release of a substance over a short time period and allows for multiple sources (Zhu et al. 2000). Instead, the CALPUFF modeling system includes three main components: CALMET, CALPUFF, and CALPOST. CALMET is the 3-dimensional meteorological model, CALPUFF is the air dispersion model and CALPOST is a post-processing package that summarizes the results of the simulation (Capelli and Sironi 2018). This model is suggested in the case of far-field applications, it is able to simulate calm wind conditions or stagnation conditions and has memory of past conditions, in other words, the pollutant concentration at a given point is given by the sum of all the puffs emitted by the sources also during the previous hours (Ranzato et al. 2012). de Melo et al. (2012) used both AERMOD and CALPUFF to model odor dispersion around a complex pig farm facility. The results showed that concentrations predicted by CALPUFF were lower than those calculated by AERMOD. They used wind tunnel data to compare and validate the results. From the comparison emerged that both models properly predict mean concentrations further downwind from the pig farm facility, whereas, closer to the buildings, the models may over- or under-predict concentrations.

Many other models have been developed to estimate odor dispersion, including *OdiGauss*. *OdiGauss* is a software developed by Danuso et al. (2015) for mapping odor dispersion from livestock waste. It could be useful in the livestock field since a model for odor emissions from poultry farms (EmiFarm) is incorporated. However, the dispersion is calculated according to a Gaussian plume model, so the software does not consider complex orography, simulate only hourly-average concentrations and the dispersion is adjusted in case of wind calm conditions. It requires data on weather and odor emission sources. The outputs generated are time-over-threshold maps with different odor threshold levels.

In general, all the above-mentioned model typologies, present advantages, and limitation in relation to the situation in which they are used. So, the choice of the most appropriate model is to be evaluated from time to time. Regardless of the type of model adopted, they are useful for the estimation of setback distances between livestock production facilities and neighbors residences, as a cost-effective odor control strategy (Nimmermark et al. 2005).

4 Setback Distances

Setback distances have been originally determined by empirical methods (experience based), as a function of some key variables, such as the number and species of animals, climatic conditions, housing characteristics (e.g. ventilation, manure collection system, etc.) and abating technologies used (Lim et al. 2000; Yu et al. 2010). For example, in Canada, Minimum Distance Separation guidelines (MDS-I and II) were developed by the Ontario Ministry of Agriculture, Food, and Rural Affairs in the 1990s (OMAFRA 1995a, b). This model has separate procedures for buildings and manure storage units. For buildings, the base distance is obtained by the product of four different tabulated values: animal species, livestock units, number of animals and manure management system. Then the resulting based distance is multiplied by another factor (Factor E) equal to 1 for nearest residence and agricultural areas and equal to 2 for residential, commercial, or urban areas. Regarding manure storage units distance is calculated according to base building distance, the type of manure storage system (e.g. open or closed) and adjusted by Factor E (Guo et al. 2004).

Then, empirical methods have been improved with dispersion models, since they a more robust tool for determining setback distances.

In USA, the Purdue model, Odor From Feedlots—Setback Estimation Tool (OFFSET), and Odor Footprint Tool (OFT) (Guo et al. 2004; Stowell et al. 2005) were developed. In particular, the OFFSET was one of the first models developed in the USA to estimate the setback distances from animal production sites. It was developed in Minnesota, taking in consideration numerous emission measurement, INPUFF-2 and historical weather data for Minnesota (Jacobson et al. 2000). Odor emissions were measured from 280 animal buildings and manure storage units on 85 farms in Minnesota from 1998 to 2001 (Jacobson et al. 2005). To determine the setback distance with OFFSET model, total odor emission rate and desired odor-annoyance-free intensity and frequencies are required (Guo et al. 2004). The total odors emission is obtained from the sum of the odor emission factors calculated for each source, while odor-annoyance-free intensity is set at 2 (faint odor = 75 OU/m³) on a 0–5 reference scale (Jacobson et al. 2005) that correspond to a free frequency high of 99% and low of 91% (Guo et al. 2005). Based on INPUFF-2, OFFSET has been validated for distances from 100 to 300 m (Zhu et al. 2000) and from 400 to 3.2 km (Guo et al. 2001). The major advantage is the easy use thanks to tabulated odor emission and tabulated odor reduction factors based on animal species and a database of emission measurements from various animal buildings, manure storage units, manure handling methods, and odor control technologies used (Nimmermark et al. 2005). The Nebraska OFT is a science-based computer resource for evaluating the potential odor impact of new and expanded animal production facilities. It utilizes AERMOD and weather databases to generate regional odor roses, odor footprints, and directional setback distance curves (Stowell et al. 2005).

The Austrian Odor Dispersion Model (AODM), a steady-state model, has been described extensively by Schaubberger et al. (Schaubberger and Piringner 2001; Schaubberger et al. 2001 2002). Schaubberger et al. (2002) used AODM to calculate

separation distance between a 1000-head pig unit and residential areas, for the city Wels. They found that distances vary mainly according to the probability of the wind direction and wind velocity. The final distance ranged between 99 and 362 m.

5 Conclusions

Odors generated by livestock farming represent a relevant air quality issue. Reducing nuisance episodes is therefore essential for sustainable livestock production. However, measuring the odor impact in the field is quite complicated, as described above. This study reviewed the main odor dispersion models commonly used to determine the extension of odor impact and related odor-annoyance-free setback distances from animal production sites.

Models may be useful tools when evaluating technologies to reduce the odor release at existing operations or when planning new operations, thus having not only a descriptive nature but also predictive. A critical element in odor modeling is the proper validation between modeled data and real nuisance perceived by the population. A better understanding of odor nuisance can be obtained combining models with odor measurements allowing a quantitative and qualitative characterization of odors.

To protect people from odor nuisance, some countries (e.g. USA, Canada, and Austria) have established guidelines based on minimum separation distances. Being setback distances generated by different models, and being scaling factors different in each country, the odor-annoyance-free level falls into a wide range. Therefore, it could be useful to develop a database of the scaling factors to ensure uniformity in approaches.

As regards future perspectives, since odors have such a big impact on the surrounding environment, it is reasonable to assess the importance of the odors also by the Life Cycle Assessment (LCA) approach, developing a dedicated impact category.

References

- Barth, C. L., Elliott, L. F., & Melvin, S. W. (1984). Using odor control technology to support animal agriculture. *Transactions of the ASAE*, 27(3), 859–864.
- Bibbiani, C., & Russo, C. (2012). Odour emission from intensive livestock production system: Approaches for emission abatement and evaluation of their effectiveness. *Large Animal Review*, 18(3), 135–138.
- Blanes-Vidal, V. (2015). Air pollution from biodegradable wastes and non-specific health symptoms among residents: Direct or annoyance-mediated associations? *Chemosphere*, 120, 371–377.
- Blanes-Vidal, V., Suh, H., Nadimi, E. S., Løfstrøm, P., Ellermann, T., Andersen, H. V., et al. (2012). Residential exposure to outdoor air pollution from livestock operations and perceived annoyance among citizens. *Environment International*, 40, 44–50.
- Capelli, L., & Sironi, S. (2018). Combination of field inspection and dispersion modelling to estimate odour emissions from an Italian landfill. *Atmospheric Environment*, 191, 273–290.

- Capelli, L., Sironi, S., Del Rosso, R., & Guillot, J. M. (2013). Measuring odours in the environment vs. dispersion modelling: A review. *Atmospheric Environment*, 79, 731–743.
- Danuso, F., Rocca, A., Ceccon, P., & Ginaldi, F. (2015). A software application for mapping livestock waste odour dispersion. *Environmental Modelling and Software*, 69, 175–186.
- de Melo, A. M. V., Santos, J. M., Mavroidis, I., & Junior, N. C. R. (2012). Modelling of odour dispersion around a pig farm building complex using AERMOD and CALPUFF. Comparison with wind tunnel results. *Building and Environment*, 56, 8–20.
- Guo, H., Jacobson, L., Schmidt, D., & Nicolai, R. (2001). Calibrating Inpuff-2 model by resident-panelists for long-distance odor dispersion from animal production sites. *Applied Engineering in Agriculture*, 17(6), 859.
- Guo, H., Jacobson, L., Schmidt, D., Nicolai, R., & Janni, K. (2004). Comparison of five models for setback distance determination from livestock sites. *Canadian Biosystems Engineering*, 46(6), 17–25.
- Guo, H., Jacobson, L., Schmidt, D., Nicolai, R., Zhu, J., & Janni, K. (2005). Development of the OFFSET model for determination of odor-annoyance-free setback distances from animal production sites: Part II. Model development and evaluations. *Transactions of the ASAE*, 48(6), 2269–2276.
- Hansen, M. J., Adamsen, A. P. S., Pedersen, P., & Feilberg, A. (2012). Prediction of odor from pig production based on chemical odorants. [Research Support, Non-U.S. Gov't]. *Journal of Environmental Quality*, 41(2), 436–443.
- Jacobson, L. D., Guo, H., Schmidt, D., Nicolai, R., Zhu, J., & Janni, K. (2005). Development of the OFFSET model for determination of odor-annoyance-free setback distances from animal production sites: Part I. Review and experiment. *Transactions of the ASAE*, 48(6), 2259–2268.
- Jacobson, L. D., Guo, H., Schmidt, D. R., Nicolai, R. E., Zhu, J., & Janni, K. A. (2000). *Development of an odor rating system to estimate setback distances from animal feedlots: Odor from feedlots-setback estimation tool (offset)*. St Joseph. <https://www.cabdirect.org/cabdirect/abstract/20003020697>.
- Kreis, R. D. (1978). Limiting the environmental impact of animal production odors. *Environment International*, 1(5), 247–275.
- Lemay, S. P. (1999). Barn management and control of odours. *Advances in Pork Production*, 10, 81–91.
- Lim, T., Heber, A., Ni, J.-Q., Grant, R., & Sutton, A. (2000). Odor impact distance guideline for swine production systems. *Odors and VOC Emissions*, 1–16.
- Mielcarek, P., & Rzeznik, W. (2015). Odor emission factors from livestock production. *Polish Journal of Environmental Studies*, 24(1), 27–35.
- Nicell, J. A. (2009). Assessment and regulation of odour impacts. *Atmospheric Environment*, 43(1), 196–206.
- Nimmermark, S. A. (2004). Odour influence on well-being and health with specific focus on animal production emissions. [Review]. *Annals of Agricultural and Environmental Medicine*, 11(2), 163–173.
- Nimmermark, S. A., Jacobson, L. D., Schmidt, D. R., & Gay, S. W. (2005). Predictions by the odor from feedlots, setback estimation tool (OFFSET) compared with observations by neighborhood monitors. [Research Support, Non-U.S. Gov't]. *Journal of the Air & Waste Management Association*, 55(9), 1306–1314.
- OMAFRA. (1995a). *Minimum Distance Separation I (MDS I)*. Toronto: Queen's Printer.
- OMAFRA. (1995b). *Minimum Distance Separation II (MDS II)*. Toronto: Queen's Printer.
- Radon, K., Peters, A., Praml, G., Ehrenstein, V., Schulze, A., Hehl, O., & Nowak, D. (2004). Livestock odours and quality of life of neighbouring residents. [Research Support, Non-U.S. Gov't]. *Annals of Agricultural and Environmental Medicine*, 11(1), 59–62.
- Ranzato, L., Barausse, A., Mantovani, A., Pittarello, A., Benzo, M., & Palmeri, L. (2012). A comparison of methods for the assessment of odor impacts on air quality: Field inspection (VDI 3940) and the air dispersion model CALPUFF. *Atmospheric Environment*, 61, 570–579.

- Schauberger, G., & Piringer, M. (2001). Predicting odour impact using the Austrian odour dispersion model (AODM). *Water Science and Technology*, 44(9), 197–204.
- Schauberger, G., Piringer, M., & Petz, E. (2001). Separation distance to avoid odour nuisance due to livestock calculated by the Austrian odour dispersion model (AODM). *Agriculture, Ecosystems & Environment*, 87(1), 13–28.
- Schauberger, G., Piringer, M., & Petz, E. (2002). Calculating direction-dependent separation distance by a dispersion model to avoid livestock odour annoyance. *Biosystems Engineering*, 82(1), 25–38.
- Schulte, D. D., Modi, M. R., Henry, C. G., Billesbach, D. P., Stowell, R. R., Hoff, S. J., & Jacobson, L. D. (2007). *Modeling odor dispersion from a swine facility using AERMOD*. Paper presented at the International Symposium on Air Quality and Waste Management for Agriculture, 16–19 September 2007, Broomfield, Colorado.
- Stowell, R. R., Koppolu, L., Schulte, D. D., & Koelsch, R. K. (2005). *Applications of using the odor footprint tool*. Paper presented at the Livestock Environment VII, 18–20 May 2005, Beijing, China.
- Wilson, J. D., and Sawford, B. L. (1996). Review of Lagrangian stochastic models for trajectories in the turbulent atmosphere: Springer.
- Yu, Z., Guo, H., & Laguë, C. (2010). Livestock odor dispersion modeling: a review. *Transactions of the ASABE*, 53(4), 1231–1244.
- Zhou, X., Zhang, Q., Guo, H., & Li, Y. (2005). *Evaluation of air dispersion models for livestock odour application*. Paper presented at the CSAE/SCGR 2005 Meeting Winnipeg, Manitoba.
- Zhu, J., Jacobson, L. D., Schmidt, D. R., & Nicolai, R. (2000). Evaluation of INPUFF-2 model for predicting downwind odors from animal production facilities. *Applied Engineering in Agriculture*, 16(2), 159–164.

Spatial Analysis of the Impact of Rural Buildings on the Agro-Forestry Landscape Using GIS



Giuseppe Cillis, Dina Statuto and Pietro Picuno

Abstract Farm buildings constitute a witness of the economic and productive organization of a specific rural territory. Designed over the centuries in order to fulfil their primary agricultural role, they now constitute a widespread heritage, which in some cases possesses an irreplaceable architectural value. Moreover, they also play a central role for the sustainability of the rural environment, since they can influence natural and semi-natural habitats, both in terms of their structure and biodiversity. Mostly in some southern European countries, these rural structures have been built basing on agricultural needs and land characteristics. Considering the land abandonment occurred during the last centuries, most of these historical farm buildings have been abandoned, causing a possible loss of the historical-cultural heritage of the rural landscape. In this paper, the potential of a Geographic Information Systems (GIS) to assess the impact of farm buildings on the surrounding agroforestry landscape has been explored with reference to a protected area of Basilicata Region, which has been considered as a case study. Through the implementation of a GIS, the land cover changes over the past 30 years—focusing mainly on the afforestation processes—have been identified and connected to the position of the geo-localized rural buildings.

Keywords Rural buildings · Cultural heritage · Agro-forestry landscape · Geographical Information System · Spatial analysis

1 Introduction

Rural buildings, realized over time in order to achieve their main agricultural role, now constitute a considerable heritage that in some cases possesses an unreplacable cultural value, playing a central role for the sustainability of the rural environment as well. Conceived to host food production, the farm building constitutes indeed a unique

G. Cillis (✉) · D. Statuto · P. Picuno

SAFE School of Agriculture, Forest, Food and Environmental Sciences, University of Basilicata, via dell'Ateneo Lucano n.10, 85100 Potenza, Italy
e-mail: giuseppe.cillis@unibas.it

© Springer Nature Switzerland AG 2020

A. Coppola et al. (eds.), *Innovative Biosystems Engineering for Sustainable Agriculture, Forestry and Food Production*, Lecture Notes in Civil Engineering 67,
https://doi.org/10.1007/978-3-030-39299-4_23

207

example in the wide epistemological sector of building construction (Picuno 2012). Designed to produce optimal environmental conditions for animals and plants, the rural building constitutes therefore a unique technological model since, at the same time, it hosts workers and inhabitants involved in the daily operations for the care of living organisms (Fuentes et al. 2010; Fuentes 2010; Picuno et al. 2015). The irreplaceable role that the buildings have historically played is strictly connected with the surrounding context as well, due to the need of the farmer to live in close contact with agricultural land and animal husbandry (Hernández et al. 2004; Jeong et al. 2012). This form of settlement has been in harmony with the environment and the agricultural land, joining the primary production needed for human nutrition with the control and care of rural land. So, the activities made by the Man have often strongly influenced the agricultural environment and the visual perception of the surrounding landscape (Statuto et al. 2016, 2019). Scientific and technological research is currently increasingly investigating the ecological impact of the rural buildings on landscape and on the importance of implementing a sustainable rural development plan to improve the conservation of habitats and ecosystem services (McKenzie et al. 2011; McCann et al. 2017). Haller and Bender (2018) showed the connection between biodiversity and conservation of grasslands habitats, which necessarily passes through the conservation of rural building heritage. This is mainly true for some *Natura2000* priority habitats, which are related to the preservation of traditional agricultural activities, such as the semi-natural dry grasslands (Calaciura and Spinelli 2008). The monitoring of the rural buildings and their surrounding landscape, considering the multi-temporal, multi-disciplinary and spatial components, may benefit from the implementation of Geographic Information Systems (GIS) tools (Cillis and Statuto 2018). In the present study, the potential of GIS and the integration of different remote sensing techniques (Statuto et al. 2018a) applied to the assessment of the rural heritage of a protected area has been explored, with the aim to assess the impact of old rural buildings on landscape diversity.

2 Materials and Methods

2.1 Study Area

The study area was identified as the *Regional Park of Gallipoli Cognato Piccole Dolomiti Lucane* (EUAP1053) of the Basilicata region (Southern Italy). The Park (Fig. 1) spans an area of 27,000 hectares within the borders of the municipalities of Accettura, Calciano and Oliveto Lucano (located in the Matera Province) and Castelmezzano and Pietrapertosa (located in the Potenza Province). The Park protects and safeguards a large area at the center of the regional territory showing an important naturalistic, historical and ethno-anthropological values. This landscape is characterized by an important rural building heritage as well, most of these constructions having been intended for shelter or as a non-stable garrison of small natural

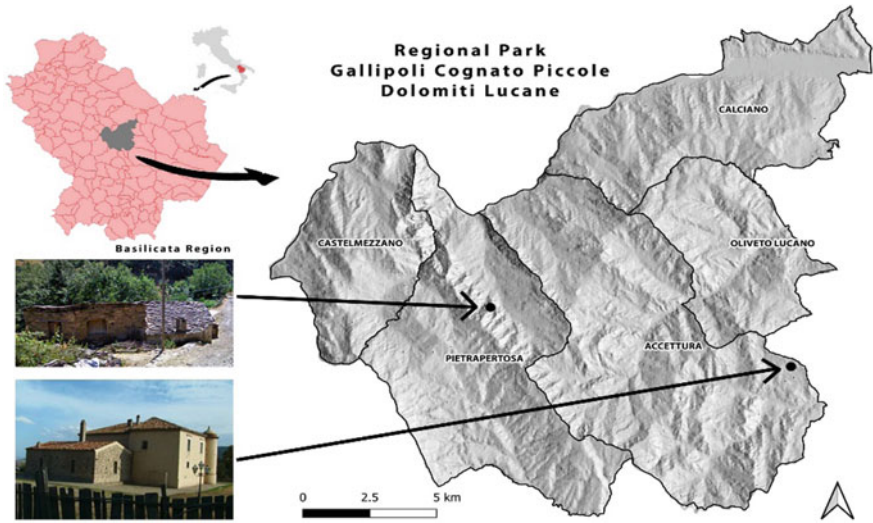


Fig. 1 Location of the study area (EPSG: 4326–40°30′48.3″N 16°07′26.9″E) and two examples of rural buildings: locality of “Casieri” (top) and a fortified farm building “Masseria Spagna” (bottom)

grasslands, used by farmers who resided permanently in the countries. These buildings are therefore very small and simple in structure, reflecting a poor family-run agriculture. Only in some well-defined areas, these buildings have stone masonry with a characteristic covering of stone slabs. This simple typology in some areas has evolved into an aggregation of more small buildings, some of which having been intended for human residence.

2.2 Data Elaboration

The elaboration has been organized in two phases performed in a GIS environment (QGIS 3.4; SNAP software for satellite images processing). In the first step, the land use datasets have been elaborated and then a database of rural buildings defined “*masserie*”—from their traditional name (Statuto et al. 2015; Statuto and Picuno 2017)—has been created. In the second phase, spatial analyses have been carried out to investigate the correlations between rural structures and the transformations of the surrounding agro-forestry landscape. The processing of land use data for 1990 and 2017 has been carried out using respectively Landsat5 TM satellite images (23 July 1990) and Landsat 8 OLI + TIRS (2 August 2017). After having completed all the pre-processing operations, a supervised classification with *Random forest* algorithm has been performed on training samples taken from high resolution orthophotos of the same period. The accuracy of classification has been verified on random sample points. The period was chosen considering the availability of satellite images

and the overlapping with high-resolution orthophotos to verify accuracy. Moreover, this was the period in which there was a greater tendency to abandon the territory because of some European agricultural policies (Statuto et al. 2018b). After the creation of the land use map (Fig. 2) a change detection was carried out, from which the necessary data for the subsequent operations have been extracted. The rural buildings database was created by a cross-search on different maps (Cillis et al. 2019a). Using topographic cartography of the Italian Military Geographic Institute (IGMI) and the regional technical cartography of the Basilicata Region related to the year 2013 in vector format, it has been possible to identify the polygons linked to rural buildings through an interrogation and subsequent selection of the individual buildings, which have been associated to specific toponyms as “*masseria*” or acronym visible on the cartography. Each one of the identified artefacts has been classified into *abandoned* and *not-abandoned* rural buildings by using high resolution orthophotos of the year 2017. Abandoned rural buildings were manually searched by visually assessing the integrity of the roof on the orthophotos. This distinction considers, among the abandoned buildings, only farms that are definitively abandoned because they are shot down or ruined. Furthermore, for each one of these constructions, a square buffer of 25 ha has been created for the subsequent spatial analysis, as proposed by McKenzie et al. (2011).

After the database creation, the spatial correlation between the abandonment of buildings and some topographical variables, such as altitude and slope, has been evaluated. The average value has been then calculated for each square buffer. Subsequently, the last analysis performed has been finalized to understand the correlation of each rural building from an ecological point of view and the surrounding landscape, highlighting the correlation between changes in land use and abandonment of rural buildings. With this aim, a geospatial intersection between land use change

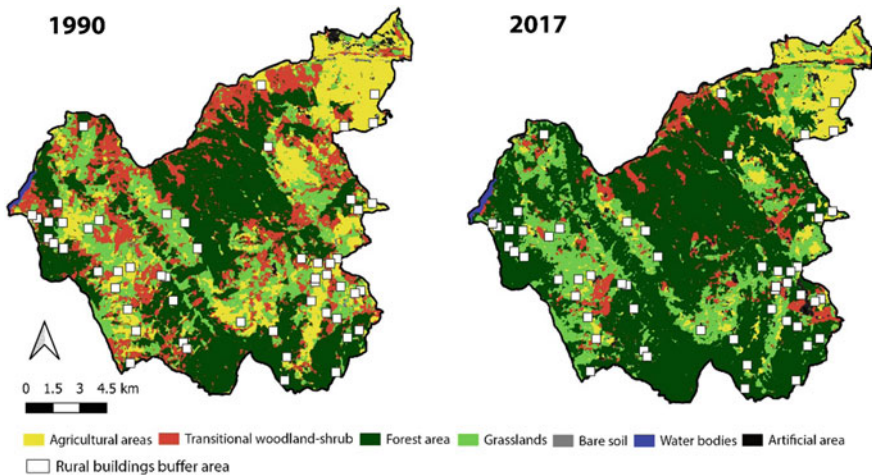


Fig. 2 Land use maps (years 1990 and 2017) and localization of rural buildings with buffer area

detection and square buffer has been carried out in the surrounding area of each abandoned and not-abandoned rural building, so as to identify any transition with repercussions on agro-forestry and habitats diversity.

3 Results and Discussion

Even if the ever-increasing number of open data has made easier to carry out a series of spatial analyzes allowing a rapid and efficient digitalization of the different types of typical rural buildings defined as *masserie* (Ruggiero et al. 2019), alongside the semi-automatic procedure here presented it has been anyway necessary to carry out a manual classification, aimed to distinguish the abandoned buildings from those non-abandoned ones. Indeed, considering the n.55 *masserie*, only n.17 of them are currently abandoned. The first spatial analysis between the buffer area around the farms and the altitude and the slope (Fig. 3) showed that the rural buildings still in use are distributed throughout all altitudinal areas and slope classes. The abandoned rural buildings are, instead, located in areas where the average slope value exceeds 20% and/or in areas with an altitude higher than 600 m.

This methodology applied on a smaller area has been useful to identify how the landscape around the farms has been transformed, mainly identifying those farms playing an important ecological role within the agro-forestry landscape. Through the construction of a geo-database including rural buildings, it has been possible indeed to carry out some spatial surveys, from a simple mapping to a more detailed geo-statistical assessments and cross detections. From this first analysis it has emerged that the areas around the abandoned buildings have undergone the afforestation process more than other areas (Table 1). In fact, from an overall assessment of all the

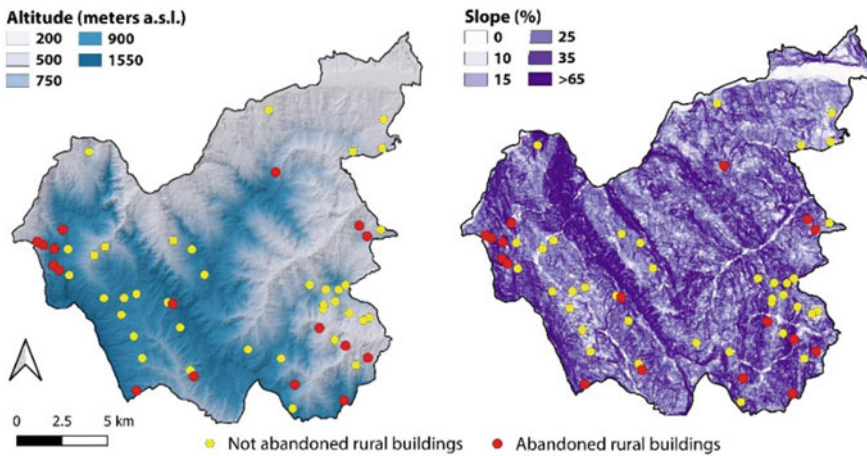


Fig. 3 Position of rural buildings related to altitude (left) and slope (right)

Table 1 Surfaces (in percentage and hectares) of the buffer areas including abandoned and not abandoned rural buildings, related to the main dynamics in the analyzed period. In “*Other changes*” all the minor dynamics in terms of surface variation were merged

	Abandoned rural buildings		Not abandoned rural buildings	
	ha	%	ha	%
Afforestation	140.18	28.8	168.17	16.4
No changes	190.61	39.2	485.84	47.1
Agricultural areas to Artificial areas	4.38	0.9	40.23	3.9
Agricultural areas to Grasslands	73.57	15.1	148.54	14.4
Agricultural areas to Transitional woodlands-shrubs	6.22	1.3	20.63	2.0
Grasslands to Agricultural areas	8.75	1.8	36.10	3.5
Grasslands to Transitional woodland-shrub	36.86	7.6	21.66	2.1
Transitional woodland-shrub to Grasslands	17.99	3.7	45.39	4.4
Other changes	12.62	1.6	63.95	6.2
	486.26		1031.50	

buffer areas, it can be noticed that between 1990 and 2017, the 28% of the examined land became a forest. Apart from this first expected conclusion, the methodology which has been implemented made also possible to evaluate other dynamics that can have an importance from the point of view of landscape and ecological diversity (Fig. 4). It has been possible to notice, in fact, that both for abandoned and non-abandoned buildings there was a transition from agricultural areas to grasslands and transitional zones (around 14–15%). This shows that the phenomenon of abandoning the territory (abandonment of agriculture and afforestation) is distributed everywhere in the study area, even in areas with farms in activity, demonstrating the widespread trend of the phenomenon (Statuto et al. 2017; Cillis et al. 2019b). This emerged process should be further investigated mostly in areas surrounding the abandoned

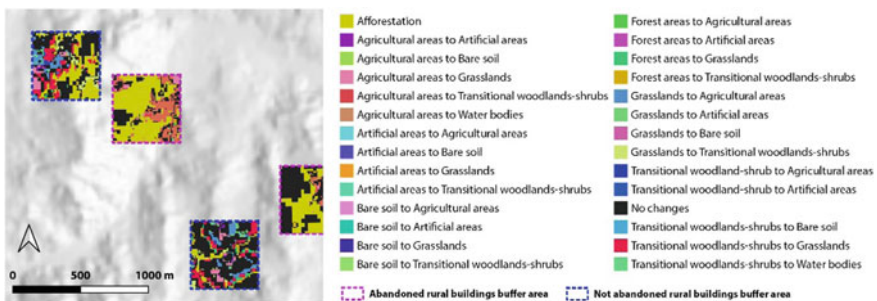


Fig. 4 Detail of a part of the study area of abandoned and non-abandoned rural buildings, with relevant land use changes in the period 1990–2017

farms in which, together with afforestation, it is visible the evolution of the grasslands towards the transitional woodlands-shrubs (7.6%). This aspect could determine on time a potential loss of habitats with an high ecological value (for example the habitat identified as “*semi-natural dry grasslands and scrubland facies*”), caused by the disappearance of traditional agricultural activities related to free-ranging and non-intensive grazing. On the contrary, in areas around active farms there is greater stability in terms of land use (no changes areas of around 47.1%), with only minor dynamics (other changes equal to 6.2%).

From this preliminary study about the impact that rural buildings could have on the landscapes of inland mountain areas, it could be concluded that the increasing abandonment of the different historical rural structures, especially in the steeper and less accessible areas such as those of Mediterranean agro-forestry landscape, often determines the land abandonment, then the consequent phenomenon of re-naturalization and afforestation. This in some cases can compromise the high biodiversity level of the grasslands semi-natural habitats, since there is a strong correlation between biodiversity conservation, traditional agriculture (including rural built heritage) and grasslands maintenance/restoration (Haller and Bender 2018).

4 Conclusions

Rural building represents the main protagonist around which the sustainable and resilient growth of agriculture can improve. The more rational consumption of resources, the fight against environmental degradation and the maintenance of stable ecosystem balances, are actions that can be carried out through the return of traditional agriculture. In this way, it is also possible to preserve the rural building heritage as an historical and architectural evidence of a certain way of living, in synergy with the surrounding natural and landscape heritage. The methodology presented in this paper can be considered as a suitable tool for planning and management of protected areas, in which there is the need to analyze many types of data with different levels of detail, in order to implement investigation and actions that can be used to preserve several important semi-natural habitats related to agricultural activities.

References

- Calaciura, B & Spinelli, O. (2008). Management of Natura 2000 habitats. 6210 Semi-natural dry grasslands and scrubland facies on calcareous substrates (Festuco-Brometalia) (*important orchid sites). *European Commission*.
- Cillis, G. & Statuto, D. (2018). Landscape protection and tourist valorisation of the cultural and natural heritage of the UNESCO site of Matera (Italy). In *Public Recreation and Landscape Protection-With Nature Hand in Hand? Conference Proceeding* (pp. 226–231).

- Cillis, G., Statuto, D., & Picuno, P. (2019a). Valorisation of historical farm buildings for protecting the rural landscape. In *proceedings of the 47rd Symposium on: Actual Tasks on Agricultural Engineering-ATAE 2109*, 5–7 March 2019, Opatija, Croatia.
- Cillis, G., Statuto, D. & Picuno, P. (2019b). Historical maps processed into a GIS for the assessment of forest landscape dynamics. In *Public Recreation and Landscape Protection - With Sense Hand in Hand? Conference Proceeding 2019* (pp. 180–184).
- Fuentes, J. M. (2010). Methodological bases for documenting and reusing vernacular farm architecture. *Journal of Cultural Heritage*, 11, 119–129.
- Fuentes, J. M., Gallego, E., García, A. I., & Ayuga, F. (2010). New uses for old traditional farm buildings: The case of the underground wine cellars in Spain. *Land Use Policy*, 27, 738–748.
- Haller, A., & Bender, O. (2018). Among rewilding mountains: Grassland conservation and abandoned settlements in the Northern Apennines. *Landscape Research*, 43(8), 1068–1084.
- Hernández, J., García, L., & Ayuga, F. (2004). Integration methodologies for visual impact assessment of rural buildings by geographic information systems. *Biosystems Engineering*, 88, 255–263.
- Jeong, J. S., García-Moruno, L., & Hernández-Blanco, J. (2012). Integrating buildings into a rural landscape using a multi-criteria spatial decision analysis in GIS-enabled web environment. *Biosystems Engineering*, 112, 82–92.
- McCann, T., Cooper, A., Rogers, D., McKenzie, P., & McErlean, T. (2017). How hedge woody species diversity and habitat change is a function of land use history and recent management in a European agricultural landscape. *Journal of Environmental Management*, 196, 692–701.
- McKenzie, P., Cooper, A., McCann, T., & Rogers, D. (2011). The ecological impact of rural building on habitats in an agricultural landscape. *Landscape and Urban Planning*, 101, 262–268.
- Picuno, P. (2012). Vernacular farm buildings in landscape planning: a typological analysis in southern Italian region. *Journal of Agricultural Engineering*, XLIII-e20, 130–137.
- Picuno, P., Stanovčić, T., Moric, I., Dimitrijević, A. & Sica, C. (2015). The valorisation of vernacular farm buildings for an innovative rural tourism. In *proceedings of the 43rd Symposium on: Actual Tasks on Agricultural Engineering-ATAE* (pp. 807–817), 24–27 February 2015. Opatija (Croatia). UDC 721:631.2.
- Ruggiero, G., Parlavacchia, P., & Dal Sasso, P. (2019). Typological characterisation and territorial distribution of traditional rural buildings in the Apulian territory (Italy). *Journal of Cultural Heritage*. <https://doi.org/10.1016/j.culher.2019.02.012>. In Press.
- Statuto D., Cillis G., & Picuno P. (2015). Historical cartography and GIS tools for the analysis of land use and landscape changes. In *Proceedings of the 43rd Symposium on: "Actual Tasks on Agricultural Engineering-ATAE"* (pp. 441–450). Opatija (Croatia), 24–27 February 2015. UDC 528.9:631.471.
- Statuto, D., Cillis, G., & Picuno, P. (2016). Analysis of the effects of agricultural land use change on rural environment and landscape through historical cartography and GIS tools. *Journal of Agricultural Engineering*, 47, 28–39.
- Statuto, D., Cillis, G., & Picuno, P. (2017). Using historical maps within a gis to analyze two centuries of rural landscape changes in Southern Italy. *Land*, 6, 65.
- Statuto, D., & Picuno, P. (2017). Valorisation of vernacular farm buildings for the sustainable development of rural tourism in mountain areas of the Adriatic-Ionian macro-region. *Journal of Agricultural Engineering*, 48, 21–26.
- Statuto, D., Frederiksen, P., & Picuno, P. (2018a). Valorization of agricultural by-products within the “energyscapes”: Renewable energy as driving force in modeling rural landscape. *Natural Resources Research*. <https://doi.org/10.1007/s11053-018-9408-1>.
- Statuto, D., Cillis, G., & Picuno, P. (2018b). GIS-based analysis of temporal evolution of rural landscape: A case study in Southern Italy. *Natural Resources Research*. <https://doi.org/10.1007/s11053-018-9402-7>.
- Statuto, D., Cillis, G. & Picuno, P. (2019). Visual quality indicators for assessing landscape characteristics and managing its protection. In *Public Recreation and Landscape Protection-With Sense Hand in Hand? Conference Proceedings* (pp. 476–480).

Milk-Production in Barns with Compost Bedding and Free Stall: A Profitability Analysis



Marcos A. Lopes, Gustavo R. de O. Silva, André L. R. Lima, Geraldo M. da Costa, Flávio A. Damasceno, Vitor P. Barros and Matteo Barbari

Abstract The objective was to analyse, comparatively, the profitability of compost barn and free stall milk-production systems. Data collected from four farms from January to December 2016 were analysed. The cost of milk production was estimated according to the operating cost methodology. Additionally, gross and net margins were estimated as indicators of profitability. The results showed that the average gross and net margins were not influenced by the type of facility; they were positive in both of the production systems. Among the components of the effective operating cost, the proportion of the “medications” item was lower in the compost barn, while the cost of bedding for the cows was lower in the free stall farms. Depreciation and total operating cost were similar in the two systems. Milk sales made up a higher percentage of the revenue in the free stall farms, while the expectations of revenues from wastes were similar in the two production systems. Given that there were no significant economic differences between the types of facilities, it is concluded that ease in management, productivity, reproductive performance, animal health, environmental issues, and availability of water and bedding material should be the motivators for choosing one system over the other.

Keywords Dairy cattle · Cost centers · Production cost · Animal facility

M. A. Lopes · G. R. de O. Silva · A. L. R. Lima · G. M. da Costa · F. A. Damasceno
Federal University of Lavras, Campus Universitário, PO Box 3037, Lavras, Minas Gerais
37200-000, Brazil
e-mail: malopes@ufla.br

V. P. Barros
Rehagro, Rua Santa Fé, 100, Sion, Belo Horizonte, Minas Gerais 30320-130, Brazil

M. Barbari (✉)
Department of Agriculture, Food, Environment and Forestry (DAGRI), Università degli Studi di
Firenze, Via San Bonaventura, 13, 50145 Florence, Italy
e-mail: matteo.barbari@unifi.it

© Springer Nature Switzerland AG 2020
A. Coppola et al. (eds.), *Innovative Biosystems Engineering for Sustainable Agriculture, Forestry and Food Production*, Lecture Notes in Civil Engineering 67,
https://doi.org/10.1007/978-3-030-39299-4_24

1 Introduction

In Brazil two intensive systems are used to produce milk from cattle in confinement, based on free stalls or compost bedding. The latter has only recently been introduced into the country. Barberg et al. (2007) reported that the first compost bedded pack barn (CBP) was built in 2001 in Minnesota, while the first CBP in Brazil was realized in 2012 (Brito 2016). This housing system in Brazil rapidly spread due to the high degree of satisfaction of producers worldwide with its functioning.

Various studies have addressed the design of the buildings, including dimensions, installation characteristics and managerial procedures. Other works cite possible advantages of the system in relation to performance, animal health (mastitis, hoof injuries), longevity (Leso et al. 2019). However, no study has reported a profitability analysis of compost barn systems. Additionally, it is known that production costs vary from year to year given that the cost depends on innumerable variables such as the price of inputs, wages, and the technology used at the time. The costs are also influenced by genetics and animal nutrition. Therefore, it is essential to conduct new research on production costs including properties of the free stall system, in order to enable the comparison of compost barn and free stall farms. Few studies adopting the cost centre methodology used in the current study are available in literature (Santos and Lopes 2012).

Thus, due to the lack of studies on economical comparison of compost barn and free stall systems, this study aimed to comparatively analyse the profitability of the two milk production systems.

2 Materials and Methods

Data from four farms were collected from January to December 2016 and analysed. Two of these farms (farms 1 and 2) use the compost barn system, and two (farms 3 and 4) use the free stall system. All the farms have the following characteristics: use of maize silage (*Zea mays*) as the main forage, herds predominantly of the 15/16HG genetic group, milking three times/day, and use of semen from Holstein bulls.

Farm 1 is using the compost barn system since September 2015. The bedding is composed of sawdust with a surface of 9 m²/cow. The daily milk production in 2016 was 8,459 kg, with an average of 27.3 kg/cow/day and an average of 310 lactating cows. On Farm 2, the coffee husks from the plantations are used as bedding for the cows and complemented with sawdust, providing 10 m²/cow. In 2016, milking 180 cows, the property produced 5,970 kg of milk per day on average with an average yield of 33.1 kg/cow/day.

On both the farms, the thickness of the bedding layer was 40 cm. The packed bedding was aerated twice a day by means of a cultivator reaching a depth of 30 cm. The quantity of new material added to bedding was 3 m³/month. The frequency of totally removing and renewing the bedding was 2 years.

In Farm 3 the free stall system has been used since 2006. The bedding consists of sand, and the stocking rate (number of animals/stalls) was 100% during the observation period. Unlike the other three properties, the facility did not have fans and sprinklers, and the animals were only cooled in the waiting room. The farm had a daily milk production of 9,693 kg, with an average of 21.1 kg/cow/day in 2016 with 459 cows milked per day on average. In Farm 4 the cows have been housed in a free stall facility since 2013. Sand is used as bedding, and the stocking rate was 100% during the study period. In 2016, daily production was 8,317 kg of milk, with an average of 23.1 kg/cow/day and an average of 360 lactating cows.

In the present study, the total operating cost (TOC) and effective operating cost (EOC) of milk production were estimated. Additionally, the gross margin and the net margin were calculated as profitability indicators, and analysis and comparison of the proportions of the items that make up the gross revenue, as well as the components of the TOC, were performed in accordance with Lopes et al. (2004).

Using the MS Excel, profitability analysis was conducted and the data were compared via descriptive analyses and grouped into tables with the aim of achieving better comparison, discussion, and presentation of the results (Lopes et al. 2004).

3 Results and Discussion

Table 1 shows the average values for the representativeness of components of Total operating cost and Effective operating cost of milk production in compost barn and free stall production systems. The feeding cost was similar in the two production systems. This occurred because in both facilities the same type of feed can be used, and feed is supplied to the animals in the same way as a total diet using a forage wagon.

The “labour” item was more representative in the farms that adopted the compost barn system. However, apart from the fact that the difference between the values is small, higher expenditure on labour does not seem to be a characteristic of the compost barn system given that the standard deviation of these properties was high ($\pm 2.83\%$) due to the high labour cost at farm 1. The “third-party services” item of this farm (4.91%) was mainly responsible for increasing the proportion of its labour force and, consequently, the average of the two farms that adopted the compost barn system. However, in farm 2, labour costs represented 13.24% of the EOC, indicating lower expenditure than in the two free stall farms, which had values of 13.33% and 14.88%. Thus, the proportion of the cost of production represented by labour costs did not appear to be significantly different in the two types of systems.

Electricity costs represented a lower percentage of the EOC in the free stall properties, but the standard deviation was high ($\pm 2.86\%$). Farm 3 was responsible for this variation because it only had fans in the waiting room, whereas in the other three farms fans were present also in the sheds housing the cows. Because fans are among the items that consume the most energy in dairy farms, in farm 3 the proportion was only 2.71% of the EOC. In farms 1, 2, and 4, electricity represented 5.93%,

Table 1 Representativeness of components of Total operating cost (TOC) and Effective operating cost (EOC) of milk production in compost barn and free stall production systems for the period January to December 2016

Specification	Compost barn ^a		Free stall ^a	
	% EOC	% TOC	% EOC	% TOC
Feed	59.06	54.6	59.37	56.46
Labour	15.24	14.14	14.10	13.46
Energy	7.05	6.50	4.74	4.48
Sanitation	2.80	2.60	6.08	5.78
Milking	3.22	2.97	3.33	3.16
bST	2.67	2.48	2.99	2.85
Reproduction inputs	1.11	1.02	2.75	2.62
Reproduction hormones	0.56	0.52	0.66	0.63
Third-party machine rental	0.18	0.17	0.02	0.02
Miscellaneous expenses	8.10	7.51	5.96	5.66
EOC	100.00	92.50	100.00	95.06
Depreciation	–	7.50	–	4.94
TOC	–	100.00	–	100.00
Milk produced (L/year) ^b	2,558,748		3,193,480	

Source Data from the study (2016)

^aInformation from two properties; bST = bovine somatotropin; sd = standard deviation

^bMilking period considered = 355 days

8.16%, and 6.76%, respectively, of the EOC. This indicates that the electricity cost proportion in the compost barn farms was close to that of the other free stall farm (farm 4). Therefore, the cost of electricity did not differ significantly between the two systems.

Expenditures for medications comprised a lower percentage of the EOC in the compost barn properties. This difference can be explained primarily by the lower expenditure on intramammary antibiotics for the treatment of mastitis. In farms 1 and 2, the cost of tubes for treating mastitis corresponded to 0.96% and 0.14% of the EOC, respectively, while in farms 3 and 4, the values were 2.30 and 3.07%, respectively. The lower expenditure for this type of medication indicates a lower prevalence of clinical mastitis, and the lower somatic cell counts (SCC) in the farms that adopted the compost barn system.

The proportions of EOC related to the cow bedding were not very significant in either system. However, in the free stall properties, the proportion was lower than in the compost barn farms. Farm 1 had the highest percentage of EOC (2.04%), while farm 2 had 0.93%, a proportion closer to that for the free stall farms (0.10% and 0.75%). This result was expected because the bedding area is smaller in the free stall system than in the compost barn and because in the free stall farms the sand was reutilized with the aid of a sand separator.

The proportion of the TOC represented by depreciation was higher in the compost barn properties than in the free stall properties. However, the standard deviation was high (3.06%). This variation occurred due to the high percentage found for farm 2 (9.66%), which had improvements and idle equipment. For farm 1, depreciation represented 5.33% of the TOC, a value close to that of farms 3 (4.01%) and 4 (5.86%). Thus, there was no significant difference in the production systems. This finding was expected because the patrimony values, which do not take into consideration the land values of the farms with compost barn and free stall facilities, were similar, as the TOC was.

The production of milk per area differed among the studied farms, but no significant difference between the production systems was observed. Farm 1, for example, had production higher than farm 3 but slightly lower than farm 4.

Regarding the operational break-even point (Lopes et al. 2015), it was not affected by the type of facility, given that farms 1 and 2 had values higher than farm 3 but lower than farm 4. This finding was expected because the depreciation also varied widely among the properties. All of the farms not only attained the break-even point but exceeded it (by 85.19%, 82.42%, 92.12%, and 83.96% for properties 1, 2, 3, and 4, respectively), indicating that all were profitable.

As a percentage of the actual revenue, revenue from milk sales was higher in the free stall properties (93.3%) than in the compost barn properties (90.85%). This was due to the higher share of the sale of animals (9.15%) in the composition of the revenues of the compost barn farms, although the standard deviation was very high (10.28%). This variation can occur because the number of animals to be sold depends on the objectives of each farm (e.g., whether the herd is stabilized or in expansion), and it also depends on the wastage rate.

Regarding the revenue from wastes, it is important to note that in the compost barn farms the bedding was not changed prior to this study. Therefore, it was not sold or used in the milk production system itself.

In the free stall properties, the slurry produced cannot be commercialized because its transport is impractical due to the low amount of dry matter. Therefore, it can be used by the fodder production cost centre and is used on the farm itself. The manure produced in these properties had already been used as fertilizer for the maize crops to reduce the cost of bulk feed, which represented 15.24% (± 2.83) and 14.10% (± 1.09) of the EOC in compost barn and free stall farms, respectively. Therefore, in the present work, expectations of revenue (if sold) from the compost barn bedding and from the free stall manure were presented separately. However, in the farms that adopted the free stall system, there were no estimated gross or net margins because the slurry could not be sold, and the manure was already used for forage production.

When the expected revenue from wastes was included, it was found that this item represented 1.23% (± 0.13) and 1.29% (± 0.01) of the revenues in the compost barn and free stall properties, respectively. Thus, a fairly similar proportion of total revenue is obtained from wastes in both types of facility, and the proportion of total revenue obtained from wastes per litre of milk was also similar.

When only the actual revenue was considered, the gross margin was higher in the free stall farms. However, the standard deviation was very high for both types of

facility (Table 2). This was expected given that the gross margin depends on various factors such as the quality of the milk produced, the price of milk in the region, and the quantity and quality of the animals sold. However, it cannot be concluded that the compost barn properties have a lower gross margin, given that farm 1, for example, had a gross margin higher than farm 4 and very similar to that of farm 3. Farm 2, in turn, had the lowest gross margin among the four due to its smaller production scale and fewer sales of animals.

Additionally, both the compost barn farms and the free stall farms had positive gross margins. This indicates that they are able to produce in the short term, given that they are capable of covering the EOC and still have surpluses.

Considering only the actual revenue, the net margin, similar to the gross margin, was higher in the free stall farms. The standard deviation was very high for both types of facility. This variation was due to the same reasons mentioned in relation to the gross margin and also to the high standard deviation of the depreciation in the

Table 2 Summary of the profitability analysis (in €) of the milk production cost centre in compost barn and free stall production systems located in the state of Minas Gerais, Brazil, for the period January to December 2016

Specification	Compost barn ^a		Free stall ^a	
	Average (€)	sd (€)	Average (€)	sd (€)
¹ Revenue	1,112,663.87	369,261.99	1,298,031.02	207,905.15
Milk	997,170.09	222,846.17	1,209,177.33	170,318.68
Animals	115,493.78	146,415.82	88,853.69	37,586.46
² TOC	738,034.98	216,687.87	877,622.03	52,749.67
³ EOC	686,028.82	223,013.41	834,628.56	61,622.03
Depreciation	52,006.16	6,325.54	42,993.46	8,872.36
⁴ Gross margin	426,635.05	146,248.58	463,402.46	146,283.12
Gross margin/ha	4,243.30	1,138.13	4,136.49	316.54
⁵ Net margin	374,628.89	152,574.12	420,409.00	155,155.47
Net margin/ha	3,716.53	1,242.88	3,727.50	495.47
Expected revenue from manure	13,412.14	3,130.09	16,673.51	2,568.40
⁶ Estimated gross margin ^b	440,047.19	149,378.67	–	–
⁷ Estimated net margin ^b	388,041.03	155,704.21	–	–

Source Data from the study (2016)

^aInformation from two properties; ^bNo gross or net margins were estimated in the free stall system because the manure had already been used in fertilizing the maize crops in these properties, thus reducing the cost of bulk feed; therefore, it could not be computed again. ¹Revenue = revenue actually received by the producer, coming only from the sale of milk and animals; ²TOC = total operating cost; ³EOC = net operating cost; ⁴Gross margin = considering only the actual revenue; ⁵Net margin = considering only the actual revenue; ⁶Estimated gross margin = considering actual revenue and expectation of revenue from wastes; ⁷Estimated net margin = considering actual revenue and expectation of revenue from wastes; sd = standard deviation; average exchange rate in 2016: 1 € = R\$ 3.858

farms studied and to the differences in production scale, given that a reduction in the product's unit cost can occur when the milk production of a farm is increased (Bressan et al. 2010) due to optimization of the physical structure of the property (Lopes et al. 2006) and keeping costs fixed (Bannock et al. 2003). Additionally, it was verified that farm 1 had a net margin close to that of farm 3, but greater than that of farm 4. Therefore, in the present work, the type of facility had no observable influence on the net margin of the properties.

It is also important to highlight that the net margin was positive in both the compost barn and free stall properties. These results show that the farms are able to produce in the medium term, given that the revenues are sufficient to cover the EOC and to replace the assets after they become worthless through depreciation (Lopes et al. 2004). In relation to the net margin/hectare, similar averages were also seen in the compost barn and free stall properties, with a high standard deviation in the former.

4 Conclusions

The gross and net margins were positive in all the production systems studied, indicating that they are able to produce in the short and medium term. By comparing the components of the TOC of the compost barn and free stall farms, it was concluded that there were differences only in the "medications" item, which constituted a lower proportion of the EOC of the compost barn properties due to the lower percentage expended for intramammary antibiotics for mastitis, and in the "bedding for cows" item, which represented the lowest proportion in the free stall system. In the costs of reproduction inputs and reproductive hormones, there were no significant differences between the farms adopting the different types of facility, although the compost barn farms had better reproductive rates. Additionally, with regard to depreciation, there was no significant difference in the production systems.

Regarding the composition of the revenue, a higher percentage came from the sale of milk in the free stall properties because the compost barn properties sold more animals. In relation to the wastes, the revenue expectations were similar in the two systems.

These results show that the revenues, EOC, depreciation, and the cost of implementing the systems may not be the major determinants in deciding which type of facility to build on a property. Thus, ease of management, productivity, reproductive performance, animal health (hoof injuries and mastitis), water availability, environmental issues, and availability of bedding material (sand, sawdust, coffee husks) should motivate the choice of one installation over the other.

References

- Bannock, G. R. E., Baxter, R. E., & Davis, E. (2003). *The penguin dictionary of economics*. 4. Ed, 7^o ed. London, *Penguin Books*, 416 p.
- Barberg, A. E., Endres, M. I., Salfer, J. A., & Reneau, J. K. (2007). Performance and welfare of dairy cows in an alternative housing system in Minnesota. *Journal of Dairy Science, Champaign, 90*(9), 1575–1583.
- Bressan, V. G. F., Braga, M. J., & Bressan, A. A. (2010). Eficiência e economia de escala em cooperativas de crédito: uma abordagem de fronteira estocástica de custo com dados em painel. *Advances in Scientific and Applied Accounting, 3*, 335–352.
- Brito, E. C. (2016). Produção intensiva de leite em compost barn: uma avaliação técnica e econômica sobre a sua viabilidade. 2016. 59 f. Master Thesis—Universidade Federal de Juiz de Fora, Juiz de Fora.
- Leso, L., Pellegrini, P., & Barbari, M. (2019). Effect of two housing systems on performance and longevity of dairy cows in Northern Italy. *Agronomy Research, 17*(2), 574–581.
- Lopes, M. A., Lima, A. L. R., Carvalho, F. M., Reis, R. P., Santos, I. C., & Saraiva, F. H. (2004). Controle gerencial e estudo da rentabilidade de sistemas de produção de leite na região de Lavras (MG). *Ciência e Agrotecnologia, 28*(4), 883–892.
- Lopes, M. A., Dias, A. S., Carvalho, F. M., Lima, A. L. R., Cardoso, M. G., & Carmo, E. A. (2006). Efeito da escala de produção nos resultados econômicos de sistemas de produção de leite na região de Lavras (MG): um estudo multicaseos. *Boletim de Indústria Animal, 63*, 177–188.
- Lopes, M. A., Moraes, F., Carvalho, F. M., Peres, A. A. C., Bruhn, F. R. P., & Reis, E. M. B. (2015). The effect of technological levels on profits of milk production systems participating in the “full bucket” program: A multicase study. *Semina: Ciências Agrárias, 36*(4), 2909–2922.
- Santos, G., & Lopes, M. A. (2012). Indicadores de rentabilidade do centro de custo produção de leite em sistemas intensivos de produção. *Boletim de Indústria Animal, 69*, 1–11.

Thermal Environment Inside Mechanically Ventilated Greenhouses: Results from a Long-Term Monitoring Campaign



Andrea Costantino, Lorenzo Comba, Giacomo Sicardi, Mauro Bariani and Enrico Fabrizio

Abstract In totally mechanically controlled greenhouses, the main indoor environmental parameters are accurately controlled for maximizing the quantity and the quality of the production. This task is challenging because values of these parameters significantly differ within the enclosure, with some spots reaching values very far from the average ones. In this work, the results from a long-term monitoring campaign in a mechanically ventilated greenhouse for floricultural production are presented. In the case study, indoor air temperature and relative humidity were measured in several spots, with different acquisition time steps. The working schedule of the evaporative pads was also monitored. The results of this work show that the thermal environment of the greenhouse was not homogeneous, especially concerning the indoor air temperature values that vary significantly inside the enclosure. This variation is more evident especially during daytime due to the presence of high values of solar radiation. Furthermore, the acquired data showed that the indoor air temperature stratification is a not negligible phenomenon inside greenhouses and has to be considered when the probes for the climate control systems are installed inside the enclosure.

Keywords Climate control · Agricultural buildings · Protected cultivation · Sensing and monitoring · Temperature distribution · Temperature gradient

A. Costantino · L. Comba · E. Fabrizio (✉)
TEBE Research Group, Department of Energy, Politecnico di Torino, Corso Duca degli Abruzzi 24, 10129 Turin, Italy
e-mail: enrico.fabrizio@polito.it

A. Costantino
School of Agricultural Engineering and Environment, Universitat Politècnica de València, Camino de Vera s/n, 46022 Valencia, Spain

G. Sicardi · M. Bariani
Munters Italy S.p.a, Via Strada Piani 2, 18027 Chiusavecchia d'Imperia, Italy

© Springer Nature Switzerland AG 2020
A. Coppola et al. (eds.), *Innovative Biosystems Engineering for Sustainable Agriculture, Forestry and Food Production*, Lecture Notes in Civil Engineering 67,
https://doi.org/10.1007/978-3-030-39299-4_25

1 Introduction

The benefit of totally mechanically controlled greenhouses relies in the control of the main indoor environmental parameters that are needed for the production, such as indoor air temperature ($t_{\text{air},i}$) and relative humidity (RH_i). These parameters are accurately controlled to overcome adverse outdoor environments and provide conditions favourable to crop production (ASHRAE 2011), even though it entails a not negligible energy consumption (Fabrizio 2012).

The climate control system of these greenhouses provides different values of $t_{\text{air},i}$ according to the cultivated crop and to the hour of the day. During daytime, in fact, $t_{\text{air},i}$ should be set for maximizing the rate of net photosynthesis and the biomass storage process. On the contrary, during nighttime hours, $t_{\text{air},i}$ must be reduced for minimizing the rate of respiration that expends glucose. The values of RH_i should be maintained between 60% and 85%. Below 60% the plant suffers from water stress, while above 85% the risk of developing pathogens increases (Hellickson and Walker 1983).

Due to the features of the greenhouses (e.g. transparent and low-insulating envelope and free cooling), maintaining the adequate indoor environmental conditions is a challenging task, especially during the warm season when high values of solar radiation are present. For these reasons, the indoor environmental conditions can vary within the enclosure and, in some spots, they can differ significantly from the average ones, as reported by previous studies in literature (García-Ruiz et al. 2018; Zorzeto and Leal 2017). The non-uniform distributions of the values of indoor environmental parameters is an issue that has recently received attention in several researches (Ahemd et al. 2016; Ma et al. 2019).

In the present work, a dataset from a long-term monitoring campaign carried out in a totally mechanically controlled greenhouse is analysed. The aim of this analysis is to evaluate the indoor environmental conditions ($t_{\text{air},i}$ and RH_i) considering the variation of the boundary conditions (e.g. activation of the evaporative pads or variation of solar radiation). Furthermore, the uniformity of the thermal environment is analyzed by evaluating the thermal gradient inside the greenhouse.

2 Materials and Methods

2.1 The Case Study

The case study presented in this work considers a greenhouse located in Veneto region, Northeast Italy. The analyzed building is part of a larger greenhouse complex for floricultural production. The monitored greenhouse is particularly interesting because is devoted to experimental cultivation of new hybrid plants (small flowers) and, consequently, climate control must provide the adequate conditions to the sensitive new cuttings.

From the geometrical point of view, the monitored greenhouse has seven bays of 6.4 m width each (the total width is 44.8 m). The height of the bays is 5.15 m at the ridge level and 3.74 m at the eave level. Four of the bays are 36 m long, while the remaining three are 39.88 m long. Thus, the total useful floor is roughly 1690 m² while the net volume is around 7500 m³.

The greenhouse has a single glazed envelope, with an average U -value (considering the metal frame) of 6.3 W m⁻² K⁻¹, while the internal areal heat capacity (κ_i) can be considered negligible. The ground is a concrete slab (200 mm of thickness) with a U -value of 2.5 W m⁻² K⁻¹ and a κ_i of 16 kJ m⁻² K⁻¹.

The heating system of the greenhouse is centralized. A gas boiler produces the supplemental heat to maintain the indoor air set point temperature. The heat is then transferred and distributed in the enclosure through a hydronic pipe system located in direct contact with the cultivation benches.

In the greenhouse, an exhaust ventilation system is adopted. The ventilation air flow rate is provided by seven direct driven fans located in the south east wall. Fans are equipped with a variable frequency speed motor that adjusts the propeller speed according to the ventilation needs. Evaporative pads are placed in the north west wall. To decrease the thermal stratification and the effect of solar radiation, the monitored greenhouse is equipped with circulating fans and solar shading screens that are activated when it is necessary. The climate control system manages also the bay openings.

2.2 The Monitoring Campaign

The monitoring campaign concerned the warm season and lasted from July 1st to October 31st 2018. In the monitored greenhouse, the indoor environmental data were obtained using the following sensors (accuracy noted in brackets):

- a thermistor for the measurement of air temperature (± 0.21 °C) and a humistor for relative humidity ($\pm 2.5\%$) embedded in the same portable logger;
- a resistance temperature detector PT1000 (± 0.15 °C) connected to an analog portable logger.

All the data loggers adopted a USB communication protocol and all the sensors were shielded from direct solar radiation. In the monitored greenhouse 15 points of measurements of $t_{\text{air},i}$ and four points of measurements of RH_i were set up in different spots and with different acquisition time steps. The outdoor conditions of $t_{\text{air},o}$, RH_o and total horizontal solar radiation ($I_{\text{sol,tot,H}}$) were provided by a third-party weather station of ARPA (Regional Environmental Protection Agency) Veneto located near the monitored case study.

To have a clearer picture of the thermal environment dynamics inside the greenhouse, the state of on/off of the evaporative pads was also monitored. This measurement was carried out through an AC current switch sensor connected to the power

cable of the circulating pump of the evaporative pads. The signal was acquired and converted by a pulse data logger.

3 Results and Discussion

In Fig. 1 the mean hourly value of $t_{air,i}$ and RH_i (the average between all the indoor measurements) and the trend of $t_{air,o}$ and RH_o are shown during the entire monitored period. From the graph it stands out that the geographical location of the analyzed greenhouse is very humid, in fact the monitored values of RH_o often reach 100%. High RH_o values should be considered during the climate control system design, because the saturation effectiveness of the evaporative pads (function of RH_o) can considerably decrease. Analyzing the trend of $t_{air,o}$, three different subperiods can be identified. They are characterized by different average values of $t_{air,o}$. The first subperiod (Subperiod A) went from July 6th to August 25th when the average values of $t_{air,o}$ was around 26.2 °C. During this subperiod $t_{air,i}$ was slightly lower than $t_{air,o}$ because evaporative pads were activated for guaranteeing adequate $t_{air,i}$. The activation of the evaporative pads was facilitated by values of RH_o that are lower than in the following days. The period from July 1st to 5th was not considered in the analysis because the production started on July 6th. For this reason, fans, evaporative cooling and shadings were not activated and temperature peaks of over 44 °C were monitored. Similar values of indoor air temperatures in free floating conditions were reported in literature (Zhou et al. 2017).

The Subperiod B is from August 26th to September 23rd, when the average $t_{air,i}$ decreased to 23.9 °C. In this subperiod, $t_{air,i}$ and $t_{air,o}$ were very similar. This similarity may depend on the high ventilation flow rates needed to guarantee the

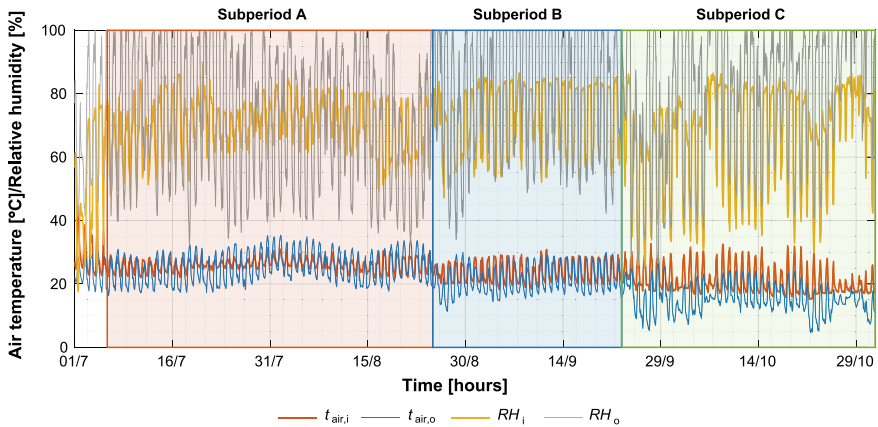


Fig. 1 Trend of $t_{air,i}$ $t_{air,o}$ RH_i and RH_o during the monitored period (hourly time step). The red frames highlight the three considered periods

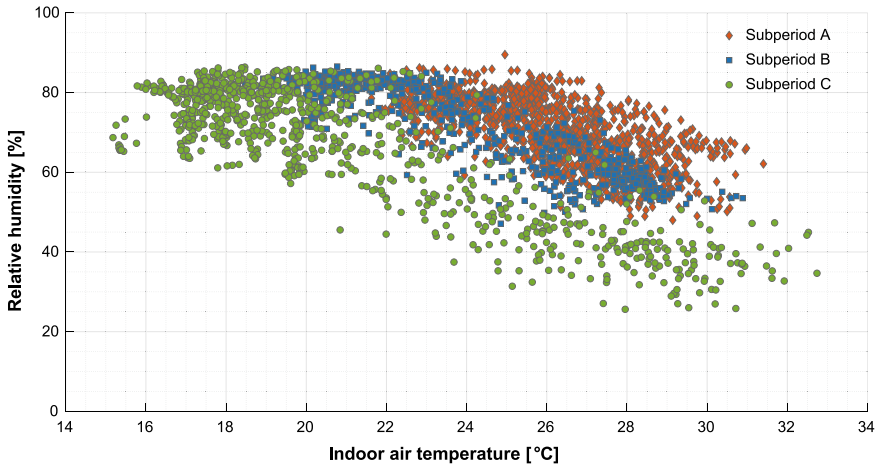


Fig. 2 Scatterplot of $t_{air,i}$ (x-axis) and RH_i (y-axis) for the three considered subperiod

indoor air set point temperature. In this subperiod, in fact, the high values of RH_o made the evaporative cooling less effective. During the last subperiod (Subperiod C, September 24th–October 31st), $t_{air,o}$ decreased to an average value of 21 °C. From the graph it stands out that in Subperiod C $t_{air,o}$ was considerably lower than $t_{air,i}$ and supplemental heating was needed to maintain the indoor air set point temperature especially during nighttime.

During the entire monitored period (with the exclusion of the first five days) $t_{air,i}$ was always in 15–33 °C range while RH_i always between 40 and 90%, but in each subperiod both the environmental parameters varied considerably. This variation is assessed through the scatterplot presented in Fig. 2. The coordinates of the points are the average hourly values of $t_{air,i}$ (x-axis) and RH_i (y-axis) monitored during the three subperiods. From the chart it stands out that the point dispersion is lower in Subperiod A, increases in Subperiod B and even more in Subperiod C. In Subperiod C $t_{air,i}$ varies from 15 to 33 °C, in Subperiod B from 18 to 31 °C and in Subperiod A from 19 to 32 °C. The range of RH_i is quite similar for Subperiod A and B (from 50 to 85%), while a greater point diffusion characterizes Subperiod C (from 30 to 85%).

The previous analyses pointed out how the indoor climate conditions vary significantly in different periods characterized by different outdoor weather conditions. As stated before, indoor environmental conditions of greenhouses are characterized also by great space variations. Analyzing the measurements of $t_{air,i}$ that were collected in the different spots of the enclosure, considerable differences can be found. In Fig. 3a, the hourly trend of $t_{air,i}$ is displayed with a focus on three days (July 29th–31st). In the graph, the trend of the hourly average value of $t_{air,i}$ is presented together with a boxplot that considers all the acquired measurements. The boxplot shows 75th and 25th percentiles of the considered measurements, the median, the upper and lower extremes and the outliers.

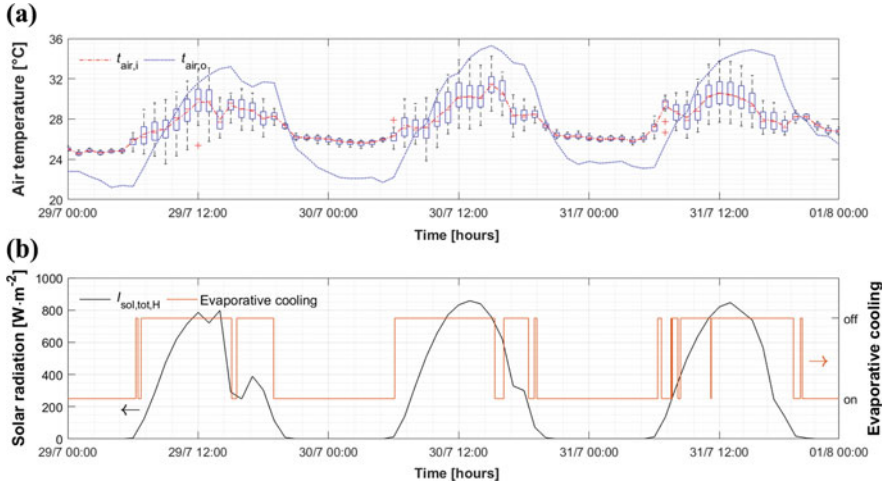


Fig. 3 Subplot a: $t_{air,i}$ (boxplot) and $t_{air,o}$. Subplot b: $I_{sol,tot,H}$ (primary axis) and activation time of the evaporative cooling (secondary axis)

A first element that stands out from that graph is that measured data have a larger dispersion during daytime than during nighttime. This issue could depend on the high values of solar radiation that were monitored during these days, which maximum exceeded $800 W m^{-2}$, as reported on the primary axis of Fig. 3b. Solar radiation is the forcing that entails an increasing of $t_{air,i}$ especially due to the glazed envelope of the greenhouse.

This temperature increase is not uniform, as shown by the boxplot and it may depend by the zenith and azimuth angles and on the presence of shadings. Furthermore, the rise of $t_{air,i}$ increases the convective motion that bring to the air stratification (vertical temperature gradient). This phenomenon is further pronounced due to the height of the greenhouse. Furthermore, also the presence of fans and of evaporative pads entail local differences in $t_{air,i}$ (horizontal temperature gradient).

Considering all the previously mentioned conditions, the variation of $t_{air,i}$ inside the enclosure could be explained. These differences are not negligible. Considering the three analyzed days of Fig. 3, the difference between the maximum and minimum monitored values of $t_{air,i}$ goes from more than $8^{\circ}C$ to around $0.4^{\circ}C$. During daytime the average difference between the maximum and the minimum values of $t_{air,i}$ was quite less than $5^{\circ}C$, while during nighttime this difference decreases to less than $1^{\circ}C$.

Another aspect that stands out from Fig. 3a is that $t_{air,i}$ was considerably lower than $t_{air,o}$ during all the three considered days. The graph shows, in fact, that during this period, the peak of $t_{air,o}$ was around $34-35^{\circ}C$ while the corresponding $t_{air,i}$ peak was generally around $30^{\circ}C$. To understand this temperature decrease, the state of on/off of the evaporative pads is reported in the secondary axis of Fig. 3b. The graph shows that the evaporative pads were activated almost without interruptions during all the

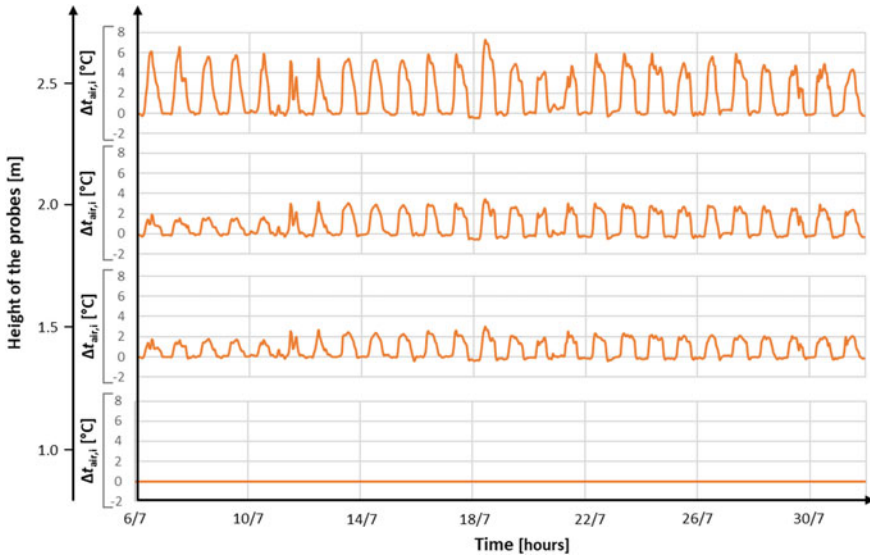


Fig. 4 Hourly differences ($\Delta t_{air,i}$) between $t_{air,i}$ monitored by probes at different heights (1.5, 2 and 2.5 m) and reference $t_{air,i}$ at bench level (1 m) during July

daytime to guarantee and adequate value of $t_{air,i}$. During nighttime, the decrease of $t_{air,o}$ and the absence of solar radiation entailed a reduction of $t_{air,i}$ that is around 23 °C without the use of evaporative cooling, as reported in Fig. 3b.

To assess the vertical variation of $t_{air,i}$ (due to the thermal stratification) in Fig. 4 the hourly differences $\Delta t_{air,i}$ between $t_{air,i}$ monitored by probes at different heights (1.5, 2 and 2.5 m) and the reference $t_{air,i}$ at the bench level (1 m) are displayed during July. From the graph it stands out that, when the solar radiation is not present, the vertical difference of temperature is at a minimum value (around 0 °C). During daytime, the differences between the various probes and the reference one are considerable. The highest probe (2.5 m) logged $t_{air,i}$ values that exceed 7 °C of difference if compared with the ones of the reference probe (cultivation bench level). The average difference between that probe and the reference one during daytime is 3.5 °C. The temperature differences between the probes at 2 and 1.5 m of height and the reference one are considerably lower, with average values during daytime of 1.8 and 1.5 °C. The maximum absolute difference does not exceed 4 °C in both of cases.

4 Conclusions

The results of a long-term monitoring campaign for the evaluation of the thermal environment inside a totally mechanically controlled greenhouse are presented. The results showed that the thermal environment of the analyzed greenhouse is not homogeneous, especially during the daytime when high values of solar radiation occur. The

analysis carried out on the acquired dataset showed a difference between maximum and minimum values of indoor air temperature of around 8 °C during daytime, both in terms of horizontal and vertical gradients. This temperature difference considerably decreases during nighttime lowering to less than 0.5 °C.

This work may represent the basis for the development of a new methodology aimed at profitably mapping the thermal uniformity in greenhouses by using a limited set of sensors, with the final aim of increasing the climate control efficiency and, thus, the production.

Acknowledgements Authors would like to thank ARPA Veneto for sharing the outdoor weather data used in this work.

References

- Ahmed, H. A., Al-Faraj, A. A., & Abdel-Ghany, A. M. (2016). Shading greenhouses to improve the microclimate, energy and water saving in hot regions: A review. *Scientia Horticulturae*. <https://doi.org/10.1016/j.scienta.2016.01.030>.
- ASHRAE. (2011). ASHRAE Handbook—HVAC Applications. In *ASHRAE*.
- Fabrizio, E. (2012). Energy reduction measures in agricultural greenhouses heating: Envelope, systems and solar energy collection. *Energy and Buildings*, 53, 57–63. <https://doi.org/10.1016/J.ENBUILD.2012.07.003>.
- García-Ruiz, R. A., López-Martínez, J., Blanco-Claraco, J. L., Pérez-Alonso, J., & Callejón-Ferre, Á. J. (2018). On air temperature distribution and ISO 7726-defined heterogeneity inside a typical greenhouse in Almería. *Computers and Electronics in Agriculture*, 151, 264–275. <https://doi.org/10.1016/J.COMPAG.2018.06.001>.
- Hellickson, M. A., & Walker, J. N. (1983). Ventilation of agricultural structures. *American Society of Agricultural Engineers*.
- Ma, D., Carpenter, N., Maki, H., Rehman, T. U., Tuinstra, M. R., & Jin, J. (2019). Greenhouse environment modeling and simulation for microclimate control. *Computers and Electronics in Agriculture*, 162, 134–142. <https://doi.org/10.1016/J.COMPAG.2019.04.013>.
- Zhou, N., Yu, Y., Yi, J., & Liu, R. (2017). A study on thermal calculation method for a plastic greenhouse with solar energy storage and heating. *Solar Energy*. <https://doi.org/10.1016/j.solener.2016.12.016>.
- Zorzeto, T. Q., & Leal, P. A. M. (2017). Wireless sensor network to map the meteorological variability in a greenhouse with evaporative cooling. *Acta Horticulturae*. <https://doi.org/10.17660/ActaHortic.2017.1154.28>.

Physical Properties of Cement Panels Reinforced with Lignocellulosic Materials



Patrícia Ferreira Ponciano Ferraz, Matheus da Rocha Coutinho Avelino, Victor Rezende Carvalho, Isabela Moreira Albano da Silva, André Luiz de Lima Domingos, Rafael Farinassi Mendes, Jaqueline de Oliveira Castro, Leonardo Conti and Giuseppe Rossi

Abstract This paper aims to compare the physical properties of panels made of lignocellulosic raw materials and cement. Density (D), water absorption (WA), and thickness swelling (TS) after 2 and 24 h of immersion in water were analyzed. These lignocellulosic materials were used to produce panels: sugarcane bagasse, eucalyptus, banana pseudostem, coconut shell, and coffee husk. Three panels of each material were produced and each sample was arranged with the following dimensions: 150 × 150 × 15 mm. Each sample was submerged in water for 2 and 24 h, and the WA and TS capacity was measured in both conditions. Coconut and banana pseudostem panels presented both the lowest D values and the highest values of WA after 2 h and 24 h of immersion. The coffee panel showed the maximum D value. About TS the eucalyptus panels presented the highest value. Sugarcane panels showed the lowest TS at 2 h according to the recommended standards related to TS for 2 h. TS resistance tends to decrease with the increase in D, so panels produced with smaller and thicker particles tend to be slenderer and to present higher resistance to perpendicular traction.

Keywords Cement composites · Density · Residues · Swelling in thickness · Water absorption

P. F. P. Ferraz (✉) · M. da R. C. Avelino · V. R. Carvalho · I. M. A. da Silva · A. L. de L. Domingos · R. F. Mendes · J. de O. Castro
Federal University of Lavras, Campus Universitário, PO Box 3037, Lavras, Minas Gerais 37200-000, Brazil
e-mail: patricia.ponciano@ufla.br

L. Conti · G. Rossi
Department of Agriculture, Food, Environment and Forestry (DAGRI), Università degli Studi di Firenze, Florence, Italy

© Springer Nature Switzerland AG 2020
A. Coppola et al. (eds.), *Innovative Biosystems Engineering for Sustainable Agriculture, Forestry and Food Production*, Lecture Notes in Civil Engineering 67,
https://doi.org/10.1007/978-3-030-39299-4_26

1 Introduction

With the increase of population density cause an increase in the development of industries and intensive methods of agriculture. These activities can be responsible for producing residues in extensive scale (Antoniolli et al. 2009).

The use of lignocellulosic material residues to produce cement composites is considered as a good option for new lignocellulosic cement formulations. According to Cesar et al. (2017), the basic principle of panel production is that most of lignocellulosic materials may be used for panel production. Besides, these panels produced with raw materials present the following advantages: good fire resistance, good thermal and acoustic insulation, good resistance to fungus and insects attack and they can be considered as good materials to work (Iwakiri and Prata 2008). Panels made of cement and lignocellulosic materials can be used in simple and complex constructions.

There are several residues with high potential for panel production. However, the majority of these materials do not have a specific application. Therefore, many researches still need to be done to analyze the potential of the use of these lignocellulosic materials in the building industry.

Among the studies for the qualification of lignocellulosic panels, the knowledge of the physical properties is crucial. However, one of the challenges for the production of cementitious composites reinforced with lignocellulosic materials is the reinforcement/matrix interaction.

Therefore, the kind of vegetal matter used in the reinforcement of panels influences the physical properties and durability of the panels made of cement and lignocellulosic materials. Thus, it is important to evaluate the effect of the use of different lignocellulosic materials in panels production and their properties (Teixeira et al. 2018). Based on water absorption (WA) and thickness swelling (TS), the use of these panels can be recommended under high or low humidity conditions (Freire et al. 2011). Based on the results obtained by Freire et al. (2011) for water absorption (WA) and thickness swelling (TS), the use of these panels can be recommended under high or low humidity conditions.

To transform residues generated by the agricultural industry and forestry sector into high quality panels is an interesting solution for solving raw material demand problem. Thus, this study aimed to compare the physical properties (density, water absorption and thickness swelling after 2 and 24 h of immersion in water) of panels produced with different lignocellulosic materials and cement.

2 Materials and Methods

The experiment was carried out on the Federal University of Lavras (UFLA), Lavras, Brazil. For the production of panels, the following lignocellulosic materials were used: sugarcane bagasse, eucalyptus, banana pseudostem, coconut shell and coffee

husk. Besides it was used high initial resistance Portland cement (CPV-ARI), as a mineral binder and calcium chloride (CaCl_2), used as an accelerator of the cement cure process.

The lignocellulosic materials were dried in stoves until 12% of humidity. After the drying process, the materials were processed in the hammer-mill to reduce the size of the material. The particulate materials were sieved through a set of two superposed sieves with 0.50 mm (top) and 0.42 mm (bottom) particle sizes for fine contents (lower than 0.42 mm) removal. The particles obtained between the sieves were used in the cementitious composites.

Five different kinds of lignocellulosic cement panels were produced. For each typology of the panel, a different lignocellulosic material residue was used: sugarcane bagasse, eucalyptus, banana pseudostem, coconut shell and coffee husk. Three repetitions for each kind of lignocellulosic material were made, totaling 15 panels (5 treatments and 3 repetitions). For the calculations of the components of each panel (lignocellulosic material, cement, water and CaCl_2), the methodology suggested by Souza (1994) was used to determine the equivalent mass of components. In the production of panels, the following parameters were applied: material and cement ratio, 1:2.75; water and cement ratio, 1:2.5; hydration water rate of 0.25; additive, 4% (based on cement mass); a percentage of losses, 6%. The calculations were performed for nominal panel density of 1.2 g/cm^3 .

In order to produce each panel, components were weighed and then mixed in a concrete mixer for eight minutes (Fig. 1a). The total mass of components for three panels equivalent to each treatment (at the same time) was mixed. After mixing, the mass of each panel was separated, weighed and randomly distributed in aluminium moulds of $480 \times 480 \times 150 \text{ mm}$. The moulding and stapling was carried out in a cold process for 24 h (Fig. 1b), and then panels were kept in a climatic room at a

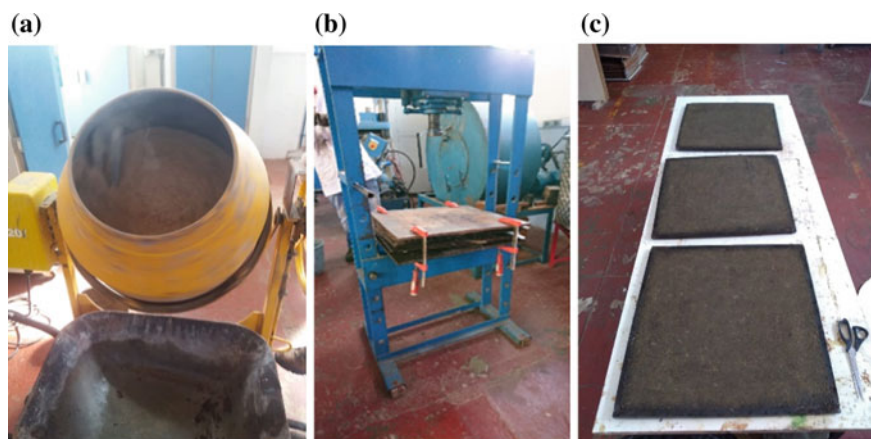


Fig. 1 Panel production: components mixed in a concrete mixer (a), cold stapling process (b), three panels kept in a climatic chamber at a temperature of $20 \pm 2 \text{ }^\circ\text{C}$ and $65 \pm 3\%$ relative humidity

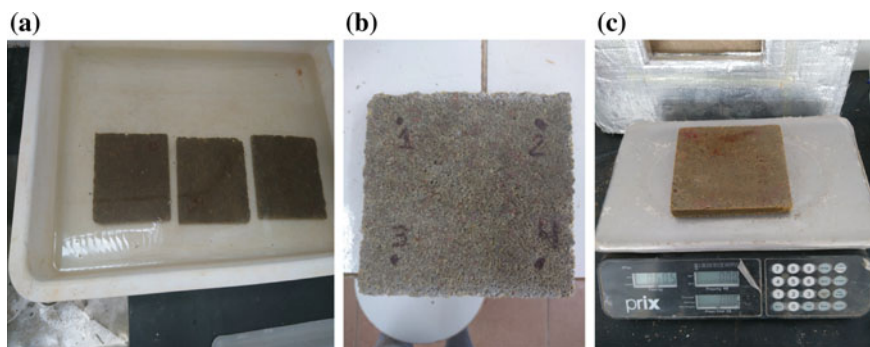


Fig. 2 Physical analysis: panel samples immersed in water (a), 4 points where the thickness measurements were done (b), panel weight measurement (c)

temperature of 20 ± 2 °C and $65 \pm 3\%$ relative humidity to ensure uniform drying for 28 days (Fig. 1c).

The following physical properties were evaluated: density of three samples (D), water absorption after immersion for 2 h (WA-2 h) and 24 h (WA-24 h) and thickness swelling after immersion for 2 h (TS-2 h) and 24 h (TS-24 h).

For the D, WA, and TS analyzes, it was necessary to cut the panels in samples with dimensions of 150×150 mm. Each lignocellulosic panel has 3 samples for each lignocellulosic material evaluated. All of these analyzes were developed based on the ASTM standard method (D1037-93, American Society for Testing and Materials—ASTM D1037 (2016) and Deutsches Institut für Normung—DIN (1982) standards.

Each sample was soaked in water for 2 and 24 h (Fig. 2a). To measure the thickness of each panel it was used a calliper in 4 points in each sample (Fig. 2b). The thickness and the weight (Fig. 2c) of each panel were measured before and immediately after soaking. The dimensional size and weight measured before and after soaking were used to calculate D, TS and WA.

D (g cm^{-3}) was calculated by the relationship between the panel mass (g) and the panel size (cm^3). The WA (%) was obtained by the difference between the panel mass (g) after immersion (2 or 24 h) and the mass (g) before de immersion. And the TS was obtained by the difference between the dimension (mm) of the panels after and before the immersion in water for 2 and 24 h.

3 Results and Discussion

Figure 3a shows different values of density and standard deviation of the lignocellulosic panels. There was a significant variation in the densities of the lignocellulosic panels. Coconut shell and banana pseudostem panels presented the smaller density with an average value of 0.984 g/cm^3 and 1.0032 g/cm^3 , respectively. Coffee husk panels presented the most significant density in comparison with the other panels

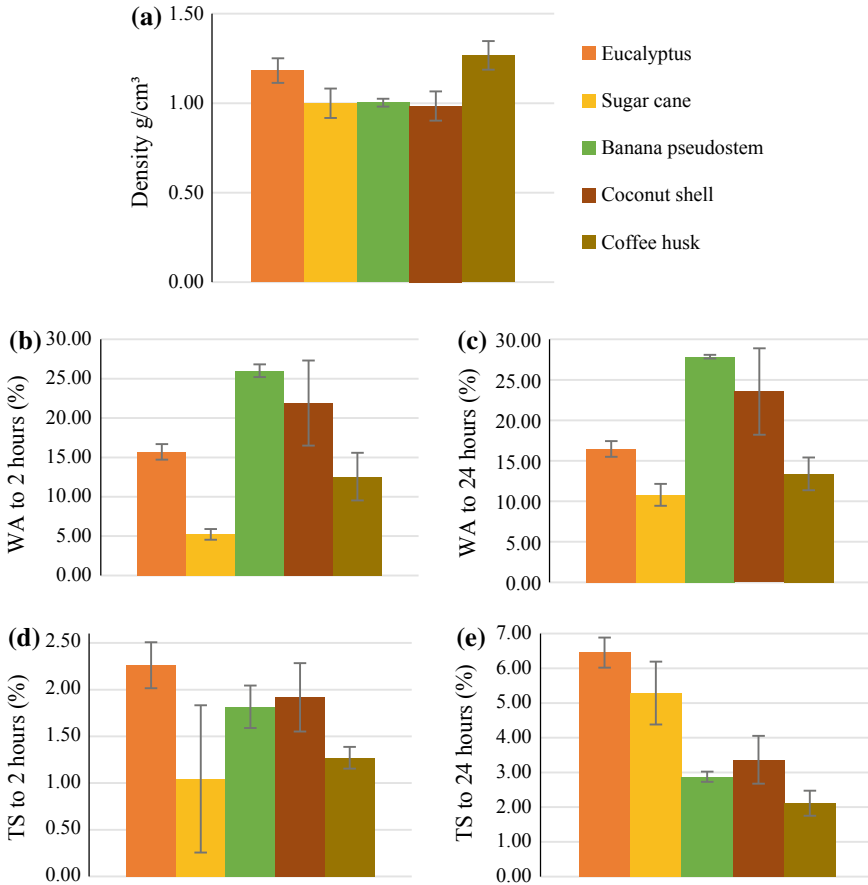


Fig. 3 Physical properties and standard deviation: **a** Density (g/cm³), **b** water absorption to 2 h (%), **c** water absorption to 24 h (%), **d** thickness swelling to 2 h (%), **e** thickness swelling to 24 h (%) of the panels made with sugar cane, eucalyptus, banana pseudostem, coconut shell and coffee husk

with an average value of 1.267 g/cm³. These results may affect the WA and TS of panels.

According to Iwakiri et al. (2005), when the panel presents a higher density, higher is the pressure required for the water to be absorbed. It means that in case of high density, it is more difficult for the panel to absorb the water. The highest values of density were found in coffee husk panels (1.267 g/cm³), and sugarcane panels (1.172 g/cm³) and these panels presented the lowest values of WA-2 h (Fig. 3b) with averages of 14.48% and 5.51%, respectively. Besides, bananas and coconut shell's panels presented the lowest density values, the highest WA-2 h (Fig. 3b) and WA-24 h (Fig. 3c) values. The same behaviour of WA can be observed after 24 h of immersion (Fig. 3c): coffee husk and sugarcane panels presented the lowest values,

15.52% and 12.14%, respectively. According to Maloney (1993), panels with more closed structure, resulting in higher densification of the particles during the pressing process, and it may have lower values of WA.

Concerning TS after 2 h and 24 h or immersion (Fig. 3d, e, respectively), the eucalyptus panels had the highest TS (2.3% and 2.1%, respectively). The sugarcane panels had the lowest TS-2 h (1.0%), and coffee (2.1%) had the lowest TS-24 h. According to Bison Wood-Cement Board (2017), panels should have TS-2 h values smaller than 1% and TS-24 h smaller than 1.5%. Standard EN 634-2 (2007) establishes that commercial cement—wood panels must present a maximum of 1.5% TS-24 h. Among tested panel, only sugarcane presented TS-2 h following the standard. All other materials showed upper results for TS-2 h and TS-24 h.

Beyond the banana pseudostem, coconut shell panels had absorbed the most significant amount of water, and they did not present the biggest values of TS. This can be explained because different lignocellulosic materials present different chemical and anatomic properties which will affect their WA and TS (Cesar et al. 2017). Besides the resistance of ST tends to decrease with the increase in density. Panels produced with smaller and thicker particles tend to be slenderer and possess higher resistance to perpendicular stress tension (Iwakiri et al. 2005).

Improvements in the production process of panels could be carried out reducing the WA and TS values, pre-treating the agricultural residues of particles for the degradation of hemicelluloses, reducing the number of hygroscopic sites (Li et al. 2011) and applying coating materials as a physical barrier to panel penetration (NEMLI 2008).

4 Conclusion

Panels with lignocellulose residues of banana pseudostem and coconut shells panels showed both the highest density values and the highest water absorption after 2 and 24 h of immersion.

Besides, sugarcane panels and coffee husk panels showed more compactness in the structural arrangement and consequently smaller ranges of water absorption after 2 and 24 h of immersion.

The eucalyptus panels presented high density and high thickness swelling after 2 and 24 h of immersion.

Only sugarcane panels presented thickness swelling after 2 in accordance following the standards recommended.

More studies need to be conducted to improve the quality of panels made of agriculture and forestry residues by treating particles and covering panels with finishing products.

Acknowledgements The authors thank, the Foundation for Research of the State of Minas Gerais (FAPEMIG) to funding this research.

References

- American Society for Testing and Material. ASTM D-1037-12. (2016). *Standard Test Methods for Evaluating Properties of Wood-Base Fiber and Particle Panel Materials*. West Conshohocken, PA: ASTM International.
- Antoniolli, Z. I., Steffen, G. P. K., & Steffen, R. B. (2009). Rice husk and cattle manure used as substrate for the *Eisenia fetida* Savigny (1826) multiplication. *Ciência e Agrotecnologia*, 33(3), 824–830.
- Bison Wood-Cement Board. (2017). Technical hand book. Bison Report. Berlin, p. 1–36.
- César, A. A. D. S., Bufalino, L., Mendes, L. M., Mesquita, R. G. D. A., Protásio, T. D. P., Mendes, R. F., et al. (2017). Transforming rice husk into a high-added value product: Potential for particleboard production. *Ciência Florestal*, 27(1), 303–313.
- Deutsches Institut für Normung. (1982). Testing of wood chipboards, bending test, determination of bending strength: DIN 52362. Berlin, 40 p.
- European Committee for Standardization. EN 634–2. (2007). Particleboard specifications. Bruxelas, 22 p.
- Freire, C. S., Silva, D. W., Scatolino, M. V., da Silva César, A. A., Bufalino, L., & Mendes, L. M. (2011). Propriedades físicas de painéis aglomerados comerciais confeccionados com bagaço de cana e madeira. *Floresta e Ambiente*, 18(2), 178–185.
- Iwakiri, S. (2005). Painéis de Madeira Reconstituída. Ajir Gráfica e Editora Ltda. 254 pp. FUFEP. Curitiba.
- Iwariki, S., & Prata, J. G. (2008). Utilização da madeira de *Eucalyptus grandis* e *Eucalyptus dunnii* na produção de painéis cimento-madeira. *Cerne, Lavras*, 14(1), 68–74.
- Li, X., Cai, Z., Winandy, J. E., & Basta, A. H. (2011). Effect of oxalic acid and steam pretreatment on the primary properties of UF-bonded rice straw panels. *Industrial Crops and Products*, 33, 665–669. <https://doi.org/10.1016/j.indcrop.2011.01.004>.
- Maloney, T. M. (1993). *Modern particleboard and dry-process fiberboard manufacturing* (p. 689). San Francisco: Miller Freeman Publication.
- Nemli, G. (2008). Factors affecting some quality properties of the decorative surface overlays. *Journal of Materials Processing Technology*, 95(1), 218–223. <https://doi.org/10.1016/j.jmatprotec.2007.05.001>.
- Souza, M. R. (1994). Durability of cement-bonded particle board made conventionally and carbon dioxide injection. These (Doctor of Philosophy)—University of Idaho, Idaho, 123p.
- Teixeira, J. N., Silva, D. W., Vilela, A. P., Junior, H. S., de Siqueira Brandão, L. E. V., and Mendes, R. F. (2018). Lignocellulosic Materials for Fiber Cement Production. *Waste and Biomass Valorization*, 1–8.

Physical Properties of Miscanthus Grass and Wheat Straw as Bedding Materials for Dairy Cattle



Patrícia Ferreira Ponciano Ferraz, Giuseppe Rossi, Leonardo Conti, Gabriel Araújo e Silva Ferraz, Lorenzo Leso and Matteo Barbari

Abstract Housing system can affect dairy cow's welfare and performance and the type of bedding material used can also affect comfort and hygiene level of the animals. A wide range of different materials can be used in bedding for dairy cattle, but their physical proprieties must be analyzed to evaluate their potential. Therefore, this study aimed to investigate the physical properties of Miscanthus grass in comparison to wheat straw, as an affordable alternative being used as bedding material in housing systems for dairy cows. Particle size, bulk density, air-filled porosity and water holding capacity from Miscanthus and wheat straw were measured experimentally in the lab of the DAGRI of the University of Florence. The particle size was determined by applying 50 g of material on six meshes. Bulk density was determined according to the ASABE Standard S269.4 DEC 91. To determine the water holding capacity and air filled porosity of bedding materials samples the Australian Standards AS 3743-2003 were used. The analysis showed that since Miscanthus presented 88% of the particle size bigger than 50 mm, it also presented higher value of water holding capacity (0.072 kg L^{-1}) in comparison with wheat straw (0.057 kg L^{-1}). Miscanthus presented higher bulk density (26 kg m^{-3}) than wheat straw (18 kg m^{-3}). Both materials presented similar air-filled porosity, around 88%. Based on these physical properties results, it was possible to demonstrate the good potential to use Miscanthus as a viable alternative to wheat straw as a bedding material for dairy cattle.

Keywords Bulk density · Dairy cows · Air filled porosity · Water holding capacity

P. F. P. Ferraz (✉) · G. A. e S. Ferraz
Departament of Agricultural Engineering (DEA), Federal University of Lavras,
Lavras, Brazil
e-mail: patricia.ponciano@ufla.br

G. Rossi · L. Conti · L. Leso · M. Barbari
Department of Agriculture, Food, Environment and Forestry (DAGRI),
Università degli Studi di Firenze, Florence, Italy

© Springer Nature Switzerland AG 2020
A. Coppola et al. (eds.), *Innovative Biosystems Engineering for Sustainable Agriculture, Forestry and Food Production*, Lecture Notes in Civil Engineering 67,
https://doi.org/10.1007/978-3-030-39299-4_27

1 Introduction

The primary function of the bedding is to provide thermal comfort and softness for the animals. It must be durable and give sufficient friction to allow rising and lying down without slipping (Van Gastelen et al. 2011). Bedding plays a crucial role in the comfort of the lying surface because cows spend more time lying down when stalls are soft and dry (Wolfe et al. 2018). Bedding material should help in keeping cows clean and healthy while minimizing daily labour requirements (Chaplin et al. 2000).

Traditionally dairy cows are bedded on straw. However, other bedding materials may perform better than straw concerning to comfort and hygiene level of the animals. Alternative materials have become attractive alternative sources as they can be obtained locally and cheaply (Kheravii et al. 2017). Some examples of alternative bedding materials used are: wood shavings, wood chips, sawdust, flax straw, spelt husks, rice hulls. According to Rauscher et al. (2016), who developed researches with alternative bedding materials for horses, *Miscanthus* grass has recently become of interest as bedding material for two reasons. First, that *Miscanthus* may cause less allergic reactions than wheat straw. Secondly, less material and time for mucking out is required. Nevertheless, to affirm that an alternative material can be used as a good bedding material, its physical proprieties must be analyzed to evaluate their potential.

Some of the keys physical parameters that contribute to the evaluation of the bedding material are bulk density (BD), air-filled porosity (AFP), particle size (PS) and water holding capacity (WHC). BD is defined as the ratio of the total weight (mass) of compost to its volume and expressed as kilograms per cubic meter (kg m^{-3}). This information is important in order to quantify volumes of products with irregular shapes. Distribution of air within the compost mix is a significant factor that can be maintained by AFP (Jain et al. 2018). The PS influences the material mass and the resistance to compaction. WHC is important because it is related to the amount of water in bedding, so affecting microbial activity, thermal insulation, gases emissions, odour emissions and friability.

Therefore, this study aimed to investigate the physical properties of *Miscanthus* grass in comparison to wheat straw, as an affordable alternative to being used as bedding material in housing systems for dairy cows.

2 Materials and Methods

The experiment was carried out in a laboratory of the Department of Agriculture, Food, Environment and Forestry (DAGRI) of the University of Florence. It was used *Miscanthus* grass and wheat straw (Fig. 1) as materials for the experimental analyses. The physical analyses were: the particle size, bulk density, water holding capacity and porosity.



Fig. 1 Experimental materials **a** Miscanthus grass and **b** wheat straw

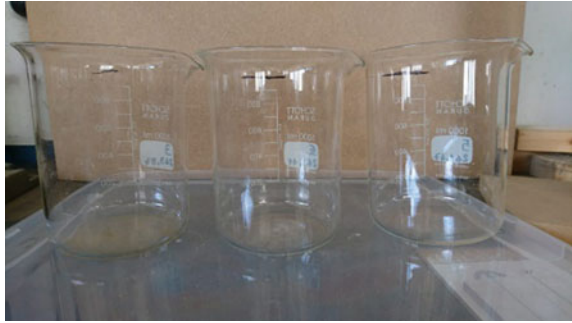
PS was determined following the methodology proposed by Jobim et al. (2007). An amount of 50 g of material (Miscanthus grass and wheat straw) was applied on a set of six meshes (50, 16, 8, 4, 2 mm, 0.425 mm) (Fig. 2) shaken 5 times in each 90° for 2 times, so the material was shaken for 40 times. After shaker, each mesh with the remaining material was weighed, and the percentage of particle size was calculated.

BD of the materials was determined according to the ASAE Standard S269.4 DEC 91 (ASABE Standards 2007). Three cylindrical glassed containers (Fig. 3) each with a specific inside diameter were used for determination of BD. The material was poured into the container from a certain height to facilitate the free flowing of the samples until the container was overflowed. The excess material was removed by striking a straight edge across the top. The weight of the material with the container was recorded. The net weight of the sample was obtained by subtracting the weight of the empty container. BD (Kg m^{-3}) was calculated by Eq. 1.



Fig. 2 Set of meshes used in the experiment

Fig. 3 Containers used to measure bulk density



$$BD = \frac{M}{V} \quad (1)$$

where:

M is the tested bedding material mass (Kg)

V is the container volume (m³).

AS 3743-2003 (appendix B method) (Standards Australia 2003) was used to determine the WHC and AFP of materials samples. Dunlop et al. (2015) described the used apparatus and methodology adopted (Fig. 4). According to them, the apparatus was realized comprising two pieces of PVC tube (internal diameter 8.7 cm, length 12.0 cm), one capped on the bottom with four holes and the second adapted so it could fit snugly over the top of the first piece (bottom tube and top tube, respectively). The volume of the bottom tube was calibrated by filling the tube with water and gravimetrically determining the volume of water added.

Each material was poured into the top of the tube (both pieces joined together at this stage) until the top section was at least half full. The apparatus was soaked three times in a container of water so that the entire litter sample was completely submerged. The top section of the tube and excess material was carefully removed and the surface of material levelled in the bottom tube. This was then lowered into the water until the water was levelled with the top surface of the material and tube. The holes were blocked as the apparatus was removed from the water. Water was



Fig. 4 Water holding capacity and porosity measurements apparatus

drained for up to 60 min into a pre-weighed container. The entire saturated sample was then poured into a pre-weighed sample dish and dried at 65 °C until it reached a stable weight. WHC (Kg L^{-1}) was calculated using Eq. 2:

$$\text{WHC} = (M_w - M_d) / V_b \quad (2)$$

where:

M_w is the mass of the saturated material in the bottom tube (kg)

M_d is the oven dry mass of the material in the bottom tube (kg)

V_b is the volume of the bottom tube (L)

AFP (%) can be calculated according to Eq. 3:

$$\text{AFP} = V_{\text{drained}} / V_b \times 100 \quad (3)$$

where:

V_{drained} is the volume of water drained from the mix (L)

V_b is the volume of the sample (the volume of the bottom tube) (L).

3 Results and Discussion

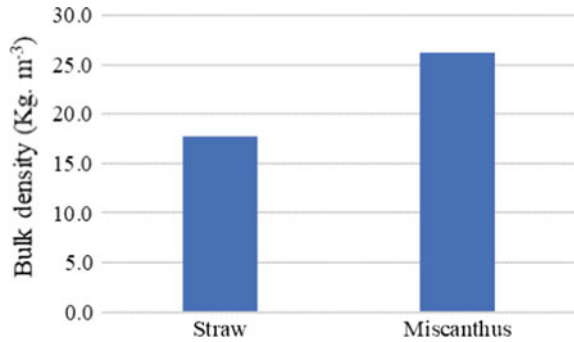
The proportion of each size of the particle can be observed in Table 1. Miscanthus grass presented a higher proportion of big particles, while wheat straw presented more distributed particles. According to Nakasaki et al. (1986), materials with a higher proportion of smallest particles should be more interesting for compost materials because the microorganisms grow primarily on particle surfaces. However, according to Agnew and Leonard (2003), if the material is too finely divided, it is likely to be easily compacted to the point where pore space becomes inadequate to allow sufficient movement of oxygen through the material and to maintain aerobic conditions around the particles.

For bedding materials, small particles could also be a problem. According to Samadi et al. (2012), bedding is known to have a significant impact on dust concentration in dairy barns. Breum et al. (1999) pointed out that straw and sawdust are the most commonly used types of bedding, and they can be very dusty. It is possible

Table 1 Particle size distribution (%) of wheat straw and Miscanthus grass

	>50(mm)	50–16 (mm)	16–8 (mm)	8–4 (mm)	4–2 (mm)	2–0.425 (mm)	<0.425 (mm)
Wheat straw	44.5	5.5	17.0	19.4	9.8	3.8	0.0
Miscanthus	88.3	3.3	2.6	3.5	1.8	0.4	0.1

Fig. 5 Bulk density of wheat straw and Miscanthus grass



to see in Table 1 that wheat straw presented 3.8% of particles with sizes between 2–0.425 while Miscanthus grass presented only 0.4 and 0.1% smaller than 0.425 mm.

BD is an important information in order to quantify volumes of products with irregular shapes. Besides, BD determines how much material can be placed at a specific site. In this study Miscanthus presented higher BD than wheat straw (Fig. 5), what means that in a volume of 1 m³ of Miscanthus this material has a mass of around 26 kg and in the same volume of wheat straw has the mass of around 18 kg. This property is important because the BD of compost is often used for design and haulage calculations as well as determining power requirements for operations such as turning and mixing (Agnew and Leonard 2003). Costs associated with transportation and storage would be lower for a denser material (Ward et al. 2000). On the other hand, higher values of BD imply an increase in mass and a decrease of porosity and air volume (Agnew and Leonard 2003).

The WHC depends on the size and distribution of both particles and pores. Since Miscanthus presented 88% of the PS bigger than 50 mm, it also presented a higher value of WHC values in comparison with wheat straw (Fig. 6). According to Agnew and Leonard (2003), these factors also influence the amount of air that can be held

Fig. 6 Water holding capacity of wheat straw and Miscanthus grass

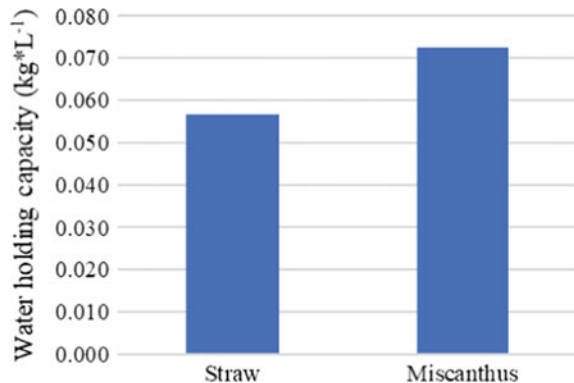
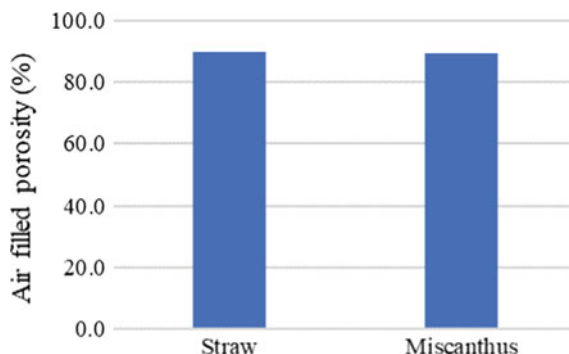


Fig. 7 Air-filled porosity of wheat straw and Miscanthus grass



in the compost and, therefore, have a direct bearing on the ability to sustain aerobic decomposition.

De Boodt and Verdonck (1972) defines AFP as a volume of air present in a drained material sample after its saturation. The wheat straw presented a value of 89.85% of AFP while Miscanthus presented a value of 89.29%, so they are very similar to this property (Fig. 7).

Therefore, based on these results, Miscanthus grass appears as a good material to be used for bedding material in comparison with the most used material (straw). Moreover, Van Weyenberg et al. (2015) stated that Miscanthus presents a low input and high yield also it can be cultivated on swampy land with a low value for crop production or livestock as well.

4 Conclusions

Miscanthus grass presented the biggest values of the following parameters: particle size, bulk density and water holding capacity. Wheat straw and Miscanthus grass had a similar behaviour related to porosity. Therefore, it is concluded that, due to the physics proprieties, Miscanthus could be applied as a bedding material for dairy cows.

Acknowledgements This research was funded by the EU program ERA-NET SUSAN and was developed within the project “FreeWalk”. The authors would like to thank Università degli Studi de Firenze (UNIFI) and Federal University of Lavras (UFLA).

References

Agnew, J. M., & Leonard, J. J. (2003). The physical properties of compost. *Compost Science & Utilization*, 11(3), 238–264.

- Breum, N. O., Nielsen, B.H., Lyngbye, M., Midtgard, U. (1999). Dustiness of chopped straw as affected by lignosulfonate as a dust suppressant. *Annales of Agriculture and Environmental Medicine*, 6(2), 133–140.
- Chaplin, S. J., Tierney, G., Stockwell, C., Logue, D. N., & Kelly, M. (2000). An evaluation of mattresses and mats in two dairy units. *Applied Animal Behaviour Science*, 66(4), 263–272.
- De Boodt, M., & Verdonck, O. (1972). The physical properties of the substrates in horticulture. *Acta Horticulturae*, 26, 37–44.
- Dunlop, M. W., Blackall, P. J., & Stuetz, R. M. (2015). Water addition, evaporation and water holding capacity of poultry litter. *Science of the Total Environment*, 538, 979–985.
- Jain, M. S., Daga, M., & Kalamdhad, A. S. (2018). Physical parameters evaluation during production of soil conditioner from aquatic waste: *Hydrilla verticillata* (Lf) Royle. *Environmental Technology & Innovation*, 11, 64–73.
- Jobim, C. C., Nussio, L. G., Reis, R. A., & Schmidt, P. (2007). Avanços metodológicos na avaliação da qualidade da forragem conservada. *Revista Brasileira de Zootecnia*, 101–119.
- Kheravii, S. K., Swick, R. A., Choct, M., & Wu, S. B. (2017). Potential of pelleted wheat straw as an alternative bedding material for broilers. *Poultry Science*, 96(6), 1641–1647.
- Nakasaki, K., Shoda, M., & Kubota, H. (1986). Effects of a bulking agent on the reaction rate of thermophilic sewage sludge composting. *Journal Fermentation Technology*, 64(6), 539–544.
- Rauscher, B., & Lewandowski, I. (2016). *Miscanthus* horse bedding compares well to alternatives. In S. Barth, D. Murphy-Bokern, O. Kalinina, G. Taylor, & M. Jones (Eds.), *Perennial biomass crops for a resource-constrained world*. Cham: Springer.
- Samadi, S., van Eerdenburg, F. J. C. M., Jamshidifard, A. R., Otten, G. P., Droppert, M., Heederik, D. J. J., et al. (2012). The influence of bedding materials on bio-aerosol exposure in dairy barns. *Journal of Exposure Science & Environmental Epidemiology*, 22, 361–368.
- Standards Australia. (2003). Potting Mixes (AS 3743–2003). Australian/New Zealand Standards (Standards Australia/Standards New Zealand, Sydney).
- Van Gastelen, S., Westerlaan, B., Houwers, D. J., & Van Eerdenburg, F. J. C. M. (2011). A study on cow comfort and risk for lameness and mastitis in relation to different types of bedding materials. *Journal of Dairy Science*, 94(10), 4878–4888.
- Van Weyenberg, S., Ulens, T., De Reu, K., Zwervaegher, I., Demeyer, P., & Pluym, L. (2015). Feasibility of *Miscanthus* as alternative bedding for dairy cows. *Veterinari Medicina*, 60(3).
- Ward, P. L., Wohlt, J. E., Zajac, P. K., & Cooper, K. R. (2000). Chemical and physical properties of processed newspaper compared to wheat straw and wood shavings as animal bedding. *Journal of Dairy Science*, 83(2), 359–367.
- Wolfe, T., Vasseur, E., DeVries, T. J., & Bergeron, R. (2018). Effects of alternative deep bedding options on dairy cow preference, lying behavior, cleanliness, and teat end contamination. *Journal of Dairy Science*, 101(1), 530–536.

Innovative Tensile Structures for Protected Crop Facilities



Silvana Fuina, Giacomo Scarascia-Mugnozza and Sergio Castellano

Abstract Greenhouse structures are complex buildings that must meet different needs, such as the microclimate control inside the greenhouse, the strength of structural elements, as well as the radiometric and mechanical features of roofing materials. The covering system must allow the transmission of solar radiation for crop needs and guarantee resistance performances in relation to external actions, such as wind and snow loads. Starting from the main characteristics of agricultural commercial greenhouses and tensile structures, the proposal concerns with an innovative tensile supporting structure designed for the covering of protected crop facilities. The innovative tensile structural configuration was first studied by means of the selection of the construction materials and the cross sections of the structural components and afterward calculated using the structural analysis software SOFISTIK. The load analysis on the structure was carried out in accordance with the European standards UNI-EN 13031-1: 2004 and the Italian Technical Construction Code of 2018 related to the Eurocodes. The main results concern the comparison with the current structural types of commercial greenhouses: analysis of the steel weight of the structure and improvement of the structural response to external actions of the innovative tensile structure.

Keywords Greenhouse structures · Load analysis · Structural behaviour

S. Fuina (✉) · G. Scarascia-Mugnozza
Department of Agricultural and Environmental Science (DISAAT), University of Bari, Via
Amendola 165/A, 70126 Bari, Italy
e-mail: silvana.fuina@uniba.it; fuina.silv@gmail.com

S. Castellano
Department of Science of Agriculture, Food and Environment (SAFE), University of Foggia, Via
Napoli 25, 71100 Foggia, Italy

© Springer Nature Switzerland AG 2020
A. Coppola et al. (eds.), *Innovative Biosystems Engineering for Sustainable Agriculture, Forestry and Food Production*, Lecture Notes in Civil Engineering 67,
https://doi.org/10.1007/978-3-030-39299-4_28

1 Introduction

Agricultural engineering, with its innovations, contributes to crop productivity by evolving the state of the art in protected cultivation systems. Factors affecting innovation in the sector include labour availability, energy costs, transport logistics, but also factors that arise from regional issues such as environmental impact, product safety and consumer demand. These are sector instances that have the effect of modifying the long-term production system (Giacomelli et al. 2012). In the world scenario the total production area in greenhouses is estimated at around 3,000,000 hectares (Kacira et al. 2016).

In the design of a controlled environment system, such as a greenhouse, structural design, covering systems, environmental control, sustainability and the cultivation system are equally important (Jensen 2002; Scarascia-Mugnozza 2003; Castellano et al. 2005; Russo and Scarascia-Mugnozza 2005; Fuina et al. 2019).

There are researches on technologies for crops in a protected environment that mainly concern the control of the microclimate, the covering materials (Fuina et al. 2016) and the structures (Cepeda et al. 2013; Waaijbergen 2004; Castellano et al. 2006; Castellano and Scarascia-Mugnozza, 1999).

From the construction point of view today the following structural types are used:

- glass or rigid plastic greenhouses are generally built as duo-pitched model or the Venlo type model;
- greenhouses covered in plastic film are generally built as arched shape structure.

This study proposes an innovative and alternative structural typology for greenhouses: a tensile structure that falls within the definition of tensegrity structures, constructions formed by cables and struts. The aim is to study the behaviour of this structural system because it allows large spans and saving of structural material and is characterized by low percentages of shading of the supporting elements.

Inspired by the construction principles of tensile structures already used in other engineering buildings such as sports arenas, airports and shopping centers (Gosling et al. 2013), we designed a greenhouse facility for protected crops.

2 Materials and Methods

2.1 Calculation Methods

The proposed structural module has been modelled using a finite element calculation program, SOFISTIK 2014, program used in previous researches on the structural behaviour of membrane structures and lightweight structures (Gosling et al. 2013; Rank et al. 2005). The finite element method (FEM) used, in the ASE analysis module of the program, is a displacement method, i.e. the unknowns are the displacements values in several selected points, the so-called nodes. The calculation of the

mechanical behaviour is based on an energetic principle minimizing the deformation energy.

In this method a configuration of n points ordered in a dimensional space is denoted as follows:

$$p = [p_1, p_2, \dots, p_n]^T \tag{1}$$

A tensegrity structure $G(p)$ is the graph on p where each edge is a cable or a strut. The cables cannot increase their length and the struts cannot decrease. A state of stress ω for $G(p)$ is a state of self-stress if the following condition is satisfied for each node i :

$$\sum_j \omega_{ij}(p_j - p_i) = 0 \tag{2}$$

where ω_{ij} is positive for cables and negative for struts.

Satisfying this equilibrium equation is necessary but not sufficient for the tensegrity structure to be in a stable equilibrium configuration. The total functional potential energy should be at a local minimum for a given stable configuration. We define the following “energetic” form associated with the stress state ω :

$$E(p) = \frac{1}{2} \sum_{ij} \omega_{ij} \|p_j - p_i\|^2 \tag{3}$$

The result is a so-called stiffness matrix. This matrix specifies the reaction forces on the nodes of an element when they are subject to known displacements. The balance of the global force is generated on the node in order to determine the unknowns.

Nonlinear effects can only be analysed with iterations. This is done in the program with the Newton method, modified with a constant stiffness matrix. This method detects the residual forces that develop during iterations and calculates the coefficients for the increments of displacement between the current configuration and the previous step.

The loads acting on the structure (Robertson et al. 2002; Scarascia-Mugnozza et al. 2017) were determined in accordance with the UNI EN standards, by the UNI 13031-1: 2004 standard: “Greenhouse: design and construction. Part 1: greenhouses for commercial production”.

2.2 Model Features

Taking into consideration the structural advantages of tensegral constructions, we set ourselves the goal of designing a “tensile” greenhouse, according to the principles of material savings, reduction of shading due to structural elements, large spans and, therefore, optimization of the functionality and performance of the structure. It was

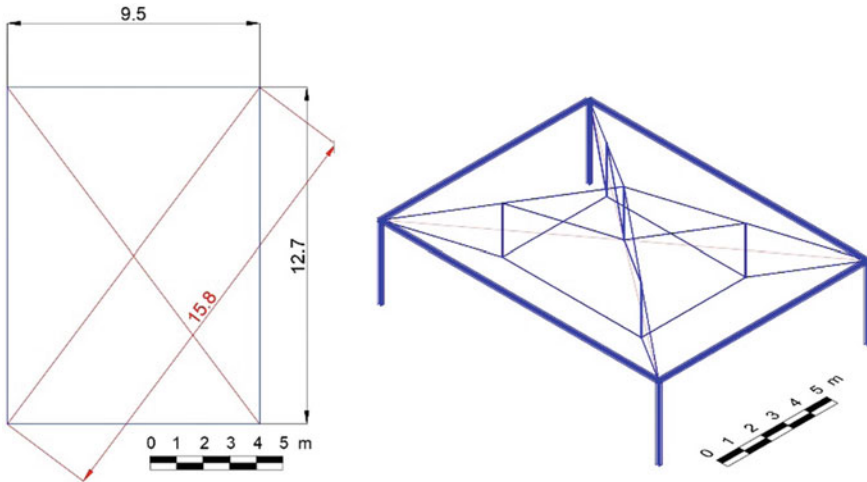


Fig. 1 Axonometric view and plan of the proposed model for the tensile-greenhouse

designed a construction module for greenhouse with the following characteristics (Fig. 1). Basing on the dimensions of the most common structures for commercial greenhouses, the proposed model has the following characteristics: rectangular plan with dimensions 12.7×9.5 m and covered surface 120 m^2 , with a gutter height equal to 3.5 m and a ridge height of 5.4 m, inclination of the roof flap relative to the horizontal of 15° . The proposed elementary element can be repeated n times to cover surfaces adapted to the production needs of the modern greenhouses settlements.

Rope cables are made of AISI 316 133 stainless steel wire with a diameter of 12 mm.

The bars are in AISI 316 hollow circular section steel, external diameter 44.5 mm thickness 2.9 mm.

The lower frame of the structure, pillars and beams, are in S355 steel with HEA 120 profiles.

3 Results

The greater displacements on the leeward side at the gutter height of the project proposal were analysed and compared with a duo-pitched greenhouse and with an arched shape greenhouse designed having the same covered area and gutter height dimensions (Fig. 2).

The results of the simulations (Tables 1 and 2) show the displacements in millimetres of the selected nodes, in the ULS and SLS combination of load a1, defined by the UNI EN 13031 standard.

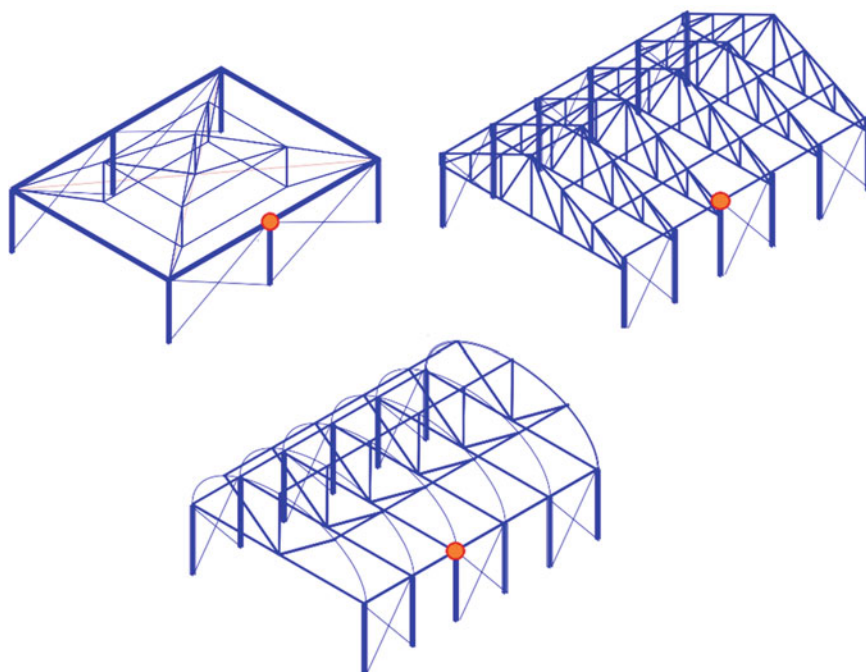


Fig. 2 Selected nodes for the displacements analysis

Table 1 Displacement in the direction of the wind at the height of the gutter of the different greenhouses in a1 ULS combination

Combination	Tunnel	Duo-pitched	Tensile
a1 ULS	63.3 mm	6.8 mm	46.9 mm

Table 2 Displacement in the direction of the wind at the height of the gutter of the different greenhouses in a1 SLS combination

Combination	Tunnel	Duo-pitched	Tensile
a1 SLS	52.8 mm	5.7 mm	39.1 mm

The nodal displacements are asymmetrical due to the non-symmetrical actions of wind and snow. The order of magnitude of the displacements of the tensile greenhouse is not compatible with the project of a glass greenhouse, but rather it is compatible with the displacements of a structure covered by a flexible material (i.e. plastic film).

4 Conclusion

The aim of this work is the design of an innovative technological typology for greenhouse roofing structures, ideal for the characteristics and functions that must have structures for protected crops. The designed covering structure has the important advantage of a better structural behaviour with regards to external actions that will act on the construction. Future research will focus on improving the structural model of the software and optimizing the structural configuration and sections of the components of the roof.

Acknowledgements The study, the data processing and the editorial work must be shared equivalently among the Authors within the areas of their expertise.

References

- Castellano, S., Candura, A., & Scarascia Mugnozza, G. (2005). Greenhouse structures SLS analysis: Experimental results and normative aspects. *Acta Horticulturae*, 691(2), 701–708.
- Castellano, S., Scarascia Mugnozza, G., & Vox, G. (2006). Prova a rottura di una struttura portante per serra a navata. *Culture Protette*, 35(1), 55–61.
- Castellano, S., & Scarascia Mugnozza, G. (1999). Analisi e progetto agli stati limite delle strutture portanti per serre alla luce dei nuovi standard europei. Atti del *Seminario AIIA “Le colture protette: aspetti agronomici, territoriali e tecnico-costruttivi”*, Ragusa, 24–26 Giugno, pp. 121–135.
- Cepeda, P., Ponce, P., Molina, A., & Lugo, E. (2013). Towards sustainability of protected agriculture: Automatic control and structural technologies integration of an intelligent greenhouse. *IFAC Proceedings Volumes*, 46(7), 366–371.
- Fuina, S., Marano, G. C., Puglisi, G., De Tommasi, D., & Scarascia-Mugnozza, G. (2016). Thermo-mechanical response of rigid plastic laminates for greenhouse covering. *Journal of Agricultural Engineering*, 47(3), 157–163.
- Fuina, S., Marano, G. C., & Scarascia-Mugnozza, G. (2019). Polycarbonate laminates thermo-mechanical behaviour under different operating temperatures. *Polymer Testing*, 76, 344–349.
- Giacomelli, G. A., Sase, S., Cramer, R., Hoogetboom, J., MacKenzie, A., Parbst, K., et al. (2012). Greenhouse production systems for people. *Acta Horticulturae*, 927, 23–38.
- Gosling, P. D., Bridgens, B. N., Albrecht, A., Alpermann, H., Angeleri, A., Barnes, M., et al. (2013). Analysis and design of membrane structures: Results of a round robin exercise. *Engineering Structures*, 48, 313–328.
- Jensen, M. H. (2002). Controlled environment agriculture in deserts, tropics and temperate regions—a world review. *Acta Horticulturae*, 578, 19–25.
- Kacira, M., Jensen, M., Robie, T., Tollefson, S., & Giacomelli, G. (2016). Use resources wisely: Waste management and organic liquid fertilizer use in greenhouse production system. In *III International Symposium on Organic Greenhouse Horticulture* 1164 (pp. 541–548).
- Rank, E., Halfmann, A., Scholz, D., Glück, M., Breuer, M., Durst, F., et al. (2005). Wind loads on lightweight structures: Numerical simulation and wind tunnel tests. *GAMM-Mitteilungen*, 28(1), 73–89.
- Robertson, A., Roux, P., Gratraud, J., Scarascia-Mugnozza, G., Castellano, S., Dufresne de Virel, M., et al. (2002). Wind pressures on permeably and impermeably-clad structures. *Journal of Wind Engineering and Industrial Aerodynamics*, 90, 461–474.
- Russo, G., & Scarascia Mugnozza, G. (2005). LCA methodology applied to various typology of greenhouses. *Acta Horticulturae*, 691(2), 837–843.

- Scarascia Mugnozza, G. (2003). Strutture e tipologie nuove negli impianti serraicoli. *Colture protette*, 32(6), 89–104.
- Scarascia-Mugnozza, G., Castellano, S., Roux, P., Gratraud, J., Palier, P., Dufresne de Virel, M., & Robertson, A. (2017). Snow distributions on greenhouses in Book Chapter: *Snow Engineering 2000: Recent Advances and Developments*, 265–274.
- Waaijenberg, D. (2004). Design, construction and maintenance of greenhouse structures. *International Symposium on Greenhouses, Environmental Controls and In-house Mechanization for Crop Production in the Tropics*, 710, 31–42.

Analysis of the Evolution of a Rural Landscape by Combining SAR Geodata with GIS Techniques



Giuseppe Cillis, Aimé Lay-Ekuakille, Vito Telesca, Dina Statuto and Pietro Picuno

Abstract In the last decades, Mediterranean rural landscapes have undergone significant changes, with relevant considerable environmental and socio-economic impacts. These phenomena are often triggered by agricultural abandonment, especially in environmentally-sensitive areas, which are usually located in marginal and less profitable regions, and which could indeed irremediably compromise the identity and role of these Mediterranean landscapes. On the other hand, the progressive increase of available multi-source geodata allows to reconstruct the landscape original structure, providing new tools able to prevent negative impacts on environment. Hence, thanks to the development of increasingly advanced and open-source GIS tools, it is possible to implement several geodata typologies that can be mutually integrated in an increasingly efficient approach. In this paper the process of landscape reshaping pattern is analyzed in a study area of Basilicata region (Southern Italy) using remote sensing. In particular, the vegetation component of a landscape has been assessed by means of SAR images by using an artificial intelligence approach, that is machine learning to understand landscape dynamics in two different time periods. In this way, it has been possible to integrate data of different source and composition into landscape analysis methodologies, hence developing a suitable tool for planning and managing the rural landscape.

Keywords Remote sensing · SAR · Geographical information system · Rural landscape · Artificial intelligence · Machine learning

G. Cillis (✉) · D. Statuto · P. Picuno
School of Agricultural, Forest, Food and Environmental Sciences - SAFE, University of Basilicata, Potenza, Italy
e-mail: giuseppe.cillis@unibas.it

A. Lay-Ekuakille
Department of Innovation Engineering, University of Salento, Lecce, Italy

V. Telesca
School of Engineering, University of Basilicata, Potenza, Italy

© Springer Nature Switzerland AG 2020
A. Coppola et al. (eds.), *Innovative Biosystems Engineering for Sustainable Agriculture, Forestry and Food Production*, Lecture Notes in Civil Engineering 67,
https://doi.org/10.1007/978-3-030-39299-4_29

1 Introduction

Agricultural activities have played an important role in the characterization of Mediterranean agroforestry landscapes. However, the increase of urbanization on one hand, and the land abandonment occurred in recent decades on the other, has negatively affected the environment, imposing irreversible changes in the landscape patterns and their relevant ecological functions. These changes are, for example, the loss of biodiversity, the hydrogeological instability and the habitat fragmentation. The change in land cover due to the abandonment of agriculture is the phenomenon that is mostly affecting scholars. In the scientific literature there are indeed many studies in which an evaluation of the positive or negative effects that the abandonment of the territory can have towards, for example, biodiversity (Queiroz et al. 2014). All techniques, for evaluating the effects of land use changes on landscape, are based on the efficient use of land use/land cover datasets. So, the first operation in most cases is based on the choice or elaboration of geodatabases that collect land use data. Moreover, GIS tools can be associated with the evaluation of landscape dynamics (Statuto et al. 2017), which allow the application of different methodologies for the evaluation of landscape dynamics; both those are based on historical approaches (Otero et al. 2015; Statuto et al. 2016) and on the use of remote sensing (Yin et al. 2018) or on an integrated approach between these different techniques. Given the need to implement new methods for collecting geodata land use, in this paper a methodology to elaborate landscape data from remote sensed images is proposed. In particular, the SAR images potentiality are explored comparing two different years (1992–1996). SAR (Synthetic Aperture Radar) images are able, thanks to appropriate processing, to point out land characters (Andria et al. 2000) and make easier its interpretation. SAR uses short physical antenna but, through modified data recording and processing techniques, they synthesize the effect of very long antenna. Hence, the used antenna should be a narrow effective antenna bandwidth, without requiring a physically long antenna (Lay-Ekuakille et al. 2002). Information captured by SAR, especially for land classification, do not need special and heavy processing, but sometimes a slightly treatments (Bhateja et al. 2015). There are different methods for treating SAR images for landscape and land information retrieval, notably traditional and innovating ones (Scheiber et al. 2008). Traditional or classical techniques are based on regular and advanced signal processing, and two broad distinctions can be recalled: (i) time-domain and frequency-domain processing; (ii) high-resolution imaging. Time-domain techniques are based on processing back-projection signals, whilst frequency-domain approaches are related to wavenumbers and motion compensation. Innovating methods are mainly based on adaptive and Artificial Intelligence (AI). AI offers possibilities to use machine learning that includes deep learning option. They exploit self-learning of a huge number of data (Zhu et al. 2017). Making a certain order in vocabulary for Machine learning, as an AI method, it is an evolution of artificial neural networks. It encompasses deep learning as one of its expressions. In turn, deep learning includes the computer vision algorithm, as classifier and processor, we have used in this paper. This algorithm possesses a paramount

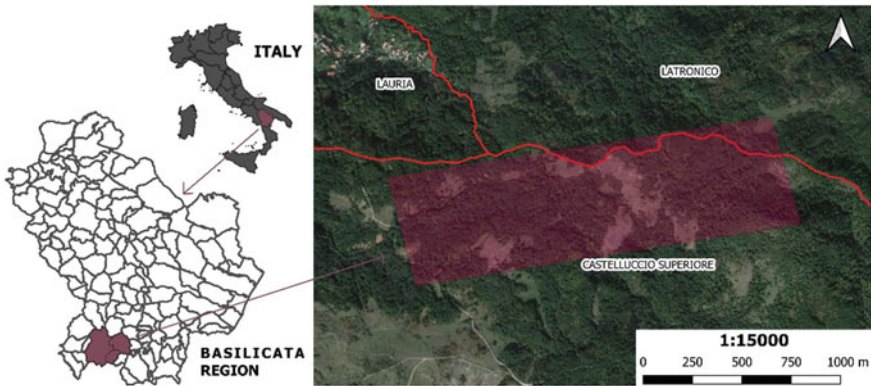


Fig. 1 Location of study area within Basilicata region and municipalities boundaries of Castelluccio Superiore and Latronico (Centroid $40^{\circ}03'07.5''N$ $15^{\circ}59'07.2''E$ – EPSG 4326)

requirement of computer vision on deep classification and processing image pixels instead many images. This requirement allows to get high accuracy in few numbers of epochs. That is the case of SAR images.

2 Materials and Methods

2.1 Study Area

The study area (Fig. 1) refers to a rural landscape included into a rectangle of about 112 ha. This area is located in the Basilicata region (Southern Italy), very close to a site registered in the Natura 2000 network: Special Areas of Conservation (SAC) of *Monte La Spina—Monte Zaccana*. It is about 1000 ha (site code: IT9210185) which also falls within the Pollino National Park and is characterized by forest habitats and mountain grasslands. The sites fall within the municipalities of Castelluccio Superiore and partly Latronico.

2.2 Land Use Data Processing

Two ERS-1/2 SAR images, captured in 1992 and 1996 respectively, have been processed in this work. These images have been acquired from a vast campaign carried out on the same study area (Losurdo et al. 2008); they are depicted in Fig. 2 where two different acquisition angles are illustrated. The strategy for processing is related to machine learning by exploiting single color reactions. The machine learning approach has been used to process a huge number of pixels encompassed in these

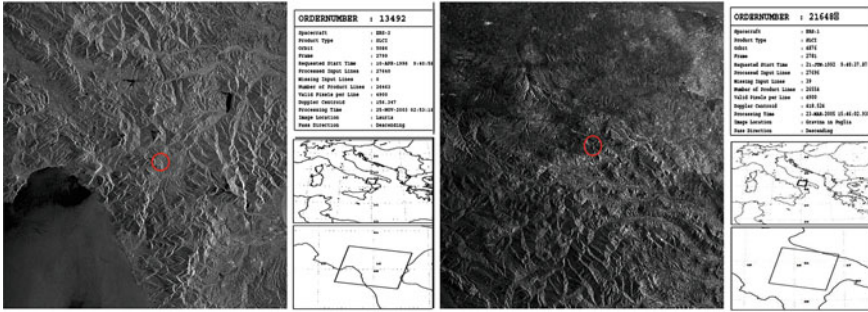


Fig. 2 ERS-1/2 SAR images of area of interest according to previous figure: Castelluccio Superiore location on April 10th 1996 (left), same area under a different angle on June 21st 1992 (right)

images, in lieu of processing as many image numbers. Then, the self-training is not on number of images, but on number of pixels. The color is here intended as frequency. We reaffirm the use of machine learning technique using Python environment (<https://pypi.org/project/pyroSAR/>), as source of major reference, and the algorithm is illustrated in Fig. 3a which is an updated and enhanced version with respect to Liu

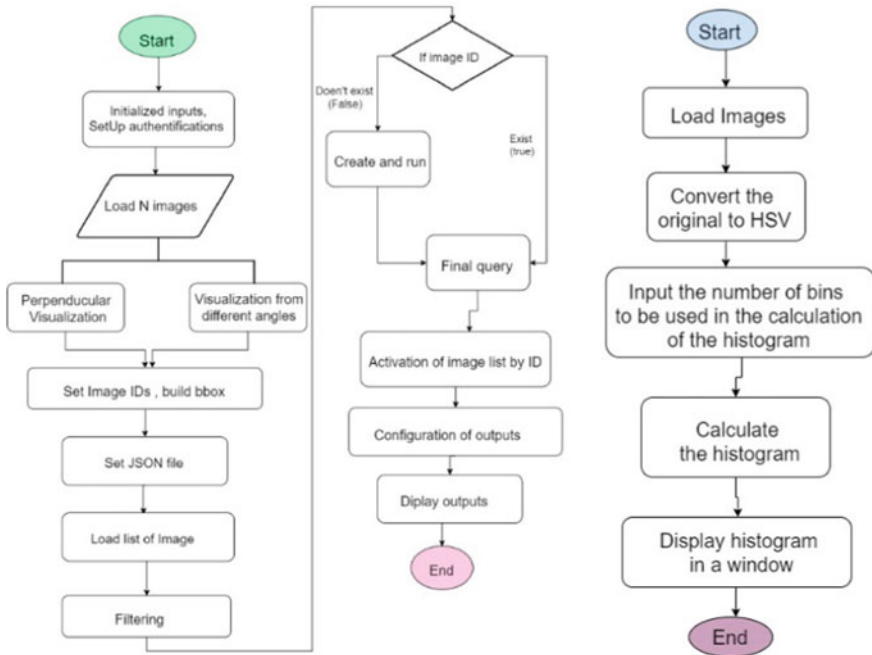


Fig. 3 Used algorithm for SAR images processing via machine learning (left), and histogram computation flowchart (right)

et al. (2019). The block works on pixels and extracts frequencies (colors) included in SAR image, namely red (C-band), green (L-band), blue (L-band) and infrared.

In this work, two primary images are used: the first taken as source image (initial state of land); in the source image we expect to find a matching with the template image. The template image is the patch image which will allow the comparison by sliding the goal to detect the highest matching area “by sliding”; the idea is to move the patch of one pixel at a given time (left to right, up to down). At each location, a metric is calculated so it represents how “good” or “bad” the matching at that location is (or how similar the patch is to that particular area of the source image). For each location of image 2 over image 1 (initial image), the metric is stored in the result matrix (R). Each location (x, y) in R contains the match metric. The output image is the result R of sliding the patch with a metric TM_CCORR_NORMED (Tan and Triggs 2010). The brightest locations indicate the highest matches. In practice, we use a dedicated function to locate the highest value (or lower, depending of the type of matching method) in the R matrix. OpenCV (open computer vision) implements template matching in the function *matchTemplate*. Several methods are available, but in the case of this work, the following formula has been used:

$$R(x, y) = \frac{\sum_{x', y'} (T(x', y') - I(x + x', y + y'))}{\sqrt{\sum_{x', y'} T(x', y')^2 \cdot \sum_{x', y'} I(x + x', y + y')^2}} \quad (1)$$

where (x, y) are coordinates of the point to be calculated, and (x', y') are coordinates of initial points. For histogram calculation, see Fig. 3b, the following steps have been performed:

1. Declare the matrices to store our images and initialize the number of bins to be used by our histogram;
2. Read the input image and transform it to HSV format;
3. Create a Trackbar for the user to enter the bin values. Any change on the Trackbar means a call to the *Hist_and_Backproj* callback function.
4. Show the image and wait for the user to exit the program;
5. *Hist_and_Backproj* functions: Initialize. The number of bins comes from the Trackbar;
6. Calculate the Histogram and normalize it to the range [0, 255];
7. Display *backproj*;
8. Draw the 1-D histogram of the image.

This first processing was subsequently combined with GIS operations to evaluate its usability with cartographical data. In particular a parallel analysis regarding land use changes between 1988 and 2017 has been carried out with QGIS 3.4, in which land use categories (agricultural areas, forest, grasslands and transitional woodlands) have been elaborated by implementing the orthophotos of 1988 and 2017 with the methodologies proposed in other works (Statuto et al. 2018).

3 Results and Discussion

First of all, for sake of clarity, it is necessary to discriminate the key objectives of GIS and machine learning processing envisaged in this paper. GIS is used here as a tool for addressing geo-referencing issues related to map information with overlapping of diverse sources, namely ortho-images. Conversely, machine learning approach is initially a stand-alone approach for processing and retrieving characters encompassed in land, to be (not necessarily) merged here in the GIS tool. As a demonstration, we include results limited to C and L bands in 1992 and 1996 SAR images (Figs. 4 and 5). Beside band-based responses, pixels histogram is also included. In the figures, reported below, a comparison between 1992 and 1996 landscape characters is exhibited. The major difference between both periods is chiefly connected to pixels histogram. Passing from 1992 to 1996, there is an improvement of landscape characters, in particular foliage and forestry coverage; suffice it to see the presence of a high peak around 250 pixels (abscissa axis), that is the vegetation/forestry response to the SAR sensor. These peaks are only noticed during 1996.

The tone index, in arbitrary scale, is here intended as the response of the item under monitoring, that is reflectivity. Similar information has been obtained through the implementation of the cartographic data into a GIS. In Table 1 and Fig. 6 the land use categories quantification is reported. It raises a progressive process of abandonment

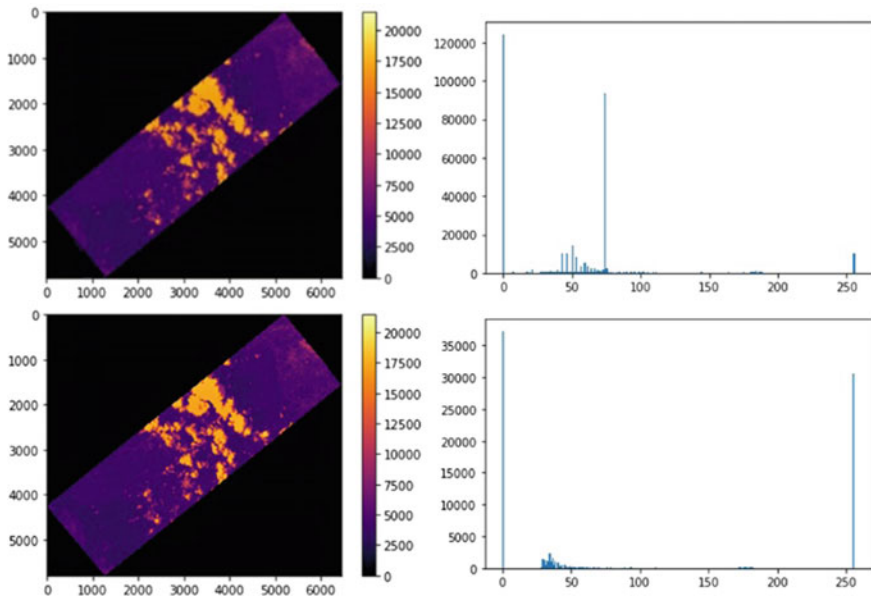


Fig. 4 (Upper-year 1992; lower-year 1996). Red band (C-band) response, left [tone index (abscissae) versus pixels (ordinates)] and related pixels histogram, right [histogram plots exhibits image grey levels (abscissae) versus pixels (ordinates)]

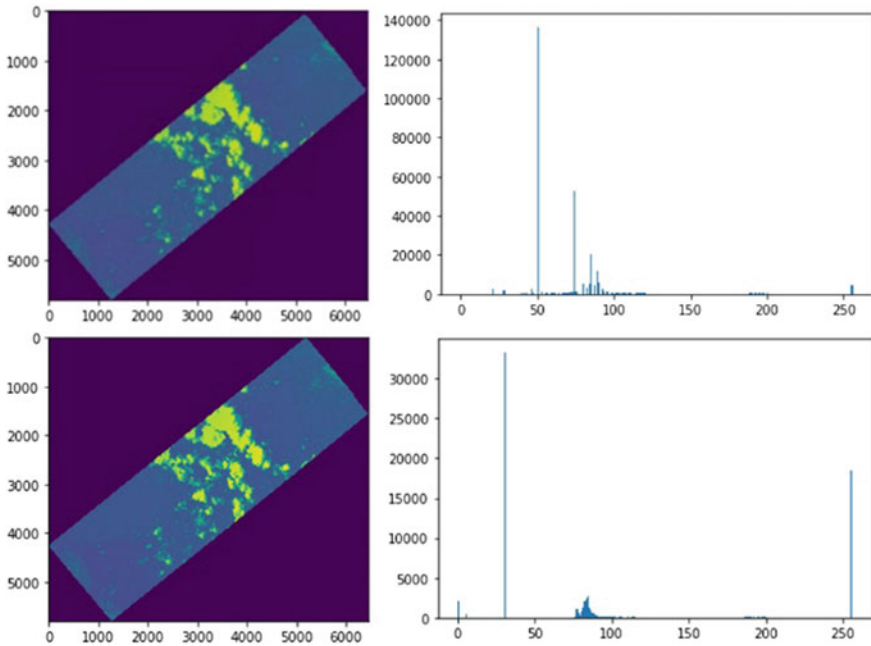


Fig. 5 (Upper–year 1992; lower–year 1996). Blue band (L-band) response, left [tone index (abscissae) versus pixels (ordinates)] and related pixels histogram, right [histogram plots exhibits image grey levels (abscissae) versus pixels (ordinates)]

Table 1 Analysis of land use categories in different time period

	1988		2017		Net change ha	Expected band
	ha	%	ha	%		
Agricultural areas	8.24	7.35	0.25	0.22	−7.99	C, L, X
Transitional woodlands	12.14	10.84	7.76	6.93	−4.38	L, P
Grasslands	26.50	23.66	15.49	13.83	−11.01	VHF, P
Forest	65.14	58.15	88.53	79.02	23.38	L
Total	112.03		112.03			

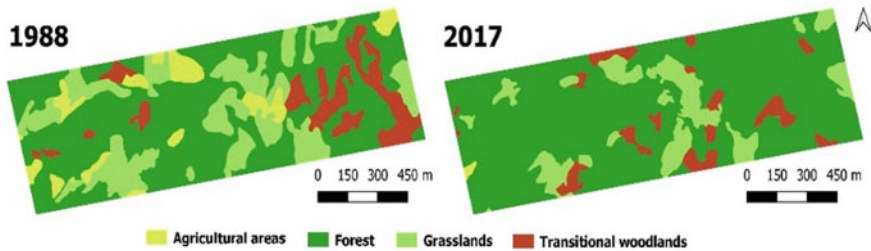


Fig. 6 Land use change in the study area in two different period (year 1988 and 2017)

of agricultural areas (-7.99 ha), grazing grasslands (-11 ha) and an increase in forests due to renaturalization processes ($+23.38$ ha). The above consideration are almost in line with the first “raw” results obtained through the implementation of SAR geodata because with GIS, hence, ortho-images, we can see a raw evolution of the land by overlapping these images. But, we cannot see details as we do with SAR approach combined with dedicated processing techniques. Moreover, results agree with the general band retrieval depicted in the rightmost column of Table 1, that is, C-band points out agriculture activities, and ocean (this area is very close to the Tyrrhenian sea) whilst L-band response exhibits agriculture activities, forestry and soil moisture.

4 Conclusions

The machine learning approach, in particular deep learning with openCV algorithm, which has been used in this work to overcome the lack of many images over the same location, has enabled to move within millions of pixels encompassed in the aforementioned two images captured in 1992 and 1996 respectively. C and L-bands have been retrieved for both years pointing out changes in tones (reflectivity) with correspondent changes in histograms, that are peaks in grey scale for pixels. That is to confirm the potential of using SAR images for the landscape dynamics investigation and to analyze some specific land components. Moreover, from this preliminary study, it emerges that one of the tools that can best exploit this source of land use data is that it definitely needing more detailed analysis is the GIS. Further improvements will face the implementation of these data into the GIS environment, to improve the accuracy of SAR images classification and to test the inclusion of these data in a more complex multi-temporal spatial framework.

Acknowledgements Authors gracefully thank Geocart Srl company for providing the SAR images used in this work.

References

- Andria, G., D’orazio, A., Lay Ekuakille, A., Moretti, M., Pieri, P., Tralli, F., & Tropeano, M. (2000). Accuracy assessment in photo interpretation of remote sensing ERS-2/SAR images. In *17th IEEE—IMTC2000*, Baltimore, USA, May 1–4.
- Bhateja, V., Tripathi, A., Gupta, A., & Lay-Ekuakille (2015). Speckle suppression in SAR images employing modified anisotropic diffusion filtering in wavelet domain for environment monitoring. *Measurement*, *74*, 246–254.
- Lay-Ekuakille, A., Pelillo, V., Dellisanti, C., & Tralli, F. (2002). Sar aided method for rural soil evaluation. *SPIE2002 Remote Sensing*, 22–27 September in Crete, Greece.

- Liu, S., Qi, Z., Li, X. & AndYeh, A. G. (2019). Integration of convolutional neural networks and object-based post-classification refinement for land use and land cover mapping with optical and SAR data. *Remote Sens*, 11, 690.
- Losurdo, A., Pacifico, S., Sarli, V., Colangelo, A., & Leggeri, M. (2008). Integration of differential SAR interferometry and ancillary GIS data for the study of superficial deformations. *EARSLe Proceedings* 7, 1/2008.
- Otero, I., Marull, J., Tello, E., Diana, G. L., Pons, M., Coll, F., et al. (2015). Land abandonment, landscape, and biodiversity: questioning the restorative character of the forest transition in the Mediterranean. *Ecology and Society*, 20(2), 7.
- Queiroz, C., Beilin, R., Folke, C., & Lindborg, R. (2014). Farmland abandonment: Threat or opportunity for biodiversity conservation? a global review. *Frontiers in Ecology and the Environment*, 12(5), 288–296.
- Scheiber, R., Hajnsek, I., Horn, R., Papathanassiou, K. P., Prats, P., & Moreira, A. (2008). Recent developments and applications of multi-pass airborne interferometric SAR using the E-SAR system. In *7th European Conference on Synthetic Aperture Radar*, Friedrichshafen, Germany, 2008, pp. 1–4.
- Statuto, D., Cillis, G., & Picuno, P. (2016). Analysis of the effects of agricultural land use change on rural environment and landscape through historical cartography and GIS tools. *Journal of Agricultural Engineering*, 47, 28–39.
- Statuto, D., Cillis, G., & Picuno, P. (2017). Using historical maps within a GIS to analyze two centuries of rural landscape changes in Southern Italy. *Land*, 6, 65.
- Statuto, D., Cillis, G., & Picuno, P. (2018). GIS-based analysis of temporal evolution of rural landscape: a case study in southern Italy. *Natural Resources Research*, <https://doi.org/10.1007/s11053-018-9402-7>.
- Tan, X., & Triggs, B. (2010). Enhanced local texture feature sets for face recognition under difficult lighting conditions. *IEEE Transactions on Image Processing*, 19, 1635–1650.
- Yin, H., Prishchepov, A. V., Kuemmerle, T., Bleyhl, B., Buchner, J., & Radeloff, V. C. (2018). Mapping agricultural land abandonment from spatial and temporal segmentation of Landsat time series. *Remote Sensing of Environment*, 210, 12–24.
- Zhu, X. X., Tuia, D., Mou, L., Xia, G., Zhang, L., Xu, F., & Fraundorfer, F. (2017). Deep learning in remote sensing: A comprehensive review and list of resources. In *IEEE Geoscience and Remote Sensing Magazine*, pp. 8–36.

Smart Dairy Farming: Innovative Solutions to Improve Herd Productivity



C. Arcidiacono, M. Barbari, S. Benni, E. Carfagna, G. Cascone, L. Conti, L. di Stefano, M. Guarino, L. Leso, D. Lovarelli, M. Mancino, S. Mattoccia, G. Minozzi, S. M. C. Porto, G. Provolo, G. Rossi, A. Sandrucci, A. Tamburini, P. Tassinari, N. Tomasello, D. Torreggiani and F. Valenti

Abstract Among the most straining trends that farmers have to face there are: on one side, to guarantee welfare and adequate life conditions for animals and to reduce the environmental footprint, on the other side, to develop new strategies to improve farm management reducing costs. The current conditions and the expected developments of the dairy sector highlight a strong need for more efficient and sustainable farming systems. Studying heat stress, herd management and housing and animals'

M. Guarino (✉)

Department of Environmental Science and Policy, Università degli Studi di Milano, Via Celoria, 10-20133 Milan, Italy

e-mail: marcella.guarino@unimi.it

D. Lovarelli · G. Provolo · A. Sandrucci · A. Tamburini

Department of Agricultural and Environmental Sciences, Production, Landscape, Agroenergy, Università degli Studi di Milano, Via Celoria, 2-20133 Milan, Italy

C. Arcidiacono · G. Cascone · M. Mancino · S. M. C. Porto · N. Tomasello · F. Valenti

Department of Agriculture, Food and Environment, Università degli Studi di Catania, Via S. Sofia, 100-95123 Catania, Italy

M. Barbari · L. Conti · L. Leso · G. Rossi

Department of Agriculture, Food, Environment and Forestry, Università degli Studi di Firenze, Via San Bonaventura, 13 50145 Florence, Italy

S. Benni · P. Tassinari · D. Torreggiani

Department of Agricultural and Food Sciences, Università di Bologna, Viale Giuseppe Fanin, 50-40127 Bologna, Italy

G. Minozzi

Department of Veterinary Medicine, Università degli Studi di Milano, Via Celoria, 10-20133 Milan, Italy

E. Carfagna

Department of Statistical Sciences "Paolo Fortunati", Università di Bologna, Via Belle arti, 41, 40126 Bologna, Italy

L. di Stefano · S. Mattoccia

Department of Computer Science and Engineering, Università di Bologna, Viale Risorgimento 2, 40136 Bologna, Italy

© Springer Nature Switzerland AG 2020

A. Coppola et al. (eds.), *Innovative Biosystems Engineering for Sustainable Agriculture, Forestry and Food Production*, Lecture Notes in Civil Engineering 67,

https://doi.org/10.1007/978-3-030-39299-4_30

productive and reproductive performances is fundamental for the economic and environmental sustainability of the dairy chain. New and effective tools to cope with these challenges have been provided by Precision Livestock Farming (PLF), which is nowadays increasingly applied and makes possible to control quali-quantitative parameters related to production, health, behaviour, and real-time locomotion per animal. The research key challenge is to turn these data into knowledge to provide real-time support in farming optimisation. This research focuses specifically on different systems to collect, process and derive useful information from data on animal welfare and productivity. A multi-disciplinary approach has been adopted to generate a decision support system for farmers.

Keywords Sustainability · Animal housing · Numerical modelling · Efficient animal production · Precision livestock farming

1 Introduction

Heat stress, herd management and housing are of major concern for milk producers. These aspects enclose the main issues that farmers are expected to deal with in the near future under the economic, environmental and social points of view. The main driver to the attention to these topics is linked to the associated decrease in milk production and the subsequent large economic losses that all these aspects involve. In addition, the environmental and social sustainability of food products is widely increasing in importance.

Traditionally, research on heat stress, for example, has focused on tracking changes in physiology and health of the cows coping with the hot environment. However, to ensure high standards of welfare for dairy cattle, a broader approach is needed in order to evaluate the affective states and the housing and thermal managements (e.g., insulation, fans, misters and shower).

The development in technology has been giving new opportunities for monitoring cow's behaviour in real time, which is known as Precision Livestock Farming (PLF). PLF is very powerful because it applies principles of control engineering to optimising production and management processes of dairy cattle and uses the resulting models to monitor, predict and control single animals and herds allowing to introduce the most adequate solutions in every herd.

Studies that have been carried out on dairy cows in intensive breeding have shown that heat stress causes unusual behaviours, a decline in their fertility and a worsening of the quality and quantity of milk produced (Gernand et al. 2019; Porto et al. 2015). Therefore, heat stress is a key point for farmers, researchers and decision makers, and monitoring the response of animals to this aspect permits to identify the most adequate solutions to adapt to it.

Other aspects that can be monitored through PLF regard animal health and fertility (Arcidiacono et al. 2017a). During the oestrus phase, which precedes the fertility state, the motor activity undergoes a variable increase that ranges between 30% and

200% respect to the usual activity. The reduced profit margins in the sale of milk had focused farmers' attention towards the reproductive performance of the herd in order to minimise costs associated with the reproduction phase. Hence, identifying the fertile period of dairy cows is an increasingly pressing need for farmers (Arcidiacono et al. 2017b; Mayo et al. 2019). Though open source algorithms were successfully developed to automatically classify standing, walking, feeding and lying down behaviour of dairy cows, hardware design can be improved to be used in the severe environment conditions of dairy barns (Trnovszky et al. 2017). Therefore, building a prototype adoptable in PLF to early detect cows' oestrus is very important.

In regard of housing and animal welfare, recent studies showed that the lack of grazing is one of the major concerns of consumers respect to intensive livestock farming. Moreover, even if consumers revealed to be particularly sensible to this aspect, grazing has been almost completely abandoned in Italy. Therefore, potential benefits of allowing the cows to access pasture should be investigated. In particular, providing access to pasture can have the potential to improve various aspects of the sustainability in dairy farming, among which animal welfare and social acceptability of intensive farming (Bargo et al. 2002; Charlton and Rutter 2017). However, grazing may limit milk production in high yielding dairy cows, reduce the control over diet composition and result in exposure to unsuitable weather conditions. Since the housing conditions affect cattle welfare, the benefits of accessing to pasture and the willingness of the cows to access to outside areas (Legrand et al. 2009) may depend on the housing system.

The general goals of this study are to identify the relationships among environmental conditions, fertility, behaviour and health state of the cow, and to find innovative solutions to ensure dairy cows' welfare and improve herd fertility by maintaining appropriate environmental conditions. To achieve this, comprehensive cow-side measurements are collected in order to obtain real-time responses to different managing solutions for housing and herd management and for high ambient temperatures that could be incorporated into heat abatement management decisions.

2 Materials and Methods

As shown in Fig. 1, the monitoring and processing of environmental parameters, behaviour and animal condition parameters represent the main points of the research.

Regarding the heat stress control, different solutions are analysed and compared to detect the animal behaviour. Eight herds that differ in design, materials, managing ventilation and cooling system are studied by measuring continuously several parameters and using wearable sensors and data loggers in the barn environment. These parameters include environmental conditions, animal activity and animal condition among which body temperature, heart rate, milk production and composition, milk somatic cell count, lameness, BCS and weight. Moreover, together with the analysis of other physiological parameters, individual monitoring of dairy-cow motor

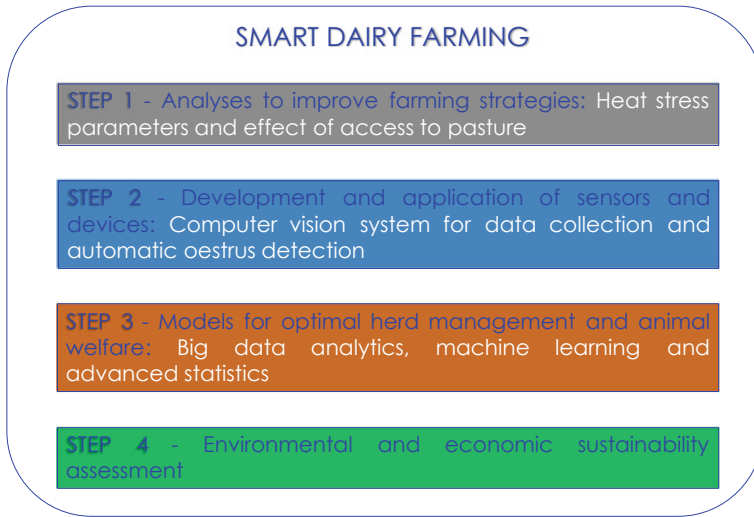


Fig. 1 Steps that define the phases of the project

activity may allow the early detection of some pathological and physiological status (Arcidiacono et al. 2017a), which also brings to a reduction in medical costs.

For the early detection of the oestrus phase, the commonly used inertial sensor-based system is improved by adding hardware and software components for storing information regarding barn environmental conditions (air temperature, humidity ratio, air velocity, etc.) that are also modified by the management of different air cooling systems (evaporative or shower type with fans) usually adopted in hot climate regions (Arcidiacono et al. 2017b).

In regard of the animal welfare, a trial is carried out by providing animals the access to pasture in order to evaluate whether there is an improvement of welfare of dairy cows. This is performed comparing the cow response when present in two different typologies of dairy barns: the compost dairy barns (CDB) that showed to improve animal welfare and especially feet and leg health, and the conventional free stall barns (FSB). Cows in CDB are provided with an open bedded pack area for resting and walking, while in FSB there are individual stalls and concrete alleys. The effects of pasture access on the performance and welfare of lactating dairy cows housed in the two housing systems are monitored with PLF sensors, to monitor behaviour and health and to measure milk yield and quality. The experiments are repeated in different periods of the year and feeding cows with the same Total Mixed Ration (TMR) ad libitum inside the barn. The preference of cows to be indoor or on pasture is assessed by monitoring the number of cows inside and outside the barn through a multi-camera video recording system.

The collected data are used to develop a fuzzy logic model for assessing the risk of reduced productivity in relation to the animals' conditions and their environment. The economic cost and the environmental impact for every strategy for mitigating

heat stress, evaluating the effect of pasture and improving herd management thank to sensors are compared using Life Cycle Analysis. Life Cycle Assessment and Life Cycle Costing will result with the environmental and economic impact of every investigated solution for understanding the most effective solution.

3 Expected Results and Applications

The automatic systems and management techniques investigated during this project represent a series of innovative tools for the process of decision making that are in line with the recent trends of breeding widespread in Europe and favoured by the modern “smart farming”. The monitoring and processing of big data is expected to furnish a large-scale modelling of animal behaviour, production and environmental conditions to keep into consideration specific livestock conditions and single animals of the herd. In particular, all collected data will be analysed as big data with advanced statistics and machine learning to develop models for real-time support.

From this research, it is expected also to identify and possibly adopt breeds of dairy cattle that are better equipped for hot environments, thus minimising the duration of compromised welfare. In addition, the comparison among data collected in the herds will show the differences related to the effect of heat stress, herd management and housing on milk production and animal health and welfare in the different contexts.

The scientific impact of the results will act in the field of PLF, since it will be possible to discern real-time data on the behavioural activities of dairy cows and facilitate the adoption of timely management protocols to safeguard animal health conditions and understand their physiological state. This will bring benefits and support to the decision making system. By promoting animal welfare, herd productivity will improve, as well as will increase the income of farmers and the environmental sustainability.

The effect on the economic and environmental points of view represents an essential aspect because consumers are increasingly demanding for sustainable intensive livestock farming systems and products. Additionally, also the social impact will emerge in regard of animal welfare because its achievement is a new requirement in those countries where animal husbandry technology has reached advanced levels that force animals to a very high productivity in environmental, physiological and food conditions that are, however, stressful.

Acknowledgements The activity presented in the paper is part of the research grant Progetti di Ricerca di rilevante Interesse Nazionale—Bando 2017 Prot. 20178AN8NC.

References

- Arcidiacono, C., Porto, S. M. C., Mancino, M., & Cascone, G. (2017a). Development of a threshold-based classifier for real-time recognition of cow feeding and standing behavioural activities from accelerometer data. *Computers and Electronics in Agriculture*, *134*, 124–134.
- Arcidiacono, C., Porto, S. M. C., Mancino, M., & Cascone, G. (2017b). A software tool for the automatic and real-time analysis of cow velocity data in free-stall barns: The case study of oestrus detection from Ultra-Wide-Band data. *Biosystems Engineering*, *173*, 157–165.
- Bargo, F., Muller, L. D., Delahoy, J. E., & Cassidy, T. W. (2002). Performance of high producing dairy cows with three different feeding systems combining pasture and total mixed rations. *Journal of Dairy Science*, *85*, 2948–2963.
- Charlton, G. L., & Rutter, S. M. (2017). The behaviour of housed dairy cattle with and without pasture access: A review. *Applied Animal Behaviour Science*, *192*, 2–9.
- Gernand, E., König, S., & Kipp, C. (2019). Influence of on-farm measurements for heat stress indicators on dairy cow productivity, female fertility, and health. *Journal of Dairy Science*, *102*, 6660–6671.
- Legrand, A. L., von Keyserlingk, M. A. G., & Weary, D. M. (2009). Preference and usage of pasture versus free-stall housing by lactating dairy cattle. *Journal of Dairy Science*, *92*, 3651–3658.
- Mayo, L. M., Silvia, W. J., Ray, D. L., Jones, B. W., Stone, A. E., Tsai, I. C., et al. (2019). Automated estrous detection using multiple commercial precision dairy monitoring technologies in synchronized dairy cows. *Journal of Dairy Science*, *102*, 2645–2656.
- Porto, S. M. C., Arcidiacono, C., Anguzza, U., & Cascone, G. (2015). The automatic detection of dairy cow feeding and standing behaviours in free-stall barns by a computer vision-based system. *Biosystems Engineering*, *133*, 46–55.
- Trnovszky, T., Kamencay, P., Orjesek, R., Benco, M., & Sykora, P. (2017). Animal recognition system based on convolutional neural network. *Digital Image Processing and Computer Graphics*, *15*(3), 517–525.

A Methodology to Support Planning and Design of Suburban Agricultural Areas



P. Russo, P. Lanteri and A. D'Emilio

Abstract The changed attitude of today's society towards environmental protection requires a reconsideration of territorial resources management, according to models characterized by an improved sustainability. Specific attention should be pointed to the recovery and redevelopment of the suburban areas, where the residual agricultural areas can have a relevant function in any land protection actions. Indeed, maintaining the productive function can contribute to support the sale and consumption of farm-to-table agricultural products. On the other hand, the addition of new social and educational functions can help to strengthen the relationship between suburban areas and urban center. In this work some design criteria are defined, which allow the introduction of new activities in suburban areas in respect of the present activities and historical landscapes. Specifically, in a first phase, the requirements of the areas intended for specific activities are determined (agricultural, on the one hand, and fruition for free time and educational activities, on the other). Subsequently, the functional and technological compatibility between the two models (agricultural and fruition) is verified, in order to allow their coexistence and integration.

Keywords Traditional agriculture · Fruition · Compatibility · Parks · Landscape project

1 Introduction

The widespread and uncontrolled urbanization has led to the creation of large fringe areas, placed on the boundary between urban and rural system, where neither the characteristics of the organized city nor those of the rural environment can be identified. Often, the modifications undergone by these areas compromised their original agricultural use, relegating them to functional and productive “marginality”. These residual areas, especially those one characterized by the persistence of agricultural

P. Russo · P. Lanteri (✉) · A. D'Emilio

Department of Agriculture, Food and Environment (Di3A), Università degli Studi di Catania, Via S. Sofia 100, 95123 Catania, Italy
e-mail: planteri@unict.it

© Springer Nature Switzerland AG 2020

A. Coppola et al. (eds.), *Innovative Biosystems Engineering for Sustainable Agriculture, Forestry and Food Production*, Lecture Notes in Civil Engineering 67,
https://doi.org/10.1007/978-3-030-39299-4_31

271

activity, are object of motivated interest, as they perform both traditional and innovative important functions, such as: the preservation of the rural territorial texture; the boundary delimitation between urban and rural areas; the establishment of green areas among urban settlements; the protection of the suburban environment in terms of both human coverage of the territory and productive support able to justify any recreational use in economic terms; the preservation of hydrogeological and climatic equilibrium at the metropolitan scale; the production of foodstuffs specifically intended for the short supply chain (Russo et al. 2014).

The recovery of these areas is significant also to avoid the formation of that “precarious landscape”, consisting of innumerable plots of abandoned land, which is a premise of further degradation. Where still evident, the historic agricultural structure should be maintained and used, as it offers a testimony of the socio-economic fabric of the region. Furthermore, these areas can contribute to restore the relationship between town and its territory, as they represent a resource for production of primary goods, as well as cultural and environmental assets (Carmona-Torres et al. 2011; Zasada 2011; Páuil and McKenzie 2013). The “identity of typical products” factor thus fits in perfectly with the “identity of the landscape” factor. Therefore, these two factors together provide concrete opportunities for possible growth in new sectors, such as tourism and recreational activities in rural environments (Erickson et al. 2011; Riguccio et al. 2015). These opportunities could further increase when these areas are part of a territorial green system, which connects them with natural reserves, parks and protected areas, creating opportunities to visit the places (Ristić et al. 2019).

However, every such proposal requires project actions, which must follow compatibility criteria between the original use and the new activities to be introduced. Specifically, the landscape project stands as an intermediate feature between general-scale planning and small-scale projects in which the details prevail over a comprehensive idea of landscape (Ghio 1999). Indeed, different authors agreed that landscape projects are useful instruments for achieving various objectives, such as: maintaining and giving added value to the specific environments; re-qualifying degraded environments; recovering ancient values and creating new ones (Leger et al. 2013; Riguccio et al. 2016). As asserted in the European Landscape Convention, the quality of the landscape plays an essential role in determining the quality of life of the local population, and thus maintaining this quality is both a social and institutional obligation (Riguccio et al. 2017).

In this context, the present study develops a methodology aimed at the integration of fruition activities in suburban agricultural areas, avoiding conflicts with the needs of environmental protection and agronomic management. The analysis of the production needs and the fruition activity to be integrated allowed to evaluate their compatibility, through the identification of reference parameters, which also take into account the aesthetic and perceptive value of the landscape.

2 Methodology

The enhancement of the suburban agricultural areas involves the drafting of projects that often require the implementation of new activities able to strengthen and diversify the anthropic presence, such as those related to leisure and free time. These activities must be introduced following criteria which allow respect and protection of the agricultural-environmental context to be preserved, so that they do not constitute disturbing factors in the management of the farm. In order to proceed with the research of design forms compatible with the reference landscape, it is necessary to analyze and compare the performance of the two environmental systems that are envisaged: the one determined by the pre-existing agricultural activity and the other that comes to be determined following the introduction of the new activities. Their compatibility can be verified by comparing some characteristic parameters.

To this aim, a method is proposed, which is structured in the following phases (Fig. 1):

- identification of the Agricultural System together with the functional, dimensional, temporal and technological characteristics of its subsystems;
- identification of the new Fruition System and its subsystems, the latter again defined according to their functional, dimensional, temporal and technological characteristics;
- study of the compatibility of the two systems on the basis of the aforementioned characteristics;
- identification of the variations or integrations necessary for the addition of the new activities.

Therefore, after identifying a reference model, the study of the characteristics of the Agricultural System requires the evaluation of its performance so as to define its subsystems, which present different potential uses.

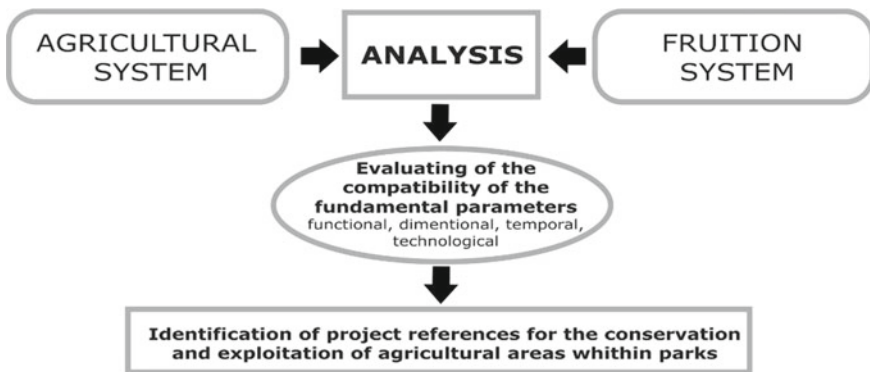


Fig. 1 Methodology flowchart

Furthermore, for each subsystem, the performance of the technical elements, which directly affect the quality of the space are identified, including: cultivation methods, size of each area with different uses, organization and dimensions of the pathways, type of greenery (agricultural or natural), service buildings (storage, cisterns etc.), building elements necessary for soil arrangement, infrastructures for irrigation and energy distribution. This makes it possible to determine the “containability” of the Agricultural System and identify the changes necessary for the addition of the new activities (Fruition System), without significant modifications of the original structure. In the same way, the definition of the performance system of places planned for free time, cultural and leisure activities, is realized from the identification and analysis of the spaces, the equipment and the services necessary for carrying out the project-based activities. Therefore, for the specific Fruition System, it is necessary to identify the spaces that constitute its subsystems, together with the related design requirements. An analysis of the two systems provides the performance parameters to be compared for assessing the suitability of the specific agricultural landscape to support the introduction of new anthropic factors. The assessment of suitability must take into account that no alterations should be planned that compromise the original functionality or the validity of the landscape.

The reference model of the Agricultural System considered in this study is the terraced citrus grove, a traditional type of plantation, which is very common in the foothills of the eastern slope of Etna. Indeed, the historical importance of these kind of agricultural areas in the aforementioned geographical context, makes particularly interesting the possibility to use them, by introducing new activities (Fruition System) related to leisure, recreation, cultural and educational fruition. Needless to say, the Agricultural System can be characterized by other cultivation types, on which to test the compatibility with a Fruition System characterized by activities that may be different from those considered in this paper.

3 Results

The first step of the proposed methodology is the identification of the Agricultural System and its subsystems. To this aim, the main aspects were considered, concerning agronomy (cultivation, climatic, installation requirements), management (cultivation times and methods, harvest, marketing) and morphology (nature of the land, slope, exposition, irrigation plants, pathways, support infrastructures) detected in the reference model (terraced citrus grove). The identified subsystems are illustrated in Fig. 2a.

For each subsystem an analysis was carried out aimed at the knowledge of the peculiar characteristics arising from the specific cultivation requirements and the particular conditions of the context. In relation to the activities carried out by the operators in each area, the necessary spaces were identified and the times they are used by those responsible were defined.

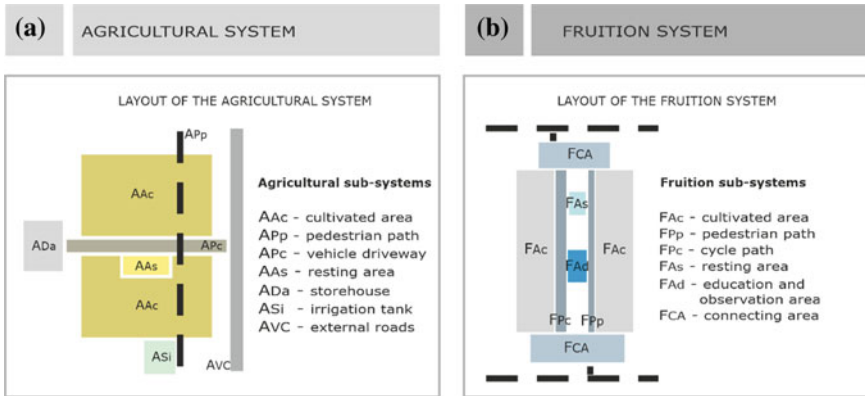


Fig. 2 Agricultural System and its subsystems (a); Fruition System and its subsystems (b)

Once the Agricultural System had been analysed, the next step consisted in assessing the new Fruition System and its subsystems, through the identification of the requirements of the educational and leisure areas and the characterisation of the necessary spaces. Making the agricultural area usable means, above all, people being able to reach it, circulate within the area and stop to observe or rest. Carrying out these simple activities within the agricultural area, requires the reference to a model for the identification of requirements and services, both at an environmental and technological level. The hypothesis is to superimpose on the described Agricultural System, a Fruition System made up of pathways, services and cultivated areas, believing that farming can be a source of interest for school children, tourists or those interested in the agricultural environment and in the historical and sociological facts connected with it. Following this model, the Fruition Subsystems were identified and reported in Fig. 2b.

Once the specific characteristics of the two systems (Agricultural and Fruition) and their respective Sub-systems (Fig. 2a and b) are known, it is necessary to identify and verify those parameters, which are considered more significant to read the compatibility levels. Specifically, the following four categories of parameters were identified:

- *functional*, referring to the intended use of each sub-system. The analysis of these parameters allows the identification and definition of areas with different functions. For the Agricultural System: cultivated areas, chargeable and pedestrian pathways, product loading and unloading areas, etc. For the Fruition System: rest and didactic areas, cycle and pedestrian paths, etc.
- *dimensional*, relative to the linear and surface dimensions, as well as to the slopes (longitudinal and transversal) of the analyzed areas of each subsystem;
- *temporal*, aiming at identifying times and seasons for carrying out the different actions. The research for compatibility between the two activities needs a detailed

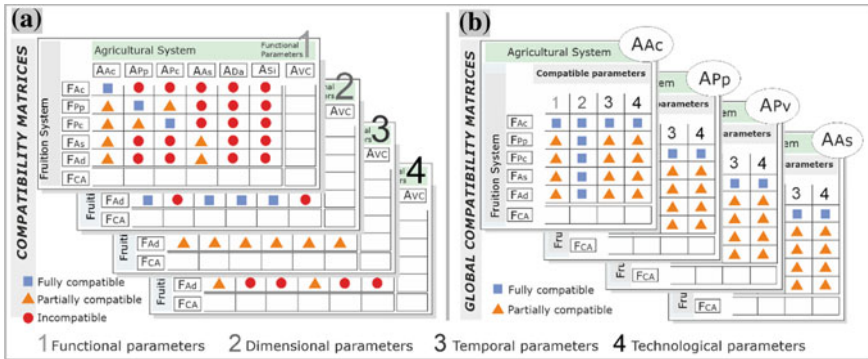


Fig. 3 Compatibility evaluation among the functional, dimensional, temporal and technological parameters of the Agricultural System with the corresponding ones of the Fruition System. Compatibility matrices for each group of parameters (a) and Global compatibility matrix for each subsystem (b)

knowledge of the time needed to carry out specific cultivation operations or processing (phytosanitary treatments, harvesting, transport, loading and unloading of products, equipment and goods, etc. The conduction of these actions, limited to short periods of the year, excludes the coexistence with other activities which, inevitably, would interfere with one another;

- *technological*, relating to the materials, systems, vehicles and vegetation existing in the referenced model for each subsystem.

The comparative analyses between the two systems, carried out through the use of four compatibility matrices—one for each group of parameters—(Fig. 3a), lead to the identification of the compatibility level between each subsystem. Three levels of compatibility were identified (*fully compatible*, *partially compatible* and *incompatible*) according to the capacity of the Agricultural System to contain the necessary spaces for other uses as well as the carrying out of the agricultural activity. The analysis made it possible to exclude all incompatible relationships. This can lead to the exclusion of entire Agricultural subsystems, when these are incompatible with all the Fruition subsystems, as happened, for example, for ADA (Storehouse) and ASi (Open-air irrigation tank built above ground) subsystems. For each subsystem remaining, a “global compatibility matrix” was created, in which the compatibility level of each Fruition subsystem is compared with each parameter group. Even in this case all incompatible relationships were excluded. On the contrary, when two subsystems are *fully compatible*, no significant intervention is necessary, but only simple maintenance activities are required.

This happened, for example, between the AAC and FAC subsystems. For all those subsystems that shows partial compatibility, a series of interventions are planned, which can be agronomic, technical-constructive, or plant and equipment related. To this aim, for all the Agricultural subsystems that are fully or partially compatibles with the related Fruition subsystems, specific sheets were created, containing the

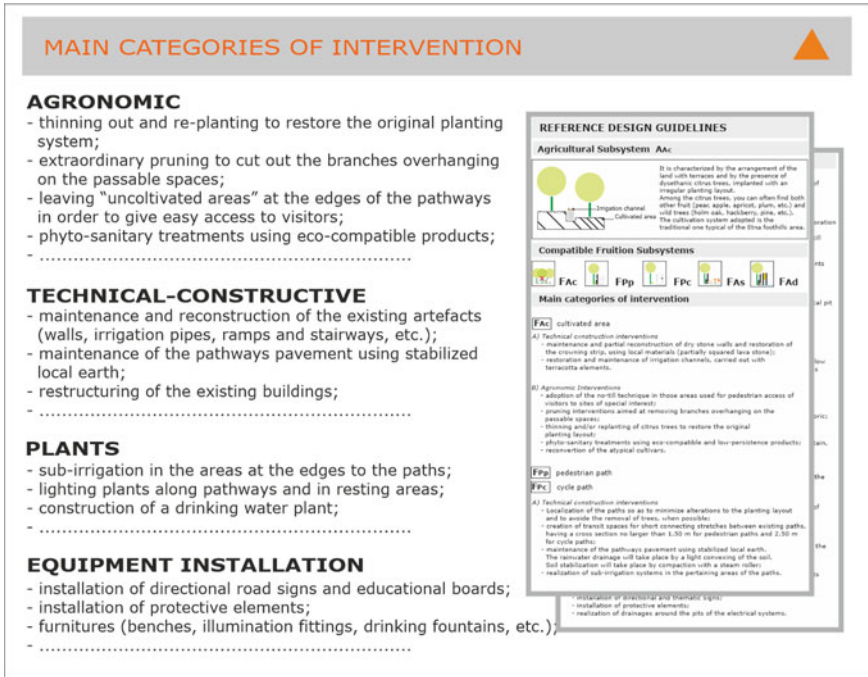


Fig. 4 Reference design guidelines for the adaptations from agricultural to fruition subsystems

main intervention categories that are necessary for the purposes of functional and technological adaptation of the reference model. A specification of the main categories of intervention, together with the sheet specific for AAc subsystem, reported as an example, are shown in Fig. 4. In detail, the Agricultural subsystem AAc is suitable for hosting both resting and educational areas (FAS, FAD), as well as pedestrian and cycle paths (FPP, FPC) of the Fruition System. However, these new functions should be introduced with caution. Indeed, building new paths along the edges of the terraces would require important changes to the pre-existing structure. Similarly, building a resting area would lead to the eradication of any plants that may be present. The existing pedestrian and vehicular pathways (APP, APC), originally used only by farmers, are fully compatible with pedestrian and cycle paths (FPP, FPC) necessary for the new Fruition System. In this case, the interventions are limited to the maintenance of the pavement, the restoration of the supporting stone-walls, the addition of furnishings and signs, together with the necessary systems.

Finally, the resting areas (AAS) of the Agricultural System are dimensionally compatible with the resting and educational areas (FAS, FAD) of the Fruition System. The main interventions consist of the installation of furniture (benches, fountains, waste bins, etc.) and of educational panels, which illustrate the characteristics of the area, the type of crop, the cultivation methods, etc.

4 Conclusions

The proposed method can provide useful guidance for the drafting of intermediate-scale projects, aimed at maintaining and developing suburban traditional agricultural areas of particular value through functional integration, targeted to the development of recreational and cultural activities. The application of the methodology proposed in this study allowed to verify the degree of compatibility that exists between two reference systems (terraced citrus Agricultural System and educational-cultural Fruition System). The reference parameters used in the proposed methodology, guarantee a flexibility of the method allowing its adaptability to different situations and contexts, with regard to both the Agricultural System and the Fruition System to be inserted.

Acknowledgements The activity presented in the paper is part of the research grant “University Research – Research Plan 2016/2018” by University of Catania.

References

- Carmona-Torres, C., Parra-López, C., Grootb, J. C. J., & Rossing, W. A. H. (2011). Collective action for multi-scale environmental management: Achieving landscape policy objectives through cooperation of local resource managers. *Landscape and Urban Planning*, *103*(1), 24–33.
- Erickson, D. L., Lovell, S. T., & Méndez, V. E. (2011). Landowner willingness to embed production agriculture and other land use options in residential areas of Chittenden County, VT. *Landscape and Urban Planning*, *103*(2), 174–184.
- Ghio, F. (1999). *Siti e paesaggi*. Firenze: Alinea Editrice. ISBN-10: 888125347X.
- Leger, A., Oueslati, W., & Salanié, J. (2013). Public tendering and green procurement as potential drivers for sustainable urban development: Implications for landscape architecture and other urban design professions. *Landscape and Urban Planning*, *116*, 13–24.
- Paül, V., & McKenzie, F. H. (2013). Peri-urban farmland conservation and development of alternative food networks: Insights from a case-study area in metropolitan Barcelona (Catalonia, Spain). *Land Use Policy*, *30*(1), 94–105.
- Riguccio, L., Carullo, L., Russo, P., & Tomaselli, G. (2016). A landscape project for the coexistence of agriculture and nature: A proposal for the coastal area of a Natura 2000 site in Sicily (Italy). *Journal of Agricultural Engineering*, *47*(2), 61–71.
- Riguccio, L., Tomaselli, G., Carullo, L., Verde, D., & Russo, P. (2017). Identifying areas suitable for wine tourism through the use of multi-criteria and geographic information system: The method and its application in the countryside around Mount Etna (Sicily). *Journal of Agricultural Engineering*, *48*(2), 88–98.
- Riguccio, L., Tomaselli, G., Russo, P., & Falanga, C. (2015). Identification of “Typical Agricultural Districts” for the development of rural areas applied to Eastern Sicily. *Land Use Policy*, *44*, 122–130.
- Ristić, D., Vukoičić, D., & Milinčić, M. (2019). Tourism and sustainable development of rural settlements in protected areas—Example NP Kopaonik (Serbia). *Land Use Policy*, *89*, 104231.
- Russo, P., Tomaselli, G., & Pappalardo, G. (2014). Marginal periurban agricultural areas: A support method for landscape planning. *Land Use Policy*, *41*, 97–109.
- Zasada, I. (2011). Multifunctional peri-urban agriculture—A review of societal demands and the provision of goods and services by farming. *Land Use Policy*, *28*(4), 639–648.

Modeling Soil Thermal Regimes During a Solarization Treatment in Closed Greenhouse by Means of Symbolic Regression via Genetic Programming



A. D'Emilio

Abstract Modeling soil thermal regimes during a solarization treatment in closed greenhouse is useful to estimate the required duration of the treatment in relation to the climatic conditions, as well as the efficacy of the technique. Several studies have been carried out, based on two main strategies: modeling the physical processes of the soil-mulch-greenhouse system or applying numerical procedures based on neural networks (NNs). However, the application and reliability of physical models require accurate knowledge of the thermo-physical properties of each component of the system, while NNs do not give any symbolic function which can be easily used. Symbolic regression via genetic programming represents an alternative method for finding a function that best fit a given set of data. In this paper, a such model is proposed, which use air temperature and global solar radiation flux outside the greenhouse, depth into the soil, existence of mulch and time of day as input variables and provides soil temperatures at different depths as output. The results allowed to obtain an easy to use symbolic function that is able to estimate soil temperature with an accuracy comparable to that one attained with other simulation models.

Keywords Soil solarization · Symbolic regression · Greenhouse · Soil temperature

1 Introduction

Soil solarization is a non-chemical method for soil disinfection that employs solar radiation to heat moistened soil, by means of a mulching film, and raises soil temperature up to deadly levels for soil-borne pathogens (Katan 1981). The efficacy of this technique mainly depends on the thermal sensitivity of soil-borne pathogens and on the level of soil infestation in relation to the soil temperature increase at various depths, the duration of the treatment and its possible integration with other plant pathogens control means (Vitale et al. 2013; Castello et al. 2017; Öz et al.

A. D'Emilio (✉)

Department of Agriculture, Food and Environment (Di3A), Università degli Studi di Catania, Via S. Sofia 100, 95123 Catania, Italy
e-mail: ademilio@unict.it

© Springer Nature Switzerland AG 2020

A. Coppola et al. (eds.), *Innovative Biosystems Engineering for Sustainable Agriculture, Forestry and Food Production*, Lecture Notes in Civil Engineering 67,
https://doi.org/10.1007/978-3-030-39299-4_32

279

2017; Öz 2018; Shi et al. 2018; Morra et al. 2018). The application of solarization in greenhouse allows to obtain higher soil temperatures in dependence on the shape and size of the greenhouse as well as by the characteristics of the covering material (Cascone et al. 2012; Miceli et al. 2008; Vitale et al. 2011; D'Emilio 2017a, b).

Modeling soil thermal regimes during a solarization treatment can be useful to estimate the required duration of the treatment in relation to the climatic conditions, as well as the efficacy of the technique. To this aim, various studies have been carried out, based on two main strategies: modeling the physical processes of the soil-mulch-greenhouse system (Mahrer et al. 1987; D'Emilio 2014) or applying numerical procedures based on Fourier series (Cenis 1989; Tiba and Ghini 2006) or on neural networks (NNs) (D'Emilio et al. 2012). However, the application and reliability of physical models require accurate knowledge of the thermo-physical properties of each component of the system, whereas NNs do not give any symbolic function which can be easily used.

Symbolic regression is an alternative method which can overcome this limitation. In conventional regression, the function used to fit data is chosen by the researcher and the goal is to determine a set of coefficients which minimizes the error. However, tackling with highly nonlinear problems and with noisy data, the choice of the function could be part of the problem. In these cases, symbolic regression can be used, as it is able to find both a symbolic function and its numerical coefficient that best fits a given set of data. Symbolic regression finds the best function starting from an initial population of expressions, formed by randomly combining primitive functions, operators, constants, and state variables. Symbolic regression is usually performed through Genetic Programming (GP) (Koza 1994; Augusto and Barbosa 2000), which use genetic algorithm to search the best function that fit the given data. GP has been used in various context of agriculture, however, to the author knowledge, no papers have used GP to model soil temperature in greenhouse neither during the growing season nor during a solarization treatment.

On this basis, the aim of this study is to develop a GP model to predict soil temperatures at different depths during a solarization treatment in closed greenhouse, based on outside air temperature, outside solar radiation flux, and time of day.

2 Materials and Methods

2.1 Field Trial

The solarization trial in which the data were collected was carried out in a closed greenhouse located in southeast Sicily, Italy, where the climate is subtropical; winters are mild with little rain and summers are hot and dry. The trial is the same as described in D'Emilio et al. (2012) so that the comparison between the results can be immediate. Specifically, it was carried out in a steel-framed tunnel greenhouse, sized 16×15 m, covering a sandy soil located on the experimental farm of the University of Catania.

The greenhouse was covered with 130 μm thick ethylene-vinyl-acetate (EVA) film. The cover material was installed at the beginning of the trial. The trial started on 15 July 2002 and ended on 26 August 2002. The soil inside the greenhouse was subdivided into 24 plots of 4.0×2.5 m each. Of these plots, 12 were mulched with a 35 μm thick EVA film and the other 12 were left uncovered. Soil temperatures were measured at 15 and 30 cm depth in a mulched plot and in a bare plot used as reference. In addition, air temperature, relative humidity, and solar radiation flux were measured inside and outside the greenhouses.

2.2 *Symbolic Regression and Genetic Programming*

The objective of symbolic regression is to determine the symbolic function that best describes a set of data, thus identifying an analytical model, which can also be used also as a predictor of response to a new set of data. Therefore, symbolic regression tries to find the best model and its parameter simultaneously.

Symbolic regression is implemented using an evolutionary algorithm, which chooses the best function using procedures inspired by natural selection. Among them, genetic programming (GP) is one of the most used and it was adopted in this study. GP is a technique whereby computer programs are encoded as a set of genes that are iteratively modified using a genetic algorithm, which selects the best programs on the basis of a fitness measure (Koza 1994). In this study, computer programs are symbolic functions and their genes are made up of primitive functions and terminals. Primitive functions include arithmetic operators, logical and basic mathematical functions. Terminals include the independent variables (inputs) of the problem and random constants.

GP starts by creating a population of randomly generated computer programs (symbolic functions) composed of the available primitive functions and terminals. In order to reduce processing times and the risk of non-convergence, it is advisable, although not mandatory, to provide a limited set of primitive functions and terminals, which are chosen on the basis of previous knowledge of the problem to be studied.

Once the first generation is obtained, each individual in the population is calculated for a set of data composed of input values, for which the corresponding output values are known. This set of data is called "training set". The ability of each function to address the problem is assessed by the fitness function, which shows how close the obtained values are to the ideal solution. Examples of fitting functions are the measure of relative and absolute error or the correlation coefficient.

The new generation is created applying genetic operations to the selected individuals. The most used genetic operations are (Augusto and Barbosa 2000): reproduction (the individual is copied to the new population), crossover (the new individual is created by recombining randomly chosen parts from two selected parent individuals), and mutation (the new individual is created by randomly mutating a randomly chosen part of one selected individual). Once the new generation has replaced the old generation, each individual is measured for fitness and the process is iteratively

repeated until a termination criterion is satisfied. Commonly used termination criteria are the achievement of a maximum generation number or of a pre-established fitness value. The symbolic function which performed the best fitness is designated as the result of the run. The generalization capability of the obtained symbolic function is evaluated by using a set of data (test set) which must not have been used during the training. In order to avoid over fitting and to improve the generalization capability a third subset of data (validation set) can be used during the iteration process for parameter optimization or model selection.

2.3 *Design of the Model*

The independent variables (inputs) chosen to be included in the terminals were air temperature outside the greenhouse, global outside solar radiation flux, existence of mulch, soil depth and time of day.

Primitive functions used to build the individuals of each population were chosen on the basis of previous studies. Specifically, the solution to the heat flow equations for the diurnal cycle is given as (van Wijk and De Vries 1963):

$$T(z, t) = T_a + A e^{-z/D} \sin(\omega t - z/D + \varphi) \quad (1)$$

where t [s] is the time, z [m] is the depth, T_a [K] is the average soil temperature, A [K] is the amplitude of the daily surface temperature fluctuations, φ is a phase constant, ω [1/s] is the angular frequency of the wave and D [m] is the damping depth that is the depth at which the amplitude of surface temperature oscillations is reduced by e^{-1} .

Therefore, the selected primitive functions were: the four arithmetic operators, sine function and exponential function. The population size was set to 1000. The Pearson correlation coefficient (R^2) was chosen as fitness function. The termination criterion was the number of generations, which was set to 5000. The study was carried out by using the open-source software package HeuristicLab 3.3.15.15587.

In order to carry out symbolic regression all data measured throughout the trial were used, with the exclusion of those data collected during the thermal transience in the soil at the beginning of the solarization treatment. Indeed, the transience is usually neglected in the evaluation of soil solarization efficacy, and therefore, it was not considered in this study. Specifically, data collected in the period 1–26 August were used. The whole dataset consisted of 4992 vectors, each containing the values of the following variables: time of day, outdoor air temperature, outdoor solar radiation flux, soil depth, soil treatment (bare soil and EVA mulched soil), and soil temperature. Dataset was randomized and, then, partitioned into three groups: the training set, made of 4224 data, the validation set and the test set, each made of 384 data.

3 Results

During the trial, the weather was characterized by clear skies for almost all the days of the treatment, and the outside values are representative of the mean seasonal climatic conditions for the area where the study was conducted.

Daily maximum values of solar irradiance ranged from 817 to 939 $W m^{-2}$ outside the greenhouse and from 637 to 783 $W m^{-2}$ inside the greenhouse. The mean value of the greenhouse transmittance was estimated at about 77%, on the basis of the ratio between inside and outside mean daily solar irradiation. The mean air temperature was 25.4 °C outside the greenhouse and 33.2 °C inside the greenhouse.

The function chosen as solution was that one corresponding to the best training solution quality, that is the highest value of R^2 calculated on the training set. Figure 1 reports the measured and estimated values both for training and test set. The results were satisfactory, as a maximum R^2 value of 0.929 was obtained for the training set, with a mean absolute error (MAE) of 0.58 °C. Correspondingly, a R^2 value of 0.915 was obtained for the test set, with a MAE of 0.62 °C. The symbolic function which represents the solution is reported in Table 1, in Excel format. The function can be copied as is in an Excel cell in any column outside the range A–E. It returns the value of soil temperature (°C) when you enter, in the same row the following inputs: outside soil temperature (°C) in column A, time of day (in twenty-fourths from 0.5 to 24) in column B, soil depth (cm) in column C, existence of mulch (1 mulched, -1 unmulched) in column D and outside solar radiation (Wm^{-2}) in column E.

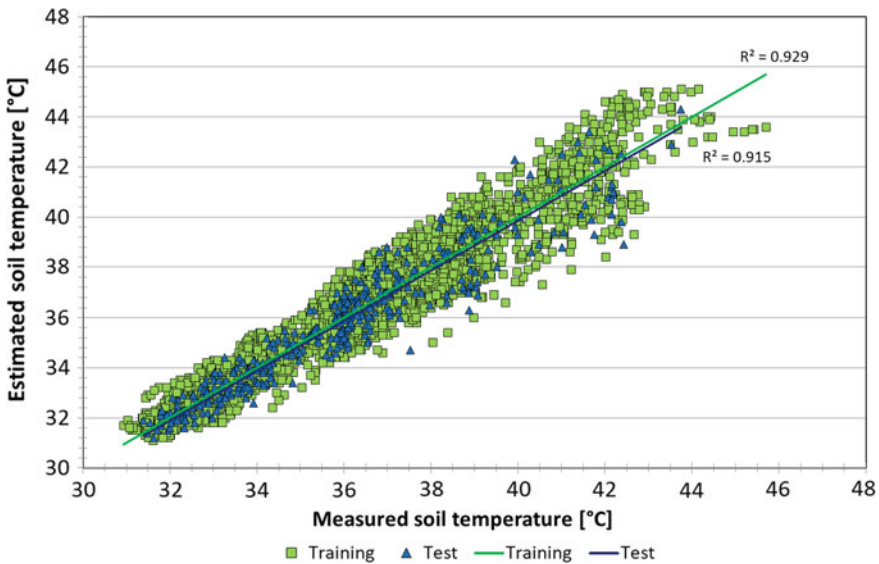


Fig. 1 Measured vs. estimated soil temperature for both training and test set

Table 1 Symbolic solution in Excel format

$$\begin{aligned}
 &= (((((-1.84864569355667 + \text{EXP}(-1.84864569355667)) / ((\text{EXP}(-1.84864569355667) - \\
 &1.79385109367038 * \$A1) + 1.04358885668898 * \$B1 * 1.63092586222355 * \$B1))) + 0.6692467997 \\
 &93663 * \$C1 * 1.04358885668898 * \$B1) - ((0.669246799793663 * \$C1 * 1.04358885668898 * \$B1 / (- \\
 &0.113950153693642 * \$A1) + (15.4430258331325 * 1.04358885668898 * \$B1 / (- \\
 &0.739524214787878 * \$D1) + (-0.737015305134327 * \$C1 - 2.55303491041863 * \$B1))) - \\
 &(((3.97272342660916 - \\
 &1.55792291866063 * \$C1) + 2.55303491041863 * \$B1) * (18.1953937287206 + 1.41261302413785 * \\
 &\$A1) + (-0.388269691129264 * \$E1))) / ((6.89152026216293 / ((-0.737015305134327 * \$C1 + (- \\
 &0.782096077199212 * \$C1 - 1.79385109367038 * \$A1) + ((-0.782096077199212 * \$C1 - \\
 &1.79385109367038 * \$A1) + 1.04358885668898 * \$B1 * 1.63092586222355 * \$B1)) / (\text{EXP}(- \\
 &1.84864569355667)) / (3.7557793115821 * \$C1)) + ((- \\
 &0.766931595010899 * \$C1 + 2.55303491041863 * \$B1) * 5.12063802234069 / (- \\
 &0.739524214787878 * \$D1) + 1.04358885668898 * \$B1 * 1.63092586222355 * \$B1) / (((1.108837052 \\
 &77595 * \$E1 / (6.89152026216293) + 15.6723299573322 * 1.04358885668898 * \$B1 / (- \\
 &0.739524214787878 * \$D1) + 1.58129712121481 * \$C1 * 1.79385109367038 * \$A1)))) / (3.6336095 \\
 &7228486 * \$C1) - \\
 &(\text{EXP}(1.10883705277595 * \$E1 / ((0.640543202985835 * \$B1 * 0.924802826260649 * \$C1 + ((3.97 \\
 &272342660916 - 1.55792291866063 * \$C1) + \text{EXP}(- \\
 &1.84864569355667) * 1.04358885668898 * \$B1 * 1.63092586222355 * \$B1) + 1.04358885668898 * \$ \\
 &B1 * 1.63092586222355 * \$B1))) + \text{SIN}(1.79385109367038 * \$A1 * 1.63092586222355 * \$B1 * 1.6309 \\
 &2586222355 * \$B1 / (0.640543202985835 * \$B1 * 1.04358885668898 * \$B1) / ((17.6964077519843 + (\\
 &17.6964077519843 + 2.55303491041863 * \$B1)))))) + ((-0.738190438967466 * \$A1 - \text{EXP}((- \\
 &0.737015305134327 * \$C1 - 0.782096077199212 * \$C1)) + 15.9512088212051 / (- \\
 &0.739524214787878 * \$D1))) * 0.0840664564909449 + 33.0019854447568)
 \end{aligned}$$

A = Outside air temperature; B = Time; C = Depth; D = Mulch; E = Outside solar radiation flux

The accuracy of the solution in estimating the data was evaluated using the mean absolute error (MAE) the root mean squared error (RMSE) and the maximum absolute error (Max AE) (Table 2). The best results were obtained for the bare soil at 30 cm depth, with the lowest values in all the error indicators for both training and test data set. The results for bare soil at 15 cm depth were very similar, with the same MAE (0.4 °C) and slightly higher MSE and Max AE.

The results for EVA mulched soil were slightly worse, although the MAE was always less than 1 °C. The results obtained in the bare soil were better than the ones

Table 2 Statistical indicators for evaluating the performance of the solution in modeling both the training and test data. All values are expressed in °C

	Training set			Test set		
	RMSE	MAE	Max AE	RMSE	MAE	Max AE
Bare soil 15 cm	0.55	0.4	2.0	0.49	0.4	1.7
Bare soil 30 cm	0.50	0.4	1.4	0.46	0.4	1.1
EVA 15 cm	1.09	0.9	3.6	1.17	0.9	3.1
EVA 30 cm	0.79	0.6	2.4	0.73	0.6	1.9

obtained in the EVA mulched soil due to the lower values of their thermal regimes. The results obtained on the training set are slightly better than those one achieved in a previous study (D’Emilio et al. 2012), carried out by using neural networks with the same data, where MAE values of 0.6 °C and slightly above 1 °C were obtained for the bare and EVA mulched soil, respectively. The results obtained on the test set are overall less accurate than those obtained in D’Emilio et al. (2012), where MAE did not exceed 0.3 °C and maximum AE was always less than 1 °C. The maximum AE values were also higher, ranging from 1.1 °C for the bare soil at 30 cm depth to 3.1 °C for the EVA mulched soil at 15 cm depth. The greatest errors occur above all in correspondence with variations in soil temperature, which are meaningful compared to the previous day. However, the greater flexibility of using a symbolic function with respect to a neural network should be considered.

The results obtained in this study are comparable with those ones obtained from physical models finalized to estimate soil temperature during a soil solarization treatment. In a previous study (D’Emilio 2014) applied to a solarization treatment in closed greenhouse, MAE values equal to 1.0 and 0.8 °C at 15 and 30 cm depth, respectively, and maximum AE equal to 2.2 and 1.8 °C were obtained in the EVA mulched soil. By applying their simulation model to a solarization treatment in a closed greenhouse, Mahrer et al. (1987) obtained a maximum RMSE of 1.2 °C and a maximum error of 1.7 °C in the estimation of soil temperature at 10 and 30 cm of depth.

4 Conclusions

In this study the estimate of soil temperature during solarization treatments in closed greenhouse is proposed, based on symbolic regression performed through genetic programming. The overall results of the validation can be considered satisfactory (MAE < 1 °C) in relation to the specific purpose of the model. The reliability of the results suggests that the proposed methodology could be used as a reference for achieving a symbolic function of wider effectiveness obtained by performing the training on a large set of data from different case studies.

Acknowledgements The activity presented in the paper is part of the research grant “University Research – Research Plan 2016/2018” by University of Catania.

References

- Augusto, D. A., & Barbosa, H. J. (2000). Symbolic regression via genetic programming. In *Sixth Brazilian Symposium on Neural Networks* (Vol. 1, pp. 173–178). IEEE.
- Cascone, G., D’Emilio, A., & Mazzarella, R. (2012). Polyamide-based film as greenhouse covering in soil solarization. *Acta Horticulture*, 927, 659–666.

- Castello, I., D'Emilio, A., Raviv, M., & Vitale, A. (2017). Soil Solarization as a sustainable solution to control tomato pseudomonads infections in greenhouses. *Agronomy for Sustainable Development*, 37(6), 59.
- Cenis, J. L. (1989). Temperature evaluation in solarized soils by Fourier analysis. *Phytopathology*, 79, 506–510.
- D'Emilio, A., Mazzarella, R., Porto, S. M. C., & Cascone, G. (2012). Neural networks for predicting greenhouse thermal regimes during soil solarization. *Transactions of the ASABE*, 55(3), 1093–1103.
- D'Emilio, A. (2014). Predictive model of soil temperature and moisture during solarization in closed greenhouse. *Transactions of the ASABE*, 57(6), 1817–1830.
- D'Emilio, A. (2017a). Soil temperature in greenhouse soil solarization using TIF and VIF as mulching films. *Transactions of the ASABE*, 60(4), 1349–1355.
- D'Emilio, A. (2017b). Parametric analysis of soil temperature in a solarization treatment in closed greenhouse. *Acta Horticulture*, 1170, 243–250.
- Katan, J. (1981). Solar heating (solarization) of soil for control of soilborne pests. *Annual Review of Phytopathology*, 19(1), 211–236.
- Koza, J. R. (1994). Genetic programming as a means for programming computers by natural selection. *Statistics and Computing*, 4, 87.
- Mahrer, Y., Avissar, R., Naot, O., & Katan, J. (1987). Intensified soil solarization with closed greenhouses: Numerical and experimental studies. *Agricultural and Forest Meteorology*, 41(3–4), 325–334.
- Miceli, A., Moncada, A., Camerata Scovazzo, G., & D'Anna, F. (2008). Influence of greenhouse volume/area ratio on soil solarization efficiency. *Acta Horticulture*, 801, 211–218.
- Morra, L., Carriero, R., Fornasier, F., Mormile, P., Rippa, M., Baiano, S., et al. (2018). Solarization working like a “solar hot panel” after compost addition sanitizes soil in thirty days and preserves soil fertility. *Applied Soil Ecology*, 126, 65–74.
- Öz, H., Coskan, A., & Atilgan, A. (2017). Determination of effects of various plastic covers and biofumigation on soil temperature and soil nitrogen form in greenhouse solarization: New solarization cover material. *Journal of Polymers and the Environment*, 25(2), 370–377.
- Öz, H. (2018). A new approach to soil solarization: Addition of biochar to the effect of soil temperature and quality and yield parameters of lettuce (*Lactuca Sativa* L. Duna). *Scientia Horticulturae*, 228, 153–161.
- Shi, C.-H., Hu, J.-R., Wei, Q.-W., Yang, Y.-T., Cheng, J.-X., Han, H.-L., et al. (2018). Control of *Bradysia odoriphaga* (Diptera: Sciaridae) by soil solarization. *Crop Protection*, 114, 76–82.
- Tiba, C., & Ghini, R. (2006). Numerical procedure for estimating temperature in solarized soils. *Pesquisa Agropecuária Brasileira*, 41(3), 533–537.
- Van Wijk, W., & De Vries, D. (1963). Periodic temperature variations in a homogeneous soil. In W. R. Van Wijk (Ed.), *Physics of plant environment* (pp. 102–143). Amsterdam: North-Holland Publishing.
- Vitale, A., Castello, I., Cascone, G., D'Emilio, A., Mazzarella, R., & Polizzi, G. (2011). Reduction of corky root infections on greenhouse tomato crops by soil solarization in South Italy. *Plant Disease*, 95(2), 195–201.
- Vitale, A., Castello, I., D'Emilio, A., Mazzarella, R., Perrone, G., Epifani, F., et al. (2013). Short-term effects of soil solarization in suppressing *Calonectria microsclerotia*. *Plant and Soil*, 368(1–2), 603–617.

Comparison of the Efficiency of Plastic Nets for Shading Greenhouse in Different Climates



Dina Statuto, Ahmed M. Abdel-Ghany, Giuseppe Starace, Paolo Arrigoni and Pietro Picuno

Abstract In order to limit the internal air temperature during summer and create optimum cultivation conditions in the greenhouses, a common solution utilized by growers is the shading against excessive solar radiation using plastic nets; this is due to their photo-selective properties. With the aim to analyse the efficacy of the shading effect of plastic nets in different climates, experimental trials have been carried out on some identical small-scale tunnels installed in two different locations, one in Mediterranean area (Acerenza—Southern Italy) and one in arid conditions (Riyadh—Saudi Arabia). These tunnels have been covered with a plastic film and shaded with a white plastic net installed either in contact or at a distance of 20 cm over the cladding film. The radiometrical characteristics of the plastic film and nets have been determined through laboratory tests, while the internal microclimatic conditions have been monitored inside these experimental tunnels in both locations. The obtained results are the base for a comparative analysis to evaluate the performance of different nets, and to explore the role of shading on the temperature reduction and quality of light in different climates.

Keywords Polyethylene nets · Crop shading · Radiometric characteristics · Micro-climatic effect

D. Statuto (✉) · P. Picuno (✉)

School of Agricultural, Forest, Food and Environmental Sciences—SAFE, University of Basilicata, Potenza, Italy
e-mail: dina.statuto@unibas.it

P. Picuno

e-mail: pietro.picuno@unibas.it

A. M. Abdel-Ghany

Department of Agricultural Engineering, College of Food and Agriculture Sciences, King Saud University—KSU, 2460, 11451 Riyadh, Saudi Arabia

G. Starace

Department of Engineering for Innovation, University of Salento, via per Monteroni, 73100 Lecce, Italy

P. Arrigoni

SACHIM s.r.l, via Mastricale 7, 70017 Putignano, BA, Italy

© Springer Nature Switzerland AG 2020

A. Coppola et al. (eds.), *Innovative Biosystems Engineering for Sustainable Agriculture, Forestry and Food Production*, Lecture Notes in Civil Engineering 67,
https://doi.org/10.1007/978-3-030-39299-4_33

1 Introduction

Agricultural production is progressively influenced by extreme meteorological phenomena and the concept of crop protection under a greenhouse, intended as a mere passive defense from hail, sun, wind, insects, birds, etc. is evolving. Greenhouse become a specialized device able to create ideal cultivation conditions thanks to a favourable microclimate, a reduction in the use of pesticides, a better exploitation of light and a controlled passage of air (Castellano et al. 2016a). The plant and/or the fruits thus become healthier, more vigorous and characterized by higher concentrations of elements beneficial for human health (e.g., antioxidants) thanks to a greater efficiency in the valorisation of natural resources and energy deriving from the sun. Cladding materials employed for covering a greenhouse destined to protect crops may play a crucial role on the quality of light arriving to the crops, reducing in different ways the radiation, mostly within the Photosynthetically Active Radiation—PAR (400–700 nm) wavebands (Schettini et al. 2011; Vox et al. 2016). Cladding materials and shading strategies may be therefore proactively selected and implemented in many Mediterranean areas, as well as in other regions (e.g., arid regions) in which the incident solar radiation during spring/summer season are often too high for a correct management of the greenhouse, to avoid undesirable effect on the crop, e.g., sunburn. A plastic net could play, if used as standalone cover or in synergy with a cladding plastic film, a fundamental role on creating more favourable microclimatic conditions during the crop growth (Castellano et al. 2016b; Picuno and Abdel-Ghany 2016) and may combine the shade effect with some specific features useful for creating suitable conditions for plants and to guarantee healthier conditions for workers. The analysis of different shading strategies has been performed by Abdel-Ghany et al. (2015), who showed that the internal position of the shading net drastically increases the generated thermal radiation within the greenhouse and the internal air temperature during the day, so the outside position for the shading net should anyway be preferred from a general thermodynamic point of view (Abdel-Ghany et al. 2016). In this paper, the results of some concerted experimental trials carried out on the basis of some previous experimental tests (Statuto et al. 2019) are reported.

2 Materials and Methods

Three identical small tunnels (Fig. 1) were realized in the experimental area of an agricultural farm located in the municipality of Acerenza (Southern Italy—40° 82' N; 15° 96' E). These small-scale tunnels, both covered with an EVAC plastic film, were left without any cultivation inside. One of them was covered only with a plastic film and was considered as the *control*, while the other two were shaded with a net overlapped on the external side, in contact with the plastic film (Fig. 1a) and at 20 cm of distance (Fig. 1b). The tested plastic net was PRISMA 90, a high density

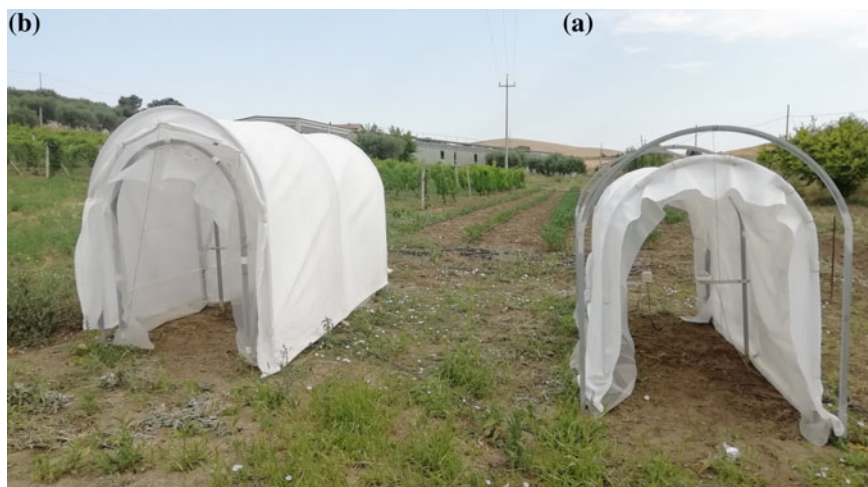


Fig. 1 Tunnels in Acerenza (Italy) covered with plastic film + net at 20 cm distance (b—left) and in contact (a—right)

thermo-reflective strong screen in HDPE flat filament net, produced by the Italian industry Sachim-Arrigoni. It is a semi-transparent milky-white colour net, with a light screening factor equal to 57% and a weight equal to 95 g/m². Both the shading plastic net and the EVAC plastic film were analyzed in the UV-VIS-NIR wavelength ranges by using a Jasco V-570 spectro-radiometer, at the Laboratory of Material Tests of the SAFE School of the University of Basilicata, Italy. The temperature (days 04 and 05 July 2019) of the external and internal air and soil were recorded by CS500-L probes (modified version of Vaisala's 50Y Humitter, Campbell Scientific Inc, Utah, USA). Relevant data were recorded by a CR10X data-logger (Campbell Sc. Inc., Utah, USA).

In parallel, another experiment was conducted in an arid climate, at King Saud University campus, Riyadh, Saudi Arabia (24° 39' N; 46° 47' E) using three identical small tunnels (Fig. 2a, b), having the same dimensions as those in Fig. 1.

These tunnels have been covered with a 200 μm thick, PE-LD film; one was kept as control and the other two were covered with a white net, with 50% nominal shading factor produced by local companies. Nets were tested in contact and at 20 cm distance from plastic film cover. In this configuration the film covered the whole side of structure and 24 holes, each of 10 cm diameter were made in the vertical sides, and roof of each tunnel for natural ventilation. The measured parameters were same as in the Acerenza experiment. In addition, the temperature of the film cover was measured using thermocouple junctions (copper constantan, type-T) attached to the outer surface of the film and protected by reflective foil.

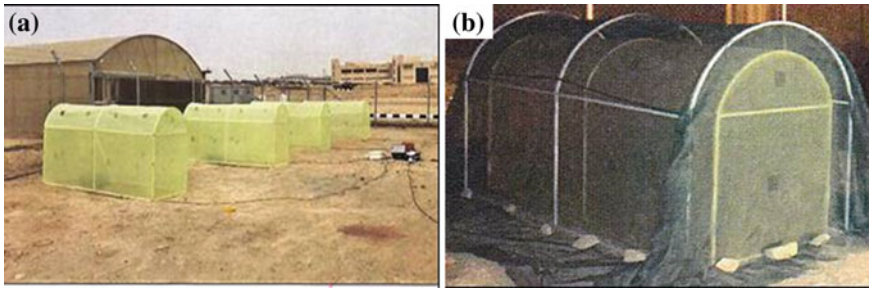


Fig. 2 Tunnels in Riyadh (Saudi Arabia) were covered with plastic film (a) and with nets at 20 cm distance over the film cover (b). The net is black—just for illustration, since the results of white-50 net are here presented for comparison

3 Results and Discussion

3.1 Experimental Tests in Acerenza (Southern Italy)

The results of the spectro-radiometrical analysis of the materials used in the experimental trials performed in Acerenza showed how the overlapping of the plastic net in contact with the cladding film has increased the shading effect in the solar range of around 36% (from 33.86 to 69.98%) that is somewhat lower than the shading effect of the net alone (57%), as it is reported by the net producer. In Fig. 3, the diagram of the solar transmittance of the plastic EVAC film and the joint combination (coupling) plastic EVAC film with the PRISMA 90 shading plastic net is reported along the whole UV-VIS-NIR wavelength [200–2500 nm].

The difference seems to have significant influence on the air and soil temperature within the two different small-scale tunnels located in Acerenza during the testing period. As shown in Fig. 4, in fact, temperatures within these close small structures were different (more than 2 °C) in the tunnel shaded with the plastic net. In particular, during daytime, it is possible to notice the shading effect of the net positioned at

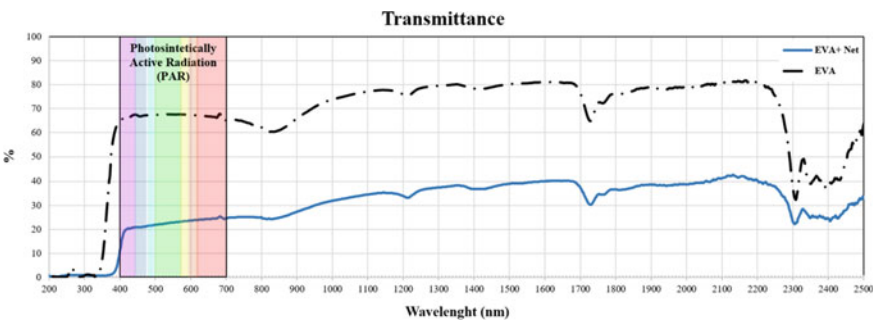


Fig. 3 Transmittance in the UV-VIS-NIR of plastic film and coupling film + net

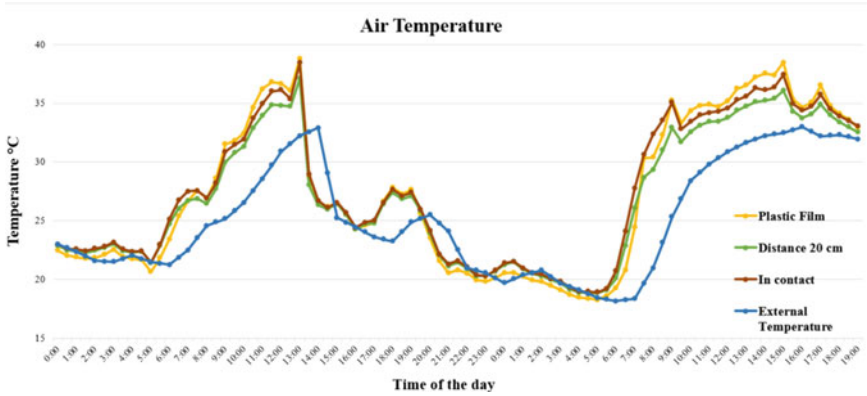


Fig. 4 Air temperature detected in the trial tunnels installed in Acerenza (Italy)

20 cm that allows a reduction of the temperature compared to the tunnel covered only with plastic film. During the night, however, the phenomenon is reversed and the temperature recorded in tunnels covered with net seems to be slightly higher than the other. The same situation appears when considering the soil temperature at the centre of each tunnel, at a depth of 5 cm (Fig. 5). Finally, in terms of the global radiation passing through the cladding surface of the small tunnels (Fig. 6), this is significantly reduced by the presence of the nets, with a slightly higher shading effect detected in the case of the net at 20 cm distance from the EVAC plastic film, probably due to some further reflections of the incoming radiation inside the air gap.

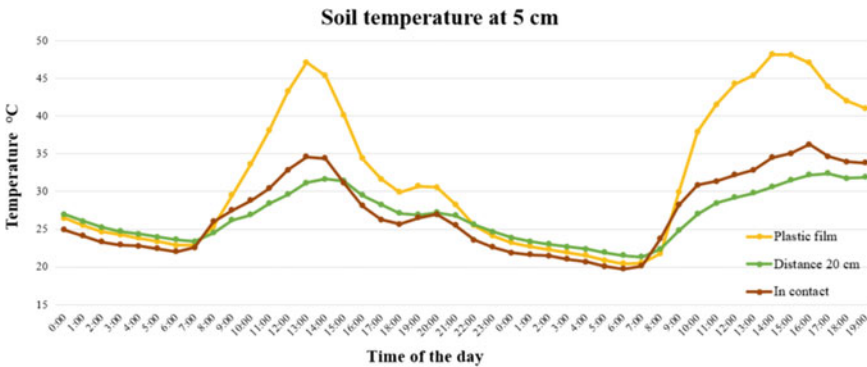


Fig. 5 Soil temperature detected at 5 cm depth in the trial tunnels installed in Acerenza (Italy)

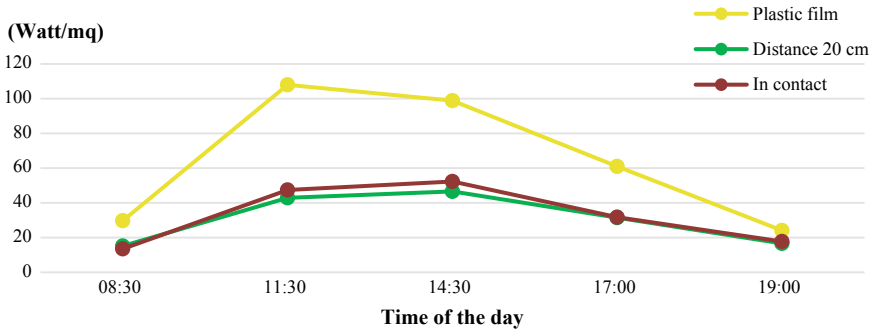


Fig. 6 Radiation inside the small tunnels installed in Acerenza (Italy)

3.2 Experimental Tests in Riyadh (Saudi Arabia)

Under intensive solar radiation flux, deploying shading nets over the cover film (in contact) reduces, of course, the transmitted radiation into the greenhouse and may not reduce the inside air temperature (Fig. 7) comparing with the control (plastic film covering). However, keeping the net apart from the film cover reduced the inside air temperature by about 5 °C, at around noon, comparing with the control (Fig. 7). The net absorbs most of the blocked solar energy by it; when the net is in contact with plastic film cover, the absorbed radiation will transfer, via convection, to the film, increase the film temperature and the thermal radiation emission into the tunnel as well. To improve the inside greenhouse microclimate, external shading is recommended and keep a distance between the net and the cover film.

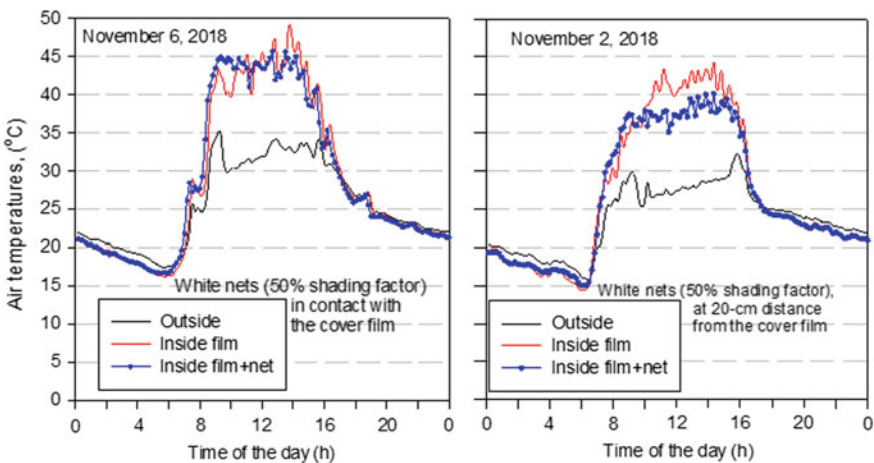


Fig. 7 Time course of air temperatures recorded outside and inside the tunnel without shading, the tunnel shading with in contact white net, and the tunnel shaded with white net at 20 cm distance

In two days (3 and 6/11/2018) having nearly the same levels of incident solar radiation flux (Fig. 8) and air temperatures, keeping the net at 20 cm distance apart from the cover film improved the microclimate, and reduced the cover and inside air temperatures (Fig. 9b). Net in contact to the film cover increased the film and inside air temperatures higher than those for net installed at 20 cm distance (Fig. 9a).

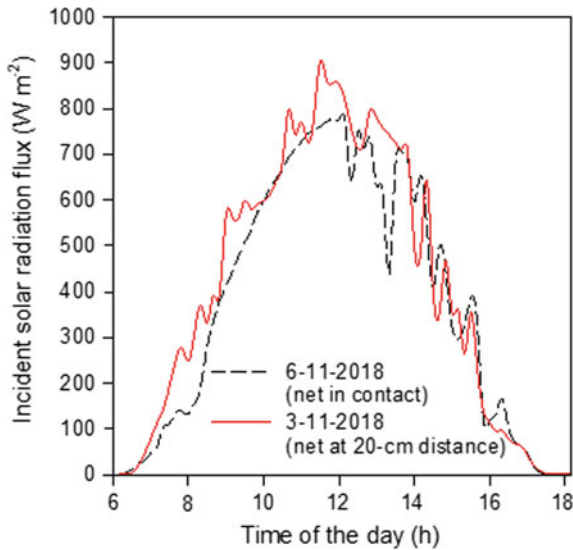


Fig. 8 Solar radiation fluxes measured in two days, at KSU campus (Riyadh) in arid climate

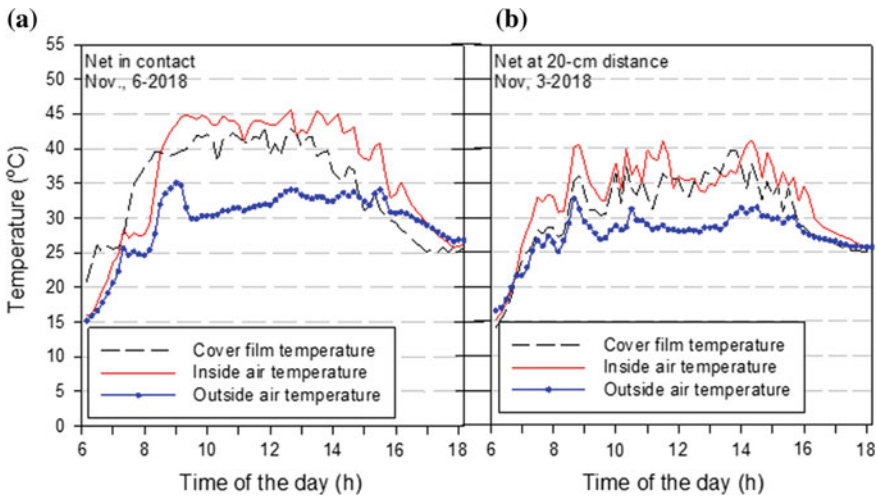


Fig. 9 Time course of the cover film, inside and outside air temperature in two cases: **a** The net is in contact to the cover film. **b** The net installed at 20 cm distance from the cover film

4 Conclusions

From the present research, it can be concluded that the shading effect of a net plays a crucial role in creating suitable conditions inside a greenhouse. Transmittance coefficients, detailed at the different wavelength ranges playing a role in the crop growth, appear as an indispensable tool, able to classify the covering material in relation to the micro-climatic parameters of the protected environment, the quality of the radiation, the temperature and the air flow. Under intensive solar radiation flux (as in arid regions), the external shading is recommended and it is suggested to keep the net apart from the film cover to achieve cooling effect in summer days. More research is anyway needed to quantify the consequences of the shading effect on the greenhouse internal climate and crop response, as well as to analyze the duration of a plastic net, depending on the site and condition of application.

Acknowledgements The Authors wish to thank the net producer SACHIM-ARRIGONI for the kind supply of the plastic nets that were tested in this experimental trial.

Many thanks to Mr. Cosimo Marano—technical staff at the SAFE School of the University of Basilicata—for his support into performing the spectro-radiometrical laboratory analysis and field tests.

References

- Abdel-Ghany, A. M., Picuno, P., Al-Helal, I., Alsadon, A., Ibrahim, A., & Shady, M. (2015). Radiometric characterization, solar and thermal radiation in a greenhouse as affected by shading configuration in an arid climate. *Energies*, 8, 13928–13937.
- Abdel-Ghany, A. M., Al-Helal, I. M., Picuno, P., & Shady, M. R. (2016). Modified plastic net-houses as alternative agricultural structures for saving energy and water in hot and sunny regions. *Renewable Energy*, 93, 332–339.
- Castellano, S., Starace, G., De Pascalis, L., Lippolis, M., & Scarascia Mugnozza, G. (2016a). Experimental results on air permeability of agricultural nets. *Journal of Agricultural Engineering*, 47(3), 134–141, 542.
- Castellano, S., Starace, G., De Pascalis, L., Lippolis, M., & Scarascia Mugnozza, G. (2016b). Test results and empirical correlations to account for air permeability of agricultural nets. *Biosystems Engineering*, 150, 131–141.
- Picuno, P., & Abdel-Ghany, A. (2016, February 23–26). Spectro-radiometrical analysis of plastic nets for greenhouse shading under arid conditions. In *Proceedings of the 44th Symposium on “Actual Tasks on Agricultural Engineering—ATAE” 2016* (pp. 469–477). Opatija (Croatia), UDC 631.234:728.98.
- Schettini, E., De Salvador, F. R., Scarascia-Mugnozza, G., & Vox, G. (2011). Radiometric properties of photosensitive and photoluminescent greenhouse plastic films and their effect on peach and cherry tree growth. *Journal of Horticultural Science & Biotechnology*, 86(1), 79–83.
- Statuto, D., Picuno, P., & Abdel-Ghany, A. M. (2019, March 5–7). Shading methods for crop protection under greenhouses in Mediterranean areas. In *Proceedings of the 47th Symposium on “Actual Tasks on Agricultural Engineering—ATAE” 2019* (pp. 297–306). Opatija (Croatia).
- Vox, G., Maneta, A., & Schettini, E. (2016). Evaluation of the radiometric properties of roofing materials for livestock buildings and their effect on the surface temperature. *Biosystems Engineering*, 144, 26–37.

Planning the Flows of Residual Biomass Produced by Wineries for Their Valorization in the Framework of a Circular Bioeconomy



Canio Manniello, Dina Statuto, Andrea Di Pasquale and Pietro Picuno

Abstract Circular economy aims to create a system that allows an optimal reuse of products and materials. In this context, the contribution provided by the valorization of residual biomass is fundamental for the production of renewable biological resources and their conversion into new added-value products. Indeed, according to an appropriate planning hierarchy, agricultural and agro-food co-products, by-products and wastes should be primarily employed to re-balance soil fertility, then valorized as new secondary raw materials used in the same agricultural sector or in different industrial chains (e.g., cosmetics, nutraceuticals, etc.). Only at the end of this process, they could be finally conveyed to energy production through co-generation. In this paper, the different residues generated by the wine production chain have been considered with reference to the Basilicata region (Southern Italy). These biomasses have been quantitatively evaluated and qualitatively classified, in order to find the most rational and convenient solution for their valorization from a technical, economic and environmental point of view. From the spatial analysis elaborated by implementing a Geographic Information System, some thematic maps have been obtained. These maps have allowed to highlight the areas with the highest concentration of residues. In this way, possible strategies for their management and valorization may be formulated, even with the support of an Internet of Things network system, aimed to allow a constant monitoring of their life cycle.

Keywords Circular bioeconomy · Agricultural biomass · Pomace · Geographic Information System · Internet of Things

C. Manniello (✉) · D. Statuto · P. Picuno
SAFE School of Agriculture, Forest, Food and Environmental Sciences, University of Basilicata,
via dell'Ateneo Lucano 10, 85100 Potenza, Italy
e-mail: canio.manniello@unibas.it

A. Di Pasquale
INNOVA Consorzio per l'Informatica e la Telematica srl, III Trav. G.B. Pirelli, snc, Z.I. La
Martella, 75100 Matera (MT), Italy

© Springer Nature Switzerland AG 2020
A. Coppola et al. (eds.), *Innovative Biosystems Engineering for Sustainable Agriculture, Forestry and Food Production*, Lecture Notes in Civil Engineering 67,
https://doi.org/10.1007/978-3-030-39299-4_34

1 Introduction

The implementation of the circular economy concept is finalized to create a system that allows for the long life, optimal reuse, refurbishment, remanufacturing and recycling of products and materials (The Ellen MacArthur Foundation 2016). The improvement of agricultural co-products, by-products and waste can play a significant role in the context of a *circular bioeconomy*, understood as the intersection of *bioeconomy* (replacement of fossil carbon with carbon from renewable biomass from agriculture, forestry and marine environment, including by-products and waste) and *circular economy*, based on the use of recycled materials to prolong their useful life and on the transformation of waste into new resources. The contribution provided by the valorization of residual biomass is indeed fundamental for the production of renewable biological resources and the conversion of these resources and waste streams into added-value products, such as food, feed, bio-based products and bioenergy (Carus and Dammer 2018).

Agricultural and agro-industrial activities generate significant quantities of residues and organic waste of different types, potentially usable not only for the production of energy but especially in high added-value molecules through biotechnological processes. The residual biomasses arise from forest waste, traditional food crops, cereal straw (e.g.: wheat, rice, barley, oats), pruning of the fruit tree (e.g.: grapes, olives, apple, peach), livestock manure (e.g.: cattle, pigs, poultry) and from the agro-food industries (olive oil mills, cellars, dairies, cereal mills, etc.). Mostly in case of residual biomass coming from the wine production chain, there are currently different possibilities of reuse of residues (Table 1) which, depending on the relevant industrial process, may have a very different environmental impact. The main outputs coming from this current scientific and technical literature show that the reuse of vinification residues could anyway find a second life in different areas, e.g.: as a substrate for the growth of plants (pomace); as a raw material for the production of tartaric acid (vinification dregs); as fuel for the electricity and the production of heat (stalks); as a raw material for the production of oil and flour (grape seeds) and fuel for the production of biogas (pomace dainty).

Some Authors (Statuto and Picuno 2015) have proposed a system for the spatial analysis of residual biomasses coming from the primary sector, identifying and including them into a Geographical Information System (GIS) aimed to the sustainable valorization of agricultural co-products, by-products and wastes produced in rural areas of the Basilicata Region from agricultural activities and small communities. These materials, after having contributed to the restoration of the level of organic matter in the soil, could be effectively exploited in different ways, e.g. as added-value components in other industrial sectors (nutraceutical, cosmetic, etc.), or in the building sector—as a natural additive that could be incorporated into clay bricks to increase their technical performance. Moreover, they would be reused in the same agricultural sector, before being considered as an alternative fuel in energy plants (Statuto et al. 2018b). Renewable energy sources represent indeed a suitable

Table 1 Main re-uses of by-products of wine production (Finesso 2015)

Residues	Possible reuse	Bibliographic source
Pomace	Wood industry or dyes for the food industry (high percentage of polyphenols)	Thorngate and Singleton (1994)
	Precursors for the synthesis of biologically active compounds (palmitic, stearic and linoleic acid)	Gallander and Peng (1980)
	Substrate favorable for plant growth	Díaz et al. (2002), Nogales et al. (2005), Bustamante et al. (2009), Paradelo et al. (2010)
	Cosmetic and nutraceutical sector	
Vinification dregs	Raw material for production of tartaric acid widely used in food sector	Braga et al. (2002)
	Bioactive functional properties (free flavonoids, anthocyanins and aglycones)	Barcia et al. (2014)
	Recovery of squalene, lipids and fatty acids useful as food additives	Gomez et al. (2004)
	Biogas production through anaerobic digestion	Rozzi and Remigi (2004)
Stalks	Compost for soil fertility restoration (high content of fiber such as lignin and cellulose and nutrients such as nitrogen and potassium)	Díaz et al. (2002), Mustin (1987)
	Substrate (in the form of compost) for the cultivation of “ <i>agaricus bisporus</i> ”, the species of mushroom most used in traditional cooking	Pardo et al. (2007)
	Fuel in electricity and heat production plants	Università Politecnica delle Marche (2013)
Grape seeds	Fuel (high calorific value)	Università Politecnica delle Marche (2013)
	Food and industrial use (grapeseed oil and grapeseed flour)	Università Politecnica delle Marche (2013)
Pomace dainty	Biogas production in anaerobic conditions	Università Politecnica delle Marche (2013)

alternative to conventional fossil fuels, due the possible advantages in terms of environmental impact reduction (Valenti et al. 2017). In this framework, different types of by-products—such as cereal straw, pruning of fruit trees, livestock manure and residues from the agro-food industries—have been recently considered at general level (Statuto and Picuno 2016; Statuto et al. 2018a). In the present paper, a further specific analysis focused on by-products generated by the wine sector only is now presented.

2 Materials and Methods

The study area consists of the total territory of the Basilicata region (Italy). It has a total geographical area of 999,224 ha, predominantly covered by rural land, with a quite low regional population medium density (57.8 inhabitants/km²). The territory of Basilicata shows wide morphological differences, mainly in elevation; it is characterized by significant seasonal variations in temperature (hot summers and very cold winters). The total agricultural area is 489,229 ha (accounting for 48.96% of the regional surface area); 368,726 ha are actually used for agricultural production (ISTAT 2011).

The analysis on the residues of the wine industry generated within this study area has been performed using a GIS (QGIS—v. 3.4) in which the municipality has been considered as the reference unit. In the year 2010, the regional surface covered by vineyards amounted to 5187.31 ha (ISTAT 2011). The area potentially producing D.O.C. (Denominazione di Origine Controllata—*Product of a Controlled Origin*) wines is 32% of the total area covered with grapes (1659.9 ha). Assuming an annual production of 8 t/ha of grapes, and calculating the territory dedicated to the whole amount of production of wine grapes (13,279.2 tons), the amount of exhausted pomace usable has been determined (Statuto et al. 2018a). Moreover, the percentage of the total amount of exhausted pomace considered in this case is the 4.6% of production of wine grapes, which means a production of about 610.8 t/year. Table 2 shows the main residual materials classifiable as by-products and the processing yields of grapes (Università Politecnica delle Marche 2013).

The pomace is produced indeed after extracting the fermented juice for white wine and after fermentation and pressing for red wine. It includes the peel, grapeseed and stems. The dreg of vinification, on the other hand, is the residue deposited after the fermentation of the wine. The stalks are composed of rachis with bunches and pedicels of the bunch. Grape seeds are essentially consisting of vine seeds. The pomace dainty, in the end, is the non-alcoholic residue of distillation.

In Table 3 (Bustamante et al. 2008) some of the typical physical and chemical characteristics of the pomace and of the various by-products are reported. They represent a significant source of organic substance, polyphenols, nitrogen, macro and microelements (Muhlack et al. 2018).

Table 2 Wine production and relevant residues from the transformation of 100 kg of grapes

Entrance (kg)	Exit (kg)	Residues classifiables as by-products (%)	
Grapes (100 kg)	Wine (77 kg)	Virgin (5, 4) and exhausted pomace (4, 6)	10
		Grape seeds	5
		Stalks	3
		Dregs	5

Table 3 Physical and chemical properties of grape pomace and other by-products

Parameter	Value	Reference	Parameter	Stalks	Pomace	Dregs	Reference
Ph	3.6 ± 0.2	Lafka et al. (2007) (red grape marc)	pH	4.4	3.8	4	Bustamante et al. (2008)
Moisture	73.6 ± 2.6% w/w		Organic substance (g/kg)	920	915	759	
Reducing sugars	1.5 ± 0.3% w/w		Oxidizable organic carbon (g/kg)	316	280	300	
Ash	4.6 ± 0.5% w/w		Water soluble carbon (g/kg)	74.5	37.4	87.8	
Cellulose	20.8% w/w	Mendes et al. (2013) (grape skins only)	Total nitrogen (g/kg)	12.4	20.3	35.2	
Hemicelluloses	12.5% w/w		P (g/kg)	0.94	1.15	4.94	
Tannins	13.8% w/w		K (g/kg)	30	24.2	72.8	
Proteins	18.8% w/w		Ca (g/kg)	9.5	9.4	9.2	
Ash	7.8% w/w		Mg (g/kg)	2.1	1.2	1.6	
			Fe (mg/kg)	128	136	357	
			Mn (mg/kg)	25	12	12	
		Cu (mg/kg)	22	28	189		
		Zn (mg/kg)	26	24	46		

3 Results and Discussion

Figure 1 shows the distribution at municipal level of the pomace, that is the main by-product arising from the transformation of the grapes. From the analysis of this map it is possible to visually identify the distribution of this resource over the whole regional territory, as well as to highlight the areas with the highest concentration of residues.

The present analysis shows how it is possible to plan a suitable system aimed to the collection and subsequent recovery of these pomace, mostly if concentrated into the two main areas of the region. Considering the north-eastern area of the region, the greater concentration of wineries and industrial areas and a radius of 10 km around a central point of the area, it is possible to identify a processing point for these easily accessible residues.

The reuse of these by-products needs to be planned also considering the spatial reference, thanks to the implementation of a GIS system, taking into account compost plants, biomass plants, distilleries and agro-food industries, together with the network analysis, with the final aim of checking distance, accessibility, and biomass amounts

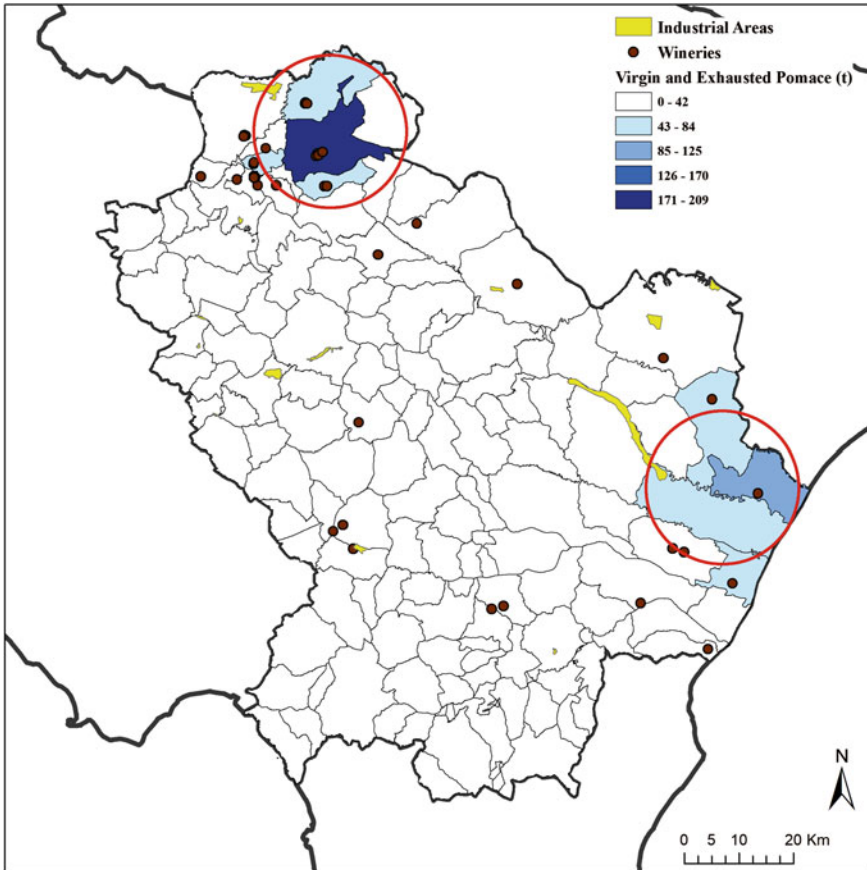


Fig. 1 Availability of pomace (virgin and exhausted) in the Basilicata region and spatial distribution of industrial areas and wineries

potentially usable, in order to facilitate and/or solve environmental issues in the process associated to their disposal.

The management of these flows would also be monitored thanks to the implementation of an Internet of Things (IoT) system, i.e. a network technology that allows the exchange of information based on sensors between objects. This technology follows all the phases of the process: from the generation of residues to collection and transport and final reuse. The advantages of this system consist in a better waste management, a better traceability of the flows during their entrainment towards the final reuse and the consequent prevention from possible illegal activities. The main disadvantage instead is linked to the operating costs, due to maintenance and renewal of the system components (Wen et al. 2018).

The final results which have been here obtained have anyway confirmed how the recovery and enhancement process of reuse of by-products is an important link

for the realization of a virtuous system aimed at improving the sustainability of the entire supply chain, enhancing its components and reducing its environmental impact (Novello 2015).

4 Conclusions

The evaluation of the possible reuse of the wine production chain residues which has been conducted in the present paper has showed as, thanks to the implementation of a GIS, several suitable hints are offered for a valorization of these agricultural biomasses. The spatial distribution, with municipal details, of these residues in the Basilicata region would therefore enable a suitable selection of the main possibilities of reuse which may be currently taken into consideration, as well as the best possible exploitation finalized to a circular economy, in which a waste becomes a new resource. This choice depends indeed on the main chemical and physical characteristics of these biomasses, which are strictly connected to the technology employed for wine production.

Finally, the IoT technology appears a very fruitful tool to be introduced as a system for evaluating the entire life cycle of these residues from their generation, to their use, transport and the best final re-use option.

Acknowledgements The activities presented in this publication have been financed by the Basilicata Region through the international research doctorate thesis financed by the Basilicata region (Innovative Doctorates Convention specializing in enabling technologies 4.0) entitled “Valorization of residual biomass generated by the primary sector for a circular bioeconomy”.

References

- Barcia, M. T., Pertuzatti, P. B., Rodrigues, D., Gómez-Alonso, S., Hermosín-Gutiérrez, I., & Godoy, H. T. (2014). Occurrence of low molecular weight phenolics in *Vitis vinifera* red grape cultivars and their winemaking by-products from São Paulo (Brazil). *Food Research International*, 62, 500–513.
- Braga, F. G., Lenskart e Silva, F. A., & Alves, A. (2002). Recovery of winery by-products in the Douro demarcated region: Production of calcium tartrate and grape pigments. *American Journal of Enology and Viticulture*, 53, 42–45.
- Bustamante, M. A., Moral, R., Paredes, C., Pérez-Espinosa, A., Moreno-Caselles, J., & Pérez Murcia, M. D. (2008). Agrochemical characterisation of the solid by-products and residues from the winery and distillery industry. *Waste Management*, 28, 372–380.
- Bustamante, M. A., Paredes, C., Morales, J., Mayoral, A. M., & Moral, R. (2009). Study of the composting process of winery and distillery wastes using multivariate techniques. *Bioresource Technology*, 100(20), 4766–4772.
- Carus, M., & Dammer, L. (2018). “The circular bioeconomy”—Concepts, opportunities and limitations. Hürth, Germany: Nova Institute. www.bio-based.eu/nova-papers.
- Díaz, M. J., Madejón, E., López, F., López, R., & Cabrera, F. (2002). Optimization of the rate vinasse/grape marc for co-composting process. *Process Biochemistry*, 37(10), 1143–1145.

- Finesso A. (2015). *Valorizzazione di scarti vinicoli per il recupero di prodotti ad alto valore aggiunto ed energia*. Tesi di laurea magistrale, Università Ca' Foscari, Venezia.
- Gallander, J. F., & Peng, A. C. (1980). Lipid and fatty acid compositions of different grape types. *American Journal of Enology and Viticulture*, 31(1), 24–27.
- Gomez, M. E., Igartuburu, J. M., Pando, E., Luis, F. R., & Mourente, G. (2004). Lipid composition of lees from sherry wine. *Journal of Agricultural and Food Chemistry*, 52, 4791–4794.
- ISTAT (Italian National Institute for Statistics). (2011). *6° Censimento Generale dell'Agricoltura. Utilizzazione del terreno dell'Unità Agricola - livello comunale*. Roma, Italy: ISTAT. <http://censimentoagricoltura.istat.it/>.
- Lafka, T. I., Sinanoglou, V., & Lazos, E. S. (2007). On the extraction and antioxidant activity of phenolic compounds from winery wastes. *Food Chemistry*, 104, 1206–1214.
- Mendes, J. A., Xavier, A. M., Evtuguin, D. V., & Lopes, L. P. (2013). Integrated utilization of grape skins from white grape pomaces. *Industrial Crops and Products*, 49, 286–291.
- Muhlack, R. A., Pothumarthi, R., & Jeffery, W. D. (2018). Sustainable wineries through waste valorization: A review of grape marc utilization for value-added products. *Waste Management*, 72, 99–118.
- Mustin, M., (1987). *Le compost: gestion de la matiere organique* (Ed. Francois Dubusc, p. 954). Paris.
- Nogales, R., Cifuentes, C., & Benítez, E. (2005). Vermicomposting of winery wastes: A laboratory study. *Journal of Environmental Science and Health Part B*, 40(4), 659–667.
- Novello, V. (2015). Filiera vitivinicola: valorizzare residui e sottoprodotti. *Disafa – Università di Torino*.
- Paradelo, R., Moldes, A. B., & Barral, M. T. (2010). Utilization of a factorial design to study the composting of hydrolyzed grape marc and vinification lees. *Journal of Agricultural and Food Chemistry*, 58(5), 3085–3089.
- Pardo, A., Perona, M. A., & Pardo, J. (2007). Indoor composting of vine by-products to produce substrates for mushroom cultivation. *Spanish Journal of Agricultural Research*, 5(3), 417–424.
- Rozzi, A., & Remigi, E. (2004). Methods of assessing microbial activity and inhibition under anaerobic conditions: A literature review. *Environmental Science and Biotechnology*, 3(2), 93–115.
- Statuto, D., Frederiksen, P., & Picuno, P. (2018a). Valorization of agricultural by-products within the “Energyscapes”: Renewable energy as driving force in modeling rural landscape. *Natural Resources Research*. <https://doi.org/10.1007/s11053-018-9408-1>.
- Statuto, D., & Picuno, P. (2016, June 26–29). Analysis of renewable energy and agro-food by-products in a rural landscape: The energyscapes. In *CIGR-AgEng Conference*, Aarhus, Denmark.
- Statuto, D., Bochicchio, M., Sica, C., & Picuno, P. (2018b). Experimental development of clay bricks reinforced with agricultural by-products. In *Symposium “Actual Tasks on Agricultural Engineering”*, Opatija, Croatia.
- Statuto D., & Picuno, P. (2015, July 19–23). Improving the greenhouse energy efficiency through the reuse of agricultural residues. In *Proceedings of the International Symposium on New Technologies and Management for Greenhouses—GreenSys 2015*, Evora (Portugal). Paper ID 236 (Acta Horticulturae).
- The Ellen MacArthur Foundation. (2016). *Intelligent assets: Unlocking the circular economy potential*. Cowes, UK: Ellen MacArthur Foundation.
- Thorngate, J. H., & Singleton, V. L. (1994). Localization of procyanidins in grape seeds. *American Journal of Enology and Viticulture*, 45, 259–262.
- Università Politecnica delle Marche. (2013). I sottoprodotti agroforestali e industriali a base rinnovabile. *Extravalore - Progetto MiPAAF Bando Settore Bioenergetico DM246/07*.
- Valenti, F., Porto, S., Cascone, G., & Arcidiacono, C. (2017). Potential biogas production from agricultural by-products in Sicily: A case study of citrus pulp and olive pomace. *Journal of Agricultural Engineering*, XLVIII, 727.

Wen, Z., Hu, S., De Clercq, D., Beck, M. B., Zhang, H., Zhang, H., et al. (2018). Design, implementation, and evaluation of an Internet of Things (IoT) network system for restaurant food waste management. *Waste Management*, 73, 26–38.

Effects of Feeding Frequency on the Behavior Patterns of Dairy Cows in an Automatic Feeding System



G. Mattachini, A. Finzi, E. Riva and G. Provolo

Abstract The objective of this study was to determine the effect of feed delivery frequency on the behavior patterns and on milk production of lactating dairy cows. The study was conducted on a commercial dairy farm. Feeding treatments of mixed ration consisted of two different frequencies replicated in two periods. Cows were fed 9 times per day (9×) and 6 times per day (6×). Lying behavior of 24 dairy cows was electronically monitored. Feeding frequency had no effect on the daily lying time and lying bouts. High feeding frequency may disturb the duration of lying bouts and alter the pattern of lying behavior throughout the day, affecting mainly the lying time before and after the provision of fresh feed. The results obtained may indicate that a very high feeding frequency disturbs the cows during their resting periods and thus influences the animal comfort.

Keywords Feed delivery frequency · Lying behavior · Dairy cow · Automatic feeding system (AFS)

1 Introduction

Feeding systems in modern dairy farms is an important issue in relation to animal welfare. Moreover the choice between the different types available on the market implies economic and technological consideration. Feeding a total mixed ration (TMR) is common practice on many farms, mostly represented by conventional manually operated mixer-feeder wagons. The delivery of feed has been shown to have the greatest influence in stimulating feeding activity in dairy cows (DeVries and von Keyserlingk 2005). Delivery of TMR in conventional feeding schedules of lactating dairy cattle for most dairy operations remains twice per day (2×). However, many farmers elect to feed their cows only once per day to minimize labor cost. Recently developed

G. Mattachini (✉) · A. Finzi · E. Riva · G. Provolo
Department of Agricultural and Environmental Sciences, Università degli Studi di Milano, via
Giovanni Celoria 2, 20133 Milan, Italy
e-mail: mxlelex@libero.it

© Springer Nature Switzerland AG 2020

A. Coppola et al. (eds.), *Innovative Biosystems Engineering for Sustainable Agriculture, Forestry and Food Production*, Lecture Notes in Civil Engineering 67,
https://doi.org/10.1007/978-3-030-39299-4_35

305

automatic feeding systems (AFS) for TMR make it easy to distribute rations frequently and manage feed intake, stimulate cow activity, reduce leftovers, adapt the volume of ration to the size of the animal group, and reduce labor costs (Belle et al. 2012).

Lying, is one of the most important behaviors performed by dairy cattle. Cows show preference for lying over feeding and social contact when subject to various time constraints, so feeding frequency is affecting lying behavior (Munksgaard et al. 2005).

Mäntysaari et al. (2006) found that cows fed five times a day increased restlessness and decreased lying time compared to cows fed once a day. In contrast, DeVries et al. (2005) and Hart et al. (2014) found that there was no change in total daily lying time with increased frequency of feed delivery, but the daily distribution of lying time was influenced. Measures of lying behavior are important indicators of cow comfort, providing valuable information on how cows interact with their environment. Total lying time (Haley et al. 2000; Fregonesi and Leaver 2001), number of lying bouts and bout duration (Haley et al. 2000) were identified as sensitive measures of stall comfort and have been evaluated as appropriate welfare indicators for lactating dairy cows (Fregonesi and Leaver 2001). Lying behavior in free-stall barns is affected by design and management factors, including milking and feeding management (DeVries and von Keyserlingk 2005; Munksgaard et al. 2005). Studies have measured lying behavior continuously over a few days by using data loggers (Ito et al. 2009), through time-lapse video (Haley et al. 2000) or by a computer vision-based system (Porto et al. 2013). Electronic data loggers are widely available and can be used to measure lying behavior accurately, including the total time spent lying down, the number of lying bouts, and the duration of each bout for individual cows (Mattachini et al. 2013).

To date, the majority of studies that have examined the effect of feeding frequency on cow behavior and performance have taken place in conventional feeding systems in combination with parlor-milking systems. The range of the feeding frequencies in these studies has been between 1× and 5×, and with cows being milked in a conventional parlor at frequencies of 2× and 3×. However, an AFS enables more frequent delivery of fresh feed compared to conventional feeding systems, and in combination with an AMS, provides cows more freedom to determine individual critical behavioral activities (feeding, lying and milking).

The objective of this study was to determine the effect of feed delivery frequency on the behavior patterns and on milk production of lactating dairy cows.

2 Materials and Methods

2.1 *Animals, Housing and Feed*

The study was conducted between December 2010 and January 2011 on a commercial dairy farm located in Friesland (The Netherlands) where animals were milked with an AMS (DeLaval VMS, DeLaval International AB, Tumba, Sweden) and fed by an AFS (Optimat Standard, DeLaval, Tumba, Sweden).

The barn housed 83 lactating Holstein-Friesian cows; 34 of these were primiparous and 49 were multiparous (at the beginning of the study parity = 2.1 ± 1.4 , DIM = 188.4 ± 128.8 ; mean \pm SD). The barn featured a loose-housing layout with a total of 129 cubicles with rubber mats. The manger, positioned sideways in the barn, had 85 feeding spaces. Twenty-four lactating cows, of which five were primiparous and 19 were multiparous (parity = 2.5 ± 1.5 , DIM = 179.4 ± 129.7 at the beginning of the data collection period) were randomly selected for behavioral tracking. The milking area consisted of two AMS units and a nearby waiting area in front of the unit entrance, with selectively guided cow traffic. All cows were fed with the same MR (44.0 kg/d per cow).

2.2 *Experimental Treatments and Behavioral Recording*

Treatments consisted of two different frequencies of MR distributions. Each treatment lasted 7 d, in which a 3 d adjustment period (Devries et al. 2005) was followed by 4 d of data collection on the treatment effects (Ito et al. 2009; Vasseur et al. 2012) replicated in two experimental periods.

The two treatments were (1) a feed delivery frequency of $9 \times$ (at 0300, 0550, 0730, 0900, 1215, 1400, 1520, 1830 and 2130 h) and (2) a feed delivery frequency of $6 \times$ (at 0550, 0900, 1215, 1520, 1830 and 2140 h). In this farm, feed was not pushed up.

Lying behavior patterns of the cows were automatically recorded using two types of electronic data loggers. HOB0 Pendant G Data Loggers (Onset Computer Corporation, Pocasset, MA) were utilized to measure the leg orientation at 1 min intervals and allowed all the lying behavior data to be collected electronically (Mattachini et al. 2013). IceTag Activity Sensors (v. 2.004, IceRobotics Ltd., Edinburgh, UK) were used to sample acceleration with a frequency of 8 Hz, and to determine the percentage of time the cows spent lying for each recorded second (Mattachini et al. 2013). Data collected by the data loggers were used to calculate lying times (h/d), bout frequency (n/d) and bout duration (min/bout) for each cow and each day of the treatment. Pre-feeding and post-feeding lying time (min) was calculated as the average lying time per cow during the 60 min before and after provision of each fresh feed delivery (feeder wagon starts automatic feed distribution). These two 60 min periods were identified in an explorative analysis as the times when behavior of cows was especially influenced by feed delivery (DeVries and von Keyserlingk 2005).

The behavioral observation period covered the days of treatment (4 d) for each feed delivery frequency in each period for a total of 16 d.

2.3 Statistical Analysis

Descriptive statistics were used to characterize the distribution of the variables in the study using the MEANS and FREQ procedures of SAS® software (Copyright© 2008, SAS Institute Inc. SAS and all other SAS Institute Inc. product or service names are registered trademarks or trademarks of SAS Institute Inc., Cary, NC, USA). Before analyses, all data were screened for normality using the UNIVARIATE procedure of SAS® software. Data transformations were applied using logarithmic transformations ($\log_{10}(x)$) to achieve normal distributions. Lying behavioral data (lying times, bout frequency, bout duration and pre-feeding and post-feeding time) and milk yield were analyzed using the GLM procedure of SAS® software for testing the effects of feeding frequency treatment (9× and 6× feed delivery), period and interaction between feeding frequency and period (Bava et al. 2012). The group of cows monitored was considered the experimental unit, and the days (in each experimental period) was considered as the replicate. Least squares means and standard errors were determined using the LSMEANS and STDERR statement in PROC GLM of SAS® software.

In the statistical analyses, significance was declared when $P < 0.05$ (* $P < 0.05$; ** $P < 0.01$).

3 Results

Feeding frequency had no effect on the daily lying time and lying bouts (bout frequency and bout duration, Table 1). We did not find an effect of high feed delivery frequency on lying time during the 60 min before and after provision of fresh feed (P

Table 1 Effect of feeding frequency on lying behavior and milk yield (least-squares means)

Variables	Feeding frequency treatment		Effect	
	9×	6×	SE	<i>P</i>
Lying time (h/d)	11.4	11.4	0.30	0.82
Bout frequency (n/d)	9.4	9.3	0.43	0.76
Bout duration (min/bout)	82.9	81.1	3.90	0.64
Pre-feeding lying (min)	28.9	29.7	1.12	0.52
Post-feeding lying (min)	25.1	24.1	1.03	0.32
Milk yield (kg/d)	28.5	28.1	0.41	0.22

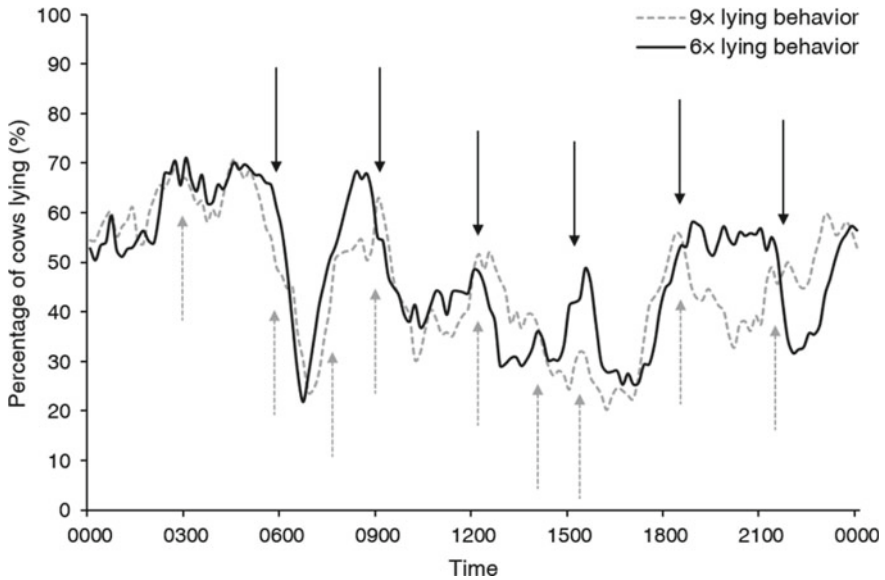


Fig. 1 Percentage of cows lying down over a 24 h period. Cows were monitored under two feed delivery frequencies (9× and 6×). Data are averaged for 4 d for each treatment and period. Solid black arrows indicate times at which the cows were fed 6× and the dashed grey arrows indicate times at which the cows were fed 9×

= 0.52 and $P = 0.32$ on the pre-feeding and post-feeding lying time, respectively; Table 1).

The differences on the pattern of lying time throughout the day (Fig. 1) between treatments were not marked. When cows were fed 6×, they took longer to lie down after the second last delivery (1830 h) and less time to lie down after the last delivery (2140 h) compared with when they were fed 9×. The average milk yields of 28.5 and 28.1 kg/d per cow for the 9× and 6× treatments, respectively, were not significantly different ($P = 0.22$).

4 Discussion

In the current study, cows spent on average 11.4 h/d lying down. These values are comparable to values ranging from 11.0 to 11.9 h/d reported in the literature for conventional milking parlors (Ito et al. 2009; Gomez and Cook 2010) and to a lying duration of 11.2 ± 2.5 h/d observed by DeVries et al. (2011) in an AMS herd. The change in feeding frequency did not result in a change in daily lying time. Our results correspond with those reported in previous studies (DeVries and von Keyserlingk 2005; DeVries et al. 2005; Hart et al. 2014), which showed that an increased frequency of feed delivery did not affect the total daily lying time. However, the studies by

Mäntysaari et al. (2006) on increasing feeding frequency from one to five times a day resulted in a decreased daily lying time.

We observed that the frequency of feed delivery affected the pattern of lying behavior throughout the day (daily distribution of lying time), although in a limited way. These patterns could reflect the periods of higher feeding activity throughout the day of the cows, which were related to feed delivery times.

We did not observe an influence of feed delivery frequency on the frequency of lying bouts or lying bouts duration. Deming et al. (2013) found that lying bout duration tended to be positively associated with increased space at the feed bunk.

Automatic milking systems in combination with AFS provide cows more freedom to determine individual moments of lying, feeding and milking. Compared to conventional dairy systems, where synchronization of behavior does still occur (particularly around times of milking and feed delivery), in AFS and AMS behavioral activity is distributed over a 24 h period. This may explain the subdued effects of feeding frequency found in this study in comparison with other studies that have examined the effect of feeding frequency in conventional feeding systems in combination with parlor-milking production systems.

5 Conclusions

In conclusion, results obtained, may indicate that a very high feeding frequency disturbs the cows during their resting periods and thus influences animal comfort. High feeding frequencies should be avoided to allow cows to distribute their lying time more evenly over the course of the day. In AFS, it is necessary to find an optimal feeding frequency that is high enough ($6\times$ feed delivery) to distribute uniformly the feeding time of cows over the course of the day, but not so high (no more than $9\times$ feed delivery) that it disturbs the pattern of cows lying behavior.

References

- Bava, L., Tamburini, A., Penati, C., Riva, E., Mattachini, G., Provolo, G., et al. (2012). Effects of feeding frequency and environmental conditions on dry matter intake, milk yield and behaviour of dairy cows milked in conventional or automatic milking systems. *Italian Journal of Animal Science*, *11*(e42), 230–235.
- Belle, Z., André, G., & Pompe, J. C. A. M. (2012). Effect of automatic feeding of total mixed rations on the diurnal visiting pattern of dairy cows to an automatic milking system. *Biosystems Engineering*, *111*, 33–39.
- Deming, J. A., Bergeron, R., Leslie, K. E., & DeVries, T. J. (2013). Associations of housing, management, milking activity, and standing and lying behavior of dairy cows milked in automatic systems. *Journal of Dairy Science*, *96*, 344–351.
- DeVries, T. J., Deming, J. A., Rodenburg, J., Seguin, G., Leslie, K. E., & Barkema, H. W. (2011). Association of standing and lying behaviour patterns and incidence of intramammary infection in dairy cows milked with an automatic milking system. *Journal of Dairy Science*, *94*, 3845–3855.

- DeVries, T. J., & von Keyserlingk, M. A. G. (2005). Time of feed delivery affects the feeding and lying patterns of dairy cows. *Journal of Dairy Science*, *88*, 625–631.
- DeVries, T. J., von Keyserlingk, M. A. G., & Beauchemin, K. A. (2005). Frequency of feed delivery affects the behaviour of lactating dairy cows. *Journal of Dairy Science*, *88*, 3553–3562.
- Fregonesi, J. A., & Leaver, J. D. (2001). Behaviour, performance and health indicators of welfare for dairy cows housed in strawyard or cubicle systems. *Livestock Production Science*, *68*, 205–216.
- Gomez, A., & Cook, N. B. (2010). Time budgets of lactating dairy cattle in commercial freestall herds. *Journal of Dairy Science*, *93*, 5772–5781.
- Haley, D. B., Rushen, J., & de Passillé, A. M. (2000). Behavioural indicators of cow comfort: Activity and resting behaviour of dairy cows in two types of housing. *Canadian Journal of Animal Science*, *80*, 257–263.
- Hart, K. D., McBride, B. W., Duffield, T. F., & DeVries, T. J. (2014). Effect of frequency of feed delivery on the behaviour and productivity of lactating dairy cows. *Journal of Dairy Science*, *97*, 1713–1724.
- Ito, K., Weary, D. M., & von Keyserlingk, M. A. G. (2009). Lying behavior: Assessing within- and between-herd variation in free-stall-housed dairy cows. *Journal of Dairy Science*, *92*, 4412–4420.
- Mäntysaari, P., Khalili, H., & Sariola, J. (2006). Effect of feeding frequency of a total mixed ration on the performance of high-yielding dairy cows. *Journal of Dairy Science*, *89*, 4312–4320.
- Mattachini, G., Riva, E., Bisaglia, C., Pompe, J. C. A. M., & Provolo, G. (2013). Methodology for quantifying the behavioral activity of dairy cows in freestall barns. *Journal of Animal Science*, *91*, 4899–4907.
- Munksgaard, L., Jensen, M. B., Pedersen, L. J., Hansen, S. W., & Matthews, L. (2005). Quantifying behavioural priorities—Effects of time constraints on behaviour of dairy cows, *Bos taurus*. *Applied Animal Behaviour Science*, *92*, 3–14.
- Porto, S. M. C., Arcidiacono, C., Anguzza, U., & Cascone, G. (2013). A computer vision-based system for the automatic detection of lying behaviour of dairy cows in free-stall barns. *Biosystems Engineering*, *115*, 184–194.
- Vasseur, E., Rushen, J., Haley, D. B., & de Passillé, A. M. (2012). Sampling cows to assess lying time for on-farm animal welfare assessment. *Journal of Dairy Science*, *95*, 4968–4977.

Shading Screens Characterization by Means of Wind Tunnel Experiments and CFD Modeling



E. Santolini, D. Torreggiani and P. Tassinari

Abstract The use of shading screens in the protected cultivation sector is widespread, due to the fact they allow both to reduce the heat load and thus to control temperature, and to have lower and uniform levels of light intensity inside greenhouses. An extended selection of shading screens is available on the market, with different colors, material, and textures. The choice of the best screen depends on the specific application and needs of the grower. Despite the positive action of the screens, some screens can also negatively affect ventilation and indoor climate, since their porosity can generate extra mass, heat and momentum transfer resistance. Most studies have evaluated the screen-related parameters, such as permeability and porosity, and the screen effect on ventilation referring to screens with simple and regular textures, which is not the case of the new screen types. The reliability of the literature models for these parameters' estimation of new type of screens is not certain. In this work, these parameters have been evaluated for three new screen types, available on the market, under different approaches. An experimental approach based on image analysis together with wind tunnel tests has been set up to yield the permeability and inertial coefficient. On the other hand, another methodology is based on the detailed modeling of the shading screen and on the CFD simulation to obtain the relation between air velocity through a screen and the relative pressure drop, avoiding any experiment. A representative section of the screen has been chosen for CFD simulations and the numerical results have been validated by comparison with Particle Image Velocimetry (PIV) data. This has allowed both to improve the model and to evaluate its effectiveness in simulating this specific fluid dynamics domain. By these novel approaches, the basis for extending this knowledge about the characterization of the screens used in agriculture have been laid.

Keywords Shading screens · Protected cultivation · Computational fluid dynamic · Wind tunnel · Particle image velocimetry · Numerical approach

E. Santolini (✉) · D. Torreggiani · P. Tassinari
Department of Agricultural and Food Sciences, University of Bologna,
Viale G. Fanin 48, 40127 Bologna, Italy
e-mail: enrica.santolini2@unibo.it

© Springer Nature Switzerland AG 2020
A. Coppola et al. (eds.), *Innovative Biosystems Engineering for Sustainable Agriculture, Forestry and Food Production*, Lecture Notes in Civil Engineering 67,
https://doi.org/10.1007/978-3-030-39299-4_36

1 Introduction

The development of new materials and technological advancements allow producing a considerable number of screen types for the agricultural sector available on the market. In the protected cultivation sector, thermal screens can be used as a cheap and effective way to reduce the night-time heat loss, shading screens can reduce the daytime heat load and thus control temperature and insect-proof screens prevent the entrance of both insects and birds (Miguel 1998). The screens usage, in particular the application of thermal and reflective screens in greenhouses, has increased in all those countries—such as Italy and other Mediterranean countries—where solar radiation would remarkably affect the possibility to control light and climate inside greenhouses and thus to obtain suitable conditions for plant growth over the entire product (Castellano et al. 2009). Considering the shading devices, the choice of the suitable screen among the various solutions available depends on the specific usage and production needs of the grower. Due to their characteristics and position, they can negatively affect ventilation and indoor climate because they can generate extra mass, heat and momentum transfer resistances (Katsoulas et al. 2006; Santolini et al. 2018). Their low porosity can affect the ventilation, reduce air velocity and modify the air patterns in the cultivation area, and consequently the indoor climatic conditions, increasing air temperature and humidity, and thus causing less favorable conditions for the crops. However, most of the case studies available in literature have been analyzed screens characterized by the regularity of weft and warp threads disposition (Miguel et al. 1998; Teitel 2010; Valera et al. 2006). Nowadays, shading screen texture presents less regular geometry and the ratio of open to total area are not easily identifiable. For these reasons, the porosity is not geometrically estimable and consequently also the other parameters related to the ventilation. Then, more sophisticated systems should be available to obtain the physical parameters driving the ventilation processes, and thus to investigate the effect of screens on ventilation and microclimate inside greenhouses. Considering the porous media approach to estimate the screen effect, the pressure drop through a porous media, depending from the fluid velocity, is defined by the Darcy-Forchheimer's law (Sobieski and Trykozko 2014a, b, b). The parameters, needed to evaluate the air flow characteristics of screens, are intrinsically related to the porosity of the surfaces and several equations are available in the scientific literature, allowing to obtain them from porosity (Miguel et al. 1997; Miguel 1998). New relations could be found also in Flores-Velazquez and Montero (2008). Several authors have used these equations to derive the parameters necessary to perform CFD studies of greenhouses with screens (Campen and Bot 2003; Fattassi et al. 2003; Molina-aiz et al. 2004). However, Teitel (2007) have demonstrated that these relations Eqs. (4)–(6) could lead to an overestimation of the parameters, between 1.5 and 5 times. Therefore, further experimental trials should be performed to assess the physical parameters of screens with complex textures and check the applicability of the existing equations relating permeability and other airflow coefficients to porosity. A CFD approach has demonstrated to be an advantageous and efficient way to simulate the airflow through the porous surface of the screens (Thaker

et al. 2019; Teitel 2010). The general goal of this paper is to define and test both experimental and simulation methodologies, aimed to assess fluid-dynamics properties of shading screens with complex textures and their relationships, suitable to evaluate their impact on ventilation in the greenhouse cultivation field. Novel methodologies have been defined in an alternative and interchangeable way for the research and definition of these specific parameters.

2 Theory

The fundamental law linking pressure drop and velocity of the fluid passing through a porous media is the Darcy's law (Gray and O'Neill 1976; Sobieski and Trykozko 2014a, b). This relation can be applied to flows of gases, liquids or mixtures:

$$\frac{\Delta p}{\Delta x} = -\frac{\mu}{K}v, \quad (1)$$

where μ is fluid dynamic viscosity (Pa s), K is permeability to the fluid (m^2) of the media and u is the fluid velocity. However, the Darcy's law suitably describes the flow in porous media for low flow velocities (Reynolds number lower than 10) if the fluid can be treated as incompressible and Newtonian (Hellström and Lundström 2006). Increasing the fluid velocity and so the Reynolds number, the discrepancies between experimental data and the Darcy's law results become significant, as presented in Hellström and Lundström (2006). These differences have been explained and described by Forchheimer, which added a term to the Darcy's law, the inertial effects, representing of kinetic energy in the equation (see Eq. 2) (Sobieski and Trykozko 2014b; Ewing et al. 1999):

$$\frac{\Delta p}{\Delta x} = \frac{\mu}{K}v + \rho\beta|v|v \quad (2)$$

$$\beta = \frac{Y}{K^{1/2}} \quad (3)$$

where K is permeability to air (m^2), μ is air dynamic viscosity (Pa s), ρ is air density and β is non-Darcy coefficient (1/m), which is specifically defined as visible in Eq. (3). This law has been applied in the modeling and characterization of various screen's types, applied in the agricultural sector (Miguel et al. 1997). The permeability and the inertial coefficient of a porous media can be derived from Eq. (2). Miguel (1998) presented a model for relating Y and K with the porosity for agricultural screens:

$$K = 3.44 \times 10^{-9}\alpha^{1.6} \quad \text{and} \quad Y = 4.3 \times 10^{-2}\alpha^{-2.13} \quad (4)$$

where α is the porosity of the samples. Valera et al. (2005) presented a similar correlation obtained by experimentally testing eleven screens in a wind tunnel:

$$K = 5.68 \times 10^{-8} \alpha^{3.68} \quad \text{and} \quad Y = 5.67 \times 10^{-2} \alpha^{-1.1604} \quad (5)$$

Flores-Velazquez and Montero (2008) suggested different relations for K and Y, based on previously published data from previous works, presented in Eq. (6):

$$K = 2 \times 10^{-7} \alpha^{3.3531} \quad \text{and} \quad Y = 0.342 \times 10^{-2} \alpha^{-2.5917} \quad (6)$$

These relations are frequently used for the determination of porous media characteristics, mainly for homogeneous texture screens.

3 Materials and Methods

The airflow related parameters of a porous media, such as porosity and permeability, are significant for understanding how the flow through it is affected. The shading screens details and the methodologies and set up applied for characterizing the airflow parameters are presented.

3.1 Shading Screens Characteristics

Three shading screens frequently used in Northern Italy region have been selected (Shading screens produced by Svensson Corporation). They are the Harmony 3647 FR, the Harmony 4215 O FR, and the Harmony 5220 O FR. These are commonly used in the cultivation of various horticultural crops, including ornamental plants, and they belong to the same family of products, with similar characteristics related to direct and diffusive sunlight. On the contrary, they present remarkable differences in terms of texture, as shown in Table 1.

3.2 Wind Tunnel Experiments and Image Analysis

The experimental tests have been conducted in a wind tunnel, placed in the Fluid-dynamics and Heat Transfer laboratories of the Department of Industrial Engineering of the University of Bologna (DIN). It is a wind tunnel with a test chamber of $30 \times 30 \times 60$ cm as dimensions. It is composed by a honeycomb of 90 cm of side, connected to a convergent channel, which is directly connected with the test section, as visible in Fig. 1, and the fan has a diameter of 45 cm and can reach the limit frequency of 50 Hz. This system has been used for the evaluation of the parameters K, Y, and

Table 1 Geometrical characteristics of the three screens investigated


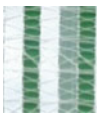
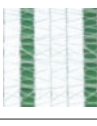
Screens	Texture	Geometry
H3647		<ul style="list-style-type: none"> - 100% Polyester - Weight 57 g/m³ - Width strips 4 mm - Pattern: 3 transparent diffuse, 1 white diffuse, 2 transparent diffuse, 1 white diffuse
H4215		<ul style="list-style-type: none"> - 100% Polyester - Weight 54 g/m³ - Width strips 4 mm - Pattern: 2 white diffuse, 1 open, 1 white diffuse, 1 transparent diffuse, 1 open
H5220		<ul style="list-style-type: none"> - 100% Polyester - Weight 61 g/m³ - Width strips 4 mm - Pattern: 3 white diffuse, 1 open



Fig. 1 Picture of the wind tunnel test chamber and the honeycomb at the beginning of the tunnel

β of the studied screens. Considering the need to obtain the relation between the frequency of the fan and the velocity of the fluid, the calibration curve of the system has been determined. The air velocity has been measured in three different positions along the width of the test chamber (3 cm from both walls and in the middle of the section), with a Pitot probe and a micro-manometer with a sensibility of 0.01 m/s (Model 8710 DP-Calc Micromanometer). The measurements have been performed every 30 s repeated for four times in each position, and they have been repeated for a fan frequency progressively higher from 5 to 30 Hz. The same data sampling has been performed with the presence of each shading screen studied. In addition to the air velocity, the pressure drop across the screen has also been collected. From the elaboration of the data collected with empty wind tunnel and with the presence of each screen, the calibration curves of the system in the four different configurations have been obtained with the relative characteristic equation of the air velocity depending on the fan frequency.

3.3 CFD Approach and PIV Test

For the CFD approach, H5220 has been modeled as study case with a scaled approach. A model 3×3 cm of the screen has been created using Autodesk Inventor, by a scanned image of the screen sample, which has been geometrically model in detail, as visible in Fig. 2.

The meshing process has been performed using ICEM CFD and the simulations have been conducted using Ansys-Inc. Fluent 17.2. The meshes are unstructured meshes of tetrahedral elements for both the approaches, obtained by the application of Robust (Octree) method.

The turbulence model used in the simulation has been the k- epsilon standard model, convergence criteria of 10^{-5} for continuity and 10^{-6} for all other parameters have been defined. The porous areas have been modeled as an interior surface and the stripes and thread as walls, impermeable to the fluid passage. The grid convergence study has been performed on seven meshes from 3×10^5 to 1.4×10^7 cells and the selected one has been of 7.6×10^6 . 2D Particle Image Velocimetry (PIV) measurements in wind tunnel have been performed to validate, from a physical point of view, the CFD model and evaluate the realistic modeling of the phenomenon by this approach. The PIV setup consists of a Dantec Dynamics System with two cameras Flowsense M2/E with Nikon lenses AF micro-Niccor 60 mm, a New Wave Research Laser with a cylindrical lens to produce a laser sheet, a synchronizing system for triggering the image acquisition with the laser shots. Flow-Manager v. 4.71 software has been used for the post-processing of the optical images. An average of a number of instantaneous experimental velocity maps is needed to compare PIV results with CFD velocity distributions. The fan frequency has been set at 10 Hz that corresponds to a 1 m/s of air velocity. In this case, the results of the test have been 40 raw velocity vector maps representative of the airflow velocity, which has been analyzed by moving average filter. Then the results have been processed through Matlab, to obtain averaged global values of velocity, considering performing an averaged picture of the phenomenon.

Fig. 2 CAD model for CFD



4 Results and Discussions

In this section, will be presented the results of the experimental and CFD approaches.

4.1 Experimental Approach

As shown in Fig. 3, the data of velocity and pressure drop have been analyzed to define the characteristics of the screens. The resulting relations by the fitting of the data have allowed deriving the values of permeability and inertial coefficient of the three cases.

From these curves, it is visible that the screens H4 and H5 have a more similar trend and coefficients of the equations. However, substituting the coefficients obtained from the fitting curves in Eqs. (7) and (8), it is possible to obtain K and Y:

$$K = \frac{\Delta x \mu}{b} \tag{7}$$

and

$$Y = \frac{a\sqrt{K}}{\Delta x \rho} \tag{8}$$

where ρ is 1.225 (kg/m³), μ is 1.81×10^{-5} (Pa s), and Δx is the thickness of samples, which has been measured by a mechanical feeler. The results have been reported in Table 2. These results outline the fact that the permeability values differ from each other by order of magnitude.

Although the permeability tends to decrease with the opening spaces reduction, the inertial coefficient does not increase according to the same trend.

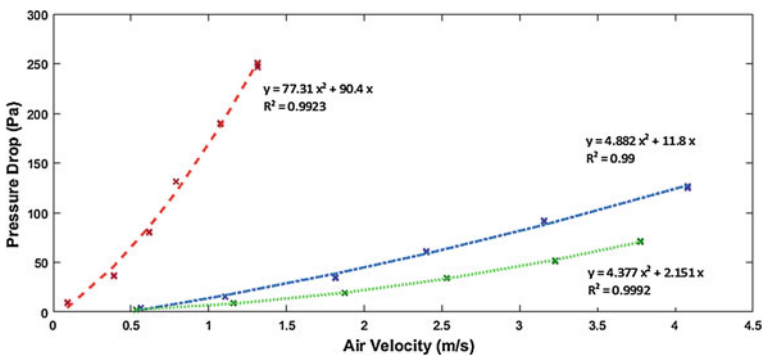


Fig. 3 Characteristic curve of screens: red curve refers to H3, green curve refers to H4 and blue one to H5

Table 2 Data obtained from the elaborations of data collected in experiments and parameters calculated

Screen	a	b	Δx (mm)	K (m^{-1})	Y (m^{-2})
H3	77.31	90.4	0.36	7.2080×10^{-11}	1.4883
H4	4.377	2.151	0.32	2.6627×10^{-9}	0.2759
H5	4.882	11.8	0.32	4.9085×10^{-10}	0.5794

4.2 CFD-PIV Approach

Two areas have been analyzed in the PIV measurements: one is immediately downstream of the screen, and the other one is the section at a distance of about 20 cm from the screen, where the flow should be less affected by the perturbation generated by the screen. Figure 4 shows the PIV results in these two different sections. The left image shows a high recirculating flow. The PIV results of the section close to the screen have been preliminary used to define the appropriate boundary conditions for the CFD simulations.

A portion equal to the dimension of the CFD model has been analyzed. The averaged velocity based on the 40 images obtained in the PIV test at 10 Hz has been calculated equal to 0.65 m/s, used then as initial velocity in the simulation. The comparison between the pressure drop measured and the one simulated with this initial velocity shows a negligible relative error (Table 3). The model can be considered validated, with reliable results.

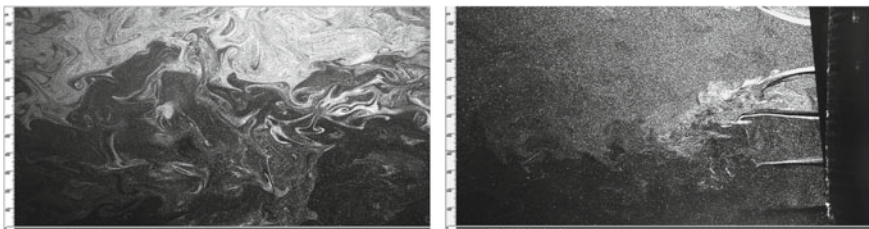


Fig. 4 Picture of the sections of PIV experiments

Table 3 Values of pressure drops measured and simulated, caused by the presence of the screens

	10 Hz
Measurent	15.48
CFD	15.3
Error	0.6%

5 Conclusions

It is well known that shading screens in greenhouses can significantly affect the air-flow patterns inside the structure. However, literature studies are mainly focused on types of screens with a regular texture, whereas new types of shading screens with more complex structure are commonly available in the protected cultivation sector. For these types, no methodology is available for their characterization. New methodologies for the characterization of the properties of complex-texture screens thus should be defined and validated. This study stemmed from this need of advancement of the knowledge in the greenhouse sector, focusing on an experimental approach and a combined experimental and numerical methodology that has been designed, tested, and evaluated. A novel approach based on wind tunnel tests has been set up to yield the permeability and inertial coefficient employing wind tunnel tests: air velocity and pressure drop measurements have allowed defining the specific behavior of each screen, which proves fundamental to investigate the specific effects of shading screens on airflows in greenhouses.

On the other hand, a computational methodology based on CFD modeling has been carried out to obtain the relation between air velocity through a screen and the relative pressure drop, avoiding any experiment. The CFD simulation has been validated by means a comparison with velocity maps obtained experimentally from PIV measurements. The proposed CFD application allows describing the fluid-dynamics phenomena, which is consistent with the results obtained through Particle Image Velocimetry, used as golden standard. Both the two methodologies presented allow deriving the parameters needed to investigate the effects of the screen on the ventilation and the indoor climatic conditions of a greenhouse.

References

- Campen, J. B., & Bot, G. P. A. (2003). Determination of greenhouse-specific aspects of ventilation using three-dimensional computational fluid dynamics. *Biosystems Engineering*, 84, 69–77.
- Castellano, S., Scarascia Mugnozza, G., Russo, G., Briassoulis, D., Mistriotis, A., Hemming, S., et al. (2009). Design and use criteria of netting systems for agricultural production in Italy. *JAE*, 518, 31–42.
- Ewing, R. E., Lazarov, R. D., Lyons, S. L., Papavassiliou, V. D., Pasciak, J., & Qin, G. (1999). Numerical well model for non-darcy flow through isotropic porous Media* 3, 185–204.
- Fatnassi, H., Boulard, T., & Bouirden, L. (2003). Simulation of climatic conditions in full-scale greenhouse fitted with insect-proof screens. *Agricultural and Forest Meteorology*, 118, 97–111.
- Flores-Velazquez, J., & Montero, J. I. (2008). Computational Fluid Dynamics (CFD) study of large scale screenhouses. *Acta Horticulturae*.
- Gray, W. G., & O'Neill, K. (1976). On the general equations for flow in porous media and their reduction to Darcy's Law. *Water Resources Research*, 12(2), 148–154.
- Hellström, J. G. I., & Lundström, T. S. (2006). Flow through porous media at moderate reynolds number, (2), 129–134.
- Katsoulas, N., Bartzanas, T., Boulard, T., Mermier, M., & Kittas, C. (2006). Effect of vent openings and insect screens on greenhouse ventilation. *Biosystems Engineering*, 93, 427–436.

- Miguel, A. F. (1998). Airflow through porous screens: from theory to practical considerations. *Energy and Buildings*, 28, 63–69.
- Miguel, A. F., Van De Braak, N. J., & Bot, G. P. A. (1997). Analysis of the airflow characteristics of greenhouse screening materials. *Journal of Agricultural and Engineering Research*, 67, 105–112.
- Miguel, A. F., Van de Braak, N. J., Silva, A. M., & Bot, G. P. A. (1998). Physical modelling of natural ventilation through screens and windows in greenhouses. *Journal of Agricultural Engineering Research*, 70, 165–176.
- Molina-aiz, F. D., Valera, D., Álvarez, A. J. (2004). Measurement and simulation of climate inside Almer' greenhouses using computational fluid dynamics. *Agricultural and Forest Meteorology* 125, 33–51.
- Santolini, E., Pulvirenti, B., Benni, S., Barbaresi, L., Torreggiani, D., & Tassinari, P. (2018). Numerical study of wind-driven natural ventilation in a greenhouse with screens. *Computers and Electronics in Agriculture*.
- Sobieski, W., & Trykozko, A. (2014a). Darcy's and Forchheimer's laws in practice. Part 1. The experiment. *Technical Sciences*, 17(4), 321–335.
- Sobieski, W., & Trykozko, A. (2014b). Darcy's and Forchheimer's Laws in practice. Part 2. The numerical model. *Technical Sciences*, 17, 321–335.
- Teitel, M. (2007). The effect of screened openings on greenhouse microclimate. *Agricultural and Forest Meteorology*, 143, 159–175.
- Teitel, M. (2010). Using computational fluid dynamics simulations to determine pressure drops on woven screens. *Biosystems Engineering*, 105, 172–179.
- Thaker, A. H., Karthik, G. M., & Buwa, V. V. (2019). PIV measurements and CFD simulations of the particle-scale flow distribution in a packed bed. *Chemical Engineering Journal*, 374, 189–200.
- Valera, D. L., Molina, F. D., Álvarez, A. J., López, J. A., Terrés-Nicoli, J. M., & Madueño, A. (2005). Contribution to characterisation of insect-proof screens: experimental measurements in wind tunnel and CFD simulation. *Acta Horticulturae*, 691, 441–448.
- Valera, D. L., Álvarez, A. J., & Molina, F. D. (2006). Aerodynamic analysis of several insect-proof screens used in greenhouses. *Spanish Journal of Agricultural Research*, 4, 273–279.

Damages to Rural Buildings and Facilities Observed in the Aftermath of 2012 Emilia Earthquakes



M. Bovo, A. Barbaresi, D. Torreggiani and P. Tassinari

Abstract In May 2012, two strong earthquakes hit the northern Italy and caused strong damage to both historical rural heritage and modern agricultural precast facilities. In this paper, damage and collapses observed in the aftermath surveys on historical rural and modern agricultural buildings, are presented and commented. It was observed that in the area hit by the earthquakes few recurrent typologies are present, and buildings of the same typology showed similar damage mechanisms. Therefore, in order to define the most typical damage affecting constructions in the agricultural sector, the stock of the historical rural buildings has been classified in different categories, based on layout and usage of each building. The outcomes presented in this paper allowed to identify the rural building typologies most vulnerable to earthquakes and to define recurring deficiencies for the various categories. The main reasons of the damage to historical buildings can be ascribed to lack of effective connections between orthogonal walls, poor connections and excessive flexibility of floor diaphragms. The main lacks observed in the precast facilities were the absence of mechanical connections between precast elements and the great flexibility of vertical elements inducing large horizontal displacements.

Keywords Rural building · Traditional technology · Precast facilities · Seismic damage · Building survey · Emilia earthquake

1 Introduction

In addition to other social and economic factors, earthquakes contribute to the transformation of rural landscape (Antrop 2005): directly, producing damages and collapses, and indirectly, pushing to intense and rapid reconstructions with no specific attention to traditional rural building criteria. In fact, after the serious seismic damages reported on traditional buildings most of them have been demolished and

M. Bovo (✉) · A. Barbaresi · D. Torreggiani · P. Tassinari
Department of Agricultural and Food Sciences, University of Bologna, Viale Giuseppe Fanin 48,
40127 Bologna, Italy
e-mail: marco.bovo@unibo.it

© Springer Nature Switzerland AG 2020
A. Coppola et al. (eds.), *Innovative Biosystems Engineering for Sustainable Agriculture, Forestry and Food Production*, Lecture Notes in Civil Engineering 67,
https://doi.org/10.1007/978-3-030-39299-4_37

323

replaced by a modern precast reinforced concrete structure, with no attention to the surrounding rural landscape. It is unnecessary to highlight that, even though it is possible to rebuild after a catastrophe, the effects of the earthquake can be permanently visible because of the relevant change left on the rural landscape. In other words, the rural landscape is changing, and the preservation of its traditional features is a delicate matter; earthquakes and other catastrophic events can accelerate the transformation progress (Picuno 2012).

In May 2012, more than 1000 seismic events with magnitude bigger than 2.0 (IESN 2018) hit the Emilia Romagna Region, in Northern Italy. Two strong earthquakes with epicenter distance equal to 11 km, characterized the sequence. The first main shock of May had local magnitude equal to 5.9 and peak ground acceleration (PGA) of 0.26 g. For the second main shock of May 29th a local magnitude of 5.8 was calculated and a $PGA = 0.42$ g was recorded (ITACA 2018). It is worth to note that the maximum PGA recorded for the second event is comparable to the expected one, following the actual Italian seismic hazard map (INGV 2018), for an event with about 1000 years return period.

The territories stricken by the earthquakes are characterized by small residential zones and medium industrial area surrounded by rural landscape. Some of the most important Italian food farming brands have their headquarters in this area, making the region one of the most densely industrialized in the northern part of the country. Several collapses and extended damages occurred to precast reinforced concrete (RC) structures (Bovo and Savoia 2018), masonry monumental heritage (Cattari et al. 2013) and historical rural buildings (Sorrentino et al. 2013), highlighting that vernacular buildings represent one of the most vulnerable categories in a geographical region where the agricultural activities play a fundamental role for the economy of the territory.

Moreover, in the aftermath of a catastrophic event, the short time imposed by reconstruction process typically makes impossible the recycling and reusing demolition waste. Consequently, metric tons of waste need to be disposed of by increasing energy and environmental impacts coming from the need for new materials (Butera et al. 2015).

The main reason of the collapse of most of the rural buildings has to be attributed to an incorrect design philosophy (Özmen and Ünay 2007), typical of past construction techniques of non-seismic zones, which considered only gravitational and wind loads. In fact, the Emilia area in the Emilia-Romagna Region was considered as a non-seismic zone by Italian regulations until 2003, therefore most of the buildings hit by the earthquake were designed without seismic rules. Moreover, old rural buildings typically represent low quality constructions built with poor construction techniques and materials.

As far as historical vernacular buildings are concerned, it was observed that, in the area hit by the earthquakes, few recurrent typologies are present, and buildings of the same typology showed similar damage or failure mechanisms. Therefore, even if every structure has its own characteristic peculiarities, it is possible to subdivide the rural building stock of the Emilia area in few categories with homogeneous use, and then connect to each category the recurrent seismic damage mechanisms. This allows

to identify the building typologies most vulnerable to earthquakes, and, from the lesson learned after recent seismic events, to plan the most effective planning strategies in order to increase the safety of historical rural constructions. This building class represents nowadays a huge cultural heritage because it represents the architectural, environmental and social distinguishing features of the Emilia landscape and history.

2 Description of Rural Buildings and RC Facilities

Earthquakes can be terrible events since they can destroy constructions in entire regions, permanently modifying the landscape, producing severe environmental and economic impacts and even killing human lives. Nevertheless, from these unfortunate experiences several information can be deducted to improve future design and define strengthening interventions on still standing buildings. First, documentation about 30 buildings, 22 vernacular buildings and 8 RC precast structures, hit by the 2012 Emilia-Romagna earthquakes has been collected by in field surveys. Then, the damages have been studied and classified; under this light, the methodology of this paper can be considered as a “lesson learned” experience, since the effects of the earthquakes have been studied to “reduce or eliminate the potential for failures and mishaps or reinforces a positive result” (Secchi 1999). For the classification and subdivision of the building stock, objective of the present study, two very simple criteria have been adopted. The first refers to geometry and plan distribution of the building, while the second to the building use.

Following the first criterion, traditional buildings are considered isolated (structurally not connected to other bodies) or composed (made up of several structurally connected bodies). According to the second criterion, the following types are identified: dwelling for residential use, stable/hayloft and building used for other services. This, because, typically, the greatest farms had other types of buildings, in order to store more hay or protect tools. The most widespread types are the “barchessa” and the “casella”, that are isolated rectangular buildings, 4–6 m high, with 6–10 m and 15–20 m plan dimensions, respectively for the transverse and the longitudinal direction. The “barchessa” was vertically closed on three façades, instead the “casella” just on one or two.

On the other hand, the modern RC precast buildings used to host agricultural process or store product, usually are isolated buildings built quite recently (usually after 1960).

3 Damages Observed During Building Surveys

3.1 Traditional Vernacular Buildings

The geographical position of the buildings, of earthquake epicenters, and some accelerometric stations are reported in Fig. 1a. As far as the isolated dwellings is concerned, the typical building has 25–30 cm thick masonry walls, made up with irregular raw bricks and poor hydraulic mortar brickworks with 2.50–2.80 m net floor height and no more than three floors. The inter-story floors are built with timber beams poorly connected to perimeter walls and pavement constituted by single layer wood plank resulting extremely flexible and unsuitable to transfer seismic actions. The typical damages observed for this class of buildings are flexure or shear mechanism in the plane of the wall, to perimeter and partition walls as depicted in Fig. 1b. Due to limited in-plane dimensions compared to thickness, the mode I (i.e. local modes) failure mechanisms usually did not appear, even if the connections between



Fig. 1 View of the area stricken by the Emilia earthquakes with **a** localization of buildings and damage to residential buildings: **b** cracks on masonry wall; **c** corner damage; **d** fall of a wooden beam

orthogonal walls are very poor, as showed in Fig. 1c. Moreover, the floor-wall connection is rather poor: in many cases, the sliding of the beams from the masonry or even the failure was observed, due to loss of support, as documented in Fig. 1d.

Most of the seismic damages in the region affected the stable/hayloft buildings. In fact, into this category, several collapses or permanent damages, and consequent building demolitions, have been reported. The structural shape of stable/haylofts makes this specific group of buildings extremely vulnerable to seismic actions. The need to achieve great volumes to store hay and wheat without introducing inner structure elements brought the adoption of long and high, usually very slender, single leaf masonry walls. In other cases, masonry columns infilled by single course (12–15 cm thick) walls were realized. The inter-story floor over the stable typically has masonry vaults surrounded by internal columns, instead, the roof has wooden trussed structure with two or four pitches. Due to the high slenderness of vertical walls and columns (the ratio height/thickness could reach values bigger than 20) and because of the distance between the masonry walls, in general the structure is expected to be horizontally very flexible, so large displacements are expected under seismic actions (see Bovo et al. 2020). In fact, the main causes of stable/haylofts collapses can be ascribed to overturning of walls, vertical and horizontal out-of-plane flexure mechanisms. A catastrophic example of collapse for overturning is reported in Fig. 2a, involving a whole façade of the buildings from foundation to roof. Figure 2b shows the global collapse of another historical rural stable/hayloft for horizontal flexure local mechanisms. As the distance from the epicenter region increases, it can be diffusely observed that vertical walls did not collapse, but the buildings reported severe damages to roof elements and in some cases the fall of the main wooden beams. This can probably be attributed to beam-wall relative displacement causing unseating and loss of support of horizontal elements. In fact, due to the building asymmetry introduced for example by non-regular infills, non-symmetric walls, presence of portico and stable, two different vertical elements could vibrate in asynchronous way, by imposing at the extremities of horizontal beams, tensile force bigger than friction force and able to activate the sliding mechanism. Figure 2c shows this situation, with pitched-roof collapsed without any apparent damaging to vertical elements. As for historical churches (Lagomarsino 2012), the unrestrained forces of the beams of a deformable pitched-roof, can cause the overturning of a limited portion of masonry panels close to the roof (see Fig. 2d).

The principal causes of collapse of these buildings must be ascribed to the high slenderness of the vertical walls or columns coupled to the absence of a rigid floor diaphragm able to prevent the relative settlements between different vertical elements and to avoid the sliding of roof beams from their seats. In some cases, the presence of steel ties avoided the overturning of the walls, but these devices were not sufficient to prevent the catastrophic scenario described above.

Similarly to some stable/haylofts, because of large slenderness of vertical walls in absence of a rigid floor diaphragm, in the “barchessa” building the out-of-plane flexure mechanism of a wall produced the complete collapse of the roof (see Fig. 3a). Figure 3b shows instead, the most important seismic-induced damages to the columns of the “casella”, caused by the asymmetric behavior of the building. Due to the torsion

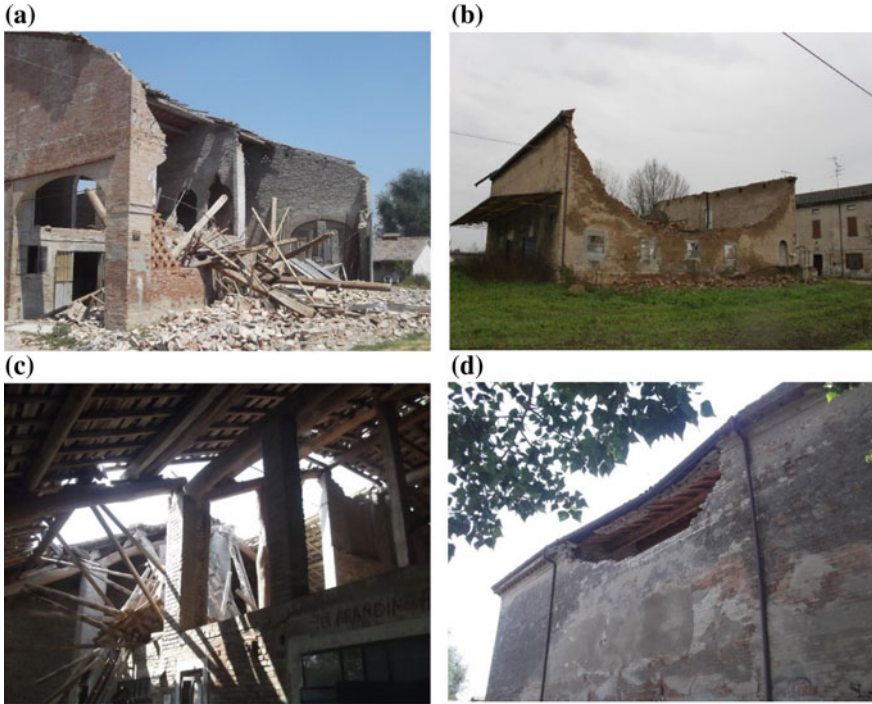


Fig. 2 Main damages to stable/hayloft buildings

effects, the corner columns were literally cut at the level of the intermediate floor, as proved by the residual settlements. As far as the smaller buildings is concerned, the typical damages are very similar to those observed for residential buildings. In fact, as depicted for example in Fig. 3c with regard to a warehouse, the collapse of the floor of roof elements is one of the most recurring mechanisms, together with the in-plane failure of walls. Then, in many cases, the overturning of the infill panels not adequately connected to vertical masonry columns was observed (see Fig. 3d). A deeper description on damage scenario can be found in Bovo et al. (2019).

3.2 Modern RC Precast Facilities

During the aftermath building surveys, eight RC precast structures used in agriculture process have been detected and inspected. The most commonly observed failures were the falling of the horizontal elements, usually constituted by RC panels or TT beams, and constituting interstorey or roof floors (see Fig. 4a). This failure mechanism was possible because of the lack in connections between precast elements which, in many cases, can be considered simply-supported pin joints based



Fig. 3 Main damages to buildings used for minor services

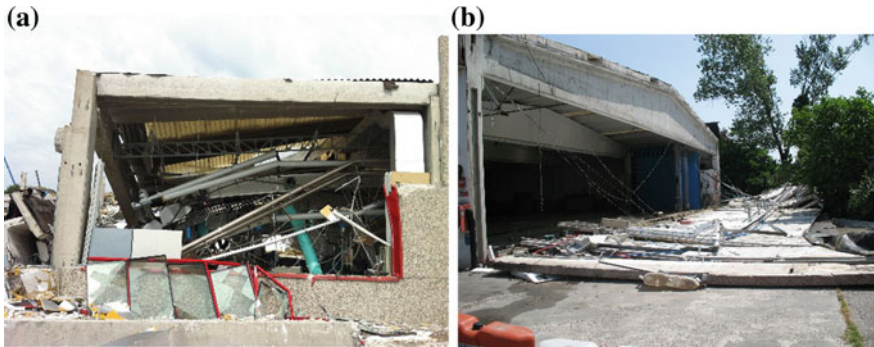


Fig. 4 Damage scenario of RC precast facilities used in agricultural process and storage

on friction resistance. In some cases, the presence of the neoprene pads typically interposed between precast elements for ease the construction process, facilitated the sliding mechanisms. Another important issue was the weak anchorage system beam-cladding panels causing partial or total detachment of the facades of the buildings (as in Fig. 4b).

4 Conclusions

In this paper, the damages and the collapses collected during the surveys on rural historical buildings in the aftermath of the 2012 Emilia earthquakes are presented and commented. It was observed that, in the area hit by the earthquake, a few recurrent typologies are present, and buildings of the same typology showed similar damage mechanisms. Therefore, in order to define the most typical damages affecting the different building typologies, the 30 structures of the building stock under study have been classified in different categories, based on layout and usage of the building. The main reason of the collapse of most of the vernacular buildings can be attributed to an incorrect design approach, typical of past construction techniques of non-seismic zones, considering only static loads. The most commonly observed collapses were walls local mechanism (i.e. single or complex overturning, horizontal or vertical flexure) and in some cases in-plane shear of flexure failure. In few cases, the presence of irregular distribution of the infill panels anticipated the failure. The failures can be ascribed to a lack of effective connections between orthogonal walls, poor connections between floor elements and walls, and excessive flexibility of floor diaphragms. In many cases the buildings were demolished because of the severe damages reported. On the other side, the main reason of the collapse of most of RC precast facilities used in agriculture can be attributed to an incorrect design philosophy since until 2003 most of the precast buildings in Emilia were designed with simply-supported slab elements with pin-joints based on friction resistance. The most commonly observed collapses were related to sliding and falling of horizontal structural elements, constituting inter-story or roof slabs, due to seismic forces exceeding the friction resistance at the support level. Sliding mechanisms were facilitated by the presence of neoprene pads between precast elements typically interposed for ease the construction process.

References

- Antrop, M. (2005). Why landscapes of the past are important for the future. *Landscape Urban Plan.*, 70(1–2), 21–34. <https://doi.org/10.1016/j.landurbplan.2003.10.002>.
- Bovo, M., & Savoia, M. (2018). Numerical simulation of seismic-induced failure of a precast structure during the emilia earthquake. *Journal of Performance of Constructed Facilities*, 32(1), 04017119.
- Bovo, M., Barbaresi, A., Torreggiani, D., & Tassinari, P. (2019). Report on earthquake-induced failures of rural buildings aimed at future preservation strategies. *Journal of Agricultural Engineering*, 50(2), 66–79. <https://doi.org/10.4081/jae.2019.930>.
- Bovo, M., Barbaresi, A., Torreggiani, D., & Tassinari, P. (2020). Collapse and damage to vernacular buildings induced by 2012 Emilia earthquakes. *Bulletin of Earthquake Engineering*, 18(3), 1049–1080.
- Butera, S., Christensen, T. H., & Astrup, T. F. (2015). Life cycle assessment of construction and demolition waste management. *Waste Management*, 44, 196–205.

- Cattari, S., Degli Abbatì, S., Ferretti, D., Lagomarsino, S., Ottonelli, D., & Tralli, A. (2013). Damage assessment of fortresses after the 2012 Emilia earthquake (Italy). *Bulletin of Earthquake Engineering*. <https://doi.org/10.1007/s10518-013-9520-x>.
- IESN (Italian Experimental Seismic Network). Retrieved from October 10, 2018, from <http://www.iesn.it>.
- INGV (Istituto Nazionale di Geofisica e Vulcanologia). Retrieved from October 10, 2018, from <http://shakemap.rm.ingv.it/shake/index.html>.
- ITACA (ITalian ACcelerometric Archive) version 2.0. Retrieved from October 10, 2018, from <http://itaca.mi.ingv.it>.
- Lagomarsino, S. (2012). Damage assessment of churches after L'Aquila earthquake (2009). *Bull Earthquake Eng*, 10, 73–92. <https://doi.org/10.1007/s10518-011-9307-x>.
- Özmen, C., & Ünay, A. I. (2007). Commonly encountered seismic design faults due to the architectural design of residential buildings in Turkey. *Building and Environment*, 24(3), 1406–1416.
- Picuno, P. (2012). Vernacular farm buildings in landscape planning: a typological analysis in a southern Italian region. *Journal of Agricultural Engineering*, XLIII, e20, 130–137.
- Secchi, P. (Ed.). (1999). Proceedings of alerts and lessons learned: an effective way to prevent failures and problems. Technical Report WPP-167. Noordwijk, The Netherlands: ESTECS.
- Sorrentino, L., Liberatore, L., Liberatore, D., & Masiani, R. (2014). The behaviour of vernacular buildings in the 2012 Emilia earthquakes. *Bull Earthquake Eng.*, 12, 2367–2382.

Proposal of a Web-Based Multi-criteria Spatial Decision Support System (MC-SDSS) for Agriculture



Giuseppe Modica, Maurizio Pollino, Luigi La Porta and Salvatore Di Fazio

Abstract The paper reports the main technological characteristics and functionalities of a web-based Multi-criteria Spatial Decision Support System (MC-SDSS) implemented on free open source software for geospatial (FOSS4G) environment. The web-based MC-SDSS was designed to perform land suitability evaluation (LSE) for olive crops and applied to the territory of Calabria (Italy). From a technological point of view, the MC-SDSS was designed on a multi-tier architecture compliant with the Open Geospatial Consortium (OGC) services (WFS, web feature service; WCS, web coverage service, and WMS, web map service. Moreover, it was enabled to processes executable via OGC web processing services (WPSs). LSE of olive crops is provided following the analytical hierarchy process (AHP) based on the different judgements obtained from experts and aggregated through the weighted linear combination (WLC). With the aim to implement an effective planning tool, the WebGIS client was designed to manage three different type of users with different level of privileges: Guest, Expert and Decision Maker. The results are expressed as multi-attribute geospatial maps (land suitability maps) and as distribution graphs according to the envisaged land suitability classes (not suitable, low, medium, high and very high suitability).

Keywords Land Suitability Evaluation (LSE) · Multi-criteria Spatial Decision Support System (MC-SDSS) · WebGIS

G. Modica (✉) · S. Di Fazio

Dipartimento di Agraria, Università degli Studi Mediterranea di Reggio Calabria, Località Feo di Vito, 89122 Reggio Calabria, Italy

e-mail: giuseppe.modica@unirc.it

M. Pollino · L. La Porta

DTE-SEN-APIC Lab, ENEA National Agency for New Technologies, Energy and Sustainable Economic Development, Via Anguillarese, 301, 00123 Rome, Italy

© Springer Nature Switzerland AG 2020

A. Coppola et al. (eds.), *Innovative Biosystems Engineering for Sustainable Agriculture, Forestry and Food Production*, Lecture Notes in Civil Engineering 67,

https://doi.org/10.1007/978-3-030-39299-4_38

1 Introduction

The main aim of the land suitability evaluation (LSE) is to give an effective support to environmental managers and planners in analysing the interactions among location, development actions, and environmental elements (Collins et al. 2001) in order to evaluate different scenarios. In this framework, Multi-criteria Spatial Decision Support Systems (MC-SDSSs) are effective tools that allow to accomplish LSE for agricultural or forest environments (Malczewski 1999; Modica et al. 2014). In this paper, we synthetically show the main characteristics and functionalities of a web-based MC-SDSS platform specifically implemented to perform LSE for olive crops (Modica et al. 2016). Such tool is based on a free open source software for geospatial (FOSS4G) environment (Steiniger and Hunter 2012), accessible through a user-friendly geographical user interface (GUI), capable to perform geospatial analyses (Pollino and Modica 2013). The MC-SDSS has been implemented with a multi-tier architecture, enabling to:

- Manage geospatial data and produce output maps via the largely used OGC (Open Geospatial Consortium) services (OGC® Standards): web feature service (WFS), web coverage service (WCS) and web map service (WMS);
- Manage processes executable via OGC web processing services (WPSs).

In the current version of MC-SDSS platform, data aggregation is provided by means of the weighted linear combination (WLC), using the different weights obtained from the judgements provided by experts (Modica et al. 2016) and following the analytical hierarchy process (AHP) proposed by Saaty (1980). To this end, the platform represents an effective solution, accessible also to non-experts, and based on specific online tools. For example, the WPS was configured to provide web-based processing (GIS geoprocessing) and multi-criteria assessment web-functions, including access to pre-programmed calculations and/or computation models, operating on geospatial data (both vector and raster formats) (Modica et al. 2016).

Taking into account the general framework and the processing steps required, the proposed WebGIS application (hereafter referred as “WebGIS Suitability-Olive”) was specifically implemented and released (Modica et al. 2016). It represents the front-end interface of the MC-SDSS platform, through which the user is able to access data, perform calculation and assess the obtained results that are constituted by land suitability maps, distribution graphs, etc. Moreover, with aim to implement an effective planning tool, the WebGIS client was designed to manage three different types of users with different levels of privileges: Guest, Expert and Decision Maker.

2 The Methodological Approach

As introduced, to perform the analyses, the WLC technique (Vizzari and Modica 2013) was implemented within the proposed MC-SDSS, specifically providing factors and criteria for the approach adopted. From a practical point of view, each factor

represents a specific map (i.e., a GIS layer) and, by means of GIS spatial overlay (Geoprocessing or Map Algebra) (Eastman et al. 1995), it is possible to integrate the variables through the use of appropriate weights, which are typically provided by one or more experts. Each attribute represents a “criterion”: to each criterion is assigned a weight, on the basis of its own relative importance. The possible options represent single parts of the analysed territory on which the variables can assume a given value, leading to the evaluation of a well-defined area in which a suitability value is assessed. The results are expressed as multi-attribute geospatial maps (land suitability maps) and as distribution graphs according to the envisaged land suitability classes (not suitable, low, medium, high and very high suitability).

Here follows an example of exploitation of a WLC: (i) a set of continuous criteria are assigned to defined intervals; (ii) the numerical ranges are combined by a weighted average; (iii) user (e.g., an expert supporting the final decision-maker), through a specific procedure, assigns weights directly to each mapped GIS layer; (iv) the overall score for each option is calculated by multiplying the weight assigned to each attribute by the (normalized) value of the attribute itself within each alternative and, then, by adding the products of all the attributes; (v) by spatially combining the evaluation criteria associated with each GIS layer, it is possible to obtain a suitability map for the area of interest.

According to the approach proposed by Saaty (1980), and based on the pairwise comparisons according to the so-called Saaty’s fundamental scale, when comparing two variables, the evaluator (i.e., the expert), has to indicate which is the most important on a scale of scores ranging from 1 to 9, which express the relative importance of the first variable with respect to the second. To compare all possible couples of variables, the scores are organized into a pairwise comparison matrix (PCM) (Modica et al. 2015).

The AHP is also a powerful tool thanks to the possibility to involve in the evaluation process multiple experts with different skills. To this end, the MC-SDSS platform has been structured to support groups of experts/evaluators, implementing a multi-user approach in which it is possible to provide individual evaluations (and to produce the related results) and then to aggregate them into a final synthetic evaluation.

The input geospatial layers (and consequent factors) considered are the following: *Elevation, Acclivity, Aspect, Land use/Land Cover* and *Pedology*. These information layers were acquired from various public data repositories (ISPRA-SINAnet, Regione Calabria, etc.). Subsequently, they were converted from their native format into raster format and resampled to a spatial resolution of 20 m × 20 m.

The evaluation workflow, on the whole, is articulated into the following steps (Modica et al. 2016):

- Step 1: Criteria definition and selection. Evaluation criteria, organised following the work of Eastman et al. (1995) as factors and constraints, are defined and selected.

- Step 2: Data Normalization. By means of a standardization procedure, all the criteria are represented within a common reference interval [0–1], through different approaches (e.g., fuzzy logic).
- Step 3: Weights Definition (AHP-based approach). To obtain the weights of the criteria considered, each expert has to provide a judgment for each pair of the n elements into the pairwise comparison matrix (PCM) (Vizzari and Modica 2013; Forman and Peniwati 1998), expressing it on the basis of the Saaty’s fundamental scale (Saaty 1980).
- Step 4: WLC and suitability maps (Map Algebra technique). According to his own evaluation, each Expert is allowed to view the obtained assessment as a land suitability map.
- Step 5: Results aggregation—Final suitability map production. Results coming from each involved expert are aggregated to obtain the final land suitability map for olive crops.

3 “Suitability-Olive”: The WebGIS Interface of MC-SDSS

The WebGIS *Suitability-Olive* was conceived and designed to share and make available territorial information and to support decision-making processes. It represents the interface of the MC-SDSS (Modica et al. 2016), also allowing processes execution. Thus, the WebGIS provides a wizard-like structure, to drive the user through a series of well-defined steps (that we called “Processing Widgets”) in order to perform the multi-criteria spatial analysis, such as:

- launch and execute data normalization processes (“Normalization Widget”);
- calculate the “WLC—Weighted Linear Combination” (“AHP Widget”).

The multi-user architecture implemented allows the experts to provide their evaluations and, at a higher level, the overall management of the platform and the synthesis of the results. To this end, three categories of users—with different roles and privileges—are defined: “*Guest*”, “*Expert*” and “*Decision Maker*” (i.e. the platform administrator) (Fig. 1).

3.1 *Expert’s Evaluations*

The so-called “Expert” users are enabled to provide their own evaluations, by performing the various steps previously described. For each of them, a specific access to the Web-GIS platform is provided by means of a username and a password. The first step that each expert must perform the normalization, managed through the “Normalization Widget”, that allows to manage the trade-off between all the evaluation factors. This Widget is organized in five different sections (TABs), each dedicated

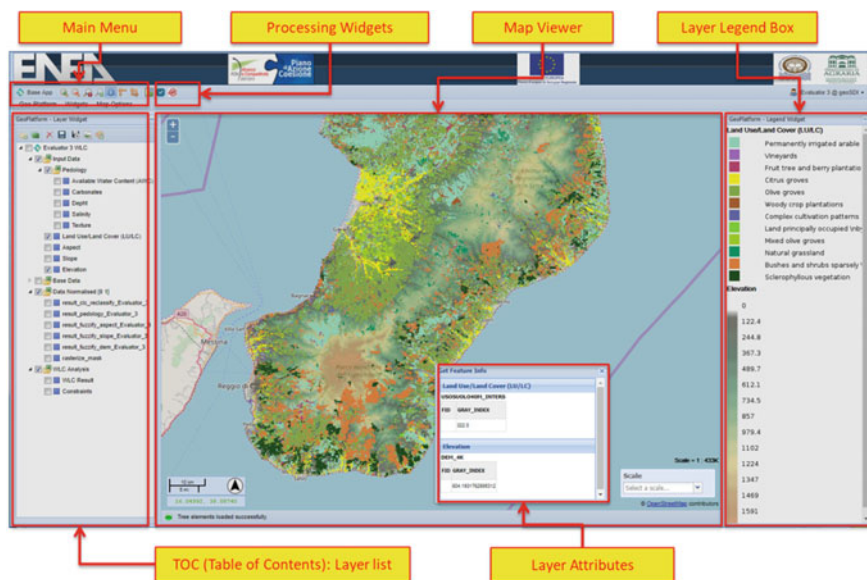


Fig. 1 WebGIS *Suitability-Olive*, example of layout with the different sub-sections labeled (red arrows). In this screenshot, the Land cover map is showed

to the normalization of a specific factor according to the most appropriate method. In particular, based on a fuzzy approach, the so-called Ordered Weighted Averaging (OWA) operators (Yager 1988) were implemented for *Elevation*, *Slope* and *Aspect* factors (Fig. 2). Thanks to this Widget, the Expert can set the “transition” from the values considered as unsuitable to those most suitable.

To normalize the *Land Use/Land Cover* factor (Fig. 3), for each class considered it is possible to indicate the relative relevance, by selecting the values in a continuous range from 0 (“Very Low”) to 1 (“Very High”). Then, *Pedology* can be normalised through a pairwise comparison between the five sub-factors characterising the layer (texture, salinity, depth, water content and carbonates).

After the normalization step, it is possible to perform the calculation of the WLC. By means of the module called “AHP Widget” the expert can assign weights to each of the five considered factors (*Elevation*, *Slope*, *Aspect*, *Land Use/Land Cover* and *Pedology*) using the pairwise comparison technique (AHP), on the basis of the reference scale indicated by Saaty (ranging from 1 = “equal importance” to 9 = “extremely more important”).

Finally, according to the parameters set-up during the above described procedure and as result of the WLC (Fig. 4), the related GIS layer (suitability Map) is produced as output and automatically made available within the WebGIS view.

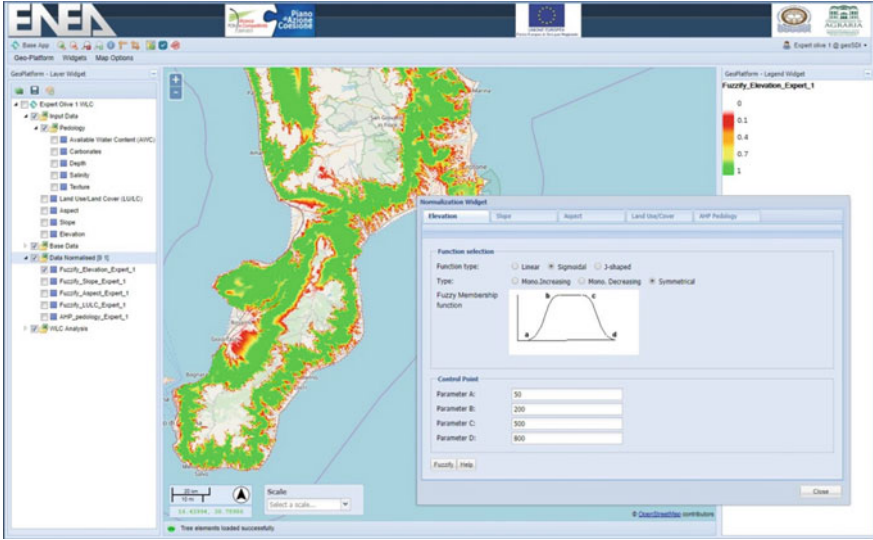


Fig. 2 Normalization Widget: example of *Elevation* factor normalization trough fuzzy logic based on linear, sigmoidal and j-shaped membership functions

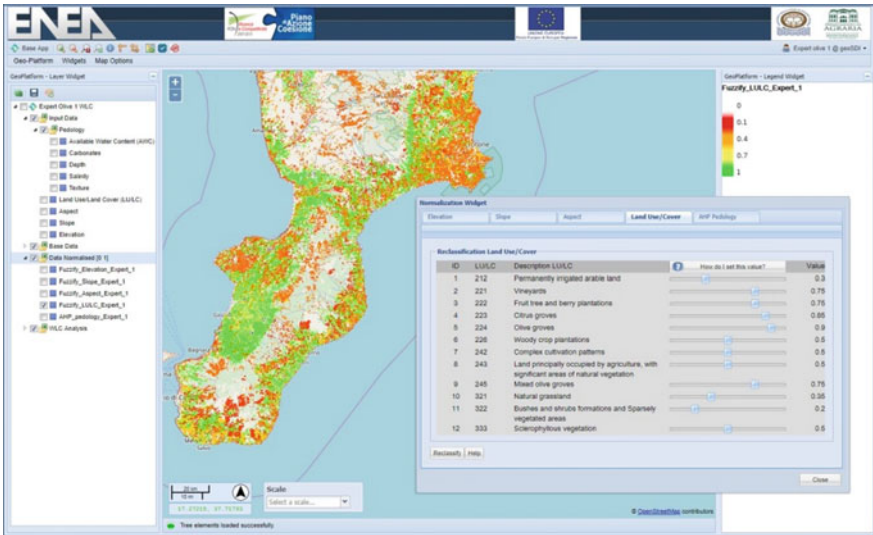


Fig. 3 Normalization Widget: example of *Land Use/Land Cover* factor normalization

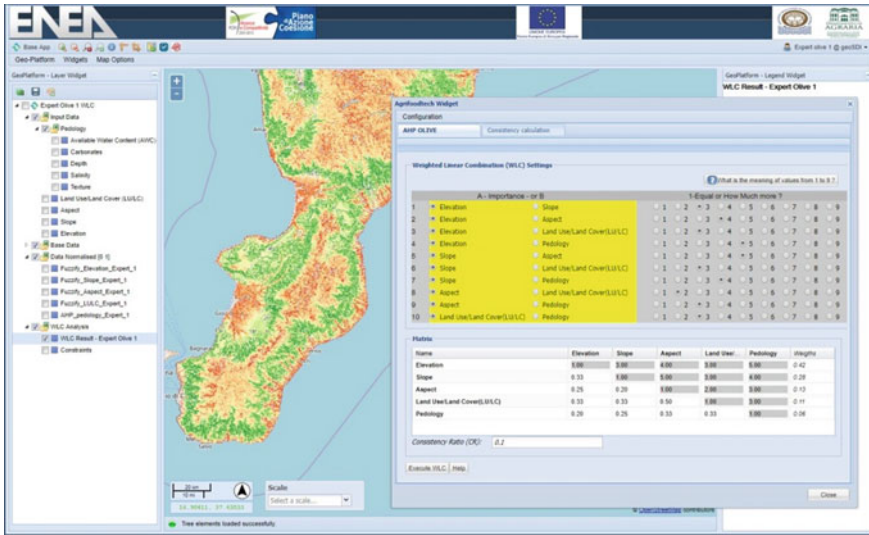


Fig. 4 Weighted Linear Combination (WLC): visualization of the Widget mask allowing an Expert to input the parameters (according to the AHP procedure) and produce its own suitability Map

3.2 Suitability Map Production

The “Decision Maker” (DM) is the *super-user* enabled to collect the results produced by each expert (according to their specific evaluations). A specific processing module, which elaborates the individual results of each expert, allows the DM to aggregate all the intermediate results (through a geometric mean) and to generate the final Suitability Map (Fig. 5), as the synthesis of the *n* evaluations provided.

4 Conclusions

In this paper we have described the design and development of a web-based MC-SDSS, relying on a FOSS4G architecture, aiming at performing spatial and environmental analyses, in order to support decision-making processes related to the agro-forestry LSE.

A WebGIS application (namely “Suitability-Olive”) was specifically implemented as multi-user interface of the MC-SDSS, to perform spatial analyses via web and to support the evaluation processes accomplished by different/multiple experts. Then, the final decision maker can easily collect and manage the results provided by the various experts involved in the evaluation phase, obtaining a final susceptibility maps as result of the overall LSE process. Feedbacks from the experts that are currently testing the application will be considered to address the future developments of the

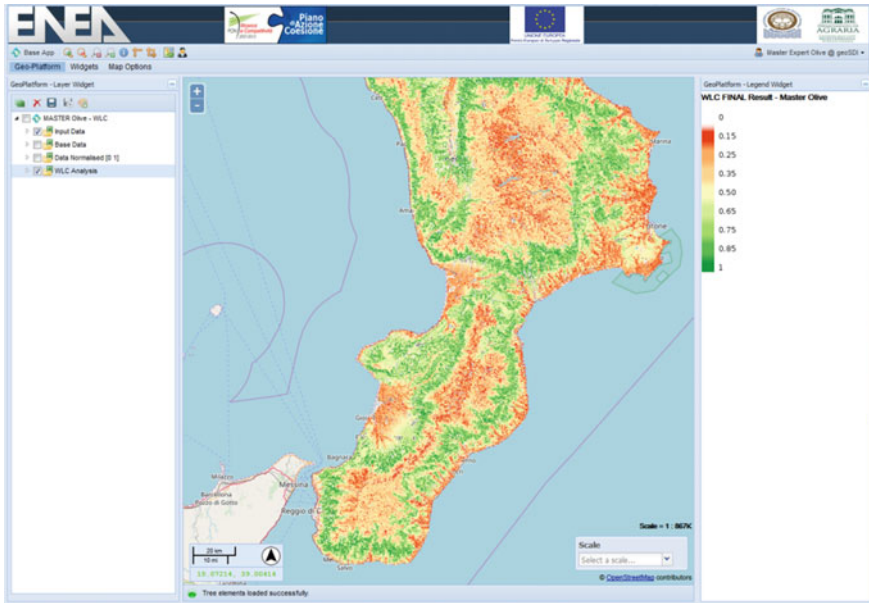


Fig. 5 Example of final Suitability Map, produced as the synthesis of the evaluations provided by the different Experts

MC-DSS, in order to enhance its capabilities. For instance, additional features may be implemented, to take into account other environmental aspects and to support more efficiently decision processes.

References

- Collins, M. G., Steiner, F. R., & Rushman, M. J. (2001). Land-use suitability analysis in the United States: Historical development and promising technological achievements. *Environmental Management*, 28, 611–621.
- Eastman, R., Jin, W., Kyem, P. A. K., & Toledano, J. (1995). Raster procedures for multi-criteria/multi-objective decisions. *Photogrammetric Engineering and Remote Sensing*, 61, 539–547.
- Forman, E., & Peniwati, K. (1998). Aggregating individual judgments and priorities with the analytic hierarchy process. *European Journal of Operational Research*, 108, 165–169.
- Malczewski, J. (1999). *GIS and multicriteria decision analysis*. New York: Wiley.
- Modica, G., Laudari, L., Barreca, F., & Fichera, C. R. (2014). A GIS-MCDA based model for the suitability evaluation of traditional grape varieties: The case-study of “Mantonico” grape (Calabria, Italy). *International Journal of Agricultural and Environmental Information Systems*, 5, 1–16.
- Modica, G., Merlino, A., Solano, F., & Mercurio, R. (2015). An index for the assessment of degraded Mediterranean forest ecosystems. *For. Syst.*, 24, 13.

- Modica, G., Pollino, M., Lanucara, S., La Porta, L., Pellicone, G., Di Fazio, S., Fichera, C. R. (2016) Land suitability evaluation for agro-forestry: Definition of a web-based multi-criteria spatial decision support system (MC-SDSS): Preliminary results. In: O. Gervasi et al. (Eds.), *Computational science and its applications—ICCSA 2016*. Lecture Notes in Computer Science (Vol. 9788). Cham: Springer.
- OGC® Standards. Retrieved from <https://www.opengeospatial.org/standards>.
- Pollino, M., & Modica, G. (2013). Free Web mapping tools to characterise landscape dynamics and to favour e-participation. In B. Murgante, S. Misra, M. Carlini, C. M. Torre, H.-Q. Nguyen, D. Taniar, B. O. Apduhan, & O. Gervasi (Eds.), *ICCSA 2013, Part III* (Vol. 7973, pp. 566–581)., LNCS Heidelberg: Springer.
- Saaty, T. L. (1980). *The analytic hierarchy process: Planning, priority setting, resource allocation*. New York: McGraw-Hill.
- Steiniger, S., & Hunter, A. J. S. (2012). Free and open source GIS software for building a spatial data infrastructure. In E. Bocher & M. Neteler (Eds.), *Geospatial free and open source software in the 21st century* (pp. 247–261). Heidelberg: Springer.
- Vizzari, M., & Modica, G. (2013). Environmental effectiveness of swine sewage management: A multicriteria AHP-based model for a reliable quick assessment. *Environmental Management*, 52, 1023–1039.
- Yager, R. R. (1988). On ordered weighted averaging aggregation operators in multicriteria decision making. *IEEE Transactions on Systems, Man, and Cybernetics: Systems*, 18, 183–190.

The Apulian Territory and the Typical Local Farmhouses: A Case of Study Through Landscape Analysis



E. Liano, I. Blanco and G. Scarascia Mugnozza

Abstract The Apulian territory is strongly characterized by a rural architectural heritage with many historical features. Rural and agro-industrial buildings, their reuse or degradation, are the testimony of a history whose investigation is complex and varied over time. The Regional Territorial Landscape Plan, which entered into force in 2015, promotes the realization of a self-sustainable and lasting socio-economic development and education for an appropriate use of the regional territory. The knowledge, conservation, use and promotion of the Traditional Apulian Architectural Heritage are among its aims. This in fact constitutes the memory of a place, culturally identifies a local community and the territory. In-depth knowledge of the identifying characteristics of the rural heritage is essential before any recovery intervention specifically aimed at protecting and enhancing the buildings, the landscape and the environmental context. A recovery activity, mindful of these issues, can generate strategic resources for reaching wider objectives of regional development. This study aims to analyze the current relationship between ancient Apulian farmhouses that have been subject to functional restoration interventions and the landscape in which they are located, in order to outline strategies for the development and promotion of the related rural area.

Keywords Architectural heritage · Rural buildings · Touristic itineraries

1 Introduction

The landscape is currently recognized as a key element for social and individual well-being. Safeguarding the landscape as a common good, its management and planning

E. Liano (✉) · G. Scarascia Mugnozza
Department of Agricultural and Environmental Science (DISAAT), University of Bari Aldo Moro,
via Amendola 165/A, 70126 Bari, Italy
e-mail: enrico.liano@uniba.it

I. Blanco
Department of Biological and Environmental Sciences and Technologies (DiStEBA), University
of Salento, S.P. 6, Lecce - Monteroni, 73100 Lecce, Italy

© Springer Nature Switzerland AG 2020
A. Coppola et al. (eds.), *Innovative Biosystems Engineering for Sustainable Agriculture, Forestry and Food Production*, Lecture Notes in Civil Engineering 67,
https://doi.org/10.1007/978-3-030-39299-4_39

involves individual and political rights and responsibilities. In particular, starting from the European Landscape Convention, new methods have been introduced for the consideration and management of the landscape dimension of the territory. The European Landscape Convention promotes “the protection, management and planning of the landscapes and organises international co-operation on landscape issues” (Council of Europe 2000).

The knowledge of territorial resources is essential for landscape preservation and for its sustainable development. It allows the revaluation of the identity of specific places and creates the prerequisites for the design of a multifunctional reuse in accordance with the European Landscape Convention policies of protection, conservation and enhancement of the environment (Caliandro et al. 2014; De Montis 2016).

With reference to agriculture, rural sustainable development must consider the interactions, within rural areas, between cultural heritage, natural resources, agricultural production and local communities (Pašakarnis et al. 2013; Ottomano Palmisano et al. 2016). Architectural and cultural heritage can be seen as fundamental tools for restoring the historical and landscape identity of a place and for defining the relative landscape image (Torreggiani et al. 2014; van der Vaart 2005).

Rural buildings are considered as key elements, with high historical and architectural value, which characterize the agricultural landscape image (Council of Europe 2000). The quality of the landscape can be significantly preserved or improved through accurate planning for reuse of buildings and through a design for new buildings aimed at a good consistency level with functions and typologies of rural settlements (Torreggiani and Tassinari 2012).

From the above issues it emerges the importance of some researches aimed at identifying and characterizing the range of existing rural constructions and elements of historical and cultural importance to be interpreted as strengths and starting points in the improvement of the rural territory (De Montis et al. 2017; Ruggiero et al. 2019).

The most significant architectural features in the Apulian rural territory are large farmhouses known as *masserie*, due to their widespread presence and the typological characteristics that give them great potential for recovery and reuse (Ruggiero et al. 2019). These farmhouses are the highest expression of the Apulian rural building, typical of the medieval age until the end of the nineteenth century (Caliandro et al. 2014). In some Apulian areas, as in the center-oriental part of the Ionian Sea province, the widespread building of agricultural settlements and of *masserie* was stimulated by the reduction of semi-nomadic sheep breeding which took place along the *tratturi*, trails used for livestock, sheep and cattle transhumance (Liano et al. 2015).

The existing relationships between Roman roads and sheep's paths, crossing the Apulia region, and *masserie*, in function of their mutual distance and of the single rural buildings importance, have been analyzed (Caliandro et al. 2014). The study results showed as the presence of the sheep's paths firstly influenced the location of the *masserie*, then secondarily the Roman roads. It also underlines that an effective strategy for promoting rural territory development could be to detect and enhance the integrated resources system constituted by the sheep's paths, the consular roads

and the valuable *masserie* falling into a restricted catchment area of these historical road tracks.

A research was carried out on the sheep trails crossing the two municipal territories of Mottola and Palagianello (Province of Taranto, South Italy), the medieval pilgrims routes in the Apulian Medieval cave settlements and cave churches sited in the Regional Natural Park of Ravines “Terra delle Gravine” (Taranto) and numerous architectural evidences belonging to the historical and cultural heritage in the Apulian rural territory. The combined detection and analysis of the above-mentioned paths and sites of interest led to propose a re-elaboration of one of the combining sheep trails linking the two cities of Mottola and Palagianello for creating a tourist path which allows the creation of a routes network and the revaluation of the landscape of the ravines (Liano et al. 2015). Moreover, the recovery of this route could allow the realization of a greenway for territorial connection (Senes et al. 2017).

This study aims to investigate the current relationship between the *masserie* that have been functionally restored and the landscape in which they are located, in order to outline strategies for the development and promotion of the related rural area. A preliminary analysis of the regional context permitted to select as case of study a restricted area of the province of Taranto (Apulia region).

2 Materials and Methods

About 5600 historic farmhouses (*masserie*) were built in the period between the medieval age and the end of 800s. About 3000 of the still existing *masserie* have been classified as assets of the regional cultural heritage due to their relevant historical architectural features (Caliandro et al. 2014).

In Italy, the “Code of cultural heritage and landscape” (Italian Regulation 2004) represents the most significant legislative instrument in the context of the evolution of Italian regulatory system following the signing of the European Landscape Convention. This tool defines two types of cultural heritage within the “national cultural heritage”: the cultural heritage of historical, artistic, archaeological interest etc., and the cultural heritage made up of Italian landscapes. The latter are defined as products of a millennial anthropization and historical stratification of the territory. The Code also includes in the cultural heritage “rural architecture with historical and ethno-anthropological interests as proof of the traditional economy”. In Apulia, the Regional Territorial Landscape Plan (PPTR) (Apulia Region 2015) introduced guidelines for the recovery, maintenance and reuse of buildings and rural assets, according to the Code.

The study was carried out on a restricted area of the Province of Taranto (Apulia region, Southern Italy) (Fig. 1a). The territory of Taranto is characterized by a widespread presence of *masserie* recognised as cultural heritage by the Apulian Regional Administration. The study area involves the municipal territory of Palagianello (Province of Taranto). The research focused on a historic *masseria*, Parco di Stalla, falling in the territory of Palagianello. Its origins are very ancient. The

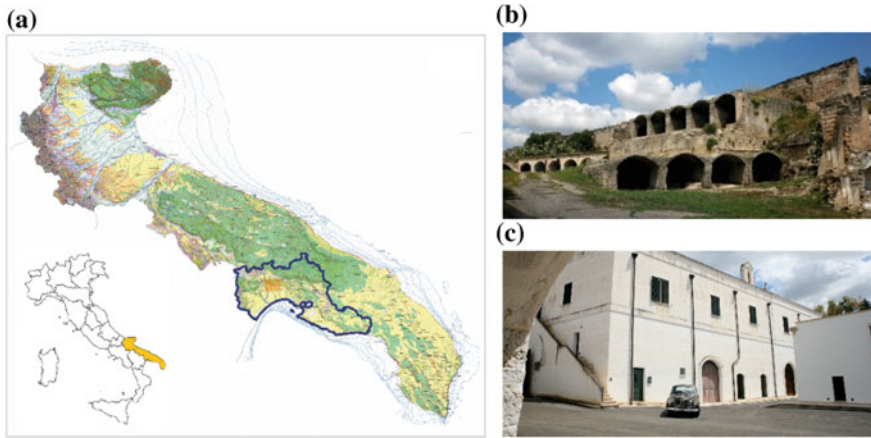


Fig. 1 Hydrogeomorphological map (drawn up in scale 1:150,000) of the Apulia region (2019), highlighting the provincial boundaries of Taranto and the study area (a); Parco di Stalla: old sheep shelters (*iazzi*) (b) and farmhouse (*masseria*) (c) (Source <http://www.parcodistalla.it/storiaita.html>)

masseria is characterized by the presence of a small church and multiple *iazzi*, rural architectures used as sheep shelters (Fig. 1b, c).

Evidences of the historical period IV—III century BC era have been found in adjacent lands that consist in the ruin of a path with roadway. In 1676 the consistency of the *masseria* is described as a set of underground reservoirs, one of which was ancient, a large pool for animals watering and a cave that was once a “taberna”. The core of the farm is described as already existing. The *tabernae* were basically resting places where people and animals travelling along the Roman roads could drink and eat. In 1811 Parco di Stalla is described as already composed of several *iazzi*, a *masseria* and a church (AA.VV 1995). Currently Parco di Stalla consists of the ancient *iazzi*, the restored church and *masseria*, an educational farm, an ancient underground oil mill and a museum of rural civilization.

Parco di Stalla was chosen as study case because it has been defined by the PPTR as “evidence of settlement stratification”, and in detail as a site “affected by the presence and/or stratification of historical cultural assets of particular landscape value as an expression of the identifying characteristics of the regional territory” (Fig. 2a, b). Moreover, it constitutes a good example of multifunctional reuse of a territorial resource.

The context in which the farm is located was analyzed using the following material:

- The official Cartography of the Military Geographic Institute (Apulia Region 2019);
- The maps of the PPTR (Apulia Region 2019);
- The maps of the Framework of Asset of the Tratturi of Puglia (Apulia Region 2019);
- The web-mapping tool Google Maps 2019.

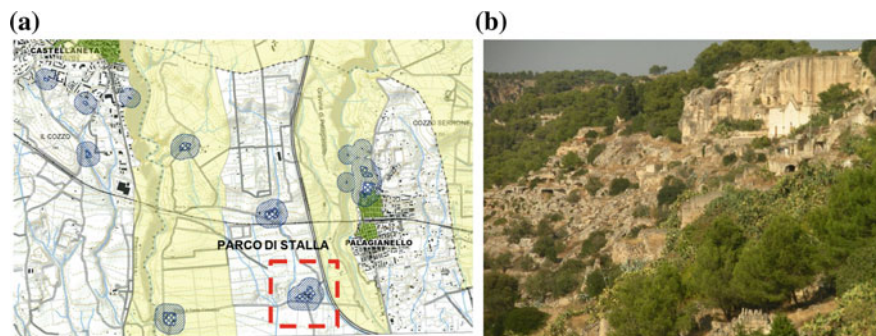


Fig. 2 Part of a PPTR map (drawn up in scale 1:50,000) showing cultural and settlement components (Apulia Region 2019) and the location of Parco di Stalla (a); the ravine of Palagianello (b)

The base maps, the infrastructural components and the main agro-environmental components characterizing the territory were managed by means of the ArcMap10 ESRI GIS software (www.esri.com). They were placed in the WGS 84/UTM zone 33 N reference system. Further data, useful for the updating of the base maps, were obtained by the photo-interpretation of the web-mapping tool Google Maps 2019.

The overlay mapping of the base map material allowed to integrate the information obtained from the aforementioned materials, to evaluate the landscape peculiarities in which Parco di Stalla is located and to outline strategies for its further development.

3 Results and Discussion

The analysis of PPTR documents showed that Parco di Stalla is located in an area close to the Regional Natural Park of Ravines. In detail, it lies between the ravine of Palagianello (Fig. 2b) and the ravine of Castellaneta, both of which have been declared areas of considerable public interest given the geomorphological and historical-cultural aspects of significant exceptionality. The whole area including the ravines and the area under study is located in the “Area delle Gravine” which is a Site of Community Importance and Special Protection Area, according to European Directives.

Numerous historical architectural evidences are located in the ravines, i.e. Medieval cave churches, cave villages, historical crypts and necropolises (Liano et al. 2015). Seventeen historic farmhouses, already present before 1810, are documented in the territory of Palagianello.

Parco di Stalla area is far from the sheep tracks that preserve the original consistency or that could be recovered, preserved and enhanced for their current historical-archaeological and touristic-recreational interest (Fig. 3a).

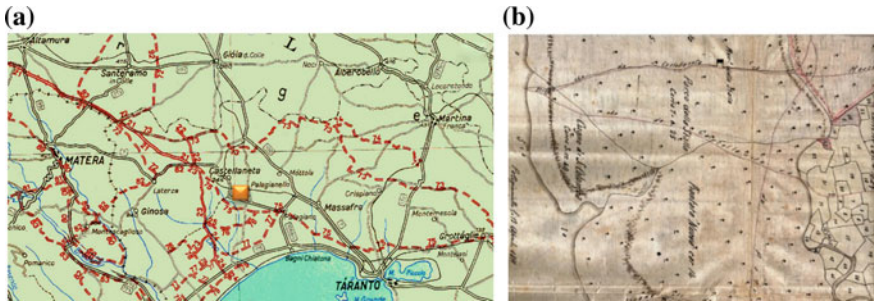


Fig. 3 Part of Sheep's paths Chart of Apulia Region (drawn up in scale 1:500,000 in 1959) and study area (a); Map dated 1811 showing the location of Parco di Stalla (Source Archivio di Stato di Lecce) (b)

Despite the great historical and cultural value of Parco di Stalla, the surrounding context is characterized by degradation and architectural elements that are not consistent with the rural context. It turns out to be distant from paths such as the *tratturi*, whose recovery and regeneration could have allowed a light and slow fruition of the surrounding extraordinary rural landscapes, or from the touristic paths already created in the area of the ravines. However, the road along the farm has ancient origins; it is in fact represented in a map dated 1811 (Fig. 3b); it represents a path to be enhanced.

For the purposes of a correct valorisation and use of the assets of Parco di Stalla therefore emerges the need to include it within a tourist route so that it can interact with the other present assets. In this way the need to make it fully usable and sustainable will be satisfied, that is to make it survive economically over time, with positive impacts on the territory and on society.

A route (Fig. 4) was therefore identified that could connect Parco di Stalla to other historic farms, and at the same time to the area of the two ravines of Castellaneta and Palagianello. In particular, the route starts from the old Bari-Taranto railway line that has been abandoned and redeveloped, becoming a cycle path.

In detail, starting from the disused railway section, the route, with its length of approximately 10 km, will skirt the Palagianello ravine and will reach the historic farmhouse Mangiaricotta (Fig. 5a); it will then pass near the ravine of Castellaneta and will reach the historic farmhouses Santa Colomba, Parco di Stalla, Serra Pizzuta (Fig. 5b–d).

The project of the route aims to protect the existing relationships between the elements of the landscape and to promote the rural tourism and the cultural exploitation of a site by enhancing the peculiarities of the rural context and allowing a slow and light use of unique historical-architectural elements and rural landscapes. Along the route, slow mobility paths must be created and construction elements with no consistency with the rural landscape, according to materials, typologies or colors, should be eliminated, as for example walls of reinforced concrete to be replaced with dry stone walls.

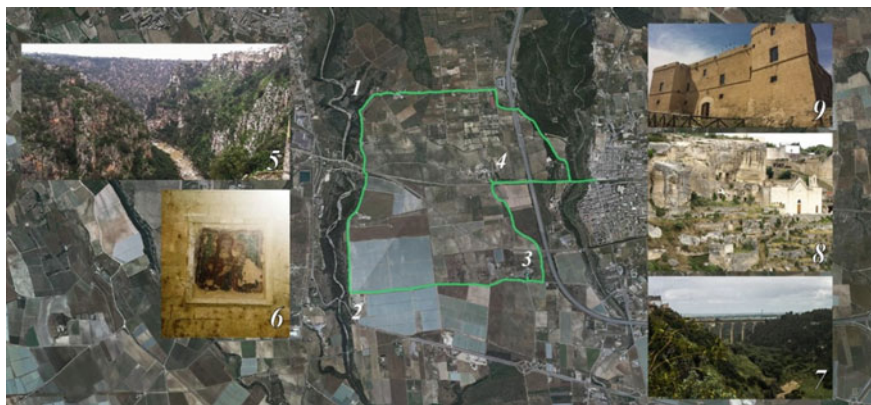


Fig. 4 Detail of the tourist route taken in consideration and sites of interest: (1) Mangiaricotta, (2) Santa Colomba, (3) Parco di Stalla, (4) Serra Pizzuta (farmhouses), (5) the ravine of Castellaneta, (6) Chiesa dell'Assunta (church), (7) the ravine of Palagianello, (8) Madonna delle Grazie (church and crypt), (9) Casale Stella-Caracciolo (castle)

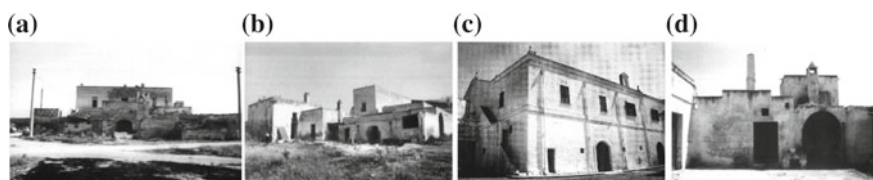


Fig. 5 The historic farmhouses Mangiaricotta (a), Santa Colomba (b), Parco di Stalla (c), Serra Pizzuta (d) (Source AA.VV. 1995)

4 Conclusions

The large farmhouses known as *masserie* are the most significant rural architectural features in the Apulian territory. Considering their widespread presence on the rural territory and their typological characteristics, they have great potential for recovery and reuse.

The designed thematic tourist route connecting various farms, recognised as cultural heritage by the Apulian Regional Administration and connected also to other routes along the ravines territory, will allow a complete cultural and touristic exploitation of historic rural buildings subject to this purpose to recovery and re-functionalization interventions.

Contributions The contribution to programming and conducting this research must be equally shared between the Authors.

References

- AA.VV. (1995). *Le Masserie storiche del territorio di Palagianello*, Catalogo Mostra Documentaria, Edizioni Grafiche Pugliesi—Mottola, Regione Puglia—Assessorato alla Pubblica Istruzione C.R.S.E.C. TA 49—Castellaneta in collaborazione con Amministrazione Comunale e Biblioteca Civica di Palagianello (In Italian).
- Apulia Region. (2015). Deliberazione Giunta Regionale n. 176, 16 Febbraio 2015. Approvazione del Piano Paesaggistico Territoriale della Regione Puglia (PPTR). Bollettino Ufficiale della Regione Puglia, n. 40, 23 Marzo 2015 (In Italian).
- Apulia Region. (2019). SIT Puglia Website. Retrieved from http://www.sit.puglia.it/portal/sit_portal.
- Calianandro, L. P., Loisi, R. V., & Dal Sasso, P. (2014). Connections between masserie and historical roads system in Apulia. *Journal of Agricultural Engineering*, 45(1), 15–23.
- Council of Europe. (2000). European landscape convention. Florence, 20/10/2000—Treaty open for signature by the member States of the Council of Europe and for accession by the European Union and the European non-member States. CETS No. 176.
- De Montis, A. (2016). Measuring the performance of planning: The conformance of Italian landscape planning practices with the European landscape convention. *European Planning Studies*, 24(9), 1727–1745.
- De Montis, A., Ledda, A., Serra, V., Noce, M., Barra, M., & De Montis, S. (2017). A method for analysing and planning rural built-up landscapes: The case of Sardinia, Italy. *Land Use Policy*, 62, 113–131.
- Italian Regulation. (2004). Legislative Decree No. 42/2004. Code about cultural heritage and landscape. Gazzetta Ufficiale, 45 (In Italian).
- Liano, E., Caragnano, D., & Scarascia Mugnozza, G. (2015). The medieval pilgrims routes in the Apulian cave settlements and their relationship with Rome and Santiago de Compostela. In *International Conference Proceedings “The European Pilgrimage Routes for Promoting Sustainable and Quality Tourism in Rural Areas*, 4–6 December 2014, Firenze, Italy.
- Ottomano Palmisano, G., Loisi, R. V., Ruggiero, G., Rocchi, L., Boggia, A., Roma, R., et al. (2016). Using analytic network process and dominance-based rough set approach for sustainable requalification of traditional farm buildings in Southern Italy. *Land Use Policy*, 59, 95–110.
- Pašakarnis, G., Morley, D., & Malienė, V. (2013). Rural development and challenges establishing sustainable land use in Eastern European countries. *Land Use Policy*, 30(1), 703–710.
- Ruggiero, G., Parlavecchia, M., & Dal Sasso, P. (2019). Typological characterisation and territorial distribution of traditional rural buildings in the Apulian territory (Italy). *Journal of Cultural Heritage*. (in press). <https://doi.org/10.1016/j.culher.2019.02.012>.
- Senes, G., Rovelli, R., Bertoni, D., Arata, L., Fumagalli, N., & Toccolini, A. (2017). Factors influencing greenways use: Definition of a method for estimation in the Italian context. *Journal of Transport Geography*, 65, 175–187.
- Torreggiani, D., & Tassinari, P. (2012). Landscape quality of farm buildings: The evolution of the design approach in Italy. *Journal of Cultural Heritage*, 13(1), 59–68.
- Torreggiani, D., Ludwiczak, Z., Dall’Ara, E., Benni, S., Maino, E., & Tassinari, P. (2014). TRuLAN: A high-resolution method for multi-time analysis of traditional rural landscapes and its application in Emilia-Romagna, Italy. *Landscape and Urban Planning*, 124, 93–103.
- van der Vaart, J. H. P. (2005). Towards a new rural landscape: Consequences of non-agricultural re-use of redundant farm buildings in Friesland. *Landscape Urban Planning*, 70(1), 143–152.

Enhancement of the Roman Bridge of Canosa in the Ofanto Valley Rural Landscape



Enrico Liano, Silvana Fuina, Marcio A. Alberti
and Giacomo Scarascia-Mugnozza

Abstract The ancient Roman Bridge, 2,000 years old, is located on the old Via Traiana route, three kilometers far from the town of Canosa (Apulia Region), and for many centuries it was the connection between northern and southern part of the Apulia Region along the Adriatic coast. It has an imposing structure stonework, with a donkey back shape, built with five round arches supported by piers sustained by rostrums. During the Second World War, a concrete access way was realized in order to let the British and American army tank pass through the bridge. The “Municipal Plan of the Tratturi” qualifies the area as “sheep trails or path” that preserves the original consistency or that can be at the same renovated. Aim of the research is the requalification of the study area through analyses, plan and restructuring the ancient routes. In this study, the current status of the area is analyzed in detail and the inconsistency of the interventions is highlighted. The project proposal provides for new tourism paths equipped with cycle/pedestrian tracks and small resting and refreshment areas, intermodal exchange car parks and management structures, allowing the creation of a green tourist-cultural route.

Keywords Roman bridge of canosa · Rural landscape · Sheep trails

1 Introduction

The Ofanto river (Fig. 1) is famous for many reasons linked to our history: the Battle of Cannae was fought by Hannibal (216 B.C.) along the bank of the river. It was celebrated several times in his lyrics by Quintus Horace Flaccus (Chelotti 1990).

Along its course were established ancient historical towns, including Compsa (present-day Conza della Campania), Canusium (present-day Canosa di Puglia) (Casano 1992), ancient Aufidena and, not distant from it, the same Venusia (or today’s Lucan city of Venosa) (Morea 1962, 1968, 1969; Sabbatini 2002).

E. Liano · S. Fuina (✉) · M. A. Alberti · G. Scarascia-Mugnozza
Department of Agricultural and Environmental Science (DISAAT), University of Bari, Via
Amendola 165/a, 70126 Bari, Italy
e-mail: fuina.silv@gmail.com

© Springer Nature Switzerland AG 2020

A. Coppola et al. (eds.), *Innovative Biosystems Engineering for Sustainable Agriculture, Forestry and Food Production*, Lecture Notes in Civil Engineering 67,
https://doi.org/10.1007/978-3-030-39299-4_40

351

The Roman Bridge, 2,000 years old (Fig. 2), is located on the Via Traiana route (Stopani 1992) about 3 km far from the town of Canosa (Fig. 3). The Via Traiana was realized between 108–110 A.D. by the Roman emperor Traianus, starting from Benevento and ending in Brindisi that was in the ancient times the boarding harbor to Greece and Middle East (Pratilli 1745; Kirsten 2003). The Via Traiana was paved with basalt stones and partly with large basole stones (Ieva 2003; Bertelli 1981; Caselli 2011). It was 4.00 m wide, with two sidewalks 2.00 m wide, and 0.50 m high, bordered by a stone curb.

The case study of the Roman Bridge, located in the relevant archaeological area of Canosa, has been carried out by means of the drone investigation technique, or unmanned aerial vehicles (UAV). The use of the drone was introduced mainly for military purposes and then was extended to numerous applications (Adams and Friedland 2011). In particular, with photographic equipment, cameras or other specialized instruments, drones allow investigations and inspections more quickly than using aircraft, helicopters or other means. It is possible to detect an entire area or a delimited area, in order to check for possible dangers of collapse or to discover hidden and undiscovered areas with laser scanning. Architecture and arts take advantage from this technology, for methods of restoration and conservation, to make it useful to an ever increasing number of people and redevelop places respecting the landscape (Toccolini et al. 2006; Fumagalli et al. 2012; Tassinari et al. 2011).

The application of the unmanned aerial vehicles (UAV) supports archeology and cultural heritage to monitor the sites and help heritage management (Stek 2016). The



Fig. 1 Giuseppe De Nittis, *Along the banks of the River Ofanto* (1867; oil on canvas Firenze, Galleria d'arte moderna)



Fig. 2 19th century painting by unknown author representing the Roman Bridge of Canosa

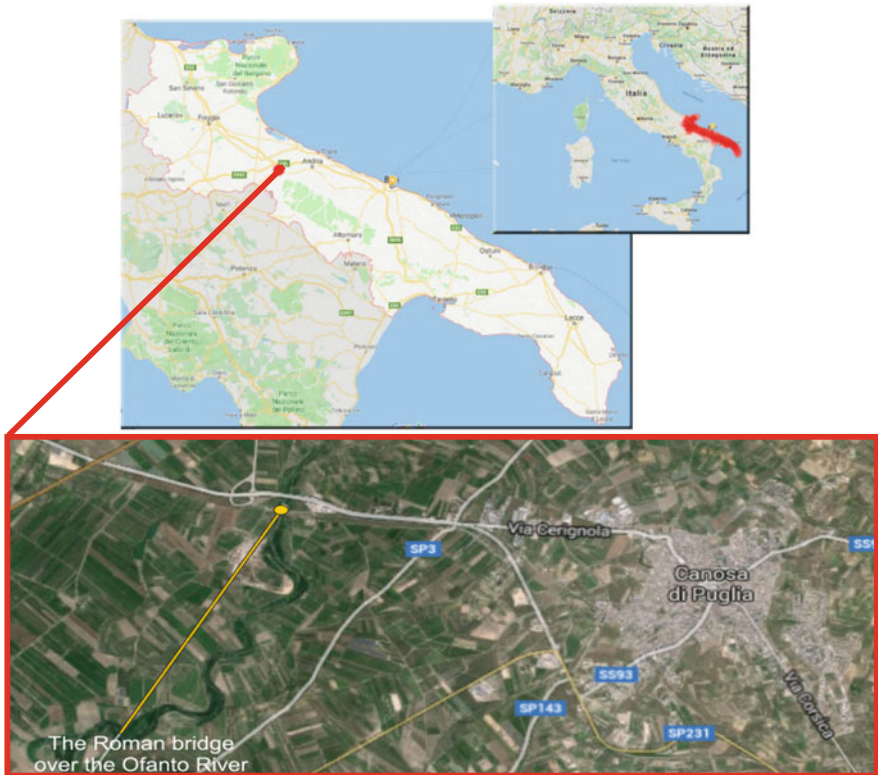


Fig. 3 Location of the bridge near the town of Canosa

possible applications are numerous: low-level photogrammetric surveys, documentation of the phases of stratigraphic archaeological excavation, analysis of ancient residential nuclei, the dynamics of the urban fabric and paleomorphologies, inspections and photo surveys graphs of architectural structures (monuments, historic buildings, aqueducts).

The integration of laser scanning technology with that of drone shots also responds to the need to obtain interior surveys of buildings that are not directly accessible. For this task “micro-drones” with a size of few cubic centimeters are generally used (Stek 2016).

The utilization of these devices together with the methods of visual anthropology are applied also to landscape management.

The main goals of this investigation are:

- To use UAV technologies in a historical important area such as the Roman bridge of Canosa;
- To identify instrument and protocol to assessment of the area of interest;

Fig. 4 Concrete route built during the Second World War for the military tanks transit Photo of 1944 of the Italian National Research Center



- To enhance the area, to identify the critical aspects of the current situation and to propose interventions suitable for a naturalistic and historic tourist itinerary.

2 The Old Roman Bridge on the Ofanto River

2.1 Construction Aspects

The Roman Bridge is 160.00 m long with a donkey's back shape. Its structure consists of 7 arches: 5 principal round arches, having different heights, and 2 lateral smaller ones. The 5 principal round arches are supported by thick massive pillars, of different dimensions, made of squared limestone blocks and equipped at the bottom with rostrum which guaranteed its stability against the stream of the river (Figs. 4, and 5). The structure is supported on a grid of wooden piles foundation filled up with concrete and coated with limestone blocks. It should be noted that during the Second World War a concrete route was built next to the bridge in the river bed to allow the military tanks to pass through (Fig. 4).

2.2 Environmental and Landscape Aspects

As a result of the survey conducted at the National State Archives of Foggia, the bridge over the centuries underwent numerous interventions of maintenance and restoration without involving the pillars, the rostrums and the foundation stalls. During the centuries the Roman Bridge was also part of the paths and livestock trails "Tratturi". From December 2015 was given the public concession of the municipal agricultural land of the town of Canosa along the "Tratturo Regio" livestock trails to voluntary organizations or social cooperatives in order to promote pedestrian or cycling tourism.



Fig. 5 Aerial view from the drone of the bridge

The purpose was to promote the area under the archaeological and agricultural productive point of view, also by means of a historical-tourist cultural itinerary. The maintenance of the area was given in concession by the Municipal Authority to the State Forestry Department. The land on the Tratturo Regio, in the section between the Roman Bridge on the Ofanto and the Mausoleo Bagnoli, should be subjected to protection, according to the “Town Plan of the Tratturi”, where they are qualified as Armento trails that preserve the original consistency or that can be restored at the same time.

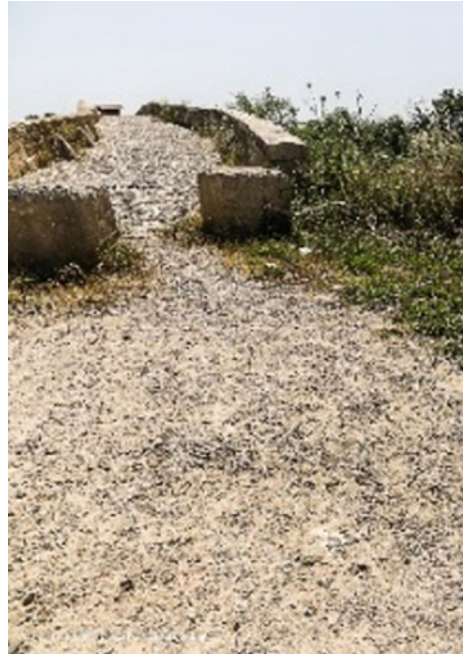
3 Design of Redevelopment of the Old Roman Bridge Area

3.1 *Materials and Methods*

The study and survey of the Roman Bridge has been carried out by means of the drone investigation technique, or unmanned aerial vehicles (UAV).

We provided a quadcopter drone with open dimensions $322 \times 242 \times 84$ mm and the flight plans were set to cover entirely the selected area, at a flight altitude of 3–10 m above ground level. The camera took pictures every 3 or 5 s with the following features: 12 million effective pixels, aperture $f/2.8$ (24 mm)– $f/3.8$ (48 mm), number of photos 100–1600 (automatic) or 100–3200 (manual).

Fig. 6 Lack of maintenance of the area



3.2 The Current Status of the Bridge Area

To date, after the field survey and the reconnaissance flight, it appears that the Roman Bridge, 2.000 years old, continues to be steady and stable but abandoned with spontaneous vegetation that covers a large part of the structure, especially the side ones (Figs. 5 and 6). Although the area is visited by tourists, the lack of a properly equipped and maintained touristic area should be pointed out.

3.3 Project Proposal

The design proposal enhances the Via Traiana through a path that involves the remaining pieces of the old sheep trails “Tratturi”.

The redevelopment of the area is based also on new infrastructures equipped with: a pedestrian and cycle trail; rest areas; intermodal exchange parking; management facilities. These equipment would allow the creation of a continuous green tourist route. The “Municipal Plan of the Tratturi” also provides for the planting of new bushy, shrubby and arboreal essences, made up of myrtle, boxwood, lavender, rosemary, holm oaks and oaks.

The criteria used for the design of the archeological path are:



Fig. 7 The design proposal of the redevelopment of the area

- Sustainable planning: services in the planning area will be based in the use of renewable sources and passive technologies, use of environment friendly technologies and materials;
- Preservation of natural resources: sustainable project should commit to the preservation of natural habitat and archeological sites as well as among the others minimizing waste, sewage, noise and maximizing of the use of renewable sources.

The proposed path starts from the town of Canosa (Fig. 7). Leaving Canosa in the direction of Cerignola, immediately after the Barletta—Spinazzola railway we meet the Arco Traiano (A.D. 109). Continuing before reaching the provincial road 231 we find Il Mausoleo Barbarossa (I century A.D.), remains of a sepulchral building. Continuing immediately after a crossroads we meet the building of the Mausoleo Bagnoli (2nd and the beginning of the 3rd century A.D.) a large two-story funerary monument with a typical pattern of tombs defined as a podium or a temple. Just turn your back to the mausoleum and turn towards the Ofanto River it is possible to admire the almost intact stretch of a sheep trail. Recently restored by the students of a Professional Institute for Agriculture and the Environment that allow us to continue either on a cycle path or a paved track (simulation of the old Via Traiana). On the entrance, RT or Regio Tratturo (4th century B.C.) is clearly marked.

Continuing along the sheep trail paths, we reach two rest areas from which we can see and reach the Roman bridge over the Ofanto River (Fig. 7).

4 Conclusions

Currently the Roman Bridge continues to be steady and stable but abandoned with spontaneous vegetation that covers a large part of the structure and lack of a properly

maintenance. The design proposal enhances the Via Traiana through a path that involves the remaining pieces of the old sheep trails “Tratturi”.

The studied area should be enhanced by means of:

- Planned green maintenance operations repeated two-three times a year;
- The correct cleaning of the bridge and the surrounding area;
- The creation of a real bike and pedestrian path;
- The strengthening of the bridge’s connection with the city of Canosa and the nearby archaeological areas;
- The realization of infrastructures equipped with a pedestrian and cycle trail, rest areas, intermodal exchange parking, management facilities;
- The realization of tourist information points;
- Event organizations that promote the area.

Acknowledgements The study, the data processing and the editorial work must be shared equivalently among the Authors within the areas of their expertise. We thank the UAV operator Vittorio Francavilla for the survey carried out with the drone.

References

- Adams, S. M., & Friedland, C. J. (2011). A survey of unmanned aerial vehicle (UAV) usage for imagery collection in disaster research and management. In *9th International Workshop on Remote Sensing for Disaster Response* (Vol. 8).
- Bertelli, G. & Castelfranchi F. M. (1981). *Canosa di Puglia e la sua storia e i suoi monumenti*, Roma, Tip.Imperia.
- Caselli, G. (2011). *La via Romea di Sigerico di Canterbury detta Via Francigena – Il percorso dell'autore rilevato nel 1985 secondo il documento del 990 “The Canterbury to Rome Pilgrims Way”*. First digital edition: Universal Library Unlimited.
- Cassano, R. (a cura di). (1992). *Principi, Imperatori e Vescovi. Duemila anni di storia a Canosa*, Ed. Marsilio, Venezia.
- Chelotti, M. (1990). *La Epigrafi romane di Canosa*. Edipuglia: Bari.
- Di Ruggiero, M.. (2016). *Correva l’anno... a Canosa, Andria*, Arts Media.
- Fumagalli, N., & Toccolini, A. (2012). Relationship between greenways and ecological network: A case study in Italy. *International Journal of Environmental Research*, 6(4), 903–916.
- Grelle, F., Giardina, A. (1993). *Canosa romana*, Roma, “L’Erma” di Bretschneider.
- Ieva, M. (2003). *Canosa dal territorio al castello: i caratteri della strutturazione del territorio in rapporto al sistema difensivo e alla nascita del castellum*. Adda: Bari.
- Kirsten, E. (2003). *Viaggiatori e vie in epoca greca e romana*, “Atti II Conv. St. Ma gna Grecia”, Taranto.
- Morea, G. (1969). *Arte e monumenti a Canosa*, a cura di Centro di servizi culturali, Canosa di Puglia.
- Morea, G. (1962). *Canosa. I suoi ruderi, i suoi monumenti*, Barletta, Ed. Rizzi.
- Morea, G. (1968). *Canosa: dalle origini all’Ottocento*, Barletta, Linotipia Rizzi & Del Re.
- Pratilli, F. M. (1745). *Della via Appia riconosciuta e descritta da Roma a Brindisi*, Giovanni di Simone, Napoli, National Central Library of Florence.
- Sabbatini, L. (2002). *Ceramiche di scavo della zona archeologica di Canosa: un’indagine archeometrica*. Proto: Bari.

- Stopani, R. (1992). *La via francigena del sud. L'Appia Traiana nel Medioevo*, Centro Studi Romei di Firenze, Le vie della storia, Le Lettere Ed. Firenze.
- Stek, T. D. (2016). Drones over Mediterranean landscapes. The potential of small UAV's (drones) for site detection and heritage management in archaeological survey projects: A case study from Le Pianelle in the Tappino Valley, Molise (Italy). *Journal of Cultural Heritage*, 22, 1066–1071.
- Tassinari, P., Torreggiani, D., Benni, S., Dall'Ara, E., & Pollicino, G. (2011). The FarmBuiLD model (farm building landscape design): First definition of parametric tools. *Journal of Cultural Heritage*, 12(4), 485–493.
- Toccolini, A., Fumagalli, N., & Senes, G. (2006). Greenways planning in Italy: the Lambro River Valley greenways system. *Landscape and urban planning*, 76(1–4), 98–111.

Mechanization and Technologies for Agricultural Production

Introduction

Prof. Marco Vieri

President of the 3rd Section of the Italian Association of Agricultural Engineering “Mechanization and Technologies for Agricultural Production”

AIIA 3rd Section proposes the development, sharing and dissemination of scientific and technical knowledge in the field of agricultural, forestry, animal husbandry and green areas, studying the possibilities to optimize the performance of agricultural production in terms of energy, environment safeguard, economic and social welfare. The Section performs its activities in the field of machinery, equipment and systems, sensors, automation and robotics, process control, logistics in agricultural, forestry and livestock supply chains.

The number of works presented in the 3rd AIIA Section highlights the intense activity of the various national universities and research institutes. Indeed, the collaboration with the industrial sector and with the territorial administrative bodies it is evident, demonstrating the role that the agricultural engineering continues to play.

The contributed works show the wide range of sectors in which the Section is currently involved, from animal husbandry to greenhouses, from open field to extreme areas cultivation, from basic experimentation on the optimization of technological apparatuses to impact assessments and efficiency studies achievable with increasingly advanced technological solutions.

Moreover, in the sector dedicated to rural activities such as agriculture and forestry, the Section maintains a strong commitment with regard to job security and eco-compatibility.

Furthermore, in the growing application of precision agriculture, the research activity gives a fundamental contribution to both the development of innovative devices and machinery and in the analysis of the correct method of new technologies use.

The development of sensors, digital models and analytical tools, brings the sector to the forefront of High-Technology Farming and digitalization development. In particular, e.g. the ISOBUS interconnection development is combined with the Farm Management Integrated System in order to create a management system in which the

skills of the 3rd Section can identify criteria and procedures for the correct allocation of technological resources so bringing added value to innovative business models of farm entrepreneurship.

Economic and Environmental Performances of a New Double Wheel Rake



J. Bacenetti, L. Bava, D. Lovarelli, A. Fusi and G. Reposi

Abstract This study presents the results of the development and testing of an innovative double-wheel rake which includes a double rotating unit that, thanks to an innovative design, aims to reduce the collection of stones and dust during the raking process. Field tests were carried out, mainly on alfalfa, comparing the Ra-Rake with different rakes (belt rake, rotary rake and comb rake). The economic and environmental performances were performed considering an increasing working area.

Keywords Raking · Life cycle assessment · Hay · Mechanization cost

1 Introduction

The quality of the forage is crucial for gaining the highest milk quality, which is increasingly important not only for health and nutritional purposes, but also for an effective recognition in terms of economic value. In this respect, the windrowing and swathing of the forage are crucial, not only in relation to the decrease in the product's mechanical loss, but also to limiting the soil contamination caused by the repeated and unavoidable handling the forage is subjected to during the haymaking operations. Timeliness is one of the key-aspects for good haymaking (Romera et al. 2005a, b). Except for machines with star wheels, it is important to focus on those equipment that minimize the inevitable contact of the working devices with the soil, bearing in mind that soil contamination facilitates the spreading of clostridial spores, which are detrimental to the production of long-ripened cheese. The availability of

J. Bacenetti (✉) · D. Lovarelli · A. Fusi

Department of Environmental Science and Policy, Università Degli Studi Di Milano, Via Celoria 2, 20133 Milano, Italy
e-mail: jacopo.bacenetti@unimi.it

L. Bava

Department of Agricultural and Environmental Science, Università Degli Studi Di Milano, Milan, Italy

G. Reposi

Reposi Macchine Agricole Srl, Via Vittorio Emanuele II, 40, Casorate Primo PV, Italy

© Springer Nature Switzerland AG 2020

A. Coppola et al. (eds.), *Innovative Biosystems Engineering for Sustainable Agriculture, Forestry and Food Production*, Lecture Notes in Civil Engineering 67,
https://doi.org/10.1007/978-3-030-39299-4_41

363

machines characterized by high field capacity and high productivity is important as it allows the reduction of product losses thanks to a good timing of the different operations carried out during the whole haymaking process. This study reports the economic and environmental results of the development and testing of an innovative rake (namely Ra-Rake) developed with the contribution of the EU project No 778475, based on a new double wheel rake with a double rotating unit that aims to reduce the collection of stones and soil during the raking process while increasing the working speed.

2 Materials and Methods

2.1 The Different Rakes

Three different rakes were compared to the double-wheel rake (or Ra-Rake): (i) a rotary rake, (ii) a comb rake, (iii) a belt rake. Table 1 reports the main rakes characteristics.





2.2 Life Cycle Assessment (LCA)

The LCA approach was applied for the environmental impact assessment. LCA, defined by specific ISO standards (ISO 2006) is, year after year, more and more used also in agricultural systems to quantify the environmental impact of products or processes (Notarnicola et al. 2015; Bortolini et al. 2014). In this study, the selected functional unit is 1 ha of raked area. The analysis is performed with a “gate to gate approach”, by focusing only on the raking operation. In more detail, the following aspects were considered in the environmental assessment: (i) production, maintenance, and end of life of the machinery used for the raking operation (rakes and coupled tractors), (ii) production of the inputs used with total wear (e.g., fuel), (iii) exhaust gases emissions from tractors’ engines.

Instead, all operations that occur before raking (e.g., sowing and crop management) and after (baling, transport, distribution, and use) were excluded. Therefore, the phases studied and outlined in Fig. 1 are: (i) Machinery manufacturing; (ii) Machinery use including the productive factors used both with partial and total wear; (iii) End of life (disposal, recycling of materials, etc.).

The following impact categories were evaluated using the characterization factors reported in the ILCD methods (EC-JRC 2012): Climate Change (CC), Ozone Depletion (OD) (depletion of the ozone layer), Particulate Matter Formation (PM) (formation of particulate matter), Photochemical Oxidant Formation (POF) (formation of photochemical smog), Acidification (TA) (terrestrial acidification), Freshwater Eutrophication (FE) (eutrophication of freshwater), Terrestrial Eutrophication

Table 1 Main characteristics of the compared rakes

	<p><i>Double-wheel rake (or ra-rake)</i> Working width 7.5 m Minimum engine power of coupled tractor 70 kW Purchase cost 19000 €</p>
	<p><i>Rotary rake</i> Working width 7.5 m Minimum engine power of coupled tractor 55 kW Purchase cost 24500 €</p>
	<p><i>Comb rake</i> Working width 7.5 m Minimum engine power of coupled tractor 40 kW Purchase cost: 20600 €</p>
	<p><i>Belt rake</i> Working width 7.3 m Minimum engine power of coupled tractor 70 kW Purchase cost 80000 €</p>

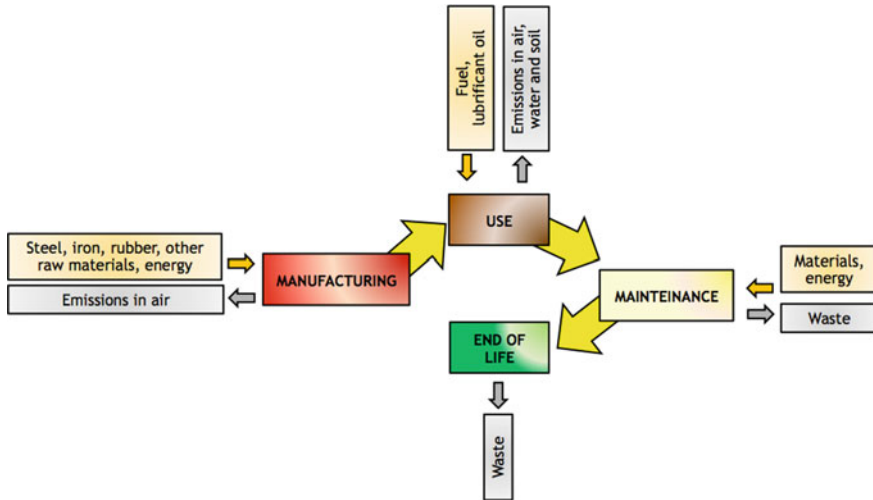


Fig. 1 Outlines the system boundary: for the different stages of the life cycle inputs and outputs are indicated

(TE) (terrestrial eutrophication), Marine Eutrophication (ME) (marine eutrophication), Mineral, Fossil and Renewable Resource Depletion (MFRD) (consumption of mineral and fossil resources).

2.3 Economic Analysis

The economic assessment, aimed at calculating the costs per hectare (€/ha) and the specific costs per unit of fodder (€/t), was carried by applying the method of fixed and variable costs (Lazzari and Mazzetto 2016) using information made available by the manufacturer (investment for the machine purchase, economic duration and lifespan, average annual use in the context in which the machine is intended to be used, maintenance and repair costs, and effective work capacity).

The economic assessment was carried out on the double-wheel rake together with different rake models available on the market. In order to verify the variation in costs at a different annually worked area, the assessment was conducted considering the use of machines on an area ranging from 200 to 2000 ha.

2.4 Data Collection

Based on specific survey forms designed by UNIMI, the following data were collected during trials performed in comparison with Repossi Machine Agricole Srl: (i)

components of the double-wheel rake characterized by a working width of 7.5 m and 6 wheels per side, (ii) mass of rakes compared to the mass of the double-wheel rake, (iii) working speed (km/h), (iv) effective work capacity (ha/h) of the different rakes by measurement of the different working times, (v) characteristics (engine power—kW, number of driving wheels WD) of tractors used during field trials, (vi) fodder losses during the raking operation, (vii) qualitative characteristics of the produced fodder by laboratory test. No statistical differences were found between the ash and the raw protein content of fodder produced using the ra-rake and the compared rakes.

In addition to the data directly collected and mentioned above, the following quantities were estimated and/or obtained from the database: (i) Fuel consumption estimated as a function of effective field capacity, power absorbed by the rake and engine power of the coupled tractor (Lazzari and Mazzetto 2016), (ii) Lubricant oil consumption for the tractor engine, (iii) “Virtual” consumption of machine (tractor and rake) calculated considering the machinery mass, their annual use, and their lifespan: $CM_{VIRT} = [M/(IM_{YEAR} \times DE)]/Co$, where: M = machinery mass (kg), IM_{YEAR} = annual use (h/year), DE = economic duration (year), Co = effective field capacity (ha/h); (iv) Emissions released in the air by the combustion of fuel in the engine calculated as a function of fuel consumption and information reported in the database Ecoinvent 3.5 (www.ecoinvent.org); (v) Energy consumed for the manufacturing of the double-wheel rake.

Table 2 reports the main materials used for Ra-Rake manufacturing while Table 3 shows the main inventory data considering an area of 2000 ha worked by the different rakes. This area takes into account the number of cuts that can be carried out per year on the different forage crops, hence, for example, the cultivation of alfalfa with a 5-cuts strategy per year corresponds to 400 ha of agricultural area (UAA). Diesel fuel consumption and emissions of exhaust gases (not shown in the table) are independent of the annual use, while the “virtual” consumption of machinery strongly depends on its use. To this end, Table 2 reports the virtual consumption considering also an annual worked land area of 1000 ha. For the tractor, a use of 600 h per year was

Table 2 Main construction materials composing the double-wheel rake (Ra-Rake)

Material	Amount	Unit
Steel S235J	559.14	kg
Steel S275J	62.39	kg
Steel S355J	1014.75	kg
Tempered steel C45	2.13	kg
Tempered steel 39NiCrMo3	22.32	kg
Steel for springs	243.01	kg
Carbon steel	459.24	kg
Aluminium	3.40	kg
Rubber	113.82	kg
Total mass	2480.20	kg

Table 3 Main inventory data for the different rakes and reported to two meadow sizes

Parameter		Rotary	Double wheel	Comb	Belt
Effective field capacity	ha/h	5.1	10.7	4.8	10.2
Mass	kg	1600	2480	1120	3200
Absorbed power	kW	35	30	22	45
Fuel consumption	kg/ha	1.55	0.63	0.98	1.04
Virtual consumption of tractor	kg/ha	0.46	0.50	0.33	0.54
Virtual consumption of rake (2000 ha/year)	kg/ha	0.5	1.705	0.35	2.00
Virtual consumption of rake (1000 ha/year)	kg/ha	1.00	3.41	0.7	4.00

assumed. Regarding the fodder losses, no statistically significant differences were found amongst the different rakes.

3 Results

3.1 Environmental Results

The absolute impact related to the raking of 1 ha with the double-wheel rake is reported in Table 4 considering two different areas (1000 and 2000 ha/year), while in Fig. 2 the contribution to the total impact of the different productive factors consumed and/or of the different emissions are reported.

The variation of impacts shown in Table 3 is due to the different mass of the rake virtually consumed considering the two areas: when doubling the area annually worked, the mass of machine virtually consumed doubles. When the environmental impact changes, also the associated production factor or emission change. However,

Table 4 Impacts related to 1 ha of worked area

Impact category	Unit	1000 ha	2000 ha
CC	kg CO ₂ eq	7.930	7.279
OD	mg CFC-11 eq	0.929	0.880
PM	g PM 2.5 eq	6.576	6.181
POF	g NMVOC eq	57.02	55.474
TA	mole H + eq	0.061	0.058
TE	mole N eq	0.177	0.172
FE	g P eq	3.225	3.021
ME	g N eq	16.40	15.951
MFRD	g Sb eq	4.164	4.118

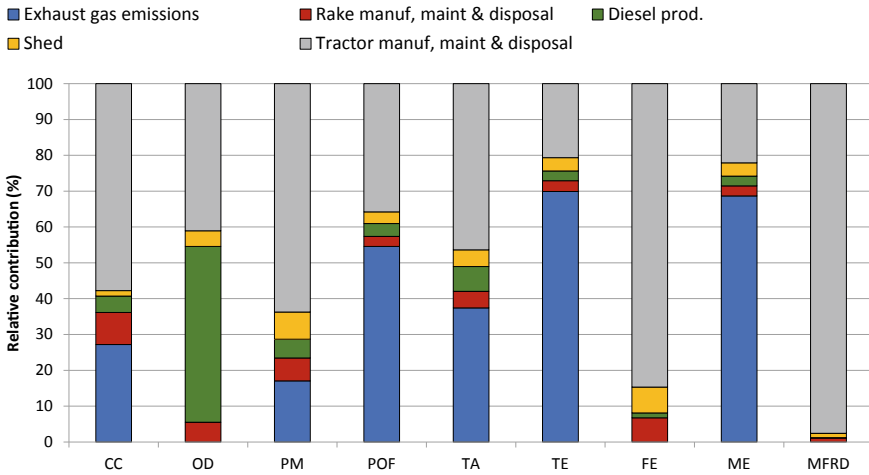


Fig. 2 Contribution analysis of the raking operation with the double-wheel rake on 2000 ha

the manufacturing, maintenance, and disposal of the machines (tractor and rake) are the processes that contribute the most to the environmental impact of the raking operation, even if the consumption of diesel (and the associated exhaust gases emissions) is low for this operation. Nevertheless, diesel consumption is responsible for about 49% of OD, and the emissions associated with its combustion in the tractor engine are responsible for 54% of POF and 68% of TE and ME.

Figure 3 shows the relative comparison amongst the different rakes when an annual worked area of 2000 ha is considered; for each evaluated impact category, the rake with the higher impact is set equal to 100% while the other rakes are proportionally scaled.

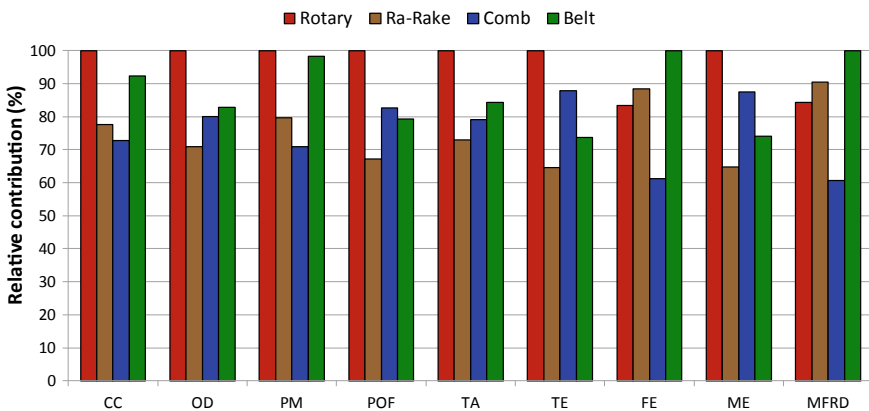


Fig. 3 Relative comparison of the environmental impact of a worked area of 2000 ha worked by different rakes

With a working area of 2000 ha, the rotary rake is the worst solution for 7 of the 9 evaluated impact categories while for the remaining two the it the belt rake that shows the higher impact. The comb rake is the best solution for CC with an impact reduction respect to the rotary harrow of about 30%. The Ra-Rake is the most sustainable solution for OD (-30% respect to the worst rake the rotary one), POF (-35% respect to the worst rake the rotary one) and TE (-33% respect to the worst rake the rotary one).

3.2 Economic Results

Figure 4 reports the economic cost considering increasing worked area. As expected, by increasing the worked area, the cost of mechanization decreases. The raking operation with the double-wheel rake has the lowest cost both for high annual surfaces (2000 ha) and for smaller surfaces (200 ha). The reason for such result lies in two factors: the greater work capacity and the lower purchasing cost.

For annual working areas wider than 600–800 ha, the differences among the Ra-Rake and comb and rotary rake are reduced but remain considerable in respect to the belt rake. For this latter the economic cost becomes similar (but however still higher) to the one of the other rakes only for annual working area of 2000 ha.

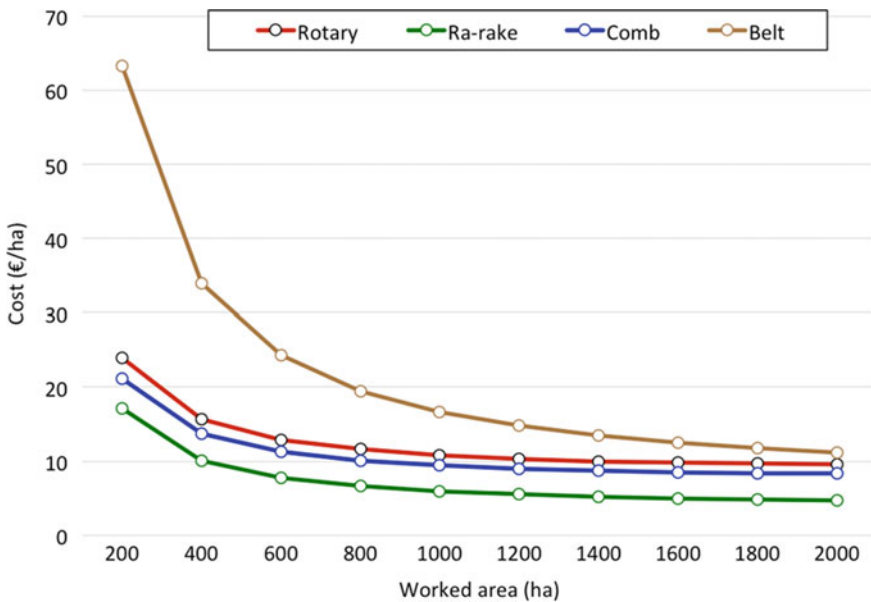


Fig. 4 Economic cost for the different rakes considering a worked area of 2000 ha

Considering an average yield for alfalfa in Lombardy of 2.8 t/ha of dry matter (14.16 t/ha of dry matter per year, considering on average 5.1 cut/year) and an annual working area of 1000 ha, the unitary cost ranges from 2.4 to 6.0 €/t of dry matter for the Ra-Rake and the belt rake, respectively.

4 Conclusions

The economic and environmental assessment carried out in the present study shows that, when compared to other three rake concepts, the double-wheel rake shows: (i) the best results for the mechanization cost of the raking operation, independently from the working area considered, (ii) a higher effective field capacity, with performances similar to the belt rake but higher than those achieved by rotary and comb rakes, (iii) an environmental impact lower than the belt rake, similar to the one achieved by the rotary rake and higher than the one of the comb rake.

Looking ahead, the development of other models of double-wheel rake with the same frame but a greater working width will allow to optimize its performance also from an environmental point of view (reduced impact).

References

- Bortolini, M., Cascini, A., Gamberi, M., Mora, C., & Regattieri, A. (2014). Sustainable design and life cycle assessment of an innovative multi-functional haymaking agricultural machinery. *Journal of Cleaner Production*, 82, 23–36.
- EC-JRC- European Commission, Joint Research Centre, Institute for Environment and Sustainability. (2012). Characterisation factors of the ILCD Recommended Life Cycle Impact Assessment methods. Database and Supporting Information. First edition. February 2012. EUR 25167. Luxembourg. Publications Office of the European Union; 2012.
- ISO 14044. (2006). *Environmental management—life cycle assessment—requirements and guidelines*. International Organization for Standardization.
- Lazzari M., Mazzetto F. (2016). *Meccanica e meccanizzazione dei processi produttivi agricoli*. Reda editore.
- Notarnicola, B., Salomone, R., Petti, L., Renzulli, P. A., Roma, R., & Cerutti, A. K. (Eds.). (2015). *Life cycle assessment in the agri-food sector: case studies, methodological issues and best practices*. Springer.
- Romera, A. J., Morris, S. T., Hodgson, J., Stirling, W. D., & Woodward, S. J. R. (2005a). Comparison of haymaking strategies for cow-calf systems in the Salado Region of Argentina using a simulation model. 3. Exploratory risk assessment. *Grass and forage science*, 60(4), 417–422.
- Romera, A. J., Morris, S. T., Hodgson, J., Stirling, W. D., & Woodward, S. J. R. (2005b). Comparison of haymaking strategies for cow-calf systems in the Salado Region of Argentina using a simulation model. 1. Effect of herbage mass at cutting and cow stocking rate under a rigid system of management. *Grass and forage science*, 60(4), 399–408.

Environmental Impact Alternatives for Soil Tillage and Sowing: Farmer or Contractor?



J. Bacenetti, D. Facchinetti, D. Lovarelli and D. Pessina

Abstract In Italy, contractors provide agricultural farms with over 40% of the mechanization needs. Compared to farmers, they can more promptly amortize their investment and help reduce the environmental impact of mechanization due to the use of better performing machinery. The goal of this study is to evaluate whether the seedbed preparation and sowing operations carried out by contractors have a lower environmental impact than those performed by farmers. Data about 20 agro-mechanical contractor companies located in Northern Italy were collected investigating technical, operating and usage machines characteristics. Regarding farmers, a typical farm (50 ha, double cropping and fleet of 4 tractors) was considered as reference. Operation sequences carried out by contractors and farmers were identified and compared through Life Cycle Assessment to evaluate their potential environmental impact. The impact of seedbed preparation and sowing resulted generally lower when carried out by contractors. Compared to farmers, Climate Change was reduced by 24.5% for conventional tillage and 9.1% for minimum tillage. The greatest reductions in environmental impact are shown for Particulate Matter production and for acidification, mostly due to the emission reduction devices available on the modern tractors mostly used by contractors.

Keywords Contractors · Farmers · Environmental sustainability · Efficiency · Machinery

J. Bacenetti (✉) · D. Lovarelli

Department of Environmental Science and Policy, Università degli Studi di Milano, Via Celoria, 2, 20133 Milan, Italy

e-mail: jacopo.bacenetti@unimi.it

D. Facchinetti · D. Pessina

Department of Agricultural and Environmental Sciences, Production, Landscape, Agroenergy, Università degli Studi di Milano, Via Celoria, 2, 20133 Milan, Italy

© Springer Nature Switzerland AG 2020

A. Coppola et al. (eds.), *Innovative Biosystems Engineering for Sustainable Agriculture*,

Forestry and Food Production, Lecture Notes in Civil Engineering 67,

https://doi.org/10.1007/978-3-030-39299-4_42

1 Introduction

In an increasingly multifunctional agriculture aimed at the sustainable production of food and feed, the role of agricultural mechanization is of great importance. The use of most suitable machinery can help carry out field operations rapidly and of good quality. Moreover, considering the high cost to get advanced agricultural machines, the role of contractors is becoming increasingly important. Till to few years ago, contractors worked almost completely only to the most demanding operations (e.g., seedbed preparation and harvesting), but recently their activity knew a remarkable expansion.

Nowadays, in Italy, contractors supply agricultural farms with over 40% of the mechanization requirements for seedbed preparation, and even more for sowing (~65%), spraying (~75%) and harvesting (~85%). Compared to a farmer, the contractor operates on big areas, hence can quickly amortize the expense for modern machinery. Furthermore, contractors can also play a role in the reduction of the environmental impact associated with mechanization, because the modern machinery they use is more efficient than that normally used by farmers.

If the environmental aspects are considered, several studies confirmed that the impact of mechanization cannot be neglected. Although less impacting than other production inputs such as the fertilizers, mechanization can affect more than 30% of the total impact of crops cultivation due to the consumption of fuel, lubricating oil and machinery and, above all, to the emission of exhaust gases released from the engines of tractors and self-propelled machines (Bacenetti et al. 2015; Bacenetti et al. 2018; Janulevičius et al. 2013; Lijewski et al. 2013).

Thanks to the reduced emissions from recent machinery equipped with efficient devices for pollutants reduction as well as to their high yearly use, contractors' activity guarantees a more limited impact on the environment than that caused by old and worn machinery with a reduced annual use frequently adopted by farmers.

Limited to the preparation of the seedbed and sowing, a study was conducted to evaluate if the operations carried out by contractors have a lower environmental impact than those performed by farmers.

2 Materials and Methods

2.1 Data Collection on Contractors

With regard to contractors, in 2018, data were collected through survey forms in 22 contractor companies located in the provinces of Bergamo, Brescia, Mantua and Reggio Emilia. These data were dealing with the technical, managing and working characteristics of tractors and machines used for seedbed preparation and sowing.

In more details, collected data for tractors are: model, year of purchase, engine power, emission stage and working time per year; for machinery: model, working

Table 1 Average values of tractors surveyed, classified per emissive stage and annual use

Emission stage	Tractors (%)	Annual use (h/year)
n/a	6.3	287 ± 35
I	9.4	713 ± 51
II	17.7	855 ± 60
IIIA	19.3	965 ± 48
IIIB	19.3	1045 ± 114
IV	28.1	1111 ± 122

Table 2 Main characteristics of the farmer tractor fleet

Engine power of tractor (kW)	Life span (years)	Field operations to be carried out	Annual use (h/year)
110	15	Primary and secondary soil tillage, transport	400
66	20	Secondary soil tillage, hoeing, fertilization, irrigation	300
60	20	Spraying, irrigation	200
50	25	Sowing	200

width, working depth, working speed and power of the tractor engine commonly coupled. The annual use and the emission stage (defined from exhaust gases emission limits (EU Directive 97/68/EC 1998)) of the tractors investigated (about 250) are reported in Table 1; almost 70% of tractors respond to an emissive stage equal to or later better than IIIA.

2.2 Data on Farmers

For farmers, no direct surveys were conducted, but the characteristics of a typical farm of the Po Valley with a cereal and cereal-livestock address was considered. In more details, this farm is characterized by agricultural area of 50 ha with double cropping and irrigated field and a fleet of 4 tractors, having the most powerful engine max power of 110 kW and belonging to IIIA emission stage (Table 2).

2.3 Seedbed and Sowing Operations

Even if an extreme variability of solutions was highlighted, the survey allowed to identify two types of soil tillage: (i) conventional, consisting of ploughing, with a

Table 3 Sequence of operations for conventional tillage (both for farmer and contractors)

Soil texture	Ploughing depth (cm)	Sowing, seeder (U = universal; P = precision)
Clayey	25	U
	35	P
	40	P
Medium textured	25	U
	35	P
	40	P
Sandy	25	U
	35	P
	40	P

Table 4 Sequence of operations for minimum tillage (both for farmer and contractors, except for the first two sequences that are performed only by contractors because it is assumed that the farmer machinery fleet does not have a tractor with the required engine power)

Soil texture	Ploughing depth (cm)	Sowing, by seeder (U = universal; P = precision)
Clayey	15	U
		P
Medium textured	15	U
		P
Sandy	15	U
		P

variable depth depending on the crop (25, 35 and 40 cm) followed by one or more harrowing (15 cm depth), (ii) minimum tillage, consisting only of a primary tillage at a depth of 15 cm. In both cases, precision and universal seeders were considered. Based on the texture and regional soil maps, three types of soil were identified: sandy, medium-textured and clayey. Combining the different field operations and soil characteristics, 28 sequences were identified (15 for conventional seedbed preparation and sowing—Table 3—and 13 for the minimum tillage—Table 4). For minimum tillage, less sequences are analyzed because it is assumed that the farmer cannot carry out some of them with his machinery fleet, namely those on the clayey soil.

2.4 Life Cycle Assessment

The environmental impact assessment was conducted using the Life Cycle Assessment (LCA) approach. LCA is defined by ISO standards (ISO 14040 series 2006)

and allows quantifying the environmental impact of a product or a process by considering all the inputs (e.g., production factors used) and the outputs (e.g., emissions into the environment) of the system.

In this case, it includes all operations for seedbed preparation and sowing. The functional unit to which the results refer is “1 ha (50 × 200 m) of worked and sown field”. For both the contractor and the farmer, the following inventory data were considered: (i) the “virtual consumption” of tractor and machine, calculated on the basis of mass, economic duration, annual use and working time, (ii) diesel consumption, estimated from tractor engine power, minimum specific fuel consumption, engine load and working time, (iii) exhaust gases emissions, calculated according to diesel consumption, the emissive stage and correction factors (Lovarelli et al. 2017).

The ILCD (Wolf et al. 2012) characterization method was adopted for translating inventory data into potential environmental impacts. The following impacts were assessed: Climate change (CC), Ozone depletion (OD), terrestrial acidification (TA), Freshwater eutrophication (FE), marine eutrophication (ME), human toxicity (HT), photochemical oxidant formation (POF), particulate matter formation (PM), metals depletion (MD) and fossil resources depletion (FD).

3 Results

The results of the LCA study show that the impact of seedbed preparation and sowing work is generally lower when mechanization is carried out by contractors.

Figure 1 shows the ratio between the environmental impact of the contractor (CT) and that of the farmer (CD). If the ratio is greater than 1 it means that the contractor has, on average, a higher environmental impact, while if it is lower than 1 the farmer has the worst environmental results.

In the case of conventional tillage, for all the environmental impacts considered, the contractor shows better results than the farmer. Instead, in the case of minimum tillage, the reduction of the environmental impact with operations carried out by the contractor occurs for 7 of the 10 environmental effects evaluated, while there is a slight increase for the remaining three because of the large machinery mass characterizing these cases. The contractor achieved the most considerable reductions in environmental impact (up to -75%) compared to the farmer for environmental impacts such as acidification (TA), marine eutrophication (ME), photochemical oxidant formation (POF) and particulate matter formation (PM) that are the categories on which the effect on the environment is linked to the emission of pollutants from the tractor engine. These differences are mainly related to the different emission reduction devices with which modern tractors are equipped (and which are mostly used by contractors with more recent fleet). In the case of other impacts such as Climate change (CC), ozone layer depletion (OD), and fossil resources depletion (FD),

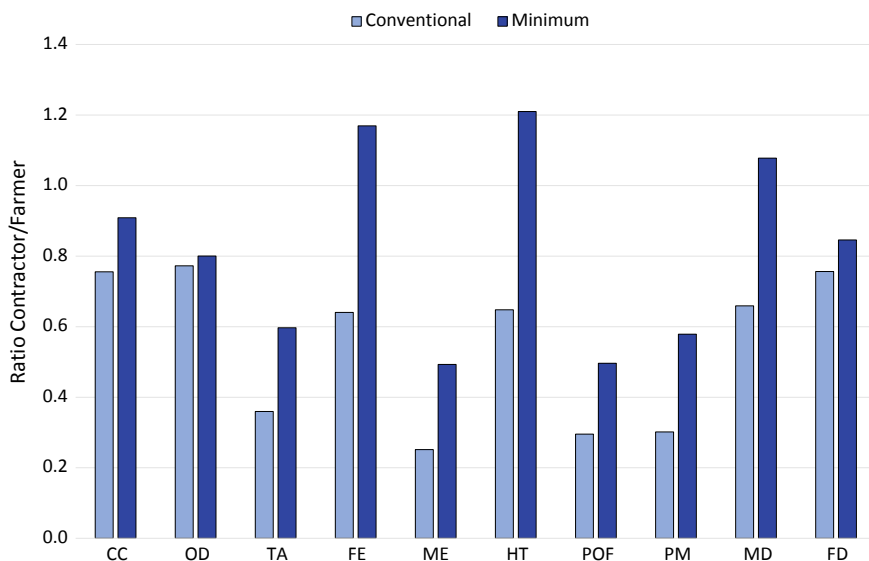


Fig. 1 Ratio between the average environmental impacts for conventional and minimum tillage, carried out by contractor and by farmer

the reduction in impact is lower (9–25%) and linked to the lower fuel consumption achieved by modern and efficient tractors coupled with implements characterized by greater productivity.

4 Conclusions

The analysis carried out shows that the contractor can significantly reduce the environmental impact due to the mechanization of seedbed preparation and sowing in the Po Valley. Therefore, increasing the operations carried out by contractors can lead to a reduction in the environmental impact of agricultural mechanization.

The results of this study may represent a starting point for the revision of the subsidies for the purchasing of agricultural equipment, that currently exclude contractors. In fact, from an environmental point of view, it is more sustainable that some field operations are carried out by a contractor. In any case, to have a more complete situation of the environmental benefits deriving from the mechanization carried out by contractors, the analysis should be extended to other areas and consider other field operations (slurry spreading, sod seeding, pesticides spreading, etc.).

Acknowledgements This activity was funded by Confederazione Agromeccanici e Agricoltori Italiani.

References

- Bacenetti, J., Fusi, A., Negri, M., & Fiala, M. (2015). Impact of cropping system and soil tillage on environmental performance of cereal silage productions. *Journal of Cleaner Production*, *86*, 49–59.
- Bacenetti, J., Lovarelli, D., Facchinetti, D., & Pessina, D. (2018). An environmental comparison of techniques to reduce pollutants emissions related to agricultural tractors. *Biosystems Engineering*, *171*, 30–40.
- European Directive 97/68/EC. (1998). On emissions from non-road mobile machinery. In: Official Journal of the European Communities 1998. L 59: 1.
- ISO 14040 series. (2006). Environmental management–Life Cycle Assessment–Requirements and guidelines. International Organization for Standardization.
- Janulevičius, A., Juostas, A., & Pupinis, G. (2013). Tractor's engine performance and emission characteristics in the process of ploughing. *Energy Conversion and Management*, *75*, 498–508.
- Lijewski, P., Merkisz, J., & Fuc, P. (2013). The analysis of the operating conditions of farm machinery engines in regard to exhaust emissions legislation. *Applied Engineering in Agriculture*, *29*(4), 445–452.
- Lovarelli, D., Bacenetti, J., & Fiala, M. (2017). Effect of local conditions and machinery characteristics on the environmental impacts of primary soil tillage. *Journal of Cleaner Production*, *140*, 479–491.
- Wolf, M. A., Pant, R., Chomkamsri, K., Sala, S., & Pennington, D. (2012). International Reference Life Cycle Data System (ILCD) Handbook–Towards more sustainable production and consumption for a resource-efficient Europe. JRC Reference Report, EUR 24982 EN. European Commission–Joint Research Centre. Luxembourg. Publications Office of the European Union.

A Biomass-Fueled Flamer for In-Row Weed Control in Vineyards: An Economic Evaluation



Gianfranco Pergher, Rino Gubiani and Matia Mainardis

Abstract Concern about the adverse effects of chemicals on the environment and on human health, and increasing restrictions of herbicide use, have led to renewed interest in non-chemical weed control, particularly under the row of vineyards. A new, biomass-fueled, flaming prototype (CS Thermos) was tested in the vineyard during spring-summer 2018, and compared with tillage and mowing. Based on the data from the field tests, an economic evaluation was conducted to compare flaming with tillage, mowing, and chemical weed control, with both one-sided and two-sided implements. The results indicated that chemical weed control was the cheapest alternative (387 €/ha or 268 €/ha, depending on the farm's size, 10 ha or 80 ha, respectively). Tillage resulted in a cost increase of 268 to 119 €/ha, which might, however, be sustainable for most growers if the better grape quality might be properly valued by the consumers. The one-sided flamer was generally more expensive than tillage, although cheaper than mowing. On the other side, the two-sided flamer version was generally more convenient than tillage (578 to 367 €/ha). Additional advantages and disadvantages of flaming versus tillage and mowing, particularly crop damage and the risk of fires, are discussed in the paper.

Keywords Weed control · Vineyard · Flaming · Economic evaluation

1 Introduction

Rising concern about the adverse effects of herbicides on the environment and on human health, and restrictions of use of some active substances, like glyphosate and glufosinate, have recently led to renewed interest in non-chemical weed control, particularly under the row of vineyards, with mechanical (tillage, mowing, brushing) or thermal methods (flaming, steaming, hot-foam machines) (Bekkers 2011; Hammermeister 2016).

G. Pergher (✉) · R. Gubiani · M. Mainardis

Department of Agricultural, Food, Environmental and Animal Sciences, University of Udine, Via delle Scienze 208, 33100 Udine, Italy
e-mail: gianfranco.pergher@uniud.it

© Springer Nature Switzerland AG 2020

A. Coppola et al. (eds.), *Innovative Biosystems Engineering for Sustainable Agriculture, Forestry and Food Production*, Lecture Notes in Civil Engineering 67,
https://doi.org/10.1007/978-3-030-39299-4_43

381

Tillage and mowing can be performed with a variety of specialized implements (Gaviglio 2007), which can be fitted with automatic vine-skipping mechanisms to reduce damage to the crop, but still have disadvantages such as: the need of repeated applications (4–6 per year), low working speeds, and limitations on wet soil and weeds. Additionally, weed control is never complete around the trunks and posts, and occasional damage to vines can still occur (Lanini et al. 2011). Brushes can do a better work around trunks and posts, but require even more frequent applications and typically cause substantial vine damage.

Thermal methods such as flaming, steaming, or hot-foam applications (Pessina et al. 2017) have been proposed and can avoid some of these problems, but require a large energy consumption from typically fossil fuels such as LPG or diesel oil.

A new, biomass-fueled, flaming prototype has been recently proposed (CS Thermos, San Vendemiano, TV). The machine was tested in the vineyard during spring-summer 2018 (Pergher et al. 2019), and compared with tillage and mowing. The results indicated that the efficacy of flaming was generally superior (64–76% of weed biomass removed or killed, depending on application date) to that of both tillage and mowing (40–60%), particularly around vines (64–75% vs. 37–48%). The study concluded that comparable weed control could be obtained with four applications per year of flaming, five of tillage, and five of mowing.

The objective of the present papers was to conduct an economic evaluation of these options, and to compare them with chemical weed control.

2 Materials and Methods

2.1 The Options Analyzed

Six options for in-row weed control were analyzed in this study, including tillage and chemical weed control (with two-sided implements), flaming and mowing (with both one-sided and two-sided implements). When possible, the same implements used in the above-mentioned field tests (Pergher et al. 2019) were considered; in the other cases, the most common models available on the market were included in the cost analysis.

The *one-sided flaming* option consisted of the biomass-fueled flamer (CS Thermos, San Vendemiano TV, Italy) tested by Pergher et al. (2019). It is a tractor-mounted implement, composed of a fuel hopper (300 dm³), an auger feeding system, a rotating-grid combustion chamber, and a horizontal chimney delivering the flame laterally onto the ground through a curved outlet (Fig. 1). Two centrifugal fans (total flow rate: 950 m³/h) provide the air for combustion and convection through the chimney and outlet. Wood pellet consumption (lower calorific value: 16.5 MJ/kg) was 32.0 kg/h in the field tests. The machine requires 10 min approx. for ignition and for reaching a stable operating temperature (900 °C at the outlet). The *two-sided flaming* option



Fig. 1 The biomass flamer in the vineyard

consisted in a different version, built by the same manufacturer, featuring two one-sided machines combined on the same frame. The length of the tubes delivering the flame to the outlets can be adjusted to suit vine row distances of 1.8–2.8 m. For both options, four applications per year were assumed, at an average speed of 4.2 km/h.

The *tillage* option included one application per year of a disc cultivator (at 4.5 km/h, two of a weeder blade (at 2.9 km/h), and two of a finger weeder (at 5.5 km/h) (all two-sided implements). *Disc cultivators* are mounted implements, carrying a concave disc on either side, designed to shuffle an amount of soil onto the row and so suffocate weeds. The resulting mound of loose soil is also useful to improve the efficacy of the following applications with the blade and finger cultivators. *Weeder blade cultivators* consist of a horizontal blade, fitted with an hydraulic vine-skipping system and designed to being slightly inserted below the soil's surface so as to sever weed shoots from their roots. *Finger weeder cultivators* are mounted implements carrying on either side a semi-horizontal disc, or "finger weeder", fitted with 20 radial, rubber spikes (diameter: 540 mm). These are entrained by the soil's reaction so as to rotate and eradicate small weeds, while bending slightly close to posts and vine trunks to avoid damage to the crop. All tillage implements considered here were two-sided.

The *mowing* option consisted of five applications per year of an undervine mower at 2.1 km/h. *Undervine mowers* are commonly designed as attachments to a standard flail mower for between-rows floor management. The undervine tool itself consists of a horizontal disc, with rubber protection edge and two axial cutting blades, driven by an hydraulic motor and provided with a mechanical vine-skipping mechanism. Both the *one-sided* version, requiring two passes on either side of the row, and the

two-sided version were analyzed. The low working speed assumed here (2.1 km/h) was found necessary in the field tests (Pergher et al. 2019) to allow the cutting discs penetrate the space between vine trunks, and to reduce the stress on the trunks themselves.

The *chemical* option consisted of three applications per year with a tractor-mounted, two-sided, shielded sprayer, at 6 km/h. Chemical weed control under the vine rows commonly includes both post-emergence herbicides, in the fall or spring before weed seeds germinate, and post-emergence herbicides in the spring or summer to control grown-up weeds. To the purposes of the present analysis, three applications per year were assumed: one in late winter, with a mix of Flazasulfuron (25% of active substance; dose rate: 0.03 l/ha) and Glyphosate (360 g/l at 1.3 l/ha); one in autumn, with the same herbicides and doses; and one in the spring—summer with Carfentrazone-ethyl (60 g/l, at 0.33 l/ha) and Cycloxydim (200 g/l at 1.0 l/ha); all doses are expressed per unit area of the vineyard, assuming application in bands over one third of total area.

To provide a correct cost comparison of the different options, the cost of shredding between the rows must be considered for all options other than mowing. Three shredding applications per year at 6.0 km/h were assumed in these cases.

The same model of specialized vineyard tractor was considered for all implements (Fendt 280P, 58 kW rated power), and a distance between the vine rows of 2.5 m was assumed.

2.2 Cost Computing

Cost calculation was performed in accordance with the method described by Srivastava et al. (2012). Cost parameters were updated, when necessary, using the latest revision of ASABE Agricultural Machinery Data (ASABE 2015). A model (Pergher 2015) was built in Excel containing all basic equations to estimate the ownership (fixed) costs (including the depreciation of the machine, interest on the investment, and cost of taxes, insurance and housing of the machine), and the operating (variable) costs (including the costs of labor, fuel and oil, other materials, and repair and maintenance).

The main data set used for cost analysis is shown in Table 1 (Tractor, Shredder, and one-sided Flamer and Mower), and in Table 2 (all other two-sided implements, including Sprayer, Flamer, Mower, Disc cultivator, Blade weeder, and Finger weeder).

Standard values, not reported in the above Tables, were defined as follows: interest rate: 5%; shelter rate: 0.5% (tractors) or 1% (implements); labor cost: 20 €/h; fuel (diesel) price: 0.9 €/kg; lubricant price: 5 €/kg; wood pellet price: 0.35 €/kg; economic life: 15 years (tractor, shredder, disc cultivator) or 10 years (all other equipment); physical life: 12,000 h (tractor) or 1,700 h (implements). Purchase cost of machinery was derived from the Manufacturers' information. All tillage implements were interchangeable, and used the same main frame; the price of this

Table 1 The parameters assumed for the Tractor, Shredder, and one-sided Flamer and Mower

Cost parameters	Symbol	Unit	Tractor	Flamer	Mower	Shredder
Engine rated power	W	kW	58	–	–	–
Purchase cost	A	€	75,000	6,500	7,000	5,000
R&m factor 1	RF 1	–	0.007	0.36	0.52	0.54
R&m factor 2	RF 2	–	2	1.14	1.76	1.50
Fuel cost (diesel)	Cf	€/h	–	4.9	7.2	8.1
Fuel cost (wood pellet)	Cp	€/h	–	10.2	–	–
Forward speed	v	km/h	–	4.5	2.3	6.0
Time efficiency	eT	–	–	0.77	0.86	0.74
Applications per year	t	–	–	4	5	3
Available field days	fd	–	–	15	12	15

Table 2 Cost parameters assumed for the two-sided implements

Cost parameters	Symbol	Unit	Sprayer	Flamer	Mower	Disc cult.	Blade weeder	Finger weeder
Engine rated power	W	kW	–	–	–	–	–	–
Purchase cost	A	€	4,500	12,000	14,000	3,400	6,600	7,500
R&m factor 1	RF 1	–	0.36	0.36	0.52	0.16	0.29	0.15
R&m factor 2	RF 2	–	1.14	1.14	1.76	1.50	1.94	1.94
Fuel cost (diesel)	Cf	€/h	4.9	4.9	7.2	4.9	4.9	4.9
Fuel cost (wood pellet)	Cp	€/h	–	20.5	–	–	–	–
Herbicide cost	Ch	€/ha	45.0	–	–	–	–	–
Forward speed	v	km/h	6.0	4.2	2.1	4.5	2.9	5.5
Time efficiency	eT	–	0.73	0.78	0.87	0.82	0.86	0.75
Applications per year	t	–	3	4	5	1	2	2
Available field days	fd	–	15	15	12	20	10	10

(15,000 €) was divided between the implements, proportionally to the number of applications.

The Tables also report the forward speeds assumed, along with time efficiency (i.e., the ratio TE/TT of actual working time, TE, to total time of use of the machine, TT) (Pergher 2015), the number of applications per year, and the available field days, i.e. the timeframe allowed for each application, considering the limitations given by rainy days or wet soil.

The model estimates the average operational cost (€/ha) of a machine as a function of the vineyard (farm) area. Whenever the vineyard area exceeds the actual area that the machine can work within the available field days, the model adds another piece of the same equipment, and re-calculates the average cost.

3 Results and Discussion

The annual operational costs (€/ha) for the six options analyzed in this study are shown in Fig. 2. For easier comparison, the cost of shredding was subtracted from the mowing options, rather than added to the other ones.

As expected, chemical weed control was the least expensive option, independently of the size of the vineyard farm, with annual costs ranging from 387 €/ha for a 10 ha farm, to 268 €/ha on 80 ha. The costs of the two-sided tillage option ranged from 656 €/ha to 387 on 10 ha and 80 ha, implying a difference of 268 to 119 €/ha, respectively. The importance of such a difference on the economic performance of the vineyard farm may vary widely, depending on the grape yield and price: from 3.7-8.4% of the value of the grapes for low prices (0.4 €/kg of grapes) and low yields (8 t/ha), depending on the farm size (80 and 10 ha, respectively), to just 0.3-0.7% for high prices (1.5 €/kg) and high yields (25 t/ha). In general, it seems that the replacement of chemical with mechanical weed control may be sustainable for most vineyard farms, especially when the “naturalness” of the product so obtained may be valued, and better priced by the consumers.

However, the use of tillage is difficult in rainy climates such as the North-East of Italy because of its limited timeframe, and is not recommended on hilly vineyards because of the risk of erosion. Here, flaming may be an interesting option. The annual costs of one-sided flaming resulted between 746 and 555 €/ha (for 10-ha and 80-ha

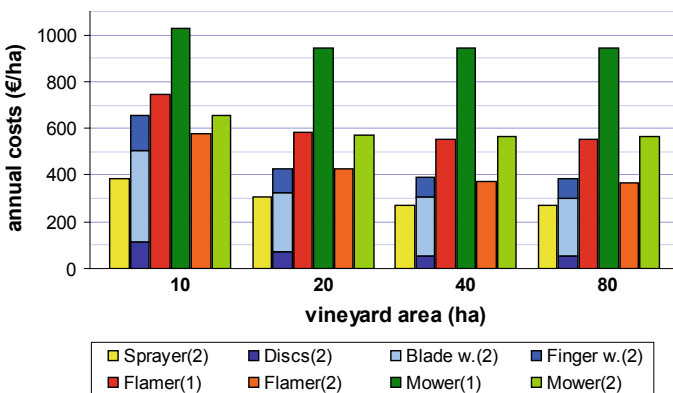


Fig. 2 Annual costs (€/ha) of the options considered. (1) one-sided, and (2) two sided implements. The cost of shredding was subtracted from the “Mower” options

farms, respectively; Fig. 2), and so always superior to that of tillage, with the gap increasing for the bigger farms, owing to the limited working width and the non-compressible cost of the wood pellet. On the other side, the two-sided flamer version was generally cheaper than tillage (578 to 367 €/ha, i.e. 77 to 20 €/ha less; as always, for 10-ha and 80-ha sized farms). Mowing was always more expensive than flaming, both in the one-sided and in the two-sided version. This was mainly owing to the low working speed assumed; it is possible that improved mowers (with hydraulic, double-acting vine-skipping mechanisms) may perform better.

Not all possible cost items could be accounted for in the present analysis because of still insufficient experimental data. This would, however, be particularly interesting for the tillage and mowing options, since the occasional damage to the vine trunks and/or roots, and incomplete weed control around trunks and posts, may generate additional costs for the replacement of damaged vines, or to manually complete the work with handheld hoes or grass trimmers.

The risk of uncontrolled fires is often reported as the main disadvantage of flaming (Lanini et al. 2011). The prototype described in this study can use an optional, front-mounted 500-L water tank, fitted with pump and nozzles to prevent risks of fire from dry weeds or debris. However, no fires were ever observed during the field tests in the 2018 season, and no damage to the vines or accessories such as shelters was reported (Pergher et al. 2019). In general, fires are unlikely to represent a serious problem in such rainy climates as in Friuli Venezia Giulia. In fact, weeds grow faster when rainy day alternate with hot, sunny days, when it is generally possible to perform flaming with moist soil and vegetation, and so avoid any risk of fires; while weed control is hardly needed during dry periods, owing to the slower weed growth rate. Nevertheless, also because of the importance of accident prevention in agricultural farms (Cividino et al. 2018), an additional safety system seems necessary, and in fact is already under study, in order to automatically exclude the flame and to prevent risks even in the case of unpredictable events, such as accidents or forced stops of the machine. Finally, the flue emissions of the flamer should be assessed, along with possible ways (Dell'antonia et al. 2013) to reduce them if necessary.

4 Conclusions

The field tests performed so far have shown that flaming has the potential of giving a level of in-row weed control comparable to that of tillage, even with a reduced number of applications (four per year, versus five; Pergher et al. 2019). Other potential advantages of flaming are: better weed control is possible around vine trunks and posts, thus eliminating the need of additional manual hoeing or weeding; a wider application time-frame is offered, since flaming can be applied even with moist soil and weeds; and a permanent sod is maintained under the vines, thus preventing soil erosion in hilly vineyards.

The economic evaluation showed that all non-chemical weed control methods analyzed were more expensive than traditional chemical weed control. The cost

increase seems, however, easily sustainable in most vineyard farms, particularly when the “naturalness” of grapes produced without chemical weed control can be valued by the consumers and so translate into a higher market price of the wine.

The use of the one-sided flaming prototype resulted in higher operational costs in comparison to tillage, while lower than those of mowing. The two-sided flaming option, on the other side, resulted in operational costs comparable to those of tillage, or even slightly less. This could make flaming a very interesting option for replacing chemical weed control, when the additional, operational advantages discussed above are considered along with economic evaluation. In conclusion, particularly if associated with improved pest control methods (Pergher and Zucchiatti 2018), flaming may further contribute to an overall reduction of chemical inputs in viticulture, with substantial environmental advantage.

References

- ASABE. (2015). D497.7: Agricultural machinery management data. St. Joseph, MI: ASABE.
- Bekkers, T. (2011). Weed control options for commercial organic vineyards. *Wine & Viticulture Journal*, 6–7, 62–64.
- Cividino, S. R. S., Pergher, G., Zucchiatti, N., & Gubiani, R. (2018). Agricultural health and safety survey in Friuli Venezia Giulia. *Agriculture*, 8(1), 10. (Paper 9).
- Dell’antonia, D., Pergher, G., Cividino, S. R. S., Gubiani, R., Cecchini, M., & Marucci, A. (2013). Characterization of biomass emissions and potential reduction in small-scale pellet boiler. *Lecture Notes in Computer Science*, 7972(2), 192–206.
- Gaviglio, C. (2007). Intérêt et limites des solutions alternatives au désherbage chimique sur le rang. *Progrès Agric. Vitic.*, 124(20), 423–427.
- Hammermeister, A. M. (2016). Organic weed management in perennial fruits. *Scientia Horticulturae*, 208, 28–42.
- Lanini, W. T., McGourty, G. T., & Thrupp, L. A. (2011). Weed management for organic vineyards. In G. McGourty (Ed.), *Organic winegrowing manual* (pp. 69–82). Richmond: University of California, Agriculture and Natural Resources.
- Pergher, G. (2015). *I costi di esercizio delle macchine agricole*. Capitolo 4 in: Appunti di meccanizzazione agricola-Parte generale. Università degli Studi di Udine, Udine, 2015.
- Pergher, G., & Zucchiatti, N. (2018). Influence of canopy development in the vineyard on spray deposition from a tunnel sprayer. *Journal of Agricultural Engineering*, 49(3), 164–173.
- Pergher, G., Gubiani, R., & Mainardis, M. (2019). Field testing of a biomass-fueled flamer for in-row weed control in the vineyard. *Agriculture*, 9(10), 210.
- Pessina, D., Facchinetti, D., Bacenetti, J., & Spezia, G. (2017). Performance of a hot-foam machine for the herbicide-free weeding of the vineyard. In *Proceedings, 11th International AIIA Conference* (pp. 343–346), 5–8 July 2016. Bari, Italy.
- Srivastava, A. K., Goering, C. E., Rohrbach, R. P., & Buckmaster D. R. (2012). Chapter 15 in Engineering principles of agricultural machines. In *Machinery selection and management* (2nd ed., pp. 525–551). St. Joseph, Michigan: ASABE.

N-TRE: A Model for the Evaluation of the Narrow Tractors Real Efficiency



Lavinia Eleonora Galli, Davide Facchinetti and Domenico Pessina

Abstract The efficiency of the so called “narrow tractors” is affected not only by their engine and transmission design evolution, but also by the usage modes adopted. In fact, especially in vineyards and orchards, many tasks do not require high engine power and traction pull, but only a remarkable oil flow, because many implements are hydraulically driven. The present work is aimed to create a model (also customizable) to evaluate the Narrow Tractor Real Efficiency (N-TRE), taking into account also different scenarios, in terms of time and intensity usage. At a first attempt, the running conditions and the power requirement of the main operations carried out in viticulture were considered on two narrow tractors, simulated in a stationary mode by means of an electromagnetic dynamometer and integrated with a device for measuring the fuel consumption. The basic output has been a series of engine performance curves (power, torque and Specific Fuel Consumption, SFC), both at full and partial loads. On these curves, some characteristic operating points were identified, simulating the typical tractor running conditions when working in vineyard.

Keywords Diesel engine · Performance curves · Fuel consumption · Narrow tractor efficiency

1 Introduction

The best coupling between the tractor and the various implements in terms of efficiency is probably the most important target to be acquired in order to reduce engine losses and therefore the overall fuel consumption. For example, in the vineyard the use of a shredder of 2 m working width could be considered, by coupling this implement to two tractors of different engine power, e.g. 90 and 50 kW. The first model could carry out the operation with no problems at a convenient travelling speed

L. E. Galli (✉) · D. Facchinetti · D. Pessina
Department of Agricultural and Environmental Sciences, Università degli Studi di Milano, Via
Celoria 2, 20133 Milan, Italy
e-mail: lavinia.galli@unimi.it

© Springer Nature Switzerland AG 2020
A. Coppola et al. (eds.), *Innovative Biosystems Engineering for Sustainable Agriculture, Forestry and Food Production*, Lecture Notes in Civil Engineering 67,
https://doi.org/10.1007/978-3-030-39299-4_44

(5–7 km/h), while with the second, due to limited engine power available, a significant reduction of the speed should be applied. It is interesting to underline that, with the more powerful tractor the percentage power usage (i.e. the efficiency) could be lower than the other smaller machine.

Several studies have been carried out on the performance evaluation and efficiency of agricultural self-propelled machinery (Lopez de Meneses 2012). From this point of view, the most popular test procedures is the OECD Code 2 (2019) and, more recently, the PowerMix settled out by DLG (Germany).

PowerMix in particular is finalized to measure the performance of agricultural tractors normally used in open field, by measuring the engine power required at the PTO, the drawbar and the hydraulic system (Degrell et al. 2011; Pieke et al. 2017). In detail, these tests are basically carried out thanks to a dynamometer wagon travelling on tracks, simulating the working field conditions. The data obtained, mainly in terms of Specific Fuel Consumption (SFC) values, allow an overall calculation of the performance and therefore the efficiency index of the tested vehicle.

The tractor efficiency based on the processing of various SFC values has been recently considered by many other organizations/laboratories. Some country as USA (Grisso et al. 2010; Howard et al. 2011), Spain (Muñoz-García et al. 2012; Ortiz-Cañavate et al. 2009), Turkey (Turker et al. 2012) and Korea defined test protocols using SFC value for evaluated the tractors efficiency.

Although several tests are already available for the assessment of the energy efficiency of agricultural vehicles and engines, they do not usually distinguish the tractor category neither their usage intensity and the most frequently working operations carried out.

An efficiency model, named N-TRE (Narrow Tractors Real Efficiency) specifically dedicated to the tractors used in orchards and vineyards was then created, taking into account their usage characteristics, both in terms of power demand and for the working time.

Tractors used in orchards and vineyards are usually included in the low-power category: recognized and shared market data have defined that, for these tractors, the engines fitted ranges normally between 35 and 90 kW, being the major part restricted between 50 and 75 kW. Due to the typical tasks carried out, the drawbar power request is frequently negligible, while those needed at the PTO and for the hydraulic systems are often remarkable.

In many working operations the size of the tractor (and as a consequence the mass and the mass distribution on the two axles) is the most important feature to be considered, because it is affecting the overall stability (and consequently the overturning risk), especially when heavy implements are coupled to the tractor at the three-point linkage. In these cases, due also to the working parameters (e.g. low travelling speed) the power request is frequently low or negligible, thus affecting negatively the engine efficiency.

Also the time used for carrying out a given operation is likewise affecting the overall machine efficiency: for example, in specialized cultivations the pruning (including also the topping) is usually executed twice in a year (before and in the middle of the

growing season), while pesticide treatments are much more frequently carried out, up to 15–20 times/year.

The aim of this paper is to present the details of the N-TRE model, finalized to compare, according to a well-defined test protocol, different tractors, in order to assess the most suitable model(s) to be used in a given cultivation area.

Moreover, the N-TRE was applied to two tractor models, equipped with engines having different anti-pollution emission stages, to point out the overall efficiency and the expected benefits (both in terms of fuel saving and pollutant production).

2 Materials and Method

In this study, 12 operations executed in vineyard have been considered. To draw suitable usage scenarios, for each of these operations the power needed to operate conveniently the implement has been assumed as well as the engine speed typically adopted by farmers to execute each operation. On the basis of these assumptions, the relevant engine load (i.e. the throttle setting) has been defined (Table 1). The engine load values were defined taking into account information provided by farmers dealing with the typical tractor usage in vineyard. Moreover, for each operation the number of repetitions over the entire season were assumed with reference to farmers' indications, to better represent the working practice, by considering the total time of execution.

Table 1 No-load engine speed and number of executions per year considered for the 12 operations to be carried out normally in the vineyard

No.	Working operation	No-load engine speed, min^{-1}	Number of executions over the season
1	Defoliation	1800	1
2	Pruning	1700	1
3	Topping	1700	1
4	Pre-pruning	1600	1
5	Shoot pruning	1800	1
6	Pneumatic spraying	1800	15
7	Duster spraying	1500	2
8	Mineral spreading	1400	2
9	Organic spreading	1450	1
10	Shredding	2000	3
11	Mechanical harvesting (towed model)	1900	1
12	Chiselling	2000	0.5 ^a

^aExecuted once every two years

In this view, three different scenarios were pointed out, taking into account the engine power request and the total time usage. They were structured as follows:

- “light” scenario: providing operations requiring low power and limited number of executions over the entire season;
- “medium” scenario: significant power and a higher frequency of execution;
- “heavy” scenario: involving high power need and a very frequent execution of some of the operations considered.

All the assumptions were referred to a conventional vineyard having 10 ha of cultivated area (Table 2).

To validate at a first step the N-TRE model, two comparable narrow tractors have been considered, showing them differences both for the technical design level and for the pollution emission stage. In detail, the two narrow tractors are coming from the same manufacturer, the tractor A was used and in good conditions and the tractor B was new (Table 3).

The performance curves (torque, power and SFC) of the two tested tractors engine were then measured at the Power Take-Off (PTO), obtaining the relevant running

Table 2 Execution time of the working operations considered in vineyard for different scenarios

No.	Working operation	“light scenario”		“medium scenario”		“heavy scenario”	
		h/year	%	h/year	%	h/year	%
1	Defoliation	35	19.4	35	13.2	35	6.8
2	Pruning	22	12.2	22	8.3	22	4.2
3	Topping	20	11.1	20	7.5	20	3.9
4	Pre-pruning	20	11.1	20	7.5	20	3.9
5	Shoot pruning	15	8.4	15	5.6	15	2.9
6	Pneumatic spraying	–		105	39.5	225	43.4
7	Duster spraying	32	17.8	–		–	
8	Mineral spreading	36	20.0	36	13.6	36	6.9
9	Organic spreading	–		12.5	4.8	25	4.8
10	Shredding	–		–		90	17.4
11	Mechanical harvesting (towed model)	–		–		15	2.9
12	Chiselling	–		–		15	2.9
	Total	180.0	100.0	265.5	100.0	518.0	100.0

Table 3 Main features of the two tractors tested

Tractor	Manufacturing year	Emission Stage	Max engine power, kW	Worked hours
A	2002	II	62.5	2900
B	2018	III B	47.8	18

points at steps of 100–200 min⁻¹. The engines were coupled with an electromagnetic dynamometer make KL-Maschinenbau GmbH (Rendsburg, Germany), mod. PT 301 MES, in combination with a fuel consumption meter of the same manufacturer, model FCM-100. The sensors and the electronics allowed a data transfer via Bluetooth every 15 s to a computer provided with a dedicated software.

The performance curves were obtained considering both that obtained at full load (i.e. at the maximum diesel delivery) both those recorded in a series of other conditions of partial load. These partial load curves were obtained by reducing the fuel delivery, in order to simulate what happens in the real execution of 12 field operations considered in the N-TRE model (Figs. 1 and 2).

For each operation the total engine power request was then calculated, taking into account, other than the power required for the implements use, also the additional power commitment to make possible the work execution (the so-called “losses”, i.e. those for the tractor travelling, the gearbox and the PTO running, the hydraulic system, the slippage).

The typical values of the 5 power-losses considered were assumed from the bibliography, considering the variations due to the different operating conditions: in Table 4 is shown an example, referred to the shoot pruning. Finally, all these assumptions were identified in given running points of the full and partial loads engine curves, to obtain the relevant SFC values. For each scenario, the typical working capacity (ha/h) of each operation considered was also defined, always referring the resulting data to a vineyard extension of 10 ha, being this figure suitable for a convenient mechanization including all (or the major part) of the 12 operations considered.

For each scenario, the SFC values were the starting data to obtain the real fuel consumption (l/year), taking into account both the whole power need and the time usage over the entire season. Considering the direct relationship between SFC and the efficiency (1), the performance of the two tractors were then ascertained.

$$\eta = \frac{1}{SFC} \cdot LCV \cdot \frac{1}{3600} \cdot 1000 \quad (1)$$

where: η = efficiency

SFC = Specific Fuel Consumption (g/kWh)

LCV = Lower Calorific Value of the diesel fuel (42.400 kJ/kg)

Finally, starting from the diesel cost, and considering the usage as constant over a period of 10 years, for the two tractors the fuel expenditures and so the savings of one in respect to the other were calculated for each scenario.

An interesting further feature concerns the environmental impact caused by the polluting gas emissions of the two tractors, according to the different intensity of use. With reference to SFC and emissive stages, the pollutant emissions for each operating scenario were estimated and compared. The emissions of pollutants were not calculated directly, but assumed equal to the limits of the correspondent engine emission stage of the two models (Stage II for the older and Stage III B for the newer).

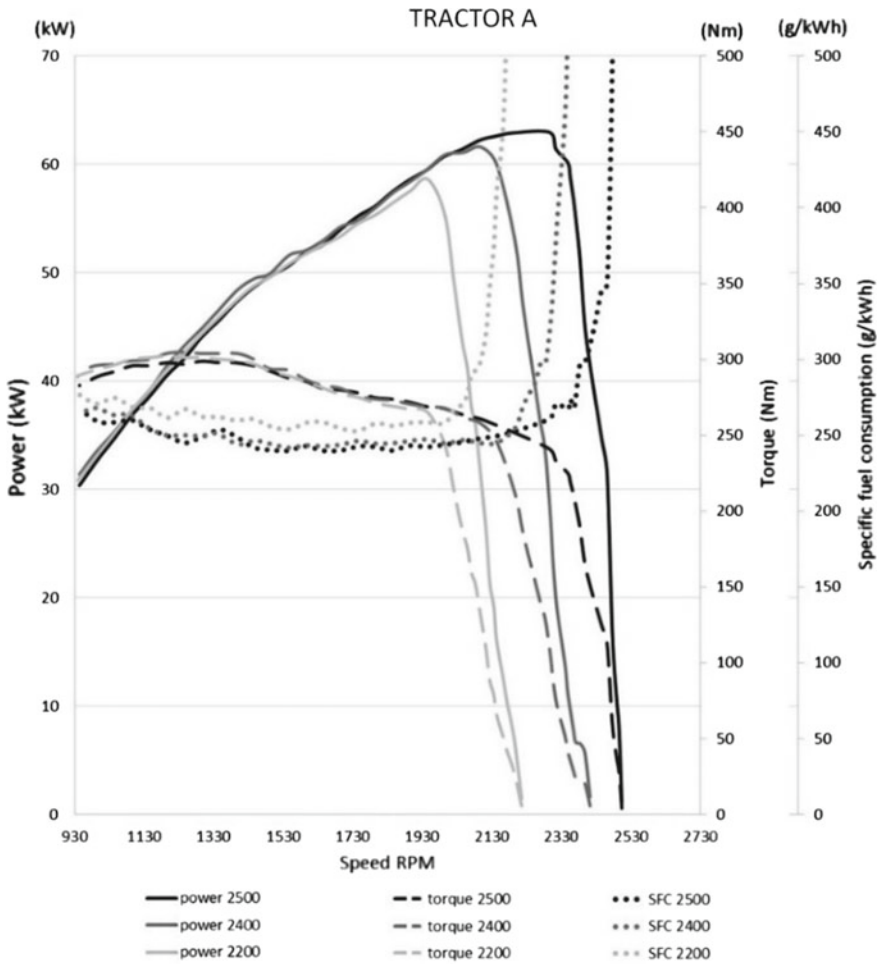


Fig. 1 Some of the engine curves of tractor A, obtained for different power ratio: those of 100% (2500 rev/min, 261.7 rad/s), 98% (2400 rev/min, 251.2 rad/s) and 93% (2200 rev/min, 230.3 rad/s) are shown in the figure

3 Results and Discussion

Although having different maximum engine power, the two tested tractors are comparable in terms of performance (Table 5). Nevertheless, they highlighted remarkable differences in developing torque and power, and consequently in terms of SFC.

As expected, the more modern tractor B showed lower SFC values (and consequently higher efficiency), both considering each single operation (Table 6) and the weighted average (Table 7), but also for the polluting gas emissions.

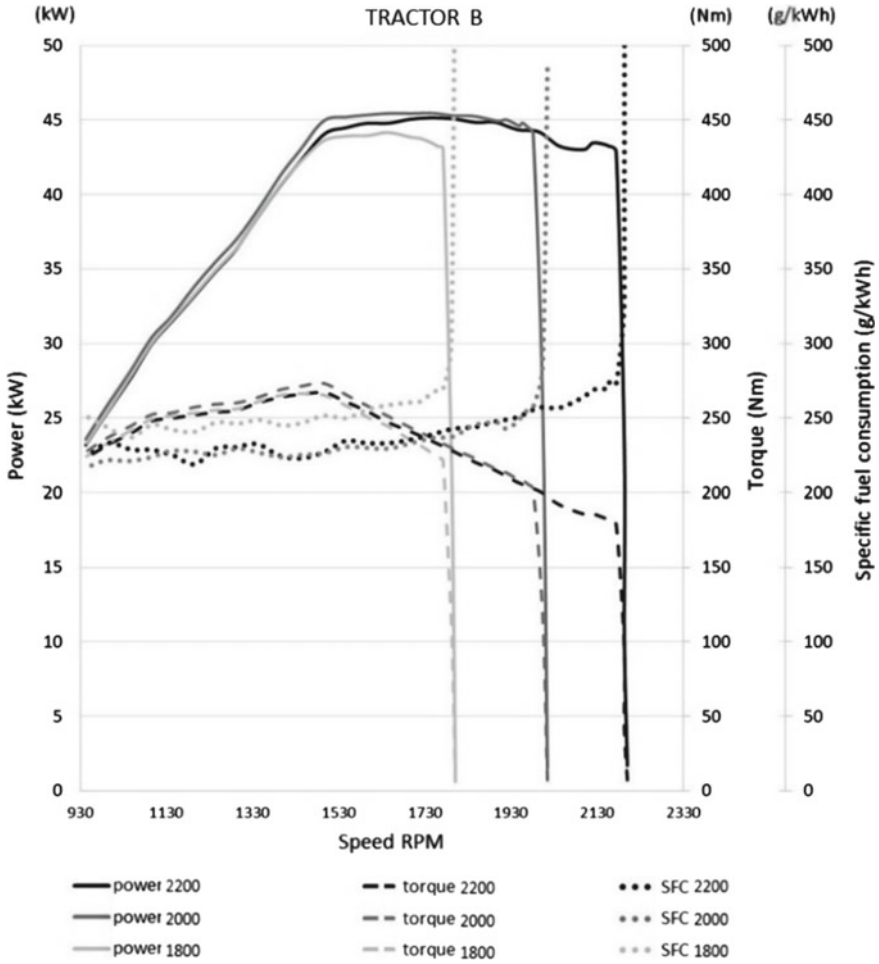


Fig. 2 Some of the engine curves of tractor B, obtained for different power ratio: those of 100% (2200 rev/min, 230.3 rad/s), 100% (2000 rev/min, 209.3 rad/s) and 98% (1800 rev/min, 188.4 rad/s) are shown in the figure

Table 4 An example of the so called “power-losses”, in this case considered for the shoot pruning

Losses	Tractor travelling	Gearbox	PTO	Hydraulic system	Slippage	Total losses	Power available for the implement working
%	10	10	5	4	4	33	67

Table 5 Engine power and its ratio in respect to the maximum of the two investigated tractors, over a range of engine speed

Engine speed, min ⁻¹	Tractor A	% of max power	Tractor B	% of max power
	Power, kW		Power, kW	
2500	62.95	100	–	–
2400	61.58	98	–	–
2300	60.46	96	45.27	100
2200	58.64	93	45.13	100
2100	57.69	92	45.38	100
2000	53.37	85	45.48	100
1900	52.59	84	45.31	100
1800	50.97	81	44.20	98
1700	50.18	80	44.46	98
1600	46.69	74	44.18	98
1500	41.43	66	43.49	96
1450	40.79	65	41.77	92
1400	38.49	61	39.88	88
1350	37.71	60	35.99	79
1200	26.71	42	32.38	72

Table 6 SFC values of the two tested tractors calculated for each working operation considered and relevant average, weighted for the assumed time usage (with reference to the heavy scenario)

No.		Tractor A	Tractor B
		g/kWh	
1	Defoliation	283.7	294.4
2	Pruning	313.3	271.8
3	Topping	291.9	261.6
4	Pre-pruning	317.1	261.6
5	Shoot pruning	325.5	305.1
6	Pneumatic spraying	281.4	268.3
7	Mineral spreading	313.8	242.4
8	Organic spreading	320.2	259.4
9	Shredding	265.7	242.9
10	Mechanical harvesting (towed model)	255.7	243.9
11	Chiselling	243.5	229.6
	Specific Fuel Consumption weighted average	285.5	262.3

Table 7 Weighted average SFC for different tractor usage intensity for the two tested tractors

Scenario		Light	Medium	Heavy
Specific fuel consumption (g/kWh)	Tractor A	308.1	295.7	285.5
	Tractor B	268.9	269.2	262.3

Table 8 Average efficiency of the two tested tractors in the 3 different scenarios considered

Scenario	Light	Medium	Heavy
Tractor A	0.276	0.287	0.298
Tractor B	0.316	0.316	0.324

In detail, tractor B highlighted efficiency index values of 31.6, 31.6 and 32.4%, respectively for the light, medium and heavy scenarios, while tractor A in the same conditions scored 27.6, 28.7 and 29.8%.

As expected, in general the engine performance is higher as the power requirements increase (Table 8).

The yearly fuel consumption of both tractors was then compared, in order to calculate the saving amount in the different scenarios, being them 9.88, 11.11 and 12.55% respectively from the light to the heavy scenarios.

Starting from a diesel cost of 0.95 €/l (VAT excluded), over a 10 years time usage the tractor B is highlighting a saving of 1844, 3567 and 8699 €, respectively passing from the light to the heavy scenarios.

On a hourly basis, it means that the burden decrease should be 1.00, 1.40 and 1.70 € in the 3 conditions, i.e. significant figures inside of the management tractor costs, also taking into account that the considered machines are included in the low-power category.

As expected, the emissions of pollutants are remarkable lower for tractor B, in accordance to the different stages, showing a reduction of approx. 94% for PM, 57% for NOx and 86% for HC.

4 Conclusions

This study showed an important decrease of SFC of tractor B in comparison with tractor A, so highlighting a significant efficiency improvement. This means a remarkable money saving for the fuel purchasing, especially if a 10 years usage is considered.

The N-TRE model demonstrated a high flexibility in its application, thanks to the possibility of modifying the variables according to the tractor usage.

The further development of the N-TRE model could provide the building of a suitable database of the most popular narrow tractor models at the moment available on the market, in order to better tune each simulation to the requirements of the single user.

The N-TRE model could have useful application for farmers evaluation and comparison of different tractor models to be purchased, to give information on the expenditure (i.e. the savings) over the entire working life of the machine, at least from the point of view of the fuel cost.

At a further step, the N-TRE model could find fruitful application in the public administration sector, to select the most efficient tractor models, to be possibly purchased by the farmers with dedicated financial supports.

References

- Degrell O, Feursten T., DLG-PowerMix. (2011). *A practical tractor test. Part I & II, DLG*, Gross Umstadt, Germany.
- Grisso R., Perumpral J., Vaughan D., Roberson G.T., & Pitman R. (2010). *Predicting tractor diesel fuel consumption*, (pp. 1–10). Virginia Cooperative Extension, Publications 442-073.
- Howard, C. N., Kocher, M. F., Hoy, R. M., & Blankenship, E. E. (2011). *Testing fuel efficiency of tractors with both continuously variable and standard geared transmissions*. Louisville, Kentucky: ASABE Annual International Meeting.
- Lopez de Meneses U.B. (2012). Characterization of farms for the machinery potential energy save and efficiency, *Bulletin UASVM, Horticulture*.
- Muñoz-García, M. A., Ortiz-Canavate, J., Gil-Sierra, J., Casanova, J., & Valle, A. (2012). *New classifications of tractors according to their energy efficiency*. Valencia: CIGR AgEng.
- OECD. (2019). OECD Standard Code for the official Testing of Agricultural and Forestry Tractor Performance, Paris.
- Ortiz-Cañavate, J., Gil-Sierra, J., Casanova-Kindelán, J., & Gil-Quirós, V. (2009). Classification of agricultural tractors according to the energy efficiencies of the engine and the transmission based on OECD tests. *Applied Engineering in Agriculture*.
- Piekie C., Stark W., Pfister F., & Schyr C. (2017). DLG powermix on the dynamometer, *ATZheavy duty worldwide*, 2/2017.
- Turker U., Ergul I., & Cumhuri Erolu M. (2012). Energy efficiency classification of agricultural tractors in Turkey based on OECD tests, *Energy Education Science and Technology*, 28(2), 917–924.

Controlled Mechanical Ventilation to Reduce Primary Energy Consumption in Air Conditioning of Greenhouses



C. Perone, P. Catalano, F. Giametta, G. La Fianza, L. Brunetti
and B. Bianchi

Abstract Air conditioning is one of the major cost in greenhouses production. One of the most interesting energy efficiency strategies is the reduction of the energy use itself. Mechanical ventilation with heat recovery could allow for a reduction in energy use for heating and cooling air inside greenhouses. After a preliminary study carried out in laboratory, a mechanical ventilation prototype was tested in a real case. The unit was installed at service of a mini-tunnel greenhouse located in Termoli (Campobasso)–Italy. The ventilation system consists of a high efficiency heat exchanger, able to recover thermal energy from the exhaust air, and a heat pump to adjust the supply air temperature before entering in greenhouse. A perforated duct was installed for the air distribution and a single grid was used to suck the indoor air. To evaluate the energy performance of the unit a supervision system allowed measuring and collecting all the thermo-physical parameters, in each side of the machine, and in the heat pump circuit. Four NTC probes were used to assess the temperature uniformity inside greenhouse. First tests were carried out on temperature control during winter season. They show that the indoor air temperature (set at 27 °C) is suitably adjusted by driving the unit with the reference probe installed on the machine recovery side. Only an offset of few Celsius degrees is observed due to duct heat loss and the recovery grid placed on one side. Furthermore, the mechanical ventilation system had also shown notable energy performance: COPs (mean value) of 5.4 and 5.7 at outdoor air temperature of 18.0 °C and 15.7 °C respectively.

Keywords Mechanical ventilation · Heat recovery · Greenhouse ventilation · Energy efficiency · Heat pump

C. Perone (✉) · P. Catalano · F. Giametta · G. La Fianza · L. Brunetti
Department of Agriculture, Environment and Food Science (A.A.A.) - University of Molise, Via
Francesco De Sanctis, 86100 Campobasso, Italy
e-mail: claudioperone@gmail.com

B. Bianchi
Department of Agro-environmental and Territorial Sciences (DISAAT), University of Bari “Aldo
Moro”, Via Amendola 165/A, 70126 Bari, Italy

© Springer Nature Switzerland AG 2020
A. Coppola et al. (eds.), *Innovative Biosystems Engineering for Sustainable Agriculture,
Forestry and Food Production*, Lecture Notes in Civil Engineering 67,
https://doi.org/10.1007/978-3-030-39299-4_45

1 Introduction

Given the rapid growth of the world population and the relative demand for food, there is a rising need to produce more by using as few resources as possible, such as soil, water and energy (Bianchi et al. 2015a). Greenhouse cultivation could meet these demands if well designed and managed. Energy saving is of vital importance for a sustainable production of protected crops. To this end several studies are developed in order to analyze the feasibility of using renewable energy for climate control inside greenhouses. Cuce et al. (2016) reported a comprehensive review on renewable and sustainable strategies for greenhouse conditioning. Environmental control of greenhouses involves the managing of temperature, humidity and carbon dioxide of the indoor air. To this purpose several systems were studied. Sethi and Sharma (2008) have classified these systems as heating system, cooling system and composite system. Regarding to ventilation systems, generally natural ventilation is the most considered. However, in line with studies on the ventilation of livestock farms (Bianchi et al. 2015b), for a better air distribution and uniformity inside greenhouse mechanical ventilation is also proposed as an alternative to natural ventilation.

Focusing deeply on ventilation systems, there is a lack of studies concerning the controlled mechanical ventilation systems, especially those that allow for air treatment before its entering in greenhouse. These systems, when compared with natural ventilation ones, ensure a better distribution and uniformity of the internal air and a substantial contribution to the reduction of the heating/cooling load. Van de Bulck et al. (2013) proposed a compact ventilation concept. The mechanical ventilation system was equipped with three intake ducts, one for outdoor air and the other two for air recirculation. Before entering the greenhouse, the supply air is pre-heated thanks to a low temperature heat exchanger. This ventilation system ensured 12% energy saving respect to reference case (natural ventilation). Coomans et al. (2013) studied a mechanical ventilation system with heat recovery through cross-flow heat exchanger in order to assess the relative energy savings compared to the reference case. Also in this case, the supply air was pre-heated through a low temperature heat exchanger. The authors found that energy saving was 28% compared to the reference greenhouse.

In this paper, the energy performances of a mechanical ventilation system, previously studied in laboratory by Fucci et al. (2016), and then installed at service of a mini-tunnel greenhouse (Perone et al. 2017), are presented in detail. Particularly, the present study focused on the energy performance of the system and its ability to control the indoor air temperature. The ventilation system is able to recover the thermal energy of the exhaust air and adjust the supply air temperature thanks to a heat pump.

2 Materials and Methods

The mechanical ventilation system analyzed in this work is that proposed by Fucci et al. (2016). The system is denominated SIVeMeC (Sistema Integrato per la Ventilazione Meccanica Controllata: Integrated System for Controlled Mechanical Ventilation). SIVeMeC is a heat recovery unit integrated with a heat pump able to adjust the supply air temperature. This system was preliminarily tested in a laboratory in which, with the aid of two climatic rooms, was possible to reproduce the boundary conditions. After that, it was optimized to be used for the conditioning of a mini-tunnel greenhouse located in Termoli (Campobasso–Italy), as reported in detail in the work of Perone et al. (2017).

For ease of understanding of the reading, in the Sect. 2, a summary of the SIVeMeC system and of the experimental apparatus installed in greenhouse are reported.

A more detailed analysis of these systems could be found in Fucci et al. (2016) and Perone et al. (2017).

2.1 SIVeMeC System

SIVeMeC (Fig. 1) is a mechanical ventilation system equipped with a counter-current heat exchanger and a heat pump consisting of a BLDC (BrushLess Direct Current) compressor, two direct expansion coils, supply and exhaust air fans with variable speed, electronic expansion valve and a 4-way valve to reverse the cycle. The two direct expansion coils are installed in series with the heat exchanger, so to ensure also a thermodynamic (active) recovery downstream of the passive one.

Thanks to by-pass ducts and internal partitions, SIVeMeC can operate according to four arrangements: (1) passive plus active recovery (by-pass ducts are closed and the compressor is active); (2) only passive recovery (when by-pass ducts are closed and the compressor is disabled); (3) only active recovery or thermodynamic recovery (by-pass ducts are open and the compressor is active); (4) freecooling/freeheating (by-pass ducts are open and the compressor is disabled). In order to adjust the system during its operation, it is possible to choose different probes as reference one: temperature (T), relative humidity (RH) and carbon dioxide (CO₂). The managing of the mechanical ventilation system prototype takes place through a suitable software programmed and installed on the electronic board of the unit. This software allows the managing of the SIVeMeC components. Moreover, it allows the communication with typical BMS (Building Management System) for the supervision of HVAC plants. Four NTC probes are connected to the electronic board to measure the temperatures of the supply, exhaust, suction and discharge airflows. Moreover, probes were installed for measuring the compressor suction and discharge temperatures, the condensation and evaporation pressure to define the compressor work zones. The optimal regulation happens with an inverter, which communicates through the Modbus serial communication protocol with the board. This connection allows the

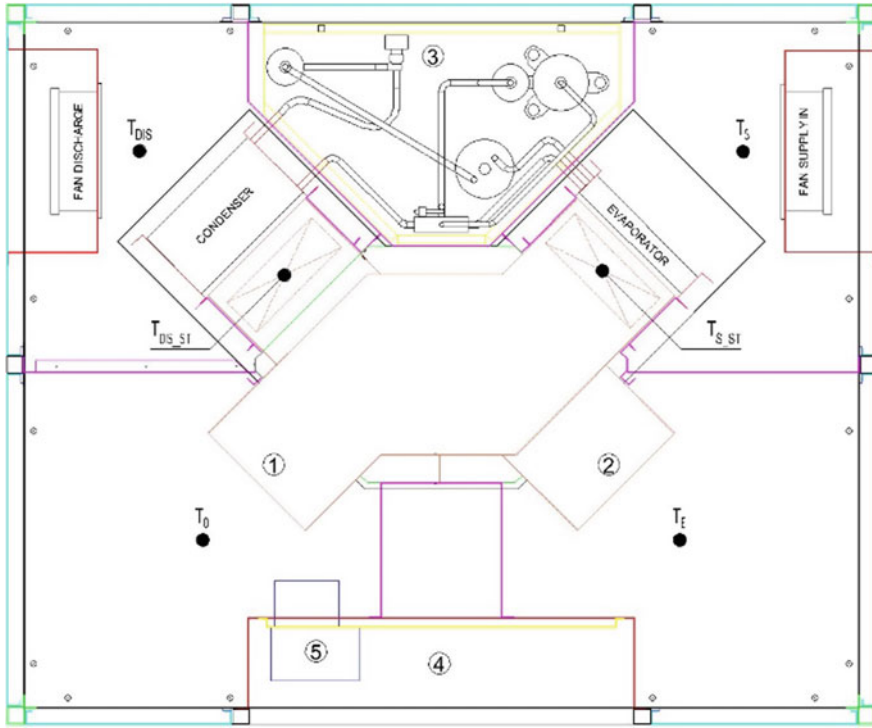


Fig. 1 SIVEMEC prototype. (1) by-pass duct for supply airstream; (2) by-pass duct for exhaust airstream; (3) heat pump compartment; (4) electrical panel; (5) inverter to modulate rotary compressor; T_S supply air temperature probe; T_0 outdoor air temperature probe; T_{S_ST} supply air temperature probe downstream the static recovery; T_E exhaust air temperature probe; T_{DIS} discharge air temperature probe downstream the static recovery. The ducts located above the heat exchanger allow its by-pass. Black circles point out where the temperature probes are placed

modulation of the load according to the climatic conditions and the maintenance of the operating parameters within the acceptable pressure and temperature limits.

2.2 Experimental Apparatus

After the first tests conducted in laboratory (Fucci et al. 2016), SIVeMeC was optimized and then installed at service of a mini-tunnel greenhouses (Perone et al. 2017). The experimental apparatus consists of the mechanical ventilation system SIVeMeC (Fig. 1a), a distribution system (Fig. 2b), a set of probes (Fig. 2b and c) and two Building Monitoring Systems (BMS), one to acquire data from field (Fig. 1a) and another to manage and supervise SIVeMeC (installed on a remote PC).

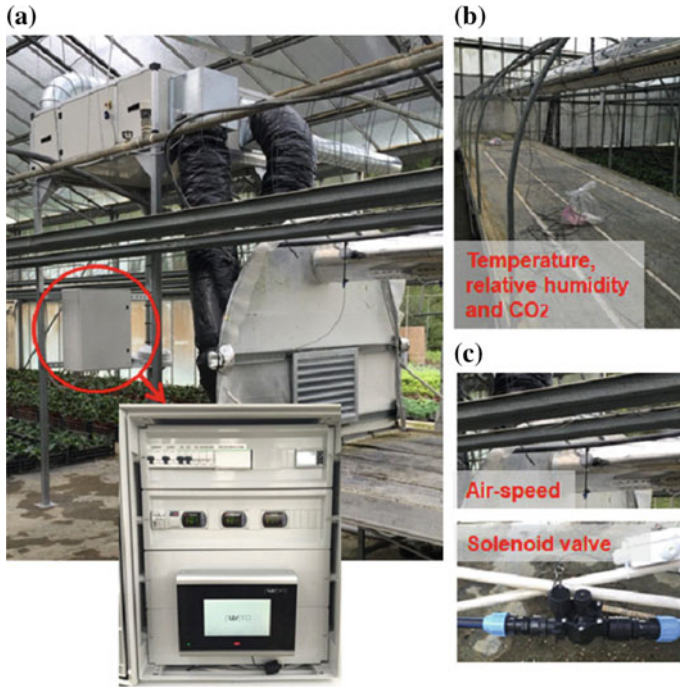


Fig. 2 SIVeMeC system and BMS for field acquisition (a), perforated duct with T, RH and CO₂ probes, air speed probe and solenoid valve to adjust RH (c)

The mini-tunnel greenhouse dimensions are 1.8 × 10 × 1.3 m (width × depth × height) and was covered with a single plastic film (thermal transmittance $U = 6 \text{ W/m}^2\text{K}$). To understand whether SIVeMeC was suitable for this application, the heat losses through the envelope was calculated. Table 1 shows the heat losses calculated based on the thermo-physics parameters of the greenhouse and by considering an air change rate of 0.5 1/h. The potential heating load supplied by SIVeMeC system is calculated according Eq. (1) and is higher than the heat losses, confirming that the

Table 1 Heat losses calculation where q_w is the heat transfer through the structural cover, U is the cover thermal transmittance, A is the exchanging area, ΔT is the temperature difference between outdoor and indoor air, $q_{v_{outf}}$ and $q_{v_{inf}}$ are the heat contained in the ventilation air exiting and entering the greenhouse respectively, c_{p_a} is the specific heat of air, n is the number of air changes per hour and V is the volume of the airspace

Heat losses		
Description	Calculation	Heat [W]
Losses through structure	$q_w = U \cdot A \cdot \Delta T$	4351.20
Losses by infiltration	$q_{v_{outf}} - q_{v_{inf}} = c_{p_a} \cdot n \cdot V \cdot \Delta T$	67.72
Total heat losses		4418.92

ventilation unit is suitable for this specific application:

$$q_{\text{VO SIVeMeC}} - q_{\text{vi SIVeMeC}} = c_{p_a} \cdot \dot{V}_s \cdot \Delta T = 5950[\text{W}] \quad (1)$$

where $q_{\text{VO SIVeMeC}}$ and $q_{\text{vi SIVeMeC}}$ represent the heat contained in the ventilation air exiting and entering the SIVeMeC system respectively and \dot{V}_s is the supply air flow rate.

The distribution of the supply air happens thanks to a perforated duct (Fig. 1b). A stainless-steel tube of diameter 250 mm, with 5 holes each side of 10 mm and with a distance of 40 mm, was installed in the ridge of the greenhouse. It was connected with the supply side of the unit through an insulate hose. The recovery side was connected to the mechanical ventilation system through a hose and a plenum. The aspiration and discharge duct are galvanized steel tubes of diameter 250 mm.

To adjust RH in greenhouse a separate line of water supply and a solenoid valve were installed and it was managed by the BMS system of Fig. 1a. The main parameters acquired are temperature, RH and carbon dioxide level values inside the greenhouse and air speed inside both supply and exhaust duct. The temperature probes are installed along the greenhouse at 2.5 m distance each other, while relative humidity and carbon dioxide level probes at 5 m. The probes were installed spaced uniformly in order to evaluate the uniformity of the indoor air parameters. The air speed probe were useful to evaluate the volumetric airflow rate of both supply and exhaust air streams. To measure and collect all the parameters related to the evaluation of the SIVeMeC energy performance a second BMS system, consisting of a software installed on a remote PC, is used. By means of this tool it is possible to choose and set the variables of interest to monitor during tests. Considering that there are two supervision systems, one for SIVeMeC, the other one for field, before starting tests we must synchronize the two BMS clocks. This procedure simplifies the following data elaboration. The temperature chosen as set point for trials is 27 °C in order to understand the behavior of the mechanical ventilation systems when the heating requirement is related to a temperature difference in the range 10–20 °C (between the set-point T_{SET} and the outdoor T_o temperature). Measurement variables acquisition begins after the clocks synchronization. The data were acquired with a sampling time of 1 s for SIVeMeC system and 30 s for field (minimum setting). Tests were carried out in heating mode by choosing as reference probe the exhaust air temperature T_e and working, as well as for laboratory tests, in passive plus active recovery mode.

3 Results and Discussion

The main aim of these first set of tests is to understand whether SIVeMeC is suitable for temperature control inside greenhouse. Another significant target is to evaluate the energy efficiency of the overall system. The most important energetic parameter is the coefficient of performance of the overall system COPs. This parameter is not directly measured, but is calculated as the ratio of the heat supplied by the system

(P_R) and its energy absorption (P_e). In this work two main representative tests carried out during winter 2016/2017 are reported and discussed.

The first test (Test 1) starts with temperature values of 17.4 and 20.3 °C for outdoor and exhaust air respectively. Moreover, the mean value of outdoor air temperature T_o was 18.0 °C. The whole Test 1 has had a duration of 44 min. Figure 3 shows the exhaust air temperature T_e , supply air temperature T_s and the coefficient of performance of the overall system COPs as the outdoor air temperature T_o changes. The test is carried out with a set point of internal air temperature of 27 °C, to ensure an adequate temperature difference (given the mild conditions of the location) and a mean airflow rate of 410 m³/h. The probe for SIVeMeC regulation is installed on the recovery side of the unit (on board). At the beginning of the test the T_s grew up quickly to balance the heating load and to bring as soon as possible T_e to the set-point. When T_e reached the set point the heat pump modulated and then deactivated. However, when only passive recovery occurred, T_e slightly decreased so the compressor turned on again. As shown in Fig. 2 the COPs, after the initial transitory (about 15 min), stabilized at about 4.6, with a compressor speed of 30 rps (minimum allowable speed). This is a very high energy performance. When the compressor shuts down COPs experiences a very high and fast increase and its mean value is of about 8.6. By considering this operating cycle the mean COPs is of about 5.4.

The second test (Test 2) started with an outdoor air temperature T_o of 16.4 °C and had a mean value of 15.7 °C during the whole test. Figure 4 shows a sudden increase of T_o at the beginning of the test, reaching about 20 °C, then return to lower values. This fact could be explained by considering that when the fans start to work, the first amount of suctioned air is the stagnant air inside duct. Particularly, only a portion of suction duct was hit by sun. The average value of the supply airflow rate, similarly to the previous one, was 418 m³/h. The boundary conditions of Test 2 are much severe. In fact, remembering that the set point temperature T_{SET} is 27 °C, the initial and mean temperature differences are of 10.6 and 11.3 °C respectively for Test 1 and 2. Figure 4 shows a very fast increase of the supply air temperature T_s . In fact, after few minutes of compressor regime (after the initial ramp) at 60 rps, the compressor experiences a

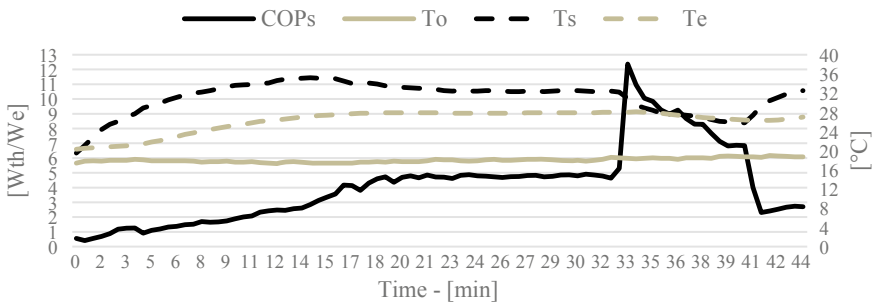


Fig. 3 Test 1—exhaust air temperature (T_e), supply air temperature (T_s) and coefficient of performance (COPs) as a function of outdoor air temperature (T_o)

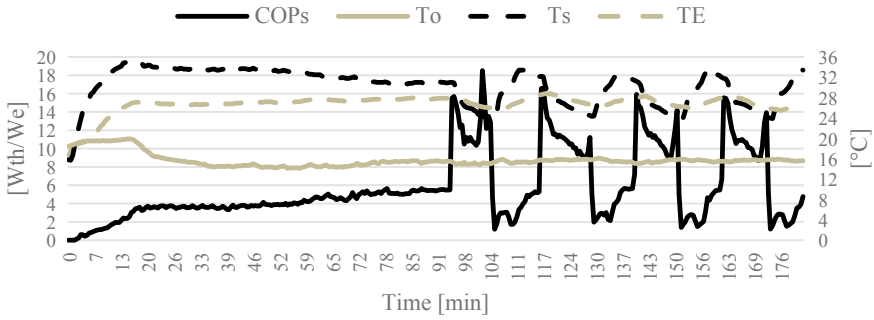


Fig. 4 Test 2—exhaust air temperature (Te), supply air temperature (Ts) and coefficient of performance (COPs) as a function of outdoor air temperature (To)

second ramp until the full load (100 rps). In this way the Te quickly reached the set point of 27 °C. Due to the thermal inertia of the system, even if the compressor was modulated and then attenuated, the exhaust air temperature exceeded the set point, so the compressor was turned off. When Te fell below the set-point the compressor was re-activated again. The energy performance evaluation of the system during the whole test (about 3 h) showed a mean COPs of 5.7. This is a very remarkable value by considering that we have no loss of the indoor air temperature control (excessive overheating).

Figure 5 shows the air temperatures (the probes are numbered in ascending order moving away from the recovery intake, from T1 to T4) inside the greenhouse during Test 1. A heat loss along the recovery duct explains a slightly higher temperature in the greenhouse respect to Te. However, it could be seen that the internal distribution of temperature is almost homogeneous. A slight gradient of temperature towards the final part of the compartment is revealed. This is mainly due to the return air system configuration. A single intake grid is installed at the beginning of the greenhouse. Thus, the air introduced in the first part of the compartment is also the first to exit. Dividing the return air system with a grid on the beginning side and a second grid on the end side could completely equalize the indoor air temperature.

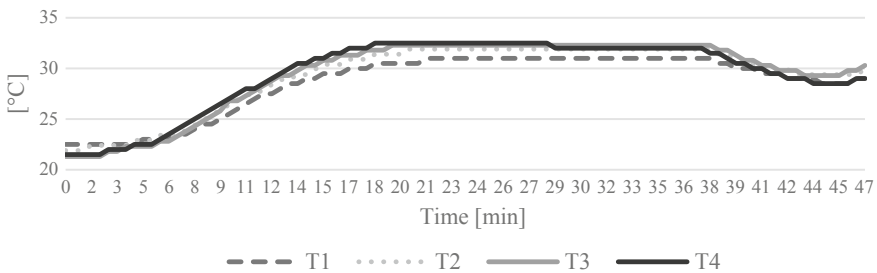


Fig. 5 Temperature distribution measured with 4 NTC probes (T1–T4) inside greenhouse during Test1

4 Conclusion

Energy savings to manage the internal microclimate conditions of greenhouses is becoming increasingly important. Thus, a new concept of mechanical ventilation with heat recovery and heat pump was installed at service of a mini-tunnel greenhouse. A first set of tests on the regulation of the indoor air temperature were carried out with a set point of 27 °C. The results show a suitable regulation when the reference probe is that installed on the recovery side, while an offset of few Celsius degree is observed with the probes inside the greenhouse. This is due to the heat loss along the recovery duct and the configuration of the recovery system (only one intake grid installed at the beginning of the greenhouse). It can be concluded that the greenhouse conditioning is possible with this system which had also shown remarkable energy performance: COPs of 5.4 and 5.7 at outdoor air temperature of 18.0 and 15.7 °C respectively.

Future tests will allow to better set up the system for a real application and make an energy comparison with other air-conditioning systems leading to an economical evaluation in terms of energy saving and increasing of crop yield.

References

- Bianchi B., Cavone G., Cice G., Tamborrino A., Amodio M., Capotorto I., et al. (2015a). CO2 employment as refrigerant fluid with a low environmental impact. Experimental tests on arugula and design criteria for a test bench. *Sustainability*, 7, 3734–3752.
- Bianchi B., Giametta F., La Fianza G., Gentile A., & Catalano P. (2015b). Microclimate measuring and fluid-dynamic simulation in an industrial broiler house: testing of an experimental ventilation system. *Rivista Veterinaria Italiana*, 51(2), 85–92.
- Coomans, M., Allaerts, K., Wittemans, L., & Pinxteren, D. (2013). Monitoring and energetic performance of two similar semi-closed greenhouse ventilation system. *Energy Conversion and Management*, 76, 128–136.
- Cuce, E., Harjunowibowo, D., & Cuce, P. M. (2016). Renewable and sustainable energy saving strategies for greenhouse systems: A comprehensive review. *Renewable and Sustainable Energy Reviews*, 64, 34–59.
- Fucci F., Perone C., Fianza G. L., Brunetti L., Giametta F., & Catalano P. (2016). Study of a prototype of an advanced mechanical ventilation system with heat recovery integrated by heat pump. *Energy and Buildings*, 133, 111–121.
- Perone, C., Fucci, F., Fianza, G. L., Brunetti, L., Giametta, F., Catalano, P., et al. (2017). Experimental Study of a Mechanical Ventilation System in a Greenhouse. *Chemical Engineering Transactions*, 58, 811–816.
- Sethi, V., & Sharma, S. (2008). Survey and evaluation of heating technologies for worldwide agricultural greenhouse applications. *Solar Energy*, 82, 832–859.
- Van de Bulck N., Coomans M., Wittemans L., Hanssens J., & Steppe K. (2013). Monitoring and energetic analysis of an innovative ventilation concept in a Belgian greenhouse, *Energy and Buildings*, 57, 51–57.

Efficiency of Tractor Drawbar Power Taking into Account Soil-Tire Slippage



M. Cutini, M. Brambilla, C. Bisaglia, D. Pochi and R. Fanigliulo

Abstract Heavy drawbar work on cultivated soil is the most critical aspect for agricultural tractors after the impairment of efficiency resulting from wheel slippage. To investigate this aspect with specific reference to cultivated soils, the data of 100 tractors of varying engine power and weight were processed to obtain a regression equation as the starting point to analyze driveline efficiency, power loss due to rolling resistance, and wheel slippage. To fit the results to soil conditions, four tractors of different mass fitted with agricultural tires of varying size and pressure settings were tested in field conditions to correlate drawbar force with wheel slippage. The algorithm obtained was introduced in the regression equation with the aim to obtain simplified algorithm for the assessment of the optimal wheel-slip value during drawbar works that enables optimal fuel consumption with minimum tractor efficiency impairment. According to the results, in case of heavy drawbar work, keeping the wheel slippage below 10% and running the tractor at low forward speeds results in greater tractor efficiency. This underlines the importance of the motion resistance of tires on the agricultural soil and the role that the proper evaluation of the drawbar force of tires plays, even at low levels of wheel slippage.

Keywords Fuel consumption · Traction · Agricultural tire · Dynamometer vehicle · Modelling

M. Cutini (✉) · M. Brambilla · C. Bisaglia

CREA Consiglio per la ricerca in agricoltura e l'analisi dell'economia agraria (Research Centre for Engineering and Agro-Food Processing), Via Milano, 43, 24047 Treviso, BG, Italy
e-mail: maurizio.cutini@crea.gov.it

D. Pochi · R. Fanigliulo

CREA Consiglio per la ricerca in agricoltura e l'analisi dell'economia Agraria (Research Centre for Engineering and Agro-Food Processing), Via Della Pascolare, 16, 00015 Monterotondo, Rome, Italy

© Springer Nature Switzerland AG 2020

A. Coppola et al. (eds.), *Innovative Biosystems Engineering for Sustainable Agriculture, Forestry and Food Production*, Lecture Notes in Civil Engineering 67,
https://doi.org/10.1007/978-3-030-39299-4_46

1 Introduction

Drawbar work is one of the primary purposes of agricultural tractors. Heavy drawbar work on cultivated soil is the most critical aspect after the impairment of efficiency resulting from wheel slippage. To mitigate high wheel slip, a number of countermeasures are taken, e.g. ballasting the tractor, reducing the forward speed or adapting the tire set (i.e. size, pressure). The adoption of standard methods of measurement, such as the OECD Code 2 International standard for the assessment of drawbar power and fuel consumption makes it possible to obtain comparable data and to develop algorithms on tractor dynamics and efficiency but, it is recommended that such measurements be carried out on asphalt or concrete test tracks. Studies on tractor efficiency have mainly focused on the improvement of engine, driveline and tire efficiency, together with optimal tractor settings (Molari and Sedoni 2008; Harris and Rethmel 2011; Smerda and Cupera 2010; Janulevicius et al. 2014; Monteiro et al. 2013), investigations have also been carried out on the effect of different fuel types on traction and emissions (Da Cunha et al. 2013). However, one of the main objectives remains that of optimizing traction performance, not only in terms of material engineering but above all with regard to labor and energy efficiency (Gil-Sierra et al. 2007; Turker et al. 2012; Grisso et al. 2004), also through the use of models (Wong and Huang 2006; Zoz and Grisso 2003) verified by experimental results or test-bench data (Sabbioni et al. 2011; Lacour et al. 2014; Tiwari et al. 2010). Furthermore, in-depth investigations on soil properties have also been intensely investigated to determine their influence on traction efficiency and performance (Lyasko 2010; Filho et al. 2010). To investigate this aspect, with specific reference to cultivated soils, the OECD Code 2 data of 100 tractors (Cutini et al. 2018) of different engine power and weight were processed to obtain a regression equation that served as the starting point to analyze driveline efficiency, the power lost as rolling resistance and the power lost due to slippage. To evaluate the results on soil conditions, four tractors equipped with agricultural tires of varying size and with different masses were tested in field conditions to correlate the drawbar force with the wheel slippage. The algorithm obtained was introduced in the previously defined equation (Cutini et al. 2018) to assess the optimal wheel-slip value during drawbar works that enables optimal fuel consumption with minimum tractor efficiency impairment. The investigation of the effect such a number of parameters have on traction required the setup of an experimental drawbar test, which consisted in the application of a horizontal force at the agricultural tractor drawbar while running it on a test track or a field (Cutini and Bisaglia 2016; PAMI 1996), and measuring the primary tractor performance outputs (i.e., drawbar force, forward speed, wheel slip and fuel consumption).

2 Materials and Methods

The OECD Code 2 standard (OECD 2018) for drawbar power and fuel consumption assessment allows comparable data to be obtained (measurements are carried out at maximum engine power), but it raises the issue that the maximum drawbar power of a tractor changes with the gear or the speed of forward movement, in case of continuously variable transmission. The data of 100 tractors of different engine power and weight from the OECD Code 2 standard test, were analyzed with the aim of evaluating the specific driveline efficiency (the net driveline power to losses due to slippage).

The drawbar test conditions were the following: (i) the engine was kept at full throttle and in different selected gears, or speeds in case the tractor had continuously variable transmission; (ii) the tractor was attached to a device generating the horizontal force at the drawbar up to a maximum wheel slip of 15% (Zoz and Brixius 1979) or the maximum drawbar power, in each gear or speed.

The records of the applied force and the forward speed were used to calculate the power at the drawbar in accordance with Eq. (1).

$$P_{db} = F_{db} \cdot \vec{v} \quad (1)$$

where P_{db} is the power at the drawbar, kW; F_{db} is the maximum force measured at the drawbar, kN, \vec{v} is the forward speed of the test tractor, ms^{-1} . The test must be carried out on a level surface, usually made of concrete or asphalt. The dataset resulted in one maximum drawbar power for each tested gear or speed for any of the 100 tested tractors so that the final dataset contained up to 584 observations. The calculation of the efficiency of the drive line was carried out following the hypothesis that the power measured at the PTO was the maximum ideally available on the test track. The power losses considered were the efficiency of the drive-line, the power used for the motion resistance and the power lost due to slip. With this aim the “expected” results would have had to follow Eq. (2):

$$P_{db} = \alpha \cdot P_{PTO} - P_{vd} - P_s \quad (2)$$

where P_{db} is the power at the drawbar (measured), kW; P_{PTO} is the maximum power at the PTO (measured), kW; P_{vd} is the power used for the displacement of the vehicle (calculated as weight and speed), kW; P_s is the power lost due to slip, kW and α is the efficiency of the driveline, dimensionless. The whole dataset underwent Linear Regression Analysis (LRA) aimed at indicating the relationship between the power at the drawbar and the losses due to slippage. The software used was Minitab 17 statistical software (Minitab 2010). The variables taken into account were:

- maximum power at the PTO: P_{PTO} , kW;
- the tractor’s mass: M , kg;
- drawbar power: P_{db} , kW;
- net traction: NT ; kN;

- forward speed: \bar{v} , ms^{-1} ;
- slip: s , %.

To manage the choice of predictive variables, stepwise regression was adopted to fit the regression models. All candidate variables were involved and the deletion of each variable using a chosen model fit criterion was tested by backward elimination, deleting the variable whose loss gave the most statistically insignificant deterioration of the model fit. The presented study highlights an example focused on wheel slippage. Although it depends on various characteristics of soil (e.g., composition, humidity, compaction) and tires (i.e., pressure, size, type), this study considers only specific tractor settings and soil characteristics, and this limits the validity of the results to the described experimentation. That's why the slippage is considered as a function of the traction force related to tractor mass only (the vertical force acting on the ground).

Regarding the assessment of the relationship between drawbar force and slippage on field, the hypothesis assumed is reported in the Eq. (3).

$$\text{Slip}(s) = f(NT, W) \quad (3)$$

where W is the dynamic wheel load in force units (kN), and it is the sum of the static load and any additional forces, such as load transfer to the vehicle, normal to the undisturbed supporting surface on which a vehicle is operating (ASAE 2003).

To define the $f(NT, W)$ term of Eq. (3) four tractors underwent drawbar test on agricultural soil (Fig. 1). Tests foresaw the use of ten sets of tires (sized 600, 650 and 710 nominal width and inflated at 0.1 MPa) and different slip rates (i.e., 15, 20, 25, 30, 35, 40%) for a total of 84 tests and the measurement of the wheel slip of the rear wheels only, which were also the only driving ones. The soil had a mean resistance to penetration of 1–1.3 MPa, 14% moisture and it contained 30% skeleton, 68% sand, 24% loam and 8% clay. The verification of the NT/W ratios calculations foresaw drawbar tests using a 4WD tractor of 73 kW maximum power at the PTO that underwent: (i) PTO test; (ii) drawbar and rolling resistance test on an asphalt track; (iii) drawbar and rolling resistance test on soil. The tractor was equipped with

Fig. 1 An example of the layout of a drawbar power test on field by dynamometer application



420/85 R24 and 460/85 R34 wheels (0.1 MPa inflated) and it underwent the tests in two ballast settings (4515 and 5722 kg). The acquired data were used to evaluate the performance of the model.

Model performance was evaluated by means of standard regression statistics (Pearson’s correlation coefficient— r —and the coefficient of determination— R^2), error indices and a dimensionless efficiency indexes such as the root mean square error (RMSE), the percent bias of prediction (PBIAS) that indicates the error of the simulations and the tendency of the simulated data to be larger or smaller than their measured counterparts and the Nash-Sutcliffe Efficiency (NSE), which indicates how well the plot of observed vs. simulated data fits the 1:1 line the scatterplot of predicted and observed data produces (Moriassi et al. 2007).

3 Results

Equation (4) shows the parameters of the regression Eq. (2) resulting from the processing of the data of the 100 OECD tractors ($R^2 = 0.99$):

$$P_{db} = 0.918 \cdot P_{PTO} - 0.026 \cdot (9.81 \cdot 10^{-3} \cdot M) \cdot \vec{v} - 0.009 \cdot P_{PTO} \cdot s \quad (4)$$

This means that, as a mean value for developing a model, it is possible to adopt $\alpha = 0.918$ as the drive-line efficiency coefficient and 0.026 as motion resistance coefficient affecting the P_{vd} . These coefficients are in line with the values reported in the ASAE standard (ASAE 2011). The coefficient of 0.009 confirms the direct correlation of power lost in slip to wheel slip: for example, 20% of slip means 18% of power lost.

In open field conditions the drawbar tests pointed out a significant role of the NT/W ratio (ASAE 2003), for the assessment of the slip (Eq. 3) so that it can be assessed as follows:

$$\frac{NT}{W} = 0.2838 + 0.008267 \cdot s \quad (5)$$

This regression equation ($R^2 = 0.652$) aims to introduce a simplification in modeling that is valid only for these experimental conditions. Merging Eqs. (1) and (5) enables the assessment of the power available at the drawbar on the field (Eq. 6):

$$P_{db} = F_{db} \cdot \vec{v} = NT \cdot \vec{v} = W \cdot (NT/W) \cdot \vec{v}$$

$$P_{db} = W \cdot (0.2838 + 0.008267 \cdot s) \cdot \vec{v} \quad (6)$$

The evaluation of the fuel consumption requires the measurement of the engine power. Equation (4) is helpful for this, but it requires the evaluation of the ratio of motion resistance on the above described soil. Because of this, the experimental

activity foresaw the measurement of the force required to pull a 4WD tractor in neutral gear and with different combinations of mass, tire pressure and speed on tilled soil. Motion resistance was between 0.06 and 0.08, reflecting what was indicated by the ASAE standard (ASAE 2011). The adopted coefficient is reported in Eq. (7).

$$P_{dc} = 0.918 \cdot P_{PTO} - 0.07 \cdot (9.81 \cdot 10^{-3} \cdot M) \cdot \vec{v} - 0.009 \cdot P_{PTO} \cdot s \quad (7)$$

The required power available at the PTO is reported in Eq. (8).

$$P_{PTO} = \frac{(P_{db} + 0.07 \cdot (9.81 \cdot 10^{(-3)}) \cdot M) \cdot \vec{v}}{(0.918 - 0.009 \cdot s)} \quad (8)$$

The simplified Eq. (9) can be obtained introducing Eq. (6) into Eq. (8):

$$P_{PTO} = \frac{W \cdot \vec{v} \cdot (0.2838 + 0.008267 \cdot s) + 0.07 \cdot (9.81 \cdot 10^{(-3)}) \cdot M \cdot \vec{v}}{0.918 - 0.009 \cdot s} \quad (9)$$

Supposing a specific fuel consumption of 300 g/kWh, the calibration of the algorithm can achieve to assess the greatest efficiency for the power at the drawbar.

Based on the simulation, the slippage value that identifies the greatest efficiency is 9%: the effect of the rolling resistance of the wheels on the soil affects this percentage so that lower values would result in higher power required for vehicle displacement.

This consideration appears valid both for heavy works (such as ploughing) and light works. The mass of the tractor to be adopted shall be 3.4 times the drawbar force required: the higher the tractor mass, the higher the rolling resistance. However, any decrease in the tractor mass would result in higher losses due to wheel slippage: it's important to point out that decreasing the slippage under the ideal value of 9% has a low impact on fuel consumption. Moreover, increasing the rolling resistance from 0.06 to 0.08 (realistic values in field conditions) results in a 5% loss of fuel consumption efficiency that is comparable with maintaining a 0.06 constant and adopting a slippage of 17%. And again, the adoption of a small ballasted tractor with low tire pressure and working with a 20% of slippage could result in a -20% fuel consumption efficiency compared to the above described ideal setting. It is important to underline that drawbar work on soft soil (e.g. arrowing after ploughing) requires attention as well. Indeed, even though the drawbar force on soft soil is not a problem, in terms of slippage, the operator could be induced to increase the forward speed of the tractor, which would lead to a significant increase in fuel consumption. Considering the ASAE standard the motion resistance ratio on soft soil could be 0.12. Figure 2 reports the fitting of the experimental observations with the linear model resulting from data processing.

On the whole, the model performed quite well as the Pearson coefficient of correlation of 0.9 points out a good degree of linear relationship between simulated and measured data. However, the R^2 of 0.65 points out that the model explains only part of the variance the measured data have. Concerning the error indices, the RMSE of

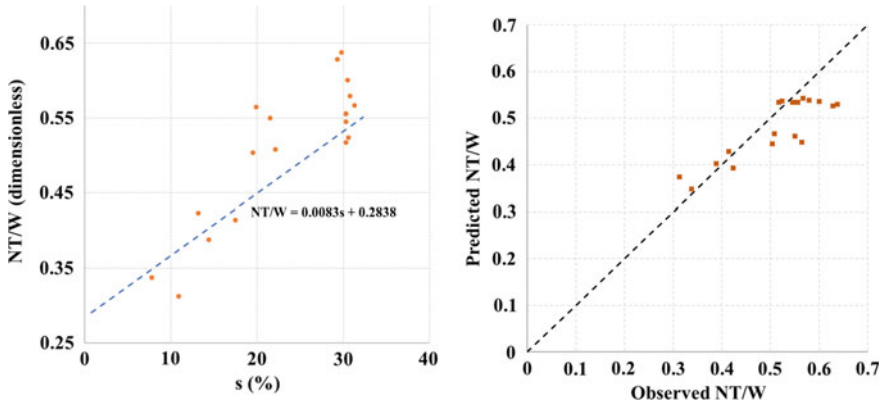


Fig. 2 On the left the fitting of the predicted model output (blue dashed line) and measured data (orange); on the right the scatter plot of predicted NT/W ratios versus the observed ones

0.0131 and the PBIAS of -6.2 indicate that the model error mostly results in underestimation of the measured data ($PBIAS < 0$). However, the value of 0.6 the NSE index achieves points out an overall acceptable level of performance: the NSE ranges from $-\infty$ to $+1$ and values from 0.0 to 1.0 refer to acceptable levels of performance (Moriassi et al. 2007).

4 Conclusions

This study presents the development of a simplified model to assess which is the optimal slip to be maintained during drawbar works to maximise the efficiency of fuel consumption. The algorithm development considered the OECD code 2 data of 100 tractors. This was implemented with a second algorithm obtained processing the output of four tractors that underwent drawbar tests in open field conditions. At the same time, model performance was evaluated comparing the output with the results of independent drawbar tests carried out in open field conditions as well. Running the model allowed to point out that, with reference to fuel consumption, the optimal wheel slip shall be in the 9–10% range. Model performance evaluation pointed out an acceptable fitting of the calculated NT/W ratios with the measured ones highlighting an underestimating trend that becomes sensible at slippages higher than 20% meaning that for such high values of wheel slippage the simplified algorithm can't consider all the factors playing. Experimental and modelling results underline the key role the wheel rolling resistance plays during field works and the importance of the testing tires' drawbar force in field conditions even at low slippage levels (i.e., lower than 10%).

Acknowledgements This work was supported by the Italian Ministry of Agriculture (MiPAAF) under the AGROENER project (D.D. no. 26329, 1 April 2016)—<http://agroener.crea.gov.it/>.

References

- ASAE D497.7 MAR2011. (R2015). Agricultural machinery management data. ASABE Standards 2018. Standards Engineering Practices Data. American Society of Agricultural and Biological Engineers. 2950 Niles Road, St. Joseph, Michigan, 49085–49659.
- ANSI/ASAE S296.5 W/Corr. 1 DEC2003. (R2013). General terminology for traction of agricultural traction and transport devices and vehicles. ASABE Standards 2018. Standards Engineering Practices Data. American Society of Agricultural and Biological Engineers. 2950 Niles Road, St. Joseph, Michigan, 49085–49659.
- Cutini, M., & Bisaglia, C. (2016). Development of a dynamometric vehicle to assess the drawbar performances of high-powered agricultural tractors. *Journal of Terramechanics*, 65(2016), 73–84. <https://doi.org/10.1016/j.jterra.2016.03.005>.
- Cutini, M., Brambilla, M., Bisaglia, C. (2018). Tractor drive line efficiency evaluation taking into account power lost in slippage. In *Proceedings of the “New Engineering Concepts for Valued Agriculture”*, 8–12 July 2018, Wageningen, The Netherlands, pp. 533–538.
- Da Cunha Siqueira, W., Fernandes, H. C., Teixeira, M. M., Santos, N. T., Abraho, S. A. (2013). Performance on the traction of an agricultural tractor drive tires fed with mixtures of petroleum diesel and raised soybean oil. *Revista Ceres*, 60(6), 793–801.
- Filho, A. G., Lancas, K. P., Leite F., Acosta J. J. B., Jesuino, P. R. (2010). Performance of agricultural tractor on three different soil surfaces and four forward speeds. *Revista Brasileira de Engenharia Agricola e Ambiental*, 14(3), 333–339.
- Gil-Sierra, J., Ortiz-Canavate, J., Gil-Quiros, V., Casanova-Kindelan, J. (2007). Energy efficiency in agricultural tractors: A methodology for their classification. *Applied Engineering in Agriculture*, 23(2), 145–150.
- Grisso, R. D., Kocher, M. F., Vaughan, D. H. (2004). Predicting tractor fuel consumption. *Applied Engineering in Agriculture*, 20(5), 553–561.
- Harris, B. J., Rethmel, B. R. (2011). Comparison of IF and standard marked metric radial ply tires. In *American Society of Agricultural and Biological Engineers Annual International Meeting 2011*, ASABE 2011 (Vol. 7, pp. 5461–5472).
- Janulevicius, A., Pupinis, G., Kurkauskas, V. (2014). How driving wheels of front loader tractor interact with the terrain depending on tire pressures. *Journal of Terramechanics*, 53(1), 83–92.
- Lacour, S., Burgun, C., Perilhon, C., Descombes, G., & Doyen, V. (2014). A model to assess tractor operational efficiency from bench test data. *Journal of Terramechanics*, 2014(54), 1–18.
- Lyasko, M. I. (2010). How to calculate the effect of soil conditions on tractive performance. *Journal of Terramechanics*, 47(6), 423–445.
- Minitab. (2010). *Minitab 17 statistical software*. State college, PA: Minitab.
- Molari, G., Sedoni, E. (2008). Experimental evaluation of power losses in a power-shift agricultural tractor transmission. *Biosystem Engineering*, 100(2), 177–183.
- Monteiro, L. A., Albiero, D., De Souza, F. H., Melo, R. P., Cordeiro, I. M. (2013). Tractor efficiency at different weight and power ratios. *Revista Ciencia Agronomica*, 44(1), 70–75.
- Moriasi, D. N., Arnold, J. G., Van Liew, M. W., Bingner, R. L., Harmel, R. D., & Veith, T. L. (2007). Model evaluation guidelines for systematic quantification of accuracy of watershed simulations. *Transactions of the ASABE*, 50(3), 885–900.
- OECD Code 2. (2018, February). OECD Standard Codes for the official testing of agricultural and forestry tractors performance.
- Prairie Agricultural Machinery Institute (PAMI). (1996, July). Research Update, Standardized Tractor Performance Testing. What it is—and isn't.

- Sabbioni, E., Negrini, S., Braghin, F., Melzi, S. (2011). A 2D model for tractor tire-soil interaction: Evaluation of the maximum traction force and comparison with experimental results. SAE Technical Papers.
- Smerda, T., Cupera, J. (2010). Tire inflation and its influence on drawbar characteristics and performance—Energetic indicators of a tractor set. *Journal of Terramechanics*, 47(6), 395–400.
- Tiwari, V. K., Pandey, K. P., Pranav, P. K. (2010). A review on traction prediction equations. *Journal of Terramechanics*, 47(3), 191–199.
- Turker, U., Ergul, I., Eroglu, M. C. (2012). Energy efficiency classification of agricultural tractors in Turkey based on OECD tests. *Energy Education Science and Technology Part A: Energy Science and Research*, 28(2), 917–924.
- Wong, J. Y., Huang, W. (2006). “Wheels vs. tracks”—A fundamental evaluation from the traction perspective. *Journal of Terramechanics*, 43(1), pp. 27–42.
- Zoz, F. M., Brixius, W. W. (1979). Traction prediction for agricultural tires on concrete. Summer Meeting of ASAE and CSAE, ASAE paper no 79–1046.
- Zoz, F. M., Grisso, D. R. (2003). Tractor and Traction 596 Performance. ASAE Publication Number 913C0403.

Design and Assessment of a Test Rig for Hydrodynamic Tests on Hydraulic Fluids



Daniele Pochi, Roberto Fanigliulo, Renato Grilli, Laura Fornaciari, Carlo Bisaglia, Maurizio Cutini, Massimo Brambilla, Angela Sagliano, Luigi Capuzzi, Fulvio Palmieri and Giancarlo Chiatti

Abstract The adoption of a new hydraulic fluid or lubricant in a productive process depends on performing tuning tests that require complex systems and often last as long as the normal lifetime of the oil itself. This is an important issue, since there is an intense activity of development of bio-based lubricants, with high biodegradability, intended to replace the conventional mineral ones. Based on this trend, CREA, Italy, developed an Oil Test Rig (OTR) for hydraulic fluids performing heavy work cycles with small oil volumes, with the aim of accelerating the fluid's aging with respect to what usually occurs, e.g., in agricultural applications. The possibility to control the hydraulic workload and to repeat the work cycles allows the comparative evaluation of fluids by observing their performances and the variations in chemical–physical properties. The OTR acceptance test was carried out using a widespread and reliable mineral fluid (assumed as a reference for future tests) in a 230 h work cycle at two operating temperatures: 50 °C (150 h) and 60 °C (80 h). The applied pressure was 40 MPa and determined a thermal leap of about 20 °C. The OTR maintained constant all functional parameters during the work cycle. It seems to be suitable for comparative tests between bio-based and conventional fluids.

Keywords High-pressure pump · Thermal jump · Flow rate · Dynamical performance

D. Pochi (✉) · R. Fanigliulo · R. Grilli · L. Fornaciari

Consiglio per la ricerca in agricoltura e l'analisi dell'economia agraria (CREA), Centro di ricerca Ingegneria e Trasformazioni agroalimentari, Via della Pascolare 16, 00015 Monterotondo, Italy
e-mail: daniele.pochi@crea.gov.it

C. Bisaglia · M. Cutini · M. Brambilla

Consiglio per la ricerca in agricoltura e l'analisi dell'economia agraria (CREA), Centro di ricerca Ingegneria e Trasformazioni agroalimentari, Via Milano 43, 24047 Treviglio, Italy

A. Sagliano · L. Capuzzi

Novamont S.p.A, Via Fauser 8, 28100 Novara, Italy

F. Palmieri · G. Chiatti

Università degli Studi Roma Tre, Dipartimento di Ingegneria, Via V. Volterra 62, 00146 Rome, Italy

© Springer Nature Switzerland AG 2020

A. Coppola et al. (eds.), *Innovative Biosystems Engineering for Sustainable Agriculture, Forestry and Food Production*, Lecture Notes in Civil Engineering 67,
https://doi.org/10.1007/978-3-030-39299-4_47

1 Introduction

The self-propelled agricultural machines require high amounts of oils for operating and lubricating the hydraulic system. When the hydraulic function of the machine is predominant, different specific products are employed. Hydraulic fluids transmit power to moving components such as pumps, valves and actuators, and must have the following characteristics: power transmission with minimum loss, lubrication of surfaces moving against each other, protection of metal surfaces from corrosion and from high temperature. The adoption of a new hydraulic fluid or lubricant in a productive process depends on performing tuning tests that require complex systems (Wan Nik et al. 2013) and often last as long as the normal lifetime of the oil itself. Suitably compressing the duration of such tests would allow to develop and evaluate a higher number of fluids. This is an important issue, since there is an intense activity of development of bio-based lubricants, with high biodegradability, intended to replace the conventional, mineral ones (Campanella et al. 2010). The characteristics of these new products will have to be evaluated to identify the best ones that must be comparable to their benchmarks (Majdan et al. 2013). The evaluation of oils suitability to the specific applications is based on the measurement of parameters defining their attitude (Birkavs and Smigins 2018). Usually, each parameter can vary within a “physiological” range of values without affecting the operative performance of the oil. The severity of the working conditions can accelerate the degradation of oil properties (Kosiba et al. 2016): high temperatures and pressures (Paredes et al. 2014) and the presence of contaminants are factors that, singularly or combined, can play an important role in the evolution of oil properties (Kučera et al. 2017; Totten et al. 2000).

The tests aimed at evaluating the suitability of hydraulic fluids to be used in agricultural machinery should be based on work cycles capable to apply, to the fluid, workloads (in terms of thermal and hydraulic stresses) similar to those borne in the normal use of hydraulic equipment and in tractors with separated hydraulic system and transmission circuits. Since these fluids are designed to have long lifetime, often extended to the lifetime of the equipment they supply, their evaluation is very difficult, given the frequent need to provide answers as much as possible quickly.

CREA, Italy, developed an Oil Test Rig (OTR) for hydraulic fluids within the project BIT³G (Industrial Bio-refinery of 3rd Generation), financed by the Italian Ministry of Education University and Research (MIUR), and coordinated by Novamont S.p.A, an Italian company engaged in the sector of the green chemistry. The OTR performs heavy work cycles with small oil volumes (20 dm³), with the aim of accelerating the aging of the tested fluid with respect to what usually occurs, e.g., in agricultural tractors (oil volume up to 180 dm³), according to a test methodology developed considering the variables characterizing the hydraulic systems (fluid pressure and flow rate, fluid operating temperatures). The possibility to control and adjust them and to repeat the work cycles allows the comparative evaluation of different fluids by observing the evolution of their performances and of their chemical-physical properties. This work describes the tests on the OTR’s functionality and a proposal

of work cycle. Such a methodological approach will be employed in the evaluation of experimental formulations of hydraulic bio-fluids with the aim of selecting the most promising ones to be tested on tractors, prior their introduction in the operative reality.

2 Materials and Methods

The Oil Test Rig has the function of applying a hydraulic workload to the fluid. It consists of a *low pressure section* and a *high pressure section*. The *low pressure section* includes; a 30 dm³ capacity oil reservoir; a centrifugal pump (max flow rate: 80 dm³min⁻¹, max pressure: 0.5 MPa) for the circulation of the oil; a digital pressure gauge (Kobold, mod. SEN-319701-B035) with a maximum pressure valve ($p \leq 0.15$ MPa); a main filter, with cellulose cartridge of 25 μm class diameter; a three-stage filter system (Rexroth 50LEN040), with fiberglass cartridges of 3, 6, 10 μm class diameter, for fractional filtration and analysis of the suspended materials; an oval gears Flow Meter (Kobold, mod. DON 215 HR 31HOMO). The *high pressure section* includes: a high-pressure radial piston pump (Atos, mod. PFR203, max. pressure 50 MPa; max. power: 5 kW; max. speed: 1800 min⁻¹; displacement: 3.5 cm³); an inverter (Toshiba, mod. VF-ASI 4055 PL-WP) controlling the pump; a distributor block with four solenoid valves directing the fluid to four high-pressure valves (Bosch Rexroth, mod. DBDS 1G &X, preloaded at 10, 20, 30, 40 MPa) or in free flow; a digital pressure gauge (Kobold, mod. SEN-319701-A165). After the *high pressure section*, the fluid is cooled by an oil-to-water heat exchanger (Pacetti, mod. BV 50) before returning to the reservoir. The thermo-regulation efficiency was improved by installing in the water inlet line a flowrate regulator and a solenoid valve. A very sensitive thermostat controls the On/Off frequency of the solenoid valve, keeping $\Delta t = 0$. The system also comprehends a series of thermocouples measuring the oil temperature at reservoir output, at circulation pump and at overpressure valves and several points for the sampling of oil destined to laboratory analyses on chemical-physical characteristics. Figure 1 shows the technical scheme of the OTR.

All sensors and instruments are connected to a data acquisition system controlling both the alarm system (mostly on the basis of the current values of temperature and pressure) and the operating conditions applied to the fluid, such as the opening sequence of the solenoid valves according to the desired pressure conditions, the setting of the high pressure pump speed, determining the flowrate and the adjustment of the oil temperature before the high-pressure pump, never exceeding 60 °C, in compliance with the its operating limits. The passage of the fluid through a high-pressure valve determines its lamination and an almost instantaneous heating, with an average thermal leap of about 20 °C with the 40 MPa valve. Controlling the operating pressure and the fluid flowrate allows the real-time calculation of the exerted hydraulic power and the hydraulic work done. Before starting a test, the OTR undergoes a deep cleaning process aimed at removing the fluid's residues of the previous test. The operation includes: (1) emptying of the OTR from exhaust fluid, at first by gravity,

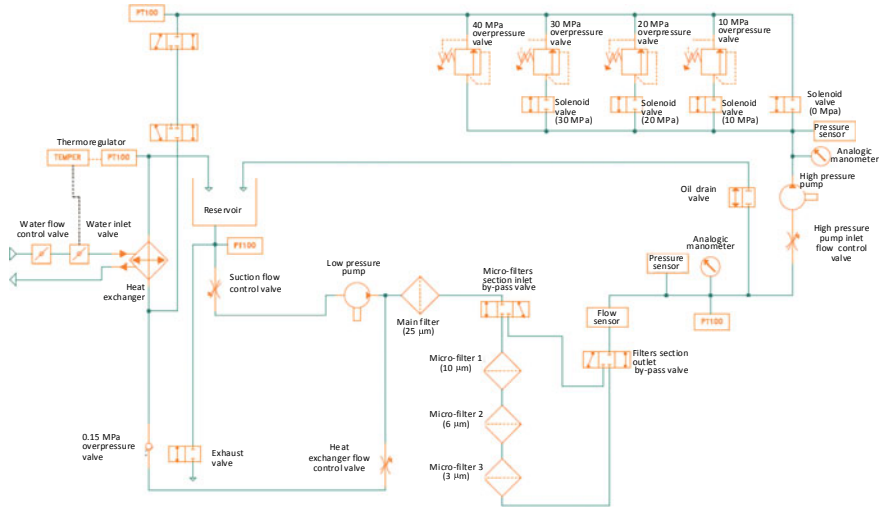


Fig. 1 Technical scheme of the OTR

then with compressed air and removal of the main filter’s exhausted cartridge; (2) circulating of 8–10 dm³ of the new fluid to be tested, to dilute the previous fluid’s residues and emptying, then repeating the operation; (3) supplying of the OTR with new fluid and installing a new main filter cartridge.

A test session was carried out to evaluate the functionality of the OTR, using a mineral fluid widespread on the market, developed for use in hydraulic systems, wet brakes and transmissions, in environmental temperature interval from –30 to +50 °C. Its main characteristics are synthesized in the Table 1.

The maximum values of flowrate, pressure, power and fluid temperature applicable with the OTR are reported in the Table 2. Basing on them, different work cycles can be defined to make the fluid undergo a process of accelerated aging. In the case of

Table 1 Main characteristics of the conventional hydraulic fluid used in the acceptance test of the OTR, reported in the technical data sheet

Properties	Values	Method
Physical state at 20 °C	Liquid and viscous	Visual
Flash point (°C)	200	ASTM D92
Kinetic viscosity at 40 °C (cSt)	44.75	ASTM D445
Kinetic viscosity at 100 °C (cSt)	6.75	ASTM D445
Viscosity index	105	ASTM D2270
Pour point (°C)	–37	ASTM D97
Specific gravity 15 °C (g cm ⁻³)	0.89	ASTM D4052

Table 2 Test conditions applicable to the fluid with the OTR. Maximum values of the parameters and values adopted in the work cycle

Main parameters of working conditions	Unit	OTR working conditions	
		Maximum	Work cycle
Tested fluid volume	dm ³	20	20
Pressure in the low-pressure section	MPa	<0.15	<0.15
Fluid temperature ^a	°C	<60	50–60
Fluid temperature ^b	°C	80	70–80
Flow rate	dm ³ min ⁻¹	6.3	5.7
Pressure applicable in the high-pressure section	MPa	10, 20, 30, 40 ^c	40
High-pressure pump maximum speed	min ⁻¹	1800	1800
Hydraulic power	kW	5.0	3.8

^aIn the reservoir/before high-pressure pump

^bAfter the lamination at 40 MPa

^cPressure values alternatively applicable by selecting one of the four high pressure valves

a hydraulic fluid, the aging should be achieved through the effects of the continuous lamination into the high-pressure section and of thermal stress.

The work cycle (Table 2) adopted in the test session was defined basing on the average power required by the different tractor functions (drive train, PTO, hydraulic system) in percent of its total power and on the average time required by the different operations in percent the total working time proposed by Renius (1994) and Osinenko (2014). According to such an assumption, the assessed average power and time required by the hydraulic system to carry out a wide range of operations (tillage, front loading, fertilizing, sowing, planting, spraying, hay making, transport with universal trailers) are, respectively, 10% of the total power and 38% of the total working time. Applying such values to a 197 kW power tractor supplied with 172 dm³ of fluid, for a working time of 800 h per year, will provide a total energy absorbed by the hydraulic system of 5988 kWh of which 5090 kWh for hydraulic work and 898 kWh for energy losses ($\eta = 0.85$, Biondi 1999). Dividing these values by the fluid volume (172 dm³) will provide a specific hydraulic work of 29.6 kWh dm⁻³ and a specific energy of 5.2 kWh dm⁻³ lost as heat. Similar values are obtained by applying the same-calculation to the work cycle conditions reported in Table 2, for 155 h, with specific hydraulic work of 29.4 kWh dm⁻³ and specific thermal energy dissipated of 5.19 kWh dm⁻³. According to these data, a 155 h work cycle at the OTR would correspond to a year of work as described in the above hypothesis. The test session consisted of a first 155 h cycle in which the oil, at operating temperature of 50 °C, reached 70 °C after the lamination, followed by a further 75 h in which the operating temperature was increased at about 60 °C and, after the lamination, reached 80 °C. Considering that a 10 °C increase in operating temperature halves the fluid's lifetime (Khonsari and Booser 2003) the 75 h cycle should correspond to about twice the 155 h cycle, i.e. a two year work according to the hypothesis. Such conditions were applied for the entire duration of the two cycles. The daily phases of starting and heating of the

OTR were excluded from the computation of the test time. The operative parameters were continuously measured (frequency of acquisition: 1 Hz) and monitored in real time to observe any variation caused by changes in fluid properties, storing the average values of 1 min acquisitions. The three micro-filters section was by-passed in this test. During the work cycle, 200 ml samples of fluid have been taken and analysed in laboratory. The samplings were carried out according to the following schedule: new oil (from the container), 1, 30, 60, 90, 120, 155, 230 h. The analyses aimed at monitoring the evolution of the main properties typical of hydraulic fluids and at providing information helpful to prevent damages of the test rig, e.g. wear process or compatibility between constituent materials and fluids. The kinematic viscosity (ASTM D445) and the Total Acid Number, TAN (ASTM D664) were measured at CREA in collaboration with NOVAMONT. MECOIL Lab. (Florence, Italy) determined the contents of wear metals and contaminants (ASTM D6595 standard), of the water (ASTM D6304), the particle counting (ASTM D7596-10) and their classification (ISO 4406/1999).

Beyond the test on the OTR's functionality, the results of the analyses on the fluid samples from the OTR were compared to those provided by the same fluid, from a different lot, that supplied the tractor described in the hypothesis above, employed in the same cited agricultural operations at CREA farm (Rome, Italy), for about 900 h, with the aim of assessing any correspondence between the applied work cycle and the working conditions. Since, as in most tractors, in this case too the fluid also operates the lubrication of the transmission, undergoing an additional mechanical stress, this comparison was not meant to validate the OTR work cycle, but rather to provide useful indications to its upgrade. The fluid samples (new from the packaging and at 900 h) were analysed at CREA laboratory to determine the TAN, the viscosity at 40 and 100 °C and the viscosity index.

3 Results and Discussion

The 230 h test with OTR was carried out under the working conditions described by the diagrams of Fig. 2. The diagrams show the trend of the daily averages of the

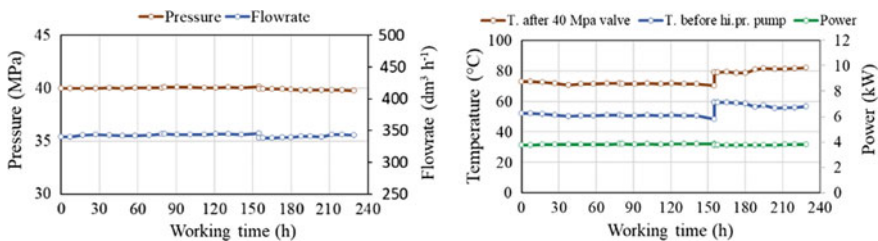


Fig. 2 Summary diagrams of the entire test, reporting the daily averages of the recorded values

Table 3 Statistical indices of the parameters shown in Fig. 3, separately considered with reference to the two interval (0–155 and 155–230 h) the test was divided in

Test (h)	Statist.	Pressure (Mpa)	Flow rate (dm ³ h ⁻¹)	Power (kW)	T. before high press. (°C)	T. after 40 MPa valve (°C)	Δt (°C)
0–155	Mean	40.02	342.99	3.81	50.78	71.64	20.86
	St. dev.	0.05	1.54	0.02	0.78	0.66	0.29
	CV	0.11	0.45	0.55	1.53	0.93	1.40
	Max	40.12	345.39	3.85	51.98	72.93	21.88
	Min	39.96	339.86	3.77	48.47	70.35	20.36
155–230	Mean	39.84	340.35	3.77	57.51	80.23	22.72
	St. dev.	0.06	2.01	0.02	1.52	1.35	2.77
	CV	0.14	0.59	0.47	2.65	1.68	12.20
	Max	39.91	343.35	3.80	59.27	82.07	25.52
	Min	39.78	338.18	3.75	55.60	78.42	19.71

operative parameters during the two intervals of the test: 0–155 and 155–230 h, as the Table 3 reports the main statistical indices.

The OTR resulted capable to maintain sensitively constant the pressure and flowrate conditions, and consequently the power, all along the 230 h test with very small variations, as indicated by the low CV values and by the small differences between maximum and minimum (Table 3).

As to the work cycle, the absence of variations in the key parameters of pressure and flowrate suggests that the fluid did not undergone appreciable variations.

The results of the samples analyses (Table 4) show that the Total Acid Number (TAN) remained nearly constant during all the test at the OTR. The viscosity at 40 and 100 °C measured on the new fluid (48.7 and 7.4 cSt) were different from the data reported in the datasheet (44.75 and 6.75 cSt) at 40 and 100 °C. However, after an increase in the very first hours of test, it remained constant in the 30–155 h interval, then it seemed to increase in the 155–230 h interval, possible consequence of the increased thermal stress. The number of particles (non-metallic) had a maximum in the first hours of test, probably due to some residues of the materials used in OTR cleaning, and decreased due to the action of the main filter: the fluid's ISO code varied accordingly, resulting in compliance with the requirements of the OTR (max. ISO Code for fluids used in "high quality reliable plants": 18/16/13).

Table 4 also reports the results of the analyses on the samples of fluid used on the tractor. With reference to the new fluid, the low TAN increase testifies the stability of the fluid toward the oxidation. As to the viscosity, in this case, the values measured on the new fluid resulted near to those on the datasheet. After 900 h of work at operative fluid temperature of about 60 °C, the viscosity at 40 °C and 100 °C increased of 14.8% and 11.26% respectively. Such increases are higher than the 10% variation considered as the caution upper limit for oil replacement (Fitch 2001), as the tractor user manual

Table 4 Results of the analyses of the samples of the fluid, carried out at MECOIL laboratory

Parameters	Time of test (h)										Tractor (h)	
	0	1	30	90	120	155	230	0	950			
Kin. visc. 40 °C (cSt) ^a	48.7	49.4	48.4	48.4	48.3	48.2	48.9	43.8	50.3			
Kin. visc. 100 °C (cSt) ^a	7.4	7.3	7.2	7.2	7.2	7.2	7.3	6.9	7.67			
Viscosity index ^a	112	108	108	108	108	108	109	114	118			
T.A.N. (mg KOH g ⁻¹) ^a	3.4	3.4	3.4	3.5	3.5	3.4	3.4	3.4	3.5			
Water K.F. (ppm) ^b	344	206	252	241	195	152	-	-	-			
Wear metals (ppm) ^b	abs.	abs.	abs.	abs.	abs.	abs.	-	-	-			
Contaminants (ppm) ^b	abs.	abs.	abs.	abs.	abs.	abs.	-	-	-			
Particles ^c	>4 µm (No. ml ⁻¹)	2401	1503	1627	750	918	-	-	-			
	>6 µm (No. ml ⁻¹)	92	731	505	215	198	-	-	-			
	>14 µm (No. ml ⁻¹)	15	26	13	5	8	-	-	-			
ISO code ^c	16/14/11	18/17/12	18/16/11	18/16/9	17/15/9	17/15/10	-	-	-			

^aAnalysis carried out by CREA lab^bAnalysis carried out by MECOIL Lab^cClassification codes according the ISO 4406/1999

Fig. 3 Aspect of the fluid used in the tests: Left: new fluid from the package; Centre: fluid after the 230 h test at OTR; Right: Fluid sampled from the tractor reservoir after 900 h in real work conditions



reported a time interval for oil change of 1500 h, and suggest that the fluid was deeply modified. This was expected and makes very difficult the comparison between the analyses results after the OTR work cycles and after the work on the tractor. The visual aspect of the OTR-230 h fluid is like the new fluid and very different from the tractor's sample that appears darker and opaque (Fig. 3), probably because of the relevant presence of contaminants.

As to their origin, it lies in the very nature of the work done by tractors. Beyond the action of the transmission, that is certainly the main factor affecting fluids characteristics and reducing their timelife, to operate different equipment by means of auxiliary distributors involves the contamination of the tractor fluid with residues of any other fluids, with different characteristics, present in the implements previously operated by other tractors. Furthermore, connecting and disconnecting the implements favour the entry of significant dust and ground amounts into the tractor's hydraulic circuit. Eventually, wet brakes and clutches are operated by the hydraulic fluid, contributing to its contamination.

4 Conclusions

An oil test rig (OTR) has been developed to evaluate the possibility of performing heavy work cycles with small oil volumes in order to concentrate in a short interval of time the stress suffered by the hydraulic fluids on tractors. As to its functionality, the OTR was tested with a mineral oil for hydraulic system and lubrication of transmissions and proved to be capable to reliably apply repeatable working cycles in which the operative conditions can be adjusted depending on the specific requirements of the tests. The work cycle applied in the tests was divided into two intervals, each designed to correspond to approximately one year of hydraulic work performed on a tractor. In the second interval (75 h) an increase in viscosity was observed, probably favoured by the setting of temperature levels higher than in the first interval (155 h). A longer test could confirm this trend. It was not possible to validate the

work cycle due to the differences between the working conditions applied with the OTR and those typical of most of tractors: transmission almost always lubricated by the same fluid, high level of contamination from dust, ground and oil residues from other implements and tractors. These factors may have caused the increase in kinematic viscosity (Khonsari and Booser 2003) observed on the tractor fluid. In their absence, the lifetime of the fluids for hydraulic machines is commonly very long, often “for life” and also in various laboratory tests they maintained their properties for several thousand hours (Kržan and Vižintin 2003). A more suitable comparison should consider a test with the same fluid on the OTR and on a tractor with separated lubrication and hydraulic systems and stably coupled with the same implement for the entire duration of the test, to avoid external interference and contamination.

The test rig seems to be suitable to the execution of comparative tests among different fluids. Further studies will aim at improving its performance and creating more severe test conditions. For example, the effect of the temperature on the aging of the fluids is an important issue to consider for any upgrade of the OTR aimed at developing effective work cycles. Moreover, the use of the OTR, suitably implemented, could be extended to the transmission lubricants, to perform tests on multifunction fluids used in tractors. At the end of this process, the OTR can be used in the evaluation of experimental formulations of bio-based hydraulic fluids and lubricants whose performances will be compared to those of the conventional fluids they should replace in the market. In the next step the most promising formulations will be tested in agricultural machines under real working conditions.

References

- Biondi, P. (1999). *Meccanica agraria - Le macchine agricole*. UTET, Torino, ISBN 88-02-05609-9, 171–174.
- Birkavs, A., & Smigins, R. (2018). Experimental research on compatibility of mineral and biobased hydraulic oils. *Agronomy Research*, 16(S1), 968–976.
- Campanella, A., Rustoy, E., Baldessari, A., Miguel, A., & Baltanás, M. A. (2010). Lubricants from chemically modified vegetable oils. *Bioresource Technology*, 101, 245–254.
- Fitch, J. (2001, May). *Trouble-shooting viscosity excursions, practicing oil analysis*. NORIA Corporation. <https://www.machinerylubrication.com/Read/185/viscosity-trouble-shooting>.
- Khonsari, M., & Booser E. R. (2003, January 9). Predicting lube life. *Machine Design*. <https://www.machinedesign.com/archive/predicting-lube-life>.
- Kosiba, J., Čorňák, Š., Glos, J., Jablonický, J., Vozárová, V., Petrović, A., et al. (2016). Monitoring oil degradation during operating tests. *Agronomy Research*, 14(5), 1626–1634.
- Kržan, B., & Vižintin, J. (2003). Tribological properties of an environmentally adopted universal tractor transmission oil based on vegetable oil. *Tribology International*, 36(11), 827–833. [https://doi.org/10.1016/S0301-679X\(03\)00100-2](https://doi.org/10.1016/S0301-679X(03)00100-2).
- Kučera, M., Aleš, Z., Mareček, J., & Machal, P. (2017). Effect of contaminants on the lifetime of hydraulic biooils and systems. *Acta Universitatis Agriculturae et Silviculturae Mendelianae Brunensis*, 65(4), 1205–1212. <https://doi.org/10.11118/actaun201765041205>.
- Majdan, R., Tkáč, Z., Kosiba, J., Abrahám, R., Jablonický, J., Hujo, Ľ., et al. (2013). Evaluation of tractor biodegradable hydraulic fluids on the basis of hydraulic pump wear. *Research in Agricultural Engineering*, 59(3), 75–82.

- Osinenko, P. (2014, October 23). *Optimal slip control for tractors with feedback of drive torque*. Thesis, Faculty of Mechanical Science and Engineering, Technische Universität Dresden.
- Paredes, X., Comunas, M. J. P., Pensado, A. S., Bazile, J. P., Boned, C., & Fernández, J. (2014). High pressure viscosity characterization of four vegetable and mineral hydraulic oils. *Industrial Crops and Products*, 54, 281–290.
- Renius, K. T. (1985/1994). Trends in tractor design with particular reference to Europe. *Journal of Agricultural Engineering Research*, 57(1), 3–22.
- Totten, G. E., Melief, H. M., & Bishop, R. J. (2000). *Hydraulic fluid qualification using the Rexroth high-pressure piston pump test* (NFPA Technical Paper Series 100-9.2), pp. 241–249.
- Wan Nik, W. B., Zulkifli, F., Ahmad, M. F., Sulaiman, O., & Rahman, M. M. (2013). Performance evaluation of hydraulic field test rig. *Procedia Engineering*, 68, 613–618.

Evaluation of Potential Spray Drift Generated by Different Types of Airblast Sprayers Using an “ad hoc” Test Bench Device



M. Grella, P. Marucco and P. Balsari

Abstract Drift is one of the most important issues to be consider for realise a sustainable pesticide application. This study proposes an alternative methodology for quantify the Drift Potential (DP) for vineyard crop sprayers, trying to avoid the difficulties faced in conducting field trials according to the reference standard protocol (*ISO 22866:2005(E): Equipment for Crop Protection—Methods for Field Measurements of Spray Drift*, International Organization for Standardization, Geneva, Switzerland, 2005). Thanks to a specific test bench device, it is possible to collect and quantify the spray fraction that remains suspended over the test bench immediately after passage of the sprayer and that can potentially be carried out of the target zone by environmental air currents, defined as “potential drift fraction”. The proposed methodology requires to made the test in absence of target and in calm of wind. Contextually, a variation of original test method (absent a target) was used to investigate both the possible effect of the target on the final results and the suitability of the test bench device to measure potential spray drift generated by multiple-row sprayers. The methodologies have been tested using two types of vineyards sprayers, namely conventional axial fan tower shaped and pneumatic single or multiple rows, in different configurations. By the comparison with the results obtained from a reference sprayer the resulting drift reduction potential (DRP), obtained from the two indirect methodologies investigated (presence or not of the target), were compared. The test bench trials confirmed the ability of the proposed methodology to discriminate the DP generated by different vineyard sprayers and their configurations tested. Furthermore, the results obtained from the two methodologies, indicate that, although the vineyard target influence the total amount of liquid collected by test bench, the absence of target is negligible and irrelevant in terms of final drift reduction sprayers classification.

Keywords Test bench method · Spray drift potential · Classification · Vineyard sprayers · Single-row hydraulic sprayer · Multiple-row pneumatic sprayer

M. Grella (✉) · P. Marucco · P. Balsari
Department of Agricultural, Forest and Food Sciences (DiSAFA), University of Turin (UNITO),
Largo Paolo Braccini, 2, 10095 Grugliasco, Italy
e-mail: marco.grella@unito.it

© Springer Nature Switzerland AG 2020
A. Coppola et al. (eds.), *Innovative Biosystems Engineering for Sustainable Agriculture, Forestry and Food Production*, Lecture Notes in Civil Engineering 67,
https://doi.org/10.1007/978-3-030-39299-4_48

1 Introduction

In 2009 the Council of the European Union adopted Directive 2009/128/EC on Sustainable Use of Pesticides (SUD) that highlighted pesticide drift risks generated during spray applications (European Community 2009). Among the pollutants from PPP use, agrochemical spray drift continues to be a major challenge because pesticides can be deposited in undesirable areas and pose risks to both the environment and bystander. Spray drift is a more constant threat in bush/tree crops than in arable field crops. Different methods to measure spray drift, both direct as spray drift field measurements and indirect as drift potential laboratory measurements, have been developed in the recent years. Direct drift measurements from field experiments utilize the complex and time-consuming standardized protocol ISO 22866 (Gil et al. 2018). It provides results that are highly affected by external factors like environmental conditions during testing (Grella et al. 2017a). In contrast, indirect methods allow drift measurements to be conducted under comparable and repeatable conditions in an easy and quick way (Nuyttens et al. 2017).

Recently, to both simplify the test procedure and reduce trial costs, authors began to develop and test an alternative methodology for quantifying the potential spray drift generated by a bush/tree crop sprayer capable of reproducing objective results independent of cultivar and canopy structure variations (Grella et al. 2017b). Simultaneously, they aimed to minimize result variability due to meteorological conditions. This new methodology implied the use of an ad hoc designed test bench device, trial layout and test protocol. The trials would be performed in absence of a crop and nearly absent of wind. The layout was specifically designed to avoid result variability due to canopy parameters that affect spray drift amounts, and to minimize the strong influence of wind velocity and direction on sprayed airborne droplets.

The aim of this study was to verify the suitability of the test bench and its methodology for two purposes: comparative assessment of potential spray drift generated by different types of vineyard crop sprayers, and classification of different sprayer configurations according to their relative Drift Reduction Potential (DRP). In addition, to validate the test bench method, the effect of the presence of the target crop on spray drift potential and consequence on DRP sprayers classification was assessed by comparing Drift Potential Values (DPV) obtained from test bench trials conducted in absence of the crop with that obtained in presence of target.

2 Materials and Methods

2.1 *Technical Characteristics of Spray Drift Test Bench Device and Potential Spray Drift Measurements*

A 20.0 m long test bench was placed transverse to the sprayer forward direction in order to catch the spray output from one side sprayer nozzles. Petri dishes aligned in an array transverse to the sprayer forward direction were placed along the test bench slots with 0.5 m distance within each other. All collectors were initially covered. The actuator of the pneumatic system for opening the collectors was activated by the sprayer pass and it was placed at a relative distance from the test bench line, so that 4 s after the sprayer passed the perpendicular line of the bench the collectors were revealed. All tests were conducted with an average wind speed $<0.5 \text{ m s}^{-1}$. Test bench estimates the spray drift risk during pesticide application through the evaluation, in calm of wind conditions, of the free floating fraction of spray cloud falling time after its discharge. The procedure is based on the assumption that longer free floating droplets lingering times might lead to a larger risk of spray drift generation in case of windy conditions. The sprayer started the application 20 m before and stopped it 20 m after the position of the collector array. The actuator of the pneumatic system for opening the collectors was activated by the sprayer pass revealing simultaneously all the collectors initially covered by the test bench sliding cover system.

2.2 *Experimental Design*

To validate the methodology for the measurements of DPV from the airblast sprayer for single row spray application, as originally proposed by Grella et al. (2017b), the effect of canopy (absence or presence) on final DPV and DRP results during test bench trials was evaluated. So, two parallel trial methodologies were arranged and compared. The first trial consisted of applying the original methodology, positioning the test bench transversely to the concrete flat lane used as the tractor track without the crop target between the sprayer and the tests bench. The second methodology introduces the crop (vineyard espalier—trained at full growth stage) between the sprayer and the test bench device; it was maintained transverse to the forward direction of the sprayer but behind the vineyard crop row (Fig. 1) (Grella et al. 2019).

Furthermore, both methodologies tested (in absence and in presence of canopy) were adapted to evaluate the potential spray drift generated by the multiple-row sprayer. For this purpose 4.3 m distance between spray output and test bench was used (1.5 m + 2.8 m—inter-row distance); the original methodology foresee a fixed distance equal to 1.5 m between the spray output and the first collectors placed on the test bench.

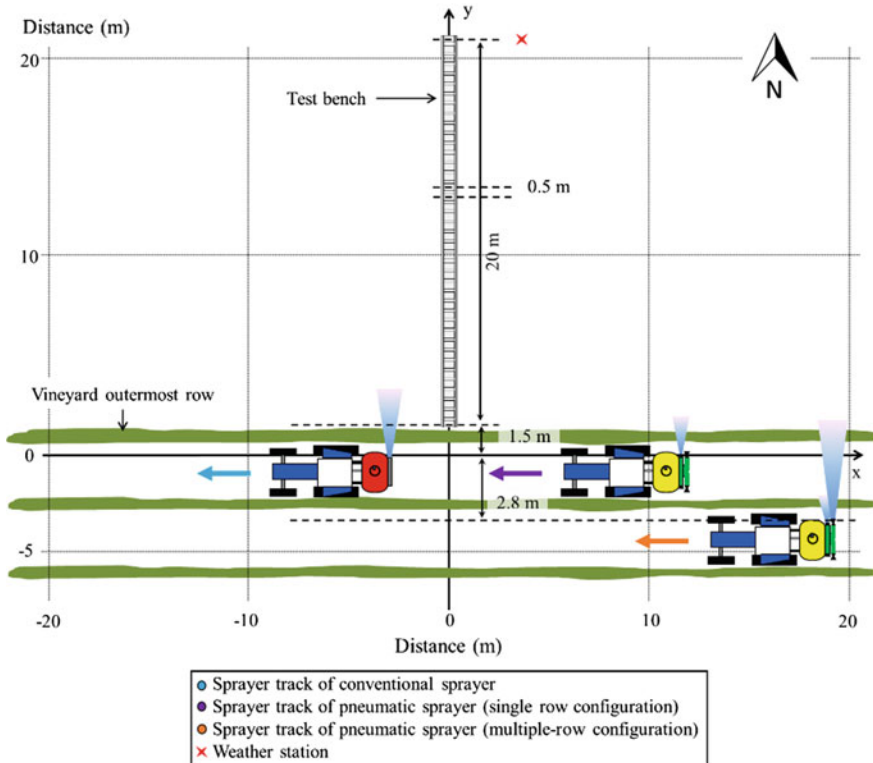


Fig. 1 Drift test bench to assess potential spray drift from vineyard sprayers and layout of field test to assess the influence of vineyard canopy using conventional airblast sprayer and multiple-row pneumatic sprayer

2.3 Characteristics of Air Blast Sprayer and Configurations Tested

Two types of vineyard sprayers characterized by different liquid atomization and passes management between rows were tested. A mounted conventional airblast sprayer Dragone k2 500 (Dragone S.n.c., Castagnole Asti, AT, Italy) with a tower shaped air conveyor and an axial fan (600 mm) and a semi-mounted multiple-row pneumatic sprayer Cima 50 Plus 400 L (Cima S.p.a., Pavia, Italy) equipped with spray head TC.2M2C and a radial fan (500 mm) were used (Fig. 2).

The Dragone k2 500 sprayer was equipped with a 200 L polyethylene tank and six nozzles on each side (Fig. 2a). Two-speed gearbox enabled the airflow rate to vary from 11,000 to 20,000 $\text{m}^3 \text{h}^{-1}$. Table 1 summarizes the configurations tested using Dragone sprayer based on combinations of two different air fan settings (airflow rate 11,000 and 20,000 $\text{m}^3 \text{h}^{-1}$) and two nozzle types, conventional hollow cone ATR 80 orange and air injection hollow cone TVI 8002 (Albuz® CoorsTek, Evreux, France),



Fig. 2 Conventional mounted airblast sprayer Dragone k2 500 (a) and multiple-row pneumatic sprayer Cima 50 Plus 400 L equipped with spray head TC.2M2C (b) during field pesticide application

used at a working pressure of 1.0 MPa and with a nominal nozzle flow rates of 1.39 and 1.46 L min⁻¹, respectively.

The pneumatic sprayer was equipped with 400 L polyethylene tank and the spray head was featured by two hand-type spouts and two cannon-type spouts placed at the bottom and at the top respectively. The hand-type nozzle is characterized by individual air spout disposed as fingers of the main spout, whose mission is to spray the row next to the sprayer pass, and the cannon-type nozzle, with main wide spout that aims at spraying the further row (Fig. 2b). Despite the spray head TC.2M2C was specifically designed for multiple-row spray purposes the possibility to disable the spouts individually give the possibility to apply a single row for each sprayer pass. So, the configurations tested using the pneumatic sprayer were based on different management of passes between the rows: 2 rows sprayed each pass activating all spouts (2 hands plus 2 cannons) and single row sprayed each pass activating only hand spouts at the bottom of spray head (Table 1). Using pneumatic sprayer, all the tests were performed with a working pressure of 0.1 MPa and with a single spout flow rate of 2.70 L min⁻¹ (disc with perimeter calibrated holes used in position 7). Based on previous research work (Grella et al. 2017a), all trials were conducted at 1.67 m s⁻¹ (6 km h⁻¹) as it is the best forward speed to measure potential spray drift of bush/tree crop sprayers using the test bench.

Table 1 Parameters of sprayers' configurations examined in trials conducted in absence and presence of canopy vineyard target: reference and candidates

Test	Config. ID	Sprayer	Nozzles/spouts		Spray pressure (Mpa)	Active nozzles (n°)	Tot. Flow rate (L min ⁻¹)	Applied volume (L ha ⁻¹) ^a	Fan air flow rate (m ³ h ⁻¹)
			Type						
Reference	ATR6H	Dragone k2 500	ATR80 orange		1.0	6	16.32	583	20,000
Candidate	ATR6L	Dragone k2 500	ATR80 orange		1.0	6	16.32	583	11,000
Candidate	TVI6H	Dragone k2 500	TVI8002		1.0	6	17.52	626	20,000
Candidate	TVI6L	Dragone k2 500	TVI8002		1.0	6	17.52	626	11,000
Candidate	MC6S	Cima 50 Plus	TC.2M2C ^b		0.1	4 ^c	10.8	193	7750
Candidate	M6S	Cima 50 Plus	TC.2M2C ^b		0.1	2 ^d	5.4	193	7750

^a2.8 m inter-row distance considered

^bMultiple-row pneumatic spray head equipped with two hand-spouts type at the bottom and two cannon-spout type at the top of spray head

^cCannon and hand spouts activated (two-rows sprayed for each sprayer pass)

^dHand spouts activated (single-row sprayed for each sprayer pass)

2.4 Sprayed Liquid and Deposition Assessment

In all trials E-102 Tartrazine yellow dye tracer—85% (w/w)—(Novema S.r.l., Torino, Italy) was added to the sprayer tank at a concentration of about 10 g L⁻¹.

60 s after the automatic opening of test bench system (complete exposure of collectors), the samples were collected and then the spray amount was determined quantifying the tracer recovered, by means of a spectrophotometer UV-1600PC (VWR, Radnor, PA, USA). The deposit on each artificial collector was then calculated to obtain the spray drift profile according each tested configuration. Five replicates were conducted for each sprayer configuration.

2.5 Drift Potential Value—DPV—and Drift Reduction Potential—DRP—Calculation Procedure for Classification Purposes

From the spray drift profiles, the related Drift Potential Values (DPVs) were calculated according the formula proposed by Grella et al. (2017b, 2019). Then, the spray drift reduction value was calculated based on the DPVs according to ISO 22369-1 formula (ISO 2006), for each sprayer configuration. The configuration chosen as reference was the ATR6H tested with Dragone sprayer. Classification was determined from comparison of the spray drift reductions achieved using the reference spray equipment and the candidate sprayer configuration. The ISO 22369-1 defines reduction classes A to F as follows: A $\geq 99\%$, B $95 \leq 99\%$, C $90 \leq 95\%$, D $75 \leq 90\%$, E $50 \leq 75\%$, and F $25 \leq 50\%$.

2.6 Statistical Analysis

The statistical analysis were performed using IBM SPSS Statistics for Windows (V.25). The statistical differences among DPVs obtained were evaluated using two-way ANOVA, considering the test bench methodology (absence or presence of target) and configurations as source of variation.

3 Results and Discussion

Irrespective of canopy target absence (Fig. 3a) or presence (Fig. 3b), the results achieved using the proposed test bench drift measurement methodology pointed out that testing the conventional airblast sprayer Dragone k2 500 both the reduction of airflow rate and the use of air injection nozzles as Spray Drift Reducing Techniques (SDRT) enable to reduce the DPV (Fig. 3), determining statistical differences among

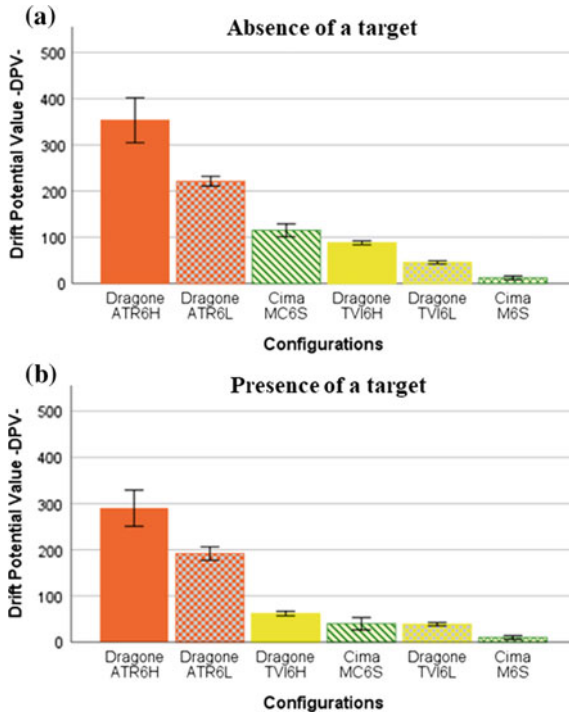


Fig. 3 DPVs obtained and bars \pm SE of the mean obtained from trials conducted in absence (a) and presence (b) of canopy vineyard target testing the conventional and pneumatic sprayer configurations

tested configurations (Table 2); this finding further confirm the previous results (Grella et al. 2017b, 2019), pointing out the repeatability of DPV measurements. Also considering the pneumatic sprayer Cima 50 Plus, the drift low-prone spray application technique tested (M6S), that foresee the application of single row for each sprayer pass using only the hand spouts placed at the bottom of spray head, allow to effectively reduce the spray drift (Fig. 3).

Even if the presence of canopy determines statistical differences between DPVs obtained from trials conducted in presence and in absence of target (Table 2), the

Table 2 Significance obtained in a two-way ANOVA for Drift Potential Values—DPV—as affected by test bench methodology applied (absence and presence of a target) and configurations tested

Source	<i>p</i> (> F)	Statistical significance ^a
Test bench methodology	0.005	**
Configuration	9.640E-21	***
Configuration x test bench methodology	0.390	NS

^aStatistical significance level: NS $p > 0.05$; * $p < 0.05$; ** $p < 0.01$; *** $p < 0.001$

Table 3 Drift reduction potential—DRP—(%) of configuration tested applying both indirect methodologies, namely absence and presence of target. Classification of the different configurations tested according to their drift risk is also provided

Test	Config. ID	Absence of target		Presence of target	
		Drift Reduction Potential-DRP-(%)	Drift class achieved ^a	Drift Reduction Potential-DRP-(%)	Drift class achieved ^a
Reference	ATR6H	–	–	–	–
Candidate	ATR6L	37	F	34	F
Candidate	TVI6H	75	D	79	D
Candidate	TVI6L	87	D	87	D
Candidate	MC6S	67	E	86	D
Candidate	M6S	97	B	97	B

^aISO 22369-1:2006

comparison of DRP values obtained from drift classification process results in an identical final classification of the tested sprayers/configurations (Table 3). Only the configuration Cima MC6S results in different final DRP according to the trials type—absence and presence of target—(Table 3); the difference could be attributable to the management of passes between the rows (one passage every two rows) that generates different spray drift profile deposition on the test bench because a double canopy wall in front of the test bench was present during vineyard trials. The identical final classification of spray application techniques tested using the two different types of sprayer, namely conventional and pneumatic, suggest that the target absence has negligible effect when test bench is used for comparative measurements aimed at determining the DRP of a given vineyard sprayer/configuration intended for single row spray application. Nevertheless, further investigations aimed to improve the test bench methodology for DPV measurements of multiple rows sprayers are needed.

4 Conclusions

The test bench method makes it possible to discriminate between potential drift generated by different vineyard sprayer types and their configurations. Furthermore, the comparison of the indirect test methods indicated that the absence or presence of a canopy affected DPVs obtained from the various configuration tested, yet calculated DRPs resulted in identical final classifications regardless of the indirect methodology tested. Therefore, the test bench methodology as originally proposed in the absence of a target was validated proving that the target absence had negligible effect when test bench is used for comparative measurements aimed to determine DRP of a given vineyard sprayer configuration when used for a single row spray application passage.

References

- European Community. (2009). Directive 2009/128/EC of the European parliament and the council of 21 October 2009 establishing a framework for community action to achieve the sustainable use of pesticides. *Official Journal of European Union*, 309, 71–86.
- Gil, E., Llorens, J., Gallart, M., Gil-Ribes, J. A., & Miranda-Fuentes, A. (2018). First attempts to obtain a reference drift curve for traditional olive grove's plantations following ISO 22866. *Science of the Total Environment*, 627, 349–360.
- Grella, M., Gallart, M., Marucco, P., Balsari, P., & Gil, E. (2017a). Ground deposition and airborne spray drift assessment in vineyard and orchard: The influence of environmental variables and sprayer settings. *Sustainability*, 9(5), 728.
- Grella, M., Gil, E., Balsari, P., Marucco, P., & Gallart, M. (2017b). Advances in developing a new test method to assess spray drift potential from air blast sprayers. *Spanish Journal of Agricultural Research*, 15(3), e0207.
- Grella, M., Marucco, P., & Balsari, P. (2019). Toward a new method to classify the airblast sprayers according to their potential drift reduction: Comparison of direct and new indirect measurement methods. *Pest Management Science*, 75, 2219–2235.
- International Organization for Standardization. (2005). *ISO 22866:2005(E): Equipment for crop protection—Methods for field measurements of spray drift*, ed. by International Organization for Standardization, Geneva, Switzerland, pp. 1–17.
- International Organization for Standardization. (2006). *ISO 22369-1:2006(E): Crop protection equipment—Drift classification of spraying equipment—Part 1: classes*. International Organization for Standardization, ed. by International Organization for Standardization, Geneva, Switzerland, pp. 1.
- Nuytens, D., Zwertvaegher, I. K. A., & Dekeyser, D. (2017). Spray drift assessment of different application techniques using a drift test bench and comparison with other assessment methods. *Biosystems Engineering*, 154, 14–24.

Influence of Ploughshare Wear on Plough Efficiency



Giovanni Molari, Massimiliano Varani and Michele Mattetti

Abstract Regarding agricultural machines, one of the main durability requirements are the wear resistance of the soil engaging tools. Wear of soil engaging tools should be minimized, since it impairs the tool specifications and affects tractor performances, tillage quality and machine maintenance costs. The purpose of this work was to investigate the impact of a worn ploughshare on tractor performances. Wear leads to a geometrical change of the soil engaging tools and previous studies investigated the relationship between the tool cutting edge geometry and the developed drought by means of trials and Finite Elements Modelling. However, no study has reported the influence of worn ploughshares on the power requirements of soil engaging tools. The methodology adopted in this study consists in a comparison of the tractor performances between its configuration with a plough equipped with a worn ploughshare and the configuration with the same plough with a new ploughshare. The tractor speed was measured with a GPS receiver and important tractor parameters such as engine torque and fuel consumption were acquired through a CAN logger.

Keywords Plough · Wear · Durability · Tractor performance

1 Introduction

Tillage tools are used to prepare the soil for seeding by means of mechanical manipulation to facilitate the crop growth. Among all the tillage machines, plough is still one of the most important and popular primary tillage tool, despite its invention was thousands of years ago (Mazoyer and Roudart 2006). The development of agricultural machines with high durability is one of the manufacturers main purpose. In fact, the achievement of this goal leads to customer satisfaction due to lower machine inactivity and call-backs (Mattetti et al. 2017a). Regarding tillage machines, soil engaging

G. Molari · M. Varani (✉) · M. Mattetti
Department of Agricultural and Food Sciences, Università di Bologna, viale G. Fanin 50, 40127
Bologna, Italy
e-mail: massimiliano.varani@unibo.it

© Springer Nature Switzerland AG 2020
A. Coppola et al. (eds.), *Innovative Biosystems Engineering for Sustainable Agriculture, Forestry and Food Production*, Lecture Notes in Civil Engineering 67,
https://doi.org/10.1007/978-3-030-39299-4_49

tools are the components more subjected to durability problems since those are subjected to severe wear (Stawicki et al. 2017). There are several wear modes on tillage tools, such as fretting or chemical action, but the predominant cause of material loss is by means of the abrasive action of soil particles (Bayhan 2006). Wear rate is mostly affected by soil texture (Richardson 1969), water content (Natsis et al. 1999), hardness of the tool material (Richardson 1967; Swanson 1993) and soil-tool pressure distribution (Mattetti et al. 2017b; Varani et al. 2017). This phenomenon should be minimized since it impairs the tool specifications and affects tractor performances, tillage quality and machine maintenance costs (Horvat et al. 2008). Plough body edges are extremely subjected to wear phenomena due to the fact that those are the most active areas during the tillage process. Previous studies investigated on the optimization of the geometric parameters of the edges of soil engaging tools by means of experiments and Finite Elements Modelling (Fielke 1999; Fielke et al. 1993). However, the ploughshare shape is deeply influenced by wear during its lifetime, nullifying the benefits brought by the optimization previously done (Cucinotta et al. 2019). Many authors developed models to predict power requirements and fuel consumption (ASABE 2006; Grisso et al. 2008) but those model has to be experimentally validated due to soil heterogeneity and the different manner in which various soil typologies fragmentate (Grisso et al. 1996). Moreover, few studies have been performed on the influence of implements wear on the tillage power requirements. The aim of this work was to investigate the impact of ploughshare wear on tractor power requirements in real field operating conditions.

2 Materials and Methods

2.1 Machines and Test Location

Tests were carried out with a 4 wheel drive New Holland T7.260 tractor (CNH Italia S.p.A, Italy) and a Nardi 4 furrows plough (Nardi S.p.A, Italy) (Table 1).

The field tests were performed in Cadriano (Bologna, Italy) on a silty-clay-loam soil as classified by the USDA Textural Soil Classification (USDA 1987). The field was divided in two areas, one for testing the Worn Ploughshare (WP) and the other for the New Ploughshare (NP). In Table 2 the characteristics of the fields measured before the tests are reported.

The two ploughshares used for the test denoted as NP and WP are shown in Fig. 1a and b. Prior of the test, they had worked for 10 and 120 ha for NP and WP, respectively. The geometrical differences between the two ploughshares are showed in Table 3. Both ploughshares were mounted on the third plough body (Fig. 1c) and the ploughshares mounted on the other plough bodies had worked for 10 ha like ploughshare NP. The tractor speed (S) was measured with an IPESpeed GPS receiver (IPETronik GmbH, Germany) coupled with a CANcaseXL CAN logger (Vector Informatik GmbH, Germany). In addition to the tractor speed, the CAN

Table 1 Tractor and plough specifications used for the test

Tractor manufacturer and model	New Holland T7.260
Nominal engine power @2200 rpm/230, 4 rad s ⁻¹ -Max Power [kW]	177–194
Max torque @1500 rpm/157, 1 rad s ⁻¹ [Nm]	1349
Transmission	Full power shift (18 forward, 6 reverse)
Mass with ballast [kg]	8900
Plough manufacturer	Nardi NX32TO-140/4T
Type of plough	Double or reversible mouldboard
Number of furrows	4
Coupling to the tractor	Semi mounted
Maximum power required by the tractor [kW]	176
Mass [kg]	1720
Width of cut [m]	2.1

Table 2 Field characteristics of both tests

Field	Worn ploughshares	New ploughshares
Field classification (USDA 1987)	silty-clay-loam	
Liquid limit (LL) [%] (ASTM 2010)	30.25	
Plastic limit (PL) [%] (ASTM 2010)	22.28	
Mean moisture content over the considered area ^a [%] (ASTM 2009)	18.36 (STD 3.20)	18.32 (STD 1.22)
Mean soil bulk density over the considered area ^a [kg m ⁻³] (ASTM 2009)	1368.14 (STD 149.62)	1460.77 (STD 67.10)

^aThis value is obtained performing the mean of the results from 9 samples collected over the considered area

logger was connected to the CAN-Bus network, so actual engine power (P), fuel consumption (F_c) and Rear Hitch Position (RHP) of the tractor were acquired. In particular, the RHP is represented in percentage, where the 0% corresponds to the full down position and 100% corresponds to the full up position.

Each pass was worked with a constant depth and with an approximately constant speed. The target ploughing speeds were 3.0, 4.5, and 6 km/h at full throttle configuration of the tractor and each level was repeated for six passes to reduce variabilities due to the soil inhomogeneities. Each pass configuration was performed for the entire length of the field, that was 100 m. The ploughing depth of all the passes were 0.27 m, this ploughing depth remained constant during the test because the draught control of the three-point hitch was disabled and its height position was fixed at 12%. For the acquired signals, only the portions corresponding to the pass were considered by defining a condition (RHP stably around 12% and the speed deviation was lower than ± 5% of the target S) (Fig. 2).

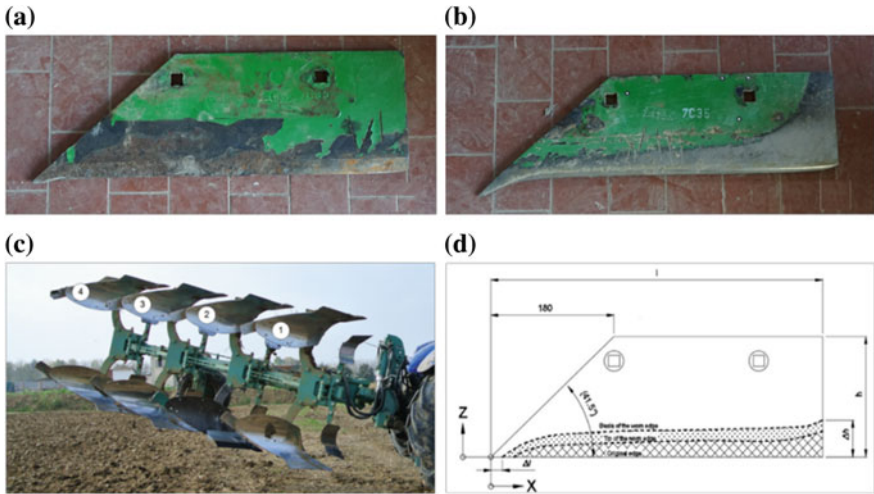


Fig. 1 New ploughshare (a) and worn ploughshare (b) used for the test. One can note the impact of the wear on the edge and blade profile (Cucinotta et al. 2019). Plough used for the test and numbering of the plough bodies (c). Technical drawing with fundamental dimensions of the tested ploughshare (d) (Cucinotta et al. 2019)

Table 3 Ploughshares dimensions

Dimension	Worn ploughshares	New ploughshares
Length in x direction (l) [mm]	478.4	478.6
Length in z direction (h) [mm]	161.1	161.9
Unworn portion of the blade profile Δl [mm]	5.7	11.5
Reduction of the trailing edge Δh [mm]	36.0	3.0

For each signal, the mean value of the selected portion was calculated and with those data, a One-Way Anova test was performed to analyze the differences between the two ploughshares on P and F_c .

3 Results

The obtained results show that the increases of P and F_c are directly correlated to the increase of S. Moreover, one can note that with an increment of speed of 3 km h^{-1} there is an increment around 55% and 69% of both P and F_c for the NP and the WP respectively (Fig. 3).

The results of the One-Way Anova test for both ploughshares at every target speed are reported in Table 4. The measured P range varies from values around 50 kW (28% of the maximum tractor power) at the lowest target speed to values around 105 kW

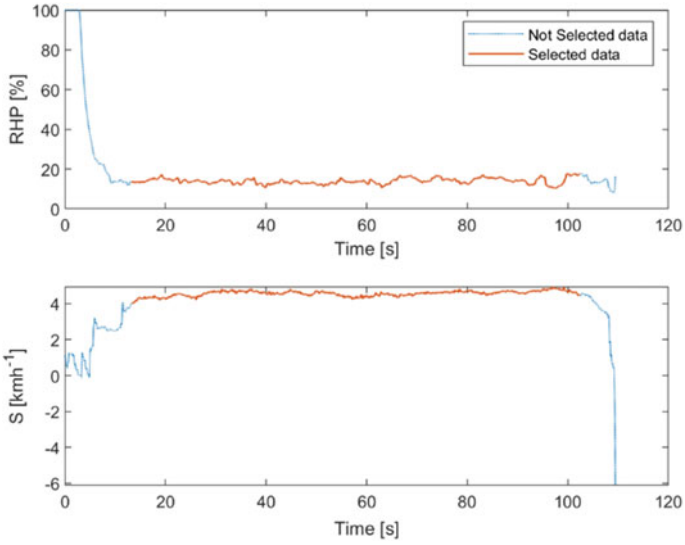


Fig. 2 Example of the methodology used to select the data of each pass

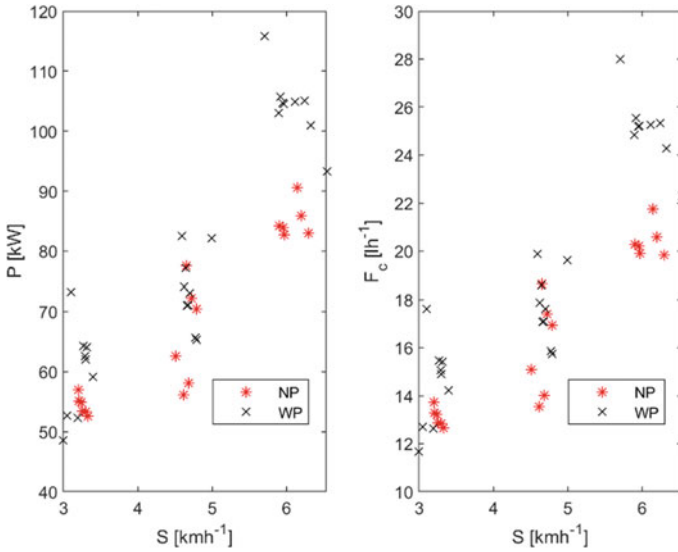


Fig. 3 Mean values of all passes for Power (P, on left) and fuel consumption (F_c, on right) in function of S for the NP and the WP

Table 4 One-Way Anova test both plowshares at every tested speed

P	F value	p value	P median value [kW]	
			NP	WP
Test @ 3 km/h	2.95	0.10	54.16	61.99
Test @ 4.5 km/h	3.80	0.07	66.52	73.08
Test @ 6 km/h	54.68	5.23 E-6	84.04	104.65
F _c	F value	p value	F _c median value [l/h]	
			NP	WP
Test @ 3 km/h	2.92	0.11	13.04	14.91
Test @ 4.5 km/h	3.84	0.07	16.01	17.61
Test @ 6 km/h	51.78	6.9 E-6	20.24	25.21

(57% of the maximum engine power) at the highest target speed. One can note from the p values of the One-Way Anova test that the P and F_c values obtained with the NP and the WP are not significantly different for 3 and 4.5 km/h speeds. On the other hand, at 6 km/h the median value of the WP is around the 24% higher than median value of the NP for both P and F_c. This high value is partially due to the position of the third body of the plough, that is where the tested ploughshares were mounted. In fact in our configuration this body had to turn over the topsoil compacted by the rear wheel of the tractor (Cucinotta et al. 2019).

The reason why only at the top tested speed there is a significant difference between the two ploughshares could be attributed to the fact that the power demand is directly correlated to the developed draught, that varies quadratically with the travelling speed (Owende and Ward 1996), so the higher the speed is, the higher is the impact of a geometry change on the developed draught. This enlarges the advantages in terms of energy efficiency produced by the NP are clearer.

4 Conclusions

In this paper, field tests were performed to investigate the impact of wear on ploughshares in terms of power requirements and tillage quality. The analysis of the results shows that both P and F_c have similar behaviors, in fact only at the highest target speed (6 km/h) there are significant differences between NP and WP. In fact, the median value of the WP is around the 24% higher than median value of the NP for both P and F_c. The results showed in this work could be useful to point out the importance of the development wear resistant implements to cut down fuel costs and CO₂ emissions. Since the influence of implements wear on the tillage power requirements is not yet fully explored in the literature, more experimental tests are necessary to investigate this phenomenon on other soil typology and with different moisture content. A further development of this work may be the investigation of the

horizontal drought developed between the tractor and the plough equipped with worn ploughshares on all its bodies. Moreover, a similar methodology could be applied with secondary tillage implements such as power harrows using blades with different wear stages.

Acknowledgements This project was supported by PRIN (Research projects of significant national interest) notification 2015 “Optimization of operating machinery through analysis of the mission profile for more efficient agriculture” Grant number: 2015KTY5NW.

References

- ASABE. (2006). Agricultural machinery management data. *American Society of Agricultural and Biological Engineers Standard ASABE, EP496.3*, 385–390.
- ASTM. (2009). *D2488—Practice for description and identification of soils (visual-manual procedure)*. West Conshohocken: ASTM International.
- ASTM. (2010). *D4318—Test methods for liquid limit, plastic limit, and plasticity index of soils*. West Conshohocken: ASTM International.
- Bayhan, Y. (2006). Reduction of wear via hardfacing of chisel ploughshare. *Tribology International*, 39, 570–574.
- Cucinotta, F., Scappaticci, L., Sfravara, F., Morelli, F., Mariani, F., Varani, M., et al. (2019). On the morphology of the abrasive wear on ploughshares by means of 3D scanning. *Biosystems Engineering*, 179, 117–125.
- Fielke, J. M. (1999). Finite element modelling of the interaction of the cutting edge of tillage implements with soil. *Journal of Agricultural Engineering Research*, 74, 91–101.
- Fielke, J. M., Riley, T. W., Slatery, M. G., & Fitzpatrick, R. W. (1993). Comparison of tillage forces and wear rates of pressed and cast cultivator shares. *Soil and Tillage Research*, 25, 317–328.
- Grisso, R. D., Yasin, M., & Kocher, M. F. (1996). Tillage implement forces operating in silty clay loam. *Transactions of the American Society of Agricultural Engineers*, 39, 1977–1982.
- Grisso, R. D., Vaughan, D. H., & Roberson, G. T. (2008). Fuel prediction for specific tractor models. *Applied Engineering in Agriculture*, 24, 423–428.
- Horvat, Z., Filipovic, D., Kosutic, S., & Emert, R. (2008). Reduction of mouldboard plough share wear by a combination technique of hardfacing. *Tribology International*, 41, 778–782.
- Mattetti, M., Molari, G., & Sereni, E. (2017a). Damage evaluation of driving events for agricultural tractors. *Computers and Electronics in Agriculture*, 135, 328–337.
- Mattetti, M., Varani, M., Molari, G., & Morelli, F. (2017b). Influence of the speed on soil-pressure over a plough. *Biosystems Engineering*, 156, 136–147.
- Mazoyer, M., & Roudart, L. (2006). *A history of world agriculture: From the neolithic age to the current crisis*. London: Earthscan.
- Natsis, A., Papadakis, G., & Pitsiliis, J. (1999). The influence of soil type, soil water and share sharpness of a mouldboard plough on energy consumption, rate of work and tillage quality. *Journal of Agricultural Engineering Research*, 72, 171–176.
- Owende, P. M. O., & Ward, S. M. (1996). Characteristic loading of light mouldboard ploughs at slow speeds. *Journal of Terramechanics*, 33, 29–53.
- Richardson, R. C. D. (1967). The wear of metals by hard abrasives. *Wear*, 10, 291–309.
- Richardson, R. D. (1969). *The wear of metal shares in agricultural soil*. Ph.D. thesis, University of London.
- Stawicki, T., Białobrzeska, B., & Kostencki, P. (2017). Tribological properties of plough shares made of pearlitic and martensitic steels. *Metals*, 7, 139.

- Swanson, P. A. (1993). Comparison of laboratory abrasion tests and field tests of materials used in tillage equipment. In A. Ruff & R. Bayer (Eds.), *Tribology: Wear test selection for design and application* (pp. 80–99). West Conshohocken, PA: ASTM International.
- USDA. (1987). *Soil Mechanics Level I*.
- Varani, M., Mattetti, M., Molari, G., & Morelli, F. (2017). Experimental evaluation of the soil pressure distribution on plough parts. *Chemical Engineering Transactions*, 58, 247–252.

Brotweg—A Path of Bread in an Alpine Environment: New Mechanical Solutions for Grain Processing in Steep Mountain Slopes



Sabrina Mayr, Riccardo Brozzi, Alice Cervellieri, Thomas Desaler, Raimondo Gallo, Josef Gamper, Bernhard Geier, Laurin Holzner, Pasqualina Sacco and Fabrizio Mazzetto

Abstract A remarkable area of the cultivable land in South Tyrol has an inclination above 30%, which precludes the use of conventional machines for its cultivation. The project “Brotweg” is facing this problem by developing technologies for grain cultivation in a steep mountain environment up to an inclination of 70%. Furthermore, a technical solution for the whole grain processing after harvesting up to the production of bread is evolved. With the help of an entire facility the grain processing can be performed directly at the farm, which allows the farmer to act more independent while increasing his profitability. The aim of this project is to offer farmers an alternative or a supplement to livestock and dairy farming. It will improve and facilitate the working condition for farmers. To reach these goals many issues must be solved: (a) Mechanical solutions for grain seeding and harvesting in steep slopes must be developed. One of the main challenges thereby is to prevent erosion. (b) A solution for grain processing and conservation on the farm must be found. The existing structures of a farm are limiting the size of the facility. (c) The grain is processed to bread directly on the farm and distributed in a further step. The whole processing path must satisfy all safety restrictions, environmental terms and consider all possible geological problems of a steep mountain slope. We present the implementation of a grain processing facility in an existing farm structure and the development of the seeding and harvesting machines for steep slopes.

S. Mayr (✉) · A. Cervellieri · R. Gallo · L. Holzner · F. Mazzetto
Faculty of Science and Technology of Free University of Bolzano/Bozen, Piazza Università 5,
39100 Bolzano, Italy
e-mail: sabrina.mayr@unibz.it

R. Brozzi · P. Sacco
Fraunhofer Italia, Via A. Volta 13 A, 39100 Bolzano, Italy

T. Desaler
Neuero Italiana S.A.S, Via Montani 7, 39012 Merano, Italy

J. Gamper
Taser Alm, Schennaberg 25, 39017 Scena, Italy

B. Geier
Geier srl, Via Prati Nuovi 13, 39020 Marlengo, Italy

© Springer Nature Switzerland AG 2020
A. Coppola et al. (eds.), *Innovative Biosystems Engineering for Sustainable Agriculture, Forestry and Food Production*, Lecture Notes in Civil Engineering 67,
https://doi.org/10.1007/978-3-030-39299-4_50

Keywords Processing cereals · Grain cultivation · Steep mountain environment · Grain seeding and harvesting · Bread

1 Introduction

South Tyrol is an alpine region where only 6% of the total area consists of level areas. The other 94% are defined as alpine areas (Autonome Provinz 2019). In the valleys farmers run mainly apple orchards and viticultures, whereas above an altitude of 500 m generally grassland is cultivated for forage production. The main income for farmers in such alpine areas are life stock and dairy farming. Though, a remarkable area of cultivable land in South Tyrol lies above 1000 m (79%) and has inclinations above 20% (64%) where the use of machines is difficult (Autonome Provinz 2019). The grassland in this regions often has to be cultivated by hand, since mechanized agriculture above an inclination of 60% is nearly impossible. Hence, agriculture in steep alpine areas is demanding and dairy farming provides inadequate income for farmers. In the past, beside dairy an stock farming, cereal was cultivated in the whole region of South Tyrol (Kulturpflanzen der Alpen 2019), which displays a serious alternative or supplement to dairy and life stock farming for farmers in alpine areas. Therefore, the project Brotweg aims to develop innovative solutions for the cultivation of cereal in extremely steep mountain environments (up to an inclination of 70%).

The cultivation of grain offers many advantages compared to dairy farming, which is illustrated in Fig. 1. The production chains of bread and cheese are compared. The gross total income is estimated to be significantly higher by cultivating cereal whereas the work effort is 10 times less than for cheese production, according to our preliminary analysis based on personal communication. The work of grain cultivation is mainly seasonal, whereas the production of cheese requires an everyday care of the animals. The conservation of the products differs for both chains. While the conservation of bread is very difficult, unprocessed cereal can be stored over a long time with low effort by using a modern conservation facility. The conservation of the products in the cheese chain is oppositely. Milk can not be stored for a long time period and must be processed quickly. The end product cheese on the other hand can be stored over a longer period of time. It must be treated regularly, though. Moreover, an European environmental analysis showed that the environmental impact of grain cultivation is less than dairy farming and the economic benefits are very high (Notarnicola et al. 2017). A mechanisation of the seeding and harvesting process diminishes the handcraft and the workload for the farmers reduces compared to dairy farming.

The focus of the project Brotweg, lies in the development of innovative machines for grain seeding and harvesting in steep mountain areas and in the design of a suitable technical solution for the grain processing after harvesting, the grain conservation and the processing to flour and bread directly on the farm. We will present the

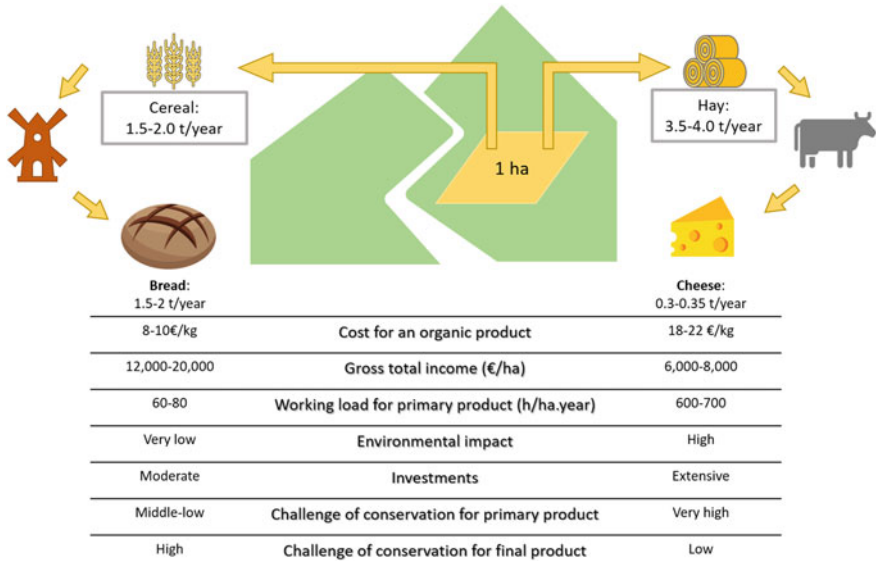


Fig. 1 Comparison of the production chains for cereal and milk for mountain farms, based on preliminary estimations of the authors and personal communication

proceedings of the seeding and harvesting machines as well as the proceedings of the grain processing and conservation facility.

2 Materials and Methods

2.1 The Project Location

The test fields for cultivating cereal are located at the Taser Alm, a modern farm above Scena (South Tyrol) on a sea level of 1450m. The fields inclination span a range between 20 and 70% and have a total area of 6 ha (Fig. 2). The post-harvest facility will be installed in a barn with a connection corridor to the in-house bakery. The processed products are distributed directly to the visitors and guests of the farm, which features a restaurant and guest houses (Fig. 3).

The farmer cultivates spelt and rye, which are suitable for this altitude and have already been cultivated in the region of South Tyrol in alpine areas (Kulturpflanzen der Alpen 2019).

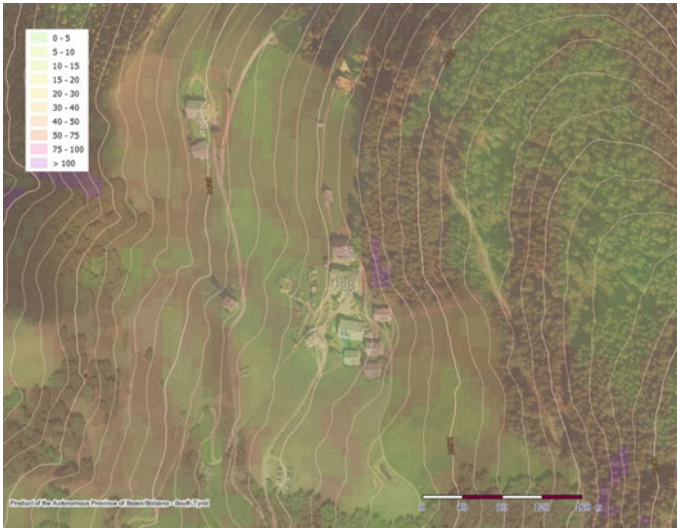


Fig. 2 The farm area with overlying contour lines and colored inclination in %



Fig. 3 The orange square marks the barn, where the grain processing facility is installed and the yellow square marks the place where the bakery is already built

2.2 Design of New Seeding and Harvesting Machines

One of the main difficulties for cereal cultivation in mountain areas is the use of machines in the field due to its steepness. Furthermore, the high risk of erosion has to be considered. For that reason, direct sowing was found to be the best method in such fields (Baker et al. 2007). In direct sowing, the soil is processed only for seed placement directly into the grass and hence, the soil has not to be ploughed. To be successful with this seeding method, it has to be combined with suitable crop

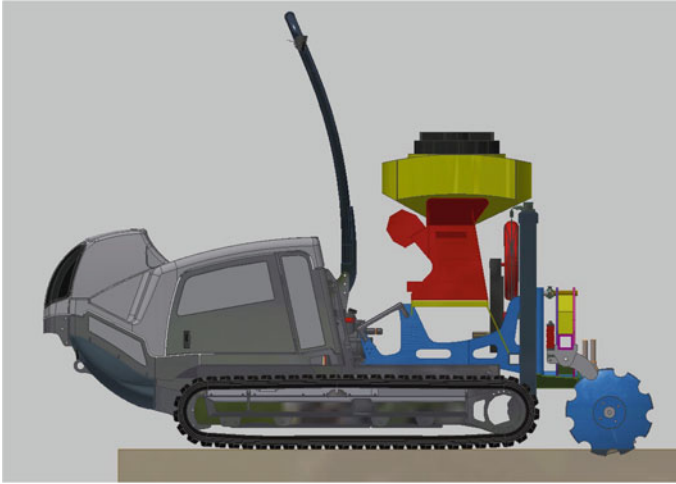


Fig. 4 Preliminary design of the seeding machine

rotations and continuous soil cover by plant residues. Direct sowing offers further advantages: a reduction of energy costs, reduction of exhaust gases, positive influence for biodiversity and reduction of fertilizers (Bodenbearbeitung und Bestellung 2015). For sowing the seeding machine is essential. Post and front tools, depth guidance, seed embedding, or the fertilizer placement are some of the components that can significantly influence the performance. Straw management and crop rotation are other critical factors in the farming system. Our investigations of the machines and coulters available on the market have led to the conclusion that a completely new seed drill has to be developed for the use on steep terrain, because the components are mostly too heavy. The seed drill consists of a disc, which is pressed in the soil (see Fig. 4). With the help of a pneumatic system, the seed and an organic fertilizer will be placed in the hole. After this process the hole is closed with two V-shaped rubber-discs. Since the self-weight of the seed is not enough to transport it from the reservoir to the soil in steep fields, the usage of a pneumatic system is essential for the process.

The stripping process emerged to be the most suitable method for harvesting grain in steep slopes. The process is relatively new and therefore needs further investigations and development (Tado et al. 1998; Mirnezami and Chegini 2016). The cereal spike is stripped through a rotary comb, which is illustrated in Fig. 5. The stalks are left in the ground, whereas the grain is transported with a pneumatic or mechanical system to a container. An advantage of this method is that the comb does not touch the ground, which prevents the crops from dirt. Furthermore, the crops contain very little straw because it is mostly left in the field and the grain is already partly threshed, which saves time in the post-harvesting process (Tado et al. 1998). Moreover, a comb enables to harvest also cereal which lies on the ground.

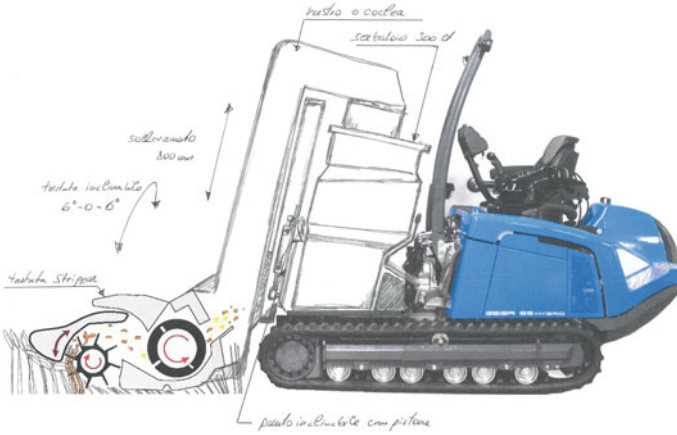


Fig. 5 Preliminary design of the harvesting machine: cereal is stripped through a rotary comb and gets transported to a container

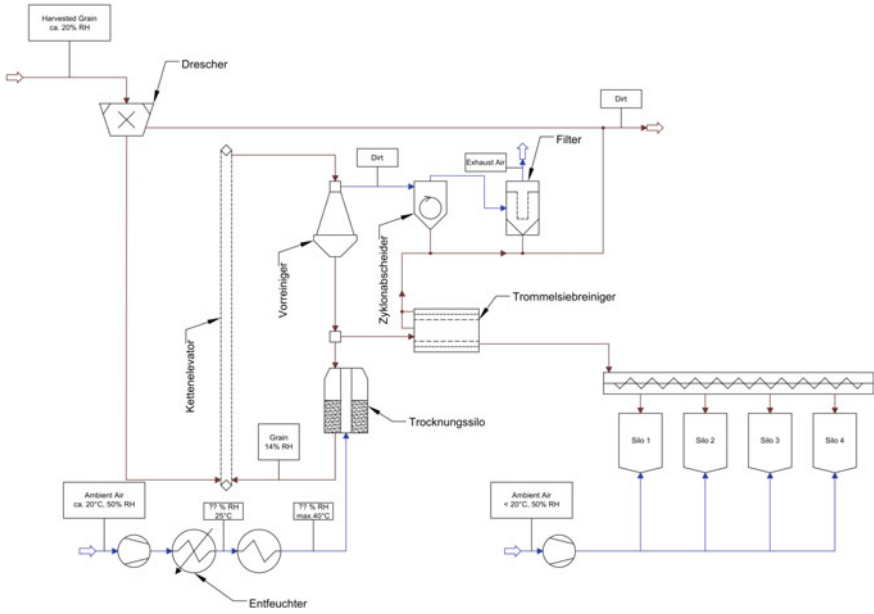


Fig. 6 Flow chart of the customized grain processing and conservation facility

2.3 Customized Grain Processing and Conservation Facility

The grain processing facility is especially designed for small farm structures which produce at maximum 10–20 t grain per year. A schematic is shown in Fig. 6. The stripped cereal is first treated in a threshing machine, which is located in the barn. Then the crop passes a pre-cleaner which extracts straw, dust and other light material from the grain. Due to unpredictable weather conditions, the relative grain humidity of the harvested grain is likely to be above the compulsory 14% for conservation (Humpisch 1998). Therefore, the grain will pass a drying facility. After the drying process, the grain is transported via a conveying system to the conservation silos. The temperature and humidity of the silos is monitored to maintain an optimal conservation environment for the grain. The most delicate component in the post harvesting process is the drying facility. Various drying techniques and the effect on grain at different drying temperatures must be evaluated to choose the most suitable drying method. Furthermore, the influence of these parameters to the flour, dough and bread quality will be examined. It poses a challenge to find a grain drying system with a high technical standard for small farm structures, since the facilities are designed mainly for huge grain processing companies. In addition it must be cost-effective for the farmer. The whole facility is expected to use mostly sustainable energy. Therefore, the drying air is heated in a heat exchanger which is supplied by hot water from an in-house wood chips facility. Typically heating systems are powered by oil burners, which enforces the design of a new supply system and to examine its efficiency.

2.4 Milling and Bread Production

The grain is extracted from the silos and transported to a mill. The flour is then processed to bread or other grocery products in the adjacent bakery and can be distributed directly at the farm. An important goal of the project is the investigation of the flour and bread quality, in correlation with the cultivation field and the post harvesting processes.

3 Summary and Outlook

The project aims to develop innovative seeding and harvesting machines for steep mountain slopes and to design a small post harvesting facility for an already existing farm building to enable farmers to cultivate cereal and to process the crops in-house. A main goal displays the development of innovative mechanization solutions, which entail a small environmental impact and high profits for the farmer. The seeding method has to be tested with the new designed machine and the harvesting machine needs further development. Afterwards the efficiency of the machines will be evalu-

ated and analysed. For the examination of the grain quality and the energy efficiency of the post harvesting facility data is collected continuously and has to be processed. A chemical analysis of the grain and flour will be performed and its correlation to the cultivation fields and post harvesting processes are examined. The dimension of automation of the facility will be examined in relation to the costs and to the investment possibilities for a small mountain farm. It is tried to find a general solution for cereal cultivation and post harvesting processing for small mountain farms, although, every single farm requires a personalized solution, since the structures and slopes are varying strongly.

References

- Autonome Provinz Bozen-Südtirol-Abteilung Landwirtschaft. Erschwernispunkte in der Berglandwirtschaft.
- Baker, C. J., Saxton, K. E., Baker, C. J., & Food and Agriculture Organization of the United Nations. (Eds.). (2007). *No-tillage seeding in conservation agriculture* (2nd ed.). Wallingford, UK; Cambridge, MA: Published jointly by Food and Agriculture Organization of the United Nations and Cabi Pub. ISBN 978-1-84593-116-2 978-92-5-105389-8. OCLC: ocm62525148.
- Bodenbearbeitung und Bestellung: Definition von Bodenbearbeitungs- und Bestellsystemen. Fachartikel, Kuratorium für Technik und Bauwesen in der Landwirtschaft, 2015.
- Humpisch, G. (1998). *Getreide lagern: Belüften und Trocknen; Einführung in Grundlagen, Technik*. Bergen/Dumme: Anwendung. Buchedition Agrimedia. ISBN 978-3-86037-090-2. OCLC: 76016894.
- Kulturpflanzen der Alpen. (2019). <http://www.provinz.bz.it/wanderausstellung/default.asp>.
- Mirnezami, S. V., & Chegini, G. (2016). Experimental comparison of combine performance with two harvesting methods: Stripper header and conventional header. *Agricultural Engineering International: CIGR Journal*, 18(1), 192–200.
- Notarnicola, B., Tassielli, G., Renzulli, P. A., Castellani, V., & Sala, S. (2017). Environmental impacts of food consumption in Europe. *Journal of Cleaner Production*, 140, 753–765.
- Tado, C. J. M., Wacker, P., Kutzbach, H. D., & Suministrado, D. C. (1998). Development of stripper harvesters: A review. *Journal of Agricultural Engineering Research*, 71(2). <https://doi.org/10.1006/jaer.1998.0318>.

The H2020 INNOSETA Project



Fabrizio Gioelli, Paolo Marucco, Floriana Nuzzo and Paolo Balsari

Abstract In the last years, a better and safer use of PPPs has become a central theme in sustainable agriculture. Spraying technologies have undergone important improvement in terms of efficiency and safety, as a consequence of the latest advances in electronics, data management and safety aspects. However, a significant gap between research & industrial innovations and farmers still exists. To enhance European agriculture sustainability, it is necessary to make the latest information available for relevant agriculture stakeholders. The objective of the H2020 INNOSETA project is to set up an innovative self-sustainable thematic network on Spraying Equipment, Training and Advising (INNOSETA) to close the gap between the available novel high-end crop protection solutions and European agriculture. A thorough inventory of EU-wide research results, relevant projects on the specific thematic, innovative industry products and available training materials was carried out by the partners. A total of 251 scientific and technical papers, 135 projects, 289 industry solutions and 315 training materials were found. Results were afterwards screened by project partners by using criteria set to select concrete, technology-ready and practical innovations. At the end of the screening process 109 articles, 55 projects, 188 industry products and all training materials were selected and will serve as inputs for an ICT tool represented by an online interactive open access platform available for all stakeholders.

Keywords Spraying equipment · Training and advising · Plant protection products · Online platform · Innovation

F. Gioelli (✉) · P. Marucco · F. Nuzzo · P. Balsari
Department of Agricultural, Forest and Food Sciences (DiSAFA), University of Torino (UNITO),
Largo Paolo Braccini, 2, 10095 Grugliasco To, Italy
e-mail: fabrizio.gioelli@unito.it

© Springer Nature Switzerland AG 2020
A. Coppola et al. (eds.), *Innovative Biosystems Engineering for Sustainable Agriculture, Forestry and Food Production*, Lecture Notes in Civil Engineering 67,
https://doi.org/10.1007/978-3-030-39299-4_51

1 Introduction

In modern agriculture, European farmers have to face major challenges: given the effects of climate change and the production rates that are needed, crop systems need to be efficient in terms of productivity and environmental sustainability, also in order to comply with recent European regulations (Directive on Sustainable Use of Pesticides 2009/128/EC 2009) that foresee the drastic reduction in use of PPPs (Plant Protection Products). To achieve this goal, the trend is to adopt Precision Agriculture (PA), a farming management concept which avails itself of technologies and practices that allow reducing the use of PPPs and shifts the farming system towards more sustainable production. In detail, for reduction and optimization of application of PPPs, PA technologies and practices aim at:

- protecting air and human health by exposure, through the reduction of spraying drift during application and operations for preparation of the mix and filling of the tank;
- protecting water bodies and soil, by preventing Point Source Pollution through proper cleaning of sprayers and remnants disposal;
- reduce the amount of utilized PPPs, by a more precise and targeted application.

The widespread adoption of PA strongly depends on the knowledge held by stakeholders: farmers, advisors, contractors. Therefore, the gap existing between the results of research (in terms of technology advancement and best practices, both achieved by research institutions and private companies) and their availability for end user must be covered. The INNOSETA project aims to close this gap in knowledge and to enhance the sustainability of European farming by gathering and selecting information about the latest innovations in terms of technology advancements in spraying and application techniques of PPPs in four cropping systems: open field, greenhouse, orchards and vineyards. Said innovations are defined as innovative SETA (Spraying, Equipment, Training and Advising) and are made available on an *open access and multi-language online platform* under the form of: (i) peer reviewed and technical papers, (ii) national and international projects, (iii) industry products, (iv) training and advising materials.

By making information easily accessible for stakeholders, an increase in the use of SETAs in European small-medium farming systems is likely to be expected. INNOSETA partners belong to Spain (UPC), Italy (DISAFA-University of Torino), France (IFV), Belgium (ILVO, CEMA, COPA-COGECA and ECPA), Greece (University of Athens and AGENSO), The Netherlands (ZLTO), Sweden (Visavi) and Poland (ZODR).

2 Materials and Methods

In order to create a dataset for the INNOSETA online platform, a thorough survey was carried out by partners by following the steps described in Fig. 1a and using the

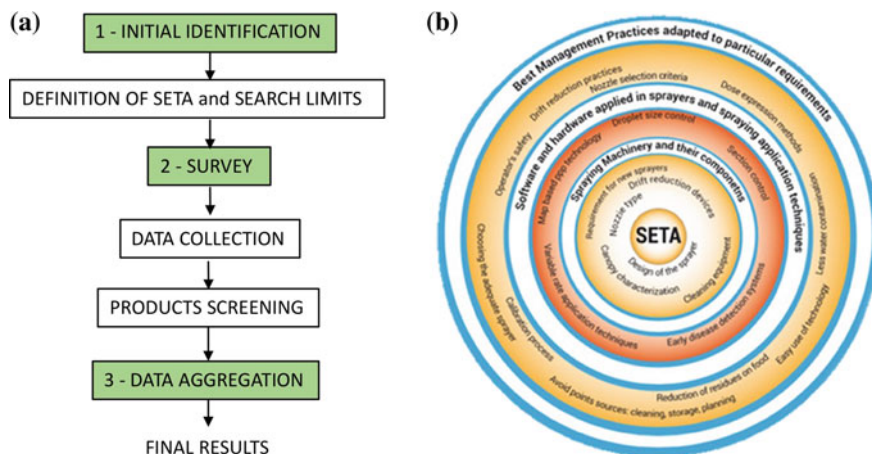


Fig. 1 Steps followed for data collection and screening (a) and keywords used for the survey (b)

keywords displayed in Fig. 1b. The basic criterion for data collection was finding *industry solutions, papers, projects advising and training materials* dealing with PPP spraying, focusing on those that allow farmers to: optimize pesticides application, avoid environmental pollution and to minimize PPPs residues on products. To narrow the search field, it was considered as a SETA: (i) whatsoever component, device, tool that can be fitted to spraying machineries; (ii) a whole sprayer that presents innovative components/accessories; (iii) devices/tools enhancing the environmental sustainability of spraying operation; (iv) training and advising material referred to sprayers, sprayers calibration and operations. The survey was carried out by considering records made available *in the reference period 2010-2018* only. For projects dealing with innovations in the spraying technology sector, data were retrieved from the available EU databases (e.g.: Cordis, EIP-Agri, etc.) and from national (or non-EU) databases. For papers, databases containing scientific peer reviewed international articles (Scopus, WoS...) as well as national databases were screened by the consortium. Industry solutions were retrieved from manufacturers' websites, direct contact with private companies or from magazines/official websites concerning national and international fairs on agricultural machinery awards and mentions (e.g. EIMA, Agritechnica etc.). At the end of the survey, records were screened to delete incomplete, double or *non-pertinent* records. The latter were considered, e.g., generic entries such as articles or projects dealing with Integrated Pest Management (IPM) or with PA in general terms (e.g. when spraying techniques were not the core part of the project or of the paper); papers, projects or industry solutions dealing with guidance and mapping systems that can be applied to a wide variety of field operations and are not exclusive for PPP application; records dealing with drones for application of PPP in compliance with the ban implemented in article 9 of Directive 2009/128/EC of the European Parliament. After screening, remaining records were

aggregated in homogeneous categories to serve as inputs for the INNOSETA online platform.

3 Results

The survey led to the collection of 250 articles, 135 projects, 289 industry solutions and 329 training materials (Fig. 2). After screening, 109 articles (peer reviewed and technical papers), 55 Projects, 188 industry solutions and 315 training materials were validated as SETAs. Considering industry products, the majority of records are represented by innovative sprayers ($n = 69$) and their components ($n = 60$) such as nozzles, filling and mixing systems etc. The same applies to articles and projects where the 50% and 37% of records deal respectively with innovative sprayers. When it comes to training materials, digital tools (websites, applications, webinar and e-learning courses) represents the 36% of the collected records, educational material (manuals, videos, presentations and case studies) the 44% and the dissemination material (leaflets and photos) the remaining 20% of the total collected information. For the selected SETAs' the predominant language for papers is English, as it is the official language for international literature. Nevertheless, about 50 articles in other languages (namely Spanish, French, Dutch, Italian, Portuguese, Polish and Chinese) are now available for the INNOSETA online platform. For training materials, the 85% of the approved records are either in English, Spanish, Italian or French. However, it must be pointed out that at present the majority of records come from Countries where at least one partner was based. In the future the records collection will be extended also to other Countries.

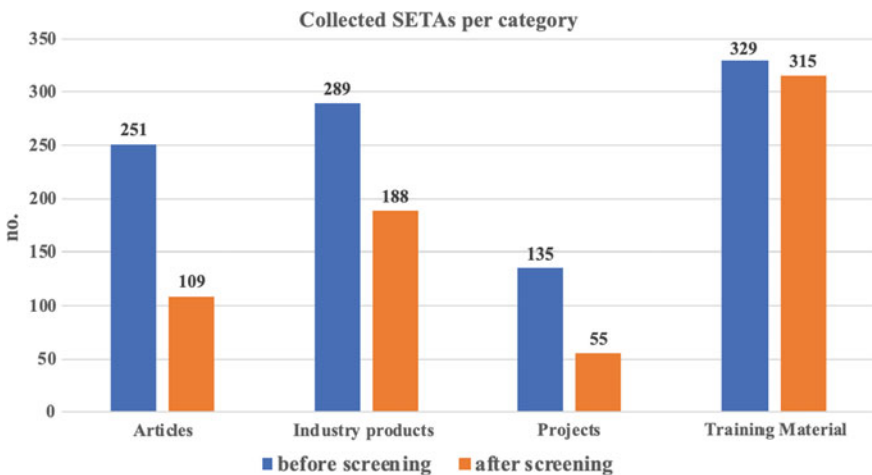


Fig. 2 Number of records per each SETAs' category before and after the screening process

4 Conclusions

In this first phase the baseline for the launch of the INNOSETA interactive online platform was set. 55 projects, 109 articles, 315 training materials and 188 industry products were selected to serve as first inputs for the platform. Records cover a wide range of technical solutions (from sprayers' components to whole machineries, from DSS to mapping systems) come from 23 countries and represent 8 different languages. Partners will keep on collecting SETAs in the upcoming years, in order to implement and to keep up to date the INNOSETA platform. Impact of the INNOSETA actions will be possible by comparing the situation about SETAs diffusion in the farming community before and after the project. To this purpose a specific survey was carried out between the farmers community in the very first months of the INNOSETA project.

Acknowledgements The activity presented in the paper is part of the research grant H2020 INNOSETA (grant agreement n° 773864).

Reference

Directive 2009/128/EC of the European Parliament and of the Council of 21. (2009). establishing a framework for Community action to achieve the sustainable use of pesticides. *Official Journal of the European Union L*, 309(71), 71–86.

Sprayer Inspection in Sicily on the Basis of Workshop Activity



Emanuele Cerruto, Giuseppe Manetto, Domenico Longo and Rita Papa

Abstract The European Directive on the sustainable use of pesticides makes mandatory the functional inspection of pesticide application equipment in all member States by the 26th November 2016. In this paper the inspection activity in Sicily region is analyzed. The test reports produced by each workshop center in the period January 2014–May 2019 have been examined. The analysis allowed knowing, on regional basis, number and type of inspected equipment, spreading of the different models of sprayer and their prevalent use. Moreover, being inspection centers mechanical workshops too, the analysis of test reports allowed knowing the condition of machines when inspected and the main repairs carried out.

Keywords Pesticide application equipment · Sustainable use of pesticides · National action plan

1 Introduction

According to the 2009/128/EC Directive for the Sustainable Use of Pesticides (SUD), all Pesticide Application Equipment (PAE) should have been inspected by the 26th November 2016 in all member States (European Commission 2009). Inspection is the means by which increasing the sprayer application efficiency and mitigating the negative effects of phytosanitary treatments on the human health and the environment (Cerruto et al. 2018). A recent survey in the European Member States and other countries in Europe (Wehmann 2018) enlightened that not all the involved countries reported the existence of a good working inspection system. Several problems are still present, regarding both the quality of the inspection system itself and a certain number of not inspected PAE which are being used. The main reasons of this status vary from lack of farmer information, to not enough high level of workshop activity

E. Cerruto (✉) · G. Manetto · D. Longo · R. Papa
Department of Agriculture, Food and Environment (Di3A), University of Catania, Via S. Sofia
100, 95123 Catania, Italy
e-mail: ecerruto@unict.it

© Springer Nature Switzerland AG 2020
A. Coppola et al. (eds.), *Innovative Biosystems Engineering for Sustainable Agriculture, Forestry and Food Production*, Lecture Notes in Civil Engineering 67,
https://doi.org/10.1007/978-3-030-39299-4_52

control, to lack of knowledge about the inspection procedure, and to lack of interest among farmers, advisors, and even authorities.

The operational framework for the SUD application in Italy has been set up by the ENAMA (National Board for Agricultural Mechanization) Working Group, coordinated by Prof. Paolo Balsari (Crop Protection Technology Research Group—Department DISAFA, University of Turin). The inspection activity received a significant boost after the Legislative Decree no. 150/2012, which incorporates the SUD and the National Action Plan (NAP). In fact, the number of inspected sprayers has increased from about 12,200 in 2012 to about 42,900 in 2017, while number of authorized workshops and licensed inspectors has increased from 148 (2012) to 255 (2016) and from 398 (2012) to 653 (2016), respectively (Allochis et al. 2017).

Sicily Region, with D.D.G. no. 6402 of 12/12/2014 (Sicily Region 2014) and subsequent amendments and additions, implemented the obligations coming from SUD and NAP regarding the mandatory and certified training system for professional users, distributors and consultants. Moreover, in order to train technicians qualified to work in fixed or mobile workshops for sprayer inspection, the Region organizes 40-hour long courses, divided between theoretical and practical section. At present, 18 workshops operate in Sicily.

In this paper the test reports produced by each workshop center in Sicily were analyzed. The analysis allowed knowing, on regional basis, number and type of inspected pesticide application equipment, results of the inspection activity, how the different models of sprayer are spread in the territory and their prevalent use.

2 Materials and Methods

Workshop centers in Sicily produce different test reports according to the sprayer type: field crop sprayers, sprayers for bush and tree crops, sprayers with oscillating jets (from February 2018), and “special” sprayers (spray lances connected to conventional sprayers or to fixed/mobile pumps and knapsack sprayers, mainly used in greenhouses). All test reports are organized into sections, referring to workshop center, sprayer owner, sprayer type, and inspection procedure. In this paper test reports produced in the period January 2014–May 2019 were analyzed (inspection activity in previous years was very limited). For each test report the following main items were extracted:

1. test center: name, city and province;
2. sprayer: brand, model, type, serial number, construction year, connection to the tractor and use (personal or as contractor);
3. test report: number and date;
4. sprayer components checked during the inspection procedure: type of defect determined, classified as “none”, “minimum”, “relevant”, and “repaired”.

For each component, in accordance to the report form used by the workshop centers, several aspects were analyzed, but the results of the control were summarized

in only one value by summing all the replays. All data were organized in an Excel spreadsheet and then processed by using the open source software R (R Core Team 2013).

3 Results and Discussion

3.1 Workshop

According to the test reports and the National Database of Authorized Workshops for Functional Inspection and Adjustment of the Sprayers (2019), 18 workshops operate in Sicily (update at 23.02.2019): seven in the province of Agrigento, two in the province of Catania, one in the province of Palermo, four in the province of Ragusa, one in the province of Siracusa, and three in the province of Trapani (Fig. 1). Seven of them are fixed workshops and eleven are mobile ones. Their distribution in the territory is therefore quite uneven, but it is conditioned by the crop typology in the different areas. In fact, workshops are mainly concentrated in the areas where vineyards (Trapani and Agrigento provinces) and greenhouse crops (Ragusa province) are more diffused.

The number of functional inspections in the period January 2014–May 2019 has been 4020, but only 3888 available reports have been analyzed. It is estimated that some 30,000 PAE operate in Sicily (Pessina and Facchinetti 2016), so less than 14% of



Fig. 1 Workshop centers in Sicily (fixed in green numbers; mobile in red numbers). The numbers are the Unique ID of the center, on Regional basis

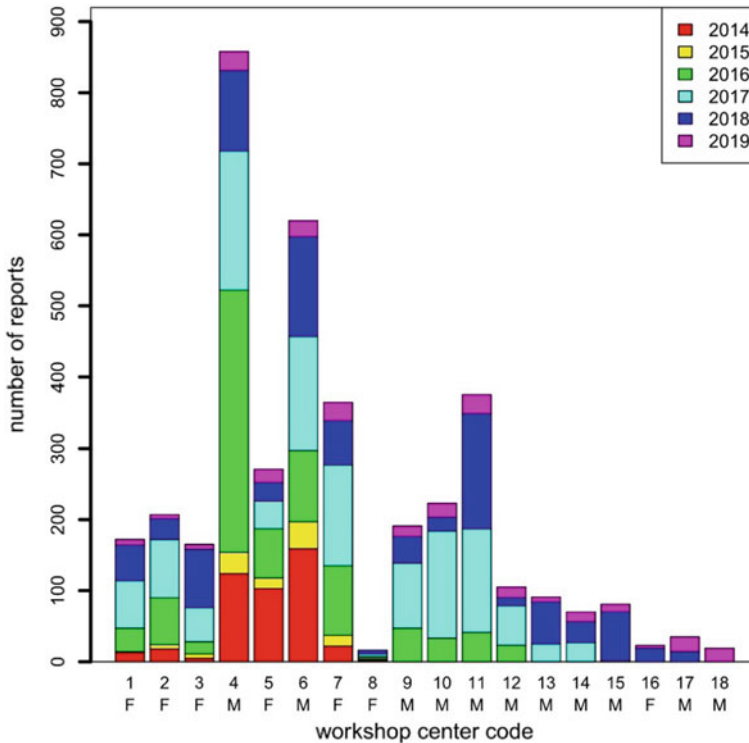


Fig. 2 Number of test reports per workshop center and per year (F: fixed; M: mobile)

equipment have been inspected. The distribution of inspected PAE among workshop centers is shown in Fig. 2. On average, about 40 functional inspections per center and per year have been carried out. Figure 2 underlines the great activity of mobile workshop centers with respect to the fixed ones: 243 functional inspections per center versus 174 (ratio 1.39) in the analyzed period. Moreover, Fig. 2 also underlines a great unevenness between workshop activities: only four of them (workshops #4, #6, #7, and #11) have produced 57% of the total test reports.

3.2 *Sprayers*

On average, 64.0% of inspected PAE are sprayers for bush and tree crops, 14.8% field crop sprayers, 1.8% with oscillating jets, and 19.4% special sprayers. Their distribution among workshop centers is reported in Fig. 3. Sprayers with oscillating jets have been mainly inspected by the workshop centers #15, #9 and #4 (operating in the province of Agrigento), #17 (Palermo), and #3 (Siracusa), where wheat production is the leading activity. The highest percentage (18.5%) was observed in workshop

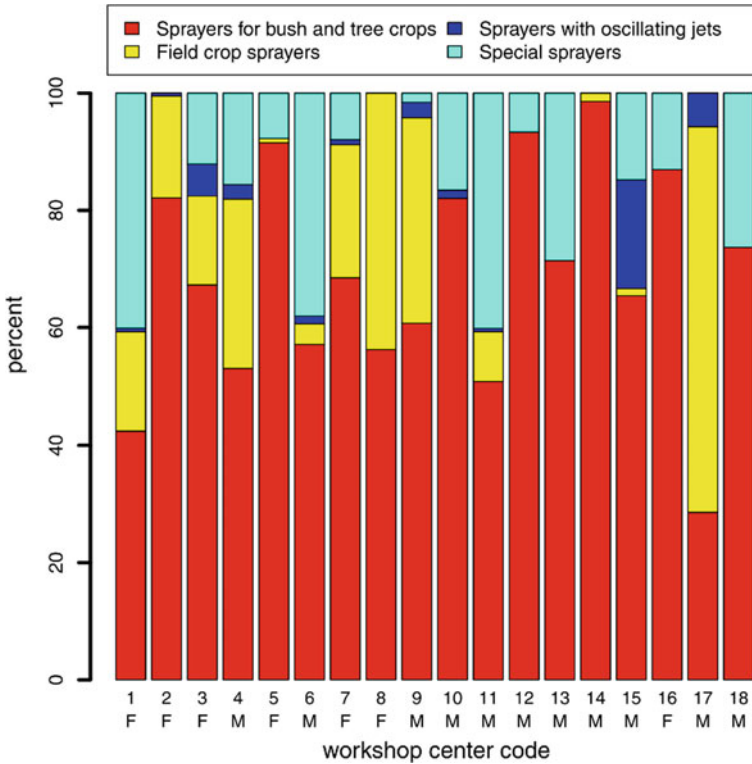
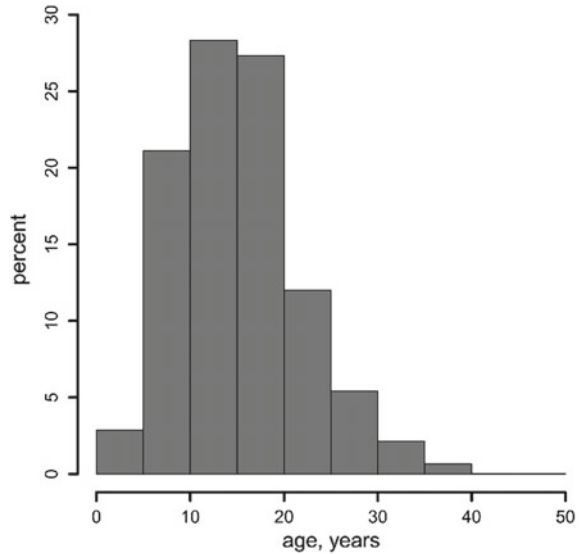


Fig. 3 Distribution of inspected sprayer types per workshop center (F: fixed; M: mobile)

center #15 located at Santa Margherita di Belice, where hilly territory is dominant. The same workshop centers (except #15), together with #8 (located at Ragusa), #7 (between the provinces of Catania and Enna) and #2 (Agrigento), have inspected the highest percentage of field crop sprayers. It must be noted the workshop center #17, located in province of Palermo, but in the central area of Sicily, that has inspected more field crop sprayers (65.7%) than sprayers for bush and tree crops (28.6%). All the other workshop centers have prevalently inspected sprayers for bush and tree crops; this is particularly true, with an incidence higher than 90%, for centers #14, #12 and #5, located in the provinces of Trapani and Agrigento, where the viticulture is more diffused. Lastly, special sprayers are inspected with an incidence higher than 30% by the workshop centers operating in province of Ragusa, where there is a high concentration of horticulture farms. Relevant percentages of inspections of these machines occur also for workshop centers #13, #18 and #10, operating in areas with orchard crops where treatments are carried out with spray lances connected to conventional sprayers.

Inspected PAE are mainly mounted on the tractor (51.2%); 48.0% are towed ones, while 0.4% are self-propelled. The remaining 0.4% are spray lances connected to

Fig. 4 Distribution of inspected sprayer age



fixed pipelines or wheelbarrows, or motorized backpack sprayers. Almost all PAE inspected (96.8%) are used directly by the owner, while only 3.2% are used by contractors. Age of PAE, when known (69.6%), ranges from 1 to 49 years (mean 15.8 years). Mean values are similar for all sprayer types: 15.7 years for bush and tree crop sprayers, 15.5 years for field crop sprayers, and 16.6 years for special sprayers; no data are available for sprayers with oscillating jets. Age distribution is reported in Fig. 4. From it emerges that 56% of PAE age ranges between 10 and 20 years, in 24% of cases it is less than 10 years, and in 20% of cases it is greater than 20 years. Unknown ages are very likely to be attributed to rather old machines, so it can be concluded that a consistent part of PAE are quite old and therefore they require important repairs.

3.3 Defects

The analysis of the reports produced by workshop centers is summarized in Fig. 5, that shows the percentage of the different types of defect determined for each component group. In this graph the “none” category is not represented, but it is the complement to 100% of the maximum percentage recorded for each component. Therefore, no interventions were necessary in more than 80% of cases, reaching 100% for the power transmission and the on/off and adjustment devices of sprayers with oscillating jets. It should be noted, however, that, according to the comments in observation fields, often “none” intervention is reported, even if substitutions or repairs are indicated.

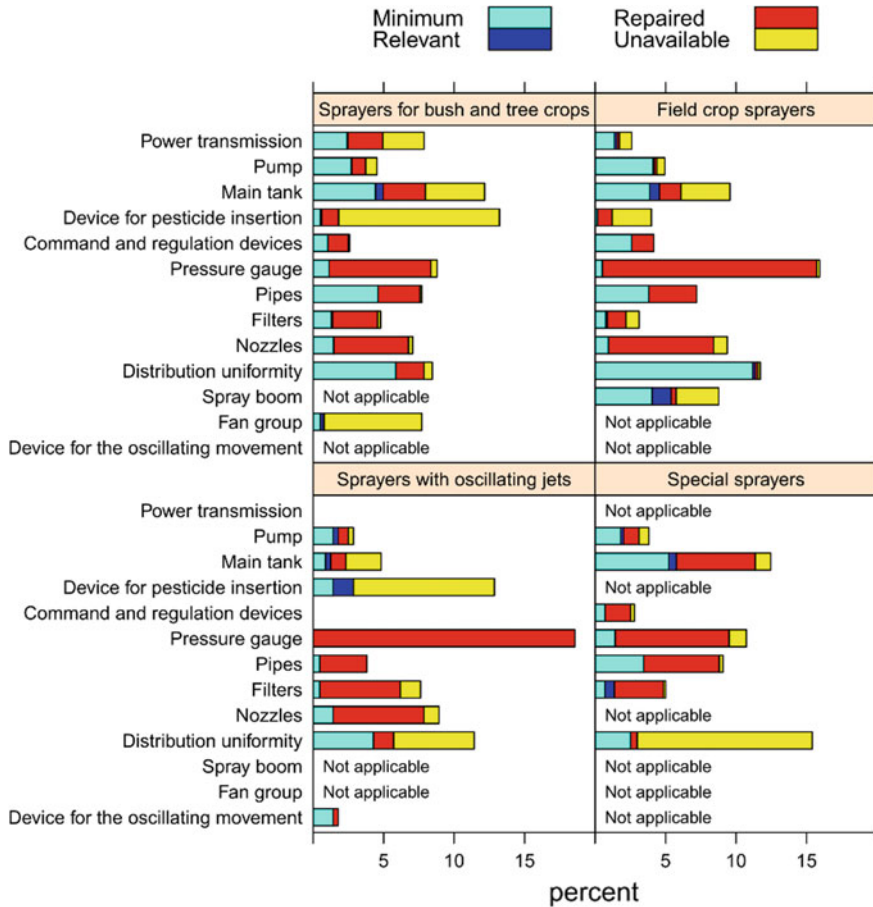


Fig. 5 Summary of workshop’s reports for sprayer type and inspected component

So, some technicians have drawn up the report referring to the condition of the machine at the end of the inspection rather than at the beginning.

A high number of repairs (substitutions) mentioned (more than 15%) concerned the pressure gauge, both in sprayers with oscillating jets and field crop sprayers; even if with a lower incidence (less than 10%), a lot of pressure gauges have been substituted in special sprayers and in sprayers for bush and tree crops, too. Many repairs have also interested nozzles and filters for all sprayer types, pipes (special sprayers and sprayers with oscillating jets) and main tank (special sprayers). Nozzles, filters and pipes have been mainly replaced, while repairs of main tank in special sprayers involved adding hand wash tank and level indicator. Distribution uniformity and pump mainly required minimum interventions; for the latter, sometimes valves were replaced and return lines were added.

4 Conclusions

In the present study, an analysis of sprayers' inspection activity in the last five years in Sicily region has been carried out. Workshop centers resulted unevenly distributed in regional area, with a higher concentration in vineyards and greenhouse crop territories. Agricultural land use had also incidence on the main sprayer types inspected by workshop centers. Up to 2019 seems that only less than 14% of the total sprayers in use estimated in Sicily region have been inspected.

The analysis of test reports has allowed identifying: the age of inspected sprayers, with 56% of them dating back from 10–20 years ago; their connection to the tractor, with 51.2% of sprayers mounted on the tractor and 48% of them being towed; the sprayer's use, with a strong predominance of owner use (96.8%). About the type of defect determined during the inspection procedure, it was verified that no interventions were needed on power transmission and on on/off and adjustment devices in sprayers with oscillating jets. In general, for the other inspected components any intervention was required in more than 80% of PAE inspected; minimum intervention was mainly reported for improve the distribution uniformity and reach the pump performance required while more severe interventions were needed for pressure gauges (10–15%), but even for nozzles, filters, pipes and main tank.

Acknowledgements The activity presented in the paper is part of the research grant “Piano della Ricerca 2016-2018 - UNICT – Innovazioni attraverso applicazioni ICT nel settore delle costruzioni rurali, della pianificazione del territorio agro-forestale e della meccanizzazione della difesa fitosanitaria. WPI – Sviluppo di tecniche e di applicazioni anche informatiche per l'innovazione nel settore della meccanizzazione della difesa fitosanitaria”. Authors wish to thank Dr. C. Ferrantello and Dr. G. Affrunti of Regional Department of Agriculture of Sicily for having made the data available.

References

- Allochis, D., Balsari, P., & Marucco, P. (2017). The Italian sprayers inspection situation after the expiry of the deadline set by the national action plan and the directive 2009/128/EC. In *11th International AIIA Conference*, 5–8 July 2017. Bari, Italy.
- Cerruto, E., Manetto, G., Santoro, F., & Pascuzzi S. (2018). Operator dermal exposure to pesticides in tomato and strawberry greenhouses from hand-held sprayers. *Sustainability*, 10(7–2273), 1–21.
- European Commission (2009). Directive 2009/128/EC of the European parliament and of the council of 21 october 2009 establishing a framework for community action to achieve the sustainable use of pesticides. *Official Journal*, L 309/71, 24/11/2009.
- National Database of Authorized Workshops for Functional Inspection and Adjustment of the Sprayers. <http://www.laboratorio-cpt.to.it/authorized-workshops/?lang=en>. Accessed 27 May 2019.
- Pessina, D., & Facchinetti, D. (2016). Verifica funzionale e taratura delle macchine per la distribuzione di fitofarmaci. <http://users.unimi.it/cirive/incontri-informativi/160413/Pessina160413.pdf>.
- R Core Team (2013). R: A language and environment for statistical computing. In *R Foundation for Statistical Computing*, Vienna, Austria. <http://www.R-project.org/>.

- Sicily Region (2014). Implementing provisions of the mandatory and certified training system for professional users, distributors and consultants. D.D.G. no. 6402, 12/12/2014.
- Wehmann, H. J. (2018). Status Quo of Inspection in EU: The Results of SPISE Enquiry. In *7th European Workshop on Standardised Procedure for the Inspection of Sprayers–SPISE 7*. Athens, Greece. (September 26–28, 9–22).

Evaluation on the Stability of Tree Used as Anchors in Cable Yarding Operations: A Preliminary Test Based on Low-Cost MEMS Sensors



L. Marchi, O. Mologni, S. Grigolato and R. Cavalli

Abstract Most of the fatal injuries that occur in cable yarding operations are related to both breakage of the skyline or failure of its anchoring system. The high forces, necessary to provide a cable path that consent an efficient transportation of the logs, are dynamically amplified by the oscillation of the moving mass (in case of fully suspended loads) and by the sudden accelerations applied to the carriage when ground obstacles are encountered (in case of semi-suspended loads). Due to the lack of effective methods that predict the actual load carrying capacity of such anchoring solution, there is the need to verify the possibility to define a system that assesses the failure of the tree used as anchors due to overturning. As a consequence, the present work aims to apply the knowledge of tree stability assessment to the case of anchors in cable yarding operations. Comparison between data on tree assessment of experimental pulling tests that simulated failure of the tree used as anchors due to uprooting and data collected from direct field measurements by MEMS sensors on tree used as anchors during real cable operation are made. The correlation between the two sets of data is made in order to develop an assessment technique, based on continuous monitoring, that guarantee a better level of safety of the anchors than actual empirical methods.

Keywords Cable logging · Precision forestry · Tree overturning · MEMS · Pulling test

1 Introduction

At different scale of applications, Precision Forestry (PF) specifies the use of modern tools and technologies to obtain real-time, non-invasive and accurate information aiming to develop decision-making processes, to verify the achievements and the

L. Marchi · O. Mologni · S. Grigolato (✉) · R. Cavalli
Department of Land, Environment, Agriculture and Forestry, Università degli Studi di Padova,
Viale dell'Università 16, 35020 Legnaro PD, Italy
e-mail: stefano.grigolato@unipd.it

© Springer Nature Switzerland AG 2020
A. Coppola et al. (eds.), *Innovative Biosystems Engineering for Sustainable Agriculture, Forestry and Food Production*, Lecture Notes in Civil Engineering 67,
https://doi.org/10.1007/978-3-030-39299-4_53

efficiency of the studied process in Forestry (Kováčsová and Antalová 2010; Lindroos et al. 2017; Marinello et al. 2017; Talbot et al. 2017).

This work deals with the applications of PF concepts to the field of cable logging harvesting systems. Several examples are available with reference to this topic that aim to investigate the productivity of the site or the safety of working operations of such harvesting systems. In the first case, combination of GPS units and Inertial Measurements Units (IMU) systems are applied to carriages in standing skyline systems to automatically determine timing of working cycles (Gallo et al. 2013; Lezier et al. 2019; Pierzchała et al. 2018). In the second, the use of high-performance tensile force load-cells are used to evaluate how and in what amount tensile force limits are exceeded during typical working cycles (Mologni et al. 2018, 2019). In this context, after breakage of ropes due to excessive tensions or usage (Tsioras et al. 2011) failure of trees used as anchors are a critical issue. These high-magnitude forces must be withstood by the anchoring system, in general consisting of a sufficiently large tree or stump available in the nearby area, over which the rope end is secured. There is a lack of information regarding this type of accidental failure and the safety of trees used as anchors in cable supported operations is still an open issue (Cavalli 2012; Marchi et al. 2018). To this aim, the application of low-cost MEMS (Micro Electro-Mechanical Systems) sensors has been recently used to evaluate stability of medium-high diameter trees subjected to high punctual forces (Marchi et al. 2019). However, application of these concepts to real case studies is still missing.

Consequently, a preliminary experimental test has been carried out involving MEMS sensors applied to the base of the anchor of a standing skyline yarding system.

2 Materials and Methods

2.1 *Layout of the Test*

The test involved the comparison between (a) the experimental data obtained from the analysis of the behavior of the trees used as anchors and subject to the controlled application of an external force (Marchi et al. 2019) similar with (b) the monitoring data of a real case study in which the behavior of the tree used as an anchor was analyzed as a function of the force applied by the carrying rope.

2.2 *Pulling Test Data*

Pulling tests data consist of definition of moment versus rotations ($M(\varphi)$) curves obtained from destructive pulling tests on mature Norway spruce (*Picea abies* (L.) Karst.) trees with medium-high diameter at breast height. The tensile force (F) was

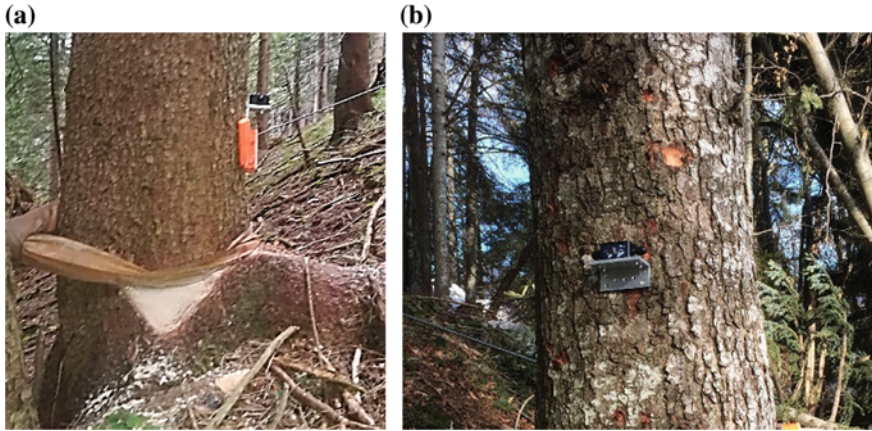


Fig. 1 Three-axis MEMS accelerometers at the tail anchor (a) and biaxial MEMS inclinometer on the tail spar (b)

applied by means of a properly designed pulley equipment capable to apply a maximum force of 400 kN to the tree being pulled. Tree displacements were measured with two 3-axis accelerometers used as tilt sensors. Details on the tests and employed equipment are available in Marchi et al. (2019).

2.3 Field Data

Field data were obtained by monitoring the anchoring system of a single-span downhill-oriented standing skyline yarding system. The same type of MEMS sensors of the pulling tests were employed as well as the load cell used to determine tensile forces in the skyline. The high-sensitivity 3-axis accelerometers have been applied at the base of the tail anchor (Fig. 1a) and to the nearby spar tree. Moreover, another type of tilt sensor built on MEMS technology capable of a precision of 0.01° , provided with a wireless connection and an integrated data logger, has been applied to the tail spar to evaluate displacement of the stem (Fig. 1b). The latter sensor could give real-time indications of the rotations reached by the base of the trunk by means of a local wireless network established through an external antenna connected to a pc.

3 Results and Discussion

Total applied force versus rotation curve were extrapolated by time-syncing of the MEMS sensors and the load cell applied to the pulling equipment (Fig. 2a). Results confirmed the difficulty in giving direct predictions on the maximum load-bearing

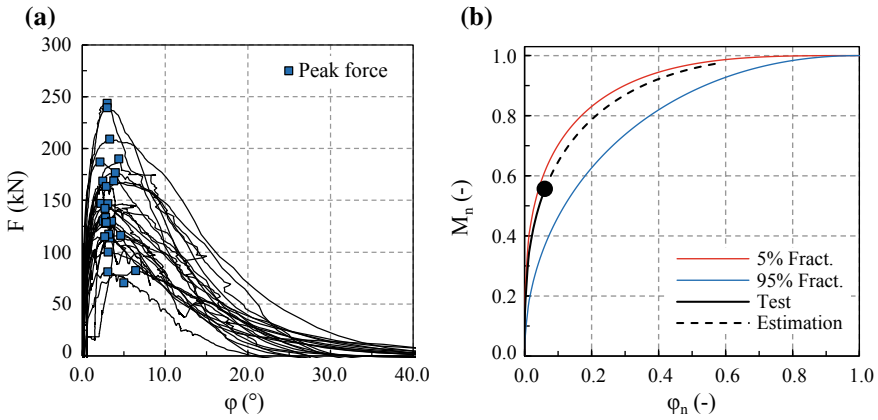


Fig. 2 Moment versus rotation curves obtained by tests (a) and dimensionless curve (b) for predictive models

capacity based only on allometric predictors. It appeared that the rotation of the root-plate follows a more reliable trend which is less site-specific and can more easily be predicted with general allometric variables as diameter over bark at breast height (DBH) and tree height (H). To this aim, the equivalent applied moment (M) was obtained by the product of the applied force and pulling height with respect to soil. Then, adimensionalized $M(\phi)$ curves were reconstructed (Fig. 2b), following similar approaches already developed for tree stability analyses on urban trees.

Main results showed that tree displacement have been correctly capture by the MEMS sensors. The same syncing process between forces and rotations used in the pulling tests have been employed in the post-processing phase (Fig. 3). The data have been pre-filtered by the internal integrated circuit of each sensor; however some additional filters have been applied to obtain an even smoother trend of the $M(\phi)$ curve shown in Fig. 4a. The origin of coordinates ($M = 0$; $\phi = 0$) has been easily

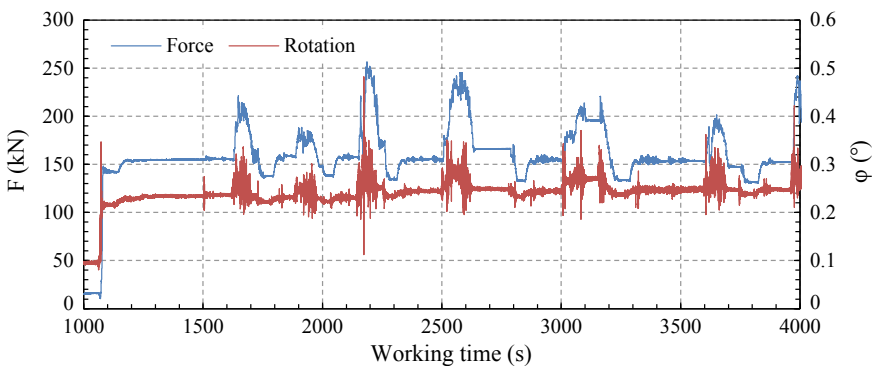


Fig. 3 Sample of tensile force and base rotation development during multiple working time

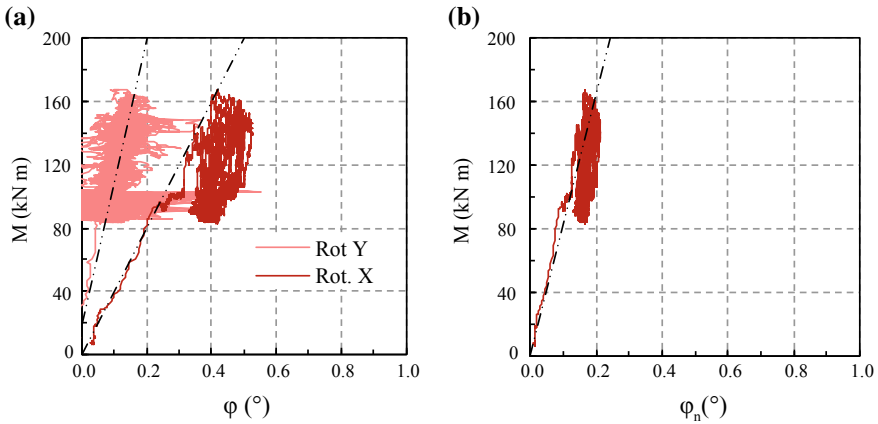


Fig. 4 Curves of the tail anchor obtained by field data expressed as $M(\varphi)$ (a) and $M(\varphi_n)$ (b)

evaluated as during the data acquisition, the skyline has been dropped to the ground and totally un-tensioned. In this way, it has been possible to recreate the general trend of the curve given by the dashed lines in Fig. 4a. Rotation X in the same figure, is referred to the rotation of the root-plate system occurring on the vertical plane parallel to the skyline and going through the anchor. The linearity of the observed curve suggests that the root-system has been working elastically, therefore the anchor could have been considered as safe, during the whole monitoring phase.

Preliminary predictions on the safety level of the anchor with respect to the load bearing capacity may be done with reference to the procedure suggested in Marchi et al. (2019) and the regressions of φ given by Lundström et al. (2007) and Marchi et al. (2019). In this case, given the anchor dimensions DBH and H, the calculated rotation at the peak tensile force φ_{peak} (i.e., the predicted maximum load bearing capacity of the tree) is equal to 2.49° . Therefore, it results that the dimensionless rotation of the given anchor ($\varphi_n = \varphi/\varphi_{peak}$) is limited to a value of 0.2 (Fig. 4b). Comparing this result with the graph of Fig. 2b—which has been constructed for Norway spruce on dry mineral soil—the registered bending moment $M \sim 160$ kNm could correspond to the 60–80% of the allowable strength offered by the anchor.

The latter paragraph is a mere example of calculation as the monitoring phase was limited to a few dozens of working cycles. More precise estimations could have been done if the monitoring phase included the initial setting phase of the skyline system and more working cycles.

4 Conclusions

In the present study, an experimental test has been carried out to evaluate the stability of a tree employed as anchor in a cable yarding harvesting operation. The low-cost MEMS sensors have been found to be suitable to monitor displacements of natural

anchors used in the cable-supported forest operations. This preliminary work has to be validated by a congruous number of field tests to provide the reliability of the presented technology. In fact, the possibility of successfully using low-cost micro sensors has been demonstrated, but in order to make the system applicable, it is necessary to set tests on different conditions of intensity and direction of the forces applied.

Again, further tests should also involve trees as anchors that are different in dimension and species. Furthermore, the transferability of the present approach also depends on the characteristics of the sensors (in term of precision and accuracy) and their efficiency to communicate even remotely in an environment such as the forest, which is complex due to the presence of obstacles such as standing trees and the morphology of the terrain.

The application of the PF can be a key element in the operational management of forestry sites. The example of MEMS sensors applied to trees used as anchors represents an important step for the creation of a real-time alert system to prevent the collapse of the structural elements—both natural like trees and artificial ones such as the pylons—that set up a cable crane.

Acknowledgements The activity presented in the paper is part of the research grant founded by the Department of Land, Environment, Agriculture and Forestry, Università degli Studi di Padova under the Grant BIRD 2017 “SLOPE: tree Stability in cable Logging and safety of Operators - Development of an alert system based on wireless and low cost sensors”.

References

- Cavalli, R. (2012). Prospects of research on cable logging in forest engineering community. *Croatian Journal of Forest Engineering*, 33(2), 339–356.
- Gallo, R., Grigolato, S., Cavalli, R., & Mazzetto, F. (2013). GNSS-based operational monitoring devices for forest logging operation chains. *Journal of Agricultural Engineering*, 44(2s), 140–144.
- Kováčsová, P., & Antalová, M. (2010). Precision forestry—definition and technologies. *Šumarski List*, 143(11–12), 603–611.
- Lezier, A., Cadei, A., Mologni, O., Marchi, L., & Grigolato, S. (2019). Development of a device based on an open-source electronics platform for the monitoring of cable-logging operations. In *Engineering for Rural Development*. May 22–24, 2019. Jelgava: Latvia University of Life Sciences and Technologies, Faculty of Engineering.
- Lindroos, O., Hera, P. La, & Häggström, C. (2017). Drivers of advances in mechanized timber harvesting—a selective review of technological innovation. *Croatian Journal of Forest Engineering*, 38(2), 243–258.
- Lundström, T., Jonsson, M. J., & Kalberer, M. (2007). The root-soil system of Norway spruce subjected to turning moment: Resistance as a function of rotation. *Plant and Soil*, 300(1–2), 35–49.
- Marchi, L., Grigolato, S., Mologni, O., Scotta, R., Cavalli, R., & Montecchio, L. (2018). State of the Art on the use of trees as supports and anchors in forest operations. *Forests*, 9(8), 467.
- Marchi, L., Mologni, O., Trutalli, D., Scotta, R., Montecchio, L., Cavalli, R., et al. (2019). Safety assessment of trees used as anchors in cable-supported harvesting operations based on experimental observations. *Biosystems Engineering*, 186, 71–82.

- Marinello, F., Proto, A. R., Zimbalatti, G., Pezzuolo, A., Cavalli, R., & Grigolato, S. (2017). Determination of forest road surface roughness by Kinect depth imaging. *Annals of Forest Research*, 60(2), 217–226.
- Mologni, O., Dyson, P., Amishev, D., Proto, A. R., Zimbalatti, G., Cavalli, R., et al. (2018). Tensile force monitoring on large winch-assist forwarders operating in British Columbia. *Croatian Journal of Forest Engineering*, 39(2), 193–204.
- Mologni, O., Lyons, C. K., Zambon, G., Proto, A. R., Zimbalatti, G., Cavalli, R., & Grigolato, S. (2019). Skyline tensile force monitoring of mobile tower yarders operating in the Italian Alps. *European Journal of Forest Research*, (on-line first).
- Pierzchała, M., Kvaal, K., Stampfer, K., & Talbot, B. (2018). Automatic recognition of work phases in cable yarding supported by sensor fusion. *International Journal of Forest Engineering*, 29(1), 12–20.
- Talbot, B., Pierzchała, M., & Astrup, R. (2017). Applications of remote and proximal sensing for improved precision in forest operations. *Croatian Journal of Forest Engineering*, 38(2), 327–336.
- Tsioras, P., Rottensteiner, C., & Stampfer, K. (2011). Analysis of Accidents during cable yarding operations in Austria 1998–2008. *Croatian Journal of Forest Engineering*, 32(2), 549–560.

Modelling of Agricultural Machinery Trends for Power, Mass, Working Width and Price



Francesco Marinello, Tatevik Yezekyan, Giannantonio Armentano and Luigi Sartori

Abstract Rural mechanisation and fleet organisation have an essential impact on agricultural production and sustainable development of farm institutions. Machine functional parameters define the fleet composition and management and, thus, play an important role in economic and environmental performance of a farm. Programming methods and decision support systems are available in the market, however, there is still a lack of applicative tools which allow modelling and forecasting of technical parameters as well as costs to complete the decision tasks. Availability of such models in relation to dimensions, mass, power or working capacity, is then particularly necessary not only to support decisions at the different applied management levels (farmer, stakeholder, policy makers), but also to study the impact of farm machine on the environment and in general to understand trends in agricultural mechanization. The present research is aimed at identifying the most relevant parameters (including working width, overall dimensions, mass and power) for different groups of agricultural machines, modelled and characterised through the application of linear regression analyses. The study is defined on the basis of a database populated on purpose with more than 5000 agricultural machines models (30 machine groups) available in the market. Extracted equations give evidence of high correlations ($R^2 > 0.75$) in particular between prices, mass and needed power, supporting the possibility of analyses on mechanisation trends, from both economical, management and environmental point of view.

Keywords Functional parameter · Operation research · Modelling · Linear programming · Fleet management

F. Marinello (✉) · T. Yezekyan · L. Sartori
Department of Land, Environment, Agriculture and Forestry, University of Padova, Via
Dell'Università 16, 35020 Legnaro, Italy
e-mail: francesco.marinello@unipd.it

G. Armentano
Edizioni L'Informatore Agrario Srl, Via Bencivenga - Biondani, 16, 37133 Verona, Italy

© Springer Nature Switzerland AG 2020
A. Coppola et al. (eds.), *Innovative Biosystems Engineering for Sustainable Agriculture, Forestry and Food Production*, Lecture Notes in Civil Engineering 67,
https://doi.org/10.1007/978-3-030-39299-4_54

1 Introduction

Economic and environmental sustainability of agricultural machinery management relies on the justified synergy of operational requirements and available resources. Definition of optimal combination is very complex due to the machinery system interaction with agronomic, biological, pedological and climatic features (Søgaard and Sørensen 2004).

The choice of the machine based on expectations of higher performances, brand, on the advanced technological devices of the implement, or available financial resources lead to the adaption of badly scaled machinery both from the dimensional and from the functional point of view (Cavallo et al. 2014). From one side, the latter can be understandable in the case of tractors, while it is unacceptable for agricultural implements which, conversely, must be optimised for well-defined operations, thus often playing a crucial role for the success of crop production. The reasons behind the unbalanced choice of the machine capacity and matching requirements have to be ascribed not only to low awareness of farmers but also to the massive information flow, lack of knowledge and reference models supporting the machine selection process (Sims and Heney 2017). Large availability and high variability of functional characteristics and prices of agricultural machines in the market make the selection process more complex and confused for the farmer. The adoption of innovative strategies for enhancement of the efficiencies applied in mechanisation system leads to the modification of machinery cost structure and price policy, impacting decision-making regarding fleet accomplishment and fleet management (Bochtis et al. 2014; Reidsma et al. 2018). Simplification of the practices for the definition of the eligible parameter-price relation for the machinery is needed and can reduce the complexity of the estimation and lead to the correct implementation of the available resources.

Technological advances adopted in agricultural production and associated units contributed to more specialized and complex farm planning management (Peart and Shown 2006). Intensification of farm practices, a saturation of machinery construction and features lead to more complex decision making phase, machinery selection process and adjustment of innovative solutions. To support and improve the managerial decision-making process for farmers and increase the quality of decisions, mathematical models and computer software packages have been widely launched in agricultural management and consultancy (Bulgakov et al. 2015; Sopegno et al. 2016). The problem-solving framework of the various programs and applications meant to optimise the farm organization, simplify the interpretation of data and adoption by users, and reduce financial expenses and environmental impact (Almansour and Jejeic 2017; Chamen 2015). A large diversity of linear and non-linear programming methods, mathematical models, computer software, integral models have been developed for optimization of machinery selection, scheduling, multi-farm crop management, simulation of agricultural in-field machinery activities and operation planning, machinery dimensioning and capacity planning intended for decision support and information conversation to the knowledge (Camarena et al. 2004; Filippi et al. 2017, Lazzari and Mazzetto 1996; Nikkila et al. 2010; Sorensen

and Bochtis 2010). However, the diversity and complexity of available systems not always meet the needs and expectations of real farms, in addition, most of them are limited to the research level or consider applied in the restricted number of experimental farms (Sopegno et al. 2016). There is a lack of consideration of functional parameters of the machine as a potential for the definition of the reference price for the implements and conversely the parameters as well. Individual farmers would need simple reference cost-based methods or tools to make an equipment investment decision. A reference model built up on the available and most predictive parameters of the machines, without a requirement of particular software/skills. Indeed, economic estimation models for machinery cost calculation and selection are based only on economic analyses of the data/operation with consideration of fixed and variable costs of machines (Edwards 2015; Tieppo et al. 2019). Thus, the management of farm fleet and machinery selection/planning, must take into account different parameters, concerning not only the cost of the machines but also their dimensions, power, mass, working width, capacity, which have impact on productivity of operation, on the return of the investment, and also on the environment (Borsato et al. 2018).

Current research is aimed to develop simplified equation models based on the analyses of functional parameters (power, mass, working width, tank capacity when appropriate) of different groups of agricultural machines, to define the impacts of technical and design parameters, to provide linear regression models for the variables with highest predictive potential, thus contributing to the optimization of the fleet selection process, evaluation and prediction of costs and performances. Linear models were chosen due to their easy understandability and versatile applicability.

2 Materials and Methods

A set of analyses was carried out considering both raw data and extracted equation models. The functionality of information source, database, has been merged with the analytical capabilities of qualitative models to provide the transformation of information into knowledge (Taechatanasat and Armstrong, 2014).

The research activity has been supported by Informatore Agrario srl (Verona, Italy), which directly and regularly contact agricultural machinery constructors in order to update with power, mass, working width, and other parameters specifications. Data presented include the technical and dimensional parameters and list prices of main groups of agricultural implements intended for soil preparation and crop cultivation. Study database consists of more than 5000 models of agricultural implements available in the market and is classified in the following six groups: soil preparation, sowing, crop protection, fertilization, irrigation, haymaking. It is worth noticing that considered implements include models both for the cultivation of herbaceous crops and for fruit tree crops or viticulture (spraying, soil preparation, etc.). Conversely, self propelled machines were not included in the study, having characteristics which might substantially deviate from other implements.

Table 1 Description of the database of agricultural implements according to the information provided by constructors

Characteristic	Description/Type
Model	Constructing company, series, name
Type of machine	Soil preparation, seeding, spraying, spreading, irrigation, haymaking
Attachment to tractor	Towed, semi-mounted, front/mid/rear mounted; minimum power of the tractor
Tank capacity	Seed, fertilizer, etc.
Distribution	Mechanical/pneumatic
Soil-engaging tools	Device type, deepness of the cultivation
Working width	The number and minimum/maximum distance of rows, number of units
Other equipment	Standard tires, hydraulics, electronic controls
Dimensions	Total length/height/width, mass
List price	Basic machine configuration

Collected raw data were sorted, edited and completed as a single databank. Further study analyses were performed for all corresponding variables as a single group (Yezekyan et al. 2018a, 2018b), as well as according to the two subgroups separately. Considered data and information related to the implements are summarized in Table 1.

Based on the characteristic classification of the implements additionally, the single database of the machines was divided into the two main groups according to the type of descriptive constructional parameters (working width/tank capacity) and analyzed separately. Soil preparation group included: plough, harrow, cultivator, strip tiller and rotary tiller; Sowing group encompassed row seeder, precision planter, combined planter and no-tillage planter; Spraying group had mistblower, tunnel sprayer and field sprayer; Spreading machine group was including mineral fertiliser spreader and organic fertiliser spreader; Haymaking group was formed by mower, tedder, shredder and baler, while Irrigation group just considered hose reel irrigator.

Data included in the analyses represent all modern market of implements thanks to the inclusion of high variation of the models and constructors as can be noticed from the summarized range of the considered variables in Table 2.

For the definition of the most correlated functional parameters for six groups of agricultural implements and their influence on the performance of the machine and price, data were statistically analysed with the application of Microsoft Excel (Microsoft Corporation, Redmond, WA, USA) program. Dependencies between considered variables were studied with the application of linear regression analyses. The relevance of the models was quantified by means of correlation studies and dependences modelled according to a linear characteristic equation defined by the slope (or linear coefficient) m_i related to the i -th independent variables and by the intercept q between y and x variables.

According to the linear regression analyses data reported regarding Pearson correlation coefficient r , slope m and intercept q of the linear models. The simplicity of linear models allows their wide application and consideration by interested parties

Table 2 The range for minimum and maximum values of the considered variables according to the dataset

	No. of models	Working width, m	Capacity, L	Power, kW	Mass, kg	Price VAT excl., €
Soil preparation	2167	0.35–12	–	7–375	94–11200	1220–136370
Seeding	463	1–9	50–4350	29–265	465–12284	4377–124000
Spraying	694	6–32	120–6000	5–100	48–4200	950–99600
Spreading	275	1.4–30	40–33000	9–147	26–12300	428–88000
Irrigation	160	–	–	2–130	220–10800	3460–93550
Haymaking	1214	0.53–9.1	–	6–190	43–16570	845–282215

(farmers, farm management applications and agencies, stakeholders, etc.) for justification of machines parameters' requirements and forecasting. The liner models considered as not large models that provide a high degree of detail and precision; nevertheless, the models are based on the defined functional parameters and represent robust and realistic output, providing sufficient details for decision making and selection optimization.

3 Results and Discussion

According to the linear correlation analyses, power, mass, working width, tank capacity and list price of the machines exhibited the highest predictable correlation properties. Main trends between mass, price and power are graphically shown in Fig. 1, in a logarithmic scale representation, in order to allow visualization of machines with parameters ranging between several orders of magnitude. Additionally, a full summary of r correlation coefficients is reported in Table 1.

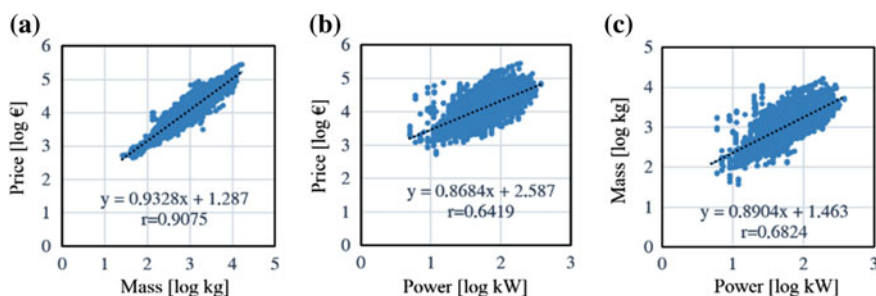


Fig. 1 General trends of correlation for all considered models of agricultural machinery in logarithmic values of **a** price versus mass, **b** mass versus power and **c** price versus power

Table 3 Distribution of high correlation coefficients r according to the considered groups of implements

	Mass/ Capacity	Mass/Power	Price/ Capacity	Price/Power	Price/ Mass
Soil preparation	N/A	0.751	N/A	0.711	0.854
Seeding	0.713	0.625	0.686	0.701	0.897
Spraying	0.825	0.426	0.704	0.454	0.918
Spreading	0.925	0.683	0.897	0.723	0.904
Irrigation	N/A	0.373	N/A	0.759	0.868
Haymaking	N/A	0.698	N/A	0.695	0.969

High correlations ($r > 0.8$) were in general arising between price and mass, between price or mass and capacity in the case of spreaders and between mass and capacity for sprayers. Other high correlations ($r > 0.7$) were also quantified as reported in Table 3. Additionally, the linear modelling and correlation analysis for spraying implements exhibited relatively high Pearson coefficients in particular between price and working width ($r = 0.85$), mass and working width ($r = 0.83$), working width and tank capacity ($r = 0.82$).

Recognised correlations are not surprising: indeed, machinery mass is clearly proportional to the working width (both in case of implements based on pulling and machines moved by hydraulic or mechanical PTO) due to larger dimensions of the implement itself. Additionally, the mass of machinery most often has to be lifted up by the tractor: since the lift capacity is physically limited by the mass of the tractor, and since tractor mass is correlated to tractor power, thus the mass of the implement eventually correlates with available power. With reference to the costs, the higher are the dimensions of machinery, the higher is the cost of material, manufacture and transport: as a consequence, the final cost of the implement is strictly correlated to the implement mass. In agreement with recognised correlations, the following models were drawn (Table 4).

As mentioned above the proposed linear models can be used in order to support decision processes, providing indications relative to different parameters. Furthermore, the same models can also be used in order to define a reference threshold for evaluating in a more general way the impact of different agricultural equipment: by way of example the line in Fig. 1a separates machinery in the upper part of the graph typically characterized by a higher technological content, by those in the lower part, characterized by a higher weight and thus a higher potential stress on soil. Similarly, the line in Fig. 1a separates implements requiring a high initial investment by those characterized by higher consumes. Thirdly, the line in Fig. 1c separates weight intensive by power intensive machinery. Thus, these and other reported models can play a relevant role in order to understand the economical and to some extent environmental sustainability of analysed agricultural machinery.

Table 4 Linear equation models for different variables according to considered groups of implements

	Mass–Capacity	Mass–Power	
Soil preparation	N/A	$M = 17.74 \cdot P - 82.06$	
Seeding	$M = 1.895 \cdot C + 531.4$	$M = 28.60 \cdot P - 318.4$	
Spraying	$M = 0.713 \cdot C - 106.5$	$M = 16.62 \cdot P + 55.09$	
Spreading	$M = 0.352 \cdot C - 80.67$	$M = 55.08 \cdot P - 285.2$	
Irrigation	N/A	$M = 35.83 \cdot P + 4447$	
Haymaking	N/A	$M = 55.54 \cdot P - 904.5$	
	Price–Capacity	Price–Power	Price–Mass
Soil preparation	N/A	$Pr = 193.3 \cdot P - 527.9$	$Pr = 9.836 \cdot M + 2190$
Seeding	$Pr = 26.68 \cdot C + 13160$	$Pr = 439.8 \cdot P - 2389$	$Pr = 13.14 \cdot M + 7584$
Spraying	$Pr = 13.77 \cdot C - 978.1$	$Pr = 402.8 \cdot P - 1513$	$Pr = 21.55 \cdot M - 499.1$
Spreading	$Pr = 2.223 \cdot C + 889.2$	$Pr = 350.6 \cdot P - 2328$	$Pr = 5.879 \cdot M + 2139$
Irrigation	N/A	$Pr = 514.9 \cdot P + 20780$	$Pr = 6.221 \cdot M + 4765$
Haymaking	N/A	$Pr = 941.4 \cdot P - 20880$	$Pr = 16.41 \cdot M - 4980$

For different groups of machines: C: tank capacity (L); M: mass (kg); P: power (kW); L: working width (m); Pr: estimated price (€)

4 Conclusions

The present research takes advantage of a database populated on purpose with more than 5000 agricultural machines models (30 machine groups) available in the market to define trends and correlations existing between main parameters of agricultural implements. Main variables include power, mass, price, working width and tank capacity (when available). Linear models analyses give evidence of high correlations ($R^2 > 0.75$) in particular between prices, mass and needed power. Such correlations can be usefully implemented whenever decision support systems have to be designed regarding the farm fleet, and can support the possibility of analyses on mechanization trends, from both economical, management and environmental point of view.

References

- Al-mansour, F., & Jejcic, V. (2017). A model calculation of the carbon footprint of agricultural products: The case of Slovenia. *Energy*, *136*, 7–15. <https://doi.org/10.1016/j.energy.2016.10.099>.
- Bochtis, D. D., Sørensen, C. G. C., & Busato, P. (2014). Advances in agricultural machinery management: A review. *Biosystems Engineering*, *126*, 69–81. <https://doi.org/10.1016/j.biosystemseng.2014.07.012>.
- Borsato, E., Tarolli, P., & Marinello, F. (2018). Sustainable patterns of main agricultural products combining different footprint parameters. *Journal of Cleaner Production*, *179*, 357–367. <https://doi.org/10.1016/j.jclepro.2018.01.044>.
- Bulgakov, V., Adamchuk, V., Arak, M., & Olt, J. (2015). Mathematical Modelling of the Process of Renewal of the Fleet of Combine Harvesters. *Agriculture and Agricultural Science Procedia*, *7*, 35–39. <https://doi.org/10.1016/j.aaspro.2015.12.027>.
- Camarena, E. A., Gracia, C., & Sixto, J. M. C. (2004). A Mixed Integer Linear Programming Machinery Selection Model for Multifarm Systems., *87*, 145–147. <https://doi.org/10.1016/j.biosystemseng.2003.10.003>.
- Cavallo, E., Ferrari, E., Bollani, L., & Coccia, M. (2014). Attitudes and behaviour of adopters of technological innovations in agricultural tractors: A case study in Italian agricultural system. *Agricultural Systems*, *130*, 44–54. <https://doi.org/10.1016/j.agsy.2014.05.012>.
- Chamen, T. (2015). Controlled traffic farming—From worldwide research to adoption in Europe and its future prospects. *Acta Technologica Agriculturae*, *18*(3), 64–73. <https://doi.org/10.1515/ata-2015-0014>.
- Edwards, W. (2015). Estimating farm machinery repair costs. *Iowa State University Extension and Outreach, Ag Decision Maker, File A3-29*.
- Filippi, C., Mansini, R., & Stevanato, E. (2017). Mixed integer linear programming models for optimal crop selection. *Computers & Operations Research*, *81*, 26–39. <https://doi.org/10.1016/j.cor.2016.12.004>.
- Lazzari, M., & Mazzetto, F. (1996). A PC model for selecting multicropping farm machinery systems. *Computers and Electronics in Agriculture*, *14*(1), 43–59. [https://doi.org/10.1016/0168-1699\(95\)00036-4](https://doi.org/10.1016/0168-1699(95)00036-4).
- Nikkilä, R., Seilonen, I., & Koskinen, K. (2010). Software architecture for farm management information systems in precision agriculture. *Computers and Electronics in Agriculture*, *70*(2), 328–336. <https://doi.org/10.1016/j.compag.2009.08.013>.
- Peart, R., & Shown, V. (2006). Agricultural systems management. optimizing efficiency and performance. In *Agricultural Systems Management*. New York: Marcel Dekker, INC.
- Reidsma, P., Janssen, S., Jansen, J., & Van Ittersum, M. K. (2018). On the development and use of farm models for policy impact assessment in the European Union. *Agricultural Systems*, *159*, 111–125. <https://doi.org/10.1016/j.agsy.2017.10.012>.
- Sims, B., & Heney, J. (2017). Promoting Smallholder Adoption of Conservation Agriculture through Mechanization Services. *Agriculture*, *7*(64). <https://doi.org/10.3390/agriculture7080064>.
- Søgaard, H. T., & Sørensen, C. G. (2004). A model for optimal selection of machinery sizes within the farm machinery system. *Biosystems Engineering*, *89*, 13–28. <https://doi.org/10.1016/j.biosystemseng.2004.05.004>.
- Sopegno, A., Busato, P., Berruto, R., & Romanelli, T. L. (2016). A cost prediction model for machine operation in multi-field production systems. *Scientia Agricola*, *73*(5), 397–405. <https://doi.org/10.1590/0103-9016-2015-0304>.
- Sørensen, C. G., & Bochtis, D. D. (2010). Conceptual model of fleet management in agriculture. *Biosystems Engineering*, *105*(1), 41–50. <https://doi.org/10.1016/j.biosystemseng.2009.09.009>.
- Taechatanasat, P., & Armstrong, L. (2014). Decision support system data for farmer decision making. In *Proceedings of Asian Federation for Information Technology in Agriculture*, 472–486.
- Tieppo, R. C., Romanelli, T. L., Milan, M., Sørensen, C. A. G., & Bochtis, D. (2019). Modeling cost and energy demand in agricultural machinery fleets for soybean and maize cultivated using

a no-tillage system. *Computers and Electronics in Agriculture*, 156, 282–292. <https://doi.org/10.1016/j.compag.2018.11.032>.

Yezekyan, T., Marinello, F., Armentano, G., & Sartori, L. (2018a). Analysis of cost and performances of agricultural machinery: Reference model for sprayers. *Agronomy Research*, 16(2), 604–614. <https://doi.org/10.15159/AR.18.049>.

Yezekyan, T., Marinello, F., Armentano, G., Trestini, S., & Sartori, L. (2018b). Definition of Reference Models for Power, Weight, Working Width, and Price for Seeding Machines. *Agriculture*, 8(12), 186. <https://doi.org/10.3390/agriculture8120186>.

High Accuracy Site-Specific Secondary Data for Mechanical Field Operations to Support LCA Studies



Marco Fiala and Luca Nonini

Abstract The aim of the study was to quantify site-specific secondary data of mechanical field operations for EU barley cropping. By the model ENVIAM v2, each operation was subdivided into 13 working times and, for each of them, the amount of total consuming inputs (fuel, lubricant and AdBlue[®]) and emissions of exhaust gases into the atmosphere were calculated. The amount of partial consuming inputs (machinery mass) and emissions of heavy metals into the soil were also quantified. Three scenarios (S) were identified: $S_1 = 50$ ha, $S_2 = 100$ ha, $S_3 = 200$ ha, with the same: agronomic conditions, operations sequence, type of machines used and cropping inputs. For each scenario, two barley ideotypes were analyzed: (i) currently in use (BarNow, 2018) and (ii) future (BarPlus, 2030). BarPlus is characterized by: (i) higher grain and straw yield, Nitrogen fertilization rate and machinery Effective Field Capacity, (ii) use of TIER 5 fuel engines, (iii) lower specific minimum fuel consumption. BarNow inputs ($\text{kg}\cdot\text{ha}^{-1}$) were: fuel = $67 \div 74$, lubricant = $0.56 \div 0.73$, mass = $7.9 \div 8.8$. BarPlus inputs ($\text{kg}\cdot\text{ha}^{-1}$) were: fuel = $55 \div 60$, lubricant = $0.53 \div 0.69$, AdBlue[®] = $2.8 \div 3.0$, mass = $7.2 \div 8.0$. The highest fuel and mass consumptions were in both cases related to tillage operations.

Keywords Barley cultivation · Mechanical field operation · Working time · Site-specific secondary data · Environmental inventory

1 Introduction

The most widespread methodology to quantify the potential environmental impacts of agricultural processes is the Life Cycle assessment (Life Cycle Analysis, LCA) (Notarnicola et al. 2017). Among the LCA phases, the Life Cycle Inventory (LCI) is the most complex to accomplish because all the system inputs (fuel, lubricant,

M. Fiala · L. Nonini (✉)

Department of Agricultural and Environmental Sciences – Production, Landscape, Agroenergy (DiSAA), University of Milan, G. Celoria 2, 20133 Milan, Italy
e-mail: luca.nonini@unimi.it

© Springer Nature Switzerland AG 2020

A. Coppola et al. (eds.), *Innovative Biosystems Engineering for Sustainable Agriculture, Forestry and Food Production*, Lecture Notes in Civil Engineering 67,
https://doi.org/10.1007/978-3-030-39299-4_55

491

masses) and outputs (emissions into the atmosphere, water and soil) have to be identified and quantified. Often, these data are not easy to collect experimentally, and long and expensive sampling are needed (Dyer and Desjardins 2003; Ossés de Eicker et al. 2010). To limit this problem, many commercial Databases that provide information about different agricultural processes (e.g. Ecoinvent, Danish LCA food, EU and DK input and output Database, Agri-footprint Database) were developed (Jannick et al. 2010; Ecoinvent 2015). Nevertheless, they usually provide simplified information about some processes and, therefore, their main deficiency is the lack of reliability. This represents a major problem for mechanical field operations, which are performed in very different conditions, both pedological (texture, water content, slope, shape and size of the field and its distance from the farm), and climatic (temperature and rainfall) (Lovarelli et al. 2016, 2017). Mechanical field operations play a crucial role in determining the environmental impacts of agricultural processes (Keyes et al. 2015) but, due to the abovementioned problems, performing reliable LCA studies using site-specific primary data is a key challenge. Therefore, it is necessary to develop models able to calculate secondary data with high accuracy, according to the different site-specific conditions (Bengoa et al. 2014). Several studies were performed to evaluate the environmental impacts of cereal cropping (Murphy and Kendall 2013; Achten and Van Acker 2016), including those related to barley cultivation (Dijkman et al. 2017). Barley is a great source of nutrients, carbohydrates and fiber (Baik and Ullrich 2008), and it is primarily used for animal feedstock and malt production (Schmidt Rivera et al. 2017). This crop is the 12th most important agricultural commodity in the world, and Europe is the largest producer (62% of the world production). The aim of the study was to quantify site-specific secondary data related to mechanical field operations for EU barley cropping (from soil tillage to grain and straw transport) to support LCA studies.

2 Materials and Methods

2.1 *The Model ENVIAM V2*

The model ENVIAM v1 (“ENVironmental Inventory of Agricultural Machinery operations”) was developed some years ago (Lovarelli et al. 2016) to calculate site-specific secondary data related to mechanical field operations, by taking into account specific working times (t_j ; h) (Reboul 1964). These data refer to both the amount of total (fuel and lubricant) and partial (mass of machinery) consuming inputs, as well as the emissions of exhaust gases (CO_2 , CO, HC, PM and NO_x) into the atmosphere, resulting from fuel combustion. ENVIAM v1 was recently implemented into a second version (ENVIAM v2); the main improvements are: (i) calculation of the working times (13 in total) in separate worksheets, specifically developed for each type of implement used. To make the further calculations feasible and accurate, a value of engine load (λ ; % tractor’s maximum engine power) must be assigned to each

working time. This is a fundamental step, since fuel consumptions—and thus exhaust gases emissions into the atmosphere—strongly depend on both tractor's engine loads and duration of each working time (Lovarelli et al. 2018). The time for transfer farm-to-field and field-to-farm (including the one for lunch breaks) was included in the calculation: it cannot be neglected for operations carried out over one day and for long distances between the farm center and the fields; (ii) calculation of AdBlue[®] consumption if the tractor is equipped with a Selective Catalyst Reduction (SCR) system; (iii) calculation—for tractors—of the mass required for production, consumption, maintenance and repair, by introducing a repair factor according to the Ecoinvent v3.2[®] Database documentation (Nemecek and Kägi 2007); (iv) calculation of the mass of tire abraded during the operation and the corresponding mass of heavy metals (Cd, Pb, Zn) released into the soil (Nemecek and Kägi 2007); (v) improvement of the general structure of the model, by removing some demanding tests, to provide a more intuitive and user-friendly interface. Other aspects are instead still under investigation: (i) calculation of the tractor's engine power losses in the case of hydraulic/mixed transmissions and (ii) calculation of consumptions and emissions for operations performed under slope conditions.

2.2 Barley Cultivation Scenarios

The analysis was based on the following assumptions about barley production in Europe: (i) the crop is cultivated on a wide range of farms whose Agricultural Area Used (AAU; ha) ranges from a few tens to a few hundred hectares (European Commission 2018); (ii) the sequence of mechanical field operations is simplified compared to other herbaceous crops and involves the use of the same types of machines; (iii) the production factors (inputs) are limited in terms of both quality and quantity (Marinussen et al. 2012); (iv) the crop is not irrigated (barley has a good resistance to drought and, usually, uses only natural water supplies); (v) grain (Y_G ; t·ha⁻¹) and straw (Y_S ; t·ha⁻¹) yields show limited variations among different cultivation areas (Marinussen et al. 2012). Three different scenarios (S) were compared (Fiala et al. 2019): (i) S1: small size cereals production farm (AAU₁ = 50 ha); (ii) S2: medium size cereals production farm (AAU₂ = 100 ha); (iii) S3: medium-large size cereals production farm (AAU₃ = 200 ha). These scenarios were all characterized by the same: (i) cultural conditions (fields characteristics and length, distance from the farm center); (ii) cultivation operations timeline and type of machines used and (iii) cropping inputs (Table 1).

Tractors and implements technical characteristics referred to EU agricultural machinery market; cropping inputs amounts referred to EU conditions. S1, S2 and S3 scenarios were different for the tractors (number, type, engine power) and implements (size) fleet. For each scenario, two barley ideotypes were taken into account: (i) currently in use (year 2018, BarNow; S1_{NOW}, S2_{NOW}, S3_{NOW}) and (ii) a future

Table 1 Agronomic parameters used for the different scenarios

	Unit	S1	S2	S3
Agricultural area used	ha	AAU ₁ = 50	AAU ₂ = 100	AAU ₃ = 200
Barley area (60% AAU)	ha	AAU _{B1} = 30	AAU _{B2} = 60	AAU _{B3} = 120
Other crops (35% AAU)	ha	AAU _{O1} = 17.5	AAU _{O2} = 35	AAU _{O3} = 70
Green crops (5% AAU)	ha	AAU _{G1} = 2.5	AAU _{G2} = 5	AAU _{G3} = 10
Fields distance	km	D = 2.0		
Fields characteristics	–	Soil texture: medium; area: flat; shape: rectangular		
Fields length	m	b _L = 800		
Cropping sequence	–	(1) NPK fertilization, (2) ploughing, (3) harrowing, (4) sowing, (5) chemical weed control, (6) N fertilization, (7) grain harvesting and (8) transport, (9) straw collection and (10) transport		
Cropping inputs	kg · ha ⁻¹	Seeding rate: 190; herbicide rate: 1.45		

ideotype (year 2030, BarPlus; S1_{PLUS}, S2_{PLUS}, S3_{PLUS}). BarNow and BarPlus cultivations were compared by introducing, for the latter, cropping and technological improvements.

2.2.1 Cropping Improvements

Grain and straw yield and dry matter (DM) content of both barley ideotypes are shown in Table 2.

The improvement of the performance of the BarPlus ideotype was pointed out in the Project “*BARPULS—Modifying canopy architecture and photosynthesis to maximize barley biomass and yield for different end-uses*” (EU FACCE-SURPLUS ERA-NET, 2015–2018). According to the results of this Project—which takes into account future climate changes in EU, as well as the evolution of barley genotype and phenotype—the increase of the biomass yield (for both grain and straw) can be achieved by a higher rate in Nitrogen mineral fertilization ($\Delta N = 20 \text{ kg} \cdot \text{ha}^{-1}$ of N) (Table 3).

Table 2 BarNow and BarPlus scenarios: grain and straw characteristics and yields

Product	BarNow (year 2018)		BarPlus (year 2030)	
	Dry matter (%)	Yield (t · ha ⁻¹) (t · ha ⁻¹ DM)	Dry matter (%)	Yield (t · ha ⁻¹) (t · ha ⁻¹ DM)
Grain	DM _G = 81.5%	Y _G = 6.5 (5.3)	DM _G = 88.0	Y _G = 7.5 (6.6)
Straw	DM _S = 84.5%	Y _S = 6.5 (5.5)	DM _S = 86.3	Y _S = 7.3 (6.3)

Table 3 BarNow and BarPlus scenarios: NPK requirements and fertilizer rates (R)

Agronomic aspects	Unit	BarNow (year 2018)	BarPlus (year 2030)
Requirements	$\text{kg} \cdot \text{ha}^{-1}$	(N) 100; (K ₂ O) 20; (P ₂ O ₅) 40	(N) 120; (K ₂ O) 20; (P ₂ O ₅) 40
1st mineral fert.	$\text{kg} \cdot \text{ha}^{-1}$	R ₁ = 150 (NPK 20-20-20)	R ₁ = 150 (NPK 20-20-20)
2nd mineral fert.	$\text{kg} \cdot \text{ha}^{-1}$	R ₂ = 220 Urea (46%)	R ₂ = 265 Urea (46%)

Table 4 BarNow and BarPlus scenarios: technological improvements in fuel engines

Technical aspects	Unit	BarNow (year 2018)	BarPlus (year 2030)
Emission stage	–	TIER 3B	TIER 5
Equipment	–	None	SCR and AdBlue® (#)
Specific fuel consumption	$\text{g} \cdot \text{kWh}^{-1}$	c _{S_{MIN}} = 200 ÷ 250	Δc _{S_{MIN}} = – 10%

Note: (#) AdBlue® consumption = 5% of fuel consumption

2.2.2 Technological improvements

Compared to BarNow, for the BarPlus scenarios the following improvements were considered (Table 4): (i) use of internal combustion (i.c.) fuel engines at TIER 5 (Emission Stage V, in force since January 2019); (ii) reduction of NO_x emissions into the atmosphere (use of SCR systems and AdBlue®); (iii) decrease of 10% of the specific minimum fuel consumption (c_{S_{MIN}}; $\text{g} \cdot \text{kWh}^{-1}$), due to improved performance of i.c. engines (Diesel cycle, in particular).

In addition, for the BarPlus scenarios, due to the technological innovations in the agricultural machinery sector, an increase of the Effective Field Capacity (EFC; $\text{ha} \cdot \text{h}^{-1}$) of the implements was introduced: ΔEFC = +10% for less complex machines (shovels plough, rotary harrow, dumper for grain and trailer for straw) and ΔEFC = + 15% for more complex ones (mineral fertilizer spreader, row seeder, herbicide sprayer, combine harvester and round baler).

2.2.3 S1, S2, S3 Machines (Tractors and Implements)

Information about the tractor fleets of S1, S2 and S3 scenarios are shown in Table 5.

For all scenarios, the following implements were used: n.1 mineral fertilizer spreader, n.1 shovel plow, n.1 rotary harrow, n.1 row seeder (mechanical type for S1; pneumatic type for S2 and S3), n.1 herbicide sprayer, n.1 combine harvester, n.1

Table 5 S1, S2 and S3 scenarios: farm tractor fleets

Scenario	Farm tractor fleet				
	Number and type	Power range (kW)	Total power (kW)	Mechanization index (kW·ha ⁻¹)	Annual use (h·year ⁻¹)
S1	3 4WD, 1 2WD	30–100	240	Pm _{AAU1} = 4.8	H _{n1} = 1000
S2	4 4WD, 1 2WD	50–150	400	Pm _{AAU2} = 4.0	H _{n2} = 1000
S3	6 4WD, 1 2WD	50–200	780	Pm _{AAU3} = 3.9	H _{n3} = 1000

dumper (for grain transport), n.1 baler (round bales), n.1 trailer (for straw transport). It was assumed that all the operations were carried out by using farm machines, except for grain harvesting (n.1 combine harvester), carried out by a contractor.

3 Results and Discussion

The Total Time (T_{TOT} ; h) spent for barley cultivation in the different scenarios were:

- S1: $T_{TOT1} = 226$ h and 209 h, for $S1_{NOW}$ and $S1_{PLUS}$, respectively. Consequently, the whole machinery chain Effective Field Capacity (EFC_1) increases from $0.13 \text{ ha} \cdot \text{h}^{-1}$ ($S1_{NOW}$) to $0.14 \text{ ha} \cdot \text{h}^{-1}$ ($S1_{PLUS}$);
- S2: $T_{TOT2} = 304$ h and 281 h, for $S2_{NOW}$ and $S2_{PLUS}$, respectively. The whole machinery chain Effective Field Capacity (EFC_2) increases from $0.20 \text{ ha} \cdot \text{h}^{-1}$ ($S2_{NOW}$) to $0.21 \text{ ha} \cdot \text{h}^{-1}$ ($S2_{PLUS}$);
- S3: $T_{TOT3} = 461$ h and 430 h, for $S3_{NOW}$ and $S3_{PLUS}$, respectively. The whole machinery chain Effective Field Capacity (EFC_3) increases from $0.26 \text{ ha} \cdot \text{h}^{-1}$ ($S3_{NOW}$) to $0.28 \text{ ha} \cdot \text{h}^{-1}$ ($S3_{PLUS}$).

The EFC_3 is practically double compared to EFC_1 ; moreover, within each scenario, the EFC related to S_{PLUS} is only 5–8% higher than the EFC related to S_{NOW} .

Fuel consumption—and thus the emissions of exhaust gases into the atmosphere—strongly depend on both tractor's engine loads and duration of each working time. The widespread assumption that engine load is constant (generally, close to 80%) for each working time (that means to assume a constant low specific fuel consumption during the whole field operation), often leads to underestimate the emissions of exhaust gases into the atmosphere.

Inputs and emissions of exhaust gases into the atmosphere amounted to (kg·ha⁻¹):

- BarNow scenarios: fuel $FC = 67 \div 74$, lubricants $LC = 0.56 \div 0.73$, mass $MC = 7.9 \div 8.8$, emissions of CO $EM_{CO} = 0.37 \div 0.61$, emissions of HC $EM_{HC} = 0.09 \div 0.11$, emissions of NO_x $EM_{NOx} = 1.11 \div 1.62$, emissions of PM $EM_{PM} = 0.01 \div 0.02$, emissions of CO₂ $EM_{CO2} = 210 \div 232$;

- BarPlus scenarios: fuel $FC = 55 \div 60$, lubricants $LC = 0.53 \div 0.69$, AdBlue® $AdB = 2.8 \div 3.0$, mass $MC = 7.2 \div 8.0$, emissions of CO $EM_{CO} = 0.29 \div 0.47$, emissions of HC $EM_{HC} = 0.08 \div 0.10$, emissions of NO_x $EM_{NOx} = 0.22 \div 0.33$, emissions of PM $EM_{PM} = 0.01 \div 0.02$, emissions of CO₂ $EM_{CO2} = 174 \div 189$.

The highest fuel (i.e. CO₂ emissions) and mass consumptions are—in any scenario—related to soil tillage (ploughing) operations (hotspot). Even if the results seem to be similar to those obtained by Niero et al. (2015), Dijkman et al. (2017) and Schmidt Rivera et al. (2017), it is not possible to do an absolute comparison because of the specificity of the methodology used in this study.

4 Conclusions

Although the use of primary data is always preferable to perform reliable LCA analysis, the collection of this type of data can be expensive and time-consuming. An alternative is the use of secondary data, related to the local working conditions, calculated by using specific models. In this study the model ENVIAM v2 was applied to calculate site-specific secondary data related to the mechanical field operations for barley cropping in EU conditions. The correct tractor-implement coupling is essential to assess the environmental performances of barley cultivation, especially if—as in this study—high accuracy calculations based on the relation between engine loads and working times are performed. By using ENVIAM v2—and commercial software—it is possible:

- to produce accurate local inventories containing complex information (mainly consumptions and emissions), thanks to the possibility of choosing—among the set of tractors and implements defined in the model—the coupling that best simulates the local working conditions;
- to quantify the potential environmental impacts related to the whole production cycle. The data provided by ENVIAM v2 can be used to carry out an LCA analysis focused on one specific operation or on the full sequence of operations composing the crop cycle. Therefore, it is possible to identify the phases (or operations) to which the highest potential impacts on the environment are associated (hotspots);
- to identify mitigation solutions: this means to re-analyze the system assuming, on one hand, to use different machines to achieve the same goal and, on the other hand, to re-define the sequence of the mechanical field operations. In the first case, different machines designed to perform the same operation could be associated with different working times, consumptions and emissions, whereas, in the second case, the same agrotechnical objective can be achieved with a different sequence of operations, making it possible to define strategies (at the farm or landscape level) with lower potential environmental impacts.

References

- Achten, W. M. J., & Van Acker, K. (2016). EU-Average impacts of wheat production. A meta-analysis of life cycle assessments. *Journal of Industrial Ecology* 20(1), 132–144.
- Baik, B. K., & Ullrich, S. E. (2008). Barley for food: characteristics, improvement, and renewed interest. *Journal of Cereal Science*, 48(2), 233–242.
- Bengoia, X., Rossi, V., Humbert, S., Nemecek, T., Lansche, J., & Mouron, P. (2014). Methodological guidelines for the life cycle inventory of agricultural products. Version 2.0, July 2014. World food LCA database. *Quantis and Agroscope, Lausanne and Zurich, Switzerland*, 1–79.
- Dijkman, T. J., Birkved, M., Saxe, H., Wenzel, H., & Hauschild, M. Z. (2017). Environmental impacts of barley cultivation under current and future climatic conditions. *Journal of Cleaner Production*, 140, 644–653.
- Dyer, J. A., & Desjardins, R. L. (2003). Simulated farm fieldwork, energy consumption and related greenhouse gas emissions in Canada. *Biosystems Engineering*, 85(4), 503–513.
- Ecoinvent (2015). Ecoinvent database. <http://www.ecoinvent.org/database/>.
- European Commission (2018). Eurostat handbook for annual crop statistics, revision 2018. https://ec.europa.eu/eurostat/cache/metadata/Annexes/apro_cp_esms_an1.pdf.
- Fiala, M., Nonini, L., & Marveggio, D. (2019). Environmental assessment. Task 4.3 final report, project “BARPLUS—Modifying canopy architecture and photosynthesis to maximize barley biomass and yield for different end-uses”, (Internal FACCE-SURPLUS ERA-NET Project report, June 2019) (pp. 122).
- Jannick, H. S., Weidema, B. P., Munõz, I., Dalgaard, R., Merciai, S., & de Saxcé, M. (2010). 2.0 LCA Consultants. www.lca-net.com.
- Keyes, S., Tyedmers, P., & Beazley, K. (2015). Evaluating the environmental impacts of conventional and organic apple production in Nova Scotia, Canada, through life cycle assessment. *Journal of Cleaner Production*, 104, 40–51.
- Lovarelli, D., Bacenetti, J., & Fiala, M. (2016). A new tool for life cycle inventories of agricultural machinery operations. *Journal of Agricultural Engineering*, 47(1), 40–53.
- Lovarelli, D., Bacenetti, J., & Fiala, M. (2017). Effect of local conditions and machinery characteristics on the environmental impacts of primary soil tillage. *Journal of Cleaner Production*, 140, 479–491.
- Lovarelli, D., Fiala, M., & Larson, G. (2018). Fuel consumption and exhaust emissions during on-field tractor activity: A possible improving strategy for the environmental load of agricultural mechanisation. *Computers and Electronics in Agriculture*, 151, 238–248.
- Marinussen, M., van Kernebeek, H., Broekema, R., Groen, E., Kool, A., van Zeist, W. J., et al. (2012). LCI data for the calculation tool feedprint for greenhouse gas emissions of feed production and utilization. <http://www.blonkconsultants.nl/wpcontent/uploads/2016/06/Cultivation-cereals-D03.pdf>.
- Murphy, C. W., & Kendall, A. (2013). Life cycle inventory development for corn and stover production systems under different allocation methods. *Biomass and Bioenergy*, 58, 67–75.
- Nemecek, T., & Kägi, T. (2007). Life cycle inventories of Swiss and European agricultural production systems. Final report ecoinvent V2.0 No. 15a, Agroscope Reckenholz-Taenikon Research Station ART, Swiss Centre for Life Cycle Inventories, Zurich and Dübendorf, CH. Retrieved from www.ecoinvent.ch.
- Niero, M., Ingvordsen, C. H., Peltonen-Sainio, P., Jalli, M., Lyngkjær, M. F., Hauschild, M. Z., et al. (2015). Eco-efficient production of spring barley in a changed climate: a life cycle assessment including primary data from future climate scenarios. *Agricultural Systems*, 136, 46–60.
- Notarnicola, B., Sala, S., Anton, A., McLaren, S. J., Saouter, E., & Sonesson, U. (2017). The role of life cycle assessment in supporting sustainable agri-food systems: a review of the challenges. *Journal of Cleaner Production*, 140, 399–409.
- Ossés de Eicker, M., Hischier, R., Kulay, L. A., Lehmann, M., Zah, R., & Hurni, H. (2010). The applicability of non-local LCI data for LCA. *Environmental Impact Assessment Review*, 30(3), 192–199.

- Reboul, C. (1964). Temps des travaux et jours disponibles en agriculture. *Economie Rurale*, 61, 50–80.
- Schmidt Rivera, X. C., Bacenetti, J., Fusi, A., & Niero, M. (2017). The influence of fertiliser and pesticide emissions model on life cycle assessment of agricultural products: The case of Danish and Italian barley. *Science of Total Environment*, 592, 745–757.

Assessment of Forest Biomass and Carbon Stocks at Stand Level Using Site-Specific Primary Data to Support Forest Management



Luca Nonini, Calogero Schillaci and Marco Fiala

Abstract To quantify and map woody biomass (WB) and forest carbon (C) stocks, several models were developed. They differ in terms of scale of application, details related to the input data required and outputs provided. Local Authorities, such as Mountain Communities, can be supported in sustainable forest planning and management by providing specific models in which the reference unit is the same as the one reported in the Forest Management Plans (FMP), i.e. the forest stand. In the Lombardy Region (Northern Italy), a few studies were performed to assess WB and forest C stocks, and they were generally based on data coming from regional—or national—forest inventories and remote sensing, without taking into account data collected in the FMPs. For this study, the first version of the stand-level model “WOody biomass and Carbon ASsessment” (WOCAS) for WB and C stocks calculation was improved into a second version (WOCAS v2) and preliminary results about its first application to 2019 forest stands of Valle Camonica District (Lombardy Region) are presented. Since the model WOCAS uses the growing stock as the main driver for the calculation, it can be applied in any other forest area where the same input data are available.

Keywords Forest modelling · Woody biomass · Carbon stock · Forest management plan · Site-specific primary data · Climate change mitigation

1 Introduction

Forests provide several Ecosystem Services (ES), commonly classified as: (i) regulating, (ii) provisioning and (iii) cultural (Costanza et al. 1997; Bennett et al. 2009; Krieger 2011). The quantification of the demand (human society) and the supply (environment) of ESs is a key challenge to define the effective environmental management practices and to identify the best institutional scale for the decision-making

L. Nonini (✉) · C. Schillaci · M. Fiala

Department of Agricultural and Environmental Sciences. Production, Landscape, Agroenergy (DiSAA), University of Milan, Via G. Celoria 2, 20133 Milan, Italy
e-mail: luca.nonini@unimi.it

© Springer Nature Switzerland AG 2020

A. Coppola et al. (eds.), *Innovative Biosystems Engineering for Sustainable Agriculture, Forestry and Food Production*, Lecture Notes in Civil Engineering 67,
https://doi.org/10.1007/978-3-030-39299-4_56

processes (Daily and Matson 2008; Swetnam et al. 2011; Kroll et al. 2012; Marchetti et al. 2012; Garcia-Gonzalo et al. 2015). In the context of the current climate change scenario, the most important forest ESs are: (i) woody biomass (WB) supply and (ii) carbon (C) stock (Nabuurs et al. 2008; Ekholm 2016; Gren and Zeleke 2016). WB supply and C stock are indicators of provisioning and regulating services, respectively, and they are competing, as an increase in WB supply generally causes a reduction of C stock in the forest (Bottalico et al. 2016). To quantify and map these two ESs, several models were developed; they differ in terms of scale of application (single tree, whole stand, regional or continental level), details related to the input data required and outputs provided (Vanclay 1994; Pretzsch et al. 2009; Klein et al. 2013; Pilli et al. 2013). In the alpine forestry region, Mountain Communities are the main Local Authorities having a key role in forest planning and management (Cantiani 2012). At this purpose, stand-level models are particularly important because stands represent the reference unit of the Forest Management Plans (FMP). FMPs make available a wide range of primary (measured) data that can be used to estimate the current WB (and the corresponding aboveground and belowground C stock), the harvested mass and their variation over time. In the Lombardy Region (Northern Italy) only a few studies were performed to assess WB and forest C stocks, and they were generally based on data coming from regional—or national—forest inventories and remote sensing (Federici et al. 2008; Colombo et al. 2009). None of these studies took into account primary data collected in the FMPs. Considering all these elements, the aims of this study were: (i) to develop a model—based on site-specific primary data—to calculate WB and C stocks at the stand level, (ii) to test the model for the Valle Camonica District (Lombardy Region) and (iii) to map the spatial distribution of these stocks at different levels (from the stand, to the municipality and to the whole forest area under assessment).

2 Materials and Methods

2.1 The Model WOCAS

A first version of an empirical stand-level model called “WOody biomass and Carbon ASsessment” (WOCAS) was developed to calculate the annual WB and C stocks in different forest pools. This model was recently improved into a second version (WOCAS v2) by: (i) adding new information (FMPs new data), (ii) defining more accurate calculation methods and (iii) improving the general structure to increase the model’s reliability and flexibility. For a generic (j) forest stand, for the year n, calculations are performed in the following pools: (i) aboveground woody biomass ($AWB_{n(j)}$), (ii) belowground woody biomass ($BWB_{n(j)}$) and (iii) dead organic matter ($DOM_{n(j)}$; dead woody biomass + litter) by applying a mass balance based on a “gain-loss” approach consistent with the 2006 IPCC Guidelines for National Greenhouse Gas Inventories (IPCC 2006; Federici et al. 2008).

For each of the j -stand, the input data required are: (i) starting ($YR_{S(j)}$) and final ($YR_{F(j)}$) year of the FMP, (ii) forest typology, (iii) forest function (e.g. production, environmental protection, recreational), (iv) forest structure (i.e. coppice, high forest), (v) area ($A_{(j)}$; ha), (vi) growing stock at $YR_{S(j)}$ ($GS_{(j)}$; $t \text{ year}^{-1}$ dry matter, hereafter DM) and (vii) harvested growing stock over time ($H_{n(j)}$; $t \text{ year}^{-1}$ DM).

For each harvesting operation, the corresponding woody residues ($HR_{n(j)}$; $t \text{ year}^{-1}$ DM)—consisting in tree stumps, tops, branches, twigs and non-commercial parts—are also calculated (IPCC 2006). Woody residues represent a loss from the living $AWB_{n(j)}$ and $BWB_{n(j)}$ pools, and—if they are left on the ground and are not extracted from the stand—a gain for the $DOM_{n(j)}$ pool.

For the year n , starting from the growing stock of the previous year ($GS_{n-1(j)}$; $t \text{ year}^{-1}$ DM), the gross annual increment ($GAI_{n(j)}$; $t \text{ year}^{-1}$ DM) is calculated by applying the first derivative of the Richards growth function (Richards 1959; Pienaar and Turnbull 1973; Birch 1999; Federici et al. 2008). Then, the net annual increment ($NAI_{n(j)}$; $t \text{ year}^{-1}$ DM)—defined as $GAI_{n(j)}$ minus growing stock losses within the same period of time due to natural mortality (UNECE/FAO 2011)—is quantified.

Two types of natural mortality are considered: (i) regular (RM), due to senescence, competition for light, water, nutrient and from the normal incidence of pests, diseases, and weather phenomena, and (ii) irregular (IM), due to wildfires, windstorms, avalanches, insect outbreaks or other disturbances (Vanclay 1994; Alenius et al. 2003). Regarding the former, the model assumes that the growing stock losses ($GS_{RMn(j)}$; $t \text{ year}^{-1}$ DM) occur each year, whereas, regarding the latter, information about: (i) year of occurrence, (ii) type of disturbance and (iii) growing stock losses ($GS_{IMn(j)}$; $t \text{ year}^{-1}$ DM) has to be defined by the user. As well as for the woody residues, natural mortality represents a loss from the living $AWB_{n(j)}$ and $BWB_{n(j)}$ pools, and a gain for the $DOM_{n(j)}$ pool. In more detail, for the regular mortality, the model assumes that all the $GS_{RMn(j)}$ are transferred to the $DOM_{n(j)}$ pool, whereas, for the irregular mortality, the model calculates the fraction of the $GS_{IMn(j)}$ transferred to the $DOM_{n(j)}$ pool according to the type of disturbance.

The growing stock in the year n ($GS_{n(j)}$; $t \text{ year}^{-1}$ DM) is then calculated starting from the $GS_{n-1(j)}$ ($t \text{ year}^{-1}$ DM), adding the $NAI_{n(j)}$ ($t \text{ year}^{-1}$ DM) and subtracting losses due to the harvested growing stock, $H_{n(j)}$ ($t \text{ year}^{-1}$ DM). The living $AWB_{n(j)}$ and $BWB_{n(j)}$ ($t \text{ year}^{-1}$ DM) stocks are calculated by multiplying the $GS_{n(j)}$ for specific coefficients (Somogyi et al. 2007; Federici et al. 2008) defined according to the stand's characteristics.

The $DOM_{n(j)}$ in the year n is calculated by taking into account, as inputs: (i) $GS_{RMn(j)}$, (ii) $GS_{IMn(j)}$ and (iii) $HR_{n(j)}$, and as output, the $DOM_{n(j)}$ decomposition, by using specific decay rates (Harmon et al. 1986; Melin et al. 2009) defined according to the stand's characteristics.

Finally, the carbon stocks in: (i) $AWB_{n(j)}$ ($C_{AWBn(j)}$, $t \text{ year}^{-1}$ C), (ii) $BWB_{n(j)}$ ($C_{BWBn(j)}$, $t \text{ year}^{-1}$ C) and (iii) $DOM_{n(j)}$ ($C_{DOMn(j)}$, $t \text{ year}^{-1}$ C) are calculated by multiplying the WB of each pool for the corresponding carbon fraction, k_C ($k_{C_{AWB(j)}}$;

$k_{C_BWB(j)}$; $k_{C_DOM(j)}$). The sum of: (i) $C_{AWBn(j)}$, (ii) $C_{BWBn(j)}$ and (iii) $C_{DOMn(j)}$ allows to calculate the total carbon content of the j -stand.

2.2 Case Study

The model WOCAS was applied to the Valle Camonica District to estimate WB and C stocks of the public forests. The total forest area is equal to 6.5×10^4 ha (52% of the total area); the public forests (managed through FMPs) cover 4.2×10^4 ha, whereas the private forests (not managed through FMPs) cover the remaining 2.3×10^4 ha. Among the coniferous, the main species are *Picea abies* L. and *Larix decidua* Mill. (30% and 20%, respectively), whereas, among the broadleaves, the main species are *Alnus viridis chaix* D.C. and *Castanea sativa* Mill. (11% and 8%, respectively). Production forests cover about 60% of the total forest area, followed by protection and recreational forests (38% and 2%, respectively).

For the study, data related to 2019 forest stands (forest area equal to 3.7×10^4 ha, approximately) were extracted from 45 FMPs collected in the Cadastral FMPs database (CPA v2) made available by the Mountain Community. The dataset covered the period from 1984 (starting year of the oldest FMP) to 2016 (no more recent data were made available from the CPA v2).

To calculate the gross annual increment, specific growth parameters were used for each of the j -stand, according to species and type of management (Vitulo 2018); these parameters were made available by the Italian Institute for Environmental Protection and Research (ISPRA) and represent the ones used for the official UNFCCC National Inventory Report (NIR) for Land Use, Land Use Change and Forestry (LULUCF) sector for the Lombardy Region. The $GS_{RMn(j)}$ ($t \text{ year}^{-1} \text{ DM}$) were assumed equal to 9.25% of the $GAI_{n(j)}$ (Tabacchi et al. 2010; Magnani and Raddi 2014). As a preliminary assessment, no differences among the stands were introduced. The $GS_{IMn(j)}$ ($t \text{ year}^{-1} \text{ DM}$) were not considered because no data were made available from the CPA v2. To calculate the $HR_{n(j)}$ ($t \text{ year}^{-1} \text{ DM}$), as well as the $AWB_{n(j)}$ and the $BWB_{n(j)}$ ($t \text{ year}^{-1} \text{ DM}$), the coefficients suggested by Federici et al. (2008) for the Italian forests were used. To simulate the $DOM_{n(j)}$ decomposition, not having specific data related to the Italian forests, the values of decay rates suggested by Harmon et al. (2001) for temperate forests were applied. Specific values of $k_{C_AWB(j)}$ were considered, by taking into account the stem of the leading species (Thomas and Martin 2012). Moreover, it was assumed that $k_{C_AWB(j)} = k_{C_BWB(j)} = k_{C_DOM(j)}$.

3 Results and Discussion

The main results of the last 2 years of the analysis (2015 and 2016)—for which the data of all the stands were made available from the CPA v2—are shown in Table 1.

Table 1 WB and forest C stocks related to the 2019 stands considered in the case study

	Unit	Year		
		2015	2016	
Harvested growing stock	H_n	$t \text{ year}^{-1} \text{ DM}$	1.5×10^4	4.1×10^3
Gross annual increment	GAI_n	$t \text{ year}^{-1} \text{ DM}$	8.6×10^4	8.6×10^4
Net annual increment	NAI_n	$t \text{ year}^{-1} \text{ DM}$	7.8×10^4	7.8×10^4
Growing stock	GS_n	$t \text{ year}^{-1} \text{ DM}$	3.1×10^6	3.2×10^6
Aboveground woody biomass	AWB_n	$t \text{ year}^{-1} \text{ DM}$	4.1×10^6	4.2×10^6
Carbon stock in the aboveground woody biomass	C_{AWB_n}	$t \text{ year}^{-1} \text{ C}$	2.0×10^6	2.1×10^6
Belowground woody biomass	BWB_n	$t \text{ year}^{-1} \text{ DM}$	9.0×10^5	9.2×10^5
Carbon stock in the belowground woody biomass	C_{BWB_n}	$t \text{ year}^{-1} \text{ C}$	4.4×10^5	4.5×10^5

For both the year 2015 and 2016, the harvested growing stock (H_{2015} and H_{2016} , respectively) is lower than the net annual increment (NAI_{2015} and NAI_{2016} , respectively) ($H_{2015} = 19.2\% NAI_{2015}$; $H_{2016} = 5.3\% NAI_{2016}$). The ratio between H_n and NAI_n represents the effective extraction rate ($EER \geq 0$) and is one of the most important indicators for the sustainable forest management. In fact, if in the short term H_n can exceed NAI_n ($EER > 1$), i.e. for years characterized by a high demand of woody biomass (for energy and/or building purposes), in the medium-long term this condition should never occur ($EER \leq 1$), to avoid the depletion of the growing stock over time and of the stand's productivity (UNECE/FAO 2011; Magnani and Raddi 2014). The EER values can be calculated with a higher accuracy by taking into account also the irregular mortality (disturbances), that strongly affects the NAI_n of the stands. Therefore, it is recommended to improve the data collection in the CPA v2 by including information about the natural disturbances. H_n , if performed in compliance with the sustainable forest management indicators, should be considered as a positive event because, besides allowing the rational use of an economically exploitable local resource, can promote a further increase of the annual increment and—as consequence—of the carbon sequestration. As a result, the homeostatic capacity of the forests can be enhanced, promoting a higher resistance to natural disturbances. The results provided by this study also show that the belowground woody biomass, generally not taken into account by the FMPs, is an important carbon pool, because it can stock about 22% of the total carbon of the aboveground biomass. These results can be obtained for each stand under analysis, single municipality, species, forest structure or function, making it possible to carry out a great deal of analysis and comparisons.

By integrating the model WOCAS with a Geographic Information System (ArcGIS®) a stand classification worksheet (SCW) was produced for each of the j -stand.

Each SCW provides two kinds of information (K_1 and K_2). K_1 contains general input information extracted from the CPA v2 (e.g. location, stands' owner); K_2 contains specific input (e.g. growing stock at the starting year of the FMP, harvested growing stock over time, forest typology, type of management) and output (calculated by the model) data, as well as information related to the mechanization (type of cutting performed and forestry machines that can be used according to the site-specific working conditions).

4 Conclusions

The use of management models able to calculate WB and forest C stocks is essential to analyze the contribution of these lands to climate change mitigation. In the alpine regions, the use of stand-level models based on data collected in the FMPs could be an interesting solution if the use of single-tree level models clashes with the technical-economic impossibility of the Local Authorities to provide the data required. In this study, the empirical stand-level model WOCAS was briefly presented and the main results about its application to a dataset of 2019 forest stands of Valle Camonica District were discussed. The main advantage of this model is that—besides being based on the international 2006 IPCC Guidelines—it uses the growing stock (generally available in any FMP) as the main driver for the calculation; as a result, it can be applied in any other forest area where the same input data are collected. Two aspects are currently under development: the first one concerns the definition of different management scenarios to quantify the masses of the woody assortments (and their carbon stock) that can be extracted from each stand and used for building and/or energy purposes. This aspect is very important, also considering that the commitments of the recent post-2012 agreements of the Kyoto Protocol include not only the need to report carbon emissions and removals related to forest management, but also the carbon stock in the harvested woody products. The second aspect consists in the definition of future scenarios based on both current and improved forest management practices (i.e. conversion of coppices to high forests) to test the model under different temporal and spatial scales and management conditions. In this way, it will be possible to make predictions and formulate prescriptions promoting an efficient use of the local forestry resources.

References

- Alenius, V., Hökkä, H., Salminen, H., & Jutras, S. (2003). Evaluating estimation methods for logistic regression in modelling individual-tree mortality. In A. Amaro, D. Reed, & P. Soares (Eds.), *Modelling forest systems* (pp. 225–236). United Kingdom: CAB International, Wallingford.
- Bennett, E. M., Peterson, G. D., & Gordon, L. J. (2009). Understanding relationships among multiple ecosystem services. *Ecology Letters*, *12*, 1394–1404.

- Birch, C. P. D. (1999). A new generalized logistic sigmoid growth equation compared with the richards growth equation. *Annals of Botany*, 83, 713–723.
- Bottalico, F., Pesola, L., Vizzarri, M., Antonello, L., Barbati, A., Chirici, G., et al. (2016). Modeling the influence of alternative forest management scenarios on wood production and carbon storage: A case study in the Mediterranean region. *Environmental Research*, 144, 72–87.
- Cantiani, M. G. (2012). Forest planning and public participation: A possible methodological approach. *iForest-Biogeosciences and Forestry* 5(2), 72–82.
- Colombo, R., Busetto, L., Migliavacca, M., Meroni, M., Della Torre, C., Tagliaferri, A., Grassi, G., & Seufert, G. (2009). Modellistica del ciclo del carbonio degli ecosistemi agro-forestali in regione Lombardia. *Forest@* 6, 277–288.
- Costanza, R., d'Arge, R., de Groot, R., Farber, S., Grasso, M., Hannon, B., et al. (1997). The value of the world's ecosystem services and natural capital. *Nature*, 387, 253–260.
- Daily, G. C., & Matson, P. A. (2008). Ecosystem services: From theory to implementation. *Proceedings of the National Academy of Sciences USA*, 105, 9455–9456.
- Ekholm, T. (2016). Optimal forest rotation age under efficient climate change mitigation. *Forest Policy and Economics*, 62, 62–68.
- Federici, S., Vitullo, M., Tulipano, S., De Lauretis, R., & Seufert, G. (2008). An approach to estimate carbon stocks change in forest carbon pools under the UNFCCC: The Italian case. *iForest-Biogeosciences and Forestry* 1, 86–95.
- Garcia-Gonzalo, J., Bushenkov, V., McDill, M. E., & Borges, J. G. (2015). A decision support system for assessing trade-offs between ecosystem management goals: An application in Portugal. *Forests*, 6, 65–87.
- Gren, I. M., & Zeleke, A. A. (2016). Policy design for forest carbon sequestration: A review of the literature. *Forest Policy and Economics*, 70, 128–136.
- Harmon, M. E., Franklin, J. F., Swanson, F. J., Sollins, P., Gregory, S. V., Lattin, J. D., et al. (1986). Ecology of coarse woody debris in temperate ecosystems. In A. MacFadyen & E. D. Ford (Eds.), *Advances in ecological research* (pp. 133–302). Orlando, United States: Academic Press.
- Harmon, M. E., Krankina, O. N., Yatskov, M., & Matthew, E. (2001). Predicting Broad-scale Carbon Stock of Woody Detritus from Plot-Level Data. In R. Lal, J. M. Kimble, R. F. Follett, & B. A. Stewart (Eds.), *Assessment Methods for Soil Carbon* (533–552). Boca Raton, United States: Lewis Publishers.
- IPCC. (2006). 2006 IPCC Guidelines for National Greenhouse Gas Inventories. Volume 4: Agriculture, Forestry, and Other Land Use. Chapter 2. Generic Methodologies Applicable to Multiple Land-Use Categories. https://www.ipcc-nggip.iges.or.jp/public/2006gl/pdf/4_Volume4/V4_02_Ch2_Generic.pdf.
- Klein, D., Hollerl, S., Blaschke, M., & Schulz, C. (2013). The contribution of managed and unmanaged forests to climate change mitigation—a model approach at stand level for the main tree species in Bavaria. *Forests*, 4, 43–69.
- Krieger, D. J. (2011). *Economic value of forest ecosystem services: A review* (1st ed.). Washington, United States: The Wilderness Society.
- Kroll, F., Müller, F., Haase, D., & Fohrer, N. (2012). Rural–urban gradient analysis of ecosystem services supply and demand dynamics. *Land Use Policy*, 29(3), 521–535.
- Magnani, F. & Raddi, S. (2014). Verso una stima della mortalità individuale e degli incrementi netti dei boschi italiani. Quale margine di sostenibilità per la gestione forestale in Italia? *Forest@* 11, 138–148.
- Marchetti, M., Sallustio, L., Ottaviano, M., Barbati, A., Corona, P., Tognetti, R., Zavattoni, L., & Capotorti, G. (2012). Carbon sequestration by forests in the national parks of Italy. *Plant Biosystems. An International Journal Dealing with all Aspects of Plant Biology: Official Journal of the Società Botanica Italiana* 146(4), 1001–1011.
- Melin, Y., Petersson, H., & Nordfjell, T. (2009). Decomposition of stump and root systems of Norway spruce in Sweden—A modelling approach. *Forest Ecology and Management*, 257(5), 1445–1451.

- Nabuurs, G. J., Thürig, E., Heidema, N., Armolaitis, K., Biber, P., Cienciala, E., et al. (2008). Hotspots of the European forests carbon cycle. *Forest Ecology and Management*, 256(3), 194–200.
- Pienaar, L. V., & Turnbull, K. J. (1973). The Chapman-Richards generalization of von Bertalanffy's growth model for basal area growth and yield in even-aged stands. *Forest Science*, 19(1), 2–22.
- Pilli, R., Grassi, G., Kurz, W. A., Smyth, C. E., & Blujdea, V. (2013). Application of the CBM-CFS3 model to estimate Italy's forest carbon budget, 1995–2020. *Ecological Modelling*, 266, 144–171.
- Pretzsch, H. (2009). *Forest dynamics, growth and yield* (1st ed.). Berlin Heidelberg, Berlin, Germany: Springer-Verlag.
- Richards, F. J. (1959). A Flexible growth function for empirical use. *Journal of Experimental Botany*, 10(2), 290–301.
- Somogyi, Z., Cienciala, E., Mäkipää, R., Muukkonen, P., Lehtonen, A., & Weiss, P. (2007). Indirect methods of large-scale forest biomass estimation. *European Journal of Forest Research*, 126(2), 197–207.
- Swetnam, R. D., Fisher, B., Mbilinyi, B. P., Munishi, P. K. T., Willcock, S., Ricketts, T., et al. (2011). Mapping socio-economic scenarios of land cover change: A GIS method to enable ecosystem service modelling. *Journal of Environmental Management*, 92(3), 563–574.
- Tabacchi, G., De Natale, F., & Gasparini, P. (2010). Coerenza ed entità delle statistiche forestali. Stime degli assorbimenti netti di carbonio nelle foreste italiane. *Sherwood*, 165, 11–19.
- Thomas, S. C., & Martin, A. R. (2012). Carbon content of tree tissues: A synthesis. *Forests*, 3(2), 332–352.
- UNECE/FAO. (2011). State of Europe's forests 2011. Status and trends in sustainable forest management in Europe. Forest Europe, UNECE/FAO, Ministerial Conference on the Protection of Forests in Europe, Oslo, Norway.
- Vanclay, J. K. (1994). *Modelling forest growth and yield: Applications to mixed tropical forests* (1st ed.). Wallingford, United Kingdom: CAB International.
- Vitullo, M. (2018). Personal Communication.

Sensors and Electronic Control Unit for Optimize Rotary Harrow Soil Tillage Operation



Francesco Marinello, Filippo Pegoraro and Luigi Sartori

Abstract Agricultural operations, and in particular tillage practices, can have a relevant influence on environmental as well as economic sustainability. The possibility of optimizing tillage operation is thus interesting in order to allow not only improvement of soil structure and cloddiness, but also better management of residues, minimization of soil disturbance and of vertical translocation of organisms, and reduction of energetic costs. The present paper reports on a research study carried out for the development of a power harrow equipped with sensors, which quantify the working depth, the height and load on the levelling bar. Data are managed by an ECU (Electronic Control Unit) which provides a feedback signal for the optimization of the working depth and the position of the levelling bar. Field tests were carried out in order to validate the effectiveness of the approach. For the scope, specific analyses were concurrently carried out to validate the proposed solution, including fuel consumption, power absorption and soil analyses (sieving, three-dimensional roughness and permanence time in the rotary harrow chamber). Finally, it is shown how the proposed approach can help maximization of the constancy of working depth and avoidance of excessive tillage intensity.

Keywords Rotary harrow · Sensors · Optimized tillage · Soil cloddiness

1 Introduction

Soil tillage is a basic and important component of agricultural production technology, playing a key role not only for the preparation of the desired seedbed, but also to manage crop residues, control weeds, alleviate compaction, optimize soil temperature and moisture regimes, improve aeration and in general soil physical structure

F. Marinello · L. Sartori (✉)

Department of Land, Environment, Agriculture and Forestry (TESAF), University of Padova,
Viale Dell'Università 16, 35020 Padova, Italy
e-mail: luigi.sartori@unipd.it

F. Pegoraro

Alpego Spa, Via Giovanni E Giuseppe Cenzato 9, 36045 Almisano, Italy

© Springer Nature Switzerland AG 2020

A. Coppola et al. (eds.), *Innovative Biosystems Engineering for Sustainable Agriculture, Forestry and Food Production*, Lecture Notes in Civil Engineering 67,
https://doi.org/10.1007/978-3-030-39299-4_57

(Lal 1991). Therefore, soil tillage operations play a key role not only from the agronomic but also from the economic point of view. Indeed, following the current and increasingly important attention to costs reduction at farm level, an optimization of the tillage operations can usefully help a simplification of the interventions and an overall reduction of related investment along with an increase of sustainability (Borsato et al. 2018). Precision agriculture techniques applied to soil processes are, at present, still relegated to an experimental stage although it is clear their importance for agricultural production in containing costs and protecting environmental resources. In such direction, there is the possibility of effective developments related to the ability to combine new approaches in tillage operations with precision agriculture practices. In particular there is a growing attention on the possibility to adjust the tillage intensity on the basis of specific crop requirements or as a function of soil characteristics variability. This is specifically interesting in the case of seedbed preparation, where often happens that the operator applies excessive soil tilling, with a consequent excessive refinement of the soil which is not of help to the plants and conversely might worsens the soil structure. The possibility of continuously monitoring a tillage operation, through implementation of specific sensing devices (Dubini et al. 2017) and resulting in an automatic correction of the implement's settings holds a high potential in terms of energy and time optimization and eventually costs reduction (Pezzuolo et al. 2017). The efforts of the research community have already produced interesting results, with direct or indirect systems proposed both for static or dynamic monitoring. Marinello et al. (2015) proposed a method based on the infrared Kinect depth camera; Moret-Fernández et al. (2016) achieved 3D reconstruction of soil aggregates through photogrammetry; Ajdadi et al. (2016) developed a machine vision approach for classification of 2D images; Kayad et al. (2019) tested implementation of RFID antennas for assessment of soil or residue movements following harrowing operations. The present work proposes indirect estimation of soil cloddiness through specific application of load cells on levelling bar.

2 Materials and Methods

Rotary harrows, driven by the power take-off, are implements which exhibit a relatively high flexibility of use, operating on soils to break the clods into small aggregates even in the case of difficult conditions, as for instance in the case of tenacious soils with very big clods, or when seedbed preparation is needed immediately after the primary tillage. On the other hand, such implements are typically characterized by high energy costs, not too high working speeds or working capacity and, depending on the types, a tendency to produce excessive reduction of aggregates with negative effects on soil structure and even erosion risks.

The implement used for the present research is a commercial rotary harrow (by Alpego spa), equipped with sensors which allow on the go monitoring of harrowing conditions and intensity. More specifically, it is equipped with:

- an ultrasonic sensor (namely S1) which measures the position of the levelling bar (see Fig. 1a, b);
- an second ultrasonic sensor (namely S2) which reveals the position of the roller (see Fig. 1a, c);
- two load cells at the end of the levelling bar and measuring the pressure of harrowed soil contained in the refining chamber and pressing on the bar itself (Fig. 1a, d).

The implemented power harrow is equipped with 10 rotors (300 rpm, 250 mm in height) and a spiral roller; the leveling bar is fixed on the roller with independent

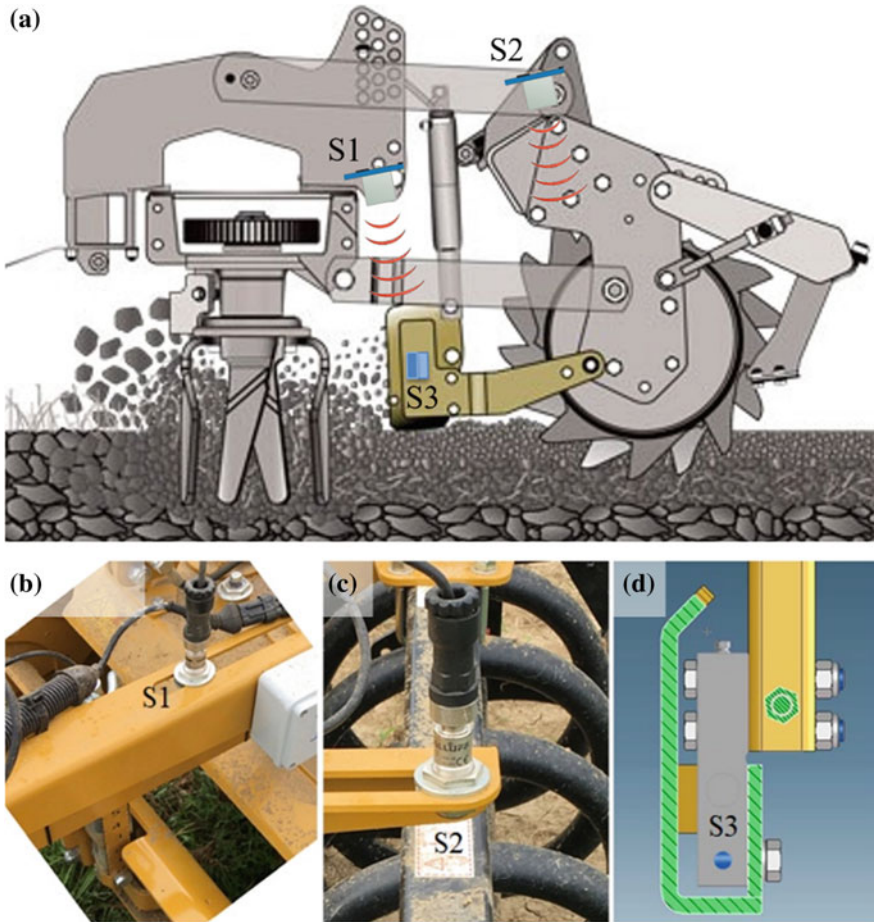


Fig. 1 On the top a schematic view of a harrowing machine and positioning of the two ultrasonic sensors (S1 and S2) and load cells (S3). On the bottom line a zoom on the levelling bar (b) and roller (c) height ultrasonic sensors. In d, schematic representation of the localization of the load cells (S3)

Table 1 Main characteristics of soil in the trials

Soil characteristics	Unit	Quantity
Sand (0.02–2.0 mm)	gg ⁻¹	0.51
Silt (0.002–0.02 mm)	gg ⁻¹	0.33
Clay (<0.002 mm)	gg ⁻¹	0.16
Dry bulk density	Mg m ⁻³	1.6
Skeleton	%	<1

adjustment. The overall working width is 2.35 m, with a typical working speed of 4–6 km/h and a working capacity of about one hectare per hour.

Research activities were carried out at the experimental farm of the University of Padova (45.3464 N, 11.9531 E), having a medium-silty texture, with an average 15% humidity in the first 10 cm (see Table 1).

A full set of parameters was collected during experiments, as described in the following. Traction force required for the operation of the harrow was measured with a dynamometer applied between the towing tractor and the tractor operating the harrow (Fig. 2a).

Time and distance for each operation was collected, allowing calculation of average forward speed along with tillage feed (i.e. the distance between two subsequent passages of rotor tools) (Fig. 3). A vibrating sieving system was applied in order to characterize soil aggregate size distribution after harrowing in the 0–5 cm soil layer. The volume of soil accumulated in the refining chamber and released with the lifting of the tool (Fig. 2b) was three-dimensionally reconstructed and quantified through implementation of a Kinect sensor (Marinello et al. 2015). A series of RFID tags inserted on cork capsules was positioned in the ground before the passage of the machine (Fig. 4c) and localized after harrowing by means of a RFID sensitive antenna: the relative shift was used in order to quantify the permanence of the clods in the refinement chamber, as described by Kayad et al. (2019). The horizontal soil resistance was measured in terms of load on the leveling bar through installed load cells (see S3 in Fig. 1), while ultrasonic sensors (S1 and S2 in Fig. 1) allowed definition of relative height of the leveling bar from the ground and of working depth.

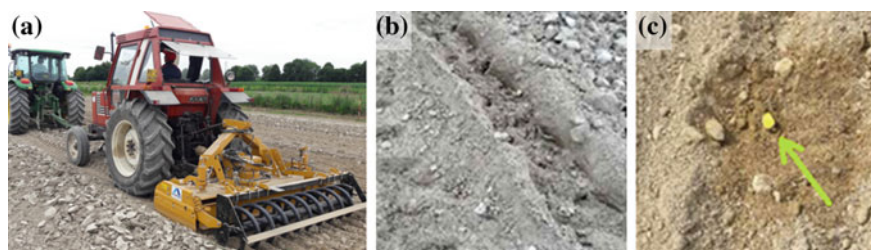


Fig. 2 The two tractors working approach for estimation of traction force (a); soil accumulated in the refining chamber (b) and RFID tags used to quantify permanence of soil within the mixing chamber (c)

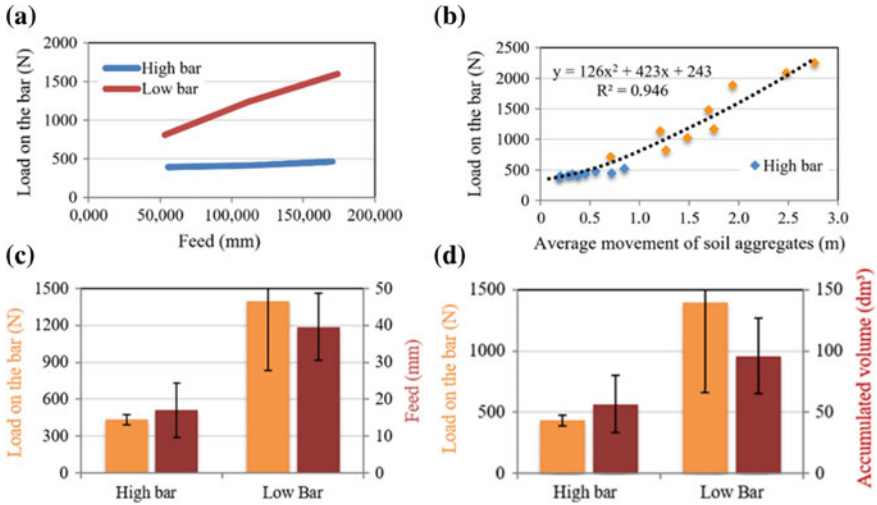


Fig. 3 On the top row: **a** effect of the bar position and cutting range on load on the bar; **b** relation between soil aggregates movements and load on the bar; on the bottom row average values for feed (c) and accumulated volume (d) at different bar positions

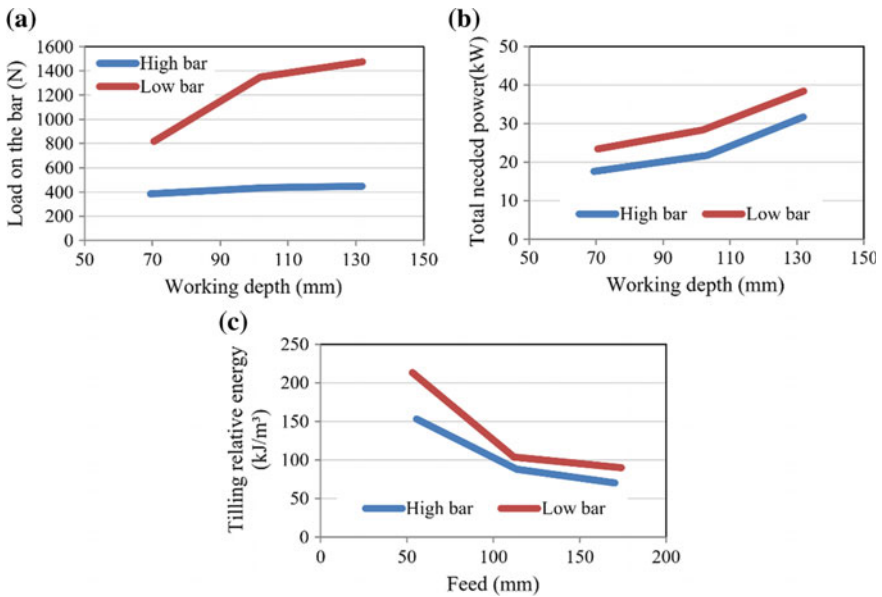


Fig. 4 Effect of working depth on load detected at the bar (a), total needed power (b) and tilling relative energy (c)

Experimental tests were carried out considering three different forward speeds (2, 4 and 6 km/h), three different working depths (7, 10 and 13 cm) and two leveling bar relative heights (8 and 14 cm).

3 Results

Experimental tests confirmed the relevance and the influence of the leveling bar on the quality of the harrowing operation both in terms of agglomerate size and needed tilling energy. The following table is a summary of the test results on the bar (Table 2).

The levelling bar in the low position causes the greatest accumulation of clods on its surface and therefore, compared to the high position, an increased permanence of the aggregates in the mixing chamber, in the near proximity of the rotors. This explains the higher load revealed when the bar is lowered during tillage, as highlighted by Fig. 3: load almost doubles (from ~800 to ~1600 N) when increasing the speed from 2 to 6 km/h (corresponding to tillage feeds respectively from 55 to 170 mm). On the other hand, when the levelling bar is raised, no soil aggregates are pressing on the bar and the detected load is almost constant (~400 N).

The effect is also confirmed by the second graph in Fig. 3, in which the load values on the bar are reported for the 18 tests performed as a function of the average displacement of soil aggregates, estimated by means of RFID tags spread over the ground before the tests. The graph reports data in different colors differentiated by the position of the bar itself. It is clear that in the raised bar position, soil aggregates have an average permanence inside the mixing chamber which varies on average between 0.5 and 1.5 s (corresponding to an average shift of clods ranging between 0.2 and 0.9 m), while the same parameter triples when the bar lays in the lower position, taking on average between 1.5 and 4.5 s (0.7–2.8 m). Averaging data, an almost linear trend can be recognized, better fitted by a second degree function: such relation is useful, as it can be implemented in order to use the load on the bar as a feedback control for the average permanence time of soil aggregates into the mixing chamber and eventually as a feedback control for the final size of aggregates themselves. This can be more clearly appreciated with the first histogram representation, which reports the direct correlation between the load exerted on the bar and the volume of soil retained in the mixing chamber as well as with the second histogram which reports the average amount (volume) of soil kept by the leveling bar within the mixing chamber during tillage (Fig. 3): in both cases the parameters assume reduced values when the bar is raised, reversing the tendency when the bar is lowered. Similarly, variations in working depth also influence the total amount of tilled soil, producing different loads on the bar, evident in particular with the bar lowered, with loads ranging from 800 N in the case of low working depth (70 mm) up to 1500 N in the case of high working depth (130 mm), as shown in Fig. 4.

It is worth noting that working conditions influencing the final size of soil aggregates and thus the load on the levelling bar, have also an effect on power need to carry out the tillage operation. Such effect is confirmed by the graphs in Fig. 4: both

Table 2 Main results from the experimental tests

Levelling bar position	Speed (km/h)	Feed (mm)	Bar height (mm)	Load on bar (N)	Clods size (mm)	Traction power (kW)	Power at the PTO (kW)	Overall power (kW)	Energy (Wh/m ³)
High	2	55.5	142.6	393.3	15.1	1.49	18.3	19.8	42.5
	4	113.5	143.1	414.1	18.7	3.53	19.5	23.0	24.4
	6	170.4	143.0	460.0	22.3	6.31	21.8	28.1	19.5
Average				422.5	18.7	3.78	19.86	23.64	28.8
Low	2	53.2	86.3	806.8	11.5	1.51	24.6	26.1	59.2
	4	111.9	87.1	1236.6	11.5	4.65	23.2	27.8	28.8
	6	174.0	87.3	1597.2	12.1	8.75	27.4	36.1	24.9
Average				1213.6	11.7	4.97	25.05	30.02	37.6

of them show how at different feeds as well as at different working depths, the lower leveling bar position produces a net increase of total needed power ranging between 25 and 30%.

Trends and correlations highlighted between field tests parameters (such as cloddiness or power consumption) and indices monitored by the sensors installed on the rotary harrow are useful for a management optimization of the implement. Indeed, controlling the working depth and the position of the leveling bar (singularly or concurrently) allows the user to control the size of soil aggregates after tilling in compliance with the agronomic needs and optimizing at the same time absorbed power and energy consumption.

4 Conclusions

The present research reports the first results obtained using after a rotary harrow equipped with specific transducers which allow on the go quantification of the working depth, of the relative height and of the load on the levelling bar. Analyses gave evidence of correlations between different analyzed parameters, opening up to the possible definition of transfer function which can be implemented for optimization of tillage operations in terms of minimization of implemented tillage power, while targeting suitable soil aggregates size.

Thus, the proposed rotary harrow sensorization and analysis approach can maintain constant the working condition (in terms of depth and clods dimensions) and avoid excessive tillage intensity.

Acknowledgements The research has been partially supported by PRIN 2015 2015KTY5NW “Optimization of operating machinery through the mission profile analysis for a more efficient agriculture”.

References

- Ajdadi, F. R., Gilandeh, Y. A., Mollazade, K., & Hasanzadeh, R. P. R. (2016). Application of machine vision for classification of soil aggregate size. *Soil and Tillage Research*, *162*, 8–17.
- Borsato, E., Tarolli, P., & Marinello, F. (2018). Sustainable patterns of main agricultural products combining different footprint parameters. *Journal of Cleaner Production*, *179*, 357–367.
- Dubbini, M., Pezzuolo, A., De Giglio, M., Gattelli, M., Curzio, L., Covi, D., et al. (2017). Last generation instrument for agriculture multispectral data collection. *CIGR Journal*, *19*, 158–163.
- Kayad, A., Rainato, R., Picco, L., & Marinello, F. (2019). Assessing crop residue movement in rotary harrowing process by RFID technique. *Agriculture*, *9*, 184.
- Lal, R. (1991). Tillage and agricultural sustainability. *Soil and Tillage Research*, *20*, 133–146.
- Marinello, F., Pezzuolo, A., Gasparini, F., Arvidsson, J., & Sartori, L. (2015). Application of the Kinect sensor for dynamic soil surface characterization. *Precision Agriculture*, *16*, 601–612.

- Moret-Fernández, D., Latorre, B., Peña, C., González-Cebollada, C., & López, M. V. (2016). Applicability of the photogrammetry technique to determine the volume and the bulk density of small soil aggregates. *Soil Research*, *54*, 354–359.
- Pezzuolo, A., Dumont, B., Sartori, L., Marinello, F., De Antoni Migliorati, M., & Basso, B. (2017). Evaluating the impact of soil conservation measures on soil organic carbon at the farm scale. *Computer and Electronics in Agriculture*, *135*, 175–182.

LIFE-Vitisom: An EU Project for the Set-up of VRT Organic Fertilization in Vineyard



Domenico Pessina, Davide Facchinetti and Lavinia Eleonora Galli

Abstract In the vineyard, the organic fertilizer spreading in VRT mode is difficult, because the various matrices used show typically a remarkable variation in their physical parameters, such as the size, water content, density, etc., mainly due to their very different original sources and managing operations. The EU LIFE-Vitisom project (LIFE15 ENV/IT/000392) focuses on the set-up of organic fertilizer spreaders, able to the distribution in VRT mode in vineyards. The VRT distribution was based on prescription maps (i.e. referred to the plant vigour) or, as an alternative at the beginning of the growing season, using a set of sensors reading locally and in real time the branches dimension. The field tests were carried out in 2017 and 2018 seasons, and were devoted to measure the spreading quality in VRT mode of three matrices (manure, solid digestate and compost), by comparing the theoretical (implemented in the software) and the real rates distributed. In respect to the acceptable deviation ($\pm 20\%$), the results show values exceeding the limit in a significant number of tested conditions. A possible solution (at present under investigation) is to vary the bulkhead speed (i.e. the matrix flow to be distributed) not only considering the prescription map or the local sensors signals, but also taking into account the material density increase from the beginning to the end of a single spreading routine.

1 Introduction

The Variable Rate Technology (VRT) is at present applied at several agricultural crops, and represents any operation which enables producers to vary the rate of inputs. Regarding the fertilization, on the market are nowadays already available many models of spreader equipped with devices able to distribute granular and powdery inorganic (mineral) fertilizers, adopting the VRT solution.

D. Pessina (✉) · D. Facchinetti · L. E. Galli

Department of Agricultural and Environmental Sciences, Università Degli Studi Di Milano, Via Celoria 2, 20133 Milan, Italy

e-mail: domenico.pessina@unimi.it

© Springer Nature Switzerland AG 2020

A. Coppola et al. (eds.), *Innovative Biosystems Engineering for Sustainable Agriculture, Forestry and Food Production*, Lecture Notes in Civil Engineering 67,

https://doi.org/10.1007/978-3-030-39299-4_58



Fig. 1 The most popular matrices used for the organic fertilization in Italy, also in vineyards and orchards

In some cases, the contribution of organic fertilization can be fully alternative to that inorganic (Celik et al. 2010; Morlat and Chaussod 2008). However, the organic matrices (especially those distributed in solid state) show very different physical characteristics. In fact, each of them can differ remarkably in size, fiber amount, water content, etc. Moreover, each of these matrices show a wide variation of the physical-chemical composition, basically function of the raw materials. As a consequence, applying the VRT to organic fertilization could become sometime quite difficult.

The most popular organic fertilizers used in Italy are manure, solid digestate and compost (Fig. 1).

More in detail:

- the manure usually derives from cattle breeding, but the fiber content depends greatly on the type of litter adopted and on the diet of the animals;
- the solid digestate is basically function of the raw materials subjected to anaerobic digestion;
- the compost characteristics depend on the nature and the amount of each single starting component, which could originate from agricultural, industrial or civil wastes.

This wide variability often implies into considerable difficulties in the application to the soil, which can be performed either with traditional methods, i.e. trying to carry out a uniform distribution over the entire surface, or by varying the dose locally in VRT mode, according to the needs of the crop (Landry et al. 2004; Metzger et al. 2010).

The organic matrices show a very complex rheological behaviour, due to a triphasic system of elements (solid components, water and air): in fact they are materials that do not behave exactly like solids, but not even like fluids. Depending on their composition, if subjected to compression or torsion stresses, they can have a so-called “Newtonian” or “non-Newtonian” behaviour (Björn et al. 2012; Mani et al. 2004).

More in detail, the manure usually has a typical size very different from the compost, being less homogeneous (Amiri et al. 2012). The water content greatly influences the reaction of this matrix. In the compression tests, the water content affects the absorbed force value, determining different levels of compaction of the sample. The behaviour features of the solid fraction of the digestate very often derive



Fig. 2 Two of the spreader prototypes manufactured for the Vitisom project: the towed self-levelling (left) and the straddle self-propelled (right) models

from the uniform feeding of the digesters with maize silage; nevertheless, being that a matrix recently introduced, there is no at present a deep knowledge on this matter.

In general, but of course also in specialized crops (vineyards and orchards), the VRT application brings significant advantages of pesticide and fertilizers (both mineral and organic) spreading (Rückamp et al. 2013). This is of great importance in the organic viticulture, of increasing interesting worldwide.

The VRT distribution is usually based on prescription maps (i.e. referred to plant vigour) or, as an alternative especially before and at the beginning of the growing season, using a set of infrared and/or optical sensors, reading locally and in real time the canopy extent and/or the branches/shoots dimension (the diameter). These data are used to determine the rate of the organic matrices to be distributed in the various area of the vineyard. The distribution is normally executed with spreaders equipped with rear rotors, fed with a bulkhead moving horizontally into the hopper, both with fixed and variable rate (Fig. 2).

The Vitisom project (LIFE15 ENV/IT/000392), funded by EU Commission inside of the LIFE framework, started in 2016 to develop an innovative technology to manage vineyard organic fertilization. The project aims to the implementation of the VRT to upgrade the vineyard organic fertilization distribution systems and to promote a more sustainable approach to vineyard soil management, also extendable at EU level. More in detail, the Vitisom project focused on the manufacturing of 5 prototypes of organic fertilizer spreaders, being them towed or self-propelled and traditional or self-levelling. They were selected for the best management efficiency, taking into account the slope and the breeding features of the Italian vineyards. The prototypes were designed to distribute the organic fertilizers in VRT mode, for a theoretical rate from 0 to 40 t/ha.

The aim of this study is to verify the distribution quality of the described models in VRT mode, for the three matrices considered, over a range of distribution rates and for different travelling speed values.

2 Materials and Method

The first spreader is based on a traditional single-axle trailer, with a wooden hopper of approx 3 m³ capacity, hydraulically driven working parts, and a series of sensors and actuators devoted to VRT distribution mode. A movable bulkhead conveys the material loaded into the hopper towards a couple of horizontal rotors, which thanks to a rear shield drop the product onto a couple of finned disks rotating in the horizontal plane, which finally provide for the spreading of the fertilizer on the ground. The fully hydraulic driving of the machine, as well as the hydraulically tiltable towbar, allow extremely reduced turning radius, assuring an excellent manoeuvrability in vineyard. Furthermore, the towed prototype is equipped with an automatic hopper levelling system and servo-controlled hydraulic brakes, so considerably improving the safety, especially when working on slope (Fig. 3). In detail, the VRT mode is managed thanks to two hydraulic motors controlled by an encoder, which varies the rotation speed of the rear distribution rotors and the translational speed of the bulkhead conveying the matrix towards the rear rotors inside the hopper. Based on the position of the machine (georeferenced by GPS), the software defines the amount distributed, which is basically inversely proportional to the canopy vigour. The canopy vigour is ascertained through previously built-up prescription maps, or alternatively using the real-time detection, thanks to a series of dedicated sensors fitted in front of the tractor. The machine is completed by a couple of sloping bulkheads, to facilitate the correct loading of the hopper, and a couple of moving chains joined by transversal bars placed on the hopper bottom, helping the matrix to be conveyed towards the rear rotors. The self-propelled version of the organic fertilizer spreader is similar to the towed model; the only (important) difference is that the distribution module is fitted on board of a straddling tool-carrier, suitable for work in vineyards having inter-rows of less than 1.8 m width, where the tractor-driven version cannot travel.

To ascertain the distribution efficiency in VRT mode of the two spreaders, two test procedures have been arranged, being them different in the detail of the data obtained.

The first method considered the material amount distributed on an entire inter-row, resulting from the difference of the measurements of the spreader gross weight at the beginning and at the end of a given inter-row travelling. The amount distributed was then compared to what expected, considering the prescription map indications for that investigated inter-row. To carry out the trials, a weighing system including four mobile digital platforms (mod. WWS, sold by Vincro Bilance, Rovereto, TN–Italy) was purchased, to be placed under the wheels of the machine (Fig. 4). In this case, only three platforms were used, and placed under the single-axle wheels of the spreader (two of them) and the third under the parking jack, assuring that all the weight was loaded on the sensors.

The second solution involved the measurement of the rate distributed in specific areas in the inter-rows, selected also in this case on the basis of the prescription maps. Some plastic sheets (length: 6 m; width: 2.5 m max, for a max covered area of 15 m²) of convenient thickness were placed in the inter-row in which the spreader

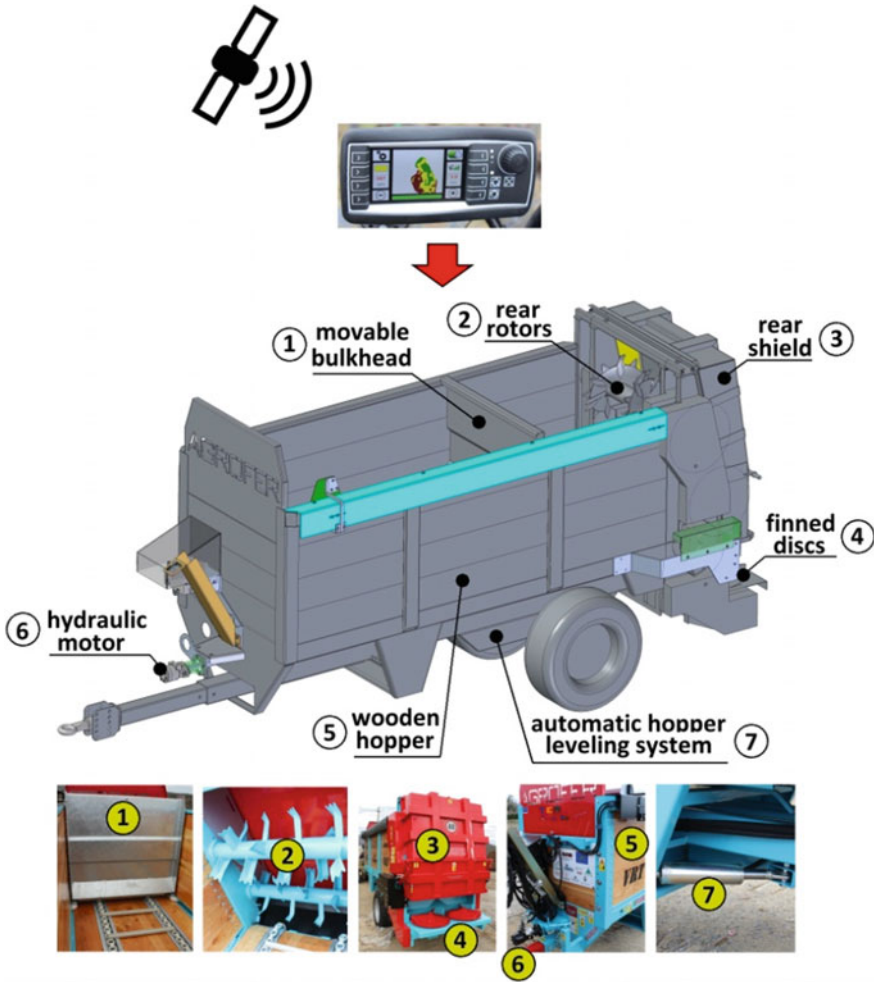


Fig. 3 Technical details of the towed self levelling version of the spreader

was travelling and in their proximal inter-row(s). The aim was to collect and weigh the amount of matrix distributed by the machine in each area surveyed (Fig. 5), and then compare the measured with the expected data. For weighing the samples, a digital dynamometer (make Marsden, Rotherham, GB, model OCS-S1, 1000 kg_f full scale) was used.

A particular care was devoted to select areas in which the due rate was constant and likewise as far as possible to its variation, in order to be sure the machine was working at the rate imposed by the correspondent reading of the prescription map. Moreover, time by time the reference working width was adjusted according to the width of the inter-rows and to the machine setting. Starting from the surface covered



Fig. 4 The weighing system including some mobile digital platforms used in the tests



Fig. 5 The amount of matrix distributed by the machine in each inter-row surveyed, and collected on the plastic sheets of known surface (left), was later weighed by using a digital dynamometer and compared with the expected figure resulting from the prescription map (right)

by the plastic sheet(s), the rate was calculated by dividing the weight of the material collected (i.e. that distributed along the length considered) for the reference area.

The described field tests were carried out in 2017 and 2018, respectively at the end of the growing season (i.e. after the grape harvesting) and before the beginning of the next one, when no canopy was present in the vineyard, so without any heavy canopy interference during the spreading.

The test was repeated in four different vineyards, located in North and Centre Italy (Guido Berlucchi, Borgonato di Corte Franca (BS); Castello Bonomi, Coccaglio (BS); Conti degli Azzoni, Montefano (MC); Premiata fattoria di Castelvecchi in Chianti, Radda in Chianti (SI)), using all the prototypes manufactured. Only the test results carried out during 2018 in the Castello Bonomi and Guido Berlucchi wine farms are reported in this paper; in any case the data obtained in the other

sites are fully in line with those shown and commented in the following. In Castello Bonomi the towed self-levelling prototype was used, while in Guido Berlucci the self-propelled straddle type has been working. In the two farms both the testing methods were applied. To assess the performance of the spreaders, for each test condition the following data were measured:

- working width, total working area and area of the sheets;
- target dose related to the test (kg/m^2 and t/ha);
- dose measured on the entire inter-row area (kg/ha) and on the sheets (kg/m^2);
- absolute deviation from the target, on the sheets and on the inter-row area.

3 Results and Discussion

Table 1 shows the data obtained at Castello Bonomi with towed self-levelling prototype, considering the two testing methods.

Taking into account the single runs, the absolute deviations from the target value varied from a minimum of 2% on manure (target 3 t/ha) to a max of approx. 67% for the digestate (target 10 t/ha).

In general, from a cultivation point of view, an absolute deviation of 20% in respect to the target dose was considered as acceptable, due to the possibility that the fertilizing potential of a matrix could share on the surroundings of the distribution point.

However, during the tests only in 4 cases on a total of 18 this limit was respected; no significant difference was highlighted considering the 3 matrices performances, but in general for the target dose of 10 t/ha for manure, 5 t/ha for compost and 3 t/ha for digestate the lowest deviation values were recorded.

For manure, a possible reason of such a behaviour may be justified considering the non-uniform texture of the material; in other words, when the dose is decreasing, the spreader shows a poor performance, highlighting wide amount variations of the material distributed along the travelling direction (Fig. 6). This feature has been detected also with the other two matrices, but the solid digestate and even more the compost show a more uniform texture, so minimizing the problem.

Another problem observed during the working was a non-uniform distribution at the starting and at the end of each single routine, mainly due to a discontinuous feeding of the rear rotors.

Moreover, it was observed that the problem becomes worse after a long transferring between two vineyards.

This is probably due to the vertical (for the gravity) and horizontal (for the movement of the bulkhead) remarkable compaction to which the matrix is subjected inside the hopper, resulting in undesired heaps along the inter-row, followed by empty areas (Fig. 7), so resulting in severe distribution errors.

In Table 2 are shown the results obtained with the self-propelled straddle prototype tested in Guido Berlucci wine farm. In this case, depending on the matrix distributed,

Table 1 Absolute deviation of the distributed dose with the towed self-levelling prototype in comparison of a range of target dose, for the three considered matrices, used in Castello Bonomi wine farm

Target dose, t/ha	10			5			3		
	Manure	Digestate	Compost	Manure	Digestate	Compost	Manure	Digestate	Compost
Entire-row method									
Absolute deviation, %	24.8	51.8	56.4	22.5	48.7	43.1	2.0	33.5	40.6
Plastic sheets method									
Absolute deviation, %	24.0	24.6	33.0	66.7	14.1	15.6	75.3	16.2	24.4

Italics and bold value indicates the not exceeding the acceptable deviation



Fig. 6 Examples of uniform (left) and non-uniform (right) distribution in the travelling direction

Fig. 7 Due to the probable vertical (for the gravity) and horizontal (for the movement of the bulkhead) remarkable compaction to which the matrix is subjected inside the hopper, the material is sometime very poorly distributed, resulting in undesired heaps along the inter-row, followed by empty areas



Table 2 Absolute deviation of the distributed dose with the self-propelled straddle prototype in comparison of a range of target dose, for the 3 considered matrices, used in Guido Berlucchi wine farm

Matrix: MANURE			
Target dose, t/ha	20	10	5
<i>Entire-row method</i>			
Absolute deviation, %	74.8	41.6	65.4
<i>Plastic sheets method</i>			
Absolute deviation, %	24.1	61.2	55.9
Matrix: DIGESTATE			
Target dose, t/ha	33	22	11
<i>Entire-row method</i>			
Absolute deviation, %	41.1	22.1	12.9
<i>Plastic sheets method</i>			
Absolute deviation, %	57.0	54.4	76.1
Matrix: COMPOST			
Target dose, t/ha	15	10	5
<i>Entire-row method</i>			
Absolute deviation, %	87.3	37.5	51.5
<i>Plastic sheets method</i>			
Absolute deviation, %	75.9	86.7	89.5

the target dose was different, but in all the cases, both for entire inter-row and plastic sheets methods, the absolute deviation exceeded (sometimes remarkably) the $\pm 20\%$ limit.

This is due to a general malfunctioning of the spreading module, that was at a first extent poorly adaptable to the tool-carrier to which it was coupled.

Moreover, with this straddle prototype a large part of the product fell on the plants, smearing them, and a significant transverse difference of the distributed product on the soil was detected.

4 Conclusions

The two tested prototypes showed a good capacity in varying the distribution rate inside of the target range. Nevertheless, due to the rheological characteristics of the organic fertilizers investigated, some difficulties in assuring a regular feeding of the rear rotors were detected, so resulting in high deviations of the materials rate distributed, when compared to those expected.

One of the probable reasons of these malfunctions is the vertical (for the gravity) and the horizontal (for the bulkhead movement) compaction to which each matrix is subjected when conveyed to the rotors.

To solve the problem, it will be necessary to pilot the speed of the base mat and the movable bulkhead, not only in relation to the dose to be distributed and to the travelling speed, but also taking into account the progressive compaction caused on the material by the two moving parts.

References

- Amiri, H., Arabhosseini, A., & Kianmehr, M. H. (2012). Determination of some rheological properties of cow manure using a shear vane. Department of Agrotechnology, College of Abouraihan, University of Tehran. *Egyptian Academic Journal of Biological Sciences* 4(1), 59–68 (2012). <https://doi.org/10.21608/eajbsz.2012.13539>.
- Björn, A., de La Monja, P. S., Karlsson, A., Ejlertsson, J., & Svensson, B. H. (2012). Rheological characterization. In Dr. Sunil Kumar (Ed.), *Biogas*. ISBN: 978-953-51-0204-5, InTech. <https://doi.org/10.5772/32596>.
- Celik, I., Gunal, H., Budak, M., & Akpınar, C. (2010). Effects of long-term organic and mineral fertilizers on bulk density and penetration resistance in semi-arid Mediterranean soil conditions. *Geoderma*, 160(2010), 236–243. <https://doi.org/10.1016/j.geoderma.2010.09.028>.
- Landry, H., Laguë, C., & Roberge, M. (2004). Physical and rheological properties of manure products. *Applied Engineering in Agriculture* 20(3), 277–288. American Society of Agricultural Engineers ISSN 0883–8542. <https://doi.org/10.13031/2013.16061>.
- Mani, S., Tabil, L. G., & Sokhansanj, S. (2004). Evaluation of compaction equations applied to four biomass species. *Canadian Biosystems Engineering*, 46(3), 55–61.
- Metzger, B., Papworth, L., Nelson, V., & Sexton, K. (2010). Calculating the Application Rate of a Manure Applicator and Why. AgTech Centre, Alberta Agriculture and Rural Development. www.agriculture.alberta.ca.
- Morlat, R., & Chaussod, R. (2008). Long-term additions of organic amendments in a Loire Valley vineyard. I. Effects on properties of a calcareous sandy soil. *American Journal of Enology and Viticulture*, 59, 353–363.
- Rückamp, D., Schick, J., Haneklaus, S., & Schnug, E. (2013). Algorithms for variable-rate application of manure. Julius Kühn-Institut, Federal Research Centre for Cultivated Plants (JKI), Institute for Crop and Soil Science.

Real-Time Measurement of Silage Moisture Content During Loading of a TMR Mixer Wagon: Preliminary Results



V. Perricone, A. Costa, A. Calcante, A. Agazzi, M. Lazzari, G. Savoini, M. Chiara, E. Sesan and F. M. Tangorra

Abstract Proper dry matter intake in dairy cows is a key factor to meet nutritional requirements and optimal performance, reducing the incidence of metabolic diseases. Moisture content of silages, can undergo variations during storing, affecting the total dry matter daily consumed by the animals. The aim of the study was to develop a system, based on microwave resonance technology, to measure the silages moisture content during feed mixer wagon loading. A commercial microwave moisture sensor for bulk materials was used. It was first calibrated over different types of silages (corn, high moisture corn, barley, soybean) using samples collected from different dairy farms located in Lombardy (Northern Italy), then it was mounted behind the loading drum of the conveyor arm of a horizontal self-propelled mixer wagon and integrated in an on-line measurement system designed to record in real-time and continuously the silages moisture content during the feed mixer wagon loading. The system was tested at the University of Milan experimental farm (Landriano, Italy). Preliminary results highlighted that the microwave sensor provided, except for soybean silage ($R^2 = 0.95$), a moderately accurate silage moisture data ($R^2 = 0.62$ for corn and high moisture corn silages; $R^2 = 0.61$ for barley silage).

Keywords Microwave sensor · Moisture · Silage · Real-time · TMR wagon

V. Perricone · A. Costa · M. Lazzari · G. Savoini · F. M. Tangorra (✉)
Department of Health, Animal Science and Food Safety, University of Milan, via G. Celoria 10,
20133 Milan, Italy
e-mail: francesco.tangorra@unimi.it

A. Calcante · A. Agazzi
Department of Agricultural and Environmental Sciences - Production, Landscape Agroenergy,
University of Milan, via G. Celoria 2, 20133 Milan, Italy

M. Chiara
PTM s.r.l, via Per Isorella 22/a, 25010 Visano, Italy

E. Sesan
Sgariboldi s.r.l, via P. Nenni 15, 26845 Codogno, Italy

© Springer Nature Switzerland AG 2020
A. Coppola et al. (eds.), *Innovative Biosystems Engineering for Sustainable Agriculture, Forestry and Food Production*, Lecture Notes in Civil Engineering 67,
https://doi.org/10.1007/978-3-030-39299-4_59

1 Introduction

Nutrient concentrations of feedstuffs can vary substantially over short periods of time (Weiss et al. 2012) influencing the total mixed ration (TMR) composition. More than half of the dry matter (DM) content of the diet fed to dairy cows is mainly provided by silages (Shaver 2004) and a change in their composition could be responsible of a substantial change in the composition of the delivered ration. DM and quality of silages can undergo reductions among time, mainly due to silo respiration and fermentation, effluent production, and oxygen exposure during storage and feed-out phase (Borreani et al. 2018). Not even a good management of the silo can prevent from DM losses during these phases due to the unavoidable aerobic deterioration of the feed-out face. These losses, along with other occurrence responsible of DM variations, such as rainfall event over uncovered silos, can modify the nutrient supply of the TMR, being the diets formulated on DM basis but the ingredients included in the mixture on as-fed basis. Therefore, if the as-fed inclusion rate is not adjusted for changes in DM concentration, the nutrient composition of the TMR would change, affecting the dairy cows' milk production as well. Short-term DM changes in silage may have short-term effects on dry matter intake (DMI) and milk yield (Barmore and Bethard 2005), albeit cows seem to quickly adapt to these changes (McBeth et al. 2013). The effects of daily silage DM fluctuations on dairy cows' performance were investigated by Mertens and Berzaghi (2009). DM variations between 8 and 16% units reduced on average DMI of 2 kg/d, with a consequent loss of milk production. The decrease of DMI of 1 kg for one day caused the loss of 0.8 kg of milk in each of the next two days.

Accurately measuring forage DM content requires the oven-dried of the forage under controlled conditions in a time-consuming process that is usually carried out in the laboratory. This makes impossible to control the moisture content of the forage during the TMR mixer wagon loading, resulting in potential dry matter and nutrients intake errors for dairy cows.

Recently a system based on a near infra-red (NIR) scanner, mounted on the scraper of the TMR wagon front miller, has been proposed to analyze forages DM content in real-time (Barbi et al. 2010). The system performs a weight-adjustment of each ingredient loaded on actual DM content contributing to improve the TMR consistency (Piccioli-Cappelli et al. 2019). Despite NIR spectroscopy has become a common method of measuring moisture content because water shows strong absorption bands in the infrared region, it has some limitation. Due to the limited penetration depth of NIR radiation the measurement is not representative of the total moisture in the product, and it is influenced by particle size. Moreover, NIR method must be calibrated versus a reference method through an intensive calibration phase that is time consuming and requires chemometrics.

An alternative for forage moisture content measuring is represented by microwave (MW) resonance technology which enables continuous, density independent moisture monitoring of solid products. This technology is based on the interaction between water molecules and changing electromagnetic fields. If a product containing water

Table 1 Main technical data of the microwave moisture sensor (MMS) used in the study

Parameter	Value
Power supply	12–24 V DC
Outputs	0–20 or 4–20 mA
Measuring range	0–100%, 0–80°C
Depth	75–100 mm
Accuracy	± 0.3%
Frequency	433.92 MHz
Dimensions	Ø: 75 mm, Length: 100 mm
Weight	1.8 kg

is passed over a MW resonance sensor, its resonance frequency decreases and the half-width of the resonance curve increases. The magnitude of these changes can be correlated to the water content of the sample (Buschmüller et al. 2007; Kocsis et al. 2008; Trabelsi et al. 2008). Contrary to NIR, MW resonance technology has some advantage. It does not need the use of chemometric analysis, making this technique more amenable for application when chemometrics software and chemometricians are not available (Corredor et al. 2011). In addition, since the microwave field penetrates a few centimeters into the sample, water is not only detected at the surface but also in the product's core.

The aim of the study was to develop a system, based on MW resonance technology, to measure the silages moisture content during TMR mixer wagon loading.

2 Materials and Methods

2.1 Microwave Sensor

A microwave moisture sensor (MMS) for bulk materials (FL-Wapp, Ludwig, Mainz, Germany), with a 75-mm diameter ceramic planar sensing face, was used. The main sensor technical characteristics are summarized in Table 1.

2.2 Sensor Calibration

The MMS was calibrated over different types of silages (corn, high moisture corn, barley, soybean) collected in different dairy farms located in Lombardy (Northern Italy) using a silage corer (Master forage probe, Dairy One, Ithaca, NY, US) from the entire front of the bunker silo, trying to gather as much as DM content variability as possible within them.

In order to avoid electrical interference effects, the sensor was flanged with a 5-cm thick holder metal ring and for each type of silage the calibration was performed according to the following procedure.

Silage samples were applied to the sensor using a 150-mm diameter \times 50-mm tall polyvinyl chloride (PVC) container. The silage was poured into the container filling it completely. A sensor raw signal (Q), function of frequency shift and amplitude attenuation of the resonance curves, was obtained for each sample reading. Four readings, achieved by a 90° rotation of the container, were performed for each silage sample and an average Q value was calculated.

After the readings, silage samples were weighed and carried to the laboratory for moisture content assessment according to Commission Regulation (EC) 152/2009. Moisture content was expressed as percentage of wet sample weight loss by the sample, i.e., wet basis (% w.b.).

The relationship between the reference moisture content and the sensor reading values was established as the calibration equation.

2.3 Integrated Measurement System

The MMS was mounted behind the loading drum of the conveyor arm of a horizontal self-propelled mixer wagon (Gulliver 6014, Sgariboldi srl, Codogno, Italy) and integrated in an on-line measurement system designed to record in real-time and continuously the silages moisture content during the TMR mixer wagon loading (Fig. 1).

The output signal from the sensor is acquired through front-end electronics. After a digital conversion, the raw sensor signal is transferred to the control unit through a PTM proprietary protocol (PTM srl, Visano, Italy). The following devices compose the system:

DRIVE 8 DRY: Through this I/O board the raw signal of the sensor is conditioned, converted in digital and then filtered. At this stage, the conditioning has the goal of providing reliable raw signal to the control unit.

ADVANCE SUPER USB: The control unit is responsible for estimating the moisture value of the loaded silage performing a real-time evaluation on the validity and

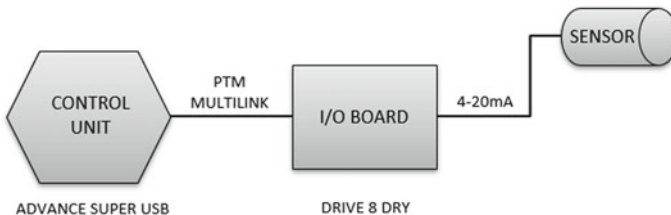


Fig. 1 Block diagram of the integrated measurement system implemented to measure the silages moisture content during TMR mixer wagon loading

Fig. 2 The microwave moisture sensor positioned behind the loading drum of the TMR mixer wagon



goodness of the data coming from the sensor. It converts the raw signal in moisture values according to the calibration curve applied. The control unit is also responsible to store and manage the moisture calibration curves of the different silages.

Figure 2 shows the MMS installed behind the loading drum of the conveyor arm of the horizontal self-propelled mixer wagon.

2.4 Field Tests

Field tests were carried out at the University of Milan experimental farm (Landriano, Italy). Samples of different types of silages (corn, high moisture corn, barley, soybean) were collected from the silo face, using a silage corer (Master forage probe, Dairy One, Ithaca, NY, US), immediately before the TMR mixer wagon loading and then they were assessed for moisture content in the laboratory according to Commission Regulation (EC) 152/2009. Moisture content was expressed as percentage of wet sample weight loss by the sample, i.e., wet basis (% w.b.).

Moisture contents of corn, high moisture corn, barley and soybean silages, recorded by the MMS during the TMR mixer wagon loading, were compared with the laboratory reference values to assess sensor performances.

2.5 Sensor Accuracy

Accuracy of the MMS was determined based on mean difference (Md) and coefficient of determination (R^2) between the moisture content recorded by the sensor and that derived from the laboratory. The coefficient of variation (CV) was calculated for repeatability.

3 Results and Discussion

Sensor performances are reported in Table 2. The negative Md values suggested that the MMS underestimated the moisture content of all silages used in the field tests. On average the moisture contents recorded by the MMS during the TMR mixer wagon loading compared with the laboratory reference values were the following: 67.18 versus 70.17% for corn silage, 34.36 versus 39.55% for high moisture corn silage, 67.78 versus 75.36% for barley silage, and 67.30 versus 72.70% for soybean silage.

The greater coefficient of determination was obtained with the soybean silage ($R^2 = 0.95$), while the microwave sensor provided a moderately accurate silage moisture data for corn and high moisture corn silages ($R^2 = 0.62$) and barley silage ($R^2 = 0.61$). The lower accuracy found for the latter silages could be due to physical and mechanical phenomena that affected the measurement during the silages loading. Analyzing the moisture tracks acquired by the sensor, discontinuous flows of material, potentially related to the irregular use of the loading drum of the conveyor arm by the TMR wagon operator when he loaded these silages from the silos, were observed on the sensor. In addition, periods in which the sensor signal remained stable at a constant value, probably due to material blocked on the sensor ceramic planar face, were recorded.

The low CV (between 2.0 and 4.0%) highlighted a good repeatability of the measurements.

Table 2 Statistical summary of sensor performances

Silage	Md (%)	R^2	CV (%)
Corn	-2.99	0.62	3.28
High moisture corn	-5.19	0.62	4.03
Barley	-7.58	0.61	2.02
Soybean	-5.40	0.95	2.92

4 Conclusions

An integrated measurement system, based on microwave resonance technology, for recording in real-time and continuously the silages moisture content during the TMR mixer wagon loading was implemented and tested. Preliminary results highlighted the potentiality of the system but its level of accuracy need to be improved for providing a reliable estimation of silages moisture content. At this purpose specific algorithms with the task of determining whether a silage sample flowing on the sensor is consistent and can contribute to the moisture estimation, or it must be discarded, should be developed. In this way the effect of physical and mechanical phenomena (e.g. discontinuous flow of the material, material blocked on the sensor) on the sensor measurement during the silages loading could be limited improving the sensor accuracy.

Acknowledgements The activity presented in the paper was co-funded by Regione Lombardia in the framework of POR FESR 2014-2020 (Axis I, Objective 1.b.1). Project P.L.U.S.—Precision Livestock Unifed System.

References

- Barbi, A., Ghiraldi, A., Manzoli, M., & Berzaghi, P. (2010). Precision feeding: NIR on line for improving TMR consistency. *The First North American Conference on Precision Dairy Management*, March 2–5, Toronto.
- Barmore, J., & Bethard, G. (2005). Performance monitoring of dairy nutrition and feeding. *Proceedings of the Tri-State Dairy Nutrition Conference*, 11–29, Ft. Wayne. Columbus: Ohio State University.
- Borreani, G., Tabacco, E., Schmidt, R. J., Holmes, B. J., & Muck, R. E. (2018). Silage review: Factors affecting dry matter and quality losses in silages. *Journal of Dairy Science*, *101*, 3952–3979.
- Buschmüller, C., Wiedey, W., Döscher, C., Dressler, J., & Breikreutz, J. (2008). In-line monitoring of granule moisture in fluidized-bed dryers using microwave resonance technology. *European Journal of Pharmaceutics and Biopharmaceutics*, *69*(1), 380–387.
- Corredor, C. C., Bu, D., & Both, D. (2011). Comparison of near infrared and microwave resonance sensors for at-line moisture determination in powders and tablets. *Analytica Chimica Acta*, *696*, 84–93.
- Kocsis, L., Schlemm, U., Richter, H., Mellmann, J., & Farkas, I. (2008). On-line microwave measurement of the moisture content of wheat. *IFAC Proceedings Volumes*, *41*(2), 631–635.
- McBeth, L. R., St-Pierre, N. R., Shoemaker, D. E., & Weiss, W. P. (2013). Effects of transient changes in silage dry matter concentration on lactating dairy cows. *Journal of Dairy Science*, *96*, 3924–3935.
- Mertens, D. R., & Berzaghi, P. (2009). Short-term changes in forage dry matter affect milk production responses in dairy cows. *Journal of Dairy Science*, *92*, 583.
- Piccioli-Cappelli, F., Calegari, F., Calamari, L., Bani, P., & Minuti, A. (2019). Application of a NIR device for precision feeding in dairy farms: Effect on metabolic conditions and milk production. *Italian Journal of Animal Science*, *18*(1), 754–765.
- Shaver, R., & Kaiser, R. (2004). Feeding programs in high producing dairy herds. *Proceedings of the Tri-State Dairy Nutrition Conference*, 143–170, Fort Wayne. Columbus: The Ohio State University.

- Trabelsi, S., Nelson, S., & Lewis, M. (2008). Microwave moisture sensor for grain and seed. *Biol. Eng., 1*(2), 195–202.
- Weiss, W. P., Shoemaker, D. E., McBeth, L. R., Yoder, P., & St-Pierre, N. R. (2012). Within farm variation in nutrient composition of feeds. *Proceedings of the Tri-State Dairy Nutrition Conference*, 103–117, Fort Wayne. Columbus: The Ohio State University.

The Response Surface Methodology as a Tool to Evaluate the Effects of Using Diesel-Biodiesel-Bioethanol Blends as Farm Tractor Fuel



Marco Bietresato, Carlo Caligiuri, Anna Bolla, Massimiliano Renzi and Fabrizio Mazzetto

Abstract The Response Surface Methodology (RSM) is used here to analyse a large set of experimental data regarding the mechanical and environmental performances of an internal combustion engine (ICE) used to power a farm tractor. The aim is twofold: (i) to demonstrate the effectiveness of RSM in quantitatively assessing the effects of biofuels on a complex system like an ICE; (ii) to supply the users with easy-to-use models to predict the effect of biofuel blends on performance and emissions of tractor engines and find an optimal blend according to given user-defined parameters. The methodology showed good prediction abilities: the calculated average errors for the first models were lower than 0.38 and 1.40% on 6 test cases, with a higher accuracy in the assessment of the ICE mechanical performance. As a result, two effective and user-friendly models for torque and NO_x emissions were developed; they were subsequently used to single out some fuel blends having interesting effects in terms of limitation of the average increment in the NO_x emissions and of the torque average decrement (here: B3E0, B11E0, B20E3).

Keywords Ternary fuel blends · Biodiesel · Bioethanol · Response surface methodology · Farm tractor · Agricultural machinery · Diesel engines emissions reduction

1 Introduction

The Response Surface Methodology (RSM), is a collection of mathematical and statistical techniques based on the fit of a polynomial equation to experimental data to yield an optimized multilinear model (i.e., an explicit polynomial regression function—the first part of the Taylor series of an unknown real function $f(x_i)$) of the behaviour of the dataset in order to carry out statistical previsions as the best approximation, in a limited validity domain, of the real function governing the phenomenon

M. Bietresato (✉) · C. Caligiuri · A. Bolla · M. Renzi · F. Mazzetto
Faculty of Science and Technology, Free University of Bozen-Bolzano, Piazza Università 5,
39100 Bolzano, Italy
e-mail: marco.bietresato@unibz.it

© Springer Nature Switzerland AG 2020

A. Coppola et al. (eds.), *Innovative Biosystems Engineering for Sustainable Agriculture, Forestry and Food Production*, Lecture Notes in Civil Engineering 67,
https://doi.org/10.1007/978-3-030-39299-4_60

539

under study (Bezerra et al. 2008; Maheshwari et al. 2011). RSM allows to obtain precise predictions (of value and derivative) of some variables that summarize the operation of a complex system, such as the torque or the NO_x emissions of the internal combustion engine (ICE) of a farm tractor fuelled with non-conventional fuels. Indeed, it is possible to predict the outputs even when using input values different from the values used to define the transfer functions coefficients (i.e., the test conditions) and to plot complete output curves/surfaces from a limited set of experimental data/cases. In particular, it was decided to apply this methodology because, although biofuels have been studied for years, much remains to be understood about their effects on engine performances especially when mixed together, and, therefore, how to fine-tune an engine fuelled this way. Indeed, biofuels are commonly considered one of the main paths towards a new sustainable paradigm in transportation technologies (Niculescu et al. 2019). With respect to the physical and chemical characteristics of alternative fuels, the aim is to obtain properties as close as possible to traditional fossil fuels in order to facilitate the use of these alternative fuels in ICEs with only minor modifications to the fuel pumping, distribution and injection sub-systems. Biodiesel, namely fatty-acid methyl-ester from transesterification of fats of different origins, has been recognized as a renewable biofuel. Its physical and chemical characteristics make it suitable to be used in compression ignition (CI) engines, the most widespread power-generation units in agricultural machines, and tractors, without any major modifications to current technologies (Tomic et al. 2013). The main chemical and physical properties of biodiesel can be empirically investigated conforming to current technical standards. Bioethanol, chemically identical to ethanol but obtained from renewable resources, has recently been attracting increasing attention. It is commonly considered a suitable biofuel for CI engines when used as an additive for diesel and biodiesel. The most important fuel properties which have a direct impact on the combustion phenomena occurring in ICEs are viscosity, density, cetane number, latent heat of evaporation, flash point and oxygen concentration (Bhuiya et al. 2014). Amongst such fuel properties, the emissions of harmful nitrogen oxides (NO_x) are correlated to the cetane number (CN), which in turn describes the auto-ignition ability of the fuel. Several studies report that biodiesel has positive effects on exhaust emissions of CI engines (Suresh et al. 2018). Nevertheless, other studies recognize (Thangaraja et al. 2016) that biodiesel addition cause a substantial relative increase in NO_x emissions, which represents one of the main cons of using biodiesel as a petro-diesel substitute: controlling NO_x emissions is crucial in order to meet the EURO and TIER emission standards. Improvements in terms of NO_x emissions can be obtained by varying the biodiesel substitution rate in diesel-biodiesel blends (Zannis et al. 2019), as well as introducing small percentages of a third alcohol-based fuel (ethanol, methanol) to produce ternary fuel blends (Caligiuri et al. 2019). It has been observed that the engine torque increases with increasing biodiesel percentage in the blends: such behaviour should be credited to the higher oxygen content, the higher biodiesel consumption, an advance of injection timing and a shorter ignition delay time (Xue et al. 2011). Instead, bioethanol addition to fuels has presented controversial results in terms of power output, which will not be discussed here. Hence, when using ternary blends, the substitution of fuels in

the mixture should respect a trade-off between the de-rating of performance and the reduction of polluting emissions. Please refer to Shahir et al. (2015) for more information regarding the potential of bioethanol. These controversial results highlight the need for further investigation in terms of assessment of emissions and performances by developing or applying numerical optimization methods (Yusri et al. 2018).

2 Materials and Methods

2.1 Experimental Setup

Tests were performed on a “T4020V” farm tractor by New Holland Agriculture (Torino, Italy) equipped with a 4-cylinder 3200-cm³ diesel engine with direct fuel injection system, gently put at the experimenters’ disposal by the “*Consorzio Agrario di Bolzano*” (Bolzano, Italy; www.ca.bz.it/). The tractor was fuelled with five fuels: pure diesel oil, two binary and two ternary blends of diesel oil (D), biodiesel (B) and bioethanol (E). Specifically, these blends were expressed in volume: B15E0 (85% D, 15% B, 0% E), B25E0 (75% D, 25% B, 0% E), B15E3 (82% D, 15% B, 3% E) and B25E3 (72% D, 25% B, 3% E). An external tank was used during these tests for rapid fuel substitution and for the measurement of the instant consumption. A description of such apparatus, based on a chrono-gravimetric principle, is available in Bietresato and Mazzetto (2018). During the tests with a PTO-dynamometer (“*SIGMA 50 Mobile*” by N. J. Froment & Co Ltd, UK), the torque at the rear PTO of the tractor and the NO_x concentration (ppm) were measured. Each dyno test started after engine warm-up and included an OECD-like test (OECD 1984): with the engine at the maximum speed and at full throttle (i.e., with fuel pump rack fully opened), an increasing braking force was applied by the dyno to the engine through the PTO. An instantaneous reading of the PTO speed allowed to modulate the braking force applied by the dyno to stabilize the tractor at six speeds of rotation of the PTO (300-400-500-600-700-800 rpm), corresponding to 822-1096-1370-1644-1918-2192 rpm for the engine, and the dyno allowed to measure the engine torque. Each operating condition was kept constant for at least 2 min to allow the gas analyser (“*Vario Plus Industrial*”, MRU Instruments, Houston, State of Texas, USA) to collect enough measurements in steady-state conditions. A total of 30 experimental cases were completed, i.e. six different speeds for each of the five above listed fuel blends. The trials were all performed on the same day to have minimal influencing effects of the external environmental conditions.

2.2 Analysis of Data by Using the Response Surface Methodology (RSM)

All the collected data concerning the mechanical and environmental performances of the engine have been elaborated statistically: (i) an Analysis of Variance (ANOVA) detected the parameters of influence on the above-mentioned response variables, (ii) the RSM allowed the calculation of the regression function coefficients that describe the effects of the statistically significant independent variables on the response. The values of the dependent variables (a) engine torque and (b) NO_x concentration in the exhaust gases were then estimated by calculating an interpolating function using the values of the independent variables (Fig. 1). Design-Expert 7.0.0 software (Stat-Ease, Minneapolis, State of Minnesota, USA) was used for these calculations.

If y and x_i are, respectively, a generic response (i.e., an independent variable) and a generic numerical factor (i.e., a dependent variable), non-coded ($i = 1$ to m , with m the number of investigated variables; $m \geq 1$), a_0 is the interception coefficient, and a_i , a_{ii} , a_{iii} , a_{ij} and a_{ijk} ($i \neq j \neq k$) are respectively the coefficients of the linear, quadratic, cubic, 2nd-order and 3rd-order interaction terms, the most generic regression model used in RSM (i.e., a “full-cubic model”) is:

$$y(x_i; i = 1 \text{ to } m) = f(x_i) = a_0 + \sum_{i=1}^m a_i x_i + \sum_{1 \leq i < j \leq m} a_{ij} x_i x_j + \sum_{1 \leq i < j < k \leq m} a_{ijk} x_i x_j x_k \quad (1)$$

For the present study, after analysing the data, the software automatically selected for most of the models a (multi-) linear 2nd-order model with interactions (more precisely, a “full-quadratic model”) as starting point to build the mathematical model for each of the investigated responses:

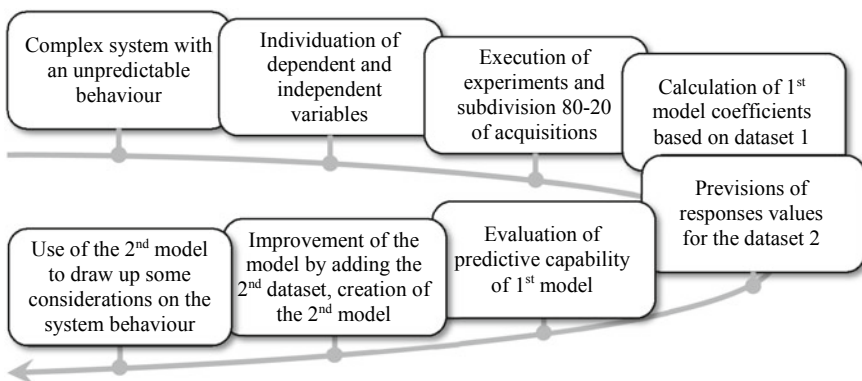


Fig. 1 Steps followed in the application of the presented mixed experimental-numerical approach

$$y(x_i; i = 1 \text{ to } m) = f(x_i) = a_0 + \sum_{i=1}^m a_i x_i + \sum_{1 \leq i \leq j \leq m} a_{ij} x_i x_j \quad (2)$$

The validity domain of each polynomial function f is given by the lower and upper values of each independent variable x_i ($i = 1$ to m). The ANOVA, which is part of this methodology, allows the analyst to identify the most significant factors and polynomial terms, thus operating a partial simplification of the resulting polynomial models based on the p-values (threshold value: 0.05).

The percentages of the three components in the fuel mixes are not fully independent from each other as their sum must be always 100. Therefore, one of these (the diesel oil percentage: D) was excluded from the analyses as it is not properly an independent variable. During each of the tests, the system tractor, fuelled with one of the presented blends, stabilizes on a different engine speed every time a new value of the load (expressed as braking torque) is applied by the PTO-dyno; therefore, the following equation holds:

$$n(\text{rpm}) = f_1[T(\text{Nm}); B(\%); E(\%)] \quad (3)$$

Thanks to the subsequent elaborations of the quadruple $[n(\text{rpm}); T(\text{Nm}); B(\%); E(\%)]$ with RSM, a model of the torque as a function of the engine speed and the blend composition (percentages of biodiesel and bioethanol) can be obtained:

$$T(\text{Nm}) = f_2[n(\text{rpm}); B(\%); E(\%)] \quad (4)$$

Considering the expression for the torque (Eq. 4) above, NO_x concentrations upon variation of the braking torque can be directly correlated to the engine speed (Eq. 6). This raises the predictive ability of these models using a parameter very easy to detect.

$$\text{NO}_x(\text{ppm}) = f_3[T(\text{Nm}); B(\%); E(\%)] \quad (5)$$

$$\text{NO}_x(\text{ppm}) = f_4[n(\text{rpm}); B(\%); E(\%)] \quad (6)$$

2.3 Validation of Numerical Models

The acquired data were randomly subdivided into two subsets: 80% of the experimental cases (24 cases) were used for building a first set of models, one per response; the remaining 20% of the experimental cases (6 test cases) were used to verify the predictive capabilities of the models constructed from the previous 24 cases. The different models were evaluated in terms of: (a) fitting of the initial set of data through

the coefficient of determination, the adjusted coefficient of determination, the average relative fitting error, the mean squared error, and (b) predictive capabilities of the values of the several responses for the 6 verification cases (through the average relative prediction error and the mean squared error). The relative error of fitting or prediction of the control cases above for the i -th case (identified by the two 4-tuples $[n(\text{rpm}); T(\text{Nm}); B(\%); E(\%)]$ and $[n(\text{rpm}); NO_x(\text{ppm}); B(\%); E(\%)]$) has been calculated. After validating the method, the RSM was applied once again to the whole dataset (30 cases). These models were evaluated using the same metrics (e.g., the coefficient of determination and the average relative fitting error) and the enhanced fitting ability, given by the addition of 6 more points to the initial dataset of 24, was also evaluated.

3 Results and Discussion: Engine Torque and NO_x Emissions as a Function of the Fuel Blend Composition

Table 1 presents the numerical regression models, based on 24 and 30 experimental cases respectively, as resulted from the backward selection of the terms forming the most complete model handled by RSM for both torque and NO_x concentrations. The equations are presented in terms of actual factors, i.e. the terms are used without any conversion, scaling or nondimensionalization. The following Figs. 2 and 3 give a graphical representation of these equations applied to the total of 30 cases, allowing the visualization of the trends and absolute values. By substituting the values of the input quantities, within the validity domains the first two numerical models can be used to predict the engine torque at the different rotational speeds and varying the fuel blend composition, whereas the second two numerical models can be used to

Table 1 Numerical models (respectively based on 24 and 30 cases) for both variables (torque and NO_x emissions)

Quantity	Model	
	nr. 1 (on 24 cases)	nr. 2 (on 30 cases)
Torque	$T[\text{Nm}] = + 749.85629 + 0.86775 \cdot B[\%] - 5.46458 \cdot E[\%] + 8.48014 \cdot 10^{-3} \cdot n[\text{rpm}] - 6.15737 \cdot 10^{-5} \cdot \{n[\text{rpm}]\}^2$	$T[\text{Nm}] = + 751.73874 + 0.77198 \cdot B[\%] - 5.63968 \cdot E[\%] + 9.55847 \cdot 10^{-3} \cdot n[\text{rpm}] - 6.24263 \cdot 10^{-5} \cdot \{n[\text{rpm}]\}^2$
NO _x emissions	$NO_x[\text{ppm}] = + 500.71510 - 0.61435 \cdot B[\%] + 25.06639 \cdot E[\%] + 0.13109 \cdot n[\text{rpm}] - 1.77110 \cdot B[\%] \cdot E[\%] - 4.43123 \cdot 10^{-4} \cdot B[\%] \cdot n[\text{rpm}] - 3.82978 \cdot 10^{-3} \cdot E[\%] \cdot n[\text{rpm}] + 0.21606 \cdot \{B[\%]\}^2 - 1.25658 \cdot 10^{-4} \cdot \{n[\text{rpm}]\}^2$	$NO_x[\text{ppm}] = + 488.75020 - 0.37219 \cdot B[\%] + 25.65112 \cdot E[\%] + 0.14445 \cdot n[\text{rpm}] - 1.81991 \cdot B[\%] \cdot E[\%] - 5.89491 \cdot 10^{-4} \cdot B[\%] \cdot n[\text{rpm}] - 4.67969 \cdot 10^{-3} \cdot E[\%] \cdot n[\text{rpm}] + 0.22224 \cdot \{B[\%]\}^2 - 1.29296 \cdot 10^{-4} \cdot \{n[\text{rpm}]\}^2$

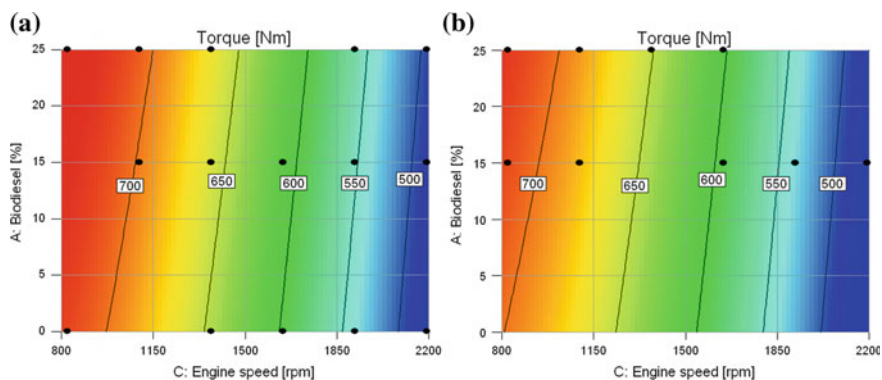


Fig. 2 Graphs (“contour plots”) of the engine torque as a function of the biodiesel percentage and of the engine speed referred to the 2nd model (30 cases), with the 0% (Fig. 2a) and the 3% (Fig. 2b) of bioethanol in the blend. The black dots represent the positions of the experimental measurements within the investigated hyperspace

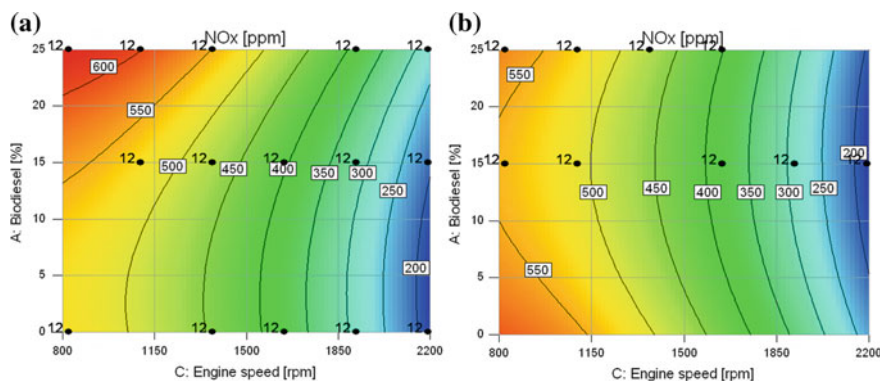


Fig. 3 Graphs (“contour plots”) of the NO_x concentration as a function of the biodiesel percentage and of the engine speed referred to the 2nd model (30 cases), with the 0% (Fig. 3a) and the 3% (Fig. 3b) of bioethanol in the blend

predict the NO_x concentration at the different rotational speeds and the variation of the fuel mix composition.

As reported in Table 2, with regards to the 24 cases used for the model building phase for the variable “torque”, the predictive capability of both the models is very high: the R^2 is 0.9918 and the Adjusted- R^2 is 0.9930. When considering the six control cases excluded in the building of the first model, the very high predictive capability of this model becomes apparent: for such cases the average error (0.38%) and the mean square error (0.01%) are very low. The prediction of the engine power at different rotational speeds and fuel mix composition can be assessed by multiplying the predicted value of the torque and the engine speed expressed in rad s^{-1} . Even for the variable “ NO_x emissions”, the values of R^2 and Adjusted- R^2 are very high for

Table 2 Experimental values from the numerical models for the variables Torque and NO_x emissions as a function of fuel blend composition and engine speed with respect to the order of the regression equations, the fitting on the available cases, and the prediction on the comparison cases

Response	Model nr., cases	Regr. Eq. order	Fitting (on model-building cases)				Prediction (on 6 test cases)	
			R ²	Adj-R ²	Average error	Mean sq. error	Ave. error	Mean sq. error
Torque [Nm]	1 (24)	2	0.9918	0.9901	0.07%	0.01%	0.38%	0.01%
	2 (30)	2	0.9930 (+0.0012)	0.9918 (+0.0017)	0.00% (-0.07%)	0.01% (+0.00%)	–	–
NO _x [ppm]	1 (24)	2	0.9825	0.9820	0.36%	0.17%	1.40%	0.25%
	2 (30)	2	0.9820 (-0.0005)	0.9816 (-0.0004)	0.11% (-0.25%)	0.15% (-0.02%)	–	–

both the models (24 and 30 cases) and approximately at the same values (ca. 0.982). The mean square error is 0.17% and the average error is 0.36%, both essentially negligible. These results suggest that the predictive capability of both the models for torque and NO_x emissions is good with respect to the cases used for the model-building phase. Secondly, concerning the very small difference of R² values, this means that the six control cases are well aligned with the calculated response surface and that the trend has been respected when including also those cases in the second model.

Thanks to the regression equations of the experimental data previously presented (2nd model, based on 30 cases), it is possible to explore the entire operating range of the engine (822–2192 rpm) with a higher resolution than the experimental one (e.g., at intervals of 100 rpm) and even at an intermediate concentrations of bioethanol (e.g., 1.5%). Moreover, with the aim of identifying a possible optimal blend composition, it is possible to estimate the percentage variations of NO_x and torque per each combination of the parameters [n (rpm); B (%); E (%)] with respect to the same speeds when the engine is fuelled with pure diesel oil, and then calculate the average variation per each mixture on the entire speed range of the engine. The results, expressed as trends in some graphs, are visible in Fig. 4.

Analysing the graphs in Fig. 4, with increasing concentration of bioethanol, a decrease in the average NO_x concentration for high percentages of biodiesel (greater than 10%) is detected. The trend is the opposite for blends with low percentages of biodiesel (i.e., lower than the indicated threshold). The increase in NO_x with 10%-biodiesel blends is almost the same (+2.3% / +2.5%) as the percentage of bioethanol in the blend varies within the validity limits explored by the model (0–3%), thus constituting a morphologically significant point in the trends of the graphs. Moreover, the effect of biodiesel is always to increase the torque on average within the engine speed range (about +1% of the torque every 8 percentage points of biodiesel in the blend), according to the cited literature references. Instead, the effect of bioethanol is opposite (about –1% of the average torque for each percentage point of bioethanol

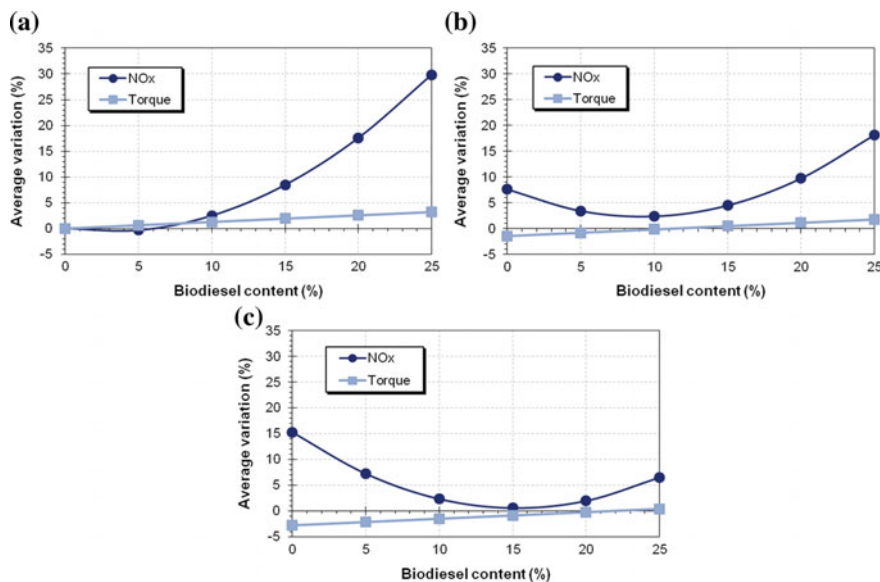


Fig. 4 Graphs of the average percentage variations of NO_x and torque as a function of the biodiesel content in the fuel blend referred to the 2nd models (30 cases), with the 0% (Fig. 4a), 1.5% (Fig. 4b) and the 3% (Fig. 4c) of bioethanol in the blend

in the blend), with an equilibrium of these antithetical effects (i.e., no average torque variations) for the mixtures B11E1.5 and B22E3. Considering together the effects on the engine performance and on the pollutants emission, it can therefore be defined as “optimal” a blend that, for example, would be able to decrease as much as possible the NO_x emission, possibly increasing also the torque. Observing the trends expressed by the graphs, the blend B3E0 meets this criterion (NO_x -0.6% , torque $+0.4\%$). It is possible to identify other points of optimality by altering the importance given to these two parameters or by introducing other criteria, for example: having the highest possible concentration of biodiesel without excessively altering the NO_x emissions (max increase $+4\%$; arbitrary threshold) and the torque (max decrease -2% ; arbitrary threshold), in order to benefit from the presence of high percentages of biodiesel thus reducing the concentration of particulate matter in the exhaust gases (not inquired in this article). With this last criterion, blends B11E0 (NO_x $+3.5\%$, torque $+1.4\%$) and B20E3 (NO_x $+2.0\%$, torque -0.2%) should be considered, for example.

4 Conclusions

The reported values of R^2 and adjusted R^2 above 0.90 demonstrate how the proposed polynomial numerical models for the torque and the NO_x concentration, within their

validity domains, are very good approximations of the real response functions. Their trends (expressed as first and second derivative or plotted in some graphs) can be used in place of the trends of the real (unknown) response functions to inquire the machine response to a change of fuelling. Finally, the same models are also applicable in formulating numerical predictions of the investigated factors and to individuate a specific blend, even different from the blends used in the experimental tests, able to maximise and/or minimise some numerical parameters. For example, if the criterion is the minimisation of the NO_x emissions over the entire speed range for the studied engine (the engine of a “*New Holland T4020V*” farm tractor), the blend to be suggested is B3E0. It is therefore possible to conclude that RSM can express its full potential also when applied to the analysis of ICEs to develop correlations involving the fuel blend composition and the engine speed. Hence, the use of RSM is highly recommended in such a scenario as the one presented in the current paper. Unexperienced users will be able to obtain reliable forecasts of engine performance and emissions when an ICE is fuelled with alternative fuel blends without the need to assess the detailed behaviour of each single sub-component, but instead by making use of few and easily-accessible input parameters. By doing so, it will be possible to apply this method also to other fuel blends and/or to other CI motors, regardless their type (e.g., direct/indirect injection, atmospheric/turbocharged) and size (i.e., light/heavy-duty).

Acknowledgements This research is part of the “BIO-TRACT-EFFICIENCY” (“*Experimental investigation on the efficiency of agricultural machines powered with different fuels*”) internal research project (grant nr. TN200F). The authors wish also to thank the “*Consorzio Agrario di Bolzano*” for having put at their disposal the farm tractor used in this study within the collaboration started with the DYNOTRACTOR 2 project (“*Experimental setup of an in-field test apparatus for farm tractors-2*”).

References

- Bezerra, M. A., Santelli, R. E., Oliveira, E. P., Villar, L. S., & Escalera, L. A. (2008). Response surface methodology (RSM) as a tool for optimization in analytical chemistry. *Talanta*, *76*, 965–977.
- Bhuiya, M. M. K., Rasul, M. G., Khan, M. M. K., Ashwath, N., Azad, A. K., & Hazrat, M. A. (2014). Second generation biodiesel: Potential alternative to-edible oil-derived biodiesel. *Energy Procedia*, *61*, 1969–1972.
- Bietresato, M., & Mazzetto, F. (2018). Ideation, realization and experimentation of prototype device for measuring farm tractor fuel consumption during dynamometer tests. In *Engineering for Rural Development* (pp. 362–372).
- Caligiuri, C., Renzi, M., Bietresato, M., & Baratieri, M. (2019). Experimental investigation on the effects of bioethanol addition in diesel-biodiesel blends on emissions and performances of a micro-cogeneration system. *Energy Conversion and Management*, *185*, 55–65.
- Maheshwari, N., Balaji, C., & Ramesh, A. (2011). A nonlinear regression based multi-objective optimization of parameters based on experimental data from an IC engine fueled with biodiesel blends. *Biomass and Bioenergy*, *35*, 2171–2183.

- Niculescu, R., Clenci, A., & Iorga-Siman, V. (2019). Review on the use of diesel–biodiesel–alcohol blends in compression ignition engines. *Energies*, *12*, 1194.
- OECD. (1984). Code 2-OECD Standard Code for the Official Testing of Agricultural and Forestry Tractor Performance. 101.
- Shahir, S. A., Masjuki, H. H., Kalam, M. A., Imran, A., & Ashraful, A. M. (2015). Performance and emission assessment of diesel–biodiesel–ethanol/bioethanol blend as a fuel in diesel engines: A review. *Renewable and Sustainable Energy Reviews*, *48*, 62–78.
- Suresh, M., Jawahar, C. P., & Richard, A. (2018). A review on biodiesel production, combustion, performance, and emission characteristics of non-edible oils in variable compression ratio diesel engine using biodiesel and its blends. *Renewable and Sustainable Energy Reviews*, *92*, 38–49.
- Thangaraja, J., Anand, K., & Mehta, P. S. (2016). Biodiesel NOx penalty and control measures-a review. *Renewable and Sustainable Energy Reviews*, *61*, 1–24.
- Tomic, M., Savin, L., Micic, R., Simikic, M., & Furman, T. (2013). Effects of fossil diesel and biodiesel blends on the performances and emissions of agricultural tractor engines. *Thermal Science*, *17*, 263–278.
- Xue, J., Grift, T. E., & Hansen, A. C. (2011). Effect of biodiesel on engine performances and emissions. *Renewable and Sustainable energy reviews*, *15*, 1098–1116.
- Yusri, I. M., Abdul Majeed, A. P. P., Mamat, R., Ghazali, M. F., Awad, O. I., & Azmi, W. H. (2018). A review on the application of response surface method and artificial neural network in engine performance and exhaust emissions characteristics in alternative fuel. *Renewable and Sustainable Energy Reviews*, *90*, 665–686.
- Zannis, T. C., Papagiannakis, R. G., Pariotis, E. G., & Kourampas, M. I. (2019). Experimental study of DI diesel engine operational and environmental behavior using blends of city diesel with glycol ethers and RME. *Energies*, *12*, 1547.

An Approach to the Development of an Integrated Real-Time Engine Test System for Agricultural Machines: Conceiving, Implementation, Set-up and First Tests



Marco Bietresato, Matteo Malavasi and Fabrizio Mazzetto

Abstract Two crucial points in the development of an experimental-test system concern specifically the instrument-management subsystem and are: (1) coordinating the acquisitions from the connected instruments and (2) making the data easily usable by the users through a rational interface. Regarding the first point, an *ex-post* synchronization of the readings previously gathered during the tests can be computationally heavy (due to: different file-formats and sampling frequencies of instruments; sometimes also non-synchronized internal clocks). Rather, a properly-said instruments synchronization during the experimentation and a unique recipient for all gatherings is certainly more effective, allowing the users to have, at the end of a test session, ready-made data for any subsequent processing phase. However, its implementation requires a lot of work concerning: the set-up/creation of hardware interfaces, the writing of a software program and the implementation of a simple and reliable user interface, but it is always preferable. This approach has been followed to propose an integrated test-system for agricultural machines and all its logical steps are illustrated here as general guidelines for any future acquisition system. The management subsystem (“TRA-LOG”) of this experimental-test system is LabVIEW-based and has a graphical user-interface, developed according to modern ergonomic design concepts. TRA-LOG is able to: (1) simultaneously acquire data from a PTO-dyno, a fuel-consumption meter, an exhaust-gas analyser, many thermocouples, (2) display in real time the value of the acquisitions, (3) plot in real time the motor-performance graphs (torque, power) and other time-dependant graphs, (4) save the data in a spreadsheet-compatible format. After illustrating the development procedure and main features of this test system, we presented also its successful validation in the test of a New Holland T4020V farm tractor.

Keywords Measurement equipment · Hardware/software interfaces · Mobile test-equipment · Engine test · Agricultural machines · LabVIEW

M. Bietresato (✉) · M. Malavasi · F. Mazzetto
Faculty of Science and Technology, Free University of Bozen-Bolzano, Piazza Università 5,
39100 Bolzano, Italy
e-mail: marco.bietresato@unibz.it

© Springer Nature Switzerland AG 2020
A. Coppola et al. (eds.), *Innovative Biosystems Engineering for Sustainable Agriculture, Forestry and Food Production*, Lecture Notes in Civil Engineering 67,
https://doi.org/10.1007/978-3-030-39299-4_61

1 Introduction

A transportable test-system for the on-site detection of many technical parameters concerning agricultural engines can be extremely interesting to widen the possibility of testing agricultural machinery by a research board. Such a test system has to be composed by many scientific instruments, which detect simultaneously different physical quantities, thus allowing the investigation of the energetic and environmental performances of an engine at different rotational speeds (Vojtisek-Lom et al. 2013), maybe also with different fuels or at different positions of the accelerator pedal. The synchronization of the readings from various instruments could surely be performed *ex post* by software, if each of these instruments had recorded also the acquisition time and their internal clocks had all been previously synchronized (Bietresato et al. 2016; Dittrich et al. 2018). However, this post-processing operation is never simple: even after selecting and purchasing only instruments with the same type of data-output (e.g., serial), the acquisition rates can be different, due to the different types of instruments and operating principles. Rather, the best solution is the development of a control subsystem with a unique interface to control specific functions of the connected instruments (Scheibelmasser et al. 2006; Mikulski and Wierzbicki 2015): the “*Instrument-management (sub)system*” or “*acquisition (sub)system*”. When designing such a system, an equal attention has to be paid to the hardware (HW) and to the software (SW); see Fig. 1. Through a fully bidirectional flow of signals (control signals, acquired data), the coordination SW/HW should be able to: (1) turn on each of the connected instruments, (2) start/stop gathering the data and (3) save them, synchronized, in a single file. However, it is also possible to use a unidirectional signal flow: all the readings are made available from each instrument

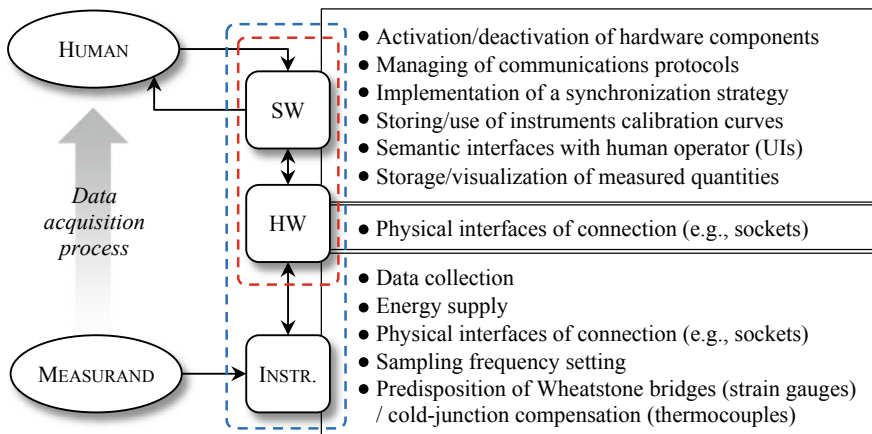


Fig. 1 Features managed by each part of an experimental-test system (in blue); the instrument-management (sub)system or acquisition system (in red) is composed only by the SW and HW

since its start and conveyed into a single storage subsystem without any control signal from the central unit. However, also in this case, the problem of communication between each measuring instrument and the central unit, even if less complex, still exists.

Moreover, even when it is possible to develop an adequate SW subsystem, little importance is given to the user interfaces, and the resulting system can be objectively difficult to be used (therefore, not very *efficient*). Indeed, who develop these interfaces is usually an expert in the systems under monitoring, but not in monitoring systems. Actually, the principles to be applied to make a better visual user interface are all simple and well codified (Oryzo Business Solutions 2019), even by international standards (ISO 9241-10/11/101, ISO 9126-1/25010) (ISO 1996, 1998, 2001, 2006, 2011). Therefore, for an acquisition system, the so-called “design” phase takes on a much broader connotation, involving aspects ranging from measurement science to electronics, from information technology to ergonomics. Hence, this work aims at presenting the approach followed in the development of an integrated test system, illustrating its application for the realization of a real-time system for the detection and recording of many engine parameters of agricultural machines during dyno tests. It connects a series of portable instruments and has an interesting layout with two expansion points and a very simple but effective interface.

2 Materials and Methods

The acquisition system of an integrated test system includes HW and SW components and it should be developed by following the four phases listed hereinafter:

1. CONCEPT OF THE SYSTEM; enumeration of the technical requirements; drafting of a basic layout (instruments, connections, control unit and data saving unit);
2. PRELIMINARY CHECKS; verification of the technical characteristics of the control unit and of the instruments (physical interfaces, communication protocols); instruments setups and possible HW modifications (e.g. creation of interfaces); analog and serial hubs predisposition; refinement of the system layout;
3. BUILDING OF THE SYSTEM; HW: procurement of all the instruments/units to be connected, creation of connections and connection-hubs; SW: creation of a program for managing the instruments: (i) setting up of a “push” or “pull” data-acquisition strategy (i.e., interrogation of the instrument or reading/interception of data already made available by the instrument), (ii) search for SW libraries or ready-made parts of code, (iii) program writing and verification, (iv) creation of a (graphical) user interface according to the main ergonomic principles, (v) creation of a data saving/export subroutine and setting of an output file structure;
4. VERIFICATION OF THE SYSTEM; verification of the correct operation of HW and of SW; verification of the correct interpretation of the signals by SW through a comparison of the readings of the same systems when stand alone; verification of

the correct operation of the whole system in a general test; setting of the optimal working parameters for all the units and of a general acquisition frequency.

In particular (**Phases 1, 2**), an acquisition system dealing with engines of agricultural machines has to detect and store many quantities related to: (i) the mechanical performances of the motor, including the brake specific fuel consumption (BSFC), measured by a chrono-gravimetric fuel-consumption meter system, (Bietresato and Mazzetto 2018), or (ii) its emissions (Table 1). It has to interface instruments of many types (analog, digital), letting also the system the possibility to be expanded in the future by adding other instruments. Concerning this last point, it is possible to notice from Table 1 that most of the instruments to be connected have a RS232 serial interface converted in USB thanks to a FTDI cable, but all thermocouples are identifiable as analogue instruments. Therefore, the layout of such a system has to present for sure *two hubs* for conveying all the gatherings, which are also two points of future expansion of the acquisition system: (1) a USB hub (or a PC with many USB ports, acting as a USB hub), and (2) a data logger (or an equivalent acquisition PC-board), able to manage the many analog signals from the thermocouples. For example, an opacity meter or an IR-thermal imaging camera could be possibly connected to the

Table 1 HW components of the developed acquisition system, with their main features

Feature	Instrument				
	PTO dyno	Scale	Gas analyser	Thermo-couples	Data logger
Model/type, Manufacturer	Sigma 50 Mobile, J. Froment & co. Ltd.	DS30K0.1L, Kern & Sohn GmbH	Vario Plus Industrial, MRU Instruments	K, J	Datataker DT85M, Thermo Fischer Scientific Australia Pty
Measured quantities	Instant torque, Instant power, Instant PTO rotational speed	Instant quantity of fuel in an external tank, BSFC	Chemical composition of the main polluting species and temperature of the exhaust gas	Temperature in several points of the motor, the exhaust line and of the fuel	Connected to the thermocouples through the cool-junction-compensated inlet ports
Instrument type	Digital	Digital	Digital	Analog	Digital
Communic. standard	RS232 + USB conv.	RS232 + USB conv.	RS232 + USB conv.	–	USB
Other specs. (BAUD rate, resolution, parity bit, flow control)	1200, 8, 0, none	2400, 8, 0, none	9600, 8, 0, none	–	–
Data format	Num. string	ASCII string	ASCII string	–	Proprietary
SW interface	VISA LabVIEW	VISA LabVIEW	VISA LabVIEW	Connected to the datalogger	LabVIEW Driver by Datataker

USB hub, an air-intake flow meter or some strain gauges to the data logger. Another possibility is using a mixed-type hub.

All these instruments had to be coordinated by a *super-subsystem* (i.e., a control unit), which can be, for example, a dedicated device or, rather, a PC with a proper SW and an adequate number of serial/USB interfaces (**Phase 3**). Hence, focussing the attention on the HW of the acquisition system, many solutions are possible. For example, a cRIO module and a digital-input 9401 board both by National Instruments can also be used (Ravaglioli et al. 2016). In the engine test bench described in (Labeckas et al. 2013) there is instead the need to have a high-performance system to measure the pressure in the injection system and in the combustion chamber, so an IndiModul 622 by AVL is used. AVL offers also an interesting SW solution, i.e. the PUMA Open System, to manage many instruments and create a so-called “*configurable device handler*” that has a unique SW interface to coordinate all the connected devices (Mikulski and Wierzbicki 2015). LabVIEW by National Instruments is another SW environment that is very used at this purpose (Emberger et al. 2016), and it has been chosen in this case because it can be installed on any PC, turning it into a signal hub, i.e. without requiring a dedicated HW but letting the experimenters use the HW already available (in this case, including a “Datataker DT85M” data logger for managing analog signals, e.g. of the thermocouples).

The acquisition system should also have a user interface (UI), i.e. a space (in its broader sense) where (tactile, visual) interactions between humans and machines/systems occur. Concerning specifically the *graphical* UI (GUI), its development should be inspired by SW ergonomic principles, which basically forecast a user-centred design and introduce the concept of *software usability*. In particular, about this topic, it is advisable to refer to the ISO 9241-10/110 standards (ISO 1996, 2006), which define the principles that characterize the so-called “*human-computer dialogue*” (Fig. 2). The goal of these standards is to have an interaction that allows effective operation and control of the system from the human, whilst the system simultaneously feeds back information that aids the operators’ decision-making and control process.

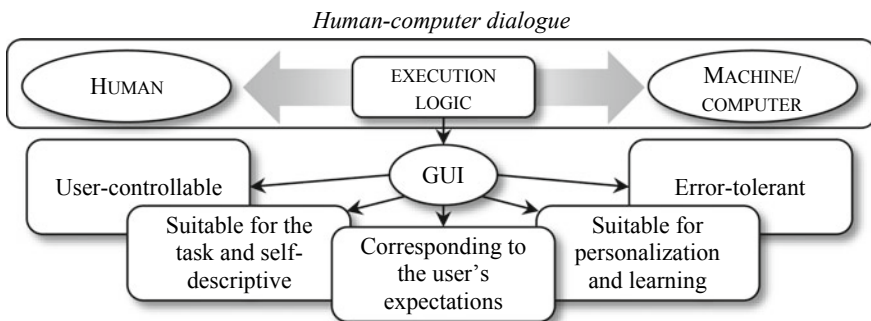


Fig. 2 Main principles present in the ISO 9241-10/110 standards, to be use in the development of a graphical user interface reflecting the execution logic used in the human/machine interactions

3 Results and Discussion

(Phase I) The integrated system is visible in Figs. 3 and 4 left. It is composed by four units physically connected to a PC on which an ad hoc-developed SW program has been installed.

The proposed solution, using a PC as *super-subsystem*, has been chosen because is more flexible and easily implementable than a layout using a data logger to coordinate all the instruments. Indeed, in the proposed general architecture of the system, the data logger is exploited firstly as an analog port multiplier, and secondly for managing the thermocouples (thanks to its cool-junction-compensated inlet ports). By the SW architectural point of view, thanks to the use of proper device drivers, the data logger is completely “transparent”, i.e. it is seen from the PC not as a connected device but as a series of channels each conveying the readings of a thermocouple. An alternative use of the data logger to coordinate all the instruments (i.e., as control unit instead of the PC) is, in this case, difficultly implementable. The PC has been given also

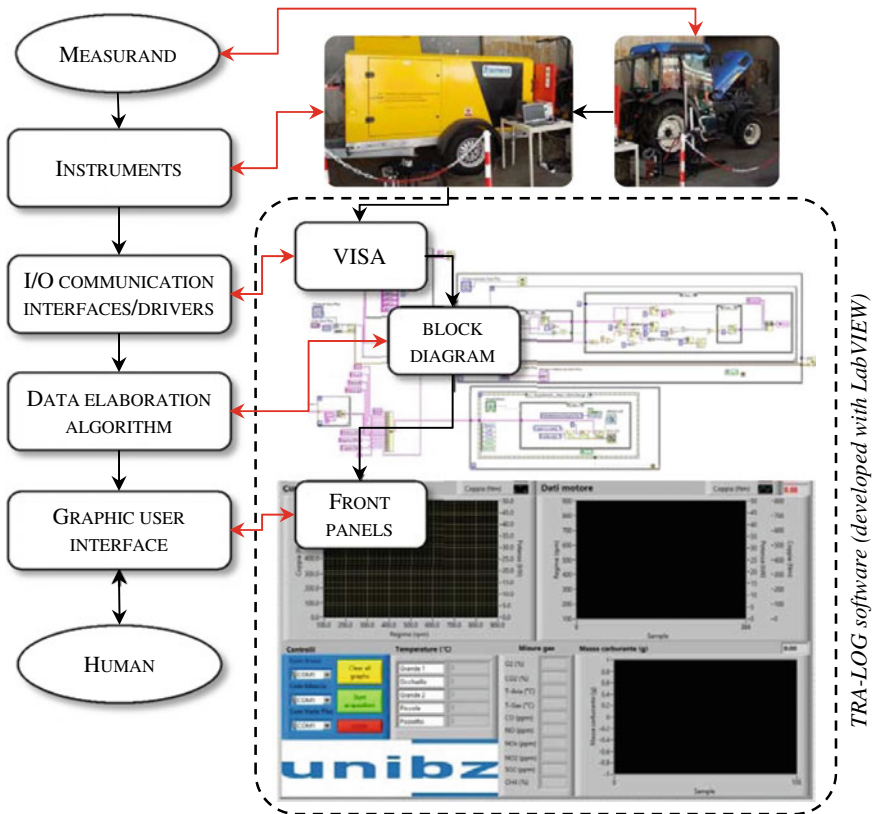


Fig. 3 “TRA-LOG” acquisition system (right) put in relation (through the red arrows) to the general parts of an experimental-test system (left); the front panels compose the first tab of the GUI

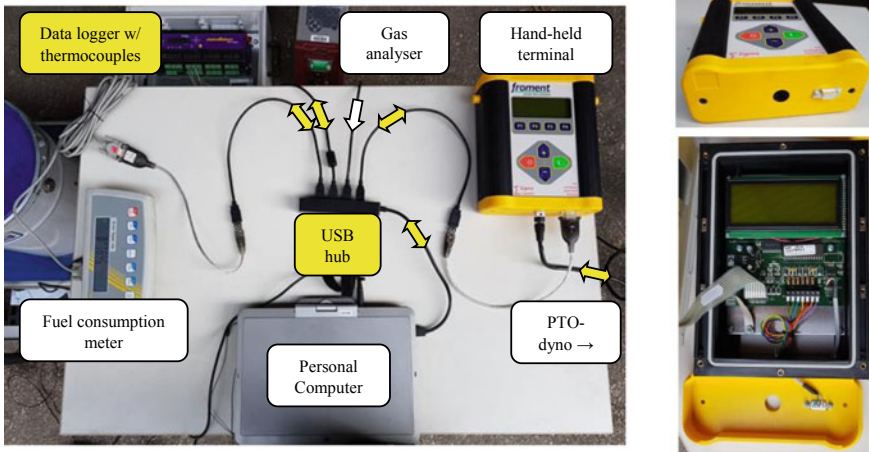


Fig. 4 (left) Wiring layout of the integrated acquisition system (white/yellow arrow: unidirectional/bidirectional flow of signals; yellow box: point of future expansion for the system); (right) hand-held terminal of the dyno with the added RS-232 serial interface on its bottom side (external/internal view)

the task to handle the human-machine interaction, thus visualizing the information to the user. Also, it is worthy to notice that an acquisition system similar to the one described here, being designed to handle several different instruments (in particular: with different interfaces and made by different manufacturers), can be difficultly found on the market and has to be necessarily developed by end-users, due to the extreme variety of instruments and systems to be monitored. The approach followed in its development is not based on the creation of an integrated circuit with an internal clock for the coordination of the peripherals, able to perform an integration at the HW-level of the signals from the instrument. Rather, it has been chosen to follow a more-powerful “mixed HW-SW approach”, in which the integration mainly takes place at the SW level, exploiting the possibility of a computer to be properly programmed, using the standard interfaces/protocols. Indeed, this solution has some interesting points that derive from its own architecture: it is extremely flexible, allowing at any time in the future the addition of other measuring instruments. In particular, any analog instrument (e.g., with a 4–20 mA current output) can be managed by the data logger and its signal can be therefore integrated/synchronized using another channel.

(Phase 2) Except for the dyno, all these units were already equipped with a serial interface for data, so their physical connection to the computer (i.e., the wiring) was very easy. Instead, the PTO-dyno had no interface to be used (1) for the collection of the data or (2) for its control, e.g. for giving a start/stop signal. For this reason, the connection of the dyno to the acquisition system had deserved a deep thinking, involving the architecture of the system on more than a level (physical connection, SW management).

(Phase 3) Therefore we thought to exploit the *additional control unit*, i.e. the hand-held terminal, which is connected via a cable to the dynamometer control panel. The communication between the dyno and the terminal is bidirectional (from the hand-held terminal to the dyno: operation-mode set-up, test-start signal; from the dyno to the hand-held terminal: measured power and torque data, PTO-speed, test-stop signal). The terminal has a simple user interface that allows configuring the dyno for the test and selecting the control mode (e.g. speed-controlled); the functionalities of this terminal are substantially the same of a proprietary SW program (Sigma DynaTest) that can be used if the hand-held cable is connected to a PC, except it does not allow a graphical representation of performances curves and a permanent data-storage (its memory is overwritten at the beginning of a new test). The need for a SW-system substituting the proprietary SW program in the full control of the dyno comes from the impossibility to modify the proprietary SW to (1) implement new functionalities and (2) let it save data from other instruments than the dyno itself. Indeed, the J. Froment & Co Ltd., manufacturer of the dynamometer, gave us access neither to the high-level communication protocol used by Sigma DynaTest to communicate with the dyno through the USB port, nor to the source-code of Sigma DynaTest, it was impossible for us to exploit this system to build a new, more integrated SW program (by extending the functionalities of Sigma DynaTest). So, we individuated, as the only viable solution to be followed in cases like the present one, not to exclude the hand-held terminal but, rather, to query it periodically to return the instant value measured by the dyno. To do so, a new RS-232 serial interface had to be added to the hand-held terminal, by manually soldering three terminals and milling an opening in the external case to accommodate the RS-232 socket (Fig. 4 right).

The management of all HW interfaces and signals, conveyed through these serial interfaces, and the creation of the GUI was carried out through a program ("*farm tractor logging software*" or, simply, "*TRA-LOG*") written in the visual-programming language "*G*" within the integrated development environment "*LabVIEW 2017*" version 17.0f32 by National Instruments Corporation (Austin, Texas, USA). The user interface has been designed according to the presented principles of user-friendliness and easy usability, by organizing hierarchically the information through the use of *colours* and *layers* (tabs, panels). In particular, in the *first tab* of the GUI (i.e. the main tab), always visible at the system start (see also in Fig. 3), there is the acquisition system control panel (in light-blue) with: three drop-down menus to setup the COM ports (respectively for: the dyno, the scale, the gas analyser), a "clear all graphs" button, a "start" button and a "stop" button, identified by the usual traffic-light colours (respectively: yellow, green, red). The rest of the interface (light-grey colour) contains some elements to display a series of parameters graphically or numerically. After the first tests, the proposed interface resulted to be very efficient by the point of view of the SW usability, i.e. in reducing possible errors made by the user. Indeed, in this case:

- the start and stop procedure is immediate and there is an immediate feedback for these actions: thanks to LabVIEW pre-set functionalities, a click on a button changes its appearance and the data recording starts;
- no unwanted action can be performed by the user (the interaction with the system is limited to three intuitive buttons and some textboxes);
- there is a coherent flow for settings (left to right), there are no submenu, the layout is simple and schematic, with only the important information and controls in the foreground.

The output is a text file with tabulation-separated values and 23 data columns: 4 for the time stamp (date, hour, minute, second), 19 for the many recorded parameters (scale: 1; data logger: 5; dyno: 3; gas analyser: 10). Except for the first line (231 characters), each line of acquisitions has a maximum length of 177 characters, with each character encoded with the ANSI character set (1 byte per character). Therefore, the memory occupancy of an acquisition file is very little (1 kb every 6 s of recording).

(Phase 4) The acquisition system was tested in all its functions in a first trial on a New Holland T4020V farm tractor put at the experimenters' disposal by the "Consortio Agrario di Bolzano" (Bolzano, Italy), fuelled with pump diesel oil and stabilized at a constant engine speed. The sampling rate of the TRA-LOG acquisition SW was set at a constant value of 1 Hz, i.e. at the lowest value of all the acquisition rates of the connected instruments, and no problem of data reception by the control unit arose. A higher sampling rate, not supported by all instruments (especially by the gas analyser), can however be managed by TRA-LOG by averaging the acquisitions of the fastest instruments but had not given any real advantage on the precision of the gathered parameters. The validation of the system was done through two OECD-like trials, in which the dyno applied an increasing braking torque to the engine at the maximum speed and at full throttle (i.e., with fuel pump rack that is fully opened). A complete trial has a duration of less than 3 min. The validation concerned specifically the torque and power data from the dyno, as this was the most critical device. TRA-LOG was used in the *first trial*, while Sigma DynaTest system was used in the *second trial*, to have data, warranted by the manufacturer of the dyno, to be used as a reference in the comparison of the acquisition systems outputs (Fig. 5).

Observing the graphs of Fig. 5 it is possible to notice that TRA-LOG gathered a lower number of experimental points than Sigma DynaTest, however sufficient to have a good delineation of the engine characteristic curves. During the same test, Sigma DynaTest stored up to 1834 points, unfortunately not with a constant sampling rate (from 8.0 to 16.1 Hz, with an average of 13.0 Hz). Comparisons were done on the basis of the absolute percentage error on the torque and power at the PTO in the 400–800 rpm PTO-speed interval, taking as a reference the acquisitions of Sigma DynaTest. As visible in Fig. 5, the maximum error of TRA-LOG is 3.1% on the torque and 3.0% on the power, the average errors are 1.1% and 1.2% respectively, thus indicating a very good reliability of this acquisition system (i.e., a high coincidence of the TRA-LOG and Sigma DynaTest outputs). The highest differences are all in the 500–600 rpm sub-range of the PTO-speed. Observing the trends recorded by the two acquisition systems, these differences seem to be due probably to an extemporaneous

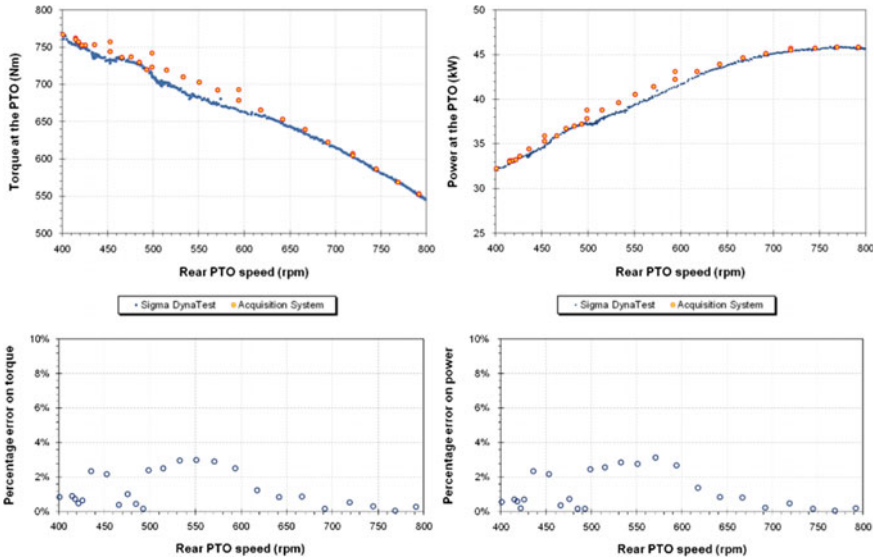


Fig. 5 Torque (*top left*) and power (*top right*) plots at the PTO of a New Holland T4020V tractor, taken with TRA-LOG and Sigma DynaTest systems; related error diagrams (*at the bottom*)

problem occurred during the test monitored by Sigma DynaTest (e.g., a temporary lower fuel flow rate having as effect an anomalous lowering of the curves, then recovered at other speeds). Indeed, in the same speed range, the points recorded by TRA-LOG are more aligned. Excluding these points, the maximum percentage error decreases to about 2%, further witnessing the reliability of TRA-LOG acquisition system and suggesting that it is fully interchangeable with Sigma DynaTest.

TRA-LOG allows also drawing many graphs, e.g. to correlate the temperature T measured at some points of the exhaust line (specifically: outside the exhaust manifold, inside the exhaust pipe through a thermowell) directly with the PTO speed or with the torque at the PTO (Fig. 6). By doing so, the experimenters were able

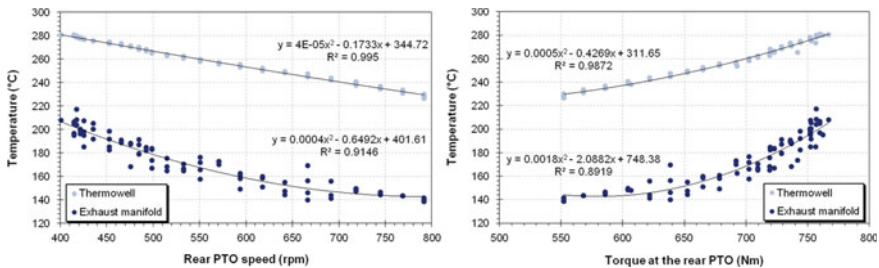


Fig. 6 Temperature of exhaust gases (measured through a thermowell) and of the exhaust manifold surface as a function of the rear PTO speed (*left*) and torque (*right*) of a New Holland T4020V tractor

to inquire the correlations $T = f(\text{speed})$ and $T = f(\text{torque})$ and thermal differences between the two considered points of measurement (75–95 °C; 87.5 °C on average), thus having an idea of the systematic error done in measuring the temperature of the exhaust gases by measuring the surface temperature of the exhaust pipe (i.e., by an experimental point of view, in a much easier way, without drilling any pipes to insert the thermowell).

4 Conclusions

A procedure for the development of an integrated test system has been presented in its principles and applicative phases. The procedure has been applied to conceive, implement and set-up an integrated test-system for agricultural machines, and all the steps and the details are illustrated here as general guidelines for any future acquisition system development. The resulting layout of this system includes many test instruments (a PTO-dyno, a fuel-consumption meter, an exhaust-gas analyser, many thermocouples connected to a data logger), which are all coordinated by a super-subsystem that is, in this case, a PC with a proper SW developed with the LabVIEW integrated development environment, acquiring also temperature data from the data logger. This solution has many advantages: (1) the data logger manages automatically the thermocouples (cold-junction compensation) and can equally easily handle possible future analog instruments/probes (e.g., load cells), it is easily managed by LabVIEW through ready-to-use drivers, (2) the whole system it has two connection hubs (a USB hub and the data logger) for conveying all the gatherings (respectively: digital and analog), which are also the two points of future expansion of the acquisition system. A special care has been devoted to the PTO-dyno, which has no native data-communication interface: a RS-232 interface has been created ex novo and was successfully used for gathering the engine performance parameters by using a “push” logic (i.e. a query-and-wait-for-the-answer logic). The whole test system was managed through a LabVIEW program (“TRA-LOG”) installed on the PC. The GUI was developed in accordance with the principles that characterize the so-called “*human-computer dialogue*” and results to be very simple but effective. The test of the system included a comparison of the TRA-LOG output with the output of the acquisition system of the dyno (“Sigma DynaTest”) during an OECD-like test on a New Holland T4020V tractor. The sampling rate was set to 1 Hz, a trade-off value to allow the correct operation of all the instruments. The TRA-LOG acquisitions of torque and power, although less numerous, were very close to the Sigma DynaTest acquisitions: the maximum differences were of 3.1–3.0%, the average differences of 1.1–1.2%, perfectly within the possible fluctuations that can be observed in the tests trials. The shape of the engine characteristic curves was well delineated and the system can be considered validated. The possibilities offered by such a system are many, thanks to the possibility to plot any quantity as a function of any other quantity. As an example, the paper shows the temperature of two points of the exhaust line as a function of the rotational speed or torque. From these graphs it was possible

to evidence the direct relation between the exhaust gas temperature and the torque, and quantify the temperature difference between the two chosen measuring points (87.5 °C), i.e. the systematic error that would be made by estimating the exhaust gas temperature with the surface temperature of the exhaust pipe.

Acknowledgements The activities presented in the paper are part of the collaboration with the “*Consorzio Agrario di Bolzano*” (www.ca.bz.it/) started on December 13, 2018 with the DYNO-TRACTOR 2 project (“*Experimental setup of an in-field test apparatus for farm tractors - 2*”). The authors wish to thank the “*Consorzio Agrario di Bolzano*” for having put at their disposal the farm tractor used in this study.

References

- Bietresato M, Mazzetto F (2018) Ideation, realization and experimentation of prototype device for measuring farm tractor fuel consumption during dyno tests. In: *Engineering for Rural Development*. pp 362–372
- Bietresato, M., Renzi, M., Mischiatti, S., & Mazzetto, F. (2016). Engine test stand layout and post processing tools for the detection of many engine performance parameters. *ARPN Journal of Engineering and Applied Sciences 11*.
- Dittrich, A., Beroun, S., & Zvolosky, T. (2018). Diesel gas dual engine with liquid LPG injection into intake manifold. *Engineering for Rural Development*, 1978–1983.
- Emberger, P., Hebecker, D., Pickel, P., et al. (2016). Emission behaviour of vegetable oil fuel compatible tractors fuelled with different pure vegetable oils. *Fuel*, 167, 257–270. <https://doi.org/10.1016/j.fuel.2015.11.071>.
- ISO. (2011). ISO/IEC 25010:2011 Systems and software engineering—Systems and software Quality Requirements and Evaluation (SQuaRE)—System and software quality models.
- ISO. (1996). ISO 9241-10:1996 Ergonomic requirements for office work with visual display terminals (VDTs)-Part 10: Dialogue principles.
- ISO. (1998). ISO 9241-11:1998 Ergonomic requirements for office work with visual display terminals (VDTs)-Part 11: Guidance on usability.
- ISO. (2006). ISO 9241-110:2006 Ergonomics of human-system interaction-Part 110: Dialogue principles.
- ISO. (2001). ISO/IEC 9126-1:2001 Software engineering—Product quality—Part 1: Quality model.
- Labeckas, G., Slavinskas, S., & Vilutiene, V. (2013). Combustion, performance and emission characteristics of diesel engine operating on Jet fuel treated with cetane improver. *Engineering for Rural Development*, 313–318.
- Mikulski, M., & Wierzbicki, S. (2015). The concept and construction of the engine test bed for experiments with a multi-fuel ci engine fed with CNG and liquid fuel as an ignition dose. *Journal of KONES powertrain and transport*, 19, 289–296. <https://doi.org/10.5604/12314005.1138136>.
- Oryzo Business Solutions. (2019). User Interface + User Experience Design A successful website begins with the experience of the customer in mind. <https://oryzo.com/user-interface-design/>.
- Ravaglioli, V., Ponti, F., Corti, E., & Cerofolini, A. (2016). Development of a torsionmeter for on-board application. *Energy Procedia*, 101, 646–653. <https://doi.org/10.1016/j.egypro.2016.11.082>.
- Scheiblmasser, A., Traussnigg, U., Schindin, G., & Derado, I. (2006). Device integration into automation systems with configurable device handler. In *Informatics in Control, Automation and Robotics I*.
- Vojtisek-Lom, M., Pechout, M., & Mazac, M. (2013). Measurement of consumption rates of viscous biofuels. *Fuel*, 107, 448–454. <https://doi.org/10.1016/j.fuel.2012.11.025>.

Development and Implementation of an Ultra-Low Volume (ULV) Spraying Equipment Installed on a Commercial UAV



Alberto Sassu, Luca Ghiani, Antonio Pazzona and Filippo Gambella

Abstract The aerial pesticide application assumes remarkable weightiness, especially in agricultural contexts, characterized by immediate interventions hardly executable through the traditional spraying techniques. The Unmanned Aerial Vehicles are versatile and easy to manage technology, capable to perform pesticide application on small and hardly attainable land parcels thanks to a specific crop spraying system. The opportunity to plan automatic flights allows performing an accurate application, optimize the quantity of pesticide applied and limit the contact between the operator and the toxic product. The objective of work was to develop a small pesticide spraying system (<1 kg weight payload), with the purpose to install it on board of a commercial drone, Phantom 4 pro DJI[®] (with a maximum payload of 3.0 kg), in order to demonstrate his potential for manage commercial bio-pesticide on horticultural crops.

Keywords UAV · Sprayer system · Ultra-Low-Volume · Water sensitive papers

1 Introduction

The growing global population and the consequent necessity of food stimulated the use of pesticides for the plant's protection, guarantee productivity and quality of the crop (Pamela et al. 2015; Glass et al. 2010). The Ultra-Low Volume (ULV) sprayers are one of the most used equipment's for control of pests (Linley and Jordan 1992) thanks to the limited volume of pesticide required and the elevated efficiency, Ahmed and Leather (1994) suggest benefits obtained by ULV methods. Despite the considerable improvements of autonomous guidance system for tractors, the GPS developments and the innovative weeds control systems described from Pérez-Ruiz

A. Sassu

Inspire S.R.L., Via XX Settembre 33/10, 16121 Genoa, Italy

e-mail: alberto_sassu@hotmail.it

L. Ghiani · A. Pazzona · F. Gambella (✉)

Department of Agriculture, University of Sassari, Viale Italia 39, 07100 Sassari, Italy

e-mail: gambella@uniss.it

© Springer Nature Switzerland AG 2020

A. Coppola et al. (eds.), *Innovative Biosystems Engineering for Sustainable Agriculture*,

Forestry and Food Production, Lecture Notes in Civil Engineering 67,

https://doi.org/10.1007/978-3-030-39299-4_62

et al. (2015), there are constraints about land spraying machines for crop protection, represented by topography, later stage of crop growth, poor field adaptability, and operational results. In this scenario, the main objective of modern agricultural aviation is to execute an efficient and effective application of chemical and biological products over the plants (Lan et al. 2017).

The Unmanned aerial vehicles (UAV), usually used in remote sensing for inspection of crop condition, can be used also for accurate application of agrochemicals thanks to the optimization of automatic guidance systems (Budiyono and Wibowo 2007; Hong et al. 2012).

Different works have been carried out about the development of pesticide spraying system, Huang et al. (2009) discussed the potential of a site-specific crop application through a small spray system installed on board of a UAV; Durham Giles et al. (2015) deployed a UAV spraying system and developed a series of spraying techniques to apply a range of liquid volume rates (l/ha); the one of Xue et al. (2016) which performed a UAV pesticide application interfacing the sprayer with the *electronic control system* to activate spray releases based on the GPS coordinates and pre-programmed spray locations; and the other of Zhang Yianlang et al. (2017) who studied electrostatic spray technology and UAV to develop a fan-shaped electrostatic spray system for crop protection operations and define a proper UAV electrostatic spray operation parameters to achieve better droplet deposition and to reduce pesticide dosage.

Despite the recent developments, there are concerns about the potential environmental contamination and limitation related to the costs, flight autonomy, payloads constraints, and aerial pesticide application regulatory.

For commercial application of biological products (i.e. *Bacillus thuringiensis*) aerial application techniques are commonly used in large scale treatment against forest pests. This is because (i) the environmental constraints faced in the blanket treatment of large areas in such operations, which mean that there is a greater tendency to use “softer” or biological sprays; (ii) the logistical pressures of aerial application encourage the adoption of low volume application techniques.

The objective of this research was to develop an Ultra-Low Volume spray system ($\leq 5\text{--}20$ L/hectare) implemented on a small and cheap UAV with low payload (<1.0 kg) for the application of biological products and evaluate its spraying performance in terms of distribution accuracy.

2 Materials and Methods

2.1 UAV Platform

The Phantom 4 Pro (DJI) is a commercial drone of 1,3 kg composed of four propellers moved by the same number of brushless motors. It includes the Main Controller, the

Table 1 The payload performance of the UAV Phantom 4 pro (DJI)

Company	UAV model	UAV Weight (kg)	Identified payload (kg)	Useful payload (kg)	Volume transported (l)
DJI	Phantom 4 pro	1.30	2.24	0.94	0.30

Table 2 WSP analysis results of the spraying operation without wind

Distribution without wind							
WSP number	1	2	3	4	5	6	
NMD	23.88	143.3	92.5	79.21	75.53	23.88	
WSP coverage (%)	0.20	1.28	1.43	0.87	0.48	0.09	
Drops per cm ⁻²	8.1	11.23	14.78	13.56	12.35	7.64	
Coefficient of variation (%)	112.45	152.64	135.72	134.70	136.97	115.41	

brain of the UAV, who communicate with the brushless motors and the Inertial Measurement Unit (IMU) which contains a Global Positioning System (GPS) module, an accelerometer and a barometer indispensable to guarantee the pilotage of the system.

DJI doesn't declare the Phantom 4 Pro payload but, after some test, it was possible to evaluate the real payload performance of the UAV reassumed in Table 1.

2.2 Spraying System Development

The spraying equipment was developed using low-cost components and materials easily available on the market. It is composed of 5 main parts installed on a plexiglass frame hooked to the base of the Phantom 4 Pro. The electric pump (normally used for aquarium refill) of 12 V and 0,1 A capable to pump the pesticide from the tank to the nozzles at a constant pressure of 1 bar. The XR-extended range nozzles (110° spray angle) produced by *ALBUZ*: a Green drift-reduction nozzle (ISO 110015), a Yellow (ISO11002), Blue (ISO 11003), Red (ISO 11004) and Brown (ISO11005) nozzles. The plastic tank of 0.3 L which represents the biggest encumbrance in terms of space and weight. The sprayer's remote activation system composed of a transmitter (*Futaba TX 8 J R2008SB*, 2.4 G) and a receiver (*Futaba R2008SB 8 ch. + S.BUS*) connected to the battery through a voltage reducer (*PALOLU-2859*, 6 V, and 2,5 A) and an SRC switch (*Alewings* company). The 2200 mAh LiPo battery to provide energy to the system.

All the components were installed on board of the Phantom 4 Pro using a plexiglass supporting plate (5 mm of thick) specifically designed from the *FabLab* (University of Sassari) with the software *Solidworks 2017* and carved with a *CNC Roland MDX 40A* (a 3 mm benchtop milling machine with square head) in order to contain all the sprayer's parts and guarantee the movement of the gimbal. The support plate

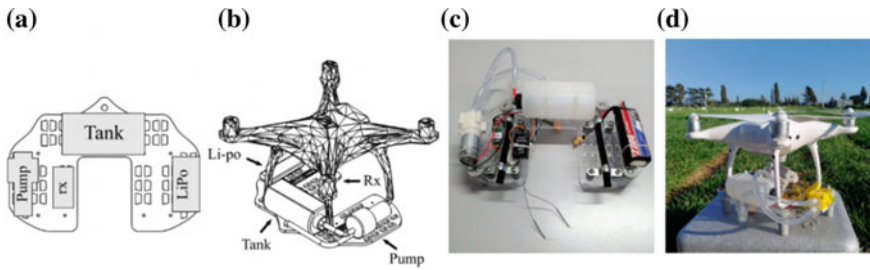


Fig. 1 The plexiglass support project with the pump and the receiver on the left, the LiPo battery on the right and the tank on the back side (a), and his installation on board of the Phantom 4 Pro in a rendering image (b). A photo of the sprayer assembled in all his parts (c) and the prototype of the Sprayer + UAV system during the field tests (d)

was hooked to the base of the UAV with four metal clamps. The battery, the electric pump, and the remote-control system were placed on the opposite side of the plate, whereas the tank was located on the back side (Fig. 1a). The weight of the sprayer with the empty tank was of 0.649 kg.

2.3 Field Test

The tests were executed in February at the experimental-didactic field “*M. Deidda*” (Ottava, Sardegna, Italy) of the Department of Agriculture, University of Sassari. The crop used for the experiments was wheat 0.30 m high in the tillering phase (29–30 of BBCH phenological scale) arranged in parcels (1.2 m × 8 m).

The first object of the field test was to check the distribution efficiency of the proposed spraying platform, assessing the number of drops per cm² and their Normal Median Diameter (NMD) over the WSP using the ALBUZ–Green drift-reduction nozzle (ISO 110015). The second goal was to verify the flight autonomy, expressed in terms of flight time, of the drone with the maximum payload.

During the experiment the spraying system (UAV + sprayer) sprinkled water flying (in manual mode) at 2 m above the ground at 2 m/s of speed over 15 WSPs (as proposed from Martínez-Guanter et al. 2018) arranged in three parallel rows of 5 WSPs each and placed inside the herbaceous crop (Fig. 2a). The WSPs were placed over a supporting structure to guarantee the uptake of the droplets produced from the sprayer (Fig. 2b and c). Three additional WSPs (n°6 in the Fig. 2a) were placed on the right (due to the wind direction from N–E as shown in Fig. 2a) from the others to catch possible drift drops.

The drop distribution on the WSPs was analyzed using the methodology proposed by Zhu et al (2011) and Ghiani et al. (2019). The scanned images (obtained with the *Canon Lide 220* scanner of 1200 dpi) of WSPs (19.86 cm²) were analyzed using a MATLAB 2018b code able to count the number of drops per cm² and measure the Normal Median Diameter of the same.

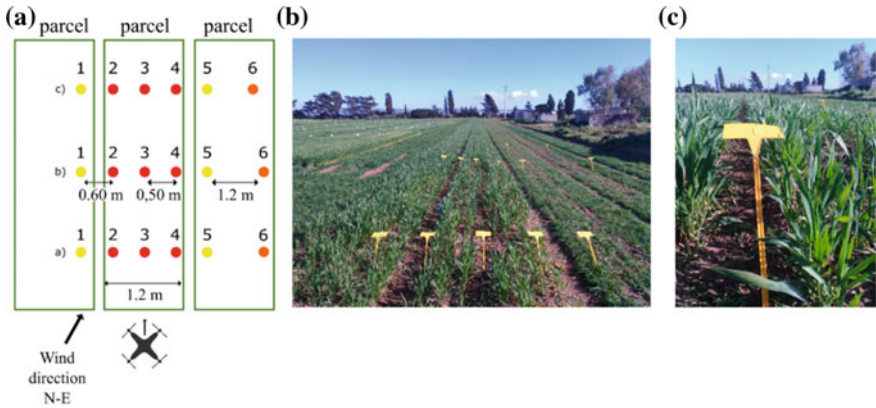


Fig. 2 The schematized disposition (a) and the photo (b) of the WSPs on the parcels of wheat and the drone’s direction above the centrals WSPs during the spraying operation. The relative photo of the supporting system of the WSP to guarantee the droplet’s uptake (c)

The UAV’s battery consumption for the treatment was calculated flying until the end (less than 30%) of battery charge with the sprayer connected to the Phantom 4 Pro and the tank of 0.3 L full of water (overall weight of 0.949 kg). All the data were collected thanks to the flight-log elaborated from the Mission Planner *DJI GO 4* (DJI) which gave a report about the consumption of battery during the entire flight.

The environmental condition (air temperature and wind speed) during the entire field test were evaluated using the *Davis-Winscribe* ultrasonic wind and temperature meter. The measured air temperature was 16.5 °C (± 0.3) and the wind speed of 1.2 m/s (± 0.5).

3 Results and Discussion

The Spraying system was transported by the UAV and it did not suffer mechanical malfunctions during the test. This result can be associated to the right choice of materials and components, and their disposition on the plexiglass support. Thanks to the WSPs analysis executed through the Matlab code, we can state that most of the drops were deposited in the three central WSPs (Fig. 3a) located under the sprayer during the water distribution. One of the biggest limiting factors of the operation was the wind, who took the drone off-course to the right and influenced the drop’s depositions on the WSPs. The drops distribution, usually obtained in the three central WSPs (n°2, 3 and 4 of Tables 3 and 4), were translated to the external WSPs on the right (Fig. 3b).

The above statement is supported by Table 3 in which the coverage (%) of the left side WSPs (n°1 and 2) and the central WSP (n°3) have very low values, and the

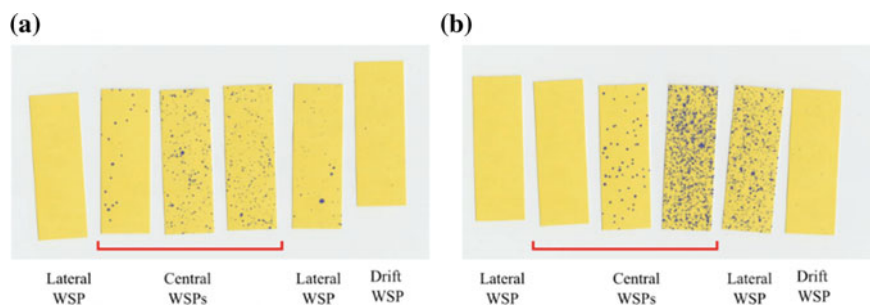


Fig. 3 Water Sensitive Papers derived from the field test using the Green nozzle ISO 110015. In absence of wind the distribution over the central WSPs resulted accurate (a) and it did not show any translation of the droplets deposition on the right like the WSPs obtained in presence of wind (b)

Table 3 WSP analysis results of the spraying operation with wind

Distribution with wind						
WSP number	1	2	3	4	5	6
NMD	33.78	33.78	53.41	106.81	312.32	114.54
WSP coverage (%)	0.02	0.03	0.04	3.47	10.47	0.20
Drops per cm^{-2}	7.64	6.88	6.88	17.26	59.97	8.45
Coefficient of Variation (%)	128.17	131.51	144.41	131.98	126.88	155.29

Table 4 Theoretical spraying performances of the UAV + sprayer system at 2.3 m/s of speed

Nozzle	Distributed volume (l/min)	Height above ground level (m)			
		1	2	3	4
		Distributed volume (l/ha)	Distributed volume (l/ha)	Distributed volume (l/ha)	Distributed volume (l/ha)
Green ISO 110015	0.4	10.00	5.12	3.40	2.52
Yellow ISO 11002	0.52	13.00	6.66	4.42	3.28
Blue ISO 11003	0.75	18.75	9.60	6.38	4.73
Red ISO 11004	1.00	25.00	12.80	8.50	6.30
Brown ISO 11005	1.25	31.25	16.00	10.63	7.88

Table 5 Flight autonomy of the Phantom 4 Pro with two different payloads

Payload	Flight autonomy (min)	Flight time reduction (%)
No payload	33.00	0
Sprayer (0.649 kg) + 0.4 kg	9.25	72

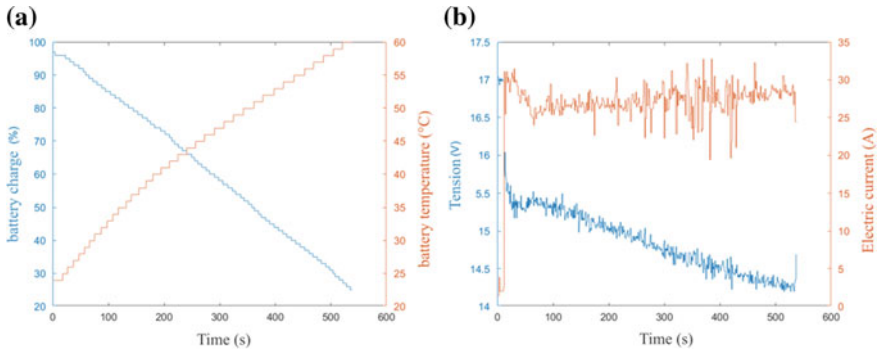


Fig. 4 The performance of the drone equipped with the sprayer system in terms of battery percentage change and temperature increase (a) and the tension variance of the 4 brushless motors and electric current change (b) during the flight

right side WSPs (n°4, 5 and 6) have high values compared to the WSP obtained in no-wind condition (Table 2).

The use of a bigger tank could reduce the number of interventions, but it could lead to more battery change operations, in fact the flight autonomy decreases proportionally to the increase of payload as summarized in Table 5.

From the field test performed with 0.5 L and 1L, the *Phantom 4 Pro* showed limited capacity to raise both weights. The 0.5 kg weight could be carried in the air by removing the camera and the gimbal (0.1 kg) but, in the second case, the drone was only capable to take-off and stay in the air only for 30 s (engine temperature recorded by AIR-Data) showing a critical temperature over 56 °C before starting an automatic landing process.

The ability of *Phantom 4 Pro* to carry the sprayer was testified from the constant electric consumption of LiPo batteries (four cells of 3, 6 V each one) and the constant increase of the temperature (Fig. 4a), the slight decrease of tension and electric current (Fig. 4b), and the absence of any meaningful variation until the full discharge.

4 Conclusions

Despite the limited ability of the Phantom 4 Pro to lift more than 0.9 kg (DJI 2016) due to the low power of the motors, it executed a distribution test efficiently and without

failures, showing the possibility to use commercial drones for Ultra-Low Volume pesticide application. These considerations foreshadow possible scenarios for the use of low-cost drones in certain agricultural operations and not only in the vegetal-productive crop monitoring (Molina 2018). The previous *Phantom 4 Pro* payload limitation could be overcome using the same sprayer equipment discussed in this work in a different low cost UAV model, like the F550 (DJI six rotor wings), a small commercial drone (2 kg of weight) able to lift 1 kg payload for 10 min (brushless motors temperature of 50 °C) using an 8400 mAh battery. The biggest limitations of the sprayer are: the storage capacity of the tank (a bigger tank would permit a greater autonomy of the system and a minor refill operation), the low pressure (only 1 bar) generated from the pump which wouldn't allow a proper use of different nozzle, and the impossibility to implement a power button in the remote controller of the drone (the DJI components are built to prevent some kind of customization) but it was necessary to use an additional one to switch on and off the spraying system. The improvement of mission planner software, making them programmable for flight operations under the limits imposed by current systems, is necessary to guarantee a more precise pesticide distribution over the crop (Tang et al. 2018) and show to the European authority how this kind of spraying equipment could be an alternative spray solution to the traditional machine's application in certain cultural contexts.

Acknowledgements This study was conducted in the framework of two projects funded by the Sardinian Regional Authority, i.e. the project POR FESR Sardegna 2014 – 2020 - “MARS - *Multiple Airdrones Response System*” and PRIN: PROGETTI DI RICERCA DI RILEVANTE INTERESSE NAZIONALE – Bando 2017 “*New technical and operative solutions for the use of drones in Agriculture 4.0*”; and the Innovative and CREAtive SEttlements in Sardinia (INCREASE) for the digital production and rapid prototyping (University of Sassari, 2019).

Bibliography

- Budiyono, A., & Wibowo, S. S. (2007). Optimal tracking controller design for a small-scale helicopter. *Journal of Bionic Engineering*, 4, 272–279.
- Ahmed & Leather. (1994). Suitability and potential of entomopathogenic microorganisms for forest pest management, some points for consideration. *International Journal of Pests Management*, 40.
- de Miguel Molina, B., & Oña, M. S. (2018). The drone sector in Europe. In *Ethics and Civil Drones* (pp. 7–33).
- DJI. (2016). User Manual Phantom 4. <https://www.dji.com/it-en>.
- Giles, D. K., & Billing, R.C. (2015). Deployment and performance of a UAV for crop spraying. *Chemical Engineering Transactions*, 44.
- Glass, et al. (2010). Recent advances in computational fluid dynamics relevant to the modelling of pesticide flow on leaf surfaces. *Pest Management Science*, 66(1), 2–9.
- Zhu, H., Salyani, M., & Fox, R. D. (2011). A portable scanning system for evaluation of spray deposit distribution. *Computers and Electronics in Agriculture*, 76(2011), 38–43.
- Martínez-Guanter, J., Agüera, P., Sassu, A., Vega, J.A., & Pérez-Ruiz, M. (2018). Design and Performance of an Unmanned Aerial System for Precision Pest Management. In *Wageningen AgEng conference*.

- Ghiani, L., Sassu, A., Piccirilli, D., Marcialis, G., & Gambella, F. (2019). Development of a mat-lab code for the evaluation of spray distribution with water-sensitive paper. In *AIIA Mid-Term Conference Matera 2019*.
- Linley, J. R., & Jordan, S. (1992). Effects of ultra-low volume and thermal fog malathion, scourge and naled applied against caged adult *Culicoides furens* and *Culex quinquefasciatus* in open and vegetated terrain. *Journal of the American Mosquito Control Association*, 8, 69–76.
- Tsimbiri, Pamela F., Moturi, Wilkister N., Sawe, Judith, Henley, Phaedra, & Bend, John R. (2015). Health impact of pesticides on residents and horticultural workers in the lake naivasha region, kenya. *Occupational Diseases and Environmental Medicine*, 3, 24–34.
- Pérez-Ruiz, M., Gonzalez-de Santos, P., Ribeiro, A., Fernandez-Quintanilla, C., Peruzzi, A., Vieri, M., et al. (2015). Highlights and preliminary results for autonomous crop protection. *Computers and Electronics in Agriculture*, 110, 150–161.
- Hong, S., Minzan, L., & Zhang, Q. (2012). Detection system of smart sprayers: status, challenges, and perspectives. *International Journal of Agricultural and Biological Engineering*, 5(3).
- Xue, X., Lan, Y., Sun, Z., Chang, C., & Hoffmann, W. C. (2016). Develop an unmanned aerial vehicle based automatic aerial spraying system. *Computers and Electronics in Agriculture*.
- Lan, Y., Shengde, C., & Fritz, B. K. (2017). Current status and future trends of precision agricultural aviation technologies. *International Journal of Agricultural and Biological Engineering*, 10(3).
- Huang, Y., Hoffmann, W. C., Lan, Y., Wu, W., & Fritz, B. K. (2009). Development of a spray system for an unmanned aerial vehicle platform. *American Society of Agricultural and Biological Engineers*. ISSN 0883-8542.
- Tang, Y., Hou, C. J., Luo, S. M., Lin, J. T., Yang, Z., & Huang, W. F. (2018). Effects of operation height and tree shape on droplet deposition in citrus trees using an unmanned aerial vehicle. *Computers and Electronics in Agriculture*, 148(2018), 1–7.
- Yanliang, Z., Qi, L., & Wei, Z. (2017). Design and test of a six-rotor unmanned aerial vehicle (UAV) electrostatic spraying system for crop protection. *International Journal of Agricultural and Biological Engineering*, 10(6).

Agricultural Electrification and Use of Energy

Introduction

Prof. Gianfranco Pergher

President of the 4th Section of the Italian Association of Agricultural Engineering 'Agricultural Electrification and Energy Usage'

Agricultural electrification and energy usage is one fundamental branch in Agricultural engineering. Founded with the purpose to initiate studies and actions to help agricultural farms in the process of electrification and the optimization of energy usage, the 4th Section of the AIIA (Italian Association of Agricultural Engineering) has changed over time its outlook, accompanying the evolution of agricultural production of agri-energy with research topics, and establishing a strong link between farming and forefront technology.

Three of the papers presented in the 4th of the International Mid-Term Conference 2019 AIIA included significant contributions about Life-Cycle Assessment (LCA) of energy conversion technologies, precision photovoltaic irrigation and carrot cultivation and processing. Three more papers were focused on energy efficiency assessment for agricultural tractors, a fully automated dairy farm and heating system for leafy vegetables.

All of these studies are significant contributions in the direction of sustainable, efficient, reliable and profitable integration of advanced energy production and management technologies into the very fabric of modern agricultural farms.

Life Cycle Impact Assessment of Carrot Cultivation and Processing: An Italian Case Study for a Small Family Company in the Marche Region



A. Ilari, D. Duca, G. Toscano, V. Vecchiarelli and E. Foppa Pedretti

Abstract Carrot environmental impact assessment was conducted using the Life Cycle Assessment (LCA) method (ISO 14040:2006; 14044:2006) and following Product Category Rules (PCR) on arable crops. SimaPro® has been used for impact assessment calculation. Goal and scope: the goal was to assess the impact of 1 kg of carrots for different packaging solutions. Life Cycle Inventory (LCI): was carried out with primary data provided by the farmers and by the processing company through interviews and consultation of official documents. Life Cycle Impact Assessment (LCIA): was carried out using CML_IA characterization model. Interpretation: results obtained were interpreted highlighting the phases of greatest impact through a contribution analysis, and the impact variability due to data uncertainties through an uncertainty analysis. The potential impact for the Global Warming (GW) category varies between 1.2×10^{-1} and 2.1×10^{-1} kg CO₂ eq, for Acidification (AC) between 7.04×10^{-4} and 1.06×10^{-3} kg SO₂ eq, for Ozone Depletion (OP) between 2.89×10^{-5} and 5.25×10^{-5} kg C₂H₄ eq, for Eutrophication (EP) between 2.19×10^{-4} and 3.05×10^{-4} kg PO₄³⁻. The greatest impacts were recorded for products with smaller sizes (0.5 kg trays). For larger formats the most impactful phase is field cultivation while for the smaller ones is packaging. As far as transport is concerned, the greatest impact is on the product coming from Mesola and not from Sicily, this is due to greater loading efficiency of transportation from Sicily.

Keywords LCA · Horticulture · Vegetables · Environmental sustainability · Comparative assessment

A. Ilari (✉) · D. Duca · G. Toscano · V. Vecchiarelli · E. Foppa Pedretti
Department of Agricultural, Food and Environmental Sciences, Università Politecnica Delle Marche, Via Breccia Bianche 10, 60131 Ancona, Italy
e-mail: ilari@univpm.it

© Springer Nature Switzerland AG 2020

A. Coppola et al. (eds.), *Innovative Biosystems Engineering for Sustainable Agriculture, Forestry and Food Production*, Lecture Notes in Civil Engineering 67,
https://doi.org/10.1007/978-3-030-39299-4_63

575

1 Introduction

Sustainability in the food sector is considered increasingly important. The reasons are different: from the marketing point of view because consumers are increasingly careful to choose products with low environmental impact but above all because according to different studies the food and beverage sector is one of the most impactful (Tukker et al. 2006). In fact, food and drink cause about 20–30% of the environmental impact of private consumption and represent more than 50% regarding the impact for the eutrophication indicator. Many authors have demonstrated that the sector requires a consistent amount of water and energy (Beccali et al. 2009; Frankowska et al. 2019a) and the production is often organized in complex processes and subprocesses with different impacts. Vegetables have an important role in human diet and have been subjected to impact assessment over the years (Beccali et al. 2009; Ilari and Duca 2018; Frankowska et al. 2019a, b) but only recently several studies were conducted about horticultural products that are considered potentially more impactful than other agricultural products (Wainwright et al. 2014). From FAOSTAT data the world carrot and turnip production in 2017 was over 42 million of tons. China is the first producer with 47% of total production. Italy is only at the 14th place with 553000 tons produced. Considering only the European level Italy is the 6th producer after UK, Ukraine, Poland, Germany and France. Considering the yield, Italy is at a medium level with 36 t/ha (FAOSTAT 2017). This paper focuses on carrot analyzing the environmental impact from field production to industry gate. Goal of the study is to evaluate the environmental impact of 1 kg of carrots at the industrial gate and in different packaging forms. The main reason is to calculate the level of environmental sustainability of the functional unit. Another goal is to identify and propose possible mitigations to the manufacturing process with significant environmental impact.

2 Materials and Methods

LCA analysis was conducted following the reference standards (ISO 2006a, b) and PCR on arable crops (EPD International 2016).

2.1 Scope Definition

The definition of the scope involves the deepening of the following issues:

- Description of the production system to be analyzed
The first step is crop cultivation that takes place in fields located in 4 different Italian regions (Lazio, Abruzzo, Emilia-Romagna and Sicily). The total yearly surface cultivated is 33 ha with a yield of 80 t/ha. The cultivation is performed in continuous cropping system. Although this practice should be avoided the cultivation systems

Table 1 LCI table for transportation (raw data referred to single trip with empty return)

	Distance (km)	Consumption diesel (kg/km)	Consumption urea (kg/km)	Gross capacity (kg)	Payload (kg)
Emilia-Romagna	300	0.28	0.015	13500	12695
Lazio	250	0.28	0.015	13500	12695
Abruzzo	150	0.28	0.015	13500	12695
Sicily	1000	0.28	0.015	25000	24650

in Italy concerning the carrot are very intensive. This is due to the added value of the product compared to other crops and to the reduced size of the fields that hinder the organization of crop rotations. Next step is transport to industry that is performed with a truck from the company excepted for the raw product from Sicily. In Table 1 is reported the raw LCI table for transportation.

The following step is the industry processing. The first elaboration is a cold storage not exceeding 6 days in winter and 24 h in summer. Second elaboration is washing to remove soil and plant residues. It is performed with three machines. First, an immersion tank removes ground, precipitated on the bottom, and leaves floating on the top. In the second machine carrots pass through a washing and brushing system that removes all the remaining ground. The third machine is also a sorter that removes all the broken carrots and small pieces. A further elaboration is a manual selection of the material washed based on the dimension of single pieces; the smaller are intended for smaller size packaging, the bigger for up to 10 kg packaging size. A last elaboration is the packaging. The company produces 8 different formats: small bags of 0.5 and 1.0 kg; trays of 0.5 (2 types) and 1.0 kg; bags of 5.0 and 10.0 kg; chest of 10.0 kg.

– Production system functions

The function of the system is to produce carrots in different packaging.

– Functional Unit (FU)

Following PCR the FU has been set on 1 kg of carrots not considering the packaging mass.

– System boundaries

The system boundaries have been set from cradle to industry gate. The analysis stops at industry gate.

– Allocation procedures

For the study was used an allocation on mass basis for what concerning the residues produced in washing phase and for the different packaging solutions.

– Impact categories and calculation methods.

The calculation method selected for this study is the CML_IA. The impact categories considered according to PCR are: Greenhouse gases emissions (GWP 100 yr kg CO₂ eq), emission of acidifying substances (AC kg SO₂ eq), gas emissions active on ozone (POCP kg C₂H₄ eq), emissions of eutrophic substances (EP

kg PO₄³⁻ eq). other indices considered are byproducts produced, land use, human toxicity (HTP kg 1–4 DB eq), freshwater ecotoxicity (FTP kg 1–4 DB eq), use of water (kg H₂O/FU).

– Data quality requirements

Data collected are primary and representative of the specific case study. The reference year is 2017. From the technological point of view the system under analysis has an average technology. All the data regarding field production, transportation and industry processing are primary data excepted water consumption that has been calculated as an average consumption from secondary data.

– Assumptions and limitations

The main limitation of this study regards the estimation of water consumption. The water used in the washing process comes from artesian aquifers for which it is difficult to assess the actual quantity extracted. In addition to this the water is often reused making it recirculate between one machine and another without an actual measurement system.

2.2 Inventory

The inventory table is calculated by dividing the inventory value of each material and operation by the total final production considering the transformation efficiency. In Tables 2a, 2b and 3 are reported the results of LCI analysis for all the considered processes.

3 Results

In Table 4 is reported the impact for 8 different types of packaging and for 11 impact categories.

From result analysis smaller format shows the greatest impacts. This is due to the larger use of packaging material, in relation to the same quantity of product. For larger format products the impact per FU is lower because of the less use of primary packaging.

Considering all the impact categories on a contribution analysis for the different products the major contributor is the open field production, the second contributor is the packaging phase. Transportation accounts for a limited impact, significant only for GWP, POCP, AP, EP. The other processing phases (temporary cool storage, washing and sorting) contribute for less than 1% for almost all the categories. As an example, contribution analysis for the two most impactful products is reported in Fig. 1.

The comparison reported in Fig. 1 is interesting because considering two alternative products. In fact, industry customers require different formats depending on

Table 2a LCI table referred to 1 kg of fresh processed product (cultivation input, emissions and primary output)

Input/output cultivation	Amount/UF	Unit		Emission to soil	Amount/UF	Unit
Land use (arable)	1.53×10^{-5}	ha		Pendimethalin	1.19×10^{-5}	kg
Soil plowing	1.38×10^{-3}	l	Diesel	Chlorantraniliprole	4.56×10^{-8}	kg
Convexing	3.07×10^{-4}	l	Diesel	Azoxystrobin	2.61×10^{-6}	kg
Sowing	1.84×10^{-4}	l	Diesel	Copper oxychloride	9.58×10^{-6}	kg
Seeds	9.20×10^{-5}	kg		Difenoconazole	1.30×10^{-6}	kg
Fertilization	9.20×10^{-4}	l	Diesel	Azoxystrobin	2.61×10^{-6}	kg
Pesticide application	5.37×10^{-4}	l	Diesel	Lambda Cyhalothrin	1.30×10^{-7}	kg
Weeding	2.30×10^{-4}	l	Diesel	Copper oxychloride	9.58×10^{-6}	kg
Irrigation	6.14×10^{-3}	l	Diesel	Emission to water		
Harvesting	9.20×10^{-4}	l	Diesel	Nitrates	2.83×10^{-4}	kg
Bins handling	4.60×10^{-4}	l	Diesel	Phosphorus total	9.11×10^{-6}	kg
Water (irrigation)	3.83	l		Phosphorus groundwater (leached)	2.81×10^{-7}	kg
Emission to air				Phosphorus river (run-off)	7.02×10^{-7}	kg
NH ₃	7.25×10^{-5}	kg		Phosphorus river (eroded)	8.13×10^{-6}	kg
N ₂ O (direct)	1.01×10^{-5}	kg		Pendimethalin	6.98×10^{-7}	kg
NO (direct)	6.42×10^{-6}	kg		Chlorantraniliprole	2.68×10^{-9}	kg
N ₂ O (indirect)	5.20×10^{-6}	kg		Azoxystrobin	1.53×10^{-7}	kg
N ₂ O (residues)	1.27×10^{-7}	kg		Copper oxychloride	5.64×10^{-7}	kg
N ₂ O (leaves)	2.84×10^{-5}	kg		Difenoconazole	7.67×10^{-8}	kg

(continued)

Table 2a (continued)

Input/output cultivation	Amount/UF	Unit		Emission to soil	Amount/UF	Unit
Pendimethalin	1.40×10^{-6}	kg		Azoxystrobin	1.53×10^{-7}	kg
Chlorantraniliprole	5.37×10^{-9}	kg		Lambda Cyhalothrin	7.67×10^{-9}	kg
Azoxystrobin	3.07×10^{-7}	kg		Copper oxychloride	5.64×10^{-7}	kg
Copper oxychloride	1.13×10^{-6}	kg		Primary output transportation		
Difenoconazole	1.53×10^{-7}	kg		Carrots	1.0	kg
Azoxystrobin	3.07×10^{-7}	kg		Carrots (losses)	1.63×10^{-3}	kg
Lambda Cyhalothrin	1.53×10^{-8}	kg		Vegetal residues	1.53×10^{-1}	kg
Copper oxychloride	1.13×10^{-6}	kg				

final purchasers (1 kg formats for large-scale retail trade, 10 kg for small markets) the 0.5 kg formats are completely alternative, and the two solutions depend only on marketing choices. Polyethylene tray carrots are from 3 to 31% less impactful. This difference is all due to the different packaging solution. In order to assess the impact variability due to the data uncertainties, a Montecarlo analysis was conducted for open field and industry phases. For open field the variability results between 5 and 23% and the only data uncertainties regard emission from fertilizers (IPCC emission factors).

For industry phase the impact variability is lower and ranges between 7 and 11%. In this case the variability is mainly due to energy (from country mix) and background processes of LCA database (included in SimaPro software).

4 Conclusions

Considering scientific literature the results of the present study are comparable or slightly lower if compared with other specific study like (Raghu, 2014).

The difference between this case study and the one cited lie in the transport phase which has much more significant incidence because carrots are transported from Sicily up to Finland. The other phases including cultivation and processing are essentially similar in the two studies. From the contribution analysis it was possible to observe which are the main causes for the absolute impact. The cultivation phase has the greatest impact, followed by packaging and transport. In cultivation there

Table 2b LCI table referred to 1 kg of fresh processed product (transportation and industry processing)

Input	Amount/UF	Unit	Transport to plant			
Fertilizers			Destination	Distance		
Dap eurochem®	1.53×10^{-3}	kg	300	km	320.71	kg km
Agromaster®	2.30×10^{-3}	kg	250	km	267.26	kg km
Entec perfect®	2.30×10^{-3}	kg	150	km	160.35	kg km
N total	9.43×10^{-4}	kg	1000	km	1069.02	kg km
P total	1.42×10^{-3}	kg	Bin HDPE	6.91×10^{-3}		kg
K total	6.21×10^{-4}	kg	Bigbag (Sicily) polyethylene	3.53×10^{-5}		kg
Pesticides			Input	Amount/UF	Unit	
Water (pesticides)	7.36×10^{-2}	l	Storage			
Stomp aqua®	3.07×10^{-5}	l	Input	Average		
Altacor®	1.53×10^{-6}	kg	Electricity	8.02×10^{-3}	kWh	
Ortiva®	1.22×10^{-5}	l	Input	Average		
Ossiclor 35WG®	3.22×10^{-5}	kg	Pre-washing	8.61×10^{-5}	kWh	
Score 25 EC®	6.13×10^{-6}	l	Washer/brusher	1.18×10^{-4}	kWh	
Ortiva®	1.22×10^{-5}	l	Sorter	1.08×10^{-4}	kWh	
Karate zeon®	1.53×10^{-6}	l	Water pumping	1.62×10^{-4}	kWh	
Ossiclor 35WG®	3.22×10^{-5}	kg	Water	$2.32 \times 10^{+1}$	l	
			Output			
			Residues (feed)	2.32×10^{-2}	kg	
			Herb and stones	2.79×10^{-3}	kg	
			Ground	3.83×10^{-2}	kg	
			Processing			
			Input	Average		
			Conveyors	1.10×10^{-4}	kWh	
Output						
Residues (feed)	4.63×10^{-3}	kg				

Table 3 LCI table for packaging referred to FU for each format

	Tray 1 kg	Tray 0.5 kg type 2	Tray 0.5 kg type 1	Bag 5 kg	Bag 10 kg	Bag 1 kg	Small bag 0.5 kg	Bo× 10 kg
LDPE tray ^a	1.6×10^{-2}	2.0×10^{-2}						
Printed paper ^a	5.1×10^{-4}	1.0×10^{-3}	1.0×10^{-3}	1.0×10^{-4}	5.0×10^{-5}	5.0×10^{-4}	1.0×10^{-3}	6.1×10^{-5}
packaging film LLDP × 10 ^a	1.0×10^{-3}	2.0×10^{-3}	2.0×10^{-3}	3.1×10^{-3}	3.8×10^{-3}	3.5×10^{-3}	3.0×10^{-3}	2.6×10^{-3}
Polystyrene ^a			8.0×10^{-3}					
Electricity ^b	1.3×10^{-3}	2.6×10^{-3}	2.6×10^{-3}			8.0×10^{-4}	1.6×10^{-3}	

^au.m. kg/FU, ^bu.m. kWh/FU

are in fact a long series of direct emissions derived both from the various field operations, but above all also from the use of fertilizers and plant protection products. In transport, the direct emissions due to fuel combustion are equally important, while the packaging assumes a considerable importance for the use of high amounts plastic material compared to the product mass. The impacts related to the refrigeration of the carrots, to the washing and to the calibration together presented a rather limited impact compared to the other phases.

Table 4 Total impact for 1 kg of carrots in different packaging formats

Category	Unit	Tray 1 kg	Tray 0.5 kg type 2	Tray 0.5 kg type 1	Bag 5 kg	Bag 10 kg	Bag 1 kg	Small bag 0.5 kg	Box 10 kg
ADP	kgSb eq	5.49×10^{-7}	5.60×10^{-7}	5.41×10^{-7}	5.10×10^{-7}	5.11×10^{-7}	5.21×10^{-7}	5.27×10^{-7}	5.17×10^{-7}
ADP (fossil fuels)	MJ eq	2.54	2.97	2.05	6.13×10^{-1}	6.61×10^{-1}	1.09	1.26	1.05
GWP100yr	kgCO ₂ eq	1.88×10^{-1}	2.06×10^{-1}	1.79×10^{-1}	1.16×10^{-1}	1.18×10^{-1}	1.35×10^{-1}	1.42×10^{-1}	1.32×10^{-1}
ODP	kgCFC-11 eq	8.16×10^{-9}	8.86×10^{-9}	7.36×10^{-9}	5.02×10^{-9}	5.04×10^{-9}	5.79×10^{-9}	6.17×10^{-10}	5.70×10^{-9}
HTP	kg1,4-DB eq	2.63×10^{-2}	2.94×10^{-2}	2.39×10^{-2}	1.49×10^{-2}	1.50×10^{-2}	1.80×10^{-2}	1.96×10^{-2}	1.71×10^{-2}
FEP.	kg1,4-DB eq	4.27×10^{-2}	4.54×10^{-2}	4.04×10^{-2}	3.17×10^{-2}	3.18×10^{-2}	3.45×10^{-2}	3.60×10^{-2}	3.41×10^{-2}
MEP	kg1,4-DB eq	$6.55 \times 10^{+1}$	$7.64 \times 10^{+1}$	$5.88 \times 10^{+1}$	$2.84 \times 10^{+1}$	$2.86 \times 10^{+1}$	$3.95 \times 10^{+1}$	$4.64 \times 10^{+1}$	$3.56 \times 10^{+1}$
TEP	kg1,4-DB eq	1.71×10^{-4}	1.87×10^{-4}	1.56×10^{-4}	1.06×10^{-4}	1.06×10^{-4}	1.23×10^{-4}	1.32×10^{-4}	1.20×10^{-4}
POCP	kgC ₂ H ₄ eq	4.78×10^{-5}	5.26×10^{-5}	4.66×10^{-5}	2.89×10^{-5}	2.92×10^{-5}	3.49×10^{-5}	3.79×10^{-5}	3.36×10^{-5}
AP	kgSO ₂ eq	9.88×10^{-4}	1.06×10^{-3}	9.40×10^{-4}	7.12×10^{-4}	7.18×10^{-4}	7.85×10^{-4}	8.17×10^{-4}	7.66×10^{-4}
EP	kgPO ₄ ³⁻ eq	2.86×10^{-4}	3.03×10^{-4}	2.70×10^{-4}	2.17×10^{-4}	2.17×10^{-4}	2.35×10^{-4}	2.44×10^{-4}	2.31×10^{-4}

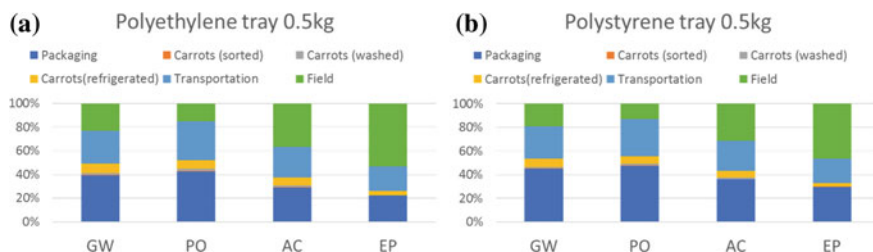


Fig. 1 GWP, POCP, AP, EP for Polyethylene tray 0.5 kg (a) and Polystyrene tray 0.5 kg (b)

Acknowledgements The activity presented in the paper has been conducted inside a bachelor's degree research program. The authors are grateful to the company C.I.L.P.O. DI VECCHIARELLI MARIO & C. S.N.C. that provided the necessary data for the analysis.

References

- Beccali, M., Cellura, M., Iudicello, M., & Mistretta, M. (2009). Resource consumption and environmental impacts of the agrofood sector: life cycle assessment of Italian citrus-based products. *Environmental Management*, 43(4), 707–724.
- EPD International. (2016). Arable Crops, product category classification UN CPC 011, 014, 017, 019. EPD website, International EPD system.
- FAOSTAT. (2017). FAOSTAT crop database for carrot and tunips access to database on 5/21/2019.
- Frankowska, A., Jeswani, H. K., & Azapagic, A. (2019a). Environmental impacts of vegetables consumption in the UK. *Science of the Total Environment* 682, 80–105.
- Frankowska, A., Jeswani, H. K., & Azapagic, A. (2019b). Environmental sustainability issues in the food-energy-water nexus in the UK vegetables sector: Energy and water consumption, Energy Procedia.
- Ilari, A., & Duca, D. (2018). Energy and environmental sustainability of nursery step finalized to “fresh cut” salad production by means of LCA. *International Journal of Life Cycle Assessment*, 23(4), 800–810.
- ISO. (2006a). ISO 14040:2006—Environmental management—Life cycle assessment—Principles and framework.
- ISO. (2006b). ISO 14044:2006—Environmental management—Life cycle assessment—Requirements and guidelines.
- Raghu, K. C. (2014). *Comparative lifecycle assessment on organic and conventional carrots case: carrots from south-savo and imported carrots from Italy*. Master's Degree: Lappeenranta University of Technology.
- Tukker, A., Huppes, G., Guinée, J., Heijungs, R., de Koning, A., van Oers, L., Suh, S., Geerken, T., van Holderbeke, M., Jansen, B., Nielsen, P., Eder, P., & Delgado, L. (2006). Environmental Impact of Products (EIPRO). Analysis of the Life Cycle Environmental Impacts Related to the Final Consumption of the EU-25, Joint Research Centre, Institute for Prospective Technological Studies.
- Wainwright, H., Jordan, C., & Day, H. (2014). Environmental impact of production horticulture. In G. R. Dixon & D. E. Aldous (Eds.), *Horticulture: Plants for people and places* (vol. 3, p. 503).

Does Precision Photovoltaic Irrigation Represent a Sustainable Alternative to Traditional Systems?



Giuseppe Todde, Maria Caria, Antonio Pazzona, Luigi Ledda and Luis Narvarte

Abstract The objective of this study was to assess whether precision photovoltaic irrigation represents a sustainable alternative to traditional systems, where the energy and environmental performances were firstly evaluated through energy and carbon payback times (EPBT and CPBT). The study involved five Photovoltaic Irrigation Systems (PVIS), ranging from 40 to 360 kW_p, installed in Spain, Portugal, Morocco and Italy. The results show an average EPBT of 3.3 years and CPBT of 6.3 years, with an energy return on energy invested (EROI) of 9.0. Additionally, the PVIS were able to achieve low emission rates with an average of 77.4 g CO₂e per kWh produced. The energy and environmental performance of the PVIS are closely influenced by weather conditions, irrigation requirements and water availability. Moreover, the implementation of precision PVIS allowed improving the irrigation practices, avoiding the exploitation of natural resources and the emissions of large amounts of GHG to the environment.

Keywords Solar irrigation · Precision agriculture · Energy and environmental emissions

1 Introduction

Over the last years, traditional agricultural production has been converted to intensive cultivation systems, characterized by high production yields and better product quality. Although this conversion is improving the profitability of farms, it requires a large amount of energy input which generates resultant environmental impacts. Among the several activities carried out on irrigated agricultural productions, water

G. Todde (✉) · M. Caria · A. Pazzona · L. Ledda
Department of Agricultural Science, Università degli Studi di Sassari, Viale Italia 39, 07100 Sassari, Italy
e-mail: gtodde@uniss.it

L. Narvarte
Solar Energy Institute, Universidad Politecnica de Madrid, Av. Complutense 30, 28040 Madrid, Spain

© Springer Nature Switzerland AG 2020
A. Coppola et al. (eds.), *Innovative Biosystems Engineering for Sustainable Agriculture, Forestry and Food Production*, Lecture Notes in Civil Engineering 67,
https://doi.org/10.1007/978-3-030-39299-4_64

pumping represents one of the main energy-demanding task (Peng et al. 2019; Singh et al. 2019; Cappelletti et al. 2014). Likewise, the improvement of the environmental burden of irrigation water pumping has been found a key factor to increase the sustainability of food productions (Benbi 2018; Xu et al. 2015).

Numerous studies have been conducted with the aim to reduce the requirements of fossil energy for irrigation practices (Chacón et al. 2019; Lima et al. 2018; Navarro Navajas et al. 2012). Moreover, the need to improve the irrigation efficiency in agricultural productions is leading farmers, stakeholders and researchers to invest and support the application of precision agriculture solutions (Sarkar and Majumder 2019) combined to the production of renewable energy (Chilundo et al. 2019; Picazo et al. 2018).

Precision agriculture is a farming management concept which implies the use of modern technologies to know precisely what inputs are needed where, in what amount and when. The goal of precision agriculture is to optimize returns of inputs while preserving the use of natural resources and the associated environmental emissions (McBratney et al. 2005). Likewise, the setting up of precision irrigation techniques contributed to mitigate negative issues related to climate change (Deligios et al. 2019).

The installation of photovoltaic (PV) systems that allow the production of renewable energy for irrigation practices is promptly increasing in the last years (Merida García et al. 2018; Sebbagh et al. 2018; Maddalena et al. 2018).

The photovoltaic electricity is considered clean energy, which does not affect the exploitation of natural resources and the related environmental impact during the operative phase. However, the manufacturing and construction of PV systems require a determinate amount of primary energy inputs, which in turn, generate the emission of pollutants to the environment (Wong et al. 2016). In order to define the energy and environmental impact of a product, the Life Cycle Assessment (LCA) methodology is considered one of the most complete tools available. A life cycle approach allows quantifying the amount of input and output throughout the entire lifetime of the PV systems, starting from raw materials extraction, manufacturing, transport, operation during its life, until its final recycling treatment.

Knowing the energy and environmental performances will enable to assess several important environmental indicators, such as the energy and carbon payback times and energy return on energy invested (EPBT, CPBT and EROI) for PVIS. Thus, the objective of this study was to assess whether precision photovoltaic irrigation represents a sustainable alternative to traditional systems.

2 Materials and Methods

This study involved five PVIS installed in the Mediterranean basin in the framework of the European Union Horizon 2020 Program's Maslowaten Project. One of the main objectives of the project was to reduce the irrigation water consumption using automatism, ICT, and precision agriculture-based solution. In order to achieve these

results, a complete fertigation controller has been implemented in the irrigation systems. This automatism allows to precisely manage irrigation and fertigation plans, processing a large number of variables related to soil humidity, air temperature, water needs, irrigation schedules, etc. The irrigation controller has also the availability to be managed from a specific app installed in mobile devices.

2.1 Data Source and Technology Description

The PVIS installations were built using the same technologies and modularity. The photovoltaic modules have a nominal power of 250 Wp, a module efficiency $\eta = 15.1\%$ and contain 60 multi-crystalline silicon cells with a total weight of 21 kg.

The PVIS are equipped with solar trackers and arranged on horizontal axis north-south (N-S).

The PVIS were installed in productive farms replacing traditional irrigation systems, which mean powered by fossil fuels and without precision based solutions.

The studied photovoltaic systems are exclusively devoted to supply energy to the irrigation systems; extra electricity production cannot be exchanged with the grid and no battery storage is allowed. Among the five sites, three of them are arranged as stand-alone PVIS, while the other two are hybrid systems. All PVIS have been installed in productive farms, where the main characteristics are described below: “Villena-360”, it represents the largest stand-alone photovoltaic system studied in this work, with a nominal power of 360 kWp, was mounted in Villena (Long 0° 50' 32" W; Lat 38° 14' 19" N) Spain. This PVIS is hosted by an irrigation community to supply water to several crop producers; “Alaejos-160”, this stand-alone PV generator, which holds 160 kWp, was installed in Alaejos (Long 5° 16' 36" W; Lat 41° 16' 21" N), Spain. The farm area is extended for 80 ha where the most representative crops are sugar beet, potato and poppy. The annual water needs were about 360,000 m³; “Uri-40”, the smallest stand-alone PV system, 40 kWp, was installed in Uri (Long 40,62° N; Lat 8,47° E), Italy. The farm, devoted to the cultivation of artichoke and wheat, holds 10 ha of land equipped with a sprinkler irrigation system; “Tamellalt-120”, it represents a hybrid (PV + grid) photovoltaic irrigation system of 120 kWp installed in Tamellalt (Long 7° 31' 12" W; Lat 31° 46' 48" N), Morocco. The farm holds 230 ha of intensive olive cultivation, divided into 8 irrigation sectors; “Alter do Chao-140”, a hydraulic hybridization of photovoltaic (140 kWp) and diesel generator, was installed in Alter do Chao (Long 7° 41' 35" W; Lat 39° 10' 0,03" N), Portugal. The farm holds about 215 ha of super-intensive olive orchards, irrigated by means of three 45 kW centrifugal pumps. The irrigation network, divided into 14 sectors, is equipped with a drip irrigation system served at constant flow and pressure.

2.2 Data Analysis and Environmental Indicators

The life cycle assessment (LCA) approach was adopted to evaluate whether precision photovoltaic irrigation represents a sustainable alternative to traditional systems. The study analyzed the primary energy embodied in the PVIS, the related environmental emissions and the advantages of using these innovative systems. In order to assess the energy and environmental load of PVIS, system boundaries were set from the extraction of raw materials through the manufacturing process, distribution, utilization and end of life treatment as recyclable waste (cradle to grave), while the functional unit was set as 1 kWp of PV power.

The type and amount of the overall components installed in each PVIS were collected during year 2017. The inventory list included: PV modules; frequency converter; solar trackers; other components (wiring, cables, controllers, etc.); civil works; pumps; fence; maintenance; waste disposal; transportation. The extended set of inputs and outputs were then multiply by the related energy and emission factors.

The impact assessment categories considered in this study were the cumulative energy demand (CED), which is used to quantify the primary energy requirements of a system and the climate change, which analyze the amount of greenhouse gases (GHG) emitted during the entire life cycle of a product. The CED is indicated as MJ of primary energy used, while the amount of GHG is quantified in kg of carbon dioxide equivalent (CO₂e), both expressed per unit of PV peak power or PV energy gained. Additionally, the energy return on energy invested (EROI), the energy payback time (EPBT) and the carbon payback time (CPBT) were assessed. The EROI indicator represents a dimensionless value where the amount of energy obtained from a generation system is divided by the amount of energy invested. The EPBT represents the time (years) necessary for PVIS to save the same amount of primary energy consumed during its life cycle, while the CPBT refers to the years necessary for PVIS to avoid the same amount of CO₂e emitted during its life cycle. The forecasted electricity and related CO₂e emissions were assessed, for 25 years of working life, considering the nominal power of the PV system, the installation site, the irrigation needs and the water availability.

Moreover, the analyses of the electricity and diesel fuel requirements and related emissions, before and after the installation of the PVIS were performed for the irrigation seasons 2016 and 2017. The cumulative energy demand and related emission rates for the electricity mix at the plant of each country involved are reported in Table 1.

3 Results and Discussions

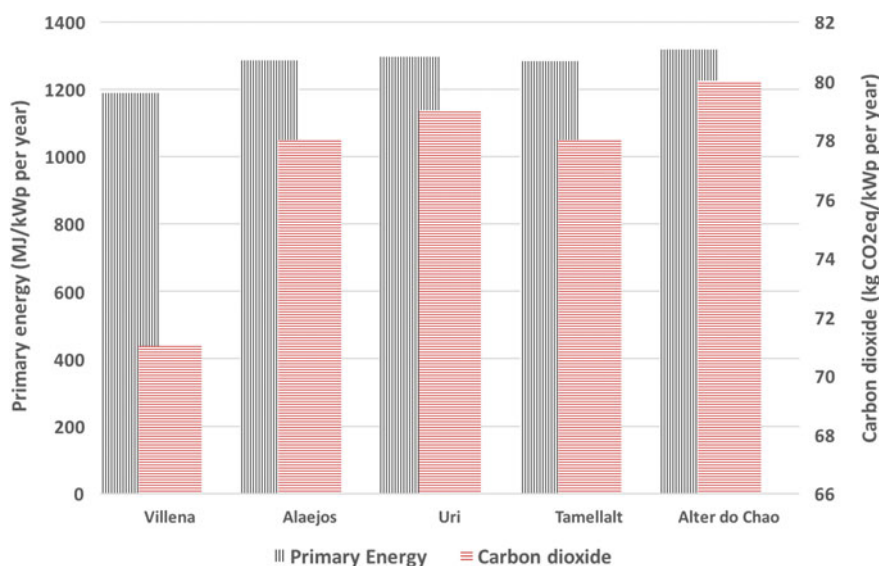
The assessment of the cumulative energy demand and the environmental impact of PVIS was carried out dividing the overall primary energy requirements and related GHG by the nominal power size of the PVIS and for the life span of each component.

Table 1 Cumulative energy demand and related emission rates of specific country mix electricity generation at the plant

Item	MJ	Unit	kg CO ₂ e	Unit	References
Electricity (Italy)	9.67	MJ/kWh	0.3306	kg CO ₂ e/kWh	Itten et al. (2014); Ispra (2017)
Electricity (Spain)	9.76	MJ/kWh	0.2483	kg CO ₂ e/kWh	Itten et al. (2014); IEA (2015)
Electricity (Portugal)	9.19	MJ/kWh	0.2827	kg CO ₂ e/kWh	
Electricity (Morocco)	9.91	MJ/kWh	0.6448	kg CO ₂ e/kWh	
Diesel fuel	36.8	MJ/L	0.280	kg CO ₂ e/kWh	ENEA (2018)

Thus, the average primary energy in PVIS was $1,274 \pm 49.5$ MJ.kWp⁻¹ per year, where the photovoltaic modules represent the main quota of the embodied energy requirements (78.2%). The other installed components (i.e. the inverters, the plant steel frame and the other items) were together responsible for about 15.5% of this distribution, while minor values were found for fence, transport and pumps.

In regards to the annual emissions of carbon dioxide from PVIS throughout its lifetime, the mean value was 77.2 ± 3.6 kg CO₂e per kWp of nominal power. Slight differences were observed, for the energy and environmental aspects, among the five systems (Fig. 1), where the lowest values were found in the largest PV plant (Villena). The assessment of energy and environmental indicators takes into account several variables that influenced the amount of energy obtained by the PVIS. In fact,

**Fig. 1** Annual embodied primary energy and related carbon dioxide emissions per kWp from cradle to grave (average among the five PVIS)

EPBT, CPBT and EROI indicators are largely affected by the irradiation and weather conditions of the specific installation site, PV efficiency, water availability and effective use of the PVIS by the farmers. The average energy and carbon payback times obtained from the five installations accounted for 3.3 ± 1.5 and 6.2 ± 3.1 years, respectively. This means that, in 25 years of lifetime, the 86.8% of the electricity produced by the PVIS will not cause the depletion of natural resources, while the 75.2% of the energy generated will not produce any emission of CO₂e. The energy and environmental benefits obtained by using PVIS are clearly highlighted by these results. However, among the EPBT and CPBT of the five PVIS, considerable differences were observed. In fact, the lowest values, both for EPBT and CPBT, were found in Tamellalt and Villena sites. These outcomes are mainly due to the large quota of electricity generated, as a result of the higher use of the PVIS. External factors and power size of PV plants may play a significant role when assessing energy and environmental indicators. Likewise, EPBT of PV plants ranging from 1.93 to 9.08 years, were found in other scientific studies (Todde et al. 2018, 2019; Yu and Halog 2015; Garcia-Valverde et al. 2009).

In references to the results related to the EROI indicator, as stated by Hall et al. (2009), this value should be at least 3:1 to be considered a viable energy source for the society. In this study, the average EROI assessed for the five PVIS accounted for 9.0 ± 3.8 , where the greater value (12.9) was found in the Villena PVIS and the lowest one in the Italian PVIS (4.8). Moreover, a study conducted on ten multi-Si photovoltaic systems reported an average harmonized EROI of 11.6 ± 5.2 (Bhandari et al. 2015).

Knowing the amount of emissions embodied in PVIS, from cradle to grave, and dividing these values by the forecasted electricity generated in the 25 years of expected operative life, an average emission rate of 78 ± 34 g CO₂e per kWh was found. This important result underlined the environmental advantages of using precision photovoltaic irrigation systems. In fact, the emission rates of the studied PVIS were from 2.7 to 13.4 times lower than those from the conventional electricity produced in the countries involved (as also reported in Table 1). The large differences obtained in these outcomes are strongly related to two main issues: first, the production of electricity from the PV plant is exclusively devoted (no battery storage is allowed or exchange with the grid) to the irrigation requirements, which in turn are closely related to external factors such as weather conditions, water needs and water availability; second, the specific emission rate of the country, since larger emission rates improve the environmental advantages of PVIS.

As also reported by other authors, similar emission rates of 37 and 44 g CO₂e per kWh were found for a simulated large scale PV system installed respectively in Morocco and France (Masakazu et al. 2016), while Beylot et al. (2014) obtained from 34.5 and 53.5 g CO₂e per kWh for a scenario involving four large size PV systems.

The data related to the amount of fossil energy requirements and related carbon dioxide emissions, before and after the installation of the five PVIS, are summarized in Table 2. Although the operational performances of PVIS are available for the firsts operative years, it highlighted the magnitude of the energy and environmental

Table 2 Direct operational fossil energy consumption and related emissions before and after installation of the PVIS, 2016–2017

Time frame	Items	Average among 5 PVIS
Before installation PVIS	Energy consumed (GJ)	2459.4
	Energy emissions (t CO ₂ e)	114.7
After installation PVIS	Energy consumed (GJ)	451.2
	Energy emissions (t CO ₂ e)	30.4
Energy-carbon balance	Energy saved (GJ)	2008.2
	Energy saved (%)	82
	Emissions avoided (t CO ₂ e)	84.3
	Emissions avoided (%)	74

advantages achieved. The installation of real-scale PVIS in productive farms allowed to save, as average of the five sites, 82% of the conventional energy requirements, also avoiding 74% of the CO₂e emissions. Thus, innovative and precision photovoltaic irrigation systems enabled to increase the economic outlook of cropping systems.

4 Conclusions

The outcomes presented in this study clearly underline the energy and environmental benefits obtained through the use of precision photovoltaic irrigation systems. The application of these innovative solutions enables to reduce the depletion of natural resources and to avoid the emission of pollutants to the ecosystem. The environmental indicators highlighted the linkage between weather conditions and irrigation management. Moreover, the implementation of precision agricultural solutions in traditional irrigation systems allowed to improve the environmental and economic sustainability of farms.

Acknowledgements This work was supported by the European Union's Horizon 2020 research and innovation program under grant agreement No. 640771.

References

Benbi, D. K. (2018). Carbon footprint and agricultural sustainability nexus in an intensively cultivated region of Indo-Gangetic Plains. *Science of the Total Environment*, 644, 611–623.

- Beylot, A., Payet, J., Puech, C., Adra, N., Jacquin, P., Blanc, I., et al. (2014). Environmental impacts of large-scale grid-connected ground-mounted PV installations. *Renewable Energy*, *61*, 2–6.
- Bhandari, K. P., Collier, J. M., Ellingson, R. J., & Apul, D. S. (2015). Energy payback time (EPBT) and energy return on energy invested (EROI) of solar photovoltaic systems: A systematic review and meta-analysis. *Renewable and Sustainable Energy Reviews*, *47*, 133–141.
- Cappelletti, G. M., Ioppolo, G., Nicoletti, G. M., & Russo, C. (2014). Energy requirement of extra virgin olive oil production. *Sustainability*, *6*, 4966–4974.
- Chilundo, R. J., Neves, D., & Mahanjane, U. S. (2019). Photovoltaic water pumping systems for horticultural crops irrigation: Advancements and opportunities towards a green energy strategy for Mozambique. *Sustainable Energy Technologies and Assessment*, *33*, 61–68.
- Chacón, M., Díaz, J. A., Morillo, J., & McNabola, A. (2019). Pump-as-turbine selection methodology for energy recovery in irrigation networks: Minimising the payback period. *Water*, *11*, 149.
- Deligios, P. A., Chergia, A. P., Sanna, G., Solinas, S., Todde, G., Narvarte, L., et al. (2019). Climate change adaptation and water saving by innovative irrigation management applied on open field globe artichoke. *Science of the Total Environment*, *649*, 461–472.
- ENEA. (2018). Agenzia Nazionale Efficienza Energetica. Poteri calorifici inferiori dei combustibili e fattori di emissione della CO₂. <http://www.ufficienzaenergetica.enea.it/>.
- Fattori di Emissione Atmosferica di CO₂e Altri Gas a Effetto Serra del Settore Elettrico. http://www.isprambiente.gov.it/files2017/pubblicazioni/rapporto/R_257_17.pdf
- Garcia Valverde, R., Miguel, C., Martinez Bejar, R., & Urbina, A. (2009). Life cycle assessment study of a 4.2 kWp stand-alone photovoltaic system. *Solar Energy*, *83*, 1434–1445.
- Hall, C. A. S., Balogh, S., & Murphy, D. J. R. (2009). What is the minimum EROI that a sustainable society must have? *Energies*, *2*, 25–47.
- International Energy Agency. (2015). CO₂ Emissions from Fuel Combustion. Statistics. # IPCC. (2006). Revised IPCC Guidelines for National Greenhouse Gas Inventories: Reference Manual. Retrieved January 16, 2018, from <https://emissionfactors.com>, <http://www.iea.org/stats/index.asp>.
- Itten, R., Frischknecht, R., & Stucki, M. (2014). Life Cycle Inventories of Electricity Mixes and Grid. Version 1.3. Retrieved February 2, 2019, from <http://studylib.net/doc/18476974/life-cycle-inventories-of-electricity-mixes-and-grid-esu>.
- Lima, F. A., Martínez-Romero, A., Tarjuelo, J. M., & Córcoles, J. I. (2018). Model for management of an on-demand irrigation network based on irrigation scheduling of crops to minimize energy use (Part I): Model development. *Agricultural Water Management*, *210*, 49–58.
- Maddalena, E. T., Moraes, C. D. S., Bragança, G., Junior, L. G., Godoy, R. B., & Pinto, J. O. P. (2018). Photovoltaic water-pumping system with low decoupling capacitance for remote communities. In *2018 IEEE industry applications society annual meeting (IAS)*.
- Masakazu, I., Lespinats, S., Merten, J., Malbranche, P., & Kurokawa, K. (2016). Life cycle assessment and cost analysis of very large scale PV systems and suitable locations in the world. *Progress in Photovoltaics: Research and Applications*, *24*, 159–174.
- McBratney, A., Whelan, B., & Ancev, T. (2005). Future directions of precision agriculture. *Precision Agriculture*, *6*, 7–23.
- Merida García, A., Fernandez García, I., Camacho Poyato, E., Montesinos Barrios, P., & Rodríguez Díaz, J. A. (2018). Coupling irrigation scheduling with solar energy production in a smart irrigation management system. *Journal of Cleaner Production*, *175*, 670–682.
- Navarro Navajas, J. M., Montesinos, P., Camacho Poyato, E., & Rodríguez Díaz, J. A. (2012). Impacts of irrigation network sectoring as an energy saving measure on olive grove production. *Journal of Environment Management*, *111*, 1–9.
- Peng, Y., Xiao, Y., Fu, Z., Dong, Y., Zheng, Y., Yan, H., et al. (2019). Precision irrigation perspectives on the sustainable water-saving of field crop production in China: Water demand prediction and irrigation scheme optimization. *Journal of Cleaner Production*, *230*, 365–377.

- Picazo, M. A., Juárez, J., & Garcia-Márquez, D. (2018). Energy consumption optimization in irrigation networks supplied by a standalone direct pumping photovoltaic system. *Sustainability*, *10*, 4203.
- Sarkar, A., & Majumder, M. (2019). Real-time monitoring of water requirement in protected farms by using polynomial neural networks and image processing. *Environment, Development and Sustainability*, *21*, 1451–1483.
- Sebbagh, T., Kelaiaia, R., Zaatri, A., Bechara, T., & Abdelouahed, L. (2018). Investigation of the use of a central unique renewable energy system versus distributed units for crop irrigation. *Clean Technologies and Environmental Policy*, *20*, 2365–2373.
- Singh, P., Singh, G., & Sodhi, G. P. S. (2019). Energy auditing and optimization approach for improving energy efficiency of rice cultivation in south-western Punjab, India. *Energy*, *174*, 269–279.
- Todde, G., Murgia, L., Carrelo, I., Hogan, R., Pazzona, A., Ledda, L., et al. (2018). Embodied energy and environmental impact of large-power stand-alone photovoltaic irrigation systems. *Energies*, *11*, 2110.
- Todde, G., Murgia, L., Deligios, P. A., Hogan, R., Carrelo, I., Moreira, M., et al. (2019). Energy and environmental performances of hybrid photovoltaic irrigation systems in Mediterranean intensive and super-intensive olive orchards. *Science of the Total Environment*, *651*, 2514–2523.
- Wong, J. H., Royapoor, M., & Chan, C. W. (2016). Review of life cycle analyses and embodied energy requirements of single-crystalline and multi-crystalline silicon photovoltaic systems. *Renewable and Sustainable Energy Reviews*, *58*, 608–618.
- Xu, Z., Sun, D. W., Zeng, X. A., Liu, D., & Pu, H. (2015). Research developments in methods to reduce the carbon footprint of the food system: A review. *Critical Reviews in Food Science and Nutrition*, *55*, 1270–1286.
- Yu, M., & Halog, A. (2015). Solar photovoltaic development in Australia—a life cycle sustainability assessment study. *Sustainability*, *7*, 1213–1247.

Development of an Energy Efficiency Index for Agricultural Tractors Based on OECD Codes Data



C. Carnevali and S. Angelelli

Abstract The need of more energy efficiency in the agricultural sector requires the use of tractors with better energy performance. The main energy losses in agriculture tractors take place at the engine and at the transmission. A possible way to merge the farmers and the Countries goals could be the introduction of an Index to help the first to choose the best tractor for their business and to help the second to evaluate the introduction of public aid. In this paper a method used for developing an energy efficiency Index (C_{APD}) is proposed. It considers the data of tractors tested in accordance with OECD (Organization for Economic Co-operation and Development) Code 2 standard. In particular the results of the P.T.O. (Power Take-off) and of the Fuel Consumption test have been used. The index, expressed in specific volumetric fuel consumption (SVFC), takes into account both the engine and the transmission influence and it is also easy to adapt for future developments. Two-hundred twelve model of tractors are analyzed and classified in five categories; from the lowest to the highest fuel consumers following this method. Almost half of the tractors with different Power (kW) are distributed close to the regression line of the index. The accuracy of the index is considered, taking into account the experiences of other international classifications. By this method, distribution of classified tractors can be used for practical application.

Keywords Fuel consumption · Tractor classification · Energy saving

1 Introduction

The challenge for many Countries is to find solutions to reduce the energy consumption and the environmental pollution in the use of vehicles.

C. Carnevali (✉) · S. Angelelli
ENAMA Ente Nazionale Per La Meccanizzazione, Agricola via Venafro 5, 00159 Rome, Italy
e-mail: carlo.carnevali@enama.it

S. Angelelli
e-mail: silvio.angelelli@enama.it

© Springer Nature Switzerland AG 2020
A. Coppola et al. (eds.), *Innovative Biosystems Engineering for Sustainable Agriculture, Forestry and Food Production*, Lecture Notes in Civil Engineering 67,
https://doi.org/10.1007/978-3-030-39299-4_65

It is common for farmers to choose the most suitable tractors according to parameters such as engine power, price, post-sale service, etc. According with the new needs, it becomes very important to give information to tractor users on the use of tractors in the view of reducing the energy consumption and to have objective criteria to classify tractors in accordance to their performances and fuel consumption related.

The interest on the tractor energy efficiency it is found in literature.

All the investigations on Energy Efficiency Index (EEI) are based on OECD Code 2 test results and the Grisso et al. (2004) equation:

$$Q \text{ (L/h)} = (0.22 X + 0.096) [1 - (-0.0045 X * N_{\text{red}} + 0.00877 N_{\text{red}})] P_{\text{pto}} \text{ (kW)}$$

where:

Q = engine fuel consumption at partial load

N_{red} = percentage of reduced engine speed for a partial load from full throttle (%)

X = ratio between the power at any partial load and at the rated power

P_{pto} = the rated power at the P.T.O

This equation is the starting point for the studies on the tractors EEI based on the OECD Code 2 test results.

The OECD Code 2 tests provide standardized and comparable data on tractor performances (power, torque, fuel consumption at the power take-off and drawbar).

Several OECD Member Countries (France, Korea, Germany, Spain and Turkey) made studies on tractors energy efficiency and classification using on OECD Code 2 test results. Most of these studies reflect the specific use of the tractor in the country of origin.

Spain and Korea finalized their studies also providing an EEI not related to the specific use of the tractor.

In both experience were used the same OECD PTO test results but different data provided by the drawbar test; Korea for the drawbar data used an own standard.

Taking into account all the experience we found in the literature a new energy efficiency index, directly related to the OECD test results given in the official reports.

The index has been compared with the Spanish one as even if the approach is different can provide comparable result.

2 Definition of an EEI

By Code 2, two main cluster of data can be considered:

- (1) P.T.O test data at the 6 points (the five extra points plus the power obtained at rated engine speed in the main test).
- (2) Drawbar fuel consumption test data at the 5 values measured at a nominal speed of 7.5 km/h and a speed between 7 and 10 km/h (for a total of 10 values).

With the aim to evaluate the energy efficiency of the tractors, we started with the following considerations:

- (a) for the index we used the “specific volumetric fuel consumption” (SVFC—l/kWh);
- (b) all power data are corrected to standard atmospheric conditions according to ISO 15550;
- (c) the type of transmissions (CVT, mechanical, etc.) is not considered as during tests must be achieved precise settings;
- (d) the final index take into account also the influence of transmissions during drawbar test;
- (e) the type of work (transport, tillage, etc.) performed by the tractors is not considered in order to define a methodology directly related to the OECD Code 2 results.

2.1 Methodology

The data are corrected to the standard atmospheric conditions of ISO 15550:2002 (25 °C temperature and 99 kPa dry pressure) and used to calculate the related SVFC (l/kWh).

Accordingly with the other experiences, the average of the 6 points, obtained during the P.T.O. test, is calculated as follows:

$$C_{6P} = \frac{\sum_{i=1}^6 SVFC_i}{6} \quad (1)$$

The drawbar power (kW) of the fuel consumption test is corrected, to take into account the transmission influence, with the addition of that part lost during the test with the slip of wheels and/or tracks, with the following formula:

$$P_{CD} = \frac{P_D}{1 - Slip\%} \quad (2)$$

where P_D is the power obtained during the fuel consumption test and $Slip\%$ is the related slip of wheels and/or tracks.

The P_{CD} values are used to correct the related fuel consumption SVFC (l/kWh).

Since the fuel consumption test is performed in 2 different speed settings it has been decided to make two averages of the SVFC results. C_{7D} and C_{10D} are both the average of the corrected SVFC (l/kWh) taken in both speed settings (7.5 and between 7 and 10 km/h):

$$C_{7D} = \frac{\sum_{i=1}^5 SVFC_i}{5} \quad (3)$$

$$C_{10D} = \frac{\sum_{i=1}^5 SVFC_i}{5} \quad (4)$$

The two averages are reported separately in order to give the possibility to adjust the index with a factor of multiplication to the fast or to low speeds. This further criteria can be a development of this index to give more weight to the results obtained during tests to lower or higher speed settings.

Since the multiplication factor is not applied, the formulas (3) and (4) can be represented as:

$$C_{FCD} = \frac{\sum_{i=1}^{10} SVFC_i}{10} \tag{5}$$

Once calculated the three (or two) averages, the efficiency of the engine and transmission is given by the average of the (1), (3) and (4) values as follows:

$$C_{APD} = \frac{C_{6P} + C_{7D} + C_{10D}}{3} \tag{6}$$

Using the data of 212 tractor models officially tested in accordance with the OECD Code 2, the results of (6) are plotted versus the corrected power at rated engine speed as shown in Fig. 1. The regression line of the model is:

$$y = 0.41803 e^{-0.00123x} \quad R^2 = 0.50541 \tag{7}$$

The C_{APD} is divided in 5 areas around the regression line with the criteria of ± 5 and $\pm 15\%$ upper and down the regression value obtained.

This classification is drawn using 212 tractor models with the aim to improve the accuracy of the methodology presented with more tractor data.

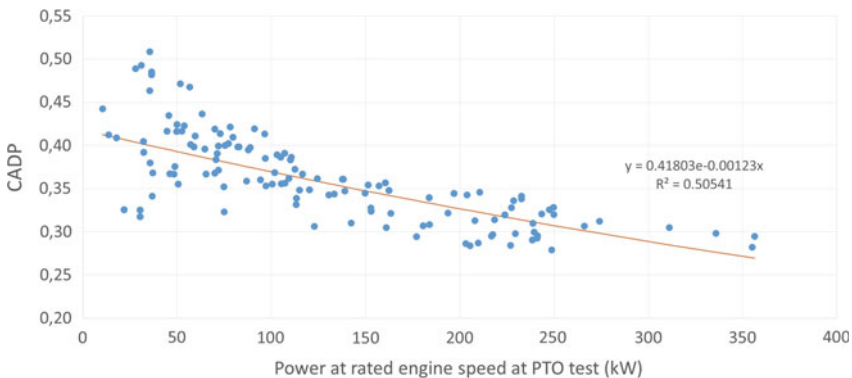


Fig. 1 Plot made with formula (6) results of the equation versus the power at rated engine speed of the tractor

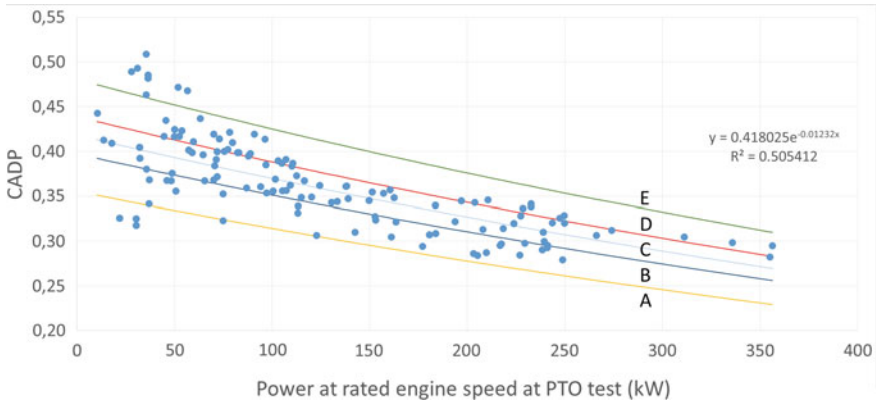


Fig. 2 Plot made with 5 areas. The criteria used is ± 5 and $\pm 15\%$ upper and down the regression value obtained

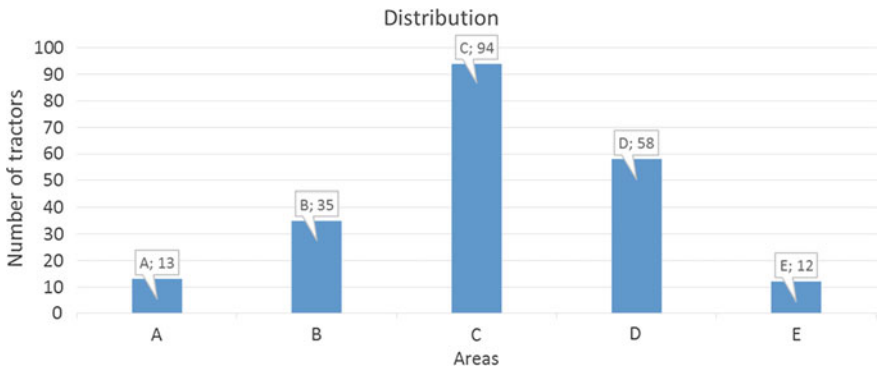


Fig. 3 Distribution of 212 tractor models in the 5 areas

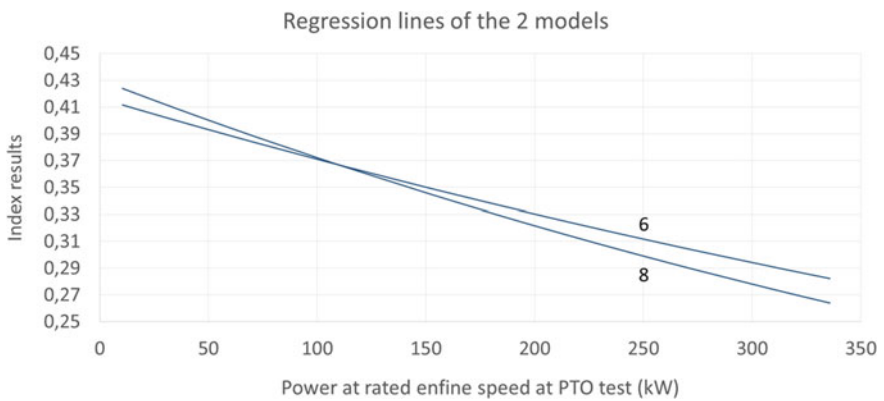


Fig. 4 Graphical result of the 2 regression lines

3 Accuracy of the Methodology Proposed

To evaluate the accuracy of the model proposed the EEI (based on a sample of 86 tractor models taken between the 212 mentioned above) has been compared with the Spanish index, which is obtained using the following formula:

$$C_{kt} = \frac{C_k}{3} \left(1 + \frac{1}{\eta_{ls}} + \frac{1}{\eta_{hs}} \right) \tag{8}$$

The formula came from:

- (8) Classification of Agricultural Tractors According to the Energy Efficiencies of the Engine and the Transmission based on OECD tests; J. Ortiz-Cañavate, J. Gil-Sierra, J. Casanova-Kindelán, V. Gil-Quirós

The formula (8) have been applied to 86 tractors, and the regression lines obtained have been compared with the (6) methodology results:

$y = 0.416027e^{-0.001122x}$	$R^2 = 0.409349$	(6)
$y = 0.430387e^{-0.001457x}$	$R^2 = 0.484722$	(8)

Plotting the 2 lines we can see that the formulas (6) and (8) have quite the same trend:

To deeply analyze the results we apply a linear regression model, plotting the data of the formulas (6) and (8).

In the linear regression formula “ $y = a + bx$ ” we consider as “ y ” (dependent values) the results of formula (8), and “ x ” (independent values) the results of (6) formula; of course “ b ” is the slop of the regression line and a is the intercept.

$y = 1.0648x - 0.0223$ $R^2 = 0.758$	
---	--

As we can see in Fig. 5 the “R squared” value is 0.758; the coefficient of determination ranges is from 0 to 1. With this result, we can consider the two model with a strong uphill (positive) linear relationship.

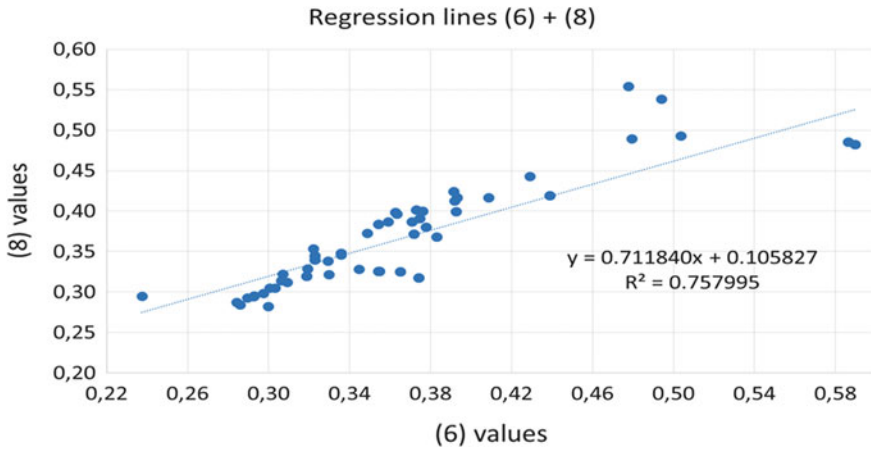


Fig. 5 Regression line of the formula results obtained with methods (6) and (8)

4 Conclusion and Future Improvements

The C_{APD} efficiency index proposed can be used to classify agricultural tractors according to their energy efficiency using the results of OECD Code 2 tests; it takes into account the engine and the transmission efficiency.

A comparison of the ENAMA proposed index with the Spanish one has been made and a “R squared” value of 0.758 has been obtained with a strong uphill (positive) linear relationship.

Acknowledgements The activity presented is part of the research activity grant by the Italian Ministry for Agriculture (MIPAAFT) under the project with the acronym of ENAGRI, articulated in several tasks aimed to improve the use of renewable energy in the agricultural sector.

References

- Energy Efficient Indexes (EEI) Applied To Agricultural Tractors. Part 1—Background Document/Literature Review. Part 2—Possibilities for harmonizing methodologies using OECD code 2 tests. TAD/CA/T(2013)4. Paris (France) OECD.
- Gil-Sierra, J., Ortiz-Cañavate, J., Gil-Quirós, V., & Casanova, J. (2007). Energy efficiency in agricultural tractors: A methodology for their classification. *Applied Engineering in Agriculture*, 23(2), 145–150.
- Grisso, R., Kocher, M. F., & Vaughan, D. H. (2004). Predicting tractor fuel consumption. *Applied Engineering in Agriculture*, 20(5), 553–561.
- IDAE. La calificación energética 2011 de tractores comercializados en España. IDAE. Madrid. 2011.
- ISO 15550:2002 Internal combustion engines—Determination and method for the measurement of engine power—General requirements.

- Muñoz-García, M. A., Ortiz-Cañavate, J., Gil-Sierra, J., Casanova, J., Valle, A. (2012). New classifications of tractors according to their energy efficiency. In *CIGR AgEng 2012 Valencia, Spain*.
- OECD. (2007). Development of indexes to classify agricultural tractors according to their energy efficiency. Spain. AGR/CA/T/RD(2007)1. Paris (France) OECD.
- OECD. (2012). Energy efficiency classification of agricultural tractors in Turkey based on OECD test. TAD/CA/T/WD(2012)1. Paris (France) OECD.
- OECD. Standard code for the official testing of agricultural and forestry tractor performance “Code 2” February 2016 and February 2017. Paris (France) OECD.
- OECD. (2012). Energy efficiency classification of agricultural tractors in Turkey based on OECD tests OECD. Turkey. TAD/CA/T/WD(2012)1. Paris (France) OECD.
- Shin, C. S., Kim, K. U., & Kim, K. W. (2012). Energy efficiency classification of agricultural tractor using OECD test data. In *Proceedings of the 6th International Symposium on Machinery and Mechatronics for Agriculture and Biosystems Engineering (ISMAB)*, June 2012, Jeonju, Korea.
- Shin, C., & Kim, K. U. (2013). A method for fuel efficiency classification of agricultural tractor. *Paper number 131621100 Proceedings of ASABE Meeting of 2013*.

Evaluation of Coaxial Pipes for Basal Heating as Alternative for Energy Saving in Heating System for Leafy Vegetables



M. Fedrizzi, C. Terrosi, S. Cacini, G. Burchi, M. Cutini, M. Brambilla, C. Bisaglia, M. Pagano, S. Figorilli, C. Costa and D. Massa

Abstract Protected horticulture is a high energy-demanding sector where the optimization of energy use and cost for heating facilities are strategic to achieve high environmental and economic sustainability of productions. The main aim of the work was to evaluate coaxial pipes, used for basal heating, as an alternative system for growing crops with small canopies such as leafy vegetables. For the tests, coaxial pipes were lied on the substrate surface in the cultivation benches of the greenhouse. In a separate area, a traditional (air-burner) heating system was installed to heat the whole greenhouse air volume. The set temperature was maintained at 15 °C by means of thermostats positioned at canopy level in the basal heating system and at a height of 1.00 m above the canopy in the traditional system. No significant difference was detected between the two systems in terms of produced yield while the energy use efficiency of the basal heating systems was significantly enhanced compared with the traditional heating. Indeed, the monitoring of temperatures by means of data loggers in both systems, confirmed that coaxial pipes used for basal heating can guarantee constant temperature at canopy level and thermal energy saving.

Keywords *Ocimum basilicum* · Mediterranean greenhouse · LPG boiler · Temperature · Canopy · Energy

M. Fedrizzi (✉) · M. Pagano · S. Figorilli · C. Costa
Consiglio per la Ricerca in Agricoltura e l'analisi dell'economia Agraria (CREA), Centro di Ricerca Ingegneria e Trasformazioni Agroalimentari (Research Centre for Engineering and Agro-Food Processing), Via Della Pascolare, 16 00015 Monterotondo (Rome), Italy
e-mail: marco.fedrizzi@crea.gov.it

C. Terrosi · S. Cacini · G. Burchi · D. Massa
Consiglio per la Ricerca in Agricoltura e l'analisi dell'economia Agraria (CREA), Centro di Ricerca Orticoltura e Florovivaismo (Research Centre for Vegetable and Ornamental Crops), Via dei Fiori, 8 51017 Pescia (PT), Italy

M. Cutini · M. Brambilla · C. Bisaglia
Consiglio per la Ricerca in Agricoltura e l'analisi dell'economia Agraria (CREA), Centro di Ricerca Ingegneria e Trasformazioni Agroalimentari (Research Centre for Engineering and Agro-Food Processing), Via Milano, 43 24047 Treviglio (BG), Italy

© Springer Nature Switzerland AG 2020

A. Coppola et al. (eds.), *Innovative Biosystems Engineering for Sustainable Agriculture, Forestry and Food Production*, Lecture Notes in Civil Engineering 67,
https://doi.org/10.1007/978-3-030-39299-4_66

1 Introduction

The world protected agriculture covers an area of 900,000, 400,000 ha of which are in Asian countries. In Italy, the heating of greenhouses currently occurs in 6,000 out of 35,000 production units. The estimated energy consumption is between 5 and 7 kg of oil equivalent (1 kgoe = 11.63 kWh) per year, or 60–80 kWh/m², while in central and northern Europe, from Germany to Holland, it reaches 40–80 kgoe (460–930 kWh/m²/year) (Campiotti et al. 2010). The energy costs of greenhouse production represent a major challenge. In cold regions, they are the second largest operating costs after labor for greenhouse production. Many studies have been conducted to reduce the heating cost of greenhouses proposing strategies such as structural design, the use of energy efficient covers, improved heating and ventilation systems, management of indoor micro-climates and the use of renewable energy sources. The focus of these techniques is mostly on (i) the reduction of farm energy requirements; (ii) the increase of energy efficiency; (iii) the reduction of energy costs. The efficiency of many solutions has been widely demonstrated but could require high investment cost. It is also essential to consider the balance between the agronomic needs of the plants and the energy saving potential the different techniques allow (Sanford 2011). For this reason this experimental work was focused on the investigation and the quantification of the energy saving potential of two conventional heating systems in an existing greenhouse during the winter season while growing a leafy vegetable. Within this approach, the paper focuses the energy consumption in terms of energy efficiency that, with specific reference to protected agriculture, is the ratio between direct energy consumption (meant as the primary consumption of fuel and/or electricity) and the production per unit of product or per unit of crop cycles (Campiotti et al. 2010). The work compares the overall energy consumption of a gas condenser boiler and basal heating system with coaxial radiant tubes and the overall consumption of a traditional heating system for air heating with a diesel burner. To achieve this goal, basil crops were cultivated in two different areas, climatically separated from each other, in the same greenhouse. The total energy consumption and yields of the two basil crops were measured.

2 Materials and Methods

A fully randomized design layout has been adopted for the experimental test. On 6th February 2017, 560 *Ocimum basilicum* L. ‘Genovese basil’ (hereinafter basil) plants were transplanted in 4 benches simultaneously (2 benches per each greenhouse section) in 4 replicates per treatment (density about 30 pl/m²). Each bench contained 140 sweet basil plants, arranged in 28 rows, 5 plants in each row. Two different treatments, consisting in different heating systems were adopted. Consequently, the 4 benches were divided in 2 benches for each treatment (280 plants). Each treatment was divided in 4 replicates (2 per each bench; 70 plants for each

replicate). Agronomic cares, such as fertigation and pest and disease control, were carried out in the same way for each treatment according to crop exigencies. During the cultivation two harvestings were planned. The first one after 30 days after transplant (DAT hereinafter), the second one at 44 DAT. At both the time of first and second harvest, plant height and yield were assessed. The trial was carried out in the experimental farm of CREA Research Centre for Vegetable and Ornamental Crops, in Pescia (province of Pistoia, Italy), in a greenhouse made of a galvanized iron structure with a polycarbonate roof and a fully automatized opening system. In the greenhouse there were rectangular concrete benches (0.70 m width \times 7.25 length m \times 0.30 m height) whose walls were coated with 30 mm thick polystyrene panels. Cement blocks kept such benches raised 0.35 m above the soil level. Polyethylene sheets 2 mm thick divided the inner space of the greenhouse in 2 separate zones of equal surface and volume (100 and 300 m³ as in Fig. 1a, b) to carry out a test with two different heating systems simultaneously: a basal heating system (BH), and a conventional air heating system (AH), used as control.

Basal heating consisted of coaxial pipes placed on the surface of the growing media, between the rows of plants (Fig. 2a, b). Heat was provided by a ECONCEPT 15A Ferroli condensation boiler Ferroli (Ferroli S.p.A., Verona, Italy), with sealed

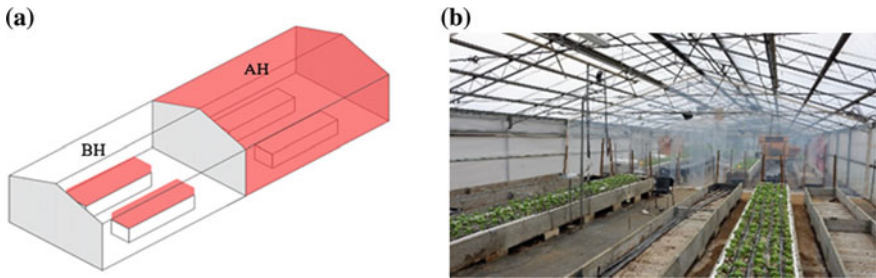


Fig. 1 The layout of the experimental greenhouse **a** colored areas highlight the different air volumes heated by BH or AH heating system. On the right **b** a general overview of the two areas with the BH area in the foreground, the polyethylene sheet and the AH area in the background

Fig. 2 a, b Positioning of heating tubes **(a)** and temperature dataloggers **(b)** in the cultivation benches

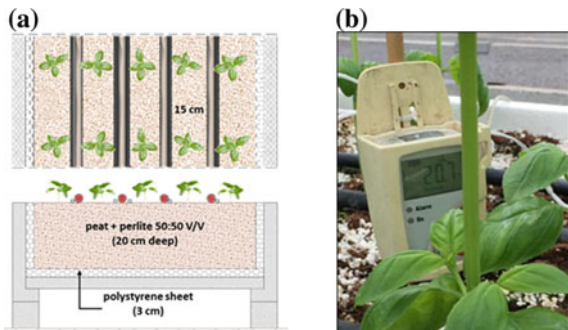


Table 1 Main characteristics of the coaxial piping system

Specification	Hydraulic delivery line (internal piping)	Hydraulic return line (interspace between the two pipes)
Outside diameter (mm)	16.0	23.2
Internal diameter (mm)	12.5	16.0
Useful section area (mm ²)	122.7	221.7

chamber, a maximum rated thermal power of 15 kW and fed with liquefied petroleum gas (LPG hereinafter) with a declared efficiency (30–50 °C) of 104.9–106.7%.

Various types of coaxial pipes have been patented in the past for various uses (Ziemek and Schatz 1972; Horton et al. 1975; Edwards 1981; Carnavos 1985; Spiegelman 1992; Wolf and Reichert 1995; Wolf 1996). The hydraulic coaxial system consisted of a PE (polyethylene) pipe with a diameter of 16 mm, in which the supply water flows, and a second PE pipe with a larger diameter (32 mm), outside the first, into which the water flowing back to the boiler (Table 1). A closing cap at the end of the outer tube let the water pass from the internal to the external pipe. Such a combination of pipes creates a characteristic condition of continuous and progressive heat exchange between the fluids flowing in opposite directions and contemporary between the outer pipe and the external environment.

A thermostat set to 15 °C for managing air temperature was positioned in the canopy of the crop at the center of the hydraulic line. An analogic gas flowmeter was installed with the purpose of monitoring the energy consumptions. In previous studies, this system had already been tested in different conditions (Fedrizzi et al. 2009, 2011). A thermostat set to 15 °C was positioned inside the canopy of the crop in the middle between two pipelines. In the AH sector of the greenhouse the plants were cultivated by heating the entire volume of the area with a Gentili Junior 85 SP fan-cooled heat generator with a power of 118 kW and efficiency of 91% fueled with diesel, whose ignitions were controlled by a room thermostat positioned at 1 m above the canopy of the culture (Fig. 3a, b). Energy consumption was monitored by

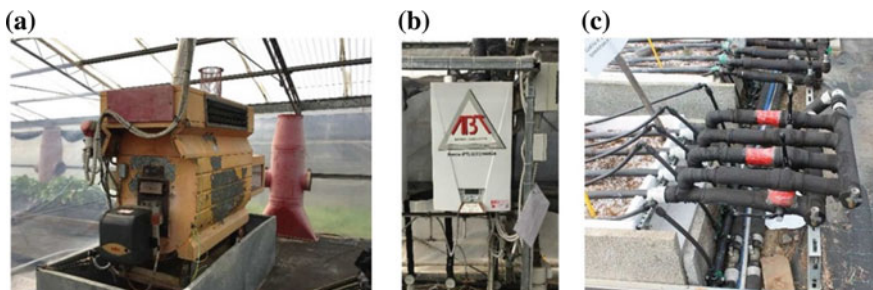


Fig. 3 a, b, c Details of the main technical solutions adopted: a the air burner; b the condensation boiler; c the basal piping coaxial system

a diesel flowmeter. In both AH and BH area, 3 Testo mod. 175T2 data loggers (Testo SpA, Settimo M.se, Italy) recorded at the same time both the canopy air temperature (10 cm above the substrate) and the substrate temperature (10 cm deep).

The air temperature inside the greenhouse was monitored with a Testo mod. 175H1 datalogger placed 2 m high above the soil level. One-way analysis of variance (ANOVA) was performed to assess the effect of each treatment on the considered parameters. Data processing was supported through Statgraphics Centurion XV (Statpoint Technologies, Inc., Warrenton, Virginia, USA) and Prism 5 (GraphPad Software, Inc., La Jolla, California USA).

3 Results and Discussions

The average air temperature outside the greenhouse during the test period was 10.2 °C. The average values of the daily minimum and maximum temperature resulted 6.1 and 14.9 °C with the absolute minimum and maximum of 1 and 21 °C. Table 2 reports the average values and the average of the daily minimum and maximum temperature inside the greenhouse during the whole period of the experimental test.

The average value of the solar radiation during the period resulted 324.8 W/m². In both systems, the target temperature value of 15 °C, maintained at canopy level, was reached successfully.

Furthermore, an analysis has been carried out to evaluate the temperatures during nighttime and daytime.

According to results, both the heating systems reached successfully the target temperature value of 15 °C to be maintained at canopy level. The mean nighttime temperature, throughout the test, was 14.8 °C for AH and 15.2 °C for BH (Fig. 3a, b). This aspect was fundamental to have comparable growing conditions in terms of air temperature in the canopy volume. As expected, BH treatment caused an increase in the substrate temperature compared with AH (Fig. 4 a and b).

Conversely, the air temperature recorded 1 m above the canopy was found to be consistently lower in the BH system during the nighttime compared with the AH system. This also resulted in higher air relative humidity in the BH system during

Table 2 Average values of ambient, canopy and substrate temperatures recorded inside the greenhouse

Average temperature values (°C)									
Section	Ambient			Canopy			Substrate		
	Mean	Min	Max	Mean	Min	Max	Mean	Min	Max
AH	18	14	25.7	17.3	13.8	24.2	16.6	15.2	18.4
BH	15.8	9.7	25.6	18.4	14.6	24.5	22.3	20.6	23.5

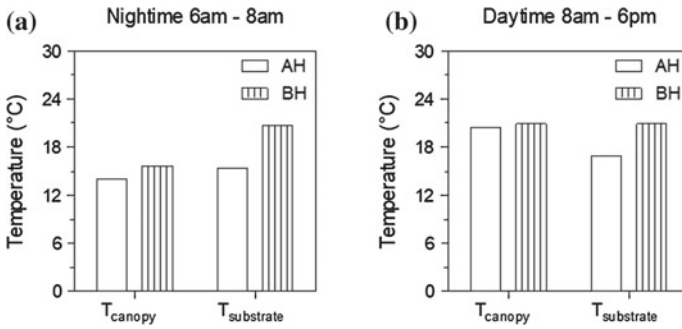


Fig. 4 a, b Mean (intra) canopy air temperature and substrate temperature recorded during nighttime (a) and daytime (b)

the night (77% for the BH side and 50% for the AH side) that however did not cause any phytosanitary problem.

Crop yield, plant biomass accumulation and energy consumption for both AH and BH systems were assessed in the experiment.

The yield biomass was evaluated both fresh and dry. In particular the fresh product of the coaxial plant resulted significantly higher.

This was possibly due to the higher mean temperature of the root zone that might have had positive effects on plant nutrient and water absorption.

The total harvested biomass has been reported as fresh weight together with the energy use efficiency (Alluvione et al. 2011), expressed as the increase in dry biomass per energy unit (Fig. 5a, b).

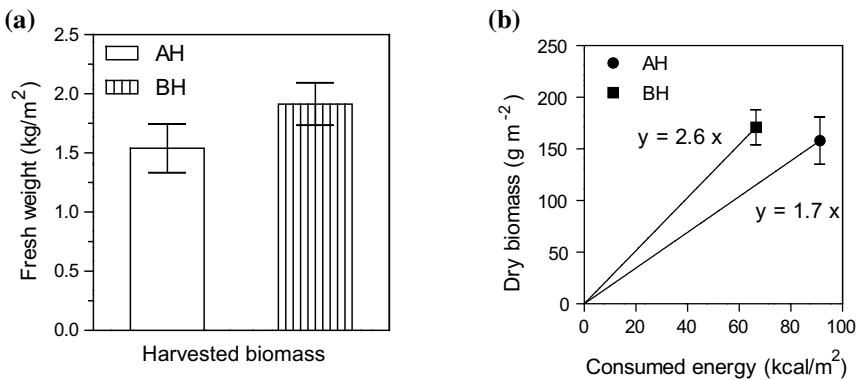


Fig. 5 a, b Total fresh biomass collected with the harvests (a) and energy use efficiency (b) of the aerial (AH) and basal (BH) heating system. In Fig. 5b, the continuous lines are linear regressions with an intercept equal to zero and a slope that represents the unit increment of biomass per unit of consumed energy for each system AH and BH. Values represent the average of four replicates (\pm SD)

The overall energy consumption, expressed as the increase in dry biomass per energy unit, in the AH system resulted higher (91293 kcal m⁻²) than BH (66538 kcal m⁻²) resulting in an average energy use of 1.7 g_{d.w.}/Mcal that in case of BH system achieves 2.6 g_{d.w.}/Mcal showing therefore a better efficiency (Fig. 5a, b).

Given this, the BH system produced the 70.5% higher quantity of fresh biomass and the 48.9% higher dry biomass per Mcal compared with the AH system thus showing better performance in terms of energy use.

4 Conclusions

The research evaluated the overall energy consumption of the heating system with coaxial radiant tubes, used for basal heating, as an alternative system for growing crops with small canopies in comparison with a traditional heating system, based on an air heating system. Temperatures were maintained at 15 °C by means of thermostats in both heating system. No significant difference was detected between the two systems in terms of produce yield while the basal heating system produced the 70.5% of fresh biomass and the 48.9% of dry biomass more per unit of heat confirming that a significant reduction of thermal energy consumption is possible. The results of this case study will stimulate further research the deepening of the knowledge of this innovative heating system and the analysis of the energy delivered to the plants and system conversion efficiency.

Acknowledgements The activity presented in the paper was supported by the Italian Ministry of Agricultural, Food, Forestry and Tourism Policies, MIPAAFT) under the AGROENER project (D. D. n. 26329, 1 April 2016)—<http://agroener.crea.gov.it/>.

References

- Alluvione, F., Moretti, B., Sacco, D., & Grignani, C. (2011). EUE (energy use efficiency) of cropping systems for a sustainable agriculture. *Energy*, 36, 4468–4481.
- Campiotti, A. C., Bibbiani, C., Dondi, F., & Viola, C. (2010). Efficienza energetica e fonti rinnovabili per l'agricoltura protette. *Ambiente Risorse Salute*, 126, 6–12.
- Carnavos, T. C. (1985). Coaxial finned tube heat exchanger. Noranda Metal Industries, Inc., Newton, CT, United States Patent no 4554969.
- Edwards, R. C. (1981). Coaxial tube in tube heat exchanger with inner tube support. Edwards Engineering Corporation, Pompton Plains, NJ, United States Patent no 4286653.
- Fedrizzi, M., Cacini, S., & Burchi, G. (2009). Heating optimization in ornamental plant production: Basal heating uniformity and energy saving in protected environments. In *Scientific Program of the GreenSys 2009 International Symposium on High Technology Greenhouse System*, “Greensys 2009” 14–19 June, Québec City (Canada) CD: Paper no. 81, pp. 1–8.
- Fedrizzi, M., Cacini, S., & Burchi, G. (2011). Root zone heating optimization in ornamental plant production. In *Proceedings of IS on High Technology for Greenhouse Systems—GreenSys2009*, *Acta Horticulturae* no 893 (ISSN 0567-7572), ISHS 2011, pp. 389–395.

- Horton, L. R., Jackson, C. A., Holcomb, W. P., & Horton, C. (1975). Coaxial Tube Coupler Assembly, *United States Patent* no 3860269.
- Sanford, S. (2011). Reducing greenhouse energy consumption an overview. *Energy* 3907: 01. Madison: University of Wisconsin Extension.
- Spiegelman, J. J. (1992). Coupling for interconnection of coaxial tubing. Tylan General, Inc., San Diego, CA, *United States Patent* no 5088774.
- Wolf, F. J., & Reichert, U. (1995). Fluid containing coaxial tube for control systems. WOCO Franz-Josef Wolf & Co., Bad Soden-Salmunster, DE, *United States Patent* no 5433252.
- Wolf, L. W. (1996). Vented bending sleeves for coaxial tubing systems, *United States Patent* no 5497809.
- Ziemek, G., & Schatz, F. (1972). Spacing in coaxial pipes system. Kabel-und Metallwerke Gutehoffnungshutte Aktiengesellschaft, Hannover, DT, *United States Patent* no 3670772.

Energy Monitoring of Fully Automated Dairy-Farm: A Case Study



Andrea Pezzuolo, Francesco Marinello, Luigi Sartori and Stefano Guercini

Abstract Automation in livestock farm is developed for various monitoring and control services such as herd management, milk production, environmental control and behaviour monitoring. In such applications, automated systems are used in order to collect data on physiological and health conditions of the animals. Subsequently they are made available to the farmer, providing a general overview of the condition of the herd as well as detailed actions on herd management. However, a more advanced use of automation devices that take part in the production process without a direct human-control relies on the most advanced automation application in dairy production involves the use of robots or intelligent machines that are capable of interacting with their work environment. The present research was focused on the energy monitoring of a fully automated dairy farm, located in the Veneto region of Italy, including automatic milking system (AMS), feeding system (AFS) and robotic scraper (ARS). The paper reports an analysis on performance indices to quantify improvements in the functionality of the automated systems, including energy consumption and man labour. Preliminary results have shown a reduction of energy consumption of at least 35% compared to conventional systems and, moreover, the energy consumption of the farm has become more regular, with the effect of a greater flexibility than conventional systems.

Keywords Dairy barn · Automatic systems · Energy consumption · Energy use

1 Introduction

The structural developments that are taking place in the livestock sector, such as enlargement of herds and land areas or reduction of family workforce, are contributing to an increasing demand for farm efficiency (Sivamani et al. 2015). The need for increased farm productivity set against a declining workforce is driving research

A. Pezzuolo (✉) · F. Marinello · L. Sartori · S. Guercini
Department of Land, Environment, Agriculture and Forestry, University of Padova, Viale
Dell'Università 16, 35020 Padua, Italy
e-mail: andrea.pezzuolo@unipd.it

© Springer Nature Switzerland AG 2020

A. Coppola et al. (eds.), *Innovative Biosystems Engineering for Sustainable Agriculture, Forestry and Food Production*, Lecture Notes in Civil Engineering 67,
https://doi.org/10.1007/978-3-030-39299-4_67

611

toward a development of fully automated dairy farm (Upton et al. 2015; Pezzuolo et al. 2018).

Automation in livestock farm is developed for various monitoring and control services such as herd management, milk production, environmental control and behavior monitoring (Kamilaris and Pitsillides 2016). However, a more advanced use of automation devices that take part in the production process without a direct human-control relies on the most advanced automation application in dairy production involves the use of robots or intelligent machines that are capable of interacting with their work environment.

Automatic concentrate dispenser and automatic milking systems (AMS) have been utilized for several years (Calcante et al. 2016). The introduction of AMS was one of the most important technological changes in the dairy production (Hogeveen et al. 2001) which can be considered not only as a substitute for milking parlors, but also as a new approach to manage dairy farms. The main factors which stimulate the introduction of AMS for dairy cows are: an improved work organization (Pezzuolo et al. 2017), an increase in milk yields and an improvement in animal behavior (Jacobs and Siegford 2012). AMS reduces heavy-workload and allows milking frequency monitoring of each individual cow, based on its production level or lactation stage, without any additional labour costs (Wagner-Storch and Palmer 2003).

More recently, automatic feeding systems (AFS) and robotic scraper (ARS) have been successfully introduced on the market (Tangorra and Calcante 2018). AFS for dairy cows gain in importance due to higher workload in farms with growing herd sizes and the possibility to feed different kind of performance groups according to their needs several times per day (Belle et al. 2012; DeVries et al. 2005). Currently, all types of AFS can be classified into three main groups characterized by different levels of automatization (Da Borso et al. 2017; Oberschätzl-Kopp et al. 2018): (i) automated feed delivery, (ii) automated mixing and distribution of the rations and (iii) fully automated filling of mixing unit, mixing and distribution of rations.

Another key point of intensive livestock production is the manure management (Chiumenti et al. 2018). For this purpose, the operation of mechanical devices for the removal of manure results in high energy consumption combined with wear of parts along with the tendency to show limited efficiency in terms of rapid and complete removal of liquid fractions. ARS instead, represent the most recent introduction among cleaning systems offered on a commercial scale. The ARS are mainly used on slatted floors in order to facilitate the removal of the solid fraction of manure from the pavement which, otherwise, reaches the removal channels underneath with more difficulty than urine (Robert and Lang 2013).

In addition to automation, efficient use of energy is another important way to improve the cost competitiveness of the dairy sector. Hence, understanding electricity consumption trends will have the potential to reduce overall energy use and reduce production costs. Studies of Oberschätzl-Kopp et al. (2018) showed an average energy consumption of AFS in dairy farms between 8.8 kWh per day for feeding systems of type 2 and 52.6 kWh per day for a fully automated system. In AMS, compared with previous studies, new models have been improved in recent years

and the energy used by AMS depends on many factors (e.g., machine generations, machine configurations and settings, and operative conditions).

To our knowledge, no research has been published that studied on-fully automated dairy farm daily electricity consumption profiles while providing detailed equipment electricity consumption information. This information, however, is required to identify strategies that reduce energy costs and that use electricity efficiently (i.e., aimed at a reduction in electricity use per kilogram of milk sold while maximizing its use).

The present research was focused on the energy monitoring of a fully automated dairy farm, located in the Veneto region (Italy), including automatic milking (AMS) and feeding system (AFS) and automatic robotic scraper (ARS). The paper reports an analysis on performance indices aimed at quantifying improvements in the functionality of the automated systems, including energy consumption.

2 Materials and Methods

2.1 Dairy Farm

The present study was carried out in April 2019 in a private dairy farm located near Treviso in Northeast Italy. The farm was characterized by a free-stall system, housing 119 Holstein-Friesian lactating cows with concrete floor. The ration for lactating cows was the typical Total Mixed Ration (TMR) normally distributed in Veneto's dairy farms and it was composed by corn silage, rye-grass hay, concentrate and cottonseed mixed to obtain TMR. Lactating cows received individual feed portions of their concentrate ration, according to their lactation period and milk yield, from the relative automatic feeder in the AMS.

2.2 Automated Technologies

Cows are voluntarily milked by two Lely Astronaut A4 (Lely Holding, Maassluis, the Netherlands) installed in the center of the housing and cows were allowed free traffic.

Vacuum for milking was supplied by a frequency-controlled lobe vacuum pump powered by a 1.5 kW motor. Compressed air for opening/closing the entrance and exit gates of the milking stall and for moving the robotic arm toward the udder was supplied by a 3.7 kW scroll compressor (SF4, Atlas Copco, Stockholm, Sweden). AMS was equipped with the "Pura Cleaning System" to clean the milk unit with hot steam (temperature about 150 °C) between every milking.

The AFS (Lely mod. Vector, Lely Holding, Maassluis, the Netherlands) consists of a mixing and feeding robot (MFR), a grabber, a crane and additional components as mineral and concentrate dispensers. According to predefined settings of feeding

groups and rations, the feed grabber filled the MFR (2 m³ filling volume) mainly with roughage. Auger systems dispensed concentrate and minerals. The MFR mixed the rations with a vertical auger system according to a default post mixing duration. Afterwards the rations were delivered in the barns. It is a battery driven feeding robot that navigates through the barns by using ultrasound sensors and outside the barns by following strips using an inductive sensor. Furthermore, silage and other roughage components were stored in blocks in a feed kitchen, which was filled by a loader and a block cutter once every three days.

The floor of the animal housing is kept clean by an ARS represented by Lely mod. Discovery (Lely Holding, Maassluis, the Netherlands) which is self-propelled and powered by electric motors connected to a 12 V gel battery. The ARS, performs the cleaning of the floor by means of an inclined scraper installed in the front of the machine that functions by pushing manure against the floor allowing it to fall through the openings. The advance speed is 11–14 m min⁻¹, and the operating width is 880 mm. The machine features an ultrasonic sensor for guidance along the walls and is accompanied by a front ring for direction change when a frontal object is detected.

2.3 Analysis of Energy Consumption and Herd Size Scenarios

The electrical energy used (kWh) by every automated system was monitored with a five seconds frequency and stored in a dedicated data logger, mod. Datataker DT80M. Data were recorded over a period of 6 days from April 22th to April 27 2019.

The total energy consumption of AMS was estimated as a combination of the contributions from the following functional components: vacuum pump, boiler unit, cleaning system, compressor and refrigeration system. As a regard the AFS, the following consumes were respectively included: mixing and feeding robot, bridge crane, feed grabber and mineral/concentrate dispensers. Finally, with regard to robotic scraper (ARS), energy consumption was estimated through the net power consumption value, expressed in kWh.

Furthermore, considering the energy consumption for each automatic system and the suggested dimensioning approaches present in the bibliography (Spencer 2011; Castro et al. 2012; John et al. 2016) is possible to obtain an estimate of the energy consumption required, depending on the size of the dairy farm. In particular the herd size (e.g. AMS and AFS) and the floor of the animal housing area (e.g. ARS) are the most important parameters by the definition of the number of automatic systems (Bisaglia et al. 2012; Buck et al. 2013; Da Borso et al. 2017).

3 Results

3.1 Energy Assessment

The two monitored AMS showed an energy consumption of 156 kWh day^{-1} AMS (Table 1). The average number of milked cows was equal to 110 ± 9 with an average number of milkings per day of 2.4 ± 0.3 and an average milk yield per animal of 27.3 ± 4.1 L of milk. Milk production for each milking amounted to 11.3 ± 0.8 L of milk.

AMS components that had the greatest impact on daily energy consumption were the air compressor ($58.32 \text{ kWh day}^{-1}$), the refrigerated tank storage ($37.66 \text{ kWh day}^{-1}$), the boiler ($35.16 \text{ kWh day}^{-1}$) and the vacuum pump ($19.40 \text{ kWh day}^{-1}$).

Such observations are in agreement with other experimental study, in which an average daily energy consumption of $81.34 \text{ kWh day}^{-1}$ was estimated by Calcante et al. (2016) for the same model of AMS, without using the present cleaning system and the refrigerated tank storage.

As for the AFS, energy consumption was slightly over 20 kWh day^{-1} (Table 2) considering an average of 23 ± 3 ration distributions and or feed pushing. Such value is relatively low if compare to a conventional feeding system (CFS), represented by a tractor- operated mixing wagon. Pezzuolo revealed daily energy consumptions equivalent to $246.64 \text{ kWh day}^{-1}$ and the CFS phase that requires more energy, is represented by the mixing, followed by loading of components (Pezzuolo et al. 2016).

Table 1 Energy consumption of Automatic Milking System (AMS)

System components	Maximum power (kW)	Operating time (h day ⁻¹)	Energy consumption (kWh day ⁻¹)
Vacuum pump	3.02 ± 0.01	21.4 ± 2.50	19.4 ± 3.41
Cleaning system	0.86 ± 0.10	13.60 ± 0.89	7.92 ± 0.22
Boiler	3.10 ± 0.04	14.0 ± 2.20	35.2 ± 3.91
Air compressor	2.83 ± 0.10	24.00 ± 0.01	58.3 ± 6.42
Refrigerated tank storage	4.20 ± 0.17	14.6 ± 4.20	37.7 ± 6.12

Table 2 Energy consumption of Automatic Feeding System (AFS)

System components		Maximum power (kW)	Operating time (h day ⁻¹)	Energy consumption (kWh day ⁻¹)
Grabber	Operating phase	0.72 ± 0.02	3.0 ± 0.40	1.04 ± 0.17
	Fixed user	0.15 ± 0.01	24.0 ± 0.01	3.67 ± 0.01
MFR	Battery charger	1.23 ± 0.09	12.5 ± 0.11	8.26 ± 0.51
Augers	Operating phase	0.66 ± 0.03	0.30 ± 0.10	0.18 ± 0.01
	Fixed user	0.31 ± 0.01	24.0 ± 0.01	7.03 ± 0.01

Table 3 Energy consumption of Automatic Robotic Scraper (ARS)

System components	Maximum power (KW)	Operating time (h day ⁻¹)	Energy consumption (kWh day ⁻¹)
Battery charger	0.52 ± 0.06	12.00 ± 0.36	6.24 ± 0.27

Surveys carried out by Oberschätzl et al. (2015) revealed daily energy consumptions of 8.8 and 42.5 kWh for two semi-automated feeding systems based on rail-mounted feed mixing and distribution carts, and 52.6 kWh for a fully automated process. Calcante et al. (2016) revealed daily energy consumption 40.2 ± 2.3 kWh per day, or 1.67 ± 0.10 kWh per hour of work.

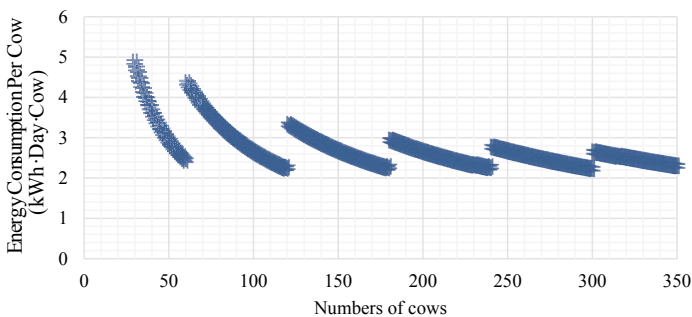
With regard to the robotic scraper (ARS), energy consumption was estimated through the net power consumption value, expressed in kWh. In this research energy consumption was just over 6 kWh day⁻¹ (Table 3) considering an average of 12 h of battery exposure. The ARS has performed 4 cleaning actions at three hours away with a working speed of about 11–14 m min⁻¹.

3.2 Energy Consumption and Herd Size Scenarios

The possible adoption of automatic systems has been simulated as a function of herd size (Fig. 1). The range of reference values represent possible Italian production scenarios, ranging between 30 and 350 lactating cows.

Combined use of automatic systems (AMS, AFS and ARS), presents a lower energy consumption per cattle herd over 120 animals. This aspect is very interesting, considering the current development of dairy farms not only in Europe but also in Italy.

Results are apparently non-linear: indeed, machines available in the market are offered with fixed size and performances. As a consequence, each machine operates with an ideal number of cows (e.g. 55–65 for AMS), which typically maximizes

**Fig. 1** Energy consumption per cow of totally automated dairy farm

the achievable performance. If the actual number of animals is lower than the ideal value, the achieved performance is slightly lower than the optimal one. Conversely if the actual number is higher than the ideal one, alternative solution or additional machines are needed in order to manage those animals which can not be managed by the available system: such case introduces a sudden increase of investments and consumes and justifies the discontinuities visible in Fig. 1.

4 Conclusions

The proposed research highlight how automated technology can represent an interesting option to improve competitiveness of dairy farms and provide useful information for farm management.

A combined use of automatic systems (AMS, AFS and ARS) presents a lower energy consumption per cattle herd over 120 animals and an energy request of 182 kWh day⁻¹ (66430 kWh-year⁻¹) could be affordable directly by the farm through a photovoltaic system or other renewable energy sources (e.g. CHP from biogas) contributing to further reduce energy costs in dairy farms and preserve environment.

However, many management factors, such as feeding ratio/strategy, cow traffic, barn layout and cow herd size, may potentially influence the operative performance of the automated technology. Further aspects to be investigated are the effect in terms of the impact of the new automatic system on the behavior of animals, and on the performance of the herd.

References

- Belle, Z., André, G., & Pompe, J. C. (2012). Effect of automatic feeding of total mixed rations on the diurnal visiting pattern of dairy cows to an automatic milking system. *Biosystems Engineering*, 111(1), 33–39.
- Bisaglia, C., Belle, Z., van den Berg, G., & Pompe, J. C. (2012). Automatic vs. conventional feeding systems in robotic milking dairy farms: A survey in The Netherlands. In *International Conference of Agricultural Engineering CIGR-AgEng: Agriculture & Engineering for a Healthier Life*.
- Buck, M., Friedli, K., Steiner, B., Gygax, L., Wechsler, B., & Steiner, A. (2013). Influence of manure scrapers on dairy cows in cubicle housing systems. *Livestock Science*, 158(1–3), 129–137.
- Calcante, A., Tangorra, F. M., & Oberti, R. (2016). Analysis of electric energy consumption of automatic milking systems in different configurations and operative conditions. *Journal of Dairy Science*, 99(5), 4043–4047.
- Castro, A., Pereira, J. M., Amiama, C., & Bueno, J. (2012). Estimating efficiency in automatic milking systems. *Journal of Dairy Science*, 95(2), 929–936.
- Chiumenti, A., da Borso, F., Pezzuolo, A., Sartori, L., & Chiumenti, R. (2018). Ammonia and greenhouse gas emissions from slatted dairy barn floors cleaned by robotic scrapers. *Research in Agricultural Engineering*, 64(1), 26–33.
- Da Borso, F., Chiumenti, A., Sigura, M., & Pezzuolo, A. (2017). Influence of automatic feeding systems on design and management of dairy farms. *Journal of Agricultural Engineering*, 48–52.

- DeVries, T. J., von Keyserlingk, M. A. G., & Beauchemin, K. A. (2005). Frequency of feed delivery affects the behavior of lactating dairy cows. *Journal of Dairy Science*, *10*, 3553–3562.
- Hogeveen, H., Ouweltjes, W. C. J. A. M., De Koning, C. J. A. M., & Stelwagen, K. (2001). Milking interval, milk production and milk flow-rate in an automatic milking system. *Livestock Production Science*, *72*(1–2), 157–167.
- Jacobs, J. A., & Siegford, J. M. (2012). The impact of automatic milking systems on dairy cow management, behavior, health, and welfare. *Journal of Dairy Science*, *95*, 2227–2247.
- John, A. J., Clark, C. E. F., Freeman, M. J., Kerrisk, K. L., Garcia, S. C., & Halachmi, I. (2016). Milking robot utilization, a successful precision livestock farming evolution. *Animal*, *10*(9), 1484–1492.
- Kamilaris, A., & Pitsillides, A. (2016). Mobile phone computing and the internet of things: A survey. *IEEE Internet of Things Journal*, *3*(6), 885–898.
- Oberschätzl-Kopp, R., Bühler, J., Gräff, A., Wörz, S., & Bernhardt, H. (2018). Studies on electrical energy consumption of an automatic feeding system in dairy cattle farming. In *ASABE (American Society of Agricultural and Biological Engineers) 2018 Annual International Meeting*.
- Pezzuolo, A., Chiumenti, A., Sartori, L., & Da Borso, F. (2016). Automatic feeding system: Evaluation of energy consumption and labour requirement in North-East Italy dairy farm. *Engineering for Rural Development Jelgava*, *15*, 882–887.
- Pezzuolo, A., Cillis, D., Marinello, F., & Sartori, L. (2017). Estimating efficiency in automatic milking systems. *Engineering for Rural Development Jelgava*, *16*, 24–26.
- Pezzuolo, A., Guarino, M., Sartori, L., & Marinello, F. (2018). A feasibility study on the use of a structured light depth-camera for three-dimensional body measurements of dairy cows in free-stall barns. *Sensors*, *18*(2), 673.
- Robert, M., & Lang, T. (2013). Development of simulation-based algorithms for livestock robots. *Landtechnik*, *68*(4), 278–280.
- Sivamani, S., Kim, H., Lee, M., Shin, C., Park, J., & Cho, Y. (2015). An android-based feed behavior monitoring system for early disease detection in livestock. In D. S. Park, H. C. Chao, Y. S. Jeong, & J. Park (Eds.) *Advances in computer science and ubiquitous computing*. Lecture Notes in Electrical Engineering, vol. 373. Springer, Singapore
- Spencer, S. B. (2011). *Milking Machines—Principles and Design*. Encyclopedia of Dairy Sciences, pp. 952–958.
- Tangorra, F. M., & Calcante, A. (2018). Energy consumption and technical-economic analysis of an automatic feeding system for dairy farms: Results from a field test. *Journal of Agricultural Engineering*, *49*.
- Upton, J., Murphy, M., De Boer, I. J. M., Koerkamp, P. G., Berentsen, P. B. M., & Shalloo, L. (2015). Investment appraisal of technology innovations on dairy farm electricity consumption. *Journal of Dairy Science*, *98*(2), 898–909.
- Wagner-Storch, A. M., & Palmer, R. W. (2003). Feeding behavior, milking behavior, and milk yields of cows milked in a parlor versus an automatic milking system. *Journal of Dairy Science*, *86*(4), 1494–1502.

Comparison of Environmental Impact of Two Different Bioelectricity Conversion Technologies by Means of LCA



Mauro Villarini, Sara Rajabi Hamedani, Vera Marcantonio, Andrea Colantoni, Massimo Cecchini and Danilo Monarca

Abstract Between the energy sources biomass waste is considered more and more important and the choice of the most appropriate energy conversion process is essential. The present paper presents a study for biomass waste to two distinguished energy conversion processes and the comparison of their environmental impact. The considered processes are gasification combined with internal combustion engine for power generation and combustion combined with an Organic Rankine Cycle (ORC) system with same electric power and same biomass flow as input to the conversion process. First, energy analysis of both mentioned systems have been investigated by means of Aspen Plus simulation. In the next step, model output is applied to evaluate the environmental profile of these small-scale biomass-based energy production systems. Environmental performance from cradle-to-gate was carried out by life cycle assessment (LCA) methodology. Results reveal that biomass production has a high influence over all impact categories. In both systems, eutrophication (EP), acidification (AP) and global warming potential (GWP) were identified as the main impacts. As a result, ORC system entails higher environmental burdens in all impacts categories.

Keywords CHP · Biomass wastes, gasification · Combustion, ORC · Impact categories

1 Introduction

Biomass has the highest potential for energy production among renewables, after wind and solar alternatives, thanks to widespread availability, annual global production and advantages regarding the environment and economics (IEA Bioenergy 2009).

M. Villarini (✉) · S. Rajabi Hamedani · V. Marcantonio · A. Colantoni · M. Cecchini · D. Monarca

DAFNE Department of Agriculture and Forest Sciences Department, Tuscia University, Via Camillo de Lellis, Viterbo 01100, Italy
e-mail: mauro.villarini@unitus.it

© Springer Nature Switzerland AG 2020

A. Coppola et al. (eds.), *Innovative Biosystems Engineering for Sustainable Agriculture, Forestry and Food Production*, Lecture Notes in Civil Engineering 67,
https://doi.org/10.1007/978-3-030-39299-4_68

Although use of energy crops entails environmental burdens, such as: land use change, damage to biodiversity, impact on food availability and real global warming potential (Popp et al. 2014; Gallagher 2008; Searchinger et al. 2008), the utilization of agricultural residues such as pruning biomass compensates these environmental costs. The energetic use of agriculture residues, is also beneficial from the farmers' perspective due to solving waste disposal problem (Spöttle et al. 2013).

Among the main biomass conversion technologies, biomass gasification is considered one of the best thermo-chemical process thanks to its ability in using a wide variety of biomass waste and for its environmental friendly relationship (Kalina 2017). Coupling biomass gasification with other systems, such as internal combustion engine (ICE) or organic Rankine cycle (ORC), gives a lot of advantages, especially in the small-scale plant. Both ORC and ICE are characterized by reliability, flexibility, mechanical simplicity, low requirement for maintenance (Chaves et al. 2016); these properties make them very useful and applicable in coupling systems. In order to predict the behaviour of biomass power plant simulative modelling can be very appropriate and ASPEN Plus is considered one of the best chemical engineering simulating software (Mazzola et al. 2016). Several works have been carried out on combined heat and power (CHP) systems modelling in order to evaluate the mechanical, electrical and thermal efficiency (Collings et al. 2016; Villarini et al. 2015).

Although studies on the techno-economic assessment of biomass cogeneration systems are widespread in literature (Kalina 2017; Chaves et al. 2016; Mazzola et al. 2016), knowledge on the environmental impact of combined technologies under a life cycle perspective for energy production is still limited. Hence, this work presents a life cycle assessment of two bioelectricity conversion systems.

2 Life Cycle Assessment Methodology

Life Cycle Assessment as the most developed approach for environmental comparison of alternative technologies following ISO standards (ISO 14040 2006a; ISO 14044 2006b) was performed in this study. The aim of this study was to compare environmental performance and to identify the environmental hotspots of heat and electricity production in two biomass-based technologies, gasification combined with internal combustion engine and combustion combined with an ORC system. The functional unit chosen for this study is 1 MWh_{PEP} (Primary Energy Production) due to ability to express the electricity and heat production through a unique term. It represents the unit of energy production corresponding with primary energy. In fact, the energy outputs are presented by equivalent primary energy production (Scott et al. 2016) where the electric and heating energy productions are reported in terms of equivalent primary energy based on the Italian national thermoelectric efficiency (AEEG, n.d.). The system boundary covers all material and emissions from grape cultivation to conversion process and energy production (cradle-to-gate).

2.1 Life Cycle Inventory

2.1.1 Biomass Production

All material and energy consumed in pruning biomass production were collected through interviewing with the farmers in 12 vineyards. This collecting data from vineyards was already carried out for environmental assessment of pellet production from pruning biomass by Hamedani et al. (2019a). In line with assumption adapted in Moreno and Dufour (2013), Martín-Gamboa et al. (2016), Hamedani et al. (2019a, b), pruning biomass is considered as a coproduct and therefore it contributes in environmental burdens caused by main product and will not be emission free. Hence, the life cycle inventory in Table 1 presents data allocated to vine pruning biomass upon an economic basis accounting for 10% of main crop (grape) price (Moreno and Dufour 2013). In addition, biomass properties are reported in Table 2.

2.1.2 Conversion Process

The values of efficiency and gas composition come out from two original simulation models implemented in ASPEN Plus software. The main assumption of the models was: steady-state and isothermal conditions while all gas behave ideally. The first model developed a CHP system coupled biomass combustion with Organic Rankine Cycle (ORC). The second one described a coupling system between steam biomass-gasifier with internal combustion engine (ICE). In both simulations, 100 kW_{th} was considered as the thermal input based on lower heating value of biomass input. The gasifier simulated was a dual fluidized bed and the ICE was represented by a turbine. The performance of the ORC unit has been evaluated using the 245fa working fluid. The operating condition of the two simulative models are reported in Table 3.

Emission factors were applied to calculate emissions (SO₂, NO_x, PM) from biomass combustor based on GJ net thermal input (IRBEA 2016). Since the sequestration of CO₂ during biomass growth offsets the emissions from burning the biomass, biogenic CO₂ from combustion of biomass and relevant gases (syngas) was considered neutral.

Table 4 reports inventory data for biomass combustor integrated with ORC (case 1) and biomass gasifier coupled with ICE (case 2). In this study, environmental results were characterized using CML-IA baseline, in line with other LCA studies on energy conversion technologies (Rajabi Hamedani et al. 2018; Tagliaferri et al. 2018). Among a total of eleven impact categories, five categories were identified for measuring the major impacts of the system studied, excluding the irrelevant categories, aquatic damage (marine and fresh water ecotoxicity), terrestrial ecotoxicity, abiotic depletion and ozone layer depletion. Therefore, following five impact categories are presented in this study:

- i. Global warming potential (GWP 100a), measured in kg CO₂ equivalent: According to the Intergovernmental Panel on Climate Change, climate change is

Table 1 Inventory data for biomass production per functional unit (1 MWh_{PEP})

Items	Unit	Quantity (Unit MWh _{PEP} ⁻¹)	
		Gasification-ICE	Combustion-ORC
A. Output	kg	225.75	276.21
B. Input from technosphere			
1. Pesticides	kg		
Insecticide			
Organophosphorus-compound		0.13	0.16
Fungicide			
Captan		0.22	0.27
2. Fertilizers	kg		
Compost			
Nitrogen fertilizer, as N		0.85	1.04
Urea		2.03	2.48
Potassium fertilizer, as K ₂ O		3.07	3.75
Phosphate fertilizer, as P ₂ O ₅		2.03	2.48
Sulfur		1.30	1.60
3. Diesel	kg	4.5E-6	5.5E-6
4. Electricity	kWh	1.30	1.60
C. Emissions to environment			
1. Emissions to air	kg		
Ammonia (NH ₃)		0.08	0.10
Nitrogen oxides (NO _x)		0.009	0.011
Carbon dioxide (CO ₂)		0.40	0.49
2. Emissions to water	kg		
Nitrate (NO ₃ ⁻)		0.25	0.31
Phosphorus		0.10	0.12
3. Emissions to soil	kg		
Pesticides		0.35	0.43

expressed in terms of global warming potential (GWP) by CO₂ equivalents for energy captured by the greenhouse gas emissions with a timeframe of 100 years. The higher the global warming potential contributes substantially to the climate change.

- ii. Human toxicity (HT), measured in kg 1,4-dichlorobenzene equivalent (1,4-DB_{eq}): This category concerning effects of toxic substances on human wellness, describes fate, exposure and effects of toxic substances for an unlimited time horizon.

Table 2 Vine pruning biomass characterization

LHV	Bulk density (kg/m ³)	Humidity (wt%)	Ash (DW%)	Volatile matter	Fixed carbon	S	H	N	O	Cl	S
18.60	260	17.60	2.62	80.84	16.54	50.84	5.82	0.88	40.08	1.87	0.05

Table 3 Operating conditions of the simulated systems

First model conditions		Second model conditions	
Gasification temperature (°C)	800	Combustion temperature (°C)	500
Gasification pressure (bar)	1	Combustion pressure (bar)	1
Syngas inlet to gas turbine engine, temperature (°C)	30	ORC mechanical efficiency (%)	17
Equivalence ratio of turbine	3	ORC thermal efficiency (%)	64
Isentropic expansion coefficient	0.9	ORC electrical efficiency (%)	16

Table 4 Inventory data per functional unit (1 MWh_{PEP})

Items	Unit	Quantity (Unit MWh _{PEP} ⁻¹)	
		Gasification—ICE	Combustion- ORC
A. Output	MWh _{PEP}	1	1
B. Input from technosphere			
1. Pruning residue	kg	225.75	276.21
2. Heat for drying	MJ	101.10	123.70
3. Electricity for grinding	kWh	9.93	12.15
4. Transport feedstock to energy conversion plant	tkm	19.86	24.30
5. Gasification			
Electricity	kWh	17.83	–
LPG	kg	6	–
Water	kg	163.5	–
Olivine	t	9.4	–
6. Combustion			
Electricity	kWh	–	24.85
C. Waste and emissions	kg		
1. Waste to treatment			
Ash to landfill		11.3	13.83
2. Emission to air			
SO ₂		0.0044	0.11
NO _x		0.055	0.58
PM			0.42

- iii. Photochemical Ozone Formation Potential (POFP), measured in kg ethylene equivalent (kg C₂H₄ eq): This category deals with the formation of reactive substances (mainly ozone), a problem indicated with “summer smog”, which damages human health, ecosystems and crops. This indicator calculates emissions arising from substances to air for a 5-day time span.

- iv. Acidification potential (AP), expressed as kg SO₂ equivalents: This category calculates emissions to air deriving from acidifying substances e.g. ammonia, nitrogen oxides, sulfur dioxide etc. for an infinite timeframe.
- v. Eutrophication potential (EP), expressed as kg PO₄ equivalents: This category contains all impacts owing to excess levels of macro-nutrients in the environment arising from emissions of nutrients to air, water and soil for an eternal life span.

In LCA studies, normalization is an optional step to simplify the interpretation of the results. Normalization shows the relevant share of each impact category to the overall impacts via application of a normalization factor. The normalization factor is defined as the impacts of all substances in their specific categories per person per year. The unit of all normalized values is [pers year/unit_{emission}], signifying the number of equivalent persons affected during one year per unit of emission (Hamedani et al. 2019c).

3 Results and Discussion

The characterization results for the two technologies indicate that all impact categories associated with 1 MWh_{PEP} from case 1 were higher than those of case 2 (Table 5).

There was also noticeable difference in the AP category between two conversion systems. The AP from case 2 was lower by 60% compared to the case 1. This difference refers to higher SO₂ and NO_x emissions from biomass combustion in case 1, comparing emissions from syngas burning in ICE in case 2.

The normalization results in Fig. 1 showed that the relative importance of EP, AP and GWP to overall impacts is more considerable than other indicators motivated by application of fertilizer and chemicals during biomass production.

The distribution of results among the different subsystems indicates that in both cases the biomass production significantly affects environmental profile, followed thereafter by biomass conversion phase. However, in combustion case, AP is highly affected by biomass conversion phase owing to airborne emissions (SO₂ and NO_x) from biomass burning (Fig. 2).

Table 5 Characterization results of two biomass conversion technologies. (FU: 1 MWh_{PEP})

Impact category	Unit	Combustion-ORC (case 1)	Gasification-ICE (case 2)
GWP100a	kg CO ₂ eq	34.6	28.3
HT	kg 1,4-DB eq	15.92	14.30
POFP	kg C ₂ H ₄ eq	0.015	0.012
AP	kg SO ₂ eq	0.61	0.27
EP	kg PO ₄ eq	0.52	0.40

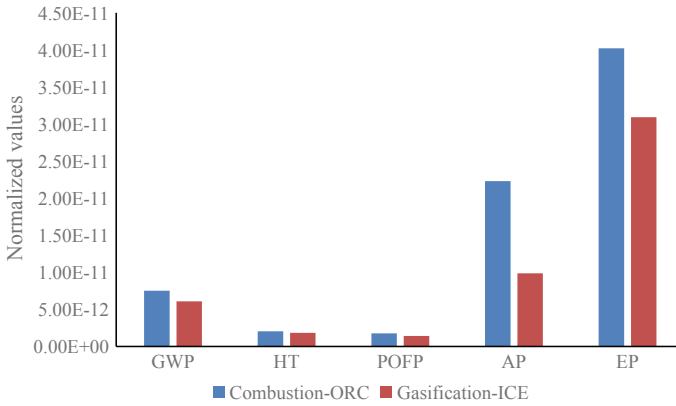


Fig. 1 Normalized impact categories in each case

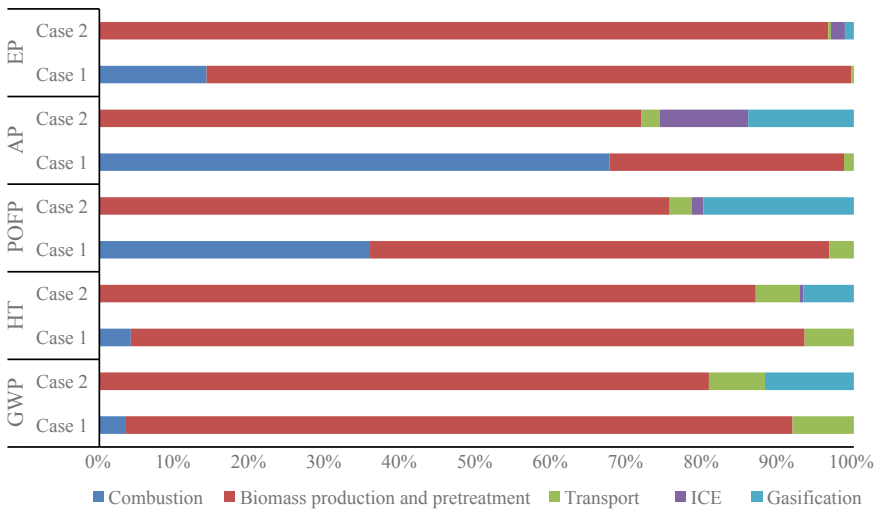


Fig. 2 Comparative contribution of processes to impact categories

4 Conclusions

A comparative life cycle assessment of two biomass-based energy conversion systems was conducted. Results signified that environmental impacts of two systems depended significantly on the biomass cultivation phase, due to impacts associated with the production and application of fertilizers. Applying ORC coupled with combustor, all impact categories were found to be higher than those of biomass gasifier integrated with ICE. The highest difference between two approaches was observed in

AP category where direct emissions from biomass combustor result in greater environmental burdens. Consequently, results of this study illuminate that bioelectricity generation via gasifier with ICE, was more environmentally compatible.

Acknowledgements The activity presented in the paper is part of the research grant by Italian Ministry for Education, University and Research (MIUR) according to the Italian Law 232/2016 within the fund for the financing of university “Departments of Excellence”. This study was also partially supported by the HBF 2.0 Project, funded in the framework of the RDS Ricerca di Sistema Programme of the Italian Ministry of Economic Development.

References

- AEEG. n.d. AEEG Resolution EEN 3/08. 01 April 2008. Retrieved October 18, 2017, from <https://www.autorita.energia.it/it/docs/08/003-08een.htm>.
- Chaves, L. I., Silva, M. J. D., Souza, S. N. M. D., Secco, D., Rosa, H. A., Nogueira, C. E. C., et al. (2016). Small-scale power generation analysis: Downdraft gasifier coupled to engine generator set. *Renewable and Sustainable Energy Reviews*, 58, 491–498. <https://doi.org/10.1016/j.rser.2015.12.033>.
- Collings, P., Zhibin, Yu., & Wang, E. (2016). A dynamic organic rankine cycle using a zeotropic mixture as the working fluid with composition tuning to match changing ambient conditions. *Applied Energy*, 171(June), 581–591. <https://doi.org/10.1016/j.apenergy.2016.03.014>.
- Gallagher, E. (2008). *The Gallagher Review of the Indirect Effects of Biofuels Production*. Renewable Fuels Agency.
- Hamedani, R., Sara, M. V., Colantoni, A., Moretti, M., & Bocci, E. (2018). Life cycle performance of hydrogen production via agro-industrial residue gasification—A small scale power plant study. *Energies*, 11(3), 675. <https://doi.org/10.3390/en11030675>.
- Hamedani, S. R., Colantoni, A., Gallucci, F., Salerno, M., Silvestri, C., & Villarini, M. (2019b). Comparative energy and environmental analysis of agro-pellet production from Orchard Woody Biomass. *Biomass and Bioenergy*, 129, 105334. <https://doi.org/10.1016/j.biombioe.2019.105334>.
- Hamedani, S.R., Del Zotto, L., Bocci, E., Colantoni, A., & Villarini, M. (2019b). Eco-efficiency assessment of bioelectricity production from iranian vineyard biomass gasification. *Biomass and Bioenergy*, 127, 105271. <https://doi.org/10.1016/j.biombioe.2019.105271>.
- Hamedani, S. R., Kuppens, T., Malina, R., Bocci, E., Colantoni, A., & Villarini, M. (2019c). Life cycle assessment and environmental valuation of biochar production: Two case studies in Belgium. *Energies*, 12(11), 1–21. <https://doi.org/10.3390/en12112166>.
- IEA bioenergy. (2009). Bioenergy—A Sustainable and Reliable Energy Source a Review of Status and Prospects. IEA bioenergy.
- IRBEA. (2016). Study on Biomass Combustion Emissions.
- ISO 14040. (2006a). Environmental Management-Life Cycle Assessment-Principles and Framework.
- ISO 14044. (2006b). Environmental Management-Life Cycle Assessment-Requirements and Guidelines. International Organization for Standardization.
- Kalina, J. (2017). Techno-economic assessment of small-scale integrated biomass gasification dual fuel combined cycle power plant. *Energy*, 141, 2499–2507. <https://doi.org/10.1016/j.energy.2017.05.009>.
- Martín-Gamboa, M., Iribarren, D., Susmozas, A., & Dufour, J. (2016). Delving into sensible measures to enhance the environmental performance of biohydrogen: A quantitative approach based on process simulation, life cycle assessment and data envelopment analysis. *Bioresource Technology*, 214, 376–385. <https://doi.org/10.1016/j.biortech.2016.04.133>.

- Mazzola, S., Astolfi, M., & Macchi, E. (2016). The potential role of solid biomass for rural electrification: A techno economic analysis for a hybrid microgrid in India. *Applied Energy*, *169*, 370–383. <https://doi.org/10.1016/j.apenergy.2016.02.051>.
- Moreno, J., & Dufour, J. (2013). Life cycle assessment of hydrogen production from biomass gasification. Evaluation of different Spanish feedstocks. *International Journal of Hydrogen Energy*, *38*(18), 7616–7622. <https://doi.org/10.1016/j.ijhydene.2012.11.076>.
- Popp, J., Lakner, Z., Harangi-Rákos, M., & Fári, M. (2014). The effect of bioenergy expansion: Food, energy, and environment. *Renewable and Sustainable Energy Reviews*, *32*, 559–578. <https://doi.org/10.1016/j.rser.2014.01.056>.
- Scott, K., Daly, H., Barrett, J., & Strachan, N. (2016). National climate policy implications of mitigating embodied energy system emissions. *Climatic Change*, *136*(2), 325–338. <https://doi.org/10.1007/s10584-016-1618-0>.
- Searchinger, T., Heimlich, R., Houghton, R. A., Dong, F., Elobeid, A., Fabiosa, J., Tokgoz, S., Hayes, D., & Yu, T. H. (2008). Use of U.S. croplands for biofuels increases greenhouse gases through emissions from land-use change. *Science*, *423*.
- Spöttle, M., Alberici, S., Toop, G., Peters, D., Gamba, L., Ping, S., van Steen, H., & Bellefleur, D. (2013). Low ILUC potential of wastes and residues for biofuels, 168.
- Tagliaferri, C., Evangelisti, S., Clift, R., & Lettieri, P. (2018). Life cycle assessment of a biomass CHP plant in UK: The heathrow energy centre case. *Chemical Engineering Research and Design*, *133*, 210–221. <https://doi.org/10.1016/j.cherd.2018.03.022>.
- Villarini, M., Bocci, E., Di Carlo, A., Savuto, E., & Pallozzi, V. (2015). The case study of an innovative small scale biomass waste gasification heat and power plant contextualized in a farm. *Energy Procedia*, *82*, 335–342. <https://doi.org/10.1016/j.egypro.2015.11.790>.

Ergonomics and Work Organization

Introduction

Prof. Domenico Pessina

President of the 5th Section of the Italian Association of Agricultural Engineering
'Improve the Working Conditions and Safety'

Section 5th of Italian Society of Agricultural Engineering aims to improve the working conditions and safety of operators and to optimize the organization and the management of the farm, through the use of field planning tools and logistics, with a system approach. The 5th Section represents the national reference platform for technicians and all operators involved in these activities. It provides the latest developments in terms of tools and methodologies for organizing work and logistics in the agricultural, forestry and agri-food sectors, ergonomics and safety of operators, through co-ordination and co-operation in the organization of conferences, seminars, workshops related to these topics.

In the Mid-Term Congress of the Italian Association of Agricultural Engineering held in Matera (Italy) in September 2019, 12 papers were presented, dealing with very different aspects in the field of occupational safety and health and work organization. Seven of them were considered suitable for publication.

Considering the **safety** topic, in the study *A bottom-up approach to tractor safety: improving the handling of foldable roll-over protective structures (FROPS) through user-centred design* an ergonomic multidimensional analysis of FROPS operation was assessed, considering users' critical behaviour and perception in their interaction with the tractor features, in order to develop user-centered design solutions to improve the manual handling of the FROPS.

In the paper *Spatial analysis for detecting recent work accidents in agriculture in Italy*, the authors applied an approach based on the spatial analysis offering several suggestions, such as where and when injuries occurred more, the socio-demographic profile of the involved people (e.g. gender, age, nationality) and additional agricultural practices (e.g. mechanization processes adopted).

In the field of **ergonomics**, two studies concern the risk for workers due to exposure to vibration. The first, entitled *Effects of rod and oscillating frequency on the vibrations transmitted to hand-arm system by two olive portable harvesters* concerns

HAV (Hand-Arm Vibration); the second, with the title *First tests on a prototype device for the active control of the vibrations on agricultural tractors* deals viceversa with WBV (Whole Body Vibration). The paper having the title *Effect of different axial fans configurations on airflow rate* concerns another important topic, involving both environment and health of workers.

Finally, two studies were more related to **work organization** aspects: *Technical and economic evaluation of urban trees pruning by climbing arborists* and *Perceived barriers to the adoption of smart farming technologies in piedmont region, northwestern Italy: the role of user and farm variables*.

All these papers contributed significantly to increase the knowledge level of the typical topics developed inside of 5th Section of the Italian Association of Agricultural Engineering. Moreover, the Research members of this Section effectively promote the dissemination of the progress in studies, by actively participating in the symposiums and conferences organized by CIGR, EurAgEng and CIOSTA.

Spatial Analysis for Detecting Recent Work Accidents in Agriculture in Italy



Massimo Cecchini, Ilaria Zambon, Danilo Monarca, Francesca Piccioni, Alvaro Marucci and Andrea Colantoni

Abstract Work safety has been recently considered a growing topic in multi-disciplinary research across different working sectors, e.g. in open-field activities in agriculture. Precise guidelines and policy strategies are stimulated with the aim of providing a greater safety for operators and a more preliminary awareness of the potential risks. Computing work accidents is regularly achieved using classical approaches. However, it is difficult to quantify potential accidents or fatalities considering several factors (e.g. age of operators, their training experience but also environmental or geo-morphological characters). The paper focuses on recent work accidents (2012–2017) that occurred in the Italian agricultural sector. It classifies the accidents at work according to their severity (e.g. fatal, with/without permanent disabilities) and the way of occurrence (e.g. overturning of the tractor). One of the approaches used was based on the spatial analysis determining numerous suggestions, such as where and when injuries happened more often, the socio-demographic profile of the involved people (e.g. gender, age, nationality) and additional agricultural practices (e.g. mechanization processes applied). Revealing inherent patterns of safe (or unsafe) working conditions at the provincial scale (NUTS level 3 as designed by EUROSTAT), results showed that training or educational programs should be planned in specific areas with the purpose of increasing awareness toward risky events in agriculture. Future scenarios can be discovered based on explicit evidences dealing with risk factors and functioning conditions at various working sites with the

M. Cecchini · I. Zambon (✉) · D. Monarca · F. Piccioni · A. Marucci · A. Colantoni
DAFNE Department, Tuscia University, San Camillo de Lellis, 01100 Viterbo, Italy
e-mail: ilaria.zambon@unitus.it

M. Cecchini
e-mail: cecchini@unitus.it

D. Monarca
e-mail: monarca@unitus.it

F. Piccioni
e-mail: francesca.piccioni@unitus.it

A. Colantoni
e-mail: colantoni@unitus.it

final goal to launch appropriate technical, legislative and operational procedures to decrease work accidents.

Keywords Spatial analysis · Work accidents · Agriculture · Ergonomics · Work organization · Italy

1 Introduction

In recent years in Europe, the safety study has revealed a constant concern (Colantoni et al. 2017). Occupational injury rates diverge seasonally (Davies and Elias 2000), geographically (Wadsworth et al. 2003), by industry sector (Davies and Elias 2000) and by job typology (Di Lorenzo et al. 1998). Furthermore, also influenced by the age where usually an increased risk is associated with younger workers (Di Lorenzo et al. 1998; Davies and Elias 2000), in earlier statistics, men recorded higher injury rates than women (Di Lorenzo et al. 1998; Akerstedt et al. 2002). However, related to older age and economic sector (Akerstedt et al. 2002), other studies proved opposed findings. Since several factors interact mutually, identifying definite accidents can be found with rigid methods and checklists. For instance, the location where agricultural, forestry and park maintenance and hobby activities occurred exposes numerous independent factors (e.g. environmental, geo-morphological) which differ from the working operator (Cividino 2014).

The present paper focused on the professional accidents happened in the last years (2012–2017) in the primary sector in all Italian provinces. Recently, literature has tried to investigate about this issue, proposing both quantitative and qualitative analysis in agriculture and forestry (Lilley et al. 2002; Thelin 2002; Neely and Wilhelmson 2006; Solomon et al. 2007; Lindroos et al. 2008; Potočnik et al. 2009; Monarca et al. 2009; Suchomel and Belanová 2009; Montorselli et al. 2010; Mann et al. 2010; Lindroos and Burström 2010; Marucci et al. 2012; Colantoni et al. 2012; Bortolini et al. 2016). The topic concerning injuries and fatalities in the primary sector is imperative today because in recent decades this sector has lost both workers and cultivated land. In fact, the lost of agricultural land, the abandonment, the deforestation, the excessive rate of land consumption and the sealing soil are some of the main European challenges (Marucci et al. 2018; Zambon et al. 2018; Cecchini et al. 2018). The need to promote the primary economic sector is relevant to endorse and preserve natural and rural landscape, guaranteeing the safety of workers.

Based on this background, possible scenarios can be explored following risk factors and operating conditions on dissimilar working sites in order to establish suitable, technical, legislative and operational explanations (Cividino et al. 2015). Several recent studies focused on explicit issues that can be correlated to highly risk operations in the agricultural and forestry sector. Firstly, didactic courses and training in occupational safety should be planned and structured by employing definite training models that suggest advanced explanations for workers (Feltrin et al. 2015). Secondly, in the last decade, the recent crisis, together with a saturated job

market, caused a major inclination in the offer fixed—term or temporary contracts in the European countries (OECD 2002). Temporary employees are less skilled and unaware towards risky operations. The widespread application of provisional work has raised worries about increased volatility of employment and the relative consequences of job quality and working conditions (Hernanz and Toharia 2006). Thirdly, the agricultural and forestry sector offer cheaper and periodical, often illegal occupations to foreigners (e.g. immigrants). In this framework, those persons are not informed enough about the danger they are dealing with. Recently, in Italy, in Lazio Region precisely, a pilot-research project regarded the training needs for different foreign workers (e.g. from India, Romania), offering classrooms with native tutors. The main purpose of this project was to comprehend the relationship among risk perception between farmers and the key risk influences which they are exposed to (Cecchini et al. 2015).

The aim of this work is to make an analysis on the injuries that arose in agriculture in Italy in the last few years. On this purpose, we used the official data provided by INAIL (National Institute for Insurance against Accidents at Work) that were related to the reference period described above. The paper made a territorial analysis to understand which areas are most affected by accidents of different nature and applying a PCA to evaluate if there is the possibility of grouping the diverse Italian provinces and to identify similar characteristics incident on accident risk.

Based on previous premises, exploring on where and when accidents occurred, knowing about the persons involved (e.g. their age, sex, nationality) and correlating these episodes with agricultural and forest data, can reveal useful and inherent information about safety work conditions in a detailed territorial area. Possible scenarios can be discovered resulting from inherent risk factors and operating conditions on divergent working area to establish suitable technical, legislative and operational explanations (Cividino et al. 2015). Personal and job characteristics tend to increase the probability of having an accident for temporary workers, but the specific influence of contract type favours the latter, who show a lower probability on this account (Hernanz and Toharia 2006). Finally, in order to provide an enhanced attention and awareness of working people, training and educational programmes should be planned and organized (Feltrin et al. 2015; Cecchini et al. 2017).

2 Materials and Methods

Compared to other European countries, Italy has a much longer historical background about recording statistical investigation of accidents at work (Jacinto and Aspinwall 2004). Thanks to the work of the National Institute of Insurance (INAIL), founded in 1883, insurance against accidents at work turned out to be enforced in 1946. The processed dataset derived from an elaboration obtained from annual data given by INAIL (National Institute for Insurance against Accidents at Work in Italy). It concerns accidents reported in Italy from 2012 to 2017. The present paper focused only on the primary sector, which can be split into three economic activities: (i)

cultivations and production of animal products, hunting and related service activities; (ii) fisheries and aquaculture; and (iii) forestry.

The dataset used gives hints to comprehend when an accident happened, its typology (mortal or not), the age, sex and nationality of the person involved. All these statistics were run in GIS program, which analyzed the data following a territorial examination.

The use of GIS is essential as in no previous study this platform was used for representing the accident data. The overlap of the accident data with information of other nature as, for example, the slope of the ground, the prevailing crops, the existence of local policies aimed to favor the training of the workers or the report of the accidents, can provide fundamental indications for the study of the prevailing causes of accidents and the development of suitable preventive measures.

In this regard, it was possible to detect where the highest number of events verified in Italy. The spatial scale was at the provincial scale. In fact, the INAIL Institution doesn't give more detailed information about the area where the critical event occurred for a question of privacy permission. However, the month when the event occurred was duly mentioned. This evidence is essential for correlating existing agricultural and forest cases with potential dangers in a precise area. Besides, further indicators were collected. They are available at ISTAT agricultural census (2011). They permit to describe the rural field (e.g. surface area cultivated). In this way, a correlation was developed between INAIL and ISTAT database. Finally, a PCA was run for classify and recognize all the Italian provinces according to the set indicators.

3 Results

Following the period of this study (2012–2017), the analysis is based on different characteristics emerging from injuries that occurred in the primary sector. In Italy, 21,100 accidents at work were verified in the past six years (of which almost 100 casualties). Then, the number of injuries (also mortal ones) followed a declining trend. This tendency can be influenced by more educational courses on safety at work towards which, year after year, the all society is more sensitive to. However, this decreasing rate may also have been affected by the economic crisis. The lower number of employees can be tied to a lower risk of accidents. Looking at the entire period in object, the months with the highest rates are: March (1,832 accidents in Italy); June (2,015); July (2,015); September (1,934); and October (1,890). These statistics clearly coincide with the major agrarian practices, such as the crop harvesting (Fig. 1).

Geographically, the greatest number of injuries was reported in Central and Northern Italy. Particularly, there were a high number of accidents in the central area, involving female population while, in all the other areas, the highest number of people injured was male. The spatial distribution of injuries explained that during the considered period (2012–2017), the region with the most accidents was the Marche region (Central Italy) with 4,825 events (Fig. 2).

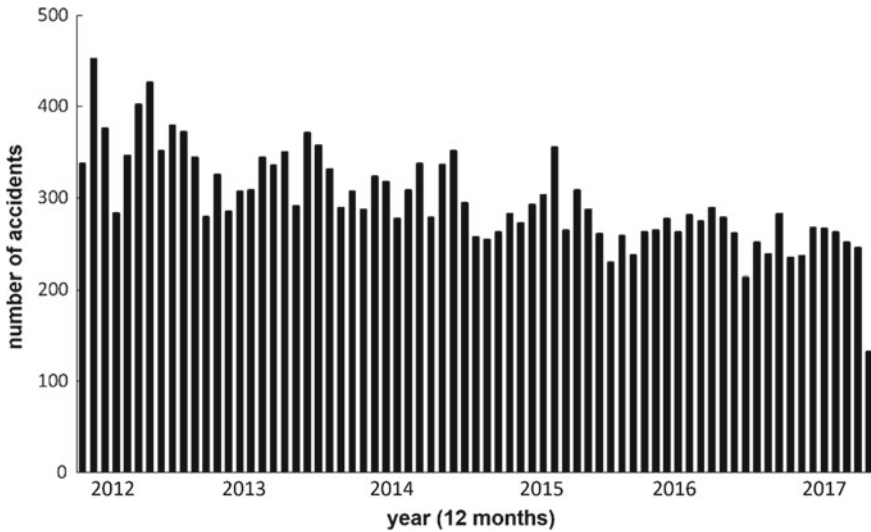


Fig. 1 Trend of number of accidents over time (2012–2017)

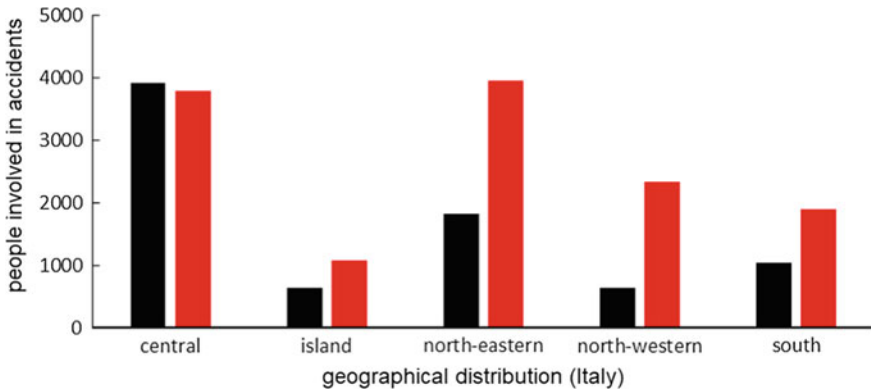


Fig. 2 People (males in black and females in red) involved in accidents for geographical subdivisions

Figure 3 shows that the groups aged between 40 and 60 years old represented the highest number of accidents in the last 5 years: in fact, there were almost 13,000 injuries of people with that age (about 60% of the sample). Moreover, map in Fig. 4 highlights the average age of the injured people being over 50 in the Sicilian provinces, whereas the age range between 45 and 50 years is recorded in the central regions, in the districts along the Po river and in Sardinian provinces.

The analysis also detected the foreign population involved in work-related injuries. The Romanian population is also the most affected group during the last 5 years. In fact, 533 persons were involved in accidents at work. In any geographical distribution

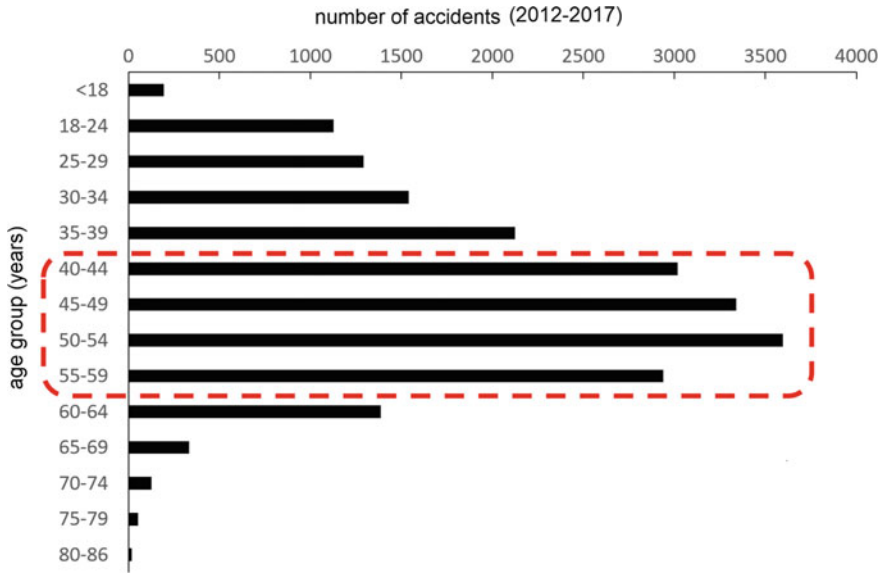
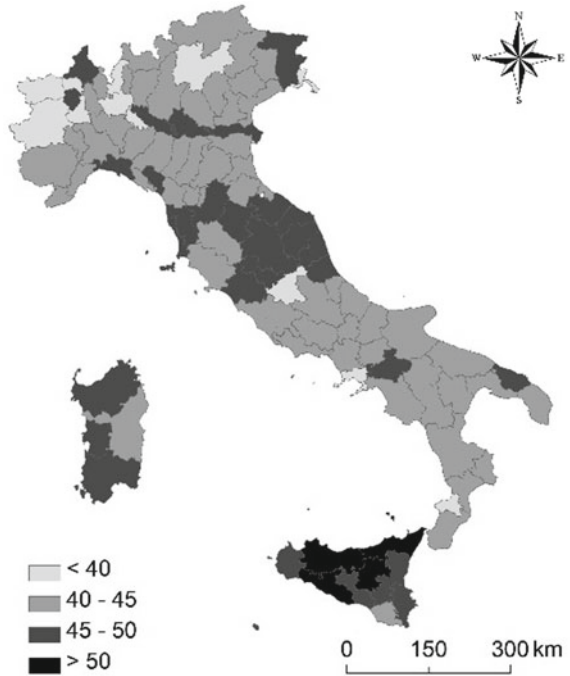


Fig. 3 Age groups of people involved in accidents

Fig. 4 Average age of the injured people at provincial level



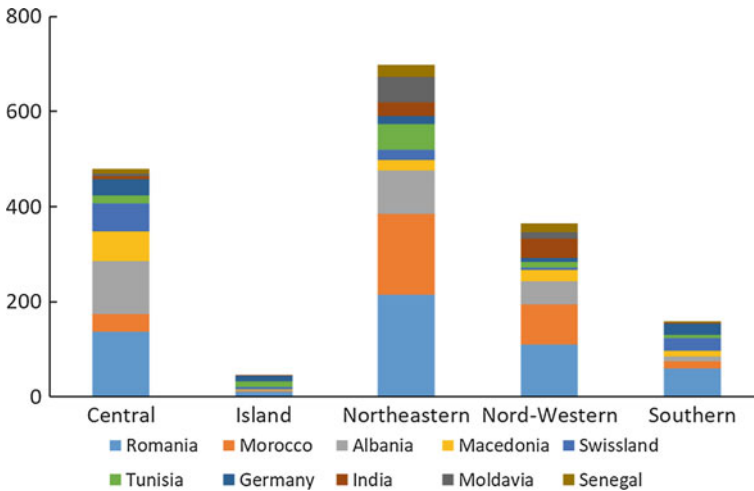


Fig. 5 Number of foreign populations involved in work-related accidents

in Italy, considering the citizenship, the Romanians represent constantly the largest number of people involved. The following group is 309 Moroccans, 261 Albanians and 121 Macedonians (Fig. 5).

A comparison with the agricultural census data is appropriate. Six indicators were then calculated:

- (a) number of people employed in agriculture on utilized agricultural area (UAA);
- (b) ratio of utilized agricultural area (UAA) on the total agricultural area (TAA);
- (c) number of accidents out of the number of people employed in agriculture per 1,000 employees;
- (d) number of accidents in relation to utilized agricultural area (UAA);
- (e) number of accidents normalized in relation to the utilized agricultural area (UAA) out of the total agricultural area (TAA);
- (f) variations among accidents occurred in 2017 (final year) and 2012 (first year of investigation).

The areas experiencing a strong incidence of workers in the primary sector in proportion to the active agricultural area (or UAA) are situated along the coastal areas, flatter lands and the main water flows (e.g. Po River). The inland mountainous regions have a lower rate for this indicator, instead. Very much cultivated rural areas are situated in the northern districts, especially along the Po River, some central provinces (e.g. Viterbo), the major islands and the Apulia region. As already mentioned above, the highest number of accidents at work calculated on the number of people employed in agriculture per 1,000 employees is recorded in the north-central areas of Italy (e.g. Aosta, big areas of Veneto, Marche and Trentino regions). The only southern province which showed a high rate is Foggia, which also stated a great occurrence of UAA on TAA. Integrating the previous ones, the fourth indicator paved the way for

emerging both the most productive areas in agricultural terms and the most dangerous contexts, linked to a higher incidence of employees. Findings also explained the riskiest provinces (Vicenza, Lucca and Roma) documenting the greatest amount of fatalities. Obtaining a normalized output, the fifth indicator has been developed expressing the number of accidents stabilized in ratio among utilized agricultural area (UAA) on total agricultural area (TAA). In this regard, the most sensitive areas towards work accidents are the central ones in Italy, especially Marche region, which has a high share of injuries at the workplace.

Following the last indicator that defines variations between the final and initial year of investigation, 11 provinces reported an increase in job-related accidents over time. Few of them are collocated in the north-western Italy (Cuneo, Aosta, Como, Monza and Brianza), while most of them are distributed in the central-southern regions (Benevento, Teramo, Matera, Isernia, Prato, Crotone, Verbanocusio-Ossola). Instead, the most virtuous provinces that have experienced a 50% decrease of work-related injuries are in the central and northern districts (e.g. Belluno, Forlì-Cesena, Siena, Rome) and in the south (e.g. Salerno, L'Aquila, Campobasso, Reggio Calabria, Barletta-Andria-Trani). Therefore, it is confirmed that 90% of Italian provinces witnessed a decrease in accidents at work overtime in the primary sector (Fig. 6).

To assess whether recent occupational accidents take on the same trends, PCA results explained the performances of each province. The PCA was chosen because it allows the identification of clusters. However, in this study no great results emerged for the very few available variables. Among these, the most important ones are those here described.

According to the first two components (PC1 highlights the areas with the highest number of accidents in the entire reference period. PC2 concerns the number of accidents per 1,000 workers), Marche region described a clearer and more detached distribution than the other Italian districts, due to the high number of accidents detected. Also, three other provinces (e.g. Forlì, Brindisi and Rome) recorded medium-large rural areas used. Besides, accidents in these areas happened particularly during autumn (e.g. October), different with winter. This situation gives us the opportunity to think about the role of specific crops whose production and harvesting can be harmful. With the third and fourth components, however, other contexts can be even better elaborated. PC3 highlighted the areas with a strong incidence of accidents in the first year of detection (2012), corresponding especially in winter e.g. December. PC4 showed the provinces with a higher accident rate in 2014, compared to 2016 (above all during February), revealing agricultural practices probably correlated to soil preparation activities that can cause accidents at work (Table 1).

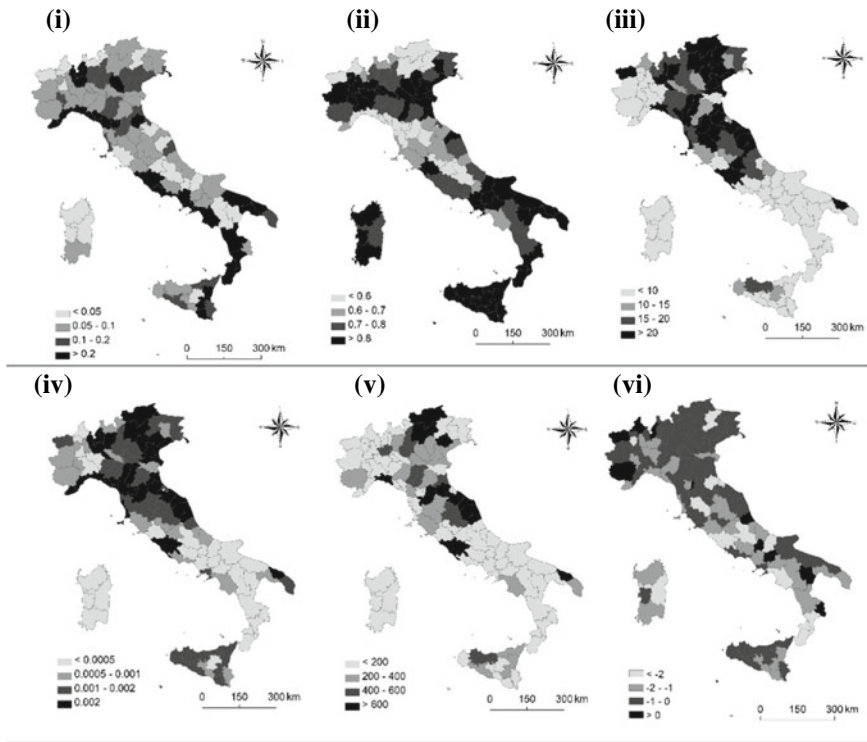


Fig. 6 Few indicators elaborated for the analysis: (i) number of people employed in agriculture on utilized agricultural area (UAA); (ii) ratio of utilized agricultural area (UAA) on the total agricultural area (TAA); (iii) number of accidents on the number of people employed in agriculture per 1,000 employees; (iv) number of accidents in relation to utilized agricultural area (UAA); (v) number of accidents normalized in relation to the utilized agricultural area (UAA) on the total agricultural area (TAA); and (vi) variations among accidents occurred in 2017 (final year) and 2012 (first year of investigation)

Table 1 Results from PCA elaboration

	PC 1	PC 2	PC 3	PC 4
Fatalities 2012			0.6	
Fatalities 2014				0.7
Fatalities 2016				-0.5
Fatalities/total fatalities	0.9			
Fatalities/n° workers per 1,000		0.9		
Total fatalities/SAU		0.7		0.7
January/total fatalities		-0.6		
Februray/total fatalities				0.7
October/total fatalities		0.5		
December/total fatalities		0.6	0.8	

4 Discussion

One of the research results highlights how the data available today do not allow correlating the accident risk indexes with factors such as the formation or the cultural level of the workers involved or the type and duration of the contract. This is a weakness of the present work, but it also represents a starting point for further research. It is suggested, therefore, to implement future and subsequent studies on this.

The analysis of statistical indicators and the exploration of data ensuing their spatial distribution make it clearly possible to distinguish the major dangerous districts. In addition to the INAIL data, an Italian Institution for collecting all the accident practices that have taken place, the census data from ISTAT allowed to normalize them with a homogeneous comparison among the Italian provinces. Geographically, the greatest number of injuries happened in central and northern Italy. The spatial distribution of work-related accidents during the reference period (2012–2017) explained that the region with the most injuries was the Marche region (Central Italy) with 4,825 events. However, it can also be necessary to integrate this data with the possible irregularity of work in certain areas (Feltrin et al. 2015). For instance, in southern Italy, work is often irregular and without a legal contract: in presence of a professional accident, the employee is obviously not protected and cannot report the episode. In this circumstance, central information is lost related to the type of contract performed. Furthermore, in Italy, as in other countries such as in France, accident statistics are also used to establish (business) contribution rates to ensure coverage of costs arising from accidents at work (Jacinto and Aspinwall 2004). Therefore, the social safety rate is variable, depending on accident costs. Such kind of policy can be used to a greater range as an economic incentive for the introduction of preventive measures (Jørgensen 2008). Conversely, the financial pressure on employers could lead to an under-declaration of accidents (Jacinto and Aspinwall 2004).

The main objective of accident research is to comprehend their causes with the aim of defining appropriate prevention measures (Jørgensen 2008; Jacinto et al. 2009). Most of accident statistics are collected and update in suitable datasets following classification systems and official registration measures (Jacinto and Aspinwall 2004). Though, talking about accidents at work, standardized legal notification and registration systems are usually not so simple (Jacinto et al. 2009) or joint in different countries, as in Europe (Dupré 2000; Jacinto and Aspinwall 2004).

Moreover, the geographical analysis of accidents at work in the primary sector is an unexplored topic in the scientific literature. Through a spatial approach, a major importance is often given to other economic sectors deemed to be hazardous, such as construction (López et al. 2008; Arquillos et al. 2012; Suárez-Cebador et al. 2014).

Analyzing work accidents in every component (e.g. place, sex, age etc. of the person involved) bring about the opportunity to examine the work environment in the primary sector in Italy and its trend over time (Cecchini et al. 2015). For instance, the influence of agricultural workplace accidents of older people can reveal a major

attention to sightsee the role that increased seniority leads to performance and attention in the workplace. Moreover, by routine, risks may be more slightly perceived during certain behavior practices but even being a potential for accident involvement. In fact, risk perception is linked to having attended training courses. However, workers that attended safety courses do not always act with a safe performance (Stoneman and Jinnah 2014; L'abbate et al. 2010). Reflecting both on the tasks to be carried out and on the quality of training is essential since information and training, at least in the primary sector, cannot be mastered mechanically but constitute real dynamic processes (Cecchini et al. 2017).

Farming activities play a greater role in economy even if it is important in taking care of workers' safety (Klepacki et al. 2008). The environment of farmer's workplace in evaluation with additional outlines of work is very explicit (Wysokiński 2015). Over time, the number of accidents has followed a declining trend. This tendency can be influenced by the presence of more educational courses on safety at work that—year after year—is more sensitive to these issues. The lower number of workers is correlated to the lower risk of accidents.

In the riskier provinces, an educational and training model should be implemented, defining a set of priorities, such as: (i) an interdisciplinary program and plan courses in addition to those programmed by law; (ii) an analysis of training with targets and profiles; (iii) a definition of degrees of knowledge and skills of trainers; (iv) development of technical sectors run by sector experts; and (v) propagation of the model in info points through regional and local awareness (Feltrin et al. 2015). Only by adopting a dynamic and contextualized model, a pilot-assessment can develop positive outcomes in the defined territorial area (Feltrin et al. 2015).

The data analyzed in the present work comes only from Italy. Findings may differ from those of other countries (Arquillos et al. 2012) but they may give some insights for sensitive common variables. Incidents that are not reported are excluded from the analysis because there are no data on them. In future researches, integrated indicators should be intended for obtaining a more accurate approach on their influence on work accidents. For instance, the climatic variable may designate whether there are variances in the severity of accidents among Mediterranean areas, e.g. Italy, and continental ones, e.g. Poland. Diverse training strategies must be considered and implemented improving the effectiveness of the training of agricultural workers.

References

- Akerstedt, T., Fredlund, P., Gillberg, M., & Jansson, B. (2002). A prospective study of fatal occupational accidents- relationship to sleeping difficulties and occupational factors. *Journal of Sleep Research, 11*, 69–71.
- Arquillos, A. L., Romero, J. C. R., & Gibb, A. (2012). Analysis of construction accidents in Spain, 2003–2008. *Journal of Safety Research, 43*(5–6), 381–388.
- Bortolini, L., Cividino, S. R., Gubiani, R., Cecchini, M., Delfanti, L. M., & Colantoni, A. (2016). Urban green spaces activities: A preparatory groundwork for a safety management system. *Journal of Safety Research, 56*, 75–82.

- Cecchini, M., Bedini, R., Mosetti, D., Marino, S., & Stasi, S. (2017). Safety knowledge and changing behavior in agricultural workers: An assessment model applied in central Italy. *Safety and Health at Work*, 9(2), 164–171.
- Cecchini, M., Monarca, D., Colantoni, A., Baciotti, B., Bedini, L., Menghini, G., & Porceddu, P. R. (2015, September 8–11). Safe in the field: A project for training and integration of foreign agricultural workers. In *Proceedings, IV International Conference Ragusa SHWA, Safety Health and Welfare in Agriculture, Agro-Food and Forestry Systems* (pp. 152–157). Lodi, Italy: Ragusa SHWA.
- Cecchini, M., Zambon, I., Pontrandolfi, A., Turco, R., Colantoni, A., Mavrakis, A., & Salvati, L. (2018). Urban sprawl and the ‘olive’ landscape: Sustainable land management for ‘crisis’ cities. *GeoJournal*, 1, 1–19.
- Cividino, S.R.S. (2014). La gestione della sicurezza sul lavoro in agricoltura; volume 1: L’azienda agricola. *Veneto Agricoltura*.
- Cividino, S. R., Colantoni, A., Vello, M., Dell’Antonia, D., Malev, O., & Gubiani, R. (2015). Risk analysis of agricultural, forestry and green maintenance working sites. *Contemporary Engineering Sciences*, 27(8), 1257–1266.
- Colantoni, A., Marucci, A., Monarca, D., Pagnello, B., Cecchini, M., & Bedini, R. (2012). The risk of musculoskeletal disorders due to repetitive movements of upper limbs for workers employed to vegetable grafting. *Journal of Food, Agriculture and Environment*, 10, 14–18.
- Colantoni, A., Mazzocchi, F., Laurendi, V., Grigolato, S., Monarca, F., Monarca, D., & Cecchini, M. (2017). Innovative solution for reducing the run-down time of the chipper disc using a brake clamp device. *Agriculture*, 7(8), 71.
- Davies, R., & Elias, P. (2000). *An analysis of temporal and national variations in reported workplace injury rates*. Warwick: Institute for Employment Research.
- Di Lorenzo, L., Zocchetti, C., & Platania, A. (1998). Minor and major work accidents in a Puglia business in the food sector: A 10-year study. *Medicina del Lavoro*, 89, 499–513.
- Dupré, D. (2000). Accidents at work in the EU in 1996. Statistics in Focus, Theme 3, *Population and social conditions*.
- Feltrin, S., Marino, M., Colantoni, A., & Cividino, S. R. (2015). *Agri-form: An innovative training model for safety in the agriculture and forestry sector*.
- Hernanz, V., & Toharia, L. (2006). Do temporary contracts increase work accidents? A microeconomic comparison between Italy and Spain. *Labour*, 20(3), 475–504.
- Jacinto, C., & Aspinwall, E. (2004). A survey on occupational accidents’ reporting and registration systems in the European Union. *Safety Science*, 42(10), 933–960.
- Jacinto, C., Canoa, M., & Soares, C. G. (2009). Workplace and organisational factors in accident analysis within the food Industry. *Safety Science*, 47(5), 626–635.
- Jørgensen, K. (2008). A systematic use of information from accidents as a basis of prevention activities. *Safety Science*, 46(2), 164–175.
- Klepacki, B. (2008). *Przestankizmianyrololnictwa w gospodarstwarodowej. V RolniczyFestiwal-Nauki (DokumenteElektroniczny)*. Warszawa: Centrum Doradztwa Rolniczego.
- L’abbate, N., Lorusso, A., & Lasalvia, M. (2010). Production cycles and risk agents in the agri-food sector. *Giornale Italiano di Medicina del Lavoro ed Ergonomia*, 32, 408–412.
- Lilley, R., Feyer, A. M., Kirk, P., & Gander, P. A. (2002). Survey of forest workers in New Zealand. Do hours of work, rest, and recovery play a role in accidents and injury? *Journal of Safety Research*, 33(1), 53–71.
- Lindroos, O., Aspmann, E. W., Lidestav, G., & Neely, G. (2008). Accidents in family forestry’s firewood production. *Accident Analysis and Prevention*, 40(3), 877–886.
- Lindroos, O., & Burström, L. (2010). Accident rates and types among self-employed private forest owners. *Accident Analysis and Prevention*, 42(6), 1729–1735.
- López, M. A. C., Ritzel, D. O., Fontaneda, I., & Alcántara, O. J. G. (2008). Construction industry accidents in Spain. *Journal of Safety Research*, 39(5), 497–507.
- Mann, C., Pouta, E., Gentin, S., & Jensen, F. S. (2010). Outdoor recreation in forest policy and legislation: A European comparison. *Urban Forestry and Urban Greening*, 9(4), 303–312.

- Marucci, A., Pagnello, B., Monarca, D., Colantoni, A., & Biondi, P. (2012). Heat stress suffered by workers employed in vegetable grafting in greenhouses. *Journal of Food, Agriculture and Environment*, 10, 1117–1121.
- Marucci, A., Zambon, I., Colantoni, A., & Monarca, D. (2018). A combination of agricultural and energy purposes: Evaluation of a prototype of photovoltaic greenhouse tunnel. *Renewable and Sustainable Energy Reviews*, 82, 1178–1186.
- Monarca, D., Cecchini, M., Guerrieri, M., Santi, M., Bedini, R., & Colantoni, A. (2009). Safety and health of workers: Exposure to dust, noise and vibration. *Acta Horticulturae*, 845, 437–442.
- Montorselli, N. B., Lombardin, C., Magagnotti, N., Marchi, E., Neri, F., Picchi, G., & Spinelli, R. (2010). Relating safety, productivity and company type for motor-manual logging operations in the Italian Alps. *Accident Analysis and Prevention*, 42(6), 2013–2017.
- Neely, G. W., & Wilhelmsen, E. (2006). Self-reported incidents, accidents, and use of protective gear among small-scale forestry workers in Sweden. *Safety Science*, 44(8), 723–732.
- OECD. (2002). *Employment Outlook 2002*. Paris: OECD.
- Potočnik, I., Pentek, T., & Poje, A. (2009). Severity analysis of accidents in forest operations. *Croatian Journal of Forest Engineering*, 30(2), 171–184.
- Solomon, C., Poole, J., Palmer, K. T., & Coggon, D. (2007). Non-fatal occupational injuries in British agriculture. *Occupational and Environmental Medicine*, 64(3), 150–154.
- Stoneman, Z., Jinnah, H. A., & Rains, G. C. (2014). Rains changing a dangerous rural cultural tradition: A randomized control study of youth as extra riders on tractors. *Journal of Rural Health*, 30, 388–396.
- Suárez-Cebador, M., Rubio-Romero, J. C., & López-Arquillos, A. (2014). Severity of electrical accidents in the construction industry in Spain. *Journal of Safety Research*, 48, 63–70.
- Suchomel, J., & Belanová, K. (2009). Influence of selected meteorological phenomena on work injury frequency in timber harvesting process. *Croatian Journal of Forest Engineering*, 30(2), 185–191.
- Thelin, A. (2002). Fatal accidents in Swedish farming and forestry, 1988–1997. *Safety Science*, 40(6), 501–517.
- Wadsworth, E. J. K., Simpson, S. A., Moss, S. C., & Smith, A. P. (2003). The Bristol Stress and Health Study: Accidents, minor injuries and cognitive failures at work. *Occupational Medicine*, 53(6), 392–397.
- Wysokiński, M. (2015). Accidents in agriculture as a socioeconomic problem. *Logistyka*, 2(1), 824–830.
- Zambon, I., Colantoni, A., Cecchini, M., & Mosconi, E. M. (2018). Rethinking sustainability within the viticulture realities integrating economy, landscape and energy. *Sustainability*, 10(2), 320.

A Bottom-Up Approach to Tractor Safety: Improving the Handling of Foldable Roll-Over Protective Structures (FROPS) Through User-Centred Design



Lucia Vigoroso, Federica Caffaro, Margherita Micheletti Cremasco, Ambra Giustetto, Giuseppe Paletto and Eugenio Cavallo

Abstract Rollover Protective Structures (ROPS) are the most effective solution to prevent fatalities in case of tractor rollover. Foldable Rollover Protective Structures (FROPS) have been developed to facilitate tractor operation in low overhead clearance zones. However, many of the fatalities and serious injuries in tractor rollover accidents occur when the FROPS is left by the operator in the folded-down position. Little is known about the reasons of such behavior and few solutions have been suggested to overcome this issue. Adopting a user-centred approach, in the present study a group of farmworkers ($n = 21$) was observed and interviewed while handling the FROPS on their own tractor, to point out critical behaviors, perceptions of effort and suggestions for technical solutions to support the manual operation of FROPS. A set of FROPS-related objective measurements were also taken. The participants reported moderate levels of perceived effort, as the entity of the force required to operate the FROPS was minimized by the low handling frequency. The observations pointed out that participants adopted some spontaneous strategies to facilitate the handling of the roll-bar during lowering and raising operations. Based on the present results some recommendations for technical adjustments are proposed to encourage the correct use of FROPS to prevent fatal accidents due to tractor rollover.

Keywords Agriculture · Foldable ROPS · Human-machine interaction · Safety · Tractor rollover · User-centred design

L. Vigoroso · F. Caffaro (✉) · G. Paletto · E. Cavallo
Institute for Agricultural and Earth Moving Machines (IMAMOTER, National Research Council (CNR)), Strada delle Cacce, 73, 10135 Turin, Italy
e-mail: f.caffaro@ima.to.cnr.it

F. Caffaro
Department of Education, Roma Tre University, Via del Castro Pretorio, 20, 00185 Rome, Italy

M. Micheletti Cremasco · A. Giustetto
Department of Life Sciences and Systems Biology, University of Torino, Via Accademia Albertina, 13, 10123 Turin, Germany

© Springer Nature Switzerland AG 2020
A. Coppola et al. (eds.), *Innovative Biosystems Engineering for Sustainable Agriculture, Forestry and Food Production*, Lecture Notes in Civil Engineering 67,
https://doi.org/10.1007/978-3-030-39299-4_70

1 Introduction

Agriculture has long been recognized as one of the most hazardous industries (Donham et al. 2016; Sanderson et al. 2006) and agricultural machinery is the major source of accidents (Abubakar et al. 2010; Reynolds and Groves 2000). Tractor rollover in particular has been reported as the main cause of unintentional fatalities and injuries among farmers in different countries (Abubakar et al. 2010; Jawa et al. 2013; Pessina et al. 2016). The most effective solution to significantly decrease the frequency of fatal rollovers is the combined use of the Rollover Protective Structure (ROPS) and the seatbelt (NIOSH, National Institute for Occupational Safety and Health 2009). The first mandatory requirement for ROPS to be fitted on newly manufactured agricultural tractors was introduced in Sweden in the 1950s (Biddle and Keane 2012). Following this experience, in the 1980s the adoption of safety structures to protect operators from injuries caused by vehicle overturns or rollovers has been generalized in most of the developed countries (Cavallo et al. 2015).

In the Scandinavian countries a significant reduction in the frequency of fatal rollovers for ROPS-equipped tractors was observed (Pessina et al. 2016). However, other European countries do not report the same positive trends and registered a high number of tractors without an adequate structure to protect the driver from overturn accidents (Mangado et al. 2007). For instance, in Italy, according to the National Institute for Insurance against Accidents at Work (INAIL, Istituto Nazionale per l'Assicurazione contro gli Infortuni sul Lavoro) database (INAIL 2018; Rondelli et al. 2018) between 2002 and 2012 there were 817 fatalities in agriculture, 205 of which were due to tractor rollover and more than 50% of the tractors involved in such accidents were not equipped with a ROPS (Pessina and Facchinetti 2011).

Overhead obstacles were reported as the most important reason for the operator not to install a ROPS (Spielholz et al. 2006). Therefore, Foldable Rollover Protective Structures (FROPS) were designed and installed on tractors to facilitate operation in low overhead clearance zone and tractor storage and transport.

In U.S. since 2005, 25% of rollover fatalities have occurred to tractors with ROPS in folded down position, and in the European countries 40% of fatalities occurred for the same reason (Ayers et al. 2017; NIOSH FACE 2015). Considering the Italian context, the few data available shows that from 2002 to 2012, 21.8% of the fatalities involved tractors with FROPS in folded-down position, and 4.8% of fatal accidents concerned tractors on which FROPS was installed but the foldable frame has been removed (INAIL 2018; Rondelli et al. 2018). Explanation for this behavior could be related to indolence or to the fact that raising and lowering the FROPS is considered a waste of time and a strenuous operation (Khorsandi et al. 2016), considering all the operation needed to fold up and fold down the FROPS (Ayers et al. 2017).

Based on these considerations, the aim of the present study was to identify the main criticalities in FROPS handling through the active involvement of a group of users, who were observed and interviewed during their interaction with the FROPS. This user-centred approach allowed to provide suggestions for targeted technical/training interventions based on the needs and capabilities of the real users to facilitate the

correct use of FROPS, with the final purpose of preventing injuries and fatalities in case of rollover accident.

2 Method

2.1 Participants

Participants in the study were recruited from different agricultural farms in Piedmont region, North western Italy, which is one of the Italian region with the higher rate of fatal tractor rollover accident (Pessina and Facchinetti 2017). Twenty-one farmers and sixteen models of tractors of different brands equipped with rear mounted FROPS according to OECD Tractor Codes (OECD 2017) were involved in the study. Only male farmers were selected, to obtain more comparable data and based on the predominance of male workers in the Italian agriculture (ISTAT, Istituto Nazionale di Statistica 2013). Inclusion criteria for the tractors were a track higher than 1150 mm (standard-track tractors, OECD 2017) and being fitted with a two posts rear mounted foldable ROPS. The socio-demographic characteristics of the participants were collected using a questionnaire and dimensions of the tractors relevant for the study were recorded using a digital laser rangefinder (Fig. 1).

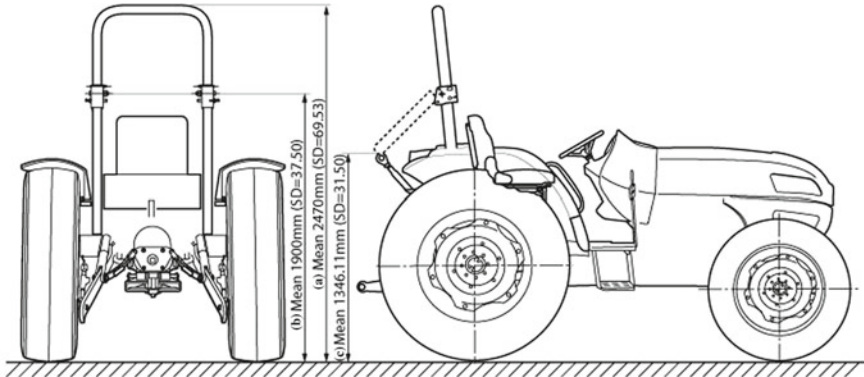


Fig. 1 Tractor dimensions recorded and their mean value: **a** overall height of tractor with FROPS in upright position, **b** vertical distance from ground-to-FROPS rotating point, and **c** vertical distance from ground-to-top of folded ROPS

2.2 Instruments

Two instruments were used to obtain data about users' perceptions, suggestions and behaviors. A semi-structured interview was used to investigate any possible source of discomfort in handling FROPS (reachability, grip, hands and/or feet placement), risk perception and suggestions to promote the correct use of FROPS. Subsequently, to collect the subjective rating of effort during FROPS handling, a Borg CR10 scale was adopted (Borg 1998). Participants were also observed and video-recorded while folding down and raising the FROPS to investigate which strategies, gestures and postures they adopted to perform the requested task and the quality of the interaction with the machinery.

3 Results

In this section, descriptive statistics related to the participants and the tractors considered in the study are reported at first. Then, the results about the interaction between the user and the FROPS are presented. Table 1 shows the main socio-demographic characteristics of the participants. Participants' stature ranged between 1600 and 1860 mm, thus including values from the 5th to the 99th percentile of the Italian male population (ISO 7250-2:2010 2010). Concerning the tractor dimensions relevant for the study, the mean values are reported in Fig. 1.

Looking at the behavioral strategies adopted by the participants to perform the FROPS handling task, some reachability and balance issues were observed, especially for the participants with a lower stature. These participants, as many of the taller ones, handled the FROPS by using some parts of the machine as a support for the feet (especially the lower links of the rear three-point linkage), exposing themselves to the risk of falling (Fig. 2). When climbing on the machine parts, the hands had no safe support, and the folding frame or the top link of the three point linkage was often used as an additional grip point (Fig. 3). Regarding operators' hands, the FROPS raising task was performed either by placing both hands on the vertical part of the roll bar or by using only one hand (the other one was used just as a support). In some cases, when there were shafts to support the rear mirror or lights mounted

Table 1 Participants' main socio-demographic characteristics

Variable	Levels	n	%	Mean	SD
Gender	Male	21	100		
	Female	0	0		
Age				49	11
Stature (cm)				175	8.43
Working experience in agriculture (years)				25.73	17.26

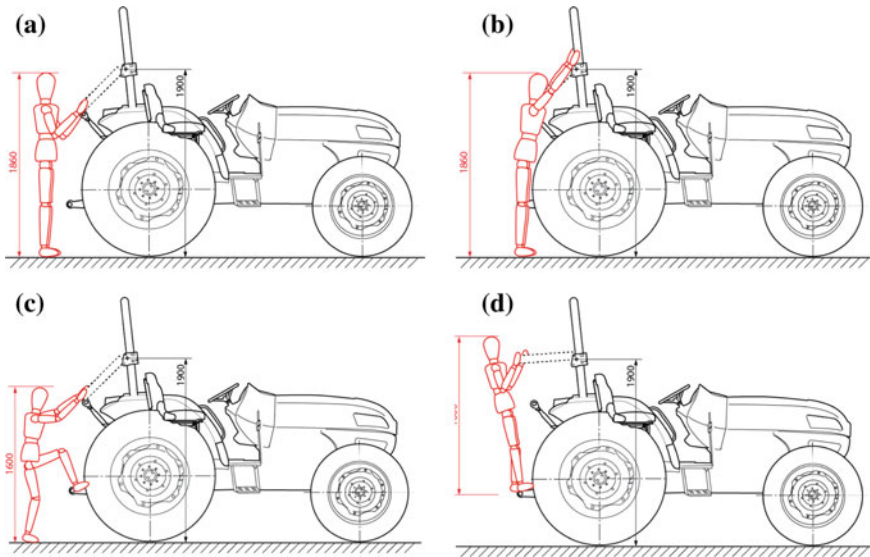


Fig. 2 Interaction between the FROPS and operators characterized by different statures: the tallest operator (1860 mm) at the beginning of the lifting operation (a) and at the end (b), and the shortest operator (1600 mm) at the beginning of the lifting operation (c) and during the operation (d). The tractor represented in the figure has been designed considering the mean value of the tractor overall height with FROPS in upright position



Fig. 3 One participant raising the FROPS, using the rear three-point lower links as a support for the feet

on the FROPS, the participants used these devices to reach and operate the folding frame (Fig. 4).

Regarding farmers' perceptions of effort, risk and discomfort in FROPS operation, some similarities emerged in the responses. Moderate levels of perceived fatigue were reported, both when lowering and raising the FROPS (mean values of 3 and 2.97 for lowering and raising, respectively, on the 0 to 10 Borg scale). However, three participants in particular reported their feeling of discomfort related to the absence



Fig. 4 One participant adopting spontaneous strategies to overcome the reachability issue

of an adequate grip point and other three participants expressed the discomfort related to the place to stand. Some examples of their answers were as follows: “I think it is uncomfortable because there is not any handle or something that helps me to climb the lower links”, “I do not know exactly where I can place my feet if there is not the equipment attached to the back of the tractor”, “This gesture is not comfortable, it is too complex”. Regarding the risky posture and behavior adopted to raise and fold down the FROPS, participants’ opinions could be divided into two main categories: the risk of being hit by FROPS during handling ($n = 4$) and the risk of falling down from the lower links ($n = 5$). Some examples of the answers were as follows: “It is not an issue of discomfort but there is the risk of getting hurt”, “If I cannot keep it up [the FROPS] it can hit my head or cut my hand”, “I do not feel safe while handling FROPS”, “It is not correct to climb on the lower links because you could fall and hurt yourself”.

Regarding the possible changes that could be made to make the handling easier, participants’ answers were rather uniform. Three farmers suggested that the adoption of a hydraulic system could be a useful solution, even if it is not a cheap device; three farmers indicated the need to use an additional support for the feet, both to increase their balance and to allow them to reach the highest points of the FROPS; nearly half of the participants ($n = 10$) expressed their preference for the addition of a handle: “You could add a handle, or a hook that allows me to lift and fold down the roll-bar without using other supports”, “Adding a handle or an anchor point would help me a lot”, “A handle or a rope to move FROPS could be useful” and “A handle could be useful but should not hinder other machinery parts”. Finally, two farmers suggested to add *something* to increase the reachability of the upper part of FROPS, but they did not express any specific suggestion about what they would change in the structure and one farmer suggested the use of a device that brakes the FROPS while it is lowering, so that it does not hit the tractor parts.

4 Discussion and Conclusions

Some previous studies focused (Ayers et al. 2017) on FROPS and methods to encourage its correct use. However, these studies were conducted starting from a technical analysis of the problem and proposed some design solutions that took into account

mainly engineering aspects. Based on the beneficial effects of a direct involvement of the users when designing interactive systems (ISO 9241-210:2010 [2010](#)), in this study we adopted a bottom-up approach to identify critical aspects in FROPS handling and to propose solutions based on real users' capabilities and behaviors.

The measurements performed in real conditions pointed out the need for an adjustment in the designing phase of the roll-bar, taking into account the anthropometric variability of the users (Ahlstrom and Longo [2003](#)). Interviews and observations showed that the issues related to FROPS lowering and raising were not due to a high level of perceived fatigue, as demonstrated by the Borg scale data, but they were mainly related to the reachability of the tractors components and FROPS parts (Micheletti Cremasco et al. [2019](#)). This was especially true for that agricultural population whose anthropometric measures belonged to the 5th and 25th percentile. The user-centred requirements shall be considered to improve the user balance, comfort and safety when performing the lowering and raising operations. The adoption of a mobile handle on the side of the FROPS would support the gesture required to reach and operate the roll bar, following the current behavior of the operators, who already perform the task by placing their hands on the vertical bars of the FROPS.

Furthermore, when lowering the FROPS, the presence of an additional handle could facilitate the task and avoid slamming the roll-bar on the mechanical parts of the tractor's back. The adoption of spontaneous strategies by some participants confirmed the feasibility of the suggestions given by many farmers involved in the study, representing a valid starting point for a subsequent phase of prototyping, development and testing of possible design solutions.

References

- Abubakar, M. S. A., Ahmad, D., & Akande, F. B. (2010). A review of farm tractor overturning accidents and safety. *Pertanika Journal of Science and Technology*, *18*(2), 377–385.
- Ahlstrom, V., & Longo, K. (2003). *Human factors design standard. For acquisition of commercial-off-the-shelf subsystems, non-developmental items, and developmental systems*. DOT/FAA/CT-96/1 HF-STD-001. US Department of Transportation Federal Aviation Administration.
- Ayers, P., Khorsandi, F., Wang, X., & Araujo, G. (2017). ROPS designs to protect operators during agricultural tractor rollovers. *Journal of Terramechanics*. <https://doi.org/10.1016/j.jterra.2017.05.003>.
- Biddle, E. A., & Keane, P. R. (2012). Action learning: A new method to increase tractor rollover protective structure (ROPS) adoption. *Journal of Agromedicine* *14*(4), 398–409. <https://doi.org/10.1080/1059924X.2012.713842>.
- Borg, G. (1998). *Borg's perceived exertion and pain scales* (H. Kinetics, Ed.). Champaign, IL: Human Kinetics.
- Cavallo, E., Ferrari, E., & Coccia, M. (2015). Likely technological trajectories in agricultural tractors by analysing innovative attitudes of farmers. *International Journal of Technology, Policy and Management*, *15*(2), 158–177. <https://doi.org/10.1504/IJTPM.2015.069203>.
- Donham, K. J., Yoder, A., & Grafft, L. (2016). Acute injuries in agriculture. In K. J. Donham & A. Thelin (Eds.), *Agricultural medicine: Rural occupational and environmental health, safety, and prevention* (p. 573). Hoboken, NJ: Wiley.

- INAIL (Istituto Nazionale per l'Assicurazione contro gli Infortuni sul Lavoro). (2018). Infor.MO. Gli infortuni mortali in agricoltura. Retrieved from <https://www.inail.it/cs/internet/docs/alg-informo-gli-infortuni-mortali-agricoltura.pdf>.
- ISO (International Organization for Standardization). ISO 7250-2:2010. (2010). *Basic human body measurements for technological design—Part 2: Statistical summaries of body measurements from national populations*.
- ISO (International Organization for Standardization). ISO 9241-210. (2010). *Ergonomics of human-system interaction—Human-centred design for interactive systems*.
- ISTAT (Istituto Nazionale di Statistica). (2013). *Atlante dell'agricoltura italiana-6° Censimento Generale dell'Agricoltura* [Atlas of Italian agriculture]. ISBN: 978-88-458-1781-6.
- Jawa, R. S., Young, D. H., Stothert, J. C., Yetter, D., Dumond, R., Shostrom, V. K., et al. (2013). Farm machinery injuries: The 15-year experience at an urban joint trauma center system in a rural state. *Journal of Agromedicine*, 18(2), 98–106. <https://doi.org/10.1080/1059924X.2013.766145>.
- Khorsandi, F., Ayers, P. D., Jackson, D., & Wilkerson, J. (2016). The effect of speed on foldable ROPS actuation forces. *Journal of Agricultural Safety and Health*, 22(4), 285–298. <https://doi.org/10.13031/jash.22.11752>.
- Micheletti Cremasco, M., Caffaro, F., Giustetto, A., Vigoroso, L., Paletto, G., & Cavallo, E. (2019). Tractor rollover protection: Is the incorrect use of foldable rollover protective structures due to human or to technical issues? *Human Factors*, 62, 64–76. <https://doi.org/10.1177/0018720819848201>.
- NIOSH (National Institute for Occupational Safety and Health). (2009). *Preventing death and injury in tractor overturns with rollover protective structures*.
- NIOSH (National Institute for Occupational Safety and Health) FACE. (2015). *Workplace Safety & Health Topics, Fatality assessment and control evaluation (FACE) program*.
- OECD (Organization for Economic Co-operation and Development). (2017). *OECD Standard Code for the official testing of agricultural and forestry tractors*. Paris: France.
- Pessina, D., & Facchinetti, D. (2011). Il ruolo del web nel monitoraggio degli incidenti mortali dovuti al ribaltamento dei trattori agricoli. *Convegno di Medio Termine dell'Associazione Italiana di Ingegneria Agraria AIIA*, 22–24.
- Pessina, D., & Facchinetti, D. (2017). A survey on fatal accidents for overturning of agricultural tractors in Italy. *Chemical Engineering Transactions*, 58, 79–84. <https://doi.org/10.3303/CET1758014>.
- Pessina, D., Facchinetti, D., & Giordano, D. M. (2016). Narrow-track agricultural tractors: A survey on the load of the hand-operated foldable rollbar. *Journal of Agricultural Safety and Health*, 22(4), 275–284. <https://doi.org/10.13031/jash.22.11709>.
- Reynolds, S. J., & Groves, W. (2000). Effectiveness of roll-over protective structures in reducing farm tractor fatalities. *American Journal of Preventive Medicine*, 18(4S), 63–69.
- Rondelli, V., Casazza, C., & Martelli, R. (2018). Tractor rollover fatalities, analyzing accident scenario. *Journal of Safety Research*, 67, 99–106. <https://doi.org/10.1016/j.jsr.2018.09.015>.
- Sanderson, W. T., Madsen, M. D., Rautiainen, R., Kelly, K. M., Zwerling, C., Taylor, C. D., et al. (2006). Tractor overturn concerns in Iowa: Perspectives from the Keokuk county rural health study. *Journal of Agricultural Safety and Health*, 12(1), 71–81.
- Spielholz, P., Sjoström, T., Clark, R. E., & Adams, D. A. (2006). A survey of tractors and rollover protective structures in Washington State. *Journal of Agricultural Safety and Health*, 12(4), 325–333. <https://doi.org/10.13031/2013.22012>.

Technical and Economic Evaluation of Urban Trees Pruning by Climbing Arborists



M. Biocca, P. Gallo and G. Sperandio

Abstract In recent years, the techniques based on access to the tree canopy with ropes (the so-called tree-climbing), have been spreading in Italy. This study evaluated the productivity and costs of tree pruning operated by professional climbing arborists. Overall, seven work sites were sampled with time studies. Work time was measured for every single phase from the beginning of pruning operations to the transport of the residual biomass to the collection and loading point, using centesimal stopwatches and video recording. Total observation time amounted to 27.78 h. The work time analysis showed that the pruning entails the main work time (about 42% of the gross time) followed by the time for setting the yards and stacking the residual wood (26%). The evaluation of the costs of each work site considered the fixed and the variable costs and the costs for the labor force. The results showed that the average gross time of the work sites was 6 h Mg⁻¹, with average productivity of 0.19 Mg h⁻¹ and an average cost of 173 € tree⁻¹. A Multiple Linear Regression modelling was adopted to predict the cost for pruning. The regression analysis provided five regressors (easily to measure) that are capable to predict the cost per tree. They were: (1) tree diameter; (2) tree height; (3) distance to the residual biomass collection point; (4) number of operators; (5) hourly cost. This paper can contribute to optimize trees maintenance methods in urban sites using tree-climbing methods.

Keywords Tree-climbing · Urban trees · Urban forestry · Tree maintenance · Work time study

M. Biocca (✉) · P. Gallo · G. Sperandio

Consiglio per la ricerca in agricoltura e l'analisi dell'economia agraria (CREA), Centro di ricerca Ingegneria e Trasformazioni agroalimentari, Via della Pascolare 16, Monterotondo, 00015 Rome, Italy

e-mail: marcello.biocca@crea.gov.it

© Springer Nature Switzerland AG 2020

A. Coppola et al. (eds.), *Innovative Biosystems Engineering for Sustainable Agriculture, Forestry and Food Production*, Lecture Notes in Civil Engineering 67,

https://doi.org/10.1007/978-3-030-39299-4_71

1 Introduction

Rope-based access methods, commonly also named “tree-climbing”, represent an assortment of techniques to ascend and operate in tree canopies.

These techniques are very appropriate to professional arborists for the maintenance of ornamental trees located in urban areas. A variety of practices such as pruning, felling of trees, cabling, phytosanitary inspections and others, can be carried out using these techniques. Tree-climbing shows several advantages compared to the traditional operations with aerial lifts: targeted and selective interventions on tree branches, reaching internal portions of the canopy without damaging branches of other trees or infrastructures, accessing to trees located in confined areas where machinery cannot enter (Biocca and Bortolini 2019). In urban forestry, operating by means of tree-climbing are often the only possible solution to maintain trees. The scientific literature about the technical and economic evaluation of maintenance operation performed by tree-climbing is rather poor. Some authors have studied either safety aspects of the method (Mazzocchi et al. 2015; Bortolini et al. 2016) or technical approaches (Anderson et al. 2015).

Pruning is performed throughout the lifetime of an urban tree for various reasons, including: improving growth form, alleviating structural problems (such as removal of deadwood), crown raising, managing pests or diseases, decreasing failure risks and resolving conflicts with infrastructures (buildings, electric cables, road signs and lights, etc.). An ideal pruning should be operated reducing to a minimum the quantity of crown removed, to safeguard the photosynthetic apparatus of the plant and to reduce the operative costs (Vogt et al. 2015). Nevertheless, the residual biomass is a potentially large and underutilized resource that could be exploited at local level for wood products and bio-based fuels for power and heat generation after the volume has been reduced by chipping (Colucci et al. 2010; Velázquez-Martí et al. 2013; Li et al. 2017; Sperandio et al. 2014; Raud et al. 2017; Bagagiolo et al. 2017). For these reasons, this study aimed at both evaluating the productivity of the observed yards in terms of produced wood and estimated costs of pruning procedures operated by professional climbing arborists.

2 Materials and Methods

Overall, seven work yards (from Y1 to Y7) were sampled with time studies (Table 1).

The trees included both evergreen and deciduous species. The work sites were located in private gardens, with different easiness of access. In fact, the distance of the plant to the collection and loading point of residual biomass ranged from 1 m (in case of full accessibility, with the possibility to place a truck for loading very close to the tree) to 60 m (where the collected biomass must be manually transported from the tree to the collection point).

Table 1 Main characteristics of the observed work yards

Work yard	Workers [No.]	Equipment	Species	Tree height [m]	Trunk diameter at 1.3 m [m]	Distance to the collection point [m]
Y1	3	manual saw; blower	<i>Cedrus libani</i>	22	0.65	15
Y2	2	manual saw; chain-saw; blower	<i>Pinus pinea</i>	22	0.70	40
Y3	3	manual saw; blower	<i>Pinus pinea</i>	15.4	0.74	35
Y4	2	manual saw; chain-saw;	<i>Tilia cordata</i>	9	0.45	1
Y5	2	manual saw; chain-saw;	<i>Pinus pinaster</i>	13.5	0.57	35
Y6	2	electric chain saw; manual saw	<i>Ailanthus altissima</i>	17	0.53	60
Y7	2	chain-saw	<i>Quercus ilex</i>	17	0.85	1

Work time was measured for every single operation carried out by a specialized worker during his activity. In particular, five main elements were identified and separated: (1) “setting and staking” (which includes yard’s preparation, transport to the collection point and stacking of residual wood), (2) “pruning” (using either manual or motorized tools), (3) “shift” (movement of the operator inside the tree crown), (4) “delay time for avoidable time losses”, (5) “delay time for unavoidable time losses”. The time elements were recorded using centesimal stopwatches and video recording. Total observation time amounted to 27.78 h.

The evaluation of the operating costs of each work yard was carried out by means of an analytical method, considering the fixed costs, the variable costs and the costs for the labor force (Spinelli et al. 2011). In Table 2, the hourly costs of workers and equipment for each work yard are reported.

A Multiple Linear Regression (MLR) modelling was adopted to predict the cost per tree. A statistical analysis of the MLR was performed with the software R (R Core Team 2013).

The residual biomass was assessed by measuring the volume of cut branches stacked at the collection point. Then the data was converted in fresh weight according to conversion tables (Tabacchi et al. 2011) for each tree species.

Table 2 Hourly costs (€ h⁻¹) of the workers and equipment employed in the observed yards

Yard	Specialized worker	Qualified worker	Chainsaw	Electric chainsaw	Blower	Total
Y1	20.00	30.00	–	–	4.00	54.0
Y2	20.00	15.00	3.00	–	4.00	42.0
Y3	20.00	30.00	–	–	4.00	54.0
Y4	20.00	15.00	3.00	–	–	38.0
Y5	20.00	15.00	3.00	–	–	38.0
Y6	20.00	15.00	–	1.95	4.00	41.0
Y7	20.00	15.00	–	–	–	35.0

3 Results and Discussion

In relation to the working time study, Fig. 1 shows the working times of the different work phases of the observed yards, with reference to the work of a specialized operator who performs the pruning operation. The main work time is the cutting of the branches, attaining about 42% of total work time, followed by the time for setting the yards and stacking the residual wood (26%), movements of the operator in the tree’s crown (20%), unavoidable delay time (10%) and avoidable delay time (2%).

The observed phases of the work included always a similar routine. A specialized worker, after wearing the personal protective equipment (PPE) approaches the tree and individuates the point to place the rope to make the first ascend. Then, he carries out the pruning operation, moving in the tree’s crown. A second operator (in some cases, two additional operators) is assisting the work from the ground and is beginning the collection of the cut branches. At the end of the pruning operation, both the operators transport the residual wood to a collection point, where the biomass is stacked for the loading, and clean the work area, removing sawdust and little branches. In this study the time (and the cost) for loading and transportation of the obtained biomass is not considered.

Fig. 1 Average time in minutes (±standard error) of the working time operations

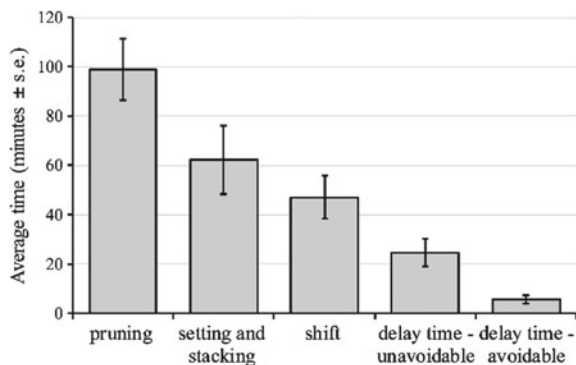


Fig. 2 Unitary time (h tree⁻¹) and productivity (Mg h⁻¹) of the seven work yards

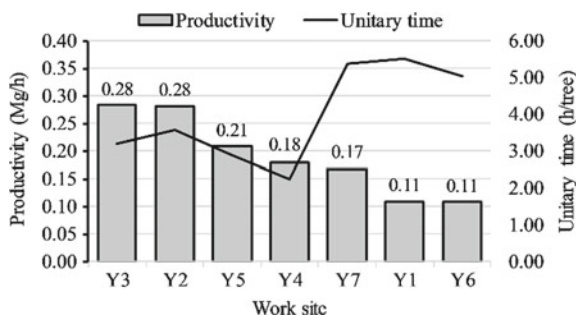
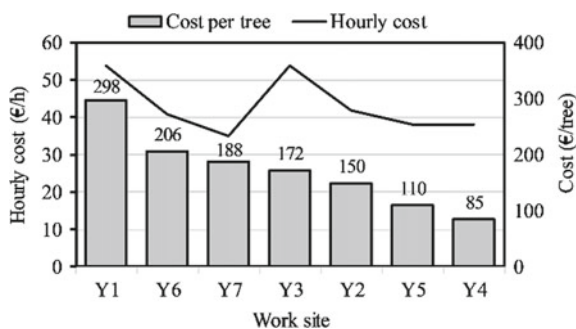


Fig. 3 Cost of the work yards in terms of cost per tree (€ tree⁻¹) and hourly cost (€ h⁻¹)



The total work time per tree was quite variable, ranging from 2.2 to 5.5 h tree⁻¹ (average 4.0 h tree⁻¹). As consequence, the obtained work productivity was also variable, with an average of 0.19 Mg h⁻¹ of residual wood from the pruning (Fig. 2).

Figure 3 shows the costs expressed in terms of cost per tree and hourly cost. Also in this case, the figures are very variable, especially when the data are expressed in terms of € tree⁻¹ (from a minimum of 85 for the work site Y4, to a maximum of 298 € tree⁻¹ for the work site Y1).

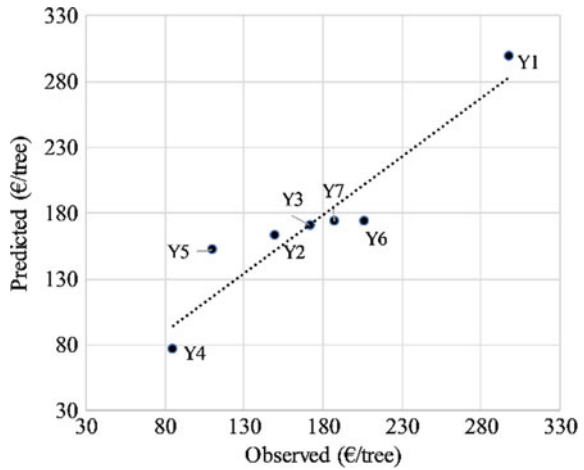
These results reflect the various yards characteristics, such as species, tree sizes, distance to the collection point and number of operators employed.

The Multiple Linear Regression (MLR) model to estimate the unitary cost (€ tree⁻¹) of the yards showed a high value of the determination coefficient (R² = 0.89). However, the value of the adjusted R² equal to 0.32, does not permit to generalize the model's prevision (Fig. 4). The regression analysis allowed to individuate five independent regressors to predict the unitary cost. They were: (1) diameter of trunk at d.b.h (m); (2) height of the tree (m); (3) distance from the tree to the wood collection point (m); (4) number of operators; (5) hourly cost (€ h⁻¹). It is noticeable that the selected variables are easily to measure, letting a practical use for estimation of costs of pruning operated by means of tree climbers.

The equation of the MLR model adopted to estimate the unitary cost necessary to pruning one tree is the followings:

Cost per tree (CT—€ tree⁻¹):

Fig. 4 Predicted and observed values of unitary cost (€ tree⁻¹). Statistics: multiple R²: 0.89, adjusted R²: 0.32, p-value: 0.5385



$$CT = -26.4255 HC + 461.293 NW + 0.95 DS - 3.1621 DI + 18.0267 HE + 137.0624;$$

where:

HC = hourly cost; NW = number of workers; DS = distance to the loading point; HE = tree height; DI = d.b.h. tree diameter.

4 Conclusions

In the present paper, urban trees pruning yards were studied. A work time analysis was carried out from the setting of the yards to the preparation for the loading of the residual wood. Time analysis can individuate weakness points in the operation and it contributes to study the work from a safety point of view. In the observed cases, the time of preparation, dismantling and transport of the cut wood to the collection point attained around one fourth of the total work time. In fact, when the operator ends the pruning, he spends additional time in collaborating to dismantle the yard, cleaning the area and transporting residual wood to the loading point. This time is largely depending from the position of the collection point of residual wood. The organization of the yard should take in account the distance from the tree to the point where the wood is stacked before the loading, and the firm should take decisions to optimize this point.

The adopted MLR model gave interesting results about the prediction of the unitary cost of urban tree pruning. However, the limited number of observed yards prevents a generalized conclusion about this point, and future studies are required to individuate a model capable to effectively predict the cost.

The possibility to reutilize the biomass for a secondary use (i.e. energy production) allows the tree owner to save the disposal charge usually paid (around 80 € Mg⁻¹).

Moreover, taking in account that the tree pruning has produced an average of 0.7 Mg tree⁻¹ (fresh wood), it is interesting to see that 200 pruned trees per year are enough to feed, with a renewable source of energy, a small size heat power plant of 232 kW_t (Verani et al. 2015).

Acknowledgements This research was funded by the Italian national project “AGROENER, Energy from agriculture: sustainable innovations for the bioeconomy”, financed by MiPAAF (D.D. n. 26329 of 01/04/2016—<http://agroener.crea.gov.it/>). Authors are grateful to the teams of arborists belonging to the following firms that actively collaborated in the project: Ecologistica s.r.l. (VT) (6 yards); Floema giardini di Emanuele Bracci, (RM) (1 yard).

References

- Anderson, D. L., Koomjian, W., French, B., Altenhoff, S. R., & Luce, J. (2015). Review of rope-based access methods for the forest canopy: safe and unsafe practices in published information sources and a summary of current methods. *Methods in Ecology and Evolution*, 6(8), 865–872. <https://doi.org/10.1111/2041-210X.12393>.
- Bagagiolo, G., Laurendi, V., & Cavallo, E. (2017) Safety improvements on wood chippers currently in use: A study on feasibility in the Italian context. *Agriculture*, 7, 98. <https://doi.org/10.3390/agriculture7120098>.
- Biocca, M., & Bortolini, L. (2019). *Macchine e tecniche per il verde urbano. Realizzazione, cura e manutenzione delle aree verdi. Consiglio per la ricerca in agricoltura e l'analisi dell'economia agraria-CREA (Ed.) (234 pp). Roma.*
- Bortolini, L., Cividino, S. R. S., Gubiani, R., Cecchini, M., Delfanti, L. M. P., & Colantoni, A. (2016). Urban green spaces activities: A preparatory groundwork for a safety management system. *Journal of Safety Research*, 56, 75–82. <https://doi.org/10.1016/j.jsr.2015.12.004>.
- Colucci, M., D'Antonio, P., D'Antonio, C., & Evangelista, C. (2010, September 16–18). The biomasses deriving from the public parks management: An hypothesis of a city-wood-energy chain in Potenza. In *Proceedings of International Conference Ragusa SHWA2010* (pp. 635–642). Italy: Ragusa Ibla Campus.
- Li, Y., Zhou, L. W., & Wang, R. Z. (2017). Urban biomass and methods of estimating municipal biomass resources. *Renewable and Sustainable Energy Reviews*, 80, 1017–1030. <https://doi.org/10.1016/j.rser.2017.05.214>.
- Mazzocchi, F., Cecchini, M., Monarca, D., Colantoni, A., Caruso, L., & Leopardi, F. (2015). An overview of risk assessment for tree climber arborists. *Contemporary Engineering Sciences*, 8(25), 1171–1177.
- R Core Team. (2013). *R: A language and environment for statistical computing*. Vienna, Austria: R Foundation for Statistical Computing. www.R-project.org.
- Raud, M., Mitt, M., Oja, T., Olt, J., Orupöld, K., & Kikas, T. (2017). The utilisation potential of urban greening waste: Tartu case study. *Urban Forestry & Urban Greening*, 21, 96–101. <https://doi.org/10.1016/j.ufug.2016.11.014>.
- Sperandio, G., Fedrizzi, M., Pagano, M., Guerrieri, M., & Verani, S. (2014). Abbattimento di palme infestate da punteruolo rosso. *Sherwood*, 204, 35–38.
- Spinelli, R., Magagnotti, N., Sperandio, G., Cielo, P., Verani, S., & Zanuttini, R. (2011). Cost and productivity of harvesting high-value hybrid poplar plantations in Italy. *Forest Products Journal*, 61(1), 64–70.
- Tabacchi, G., Di Cosmo, L., Gasparini, P., & Morelli, S. (2011). Stima del volume e della fitomassa delle principali specie forestali italiane. Equazioni di previsione, tavole del volume e tavole della

- fitomassa arborea epigea. CRA, Unità di Ricerca per il Monitoraggio e la Pianificazione Forestale. Trento. 412 pp.
- Velázquez-Martí, B., Sajdak, M., & López-Cortés, I. (2013). Available residual biomass obtained from pruning *Morus alba* L. trees cultivated in urban forest. *Renewable Energy*, *60*, 27–33. <https://doi.org/10.1016/j.renene.2013.04.001>.
- Verani, S., Sperandio, G., Picchio, R., Marchi, E., & Costa, C. (2015). Sustainability assessment of a self-consumption wood-energy chain on small scale for heat generation in central Italy. *Energies*, *8*(6), 5182–5197.
- Vogt, J., Hauer, R. J., & Fischer, B. C. (2015). The costs of maintaining and not maintaining the urban forest: A review of the urban forestry and arboriculture literature. *Arboriculture & Urban Forestry*, *41*(6), 293–323.

First Tests on a Prototype Device for the Active Control of Whole-Body Vibrations on Agricultural Tractors



Daniele Pochi, Laura Fornaciari, Renato Grilli, Monica Betto, Stefano Benigni and Roberto Fanigliulo

Abstract In old tractors, apart from tires, the only means for the reduction of vibration was a seat consisting of a sheet metal shell supported by a simple U-shaped spring. Today, the effects of seats, cabins, axles, suspensions and tires combine to increase comfort and safety at levels that were once unimaginable. Trying to improve the safety and comfort levels in the work-places, this work describes a first experience on the application of a vibration active control system (AVC) on a medium-power agricultural tractor. Its seat's suspension was integrated by an electromagnetic actuator generating movements opposing to those caused by soil unevenness, based on the signals received from two accelerometers measuring the vibrations at the seat and at the cab platform. A further instrumentation measured the driver whole-body vibration providing the frequency analysis and the calculation of the weighted accelerations and the acceleration sum vector (a_v). The tests were carried out on a compacted ground circuit with a section with natural unevenness. They aimed at evaluating the effects of the AVC system by comparing the whole-body vibrations measured in "ON" and "OFF" modes. The maximum accelerations always occurred at 2.5 Hz. The reduction mostly regarded the a_z component ("ON": 0.66 m s^{-2} ; "OFF": 0.94 m s^{-2}). The resultant a_v were 1.47 m s^{-2} and 1.97 m s^{-2} respectively for "ON" and "OFF" modes. In both tests, the differences between the values of weighted accelerations were lower due to the effect of the filter "A". The above data resulted from the acquisition along the entire established paths. Since only limited sections of the tracks were uneven, the results underestimated the actual reduction achieved on the obstacles, which becomes more evident by observing the FFT diagrams.

Keywords Vibration · Active vibration control · Tractor · Driver comfort

D. Pochi · L. Fornaciari · R. Grilli · M. Betto · S. Benigni · R. Fanigliulo (✉)
Consiglio per la ricerca in agricoltura e l'analisi dell'economia Agraria (CREA), Centro di ricerca Ingegneria e Trasformazioni agroalimentari (Research Centre for Engineering and Agro-Food Processing), Via della Pascolare 16, Monterotondo, 00015 Rome, Italy
e-mail: roberto.fanigliulo@crea.gov.it

© Springer Nature Switzerland AG 2020
A. Coppola et al. (eds.), *Innovative Biosystems Engineering for Sustainable Agriculture, Forestry and Food Production*, Lecture Notes in Civil Engineering 67,
https://doi.org/10.1007/978-3-030-39299-4_72

1 Introduction

A long time has passed since, apart from tires, the only means for the reduction of vibration on tractors was a seat consisting of a sheet metal shell supported by a simple U-shaped spring. Today, the effects of seats, cabins, axles, suspensions and tires combine to increase comfort and safety. However, even after the entry into force of the Italian Legislative Decree 81/08 (D.Lgs. n. 81 2008), the levels of vibration at the driver seat, often exceeding the law limits, keep on causing negative effects on the health of the drivers. Low back pain is commonly spread among workers subjected to whole body vibrations on vehicles. Studies on this problem started since a long time (Hulshof et al. 1987; Pope et al. 1999) and led to an improvement of the methods for the evaluations of the vibrations on the vehicles (Paddan and Griffin 2002) and of the effectiveness of the suspensions adopted to reduce them. The progress regarded both passive (Maciejewski et al. 2009) and active suspensions. The first studies on active suspension concerned the automotive sector (Hohensee et al. 1989; Buma 1991; Ballo 1993) and were focused on the development of pneumatic systems (Horvat 1980; Cho and Hedrick 1985; Sharp and Hassan 1988). They progressively extended to other types of vehicle.

Nowadays, the reduction of the vibrations on the driver seat of agricultural tractors is still achieved mostly by means of passive suspensions adopting mechanic or pneumatic springs, effective on the vertical axis at frequencies higher than 8–10 Hz. Due to the still high cost of active suspensions, only a few models of high-end tractors are equipped with them, mainly based on pneumatic systems. Trying to contribute to improve the safety and comfort levels in the work-place, this work reports the results of the first test on a tractor with the driver seat integrated with an active vibration control (VAC) system based on an electromagnetic actuator used as an active suspension.

2 Materials and Methods

The tests were carried out using the Landini Legend 145, a 4WD tractor with cab and nominal power of 107 kW. The original driver seat was replaced by a seat Grammer, mod. Compacto XXM (Fig. 1a), equipped with a spring suspension system whose stiffness (Fig. 1b) can be adjusted basing on the driver's mass. The overall excursion of the seat is 110 mm. The suspension of the seat was integrated with an electromagnetic actuator (LINMOT PO1-48 × 360F-C, Fig. 1d) capable to exert a maximum force (1024 N) for a 180 mm stroke (max stroke: 330 mm), enough to cover the overall excursion of the seat. The characteristics of the actuator are reported in the Table 1. The Fig. 1e shows how the actuator has been installed. The stator was fixed to the steel support of the seat cushion by means of a steel block suitably shaped, with the aim of following the movement of the seat, while one end of the slider was hinged on the steel plate base of the seat and hence, to the cab floor.

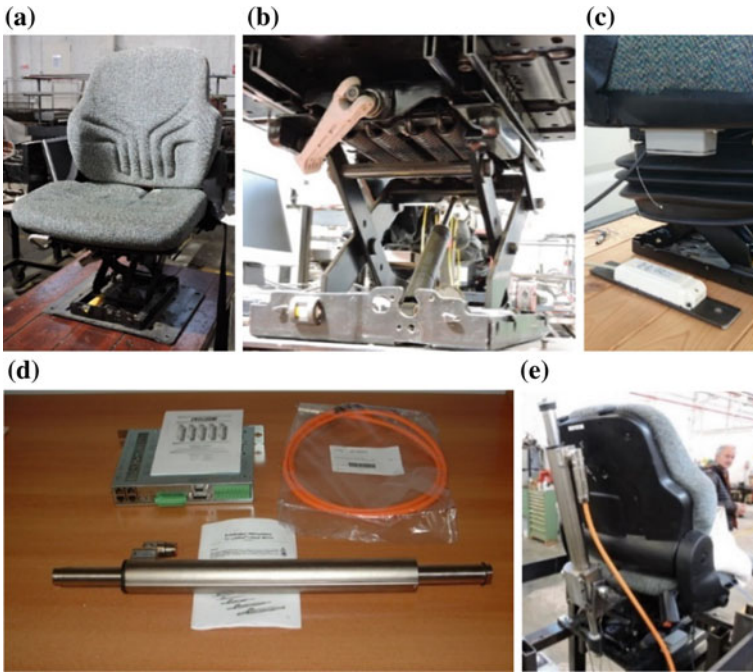


Fig. 1 **a** the seat Grammer Compacto XXM used in the study; **b** spring suspension of the seat; **c** three-axial accelerometers applied to the seat and to the cab floor; **d** actuator LINMOT and servo-controller LINMOT Series E1200; **e** actuator applied to the driver seat

Table 1 Main characteristics of the actuator LINMOT PO1-48 × 360F-C

Stator	Diameter (mm)	48
	Length (mm)	410
	Mass (g)	2880
Slider	Diameter (mm)	28.1
	Length (mm)	620
	Mass (g)	2720
Stroke	Maximum (mm)	330
	Max Force (mm)	180
Peak force (N)		1024
Cont. force (N)		203
Force constant (N/A)		32
Max. current @ 72 V DC (A)		32
Max. velocity @ 72 V DC (m s ⁻¹)		2.1
Position repeatability (mm)		±0.05
Linearity (%)		±0.20

In the new suspension resulting from the combination of the spring system and the actuator, the stiffness of the springs was adjusted so that the seat, with the driver seated, without shocks, was in the middle of its 110 mm stroke, with possible excursion of ± 55 mm. Thus, the springs system supports all driver's mass, while the function of the actuator is to counteract, mainly on the vertical axis (Z), the effects of any shocks due to soil unevenness.

The system is completed by: switching power supply for the mechanics (power: 800 W, output: 72 V DC, input: 230 V DC); power supply for the control system (power: 100 W, output: 24 V CC, input: 230 V DC); DC/AC Inverter, (power: 2000 W, input: 12 V, output 230 V); servo-controller LINMOT (Fig. 1e); Data Acquisition System (DAS—sampling frequency: 500 kHz; 16 analogic single ended, or 8 differential, input channels; 2 analogic output channels; 8 digital output channels; two 32 bit counters; USB interface). All components can be shipped on the tractor. The feedback intervention of the actuator (force, speed, position) is based on the measurement of the accelerations on the seat and on the floor of the cabin. On purpose, a three-axial accelerometer (frequency of measurement: 500 Hz; range of meas.: ± 6 g; sensitivity: 206 mV g^{-1}) was installed under the seat cushion and another on the floor, on the same vertical axis (Fig. 1c). The vertical oscillation of the seat, referred to the cab floor, was monitored by a position transducer (CELESCO, mod. VT 2101-0025-111). Basing on the signals provided by these sensors the data acquisition system generates the countersignals. These are sent to the servo-controller that modulates the interventions of the actuator which are meant to minimize/nullify the shocks on the seat. The characteristics of the countersignals can be varied by means filters controlled by a module inserted in the DAS. Such filters concern: (1) "Threshold": level of acceleration, expressed as fraction of the gravity acceleration, "g", below which the system does not work; (2) "P": percent of the maximum force providable by the actuator; (3) "R": delay of the countersignals referred to the signal. A second instrumental chain was employed to evaluate the effects of the actuator on the level of vibration (on the cab floor and on the driver whole-body). It consists of an 8 channel data acquisition system (Soundbook) with data processing software (Samurai); a three-axial accelerometer (Brüel & Kjær, mod. 4322) configured for seat measurements; a three-axial accelerometer (Brüel & Kjær, mod. 4321) fixed on the cab floor; a calibrator (PCB mod. 394 C 06). The accelerometers were oriented according to the standard UNI ISO 2631-1:2014. The measurements were made to compare the obtained results. When the AVC is "OFF", only the spring suspension of the seat is working. The first data processing provided the Fast Fourier Transform (FFT) of the linear accelerations in the three spatial axes. In the abscissas of the resulting diagrams, the time was replaced by the corresponding distance traveled by the tractor to show the variation of the acceleration along the test track. Then, the frequency analysis of the three axial components of the acceleration (a_x , a_y , a_z) was carried out for the linear data and the data weighted in the interval 0.5–80 Hz. The filters used (W_k for Z axis and W_d for X and Y axes) are commonly adopted in the evaluation of the comfort and on the evaluation of the possible occurrence of damage to the health. Eventually, the average axial accelerations (a_{wx} , a_{wy} , a_{wz}) and the resultant acceleration vector (a_v) were calculated according to the above mentioned

standard. The tests track consisted of a closed path (length: 206 m). About half of the path had the surface in compact ground and presented a natural unevenness, while the remaining part was plane with a macadam surface. Each test consisted of a lap of this circuit, at a speed of about 3.3 m^{-1} chosen by the driver to deal with the irregularities of the test track under safety conditions. The data recorded with AVC in “OFF” mode were compared with those in “ON” mode, recorded under different settings of the system (threshold of the signal (T), intensity (P) and delay (R) of the countersignal). Many trials have been executed to explore the capabilities of the actuator. Three settings provided good results and will be described in the following.

3 Results and Discussion

The Fig. 2 shows an example of the accelerations measured in the test track by the two accelerometers connected to the AVC system. The unit adopted is “g” (gravity acc.).

The interventions of the actuator are based on the values at the cab floor, while those at the driver seat describe the trend of the parameter, that is similar in “ON” and “OFF”, reflecting the trend of the track with the first half more uneven. However, the peaks of acceleration at the seat in “ON” are lower than in “OFF”. The values of the accelerations observed in the same tests of Fig. 2 were processed to obtain the frequency distribution for classes of 0.013 g (0.127 m s^{-2}) in the interval between $\pm 0.19 \text{ g}$. The results are reported in the Fig. 3.

The comparison between the frequency distributions of the accelerations at cab floor and at the seat is reported in the left diagrams of Fig. 3 for “ON” and “OFF” modes. In “ON” the frequency distributions are similar and concentrated around 0 g, while in “OFF” the seat acceleration is more dispersed, indicating higher accelerations occurring for effect of the spring suspension. On the other hand, the comparison between “ON” and “OFF” (right diagrams of Fig. 3) show that, both at the driver seat and at the cab floor, the frequency distribution of the accelerations is clearly more concentrated around 0 in “ON” than in “OFF”. This means that the actuator is effective in modifying the level of vibration, but probably, part of its action is directed

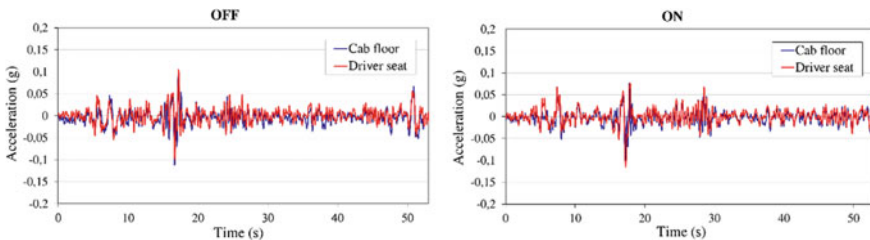


Fig. 2 Example of measurements made by the two accelerometers of the AVC system, in “OFF” and “ON” mode. The AVC setting was: R 8 (0.08 s), P 83 (%), T 0.01 g (0.0981 m s^{-2})

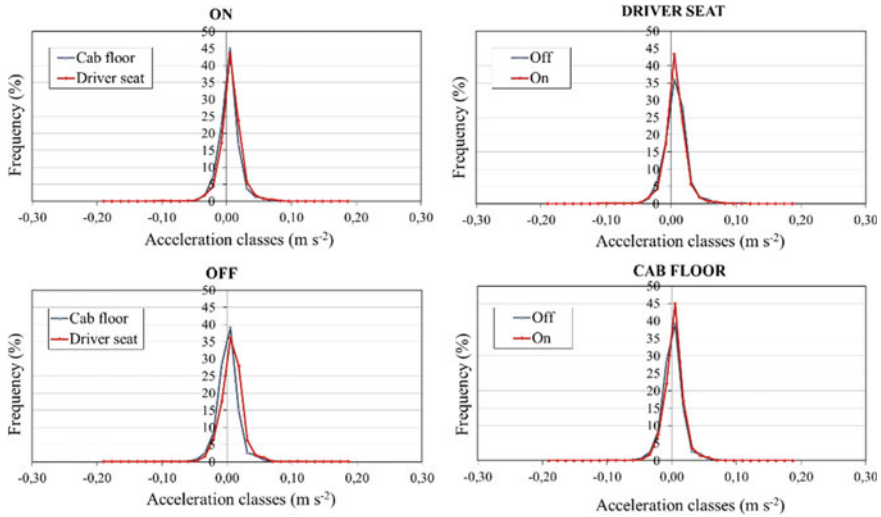


Fig. 3 Frequency distribution of the values of accelerations provided by the two accelerometers of the AVC system. Comparison between Cab Floor and Seat in “ON” and in “OFF” modes and between “OFF” and “ON” modes both at driver seat and cab floor level

toward the cab platform. Improving the quality of the connection between actuator and cab floor (e.g. by interposing a seismic mass) could increase its effectiveness toward the seat.

The effects of the active system on the level of vibration in the cab were evaluated through the analysis of the data collected and processed by the second instrumentation described in “Materials and Methods”. With reference to three AVC settings (“ON”) compared to “OFF” mode, the Fig. 4 reports the FFT diagrams of the three-axial components of the accelerations at driver seat. In order to spatially refer the accelerations, the scale of the distance covered in the time considered for the FFT elaboration is reported at the bottom of Fig. 4. The difference between “ON” and “OFF” is clear on the X and, mostly, the Z axis, with significant reduction of the higher peaks in “ON” occurring in the most uneven section of the test track (20–120 m), while the trends are similar in the remaining, more regular section of the track.

The results of the frequency analysis of the accelerations at the driver seat, in “ON” and “OFF” modes, are reported in the Fig. 5 for the three AVC settings of Fig. 4. They confirm the above considerations: some differences can be observed in the X, but the major reductions occur on the Z axis and concern the low frequencies (below 12.5 Hz), with highest values always at 2.5 Hz. The diagrams also show the different behaviours of linear and weighted accelerations, due to the weighting filter that emphasizes the effect of the high frequencies. Consequently, the differences between “ON” and “OFF” are lower for the weighted than for the linear accelerations. The “R2-P69- T0.01 g” AVC setting (Fig. 5, right diagrams) provided the higher reductions on all spatial axes, with some visible effects also on the Y.

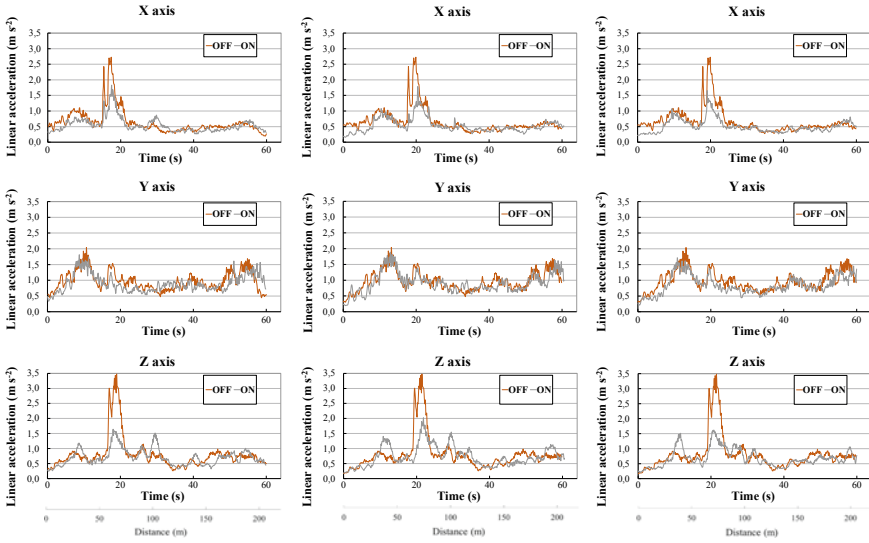


Fig. 4 FFT diagrams of the axial acceleration as a function of the distance. The diagrams refer to three AVC settings that provided the higher reduction of the level of vibration. From the left: R8-P83-T0.03 g (0.294 m s^{-2}); R2-P88-T0.01 g (0.098 m s^{-2}); R2-P69-T0.01 g (0.098 m s^{-2})

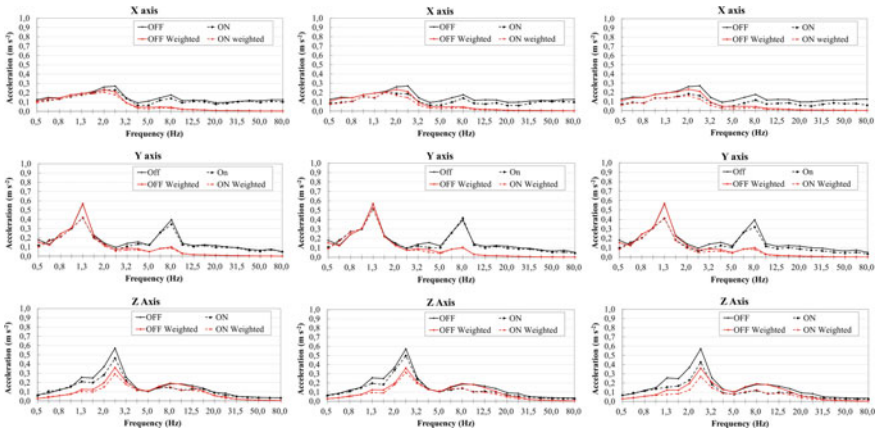


Fig. 5 Diagrams of the frequency analysis of the accelerations in the interval 0.5–80 Hz. The analysis regarded the three axial components of linear and “A” weighted accelerations observed in the three AVC settings that provided the higher reduction of the level of vibration: R8-P83-T0.03 g (0.294 m s^{-2}); R2-P88-T0.01 g (0.098 m s^{-2}); R2-P69-T0.01 g (0.098 m s^{-2})

Table 2 Comparison of the accelerations observed with AVC system in “OFF” and “ON” modes

Actuator's setting	Linear acceleration ($m\ s^{-2}$)						“A” weighted acceleration ($m\ s^{-2}$)									
	a_{wx}		a_{wy}		a_{wz}		a_v		a_{wx}		a_{wy}		a_{wz}		a_v	
	On	Off	On	Off	On	Off	On	Off	On	Off	On	Off	On	Off	On	Off
R8-P83-T0.03 g	0.64	0.73	0.85	0.99	0.78	0.94	1.68	1.97	0.47	0.53	0.65	0.79	0.53	0.64	1.25	1.48
R2-P88-T0.01 g	0.55	0.73	0.95	0.99	0.8	0.94	1.74	1.97	0.41	0.53	0.75	0.79	0.54	0.64	1.32	1.48
R2-P69-T0.01 g	0.47	0.73	0.8	0.99	0.66	0.94	1.47	1.97	0.36	0.53	0.64	0.79	0.44	0.64	1.11	1.48

The series of values of linear and weighted axial accelerations were used to calculate the average axial accelerations (a_{wx} , a_{wy} , a_{wz}) and the resultant a_v . The results of calculation (Table 2) confirm that the “R2-P69-T0.01 g” setting provided the best performance, with higher reduction of the whole-body vibration.

4 Conclusions

This work describes the first tests of an active vibration control system applied at the seat of an agricultural tractor, based on an electromagnetic actuator. The tests, aimed at exploring the potentiality of the actuator, allowed to identify some promising configurations of the AVC system. A significant reduction of the whole-body vibration was observed for frequencies below 12.5 Hz. As to the resultant acceleration, a_v , the highest reductions were 0.49 m s^{-2} and 0.36 m s^{-2} respectively for linear and weighted accelerations. Limiting the data analysis to the most uneven section of the test track would probably increase such differences. However, further investigations are needed to increase the knowledge of the system with the aim of improving its effectiveness.

Acknowledgements This work was supported by the sub-project AgriDigit financed by the Ministry of Agricultural, Food and Forestry Policies (MiPAAF) (DM 36503/7305/2018).

References

- Ballo, I. (1993). Active vibration control system for driver's seat of earth-moving vehicles. *Archives of Acoustic*, 18(2), 183–195.
- Buma, S. (1991). Toyota active suspension system for the 1989 celica. In *Proceedings of the International Symposium on Active Control of Sound and Vibration* (pp. 517–521). Tokyo, Japan.
- Cho, D., & Hedrick, J. K. (1985). Pneumatic actuators for vehicle active suspension applications. *Journal of Dynamic Systems, Measurement, and Control*, 107(3), 67–72.
- D. Lgs. 9 aprile 2008 n. 81. Attuazione dell'articolo 1 della Legge 3 agosto 2007. n. 123 in materia di tutela della salute e della sicurezza nei luoghi di lavoro. G. U. n. 101 del 30/4/2008.
- Hohensee, H. J., Jaker, H. P., Rutz, R., & Gaedtke, T. (1989). Aktive Fahrzeugfederung. *VDI Bericht 778 in Reifen*, Fahrwerk, Fahrbahn (pp. 357–377). VDI Verlag.
- Horvat, B. (1980). Pneumatisches aktives Federungssystem. *VDI Bericht*, 369, 1–8.
- Hulshof, C., & van Zanten, B. V. (1987). Whole-body vibration and low back pain—A review of epidemiologic studies. *International Archives of Occupational Health*, 59, 205–220.
- Maciejewski, I., Meyer, L., & Krzyzynski, T. (2009). Modelling and multi-criteria optimisation of passive seat suspension vibro-isolating properties. *Journal of Sound and Vibration*, 324, 520–538.
- Paddan, G. S., & Griffin, M. J. (2002). Evaluation of whole-body vibration in vehicle. *Journal of Sound and Vibration*, 253(1), 195–213.
- Pope, M. H., Wilder, D. G., & Magnusson, M. L. (1999). A review of studies on seated whole body vibration and low back pain. *Proceedings of the Institution of Mechanical Engineers. Part H, Journal of Engineering in Medicine*, 213(6), 435–446.

Sharp, R. S., & Hassan, J. H. (1988). Performance predictions for a pneumatic active car suspension system. *Proceedings of the Institution of Mechanical Engineers, Part D: Journal of Engineering in Medicine*, 202(4), 243–250.

UNI ISO 2631-1:2014 - Vibrazioni meccaniche e urti - Valutazione dell'esposizione dell'uomo alle vibrazioni trasmesse al corpo intero - Parte 1: Requisiti generali.

Effects of Rod and Oscillating Frequency on the Vibrations Transmitted to Hand-Arm System by Four Olive Portable Harvesters



Giuseppe Manetto, Emanuele Cerruto and Rita Papa

Abstract This research aims to evaluate the vibration transmitted to the hand-arm system by four electric portable harvesters, mainly different for kinematics of the harvester head (synchronous or opposite), rod material (aluminum or carbon fiber), and rod configuration (fixed length or telescopic). Models with telescopic rods were tested at minimum and maximum length. All models were driven at two running frequencies: 1050 and 1200 oscillations per minute. Accelerations were measured at different times and at no-load condition in two points, 0.5 m apart, next to the hand positions. The results showed that the main difference in acceleration values was due to the kinematics of the harvester heads: 21.80 versus 6.27 m s⁻² for synchronous and opposite movement, respectively. Differences between rod configurations were on average not statistical significant, as well as those between running frequencies. For each machine, acceleration values in front position (on the rod) were higher than in rear position (near the hand-grip). The differences in kinematics of the harvester head also affected acceleration component values: acceleration was higher along x-axis (19.27 m s⁻²) when arms carrying sticks moved synchronously and higher along y-axis (5.11 m s⁻²) when arms moved in opposition.

Keywords Safety · Health · Exposure · Acceleration · HAV

1 Introduction

The use of electrical portable harvesters for olives is quite common, mainly due to the availability and spreading of the new long life lithium batteries, whose reduced mass allows them to be carried by the worker himself. Moreover, all the main manufacturers have introduced new models of these machines, made of carbon fibers, plastic, and aluminum to reduce the total mass. To satisfy the market requests, many models have telescopic rods that make the use of stairs unnecessary during the harvesting.

G. Manetto (✉) · E. Cerruto · R. Papa
Department of Agriculture, Food and Environment (Di3A), University of Catania, Via S. Sofia
100, 95123 Catania, Italy
e-mail: gmanetto@unict.it

© Springer Nature Switzerland AG 2020
A. Coppola et al. (eds.), *Innovative Biosystems Engineering for Sustainable Agriculture, Forestry and Food Production*, Lecture Notes in Civil Engineering 67,
https://doi.org/10.1007/978-3-030-39299-4_73

Harvester heads are of different types (comb, hook, flap, beater), with different number and shape of sticks and with different kinematics, many of which have been investigated by researchers to assess productivity (Famiani et al. 2014; Sperandio et al. 2017) and safety aspects (Pascuzzi et al. 2009; Çakmak et al. 2011; Cerruto et al. 2012; Manetto and Cerruto 2013; Calvo et al. 2014; Deboli et al. 2014a; Catania et al. 2017).

Unfortunately, safety aspects of portable harvesters are often underestimated by users, mainly interested in productivity. The most important risk connected with their use is probably the vibration transmitted to the hand-arm system, being noise greatly reduced with the adoption of electrical motors instead of internal combustion engines (Biocca et al. 2008). Vibration can be reduced after a proper design of the machine or an optimal choice of the operating parameters (Monarca et al. 2007; Aiello et al. 2019).

Regular exposure to hand-transmitted vibration can lead to a variety of signs and symptoms, including vascular and neurological disorders, muscle and tendon disorders, bone and joint disorders, collectively known as the “Hand-Arm Vibration Syndrome” (HAVS) (Griffin 2008; Calvo et al. 2018). The disease shows itself after a latency period and the prevention of injuries or disorders requires the implementation of administrative, technical and medical procedures, including technical measures aimed at eliminating or reducing vibrations at the source, appropriate information and advice to employers and employees, instruction to adopt safe and correct work practices, and medical preventive guidance (Bovenzi 2005).

Vibration level produced by portable harvesters for olives is mainly affected by the kinematics of the harvester head, but also the rod material, its geometry (length and diameter) and its configuration (fixed length or telescopic) play a relevant role. Other aspects to be considered are the working conditions (load or no-load) and the operator characteristics (weight, grip force, ability), so the assessment of the effective risk requires the direct measurement under real working conditions or the definition of standardized procedures able to provide reliable acceleration values (Deboli et al. 2014b).

In this paper vibrations transmitted to the hand-arm system by four electrical olive portable harvesters are analyzed. The study concerns this safety aspect only. No tests on their effectiveness during harvesting have been carried out, but all models are equally marketed in Mediterranean countries, so equal appreciation by users must be expected.

2 Materials and Methods

2.1 *The Portable Harvesters*

Four models of electric portable harvester, assembled by a local manufacturer, were investigated. Main differences between the four models were rod material (carbon

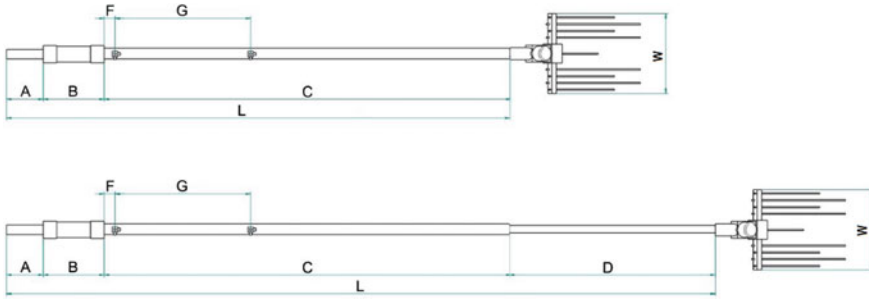


Fig. 1 General scheme of the portable harvesters in fixed length and telescopic rod configuration

fiber or aluminum), rod configuration (fixed length or telescopic), and kinematics of the harvester head (movement of the arms carrying the sticks: synchronous or opposite). More specifically, the four models derived from the combination of two harvester heads, labeled as H1 (synchronous movement) and H2 (opposite movement), and two rod configurations, labeled as F (fixed length) and T (telescopic). In addition, harvester head H1 is marketed combined with carbon fiber rod and harvester head H2 with aluminum rod. Finally, each harvester head can be driven at two nominal arm oscillations (pulses) per minute (ppm): 1050 or 1200.

A general scheme of the portable harvesters is shown in Fig. 1, whereas their main characteristics are summarized in Table 1. All models are driven by an 800 W electric motor with nominal rotating speed of 710 rad s^{-1} , installed on the harvester head and powered by a 12 V lithium battery. On the opposite side of the rod, a plastic handgrip (B, Fig. 1) carries a switch for activating or stopping the motor and choosing between the two operating conditions of 1050 or 1200 ppm.

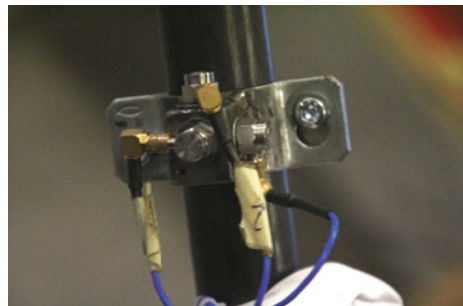
2.2 Vibration Measurements and Data Analysis

To smooth the influence of external factors, acceleration measurements were carried out at no-load condition, keeping the rod angled of about 45° , and with all the machines driven by the same person. Each harvester was tested at both running frequencies; moreover, harvesters with telescopic rod were analyzed at both shortened and extended configurations.

Accelerations were measured, at different times, in two points next to the hand positions, 0.5 m apart (distance G, Fig. 1), labeled as M1 (rear position, near the hand-grip) and M2 (front position, on the rod). Three mono axial accelerometers (DJB, model A/123/S, DJB Instruments Ltd., Suffolk, UK), screwed on the faces of a small cube tied to the rod with a metallic clamp, were used. Reference axes were fixed according to the basicentric coordinate system defined by the UNI EN ISO 5349-1:2004 regulation (Fig. 2). Each measurement session lasted no less than 60 s and it was repeated at least 4 times. Acceleration signals were sampled at 5 kHz

Table 1 Main technical features of the portable harvesters (refer to Fig. 1 for geometric aspects)

	H1F	H1T	H2F	H2T
Total mass (kg)	2.4	2.5	2.9	3.0
Rear extension length (A, mm)	135	135	135	135
Rear extension section (diameter × thickness, mm)	35 × 1	35 × 1	35 × 1	35 × 1
Rear extension material	aluminum	aluminum	aluminum	aluminum
Hand-grip length (B, mm)	225	225	225	225
Rod length (C, mm)	1730	1860	1540	1490
Rod section (diameter × thickness, mm)	35 × 1.2	35 × 1.2	35 × 1	35 × 1
Rod material	carbon fiber	carbon fiber	aluminum	aluminum
Extension rod length (D, mm)	–	765	–	760
Extension rod section (diameter × thickness, mm)	–	28 × 1	–	28 × 1
Extension rod material	–	aluminum	–	aluminum
Rod total length (L, mm)	2090	2985	1900	2610
Head maximum width (W, mm)	295	295	295	295
Kinematics of harvester head	synchronous	synchronous	opposite	opposite
Stick number	8	8	8 + 1 (1 fixed)	8 + 1 (1 fixed)
Stick length (mm)	360	360	360 (180 fixed)	360 (180 fixed)
Stick diameter (mm)	5	5	5	5
Stick material	carbon fiber	carbon fiber	carbon fiber	carbon fiber

Fig. 2 The three monoaxial accelerometers applied to the rod

by means of a dB4 four-channel acquisition unit and the recording module of the dBFA Suite software (01 dB-Metravib, Lyon, France) and then recorded on the hard disk of a PC. Subsequently, they were post-processed according to the UNI EN ISO 5349-1:2004 regulation by using the post-processing module of the same dBFA Suite software, in the frequency range 5.6–1400 Hz (third of octave bands from 6.3 to 1250 Hz).

Frequency weighted root mean square (RMS) accelerations a_{hwx} , a_{hwy} , and a_{hwz} were computed via third octave analysis for each axis, and then the global weighted acceleration a_{hw} was calculated according to:

$$a_{hw} = \sqrt{a_{hwx}^2 + a_{hwy}^2 + a_{hwz}^2}. \quad (1)$$

The daily vibration exposure value, $A(8)$, standardized to a reference period of 8 h, was computed according to:

$$A(8) = a_{hw} \sqrt{\frac{T_e}{T_0}}, \quad (2)$$

being T_e the daily exposure time (h) and $T_0 = 8$ h the reference period.

Global values were statistically analyzed by means of the Kruskal-Wallis test to detect any significant difference related to harvester head, running frequency, rod configuration and measuring point. All statistical analyses and graphical representations were carried out by using the open source software R (R Core Team 2013).

3 Results and Discussion

Box plots and mean values of global weighted acceleration values are reported in Fig. 3 and Table 2, respectively. The results showed that the most significant differences in global weighted acceleration values were due to the harvester head: 21.80 m s^{-2} (H1) and 6.27 m s^{-2} (H2). The opposite oscillations of the two arms carrying the sticks allow for a partial compensation of the vibration transmitted to the hand-harm system, and this means that the best way to reduce vibration is to act in the design of the machine.

On average, the differences between the three rod configurations were not statistically significant (mean values ranged from 13.20 to 15.35 m s^{-2}). When harvester head H1 was used, acceleration values were higher with the telescopic rod in extended configuration (25.14 m s^{-2}), whereas they were lower (on average 20.57 m s^{-2}) with the telescopic rod in shortened configuration or with fixed length rod. When harvester head H2 was used, acceleration values were higher with fixed length rod (6.97 m s^{-2}), whereas they were lower (on average 5.70 m s^{-2}) with the telescopic rod. The difference between the two measuring points was not statistical significant: 13.77 m s^{-2} in M1 and 14.57 m s^{-2} in M2. However, for each harvester head, acceleration values in

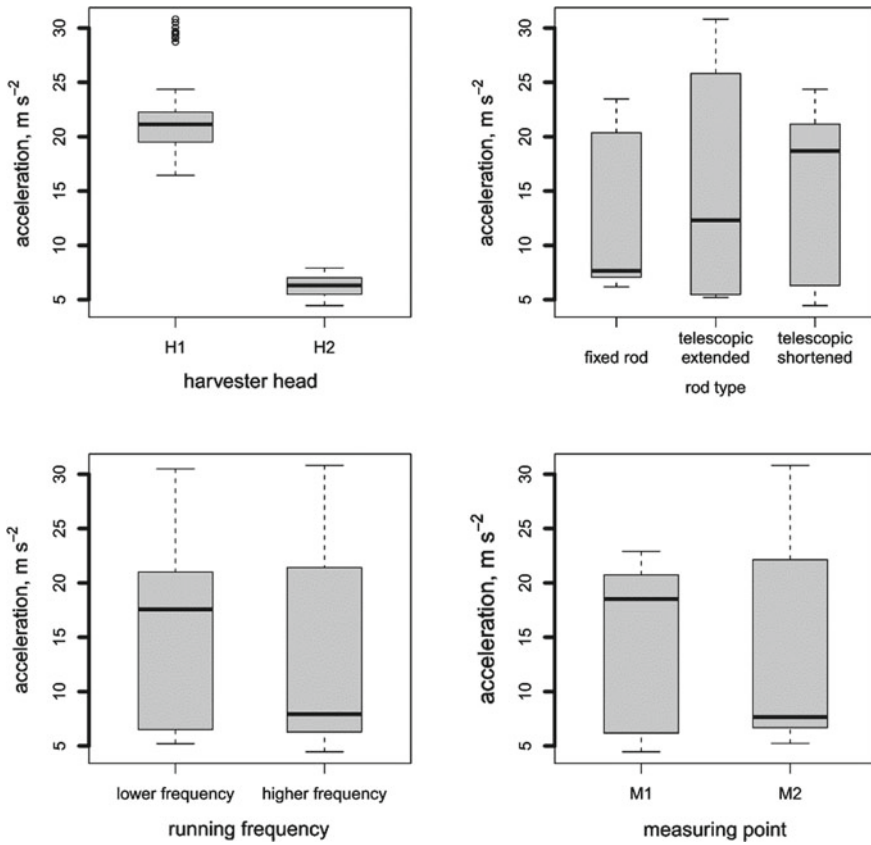


Fig. 3 Box plots of global weighted acceleration as affected by harvester head, rod type, running frequency and measuring point

Table 2 Mean values of global weighted acceleration ($m s^{-2}$) (mean separation by Kruskal-Wallis test at p -level = 0.05; comparison between harvester heads, rod types, measuring points, running frequencies, and first order interactions with harvester heads)

Rod type								
Harvester head	Fixed length		Telescopic extended		Telescopic shortened		Mean	
H1	20.32	b	25.14	a	20.82	b	21.80	a
H2	6.97	c	5.56	d	5.85	d	6.27	b
Mean	13.20	ns	15.35	ns	14.31	ns	14.14	
Measuring point								
	M1		M2		lower		higher	
H1	20.45	b	23.57	a	21.63	a	21.98	a
H2	5.97	d	6.57	c	6.40	b	6.13	b
Mean	13.77	ns	14.57	ns	14.32	ns	13.95	ns

M2 were always significantly higher than acceleration values in M1. Finally, differences between running frequencies were not statistical significant, probably because the two frequencies were not too different: 14.32 m s^{-2} at 1050 ppm and 13.95 m s^{-2} at 1200 ppm. The difference was also not statistical significant for each harvester head.

The daily vibration exposure values $A(8)$, assuming a daily exposure time of 4 h, ranged on average from 14.4 to 17.8 m s^{-2} when using the harvester head H1 and from 3.9 to 4.9 m s^{-2} when using the harvester head H2. These values will have to be compared with the daily exposure action value of 2.5 m s^{-2} and the daily exposure limit value of 5.0 m s^{-2} established by the European Directive 2002/44/EC (European Commission 2002) in order to implement proper safety actions. All considered, from safety point of view, the use of harvester head H1 should be avoided: it exposes operators to a level of acceleration 3.6 times higher than H2. A more comprehensive evaluation can be performed after field tests and productivity assessment.

Figure 4 reports the x -, y - and z -axis acceleration components at varying harvester head, rod type and measuring point. From it emerges that with H1 the highest acceleration was measured along the x -axis (19.27 m s^{-2}), followed by z -axis (8.81 m s^{-2}) and y -axis (2.83 m s^{-2}). With H2 harvester head, instead, due to the opposite movement of the arms carrying the sticks that determined a partial compensation of transversal components, the highest acceleration was measured along the y -axis (5.11 m s^{-2}); acceleration values along x - and z -axis were 2.90 and 1.86 m s^{-2} , respectively, and lower or comparable with those due to the H1 harvester.

4 Conclusions

The main results of the present study can be summarized as follows:

- The main factor affecting acceleration values is the kinematics of the harvester head. When the arms carrying the sticks moved synchronously, acceleration value was on average 21.80 m s^{-2} , whereas when they moved in opposition, it was on average 6.27 m s^{-2} . This confirms that the best way to reduce vibration is to act in the design of the machine.
- Differences between rod types and between running frequencies were on average not statistical significant. Acceleration values in front position were higher than in rear position for each machine, implying different exposure of operator hands.
- A more comprehensive evaluation of the four machines can be performed also taking into account vibration measurement during harvesting and after assessing productivity, even if these are equally appreciated by the markets.

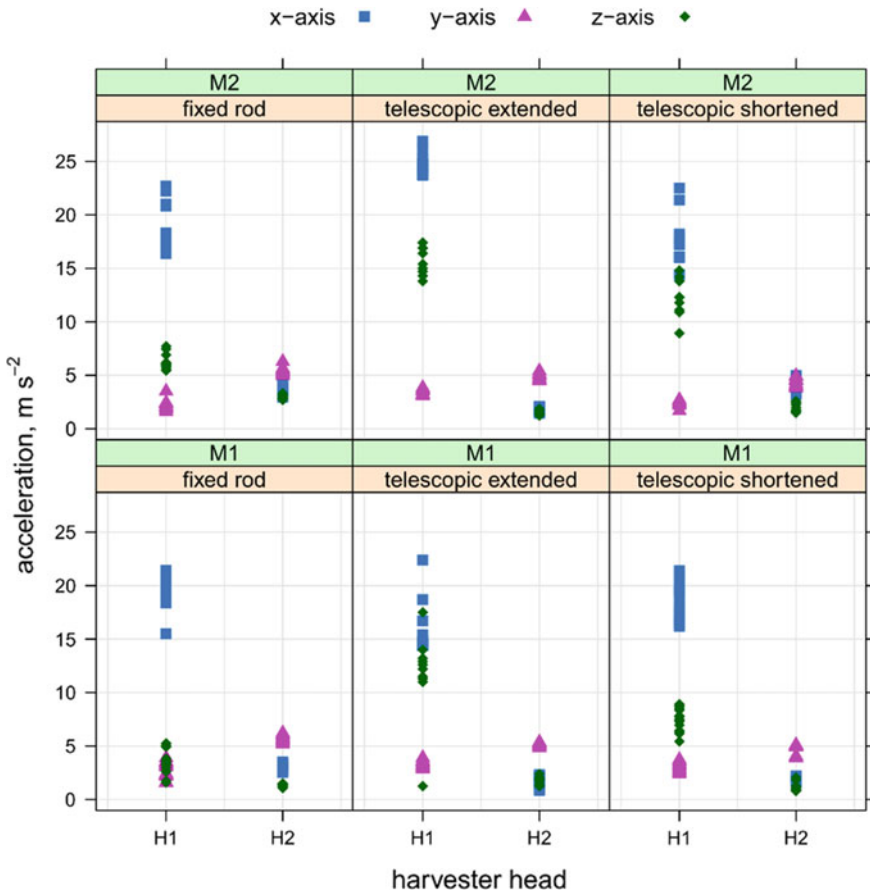


Fig. 4 Components of weighted acceleration as affected by harvester head, rod type and measuring point

References

- Aiello, G., Vallone, M., & Catania, P. (2019). Optimising the efficiency of olive harvesting considering operator safety. *Biosystems Engineering*, *185*, 15–24.
- Biocca, M., Fornaciari, L., & Vassalini, G. (2008, June 23–25). Noise risk evaluation in electrical hand-held picking machines for olive harvesting. In *Proceedings of International Conference on Agricultural Engineering "Agricultural and Biosystems Engineering for a Sustainable World"*. Hersonissos, Crete, Greece.
- Bovenzi, M. (2005). Health effects of mechanical vibration. *Giornale italiano di medicina del lavoro ed ergonomia*, *27*(1), 58–64.
- Calvo, A., Deboli, R., Preti, C., & De Maria, A. (2014). Daily exposure to hand arm vibration by different electric olive beaters. *Journal of Agricultural Engineering*, *45*, 103–110.
- Calvo, A., Romano, E., Preti, C., Schillaci, G., & Deboli, R. (2018). Upper limb disorders and hand-arm vibration risks with hand-held olive beaters. *International Journal of Industrial Ergonomics*, *65*, 36–45.

- Çakmak, B., Saraçoğlu, T., Alayunt, F. N., & Özarslan, C. (2011). Vibration and noise characteristics of flap type olive harvesters. *Applied Ergonomics*, *42*, 397–402.
- Catania, P., Bono, F., & Vallone, M. (2017). Evaluation of the vibrations transmitted to the hand-arm system in the use of portable harvesters for olives. *Agricultural Engineering International: CIGR Journal*, *19*(2), 129–138.
- Cerruto, E., Manetto, G., & Schillaci, G. (2012). Vibration produced by hand-held olive electrical harvesters. *Journal of Agricultural Engineering*, *43*, 79–85.
- Deboli, R., Calvo, A., Gambella, F., Preti, C., Dau, R., & Casu, E.C. (2014a). Hand arm vibration generated by a rotary pick-up for table olives harvesting. *Agricultural Engineering International: CIGR Journal*, *16*(1), 228–235.
- Deboli, R., Calvo, A., Preti, C., & Inserillo, M. (2014b). Design and test of a device for acceleration reproducibility of hand held olive harvesters. *International Journal of Industrial Ergonomics*, *44*, 581–589.
- European Commission. (2002, July 6). European directive of 25 June 2002 on the minimum health and safety requirements regarding the exposure of workers to the risks arising from physical agents (vibration) 2002/44/EC. *Official Journal, L 177/13*, 13–19.
- Famiani, F., Farinelli, D., Rollo, S., Camposeo, S., Di Vaio, C., & Inglese, P. (2014). Evaluation of different mechanical fruit harvesting systems and oil quality in very large size olive trees. *Spanish Journal of Agricultural Research*, *12*(4), 960–972.
- Griffin, M. (2008). Measurement, evaluation, and assessment of peripheral neurological disorders caused by hand-transmitted vibration. *International Archives of Occupational and Environmental Health*, *81*, 559–573.
- ISO. (2004). Mechanical vibration measurement and evaluation of human exposure to hand-transmitted vibration—Part 1: General requirements. *Norm ISO 5349-1:2004*. Geneva, Switzerland: International Organization for Standardization Publication.
- Manetto, G., & Cerruto, E. (2013). Vibration risk evaluation in hand-held harvesters for olives. *Journal of Agricultural Engineering*, *44*, 705–709.
- Monarca, D., Cecchini, M., & Colantoni, A. (2007, September 17–19). Study for the reduction of vibration levels on an “olive electrical harvester”. In *Proceedings of the XXXII CIOSTA-CIGR Section V Conference* (pp. 503–509). Nitra, Slovakia, Part II.
- Pascuzzi, S., Santoro, F., & Panaro, V. (2009). Investigation of workers’ exposure to vibrations produced by portable shakers. *Agricultural Engineering International: CIGR Journal*, *11*, 1–10.
- R Core Team. (2013). R: A language and environment for statistical computing. *R Foundation for Statistical Computing*, Vienna, Austria: Available from <http://www.R-project.org/>.
- Sperandio, G., Biocca, M., Fedrizzia, M., & Toscano, P. (2017). Economic and technical features of different levels of mechanization in olive harvesting. *Chemical Engineering Transactions*, *58*, 853–858.

Perceived Barriers to the Adoption of Smart Farming Technologies in Piedmont Region, Northwestern Italy: The Role of User and Farm Variables



Federica Caffaro and Eugenio Cavallo

Abstract Smart Farming Technologies (SFTs) can increase the sustainability of agricultural production, based on a more precise and resource-efficient approach. However, previous studies pointed out a low level of SFTs adoption, often highlighting that technologies and innovations successfully adopted may be rejected by the users, who go back to the traditional practices even where benefits were being enjoyed. This study aimed at investigating the role played by individual variables, farming system characteristics, and perceived barriers in affecting the adoption of SFTs in a sample of Italian farm operators. Three-hundred and ten participants were administered a paper-and-pencil questionnaire addressing perceived economic, market and data management barriers in the adoption of SFTs. At the same time a set of user and farm-related variables was collected. The analyses showed that farm size and the perception of economic barriers affected the adoption of SFTs. Larger farms were more likely to adopt the SFTs investigated. The present results pointed out some critical aspects which may benefit from tailor-made interventions in terms of policies, work re-organization and/or operators' training, to support and widen the use of SFTs in the Italian context.

Keywords Barrier to innovation · Innovation adoption · Smart farming · Survey · Italy

1 Introduction

Smart Farming may be defined as the application of a large set of technologies such as sensors and actuators, geo-positioning systems, aerial and terrestrial autonomous vehicles, robotics, ICT (Information and Communication Technologies), the IoT

F. Caffaro (✉) · E. Cavallo
Institute for Agricultural and Earth Moving Machines (IMAMOTER) - National Research Council of Italy (CNR), Strada delle cacce, 73, 10135 Turin, Italy
e-mail: f.caffaro@ima.to.cnr.it

F. Caffaro
Department of Education, Roma Tre University, via del Castro Pretorio 20, 00185 Rome, Italy

© Springer Nature Switzerland AG 2020
A. Coppola et al. (eds.), *Innovative Biosystems Engineering for Sustainable Agriculture, Forestry and Food Production*, Lecture Notes in Civil Engineering 67,
https://doi.org/10.1007/978-3-030-39299-4_74

(Internet of Things), Big Data analytics, and Cloud Computing (Pierpaoli et al. 2013) to agriculture. These technologies, together with synthetic biology, neurotechnologies, nanomaterials, advance energy and storage technologies are expected to disrupt and greatly affect economies and societies over the next future (10–15 years) unfolding their effects on many fronts, including the agricultural business (OECD 2016). Smart Farming Technologies (SFTs) have been recognized as having a real potential to deliver a more productive and sustainable agricultural production, based on a more precise and resource-efficient approach (Knickel et al. 2017; The White House 2014).

A still limited amount of empirical research is available about farmers' view on the adoption of such disruptive technologies and innovations in developed and developing countries. Overall, the previous research pointed out a low level of SFTs adoption, and the core factor which has been investigated to interpret this evidence is farmers' perception of the financial cost of technological innovation, its economic benefits, and its appropriateness in fitting the 'day-to-day' reality on a farm (Adrian et al. 2005). Beside the economic concern, some studies have pointed out other relevant variables which could hinder the uptake of technological innovation in agriculture, which have been nonetheless underinvestigated in this sector. Market-related barriers such as the use of an overly scientific language or jargon in presenting the technology to the consumers and the difficulties in being trained and supported in case of malfunction may make the potential users feel they do not have the necessary skills and capabilities to integrate and use the innovation (Long et al. 2016). Furthermore, data management and usability were frequently mentioned in a previous study involving groups of farmers from different European countries as deserving further improvement, especially with regard to simplification of data collection and legibility and compatibility between devices (Kerneckner et al. 2019).

1.1 Context and Aim of the Study

As regards the adoption of technological innovation, available statistics show that while in the USA possibly up to 80% of farmers use some kind of SFTs, in European Union Countries farms, the rate is no more than 25% (European Parliament 2016).

Italy is the second agricultural power in the EU-28, and as regards the use of SFTs, the last agricultural census reported that only 61,000 out of 1.6 million farms recorded in the census were using Information and Communication Technologies (ICT) (ISTAT 2010). The Piedmont region is on the North West part of Italy and it covers 35% of the Po River catchment, with agriculture taking place on the plain (41% of Utilized Agricultural Area – UAA), mainly with maize-based systems, and on the hills (31% of UAA), mainly with vineyards and winter cereals. Piedmont includes approximately 10% of the total Italian UAA, and over 61,000 out of the 1,620,884 Italian agricultural holdings operate in this region (INEA 2014). The average standard output of farms from Piedmont is approximately 60,000 €: it can be considered representative of the Italian national average (35,000 €) when

compared to the outperforming (Lombardia, 135,000 €; Emilia Romagna, 90,000 €) or underperforming (Liguria and Puglia, 12,000 €; Calabria 10,000 €) regions (ISTAT 2019). The composition of the average Piedmont farm standard output is very similar to those from other Northern Italian regions (Veneto, Emilia Romagna, Friuli-Venezia Giulia) and to the Italian average: 50% from plant/vegetable, 40% from livestock and 10% from mixed systems (INEA 2014). Even in Piedmont, as reported also at the national level, Smart Farming is struggling to spread among end users (Cavallo et al. 2014). This phenomenon is observed despite the fact that there are numerous initiatives at the regional level to promote the creation of innovative firms in the agricultural sector (Regione Piemonte 2017).

Based on the previous considerations, this study aimed at investigating the role played by users' variables, farming system characteristics, and subjective factors (perceived barriers) in affecting the adoption of two types of SFTs in a sample of farm operators in the Piedmont region.

2 Materials and Methods

2.1 Participants

Three-hundred and ten farm operators participated in the study. The participants were recruited among the visitors of the National Exhibition of Agricultural Mechanization in Savigliano, the largest agricultural machinery exhibition in the Piedmont region. Since the agricultural population is spread across the country and have varying operating schedules, agricultural machinery exhibitions are one of the best occasions where a large and wide-ranging group of farmers, agricultural workers and other agricultural business operators come together. Therefore, such events provide a suitable place to conduct surveys and other data-collection activities (Caffaro et al. 2018; Cavallo et al. 2014; Reichardt and Jürgens 2009).

2.2 Instrument

Participants were administered a 34-item paper-and-pencil questionnaire. Only those items related to the aims of the present study were considered for analysis and will be described in the next paragraphs. Before starting the questionnaire, two groups of images printed on two A4 papers were shown to each participant. The images were developed based on the range of technology fields encompassed by the definition of Smart Farming (Pierpaoli et al. 2013) and considering previous evidence from a survey performed in different European countries on the most and less important technologies for farm operation (Kerneckner et al. 2019). In group 1, images represented the management information systems (SFT Type 1), depicting drones,

sensors for data acquisition and automatic download, and agricultural apps. In group 2, in-field advanced working tools technologies (SFT Type 2) were represented, with agricultural robots and autonomous machines, and tractors equipped with CAN-bus. The participants were asked to choose one group of images based on the fact that they have either already adopted any of the depicted SFTs on farm, or they have heard about them. After this choice, the participants were asked about their actual adoption of some of the technologies belonging to the SFTs type they have chosen (0 = do not use, 1 = use it at least some times a year). Then, participants had to indicate on a 2-category format (0 = no, 1 = yes) whether they considered (in case of actual users)/would consider (in case of non-users) any of the following aspects as regards the adoption of the selected group of SFTs: low cost-benefit ratio, insufficient external subsidy, uncertain results, lack of other farmers to share the costs with, scarce matching with farmers' needs, low after-sale technical support, hard to be trained, and inaccessible language. Participants' scores on these scales (first 5 items representing economic barriers, Cronbach's $\alpha = 0.530$; the other three the market barriers, Cronbach's $\alpha = 0.478$) were computed as a mean of the scores given for each item. Finally, the participants had to indicate on a 4-point scale (1 = not at all important, 4 = very important) how much the following aspects should be improved to encourage the uptake of SFTs: data safety, data collection, data transfer, shared databases, data legibility, privacy (data management/usability barriers, Cronbach's $\alpha = 0.735$, mean score computed). A standard socio demographic form, assessing also participants' relation with work (on-farm occupation, farm size and being a sole farmer) closed the questionnaire.

2.3 Procedure

Trained research assistants provided the questionnaire to exhibition attendees. The assistants explained the aims of the study and informed the participants that the questionnaire was anonymous. The questionnaire was in Italian, and its completion took approximately 3–4 min. No incentive was offered to participate in the survey. The response rate was approximately 80%.

2.4 Data Analysis

Descriptive statistics were calculated for the variables of interest and then a logistic regression computed, in which the dependent variable was the adoption of the technology, and the independent variables were the type of technologies, the users and farm characteristics and perceived barriers, i.e.: age, education, farm size, being a sole farmer, being a professional or a part-time farmer, and economic, market and institutional barriers.

3 Results

The main characteristics of the participants are reported in Table 1. With regard to SFTs, 37.1% of the participants focused on SFTs Type 1, whereas 62.9% chose SFTs Type 2. Overall, 74.8% of the interviewed people reported not to use the type of SFTs they have chosen (in particular, 75.7% for Type 1 and 74.4% for Type 2).

Regarding economic and market barriers to technology adoption perceived by the participants, problems with accessing subsidies and overly complex language were the most often cited criticalities. Accuracy in data collection and legibility of collected data were the most urgent issues regarding data management (see Fig. 1a, b, c).

The regression analysis showed a significant effect of farm size ($B = 0.379$, $p = 0.004$) and of perceived economic barriers ($B = -2.135$, $p = 0.000$) on SFTs adoption: in particular, larger farms were associated with a higher adoption, whereas a higher

Table 1 Main sociodemographic characteristics of the participants

Variable	Level	%		
Gender	Male	97.1		
	Female	2.9		
Education	None	0.6		
	Primary school	2.9		
	Secondary school	29.7		
	High school	59.0		
	Degree and over	7.8		
On-farm profession	Professional operator	47.7		
	Part-time farmer ^a	52.3		
Farm size (ha)	Up to 2	15.8		
	2–9	37.4		
	10–29	22.6		
	30–49	11.9		
	50 and over	12.3		
Working alone	Yes	27.1		
	No	72.9		
Variable			Mean	SD
Age			39.9	17.4
Economic barriers			0.6	0.3
Market barriers			0.4	0.3
Data manag. barriers			3.2	0.5

^aThe so called ‘part-time’ farmers are those who do not have an official role in the agricultural industry but, in addition to their main occupation, spend time working in agriculture and using agricultural machinery (Caffaro et al. 2018)

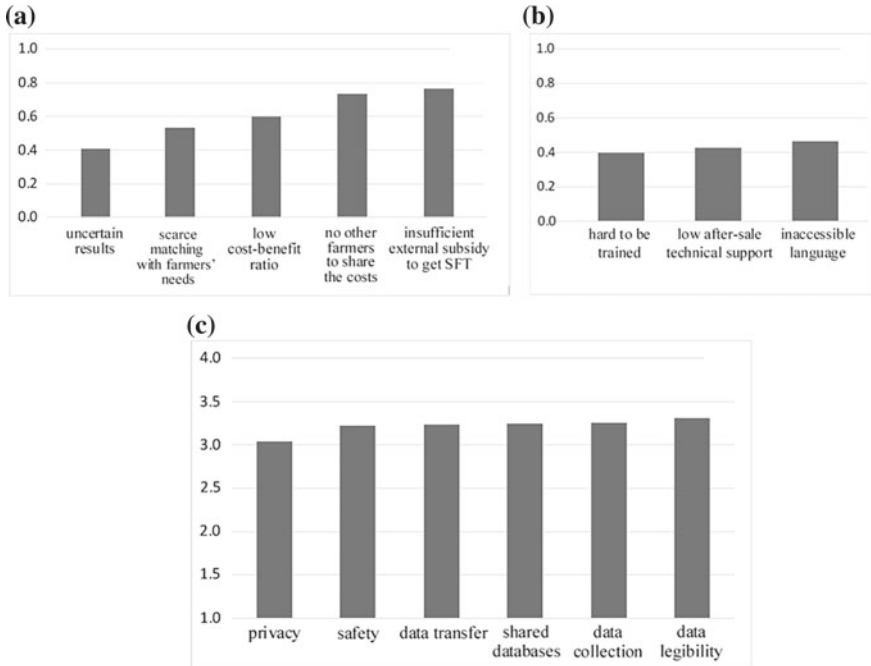


Fig. 1 Mean ratings for the different perceived barriers to SFTs adoption considered in the study: **a** economic, **b** market, **c** data management

perception of economic barriers hindered the adoption of SFTs. No significant effects were reported for the other variables considered.

4 Discussion

The present study investigated how user's and farming characteristics and perceived economic, market and data management/usability barriers affected the adoption of different SFTs in a sample of Italian farmers. Overall, consistent with previous studies performed in different countries (Cullen et al. 2013; Sneddon et al. 2011), the results showed a low uptake of both types of the investigated technologies, stressing the importance of targeted interventions to encourage the adoption of technological innovations in agriculture in Piedmont region.

The analyses showed that farm size and perceived economic barriers affected the adoption of the investigated SFTs. As with any business, farmers have an interest in maximizing production and making a profit (Pierpaoli et al. 2013), thus governmental policies and financial support are needed to reduce the actual economic barriers, but also factors related to the 'cultural accessibility' of SFTs should be taken into account and addressed, with both a restyling of the way in which SFTs are presented

on the market, and the promotion of targeted information campaigns to maximise the perceived economic benefit of SFTs.

With regard to farm size, the present study showed that working on a small farm lowered the adoption of SFTs. This result is consistent with previous evidence (Adrian et al. 2005) and the same pattern has been observed in different countries whose agricultural systems are characterized by small farms rather than big plots of land (Giannakis et al. 2016). Smaller farmers are typically not able to keep up with new technologies because of the lack of investment capital or knowledge, thus creating a large digital divide between big and small farmers (Daberkow and McBride 2003). Strong governmental intervention will be needed to create new business models and new economic opportunities, so that the new technologies might not be costly and for large scale operations only, but also be 'small and cheap'. Furthermore, stimulate international exchange of knowledge and ideas and new forms of cooperation between farmers and farms, and encourage global collaboration may all be effective ways to reach out to smaller farms. New education forms such as those focusing on the role of experienced farmers as mentors (Lundqvist and Svennefelt 2012) may be particularly useful, since smaller farmers often find it challenging to participate in costly and time-intensive traditional training forms. Access to new technologies could also be encouraged by targeted incentives and support programs. Strong public intervention will be needed to create the suitable conditions for new business models and new economic opportunities along the agriculture value chain, so that new technologies might not be developed, marketed and adopted by large scale operations only (Pham and Stack 2017). Relevantly, no effect of the two different types of SFTs considered was detected, which may suggest that innovation adoption is a general process which displays patterns and regularities, not bound by the type of innovation studied (Rogers 2003). Further investigations, widening the range of SFTs surveyed, will be interesting.

5 Conclusions

Smart Farming applications do not target large, conventional farming exploitations only, but could also be new levers to boost other common or growing trends in agricultural exploitations, such as family farming and organic farming. Previous studies performed in Italy reported low levels of SFTs adoption, but factors affecting this adoption have been underinvestigated. The present study focused on the Piedmont region, northwest Italy, to point out some critical variables which should be addressed to increase SFTs adoption among farmers. Farm size and perceived economic barriers showed to play a relevant role in affecting SFTs uptake, pointing out the relevance of institutional interventions and policies to encourage the use of SFTs.

References

- Adrian, A. M., Norwood, S. H., & Mask, P. L. (2005). Producers' perceptions and attitudes toward precision agriculture technologies. *Computer and Electronics in Agriculture*, 48(3), 256–271.
- Caffaro, F., Roccato, M., Micheletti Cremasco, M., & Cavallo, E. (2018). Part-time farmers and accidents with agricultural machinery: a moderated mediated model on the role played by frequency of use and unsafe beliefs. *Journal of Occupational Health*, 60(1), 80–84.
- Cavallo, E., Ferrari, E., Bollani, L., & Coccia, M. (2014). Attitudes and behaviour of adopters of technological innovations in agricultural tractors: A case study in Italian agricultural system. *Agricultural Systems*, 130, 44–54.
- Cullen, R., Forbes, S. L., & Grout, R. (2013). Non-adoption of environmental innovations in wine growing. *New Zealand Journal of Crop and Horticultural Science*, 41(1), 41–48.
- Daberkow, S. G., & McBride, W. D. (2003). Farm and operator characteristics affecting the awareness and adoption of precision agriculture technologies in the US. *Precision Agriculture*, 4(2), 163–177.
- European Parliament. (2016). Precision agriculture and the future of farming in Europe. Scientific Foresight Study. STOA IP/G/STOA/FWC-2013-1/Lot 7/SC5. Scientific Foresight Unit (STOA), European Parliamentary Research Service. [http://www.europarl.europa.eu/RegData/etudes/STUD/2016/581892/EPRS_STU\(2016\)581892_EN.pdf](http://www.europarl.europa.eu/RegData/etudes/STUD/2016/581892/EPRS_STU(2016)581892_EN.pdf).
- Giannakis, E., Bruggeman, A., Djuma, H., Kozyra, J., & Hammer, J. (2016). Water pricing and irrigation across Europe: Opportunities and constraints for adopting irrigation scheduling decision support systems. *Water Science and Technology: Water Supply*, 16(1), 245–252.
- INEA. (2014). *Italian agriculture in figures 2013*. Roma: Istituto Nazionale di Economia Agraria. http://dspace.crea.gov.it/bitstream/inea/8431/1/Italian_agriculture_figures_2013.pdf.
- ISTAT. (2019). *Censimento Agricoltura 2010* [Agricultural Census 2010]. Data Warehouse. <http://dati-censimentoagricoltura.istat.it/Index.aspx>.
- Kernecker, M., Knierim, A., Wurbs, A., Kraus, T., & Borges, F. (2019). Experience versus expectation: Farmers' perceptions of smart farming technologies for cropping systems across Europe. *Precision Agriculture*, 1–17. <https://doi.org/10.1007/s11119-019-09651-z>.
- Knickel, K., Ashkenazy, A., Chebach, T. C., & Parrot, N. (2017). Agricultural modernization and sustainable agriculture: contradictions and complementarities. *International Journal of Agricultural Sustainability*, 15, 575–592.
- Long, T. B., Blok, V., & Coninx, I. (2016). Barriers to the adoption and diffusion of technological innovations for climate-smart agriculture in Europe: Evidence from the Netherlands, France, Switzerland and Italy. *Journal of Cleaner Production*, 112, 9–21.
- Lundqvist, P., & Svennefelt, C. A. (2012). Health and safety strategy in Swedish agriculture. *Work*, 41(Supplement 1), 5304–53072012.
- OECD. (2016). *OECD science, technology and innovation outlook 2016*. Paris: OECD Publishing. https://doi.org/10.1787/sti_in_outlook-2016-en.
- Pham, X., & Stack M. (2017). How data analytics is transforming agriculture. *Business Horizons*, 61(1), 125–133.
- Pierpaoli, E., Carli, G., Pignatti, E., & Canavari, M. (2013). Drivers of precision agriculture technologies adoption: A literature review. *Procedia Technology*, 8, 61–69.
- Regione Piemonte. (2017). *Il sistema dei Poli di Innovazione regionali* [Innovation clusters in Piedmont]. <https://www.regione.piemonte.it/web/temi/fondi-progetti-europei/fondo-europeo-sviluppo-regionale-fesr/sistema-dei-poli-innovazione-regionali>.
- Reichardt, M., & Jürgens, C. (2009). Adoption and future perspective of precision farming in Germany: results of several surveys among different agricultural target groups. *Precision Agriculture*, 10(1), 73–94.

- Rogers, E. M. (2003). *Diffusion of innovations* (5th ed.). New York: Simon and Schuster.
- Sneddon, J., Soutar, G., & Mazzarol, T. (2011). Modelling the faddish, fashionable and efficient diffusion of agricultural technologies: A case study of the diffusion of wool testing technology in Australia. *Technological Forecasting and Societal Change*, 78(3), 468–480.
- The White House. (2014). *Big data: Seizing opportunities, preserving values*. Washington DC: The Executive Office of the President. Retrieved October 24, 2018, from https://obamawhitehouse.archives.gov/sites/default/files/docs/20150204_Big_Data_Seizing_Opportunities_Preserving_Values_Memo.pdf.

Effect of Different Axial Fans Configurations on Airflow Rate



S. Failla, E. Romano, D. Longo, C. Bisaglia and G. Schillaci

Abstract The general objective of the research is to contribute to a fewer impacting methods for pest and disease management in tree crops, optimizing the air flows in relation to the canopy characteristics, and reducing the risks of drift. The aim of the work was to assess the airflow rate of different axial fan configurations in order to reduce energy consumption by assuring the adjustment of the right rate. Different configurations in terms of pitch angles and rotation speed of the blades as well as air outlet sections were taken into consideration. The tests were carried out at an Inspection Center for sprayers, Catania province (Italy) with a conventional sprayer machine. The methodology followed the ISO/FDIS 9898 International standard (1999) for the measurement of the flow rate at the suction side of the fan. A special frame was realised for measuring of air velocity at outlet side of the fan. In order to study the correlation between fan configuration and energy consumption a mechanical torque-meter and a speedometer were used. Preliminary results highlighted the performance of a fan used in sprayers for orchards and vineyard and tested to reducing energy consumption and environmental impact.

Keywords Sprayers · Axial fan · Airflow rate · Energy consumption · Environmental impact

1 Introduction

An accurate crop protection requires careful calibration of sprayers, which takes into account the characteristics of the crops (shape and size of the plants, distances

S. Failla (✉) · D. Longo · G. Schillaci
Department of Agricultural, Food and Environment (Di3A), University of Catania, Via S. Sofia
100, 95123 Catania, Italy
e-mail: sfailla@unict.it

E. Romano · C. Bisaglia
Consiglio per la ricerca in agricoltura e l'analisi dell'economia agraria, Centro di Ricerca
Ingegneria e Trasformazioni agroalimentari (CREA-IT), Via Milano, 43, 24047 Treviglio, BG,
Italy

© Springer Nature Switzerland AG 2020

A. Coppola et al. (eds.), *Innovative Biosystems Engineering for Sustainable Agriculture, Forestry and Food Production*, Lecture Notes in Civil Engineering 67,
https://doi.org/10.1007/978-3-030-39299-4_75

between the plants and between the rows, age and vegetative stage) as well as their periodic inspection, as already provided for the current legislation (Dir. 2009/127/CE, Dir. 2009/128/CE, Legislative Decree No. 124 of 22/06/12, Legislative Decree No. 150 of 14/08/12, Ministerial Decree No. 4847 of 03/03/2015). Although the interest towards environmental aspects among farmers and researchers has increased considerably, pesticides distribution on tree canopy is a practice still today characterized by low efficiency, i.e. a low and uneven deposit and consequent high environmental impacts.

Airflow rate supplied by the fan of a sprayer represents the parameter that most affect the quality of a treatment (Hołownicki et al. 2017; van de Zande et al. 2018): its correct management, according to the tree canopy characteristic, helps to minimize off-target losses (on the ground or in the air) and improve deposit uniformity (Cerruto et al. 2016; Felsot et al. 2010; Grella et al. 2017; Miranda-Fuentes et al. 2018; Moltó et al. 2017; Nuyttens et al. 2007; Qiu et al. 2016). In particular, air volume settings seem to be more important for spray deposition in tree leaf canopy than nozzles type (van de Zande et al. 2018).

In a Precision Agriculture (PA) perspective, air volume calibration appears more fitted for Variable Rate Technology (VRT) systems working in orchards and vineyards. Moreover, the use of more efficient Variable Air Assistance (VAA) systems in orchard sprayers could decrease by 50% the power requirements of tractors, which are influenced by the power demand of the fan, and, consequently, it also could reduce fuel consumption (Hołownicki et al. 2017).

In this direction, our work was carried out with the aim to assess:

- the air velocity and airflow rate at the intake, and the air velocity at the outlet side of the sprayer, by changing the gear ratio and the pitch angle of the fan blades;
- the influence of the air exit section on air velocity and energy consumption, by regulating its width at three different positions;
- the energy consumption with the different configurations.

2 Materials and Methods

2.1 *The Laboratory for Measurements*

The experimental activity was carried out at the Inspection Center for sprayers and sprayer machine manufacturer “Officina Antonino Turrisi” sited in Catania province in eastern Sicily (Italy). The tests were carried out with an axial helical fan (700 mm in diameter, with 8 adjustable pitch blades in polyethylene, 130 mm long, clockwise rotation, 38,000 m³ h⁻¹ peak flow rate) usually mounted on conventional sprayer machines (hydraulic pulverization) and commonly used in vineyard and orchard (Fig. 1a). The blades can assume five different tilt angles: 20, 26, 34, 40 and 44 degrees.

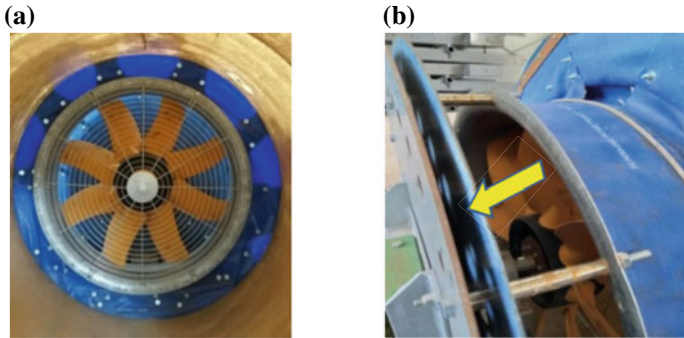


Fig. 1 a The axial helical fan of our study. b The metal sheet behind the fan

The air outlet section can be increased or decreased by means of a metal sheet placed behind the fan; it can be adjusted from 40 mm to 110 mm (Fig. 1b).

The fan was powered by the PTO of a tractor at 56 rad s^{-1} by means of a gearbox with two transmission ratios ($\tau_1 = 3.8$ and $\tau_2 = 4.53$). The tractor has a power of 35 kW and a mass of 1900 kg.

According to ISO/FDIS 9898 International Standard (1999), a 1000 mm diameter pipe (“1.5 times of the suction diameter of the fan”) 2.5 m length, connected to the suction side of the fan, was used for measuring airflow inside the pipe by means of three hot wire anemometers (Fig. 2a). The measurement range of these instruments is $0\text{--}50 \text{ m s}^{-1}$ and the measuring error is $\pm 3\%$.

A purposely designed frame was used for measuring air velocity at outlet side of the fan by means of a three-cup anemometer, suitably mounted on the frame (Fig. 2b). The measurement range of the anemometer is $0\text{--}40 \text{ m s}^{-1}$ and the measuring error is $\pm 1\%$. In particular, the frame is able to make a 180° rotation, allowing to measure on both sides of the sprayer at different distances from the center of the fan (radial adjustment) in two directions: the first allows discrete measurements up to 1.80 m

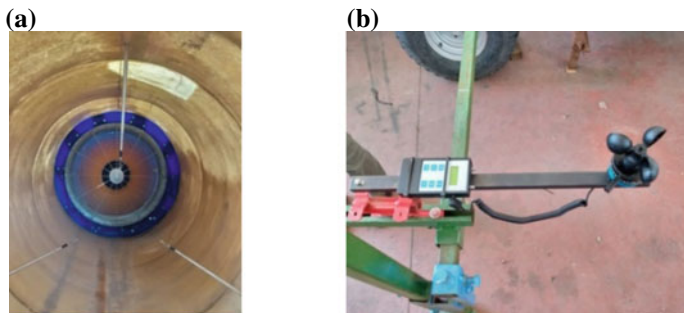


Fig. 2 a The thermo-anemometers inside the pipe. b The three-cup anemometer mounted on the frame

(horizontal adjustment); and the second (transverse adjustment) allows to position the anemometer transversely, forwards or backwards respect to the air outlet section.

A torque-meter and a speedometer were used to measure torque and rotation speed at PTO, in order to calculate the energy requirements during fan operating at the different configurations (Andersson et al. 2012).

2.2 The Tests

The methodology for air flow measurement at the intake side of the fan followed the ISO/FDIS 9898 International Standard. In particular, the probes of the three hot wire anemometers were placed at an angular distance of 120° to each other in order to measure the air velocity and flow in the five measuring points (y_1, y_2, y_3, y_4, y_5) along the radius, where y_1 is the nearest position to the pipe wall, as indicated by the ISO and showed in Fig. 3a. For each measuring point, 60 samples data (with a period of 60 s) were taken from every anemometer (Fig. 3b) at the same time.

As concern the measures at the outlet side of the fan, assuming a 2 m vineyard inter-row spacing, a first set of measurements was carried out at 4 different distances (0.50–1.00–1.50–1.80 m) from the center of the fan, both on the right and on the left side by means of the three-cup anemometer. To this scope, the rod of the frame was placed at zero degrees, parallel to the ground, and at a 0.73 m height from the ground.

The tests were carried out with the blade pitch angle most used (40 degrees) and with the others possible blade tilt angles; and with two transmission ratios ($\tau_1 = 3.8$ and $\tau_2 = 4.53$). The width of fan outlet section was adjusted based on the maximum opening (110 mm), the average (60 mm) and the minimum (40 mm), allowed by the

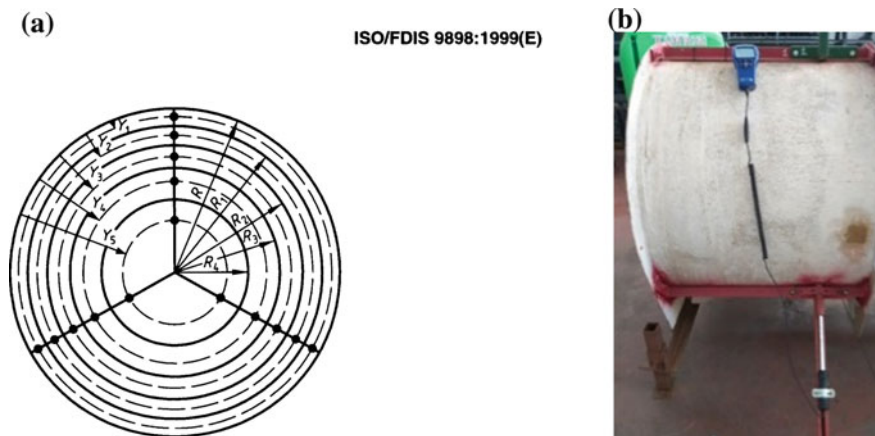


Fig. 3 **a** Cross section for measuring, position of measuring points (ISO/FDIS 9898). **b** The probe inside the tube

Table 1 The scheme of the 6 tests

Test	Transmission ratios	Blade angle	Outlet section
1	τ_2 (4.53)	40°	Max (11 cm)
2	τ_2 (4.53)	40°	Mean (6 cm)
3	τ_2 (4.53)	40°	Min (4 cm)
4	τ_1 (3.8)	40°	Max (11 cm)
5	τ_1 (3.8)	40°	Mean (6 cm)
6	τ_1 (3.8)	40°	Min (4 cm)

specially designed system (Fig. 1b). 30 tests were performed by combining these configurations, but only six of those are analysed in the present paper (Table 1).

During the tests, air temperature and relative humidity were recorded.

All the data were statistically analysed with the open source software R (R Development Core Team 2012). The ANOVA was performed to test the main effect of the different fan configurations. The statistically significant difference between tests was estimated using Duncan test with a probability level $p \leq 0.05$ and $p \leq 0.01$.

3 Results

The air velocity and flow rate values were significantly influenced by the outlet section (p -value < 0.01), with a directly proportional effect. As expected, overall, the smaller section (4 cm) recorded an average speed of 4.03 m s^{-1} and a flow rate of $7,880.97 \text{ m}^3 \text{ h}^{-1}$, the intermediate one (6 cm) showed an average speed of 4.85 m s^{-1} and a flow rate of $9,320.96 \text{ m}^3 \text{ h}^{-1}$, the largest section (11 cm) involved an average speed of 6.78 m s^{-1} and a flow rate of $13,590.62 \text{ m}^3 \text{ h}^{-1}$ (Figs. 4a and 5a).

The shift from the τ_1 to τ_2 gear ratio also had directly proportional and significant influence (p -value < 0.01), showing an average air velocity values of 4.75 m s^{-1} and

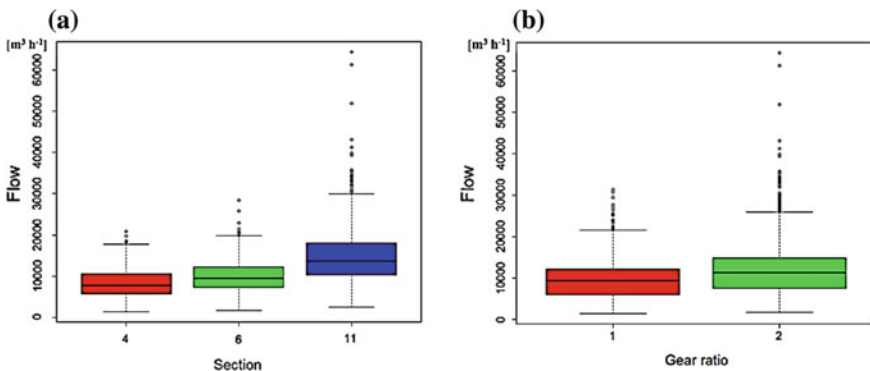


Fig. 4 a Airflow rate at the different sections. b Airflow rate at the two gear ratio

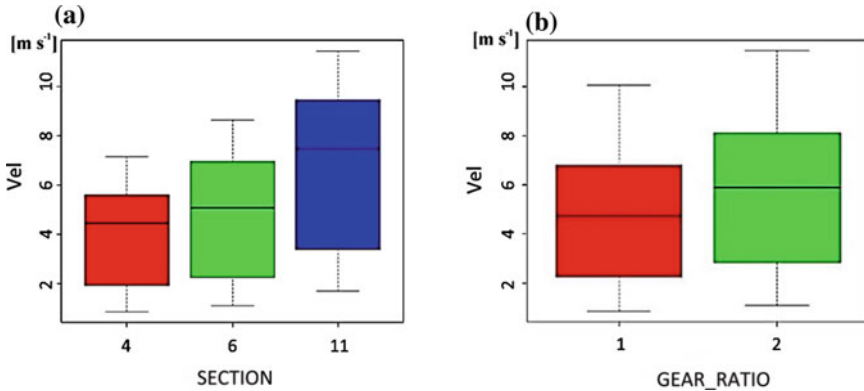


Fig. 5 a Air velocity at the different sections. b Air velocity at the two gear ratio

5.71 m s^{-1} with a flow rate of 9,234.70 $\text{m}^3 \text{h}^{-1}$ and 11,293.66 $\text{m}^3 \text{h}^{-1}$, respectively (Figs. 4b and 5b).

In terms of air flow and air velocity, the six tests were statistically different (p -value < 0.05), except the tests 3 and 5, as showed in Figs. 6a and 7a. In particular, according to the Duncan test, test 3 with τ_1 and medium outlet section (6 cm) was not statistically different compared to test 5 with τ_2 and minimum outlet section (4 cm).

The airflow rate showed different statistically data at the different depths inside the tube, with an average maximum value of 14,098.17 $\text{m}^3 \text{h}^{-1}$ at 146 mm (y_3 medium position) and an average minimum value of 2221.95 $\text{m}^3 \text{h}^{-1}$ at 342 mm (y_5 central position) (Fig. 6b). Similarly, the air velocity showed different statistically data at the different depths inside the tube, passing from 8.0 m s^{-1} at 342 mm (y_5 position) to 1.9 m s^{-1} at 26 mm (y_1 position) (Fig. 7b).

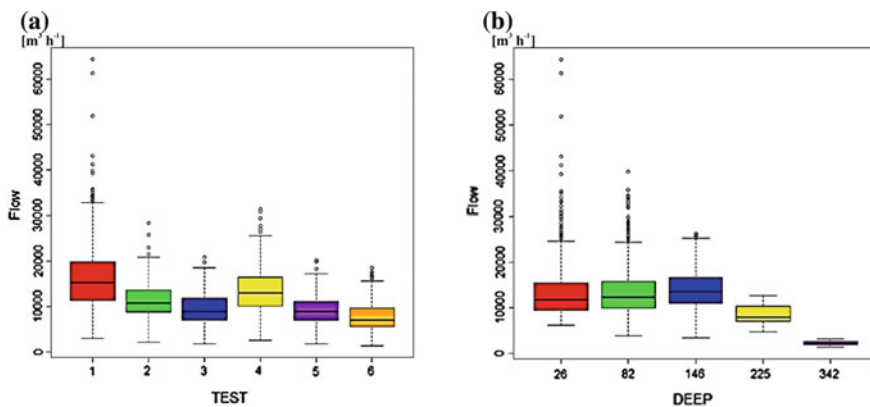


Fig. 6 a Mean airflow rate in the different tests. b Mean airflow rate in the five measuring points inside the pipe

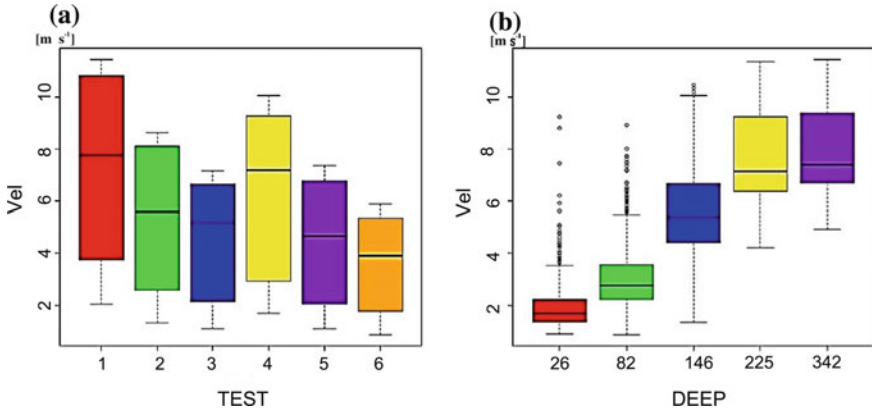


Fig. 7 a Mean air velocity in the different tests. b Mean air velocity in the five measuring points inside the pipe

As concerns power consumptions (Fig. 8), the values were statistically influenced both by the gear ratio and by the outlet section, as expected. In particular, a statistically lower average value of 8.68 kW ($p < 0.05$) was recorded using τ_1 in respect to 11.30 kW with τ_2 . Moreover, the variation of the outlet section produced values statistically discretized according to the Duncan test, with an average value of

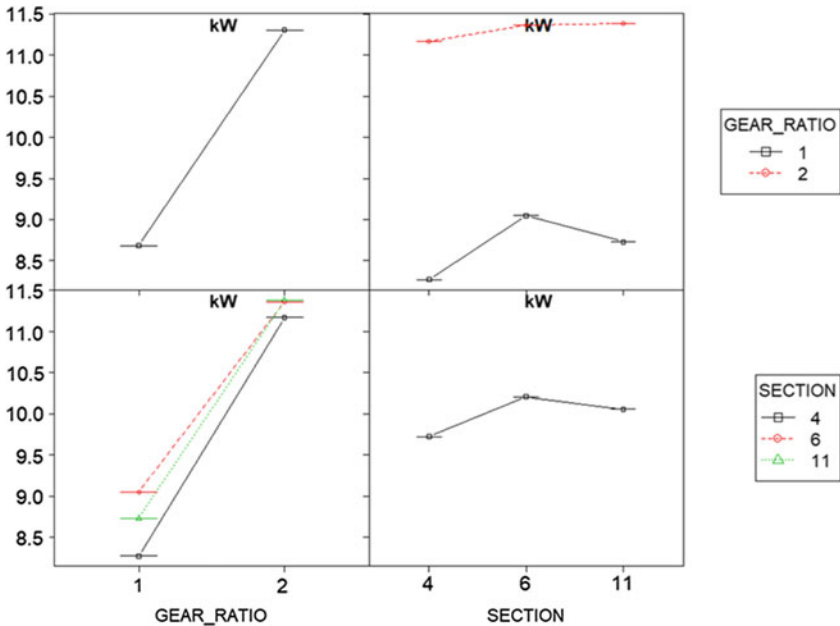


Fig. 8 Power consumption at the two gear ratio and at the three outlet sections

10.20 kW in the case of the medium section (6 cm), greater than 10.06 kW with the widest section (11 cm) and 9.72 kW with the minimum section (4 cm). The tests showed higher absorbed power values with the medium section (6 cm), indicating a significative interaction between gear ratio and section.

Regarding the air velocity at the outlet side of the fan, a value greater than 40 m s^{-1} was recorded in all the different outlet sections, with τ_2 and at 0.5 m even if the data show a certain asymmetry between the right and the left side. The highest average data are shown for the medium outlet section (6 cm) with both τ_1 and τ_2 .

4 Conclusions

The present paper reports only partial results with respect to the whole experimental study. The preliminary results starting to highlight the relationships between the configuration parameters of a 70 cm diameter fan; e.g. the relationship between gear ratio and air output sections has provided preliminary insights with the aim of reducing energy consumption. Because, there is not statistically differences in terms of airflow rate, between the tests 3 and 5, conducted with the same tilt angle but with different transmission gear ratios and outlet section, this result could represent an interesting result with the aim of reducing energy consumption.

We believe that this knowledge will be useful in subsequent field tests, with the aim of regulating the airflow rate and air velocity in relation to the characteristics of the crop.

Further analysis will be developed on the relation between the different fans configurations, in particular working on the air outlet section, a parameter that does not appear particularly taken into consideration by the literature.

In other words, these results will be validated in the field to find the best configurations as a function of tree canopy in a PA perspective.

Finally, the work could be functional to test the methodology to use in the spraying machine inspection centers.

Acknowledgements The authors thank R. Papa for her contribution during the tests. The activity presented in the paper is part of the research project titled “Innovazioni attraverso applicazioni ICT nel settore delle costruzioni rurali, della pianificazione del territorio agro-forestale e della meccanizzazione della difesa fitosanitaria. WP1—Sviluppo di tecniche e di applicazioni anche informatiche per l’innovazione nel settore della meccanizzazione della difesa fitosanitaria.” Piano della Ricerca 2016-2018 of the University of Catania (Italy).

References

- Andersson, I., Thor, M., & McKelvey, T. (2012). The torque ratio concept for combustion monitoring of internal combustion engines. *Control Engineering Practice*, 20(6), 561–568.
- Cerruto, E., Failla, S., Longo, D., Manetto, G. (2016). Simulation of water sensitive papers for spray analysis. *E-JOURNAL – CIGR*, 18(4), 22–29. ISSN 1682-1130.
- Felsot, A. S., Unsworth, J. B., Linders, J. B. H. J., Roberts, G., Rautman, D., Harris, C., et al. (2010). Agrochemical spray drift; assessment and mitigation—A review. *Journal of Environmental Science and Health, Part B*, 46(1), 1–23.
- Grella M., Gil E., Balsari P., Marucco P., & Gallart M. (2017). Advances in developing a new test method to assess spray drift potential from air blast sprayers. *Spanish Journal of Agricultural Research*, 15(3), e0207, 16.
- Hołownicki, R., Doruchowski, G., Swiechowski, W., Godyn, A., & Konopacki, P. J. (2017). Variable air assistance system for orchard sprayers; concept, design and preliminary testing. *Biosystems Engineering*, 163, 134–149.
- International Standards ISO/FDIS 9898. (1999). Equipment for crop protection—Test methods for air-assisted sprayers for bush and tree crops.
- Miranda-Fuentes, A., Marucco, P., González-Sánchez, E. J., Gil, E., Grella, M., & Balsari, P. (2018). Developing strategies to reduce spray drift in pneumatic spraying in vineyards: Assessment of the parameters affecting droplet size in pneumatic spraying. *Science of the Total Environment*, 616–617, 805–815.
- Moltó, E., Chueca, P., Moltó, E., Chueca, P., Garcerá, C., Balsari, P., et al. (2017). Engineering approaches for reducing spray drift. *Biosystems Engineering*, 154, 1–2.
- Nuyttens, D., Baetens, K., De Schampheleire, M., & Sonck, B. (2007). Effect of nozzle type, size and pressure on spray droplet characteristics. *Biosystems Engineering*, 97(3), 333–345.
- Qiu, W., Sun, C., Lv, X., Ding, W., & Feng, X. (2016). Effect of air-assisted spray application rate on spray droplet deposition distribution on fruit tree canopies. *Applied Engineering in Agriculture*, 32(6), 739–749.
- R Development Core Team. (2012). R: A language and environment for statistical computing. R Foundation for Statistical Computing, Vienna, Austria. <http://www.R-project.org>.
- van de Zande J. C., Michielsen J. M. G. P., Stallinga H., van Dalfsen P., Wenneker M. (2018). Effect on air deposition and spray liquid distribution of a cross flow fan orchard sprayer on spray deposition in fruit trees. In *Proceedings of VII SPISE* (pp. 24–26 IX). Athens.

Machines and Plants for Processing Agricultural Production

Introduction

Prof. Giovanni Carlo Di Renzo

President of the 6th Section of the Italian Association of Agricultural Engineering 'Machines and Plants for Processing Agricultural Production'.

The AIIA 6th Section studies and investigates the engineering aspects related to machinery and plants in the agri-food production processing. The typical approach to the topics of this section is the following:

- how the machine, the plant, and the device developed and tested, helps to improve the product quality, the workers' productivity or the performed operation efficiency/efficacy;
- how the operating parameters (as temperature, pressure, flow rate, torque, number of revolutions, etc.) optimization affects the product quality or the process efficiency;
- how the result of simulations performed contributes to the manufacturing improvement and to the technological development of machine, plant or device.

The task of the Section is to encourage the exchange of ideas among researchers and professional operators interested in these topics: engineers, agronomists and food technologists. The Section has always paid particular attention to the systems used in the sector of the so-called 'agri-industries' (dairy, wine, oil): there are numerous research groups, created within the Association and in the various University Departments or other research Centers, involved in developing and/or evaluating innovative technologies so providing useful information for their optimization. For example, studies related to machines optimization, extra virgin olive oil extraction and oenological processes management can be traced back to members of this Section.

Furthermore, the evolution of the agri-food sector has expanded the Section's interests also within the whole food production system: more and more frequently researchers (members of the VI Section) are involved in study of problems related, for example, to transformation of meat, to production of flour and pasta, but also to the world of catering, logistics and to large-scale distribution (GDO) problems. The plant engineering approach has led to in-depth researches aimed at evaluating the

interaction among the machine/product and process required. The working capacity or the plant productivity (in terms of processing yield and/or reduction of cost) still represents one of the most important targets of the research activity with an increasing number of papers treating the final product quality in terms of organoleptic and nutritional value, the by-products produced, the food safety, the operator safety and the sustainability of the entire production cycle. The research done presents a wide interdisciplinary approach that generally requires a multidisciplinary composition of the research group as in the Authors of the papers. Agricultural Engineers are often required to work with the support of food technologists, microbiologists and Electronic and Computer Science Engineers.

The research activity here presented is related to different subjects. It ranges from energy-type assessments to design some plant components, also through the application of forecasting models, to the optimization of the control and monitoring of processes. In addition to the traditional agricultural industries, the machines and plants for the sector of post-harvest of fresh fruit and vegetables represent an important research area inside the member of the 6th Section. The studies carried out concerning the optimization of both sorting and selection systems, with particular regard to the development of new non-destructive techniques, the storage technologies (modified atmospheres, refrigeration systems, etc.), and innovative solutions for packaging and product logistic. Recently the interest was particularly focused on the development of technologies supporting the production in the ready to Eat produces which represent one of the most interesting challenges for the entire agricultural sector and for the agricultural areas within Mediterranean Climate conditions.

The Section promotes the dissemination of its findings among researchers from both the academic world and the industrial sector, with seminars and scientific conferences. The members are active both in the EurAgEng Working Groups (European Society of Agricultural Engineers) related to the themes of 'food engineering' (AP06 Innovative technologies for dairy farming, PM11 Fruit and vegetable production engineering, etc.) and in the CIGR (International Commission of Agricultural and Biosystem Engineering) VI section (Postharvest Technology and Process Engineering).

Use of Ultrasound in the Extraction Process of Virgin Olive Oil and Influence on Malaxation Time



Mauro Pagano, Roberto Tomasone, Carla Cedrola, Marco Fedrizzi, Gianluca Veneziani and Maurizio Servili

Abstract The use of power ultrasonic in the olive oil industry is an innovative technique applied for the treatment of olive paste. The high-intensity sound waves exert a mechanical action by means of acoustic cavitation. Different operating parameters were applied in the milling operations to test the impact of the ultrasound treatment on the physical and chemical characteristics of the oils. The extraction tests were carried out with olives harvested at three different maturity stages and with three different durations for the malaxation phase, whereas the sonication time was the same for all treatments. The ultrasound US treatment was applied to the olive paste flowing through connection pipes in continuous operation, at 20 kHz frequency and 2.8 kW power. The yield and the organoleptic quality of the virgin olive oils extracted (VOO) were evaluated according to standard procedures. Three different malaxation times were used in oil extraction. The oil extraction yields progressively decreased with shorter malaxation time. The US treatment increases olive oil yield up to 22.7% when milling olives at an early ripening stage. In general, the ultrasonic treatment was found to increase the efficiency and speed of extraction, also giving olive oils enriched in bioactive compounds.

Keywords Oil extraction yield · Ultrasounds · Quality parameters · Maturity index · Malaxation time

M. Pagano (✉) · R. Tomasone · C. Cedrola · M. Fedrizzi

Consiglio per la ricerca in agricoltura e l'analisi dell'economia agraria (CREA), Centro di ricerca Ingegneria e Trasformazioni agroalimentari (Research Centre for Engineering and Agro-Food Processing), Via della Pascolare 16, 00015 Monterotondo (Roma), Italy
e-mail: mauro.pagano@crea.gov.it

G. Veneziani · M. Servili

Dipartimento di Scienze Agrarie, Alimentari e Ambientali Università degli Studi di Perugia, Via S. Costanzo, s.n.c., 06126 Perugia, Italy

© Springer Nature Switzerland AG 2020

A. Coppola et al. (eds.), *Innovative Biosystems Engineering for Sustainable Agriculture, Forestry and Food Production*, Lecture Notes in Civil Engineering 67,
https://doi.org/10.1007/978-3-030-39299-4_76

1 Introduction

The goal of recent technological innovations introduced in the virgin olive oil (VOO) extraction process is to increase olive oil extractability, while maintaining or improving the quality characteristics of the extracted VOO. The technologies tested in the olive mill include: microwave, pulsed electric field and ultrasound technologies. The common action of these technologies causes a significant disruption in the olive cells to enhance the release of the intracellular content and increase the yield in olive oil (Clodoveo et al. 2017; Puertolas and Martinez de Maranon 2015; Leone et al. 2018).

These technologies affect the cellular structure of the drupes in different ways. These treatments cause sudden and rapid alterations in the physical parameters: temperature, pressure, energy, electrical potential. The extraction technologies induce structural modifications in olive tissues, such as the development of pores, the increase of cellular permeability, the collapse of cellular membranes (Chemat et al. 2017).

These treatments are intended to improve the release of the oil drops that are principally positioned inside the vacuoles found in the mesocarp cells of the olive drupes. The breakage exerted by these processes also produces the simultaneous release of additional intracellular matter, thus allowing different antioxidant compounds to diffuse into the aqueous and oily phases (Chemat et al. 2017).

Besides increasing oil yield, recent studies conducted to test the use of heat exchangers, pulsed electric fields and ultrasounds showed that the quality of the VOO improves thanks to the increase in the relative content of α -tocopherols and/or hydrophilic phenols, that are quality parameters closely related to the product's health and sensory properties (Iqdiem et al. 2018; Puertolas and Martinez de Maranon 2015; Almeida et al. 2017; Esposto et al. 2013; Veneziani et al. 2018a).

Ultrasound-assisted extraction, which is based on the mechanical action of high-intensity sound waves whose effect is to cause acoustic cavitation in plant tissues, enables accelerated heat and mass transfers in olive paste. The ultrasound treatment (US) is an example of the new technologies applied in the mechanical extraction process of VOO. The US treatment can be applied either before or after the malaxation phase. Very recent tests have further improved the working efficiency of ultra-sound systems, increasing oil yields and also the phenolic fraction in the extracted oil.

The present paper examines the impact of a high-power ultrasound technology on the physicochemical characteristics of VOO extracted in an industrial processing plant. Large-scale extractions were carried out using different olive batches, at three ripening stages. Three malaxation durations were applied to evaluate the combined effect of the US treatment and malaxation time on the oil extraction yield (Taticchi et al. 2019). Many olive oil samples were analyzed to establish the effects of the treatments on the release of extractable compounds and on the modification of VOO quality.

2 Materials and Methods

The experimental tests were carried out using a high-power UIP4000 hdT ultrasound system. The ultrasound industrial equipment produced by Hielscher GmbH—Teltow, and installed by Seneco srl—Milano, is for continuous operation, and is composed by a generator and a transducer having 4 kW of power and 20 kHz frequency. The generator is equipped with a touch screen control panel and an ethernet connection for remote control of the main process parameters. A specially designed flow cell enables the ultrasound equipment to work in continuous operation. The apparatus is provided with a bottom inlet and a top outlet, with a DN90 connection. Specific connections for the temperature and pressure probes are inserted on the outlet side of the flow cell. A pinch valve regulates the pressure inside the flow cell. A specially designed radial “cascatrode”, made in titanium, is located inside the flow-cell to provide an adequate cavitation. The settings for cavitation amplitude are accessed through a touch-screen control panel. The US unit is positioned between the hammermill unit (model FP HP 30 INOX crusher) and four MOLINOVA TG MOD 600 malaxers. The connections between the components of the olive mill line are made with food-grade pipes only.

Different centrifugation systems are used in olive mills to separate the olive oil: two-stage, three-stage and multi-phase centrifugation. The two-phase centrifuge separates the oil fraction from an aqueous solid fraction comprising solid material and vegetation water. The three-phase centrifuge separates three parts: olive oil, solid material, vegetation water. The multi-phase centrifuge separates the oil from the solid material and an additional solid fraction consisting of olive flesh, without pits.

In this study, the centrifuge model installed in the olive mill is a Leopard decanter (Pieralisi S.p.A., Jesi, Ancona, Italy), which is a multi-phase decanter (DMF). In particular, this is a two-phase centrifuge, capable of producing a slightly hydrated pomace, like the one obtained from a three-phase decanter. The multi-phase technology is based on the production of an oily phase, a dehydrated husk and another phase represented by a certain amount of pulp from the husk referred to as “paté”, characterized by a high moisture content, without the presence of olive pits. The bowl discharging device used in the DMF technology is automatically controlled and allows to extract the olive oil without the addition of water, this process guarantees the advantages of a two-phase decanter extraction technology plus the versatility of an extractor able to operate both in continuous and in batch processing.

The olive paste, flowing from the hammer mill was processed in continuous mode with the ultrasound system set at a frequency of 20 kHz, a power of 2.8 kW, with 3 bars of pressure and an 80% of amplitude. The ultrasound treatment was followed by a malaxation phase regulated at a kneading time of 30 min with a controlled temperature of 25 °C. The olive batches characterized by an early ripening stage (having a maturity index of 0.88 MI) were also processed applying two additional malaxation duration times, i.e. 10 min and 20 min, in addition to the above mentioned 30 min.

2.1 Quality Indices

The values of free acidity, peroxide value, K232, K270 and ΔK were detected according to the analysis methods described by Regulation (EU) 2015/1830 (OJEC 2015). The sterol composition, total sterols, amount of erythrodiol and uvaol, and waxes were detected using the official methods of analysis according to Regulation (EU) 2015/1830, OJEC (2015).

The VOOs extracted in the trials were evaluated using the methods of analysis described by the IOC (2013); the quantities of Chlorophylls and carotenoids, α -Tocopherol, Hydrophilic phenols and Volatile compounds were also analyzed.

2.2 Statistical Analysis

The physicochemical data related to the olive oils extracted, treated with ultrasound-assisted extraction or untreated, were analyzed using SigmaPlot Software 12.3 (Systat Software Inc., San Jose, CA, USA), by means of one-way analysis of variance (ANOVA), and differences considered significant with $p < 0.05$. (Taticchi et al. 2019).

3 Results and Discussion

3.1 Physicochemical Characterization of VOO

The impact of the ultrasound-assisted extraction on the physicochemical composition of the VOOs was evaluated in an industrial plant, where olives of cultivar *Ogliarola garganica* were processed at a working capacity of 2 tons/h. These olives were characterized by an early maturity index of 0.88 MI, for which a conventional malaxation time of 30 min was applied. The ultrasound treatment did not modify the legal quality indices, including free acidity, peroxide value and spectrophotometric constants.

The cavitation process induced by the ultrasound waves causes a sudden increase in temperature and disruptive effects on the olive's skin, that did not however change the waxes content in any of the VOOs extracted. The different parts of the olive fruit (skin, pulp and seed) are characterized by different concentrations of sterols, that are mainly represented as β -sitosterol, campesterol, delta-5-avenasterol and stigmasterol. The highest total content of sterols is found in the endocarp oil, which is approximately two-fold higher than that detected in mesocarp and epicarp oil fractions. Following the ultrasound treatment (US), there is a more abundant extraction of oil from the cells composing the skin and seed tissues, which are characterized by different concentrations of sterols. However, the treatment did not determine any significant alteration in the composition in sterols of the extracted oils, compared to the control test (C).

Also, the technological factors of the extraction process have been seen to influence the sterol content (Guillaume et al. 2012). All these factors suggest that the ultrasound treatment may have an impact on the content of triterpene dialcohols, but the chemical analysis on the different oil samples showed no differences in these compounds in relation to the ultrasound extraction. Ultrasound-assisted extraction can modify the chemical structure of some compounds during the treatment of the food matrix, because it can induce isomerization or degradation effects.

3.2 Innovative Technological Treatment

The innovative US technological treatment improves the separation of the water phase from the oil phase. This effect is highlighted by a significant reduction in the turbidity of oil extracted and also moisture levels. The data relating to the CIELAB coordinates show slight increases in lightness (L^*), green value (a^*) and yellow value (b^*) of the VOOs obtained from the ultrasound treated olive paste. These changes are probably related to the reduction in the degree of turbidity and are also likely connected to oil transparency (Gordillo, et al. 2011) and to the increase in the pigment contents (chlorophylls and carotenoids). The chroma value was also enhanced by the ultrasound-assisted extraction, while the hue data showed no difference when compared to the control. The analysis regarding the content in chlorophylls and carotenoids show a 21.5% and 15.4% increase, respectively, in the US treated VOOs, confirming as mentioned above the changes induced in the color of the extracted oil, due to the impact of ultrasound technology. The physical and chemical effects of the cavitation phenomenon caused by the ultrasound treatment resulted in a significant increase in extraction yield, from 11.9 kg to 14.6 kg of oil per 100 kg of olives, with a 22.7% increase when compared to the oil obtained in the control test (Table 1).

The residual oil content measured in the olive pomace and paté also confirm the extraction yield data. Residual oil values in pomace and paté were lower in the US treated samples compared to the control C sample. The ultrasound treatment

Table 1 VOO extraction yield, moisture and oil content of paté and pomace^a

Maturity index	Control			Ultrasound		
	0.88					
Extraction yield (%)	11.9	±	0.3a	14.6	±	0.3b
Paté moisture content (%)	74.8	±	3.5a	77.6	±	2.1a
Paté oil content (% db)	26.2	±	2.3a	20.4	±	2.2b
Pomace moisture content (%)	50.8	±	3.5a	46.8	±	0.5a
Pomace oil content (% db)	3.9	±	0.4a	4.0	±	0.1a

^aThe data are the mean values of three independent extractions, ± standard deviation. For each different maturity index the values in each row having different letters (a – b) are significantly different from one another ($p < 0.05$). C = control test; US = ultrasound test; db = dry basis

applied to the crushed olive paste during the mechanical extraction process determined a release of phenolic compounds into the oily phase, increasing the amount of hydrophilic phenols in US treated VOO, compared to the corresponding control oil.

A 9.8% increase was measured, which was mainly attributed to the aglycon derivatives of oleuropein that are among the most important bioactive molecules, characterized by biological activity providing health and sensory benefits (Di Maio et al. 2011). The lipophilic fraction, mainly represented by α -tocopherol, was also positively enhanced, with an increased concentration of approximately 30 mg/kg, representing an 11.3% increase compared to the lipophilic content in the control sample. Increases in both hydrophilic and lipophilic concentrations of VOO phenols are attributed to the improvement of cellular degradation of the US treated olive drupe (Table 2).

3.3 Impact of Ultrasound System on VOO Extracted at Different Malaxation Times

The relevant increase in extraction yield obtained in the US VOO suggested that a supplementary investigation should be pursued on the impact on oil extractability, using the same technology with the same cultivar at the same maturity index (0.88), but with a reduction in the time of malaxation to determine how a hypothetical conversion of the traditional mechanical extraction process to a continuous extraction system might be achieved. The yield in oil extraction decreased progressively with the reduction in the malaxation time. A decrease in malaxation time also determined a progressive reduction of the content in hydrophilic phenols, for both the control and ultrasound VOOs. A reduction in malaxation duration from 30 min to 10 min produced the decrease in hydrophilic phenols content equal to 11.8% and 17.9%, respectively.

3.4 Impact of Ultrasound System Processing Olives at Different Maturity Indices

This experiment also studied the changes in extraction yields measured using cultivar *Ogliarola garganica* olives, at two other maturity indices: 2.82 and 3.31. The improvement of the oil yield due to the ultrasound treatment decreased with olive ripeness. The higher maturity indices are related to lower oil yields, compared to oil extracted from olives at 0.88 MI. Overall, the turbidity levels were higher than the values obtained for the early ripening stage of olives and the same reduction effect of US treatment was detected for both the other VOOs, even if the data was not statistically significant for the VOO obtained from fruits at 2.82 MI. The results

Table 2 Physicochemical parameters of VOOs, control and ultrasound treatment^a

Maturity index	C			US		
	0.88					
Turbidity (NTU)	131	±	28a	64	±	24b
Oil moisture content (%)	0.16	±	0.01a	0.13	±	0.01b
Free fatty acid (% oleic acid)	0.25	±	0.00a	0.25	±	0.00a
Peroxide values (meqO ₂ /kg)	4.7	±	0.6a	4.9	±	0.7a
K ₂₃₂	1.974	±	0.011a	1.968	±	0.019a
K ₂₇₀	0.195	±	0.003a	0.197	±	0.003a
ΔK	-0.006	±	0.000a	-0.006	±	0.000a
Waxes (mg/kg)	19.9	±	0.8a	18.2	±	0.2a
Cholesterol (%)	0.2	±	0.1a	0.2	±	0.1a
Brassicasterol (%)	0.0	±	0.0a	0.0	±	0.0a
24-Methylenecholesterol (%)	0.1	±	0.0a	0.1	±	0.0a
Campesterol (%)	3.3	±	0.2a	3.2	±	0.0a
Campestanol (%)	0.2	±	0.0a	0.2	±	0.0a
Stigmasterol (%)	0.5	±	0.0a	0.5	±	0.0a
Δ7-Campesterol (%)	0.0	±	0.0a	0.0	±	0.0a
Δ5,23-Stigmastadienol (%)	0.0	±	0.0a	0.0	±	0.0a
Cholesterol (%)	1.0	±	0.0a	1.1	±	0.1a
β-Sitosterol (%)	85.0	±	0.2a	85.5	±	0.3a
Sitosterol (%)	1.3	±	0.1a	1.3	±	0.0a
Δ5-Avenasterol (%)	6.4	±	0.1a	6.2	±	0.1a
Δ5,24-Stigmastadienol (%)	1.1	±	0.0a	1.0	±	0.1a
Delta-7-Stigmastenol (%)	0.3	±	0.0a	0.2	±	0.1a
Delta-7-Avenasterol (%)	0.7	±	0.0a	0.5	±	0.2a
App β-sitosterol (%) ^b	94.8	±	0.2a	95.1	±	0.4a
Total sterols (mg/kg)	1273	±	33a	1302	±	31a

(continued)

Table 2 (continued)

Maturity index		C			US		
		0.88					
Erythrodiol and uvaol (%)		1.4	±	0.0a	1.1	±	0.5a
Chlorophyll (mg/kg)		4.0	±	0.1a	4.9	±	0.4b
Carotenoid (mg/kg)		3.1	±	0.0a	3.7	±	0.3b
Colour:	L*	90.2	±	0.1a	93.2	±	1.6b
	a*	-5.3	±	0.2a	-5.6	±	0.1b
	b*	48.3	±	0.5a	53.2	±	2.0b
	C*	48.7	±	0.4a	53.5	±	2.1b
	h	96.2	±	0.2a	96.1	±	0.4a

^aThe data are the mean values of three independent extractions, ± standard deviation. The values in each row having different letters (a – b) are significantly different from one another ($p < 0.05$)

^bApp β -sitosterol: $\Delta 5,23$ -stigmastadienol + chlerosterol + β -sitosterol + sitostanol + $\Delta 5$ -avenasterol + $\Delta 5,24$ -stigmastadienol.; L*a*b* = CIE coordinates; C* = chroma; h = hue

suggest a more intensive effect of ultrasound treatment on the release of waxes and sterols into the water/oily phase from olive cells at a late ripening stage, when the different tissues of fruit are subjected to high levels of depolymerizing enzymatic activities. However, the sterol content, that decreased during the olives ripening in both US and C tests, did not modified its percentage composition after the ultrasound treatment for all the VOOs extracted from fruits at different maturity indices. The high percentage increase of waxes compared to control at the highest maturity index did not compromise the quality of the product with a content (15.3 mg/kg) abundantly below the limit (≤ 150 mg/kg) fixed by the regulation of European Union (OJEC 2015; Taticchi et al. 2019).

4 Conclusions

The ultrasound treatment showed a positive impact on VOOs obtained from the olive fruits in their early ripening stage, because it exerts a highly disruptive effect on the cells, thus causing an abundant release of intracellular contents into the liquid medium. The impact of high-power ultrasounds on oil yield and quality parameters was evaluated along with other physicochemical characteristics of the VOOs extracted from olives having different maturity indices. The US treatment increases oil yield and significantly improves the extraction of the phenolic fraction. The US technology causes cavitation and shockwaves, improving the mechanical extraction process in general. The positive impact of the ultrasound treatment on oil extractability and on quality parameters progressively decreases during olive fruit ripening, with no extra gain as the olive drupes ripen. The effects of the US technology should be

further evaluated on more cultivars at different maturity indices, to investigate the effects on quality and extraction yield at the medium to late ripening stages.

Acknowledgements This study was funded and developed by the project INFOLIVA (D.M. n.12479) funded by the Italian Ministry of Agriculture (MiPAAF).

References

- Almeida, B., Valli, E., Bendini, A., & Toschi, T. G. (2017). Semi-industrial ultrasound assisted virgin olive oil extraction: Impact on quality. (Special Issue: Olive oil). *European Journal of Lipid Science and Technology*, *1600230*, 119–125.
- Chemat, F., Rombaut, N., Sicaire, A.-G., Meullemiestre, A., Fabiano-Tixier, A.-S., & Abert-Vian, M. (2017). Ultrasound assisted extraction of food and natural products. Mechanisms, techniques, combinations, protocols and applications. A review. *Ultrasonics Sonochemistry*, *34*, 540–560.
- Clodoveo, M. L., Moramarco, V., Paduano, A., Sacchi, R., Di Palmo, T., Crupi, P., et al. (2017). Engineering design and prototype development of a full scale ultrasound system for virgin olive oil by means of numerical and experimental analysis. *Ultrasonics Sonochemistry*, *37*, 169–181.
- Di Maio, I., Esposito, S., Taticchi, A., Selvaggini, R., Veneziani, G., Urbani, S., et al. (2011). HPLC–ESI-MS investigation of tyrosol and hydroxytyrosol oxidation products in virgin olive oil. *Food Chemistry*, *125*, 21–28.
- Esposito, S., Veneziani, G., Taticchi, A., Selvaggini, R., Urbani, S., Di Maio, I., et al. (2013). Flash thermal conditioning of olive pastes during the olive oil mechanical extraction process: Impact on the structural modifications of pastes and oil quality. *Journal of Agricultural and Food Chemistry*, *61*, 4953–4960.
- Gordillo, B., Ciaccheri, L., Mignani, A. G., Gonzalez-Miret, M. L., & Heredia, F. J. (2011). Influence of turbidity grade on color and appearance of virgin olive oil. *Journal of the American Oil Chemists' Society*, *88*, 1317–1327.
- Guillaume, C., Ravetti, L., Lala Ray, D., & Johnson, J. (2012). Technological factors affecting sterols in Australian olive oils. *Journal of the American Oil Chemists' Society*, *89*, 29–39.
- IOC. (2013). International Olive Council. Determination of composition of triacylglycerols and composition and content of di-acylglycerols by capillary gas chromatography, in vegetable oils. COI/T.20/Doc. No 32, November 2013.
- Iqdiyam, B. M., Mostafa, H., Goodrich-Schneider, R., Baker, G. L., Welt, B., & Marshall, M. R. (2018). High power ultrasound: Impact on olive paste temperature, malaxation time, extraction efficiency, and characteristics of extra virgin olive oil. *Food and Bioprocess Technology*, *11*(3), 634–644.
- Leone, A., Romaniello, R., Tamborrino, A., Urbani, S., Amarillo, M., Grompone, M. A., et al. (2018). Application of microwaves and megasonics to olive paste in an industrial olive oil extraction plant: impact on virgin olive oil quality and composition. *European Journal of Lipid Science and Technology*, *120*, 1700261–1700269.
- OJEC. (2015). Official Journal of the European Community Commission Delegated.
- Puertolas, E., & Martinez de Marañon, I. (2015). Olive oil pilot-production assisted by pulsed electric field: Impact on extraction yield, chemical parameters and sensory properties. *Food Chemistry*, *167*, 497–502.
- REGULATION (EU) 2015/1830 of 8 July 2015 amending Regulation (EEC) No 2568/91 on the characteristics of olive oil and olive-residue oil and on the relevant methods of analysis.
- Taticchi, A., Selvaggini, R., Esposito, S., Sordini, B., Veneziani, G., Servili, M. (2019). Physicochemical characterization of virgin olive oil obtained using an ultrasound-assisted extraction at an industrial scale: Influence of olive maturity index and malaxation time. *Food Chemistry*, *289*, 7–15.

- Veneziani, G., Esposto, S., Taticchi, A., Urbani, S., Selvaggini, R., Sordini, B., et al. (2018a). Characterization of phenolic and volatile composition of extra virgin olive oil extracted from six Italian cultivars using a cooling treatment of olive paste. *LWT—Food Science and Technology*, *87*, 523–528.
- Veneziani, G., Esposto, S., Minnocci, A., Taticchi, A., Urbani, S., Selvaggini, R., et al. (2018b). Compositional differences between veiled and filtered virgin olive oils. *LWT—Food Science and Technology*, *94*, 87–95.

An Innovative Vat for the Continuous Recovery of Volatile Compounds During Fermentation



Giulia Angeloni, Lorenzo Guerrini, Piernicola Masella, Agnese Spadi, Fabio Baldi and Alessandro Parenti

Abstract During the production of fermented alcoholic beverages a part of the volatile organic compounds, that represent the aromas of the product being processed, are dispersed with the gaseous phase. The loss of volatile compounds has a significant impact on the overall product aroma. The preservation of beverage aroma and the loss recovery during processing is a key issue that is becoming increasingly important in the beverages technology. This loss is mostly due to the leakage of carbon dioxide, that drag out the aromatic compounds. To date all solutions proposed for the recovery of aromas by condensing the gases are equipped by systems separated from fermentation tank. A new apparatus for fermentation of beverages, equipped internally with a system for reducing the losses of the volatile organic compounds, has been designed, tested and patented. This apparatus comprises a container having a single inner chamber for the fermentation of liquids and for the continuous condensation of fermentation vapors, with relapse of volatile organic compounds directly in the mass under fermentation. The condensation of the vapors is realized thanks to a cooling jacket at the top portion of the tank, able to cool and condense the fermentation vapors. The system has been developed and tested by several trials performed on wine and beer fermentations. Esters, acids, terpenes, alcohols, and lactones can be recovered with a condensation device. Moreover, the recovery system stimulated the de novo synthesis of esters from carboxylic acids and alcohols. Thus, using different temperatures, the condensation of the gasses escaping during the fermentation can be used as a tool to modulate the final aroma of the beverages.

Keywords Volatile compounds · Brewing · Alcoholic beverage · Aroma losses

G. Angeloni (✉) · L. Guerrini · P. Masella · A. Spadi · F. Baldi · A. Parenti
Dipartimento di Scienze e Tecnologie Agrarie, Alimentari Ambientali e Forestali (DAGRI),
Università degli Studi di Firenze, Piazzale delle Cascine 15, 50144 Florence, Italy
e-mail: giulia.angeloni@unifi.it

© Springer Nature Switzerland AG 2020
A. Coppola et al. (eds.), *Innovative Biosystems Engineering for Sustainable Agriculture, Forestry and Food Production*, Lecture Notes in Civil Engineering 67,
https://doi.org/10.1007/978-3-030-39299-4_77

1 Introduction

The preservation of beverage aroma and the recovery of aroma losses during processing is a key issue that is becoming increasingly important in food technology.

The aromatic profile, generally considered to be one of the most individual characteristics of wine and beer, is the result of the concentrations of different volatile compounds and their sensory interactions. Through the production of fermented alcoholic beverages, such as wine or beer, the loss of volatile compounds has a significant impact on the overall product aroma.

The quantity of each volatile compound in wine mainly depends on its initial content in the grape, and/or its production (by yeast fermentation), and the activity of specific enzymes. However, in wines the level of each volatile compound is affected by many variables. During the alcoholic fermentation the rapid emission of large quantities of CO₂ in tumultuous fermentation leads to continuous stripping of volatile compounds with uncontrolled consequences for the aromatic profile.

In wine production this phenomenon is widely studied. For instance, Mouret et al. (2014) evidenced the losses of aromatic compounds in the gas phase produced by the fermentation mass. In scientific literature are proposed few methods to recover these aromatic compounds condensing them in an external container by cooling the gas that draws them out of the container. A large number of studies focused on the modulation of the secondary aroma. Post-harvest degradation of grapes (Moreno et al. 2008), yeasts inoculum, fermentation temperature control (Guerrini et al. 2017a), stem contact fermentation (Guerrini et al. 2018a) can all be considered traditional oenological practices aimed to change the final wine aroma. Gomez and co-authors (Gomez et al. 1993), have focused on the recovery of such volatile compounds and have shown that they are primarily esters and alcohols, which are particularly important for wine aroma (Sumby et al. 2010; Capone et al. 2013). However, in this study Gomez et al. (1993) did not test the effect of the addition of these compounds back to the wine. In recent study (Guerrini et al. 2019) it was investigating the comparison between a traditional red grape fermentation and a fermentation during which the volatile compounds escaping from the tank were recovered and condensed back into the wine.

Based on the studies conducted, it has been proposed an innovative condensation device designed to recover the aroma active compounds (AACs) stripped-off by carbon dioxide emission during fermentation. They patented this solution as “fermentation apparatus able to reduce the aroma loss” (Parenti and Guerrini 2016). This technological solution was also applied in another work, with the aim of recovering AACs lost during wort fermentation in beer.

Fig. 1 System above a fermentation tank



2 Materials and Methods

2.1 Wine Experimental Test

The aim of the trial was the comparison between a traditional red grape fermentation, namely “Control”, and a fermentation during which the volatile compounds escaping from the tank were recovered and condensed back into the wine, namely “Condensed”. Fermentations were conducted in stainless steel tanks of nominal capacity of 1000 l. On the top of the tanks of the Condensed samples a heat exchanger was placed to recover the volatiles (Fig. 1). Each fermentation tank was filled with 540 kg of grapes. During the trials, Sangiovese, Cabernet Sauvignon, and Merlot grapes were used for a total of 6 fermentations (3 Control and 3 Condensed). The musts were inoculated with 20 g/100 kg of grapes of a commercial yeast (Red Fruit, Enartis, Italy), and 10 g/100 kg of grapes of potassium metabisulfite were added. During the fermentations, the temperatures of all tanks were controlled at 32 °C, while in the Condensed samples, the condensation temperature was fixed to 5 °C. The cooling fluid was propylene glycol. Two pump-overs every day, of 5 min each were done to all tanks.

The obtained wines were stored for 11 months in 100 l stainless steel tanks. The head space of the tanks was blanketed with nitrogen to avoid oxidations. Analyses were done immediately after the fermentations, after 6 months, and after 11 months of storage.

2.2 Beer Experimental Test

Wheat beer samples were prepared using a system that allows the continuous recovery by condensation of vapors escaping from fermenters during fermentation. These samples were compared with the standard brewing procedure (i.e., where vapors are free to escape from fermenters). Samples were brewed at laboratory scale using commercial home-brewing equipment (Muntions malt for premium beer. Muntions

Plc, Cedars Maltings, Suffolk, England). A mass of 1.8 kg of malt extract (containing, as reported in the label: malted barley, wheat, and dry hop extract) and 1 kg sugar were dissolved in 3 l water. This solution was transferred to a stainless-steel tank and supplemented with 23 l water. Then, 5 g of active dry yeast (*Saccharomyces cerevisiae*, Safbrew WB-06, Lesaffre, France) were re-hydrated and added to the wort.

Three replicates have been performed. In three of the six tanks, fermentation took place under standard conditions (i.e., with no vapor condensation); these were the control samples. The remaining tanks constituted the test condition. In the test condition, Allihn condensers were placed on top of the three tanks. These condensers allow heat exchange between the vapors escaping from the tanks and the cooling liquid. Condensed vapors fall back into the fermenting wort.

Cold water at 3–8 °C was used as coolant and flowed in countercurrent with respect to vapors (i.e., from the top) in order to increase cooling efficiency. Tanks were maintained at 20 °C for the duration of the experiment. At the end of the six fermentations, a sample was taken from each tank. The three condensed beer samples and the three control beer samples were then analyzed separately and compared.

2.3 Chemical Analyses

The AAC profile was determined by gas chromatography with mass spectrometry detection (GC-MS) after solid-phase microextraction (SPME) sampling of the headspace of sampling vials in equilibrium with the liquid (HS-SPME-GCMS), in both experimental tests, i.e. wine and beer.

2.4 Sensory Analyses

The differences between the Condensed and the Control samples for each grape cultivar, and for each samples of beer, were assessed using a triangular test (UNI 0590 A2520 2001). The selection criterion was regular consumption of wine and/or beer. Samples were presented in glass cups with a plastic cover at room temperature (20 °C).

2.5 Statistical Analysis

For the wine experimental test, data were analysed with a two-way Analysis of Variance (ANOVA) considering the condensation treatment (2 levels, Condensed and Control) and the storage time (3 levels, 0-6-11 months) as independent variable.

Data were tested for the two main effects of the independent variables and for their interaction. When $p < 0.05$ a Tukey HSD post hoc test was used.

For the beer experimental test, AACs were analysed individually. For each compound, an independent t-test for two samples ($p < 0.05$) was performed to detect significant differences between the control and condensed beer samples.

3 Results

3.1 Wine Experimental Test Results

Immediately after the production, no significant difference was found in wines for total ethanol, pH, total acidity, volatile acidity, free and total sulfur dioxide and residual sugars.

During the wine storage, no significant difference in the above reported parameters was found (data not shown). During the storage, no significant interaction between treatment and time was assessed; the compounds higher immediately after the fermentation remain higher after 1 year of storage.

The volatile profile has been analyzed for 18 compounds considered important on the basis of a previous work (Guerrini 2017b). Among these, 7 increased significantly in the Condensed samples, while no compound was found at higher concentration in the control. The volatile concentration immediately after the wine production is reported in Table 1. The concentration of four esters, acetic acid hexyl ester, ethyl octanoate, ethyl hexanoate, and ethyl acetate, was found to be significantly increased by the condensation. These compounds can be considered positive for the wine flavor since they are usually related to fresh, sweet, and fruity flavors (the good scent company database).

Two alcohols (i.e. propanol and hexanol) were found at significant higher concentrations in Condensed wines than in the Control. As well as the above discussed esters, both these alcohols are related to fruity flavors. Thus, the recovered alcohols

Table 1 Mean and standard deviation of selected wine volatile compounds immediately after the production

Compound (mg/kg)	Condensed	Control	p-value	Ratio
Acetic acid hexil ester	0.06 (0.02)	0.05 (0.02)	0.04	1.18
Ethyl octanoate	19.07 (13.33)	16.58 (9.78)	0.04	1.15
Ethyl hexanoate	3.41 (0.31)	3.00 (0.45)	0.04	1.14
Ethyl acetate	66.19 (19.68)	59.05 (14.26)	0.05	1.12
Propanol	26.95 (5.93)	22.30 (3.55)	0.001	1.21
Hexanol	1.37 (0.37)	1.17 (0.25)	0.007	1.17
Hexanoic acid	2.18 (0.23)	1.79 (0.23)	0.001	1.22

and esters can enhance the fruity flavor of the tested wines. Finally, the hexanoic acid was higher in Condensed samples than in the Control. Hexanoic acid is related to the “cheese” flavor and its occurrence in wines at higher concentrations can be considered negative for the wine flavor.

Being the difference measured with the aromatic analysis small (the ratios between Condenser and Control ranged from 1.12 to 1.21) we performed a panel test to understand if they can be perceived by wine tasters. Immediately after the wines production, tasters were able to found the difference in Sangiovese and in Merlot ($p < 0.05$), while Cabernet Sauvignon Condenser and Control were perceived as equal.

3.2 Beer Experimental Test Results

Significant differences were found for 24 compounds (in Table 2, we report only the compounds showing significance at the statistical test, while the others are not reported), belonging to several chemical classes (esters, alcohols, aromatic compounds, sulfur compounds, acids, and terpenes) (Guerrini et al. 2018b).

Unexpectedly, four compounds (butanal, 3-methyl, 1-propanol, 2-methyl, geraniol, and citronellol) were higher in the control samples. Eleven of the 16 compounds with higher concentrations in condensed samples (shown in Table 2) were esters: 4

Table 2 Significant results of the t test. Mean peak area and standard deviation (number of counts). Nd not detected

Compounds		Condenser		Control		p-value	Condenser/Control
		Mean	sd	Mean	sd		
Dimethyl	Sulfide	1,977,128	660,423	158,303	25,166	0.009	12.5
Ethyl	Acetate	8,091,706	1,259,693	2,085,467	662,536	0.002	3.9
Isoamyl	Acetate	2,037,411	1,236,571	240,495	130,162	0.07	8.5
Isobutyl	Acetate	2,237,190	824,110	Nd	Nd		
Propyl	Acetate	443,020	250,240	Nd	Nd		
Butanoic acid, ethyl ester		11,542,804	4,662,849	1,476,968	11,280,565	0.02	7.8
Isopentyl hexanoate		5,950,310	926,449	1,446,478	223,240	0.001	4.1
Octanoic acid, 3-methylbutyl ester		9,952,198	246,769	5,916,665	2,575,155	0.05	1.7
1-propanol, 2-methyl		95,220	5483	163,361	36,391	0.03	0.6
1-heptanol		18,819,205	4,407,407	9,866,241	3,254,238	0.05	1.9
1-octanol		26,029,950	8,689,527	12,238,065	2,286,123	0.06	2.1
Benzeneacetaldehyde		7,547,953	2,931,705	2,457,117	535,807	0.04	3.1
Butanal, 3-methyl		2,779,875	1,263,792	26,894,303	4,054,566	0.001	0.1
Linalool		367,124	142,543	97,602	18,460	0.03	3.8
Citronellol		369,505	141,479	686,893	26,490	0.02	0.5
Geraniol		341,915	110,745	546,859	30,678	0.04	0.6

acetates, 5 ethyl esters, and 2 other esters. On the other hand, in control samples, four of the eight compounds with higher concentrations were acids. Higher concentrations of ethyl esters were found in condensed samples ethyl hexanoate, ethyl octanoate, ethyl decanoate, and ethyl dodecanoate.

The condenser system highlighted two effects, both have the potential to change the flavor of the beer:

- the recovery of some volatile compounds that would otherwise escape during fermentation.
- the production of esters from carboxylic acids, ethanol, and alcohols.

3.3 *Vat Design*

The experimental tests conducted with the wine and beer fermentations allowed to design an appropriate vat for the recovery of aromas.

The vat comprises a container having a single inner chamber adapted to carry out the fermentation. The vat is surmounted by a portion provided with an outlet for the gases coming out of the liquids under fermentation. It's further characterized by the presence of a cooling jacket in the top portion of the container, able to cool and condense the fermentation vapors comprising gases and volatile organic compounds, and to let a liquid condensate falling together with a part of volatile organic compounds into the liquid under fermentation, while the uncondensed gases go away. In Fig. 2 is represented the prototype of the fermentation vat.

4 Conclusions

The recovery of aromatic active compounds (AACs) lost during fermentation appears to have a perceivable impact on the sensorial profile of the produced beer and wine. Moreover, the AACs could be condensed back into the fermenting wort but they also react with each other and increase in concentration.

In particular, the condensation device placed on the top of the fermenter is able to recover some of the volatile compounds escaping from the tank during the alcoholic fermentation.

The studies conducted on the loss and recovery of AACs during fermentation, both in wine and in beer, have permitted to develop and patent a vat for the continuous recovery of volatile compounds during fermentation, that can be considered a valuable tool to change the aroma profile of the beverage.

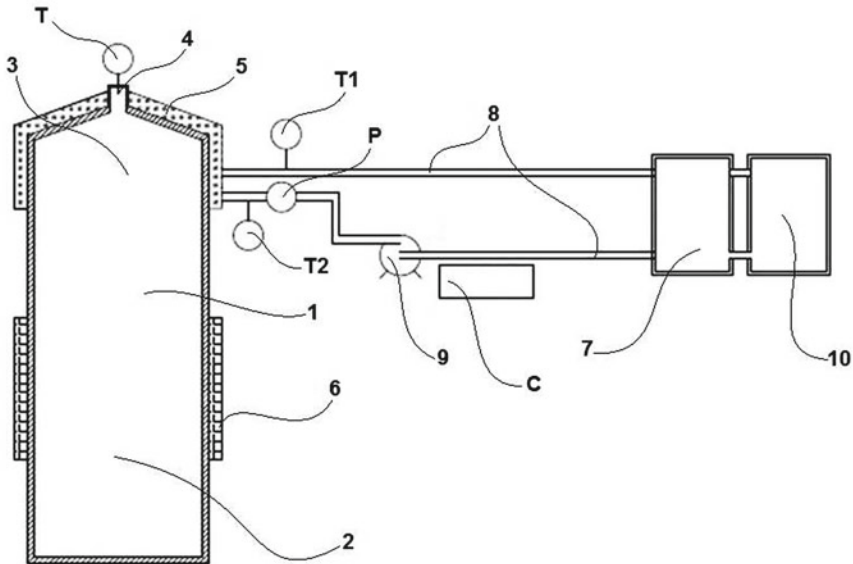


Fig. 2 The container (1) having a single inner chamber wherein are defined the bottom portion (2) and a top portion (3) provided with a cooling jacket (5) and with an outlet (4) for the gases coming out of the liquids under fermentation; the storage tank (7) connected to jacket through pipes (8) wherein the fluid is made to circulate by using a pump (9) and cooled by a cooling unit (10)

References

- Capone, S., Tufariello, M., & Siciliano, P. (2013). Analytical characterisation of Negroamaro red wines by "Aroma Wheels". *Food Chemistry*, *141*, 2906–2915.
- Gomez, E., Martinez, A., & Laencina, J. (1993). Recovery of wine volatile compounds during the vinification. *J Int Sci Vigne Vin*, *7*, 219–224.
- Guerrini, L., Angeloni, G., Baldi, F., & Parenti, A. (2017a). Thermal effects of pump-overs during red wine fermentation. *Applied Thermal Engineering*, *112*, 621–626.
- Guerrini, L., Masella, P., Angeloni, G., Cini, E., & Parenti, A. (2017b). A device for the monitoring of the cap buoyancy during the red grapes fermentation. *Chemical Engineering Transactions*, *58*, 427–432.
- Guerrini, L., Masella, P., Angeloni, G., Calamai, L., Spinelli, S., Di Blasi, S., et al. (2018a). Harvest of Sangiovese grapes: The influence of material other than grape and unripe berries on wine quality. *European Food Research and Technology*, *244*, 1487–1496.
- Guerrini, L., Angeloni, G., Masella, P., Calamai, L., & Parenti, A. (2018b). A technological solution to modulate the aroma profile during beer fermentation. *Food and Bioprocess Technology*, *11*, 1487–1496.
- Guerrini, L., Masella, P., Angeloni, G., Baldi, F., Calamai, L., & Parenti, A. (2019). Stability of volatile compounds recovered during the winemaking process. *Chemical Engineering Transactions*, *75*, 49–54.
- Moreno, J. J., Cerpa-Calderón, F., Cohen, S. D., Fang, Y., Qian, M., & Kennedy, J. A. (2008). Effect of postharvest dehydration on the composition of pinot noir grapes (*Vitis vinifera* L.) and wine. *Food Chemistry*, *109*, 755–762.

- Mouret, J. R., Perez, M., Angenieux, M., Nicolle, P., Farines, V., & Sablayrolles, J. M. (2014). Online-based kinetic analysis of higher alcohol and ester synthesis during winemaking fermentations. *Food Bioprocess Tech*, 7, 1235–1245.
- Parenti, A., & Guerrini, L. (2016). Domanda No. (Patent number) 102016000122743. Ministero per lo sviluppo economico. Repubblica Italiana.
- Sumby, K. M., Grbin, P. R., & Jiranek, V. (2010). Microbial modulation of aromatic esters in wine: Current knowledge and future prospects. *Food Chemistry*, 121, 1–16.

Effect of Packaging Technology on the Quality of Pre-cooled Clementine Fruit



F. Genovese, G. C. Di Renzo, G. Altieri, L. Scarano and M. C. Strano

Abstract This paper reports the results of comparative tests using pre-cooling and an innovative packaging device on Clementine fruit (*Citrus clementina* Hort. ex Tan.) aiming to reduce the weight loss and to preserve fruit quality. The tests were carried out by dividing Clementine fruits into six homogeneous lots: three lots were subjected to the pre-cooling (using a cooling unit prototype) followed by controlled temperature storage (6 ± 0.5 °C, RH 90–95%), three lots were directly stored in cold storage room without pre-cooling. Moreover, in order to verify the effect on fruit weight loss, traditional HDPE bags and the same bags improved with an innovative breathable device were used for the packaging. To evaluate the effect of the treatments were used: fruit weight, peel and pulp colour, deformation, firmness, juice yield, total soluble solids content, pH and titratable acidity. After 15 and 30 days of cold storage, plus 7 days of shelf-life, were assessed: VOC, O₂ and CO₂ concentration inside the packaging, weight loss, decay incidence and physiological disorders. Results showed that during the storage using HDPE bags the fruit weight loss, chilling injury and ageing were significantly reduced with respect to unwrapped fruit. However, a higher presence of total decay was observed in all wrapped fruit, although it was absent on precooled fruit, up to 15 days of cold storage. Precooling reduced significantly ethylene production inside packaging.

Keywords Citrus fruit · Postharvest · Smart packaging · Fruit quality · Shelf-life

F. Genovese (✉) · G. C. Di Renzo · G. Altieri · L. Scarano
Scuola di Scienze Agrarie, Forestali, Alimentari ed Ambientali (SAFE), Università degli Studi della Basilicata, Via dell'Ateneo Lucano 10, Potenza, Italy
e-mail: francesco.genovese@unibas.it

M. C. Strano

Consiglio per la ricerca in agricoltura e l'analisi dell'economia agraria (CREA), Centro di ricerca Olivicoltura, Frutticoltura e Agrumicoltura, Corso Savoia 190, 95024 Acireale (CT), Italy

© Springer Nature Switzerland AG 2020

A. Coppola et al. (eds.), *Innovative Biosystems Engineering for Sustainable Agriculture, Forestry and Food Production*, Lecture Notes in Civil Engineering 67,
https://doi.org/10.1007/978-3-030-39299-4_78

723

1 Introduction

Clementine (*Citrus clementina* Hort. ex Tan.) is a citrus variety grown in the Southern regions of Italy. Fruits are highly appreciated by consumers for their taste, easy-peeling aptitude, seedless and the positive health value, representing a rich source of bioactive substances including vitamin C and phenolic compounds (Fabroni et al. 2016). These fruits are very perishable with a short shelf-life, due mainly to weight loss during storage, responsible for their deterioration, and the occurrence of various fruit diseases and physiological disorders affecting their marketing value.

Fungal pathogens are considered the main cause of postharvest losses of citrus fruit (Scheda et al. 2011; Strano et al. 2017). Green mould (*Penicillium digitatum* Sacc.), blue mould (*P. italicum* Weh.) and sour rot (*Geotrichum candidum* Link), represent the most important clementine postharvest diseases (Eckert and Eaks 1989). Minor rots such as Brown rot (*Phytophthora* spp.), Alternaria rot (*Alternaria* spp.), Stem-end rot (*Phomopsis citri* Fawcett, *Diplodia natalensis* Pole-Evans), and Grey mould (*Botrytis cinerea* Pers.) are considered pre-harvest infections that develop after harvest. Their incidence is generally low but becomes a serious problem in warm and wet years (Ismail and Zhang 2004).

Moreover, some fungicide and/or ozone treatment can be used satisfactorily on citrus fruit in order to prolong its cold storage (Strano et al. 2017; Altieri et al. 2016; Genovese et al. 2015; Altieri et al. 2005, 2013; Di Renzo et al. 2005a, 2006, 2011b).

In addition, during the fruit storage, water loss and firmness decrease cause fruit texture change bringing to severe fruit quality loss (Toivonen and Brummell 2008).

Physiological disorders (i.e. chilling injury and ageing) develop when clementine is held at inadequate temperature and low humidity levels during cold storage, making the fruit unmarketable. Chilling injury (CI) is characterized by brown colour areas of the rind that collapse and darken to form pit, with the consequence of an increase in mould development on fruit surface; ageing indicated by the shrivelling and collapse of the button tissue, is the consequence of prolonged storage at low humidity (Lafuente and Zacarias 2006).

To reduce physiological disorders and fruit rots of clementine a reliable solution is given by the rapid cooling (precooling) of fruit soon after the harvest, so to quickly remove field heat of fresh fruit prior to be refrigerated, transported or cold-stored (Thompson et al. 2008). Among the various types of precooling available, forced-air cooling (FAC) represents the most effective method for citrus fruit (Brosnan 2001; Di Renzo et al. 2005a, 2007; Tauriello et al. 2015; Wu et al. 2018). It is used in conjunction with a cooling room, and it consists of the use of fans and strategically placed barriers so that cold air is forced to pass through the containers of fruit with a remarkable reduction of the time required to cool produce by passive room cooling.

Moreover, the use of an appropriate packaging can reduce fruit water loss and minimize shrinkage and softening, caused by cold storage. In particular, the usage of High-density polyethylene (HDPE) films allows depletion of oxygen and accumulation of carbon dioxide within the package (modified atmosphere packaging, MA) with the consequence to maintain fruit quality longer during cold storage.

The aim of this study was to evaluate the effectiveness of precooling combined with HDPE packaging improved with an innovative breathable device on fruit weight loss reduction and clementine quality improvement as the extension of fruit shelf-life represents an opportunity to increase the marketability of Clementine mandarins grown in South Italy.

2 Materials and Methods

Clementines cv. Rubino were harvested at maturity stage from the experimental orchard of CREA (Lentini, SR, Italy) and transported within two hours to CREA laboratories (Acireale, CT, Italy). Fruit was selected accordingly to its uniformity in size, colour and lack of defects (blemishes, lesions and/or rot symptoms), then divided into six homogeneous groups of 280 fruits each and placed in plastic boxes (70 fruits per each box). Four replicates were used in each group. For each box 10 fruit were numbered to determine weight loss. Three groups were subjected to the precooling followed by cold storage at 6 ± 0.5 °C and relative humidity (RH) 90–95% for 30 days, whereas the other three groups were directly stored in cold storage room without pre-cooling. To simulate the period on the market, all the fruits followed 7 days of shelf-life at 20 ± 2 °C and RH 75%. Additionally, in order to reduce fruit weight loss, HDPE bags (180 μ m thickness) were used for wrapping and an innovative device (Blow) was applied in two bags (P + B and R + B), following the scheme described in Table 1.

Blow is an innovative device that allows the bidirectional gas exchange across a sealed package. The device results particularly useful for managing the atmosphere in the package headspace of fruit and vegetables packed in modified atmosphere, with

Table 1 Treatments performed

Treatment	Description
P	Fruits pre-cooled (speed approx. 3 m/s) and subsequently kept at 6 ± 0.5 °C and RH 90–95% (room cooling storage)
P + S	Fruits pre-cooled (speed approx. 3 m/s), subsequently packed with HDPE bags (S), then kept at 6 ± 0.5 °C and RH 90–95%
P + B	Fruits pre-cooled (speed approx. 3 m/s), subsequently packed with HDPE bags with Blow device (B), then kept at 6 ± 0.5 °C and RH 90–95%
R	Fruits stored in cold storage room at 6 ± 0.5 °C and RH 90–95%, without pre-cooling
R + S	Fruits stored in cold storage room at 6 ± 0.5 °C and RH 90–95%, without pre-cooling and packed with HDPE bags (S), after 24 h of room cooling storage
R + B	Fruits stored in cold storage room at 6 ± 0.5 °C and RH 90–95%, without pre-cooling and packed with HDPE bags with Blow device (B), after 24 h of room cooling storage

a high level of carbon dioxide or low level of oxygen (Altieri et al. 2018; Matera et al. 2017).

Pre-cooling was carried out using a cooling unit prototype, installed in a cold room settled to 0.5 °C. The prototype consisted of a centrifugal blower (Nicotra ADH250, 5500 m³/h, 2081 RPM) capable of delivering a static pressure of 1000 Pa, coupled to a three-phase 4 kW asynchronous electric motor managed by a variable frequency driver (Siemens Micromaster Vector, 5 kW) (Di Renzo et al. 2011a).

Before treatments (T0), a total amount of 50 fruits were used for the following assessment: fruit weight, peel and pulp colour, initial and residual deformation, firmness, juice yield, total soluble solids content (TSS), pH and titratable acidity (TA). The following determinations were carried out during the cold storage, with frequency of 15 days, up to 30 days (T15, T30) plus 7 days of shelf life (T30 + 7) at 20 °C and 75% RH: Volatile organic compounds (VOCs), O₂ and CO₂ concentration inside the packaging, weight loss, decay incidence (*Penicilli* decay and minor decay), physiological disorders (chilling injury and aging), fruit weight, peel and pulp colour, initial and residual deformation, firmness, juice yield, TSS, pH and TA. RH%, cooling room temperature and internal fruits temperature were monitored and recorded daily using data loggers.

The development of VOCs inside the packaging was monitored using a ppb RAE device; the O₂/CO₂ concentrations were measured by Checkmate (Dansensor). Fruit weight loss in percentage was calculated from the initial weight and the weight taken at each interval. The number of decays was recorded at each interval and decay incidence percentage was calculated from the total number of fruits. The severity of CI was determined with visual examination of the fruit pericarp, using the following four-grade scoring system to estimate the damage: 0 = none, 1 = light, 2 = moderate, and 3 = severe. A light rating (less than 5% of the rind surface) indicated that damage was not perceived from the consumer, while a severe rating (over 25% of the rind surface) indicated a damage leading consumer to reject the product. CI index was calculated as follows: CI index = Σ (CI level) \times (number of fruit at each CI level)/total number of fruits. The incidence of the fruit affected by ageing was expressed as a percentage.

To measure the variation of the external (peel) and internal (pulp) colour, 30 fruits were randomly selected from each box. They were then divided into 3 groups of 10 fruits each. CIELAB coordinates L* (lightness), a* (red-green component) and b* (yellow-blue component) were determined as the average of three measurements per fruit using a Minolta Spectrophotometer CM-2500d (Minolta, Milan, Italy). Results were expressed as Citrus Colour Index (CCI) (Jiménez-Cuesta et al. 1981), both for the peel and for the pulp and calculated as follows: CCI = 1000 \times a*/L* \times b*.

Firmness and deformation were tested with a dynamometer (Zwick/Roell DO-FB0.5 TS model 2002, Genova, Italy). Fruit firmness was recorded using an 8 mm flat probe (area of 50.24 mm²) with the maximum penetration force of the peel. Two measurements were made on two opposite of the equatorial zones of the fruit. The results were reported as the peak force in newton (N). Softness represents the shrinkage of fruit in diameter (mm) after the compression on the equatorial axis for 30 s with a 29 N load. The deformation is the residual deformation (express in mm)

on the recovering for 30 additional sec after the removal of the load (Mitcham et al. 1996).

The juice was extracted using a domestic citrus fruit squeezer and the pooled juice of five fruits per replicate was analysed. The juice yield was calculated as follows: juice yield (%) = (juice weight/fruit weight) × 100. TSS content was determined using a digital refractometer (ATAGO RX-5000, Atago, Japan) and results expressed as °Brix. TA was determined by potentiometric titration (Automatic Titrator, Mettler Toledo T50) with 0.1 N sodium hydroxide solution to the titration endpoint of pH 8.1 according to the AOC method (AOAC 1995) and results were expressed as % (w/v) of citric acid equivalent (Ladaniya 2008).

Statistical analysis of the results was performed using one-way analysis of variance (ANOVA), and Tukey's HSD post hoc test for means separation (significance level $P \leq 0.01$ and ≤ 0.05). The statistical software was IBM SPSS Statistics for Windows, version 20 (IBM Corp., Armonk, N.Y., USA).

3 Results

The percentage cumulative weight loss of clementine during storage is presented in Fig. 1. During the cold storage, the use of HDPE bags and the Blow device significantly reduced fruit weight loss (1–2%) with respect to the unwrapped fruit (5–8%). The same statistical difference for weight loss was maintained after the week of shelf-life.

In Fig. 2 is reported the susceptibility to CI of clementine expressed as an index. During the cold storage a higher significant CI index was observed for the unwrapped precooled fruit (P) if compared to the precooled fruits with HDPE bags (P + S) and the wrapped refrigerated fruits (R + S and R + B). After the week of shelf-life

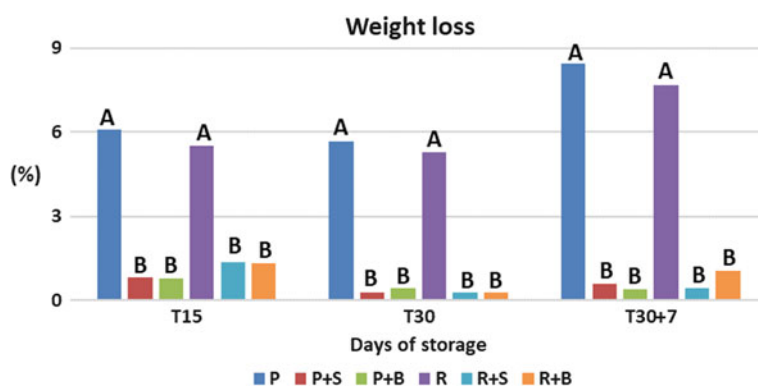


Fig. 1 Clementine weight loss percentage after cold storage and shelf-life. Different letters within the same interval time indicate significant differences ($P \leq 0.01$) based on Tukey's HSD test

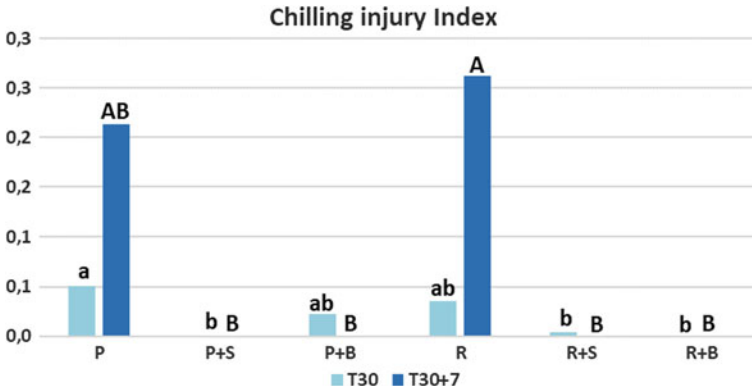


Fig. 2 Effect of packaging on chilling injury of precooled clementines with respect to the conventional refrigeration. Different letters within the same interval time indicate significant differences ($P \leq 0.05$ for the cold storage and $P < 0.01$ for the shelf-life) based on Tukey’s HSD test

(T30 + 7), all wrapped fruits showed lower significant values if compared to the refrigerated fruits (R).

Regarding the ageing, during the storage (T30 and T30 + 7), no presence was observed in wrapped fruits, significantly different if compared to the unwrapped fruits (P and R) (Fig. 3).

A higher presence of total decay was observed in all wrapped fruit (18–23% after 30 days and 68–75% after shelf-life), although it was absent on precooled fruit up to 15 days of cold storage (Fig. 4). The pathogen predominance registered was represented by *P. italicum* (blue mould), whom growth is favourite even at low temperature.

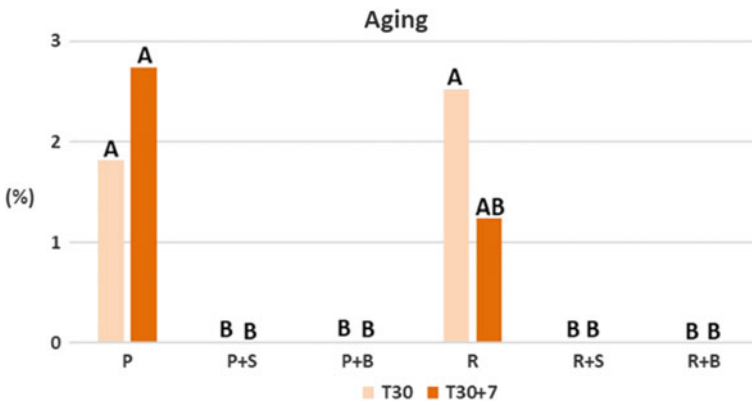


Fig. 3 Effect of packaging on the presence of ageing of precooled clementines with respect to the conventional refrigeration. Different letters within the same interval time indicate significant differences ($P \leq 0.01$) based on Tukey’s HSD test

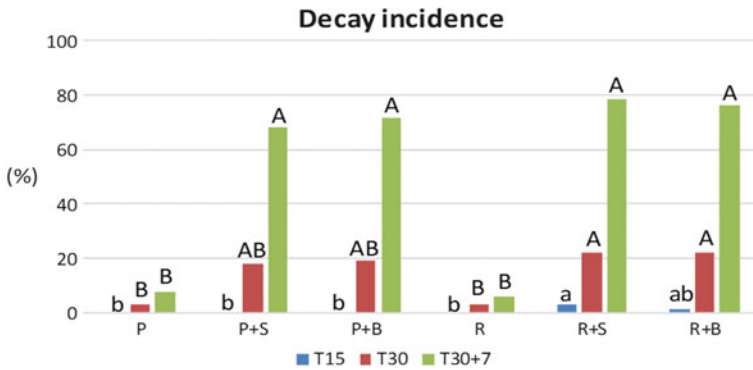


Fig. 4 Effect of packaging on total decay incidence percentage due to the presence of *P. digitatum* (green mould), *P. italicum* (blue mould), and minor decay. Different letters within the same interval time indicate significant differences ($P \leq 0.05$ at T15 and $P < 0.01$ at T30 and T30 + 7) based on Tukey’s HSD test

Precooling reduced significantly ethylene production inside the fruit wrapped if compared to R + S (Fig. 5).

Table 2 shows the results of the variation of fruits colour index, initial and residual deformation, and firmness during the cold storage and the shelf-life. Regarding CCI peel no visible variations were observed among treatments although a significant difference was registered at T15 between P + B and R, at T30 among P + S, P + B, R and R + B, and at T30 + 7 among P + B, R, R + S and R + B. For CCI pulp a significant difference was observed only at T15 between P and P + S.

Concerning initial and residual deformation and firmness, significantly statistical values were observed among treatments at each interval time. However, the registered differences among treatments at T15 were not the same at the next control, probably due to the fruit sampling.

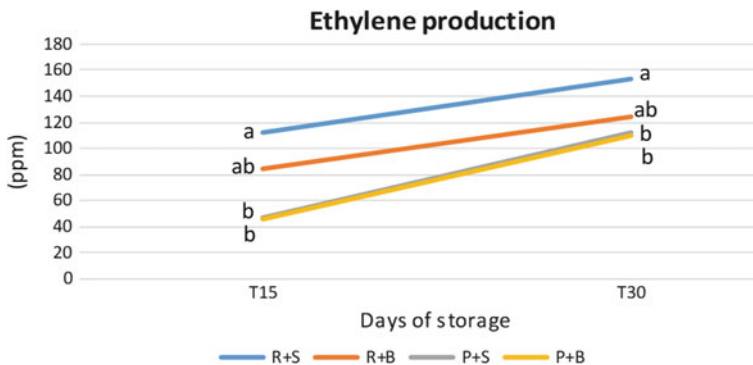


Fig. 5 Effect of packaging on ethylene production. Different letters within the same interval time indicate significant differences ($P \leq 0.05$) based on Tukey’s HSD test

Table 2 Fruit colour, deformation and firmness variation during the cold storage and the shelf-life

Treatment	CCI peel	CCI pulp	Initial deformation (mm)	Residual deformation (mm)	Firmness (N)					
T15										
P	16.6	AB	18.0	b	4.2	AB	1.4	AB	16.5	
P + S	15.9	AB	20.1	a	2.7	B	0.6	C	15.4	
P + B	15.7	B	18.6	ab	3.0	B	0.7	BC	15.7	
R	18.2	A	18.1	ab	4.8	A	1.6	A	16.7	
R + S	16.1	AB	18.3	ab	3.4	AB	0.9	ABC	15.7	
R + B	16.2	AB	19.4	ab	3.9	AB	1.1	ABC	16.0	
T30										
P	15.9	AB	11.3		4.5	AB	1.3	AB	16.3	AB
P + S	16.3	A	11.1		3.5	AB	0.9	AB	14.0	B
P + B	14.4	B	12.0		3.2	B	0.7	B	16.9	AB
R	9.6	C	11.1		3.9	AB	1.1	AB	17.5	A
R + S	14.7	AB	11.5		3.3	AB	0.7	AB	16.4	AB
R + B	9.7	C	11.4		4.7	A	1.4	A	14.0	B
T30 + 7										
P	17.4	AB	10.6		5.4	A	1.8	A	17.2	A
P + S	17.5	AB	11.0		3.7	BC	0.9	BC	14.4	AB
P + B	10.8	C	11.6		3.3	C	0.7	C	13.7	B
R	19.5	A	10.5		5.0	AB	1.5	AB	16.7	AB
R + S	11.9	C	11.4		4.4	ABC	1.3	ABC	14.2	AB
R + B	16.3	B	11.5		3.6	BC	0.8	C	14.8	AB

For internal quality parameters (i.e. juice yield, TSS, pH and TA), no relevant significant differences were observed among treatments during the storage of the fruits (data not shown).

4 Discussion and Conclusions

Postharvest fruit quality is strictly related to the correct handling of the product, starting from the harvest up to the commercialization. After fruit harvest, metabolic processes increase, it could be due to many different reasons the most frequent are mechanical injury; wrong temperature management and pathological diseases (Li et al. 2012). Temperature control as soon as possible after harvest is one of the most important factors affecting metabolism in fresh products as metabolism increases two to threefold for every 10 °C rise in temperature (Saltveit 2004).

Thus, cooling represents a crucial step to obtain a high qualitative product: the wrong combination of temperature and humidity during cold storage can increase the presence of physiological and pathological disorders with the consequence of a higher decay incidence and a low quality of fruits. Precooling by forced-air cooling treatment, followed by cold storage, is a reliable postharvest technology to effectively reduce citrus fruit chilling injury and prolong their shelf-life.

In the present study forced-air cooled treatments of packaged clementine reduced weight loss, physiological disorders and maintained fruit quality. Within the period of 30 days of cold storage, weight loss was limited to a value of 1–2% for precooled and wrapped fruits compared to 5–8% on unwrapped fruits. In addition, a good control of physiological disorders and maintenance of quality parameters was obtained, even after one week of shelf-life. However, the presence of higher decay incidence in wrapped fruit suggests an improvement of the breathable properties respect to the breathable device applied on HPDE package. The accumulation of humidity inside the package resulted in the increasing of the pathological disorder in all the packed lots.

Moreover, citrus fruit usually matures at the end of September, when high temperatures are still registered. Precooling could be useful to quickly remove the “field heat” associated with the fruit thermal rising due to the metabolism acceleration consequent to the harvest stress. Our findings indicate that clementine quality was significantly improved by precooling treatment and, according to different authors (Lallu et al. 2000; Kalbasi-Ashtari 2004; Rab et al. 2013), clementine should be precooled immediately after harvest to maintain fruit quality during cold storage and to prolong shelf-life.

References

- Altieri, G., Di Renzo, G. C., Genovese, F., Calandra, M., & Strano, M. C. (2013). A new method for the postharvest application of imazalil fungicide to citrus fruit. *Biosystems Engineering*, *115*, 434–443.
- Altieri, G., Di Renzo, G. C., & Lanza, G. (2005). Imazalil on-line control in post-harvest treatments of citrus fruit. *Acta Horticulturae*, *682*, 1773–1780.
- Altieri, G., Genovese, F., Matera, A., Tauriello, A., & Di Renzo, G. C. (2018). Characterization of an innovative device controlling gaseous exchange in packages for food products. *Postharvest Biology and Technology*, *138*, 64–73.
- Altieri, G., Genovese, F., Tauriello, A., Di Renzo, G. C., Strano, M. C., & Romeo, F. V. (2016). Effectiveness of thin film application of imazalil fungicide on decay control of Tarocco orange fruit. *Biosystems Engineering*, *151*, 399–408.
- AOAC. (1995). *Official methods of analysis* (16th ed.). Washington, DC: Association of Official Analytical Chemists.
- Brosnan, S. (2001). Precooling techniques and applications for horticultural products—A Review. *International Journal of Refrigeration*, *24*, 154–170.
- Di Renzo, G. C., Altieri, G., D’Erchia, L., Lanza, G., & Strano, M. C. (2005a). Effects of gaseous ozone exposure on cold stored orange fruit. *Acta Horticulturae*, *682*, 1605–1610.
- Di Renzo, G. C., Altieri, G., & Genovese, F. (2005b). Conservazione dei prodotti agro-alimentari. *Ottimizzazione degli aerorefrigeranti. Zerosottozero*, *6*, 60–66.
- Di Renzo, G. C., Altieri, G., & Genovese, F. (2011a). Innovazione tecnologica degli impianti per le industrie agro-alimentari in Basilicata. In M. Maldonato (Ed.), *Fenomenologia della scoperta* (pp. 265–273). Milan: Bruno Mondadori.
- Di Renzo, G. C., Altieri, G., Genovese, F., & Tauriello, A. (2011b). Realizzazione e controllo di un impianto di prerrefrigerazione ad aria in depressione per gli agrumi. AIIA Mid-Term Conference, “Gestione e controllo dei sistemi agrari e forestali”, Belgirate (VB), 22–24 settembre 2011. Lecture n. 81. <http://www.aiaa2011.unimi.it/chiave/memorie/81.pdf>.
- Di Renzo, G. C., Altieri, G., Lanza, G., Di Martino Aleppo, E., & Strano, M. C. (2006). Il controllo in continuo dell’ozono e dell’Imazalil impiegati nella postraccolta degli agrumi. *Italus Hortus*, *13*, 48–53.
- Di Renzo, G. C., Altieri, G., Lanza, G., Genovese, F., & Strano, M. C. (2007). Problematiche del settore postraccolta. *Italus Hortus*, *14*, 47–49.
- Eckert, J. W., & Eaks, I. L. (1989). Postharvest disorders and diseases of citrus fruits. In W. Reuter, E. C. Calavan, & G. E. Carman (Eds.), *The citrus industry* (Vol. 5, pp. 179–260). Berkeley, CA, USA: University of California Press.
- Fabroni, S., Romeo, F. V., & Rapisarda, P. (2016). Nutritional composition of clementine (*Citrus x clementina*) cultivars. In M. S. J. Simmonds & V. R. Preedy (Eds.), *Nutritional composition of fruit cultivars* (pp. 149–172). Cambridge, MA: Academic Press. ISBN: 9780124081178.
- Genovese, F., Altieri, G., Admane, N., Salamon, I., & Di Renzo, G. C. (2015). Processing plants and technologies for a sustainable Mediterranean food chain. In A. Vastola (Ed.), *The Sustainability of Agro-Food and Natural Resource Systems in the Mediterranean Basin* (pp. 339–351). Cham: Springer.
- Ismail, M., & Zhang, J. (2004). Postharvest citrus diseases and their control. *Outlooks on Pest Management*, *15*(1), 29–35.
- Jiménez-Cuesta, M., Cuquerella, J., & Martínez-Jávega, J. (1981). Determination of a color index for citrus fruit degreening. *Proceedings of the International Society of Citriculture*, *2*, 750–753.
- Kalbasi-Ashtari, A. (2004). Effects of post-harvest pre-cooling processes and cyclical heat treatment on the physico-chemical properties of “Red Haven Peaches” and “Shahmiveh Pears” during cold storage. *Agricultural Engineering International*, *6*, 1–17.
- Ladaniya, M. S. (2008). *Citrus fruit: Biology, technology and evaluation*. San Diego: Academic Press.

- Lafuente, M. T., & Zacarias, L. (2006). Postharvest physiological disorders in citrus fruit. *Stewart Posthar. Rev.*, 2(1), 1–9.
- Lallu, N., Yearsley, C. W., & Elgar, H. J. (2000). Effects of cooling treatments and physical damage on tip rot and postharvest quality of asparagus spears. *New Zealand Journal of Crop and Horticultural Science*, 28(1), 27–36.
- Li, J., Yan, J., Cao, J., Zhao, Y., & Jiang, W. (2012). Preventing the wound-induced deterioration of Yali pears by chitosan coating treatments. *Food Science and Technology International*, 18(2), 123–128.
- Matera, A., Genovese, F., Altieri, G., Tauriello, A., & Di Renzo, G. C. (2017). An innovative smart device to control modified atmosphere packaging (MAP) of fruit and vegetables. *Chemical Engineering Transactions*, 58, 193–198.
- Mitcham, B., Cantwell, M., & Kader, A. (1996). Methods for determining quality of fresh commodities. *Perishables Handling Newsletter*; 85, 1–5.
- Rab, A., Rehman, H., Haq, I., Sajid, M., Nawab, K., & Ali, K. (2013). Harvest stages and pre-cooling influence the quality and storage life of tomato fruit. *Journal of Animal and Plant Sciences*, 23(5), 1347–1352.
- Saltveit, M. E. (2004). Respiratory metabolism. In K. C. Gross et al. (Ed.), *The commercial storage of fruits, vegetables, and florist and nursery stocks*. USDA Agricultural Handbook Number 66 (pp. 68–76). Beltsville, MD: USDA/ARS.
- Schena, L., Strano, M. C., Sanzani, S. M., & Ippolito, A. (2011). Le malattie degli agrumi in postraccolta. *Protezione delle Colture, Anno IV*(9), 30–41.
- Strano, M. C., Altieri, G., Admane, N., Genovese, F., & Di Renzo, G. C. (2017). Advance in citrus postharvest management: Diseases, cold storage and quality evaluation. In H. Gill & H. Garg (Eds.), *Citrus Pathology*. IntechOpen. <http://dx.doi.org/10.5772/66518>.
- Tauriello, A., Di Renzo, G. C., Altieri, G., Strano, M. C., Genovese, F., & Calandra, M. (2015). Simulation of cold treatment during a cargo shipment of citrus fruit. *Acta Horticulturae*, 1065, 1685–1692.
- Thompson, J. F., Mitchell, F. G., Rumsey, R. T., Kasmire, R. F., Crisosto, C. H. (2008). *Commercial cooling of fruit, vegetables and flowers* (p. 61). California: University of California.
- Toivonen, P. M. A., & Brummell, D. A. (2008). Biochemical bases of appearance and texture changes in fresh-cut fruit and vegetables. *Postharvest Biology and Technology*, 48(1), 1–14.
- Wu, W., Haller, P., Cronje, P., & Defraeye, T. (2018). Full-scale experiments in forced-air precoolers for citrus fruit: Impact of packaging design and fruit size on cooling rate and heterogeneity. *Biosystems Engineering*, 169, 115–125.

Optimization of Donkey Milk Pasteurization Process



A. Matera, G. Altieri, F. Genovese and G. C. Di Renzo

Abstract Donkey milk represents an attractive solution as new-born feeding, mainly if occur physiological limitations concerning the milk availability in post-pregnancy or bovine's milk proteins linked to immune diseases. At present, the producers use custom-made batch pasteurization plant, with a poor temperature control system and very high time required to carry out the pasteurization process. It is due to the low availability of raw materials due to limited donkey livestock and low milk's yield and the lack of high technology UHT pasteurization plants with limited processing capacity. In this work, an innovative low capability (30 l/h) continuous flow pasteurization plant, designed and built for High Temperature for Short Time (HTST) treatments, was characterized in the MACLab of UNIBAS. To test the plant, a matrix with three pasteurization temperatures (75, 85, 92 °C) and times (3, 7, 14 s) was tested, and the efficacy of the treatments was evaluated on microflora enumeration (*L. monocytogenes*, *Enterobacteriaceae*, total aerobic bacteria) as soon as after the treatments and over 30 days-storage at 4 °C. The HTST apparatus showed high performance; the complete eradication of *Enterobacteriaceae* detected the efficacy of the treatments at every time and temperatures tested. Decreasing in total bacterial count and lysozyme content was affected by treatment size. Through this methodological approach, it was possible to investigate the effect of HTST treatments (following by cooling soon) on the primary chemical and microbiological standard for donkey milk, to set up an official sanitation protocol that allows optimizing its nutritional value.

Keywords Plate heat exchanger · Donkey milk · Pasteurization · HTST

1 Introduction

Donkey milk production, with particular reference to southern Italy, is mostly performed in small livestock farms with no more than 60 animals. Moreover, as the

A. Matera (✉) · G. Altieri · F. Genovese · G. C. Di Renzo
Scuola Di Scienze Agrarie, Alimentari Ed Ambientali (SAFE), Università Degli Studi Della Basilicata, via Dell'Ateneo Lucano 10, Potenza, Italy
e-mail: attilio.matera@unibas.it

© Springer Nature Switzerland AG 2020

A. Coppola et al. (eds.), *Innovative Biosystems Engineering for Sustainable Agriculture, Forestry and Food Production*, Lecture Notes in Civil Engineering 67,
https://doi.org/10.1007/978-3-030-39299-4_79

735

typical composition of milk makes it very perishable, it has to be processed into a more stable product (Di Renzo et al. 2007). Among the several technologies available, spray-drying offers many benefits but it is very expensive (Altieri et al. 2007; Di Renzo et al. 2008, 2013).

The traditional UHT pasteurization plants available on the market, based on a plate heat exchanger and the tubular stop, are commonly exploited in dairy factories for bovine milk and other no-packed liquid food, have a processing capacity over than 600 l/h.

They are based on the dynamic Short Time High Temperature (STHT) principle which involves heating the mass to a temperature of 72–74 °C with a stop of 12''–15'' followed by rapid cooling. It is equivalent to the Low Temperature Long Time (LTLT) at 60 °C for 30', or any other time-temperature combination that allows obtaining an equivalent effect, so that the products give, if necessary, a negative reaction to the alkaline phosphatase test immediately after undergoing such treatment (EU Reg 2074/2005). FAO/WHO (2004) defined pasteurization as "A microbiocidal heat treatment aimed at reducing the number of any pathogenic microorganisms in milk and liquid milk products, if present, to a level at which they do not constitute a significant health hazard".

The HTST pasteurization kills 99.999% of pathogens (FDA 2011) and is effective in reducing the viable population of *Mycobacterium avium* subsp. *paratuberculosis* (4–5 logs).

Scale-up in-continuous treatments allow the reduction of at least 4 logs of the bacterial load initially present in the milk and, compared to in batch custom-made pasteurization system (in heated tanks or insulated multi-purpose tanks), guarantee more significant nutritional and sensorial characteristics in the ended product. As known, due to the heating and cooling steps that are not instantaneous, the temperatures of the treatments using custom-made plants are difficult to manage, especially the cooling phase which is not sudden, causing a substantial modification of the nutritional characteristics and organoleptic characteristics of the product.

The absence of alkaline phosphatase enzyme in donkey's milk and the lack microbiological criteria referring to pasteurized product, they both determine the complication in defining the target of the donkey's milk pasteurization process and develop "equivalent" pasteurization protocols, as it is for bovine milk.

The plants designed and manufactured for bovine milk processing have production capacity, even in the smallest versions, that far exceeds the production capacity of the largest donkey's milk factory.

Donkey's milk sanitation process is subordinate to the availability and sizing of the plants which allow the processing of the small amount productions, including those obtained in small production units characterized by high dispersal at the national level.

Increasing in small donkey farms in Italy pushes the stakeholder to ask for more advanced, reliable, and reproducible technologies and devices analogues to the bovine milk industry. The capability to sanitize a low amount of product involving technologies which not significantly exceed the final costs of the product is essential.

Alternative to thermal ones' treatments for liquid food sanitation, "mild" technologies (i.e. supercritical CO₂, high hydrostatic pressure processing, pulsed electrical field, microfiltration), have been developed and are widely exploited, in combination or alone, both in pharma and food industry, as they preserve the organoleptic and nutritional properties of a food/drug target, at ambient or moderate temperature. However, these methods suffer from some limitations which hamper their implementation in the food industry (e.g. treatment time, input energy, extreme processing conditions) (Devlieghere et al. 2004; Lopes et al. 2018).

For these reasons donkey milk pasteurization is carried out using custom-made batch pasteurization plant, with a poor temperature control system and low efficient heat exchanger. In these conditions, dramatic uncontrolled thermal damage of the bioactive molecule occurs that however could be still easily under control if using the newly developed sensors by means of the near infrared spectra (Di Renzo et al. 2011; Altieri et al. 2011, 2016).

Therefore, in the MACLab of UNIBAS, a low capacity, in-continuous, plate heat exchanger pasteurization plant was designed and built. It works according to the HTST principle, processing a low flow rate of liquid food products, to guarantee the integrity of the nutritional properties of particular interest.

The plant temperature profile during the treatments was measured. Nutritional and microbiological quality of donkey milk produced, using three-time and -temperature, was verified. In the present paper the preliminary results of the effects of the treatments on the microbiological quality of the milk at the end of the process and after the cool-storage are discussed.

2 Materials and Methods

2.1 Test Protocol

Raw donkey milk (31,5 l) was collected from the livestock "La Valle degli Asini" in Laterza (TA), refrigerated at 4 °C within 10 min from the milking operation and maintained at 4 °C till the test.

The milk, mechanically stirred in the tank to avoid separation of the different fractions were used for nine different pasteurization treatments. The test protocol was based on a matrix with three pasteurization treatment (Temperature: 75, 85, 92 °C) and three treatment times (treatment stop: 3, 7, 14 s). The pasteurization time was controlled with the change of the stop section. For each test were used an amount of 3.5 l using a flow rate of 32 l/h, that means a treatment time of about 6.5 min for each test.

To control the treatment efficiency and efficacy, the data of inlet/outlet temperature and pressure of each section were measured and recorded and, using a sample taking faucet, every 5 min the milk samples were collected during every treatment and analyzed as soon as the experiment. Moreover, the milk was bottled and stored for 30-days at 4 °C. At the day 0, 15, and 30 the milk was sampled to test the quality

parameters and the microflora enumeration (*L. monocytogenes*, *Enterobacteriaceae*, total aerobic bacteria).

2.2 Processing and Equipment

The first section of the pasteurization plant is the refrigerated raw milk tank equipped with a mechanical overhead stirrer. From this tank, the inlet of the milk in the pasteurization plant is guaranteed by the flow-rate adjustable pump, feeding the raw milk in the thermal recovery section of plate exchanger. In the heat exchanger inlet milk is upstream preheated using the pasteurized outlet milk to get a heat recovery.

Then the preheated milk enters in the heating section of the plate exchanger where it is upstream heated using hot water to the pasteurization temperature. To exactly control the water temperature, hot water is produced in the generating unit using steam injection. This section of the plant is composed by an electric circulation pump, steam injector, insulated water storage tank, condensate drainage system, modulating pneumatic valve and a PLC with control software to manage the steam flow with the required water temperature. The milk at pasteurization temperature flows through the stop section where it stays the required time adjusted by managing the upstream milk flow and the stop pipe length (the stop section is interchangeable due to the experimental purpose of the plant). After the stop section, the pressure of the pasteurized milk is increased to guarantee a greater pressure of pasteurized milk compared to non-pasteurized milk. Pasteurization temperature is measured by high precision temperature probe, controller, and logger. The pasteurized milk outlet from the stop section returns to the recovery section of plate exchanger where it is upstream cooled using the raw milk.

Considering the experimental purpose of the plant, a pressure-regulating valve allows the pressure difference between the inlet raw milk and outlet pasteurized and refrigerated milk from the plate exchanger.

A three-way valve controlled by the temperature/pressure controller guaranteed the proper processed milk flow. If pasteurization temperature was not reached or pasteurized outlet milk pressure was lower than those of the inlet raw milk, the valve deviates milk, recycling in the raw milk tank until were reached the required pasteurization conditions (temperature or pressure).

The final section is the pasteurized milk tank, that is refrigerated and equipped with a mechanical overhead stirrer.

2.3 Microbiological Analysis

Five replicates (50 ml/replicate) from each treatment were analyzed in duplicate for the microbiological analysis at day 0, 15, and 30. The first decimal dilution was

carried out in sterile 2% trisodium citrate, while further dilutions were carried out in sterile quarter-strength Ringer solution.

Enterobacteriaceae were enumerated by pour plating in Violet Red Bile Glucose Agar (VRBGA), with incubation at 30 °C for 24 h (ISO 21528-2:2004). Total mesophilic counts were carried out in Plate Count Agar standard for raw milk with incubation at 30 °C for 48 h (ISO 4833:1-2013). Enumeration of *L. monocytogenes* was carried on PALCAM media with Palcam selective supplement and incubated at 37 °C per 48 h (ISO 11290-1:1996/Amd 1:2004). Except for *Enterobacteriaceae* enumeration was carried out by spiral plating (WASP Spiral Plater, bioMérieux Italia SpA, Bagno a Ripoli, Firenze, Italy) and a digital colony counting (EasyCount 2, bioMérieux Italia). All microbiological media were obtained from Oxoid (Oxoid SpA, Rodano, MI, Italy) and reagents from SigmaAldrich (Milan, Italy).

2.4 Thermal Death Kinetics

Heat resistance study was carried out respect to the aerobic mesophilic population detected by PCA. The reaction of thermal degradation of microorganisms follows the laws of a first-order reaction where the reaction rate is proportional to the amount of population to be inactivated, according to the general law:

$$-\frac{dN}{dt} = kN \quad (1)$$

which can be written as:

$$-\frac{dN}{N} = kdt \quad (2)$$

where t is the reaction time, k is the rate constant, and N is the microbial population.

The integration (1) between N_0 and N_t , which represent, respectively, the initial cellular concentrations and after the treatment time t , leads to:

$$\frac{N}{N_0} = \exp(-kt) \quad (3)$$

Or

$$\ln\left(\frac{N}{N_0}\right) = -kt \quad (4)$$

Switching to decimal log,

$$\text{Log}\left(\frac{N}{N_0}\right) = -kt / 2.303 \quad (5)$$

this relation allows to calculate the concentration microbial N_t resulting from the application of a lethal temperature for a time t , note the initial concentration N_0 and the value of speed constant k .

In this equation, the ratio $-k/2.303$ is called D-value; it is the time required at a specific temperature for a one-log reduction in the microorganism population.

The exposure time t_T necessary to obtain the aimed reduction of a given microbial population at pasteurization temperature T is the “biological” equivalent time, F_{BIO} .

When D_T is known at a given experimental temperature T , then F_{BIO} is given by the formula (European Pharmacopoeia 9.2, 2017):

$$F_{BIO} = D_T(\text{Log}N_0 - \text{Log}N) \quad (6)$$

3 Results

3.1 Assessment of the Heat Treatments on Microbiological Quality

Tables 1 and 2 report the results for the PCA and VRBGA before (control) and after the treatments, and over 15 and 30 day-storage. The microbiological quality of the raw milk was characterized by the moderate presence of the *Enterobacteriaceae* (2.8 logs [cfu/ml]) and of a greater mesophilic bacteria community (4.2 logs [cfu/ml]). Despite all the treatments produced the viable cells number reduction, the temperature

Table 1 Experimental and modelling data of the thermal death kinetic referring to the total mesophilic aerobic population

T (°C)	Time (s)	Log (cfu/ml) exp	k (-)	Log (cfu/ml) model	Survival (%)	D-value (s)	R ² (-)	¹ F _{Bio} (s)
Control	—	4.22	—	4.22	100	—	—	—
75	3.2	3.95	0.17	3.69	29.5	6.05	0.99	30.27
	7.2	3.19		3.03	6.4			
	14.5	1.90		1.82	0.39			
85	3.2	3.80	0.47	2.72	3.16	2.13	0.89	10.64
	7.2	0.90		0.84	0.04			
	14.5	<0.1		-2.60	1.51E-05			
92	3.2	3.72	0.50	2.62	2.51	2.00	0.90	10.00
	7.2	0.66		0.62	0.025			
	14.5	<0.1		-3.03	5.62E-06			

¹Value computed respect to 5 logs reduction

Table 2 Enumeration of *Enterobacteriaceae* (VRBGA) and total mesophilic aerobic bacteria (PCA) after the thermal treatments and over 30-days storage

T (°C)	Time (s)	VRBGA Day0	VRBGA Day15	VRBGA Day30	PCA Day0	PCA Day15	PCA Day30
Control	–	2.8	>5.48	>5.48	4.22	5.21	5.55
75	3.2	<0.1	<0.1	<0.1	3.95	>5.48	>5.48
	7.2	<0.1	<0.1	<0.1	3.19	3.51	4.24
	14.5	<0.1	<0.1	<0.1	1.90	2.20	2.75
85	3.2	<0.1	<0.1	<0.1	3.80	>5.48	>5.48
	7.2	<0.1	<0.1	<0.1	0.90	1.08	1.74
	14.5	<0.1	<0.1	<0.1	<0.1	0.8	1.06
92	3.2	<0.1	<0.1	<0.1	3.72	>5.48	>5.48
	7.2	<0.1	<0.1	<0.1	0.66	0.84	1.10
	14.5	<0.1	<0.1	<0.1	<0.1	0.62	0.94

level at 75 °C per 3.2, 7.2 and 14.5 s stop did not ensure the complete inactivation of the mesophilic population, it produced a reduction in the range between 0.53 and 2.5 logs(cfu/ml). The stop for 3 s was not efficacy neither at the 85 and 92 °C, as the reduction was in both the condition close to 1.5 logs(cfu/ml). When those temperatures were tested using a stop time of 7.2 and 14.5 s, a significant reduction in mesophilic population was detected, ranging between 3 and 5 logs(cfu/ml), ensuring the milk sanitation relatively to the mesophilic aerobic populations.

The genus *Enterobacteriaceae* was detected on VRBGA and were below the detection limit (0.1 log[cfu/ml]) in the samples collected in all the treatment, suggesting as the weakest treatment (75 °C per 3 s) was sufficient to inactivate the initial population. It is in agreement with data reported in the literature as D-values of 0.10 and 0.004 min at 62.8 and 71.7 °C, respectively, were computed for *Salmonella* spp (Doyle and Mazzotta 2010), and between 0.7–17.8 s at 62.8 °C for *Yersinia enterocolitica* (Francis et al. 1980).

In all samples analyzed (before and after the treatments) *L. monocytgenens* was undetected in 25 g of analyzed sample (data not shown), confirming the absence of the bacterium in the milk, and the absence of contamination in the milking, transport and treatment phases inside the pasteurization plant.

3.2 Heat Resistance Modeling

Table 1 also shows the decimal reduction times D-values computed from the reductions of the mesophilic aerobic population independence on the heating time. Only the linear part of the measured survivor curves was included in the calculations. D-value computed at 75, 85, and 92 °C were 6.05, 2.13 and 2.0 s, suggesting as 85

and 92 °C treatment lead to similar death kinetics of the total mesophilic population in this experiment. The detected values for the sample analyzed after 14.5 s of treatment for both the treatment (85 and 92 °C) for the microbiological plate count, resulted similar because the limit of detection of the used measuring method was 0.1 log(cfu/ml).

Furthermore, the output of the modeling suggests as after 14.5 s, the survival colony are ten times greater at 85 than 92 °C. Using a probabilistic interpretation of the fractional survival values results that 0.1 surviving cell per reference unit (ml, in this experiment) will mean survival of 1 cell on 10 ml of treated milk ($0.1 = 1/10$). In case of 85 °C per 14.5 s treatment, it allows to obtain one viable cell every 10^5 ml of milk treated (10 l), while 92 °C per 14.5 s thermal treatment guarantees one survival every 10^6 ml (100 l). F_{BIO} values indicate the time to set in the treatment to get 5logs reduction of the population respect to D_T -value computed at every given T temperature.

3.3 Evolution of Bacterial Count During the Storage

The bottled milk samples stored at 4 °C were analyzed after 15 and 30 days of storage. Bacterial growth in the control sample after 15-days storage was characterized by increasing of more than three times log(cfu/ml) referring to *Enterobacteriaceae* and about 1 log(cfu/ml) total mesophilic bacteria. The increasing of *Enterobacteriaceae* is not surprising, as lysozyme which donkey milk is very rich, does not affect the viability of Gram- bacteria, of which the *Enterobacteriaceae* belong, while has bactericidal effect against Gram+ . Although it is of great interest, there are few studies on pasteurized donkey milk stored for long term in refrigerated conditions. Instead, many works agree in establishing that raw donkey milk has excellent stability inherently linked to the concentration of lysozyme. Salerno et al. (2011), in fact, found a shelf-life of more than 15 days for 3 samples of raw donkey milk containing 3000 mg/l of lysozyme, corresponding to total aerobic mesophilic, *Enterobacteriaceae*, *Lactococcus* and *Lactobacillus* species count less than 1 log(cfu/ml). 75 °C treatments, as observed, allows to inactivate the pathogenic species investigated, but the total bacterial count was still viable. For many food products, the total aerobic bacterial count is not a legal parameter, however, depending on the products, values between 3–6 logs(cfu/ml) are considered satisfactory (Gilbert et al. 2000), to the detriment of the storage time that could drastically decrease.

4 Conclusion

The preliminary results of this study are aimed to verify the efficacy and efficiency of the pasteurizer designed and built to treat small quantities of food liquid with a very high content of bioactive molecules with thermal sensitivity. Also, a matrix of

temperature and time pasteurization trial were carried out to optimize the process protocol for donkey milk pasteurization. The main target of the pasteurization is the 5 logs reduction of the pathogenic species, eventually, present in the product. At present, the main limitation in donkey milk is the absence of a thermal treatment indicator, like the alkaline phosphatase enzyme. Future studies must be taken into account alternative references to establish guidelines for the pasteurization of this product. *L. monocytogenes* and *Enterobacteriaceae* are bovine pasteurized milk's control microbial criteria, thus in this experiment to they were enumerated. The pasteurization plant and the treatment over 85 °C achieved satisfactory results concerning those microorganisms; furthermore, results suggest as satisfactory results can be reached from the treatments with the lowest energy demand, but their sanitation efficacy depends on the initial viable concentration. Jointly to microbiological analysis, nutritional indexes analysis (i.e. lysozyme, thiol, β -lactoglobulin), energy efficiency and operating and maintenance costs analysis may help to improve the innovative pasteurization plant and design a proper protocol for donkey milk pasteurization.

References

- Altieri, G., Di Renzo, G. C., & Genovese, F. (2007). Spray dryer process performance optimization for producing milk powders from cow, goat and she-ass milk concentrates. In *Food and agricultural products: Processing and innovations*, 24–26 September. Naples, Italy.
- Altieri, G., Di Renzo, G. C., & Genovese, F. (2011). Preliminary evaluation of donkey's milk properties through near infrared spectrometry. In *Towards a sustainable food chain food process, bioprocessing and food quality management*, 18–20 April. Nantes, France.
- Altieri, G., Genovese, F., Admane, N., & Di Renzo, G. C. (2016). On-line measure of donkey's milk properties by near infrared spectrometry. *Lebensmittel-Wissenschaft & Technologie*, 69, 348–357.
- Devlieghere, F., Vermeiren, L., & Debevere, J. (2004). New preservation technologies: Possibilities and limitations. *International Dairy Journal*, 14, 273–285.
- Di Renzo, G. C., Altieri, G., & Genovese, F. (2007). Tecniche per il trattamento del latte d'asina. Risultati di prove preliminari [In Italian: The she-ass milk treatment techniques. Preliminary results]. In Proceedings of II° Convegno Nazionale sul Latte d'Asina – “Latte d'asina perché”, Centro Congressi Coldiretti, Rome, 22 March.
- Di Renzo, G. C., Altieri, G., & Genovese, F. (2008). Preliminary results about a new method to optimize a spray dryer process for producing high quality milk powders from cow, goat and she-ass milk concentrates. *Journal of Agricultural Engineering*, 39, 35–41.
- Di Renzo, G. C., Altieri, G., & Genovese, F. (2011). Prove preliminari per lo sviluppo di un sensore NIR per l'analisi dei parametri costitutivi nel latte di asina [In Italian: Preliminary trials for the development of a NIR sensor for the analysis of the donkey milk]. In *Gestione e controllo dei sistemi agrari e forestali – Memorie*, p. 36, Belgirate (VB), 22–24 September.
- Di Renzo, G. C., Altieri, G., & Genovese, F. (2013). Donkey milk powder production and properties compared to other milk powders. *Dairy Science & Technology*, 93(4–5), 551–564.
- Doyle, M. E., & Mazzotta, A. S. (2000). Review of studies on the thermal resistance of salmonellae. *Journal of Food Protection*, 63, 779–795.
- European Pharmacopoeia 9.2 Supplement Implementation: 7/2017, Chapter 5.1.2 “*Biological Indicators and related microbial preparation used in the manufacture of sterile products*”.
- FAO/WHO. (2004). Code of hygienic practice for milk and milk products. *Joint FAO/WHO Food Standards Programme-Codex Committee on Food Hygiene, 26th Session*, March 29–April 2. Washington, DC, USA.

- Francis, D. W., Spaulding, P. L., Lovett, J. (1980). Enterotoxin production and thermal resistance of *Yersinia enterocolitica* in milk. *Applied and Environmental Microbiolog.* 40(1), 174–176.
- FDA. (2011). *Fish and fisheries products hazards and control guidance*, 4th ed. U.S. Food and Drug Administration, Department of Health and Human Services. Available at <http://www.fda.gov/downloads/food/guidanceregulation/ucm251970.pdf>.
- Gilbert, R. J., de Louvois, J., Donovan, T., Little, C., Nye, K., Ribeiro, C. D., Richards, J., Roberts, D., Bolton, F. J. (2000). Guidelines for the microbiological quality of some ready-to-eat foods sampled at the point of sale. *Communicable Disease and Public Health*, 3, 163–167.
- Lopes, R. P., Mota, M. J., Gomes, A. M., Delgadillo, I., & Saraiva, J. A. (2018). Application of high pressure with homogenization, temperature, carbon dioxide, and cold plasma for the inactivation of bacterial spores: A review. *Comprehensive Reviews in Food Science and Food Safety*, 17, 532–555.
- Salerno, M., Paterlini, F., & Martino, P. A. (2011). Microbiologia e attività battericida del latte di asina. *Latte d'asina: produzione, caratteristiche e gestione dell'azienda asinina*, 193–205.

Effect of Materials and Assembly Methods on Gas Selectivity of Blow[®] Device



A. Matera, G. Altieri, F. Genovese and G. C. Di Renzo

Abstract In the present paper, the effect on gas selectivity using different materials of the patented Blow[®] device is described. Blow[®] is an innovative device that allows the bidirectional gas exchange across a sealed package. The device results particularly useful for managing the atmosphere in the package headspace of fruit and vegetables packed in modified atmosphere, with a high level of carbon dioxide or low level of oxygen. The latest device version is produced by assembling two different parts; preliminary tests showed that the device's material and the assembly procedure affects the gas selectivity of the device. To evaluate the effect of material and welding system on the breathable characteristics of the device, three plastic- (PP, LDPE, ABS) and bio- (Mater-Bi[®]) based materials and three different levels of welding pressure were used for comparative tests. For each material and test condition, the diffusion of oxygen (O₂) and carbon dioxide (CO₂) has been measured by the pressure discharging time measured in the range from 400 to 10 Pa of differential pressure from inside to outside of the package.

Keywords MAP · Bioplastic · Food packaging

1 Introduction

Blow[®] is a patented microtechnology intended for both passive and active control of the surrounding headspace in fruit and vegetable packaging (Di Renzo et al. 2015, 2016). This microtechnology and the testing involved to assess its physical properties (hydro-dynamic behaviour and gas diffusivity) have been deeply described, and it has pointed out as the gaseous permselectivity and the bidirectional flow are distinctiveness characteristics of Blow[®] (Altieri et al. 2018), and made this device unique among the ones designed for food packaging. Additionally, Blow[®] prevents the increasing of partial pressure inside the container and the stacking of water vapour

A. Matera (✉) · G. Altieri · F. Genovese · G. C. Di Renzo
Scuola di Scienze Agrarie, Alimentari ed Ambientali (SAFE), Università degli Studi della Basilicata, via dell'Ateneo Lucano 10, Potenza, Italy
e-mail: attilio.matera@unibas.it

© Springer Nature Switzerland AG 2020

A. Coppola et al. (eds.), *Innovative Biosystems Engineering for Sustainable Agriculture, Forestry and Food Production*, Lecture Notes in Civil Engineering 67,
https://doi.org/10.1007/978-3-030-39299-4_80

745

in the package and, thus, delays the decay or rotten due to mould growth. When combined with MAP, Blow[®] exhibited excellent performance, as the storage period of organic table grapes with Blow[®] was increased up to 100% if compared with the macro perforated film (Di Renzo et al. 2019).

The packaging design for climacteric fruit and vegetables must take into account for the need to avoid both “too closed” packaging because it involves high levels of CO₂ (phytotoxic), low levels of O₂ (organoleptic anomalies) and excessive humidity (increase in rot), and “too open” packaging because it does not reduce the onset of senescence and facilitate the mass loss.

In packaging design and development, the knowledge of the gaseous permeability of the layer or a film involved is unavoidable. The β value of an extruded material represents the permselectivity factor, it represents the ratio between CO₂ and O₂ permeability coefficient PCO_2/O_2 (ml $\mu\text{m cm}^{-2} \text{ atm}^{-1} \text{ day}^{-1}$) and it must be taken into account in evaluating the suitability of a material for food packaging design, especially for any food product showing high metabolic activity due to microflora or product respiration. Thus, the packaging design or improvement cannot leave β out of consideration, as it determines the proper gaseous mixture, the product mass and the size of the bag or pack to be used in the calculation.

Micro-perforated films (hole diameter < 200 μm) have β value of 1, which means high (> 18%) CO₂ and low (<3%) O₂ content at steady-state, and this property is of great interest as low O₂ content avoid fermentation process by anaerobic bacteria and contributes to maintain the produce “live”, whereas medium-high partial pressure values of CO₂ have fungistatic effect, but caused the onset of anomalous flavours in the grapes and the browning of rasp and berry in table grapes (Mari et al. 2010).

Conversely, macro-perforated films (hole diameter > 200 μm) have β value < 1, corresponding to a high O₂ and low CO₂ partial pressure at steady-state.

However, *ad hoc* design of micro- and macro- perforated film for a target product needs the knowledge of holes' density and size to perform on the film by laser incision.

The β value of Blow[®] made up of acetalic resin was 1.46 and 1.50 for S-MMD and L-MMD version respectively, which means that the permselectivity of Blow[®], due to the fluid dynamic properties of the device, determines the faster flushing of CO₂ with respect to O₂ (Altieri et al. 2018). These properties result in lower CO₂ of and higher O₂ content at steady-state in the container if compared with a micro-perforated film.

Among the polymeric packaging films, the mostly used are coextruded or laminated made up of polypropylene (PP), polyethylene (PE), ethylene vinyl alcohol (EVOH), oriented polypropylene (OPP). The suitability of these films to support an industrial process or treatment depends on their properties such as film permeability to O₂ and CO₂, mechanical properties, degree of recyclability. The final target is the slowing of the respiration, moisture loss and decay, which results in product' shelf-life extending. However not many films offer all of the required properties for a MAP packaging and in general, their use is not common due to the many problems related to their use (cost, affinity with the ink used, coefficient of friction required by the packaging machines, etc.). Therefore, to provide better properties and extend the shelf life of products, many films are combined with lamination, co-extrusion

(Mario Ščetar et al. 2010), bioactive compounds, or the Blow[®] technology (Matera et al. 2017).

The S-MMD and L-MMD micro technology have huge potential because its design made it suitable to be fixed on any film using the glue, whatever is the material of the layer. However, these versions cannot be exploited for industrial purpose because the insertion process on a film requires a trained operator, determining a production slowdown in the factory. Thus, the device's design has been ameliorated by replacing the manufacturing material to obtain improved mechanical and biodegradability properties, and by covering the main body containing the microtechnology with an ultrasonically sealed lid, to increase the welding speed on the film needed when dealing with flow pack machinery. Only after the application of the lid on the upper side of the Blow[®] device, it has the breathable property that makes it an innovative system for fruit and vegetable packaging.

This work aimed to assess the performance of this Blow[®] restyling, in terms of hydrodynamic behaviour, gaseous mixture diffusivity across the main body and changes in the structure after ultrasonic welding of the various tested materials.

2 Materials and Methods

2.1 Materials

The materials used for the restyling were three fossil fuel (Low-Density Polypropylene LDPE, Riblene[®]; Polypropylene PP, BD310MO; Acrylonitrile Butadiene Styrene ABS, Terluran[®] GP-35) and one bio-based plastic (Mater-Bi[®]—PT MYPACK 004). The raw materials (spherical pellets) were purchased from their respective manufacturers (Italy) and have been delivered to the Blow[®] device manufacture to obtain the end product with the patented characteristics. First, the main body and the lid were built separately and subsequently they were ultrasonically welded at 20 kHz per 1.5s. Once Blow[®] was assembled it was thermally welded on the films by means of a dedicated semi-automatic prototype welding machine, allowing various pressures and holding times, as described in 2.2. The films used had chemical characteristics similar to the materials with which Blow[®] was manufactured. Fossil fuel-based devices were welded with PET (12 μm)/PP (50 μm) film, characterized by a O₂ and CO₂ permeability of, respectively, 110 and 500 mL/m²/24 h/bar at 23 °C, and water permeability of 3 g/m²/24 h at 38 °C (data provided by the manufacturer Gopack, Italy). The bio-based device was welded on polylactic acid (PLA) based film (40 μm thickness) with O₂ permeability of 540 cm³/m²/24 h/bar at 23 °C, and water permeability of 200 g/m²/24 h at 38 °C (data provided by the manufacturer Corapack, Italy).

2.2 *Welding Process*

The welding process was carried out using a dedicated prototype machine, adjusting the temperature, pressure and holding time. The welding temperatures were chosen accordingly to the melting temperature of the material and were set up at 200 °C and 130 °C for the fossil fuel- and bio- based Blow[®], respectively. Three levels of pressure (2, 3.5, 5 bar) and holding time (2, 4, 6s) were tested.

2.3 *Performance Assessment of the Produced Device*

Ultrasonically sealed Blow[®] made of the above-cited materials were checked out. A preliminary assessment was obtained by the image analysis of the Blow[®] cross-section with Supereyes 3.5 and its dedicated software, in order to observe if the ultrasonic sealing process affected the micro-incision of the device.

The Blow[®]/Film device represented the output of the welding process.

The device fluid-dynamic behaviour was investigated measuring its hydrodynamic parameter H: trials were carried out using pure air to eliminate the effect of the diffusion term, starting with a differential pressure of approximately 400 Pa decreasing up to 10 Pa. Data were collected using a DAQCard acquisition board (AI-16X-E50, 16 ADC channels, 16 bits resolution, National Instrument S.r.l., Italy) and a differential pressure sensor (Gems Sensors 5266500LBHTI, ± 500 Pa, RS Components S.r.l., Italy).

The apparatus consists of two stainless steel plates sealing the Blow[®]/Film device, as described by Altieri et al. (2018). The gas is charged from one end (gas loading) into the internal apparatus volume, and the discharge begins through the Blow[®]/Film after closing the inlet valve. The apparatus was enclosed into a thermostatic chamber settled at 20 °C; 5 devices were tested and 5 repetitions were carried out on every test. Subsequently, the diffusion parameters F_{im} have been measured: one container (internal volume of 1050 mL) was sealed applying the Blow[®]/Film device. The container has been flushed (2 min at 50 L/h) with three types of commercial gaseous mixtures (5% CO₂–5% O₂, 10% CO₂–10% O₂). Subsequently, the container has been enclosed into a thermostatic chamber settled at 20 °C. Three trials for each of device version have been carried out with a duration of approximately 7 d. A CheckMate3 instrument (Dansensor Italia S.r.l., Italy) has been used to measure the gas concentration (O₂% and CO₂%) hourly inside the container. The average Lab atmospheric pressure was 919.0 hPa. Blow[®]/Film device sealed with glue represented the control.

3 Results and Discussions

3.1 Hydro-Dynamic Behaviour

Figure 1 shows the trend of gaseous mixture flushing across the Blow[®] made of Mater-Bi[®], PP, LDPE and ABS and welded with glue. As expected, the null hypothesis that the material did not have a significant effect on the time constant was rejected ($p < 0.01$). The pressure across the device decrease with a characteristic time constant (Table 1) that was the highest for Mater-Bi[®] (93.55s) and the slowest for PP (1.02s), while LDPE and ABS based devices showed the highest variability (Coeff. Var. > 40%), these devices were not considered for further test (i.e. gaseous mixture diffusion test). These results are effectively affected by both materials used and their behaviour under ultrasonic welding. Image analysis shown in Fig. 2 clearly highlights as the section of the capillary duct, across which the gaseous mixture flushes, it is well defined and larger in PP than other materials. The lower time constant computed for Blow[®] made of PP is probably a consequence of the ultrasonic process, which did not melt completely the duct and did not affect its structure, bringing to a

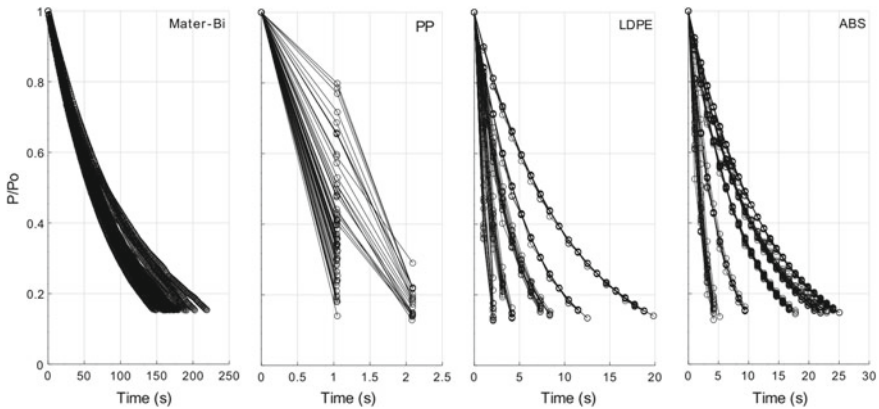


Fig. 1 Pressure discharging time measured in the range from 400 to 10 Pa of differential pressure across Blow[®]'s capillary duct

Table 1 Characteristic time constants (τ) of the control devices computed fitting the data to the model “ $a \cdot \exp(t/\tau)$ ”. Results are expressed in seconds (s); means not sharing the same letter are significantly different (Tukey’s HSD, $p < 0.01$)

	Mater-Bi [®]	PP	LDPE	ABS
Runs	65	68	79	80
Mean (τ), s	93.55 ^a	1.02 ^b	4.64 ^c	8.15 ^d
St. Dev. (τ)	10.72	0.26	3.18	4.02
Coeff. Var (%)	11.46	25.94	68.53	49.35

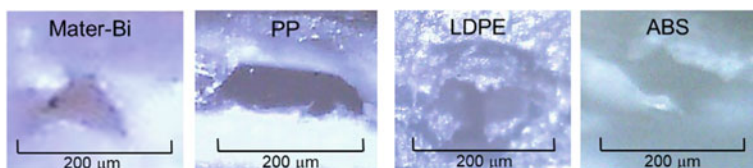


Fig. 2 Detail of the cross-section of the Blow[®] devices made of Mater-Bi[®], PP, LDPE, ABS. The shaded area represents the duct section after the ultrasonic welding of the main body with the lid

larger section than the other materials and, thus, to a reliable device with reproducible performance.

3.2 Gas Diffusivity and Selectivity

Gaseous mixtures spread out across Blow[®] with time characteristic depending upon the version and material involved, as highlighted by the hydro-dynamic results.

With respect to the permselectivity properties (Table 2), the acetal resin based Blow[®] (S, L-MMAD) reported the highest β values, making it very suitable for the storage of highly perishable products (i.e. with high respiration rate), wherein the uptake of CO₂ is too much fast, they may not tolerate a high percentage of CO₂ in the package, determining the onset of organoleptic defects. The results of gaseous diffusion across PP- and Mater-Bi[®]- based Blow[®] indicate as the gas selectivity property is negligible since a β value close to 1 was measured, suggesting as these devices had not selectivity property among O₂ and CO₂, whatever is the gaseous concentration inside the container, O₂ and CO₂ diffuse through the device at a similar rate, so it's impossible to achieve low O₂ (1–5%) without accumulating high CO₂ (15–20%), as for the micro-perforated film (Robertson 2009).

Table 2 Results of the trials carried out to measure the time constant τ and the diffusion parameter F_{im} for each gas (O₂, CO₂, N₂) of the Blow[®]. Data were fitted using Eq. (7) by Altieri et al. 2018. Matlab's Curve Fitting Toolbox was used to fit the data to the model "exp(-t/ τ)"

Blow [®] version	O ₂		CO ₂		N ₂		β P_{CO_2}/P_{O_2}
	F_{im} (m ³ s ⁻¹)10 ⁻⁹	τ (h)	F_{im} (m ³ s ⁻¹)10 ⁻⁹	τ (h)	F_{im} (m ³ s ⁻¹)10 ⁻⁹	τ (h)	
S-MMAD ¹	1.51	193.5	2.21	132.0	263.9	1.1	1.46
L-MMAD ¹	1.38	211.6	2.06	141.6	274.8	1.0	1.50
Mater-Bi [®]	3.59	81.2	3.74	78.2	3.51	83.0	0.94
PP	4.56	64.0	4.33	67.4	4.72	61.8	1.04

¹Altieri et al. (2018)

3.3 Evaluation of the Welding Process

The experimental design was preliminary arranged to test the welding of all the plastic- and bio- based Blow[®] on an adequate film. The test on control sample (paragraph 3.1) showed high variability between the replications, highlighting a statistically uncontrolled manufacturing process, leading to ended device ABS- and LDPE- based that was rejected by our test. Thus, we expected similar performances after performing the welding process of Blow[®] on the films with the prototype machinery. Effectively, PP had lower variability among the treatments (Fig. 3), LDPE led to uncertain results (data not shown), ABS was not suitable at all for sealing with the prototype machinery because of the size and the hardness of the material, which contributes to partially weld the crown of the device on the film (Fig. 4c). The most surprising result concerned Mater-Bi[®] based Blow[®] thermally sealed on the PLA bio-based film. In this case, the holding time was set up to 4s, and the sealing temperature and pressure were modified to find a compromise among the working parameters which guaranteed the device welding without detachment. Although these samples are made up of bio- based materials, they did not weld to each other and exhibited weak seal strength (Fig. 4d), thus were not analysed for the characterization of τ . Since the Mater-Bi[®]'s manufacturer provides a wide range of this material, owning different physical-chemical properties, by supplying alternative pellets or welding on other bio-based films could be possible to evaluate the feasibility of Mater-Bi[®] based Blow[®] for welding processes.

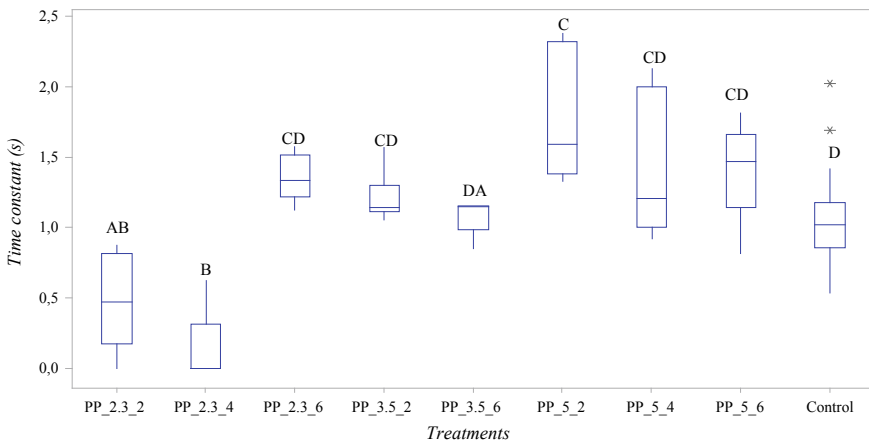


Fig. 3 Box plot of the time constant referred to the air flush across the thermally sealed PP based Blow[®] on PP-PET film (5 replications). For every treatment, the number in the middle is the pressure value (bar), the second one the holding time (s). Treatments not sharing the same letter are significantly different (Tukey's HSD $p < 0.05$)

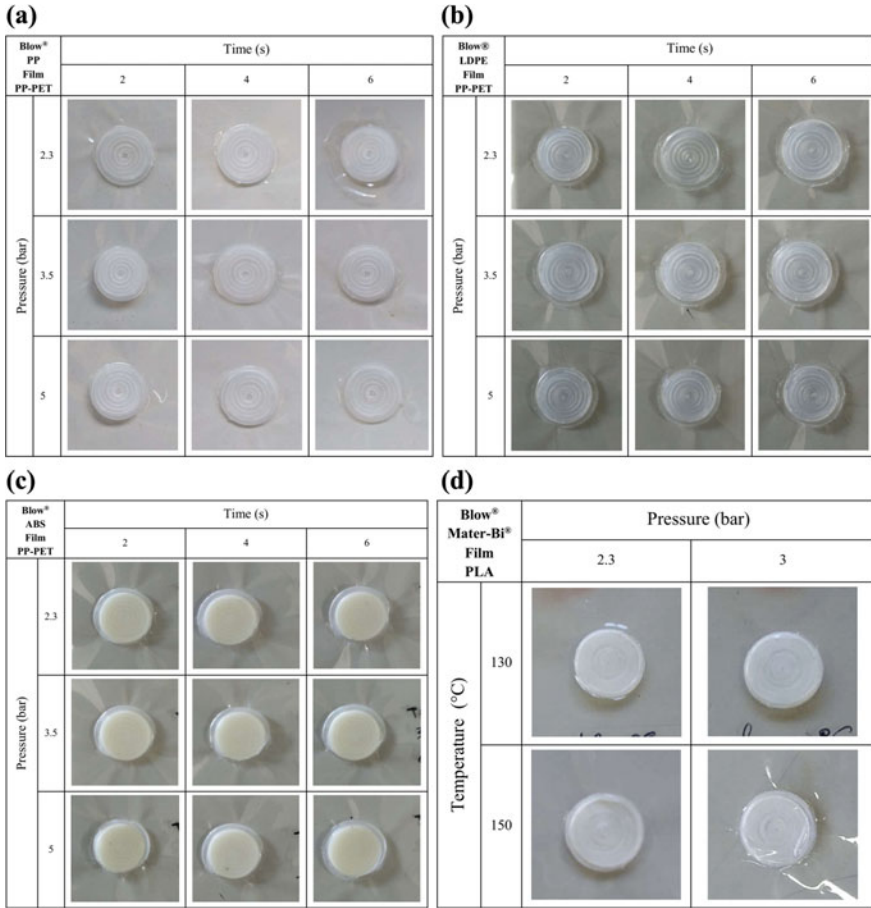


Fig. 4 Pictures of the Blow[®] sealed on the films involving different levels of pressure, temperature and time. The sealing temperature of PP (a) LDPE (b) and ABS (c) was 200 °C. Holding time of Mater-Bi[®] based Blow[®] was 4s

4 Conclusion

This work represents a research activity aimed to improve the functionality of Blow[®] device, both in terms of performance and design. To date, great results were achieved with the S, L—MMAD type, but the design of these version doesn't allow the industrial exploitation. Moreover, market demands for new recyclable and bio-based material. The restyling of the invention with other materials and combining with an ultrasonically sealed lid, they brought advances in the study of packaging solutions for food products. The choosing of materials has great importance, since their suitability to be ultrasonic or thermal welded determine a changing on the performance, in particular, the gas permselectivity was conditioned. PP and Mater-Bi[®] are the

materials that guaranteed lower variability in the performance of the end product, but, in the latter case, the welding on bio-based film has still to be investigated as unsatisfactory results were obtained. PP based Blow[®] was the product with lower variability in terms of hydrodynamic behaviour. By setting up the welding process of the PP based Blow on PP-PET film in a specific working range, the fluid dynamic properties across the capillary duct are constant and similar to the control sample.

Acknowledgements The activity of this paper was carried out in the framework of the MyPack Project “Best markets for the exploitation of innovative sustainable food packaging solutions”. It is a four-year project started on November 1st 2017, and funded by European Union’s H2020 research and innovation programme under grant agreement no. 774265. The information contained in this document only reflects the author’s view.

References

- Altieri, G., Genovese, F., Matera, A., Tauriello, A., & Di Renzo, G. C. (2018). Characterization of an innovative device controlling gaseous exchange in packages for food products. *Postharvest Biology and Technology*, 138, 64–73.
- Di Renzo, G. C., Altieri, G., & Genovese, F. (2015). Dispositivo per controllare scambi gassosi fra l’interno e l’esterno di un contenitore per prodotti alimentari solidi o liquidi. Patent: 102015000018707 (in italian).
- Di Renzo, G. C., Altieri, G., & Genovese, F. (2016). Device for controlling gaseous exchanges between the inside and outside of a container for solid or liquid food products. Patent: PCT/IB2016/0506600.
- Di Renzo, G. C., & Matera, A. (2019). Le nuove tecnologie per la gestione post raccolta dell’uva da tavola. *Uva da tavola... Rutigliano oggi e domani*, 24–27.
- Mari, M., & Neri, F. (2010). Nuove tecniche di confezionamento per la GDO. *Metodi innovativi di gestione dei frutti nella fase post-raccolta*, 89–91.
- Matera, A., Genovese, F., Altieri, G., Tauriello, A., & Di Renzo, G. C. (2017). An innovative smart device to control Modified Atmosphere Packaging (MAP) of fruit and vegetables. *Chemical Engineering Transactions*, 58, 193–198.
- Robertson, G. L. (2009). *Food packaging and shelf life: A practical guide*. ISBN 9781420078442.
- Ščetar, M., Kurek, M., & Galić, K. (2010). Trends in fruit and vegetable packaging—A review. *Croatian Journal of Food Technology, Biotechnology and Nutrition*, 5(3–4), 69–86.

Information and Communication Technologies

Introduction

Prof. Fabrizio Mazzetto

President of the 7th Section of the Italian Association of Agricultural Engineering 'Information and Communication Technologies'

The purpose of the 7th Section is to promote the use of Information and Communication Technologies (ICT) to optimize the management of all agricultural and agri-food production processes, in order to improve their quality and sustainability. The effective adoption of ICT in this sector requires the combination of tools and knowledge applied to biological systems including: advanced sensors, control and monitoring techniques, Automation, Robotics, Artificial Vision, advanced data and information management, use of new communication networks. The activities of the 7th Section, therefore, require an active cooperation with all the other sections of the AIIA, and therefore of the CIGR, for a complete harmonization in the use of ICT in the different production phases of each agri-food chain.

The 7th Section promotes information and communication technologies both through dissemination in the academic and post-university fields, and through research and development of new systems and applications, with reference to the following sectors: (a) In situ and remote sensors, from land, UAVs (drones), airborne and satellite platforms; (b) Information Processing Technologies; (c) Simulation and Modelling; (d) Applications of Information Management Systems, including Knowledge-Based Systems and Decision Support Systems; (e) Computer Vision and Artificial Intelligence; (f) Geographic Information Systems (GIS); (g) use of Global Navigation Satellite Systems (GNSS) for land planning and management; (h) applications of Precision Agriculture and Precision Forestry techniques; (i) Networks for data sharing and data mining to manage issues in agricultural, forestry and environmental contexts. The 7th section organizes and coordinates meetings, seminars and scientific conferences both nationally and internationally, also in collaboration with related associations, and promotes the formation of interdisciplinary groups for participation in research projects.

Among the 14 papers presented to the 7th Section in the 4th of the International Mid-Term Conference 2019 AIIA, a large number of contributions (about 60%) dealt

with topics related to remote sensing applications with UAVs for crop monitoring tasks. The other 3 papers considered conventional problems of Information Management and Precision Agriculture, including site-specific farming approaches. The remaining contributions dealt with Precision Forestry, automation and issues related to sprayers' performances. All considered, all they are in line with the hot topic trends of the research currently worldwide applied in the sector.

Monitoring of Coffee Tree Growth Through Crop Surface Models and MGRVI with Images Obtained with RPA



Gabriel Araújo e Silva Ferraz, Luana Mendes dos Santos, Marco Thulio Andrade, Letícia Aparecida Gonçalves Xavier, Diogo Tubertini Maciel, Patrícia Ferreira Ponciano Ferraz, Giuseppe Rossi and Matteo Barbari

Abstract For precision agriculture to monitor the crops during the vegetative and reproductive period is very important. Currently, remote sensing platforms such as remotely piloted aircraft (RPA) have stood out. The aim of this work was to evaluate the application of Modified Green Red Vegetation Index (MGRVI) vegetation index and Crop Surface Models (CSM) with images obtained by an RPA, to monitor the growth of coffee trees in three different seasons. The experiment was carried out at the Federal University of Lavras, Lavras, Minas Gerais, Brazil, in an area cultivated with coffee species *Coffea arabica* L. A RPA equipped with a digital camera was used to take photos, and Agisoft PhotoScan software was used to build the mosaic of photos and CSM. QGIS was used to obtain the height of the plants, application of the index MGRVI and the preparation of the map layouts by images processing. It was possible to identify the crop failure areas with the CSM. Crop Surface Models (CSM) showed to be a promising technique for the monitoring of coffee tree growth, making it possible to identify crop failures and growth variations. The MGRVI index failed to identify crop failures. The index did not recognize the difference between soil and vegetation, possibly due to the light variations in the area.

Keywords Precision agriculture · Plant height · Remote sensing · UAS · Vegetation index · Crop monitoring

G. A. S. Ferraz (✉) · L. M. dos Santos · M. T. Andrade · L. A. G. Xavier · D. T. Maciel · P. F. P. Ferraz
Federal University of Lavras, Campus Universitário, PO Box 3037, Lavras, Minas Gerais, CEP 37200-000 Lavras, Brazil
e-mail: gabriel.ferraz@ufla.br

G. Rossi · M. Barbari
Department of Agriculture, Food, Environment and Forestry (DAGRI), University of Florence, Via San Bonaventura, 13-50145, Florence, Italy

© Springer Nature Switzerland AG 2020
A. Coppola et al. (eds.), *Innovative Biosystems Engineering for Sustainable Agriculture, Forestry and Food Production*, Lecture Notes in Civil Engineering 67,
https://doi.org/10.1007/978-3-030-39299-4_81

1 Introduction

Crop monitoring during the vegetative and reproductive period is necessary for precision farming (Mulla 2013; Bendig et al. 2014). Currently, remote sensing platforms with high spatial and temporal resolution have been highlighted. Remotely piloted aircraft (RPA) allow the shipment of RGB-cameras and other sensors, and it can collect agricultural data with low cost and with the flexibility (Sankaran et al. 2015).

The images obtained by the RPA, undergo a mosaic process, resulting in orthomosaic and Digital Elevation Models (DEM). So, with orthomosaic and DEM, the height of the canopy can be obtained by the Crop Surface Models (CSM). Bendig et al. (2013) used the CSM to monitoring the rice crop growth through images obtained with RPA and showed the viability of this technique. Bareth et al. (2016) used CSM to predict maize production. The authors highlighted that the method was suitable for the non-destructive determination of plant height.

Thus, this approach can also be extended to coffee cultivation. According to Ramirez and Zullo Júnior (2010), coffee plant height is an important parameter for crop prediction and monitoring methods.

Vegetation indexes (VI) help to differ in digital images the vegetation from other variables (Xiao and Moody 2005). The Modified Green Red Vegetation Index (MGRVI) is defined as the standardized difference from green to square reflectance and squared red reflectance. MGRVI was developed by Bendig et al. (2015) in and it presents promising results as a vegetation index; however, it requires more researches applying this index.

Both CSM and VI application are processes that aid in crop monitoring, however, VI are not efficient in non-uniform illumination conditions (Romeo et al. 2013). Thus, surface modelling can be an alternative when there are lighting hints on images obtained by RPA.

The aim of this work was to evaluate the application of MGRVI vegetation index and CSM in images obtained by an RPA to monitoring coffee tree growth in three different seasons.

2 Materials and Methods

The study was carried out at the Federal University of Lavras (UFLA), in the city of Lavras, Minas Gerais, Brazil. The study was developed in 0.13 hectares of an experimental area, cultivated with *Coffea arabica* L., cultivar Travessia, with 2.60 × 0.60 m spacing, under the coordinates: at 21°13'33.23" South latitude, 44°58'17.63" West longitude, and 936 m altitude. The images were taken with a Sony digital camera, model EXMOR 1/2.3", with 12 megapixel resolution, obtaining images in true colour (red-R, green-G, blue-B) and 8-bit radiometric resolution; 20 mm lens with an f/2.8 aperture and a maximum image resolution of 4000 × 3000 pixels, and its photos are stored on an SD card. The camera was coupled to a Phantom

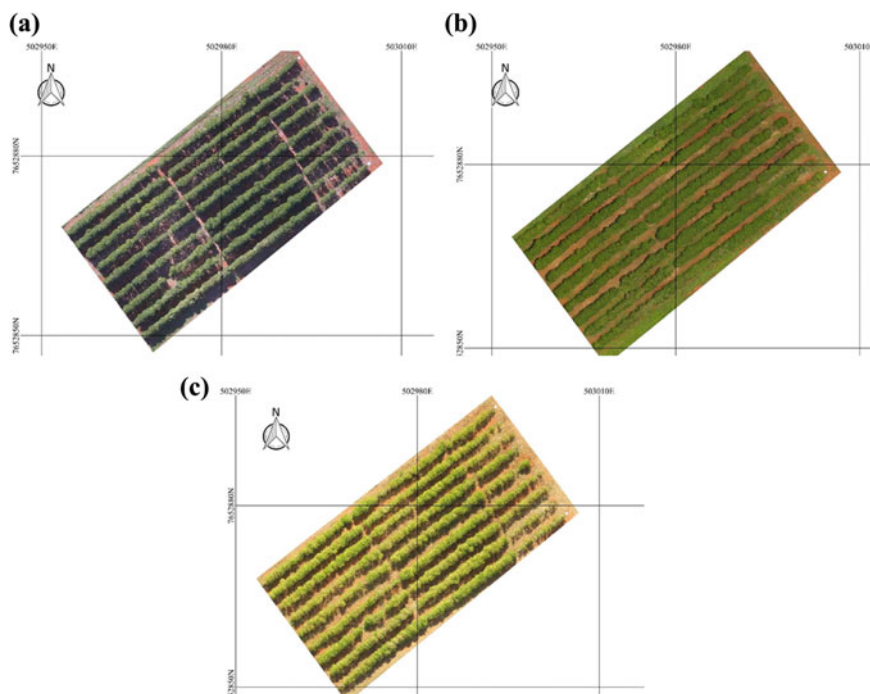


Fig. 1 RGB images of coffee crop area in **a** June 2017, **b** December 2017 and **c** May 2018

3 Professional Remotely Piloted Aircraft (RPA). To capture the images, the flight height was standardized to an altitude of 30 m from the ground with a constant travel speed of 3 m/s, with image overlap (Longitudinal Overlap and Lateral Overlap) of 80/80%. Three collections were carried out in the study area, in June 2017, December 2017 and May 2018 (Fig. 1).

Six control ground points (CGP) were demarcated in the soil, with coordinates collected by GPS L1 and post-processed (0.07 m precision). It was placed at each CGP a 0.16 m² target that can be seen at the image and was used for georeferencing correction. It was performed to all three flights.

The images were processed in Agisoft PhotoScan (2018) version 1.25 software. This software identifies homologous points in the overlapping images. So, it creates a continuous region by stereoscopy, and then it is possible to obtain a point cloud. The next step is to create a dense point cloud. From this dense point cloud was possible to create the Digital Surface Model (MDS), the Digital Terrain Model (MDT) and the orthomosaic, with a high spatial resolution (0.012 m).

The software QuantumGis (QGis, 2018) version 2.14.22 was used to obtain the plant height. So, it was used the methodology proposed by Panagiotidis et al. (2017), in which a Crop Surface Models (CSM) is obtained by subtracting the MDS from MDT. Then, with the orthomosaic, the MGRVI (Modified Green Red Vegetation Index) (Bendig et al. 2015) was calculated in the QGis software. This index facilitates

to differ the soil and vegetation in a crop area Eq. (1):

$$\text{MGRVI} = \frac{G^2 - R^2}{G^2 + R^2} \quad (1)$$

where R is the red band and G is the green band.

According to Barbosa et al. (2019), the MGRVI has potential for studies of agricultural productivity and, according to Bendig et al. (2015), this VI is promising for the prediction of barley biomass. As this study used a conventional camera, the electromagnetic radiation spectrum was detected in the portion of the visible (Red-R, Blue-B and Green-G). The MGRVI index differs from NDVI (which is the VI most used in the research) because NDVI needs the infrared spectrum, that is not available in conventional cameras but expensive cameras. Ballesteros et al. (2014) state that the use of RPA with RGB (Red, Green, Blue) spectrum camera is a cheaper alternative than a PRA with infrared (IR) spectrum camera. Therefore, based on these statements, it is interesting to apply the MGRVI and also compare with Crop Surface Models (CSM).

3 Results and Discussion

In the delimitations highlighted in Crop Surface Models (CSM) (Fig. 2) was possible to observe some failure in the crop field. Due to coffee being a perennial crop, this failure remained throughout the monitoring period. Figure 2 shows the development of coffee tree growth during the experimental period. There was an increase in plant height in the evaluated period. It is highlighted by a greener colouration in most of the plants in Fig. 2c.

In addition, it is possible to identify the exposed soil sites or undergrowth vegetation between the coffee trees rows. These places presented the lowest values of height, and the red colouration represents it. The coffee crop underwent a pruning process, called “esqueletamento”, in which it is pruned about 20 cm at the top, and end with 40 cm in the lower branches. So, it was possible to observe in Fig. 2 that the light yellow colour represents an intermediate height that refers to these low branches or the climbing plants in the area.

According to Bendig et al. (2014), the RGB images obtained with RPA are highly suitable to derive height of plants with high resolution (1 cm), enabling to obtain information of the entire canopy, unlike data obtained in the field that requires interpolation.

The enhancement of the images from the vegetation index is shown in Fig. 3. The MGRVI vegetation index was affected by the illumination variations in the images. It is possible to observe in Figs. 1a and 3a and Figs. 1c and 3c that there was shading in the interline of the coffee trees, so the index classified the shade as vegetation. In the other hand, Fig. 3b resulted in a correct index classification. The images were collected in a day with little variation of the lighting, that is, totally cloudy. The

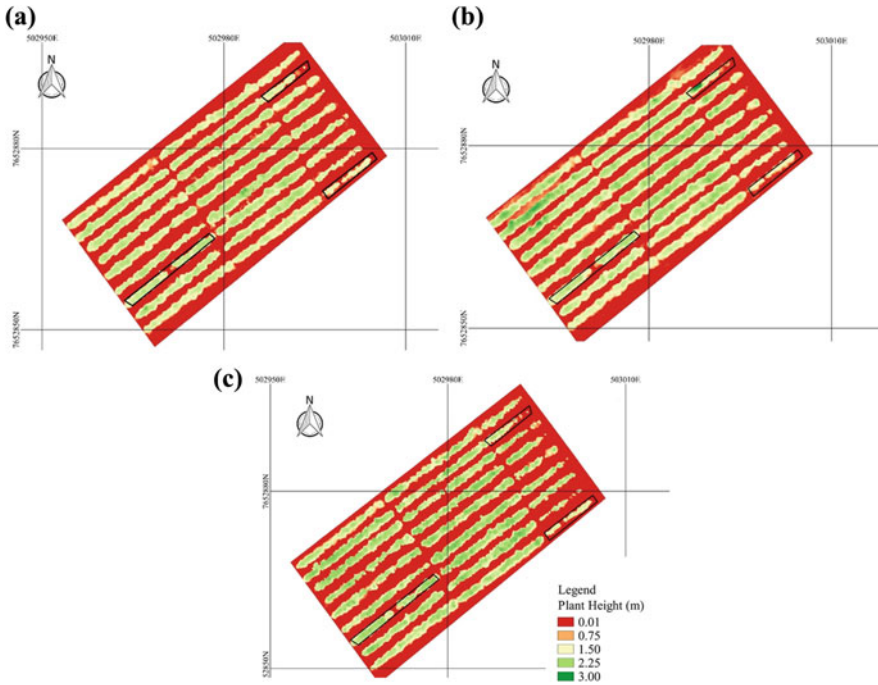


Fig. 2 Plant height obtained by CSM in **a** June 2017, **b** December 2017 and **c** May 2018

variation of the solar incidence in RPA images was studied by Rasmussen et al. (2016), the authors recommended that the images need to be obtained on totally cloudy days or with the incidence of light angle needs to be the same of the camera positioning, so that the lighting conditions are constant, or calibrating the images with monitoring of lighting conditions. Another recommendation of the authors Dandois et al. (2015) is to collect the photos under conditions of uniformly clear or evenly cloudy light.

However, MGRVI did not allow to observe crop field failures, as could be observed in the CSM. This is due to another misclassification, in which the index classifies vegetation as coffee trees.

This index considered any vegetation as green, even in Fig. 3b, where the index was able to differentiate exposed soil from vegetation. Romeo et al. (2013), pointed out that VIs are not efficient under nonuniform lighting conditions, so surface modelling may be an alternative when there are variations of illumination in images obtained by RPA to identify faults or growth variations due to plagues, diseases or nutritional and water deficiencies.

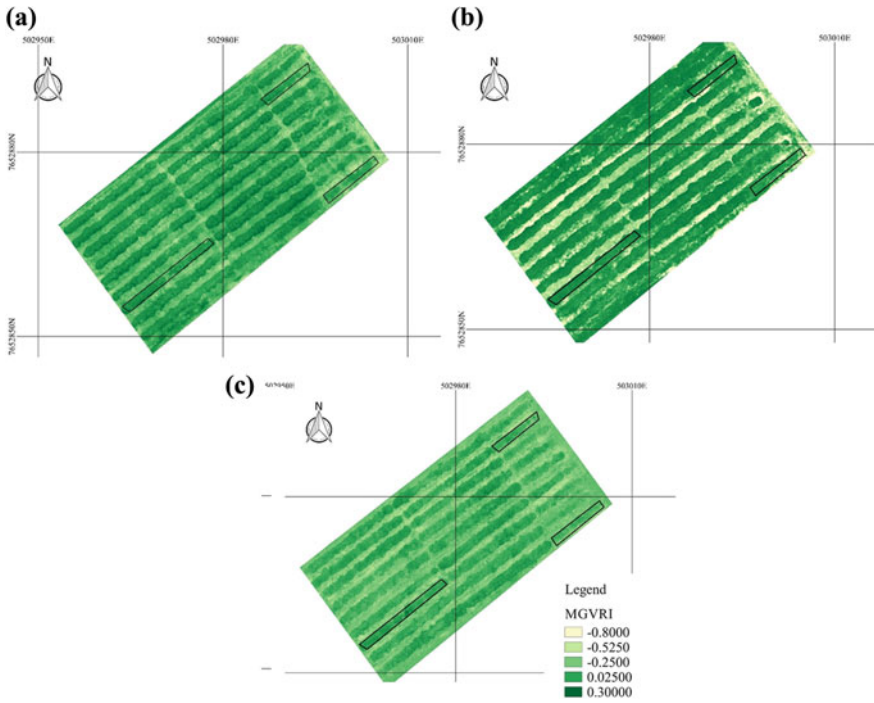


Fig. 3 Coffee crop area with MGRVI spectral enhancement in **a** June 2017, **b** December 2017 and **c** May 2018

4 Conclusions

Crop Surface Models (CSM) showed to be a promising technique for monitoring coffee tree growth. This model allowed to identify crop failures and growth variations. The MGRVI index failed to identify crop failures, and in some moments, this index did not recognize the difference between soil and vegetation due to the lighting variations in the area. Future studies related to the integration of biophysical parameters (CSM) and vegetation indices such as MGRVI are recommended for evaluation of coffee tree vigour.

Acknowledgements The authors thank, the Foundation for Research of the State of Minas Gerais (FAPEMIG) to funding this research, the National Council for Scientific and Technological Development (CNPq), the Coordination for the Improvement of Higher Education Personnel (CAPES), the Federal University of Lavras (UFLA) and University of Florence (UniFI).

References

- Ballesteros, R., Hernández, D., Ortega, J. F., & Moreno, M. A. (2014). Applications of georeferenced high-resolution images obtained with unmanned aerial vehicles. Part II: Application to maize and onion crops of a semi-arid region in Spain. *Precision Agriculture*, *15*, 593–614.
- Barbosa, B. D. S., Ferraz, G. A. S., Gonçalves, L. M., Marin, D. B., Maciel, D. T., Ferraz, P. F. P., et al. (2019). RGB vegetation indices applied to grass monitoring: A qualitative analysis. *Agronomy Research*, *17*(2), 349–357.
- Bareth, G., Bendig, J., Tilly, N., Hoffmeister, D., Aasen, H., and Bolten, A. (2016). A comparison of UAV-and TLS-derived plant height for crop monitoring: Using polygon grids for the analysis of crop surface models (CSMs). *Photogrammetrie-Fernerkundung-Geoinformation*, *2*, 85–94.
- Bendig, J., Bolten, A., Bennertz, S., Broscheit, J., Eichfuss, S., & Bareth, G. (2014). Estimating biomass of barley using crop surface models (CSMs) derived from UAV-based RGB imaging. *Remote Sensing*, *6*, 10395–10412.
- Bendig, J., Willkomm, M., Tilly, N., Gnyp, M. L., Bennertz, S., Qiang, C., et al. (2013). Very high resolution crop surface models (CSMs) from UAV-based stereo images for rice growth monitoring in Northeast China. *International Archives of the Photogrammetry, Remote Sensing and Spatial Information Sciences*, *40*, 45–50.
- Bendig, J., Yu, K., Aasen, H., Bolten, A., Bennertz, S., Broscheit, J., et al. (2015). Combining UAV-based plant height from crop surface models, visible, and near infrared vegetation indices for biomass monitoring in barley. *International Journal of Applied Earth Observation and Geoinformation*, *39*, 79–87.
- Dandois, J., Olano, M., & Ellis, E. (2015). Optimal altitude, overlap, and weather conditions for computer vision UAV estimates of forest structure. *Remote Sensing*, *7*, 13895–13920.
- Mulla, D. J. (2013). Twenty five years of remote sensing in precision agriculture: Key advances and remaining knowledge gaps. *Biosystems Engineering*, *114*, 358–371.
- Panagiotidis, D., Abdollahnejad, A., Surový, P., & Chiteculo, V. (2017). Determining tree height and crown diameter from high-resolution UAV imagery. *International Journal of Remote Sensing*, *38*, 2392–2410.
- Ramirez, G. M., & Zullo Júnior, J. (2010). Estimation of biophysical parameters of coffee fields based on high-resolution satellite images. *Engenharia Agrícola*, *30*, 468–479.
- Rasmussen, J., Ntakos, G., Nielsen, J., Svendsgaard, J., Poulsen, R. N., & Christensen, S. (2016). Are vegetation indices derived from consumer-grade cameras mounted on UAVs sufficiently reliable for assessing experimental plots? *European Journal of Agronomy*, *74*, 75–92.
- Romeo, J., Pajares, G., Montalvo, M., Guerrero, J. M., Guijarro, M., & de la Cruz, J. M. (2013). A new Expert System for greenness identification in agricultural images. *Expert Systems with Applications*, *40*, 2275–2286.
- Sankaran, S., Khot, L. R., Espinoza, C. Z., Jarolmasjed, S., Sathuvalli, V. R., Vandemark, G. J., et al. (2015). Low-altitude, high-resolution aerial imaging systems for row and field crop phenotyping: A review. *European Journal of Agronomy*, *70*, 112–123.
- Xiao, J., & Moody, A. (2005). A comparison of methods for estimating fractional green vegetation cover within a desert-to-upland transition zone in central New Mexico, USA. *Remote Sensing of Environment*, *98*, 237–250.

A Prototype of Service Oriented Architecture for Precision Agriculture



S. Lanucara, A. Oggioni, S. Di Fazio and G. Modica

Abstract Precision Agriculture (PA) takes advantage of digital technologies to improve agricultural production and its economic and environmental sustainability. The main issues in the implementation and spread of PA include (a) harmonization and (b) interpretation of heterogeneous data collected from different sources; (c) interoperability of systems and data; (d) implementation of new algorithms and methodologies coming from research projects; (e) semantic enablement of meta-data. To help solve these issues we propose a software infrastructure prototype developed in the framework of the SATFARMING project, and based on Service Oriented Architecture (SOA) concept, free open-source software (FOSS), interoperability of data and web services through the accomplishment of international standards, semantic enablement of data description.

Keywords Precision Agriculture (PA) · Service Oriented Architecture (SOA) · Open Geospatial Consortium (OGC) · Free and Open Source Software (FOSS) · Interoperability · Semantic Enablement

1 Introduction

With an expected global population of over nine billion by 2050 (FAO 2009), food production is a major challenge that will be further exacerbated by climate change, reduced water supply, and the environmental impacts of intensive plant and livestock production. The United Nations Food and Agriculture Organization (FAO) recommends adopting digital technologies to increase productivity and address the risk of

S. Lanucara (✉) · A. Oggioni
Istituto per il Rilevamento Elettromagnetico dell'Ambiente, Consiglio Nazionale delle Ricerche (IREA-CNR), Via Bassini 15, 20133 Milan, Italy
e-mail: lanucara.s@irea.cnr.it

S. Di Fazio · G. Modica
Dipartimento di Agraria, Università degli Studi Mediterranea di Reggio Calabria, Località Feo di Vito, 89122 Reggio Calabria, Italy

© Springer Nature Switzerland AG 2020
A. Coppola et al. (eds.), *Innovative Biosystems Engineering for Sustainable Agriculture, Forestry and Food Production*, Lecture Notes in Civil Engineering 67,
https://doi.org/10.1007/978-3-030-39299-4_82

food security (FAO 2017). This is also in line with the recent Italian official guidelines for Precision Agriculture (PA) (Ministero delle politiche agricole alimentari, forestali e del turismo 2017).

From a technological perspective, PA is a data-intensive discipline characterized by the collection, storage, processing and dissemination/sharing of digital data collected from various sources with the aim to (1) analyze and understand the space-temporal variability in agricultural production inter and intra-field; (2) implement sound strategies for field management; (3) monitor the outcome of the implemented strategies. Several authors (e.g., Murakami et al. 2007; Nash et al. 2009; Nikkilä et al. 2010; Chen et al. 2015) have recently addressed main technological requirements for the diffusion of PA, which include: (a) harmonization of data; (b) friendly user interfaces; (c) simple methods for executing algorithms; (d) simple methods for implementing new methodologies; (d) interoperability between system; (e) scalability; (f) support for metadata. It is improbable that a single vendor will develop a comprehensive system that meets all these requirements; a free and open-source software (FOSS) platform could be a solution (Murakami et al. 2007). To tackle the aforementioned issues, we propose a prototype of SOA for PA developed in the framework of the SATFARMING project.

2 Materials and Methods

2.1 Study Area

The study area is a portion of territory within the Municipality of Jolanda di Savoia, a large plain located in the northern part of Italy (Fig. 1). The study area of about 40 km², has a flat morphology, with an average altitude of about -1 m a.s.l., in fact in the nineteenth century it was a territory covered by water and marshes that was reclaimed in the twentieth century. Within the study area we collected data on 27 fields planted with durum wheat, for a total of 512 Ha (Fig. 1).

2.2 Dataset

In the framework of SATFARMING project, we have collected different datasets concerning 27 fields cultivated with durum wheat sown in November 2018 and harvested in June 2019. The multi-dimensional data, collected from different sources and elaborated by advanced geomatic techniques, are relative to: (a) soil properties; (b) fields boundaries; (c) agronomic operations; (d) meteo-climatic variables; (e) earth observation. The collected data allowed us to test the interoperability of the prototype and also, are valuable, to analyze the space-time variability intra-fields and inter-fields.

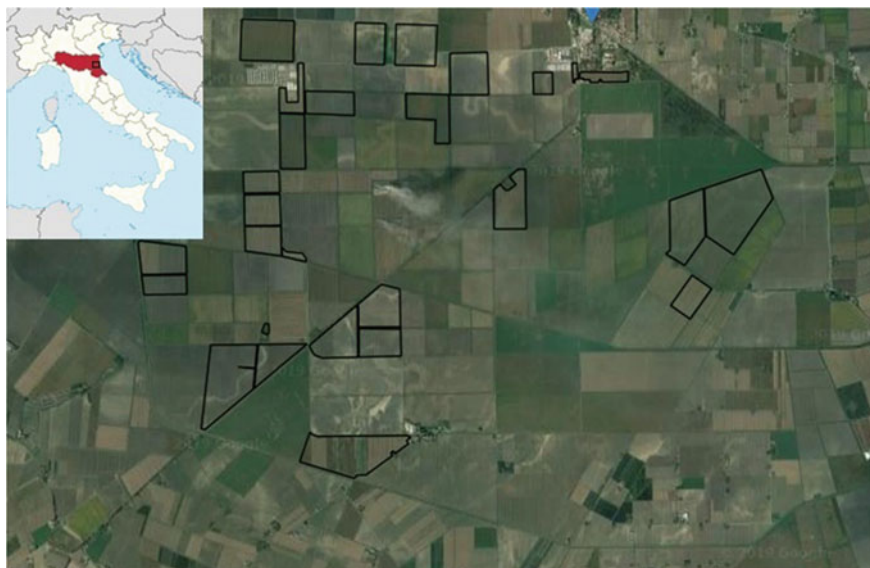


Fig. 1 Study Area, Jolanda di Savoia, upper left of figure; fields with durum wheat cultivar, black polygons, center of figure

Table 1 Data types, files format, and source of data collected

Data type	Format	Source
Fields	Shapefile	Digitalization
Cultivation plan	Shapefile	Digitalization
Soil pedology	Shapefile	Sampling
Soil resistivity	GeoTIFF	Resistivity sensors
Agronomic operations	Shapefile	Agricultural machines
Meteo-climatic	Json	FieldClimate API
Earth observation	GeoTIFF	Sentinel open access hub Planetscope API

The complete list of data types, file format, and sources are shown in Table 1.

2.3 Service Oriented Architecture

Service Oriented Architecture (SOA) can be defined as multi-tier architecture comprised of services: (a) independent from software; (b) interoperable; (c) discoverable and (d) reusable (Erl 2005). Several authors (Papazoglou 2003; Erl 2005; Papazoglou et al. 2007), proposed SOA composed by three tiers: (a) storage, for data; (b)

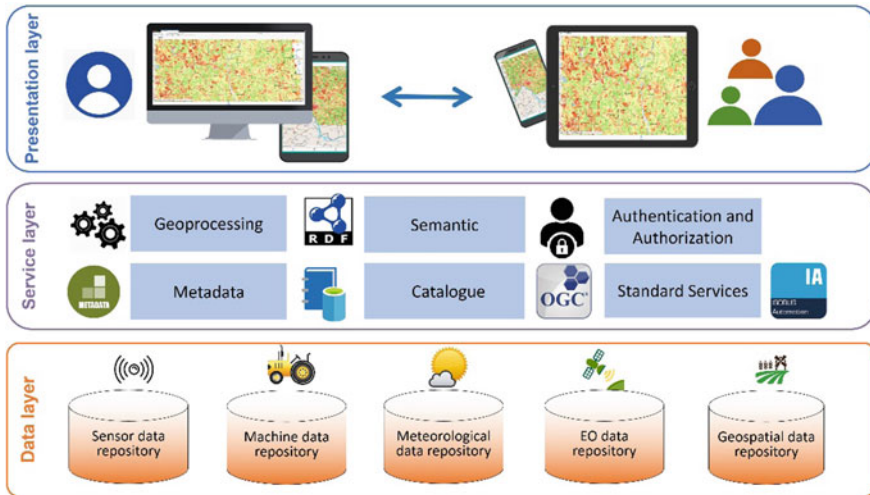


Fig. 2 General scheme of the proposed modular, three-tier Service Oriented Architecture (SOA) based on free and open-source software (FOSS)

service, for business logic and service interoperability (c) front-end, for graphical user interfaces (GUI). The same architecture is envisaged by INSPIRE EU Directive specifications (European Commission 2007).

Based on these premises, and on previous researches (Lanucara et al. 2018; Modica et al. 2016; Pepe et al. 2019) we designed a three-tier SOA, composed by different modules (Fig. 2) independent from software that enables them:

- *Data archive*: It allows the storage of data in the geospatial database and structured file system. Data can be provided from: (i) local sensors such as, for example, meteorological sheds, humidity sensors, multi-parametric sensors; (ii) machinery such as yield data, agronomic application data; (iii) earth observation analysis from satellites, such as Normalized Difference Vegetation Index (NDVI), Modified Soil-Adjusted Vegetation Index (MSAVI) and other vegetation index; (iv) other geospatial data such as field and parcel boundaries, soil data, variable rate technology (VRT) prescription maps; (v) provider of data as service (i.e., REST API) such as meteorological data and weather forecasts.
- *Semantic*: Enables the creation and management of code-lists, controlled vocabularies, and thesauri used by meta-dating systems for a multilingual semantic enabling data descriptions.
- *Metadata*: Enables the meta-dating of data according to standard profiles, using the Semantic module for data description, and the conversion between metadata schemes.
- *Catalogue*: Performs the collection and cataloging of data and relevant metadata, allowing univocal and detailed research of web services and data.
- *Services*: Transforms data into interoperable web services.

- *Geo-Processing*: Enables the execution of geospatial processing and algorithms for the production of digital data from knowledge, such as, for example, delineation of management zones, prescription maps for agronomic operation (i.e., VRT maps for soil treatment, sowing, fertilization, plant defense, differential harvest).
- *Authorization and authentication*: Enable authentication and authorization of users, data, and applications.
- *Front-End*: Access portal allowing the users to insert, view, query, process, and download data.

2.4 Service and Data Interoperability

The interoperability of services and related data is obtained by adopting international recognized standards. To this regards, the Open Geospatial Consortium (OGC) and the International Organization for Standardization (ISO) work from more than twenty years to improve geospatial, sensor, satellite and agricultural machinery data interoperability. In this work, taking advantage of existing ISO and OGC standard, we have identified which standard is most suitable for the following issues:

- *Sensors data*. OGC Sensor Web Enablement (SWE) allows us to search and retrieve data such as weather time series, soil moisture and also allows the semantic description of the different employed sensors.
- *Agricultural machinery data*, such as application data for fertilizers, seeding, weeding and yield. The reference standard is the protocol ISOBUS (ISO 11783, commonly referred to as standard “ISO Bus” or “ISOBUS”) (www.iso.org/standard/57556.html, last access 10 July 2019). By this standard, data can be provided to, or retrieved from, agricultural machinery, i.e. prescription data for the different agronomic operations. Also, this standard enables telemetry for agricultural machinery.
- *Earth observation data* such as satellite data and data collected by unmanned aerial vehicles (UAVs) and their related products, such as vegetation indices maps (NDVI, MSAVI, etc.). In this case, the most appropriate standards are (a) OGC Web Map Service (WMS), with multi-temporal enabling allowing their thematic spatial representation; (b) OGC Web Coverage Service (WCS) for data extraction and downloading.
- *Other geospatial data*, such as field and parcel boundaries identification. The most appropriate standards are the WMS for their thematic spatial representation, the Web Feature Service (WFS) standard for their downloading and updating.

2.5 Free and Open Source Software

Since today there are many FOSS for geospatial application (Brovelli et al. 2017), in choosing the one that fitted our needs, we filtered them according to the following criteria: (a) multi-dimensional geospatial data support; (b) compatibility and support with OGC and ISOBUS standards; (c) well-structured developer community support; (d) easy implementation. Each software enables the functionalities of the modules described in Sect. 2.3. In particular, PostGIS enable the storage and indexing of geospatial (earth observation, sensors, agricultural machinery, meteorological, weather forecast, elaboration) data and related meta-data, while EDI (Pavesi et al. 2016) facilitates the editing of rich and standard metadata for geospatial resources. Apache Jena allows the enabling of the semantic web, Apache Airflow programmatically schedules workflows enabling the execution of elaboration pipeline, 52° North WPS enables the deployment of geo-processes on the web supporting OGC Web Processing Standard (WPS), Geonetwork OpenSource facilitates the creation of a web catalogue of resource also supporting the OGC Catalogue Service for the Web Standard (CSW). Moreover, GeoServer and 52° North Open Source enable the transformation of geospatial and sensor data into interoperable OGC web services (WMS, WFS, WCS, TMS, SWE), respectively, and KeyCloak allows for authentication and authorization of users, data and applications also supporting OAUTH2 and Open-ID protocols.

The complete list of software, their related modules, and the URL of source code are summarized in Table 2.

Table 2 Modules and corresponding software implemented in the proposed Service Oriented Architecture. For each of them, the source code URL is also provided

Module	Software	Source code URL
Data archive	PostGIS	https://github.com/postgis/postgis
Geo-processing	52° North WPS Apache Airflow	https://github.com/52North/WPS https://github.com/apache/airflow
Semantic	Apache Jena	https://github.com/apache/jena
Metadata	EDI	https://github.com/SP7-Ritmare/EDI-NG_client
Catalogue	GeoNetwork OpenSource	https://github.com/geonetwork
Services	Geoserver 52° North SOS	https://github.com/geoserver https://github.com/52North/SOS
Authorization and authentication	Keycloak	https://github.com/keycloak/keycloak

The technological platform on which the prototype was implemented is a cloud environment, provided by IBF Servizi S.p.A. The cloud environment allows the creation of virtual applications and their use in a simple and intuitive way by a GUI. The environment includes services for data security, disaster recovery, and backup of the virtual application. Within the cloud, we implemented the SOA by docker (<https://docs.docker.com>) which provides: (a) scalability; (b) independence from operative system; (c) easy software deployment; (d) and network communication among modules.

It is worthy of notice that, about ISOBUS services, we did not find a FOSS solution. Instead, we identified a programming library, the ISOAgLib (<http://isoaglib.com>), that implements all functions according to the ISOBUS standard, thus facilitating the access to the ISOBUS software development.

3 Discussion and Final Remarks

PA can improve the sustainability of agriculture productions; anyway the spread of PA practices is hindered by many issues described in Sect. 1. To overcome this issues, we: (a) developed a prototype of SOA composed by three tiers and different modules, described in Sect. 2.3; (b) identified the international standards to improve data and service interoperability, described in Sect. 2.4; (c) identified and implemented the FOSS that provides the modules functions, described in Sect. 2.5.

The methodology we adopted can improve: (a) standardization, exploiting international reference standards, (b) scalability, since the presence of separate modules makes easier to scale the architecture or a particular module, (c) decoupling, since the infrastructure and architecture are divided into various modules, and so the FOSS can be freely coupled, (d) data identification by meta-data and semantic enablement, (e) implementation of new methods by data processing.

A significant point that favors a FOSS modular solution is that PA still has many uncertainties that are the focus of current research. As a result, new workflow, methodologies, and algorithms could need to be incorporated into SOA as they become accessible. Moreover, the FOSS solution, i.e. without licensing fees, could represent a reliable platform to manage PA even in low-income concerns, regions or countries.

Through the SOA prototype described here, it is possible to search, visualize, analyze and download data from different sources such as (a) sensors in the field, (b) Earth observation, (c) agricultural machinery (Fig. 3), (d) processed on GIS systems, (e) service providers by OGC/ISOBUS standards. It is also possible to implement and run data processing algorithms for the creation of digital products such as: (a) satellite vegetation indices (Fig. 4), (b) management unit zones (MUZs) (Fig. 5), (c) intra- and inter-field variability, (d) prescription maps, (e) comparison of prescription maps, and (f) application maps. Finally, it is possible to enable tools such as semantic dashboards (Lanucara et al. 2018) for dissemination of PA knowledge. Summing up, the SOA prototype could be used as a comprehensive tool for monitoring and managing PA practices and as spatial decision support system (SDSS). In this latter

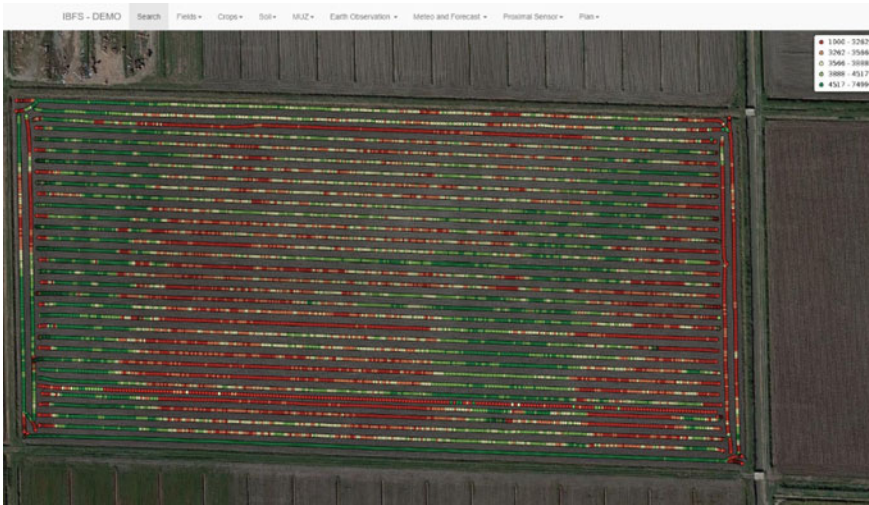


Fig. 3 Graphical user interface showing agricultural machine data, yield, for one field

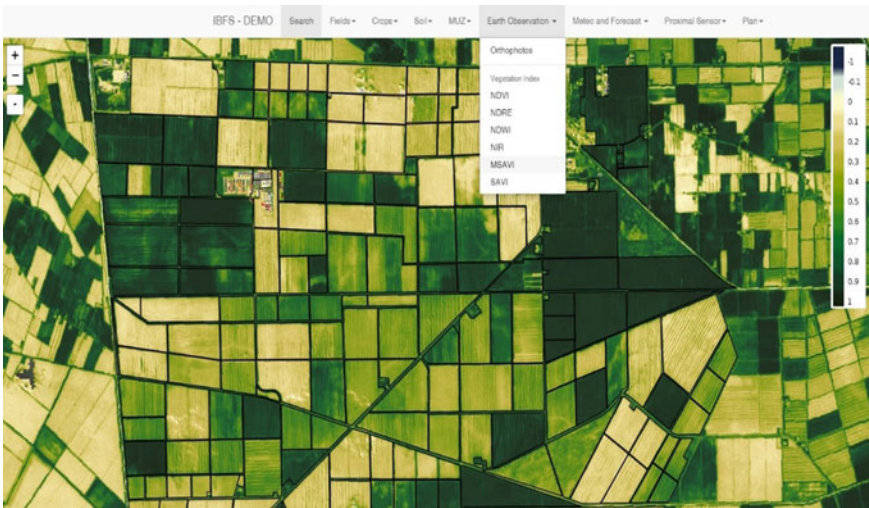


Fig. 4 Graphical user interface showing the module allowing the satellite monitoring implemented on a set of several vegetation indexes, such as the Modified Soil-Adjusted Vegetation Index (MSAVI). Superimposed to the VI map, the field boundaries (showed in black in the figure) are also provided on the platform



Fig. 5 Graphical user interface showing the module allowing the elaboration of Management Unit Zones (MUZs) for two fields cultivated with durum wheat

case, a specific multi-criteria module can be implemented to assess the suitability of a given territory for a specific crop (e.g., Modica et al. 2014, 2016).

Acknowledgements The activity presented in the paper is part of the research grant SATFARMING-2017–19.

References

- Brovelli, M. A., Minghini, M., Moreno-Sanchez, R., & Oliveira, R. (2017). Free and open source software for geospatial applications (FOSS4G) to support future earth. *International Journal of Digital Earth*, 10, 386–404.
- Chen, N., Zhang, X., & Wang, C. (2015). Integrated open geospatial web service enabled cyber-physical information infrastructure for precision agriculture monitoring. *Computers and Electronics in Agriculture*, 111, 78–91.
- Commission, European. (2007). Establishing an Infrastructure for Spatial Information in the European Community (INSPIRE), Directive 2007/2/EC, Official. *Journal of European Union*, 50, 1–14.
- Erl, T. (2005). *Service-oriented architecture: Concepts, technology, and design*. Prentice Hall PTR.
- FAO. (2009). How to feed the world in 2050, Rome: s.n.
- FAO. (2017). Information and Communication Technology (ICT) in Agriculture, Rome: s.n.
- Lanucara, S., Fugazza, C., Tagliolato, P., & Oggioni, A. (2018). Information systems for precision agriculture: Monitoring computation of prescription maps. *ERCIM News*, 113, 24–25.
- Ministero delle politiche agricole alimentari, forestali e del turismo. (2017). Linee guida per lo sviluppo dell'Agricoltura di Precisione in Italia, Rome: s.n.

- Modica, G., Laudari, L., Barreca, F., & Fichera, C. R. (2014). A GIS-MCDA based model for the suitability evaluation of traditional grape varieties: The case-study of 'Mantonico' grape (Calabria, Italy). *International Journal of Agricultural and Environmental Information Systems*, 5, 1–16. <https://doi.org/10.4018/ijaeis.2014070101>.
- Modica, G., Pollino, M., Lanucara, S., La Porta, L., Pellicone, G., Di Fazio, S., et al. (2016). Land suitability evaluation for agro-forestry: Definition of a web-based multi-criteria spatial decision support system (MC-SDSS): Preliminary results. In *International Conference on Computational Science and Its Applications—ICCSA 2016. Lecture Notes in Computer Science*, vol 9788. Cham: Springer.
- Murakami, E., Saraiva, A. M., Ribeiro, L. C. M., Cugnasca, C. E., Hirakawa, A. R., & Correa, P. L. P. (2007). An infrastructure for the development of distributed service-oriented information systems for precision agriculture. *Computers and Electronics in Agriculture*, 58, 37–48.
- Nash, E., Korduan, P., & Bill, R. (2009). Applications of open geospatial web services in precision agriculture: A review. *Precision Agriculture*, 10, 546–560.
- Nikkilä, R., Seilonen, I., & Koskinen, K. (2010). Software architecture for farm management information systems in precision agriculture. *Computers and Electronics in Agriculture*, 70(2), 328–336.
- Papazoglou, M. P. (2003). Service-oriented computing: Concepts, characteristics and directions. In *Proceedings of the Fourth International Conference on Web Information Systems Engineering, 2003. WISE 2003*. IEEE.
- Papazoglou, M. P., Traverso, P., Dustdar, S., & Leymann, F. (2007). Service-oriented computing: State of the art and research challenges. *Computer*, 40(11), 38–45.
- Pavesi, F., Basoni, A., Fugazza, C., Menegon, S., Oggioni, A., Pepe, M., Tagliolato, P. and Carrara, P., 2016. EDI—A Template-Driven Metadata Editor for Research Data. *Journal of Open Research Software*, 4(1), e40. <http://doi.org/10.5334/jors.106>.
- Pepe, M., Candiani, G., Pavesi, F., Lanucara, S., Guarneri, T., & Caceffo D. (2019). SDI and smart technologies for the dissemination of EO-derived information on a rural district. *New Metropolitan Perspectives. ISHT 2018. Smart Innovation, Systems and Technologies*, vol 100. Cham: Springer.

A Method to Implement a Monitoring System Based on Low-Cost Sensors for Micro-environmental Conditions Monitoring in Greenhouses



Elio Romano, Massimo Brambilla, Pietro Toscano and Carlo Bisaglia

Abstract The precise monitoring of the inner microclimate of a greenhouse implies an increase of the production costs following the expensive needed sensor arrays. Currently, there is availability of low-cost sensors and cards for data storage and processing, but their application in real scale facilities is still under study. This research aimed to find a solution to manage and implement the outcome of various information (i.e. luminosity as well as air humidity and temperature) on the internal environment of a tunnel greenhouse to point out the most critical dynamics occurring during the growth cycle of basil plants in summer. Placing low-cost sensors inside a tunnel greenhouse made it possible to acquire data with an adequate rate (0.1 min^{-1}) and spatiotemporal distribution throughout the facility. Data storage and processing took place thanks to an on purpose created weather station based on Arduino Yun Rev2 board. The highest variability of air temperature and moisture inside the greenhouse occurred when the solar radiation begins to heat the cover of the greenhouse (between 6.00 and 7.00 AM) and few hours after the maximum peak of solar radiation ($843.4 \pm 133.3 \text{ W/m}^2$). Low-cost sensors combined with spatial fitting of the data provided insights about the effective microenvironmental conditions occurring on daily basis. This, implemented with IoT technologies, will be the base for the realization of economic monitoring systems.

Keywords Air temperature · Air moisture · Protected crops · Arduino board · Remote control

1 Introduction

Greenhouses, protecting plants against diseases and adverse environmental conditions, represent a feasible solution as they make it possible to control the optimal temperature for crop cultivation (Oliveira et al. 2016). However, changes in climate

E. Romano (✉) · M. Brambilla · P. Toscano · C. Bisaglia
Consiglio per la ricerca in agricoltura e l'analisi dell'economia agraria (CREA), Research Centre for Engineering and Agrofood Processing, Via Milano 43, 24047 Treviglio, BG, Italy
e-mail: elio.romano@crea.gov.it

© Springer Nature Switzerland AG 2020

A. Coppola et al. (eds.), *Innovative Biosystems Engineering for Sustainable Agriculture, Forestry and Food Production*, Lecture Notes in Civil Engineering 67,
https://doi.org/10.1007/978-3-030-39299-4_83

775

can interact with other greenhouse stressors and affect plant growth, yield and quality of produce (Gruda et al. 2019).

Researchers have shown an increased interest in monitoring greenhouse temperature using different sensor configurations, hardware architectures, and control techniques (Shamshiri et al. 2018) as the non-uniform distributions of microclimate parameters affect the greenhouse environment impairing crops' production and quality. Temperature and irradiation are considered as two major factors relating to microclimatic effects (Ahemd et al. 2016).

Currently, monitoring greenhouse temperature is complex in terms of sensing technology (Postolache et al. 2012). Increasing the number of installed sensors, if on the one hand results in improved monitoring capacity, on the other causes engineering and management costs to increase. Furthermore, the sensors' exposure to environmental factors (e.g. direct sunlight and humidity) may lead them to malfunction or damage with unexpected failures and economic damage for farmers. Environmental modelling and virtual sensing may represent a solution to this (Guzmán et al. 2018) provided that high calculation power is available (Carvajal-Arango et al. 2016). The sensing concept has enabled the production of robust, small, and reliable low-cost sensors that, conveniently connected to any hub (e.g. Arduino and Raspberry boards), make it possible to implement a monitoring network with reduced power consumption, maintenance and complexity (Sowmya and Praveen Sam 2018).

The presented study deals with the set-up of a simple, low cost, Arduino based system to monitor the environmental parameters in a small-scale greenhouse to evaluate the feasibility of the low-cost sensors for the continuous monitoring aimed at achieving optimum plant growth and yield.

2 Materials and Methods

A greenhouse (12 m long, 2.5 m wide and 2 m high), made of a metal structure and with plastic covering, was set up at the CREA-IT facility of Treviglio (45°31'17.18 N; 09°33'50.82 E). Inside it, 24 pots of basil plants, grown in a substrate made of peat and perlite (50% v/v), were placed on a shelf 1 m above the ground high and as long as the greenhouse. It was subdivided into three longitudinal sectors (S1 and S3—lateral; S2—central), so that each sector had 8 identical pots.

The low-cost sensors used to monitor the greenhouse micro-environment were all based on the Arduino board (www.arduino.cc) and made it possible to measure air and soil moisture content and the amount of incident light.

The YL-69 hygrometer sensor (Fig. 1a) assessed the soil moisture measurements. It measures the soil resistance (Rs), which is directly proportional to the moisture present in the soil (Kolapkar et al. 2016). To verify the difference in humidity of the soil between the sectors and in the same thesis, three humidity sensors have been positioned for each sector compared.

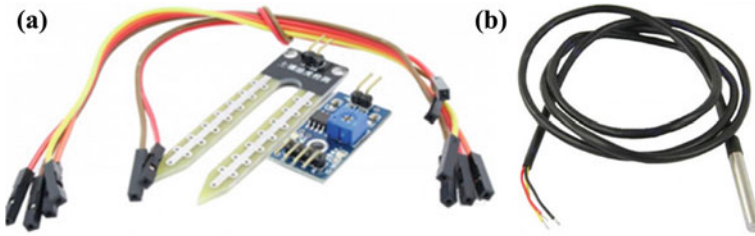
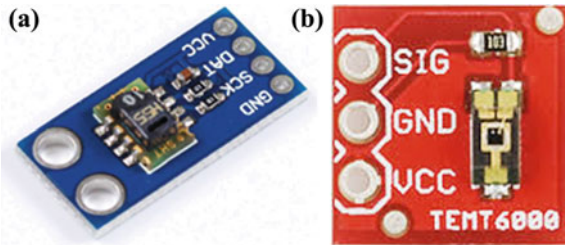


Fig. 1 The modules to measure the soil moisture content (a) and the probe to read the soil temperature (b)

Fig. 2 The CJMCU-SHT10 sensor to read the air moisture and temperature (a), the TEMT 6000 sensor for light intensity measurement (b)



The *DS18B20* probe (Maxim Integrated Products, Inc., USA—Fig. 1b) measured the temperature of the growing substrate. Its precision is $\pm 0.5\text{ }^{\circ}\text{C}$ in the range from $-10\text{ }^{\circ}\text{C}$ to $+85\text{ }^{\circ}\text{C}$. The probe is made of stainless steel, however since it had to remain immersed in the ground, the surface was previously covered with a layer of Parafilm® (Bemis Company, Inc., USA). To study the homogeneity of the temperature in the ground over the entire observed surface and to detect any differences throughout the length of the greenhouse, three soil temperature sensors were inserted into just as many pots placed in the center of the shelf of the series in each sector.

The sensor *CJMCU-SHT10* (Sensirion AG, CH—Fig. 2a) made it possible recording air moisture and temperature. Both sensors were seamlessly coupled to a 14 bit analog to digital converter and a serial interface circuit. Three tunnel sections of 2 meters in length were chosen: within each section, six air humidity and temperature sensors were placed in three different heights from the shelf surface where pots were placed (30, 60, 90 cm).

The amount of incident light was monitored by a *TEMT6000* sensor (Vishay Semiconductor GmbH, Germany—Fig. 2b). It is based on a phototransistor that produces a voltage output between 0 V and +5 V that is directly proportional to the incident light.

Air temperature and moisture acquisitions occurred at the rate of 6 acquisitions per hour. The recorded data, after preliminary processing with MS Excel spreadsheet, underwent statistical processing using R software (R Core Team 2018) and Minitab 17® (Minitab 2010), to study averages, standard deviations and coefficient of variation (CV%). Analysis of variance followed by Tukey and Duncan post hoc comparisons ($p < 0.05$) were carried out on air and substrate temperature and air

humidity. To study the distribution of the microclimate inside the greenhouse, the Surfer® software (Golden Software, LLC) was used for the realization of interpolated graphs through the kriging algorithm (Wackernagel 1995) after data standardization with respect to their average and standard deviation.

3 Results and Discussion

The top part of Fig. 3 shows the hourly average air and soil temperatures together with air relative humidity (RH). In the bottom one there are the hourly CVs of the same variable that allowed choosing the hours to study the occurring dynamics.

Soil moisture data could not be processed as the chosen sensor turned out to be very sensitive to the variations resulting from pot irrigation. As a matter of fact, to grow basil seedlings, fertilizing solutions with hydro soluble mineral elements were used. These might have caused a failure in sensor response causing it to misread soil moisture because of both the effect dissolved ions and solids have on Rs (Cloete et al. 2016; Roberts Alley 2007) and the unavoidable oxidation process that affects resistive sensors performance and lifespan (Yeow Tan et al. 2018).

Substrate temperature records were in the 16.6–36.6 °C range: the position of the pots along the greenhouse significantly affected the maximum average temperatures achieved in each sector (32.3 °C on average for S1 and S3 and 28.0 °C for S2) but it turned out not to be significant minimum averages (18.8–20.1 °C range). However, with reference to the hourly averages, it turned out that at 8.00 AM the high CV results from the difference between S1 and S3 (29.4 ± 3.9 °C and 26.1 ± 5.5) and S2 (23.2 ± 2.1) while at 6.00 PM the lowest CV comes from the substantial homogeneity of temperatures along the greenhouse (25.6 ± 3.8 °C, 25.8 ± 2.6 °C and 25.8 ± 4.0 °C for S1, S2 and S3).

Plotting the isocurves of the average t° and RH throughout greenhouse width and height made it possible to evaluate the dynamics of air temperature and RH distribution longitudinally and transversely to the greenhouse volume, (Fig. 4). As expected, the observed temperature and humidity showed two opposite behaviors. When the CV of micro-climatic observations was higher (8.00 AM and 3.00 PM for temperature and RH) the analysis pointed out a high variability of values lower than the related hourly average value. In the hours of minimum CV (6.00 PM and 5.00 AM for temperature and RH), in all the observed sections, the RH had a decrease in the areas most close to the average value, therefore to the zero value. The temperature instead showed the opposite, but with values higher than the average value.

As expected, such variabilities occurred when the solar radiation began to heat the cover of the green-house (between 6.00 and 7.00 AM) and few hours after the maximum peak of solar radiation (843.4 ± 133.3 W m⁻²). The analysis of the variance carried out on the response values of the temperature and of the recorded humidity showed statistical significance for the effect of the position of the sensors both longitudinally and transversally. The Duncan test, conducted in both the directions of

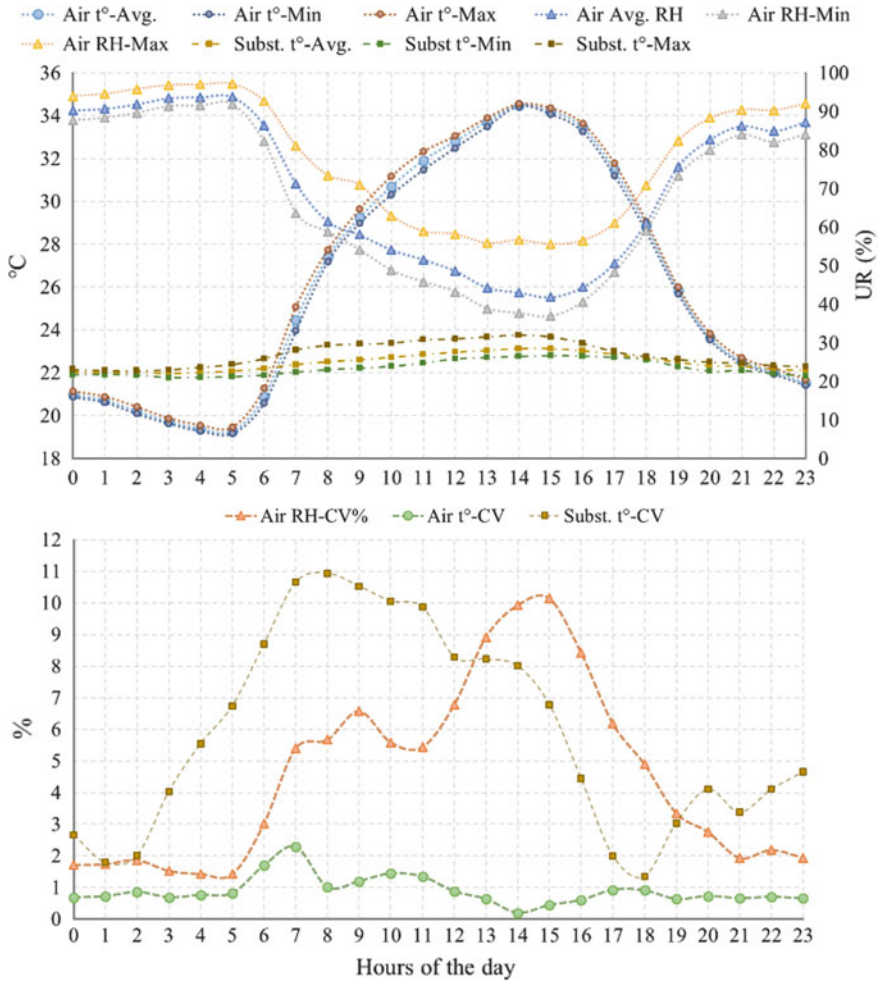


Fig. 3 Trends of average hourly temperatures of air and substrate and relative humidity of air (above) together with the related per cent CV (below) measured during the observation period

sensor’s distribution, showed a statistically significant difference between the three sectors of the greenhouse.

The tests carried out with the *TEMT6000* sensor aimed to verify its capability in measuring the amounts of incident light. It resulted that: if, on the one hand, it could react very well to small light changes at sunrise and sunset, on the other, it was found not to be able to produce accurate during the daytime despite the reported successful application in agriculture (Ray 2018). In our case, in line with the findings of Gao et al. (2019), the reduced sensitivity range of the sensor, 0–250 lx (Kumar 2014) caused it to give rise to unacceptable illuminance deviation under direct sunlight when its response compares with the agrometeorological data from ARPA Lombardia (www.arpalombardia.it). However, with scattered sunlight, the algorithm the sensor

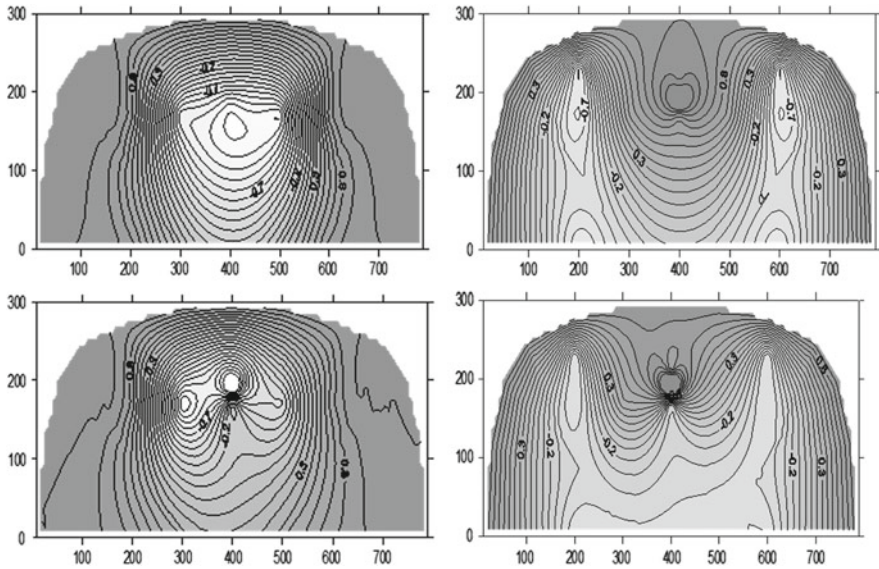


Fig. 4 Example of the distributions of air temperature (on the left) and humidity (on the right) throughout the central sector (S2) when the CV of the acquisitions was highest (above) and lowest (below). Horizontal and vertical axes report the width and the height (cm) of the inner greenhouse space

manufacturer proposes, followed quite well the illuminance trend even without cosine correction and this led us deepening the sensor responsivity in terms of $mV\ lx^{-1}$ comparing the output of the sensor (mV) with the illuminance (lx) derived from the official data. The ANOVA pointed out that sensor responsivity significantly changes during the day (Table 1) so that it can be possible setting up a specific calibration process for this sensor.

Table 1 The TEMT6000 average hourly responsivity ($mV\ lx^{-1}$). Means that do not share a letter are significantly different ($p < 0.05$)

Hour	$mV\ lx^{-1}$		Hour	$mV\ lx^{-1}$	
5	0.49 ± 0.25	a	14	0.014 ± 0.02	d
6	0.15 ± 0.06	b, c	15	0.023 ± 0.05	d
7	0.074 ± 0.03	c, d	16	0.021 ± 0.03	d
8	0.032 ± 0.02	c, d	17	0.032 ± 0.04	c, d
9	0.020 ± 0.01	d	18	0.054 ± 0.08	c, d
10	0.016 ± 0.02	d	19	0.086 ± 0.07	c, d
11	0.015 ± 0.02	d	20	0.214 ± 0.24	b
12	0.011 ± 0.02	d	21	0.37 ± 0.16	a
13	0.010 ± 0.01	d			

4 Conclusions

In this study the use of a low-cost Arduino based suite of sensors for greenhouse microclimate monitoring is presented. Based on the results, the system was able to detect the different conditions existing in each greenhouse sector during the day and to catch the dynamics of air humidity and air and substrate temperatures so that it provided insights about the effective microenvironmental conditions occurring on daily basis. However, further improvements of the system architecture need to be set up in particular with reference to data storage and processing that could be improved thanks to wireless connection and on line processing software whose results could support the farm management with IoT technologies. Further studies on sensor calibration are however required to better point out the reliability and the efficacy of this kind of sensors.

Acknowledgements This work was supported by the Italian Ministry of Agriculture (MiPAAF) under the AGROENER project (D.D. n. 26329, 1st April 2016)—<http://agroener.crea.gov.it/>.

The authors are very grateful to Mr. Gianluigi Rozzoni, Mr. Ivan Carminati, Mr. Stefano Basile, Mr. Alex Filisetti, Mr. Elia Premoli and Mr. Walter Antonioli for their valuable help in the setting up of the experimental greenhouse.

References

- Ahmed, H. A., Al-Faraj, A. A., & Abdel-Ghany, A. M. (2016). Shading greenhouses to improve the microclimate, energy and water saving in hot regions: A review. *Scientia Horticulturae*, 201, 36–45.
- Carvajal-Arango, R., Zuluaga-Holguín, D., & Mejía-Gutiérrez, R. (2016). A systems-engineering approach for virtual/real analysis and validation of an automated greenhouse irrigation system. *International Journal on Interactive Design and Manufacturing*, 10, 355–367.
- Cloete, N. A., Malekian, R., & Nair, L. (2016). Design of smart sensors for realtime water quality monitoring. *IEEE Access*, 4, 3975–3990.
- Gao, Y., Cheng, Y., Zhang, H., & Zou, N. (2019). Dynamic illuminance measurement and control
- Gruda, N., Bisbis, M., & Tanny, J. (2019). Influence of climate change on protected cultivation: Impacts and sustainable adaptation strategies—A review. *Journal of Cleaner Production*, 225, 481–495.
- Guzmán, C. H., Carrera, J. L., Durán, H. A., Berumen, J., Ortiz, A. A., Guirette, O. A., Arroyo, A., Brizuela, J. A., Gómez, F., Blanco, A., Azcaray, H. R., & Hernández, M. (2019). Implementation of virtual sensors for monitoring temperature in greenhouses using CFD and control. *Sensors*, 19, 60. <https://doi.org/10.3390/s19010060>
- Kolapkar, M. M., Khirade, P. W., & Sayyad, S. B. (2016). Design and development of embedded system for measurement of humidity, soil moisture and temperature in Polyhouse using 89E516RD microcontroller. *International Journal of Advanced Agricultural Sciences and Technology*, 5(1), 96–110.
- Kumar, S. (2014). *Mobile sensor systems for field estimation and “hot spot” identification*. Thesis: Ph.D., Massachusetts Institute of Technology, Department of Mechanical Engineering, 2014. <https://dspace.mit.edu/handle/1721.1/87977>. Accessed June 2019
- Minitab. (2010). *Minitab 17 statistical software*. State college, PA: Minitab.

- Miranda, J., Ponce, P., Molina, A., & Wright, P. (2019). Sensing, smart and sustainable technologies for Agri-Food 4.0. *Computers in Industry*, 108, 21–36.
- Oliveira, J., Boaventura-Cunha, J., & Oliveira, P. M. (2016). Automation and control in greenhouses: State-of-the-art and future trends. In *CONTROL 2016, Lecture Notes in Electrical Engineering*; Springer: Berlin/Heidelberg, Germany, 2017; Volume 402, pp. 597–606.
- Postolache, O., Pereira J. M., Girão P. S., & Monteiro A. A. (2012). Greenhouse environment: Air and water monitoring, In *Smart Sensing Technology for Agriculture and Environmental Monitoring*. Mukhopadhyay, S. C. Ed. 81–102. Springer.
- R Core Team. (2018). R: A language and environment for statistical computing. R Foundation for Statistical Computing, Vienna, Austria. URL <https://www.R-project.org/>.
- Ray, P. P. (2018). Internet of Things-based approximation of sun radiative-evapotranspiration models. *Journal of Agrometeorology*, 20(2), 171–173.
- Roberts, Alley E. (2007). Pollutant classification. *Water quality control handbook*, Alexandria (2nd ed., pp. 42–51). Virginia: McGraw-Hill.
- Shamshiri, R., Kalantari, F., Ting, K., Thorp, K. R., Hameed, I. A., Weltzien, C., et al. (2018). Advances in greenhouse automation and controlled environment agriculture: A transition to plant factories and urban agriculture. *International Journal of Agricultural and Biological Engineering*, 11, 1–22.
- Sowmya, D., & Praveen Sam, R. (2018). Low Cost and PI based smart home garden watering system using IoT. *International Journal of Recent Technology and Engineering (IJRTE)*, 7(6S), 399–402.
- Used for smart lighting with LED, *Measurement*, 139, 380–386
- Wackernagel, H. (1995) Ordinary Kriging. In *Multivariate Geostatistics*. Springer, Berlin, Heidelberg
- Yeow Tan, W., Lung Then, Y., Long Lew, Y., & Siang Tay, F. (2018). Newly calibrated analytical models for soil moisture content and pH Value by Low-Cost YL-69 hygrometer sensor. *Measurement*. <https://doi.org/10.1016/j.measurement.2018.10.071>.

An Innovative Methodology to Be More Time-Efficient When Analyzing Data in Precision Viticulture



Monica F. Rinaldi, Raimondo Gallo, Gabriele Daglio and Fabrizio Mazzetto

Abstract Remote Sensing tools in Precision Viticulture to detect disease levels of plants implies big data-sets and time-consuming analysis of data. In this study, we used remote images collected by an Unmanned Aerial Vehicle equipped with a Micasense RedEdge.MXTM multispectral camera and a Terrestrial Laser Scanner (TLS). These tools gave us large amounts of data in a short period. The aim of this research was to develop a methodology that shortens the post-processing phase of data. The data sets were taken from a vineyard during two crop monitoring surveys in June and August 2018. The monitored vineyard is situated in the Piedmont region (Italy). As a first step in the data analysis procedures, we used photogrammetry approaches, as well as the Digital Terrestrial Model and the Digital Surface Model to detect the shape of single plants. The achieved results were then validated with the analysis obtained through the TLS. We then analyzed the reflectance of the canopy using open source software, to detect changes in the pixels about the reflectance curve between healthy plants and plants with disease. We expect that the proposed methodology will help us to be time-efficient and to detect condition of vegetative changes.

Keywords Unmanned aerial vehicle (UAV) · Terrestrial LIDAR scan (TLS) · Multispectral camera

1 Introduction

Precision viticulture nowadays implies big datasets and the possibility to choose many different sensors that describe the land situation remotely. Industry 4.0 and real-time data require not only experts taking data and analyzing the information (Mazzetto et al. 2019), but also software and post-processing methodologies able to analyze datasets and give output in a short period of time (Rosell et al. 2011).

M. F. Rinaldi (✉) · R. Gallo · G. Daglio · F. Mazzetto
Faculty of Science and Technology - Fa.S.T, Free University of Bozen – Bolzano, Piazza
Università 5, 39100 Bolzano, Italy
e-mail: MonicaFernanda.Rinaldi@unibz.it

© Springer Nature Switzerland AG 2020
A. Coppola et al. (eds.), *Innovative Biosystems Engineering for Sustainable Agriculture, Forestry and Food Production*, Lecture Notes in Civil Engineering 67,
https://doi.org/10.1007/978-3-030-39299-4_84

Participatory Sensing (PS), through which geodata is gathered using mobile devices and shared with peers, will increase this necessity (Kotovirta et al. 2012; Mark et al. 2016). In our project we used UAS transporting multispectral cameras, which require not only a licensed pilot but also trained technicians who can analyze the datasets and using appropriate and calibrated crop models. The aim of this study was to find and develop a methodology that shortens the post-processing phase of data. Our team decided to explore possibilities to interpret data in a way that allows technicians and owners to have a quick overview of the situation of their vineyard and detect changes in the canopy.

2 Methods

2.1 Study Area and Sites

The study area is a vineyard with two varieties of grapevine (Dolcetto and Barbera), situated in the Ovada municipality (Piedmont region, North-west of Italy) placed at 470448.80 (E), 4947856.1721 (N), UTM32N-ETRS89 (Fig. 1). This area is an ancient region of wine production, where the Dolcetto DOC is being cultivated on the hills below 600 m.a.s.l. The vineyard area was approximately 2.75 ha. The vineyard is a trellis training system with 2.8 m between rows and approximately 0.9 m between plants each row. The surveys were conducted in June and August 2018, when the grapevine was in the following growth stages: fruit set (stage BBCH 71) and beginning of ripening (BBCH 81). The particularity of this vineyard is the level of infected plants with the Esca disease produced by *Phaeoacremonium aleophilum*, *Phaeoaniella chlamydospora* and *Fomitiporia punctata*. This disease produces chlorotic and necrotic spots on leaves and dark brown areas on woody parts. The chronic Esca syndrome occurs in late spring and increases during summer, whereas the acute Esca occurs at the beginning of July. Within this context, we



Fig. 1 The study area: **a** Piedmont Region (Italy), **b** Vineyard's area (zooming in) using RGB images with different spatial resolution (10 m and 0.03 m), **c** Row view (zooming in), scanned with the TLS over a RGB image (0.03 m)

randomly chose six study areas where the TLS was conducted. Each site included a total of twelve grapevines, in some cases with more than one absence of plants and different numbers of plants with different levels of disease in each row. The total number of plants monitored within the study area was 288 on both monitoring dates. All plants were georeferenced on each date using a Zenith35 Pro—Geomax GNSS device.

2.2 Remote Sensing Instruments

The vineyard was monitored on two dates in June and August 2018, using an Unmanned Aerial Vehicle (UAV), which carried a multispectral camera Micasense RedEdge.MX™. Additionally, our team conducted a survey with a Terrestrial LIDAR Scan (TLS). Each time two flights were undertaken, with a quadcopter called MAVTech Q4E. This four rotary-wing UAV has the capacity to take-off and land in narrow places (Gallo et al. 2019). It has a Maximum Take-Off Mass (MTOM) of 3.5 kg, a diagonal wheelbase of 0.590 m and an endurance of 20–25 min with a survey speed of 6 m/s and an estimated autonomy of 4 ha. The flight altitude was 30 m with a ground sample distance (GSD) of 0.3 cm. The sensor carried a multispectral camera with 231.9 g of weight and a field of view (HFOV) of 47.2°. The spectral bands captured were Blue (475 μm ± 20 μm), Green (560 μm ± 20 μm), Red (668 μm ± 10 μm), Red-Edge (717 μm ± 10 μm), and near-IR (840 μm ± 40 μm). The images were geometrically corrected and radiometrically calibrated using the Pix4D software (Fig. 2). Geometrical calibration 2D (x, y) was based on overlapping the information of Global Control Points (GCPs), circular targets randomly positioned in the vineyard, and the images. 3D calibration (x, y, z) was realized using the position of 12 targets captured with the GPS. In June, the flight area covered was 3.025 ha with a total dataset of 3270 images, which implies a total dataset of 7.74 GigaByte (GB). These images were georeferenced using seven GCPs with a

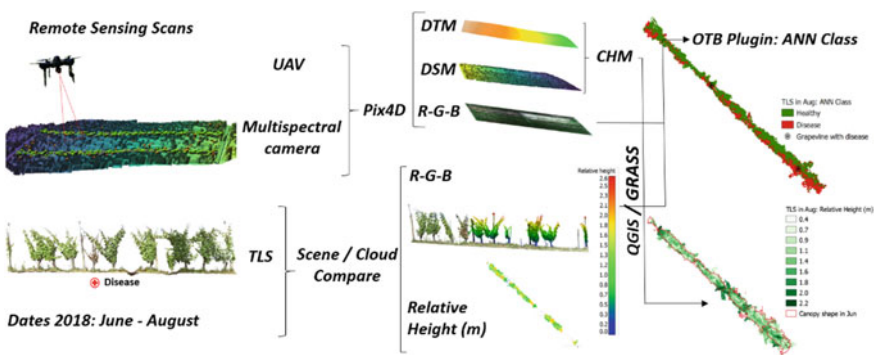


Fig. 2 The workflow of the proposed methodology

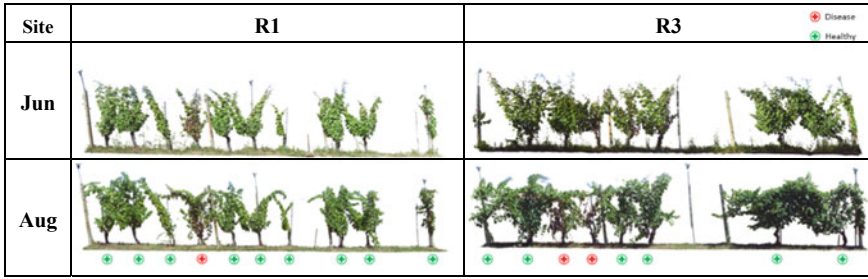


Fig. 3 3D View of the sites scanned with the TLS in both periods June and August. Red dots are grapevines with disease and green dots are healthy plants

root mean square error (RMSE) = 0.024 m. In August, the area was 2.76 ha, with 2845 images (6.61 GB), which were georeferenced with a RMSE = 0.041 m. With this software used, we obtain not only the images but also the NDVI, DTM, and DSM. The time used in the calibration of the images and photogrammetric orthomosaicking procedures, using a laptop with 8 GB of ram, took approximately 5 h after each monitoring visit in June and August. All the data was then processed later QGIS-GRASS GIS. The ground sensor used was a Terrestrial Laser Scanner called Faro Focus3D X 330 HDR, it has ±1 mm of measurement accuracy. This scanner was placed between rows at 1.2 m from the row with a horizontal FOV of 360°, in six different locations, randomly positioned and georeferenced in the vineyard. Each scan covered twelve grapevines. The output was a .fls file with data organized in a matrix (rows/columns). The scan registered data position and reflectivity of each value. The collected data was analyzed using Scene software, and exported in a .xyz file, which was then analyzed using QGIS-GRASS software.

2.3 Interpretation of the Datasets

A visual survey of the grapevines was conducted, using a disease severity index (DSI), which allowed us to analyze the Grade (G) of identified disease. We used a four-scale grading system to describe the level of Esca infection of the plant. A total of 144 plants were monitored in June and August; in June of 12.5% was infected with the disease, in August 15.28%. The visual also focused on identifying the absences of grapevines in the rows. With then combined the visually obtained information with the data obtained through the sensors in GIS, to start detecting changes in the canopy (Fig. 2).

As a first step, the area of the canopy was extracted based on the data obtained through both sensors and the visual survey, which were then compared. Each TLS was rasterized using Cloud Compare software at the same resolution as the Micasense data. The total datasets were six in each season.

To compare the area of the canopy, we calculated the Canopy Height Model (CHM) using the multispectral data on each date as follows:

$$CHM = DSM - DTM \quad (1)$$

where CHM is the Canopy Height Model; DSM is the Digital Surface Model, and DTM is the Digital Terrain Model. Buffering the CHM in each TLS site, we obtained the six-study area for June and August. Using the data from each sensor, we extracted and calculated the canopy area (m²). With these two datasets, we were then able to compare both shapes of the canopies and do a quick check to detect the absence of grapevine. The differences of the canopy shapes between CHM and TLS measured in area are described in Table 1. The percentage was calculated, selecting the maximum area of each site in August. The last columns relate to the visual survey calculation taking into account the numbers of plants with disease, the absence of grapevines in the rows and the healthy plants in the rows. This measurement was the result of a mean value of the categorized plants and the distance between plants in each row. The mean value of the width was computed using the shape of the canopy of plants categorized as healthy or with disease. In our case the absence of plants was computed with the value zero. The distance between plants is an average of the GPS data.

The area of the plants was calculated as followed:

$$A = H * w_{\bar{x}} * d_{\bar{x}} + D * w_{\bar{x}} d_{\bar{x}} \quad (2)$$

where A is the area measured in square meters; H is the number of healthy plants; w is the width, d is the distances between plants; \bar{x} is the mean value of the samples; D is the number of plants with the disease.

The next step was to extract Red, Green, and Blue band from the area of the canopy. We decide to use a non-parametric classifier using the OTB plugging in QGIS. Choosing the machine learning framework classifier, we compared the performance (time-consuming) and accuracy to distinguish canopy with disease as well as absences of grapevines in the rows. We used OTB plugging with a learning section, which includes an Artificial Neural Network (ANN) classifier. Based on the data collected from the vineyard, we then created two vector layers representing the Region Of Interest (ROI) for each specific location, where the plants were cataloged in two classes: healthy or, with disease. The pixels selected in the polygons were a mix of reflectances which help identify the condition of each plant. One ROI was built with 80% of the samples and denominated: training vector. The rest of the data (20%) was used to create a true vector to validate the classification. As next step in the process, we computed the image statistics. The application computes a global means and standard deviation for each band saved in.xml file. Then, to train the machine learning model, we used the train images classifier with the input of the training vector and true vector for validation. The input parameters of the ANN were two classes (healthy and with disease), and we chose 100 neurons in each intermediate layer. This number of neurons was chosen to increase the accuracy of the classifier,

Table 1 Total area (m²) site-specific measured using CHM and TLS in both periods (Jun–Aug)

	CHM from Micasense			TLS			Visual survey		
	Jun	Aug	Diff. Aug–Jun	Jun	Aug	Diff. Aug–Jun	Jun	Aug	Diff. Aug–Jun
	Area (m ²)	Area (m ²)	Area (%)	Area (m ²)	Area (m ²)	Area (%)	Area (m ²)	Area (m ²)	Area (%)
R1	2.139	5.572	61.61	4.260	5.889	27.66	5.08	7.42	31.45
R2	3.895	8.204	52.52	5.945	8.580	30.71	5.63	8.23	31.63
R3	4.576	11.27	59.40	6.318	9.409	32.85	4.11	6.35	35.35
R4	3.446	8.227	58.11	5.309	6.096	12.91	3.60	5.24	31.39
R5	5.885	11.00	46.50	6.875	9.679	28.97	4.72	7.52	37.31
R6	1.975	3.208	38.44	4.742	6.268	24.35	3.77	4.02	6.30

Table 2 Kappa Index in each site in June and August

Site	Kappa Index			
	June		Aug	
	TLS	CHM	TLS	CHM
R1	0.8	1	0.87	0.83
R2	0.82	1	0.77	0.75
R3	0.71	0.87	0.91	0.88
R4	0.90	0.63	0.8	0.86
R5	0.92	0.91	0.86	0.89
R6	0.95	1	1	1

and because big numbers in our case do not ensure good results. The train method type used was a resilient backpropagation algorithm (RPROP) with neuron activation function type symmetrical sigmoid function. Riedmiller et al. (1993) describe that the resilient backpropagation RPROP updates the weights according to the behavior of the error function. As last step in the classification we used the image classification with a mask of the shape of the canopy extracted in a raster and the model obtained from the training phase. The validation of the classification was based on the confusion matrix and the Kappa index of the global performance (Table 2). The confusion matrix was the result of the computing differences between the references (rows), and the produced classes (columns).

The Cohen’s Kappa index was calculated as followed:

$$k = \frac{p_o - p_e}{1 - p_e} = 1 - \frac{1 - p_o}{1 - p_e} \tag{3}$$

where k is the Kappa index; p_o is the observed class; p_e is the expected class. The data interpretation is using the scheme described by Landis and Koch (1977), which were values between 0.81–1 as considered almost perfect and values between 0.61–0.80 as substantial.

3 Results

TLS data for each scan was approximately between 3.812.297 points in June and 7.030.009 in August. The 3D view of each scan in each site on both dates was accurate (Fig. 3). This information was very useful to compare with the dataset of the visual surveys, which described the different levels of disease and the absence of plants.

The differences of the canopy shapes between CHM and TLS measured in the area (m²) are described in Table 1.

The area calculation was done using GRASS commands and paying attention to the denomination of maps. With these results, CHM shows five sites where the

canopy grew around 50% between June and August, which we could consider a normal growth. One site shows a growth of 38.44%, which could be considered as a problem. Checking this result with the 3D TLS view, we saw that this is the row with more absence of plants. Also, the CHM in June lacked some areas of the canopy due to a problem with the DTM, which increased the problem. When analyzing TLS data, the measured area of canopy growth between seasons is smaller compared to CHM, showing values between 32.85 and 24.35%. Also, the smallest area when using TLS was different from CHM (see highlighted sizes in Table 1). To understand this, we compared this result with the data from the visual survey. When looking at grapevines with disease and absences of grapevines in the row on each date and grapevines who changed between seasons (i.e., catalogued healthy in June and with disease in August), we realized that the low value of 12.91% from the TLS data was influenced by the actual visually observed state of the canopy in June. Though this analysis of the areas we realized that the CHM could be an easy tool to detect absences and some problems in the canopies. TLS, on the other hand, is accurate in its calculation of the canopy area when comparing it with the visual results. It could be a great tool if one needs to calculate these elements for vineyard management purposes canopy for spray control for example. The weakness of this methodology is the time-consuming process of post-processing data with a large number of files in xyz to be analyzed. Using OTB plugging, the RGB data from TLS and CHM was analyzed. First, we computed the statistics of each RGB image. Performance of the total image of the vineyard took 3.62 s, layer sized w:6136 h:6078. Performance of a small image with a mask (i.e., 302×302) only took 1.27 s. Secondly, we trained the images classifier choosing our training and true ROI and selecting ANN.

The command was completed in 6.22 s without and 1.31 s with a canopy's mask. Finally, it was the classification that was most time-consuming reaching values of 177.63 s/0.41 s (Fig. 4).

The results had strong statistics, as showed in Table 2, but still remain uncertainties when we wanted to compare these classifications with the real state of the canopy. i.e., we did not have a canopy taken from above, showing the areas of disease. The classifier can distinguish both classes in the canopy, but we could not link all the pixels to the Esca disease. An important step in the process is how we created the ROI's. The approach was to choose small polygons into the canopy, comparing them with pictures and TLS. Another adjustment made was choosing 100 intermediate neurons during the train image classification, which gave us more accuracy.

Although, there are uncertainties related to the quantification of the canopy with the disease until new monitoring data using different approaches are conducted. This result shows that we need to follow an adjusted of refined methodology to identify only Esca disease or also consider other vegetative problems.

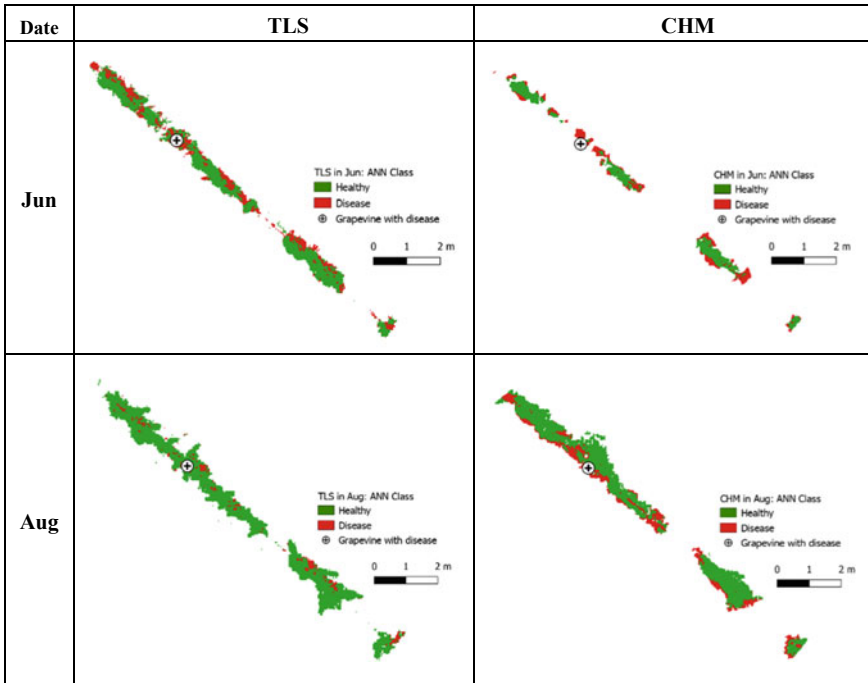


Fig. 4 Artificial Neural Network classification in TLS and CHM in June and August in site R1

4 Conclusions

The followed methodology in this research has strong outputs, showing how we could analyze large datasets and detect changes in the canopy. The use of multispectral cameras mounted in a UAS at 30 m of altitude brings enough accuracy to detect problems of disease in the canopy, using the CHM or RGB bands. Further analysis is needed to reach a good quantification in terms of area or volume of the grapevine affected with Esca disease as well as an analysis of possible other problems. Based on in-depth knowledge the Esca disease and using an accurate classification, it is important for technicians to develop 3D maps showing the levels of disease in the canopy, to be able to compare them with data obtained with sensors. When extracting information at many sites using multitemporal datasets, technicians need to know how to build a database and how to insert results into the system, to gain time. In this regard, our advice is to first think about the variables (sites, sensors) and times (date of surveys). Secondly, build a name easily changeable between the variables. It is better to lose time, in the beginning, to think about the desired output, then to lose time changing names or overlapping information at a later stage in the process.

References

- Gallo, R., Bojeri, Z., Rinaldi, S., & Mazzetto. (2019). Design a web platform to manage environmental monitoring information to be used in Multicriteria evaluations of Green infrastructures. *IOP Conference Series: Earth and Environmental Science*, 275, 012005 (2019). Web.
- Kotovirta, V., Toivanen, T., Tergujeff, R., & Huttunen, M. (2012). Participatory sensing in environmental monitoring: experiences. Palermo, Italy. In *Sixth International Conference on Innovative Mobile and Internet Services in Ubiquitous Computing*.
- Landis, J. R., & Koch, G. G. (1977). The measurement of observer agreement for categorical data. *Biometrics*, 33(1), 159–174 (1977). Web.
- Marx, S., Hämmerle, M., Klonner, C., & Höfle, B. (2016). 3D Participatory sensing with low-cost mobile devices for crop height assessment—a comparison with terrestrial laser scanning data. *PLoS One*, 11(4), e0152839. Published 2016 Apr 13. <https://doi.org/10.1371/journal.pone.0152839>.
- Mazzetto, F., Gallo, R., Riedl, M., & Sacco, P. (2019). Proposal of an ontological approach to design and analyses farm information systems to support precision agriculture techniques. *IOP Conference Series: Earth and Environmental Science*, 275, 012008 (2019). Web.
- Riedmiller, M., & Braun, H. (1993). A Direct Adaptive Method for Faster Backpropagation Learning: The RPROP Algorithm. 0-7803-0999-5/93/\$03.00©1993 IEEE.
- Rosell, & Sanz. (2011). A review of methods and applications of the geometric characterization of tree crops in agricultural activities. *Computers and Electronics in Agriculture*, 81.C, 124–141 (2011). Web.

AgroBot Smash a Robotic Platform for the Sustainable Precision Agriculture



D. Sarri, S. Lombardo, R. Lisci, V. De Pascale and M. Vieri

Abstract The growing need for production processes oriented to environmental sustainability is leading to the quickly spreading of robotic solutions. In this scenario, the Smart Machine for Agricultural Solutions High-tech SMASH project is focusing on the development of a robotic collaborative ecosystem. It consists of four main modules: an unmanned ground vehicle (AgroBot), a soil monitoring unit (Plantoid), an aerial unit (FlyBot), and a mobile service unit on the field (AncillaryBot). Furthermore, the SMASH project is implementing technological solutions with a view to resolve some issues related to nutrition safety (e.g. nitrate content on the vegetable) and environmental sustainability (e.g. pesticide use, production process waste) in two representative scenarios of specialty crops (viticulture) and vegetables (spinach). The present work reports the results concerning the design stage and development of the robotic terrestrial platform AgroBot and their implements for the crop protection management and physical control of weeds. A system made of a terrestrial wheeled platform with an innovative perception system and three types of implements have been built to make sustainable agronomic practices.

Keywords Precision farming · Monitoring · Viticulture · Agricultural robots · Automation

1 Introduction

In the reference framework of the last 15 years, European institutions, in collaboration with member states and researchers, raised more awareness of the use of pesticides in agriculture. At first, starting from more punctual legislation (EU, 2007) to reduce the use of pesticides, with the aim of opening new markets and promoting environment and citizens' health security. In this path, some of the calls from the projects of Horizon 2020 (RHEA project) (Gonzalez-de-Santos et al. 2016; Vieri et al. 2013), but

D. Sarri (✉) · S. Lombardo · R. Lisci · V. De Pascale · M. Vieri
Department of Agriculture, Food, Environment and Forestry DAGRI, University of Florence,
Piazzale delle Cacine 15, 50144 Florence, Italy
e-mail: daniele.sarri@unifi.it

© Springer Nature Switzerland AG 2020
A. Coppola et al. (eds.), *Innovative Biosystems Engineering for Sustainable Agriculture, Forestry and Food Production*, Lecture Notes in Civil Engineering 67,
https://doi.org/10.1007/978-3-030-39299-4_85

also some directly founded in regional systems (even through European balance) (i.e. POR CREO—FSE Tuscany) are oriented to find innovative solutions for minimizing agricultural impacts. With those premises, the largest part of robotics applied to agriculture tries to bring an innovative approach and practical solutions for farmers who need to apply pesticides in the safest and more precise way. Not only robots are going to radically change the machinery sector: innovation is actually running in the direction of using fleets of robots for field operation, instead of tractors. This, if it became real, could mean that abilities in the field, for technicians and farmers, should change too. Currently, there are different kinds of robots, which make different operations but two are the main functioning: only sensing or monitoring and field works. Robots for monitoring are usually able to map and scan the canopy, to estimate the production, to evaluate water content and other parameters by several kinds of sensors. Those particular sensors are better than human eyes and may help in the decision process. Only in the viticulture sector, there are different projects and we cite the most innovative as Vinbot (2019) and Saiz–Rubio et al. (2017). Robot for both monitoring and field operations have been mainly developed for one field operation, but they have mounted on a lot of different sensors that help the decision process of the machine (in some cases it is real-time elaboration). Even in the viticulture sector, there are Vitirover (2019) or Agrirobot (Agrirobot 2019), a set of sensors (GNSS included) that help the robots decide when and where to cut grass under the single vine. The GNSS helps the robot to be autonomous, but in some cases, it could be beneficial to have the machine guided in remote mode, and for this reason Vitirover has a dedicated app and a platform on PC. There are many other best cases of robots in the viticulture sector, such as the French Wall-YE, which with its sensors and arms can practice precision pruning (Diago and Tardaguila 2015). It is also interesting the experience made with the development of Vineguard: its aim, achieved, was to develop a robot able to use variable rate treatments on leaves in the vineyard. SMASH (Smart Machine for Agricultural Solutions High-tech) is a project funded by Tuscany region and its objective is to introduce innovative technologies to realize sustainable agricultural practices to reduce the input needed in terms of products applied. The SMASH Project has the following aims: 1. Creating a robotic collaborative ecosystem. 2. Monitoring and managing modular and integrated systems for sustainable agricultural crops through precision agriculture techniques. In addition, SMASH will try to solve problems related to food security as nitrates concentration and the use of chemicals over crops starting from two study cases on vineyards and spinach cultivation. The robot is going to be a modular tool with a ground mobile unit (AgroBot), a unit devoted to the soil inspection (Plantoide), a flying unit (Flybot) e a unit for field boundaries (AncillaryBot).

2 Material and Method

The project development is articulated in two main tasks, i.e. the design of unmanned ground vehicle (AgroBot) and the implements used to perform field activities. This

was achieved in four main steps, i.e. (a) definition of technical and functional specification, (b) design, (c) manufacturing, (d) field tests.

2.1 AgroBot System Architecture

The AgroBot design followed the overall criterion used for agricultural machines but with particular attention paid to the carrying out of low impact agricultural activities. Therefore, it was chosen to develop an electrical power-driven robot, wheeled, with two axles and light mass to limit the issues of soil compaction. Other design criterions were the ability to maintain stability on the asperities that can be found in specialized and open field cultivation, without losing out on performance in terms of autonomy, load-carrying capacity, tractive power and actuation of certain implements. Further design specification was the capacity to perform both monitoring and execution of some cultural interventions. The last point required the adaptation of variable wheel tracks to the vegetable scenario. This was characterized by a seeding layout of 0.6 m between three rows and 0.2 m on the line used in the farm which held the field test. Finally, the robot should be able to geo-locating and moving independently using dedicated sensors and planning strategies, route and obstacle management based on the latest generation control algorithms. The robot environment and target perception were designed to get a forward-looking view of the crop rows and obstacle avoidance. Another essential design criterion was the communication system. The AgroBot had to be able to collect data and communicate remotely with the AncillaryBot all the data acquired during the working stages. Besides, the AgroBot had the function of carrying the actuation equipment, which consists of physical (mechanical) and chemical tools to destroy weeds or apply pesticide and non-thermal plasma mixture (NTP).

2.2 Implements Design Specifications

2.2.1 RoboSpray

As regards the RoboSpray design, the main constraint was the development of a spraying system that fulfilled the following requirements:

- Spot spray technique assisted by a vision disease identification system;
- Pulverization by pressure to get the wider spectrum of drops;
- Airflow generator;
- On-demand spraying system; so as not to have a continuous absorption of electric power;
- 12 and 48 Vdc hardware elements power supplies;
- Possibility of the continuous orientation of the diffuser;
- Installation on a robotic arm.

The need to limit drift as much as possible is obtainable with intelligent spraying systems capable of identifying the infection outbreaks and spraying timely. The criterion of orientation versatility of the diffuser is advantageous to ensure a greater number of degrees of freedom and a broad adaptability of the RoboSpray to the different operating scenarios. The RoboSpray must not only spray a specific pesticide but also distribute, in a targeted way to the ground, the ionized water produced by the NTP system with punctual volumes. Finally, considering the general objective of designing a robot capable of effectively performing some cultivation interventions in a real agricultural context, technical solutions have been chosen to standardize the power supply to the AgroBot energy sources and calculate the components' adsorption to guarantee practicable autonomy.

2.2.2 DiserBot for Specialty Crops

The weed control management on tree crops was based on the methodology oriented towards the mechanical control of weeds along the row. The weed control in such zones has been chosen as it represents one of the main critical farmers' issues, being a time and energy-consuming work. The weeds in the crop rows determine issues for water competition, induction of a microclimate favorable to the diffusion of the main pests and diseases. The chemical weed control has been excluded as it is not in line with the general objective of the project: identifying innovative robotic solutions for the development of sustainable agriculture. Therefore the choice fell on the type of passive mechanical weeding in consideration of the right compromise regarding sustainability, efficacy, energy requirements and masses.

2.2.3 DiserBot for Vegetable

Weed control on the row of open-field vegetable crops was of a passive mechanical type. The advantages are the same as those shown for the specialty crops DiserBot. The equipment had to be able to perform weed control in the seeding row in the early stages of development so as to increase the effectiveness of control. The equipment must be light with an overall mass such that it can be raised at the end of the plots and allow easy turns. Furthermore, the implementation must have adjustments to be able to adapt to the different sowing layouts, soil textures and irregularities of the ploughed soil to guarantee a constant working height.

3 Results and Discussion

On the basis of the design methodology followed, a robot was built with a central body connected to four electric drive wheels mounted on a double axel, one rigid and the other oscillating. The solution identified allows to deal with lateral inclinations

of $\pm 20^\circ$ guaranteeing stability in the forwarding. In this perspective, it was considered that the AgroBot should be equipped with four independent drive wheels, so as to ensure greater mobility and an ability to perform maneuvers in narrow spaces. This was achieved by drive wheels, which individually provided tractive power and allowed rotations up to 270° . To make the AgroBot applicability as flexible as possible to the different scenarios, a modular structure, was designed. It allowed the mounting of two types of axels whose size varies according to the scenario. The overall dimensions of the wheel track range from a minimum of 1.144 mm for specialty crops scenario and a maximum of 1.800 mm for the vegetable, while the length was 1.400 mm. The height from the ground for specialty crops scenario was set at 250 mm to guarantee the vehicle greater stability and adaptability on tilled soils or with plant residues and of 500 mm for the horticultural scenario. The final mass of AgroBot was 800 kg including all the equipments and implementation-perception systems. This architecture limited the problems of soil compaction induced by conventional means to a specific pressure value on the ground of 0.35 kg cm^2 . The maximum operating speed was 6 km h^{-1} at the maximum permitted gradient of 15%. The central body of the robot consists of a steel frame, where the power supply system for the equipments and handlings were installed. The main components, positioned inside the steel protection frame, for powering and controlling the vehicle, were (a) battery chargers, (b) a battery Management System, (c) motor inverters, (d) battery pack. The theoretical autonomy was variable according to the activity carried out and the operating scenario from a minimum of 4 h to a maximum of 5.5 h. An inertial geo-localization system with GNSS receiver (double-antenna INS-GNSS) allows estimating the position and orientation of the AgroBot (Fig. 1).

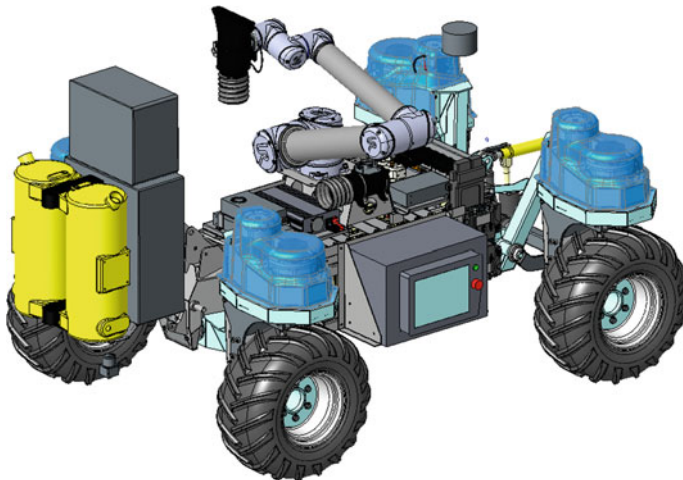


Fig. 1 Agrobot ground unit for specialty crop. In the central body, it is possible to view the RoboSpray set up on the robotic arm. On the three hitch point the tank and the electronics

The localization system is a GNSS-RTK (Real Time Kinematic) with positioning accuracy ± 0.02 m. Navigation takes place based on a georeferenced map of the field on which the main path nodes are loaded. A communication system based on both GPRS-GSM and WiFi technology was implemented in order to transmit all the data acquired during the working stages. The AgroBot have been equipped with a double sensing system. The first, based on vision and laser components, allowed the accident prevention to the plant, humans and animals. The second performed the screening of specific target (pests on vineyard and weeds on vegetable) through stereo-camera and RGB camera supported by advanced algorithms.

3.1 *RoboSpray*

The RoboSpray was developed referring to a versatile and controllable pressure system. This combined with a general pressure regulation system, allowed the managing of volumes and the quality of the spray. In the end, RoboSpray presents a sprayer group that permits high configuration in terms of pressure, volumes, and kind of droplet size to use the robot with several pesticides type and crops. This kind of choice is the answer to the need of using the robot for both spraying crop protection products and spraying ionized water. Furthermore, were implemented an electrostatic charging system to increase the droplet deposit and a tool for intermittent spraying (solenoid valve) to modify the liquid flow. RoboSpray parts were a tank (more less 30 L) posed in vertical (to avoid problems connected to the draft of the liquid when transversal and longitudinal slope occur), a filter for impurities, a diaphragm pump 12 Vdc able to provide variable continuous pressure and variable flow in relation to the needs, a manual pressure regulator, a standard ISO nozzle manually interchangeable and a solenoid valve for regulating and interrupting the liquid flow. An electrical fan was mounted to direct drops produced by the spraying system. This tool seems to be essential to be able to give a warranty for the correct direction of spray on targets to permit the right penetration inside the canopy and coverage on vegetal elements. For this purpose, an axial turbine with a 48 Vdc electric drive was chosen, with the possibility of being regulated on time in relation to the distance of the target and the thickness of vegetation to be penetrated. To limit pitching problems during the advancement of the robotic platform and in consideration of the need to install RoboSpray on the robotic arm universal robot UR10 hydraulic components (excluding pulverization system and solenoid valve) were positioned on the rear linkage to optimize dell' AgroBot spaces. The turbine, the atomization system, and the solenoid valve were instead set up at the end of the robotic arm. The electrical components are electronically managed and controlled in the different stand-by, idle and working phases to obtain the maximum energy yield and to safeguard as much as possible the energetic autonomy of the terrestrial mobile unit. The whole is assembled as a "kit" to facilitate coupling operations.

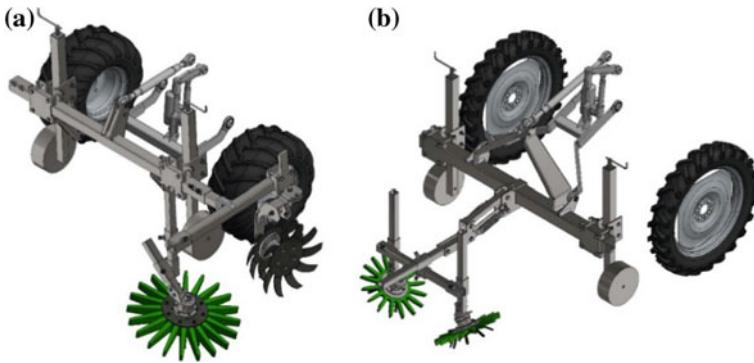


Fig. 2 Implements for mechanical weed control **a** on the row on specialty perennial crops and **b** on the row for vegetable crops

3.2 *DiserBot: Specialty Perennial Crops*

The passive mechanical control was carried out by shaped mechanical tools in neutral mounted on a support arms with a variable inclination with respect to the direction of forward motion. The actuators used were of the star-shaped finger type. These elements exploit the advancement of the vehicle. The resultant forces determine a rotation induced by the advancement of the AgroBot therefore they do not need direct supply and continuous energy for their actuation. The star-shaped finger tools, with their particular shape, penetrate the ground below the plant and thanks to the steel teeth placed underneath, work the ground superficially (0.05 m). To improve the weed removal action, a double idle toothed steel wheel has been applied at the front which coarsely breaks the soil. A support frame with adjustments to the working and positioning heights was developed to plug the implements to the AgroBot. The star-shaped finger rotor provides for the shredding of the particles in smaller aggregates and the filling of weeds. Based on the existing applications used in the specialty crops scenario, the expected forwarding speed of advancement of the AgroBot (4.5 km h^{-1}) is compatible with the operation of the identified solution. This peculiarity allowed high autonomy to the terrestrial unit with considerable advantages in terms of performance and work productivity (Fig. 2).

3.2.1 *DiserBot: Vegetable*

The DiserBot weed control on the row of open field vegetable was achieved by passive mechanical equipment. The working elements of this type of operator were composed of opposing rotating metal plates neutral mounted on an axis inclined with respect to the surface of the ground and connected to a mainframe by adjustable arms. The motion of the weed spreader is guaranteed by the resistance offered by the ground during the advancement of the AgroBot towards specific metal spikes,

mounted on the lower part of the support plate so as to penetrate for a few centimeters inside the soil. Along the external circumference of the rotating plates are mounted the flexible elements (fingers), made of plastic material so as not to damage the stem of the crop. Furthermore, to adapt to the different sowing layouts and irregularities of the worked soil, a double regulating system was developed. The first is of manual type and consists of a support wheel adjustable in height, the second is of the type with automatic mechanical damping to contain the possible asperities on the transplant bed. The total mass of the tool was 90 kg. This made it possible to use an electric-type linear actuator for lifting on the three-point hitch. This has made it possible to obtain a compact and light and versatile system that can be raised at the end of the field and allow easy turns. The implements perform weed control for a maximum of three rows in a single passage.

4 Conclusion

In the present study, the result related to the development stage of a robotic platform for sustainable precision agriculture were shown. The ground unit has high performances and innovative operating characteristics among the robotic solutions developed to date. The AgroBot allows both the scouting phase and the execution of cultivation interventions in a precise manner and at a variable rate. This, together with the other modules of the robotic platform, represents an articulated and intelligent system able to offer decision-making and operational support to farmers who can implement agricultural processes with reduced environmental impact.

Acknowledgements The activity presented in the paper is part of the research grant POR CReO FESR Toscana 2014–2020 AZIONE 1.1.5 sub azione 11—RS 2017 Progetti Strategici di ricerca e sviluppo Bando 1 project Smart Machine for Agricultural Solutions High-tech (SMASH) CUP D51B17002350009.

References

- Agrirobot. (2019). Last accessed on 2019 July the 5th <https://ambrogiorobot.weebly.com/agrirobot.html>.
- Diago, M. P., & Tardaguila, J. (2015). A new robot for vineyard monitoring. *Wine Viticulture Journal*, 30(3), 38.
- Gonzalez-de-Santos, P., Ribeiro, A., Fernandez-Quintanilla, C., Lopez-Granados, F., Brandstoetter, M., Tomic, S., Pedrazzi, S., Peruzzi, A., Pajares, G., Kaplanis, G., Perez-Ruiz, M., Valero, C., Del Cerro, J., Vieri, M., Rabatel, G., & Debilde, B. (2016). Fleets of robots for environmentally-safe pest control in agriculture. *Precision Agriculture*. pp. 1–41. <https://doi.org/10.1007/s11119-016-9476-3>.
- Saiz-Rubio, V., Rovira-Más, F., & Millot, C. (2017). Performance improvement of a vineyard robot through its mechanical design. Paper presented at the 2017 ASABE Annual International Meeting. <https://doi.org/10.13031/aim.201701120>.

- Vieri, M., Sarri, D., Rimediotti, M., Perria, R., & Storchi, P. (2013). The new architecture in the vineyard system management for variable rate technologies and traceability. *Acta Horti*, 978, 47–53. <https://doi.org/10.17660/actahortic.2013.978.3>.
- Vinbot. (2019). Last accessed on 2019 July the 5th <http://vinbot.eu/>.
- Vitirover. (2019). Last accessed on 2019 July the 5th <https://www.vitirover.fr/>.

Use of a Multirotor-UAV Equipped with a Multispectral Camera to Detect Vineyard Diseases: A Case Study on Barbera and Dolcetto Cultivars



Gabriele Daglio, Raimondo Gallo, Monica F. Rinaldi, Nadia Massa, Valeria Todeschini and Fabrizio Mazzetto

Abstract Viticulture is one of the most important productive sectors of agriculture. The vineyards can be subject to a large production of losses, mainly due to vegetative stress or diseases. Esca disease (ED) is one of the most widespread diseases in the vineyards and it is difficult to be predicted. The main symptoms appear at level of wood and leave starting to the end of showing yellow spots which turn to red—brown before their complete drying. This research aims to develop and validate a fast and reliable system able to recognize diseased plants in the vineyard through remote sensing applications. This experiment was carried out in a vineyard in the North–West of Italy on rows of *V. vinifera* plants cv. Dolcetto and Barbera using a multirotor-UAV (Unmanned Aerial Vehicle) equipped with a multispectral camera. A ground survey was performed in order to assess the plant's health status and georeference their position. During the field test, the UAV flew at three different flying altitude: 30–50–70 m. The collected images were elaborated using Pix4Dmapper software in order to: (i) extract the vineyard rows, (ii) identify their surface covered by a plant, and (ii) calculate a NDVI map for each plant.

Keywords Precision viticulture · NDVI · UAV · Remote sensing · Esca disease

1 Introduction

Vitis vinifera is one of the most profitable cultures present on the Italian territory. The most popular Piedmont areas for wine production are those located within Alessandria. One of the most important and widespread diseases that can affect

G. Daglio (✉) · R. Gallo · M. F. Rinaldi · F. Mazzetto
Faculty of Science and Technology, Free University of Bozen (FUB), Piazza Università 5, 39100 Bolzano, BZ, Italy
e-mail: gabriele.daglio@unibz.it

N. Massa · V. Todeschini
Dipartimento di Scienze e Innovazione Tecnologica (DISIT), Università del Piemonte Orientale, Viale T. Michel 11, 15121 Alessandria, AL, Italy

© Springer Nature Switzerland AG 2020
A. Coppola et al. (eds.), *Innovative Biosystems Engineering for Sustainable Agriculture, Forestry and Food Production*, Lecture Notes in Civil Engineering 67,
https://doi.org/10.1007/978-3-030-39299-4_86



Fig. 1 Esca disease symptoms: grapevine leaf stripe disease on the left, apoplectic form on the right

grapevine is Esca disease (ED). It is caused by several fungi (*Fomitoporia mediterranea*, *Phaeomoniella chlamydospora* and *Phaeoacremonium minimum*) and its symptoms included: wood decay and grapevine leaf stripe disease (GLSD). The main GLSD symptoms are decline in vegetative vigor, growth stop, foliar interveinal necrosis (tiger stripe appearance) and drying fruit cluster (Bertsch et al. 2013; Di Gennaro et al. 2016). In general, the ED symptoms are observable on leaves and fruits and in the most acute form sometimes the plant quickly dies (Fig. 1). The strategy that is usually applied to manage the ED disease spread, is principally based on the individuation of the diseased plants through manual surveys and on the application of new pruning practices (Bertsch et al. 2013).

Considering the damage that ED disease can cause to the vineyards and the entire wine sector, it is fundamental to find new solutions to limit its spread and to identify the symptoms quickly and accurately. Techniques and tools derived from precision agriculture (PA) as remote-sensing technologies can be used to reduce the time needed for crop monitoring. Using optical sensors installed on vehicles (aerial or terrestrial), it is possible to obtain punctual information, about a crop, canopy volume, distance between plants, number of plants, or health status and to optimize the use of fertilizers (Rosell et al. 2009; Mazzetto et al. 2010, Di Gennaro et al. 2016; Albetis et al. 2017; Gallo et al. 2017; Ristorto et al. 2017). Optical sensors can provide information about: crop health status plants and geometry. From the data collected by sensors it is possible to compute vegetative indices, for example the Normalized Difference Vegetation Index (NDVI) that are able to give information about the health status of the crop (D'Auria et al. 2016; Mazzetto et al. 2010). Several authors tested different optical sensors on *V. vinifera* plants. Mazzetto et al. (2010) used several proximal sensing technologies in order to evaluate the health and

vigor canopy in plants infected by *Plasmopora viticola*, reporting lower NDVI values in plants infected if compared to the healthy ones, according to the observations obtained during the manual observations. Albetis et al. (2017) used multispectral images obtained by Unmanned Aerial Vehicle (UAV) equipped with multispectral camera to detect plants affected by Flavescence Dorée considering eleven vegetation indices, in different cultivars of *V. vinifera*. Di Gennaro et al. (2016) studied the relationships between NDVI, acquired by remote sensing technologies, and ED symptomatic plants monitored by ground observation and they obtained promising results. This research aims to develop a fast and reliable system able to recognize diseased plants in vineyard through remote sensing applications.

2 Materials and Methods

2.1 Experimental Site

The experimentation was carried out in a vineyard of *V. vinifera* cv_s. Dolcetto and Barbera, in Piedmont (Italy) (Carpeneto—AL), where many cases of vines suffering from ED are documented. The vineyard was planted in 1988, with rows aligned NW-SE and 2.8×1 m of planting layout, average slope 10% at 329 m. a.s.l., Guyot trained system. The activities were carried out at the end of August 2018. While the survey was done on the entire vineyards, in this paper only 6 rows of the 42% ones in the vineyard are considered. The rows considered are the numbers: 18, 19 and 20 (cv. Dolcetto) and 38, 39, 40 (cv. Barbera).

2.2 Instrumentation

For the monitoring activities of the vineyard a UAV multirotor (4 rotors) Mavtech Q4Light equipped with a multispectral sensor, Micasense-RedEdge was used (Fig. 2).

The multicamera capture images in 5 different bands: Blue, Green, Red, RedEdge, and Nir. Also, a unit RTK-GNSS, GEOMAX Zenith 35 Pro, was used to georeference the plants and consider the faults in the rows.

2.3 Ground and Aerial Survey

Before performing the aerial survey, two technicians carried out a ground survey in order to assess the health status of the plants and to identify the missing plants of the row. All the plants which had disease symptoms, in this case, study plants affected by ED were georeferenced and classified (from 1 to 4) as follows according to the



Fig. 2 On the left the UAV equipped with the multi-camera, on the right, in detail, the Micasense-RedEdge used during the survey

Table 1 Flight specification

Flight altimetry (m)	30	50	70
Flight time (min.)	19 min	10 min	8 min
Cruise Speed (m/s)	4	5	5
Multispectral images acquired	638	240	132
Ground Sampling Distance (cm/pixel)	2.05	3.41	4.77

level of disease: (1) few symptoms on some leaves and not very evident, (2) some symptoms and canopy not dry, (3) general widespread symptoms, canopy partially dry, (4) canopy totally dry.

The aerial surveys were performed at three different heights: 30–50–70 m. The table below shows the information about the flight altitude, cruise speed, flight time, number of multispectral images acquired, and the ground sampling distance (Table 1).

Survey missions have been planned using Mission Planner software and the flights have been performed in automatic mode, except for take-off and landing phases. Moreover, values have been set equal to 75% for overlap (along drone progress direction) and side-overlap.

2.4 Data Processing

The images acquired during the flights have been processed with Pix4D software. First of all, with the software, using camera specifications, it was possible to assemble and georeference the images acquired during the flights. After the second processing in Pix4D it was possible to obtain: image in the bands of Blue, Green, Red, RedEdge and Nir, maps of Normalized Difference Vegetation Index (NDVI), Digital Terrain Model (DTM) and Digital Surface Model. These outputs were used for final processing in QGIS 3.6 software. Computing the Canopy Height Model (CHM) it was possible to obtain information about the canopy area and perimeter of the plants

without considering the grassing of the rows.

$$NDVI = \frac{NIR - RED}{NIR + RED} \tag{1}$$

where NDVI is the Normalized Difference Vegetation Index, NIR is the reflectance value in the Near-Infrared spectrum, and the RED is the reflectance value in the RED spectrum.

In order to obtain information about the canopy surface and perimeter the Computing the Canopy Height Model (CHM) we computed Eq. (2). CHM it was possible to obtain the plants without considering the grassing of the rows.

$$CHM = DSM - DTM. \tag{2}$$

where *CHM* is the Canopy Height Model, *DSM* is the Digital Surface Model and *DTM* is the Digital Terrain Model

The obtained maps were cut in order to extract the information relating to the six rows considered for this analysis. Overlaying a grid with a known size (1 m × 1 m) it was possible to extract the NDVI values associated with each plant. The same grid was used to calculate the surface of the canopy of each plant through CHM values. The NDVI values associated with each plant were compared with the information collected during manual surveys (state of health of the plants and degree of symptoms). The diseased plants, which, according to the degree of symptomatology had previously been classified into four categories, were reclassified according to two categories: high disease degree and low disease degree. The NDVI values obtained were then analyzed to compute the NDVI average value for each row for each flight altimetry and each one of the plant’s health status categories.

3 Results

From the data elaboration, we obtained the NDVI values, which represent the two cultivars classified as Healthy, High and Low diseased (Tables 2, 3 and 4). Moreover the values are divided by altimetry of the flights and single row.

Table 2 NDVI: Healthy Plants

Altimetry (m)	Dolcetto				Barbera			
	R18	R19	R20	Mean	R38	R39	R40	Mean
30	0.74	0.73	0.78	0.75	0.71	0.83	0.84	0.79
50	0.73	0.76	0.77	0.75	0.70	0.76	0.82	0.76
70	0.72	0.73	0.68	0.71	0.67	0.72	0.79	0.73

Table 3 NDVI: Plants with High disease degree

Altimetry (m)	Dolcetto				Barbera			
	R18	R19	R20	Mean	R38	R39	R40	Mean
30	0.64	No Data	No Data	0.64	0.65	0.70	0.79	0.71
50	0.64	No Data	No Data	0.64	0.63	0.69	0.76	0.70
70	0.72	No Data	No Data	0.72	0.62	0.68	0.75	0.68

Table 4 NDVI: Plants with Low disease degree

Altimetry (m)	Dolcetto				Barbera			
	R18	R19	R20	Mean	R38	R39	R40	Mean
30	0.75	0.87	0.76	0.79	0.72	0.75	0.84	0.77
50	0.73	0.86	0.74	0.78	0.71	0.75	0.81	0.76
70	0.74	0.84	0.72	0.77	0.67	0.73	0.79	0.63

The Dolcetto cv shows NDVI values lower than the Barbera cv ones. If we relate to the NDVI on the altimetry, we could see higher NDVI values in 30 m if compared with the other altimetry.

In Dolcetto cv in 19 and 20 rows, we didn't find plants with a high disease degree, that is why we use the label No Data.

The Dolcetto cv shows lower NDVI values compared to the Barbera cv ones. Although, in Dolcetto, we only monitored one row. If we relate to the NDVI on the altimetry, we could see similar NDVI values in each altimetry 30.

The NDVI values in Dolcetto cv are higher than the Healthy ones probably because the symptoms are still not evident enough. The Barbera cv shows lower values, which represent the presence of disease.

4 Conclusions

Observing the results, it is possible to affirm that the system tested is already able to give indications about the state of health of the observed plants. With this system, it is possible to monitor large areas in a short time. Normally two specialized technicians take about 3 h to assess the state of health of the six rows taken into account for this test, while the proposed instruments only require few minutes. Based on the results obtained in this work, it is possible to observe that the system used in this experimentation can give punctual indications about the health status of the vines. The NDVI values calculated for plants with a high degree of disease are always low if compared to the values of healthy plants, while plants with a low disease degree show values similar to those of healthy plants hence the used system is not able to identify plants when the disease is not very evident.

In the next studies the data obtained from the analysis of the areas of the canopy, that have not been shown in this paper, will be used to verify if the proposed system is able to discriminate plants from the faults. Also, other vegetation indexes will be tested to improve the ability of our system to identify plants that show few symptoms on the canopy to realize an early detection system for plant diseases.

References

- Albetis, J., Duthoit, S., Guttler, F., Jacquin, A., Goulard, M., Poilvé, P., et al. (2017). Detection of Flavescence dorée grapevine disease using Unmanned Aerial Vehicle (UAV) multispectral imagery. *Remote Sensing*, 9, 308.
- Bertsch, C., Ramírez-Suero, M., Magnin-Robert, M., Larigno, P., Chonga, J., Abou-Mansour, E., et al. (2013). Grapevine trunk diseases: Complex and still poorly understood. *Plant Pathology*, 62, 243–265.
- D’Auria, D., Ristorto, G., Persia, F., Vidoni, R., & Mazzetto, F. (2016). Development and preliminary tests of a crop monitoring mobile lab based on a combined use of optical sensors. *International Journal of Computer & Software Engineering*, 1, 103.
- Di Gennaro, S. F., Battiston, E., Di Marco, S., Facini, O., Matese, A., Nocentini, M., et al. (2016). Unmanned Aerial Vehicle (UAV)-based remote sensing to monitor grapevine leaf stripe disease within a vineyard affected by esca complex. *Phytopathologia Mediterranea*, 55, 262–275.
- Gallo, R., Ristorto, G., Daglio, G., Massa, N., Berta, G., Lazzari, M., et al. (2017). New solutions for the automatic early detection of diseases in vineyards through ground sensing approaches integrating lidar and optical sensors. *Chemical Engineering Transactions*, 58, 673–678.
- Mazzetto, F., Calcante, A., Mena, A., & Vercesi, A. (2010). Integration of optical and analogue sensors for monitoring canopy health and vigour in precision viticulture. *Precision Agriculture*, 11, 636–649.
- Ristorto, G., Gallo, R., Gasparetto, A., Scalera, L., Vidoni, R., & Mazzetto, F. (2017). A mobile laboratory for orchard health status monitoring in precision farming. *Chemical Engineering Transactions*, 58, 661–666.
- Rosell, J. R., Llorens, J., Sanz, R., Arnó, J., Ribes-Dasi, M., Masip, Escolá, A., Campc, F., Solanelles, F., Grá, F., Gil, E., Val, L., Planas, S., & Palac, J. (2009). Obtaining the three-dimensional structure of tree orchards from remote 2D terrestrial LIDAR scanning. *Agricultural and Forest Meteorology*, 149, 1505–1515.

An Ontology-Based Study for the Design of a Database for Data Management in Precision Farming



S. Chiappini, A. Galli, E. S. Malinverni, P. Zingaretti, R. Orsini,
M. Fiorentini and S. Zenobi

Abstract Precision Farming is nowadays an important challenge aiming to improve environmental quality in rural areas, giving more sustainability to agricultural operations by improving the quality of fieldworks and increasing the food safety and security for social life. To these purposes, the setting up of specific methodologies, for precision Farming Management System (FMS), is required the use of sensors and Geomatics techniques and optimization of field operation with the aim to build a precision Farming Management System (FMS) enhancing the agricultural performance and ability to predict and mitigate environmental risks. The research activities here presented belong to a multidisciplinary project named “PFRLab: Setting of a Precision Farming Robotic Laboratory for cropping system sustainability and food safety and security” founded by the Università Politecnica delle Marche during the period 2017–2020. The main goal of the research is to design a database for data management based on agriculture ontology, using as case study the experimental farm of Università Politecnica delle Marche. To solved this task, many data have been connected by advanced technologies like Unmanned (UAV), Internet of Things (IoT), Remote Sensing and field sensors. In the future, the big amount of field data

S. Chiappini (✉) · E. S. Malinverni
Dipartimento d’Ingegneria Civile, Edile e Architettura (DICEA), Università Politecnica delle Marche, Via Brecce Bianche 10, Ancona, Italy
e-mail: s.chiappini@staff.univpm.it

E. S. Malinverni
e-mail: e.s.malinverni@univpm.it

A. Galli · R. Orsini · M. Fiorentini · S. Zenobi
Dipartimento di Scienze Agrarie, Alimentari ed Ambientali (D3A), Università Politecnica delle Marche, Via Brecce Bianche 10, Ancona, Italy
e-mail: a.galli@univpm.it

R. Orsini
e-mail: r.orsini@staff.univpm.it

P. Zingaretti
Dipartimento di Ingegneria Informatica (DII), Università Politecnica delle Marche, Via Brecce Bianche 10, Ancona, Italy
e-mail: p.zingaretti@univpm.it

© Springer Nature Switzerland AG 2020
A. Coppola et al. (eds.), *Innovative Biosystems Engineering for Sustainable Agriculture, Forestry and Food Production*, Lecture Notes in Civil Engineering 67,
https://doi.org/10.1007/978-3-030-39299-4_87

allow building a Decision Support System to increase the performances of precision farming experimental trials and making farm's decision potentially more productive and efficient.

Keywords Geodatabase · Data processing · GIS · Remote sensing · Precision farming · Ontology

1 Introduction

Precision farming is defined as the application of technologies and principles to manage spatial and temporal variability associated with all aspect of agricultural production (Pierce and Novak 1999). In Italy is a topic still little known, nevertheless it seems to be able to increase the sustainability of agricultural models by taking the innovation as one of the most important challenges of the near future for improving the quality of agricultural production and protect the environment at the same time (Kunal et al. 2015). Thanks to Horizons 2020 that is the European Strategy for the research, with the collaboration with the “Pasquale Rosati Farm” (based in Agugliano, Province of Ancona, Marche Region, Italy) of the Università Politecnica delle Marche, an innovative study on precision farming has been launched in 2017. The aim of Horizon 2020 is to support research and innovation. In line with this Strategy, Horizon aims to contribute, in particular, to the realization of smart, sustainable and inclusive growth. Europe is facing with an increasing competition to handle limited natural resources. One of the specific challenges is to help attain high levels of precision in modern farming through the smart use of informatics, geomatics and robotics. Robotised precision farming involves the use of technology for optimizing field-level operation management, enhancing agricultural performance, predicting and mitigate environmental risks, increasing crop yields by optimizing crop growth so they could lead to lower fertilizer/pesticides usage, improve food safety, boost for an integrated farming management system (FMS). Since in precision farming information resources are not centrally organized and heterogeneous, an innovative approach to manage this knowledge is needed (Udsanee et al. 2018). This research is based on the ontology knowledge by means of agronomic protocols, experimental scheme, data collection, data processing following in a manage geodatabase for the quality and human health risk assessment and, finally, economic meaning. The data collected during the first step of the project have been stored in a relational database organized in a set of multi-tables, created on Microsoft Access. Users can manage the database using as field key the agricultural operation of interest and the year of the event for each parcel of the farm. All the queries are exportable in a GIS open source software through .csv format files. In this way a Farming Management System has been created and farmers are fostered to organize their own geodatabase of the farm, with the aim to improve the management of all activities they have to perform also reinforcing all decision-making processes through more knowledge.

2 Background and Related Works

IoT in agriculture is growing quickly, improving farm productivity and increasing farm benefit. In particular includes vehicle tracking, farm and livestock monitoring, storage monitoring and much more in producing food products (Jayaramanp et al. 2016). IoT, in that way, has an important role in smart farming, collecting different type of information. Different datasets create challenges to integrate them into a useful system for the end consumer (Hung et al. 2018). To achieve such target, ontologies are used as repositories to organize knowledge and information based on shared common vocabulary. Several works have been promoted to develop vocabulary. For example, there is AGROVOC (Nations FaAOtu 2018) by the FAO, composed of topics relevant in agriculture, fisheries, forestry and environment. One of the first important introduction in these datasets is the Thai rice ontology for the management of knowledge of Thai rice production research, even if focused only on that type of production it's an innovation for whoever is interested in (Thunkijjanukijj et al. 2009). Another important case is the developed ontology as a knowledge repository of agricultural information, including farming stages varying from crop selection to the selling stage (Walisadeera et al. 2015). There is also an ontology for crops production cycle which is used as a building block driver for an Agriculture Information System (Bansal et al. 2011). Another interesting application is the ontology-based knowledge to organize standard way for the crop cultivation (Li et al. 2013).

3 Data Collection

There is some ontology literature that defines as a starting point the acquisition methodology (Xie Nengfu et al. 2007). The equipment for the data acquisitions during the test are: unmanned aerial vehicle (UAV), SPAD chlorophyll meters, GNSS in mode Real-Time Kinematic and a meteorological station. The area is divided into two equal parts, where a rotation between wheat and corn is carried out from year to year. This area is divided into four macro areas where three different types of processing are carried out: traditional tillage, minimal tillage and sod seeding. Each macro area has three main plots and inside there are three plots smaller with three different sampling points and three levels of fertilization, with 0, 90 and 180 kg of nitrogen per hectare. Data acquisition depends basically on two technologies: GNSS and Remote Sensing. GNSS makes possible to record the in-field variability as geographically encoded data. It is possible to determinate and to record the correct position of each observation recurrent. The use of a GNSS receiver can find different applications in agriculture that are soil sampling, detection and definition of boundaries and areas. This technology has allowed, during this first stage of the research, to consider each experimental parcel of wheat (*Triticum durum*) growing, in detail. In addition, Remote Sensing techniques provide the solutions for monitoring spectral and spatial changes within the crops at high resolution (Moran et al 1997). In this research UAV

technology has been used, in particular the sensor is based on the MATRICE 600, as flying platform, equipped with the MicaSense multispectral camera. Each survey took place simultaneously with GNSS (WGS84/UTM33N) and UAV instruments in three different periods: March (before nitrogen fertilization), April (after nitrogen fertilization) and May (before harvesting). In addition, where each GNSS point was recorded, different samples of the crop canopy were taken a then examined into a laboratory.

4 Geodata Base Conceptual Modelling

The next step is the conceptualization, that is a process to build a conceptual ontological model consisting of the concepts in the domain and the relationships between those concepts (Udsanee et al. 2018). This step has concerned the geodatabase conceptual modelling, assigning specific attributes to each different geographical element, in order to organize and built it in the GIS (Malinverni et al. 2009). The database design was developed in Microsoft Access 2016 platform, adopting a simple structure with horizontal hierarchical data entry and minimal data redundancy. This means that the integrity of the data is important, as well as the maintenance of its correctness and consistency, to avoid possible mistakes. This makes easy the data management and provides excellent accessibility, reliability and independence of the data. Conceptual models for geo-database may take several forms, in this case the entity-relations model has been used, respecting the relationships One-to-Many. The conceptual model for the database subdivides the objects of interest in three topics: arable land, horticulture and viticulture; in this case only arable land database has been developed. Each part organizes, at different levels of detail, the related tables, to manage the single components with own attributes and specific characteristics. Each table is divided into several fields according to the data collected. In relation to a logical structure (Fig 1), the tables will be linked to the georeferenced vector data (points, polylines and polygons) which represent the single objects in the field,

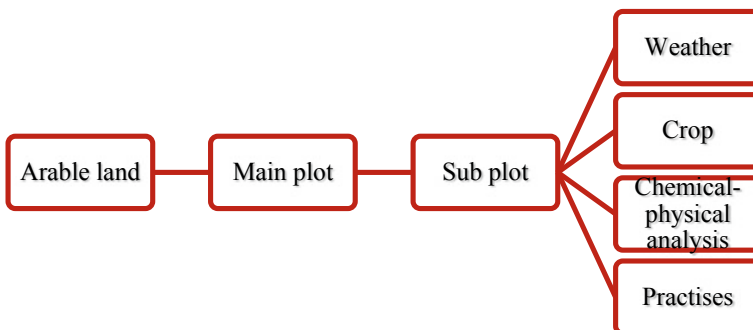


Fig. 1 Conceptual model of the database

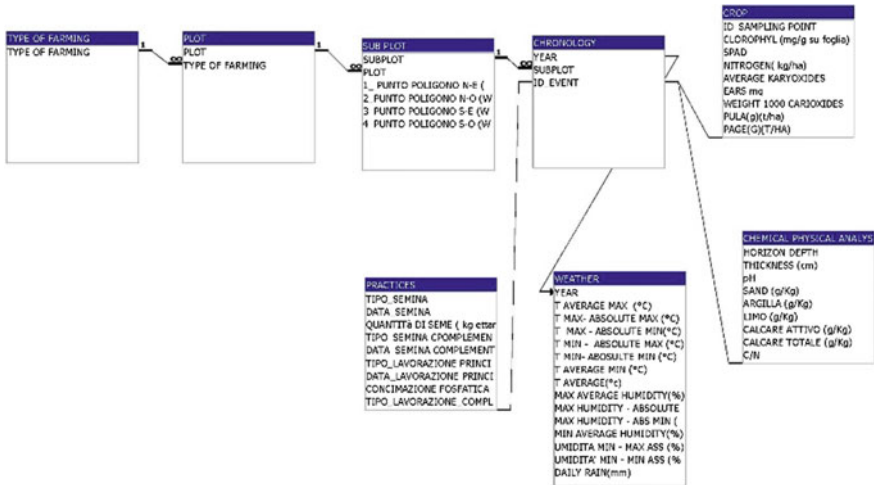


Fig. 2 Relationships of Agriculture conceptual model

identifying the correct relationship by means a univocal identification (ID_EVENT) code, allowing to identify the correct relationships among spatial and alphanumeric data.

Therefore, the most important elements by which is possible to create an entity-relationships model are the alphanumeric attributes, describing the properties of each entity and the relationships considered of relevant interest for the description of the real world. Another consistency of the entity-relationships model is the cardinality among relations and attributes (Fig 2). In fact the geodatabase represents a fundamental tool for different end-users because it can facilitate the management of local resources. Taking into account the time, the attribute that identifies the type of plot and the crop changes over the time is stored in the geodatabase and in a very, fast and simple way the farmer can retrieve data by doing simple queries for fostering all kinds of monitoring purposes (Figs. 3 and 4).

5 Geodata Base Implementation

After the creation of the database conceptual modelling, all collected data are inserted and processed in a GIS software, using the software open-source Quantum GIS. A Geographic Information System is a powerful set of tools for collecting, storing and retrieving, transforming and displaying the spatial data for particular purposes (Burrough and McDonnel 1998). The database organization (tables and features) facilitates the data entry and particularly simplifies the extraction of thematic data by means of queries or filters. In a GIS, each vector layer corresponds to a table which deals with the attributes of feature giving real meaning to the geometric entities that, otherwise,

Arable land	Main plot	Sub Plot	Year	ID. Event	Sowing date	Quantity of seed	Type of crop
Crop	116	21	2014	1	04/11/2013	220	Durum wheat
Crop	116	34	2014	2	04/11/2013	220	Durum wheat
Crop	116	21	2016	3	17/11/2015	220	Durum wheat
Crop	116	34	2016	4	17/11/2015	220	Durum wheat

ID. Event	Point sampled	Grain (g *0,25 mq)	Straw (g*0,25mq)	Nitrogen supply (kg/ha)
1	M	99,20	264,59	180
1	C	69,93	174,65	180
1	V	86,15	251,44	180

Fig. 3 Example of a yield query following the previous one

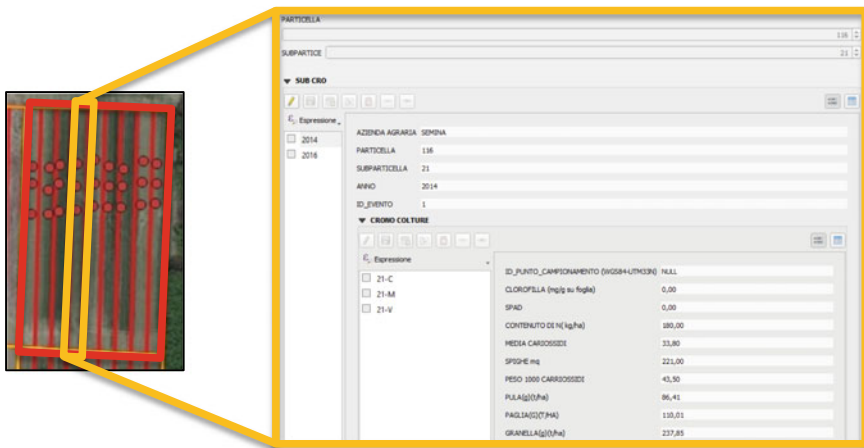


Fig. 4 An example of the subplot mask of chemical-physical analysis in QuantumGIS

would be undifferentiated. Each element of a layer is associated with a record in the table, composed of one or more fields. After creating the different layers, the data has been assigned. The operation uses the .csv file extracted from Microsoft Access and the command relations from project properties, to associate the attributes to the various objects. The final table is built by the information retrieved from other tables all related in the conceptual model one to each other (Fig. 4). All data are stored within a database management system (DBMS), completely organized avoiding the loss of information for farm management.

6 Towards a Spatial Decision Support System (SDSS)

All data of the Geodatabase can be queried by using SQL language to extract a subset of elements that are useful to perform spatial analysis and thematic classification. This makes the GIS designed for farming management system applications a powerful tool available for technicians and farmers to program operations, predict results and define strategies. The possibility to manage dynamic monitoring, based on remote sensing and field data, represents a first step towards the building of a Spatial Decision Support System (SDSS) useful to guide the agricultural operations such as sowing, fertilizing and pesticides distribution, harvesting, in the more effective way. Spatial queries and visualization allow farmers to analyse and evaluate the real situation in each crop parcel, showing the spatial distribution of the inputs, like fertilizers and pesticides, and related performances of crops, finally making possible to implement specific actions able to increase their efficiency in order to reduce the environmental pollution while boosting the quality of products. Furthermore, the system has the ability to generate relevant reports, statistical analysis and figures, as well as thematic maps. However, this new way to manage crop production needs to be supported by robust scientific and technical tools, to achieve economic, social and environmental benefits really durable.

7 Conclusions

As a matter of fact, the integration of GNSS, remote sensing, and GIS in combination with ground monitoring systems has proved from a long time to be an efficient method of managing, analysing, and outputting spatial data on landscape resources at wide-scale level (e.g. region or province) as was pointed out by Chen et al. (1997) for water resources. More recently, through the Precision Farming approach, new challenges invested the farm's scale, by focusing on the management of single parcel of crops. At parcel level, indeed, such integration is indispensable in devising an effective approach for selectively applying pesticides and fertilizers to improve farming efficiency and reduce environmental hazards (Runyon et al. 1994). The overall purpose is to design an ontology that integrates all stages and field of farm and to provide agriculture information and knowledge to end-users. The integration of those technologies may lead to an intelligent farming management system ables to solve complex spatial problems and to allow decisions concerning the pest management, hotspots identification, niche areas identification for disease outbreaks, irrigation, fertilization and other chemical usages. Actually, this is the main goal and the preliminary results of the briefly reported research, which is still ongoing in the framework of the project "PFRLab: Setting of a Precision Farming Robotics Laboratory for cropping system sustainability and food safety and security" founded by the Università Politecnica delle Marche in the 2017–2020 years (Orsini et al. 2019).

References

- Bansal, N., Malink, S. K. (2011). A framework for agriculture ontology development in semantic web. In *2011 International Conference on Communication Systems and Network Technologies (CSNT)*.
- Burrough, P.A., McDonnell. (1998). *Principles of geographic information systems*, 2nd ed. Oxford University Press, New York.
- Chen, X., Zhou, D., Zhou, N., & Tan, Z. (1997). Systematic analysis model for regional water resources based on a spatial information system, Proceedings of International Symposium, Remote Sensing and Geographic Information Systems for Design and Operation of Water Resources Systems, (M.F. Baumgartner, editor), Rabat, Morocco (IAHS Publication 242), pp. 43–51.
- Hung, Q. N., Nhien-An, L.-K., Tahar, K. (2018). *Ontology based approach for Precision Agriculture: 2th International Conference*, MIWAI 2018, Hanoi, Vietnam, November 18–20, 2018, Proceedings. https://doi.org/10.1007/978-3-030-03014-8_15.
- Jayaraman, P. P., Yavari, A., Georfakopoulos, D., Morshed, A., & Zaslavsky, A. (2016). Internet of things platform for smart farming: Experiences and lessons learnt. *Sensors*, 16(11), 1884.
- Kunal, S., Sharda, S., Ranbir Singh, R., Aditya, R., Vaibhav, K., & Arun, K. (2015). *Application of GIS in precision agriculture*. Conference Paper October 2015. <https://doi.org/10.13140/rg.2.1.2221.3368>.
- Li, D., Kang, L., Cheng, X., Li, D., Wang, K., et al. (2013). An ontology-based representation and implement method for crop cultivation standard. *Mathematical and Computer Modeling*, 58(3–4), 466–473.
- Malinverni, E. S., Chiappini, S., Pierdicca, R. (2019). *A Geodatabase for multisource data management applied to cultural heritage: The case study of Villa Buonaccorsi's historical garden* The International Archives of the Photogrammetry, Remote Sensing and Spatial Information Sciences, Volume XLII-2/W11, 2019 GEORES 2019—2nd International Conference of Geomatics and Restoration, 8–10 May 2019, Milan, Italy.
- Moran, M. S., Inoue, Y., & Barnes, E. M. (1997). Opportunities and limitations for image-based remote sensing in precision crop management. *Remote Sensing of Environment*, 61, 319–346.
- Nations FaAOotU. *Multilingual Agricultural Thesaurus (AGROVOC)*. [cited 5 March 2018]. <http://aims.fao.org/est-egistry/vocabularies/agrovoc-multilingual-agriculturalthesaurus>.
- Orsini, R., Basili, D., Belletti, M., Bentivoglio, D., Bozzi, C. A., & Chiappini, S. et al. (2019) *Setting of a precision farming robotic laboratory for cropping system sustainability and food safety and security: Preliminary results*. In *1st Workshop on Metrology for Agriculture and Forestry (METROAGRIFOR) IOP Conf. Series: Earth and Environmental Science* 275, 012021 IOP Publishing (2019). <https://doi.org/10.1088/1755-1315/275/1/012021>.
- Pierce, F. J., & Nowak, P. (1999). Aspects of precision agriculture. *Advances in Agronomy*, 67, 1–85.
- Runyon, T., Hammitt, R., & Lindquist, R. (1994). Buried danger: Integrating GIS and GPS to identify radiologically contaminated sites. *Geo Info Systems*, 8(4), 28–36.
- Thunkijjanukij, A., Panichsakpatana, S., & Veesommai, Uamporn. (2009). *Ontology development: A case study for thai rice*. Kasetsart Journal—Natural Science. 43.
- Pakdeetrakulwong, Udsanee, & Hengpraproh, Kairung. (2018). An ontology-based knowledge management for organic and good agricultural practice agriculture: A case of study of Nakhon Pathom Province, Thailand. *Journal of Thai Interdisciplinary Research*, 13(4), 26–34.
- Walisadeera, A. I., Ginige, A., & Wikramanayake, G. N. (2015). User centered ontology for Sri Lankan farmers. *Published in Ecological Informatics*. <https://doi.org/10.1016/j.ecoinf.2014.07.008>.
- Xie, Nengfu et al. *Ontology-based agricultural knowledge acquisition and application*. CCTA (2007).

A Skyline Deflection Analysis Methodology for Timber Volume Estimation in Yarding Operations



Raimondo Gallo, Luca Marchi, Stefano Grigolato, Raffaele Cavalli
and Fabrizio Mazzetto

Abstract This paper describes the approach followed to perform an automatic load monitoring during yarding activities. The goal of this methodology is the weight assessment of the loaded biomass during the inhaul phase in cable logging operations. The approach is based on the development of dedicated mathematical models that assessing the skyline deflection, tension, and slope permit to estimate the hauled load through an indirect approach. To carry out this experience an in-scale standing skyline system with single-span was set-up. The experiment was conducted at 0%, 10% and 20% of slope, respectively, and the skyline deflection was measured during travels with 0, 5, 10, 20, 30 and 40 kg of fully suspend loads. Besides these, the assessment was performed at mounting tensions of 10 and 100 kg. According to the different estimative models and the operative context, the collected results showed a difference between the estimated load and the reference one lower than 20% in terms of mass. In conclusion is possible to affirm that the proposed approach can be a suitable compromise for the indirect estimation of timber during fully suspended yarding operations.

Keywords Operational monitoring · Precision forestry · Productivity · ICT · Sensors

1 Introduction

In the Alpine Region, the use of aerial technologies is very common for timber logging operations. Indeed, the transportation of trees using helicopter or yarding systems permits to reach forestry areas characterized by extreme terrain conditions

R. Gallo (✉) · F. Mazzetto
Faculty of Science and Technology, Free University of Bozen-Bolzano, Piazza Università 5,
39100 Bolzano, Italy
e-mail: raimondo.gallo@unibz.it

L. Marchi · S. Grigolato · R. Cavalli
Department Land, Environment, Agriculture and Forestry, University of Padova, Viale
dell'Università 16, 35020 Legnaro, PD, Italy

© Springer Nature Switzerland AG 2020
A. Coppola et al. (eds.), *Innovative Biosystems Engineering for Sustainable Agriculture, Forestry and Food Production*, Lecture Notes in Civil Engineering 67,
https://doi.org/10.1007/978-3-030-39299-4_88

where the trafficability for terrestrial forestry equipment is not possible. Terrain steepness and soil roughness are the most common physical constraints for forestry tractors coupled with winch or trailers, skidders or forwards (Cavalli et al. 2009; Foderi and Marchi 2016). To overpass these operative constraints the yarding logging systems are generally used because they can ensure good productivity, short time for mounting and dismounting operations, and affordability. This logging technologies are characterized by the use of several steel cables with different tasks: (i) to support as well as to permit the displacements of the forestry carriage towards the felling area and the landing area, (ii) to command the movements of the carriage in forward or backward direction, and (iii) to anchor all the vertical components of the line (e.g. tower, intermediate supports, spars). In a standing skyline system, the skyline is that steel wire stood with an appropriate mounting tension between two spars, on which the forestry carriage runs. In the case of long yarding lines or not appropriate terrain profile conditions, one or more intermediate supports can be used to lift the skyline to avoid the risk of contact between carriage (loaded or unloaded) and ground. According to the number of intermediate supports a single or multiple span line can be set-up.

In every line section, the passage of the empty or loaded carriage determines a deflection proportional to the load, to the linear weight of the rope, the position of the carriage along the line portion, and the horizontal component of the tension on the skyline (Samset 1985). To calculate the horizontal tension on the skyline, it is necessary to understand first the tension on the skyline as well as the angle between this force and the reference plane. The aims of the present work are to define a set of simplified mathematical model capable to estimate indirectly the hauled mass knowing the mounting tension, the skyline's deflection and the slope of the line.

2 Materials and Methods

As reported in Samset (1985), to carry out the computation of the deflection is necessary to know the transported mass, the total length of the yarding line, the instantaneous distance from one extremity, the linear weight of the skyline rope and the horizontal component of the tension generated on the wire due to the load. Among all these parameters, as already said, the horizontal component of the tension is not easy to be calculated for the complexity of the measurement of the angle. As consequence of this limitation an in-scale single-span yarding line has been set-up in a controlled environment to monitor all the parameters necessary to develop specific models able to estimate the mass of the loads at different distances from the landing area.

The in-scale system is about 7 m lengths, the skyline has been stood between two pillars of concrete at three heights to obtain around 0° , 5° and 10° of skyline's slope. The skyline was manually pre-tensioned and then tensioned at about 10 and 100 kg thanks to a manual hoist. The skyline tension has been constantly monitored through a load cell. These tensions have been the operative ones. The highest represents the

most appropriate if considered the best practice for yarding installation, while the lowest is not appropriated for the same rigging configuration (Fabiano and Marchi 2001; Hippoliti 1988). Three repetitions at 0, 5, 10, 20, 30, and 40 kg of loads have been carried out for each tension and slope conditions considering both logging directions. The movement of the carriage has been ensured thanks to the gravity or through a manual pushing. During the experiment the advancement speed has been kept as possible constant. Since the in-scale yarding line has been set-up indoor the use of a GNSS for the identification of the carriage's behavior has not been possible (Gallo et al. 2013, 2018), therefore through motion analysis the behavior of the carriage under different loads and operative conditions has been evaluated. Hence, during the experiment all travels have been video recorded using a digital camera and analyzed using the software Tracker, a free tool for video analysis (<https://physlets.org/tracker/>). This software, after the video uploading and the setting of necessary parameters (such as the origin of the system, the distance calibration and the recognition of target attached on the carriage to be followed) starts to collect the coordinates of the trajectory of the carriage during the displacements (Fig. 1).

The obtained dataset, beside the quote, also contains the distances from the pre-set origin of the system and the relative time. All these acquisitions have been used to develop five mathematical models suitable to estimate the load at 10, 30, 50, 70, and 90% of the yarding line length. These distances have been arbitrarily selected as representative to assess if models can estimate the mass properly along the entire line considering their precision and accuracy. To build the model all the acquisitions related to the loads of 0, 5, 20, and 40 kg have been used for the different operative conditions, whereas those related to 10 and 30 kg have been used for the validation

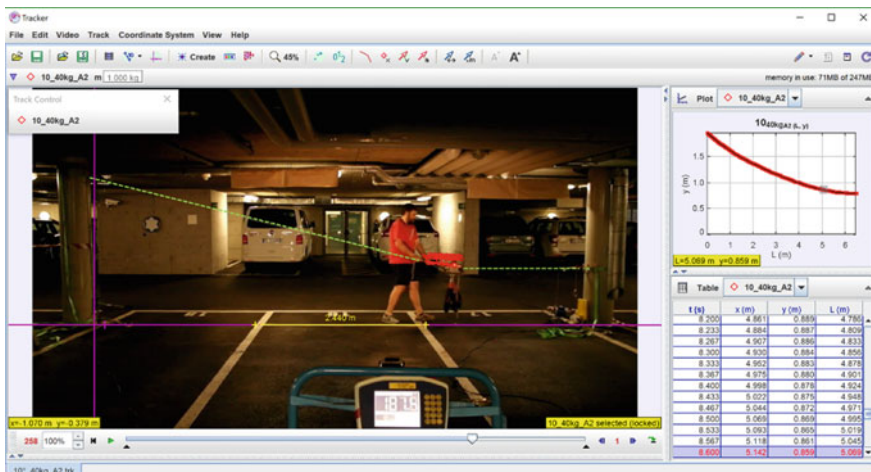


Fig. 1 The Tracker software during the video analysis. In pink, the coordinate axes (the origin refers to the landing area), in yellow the calibration distance, the red dots are the trajectory related to the followed target (the carriage), and the dashed green line is the skyline. In the right upper portion the trajectory of the carriage is reported

procedures. In Eqs. (1), (2) are reported the proposed general formulas for the indirect estimation of the mass of the carried loads. The Eq. (1) considers all the collected parameters, whereas the Eq. (2) does not consider the mounting tension. Authors decide to develop two different models to consider if the different mounting tensions can cause sensitive differences in mass estimation.

Here, $W_{\%L}$ is the load’s mass at the defined length, $D_{\%L}$ is the deflection due to the load occurred at the same length, S is the slope of the line, T is the mounting tension and a, b, c, d are the respective regression coefficients.

$$W_{\%L} = a + b \cdot D_{\%L} + c \cdot S + d \cdot T \tag{1}$$

$$W_{\%L} = a + b \cdot D_{\%L} + c \cdot S \tag{2}$$

Through multiple linear regression, all the regression coefficients have been calculated and reported in Table 1. While S and T are well known because set during the line installation, the $D_{\%L}$ has been calculated by the difference between the geometric cord of the skyline for the three slopes and the quote of carriage’s trajectory achieved during the travels.

Table 1 Results of the regression coefficients computation

	$W_{\%L}$ (%)	a	b	c	d	R^2_{adj} (%)
Equation (1)	10	-23.8223	200.587	-1.54618	0.287287	88.48
	30	-34.4956	140.682	-0.879798	0.306792	94.29
	50	-36.698	130.048	-0.627509	0.315091	94.67
	70	-39.8965	145.57	-0.321224	0.34733	95.13
	90	-40.3073	221.216	0.326995	0.394659	94.15
Equation (2) for T = 10 kg	10	-46.8304	284.14	-1.78548	-	89.21
	30	-29.5101	141.698	-1.33847	-	93.12
	50	-32.4234	131.526	-0.972563	-	92.98
	70	-35.8839	148.393	-0.639655	-	92.91
	90	-35.0541	216.515	0.285811	-	90.91
Equation (2) for T = 100 kg	10	-0.59045	222.679	-0.866978	-	96.01
	30	-6.56157	143.834	-0.440364	-	98.26
	50	-6.9778	130.714	-0.294887	-	97.79
	70	-6.59004	144.905	-0.014895	-	98.56
	90	-1.21163	226.078	0.369848	-	97.21

3 Results and Discussions

During the experiment, a total of 108 analyses have been done. The records obtained for the loads of 0, 5, 20, and 40 kg have been considered for mathematical models development. The entire dataset has been used to develop Eq. (1), while the Eq. (2) has been developed considering separately dataset collected with tension of 10 kg and 100 kg, respectively. The obtained models have been then used to estimate the load’s mass related to the deflections occurred during hauling of 10 and 30 kg of loads. In Fig. 2 a graphical summary of the obtained results has been reported.

As is possible to see, it is very clear that the results obtained applying the Eq. (2) for mounting tension equal to 10 kg shown high variability in the mass estimation if compared with the others. The highest discrepancy has been recorded for the assessment performed at 10% of the total length. Indeed, the standard deviations are higher than 10 kg for both reference loads. These values correspond at a difference in term of mass equal to 8.3 and 6.9 kg for the reference loads of 10 and 30 kg, respectively. The estimations performed for the other lengths shown standard deviations around 5 and 4 kg for the same loads. In contrast, the results obtained by applying the Eq. (2) for mounting tension equal to 100 kg shown low variability. Also in this estimation the highest variability has been recorded at 10% of the total length, with a standard deviation of 2.5 kg for both loads. For the other lengths the standard deviations have resulted around 1.5 kg. Considering the results obtained from the Eq. (1) the tendency is always the same: highest standard deviations have been recorded at 10% of the total length for both loads, meanwhile the results for the other lengths shown standard deviations around 4.3 kg and 3.3 kg for 10 kg and 30 kg of load, respectively.

In Table 2 a summary of the obtained results has been reported. In conclusion, considering the standard error for the different lengths of assessment it is possible

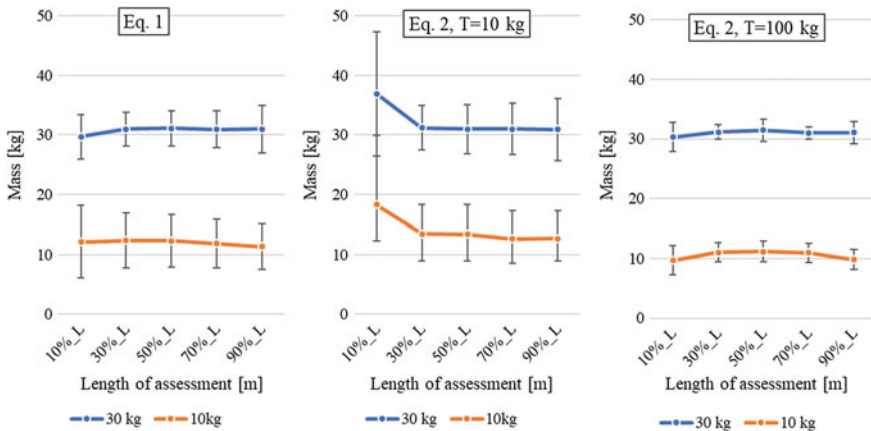


Fig. 2 Box-plots of the obtained results. The figures above and below represent the results obtained for the loads of 10 kg and 30 kg, respectively. The different colors are related to the distance at which the assessments have been performed applying the three developed models

Table 2 Summary of the results obtained from the three models. The results have been displayed separately considering the hauled loads and the mounting tensions. All the results are reported in kg

	W _{%L} (%)	Reference load of 10 kg				Reference load of 30 kg			
		Avg.	St.dev.	St.err.	Diff.	Avg.	St.dev.	St.err.	Diff.
Equation (1)	10	12.1	6.1	1.7	-2.1	29.7	3.7	1.1	0.3
	30	12.3	4.6	1.3	-2.3	30.9	2.8	0.8	-0.9
	50	12.3	4.4	1.3	-2.3	31.1	3.0	0.9	-1.1
	70	11.8	4.1	1.2	-1.8	30.9	3.1	0.9	-0.9
	90	11.3	3.8	1.1	-1.3	31.0	4.0	1.2	-1.0
Equation (2) for T = 10 kg	10	18.3	11.6	4.7	-8.3	36.9	10.5	4.3	-6.9
	30	13.5	4.9	2.0	-3.5	31.2	3.7	1.5	-1.2
	50	13.4	4.9	2.0	-3.4	31.0	4.2	1.7	-1.0
	70	12.6	4.7	1.9	-2.6	31.0	4.3	1.8	-1.0
	90	12.7	4.6	1.9	-2.7	30.9	5.2	2.1	-0.9
Equation (2) for T = 100 kg	10	9.7	2.4	1.0	0.3	30.3	2.5	1.0	-0.3
	30	11.0	1.6	0.7	-1.0	31.1	1.2	0.5	-1.1
	50	11.2	1.7	0.7	-1.2	31.4	1.9	0.8	-1.4
	70	11.0	1.6	0.7	-1.0	31.0	1.0	0.4	-1.0
	90	9.8	1.7	0.7	0.2	31.0	1.9	0.8	-1.0

affirm that the estimations done at 10 and 90% of the total lengths should not be taken into account for an indirect mass assessment of the load during yarding operation. Probably, deflection evaluations are negatively affected by a not controllable behavior of the system due to the proximity with the skyline's extremities (e.g. the change in yarding direction or the manual pushing of the carriage during the approaching operations).

4 Conclusions

In the present research, preliminary results on the indirect mass assessment during yarding operations have been presented. The general concept deals with the definition of models able to estimate the mass of the transported loads knowing the slope of the skyline, the mounting tension, and the skyline's deflection. The results have highlighted that the tension applied during the skyline installation affects the precision of the assessments but not the accuracy. Considering the outputs achieved with the Eq. (2) the lowest precision, and accuracy has been recorded for light load. Indeed, small transported mass do not permit an increase of the skyline's tension up to a tension which limits the bouncing and fluctuation effects of the carriage on the rope. Consequently, the deflection assessment could be affected by errors. Nevertheless the Eq. (1), which takes into account both operative conditions, proper and no proper mounting tensions, can be considered as a good estimator since has ensured pretty good accuracy and sufficient precision, with a mass difference around 20% and 10%, which can be considered acceptable.

Further considerations will take into account the application of this approach to multiple spans line since their behavior is very different from the single one (Pestal 1961; Hippoliti et al. 1984) as well as to partially suspended loads. With these new operative conditions all the actual skidding logging conditions have been considered.

To apply the proposed application to actual yarding systems, it is necessary to find a solution able to calculate, with high accuracy, skyline's deflections. For this aim, experiences, where RTK-GNSS unit installed on the carriage, will also be conducted and tested.

References

- Cavalli, R., Grigolato, S., & Bergomi, L. Z. (2009). *Esbosco in ambiente montano con Cable-Forwarder*. Taormina (ME): In Atti del Terzo Congresso Nazionale di Selvicoltura.
- Fabiano, F., & Marchi, E. (2001). *Note pratiche sul dimensionamento di gru a cavo* (forestali ed.). Arezzo: Compagnia delle Foreste.
- Foderi, C., & Marchi, E. (2016). Stima dei costi di utilizzazione del materiale legnoso danneggiato dal vento in regione toscana a seguito dell'evento del 5 marzo 2015. *L'italia forestale e montana*, 71(4).

- Gallo, R., Grigolato, S., Cavalli, R., & Mazzetto, F. (2013). GNSS-based operational monitoring devices for forest logging operation chains. *Journal of Agricultural Engineering*, 43.
- Gallo, R., Carabin, G., Vidoni, R., Sacco, P., & Mazzetto, F. (2018). Solutions for the automation of operational monitoring activities for agricultural and forestry tasks. *Die Bodenkultur: Journal of Land Management, Food and Environment*, 69.
- Hippoliti, G., Uzielli, L., Bronzi, A., & Piegai, F. (1984). Messa a punto di moderne attrezzature per l'esbosco dei prodotti forestali. I.S.E.A (BO).
- Hippoliti, G. (1988). *Appunti di meccanizzazione forestale*. Ed. CUSL, (FI).
- Pestal, E. (1961). *Seilbahnen und Seilkrane für Holz—und Materialtransport* – Verlag Georg Fromme & Co. Wien und München.
- Samset, I. (1985). *Winch and cable systems*. Martinus Nijhoff/Dr W.” Junk Publishers.

Neural Network Algorithms for Real Time Plant Diseases Detection Using UAVs



Mariano Crimaldi, Vincenzo Cristiano, Angela De Vivo, Marco Isernia, Plamen Ivanov and Fabrizio Sarghini

Abstract Precision agriculture aims to optimize investments and yields taking into account environmental and conditions variability between different agronomic substrates. It has influenced every aspect of agriculture such as tillage, seeding, fertilization, irrigation and pesticide spraying. The crop management optimization is the main goal of precision agriculture and it could be achieved from a triple point of view: (i) Agronomic: improvement of inputs/yields efficiency such as the choice of varieties more adapted to agricultural context; (ii) Environmental: reducing the risks to human health and environment minimizing the use and release of nitrates, phosphates and pesticides; (iii) Economic: reducing energy consumption and chemical inputs while increasing yields. In recent years, Unmanned Aerial Vehicles (UAVs) have been used in agriculture as part of photogrammetric and remote sensing tasks, but new opportunities arise also in real time pathogen detection and pesticide distribution. To this purpose, high resolution images are required, introducing a technical complexity linked to data transfer and storage. One possibility is to store only images requiring eventually a post processing operation, dropping all images proposing a standard healthy crop. The use of Artificial Intelligence (AI), and Deep Learning (DL) in particular, allows larger learning capabilities and thus higher performance and precision of real-time classification and detection. The aim of this work is to develop and test a DL model in order to detect in real-time plants diseases. The neural network proposed in this work has been trained using a dataset of RGB images, then tested on a test set. The system adopted a Convolutional Neural Network (CNN) as feature extractors from the input images and TensorFlow as framework, showing good results in disease detection.

Keywords Agriculture · UAV · Deep learning · AI · Plant disease · Remote sensing

M. Crimaldi · V. Cristiano · A. De Vivo · F. Sarghini (✉)
Department of Agricultural Sciences, University of Naples Federico II, Via Università 100, 80055 Portici, Italy
e-mail: fabrizio.sarghini@unina.it

M. Isernia · P. Ivanov
Desà SrL, Naples, Italy

© Springer Nature Switzerland AG 2020
A. Coppola et al. (eds.), *Innovative Biosystems Engineering for Sustainable Agriculture, Forestry and Food Production*, Lecture Notes in Civil Engineering 67,
https://doi.org/10.1007/978-3-030-39299-4_89

1 Introduction

The identification and diagnosis of the health status of plants is in great demand in the field of agricultural information.

Deep Learning (DL) algorithms can efficiently solve these challenges in plant pathology identification. The traditional method of detection of plant diseases requires a great deal of experience and knowledge by expert agronomist. With the development of information technology and the internet, farmers can search the image database of plant diseases or consult plant pathologists to identify diseases at a distance. In order to improve the accuracy and speed of diagnosis results, many researchers have studied automated diagnosis of plant diseases based on pattern recognition and automatic learning.

Such as, for example, using pattern recognition techniques, Support-Vector Machines (SVM), Digital image processing and Computer Vision. Meanwhile, these advanced techniques are applied to the diagnosis of plant diseases, such as wheat, corn, cotton, tomato, rice etc. In this paper we propose a method of plant disease classification based on deep convolutional neural networks DCNN. Using a dataset of images of healthy leaves, Early Blight (*Alternaria solani*), Late Blight (*Phytophthora Infestans*), Septoria Leaf Spot (*Septoria lycopersici*), Yellow Leaf Curl Virus (*Family Geminiviridae genus Begomovirus*), Bacterial Spot (*Xanthomonas campestris pv. vesicatoria*), Target Spot (*Corynespora cassiicola*), Spider Mite (*Tetranychus urticae*) damages and undefined class, we adopted the transfer learning method, consisting in the use of pre-trained models over new type of data. This approach results very efficient for a lot of cases. Among several DL models, a promising one is GoogleNet Inception V3, under TensorFlow framework. Several other models could be used, with different number of parameters, depending on the type of application: in mobile devices it is preferred light-with models with small number of layer and parameters, picking up a trade-off between accuracy and speed of the predictions.

2 Materials and Methods

From a mathematical point of view, CNNs are regularized versions of multilayer perceptrons. Multilayer perceptron usually refers to fully connected networks, that is, each neuron in one layer is connected to all neurons in the next layer.

The “fully-connectedness” of these networks make them prone to overfitting data.

Typical ways of regularization include adding some form of magnitude measurement of weights to the loss function. However, CNNs take a different approach towards regularization: they take advantage of the hierarchical pattern in data and assemble more complex patterns using smaller and simpler patterns.

Therefore, on the scale of connectedness and complexity, CNNs are on the lower extreme. The training of the CNN model is a process that consists in finding the optimal parameters of the DL model that classify correctly all the labels of the

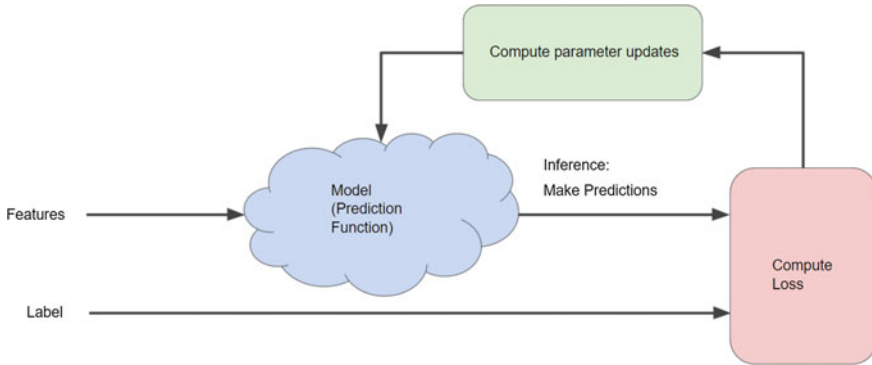


Fig. 1 Gradient Descent algorithm used for DL training process

previously selected images, also known as Supervised Learning (Jordan et al. 1992; Caruana et al. 2006). These parameters are known as weights of the model. These models are commonly stack of convolution filters with weight initialized with normal distribution values, then the weights are updated in each iteration of the training process.

The first phase the system analyses all the images in the memory and calculates bottlenecks in the last layer of the model, and the performs the classification. Images were divided into three subsets (Witten et al. 2016), i.e. train, validation and test set.

The largest set is usually the training set, approximately 80% of the all dataset. In fact, one of requirements of a correct CNN training is the non-overlapping of the three different subset, to avoid any possible interpolation in NN training.

The Fig. 1 suggests the iterative process (gradient descend algorithm) that ML and DL are using for training process.

The main goal is to define a good loss function and to minimize it, finding the optimal parameters of the model. The most popular and used loss function in the classification problems is a cross entropy loss between two probability distributions p and q that are labels and predictions, which is given by (Eq. 1):

$$Cross\ Entropy\ Loss(p, q) = - \sum_i p_i \log(q_i) \tag{1}$$

If the two distributions are similar than the loss is close to zero. On the other hand, if the distributions are significantly different, the loss results in a very large number asymptotically tending to infinity. During the training process, a Stochastic Gradient Descent (SGD) optimizer for minimizing this loss function has been used. This optimizer tunes the model parameters in each training approaching the Ground Through (Images Labels).

For modeling and training of the CNN architecture an HP Workstation was used with the following configuration:

- Two Nvidia Quadro P5000 GPU's 16 GB GDDR5, 2560 Cuda Cores, FP32 8.9 TFLOPS each of them Intel Xeon Silver 4108 CPU 1.8 GHz up to 3.0 GHz, 8 Core 16 threads, 64 Gb of RAM.
- Python with Tensorflow GPU version with CUDNN, Cuda Drivers and toolkit.

The trained networks were then deployed on low-consumption optimized hardware Nvidia Jetson TX2 onboard computer for the UAV for real time classification and storage of the data. It is a CPU 256-core NVIDIA Pascal GPU, a pair of 64-bit NVIDIA Denver 2 ARM-compatible cores, and four 64-bit ARM A57 cores. It can deliver 2 TFLOPs of single precision performance, using mathematical libraries as OpenCV, NumPy, SciPy and Matplotlib.

The training process has been re-trained starting from a pre-trained model (InceptionV3 for Image-Net) on standard dataset images (Transfer Learning) in order to reuse lower layers that have been trained to distinguish between some other objects.

2.1 *Bottlenecks*

The training script during the first phase analyzes all the images on disk and calculates and caches the bottleneck values for each of them. '*Bottleneck*' is an informal term often used for the layer just before the final output layer that does the classification. This pre-final layer has been trained to output a set of values that's good enough for the classifier to use to distinguish between all the classes it's been asked to recognize. That means it has to be a meaningful and compact summary of the images, since it has to contain enough information for the classifier to make a good choice in a very small set of values.

2.2 *Training Dataset*

The data records contain 54309 images. The images span 14 crop species: Apple, Blueberry, Cherry, Corn, Grape, Orange, Peach, Bell Pepper, Potato, Raspberry, Soybean, Squash, Strawberry, Tomato. It contains images of 17 fungal diseases, 4 bacterial diseases, 2 mold (oomycete) diseases, 2 viral disease, and 1 disease caused by a mite. 12 crop species also have images of healthy leaves that are not visibly affected by a disease.

Figure 2 shows the 38 classes of crop disease pairs that the dataset is offering. (Hughes et al. 2016; Witten et al. 2016).

The training of the top layer of the network begins once the bottlenecks are completed. The training steps have been set equal to 500 each one with a training accuracy and cross entropy output. The training accuracy shows what percent of the images used in the current training batch were labeled with the correct class. Cross



Fig. 2 Classes of crop diseases in dataset

entropy is a loss function which gives a glimpse into how well the learning process is progressing.

The training's objective is to make the loss as small as possible, in order to tell if the learning is working. All the training process data have been stored as TensorBoard log file in order to be visualized as graph for better understanding the process. Figure 3 shows the NN graph (last layers) used to train the model.

The trained model has been subsequently validated calculating the accuracy on a randomly selected group of images from a different set.

3 Results and Discussion

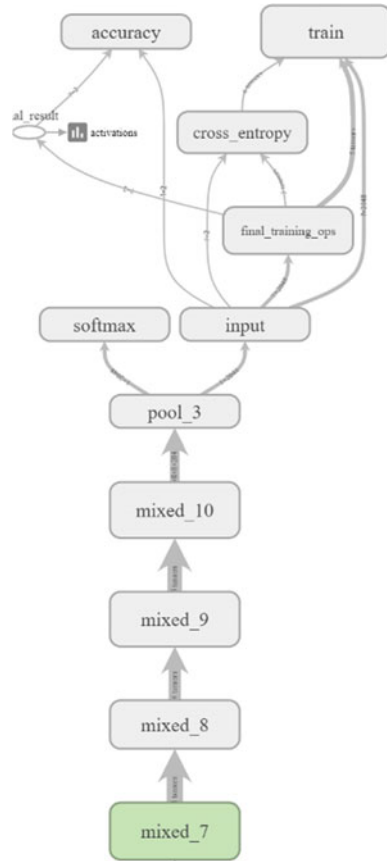
In this work we focused the application on the rice plant diseases. The most dangerous disease in this field is the rice blast, this is plant-pathogenic fungus that causes economically significant crop losses annually. Each year it is estimated to destroy enough rice to feed more than 60 million people. This fungus is known to occur in 85 countries worldwide (Scardaci et al. 1997)

After the training dataset was prepared, the training step was performed.

As previously mentioned, a pre-trained models Inception V3 model, based on transfer learning, was adopted.

Inception V3 is a widely-used image recognition model that has been shown to attain greater than 78.1% accuracy on the ImageNet dataset. The model is the

Fig. 3 Neural Network structure: last layers nodes



culmination of many ideas developed by multiple researchers over the years. It is based on the original paper: “Rethinking the Inception Architecture for Computer Vision” by Szegedy et al. (2016).

The model itself is made up of symmetric and asymmetric building blocks, including convolutions, average pooling, max pooling, concats, dropouts, and fully connected layers. Batchnorm is used extensively throughout the model and applied to activation inputs. Loss is computed via Softmax.

In the first phase all the images are analyzed by the system in the memory and bottlenecks are evaluated in the last layer of the model, and then the classification is performed. Images were divided into three subsets (Witten et al. 2016), i.e. train, validation and test set.

The largest set is usually the training set, approximately 80% of the all dataset. In fact, one of requirements of a correct CNN training is the non-overlapping of the three different subset, to avoid any possible interpolation in NN training. One might wonder why all the images were not used in the training process. As a matter of fact in machine learning the model may store irrelevant details of the training images to find

the right answers. For example, the model could identify patterns in the background of each image classified as correct answer due to the presence of a pest, and then use these details to match labels with objects.

It could produce good results on all images because it has not learned the general characteristics of the objects, but only stored unimportant details of the training images.

This problem is note with the name of overfitting, (Srivastava et al. 2014), and to avoid it we must keep data separate from the training process, so that the model cannot store them. Typically, 80% of the images are used for training, 10% for validation and 10% for test the performance on real data (Witten et al. 2016).

Once the training shows a good performance in terms of accuracy, the model is frozen and all the model weights are recovered, ready to be transferred into the mobile hardware (Nvidia Jetson mainboard).

The application in rice pathologies identification showed a percentage of correct identification of 98%, and the average identification time was 200 ms on the mobile board. Such time can be considered very small, but as a matter of fact is still high to decide if an image contains a possible pathogen and must be retained or is a healthy crop and it can be dumped.

The model training started with the analysis of all the images and calculation of bottlenecks which performs the classification. The images have been divided into three subsets of images (train, validation and test) (Srivastava et al. 2014). The training stops after 500 training steps, reaching an accuracy of 0.92 (Fig. 4). Once we have reached good performance in terms of accuracy of the model we can freeze all the model weights (variables) as file *graph.pb* and textual file *lab.txt* with the images labels. These files can be transferred on UAV onboard computer for real time classification of on-field recorded images. Also, during the training phase, the cross-entropy has been calculated after 500 training steps as shown in Fig. 5.

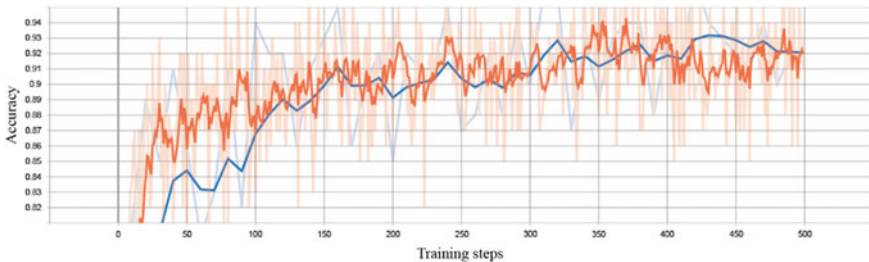


Fig. 4 Accuracy of training process with 500 training steps (The accuracy represents the percentage of recognized samples during training process, the higher the better)

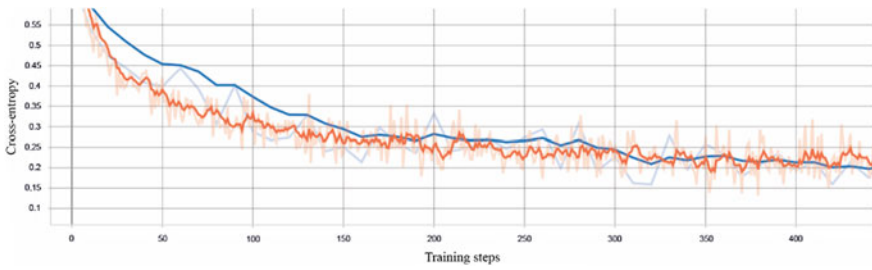


Fig. 5 Cross-entropy of 500 training steps. Cross-entropy loss, or log loss, measures the performance of a classification model whose output is a probability value between 0 and 1. Cross-entropy loss increases as the predicted probability diverges from the actual label. A perfect model would have a log loss of 0

4 Conclusions

The application of DL in real time identification of crop diseases open new possibility to identify possible infestations the early phase, allowing to provide remedies immediately, reducing the environmental impact in terms of overall pesticides quantities and increasing the final quality of the product. Convolutionary neural network seems to be an appropriate approach for pathogen identification, and the actual bottleneck seems to be related to the existence of reliable dataset of images for each possible pathogen at the resolution required by the observation system (drone, rover) rather than of the power of the DL algorithms adopted. In practical cases, in authors' opinion, the application of the proposed approach requires a multidisciplinary team, where pilots and engineers are in charge of obtaining images according civil aviation rules and perform the technical analysis. Agronomists, based on observations and information provided by the on field analysis, can suggest the appropriate treatment including specific pesticides and dosing. Following this multidisciplinary operative framework, the agronomical entrepreneur is not supposed to acquire the all knowledge of systems, data treatment and storage, but he can buy a pay per number of mission service reducing implementation and operative costs. As a consequence, early detection of pathogens and pests can reduce strongly the amount and number of pesticide treatments, producing a higher quality production at reduced environmental impact.

References

- Caruana, R., & Mizil, A. N. (2006). An empirical comparison of supervised learning algorithms. In *Proceedings of the 23rd International Conference on Machine Learning*.
- Hughes, D. P., & Salathe, M. (2016). An open access repository of images on plant health to enable the development of mobile disease diagnostics. *arXiv preprint arXiv:1511.08060*.

- Jordan, M., & Rumelhart, D. E. (1992). Forward models: Supervised learning with a distal teacher. *Cognitive Science*, *16*(3), 307–354.
- Scardaci, S. C., et al. (1997). Rice blast: A new disease in California. *Agronomy Fact Sheet Series*, *2*, 1–2.
- Srivastava, N., Hinton, G., Krizhevsky, A., Sutskever, I., & Salakhutdinov, R. (2014). Dropout: A simple way to prevent neural networks from overfitting. *The Journal of Machine Learning Research*, *15*(1), 1929–1958.
- Szegedy, C., Vanhoucke, V., Ioffe, S., Shlens, J., & Wojna, Z. (2016). Rethinking the inception architecture for computer vision. In *Computer Vision and Pattern Recognition*.
- Witten, I. H., Frank, E., Hall, M. A., & Pal, C. J. (2016). Data mining: Practical machine learning tools and techniques. *Morgan Kaufmann*.

Use of UAVs and Canopy Height Model Applied on a Time Scale in the Vineyard



Luca Ghiani, Alberto Sassu, Vanessa Lozano, Giuseppe Brundu, Davide Piccirilli and Filippo Gambella

Abstract Among the main objectives of “Precision Farming”, there is a more rational use of plant protection products, including a better application in the field. The benefits that can be achieved are various: from best product quality and reduced costs, up to an increase in productivity with considerable advantages both from an economic point of view and in terms of lower environmental impact. Currently, field measurements in agriculture are carried out using mathematical formulas that require direct measurements of crown height, thickness and distance between canopies (e.g., the Tree Row Volume or TRV). These methods are used e.g. to estimate adequate dosages treatments and to manage the canopy of vineyards. The present research describes the development of a methodology for the computation of the volumes through remotely sensed imagery acquired with UAV RGB digital camera, analyzed with MATLAB scripts and ArcGIS. Preliminary results show that the volumes obtained with this 3D reconstruction are 50% lower than those directly measured in the field (TRV), therefore promoting a limitation of the use of chemicals.

Keywords Unmanned Aerial Vehicle (UAV) · Canopy cover · Tree Row Volume (TRV) · Digital Surface Model (DSM) · Digital Elevation Model (DEM) · Precision Viticulture (PV)

1 Introduction

The measurement and structural characterization of plants can be carried out remotely using several detection tools, including image analysis techniques, stereoscopic photography, analysis of the light spectrum, ultrasonic ranging, and optical ranging (Mathews and Jensen 2013; Torres-Sánchez et al. 2015). Previous studies have used the Structure from Motion (SfM) technique to create a 3-D vineyard point cloud

L. Ghiani · V. Lozano · G. Brundu · D. Piccirilli · F. Gambella (✉)
Department of Agriculture, University of Sassari, Viale Italia 39, 07100 Sassari, Italy
e-mail: gambella@uniss.it

A. Sassu
Inspire s.r.l, Via XX Settembre 33/10, 16121 Genoa, Italy

© Springer Nature Switzerland AG 2020
A. Coppola et al. (eds.), *Innovative Biosystems Engineering for Sustainable Agriculture, Forestry and Food Production*, Lecture Notes in Civil Engineering 67,
https://doi.org/10.1007/978-3-030-39299-4_90

and to estimate grape vine canopy volume and LAI (Mathews et al. 2013). These techniques allow to optimize canopy management and pest control (spray application), especially when the variable rate techniques (VRT) are used (Gil al. 2007). The Tree Row Volume is the total vegetation volume by ground unit ($\text{m}^3 \text{ha}^{-1}$) in vineyard crown height (h), vineyard width (w) and inter-row distance (ir) (Sutton and Unrath 1984) and can be calculated by manual measurements, but this method is labor intensive and time-consuming (Andùjar et al. 2019). Recently, the acquisition of high-resolution RGB images of the canopy derived from UAVs has proved to be an effective tool for estimating plant architecture through the computation of a Digital Surface Model (DSM) (Bending et al. 2013; Zarco-Tejada et al. 2014) and the use of Ground Control Points (GCP) located within the scene are recommended as best-practice for spatial accuracy and minimization of model error.

The aim of the present research was to test the use of DEM, DTM and normalized nDSM derived by SfM techniques (Canopy Height Model) in different years and the analysis of the row volume using a MATLAB script and ArcGIS software to compare the volume of the canopy measured in the field by TRV.

2 Materials and Methods

This study was carried out during the 2016 growing season in July, and August, under sunny clear sky conditions, and on July 2017 and June 2019. The experimental field was located in the municipality of Usini (Fig. 1), Sardinia Region, Italy (Lat. $40^\circ 40' 10.13''$, Long. $8^\circ 29' 37.35''$, 144 m s.l.m.). Grape vines were planted in a clay-loam soil at a 0.9×2.1 m spacing (North-South row orientation) and pruned according to the *Guyot* system. Six Ground Control Point (GCP) were georeferenced through the use of a GNSS Leica 900 real-time kinematic receiver (Leica Geosystems, Switzerland). Twenty-four single sample points were identified in the parcel to characterize the canopy after every single flight.

2.1 UAV-Based System

A DJI Phantom 4 Pro equipped with a digital camera resolution of 21 Megapixel was used for data acquisition. Images with front overlap and side overlap (75% and 80% respectively), were acquired at midday under clear sky conditions. The images guaranteed optimal photogrammetric processing at a height of 35 m Above Ground Limit (AGL) in 2016, 2017, and 2019 and 50 m in 2017. The flights were made (Table 1) on 2016, DOY 189 (07 July), BBCH 79 (beginning of bunch closure) and GDD 798 and finally at DOY 215 (02 August), BBCH 81 (veraison, berries developing color) and GDD 1176 (Lorenz et al. 1994). The GSD of the models is reported in Table 1.

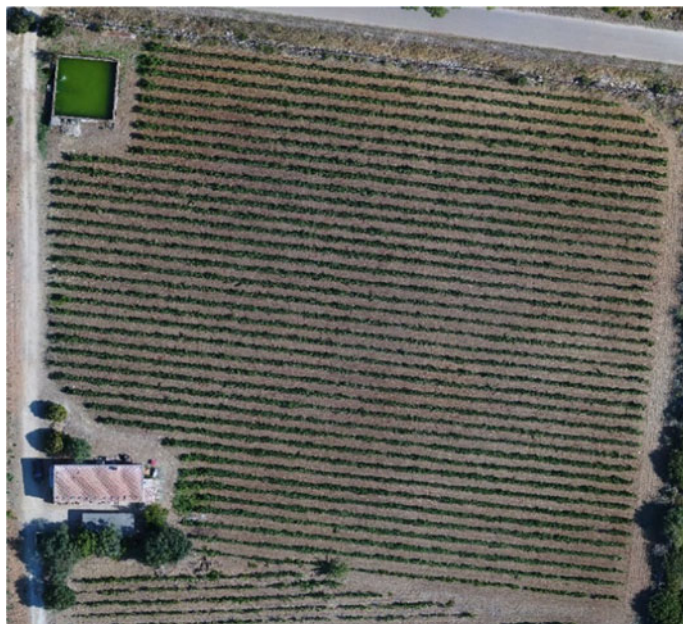


Fig. 1 Experimental field in the municipality of Usini

Table 1 Flight survey, orthophoto properties, Ground Sample Distance (GSD) and vineyard Day of the Year, BBCH and Ground Degree Day values

Year	Where	When	Orthophoto		Vineyard		
			GSD (cm)	RMSE (cm)	DOY	BBCH	GDD
2016	Usini	07/07	0.26	3.3	189	79	798
		02/08	0.26	0.07	215	81	1176
2017	Usini	17/07	0.90	6.4	198	79	798
		31/07	1.22	5.7	212	81	1282
2019	Usini	26/06	0.92	2.5	177	71	665

2.2 Extraction of the Canopy Height Model (CHM)

In literature the terminology used to describe the different differential 3D models created in SfM processing and the use of the Crop Surface Model (CSM), (Bendig et al. 2104; Geipel et al. 2014) describes the absolute height of crop canopies and define a CSM as the difference between the Digital Elevation Model (DEM) and the Digital Terrain Model (DTM). The 3D differential model that calculates the altimetric profile of the vineyard (Canopy Height Model) was the normalized n DSM obtained by difference between DEM and DTM values processed in Agisoft Photoscan© (St. Petersburg, Russia). The major approximation is due to the fact that, in

a reconstruction based on nadiral images taken from above, it is not possible to see (and therefore reconstruct) the lower part of the plants. The calculation in ArcGIS was performed with a deduction of the quota values included in the “first basic input raster” (DEM), versus a “second input raster” (DTM) from the values of the cell by cell, generating an ASCII file containing the height values on the reference plane (height of the vine-farming system measured in the field at 0.90 m). Both the software analysis procedure in ArcGIS and in MATLAB, extract numerical information from the vineyard rows to calculate the covered area heights of the single rows (Canopy Height Model) integrating the volume of all of individual pixels above the top of the vineyard. The information contained in the *n*DSM concerns the variations in height without interference by the colors or shadows or other types of plants in the area being analyzed (at least until their height exceeds the set limit 0.90 m). The analysis procedure in MATLAB was run only on the DEM. We estimated the quota values for each row (vineyard wasn't flatness), by averaging the values of visible land between which that particular row was found. The values in meters in the DEM were calculated by a $R \times C$ pixel matrix (R rows and C columns) knowing GSD (0.26 cm/pixel) and dividing the matrix into blocks formed by a number y of rows and x of columns (in pixels), respectively the x and y values parallel and perpendicular to the rows, corresponding to values of field spacing ($0.9 \text{ m} \times 2.1 \text{ m}$) including one small part of the ground present inside each block (Fig. 2a). The minimum value of each block can, therefore, be taken as a reference zero, to extract the values that exceed the cutting height of 0.90 m (Fig. 2b). Compared to the classic methods of calculating volumes (such as the Tree Row Volume or TRV) these two methods were more reliable. Moreover, selected pixels allow obtaining an excellent segmentation of the rows, as shown where the edge of the selected area has been superimposed on the corresponding orthophoto (Fig. 2c).

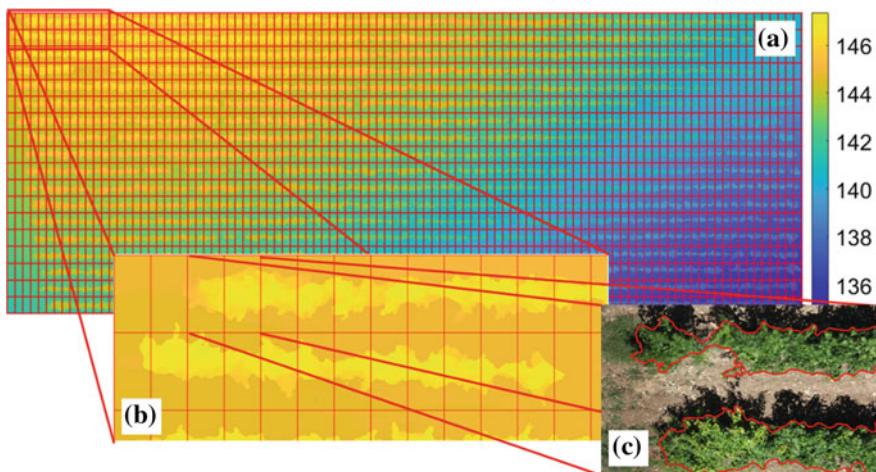


Fig. 2 a DEM analyzed in MATLAB (each rectangle is 2.1 m high and 0.9 m wide), b zoom of the upper-left part, c example of the overlapping of the rows considered

Table 2 The tree row volume (TRV) measured in the field compared with the grape vine volumes calculated by ArcGIS and MATLAB, and GCC, on 4 different dates

Date	Field TRV (m ³ ha ⁻¹)	MATLAB TRV (m ³ ha ⁻¹)	Green canopy cover (%)	
			MATLAB	Field
07/07/2016	9679 ^a	3115	29	42
17/07/2017	1994 ^b	2690	24	17
26/07/2019	3532 ^b	2731	32	27
02/08/2016	9498 ^b	2595	26	42
31/07/2017	1962 ^b	2624	30	17

^a12 measurements for nine rows used to extract the value of TRV in 2016.

^b100 for four rows used to extract the value of TRV 2017 and for six rows in 2019

3 Experimental Results

The data values are presented in the table (Table 2). More precisely, the volumes have been determined both for single rows and for all grape-vine rows in the field. Furthermore, the average percentages of the Green Canopy Cover (GCC) area of 4 single rows concerning the field area have also been included, determined by ArcGIS and MATLAB. Regarding the two methods presented, any absence of plant or variation in the thickness of the canopy was easily detectable and analysis of this type, very simple with the tools we have used, becomes much more complex if we do not have an image from the top or better yet a DEM.

4 Discussion

The difference between the three years is the result of plant growth and management of the vineyard. During the month of July for the years 2016, 2017 and 2019 values were, respectively, 9679 (m³ ha⁻¹), 1994 (m³ ha⁻¹), and 3532 (m³ ha⁻¹) in field. The row volume calculated with ArcGIS and MATLAB went from 3115 (m³ ha⁻¹) to 2690 (m³ ha⁻¹) to 2731 (m³ ha⁻¹) with a reduction of the canopy volume of more than fifty percent only in 2016. In fact, in the TRV estimation field, workers tend to measure the maximum width and maximum height, and this might produce an overestimate of the volume of the plants. Similar values of TRV were obtained in July-August 2016, 9679 (m³ ha⁻¹), and 9498 (m³ ha⁻¹) in field versus 2690 (m³ ha⁻¹) and 2595 (m³ ha⁻¹) determined by MATLAB and ArcGIS (12 measures versus 116 measures). In 2017 the TRV values were 1962 (m³ ha⁻¹) in field in July (31st) versus 2624 (m³ ha⁻¹) (August 2nd) calculated by MATLAB and ArcGIS with the same set of measures (116, all the plants in the row). These different trends are due to the great difference between the calculation methods. More precisely, if through the use of these software one goes to evaluate quantitatively the centimeter by centimeter

volumes analyzing them then in the smallest details (at least in the visible parts from the top), through the TRV method we limit ourselves to the determination of the volume through systems of sample sizes. The GCC percentage in July and August range between 24.0 and 32.0 was similar to value obtained by other authors in red vine Tempranillo and Cabernet Sauvignon and correlated with LAI (Ballesteros et al. 2015). Field data in 2017 and 2019 present a much higher similarity with the values obtained by software. This is mainly due to the different measure extraction process and also to the fact that we extended measures to all the plants in the investigated rows (4 in 2017 and 6 in 2019). In 2019 we also applied 20 orange cards in different plants in vineyard to evaluate the precision in the *n*DSM reconstruction. The comparison between the height values extracted by ArcGIS and MATLAB software and those measured in the field confirm the precision of the *n*DSM model with a Pearson correlation $r^2 = 0.80$, $p = 0.000$, and $RSME \pm 10.28$. In order to confirm the validity of the height set as a reference for the volume calculation in the 2016, in 2017 and in the 2019 4 rows were selected (16, 18, 20 and 22) and the variations of surfaces and volumes were calculated in MATLAB for variable cutting heights from 0.4 m up to 1.0 m with 0.1 m intervals for a total of 7 different values. As can be seen from Fig. 3, the volumes (July 2019) vary almost linearly, while the variation in surfaces is limited in the early stages and then decreases more and more clearly, with same variation observed for the years 2016 and 2017.

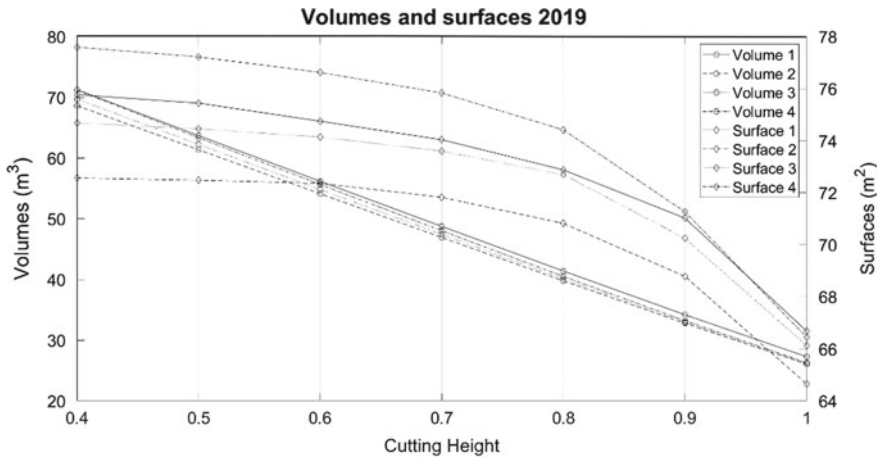


Fig. 3 Variation in volume (m³) and surface area (m²) in four-row in vineyard with imposed cutting height in MATLAB

5 Conclusions

In three years (2016, 2017, and 2019) we observed both volume and area growth until when in-field grapevine canopy management operations were carried out for leaf removal until the grape harvesting season. Using high-resolution images from UAVs provides accurate geo-referenced imagery with high spatial and temporal resolution that is delivered in near-real-time. The MATLAB procedure resolve problems due to the presence of shadows or other non-target plant species (weeds) in the area analyzed. The high resolution of the model (GSD) was comparable to the results obtained with the use of more expensive and precise sensors (e.g., Lidar). Furthermore, the operational performances of the single computers destined for processing do not represent a limit (for the models proposed from 2 h to 4 h) of processing as a function of the desired cm/pixel resolution; they are, in any case, advantageous compared to the measurements in the field. The advantage to procedure and to the consequence analysis of the values was extended to every centimeter of the entire analyzed surface (*n*DSM). This technology will help farmers control grapevine vigor and growth patterns and support decisions to improve crop management, optimize pesticide and fertilizer applications, and enhance forecast yield. UAV use is advantageous for measuring GCC and volume because it describes canopy structure for the whole vineyard and by SfM algorithm can be derived terrain and canopy data sets. Traditional methods for technological and physiological variables estimation used by the winemaker are often time-consuming and require difficult procedures in both field and laboratory. Moreover, canopy evaluation using UAV-based imagery allows a non-destructive, which is beneficial for the farmers.

Acknowledgements This study was conducted in the framework of projects funded by the Sardinian Regional Authority, i.e. the project (a) POR FESR Sardegna 2014–2020—“MARS—*Multiple Airdrones Response System*” and (b) National project PRIN: Progetti di Ricerca di Rilevante Interesse Nazionale—Bando 2017 Title: “*New technical and operative solutions for the use of drones in Agriculture 4.0*”.

References

- Andújar, D., Moreno, H., Bengochea-Guevara, J. M., de Castro, A., & Ribeiro, A. (2019). Aerial imagery or on-ground detection? An economic analysis for vineyard crops. *Computers and Electronics in Agriculture*, *157*, 351–358.
- Ballesteros, R., Ortega, J. F., Hernández, D., & Moreno, M. Á. (2015). *American Journal of Enology and Viticulture*, *66*, 120–129. <https://doi.org/10.5344/ajev.2014.14070>
- Bendig, J., Bolten, A., & Bareth, G. (2013). UAV-based imaging for multi-temporal, very high resolution crop surface models to monitor crop growth variability. *Photogramm. Fernerkund. Geoinf.*, *6*, 551–562.
- Geipel, J., Link, J., & Claupein, W. (2014). Combined spectral and spatial modeling of corn yield based on aerial images and crop surface models acquired with an unmanned aircraft system. *Remote Sensing*, *6*, 10335–10355.

- Gil, E., Llorens, J., & Llop, J. (2009). Precision Viticulture: use of new technologies to improve efficiency in spray applications in vineyard. In *Conference "Technology and Management to Increase the Efficiency in Sustainable Agricultural Systems"*, Rosario, Argentina, 1–4 September 2009.
- Mathews, A. J., & Jensen, J. L. R. (2013). Visualizing and quantifying vineyard canopy LAI using an Unmanned Aerial Vehicle (UAV) collected high density structure from motion point cloud. *Remote Sensing*, 5, 2164–2183.
- Sutton, T. B., & Unrath, C. R. (1984). Evaluation of the tree-row-volume concept with density adjustments in relation to spray deposits in apple orchards. *Plant Disease*, 68(6), 480–484.
- Torres-Sánchez, J., Peña, J. M., De Castro, A. I., & López-Granados, F. (2014). Multi-temporal mapping of the vegetation fraction in early-season wheat fields using images from UAV. *Computers and Electronics in Agriculture*, 103, 104–113.

Development of a Matlab Code for the Evaluation of Spray Distribution with Water-Sensitive Paper



Luca Ghiani, Alberto Sassu, Davide Piccirilli, Gian Luca Marcialis and Filippo Gambella

Abstract One of the biggest problems of agriculture is the reckless use of pesticides and their incorrect application with consequent waste of product and environmental pollution. The spray application characterization is a good preventive technique to limit the volume of a distributed product, to perform a more efficient application and to restrict the spray drift. Since there is no specific sampling technique useful for every context, it is necessary that every methodology is known in all its aspects before being employed. The colorimetry, fluorimetry and spectrometry methods are very accurate, but they are costly and time-consuming compared to a Water-Sensitive Paper (WSP) assessment performed by an image analysis software. This kind of software can detect and estimate many drops features using an image often obtained from a scanner. The objective of work was to develop a MATLAB code to evaluate the spray distribution over WSPs. After a pre-processing step in which the WSPs were isolated inside the image, the individual drops were identified using the difference between their color (blue) and the remaining dry part of the paper (yellow). Once the surface of every drop was estimated, it was possible to assess the number of the drops per cm^2 , the Normal Median Diameter (NMD) and the Normal Volume Diameter (VMD).

Keywords Image-processing · Water-Sensitive paper · MATLAB · Pesticide spraying analysis · Deposition analysis

L. Ghiani (✉) · D. Piccirilli · F. Gambella
Department of Agriculture, University of Sassari, Viale Italia 39, 07100 Sassari, Italy
e-mail: lghiani@uniss.it

A. Sassu
Inspire s.r.l, Via XX Settembre 33/10, 16121 Genoa, Italy

G. L. Marcialis
Dipartimento Ingegneria Elettronica, University of Cagliari, Piazza D'Armi snc, 09123 Cagliari, Italy

© Springer Nature Switzerland AG 2020
A. Coppola et al. (eds.), *Innovative Biosystems Engineering for Sustainable Agriculture, Forestry and Food Production*, Lecture Notes in Civil Engineering 67,
https://doi.org/10.1007/978-3-030-39299-4_91

1 Introduction

Pesticides are a useful tool for pests and disease control in commercial crop system (Witton et al. 2018) but, due to their effect on the environment, they represent one of the major concerns in the world. For this reason, in 2009 the European Union regulated the reduction of pesticide usage through the Directive 2009/128/CE (European Parliament 2009).

The improvements in spray application analysis seem to be the best method to achieve a pesticides reduction. Aerial spraying application of chemical and biological products can help to execute efficient and effective (Lan et al. 2017) control over severe disease and insect pests. Compared with manned aircraft, the Unmanned Aerial Vehicles (UAV), can perform accurate application of agrochemicals thanks to the optimization of automatic guidance systems (Budiyono and Wibowo 2007; Hong et al. 2012), a very low altitude fly operations (Lou et al. 2018), a good mobility, a lightweight and the low-cost.

The information about the distribution performance and spray deposition can help to reduce the volume of the product during the application and execute a more accurate and effective application. Various methods could be used to investigate spray patterns like deposition and coverage.

The quality of spray application in the field may be deduced using a Kromekote® card or a Water Sensitive Paper (WSP), a yellow card which turns from yellow to blue on contact with water thanks to a bromophenol surface. These tools can be attached to selected target areas or leaves and inspected after spraying (Aglieco and Cerruto 2011; Otto et al. 2018).

Different works were assessed about the use of WSP and their analysis methods. Heping Zhu et al. (2011) developed a portable scanning system (composed of handheld business card scanner, deposit collectors, a laptop computer, and a custom-designed software entitled “*DepositScan*”) to quickly evaluate spray deposit distribution and coverage area of WSP or Kromekote® card. Salyani et al. (2013) highlighted the limitations of WSP for spray droplet characterization compared to Absorbent Paper (AP), using a spray solution containing a fluorescent tracer. The spray drops over the WSP were assessed by three independent image analysis systems, while the data from AP were obtained by fluorimetry. Cuhna et al. (2012) compared the performance of several commercial and experimental software for WSP analysis (*Gotas*, *StainMaster*, *ImageTool*, *StainAnalysis*, *AgroScan*, *DropletScan* and *Spray_image I* and *II*) against known coverage, droplet size spectra and class size distribution verified through manual counting. The results showed the accuracy derived by the artificial targets coupled with an appropriate image system.

The objective of this work was to develop a fast and cheap image processing method based on a MATLAB code to evaluate the spray distribution over a WSPs (26 × 76 mm) images, obtained from an office scanner.

2 Materials and Methods

The Water Sensitive Paper analyzed through the MATLAB code were obtained from a UAV water spray application with a Green drift-reduction nozzle (ALBUZ, ISO 110015) over a wheat crop in the tillering phase arranged in parcels (1.2 m × 8 m). Fifteen WSPs, disposed in three parallel rows of 5 WSPs each, were placed over a supporting structure to guarantee the uptake of the droplets produced from the sprayer inside the herbaceous crop. Every row (composed of 5 WSP) was then scanned and analyzed individually (Fig. 1a) as reported in the section below.

2.1 Analysis of Water-Sensitive Paper (WSP) Through a MATLAB Code System

The following analysis was performed scanning images of WSPs (19.86 cm²) with the *Canon Lide 220* scanner of 1200 dpi (dots per inch) resolution. Given that, one inch corresponds to 25.4 mm, with a resolution of 1200 dots per inch, the size of the single pixel is about 21.17 microns (obtained by dividing 25.4/1200).

The WSPs used for the test were then analyzed through a MATLAB 2018b code, able to investigate the WSP images (with a white background) characterized by a yellow dry part and blue wet parts (Fig. 1b).

The WSP analysis using the MATLAB code was divided in three phases. In the first one, the *preprocessing phase*, each WSP were first isolated in the image creating a mask (Fig. 2a). The part of the image selected by the mask (Fig. 2b) was then processed using the three RGB channels to isolate the blue parts (channel B predominant on the other two) and the yellow parts (derived from the combination of R and G channels).

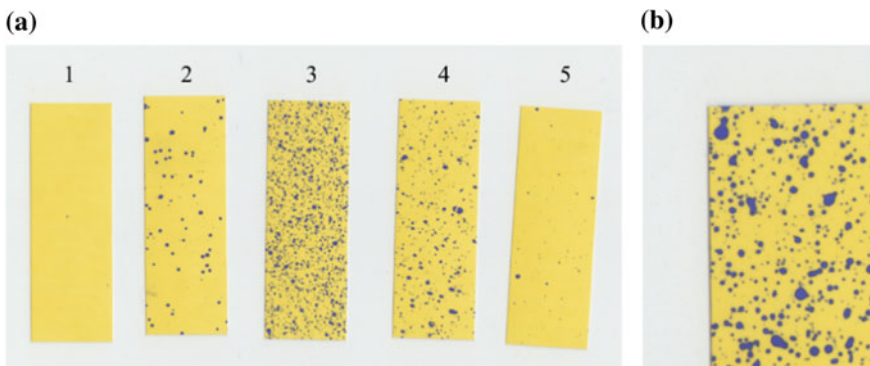


Fig. 1 A row of five Water-Sensitive Papers **a** scanned with *Canon Lide 220*, and the top corner enlargement of a WSP **b** with the grey background and the the shadow of a darker grey

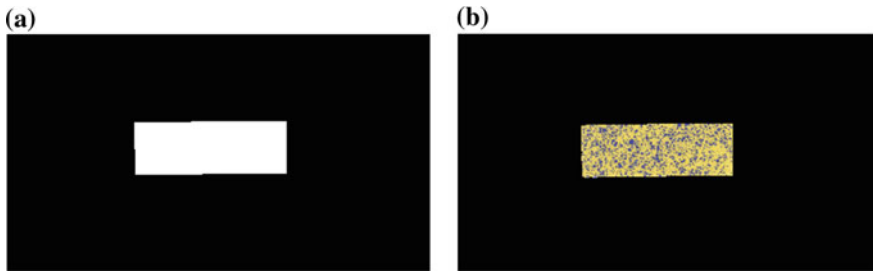


Fig. 2 An example of a mask to isolate one WSP from the rest of the image (a) and the same WSP isolated after the masking process (b)

The next *analysis phase* was performed to detect the part affected by the blue stains over the yellow WSP surface using the Red channel to identify with a bigger precision the stains on the WSP, searching not the presence of blue color (blue pixels) but his absence and deleting the parts with no color (Fig. 3).

The result of these first two steps (Fig. 4a) was the isolation of water altered parts (in white) from the WSP dry parts and the background (both in black).

The *measurement of the stain* was the last phase and, once all the elements were isolated, permitted to estimate the diameter of the drops as defined by the Eq. 1, where “d” is the diameter and “A” is the stain’s area.

$$d = \sqrt{\frac{4A}{\pi}} \quad (1)$$

The Eq. 1 is the reverse of the one used for the area of the circle: $A = \pi \left(\frac{d}{2}\right)^2$.

The diameter measure was acquired indirectly from the area of the stains (Table 1) converting the image dimension from pixel to micron meter (μm). Another important

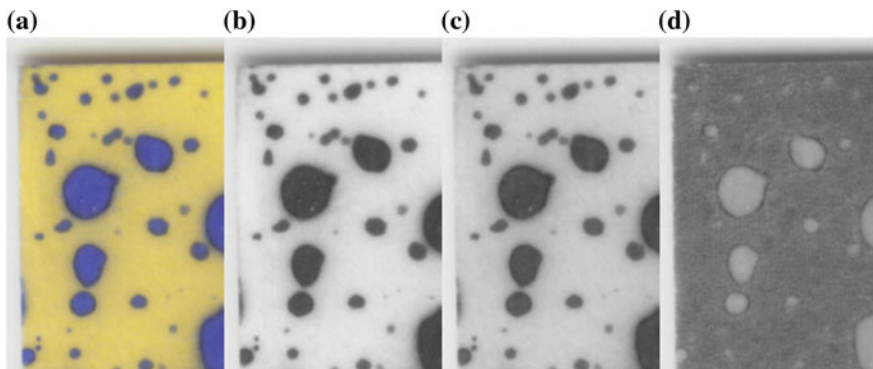


Fig. 3 A WSP vertex enlargement (a) and the corresponding Red (b), Green (c) and Blue (d) channels

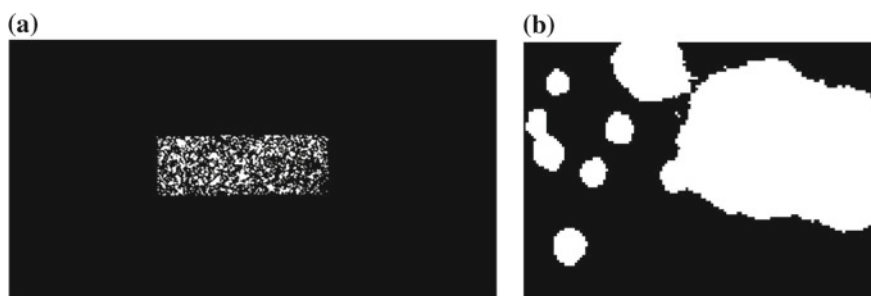


Fig. 4 WSP image binarization (a) with the drops showed in white color and the dry part of the WSP and the background in black color. In (b) the zoom of part of the image showing a few drops

Table 1 The stain area in pixel, his relative diameter (μm) and the derived drop diameter (μm)

Area (number of pixel)	Stain diameter (μm)	Spread factor ^a	Drops diameter (μm)
40	151.06	1.7	88.86
110	250	1.8	138.89
281	400.37	2.0	200.19
439	500.43	2.1	238.30

^aThe spread factor used in the equation ($\text{drop diameter} = \frac{\text{stain diameter}}{\text{spread factor}}$) is referred to water at 20 °C, a Relative Humidity (RH) about 40%, and droplets reaching sedimentation velocity on the Water-Sensitive Paper (*Syngenta*)

value is the percentage of WSP surface hit by water drops, derived by the ratio between the number of blue pixels and all the WSP. Thanks to this information and the WSP dimensions it was possible to convert the covered area data from the number of pixels to cm^2 and transform the stain diameter into the relative drop diameter (as shown in Table 1) using the spread factor (Fig. 5) provided by *Syngenta* (*Crop Protection AG, CH-4002, Basel, Switzerland*).

The basic steps of the algorithm are described in Fig. 6.

Two different types of WSP reference (Fig. 7) were used to verify the accuracy of the MATLAB code and validate the proposed methodology. Three WSP containing circles of different diameters each (100, 300, and 600 μm) were drawn, (Fig. 7a–c) using WSPs spotted by stains produced with a laboratory pipette (*Eppendorf® 2 Variable Volume Pipettor 0.5–20 μl*). All the diameters were first measured manually with a digital caliper (*Wurth*) and then analyzed with the code. The second type of reference (Fig. 6d) was composed by digitally designed WSPs with stains of known diameter (100, 300, and 600 μm), obtained using open-source vector software (*Inkscape*). The output pdf image file (210 mm \times 297 mm, 1200 dpi) was printed with a laser printer and then scanned to simulate the analysis procedure followed for the real WSPs.

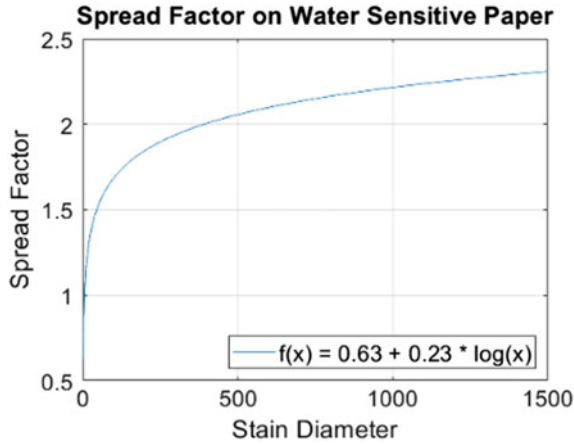


Fig. 5 The spread factor curve used to obtain the drops diameters starting from the WSP’s stains

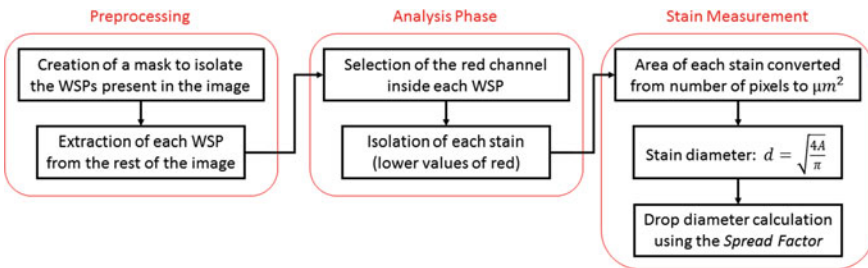


Fig. 6 Basic steps of the proposed method

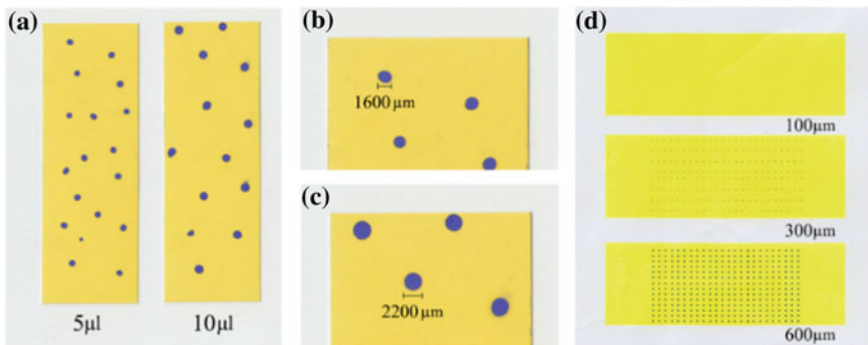


Fig. 7 The WSP reference with stains of know diameter and volume obtained with a laboratory pipette (a), an enlargement of the stains of 1600 μ m (b) and 2200 μ m (c), and the three WSP digital obtained reference (d) with stains of 100, 300 and 600 μ m

Table 2 Some results derived from the WSP analysis through the MATLAB code

Position a, test #2					
N° of WSP	1	2	3	4	5
NMD	27.88	71.49	157.42	138.19	44.51
VMD	191.31	479.54	407.08	490.76	390.01
Covered area (%)	0.04%	2.40%	15.95%	5.46%	0.42%
Drops cm ⁻²	3.19	11.79	89.32	31.78	16.04

3 Results and Discussion

The developed MATLAB code showed the possibility to obtain different drops properties like the Normal Median Diameter (NMD), the Normal Volume Diameter (VMD), the number of drops cm⁻², the percentage of covered area, and the variation coefficient (Table 2).

The main problem related to the WSP analysis was the limited code ability to discriminate all the stains characterized by different sizes and especially by different shapes (Fig. 4b) due to the impact of the drops over the WSP surface and the overlapping of many of them. A positive consideration regarding the analysis process is about the quality of the image. As a matter of fact, thanks to the high resolution employed during the scanning operation (1200 dpi), it was possible to identify and measure the smaller stains, and overcome or limit problems like deformation and exposure (the use of a scanner to obtain the images instead a camera, permitted to have a standard light condition). The WSP reference analysis results showed (Fig. 8) a high accuracy of the software to detect and measure the stains present on their surface and permit to state the enormous potential of the image analysis process.

4 Conclusions

The developed MATLAB code was able to detect and analyze different features of droplets deposit on the WSP with high accuracy and precision.

Because of pixel limitations, the accuracy of the MATLAB code decreased with the decrease of stain size. Another important limitation is referred to the low capacity to discriminate the overlapped stains and distinguish the blue humidity patches from the real stains. The WSP reference (Fig. 5) used to verify the coding precision, highlighted a high discrimination ability to detect stains of small dimension (<100 μm). A future intention will be to use an ISO procedure to verify the precision of the proposed analysis process. The analysis of the WSP images permitted a complete description of the spraying activity in terms of covered area, drop diameter and impact density. The use of this analysis method could improve the accuracy of pesticide spray applications and help to save the volume of the products and his dispersion into the environment.

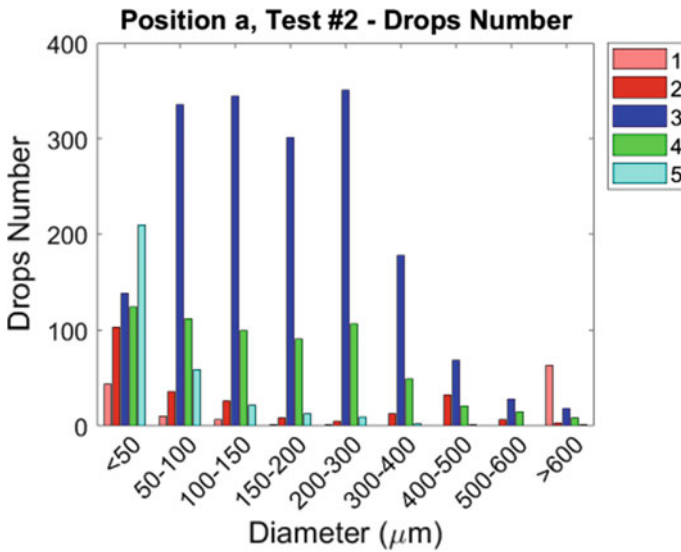


Fig. 8 Histogram shows the percentage of drops for each size segment over the five WSP represented in different colors

Future studies will be realized to overcome the code limitation, to cover other spraying situations and to develop an automatic procedure usable without specific coding competence.

Acknowledgements This study was conducted in the framework of two projects funded by the Sardinian Regional Authority, i.e. the project POR FESR Sardegna 2014–2020—“MARS—*Multiple Airdrones Response System*” and PRIN: PROGETTI DI RICERCA DI RILEVANTE INTERESSE NAZIONALE—Bando 2017 “*New technical and operative solutions for the use of drones in Agriculture 4.0*”; and the Innovative and CREative SEttlements in Sardinia (IN. CREA. SE) for the digital production and rapid prototyping (University of Sassari, 2019).

References

- Aglieco, C., & Cerruto, E. (2011). Analisi Teorica Degli Spray Tramite Simulazione Su Cartine Idrosensibili. Convegno di Medio Termine dell'Associazione Italiana di Ingegneria Agraria.
- Budiyono, A., & Wibowo, S. S. (2007). Optimal tracking controller design for a small-scale helicopter. *Journal of Bionic Engineering*, 4, 272–279. [https://doi.org/10.1016/S1672-6529\(07\)60041-9](https://doi.org/10.1016/S1672-6529(07)60041-9).
- Cunha, M., Carvalho, C., & Marcal, A. R. S. (2012). Assessing the ability of image processing software to analyse spray quality on water-sensitive Papers used as artificial targets. *SciVerse ScienceDirect, Biosystem Engineering*, III, II–23.
- Hong, S., Minzan, L., & Zhang, Q. (2012). Detection system of smart sprayers: Status. Challenges. and perspectives. *International Journal of Agricultural and Biological Engineering*, 5(3). <https://doi.org/10.25165/ijabe.v5i3.585>.

- Lan, Y., Shengde, C., & Fritz, B. K. (2017) Current status and future trends of precision agricultural aviation technologies. *International Journal of Agricultural and Biological Engineering*, 10 No. 3. <https://doi.org/10.3965/ijabe.20171003.3088>.
- Lou, Z., Xin, F., Han, X., Lan, Y., Duan, T., & Fu, W. (2018). Effect of Unmanned Aerial Vehicle Flight Height on Droplet Distribution. Drift and Control of Cotton Aphids and Spider Mites. *Agronomy*, 8, 187. <https://doi.org/10.3390/agronomy8090187>.
- Otto, S., Loddo, D., Schmid, A., Roschatt, C., Venturelli, M., & Innerebner, G. (2018). Droplets deposition pattern from a prototype of a fixed spraying system in a sloping vineyard. *Science of the Total Environment*, 639(2018), 92–99. <https://doi.org/10.1016/j.scitotenv.2018.05.167>.
- Salyani, M., Zhu, H., Sweeb, R. D., & Pai, N. (2013). Assessment of spray distribution with water-sensitive paper. *Agricultural Engineering International: CIGR Journal*, 15(2), 101–111.
- The European Parliament. (2009). Directive 2009/128/ce. Official European Union Gazette. Yu Xue, Droplet deposition and control effect of insecticides sprayed ith an unmanned aerial vehicle against plant hoppers. *Crop Protection*, 85, 79–88.
- Witton, J. T., Pickering, M. D., Alvarez, T., Reed, M., Weyman, G., Hodson, M. E. et al. (2018). Quantifying pesticide deposits and spray patterns at micro-scales on apple (*Malus domestica*) leave with a view to arthropod exposure. *Pest Management Science. Society of Chemical Industry (wileyonlinelibrary.com)*. <https://doi.org/10.1002/ps.5136>.
- Zhu, H., Salyani, M., & Fox, R. D. (2011). A portable scanning system for evaluation of spray deposit distribution. *Computers and Electronics in Agriculture*, 76(1), 38–43.

Detection and Monitoring of Alien Weeds Using Unmanned Aerial Vehicle in Agricultural Systems in Sardinia (Italy)



Vanessa Lozano, Giuseppe Brundu, Luca Ghiani, Davide Piccirilli, Alberto Sassu, Maria Teresa Tiloca, Luigi Ledda and Filippo Gambella

Abstract Emerging technologies such as high-resolution Unmanned Aerial Vehicles (UAVs) surveys combined with object-based image analysis, and field surveys could represent a reliable, precise, and effective tool to support land management in agricultural systems. The technological advances of UAVs can also promote the detection and regular monitoring of invasive alien plants and agricultural weeds. The objective of the study has been to identify, map and monitor alien weed species in agricultural systems to provide an overview of the future applications and challenges of precision farming. In particular, we evaluated how UAV imagery can be used to assess the cover of *Oxalis pes-caprae*, present in several crops in Sardinia as an alien invasive weed, with negative direct and indirect effects on the affected crops. Our core assumption is that the most reliable species discrimination can be achieved by targeting flights during flowering to allow easier detection due to species-specific spectral differences. Therefore, *O. pes-caprae* infestation was acquired using RGB camera installed on board a Phantom 4 pro. As a result, we presented the mapping of *O. pes-caprae*, highlighting the cost-effectiveness and replicability of this approach to detect the presence of this alien weed in agricultural fields.

Keywords Alien weeds · Drone · Object-based image · UAV-imagery weed monitoring

1 Introduction

Nowadays, one of the most promising and innovative technology in weed management is the use of Unmanned Aerial Vehicles (UAVs or drones). The images captured with the UAVs can be used for the design of appropriate site-specific control measures. Compared with other remote platforms (e.g. satellites or piloted aircraft),

V. Lozano (✉) · G. Brundu · L. Ghiani · D. Piccirilli · M. T. Tiloca · L. Ledda · F. Gambella
Department of Agriculture, University of Sassari, Viale Italia 39, 07100 Sassari, Italy
e-mail: vlozano@uniss.it

A. Sassu
Inspire s.r.l, Via XX Settembre 33/10, 16121 Genoa, Italy

© Springer Nature Switzerland AG 2020

A. Coppola et al. (eds.), *Innovative Biosystems Engineering for Sustainable Agriculture, Forestry and Food Production*, Lecture Notes in Civil Engineering 67,
https://doi.org/10.1007/978-3-030-39299-4_92

UAVs can operate at low altitudes (e.g. below 100 m) and can provide an ultra-high geometric resolution image of the entire crop field (Peña et al. 2015). The UAVs can collect remote imagery of crops and weeds at critical times in the growing season, thus improving the decision-making process (Lelong et al. 2008).

Native and non-native weeds pose globally an important environmental and economic threat to crop production in agricultural systems as they compete for space, light, water, and nutrients from the soil. The ratio between native and non-native weeds in agricultural cropping systems has been only scarcely studied as the weed flora is more frequently considered as a single unit. Agricultural areas can be places of introduction of new alien species, therefore worth to be periodically monitored or they could act as reservoirs of alien species that can also invade adjacent semi-natural to natural areas, thus specific management plans are to be put in place.

This study focuses on analyzing UAV imagery with a combined spectral and spatial analysis to inspect the status of globe artichoke fields in terms of *Oxalis pes-caprae* coverage, present in several crops in Sardinia as an invasive alien weed. We focused the detection and monitoring the spread of the invasive species on an object-based classification system, making a site-specific control for distinguishing crops and *O. pes-caprae* in RGB imagery of agricultural fields.

2 Experimental Section

2.1 UAV Flights and Data Acquisition

The UAV platform, a Phantom 4 pro (DJI) equipped with an RGB camera (FOV 1.46 rad) was tested in a cropping system of globe artichokes located in Sardinia at the agricultural experimental station “Mauro Deidda” of the University of Sassari, Italy (40° 46′ N, 8° 29′ E; 81 m a.s.l.). The aerial images were collected in 2019 during early spring (full-flowering) when the artichoke crop was naturally infested by *Oxalis pes-caprae*. The UAV flew at 15 m (85% side overlap and 75% front overlap) for 10 min at 2 ms⁻¹ over an experimental plot of 90 × 30 m (Fig. 1).

Thanks to the GPS installed on board the Phantom 4 Pro, with an accuracy of the orthomosaic of 3.37 mm/pix, it was possible to obtain georeferenced imagery of the field. In fact, every time the drone shoots a photo, it associates that photo with the global position in that moment. This tool allows accelerating the alignment of the photos during the image processing because the software reads the exact position of each photo in a 3D space.

Each flight route was programmed into the UAV mission planner (DJI pro) so that the vehicle ascended vertically above a fixed point in the globe artichoke field. Once the UAV achieved each scheduled altitude, a unique shot was captured as the vehicle stopped. In total, 284 images (i.e. each one of 5472 × 3648 pixels) were taken and analyzed and were geo-referenced by identifying a set of ground control points

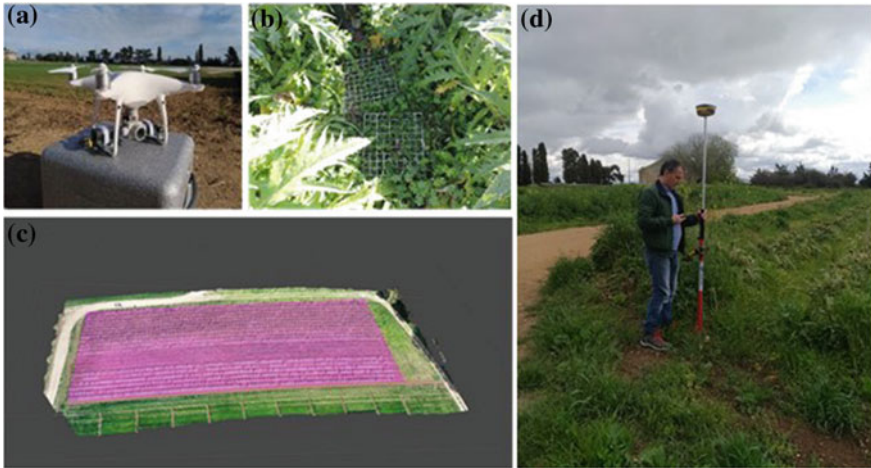


Fig. 1 **a** The Unmanned Aerial Vehicle (Phantom 4 pro, DJI) used to monitor the invasion of *Oxalis pes-caprae*; **b** in-field view of the study site, showing the artichoke crop-rows and *Oxalis pes-caprae*; **c** orthomosaic of the field under investigation (RGB composition) collected by the UAV at 15 m altitude; **d** ground control points (GCP) located in the field by using a GPS

(GCP) located in the field by using a GPS (TOP CON HIPER II). We used 5 GPC disposed in the four corner of the field and one in the middle of the same (Fig. 1d).

2.2 Image Pre-processing

All the collected photos were used to build an orthomosaic image of the field. The software used for the elaboration, Agisoft Metashape v 1.5.2, permits to align all the photos in a georeferenced space, build a 3D point cloud and a 3D mesh. The 3D mesh is converted into a Digital Elevation Model (DEM) with a 1.37×1.37 cm resolution. We used the maximum definition given by the software Agisoft. The spec. (a camera of “20 megapixels, lens-24 mm, Sensor size-1” CMOS, ISO 100/12800, Aperture f/2.8-f/11) of the camera affect the resolution of the entire model (Dense Cloud, Mesh, DEM). The DEM is then used for orthorectification and the production of the orthomosaic (Fig. 2).

2.3 Image Classification and Weed Detection

The proposed approach of image classification aims to identify the alien weed *Oxalis pes-caprae* in globe artichoke crops in order to provide a tool for quantification of the level of invasion and accurate monitoring of the cultivated field. The objective

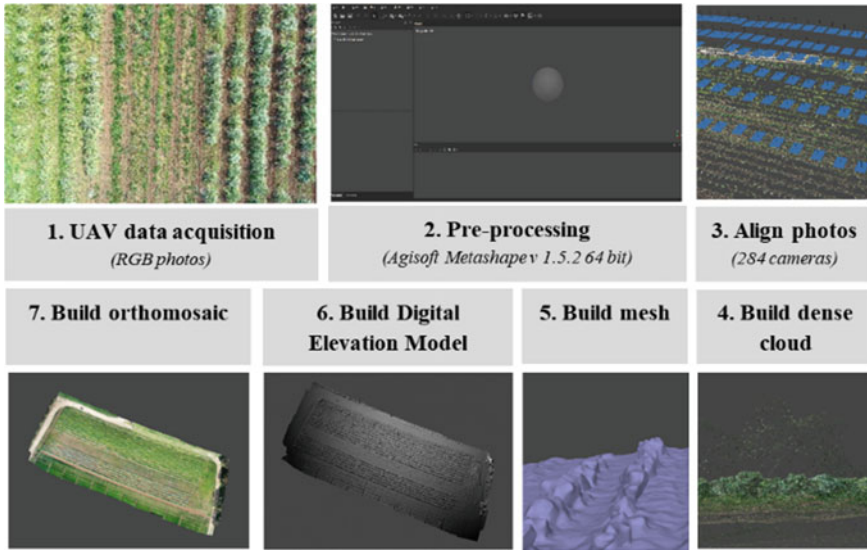


Fig. 2 Workflow of the UAV flight, data acquisition (RGB photos) and image processing with Agisoft Metashape to obtain the DEM and the orthomosaic of the field

is to produce a map of the crop and weeds from the image, including weeds located in the intra-row space. The proposed system to disentangle the two components of the vegetation (i.e. crops vs. weeds) computes a set of features for the image regions that correspond to vegetation and classify the image matrix using an object-oriented analysis approach (i.e. identifies spatially and spectrally similar objects created by grouping adjacent pixels according to a classification per segments) basis in the RGB camera images which leads to a vegetation mask. This step is highly effective as it allows us to compute the features on the subsequent processing steps only for the regions that correspond to vegetation.

We followed the object-based image analysis approach used by Peña et al. (2013), using UAV imagery and a three-step classification approach and the threshold was selected using the Otsu (1979) algorithm: (1) discrimination of vegetation objects based on RGB and DEM information (hereon Vegetation detection), (2) image segmentation into multi-pixel regions that define plants (crop and weeds) (hereon Feature extraction), and (3) classification distinguishing crop and weed based on obtention of an index of vegetation and detection of object-based image (Fig. 3).

The data extracted were integrated from the orthomosaic with the corresponding DEM values and took advantage of the a priori knowledge of the vegetation present in the field (ground-truth data). At the time of the data collection, we marked as globe artichoke every point of the DEM with a height of more than 30 cm over the DTM (terrain level). The remaining vegetation is identified with the Excess Green Index (ExG), Eq. (1), extracted from the RGB bands values (Woebbecke et al. 1995):

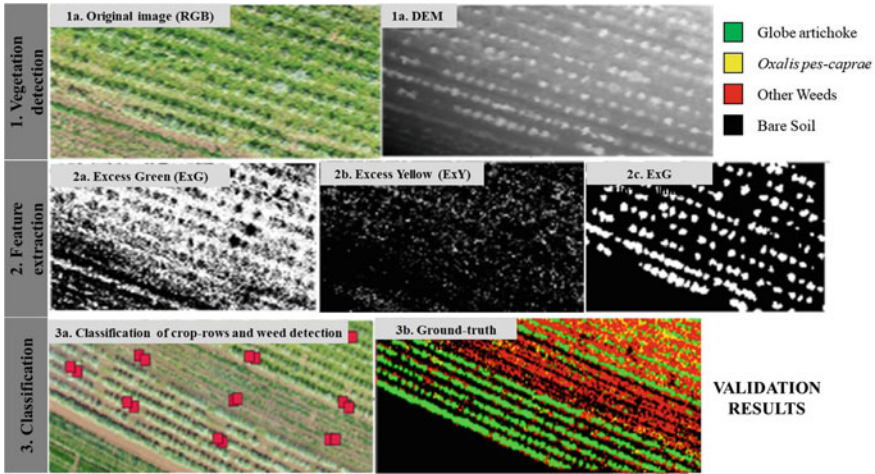


Fig. 3 Representation of the different steps for the classification procedure considered for selecting the training patterns. In step 3, green-colored pixels represent globe artichoke crop, yellow ones represent *Oxalis pes-caprae*, red ones correspond to other weeds, and black represent the bare soil

$$ExG = 2g - r - b \text{ where } r = \frac{R}{R + G + B}, g = \frac{R}{R + G + B}, b = \frac{R}{R + G + B} \tag{1}$$

The ExG values are not sufficient to distinguish the presence of *Oxalis pes-caprae* from other weed species. Therefore, since we know that during the time of the survey, *O. pes-caprae* is characterized by the presence of a great number of little yellow flowers, we added the detection of yellow pixels to the orthoimage analysis. Those pixels were detected extracting an Excess Yellow Index (ExY), Eq. (2), (Wobbecke et al. 1995):

$$ExY = g + r - 2b \text{ where } r = \frac{R}{R + G + B}, g = \frac{R}{R + G + B}, b = \frac{R}{R + G + B} \tag{2}$$

Finally, the classification was performed on each 500×500 pixel block by the following discrimination rules:

- if more than 50% of the pixels of the block contains DEM values above 30 cm, the block is classified as globe artichoke;
- otherwise, if more than 20% of the RGB values are green and at least 4 pixels are yellow, it is *Oxalis pes-caprae*;
- otherwise, if more than 20% of the RGB values are green, it is another type of weed;
- In any other case, it is bare soil.

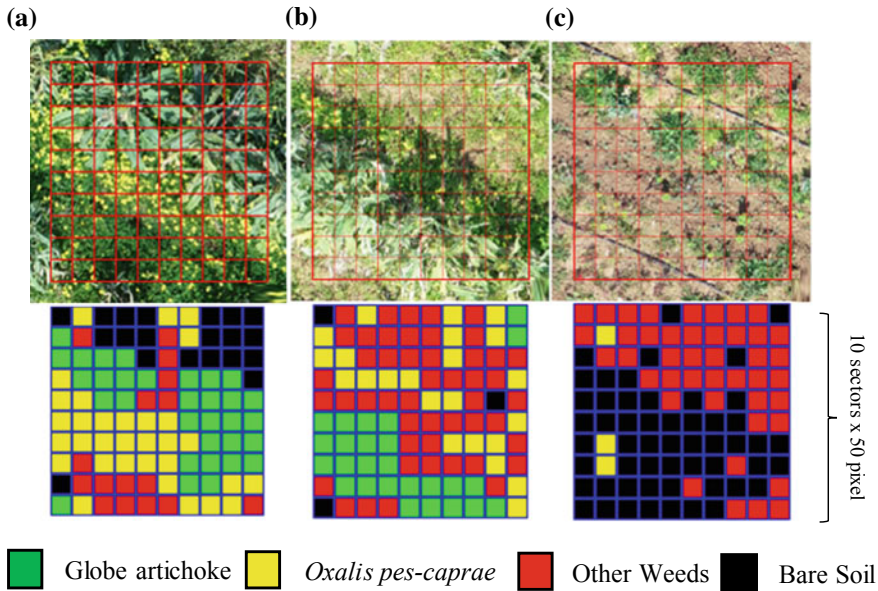


Fig. 4 In the top: RGB images with globe artichoke plants and *Oxalis pes-caprae* (a, b), other weeds, and bare soil (c) from the UAV flight at 15 m altitude with visible-light camera. In the bottom: the respective classified images (i.e. 100 sectors, each one of 50 × 50 pixels) sin crop-rows of artichoke (green), *Oxalis pes-caprae* (yellow), other alien weeds (red), and bare soil (black)

3 Results and Discussion

3.1 Classification of Crop and Weed Detection in the Covered Area

As described above, weed identification and mapping were based on two major steps: vegetation detection and crop row recognition. After these steps have been performed, vegetation growing outside the row structure is classified as a weed. Each 500 × 500 pixel block was divided into 100 sectors (i.e. each one of 50 × 50 pixels, Fig. 4a–c). For each block we obtained two images, one is the RGB image of the block divided into sectors while the other is a single band colored to represent the classification of crop-rows and weed detection, of the sectors we have obtained.

3.2 Accuracy of the Classification

Accuracy on weed discrimination achieved from analyses of the UAV images captured by the camera on the flight is shown in Table 1. A weed was classified as

Table 1 Accuracy assessment of artichoke crop, *Oxalis pes-caprae*, other weeds and bare soil detection as affected by the camera

UAV system	Presence vegetation	Flight altitude (m)	Visible-Light		
			Correct (%)	False + (%)	False (%)
Phantom 4 pro	Crop-row	15	50.00	13.04	36.96
Phantom 4 pro	<i>Oxalis pes-caprae</i>	15	49.40	20.48	30.12
Phantom 4 pro	Other weeds	15	52.45	22.38	25.17
Phantom 4 pro	Bare soil	15	48.15	46.91	4.94

correct if all the weed plants within the frame were correctly attributed to weed objects. Otherwise, the frame was labeled as either underestimated, false negative or false positive according to the error observed (Fig. 4). From an agronomic point of view, the false positive errors (overestimation of weeds) might be more acceptable than false negative errors (non-detection of weeds) for generating the weed maps in practice, assuming that farmers would choose to treat weed-free areas rather than risk allowing weeds to go untreated (Gibson et al. 2004). The camera and the image processing methodology identify *O. pes-caprae* area with an accuracy of 49.4% and for artichoke was 50%. This demonstrated the efficiency of the procedure developed for weed classification. After the importance of efficient classification, spectral information derived from ExG and ExY indices (in the visible-light images) could initially be considered the primary factor affecting weed identification. Additionally, the data extracted and classified from the orthomosaic was compared with the vegetation present in the field (ground-truth data) using ANOVA and we obtain no significant differences for classification in the field (*O. pes-caprae* p-value: 0.17, other weeds p-value: 0.67 and bare soil p-value: 0.10).

4 Conclusions

This paper has explored the use of UAV-imagery for weed monitoring in globe artichoke crops. The procedure identified the crop-rows and made errors in the extremes because of the short size of these rows. The detection process of *Oxalis pes-caprae* in the artichoke field is strongly affected by the presence of other weeds plants very close or within the crop-rows. Therefore, weed discrimination was effective in the frames with low weed infestation but decreased in the frames with moderate or high weed infestation. However, these results showed that this procedure might be very useful for further discrimination and classification of other weeds and crop plants. To improve our future work, we considered that a high degree of accuracy in the detection of weeds is needed. Nevertheless, the information reported in this article might be very useful to give farmers details on the type of camera (i.e. spatial and spectral

sensor resolution), procedure, and the optimal flight altitude needed to generate a suitable weed map in the season to apply site-specific weed management operations.

Acknowledgements This study was conducted in the framework of two projects funded by the Sardinian Regional Authority, i.e. the project POR FESR Sardegna 2014–2020—“MARS—*Multiple Airdrones Response System*” and the project “CarBio—*Carciofo Biologico: innovazione e sostenibilità di filiera*”.

References

- Gibson, K. D., Dirks, R., Medlin, C. S., & Johnston, L. (2004). Detection of weed species in soybean using multispectral digital images. *Weed Technology*, *18*, 742–749.
- Lelong, C. C. D., Burger, P., Jubelin, G., Roux, B., Labbé, S., & Baret, F. (2008). Assessment of unmanned aerial vehicles imagery for quantitative monitoring of wheat crop in small plots. *Sensors*, *8*, 3557–3585.
- Otsu, N. A. (1979). Threshold selection method from gray-level histograms. *IEEE Transactions Systems Man Cybernetics*, *9*, 62–66.
- Peña, J. M., Torres-Sánchez, J., de Castro, A. I., Kelly, M., & López-Granados, F. (2013). Weed mapping in early-season maize fields using object-based analysis of unmanned aerial vehicle (UAV) images. *PLoS ONE*, *8*, e77151.
- Peña, J., Torres-Sánchez, J., Serrano-Pérez, A., de Castro, A., & López-Granados, F. (2015). Quantifying efficacy and limits of unmanned aerial vehicle (UAV) technology for weed seedling detection as affected by sensor resolution. *Sensors*, *15*(3), 5609–5626.
- Woebbecke, D. M., Meyer, G. E., von Bargen, K., & Mortensen, D. A. (1995). Color indices for weed identification under various soil, residue, and lighting conditions. *Transactions of the American Society of Agricultural Engineers*, *38*, 259–269.

Experimental Methodology for Prescription Maps of Variable Rate Nitrogenous Fertilizers on Cereal Crops



Costanza Fiorentino, A. R. Donvito, P. D'Antonio and S. Lopinto

Abstract Agricultural fields have been always considered as uniform entities and managed accordingly. However, uniform agronomic management in fields where spatial variability is present, is economically and environmentally inefficient. The study was carried out on a 18 ha field located in Melfi (PZ, Basilicata), Southern Italy during six years of alternate cultivation of wheat and forage. Spatial maps of grain yield, normalized difference vegetation index (NDVI) and topography were collected. The spatial maps were used to define spatial and temporal yield variability and to identify two stable zones within the field, “low yield stable” (LS) and “high yield stable” (HS). Short fallow rainfall was correlated with grain yield of HS. Both zones were negatively correlated to vegetative growing season (Dec-Gen-Feb cumulative rainfall). Wheat yield production in Mediterranean environment is highly affected by rainfall and amount of soil water stored into the soil before and during the growing season. The objectives of this study were to identify spatio-temporal stable areas throughout the field, understanding the influence of rainfall on wheat yield. Starting from this map, prescription maps are produced to experiment the distribution of variable-dose nitrogenated fertilizers with the Kverneland GEOSPAT Exacta TL Fertilizer spreader. This operation in the case of cereal crops, today still represents a highly impacting intervention from the economic and environmental point of view.

Keywords Remote sensing · Management zone · Fertilization

C. Fiorentino (✉) · A. R. Donvito
Digimat SPA, via delle Officine, Matera, Italy
e-mail: costanza.fiorentino@digimat.it

P. D'Antonio
Università degli Studi della Basilicata, Macchia Romana, viale dell'Ateneo Lucano, Potenza, Italy

S. Lopinto
Azienda Lopinto, Melfi, Potenza, Italy

© Springer Nature Switzerland AG 2020
A. Coppola et al. (eds.), *Innovative Biosystems Engineering for Sustainable Agriculture, Forestry and Food Production*, Lecture Notes in Civil Engineering 67,
https://doi.org/10.1007/978-3-030-39299-4_93

1 Introduction

Agricultural fields have been always considered as uniform entities and managed accordingly (Mulla 2013). However, uniform agronomic management in fields where spatial variability is present, is economically and environmentally inefficient (Pierce and Nowak 1999). In Mediterranean environments the benefit of managing the field in zones can only be achieved by dividing the fields in areas that are consistent in yield performance (Robertson et al. 2005; Ritchie and Basso 2008).

Commonly, yield maps are acquired at harvesting and segmentation techniques are applied to delineate the Management Zones (MZ). Yield data have significant error sources, such as via sensor, georeferencing, operator or data processing errors (Simbahan et al. 2004), and are also complicated to prepare (Blackmore and Marshall 1996). Moreover, the irregular distribution of data points in regard to the spatial variation in yield can impede accurate interpolation, which is a necessity for most spatial analyses. The use of soil sampling data and soil maps for delineation of MZ is also a common approach, especially if yield maps are not available. Electrical resistivity tomography (ERT) maps can also be used for successful MZ delineation. They reflect soil differences due to such factors as moisture content, salinity and texture. However, even if these characteristics influence crop growth significantly, ERT maps may not always give a direct picture of in-season vegetation patterns. In addition, ERT of soil is influenced by a number of complex and mostly inter-related parameters (Lück et al. 2009), therefore interpretation is not necessarily straightforward. Since spatial patterns in ERT measurements are affected by seasonal effects (e.g. weather conditions; Lück et al. 2009).

Satellite remote sensing provides spatial continuity and extent, spectral crop information and low cost. When analyzing time series, satellite remote sensing is often more cost-effective and offers an archive of already acquired data by operating sensors. When it comes to determining MZ on the basis of actual crop growth patterns, satellite imagery applications are valuable tools in precision farming (Basnyat et al. 2005). The major disadvantage of optical satellite imagery however is the dependence on a clear, cloud-free view. A considerable number of studies related to crop growth and yield (Hank et al. 2015; Lobell et al. 2015) are based on satellite images within one growing season (Song et al. 2009). However, Thenkabail (2003) pointed out the potential of multi-temporal analysis of archived remote sensing data in combination with real-time data.

The delineation of zones based on remotely sensed images confirms large differences in canopy growth that lead to yield variability (Basso et al. 2007; Andersen et al. 2005; Blackmore et al. 2003). Such images taken during key growing stages might help to characterize the spatial variability of crops and delineate areas with similar response. Robertson et al. (2007) using spatial information from remote sensing and soil attributes at whole-farm and catchment scale showed the presence of spatial patterns of soil landscape useful to identify areas with both low productivity and excessive nitrate leaching.

The objective was the delineation of a field homogeneous zones based only on satellite data. In the optics of remote sensing open data (Copernicus and Landsat missions) of earth observation, an automatic segmentation algorithm, for within-field crop patterns delineation, was developed by using only multi-temporal and multi-spectral satellite images. Yield maps, rainfall and topographic data were used to characterize and validate the spatially and temporally stable areas. This study makes it possible to attribute the correct nitrogen fertilization rate to each zone.

2 Materials and Methods

2.1 Site Description and Agronomic Management

The study was carried out on a 18 ha field located in Melfi, Potenza-Italy during six years of alternate cultivation of wheat and forage. In particular, wheat has been sown in 2013/14 (Anco Marzio), 2015/16 (Core), 2017/18 (Core) and 2018/19 (Core) growing season. Every year sod sowing was carried out between the last week of November and the first week of December. Digestate was applied in pre-sowing each year from 2016 to 17. The nitrogen (N) fertilization consisted in one slow release fertilizer applications, at the beginning of February with a homogeneous rate of 4 Q ha⁻¹. Only in 2014 the nitrogen (N) fertilization consisted in two split applications, one as ammonium nitrate 33.5% (1.5 Q ha⁻¹) and another at tillering as urea (1.5 Q ha⁻¹). The crop was harvested between the second and the third week of June for the six years. The mean yield was about: 61.8 Q ha⁻¹ in 2019, 49.1 Q ha⁻¹ in 2017, 69.6 Q ha⁻¹ in 2016, 39.5 Q ha⁻¹ in 2014.

2.2 Field Data

Soil samples were taken for determination of soil texture and soil organic matter. The soil is a sandy clay loam, with: 61.2% of sand, 16.3 of silt and 22.5% of clay. The soil was calcareous and chlorosant with alkaline PH. It was poor in organic matter, with low values of nitrogen, phosphorus, potassium and magnesium content.

Multitemporal remote sensing images from Landsat8 satellite (30 mt spatial resolution) were acquired from 2014 to 2019. A yield map in 2019 was acquired and it was processed by ordinary kriging technique at the spatial resolution of 10 m. A Digital terrain Model (DTM) was downloaded from the web-gis of the official website of the Basilicata Region. It was elaborate to compute the topographic wetness index (TWI; Sørensen et al. 2006). All data and images were georeferenced and registered in UTM WGS 84 zone 33 N. Weather data were recorded by the nearest on-site station of the Lucana Agency for Development and Innovation in Agriculture

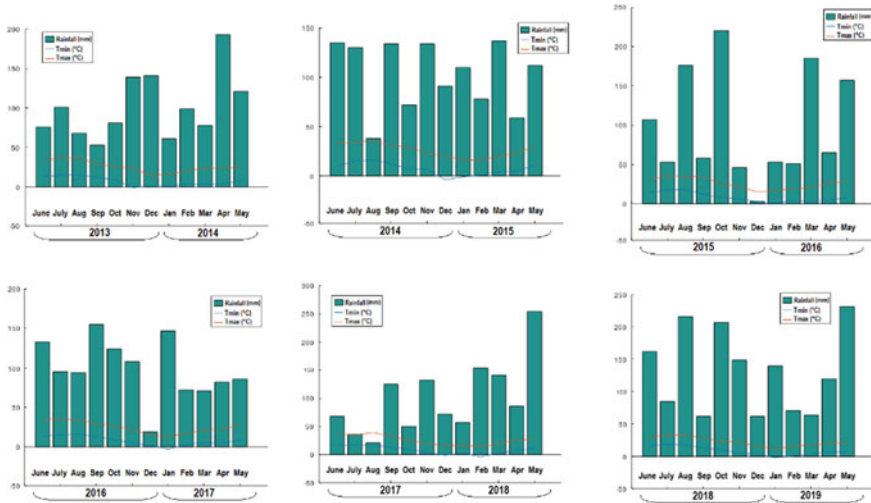


Fig. 1 Monthly rainfall average and minimum and maximum temperature for the growing seasons from 2013 to 2019

(ALSIA) network. Total growing season rainfall was divided into long fallow (June–November) and growing season rainfall (December–May). Detailed monthly rainfall average and minimum and maximum temperature for the six growing seasons are reported in Fig. 1.

3 Results and Discussion

The spatial variability of soil properties and the distribution of the rainfall influenced both the spatial and temporal variability of grain yield. The analysis allowed the identification of two spatial and temporal stable zones and one unstable zone (Fig. 2a). High level of clay in soil has an important implication in terms of water stored into the soil during the fallow period or growing season, and in terms of rooting depth. The crop response to rainfall is the result of dynamic interaction of spatial static properties (soil texture, position in the landscape) and dynamic properties (soil water content, infiltration and crop water use). In Mediterranean environment, wheat yield is influenced by rainfall and amount of water stored in the soil before the growing season and soil water availability during the growing season (Basso et al. 2012). Wheat yield response to stored soil water varies according to the site and the soil type (Anderson 2010). The balance between fallow rain and growing season rainfall plays an important role in determining grain yield. The amount of rain stored in the short fallow period (September–November) was an important factor affecting the spatial and temporal variability of wheat yield. Sadras et al. (2012) have demonstrated that there are no beneficial effects of the long fallows water storage and concluded that the

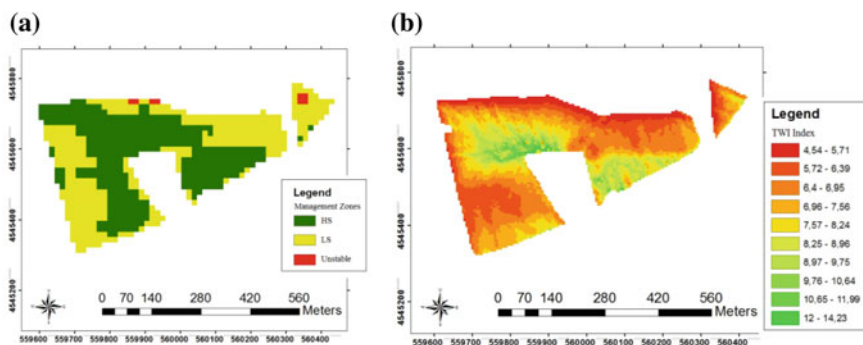


Fig. 2 **a** Management zone map, in green is reported the high yield and time stable zone, while in yellow is shown the Low yield and time-stable zone. **b** TWI index elaborated from the digital terrain model

benefits of fallow rainfall declined with the increase of seasonal rainfall. Crops that rely on fallow rainfall lose much less in soil evaporation during the growing season, although evaporative losses before sowing could be significant (Hatfield et al. 2001). Once the homogeneous areas were identified (by processing the data from 2013/14 to 2017/18 growing season), a correlation analysis was carried out between mean estimated yield and rainfall for each zone. The total rainfall was divided into fallow and growing season rainfall. The fallow rainfall was sub-divided in two periods, long fallow (June–November), and short fallow (September–November). Growing season rainfall (December–May) was sub-divided into vegetative rainfall (December–February) that corresponds to the rainfall period from sowing to end of tillering, and reproductive rainfall (March–May) that is the rainfall period between stem elongation and maturation. Growing season rainfall and fallow rainfall from 2013 to 2019 were reported in Table 1. These rainfall periods were correlated to grain yield of each zone through the Pearson’s coefficients. This analysis showed a significant, negative correlation between estimate average yield and vegetative growing season rainfall. The negative correlation was higher for the HS zone. This was probably due to the clayey soil component and the lower altitude of the HS zone (Fig. 2b). By removing

Table 1 Mean growing season rainfall and fallow rainfall (mm) from 2013 to 2019. In the years highlighted in italic wheat crop was seeded

Rainfall year	Tot. fallow	Short fallow	Grow. season	Veg. grow. seas.	Rep. grow seas.
<i>2013/14</i>	518	273	693	301	392
2014/15	643	340	587	279	308
2015/16	660	324	514	107	407
2016/17	709	387	477	238	239
2017/18	432	307	764	283	481
2018/19	881	418	577	273	304

from the analysis, the growing seasons with the highest level of short fallow rainfall (Table 1: 2018/19, 1016/17 and 2014/15) the correlation between average yield and short fallow rainfall per zone became significant.

The correlation analysis between average estimated yield per zone and TWI index (Fig. 2b) showed a significant positive correlation of HS zone with TWI for all study years, it was very low only in 2014/15 growing season. The Pearson correlation coefficient was higher than the others during the most productive growing season (2015/16) reaching the value of 0.63. The 2015/16 growing season was the driest during vegetative growing season. The lowest value of the Pearson correlation coefficient was reached for the 2013/14 growing season (0.32). It was the wettest during vegetative growing season.

Kaspar et al. (2003) related six years of corn yield data with soil attributes. They found that in four years, where rainfall was lower than the average, corn yield showed negative correlations with elevation, slope and soil curvature, and in the two years with abundant rainfall, the yield was positively correlated with those parameters. Kravchenko et al. (2005) found that the coefficient of variation increased in years with low rainfall (45%) and decreased in years with high rainfall (14%). Therefore, the effect of weather patterns on both crop growth and development and its interaction with soil type causes bias in the assessment of homogeneous management zones.

Adequate rainfall before sowing provides proper condition for good seed germination and enough supply of water for later growth. All of them (Angus and van Herwaarden 2001; Sakamoto et al. 2013).

In Fig. 3a, the yield map of 2018/19 growing season was reported, it was used to validate the methodology proposed in this work. In Fig. 3b, c and d it was shown the NDVI index for growing season 2018/19 at different dates, from the end of March to the end of April. It is possible to observe the very similar pattern of NDVI maps and yield, despite the different spatial resolution.

In Fig. 4a the graph of mean NDVI values for HS and LS zone for each study year was shown. The HS zone always produces more than the LS. The higher values of grain yield from 2015/16 growing season are probably due to the pre-sowing digestate application.

it is interesting to note the very low average NDVI value associated with the LS zone in the year 2016/17, while the HS zone maintains an average NDVI value comparable with that of the following years.

During this year the rain in March and April was the lowest compared to the others studied years: 71 mm in April with a single event of 36 and 82 mm in April with 2 events exceeding 15 mm of rain. Probably due to the slope this area has suffered from the lack of rain. In the graph, in Fig. 4b, the average field yield vs average NDVI was reported. The average yield estimated for 2018/2019 growing season was about 61.4 Q ha⁻¹ with the HS zone which produces about 10% more than the LS. The measured average value of grain yield in 2019 was about 61.8 Q ha⁻¹.

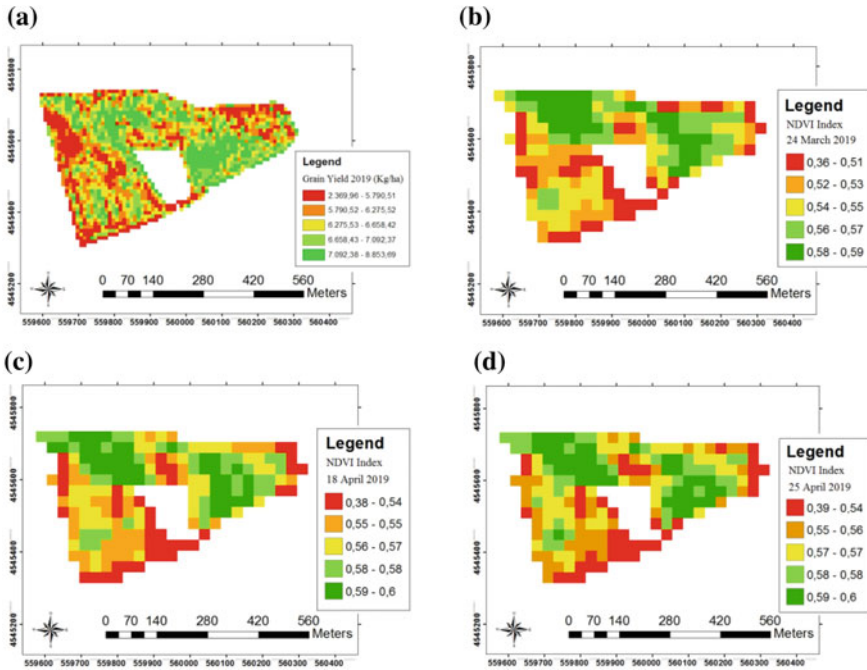


Fig. 3 In **a** is shown the 2019 grain yield map. In **b**, **c** and **d** are shown the NDVI (Rouse et al. 1974) indices acquired during 2019 growing season from Landsat8 satellite on: 24 of March, 18 and 25 of April

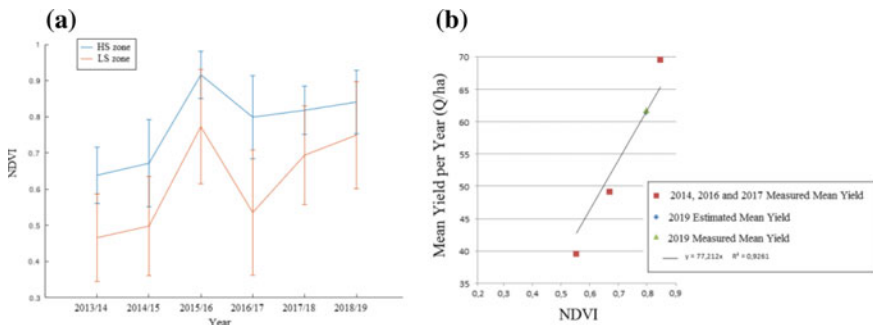


Fig. 4 The graph of mean NDVI values for each study year and for both, HS and LS zone, is reported in **(a)**. **b** shows, in red, the mean field NDVI versus measured average grain yield for 2014, 2016 and 2017 growing seasons. In the graph the measured and the estimated average grain yield are also reported

4 Conclusions

In this paper a semi-automatic procedure for the production of variable nitrogen rate fertilization prescription maps is reported. The algorithm is currently being validated, and it will soon be delivered as Digimat Cloud Service.

The Service will be supplied through a WEB-GIS where the user can select the boundaries of the fields of interest and request the provision of the service. The user must also provide information on the management of the fields.

Three levels of services have been set up:

1. prescription map based on the state of the vegetation evaluated (from a remote sensing image) few days before the nitrogen fertilization is scheduled;
2. prescription map based on the spatio-temporal homogeneous management zones map. This map is elaborated by using only multitemporal series of remote sensing images;
3. prescription map obtained by combining the two approaches.

The choice of the level of service available depends on the type of management that the farmer intends to carry out.

The procedure that implements all service levels is completely automatic. Only for levels 2 and 3, when the rate of nitrogen fertilization for each zone has to be defined, a preliminary study by a team of expert operators is necessary. To understand the delineated field patterns properties and define the correct nitrogen rate, it is necessary to analyze the MZ map by using further information: weather pattern, topography, chemical and physical properties of soil, etc.

Only for this reason the procedure is defined as semi-automatic.

This procedure has been developed according to the smart farming and it addresses upcoming important developments of big data and open source satellite images access. Furthermore, the algorithm can be applied in any field of cereals, wherever it is, because the map of homogeneous areas is processed only starting from satellite images. The expert operator intervenes only to attribute to each zone the correct nitrogen rate.

Acknowledgements The activity presented in the paper is part of the research grant PSR Basilicata Mis. 16.1 GO AGROTCH.

References

- Andersen, A., Persavento, U., & Wang, Z. J. (2005). Unsteady aerodynamics of fluttering and tumbling plates. *Journal of Fluid Mechanics*, 541, 65–90.
- Anderson, W. K. (2010). Closing the gap between actual and potential yield of rain-fed wheat. The impacts of environment, management and cultivar. *Field Crop Research*, 116, 14–22.
- Angus, J. F., & van Herwaarden, A. F. (2001). Increasing water use and water use efficiency in dryland wheat. *Agronomy Journal*, 93(2), 290–298.

- Basnyat, P., McConkey, B., Selles, F., & Meinert, L. (2005). Effectiveness of using vegetation index to delineate zones of different soil and crop grain production characteristics. *Canadian Journal of Soil Science*, 85(2), 319–328.
- Basso, B., Fiorentino, C., Cammarano, D., Cafiero, G., & Dardanelli, J. (2012). Analysis of rainfall distribution on spatial and temporal patterns of wheat yield in Mediterranean environment. *The European Journal of Agronomy*, 41, 52–65.
- Basso, B., Bertocco, M., Sartori, L., & Martin, E. C. (2007). Analysing the effects of climate variability on spatial pattern of yield in a maize–wheat–soybean rotation. *European J. of Agronomy*, 26, 82–91.
- Blackmore, B. S., & Marshall, C. J. (1996). Yield mapping; errors and algorithms. In P. C. Robert, et al. (Eds.), *Precision Agriculture: Proceedings of the 3rd International Conference* (pp. 403–416). Madison, WI, USA: American Society of Agronomy, Crop Science Society of America, Soil Science Society of America (ACSESS publications).
- Blackmore, S., Godwin, R. J., & Fountas, S. (2003). The analysis of spatial and temporal trends in yield map data over six years. *Biosystems Engineering*, 84, 455–466.
- Hank, T., Bach, H., & Mauser, W. (2015). Using a remote sensing-supported hydro-agroecological model for field-scale simulation of heterogeneous crop growth and yield: Application for wheat in Central Europe. *Remote Sensing*, 7(4), 3934–3965. <https://doi.org/10.3390/rs70403934>.
- Hatfield, J. L., Sauer, T. J., & Prueger, J. H. (2001). Managing soils to achieve greater water use efficiency. *Agronomy Journal*, 93(2), 271–280.
- Kaspar, T. C., Colvin, T. S., Jaynes, D. B., Karlen, D. L., James, D. E., Meek, D. W., et al. (2003). Relationship between six years of corn yields and terrain attributes. *Precision Agriculture*, 4(1), 87–101.
- Kravchenko, A. N., Robertson, G. P., Thelen, K. D., & Harwood, R. R. (2005). Management, topographical, and weather effects on spatial variability of crop grain yields. *Agronomy Journal*, 97(2), 514–523.
- Lobell, D. B., Thau, D., Seifert, C., Engle, E., & Little, B. (2015). A scalable satellite-based crop yield mapper. *Remote Sensing of Environment*, 164, 324–333. <https://doi.org/10.1016/j.rse.2015.04.021>.
- Lück, E., Gebbers, R., Ruehlmann, J., & Spangenberg, U. (2009). Electrical conductivity mapping for precision farming. *Near Surface Geophysics*, 7(32), 15–25. <https://doi.org/10.3997/1873-0604.2008031>.
- Mulla, D. J. (2013). Twenty five years of remote sensing in precision agriculture: Key advances and remaining knowledge gaps. *Biosystems Engineering*, 114(4), 358–371. <https://doi.org/10.1016/j.biosystemseng.2012.08.009>.
- Pierce, F. J., & Nowak, P. (1999). Aspects of precision agriculture. *Advances in Agronomy*, 67, 1–85.
- Robertson, M., Isbister, M., Maling, I., Oliver, Y., Wong, M., Adams, M., et al. (2007). Opportunities and constraints for managing within-field spatial variability in Western Australian grain production. *Field Crops Research*, 104, 60–67.
- Ritchie, J. T., & Basso, B. (2008). Water use efficiency is not constant when crop water supply is adequate or fixed: the role of agronomic management. *European J. of Agronomy*, 28, 273–281.
- Robertson, M., Isbister, M., Maling, I., Oliver, Y., Wong, M., Adams, M., et al. (2005). Managing spatial and seasonal variability within field can improve the profitability of WA grain production. In: N. Turner & T. Acuna (Eds.), *Groundbreaking Stuff. Proceedings of the 13th Australian Agronomy Conference*, September 10–14, 2006, Perth, Western Australia.
- Rouse, J. W., Haas, R. H., Schell, J. A., & Deering, D. W. (1974). Monitoring vegetation systems in the Great Plains with ERTS. In *Third ERTS Symposium, NASA SP-351 1* (pp. 309–317).
- Sadras, V. O., Lawson, C., Hooper, P., & McDonald, G. K. (2012). Contribution of summer rainfall and nitrogen to the yield and water use efficiency of wheat in Mediterranean-type environments of South Australia. *European Journal of Agronomy*, 36(1), 41–54.

- Sakamoto, T., Gitelson, A. A., & Arkebauer, T. J. (2013). MODIS-based corn grain yield estimation model incorporating crop phenology information. *Remote Sensing of Environment*, *131*, 215–231. <https://doi.org/10.1016/j.rse.2012.12.017>.
- Sørensen, R., Zinko, U., & Seibert, J. (2006). On the calculation of the topographic wetness index: Evaluation of different methods based on field observations. *Hydrology and Earth System Sciences*, *10*, 101–112.
- Simbahan, G., Dobermann, A., & Ping, J. (2004). Site-specific management—Screening yield monitor data improves grain yield maps. *Agronomy Journal*, *96*(4), 1091–1102.
- Song, X., Wang, J., Huang, W., Liu, L., Yan, G., & Pu, R. (2009). The delineation of agricultural management zones with high resolution remotely sensed data. *Precision Agriculture*, *10*(6), 471–487. <https://doi.org/10.1007/s11119-009-9108-2>.
- Thenkabail, P. S. (2003). Biophysical and yield information for precision farming from near-real-time and historical Landsat TM images. *International Journal of Remote Sensing*, *24*(14), 2879–2904. <https://doi.org/10.1080/01431160710155974>.

Monitoring Onion Crops Using UAV Multispectral and Thermal Imagery: Preliminary Results



Gaetano Messina, Salvatore Praticò, Biagio Siciliani, Antonio Curcio,
Salvatore Di Fazio and Giuseppe Modica

Abstract Agriculture constitutes one of the most important fields where Remote Sensing is employed, particularly in the aspects related to precision agriculture (PA). PA means a management strategy that aims at carrying out agronomic interventions in compliance with the actual crop needs and the biochemical and physical characteristics of the soil. PA analyses and manages the spatial variability of the field to optimize profitability, sustainability, and protection of agro-ecological services. The present paper shows the potentiality of coupling multispectral and thermal imagery acquired by an unmanned aerial vehicle (UAV) in monitoring crops. A case study in onion crop (Cipolla rossa di Tropea IGP) is provided. Multitemporal surveys were carried out by means of a fixed-wing UAV, equipped with a multispectral camera Sequoia Parrot (R-G-RedEdge-NIR) and a quadcopter equipped with a thermal camera Flir Vue Pro 640 R. Prior to proceeding with UAV surveys, soil characteristics were analysed on the basis of systematic sampling. According to the characteristics of thermal cameras, aluminum is used as the material of control targets with their size identified clearly in the thermal images. UAV multispectral imagery was calibrated with a panel with known reflectance, and verified with a spectroradiometer (Apogee Ps-300) on bare soil and vegetation. With regard to thermal ground truths, wet and dry panels/surfaces have been used as references, measuring their temperature before and after UAV thermal flights by means of a handheld infrared thermometer.

Keywords Precision agriculture (PA) · Remote sensing (RS) · Unmanned aerial vehicle (UAV) · Thermal surveys · Multispectral surveys · Onion crop

G. Messina · S. Praticò · S. Di Fazio · G. Modica (✉)
Dipartimento Di Agraria, Università Degli Studi Mediterranea Di Reggio Calabria, Località Feo
Di Vito, 89122 Reggio Calabria, Italy
e-mail: giuseppe.modica@unirc.it

B. Siciliani · A. Curcio
DR-One S.R.L., Via Card. F. Ruffo N. 6 I-87033 - Belmonte Calabro, Cosenza, Italy

© Springer Nature Switzerland AG 2020
A. Coppola et al. (eds.), *Innovative Biosystems Engineering for Sustainable Agriculture,
Forestry and Food Production*, Lecture Notes in Civil Engineering 67,
https://doi.org/10.1007/978-3-030-39299-4_94

1 Introduction

Remote sensing (RS) is the practice of obtaining information about an object, an area, or a phenomenon through the analysis of images acquired using a device without making physical contact with them (Lillesand et al. 2015). RS investigations are mostly based on the development of a deterministic relationship between the amount of reflected emitted or backscattered electromagnetic energy, in specific bands or frequencies, and the chemical, biological, and physical characteristics of the studied phenomena. Agriculture constitutes one of the most important fields where RS is employed, particularly in the aspects related to precision agriculture (PA) (De Montis et al. 2017). PA means a management strategy that, using modern instruments, aims at carrying out agronomic interventions in compliance with the actual crop needs and the biochemical and physical characteristics of the soil. PA analyses and manages the spatial variability of the field to optimize profitability, sustainability, and protection of agro-ecological services. Conventionally, RS has been associated with satellites and manned aircrafts equipped with different sensors (Pajares 2015). In recent years, considerable technological developments particularly concerned with the use of unmanned aerial vehicles (UAVs) platforms, has been registered (Chen et al. 2016). Various types of sensors have been tested for their ability to detect early changes in plant physiology caused by biotic and abiotic stress (Mahlein 2016). Today, multispectral (MS) cameras mounted on board of UAVs represent the most commonly used RS systems in agriculture (Khanal et al. 2017). Optical RS is based on the detection of the reflected energy from an area of interest (AOI) in the electromagnetic (EM) regions of visible (380–720 nm), near-infrared (NIR) (750–1400 nm) and in the short wave infrared (SWIR) (1400–3000 nm) (Prasad et al. 2011). However, especially in PA applications, results coming from visible and NIR spectrum often are not sufficient (Stark et al. 2014). In contrast, the surface temperature detected by thermal sensors was found to be a rapid response variable to monitor plant growth and stress (Anderson et al. 2013; Stark et al. 2014). Nevertheless nowadays there are very limited studies focused on UAV acquired thermal images in PA (Khanal et al. 2017). Thermal RS deals with the study of data obtained measuring the emitted radiation from the surface of an object, in the thermal infrared (TIR) region of the EM spectrum (Prakash 2000), and its conversion into temperature without establishing a direct contact with the object itself (Khanal et al. 2017). The potentialities of application of thermal UAV RS concern several mapping and monitoring issues: plant water stress, drought, plant disease detection, soil characteristics, residue cover and tillage, field tile, crop maturity, and yield estimation. The present paper shows the potentiality of coupling multispectral and thermal imagery acquired by UAVs in monitoring crops.

2 Materials and Methods

2.1 Study Site

The study was performed in an onion field located in Campora S. Giovanni, in the municipality of Amantea (Cosenza, Italy). Since 2008, the onions here produced are labeled with the European Protected Geographical Indication label “Cipolla Rossa di Tropea IGP.” The producer farms are organized in a consortium with a crop surface of 500 hectares. The experiment site has an area of 2 hectares (Fig. 1). The UAV flights were carried out three times two months after the transplant of onions (Fig. 1a and b), which took place in early September, operating the first flight on 23 November 2018 and performing two other flights on 19 December 2018 and 18 January 2019.

Multispectral surveys were carried out at 50 m of flight height by means of the fixed-wing UAV Parrot Disco-Pro AG equipped with a multispectral camera Sequoia

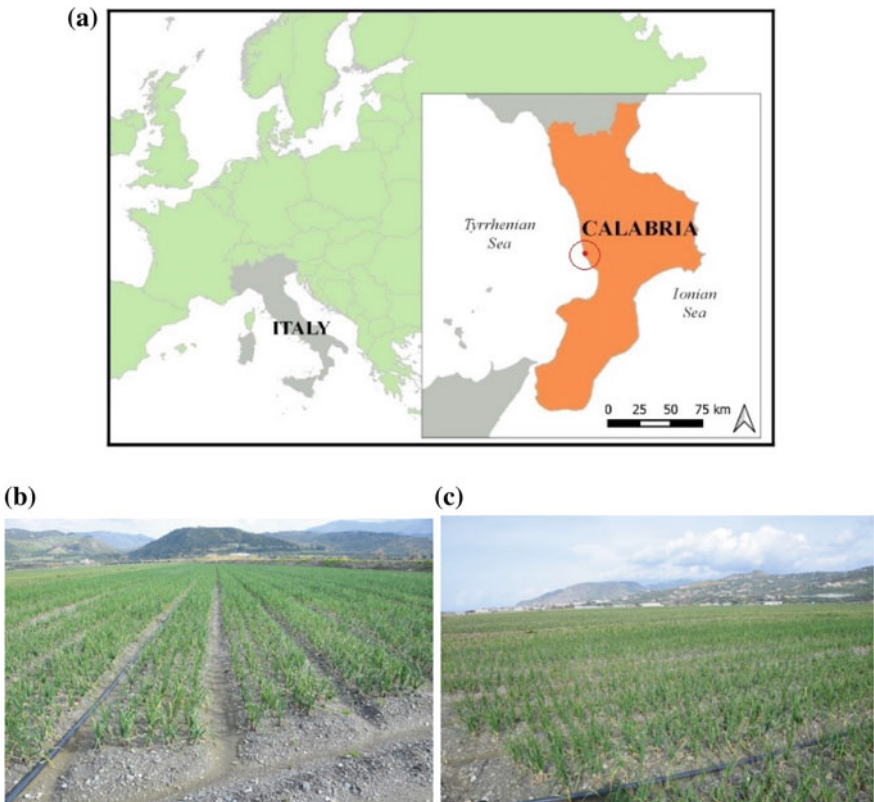


Fig. 1 a The localisation of the study site. b–c The Onion field in which the experiments were carried out (Campora S. Giovanni, CS–Italy)

Parrot (Fig. 2b). The Parrot Sequoia MS has four different channels, each with 1.2 Mpx of resolution: green (530–570 nm), red (640–680 nm), red edge (730–740 nm) and near-infrared (770–810 nm). Furthermore, it is also equipped with a RGB composite sensor, and an external irradiance sensor with GPS and IMU placed on top of the UAV. The latter is used to capture sensor angle, sun angle, location, and irradiance for every image taken during flight. Thermal surveys were carried out using a quadcopter DJI Phantom 4 (Shenzhen, China), equipped with a thermal camera Flir Vue Pro R 640 (Fig. 2a) (FLIR Systems, Inc., Wilsonville, Oregon, USA). The thermal camera captures temperature with a spectral range of 7.5–13.5 μm with a resolution of 640×512 pixels and a thermal accuracy of ± 5 °C. The model used in our experiments was equipped with a 9 mm focal lens, offering a field of view (FOV) of $69^\circ(\text{H}) \times 56^\circ(\text{V})$. The camera has been set by means of Flir Vue Pro APP that is the primary control interface available. The JPEG format selected has both the compressed 8-bit processed JPG image and 14-bit raw sensor data that provide data about Scene, Palette, and Telemetry. About radiometry settings, humidity was set on medium value (45%), air temperature at 25 °C and emissivity on 98%. The UAV equipped with thermal camera was flown two times during the 23 November between 12:28 and 12:50 (local time). The flight height was set to 40 m, while the interval timer shooting was set to 2 s.

Over the field plot, a total of 9 GCP were placed and geo-referenced using a Leica RTK GPS with a planimetric accuracy of 0.03 m. For each GCP were used two different targets, i.e. for multispectral and thermal surveys (Fig. 3b). In particular, GCPs were made using 50 cm \times 50 cm white polypropylene panels and covering two quadrants by respectively black cardboard and aluminum sheets in multispectral and thermal GCPs to locate the point. According to the characteristics of thermal cameras, aluminum is used as the material of control targets with their size identified clearly in the thermal images. In fact since aluminum material has a low emissivity, the target appears distinctively as a cold object in thermal imagery.

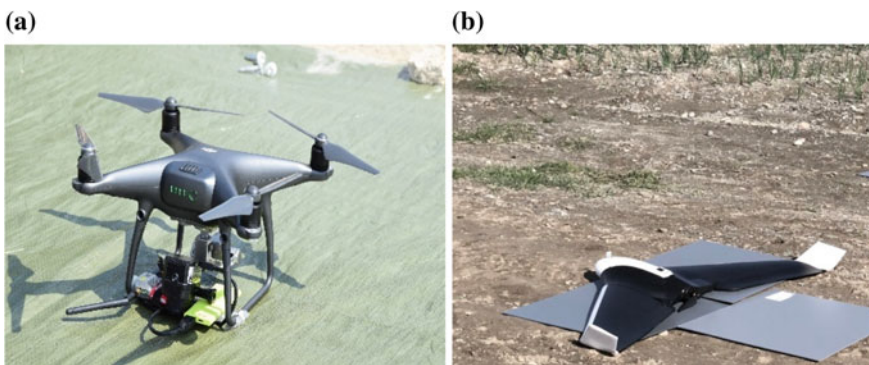


Fig. 2 **a** DJI Phantom 4 equipped with the thermal camera Flir Vue Pro R 640. **b** Parrot Disco-Pro AG equipped with the Multispectral camera Parrot Sequoia

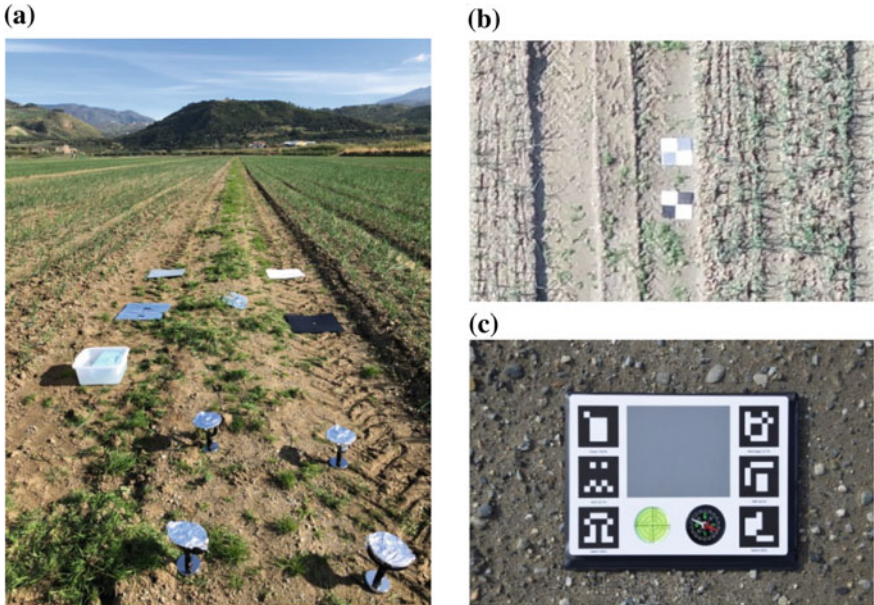


Fig. 3 **a** Temperature reference targets used during thermal surveys. **b** Thermal (above) and multispectral (below) targets used to survey the ground control points (GCPs) in the onion field. **c** The Parrot Sequoia calibration target

Furthermore, being thermal cameras on UAVs typically equipped with uncooled microbolometer sensors the thermal signal can be highly influenced by the temperature of the sensor, body, and lens. For this reason wet and dry reference panels/surfaces with known temperatures have been used by taking images of them before and after the flights. Reference surfaces (Fig. 3a) were placed near the UAV take-off, and landing point and their temperature were measured three times by means a handheld infrared thermometer (FLIR E6): at take-off, during and at the end of every flight. These measurements can then be used to compensate for changes in sensor temperature. For this purpose, four reference surfaces were used. Three of them were dry: three panels of polypropylene (white, grey, and black). The fourth target was created delimiting with circular targets, covered with aluminum, a square piece of ground keeping it constantly wet for the duration of the flight.

Furthermore, the temperature of the dry soil near the targets was measured using a probe thermometer.

UAV multispectral imagery was calibrated with a panel with known reflectance and using a spectroradiometer for ground truth measurements (Apogee Ps-300) on bare soil, vegetation, and using Parrot Sequoia calibration target (Fig. 3c).

All consecutive images were processed via aerial image triangulation with the geo-tagged flight log and the GCPs using the software Pix4D. The digital elevation model (DEM) was obtained from the dense point cloud with a ground sample distance (GSD) of 5 cm/pixel and a mean geolocation accuracy of 0.37 m for X/Y axes and

0.43 m for Z axis. Then, the orthomosaic was built using the DEM as the surface reference.

3 Preliminary Results and Future Developments

Orthomosaics obtained from both thermal and multispectral and characterized by 8.5 and 5 cm of GSD, respectively, showed a clear difference in both temperature and vegetative state of the crop in two distinct areas of the experimental field (Fig. 4).

Moreover, a geographical object-based image classification (GEOBIA) procedure for the identification and classification of onions and weeds was performed. Differently from previous research carried out by the research group and using Orfeo Toolbox (De luca et al. 2019) or Erdas Imagine Objective (Solano et al. 2019), in this case, GEOBIA was implemented through eCognition Developer 8 (Trimble GeoSpatial, Munich, Germany). The classification was developed starting from images in the bands Green, NIR, Red, RedEdge using only the spectral response of the vegetation in the different bands. The images were segmented into uniform multi-pixel objects using the multiresolution algorithm (Baatz and Schäpe 2000) and setting the following parameters: 1, 0.1, and 0.5 for scale, shape, and compactness, respectively. After segmentation, onions were classified according to GNDVI values. In particular onions objects were attributed to $GNDVI \geq -0.15$.

In view of these results, a monitoring plan was prepared to detect the presence of any diseases that often cause damage to the production of the farm (for example the *Onion Yellow Dwarf Virus-OYDV* and the fungus *Sclerotinia Cepivorum*) and other causes and concauses that determine conditions of vegetative stress of a part of the crop as can be seen. The plan provides for the monitoring of the crop from the transplantation phase to harvesting. The first step involves a systematic sampling of soil. Sampling will consist of collecting 56 soil samples distributed according to a grid pattern 10 m × 50 m. On each row, each sample will be collected at a distance of 10 m from the next one. For each sample, the corresponding position will be stored using GNSS.

The soil samples will be subjected to the following analyses:

- Determination of total or organic carbon and total nitrogen;
- Determination of nitrate ion content;
- Determination of ammonia nitrogen;
- Determination of assimilable phosphorus (Olsen method);
- Determination of infiltration rate;
- Determination of electrical conductivity;
- Resistance to penetration;
- Particle size analysis.

Following the soil analysis, constant UAV multispectral and thermal surveys (weekly or fortnightly) will be carried out until the harvesting to verify the state of growth and the phytosanitary status of the crop.

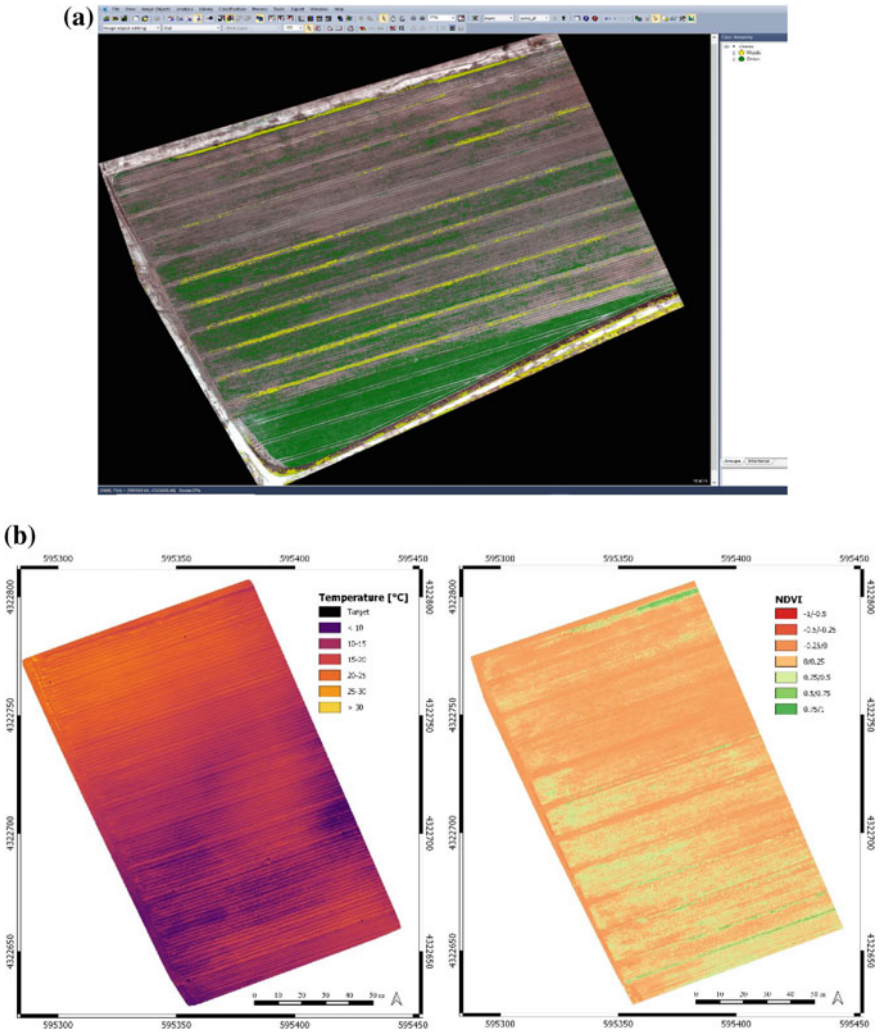


Fig. 4 **a** A map showing the image-object classification of weeds (yellow) and onions (green) performed in eCognition suite. Below, the two obtained orthomosaics from the UAV surveys carried out on 23 November 2018. **a** map of the temperatures [°C]. **b** map of the normalized difference vegetation index (NDVI)

At the same time as monitoring on the same field, suitably divided into 3 streaks and 27 plots, two different tests will be carried out. Along with the three streaks three different treatments will be carried out from the phytosanitary point of view using a biological fungicide product (still to be selected), a fungicide product usually used by the company and finally a non-treatment using water. In the 27 plots chosen in such a way as to have 3 repetitions, a different dose of nitrogen fertilizer will be

administered. The 3 doses will be one corresponding to the one used by the company and the other two respectively higher and lower than 10% of the former.

The proposed methodology, especially in presence of an area with homogeneous soil characteristics, could be an useful tool in the study of the response of various crops to phytosanitary and fertilizer treatments in different areas.

References

- Anderson, M. C., Hain, C., Otkin, J., Zhan, X., Mo, K., Svoboda, M., et al. (2013). An intercomparison of drought indicators based on thermal remote sensing and nldas-2 simulations with u.s. drought monitor classifications. *Journal of Hydrometeorology*, *14*, 1035–1056. <https://doi.org/10.1175/JHM-D-12-0140.1>.
- Baatz, M., & Schäpe A. (2000). Multi-resolution segmentation: An optimization approach for high quality multi-scale segmentation. In *Beiträge zum, AGIT XII Symposium* (pp. 12–23). Salsburg.
- Chen, S., Laefer, D. F., & Mangina, E. (2016). State of technology review of civilian UAVs. *Recent Patents on Engineering*, *10*, 160–174. <https://doi.org/10.2174/1872212110666160712230039>.
- De Montis, A., Modica, G., & Arcidiacono, C. (2017). AgInformatics. In L.A., Schintler, & C.L. McNeely (Eds.), *Encyclopedia of Big Data* (pp. 1–4). Springer International Publishing, Cham. https://doi.org/10.1007/978-3-319-32001-4_218-1.
- De Luca, G., N. Silva, J.M., Cerasoli, S., Araújo, J., Campos, J., Di Fazio, S., & Modica, G. (2019). Object-Based Land Cover Classification of Cork Oak Woodlands using UAV Imagery and Orfeo ToolBox. *Remote Sens* *11*, 1238. <https://doi.org/10.3390/rs11101238>.
- Khanal, S., Fulton, J., & Shearer, S. (2017). An overview of current and potential applications of thermal remote sensing in precision agriculture. *Computers and Electronics in Agriculture*, *139*, 22–32. <https://doi.org/10.1016/j.compag.2017.05.001>.
- Lillesand, T., Kiefer, R. W., & Chipman, J. (2015). *Remote sensing and image interpretation* (7th ed.). New York: Wiley.
- Mahlein, A.-K. (2016). Present and future trends in plant disease detection. *Plant Disease*, *100*, 1–11. <https://doi.org/10.1007/s13398-014-0173-7.2>.
- Pajares, G. (2015). Overview and Current Status of Remote Sensing Applications Based on Unmanned Aerial Vehicles (UAVs). *Photogrammetric Engineering & Remote Sensing* *81*, 281–330. <https://doi.org/10.14358/PERS.81.4.281>.
- Prakash, A. (2000). Thermal remote sensing: concepts, issues and applications. In: *International Archives of Photogrammetry and Remote Sensing* (Vol. XXXIII, pp. 239–243).
- Prasad, S., Bruce, L.M., & Chanussot, J. (Eds.). (2011). *Optical Remote Sensing*. Springer, Berlin. <https://doi.org/10.1007/978-3-642-14212-3>.
- Solano, F., Di Fazio, S., & Modica, G. (2019). A methodology based on GEOBIA and WorldView-3 imagery to derive vegetation indices at tree crown detail in olive orchards. *International Journal of Applied Earth Observation and Geoinformation*, *83*, 101912. <https://doi.org/10.1016/J.JAG.2019.101912>.
- Stark, B., Smith, B., Chen, Y. (2014). Survey of thermal infrared remote sensing for Unmanned Aerial Systems. In: *2014 International Conference on Unmanned Aircraft Systems*. (pp.1294–1299). <https://doi.org/10.1109/ICUAS.2014.6842387>.